FACULTAD DE INGENIERIA U.N.A.M.
DIVISION DE EDUCACION CONTINUA

CURSOS ABIERTOS

DESARROLLO Y OPERACIÓN DE SENSORES PARA CONTROL DIRECTO Y CONTINUO EN PLANTAS DE BENEFICIO DE MINERALES Y EN LA RESTAURACIÓN DEL MEDIO AMBIENTE

Del 18 al 23 de mayo de 1998

TEMA:BAFFLED - COLUMN FLOTATION OF A COAL PLANT FINE - WASTE STREAM

EXPOSITOR :DR. KOMAR KAWATRA

1998

Minerals and Metallurgical Processing
Vol. 12, No. 3, Aug. 1995, pp 103-107

Baffled-Column Flotation of a Coal Plant Fine-Waste Stream

T. C. Eisele and S. K. Kawatra
Department of Metallurgical and Materials Engineering
Michigan Technological University
Houghton, Michigan

Abstract. It is common in coal-cleaning operations to produce a fine waste stream which contains a considerable amount of coal, but which is not economical to recover both because it is mixed with large amounts of difficult-to-remove clay slimes, and because the fine coal is often heavily oxidized or contaminated. Conventional froth-flotation machines cannot produce an acceptable product from such material in a single stage of flotation, and even flotation columns often have difficulty cleaning this type of feed.

A new type of flotation column was designed specifically to deal with these problems, and was installed and tested in a coal-cleaning plant in Ohio. The feed coal contained 39.8% ash as fine clay, 2.83% total sulfur, was 80% passing 176 micrometers, and had a heating value of 8401 BTU/lb. The coal was the tailings thickener product for the plant. Plant personnel felt that the coal was too heavily oxidized and contaminated for flotation to be effective, as previous attempts at conventional flotation of this material in the plant had been abandoned. However, using the new column it was possible to recover up to 85% of the calorific value in a product containing less than 11% ash, and up to 60% of the calorific value in a product of less that 8% ash. The bulk of the pyritic sulfur was rejected from the coal as well.

Introduction

Flotation columns have been widely adopted in many mineral beneficiation applications in recent years, because they are more efficient separators than conventional flotation machines (Parekh et al., 1990; Groppo et al., 1994). Columns are more effective because they establish a long concentration gradient between the froth product and the sinks product. This is in contrast to conventional flotation machines, where the separation mainly occurs at the pulp/froth interface.

Froth washing in the columns, which reduces entrainment of gangue into the froth, further improves the separation.

As columns are increased in size from laboratory or pilot scale to full scale, their performance tends to be degraded by increasing axial mixing. In this paper, the use of horizontal baffles is described, which reduce axial mixing by a method that is expected to be suitable for retrofitting existing larger columns.

Theoretical Discussion

In flotation columns, vertical mixing along the axis of the column (axial mixing) is generally harmful, as it tends to reduce the product recovery and to make the separation less selective (Finch and Dobby, 1990). In the most common type of flotation column, shown in Figure 1, there is no restriction to flow of air and water along the axis of the column. Rising air bubbles therefore are free to carry slurry up along the axis, which then returns to the bottom along the sides of the column, producing strong axial mixing. Considerable effort has been made to minimize this effect by means such as the use of microbubble generators, by multi-level air injection, and by uniformly dispersing the bubbles across the entire cross-section of the column so that there are no areas where unusual numbers of bubbles are rising and producing a vertical current. While these measures have been reported to show a certain degree of success in columns that are kept in perfect working order at all times, any malfunctions that either allow large air bubbles to form, or that make the distribution of air bubbles non-uniform, will cause axial mixing to occur again. It is therefore important that the column be designed not only to minimize axial mixing when everything is working well, but also to suppress any axial mixing that is produced by equipment imperfections or malfunctions.

Work has been done in the past using vertical baffles to subdivide the column and reduce the apparent diameter, with the goal of reducing axial mixing, but this has been found to introduce bubble-distribution problems (Finch and Dobby, 1990) and has been found to have only a small effect on performance in any case (Alford, 1992).

In attempts to design columns that would inherently prevent axial mixing, two different approaches were taken, by Yang (1988) and Dell (1976). Yang (1988) used packing similar to that used in packed distillation columns. While Yang's column was effective for ultrafine particles finer than 20 micrometers, the packings were very prone to plugging by solids, and so maintenance costs would be high. Coal flotation is typically carried out with a top particle size of nearly 0.5 millimeter, which is far too coarse for the packed column to handle without plugging, Therefore, Yang's column is not suitable for existing coal-cleaning operations. In the Leeds column, designed by Dell (Degner and Sabey, 1988), a combination of fixed and movable rods in discrete racks was used to horizontally divide what was essentially a conventional flotation machine into a series of stacked chambers. The goal was to mimic the performance of a multi-stage flotation circuit with several stages of froth recleaning. In the Leeds column, the feed was introduced in the bottom chamber which resulted in a considerably cleaner froth, although no attempt was made to improve recovery. Because the rod-racks are fairly thick, the machine is only sectioned into a few chambers. The use of moving parts in the rod-racks is also likely to contribute to excessive wear. Because of these problems, neither of the above columns have been adopted commercially by the coal industry.

The horizontal baffles described in this paper provide many of the advantages of both the regular column and the packed column, while minimizing the drawbacks. The horizontal baffles consist of simple perforated plates, with openings large enough to keep them from being plugged by solid particles, but small enough to break up vertical mixing currents, as shown in Figure 1, so that slurry cannot be rapidly swept along the axis of the column. This provides a much closer approximation to plug flow, and therefore improves the separation. The perforated-plate baffles are much simpler and take up less volume than the rod-racks used in the Leeds column (Dell, 1976), and are much more resistant to plugging and wear than closely-spaced packing material. They are also more suitable for retrofitting existing columns, as they are simple to make and install.

In previous work by the authors (Kawatra and Eisele, 1993; Eisele, 1992), it was found that the best results were obtained in the laboratory when the baffles had between 29 and 38% open area and were present both above and below the feed inlet. In the work described in this paper, a pilot-scale column of the same basic design as the laboratory column was tested in an operating coal-cleaning plant, to determine whether there were any obvious scale-up difficulties, such as plugging, with the baffles.

Procedures

Plant Characteristics

Based on the results of previously-described laboratory studies (Kawatra and Eisele, 1993), a pilot-scale Deister Flotaire column (20.3 cm diameter) was modified and installed in the Empire Coal processing plant, Gnadenhutten, Ohio. The flowsheet of the Empire fine coal cleaning circuit is given in Figure 2.

Feed Characteristics

This plant processes a mixture of bituminous coals from the Lower Kittanning (#5) seam and the Middle Kittanning (#6) seam, with the main gangue mineral being fine clay. The feed used for the tests described in this paper was collected from the plant filter-press, which dewatered the solids from the plant tailings thickener. This material contained 39.8% ash, 2.83% total sulfur, 2.04% pyritic sulfur, and 8401 BTU/lb. The size distribution was 80% passing 176 micrometers, and 10% passing 3.7 micrometers. The plant had originally included conventional froth flotation in its flowsheet, but the flotation circuit had to be abandoned because it could not produce a sufficiently high-quality product from the coal being processed. Plant personnel felt that the fine coal was too heavily oxidized and contaminated by flocculants and dewatering aids to be floatable by conventional flotation.

Pilot-Scale Column Design

The column was derived from a Deister Flotaire unit, 20.3 cm in diameter and 9.1 meters tall. A schematic of the column is given in Figure 3. Air bubbles were injected at 4.5 meters and 9.1 meters below the froth overflow lip. The column contained 9 upper baffles, and 17 lower baffles, as shown in Figure 3, each with 34% open area. The bubble generators were manufactured by the Deister Concentrator Co, which injected an air-water mixture at a volume ratio of 7.5/1. The two bubble generators used each had maximum flowrates of 28.3 standard liters/min of air, and 3.78 liters/min of water (Eisele, 1992).

The column was operated with a froth depth of 61 cm. Measuring from the froth overflow lip, the end of the feed inlet tube was at a depth of 122 cm. This long feed tube was needed so that there would be enough room between the froth base and the feed inlet to install baffles. The upper baffles extended from a depth of 71 cm to 117 cm, and the lower baffles extended from 147 cm to 234 cm. The washwater spray ring was immersed 5 cm below the froth surface, and the washwater flowrate was maintained at 7.57 liters/min.

In initial tests, it was found that the clean-coal froth would immediately collapse unless frother was added to the washwater. This was due to the upper baffles increasing the effectiveness of the washwater, such that the frother rising from the feed slurry or the bubble generator water was flushed back down before it could reach the froth.

The baffles also caused the froth to be much more stable, because they broke up large bubbles into smaller bubbles, and made them rise more slowly. This was beneficial, as it prevented the bubbles from entering the froth layer at high speeds, and disrupting the froth. However, it also allowed parts of the top of the froth to dry slightly into a semisolid mass that stuck to the feed tube. Over time, this would form a cap and eventually plug the top of the column. This was prevented by installing additional spray nozzles above the froth, spraying a mist of water at 1 liter/min to keep the top of the froth moist and fluid, so that it would not become sticky. This spray was in addition to the main washwater ring.

No operational problems were encountered with plugging of the baffles in any of the tests, even when large particles of approximately 1 millimeter in diameter were present in the feed.

Feed Preparation and Reagents

For the series of tests described in this paper, approximately 1 metric ton of filtered solids was collected from the plant fine-tailings filter-press, and thoroughly mixed. The collector used was a mixture of 80% #2 fuel oil and 20% Dow M210 froth conditioner (which is more effective for difficult-to-float coal than fuel oil alone). In addition, DF1012 (a very strong polypropylene-glycol-based frother manufactured by the Dow Chemical Co) was also used. This frother was selected because the presence of a dewatering aid in the column feed made it necessary to use a very strong frother in order to maintain a satisfactory froth.

The column was run by preparing a large volume of feed slurry in a 55-gallon drum, and continuously pumping slurry into the column during each test, so that random variations in the plant feed would not disturb the column operation. For each test, 190 liters of a 10% solids slurry was prepared, and conditioned for 5 minutes with the desired reagents. The column was first filled with plant process water and operated until a stable froth layer had formed. The feed slurry pump was then started, with the feed slurry pumped into the cell at a steady flowrate of 7.6 liters/min for 25 minutes. Froth and tailings samples were collected after 20 minutes, which provided sufficient time for the column to reach steady-state. The residence time of slurry in the column was calculated to be approximately 15 minutes.

Two sets of tests were carried out with this feed. The first set was carried out at a constant reagent dosage while the baffle configuration and bubble-generator configuration was varied. The reagent dosage was selected to be less than optimum for these tests, so that the effect of the baffles on the recovery could be clearly seen. The second series of tests used a constant baffle configuration while the reagent dosage was changed, so that the ultimate ability of the column to recover clean coal from this feed could be determined.

Series 1: Baffle Variation

The first test series used a constant reagent dosage (80% #2 fuel oil/20% M210 at 1.1 kg/mt; DF 1012 at 0.36 kg/mt), and duplicate tests were run with each of the following conditions:

1: No baffles, both bubble generators used;

2. Upper baffles installed, both bubble generators used;

3. Lower baffles installed, only upper bubble generator used;

4. Both upper and lower baffles installed, only upper bubble generator used.

When the lower baffles were installed, only the upper bubble generator was used. This was done to determine whether there was any potential for reducing the necessary height of the column when baffles were installed. As a result, the comparison is essentially between an unbaffled column 9.1 meters tall, and a column with lower baffles and an active height of only 4.6 meters. When both bubble generators were used, the air flow was evenly divided between them. The total air flowrate with both generators operating was 35.5 standard liters/min, while the air flowrate with only the upper bubble generator running was 28.3 standard liters/min.

Series 2: Reagent Variation

The tests in the second series were all carried out with all of the baffles in place, and with only the upper bubble generator used. Eleven single-stage tests were carried out in this series, with the collector and frother dosages varied as shown in Table 1, along with the BTU recoveries obtained with each reagent dosage. In two additional tests, the froth product from the column was refloated, to determine whether any significant grade improvement would result from 2-stage flotation.

Results

The effect of the baffles on the column operation is clearly seen in Figure 4. When the baffles are installed in the column, the BTU recovery is increased markedly, from only 15% without baffles, up to 54% with baffles, even though the reagent dosage is unchanged. The reagent dosages used in the baffle variation tests (1.1 kg/mt collector, and 0.36 kg/mt frother) were lower

than the values that were later determined to be needed for high BTU recovery (2.25 kg/mt collector, and 1.26 kg/mt frother), as can be seen in Table 1.

The reagent-variation studies (Figure 5) showed that the column could produce good results in a single stage, even when processing a very high-ash and difficult-to-float coal. With the proper reagent dosage, a product of 10.5% ash could be produced at 85% BTU recovery from the 39.8% ash feed stream. This feed was not considered by plant personnel to be treatable by froth flotation, and was being discarded, but the column flotation product was sufficiently clean to be salable. Reflotation of the froth product in the column did not produce a significant improvement in the grade of the clean coal at a given recovery.

Figure 6 shows that the column is also quite effective for rejecting pyritic sulfur from the coal, where rejection was calculated as:

$$\%\text{Rejection} = \frac{(\%\text{Wt Pyrite in Tails} \times \text{Tails Wt.})}{(\%\text{Wt Pyrite in Feed} \times \text{Feed Wt.})} \times 100$$

The feed contained 2.04% pyritic sulfur, and over 50% of this was rejected while recovering 85% of the calorific value. Pyrite rejections as high as 70% could be achieved at approximately 60% BTU recovery

Conclusions

The baffled column was tested on a pilot scale in an operating coal-processing plant, to recover clean coal from a high-ash, difficult-to-float coal. No serious operating problems were observed in the course of the tests, and the baffles did not plug or show any buildup of solids. The baffles were found to be effective in increasing the BTU recovery of this difficult-to float coal compared to operating with the same reagent dosages but without baffles.

The baffled column recovered up to 85% of the calorific value from this fine waste without exceeding 10.5% ash, and simultaneously rejected over 50% of the pyritic sulfur. Reflotation of the froth product showed no further improvement in the grade/recovery performance.

Acknowledgments

Support for this research was provided by the Empire Coal Co. and the Ohio Coal Development Office. The authors would also like to thank Ms. J. F. Bird and Dr. Howard Johnson of the Ohio Coal Development Office, Dr. R. R. Klimpel of the Dow Chemical Co., and Dr. B. K. Parekh of the Center for Applied Energy Research, for their useful suggestions and critical discussion of this project.

References

1. Alford, R. A., 1992, "Modelling of Single Flotation Column Stages and Column Circuits," International Journal of Mineral Processing, 36 pp 155-174
2. Degner, V. R. and Sabey, J. B., 1988, "WEMCO/Leeds Flotation Column Development," Column Flotation '88 (K. V. S. Sastry, editor) Society of Mining Engineers, Littleton, CO, pp 267-280
3. Dell, C. C., 1976, Froth Flotation, British Patent No. 1,519,075
4. Eisele, T. C., 1992, "Coal Desulfurization by Bacterial Treatment and Column Flotation," Ph. D. dissertation, Michigan Technological University
5. Finch, J. A., and Dobby, G. S., 1990 Column Flotation, Pergamon Press, Oxford
6. Groppo, J. G., Parekh, B. K., Peters, W. J., and Kennedy, D., 1994 "Three Years of Column Flotation Operating Experience at Powell Mountain Coal Co.," Proceedings, Coal Prep '94, pp 258-267
7. Kawatra, S. K., and Eisele, T. C., 1993 "The Use of Horizontal Baffles to Improve the Effectiveness of Column Flotation of Coal," XVIII International Mineral Processing Congress, Sydney, 23-28 May, pp 771-778
8. Parekh, B. K., Groppo, J. G., and Peters, W. J., 1990, "Column Flotation Circuit Installation at Powell Mountain Coal," Proceedings of the 11th International Coal Preparation Congress, pp. 267-270
9. Yang, D. C., 1988, "A New Packed Column Flotation System," Column Flotation '88 (K. V. S. Sastry, editor) Society of Mining Engineers, Littleton, CO, pp 257-266

Table 1: Reagent dosages used in column flotation tests with a complete set of baffles, and the corresponding results.

Collector Kg/mt	Frother Kg/mt	%BTU Recovery	% Pyrite Rejection	%Ash Rejection
0.55	0.18	18.19	94.6	98.1
0.55	0.36	45.55	81.4	94.5
0.55	1.26	70.55	65.8	88.2
1.10	0.18	11.33	98.2	98.9
1.10	0.36	55.90	80.3	93.9
1.10	1.26	65.26	70.6	91.0
1.30	0.36	30.31	92.4	97.3
2.25	0.54	24.65	94.9	98.0
2.25	0.72	51.12	84.1	95.6
2.25	1.26	83.57	53.3	85.3
2.25	2.52	85.26	51.7	84.0

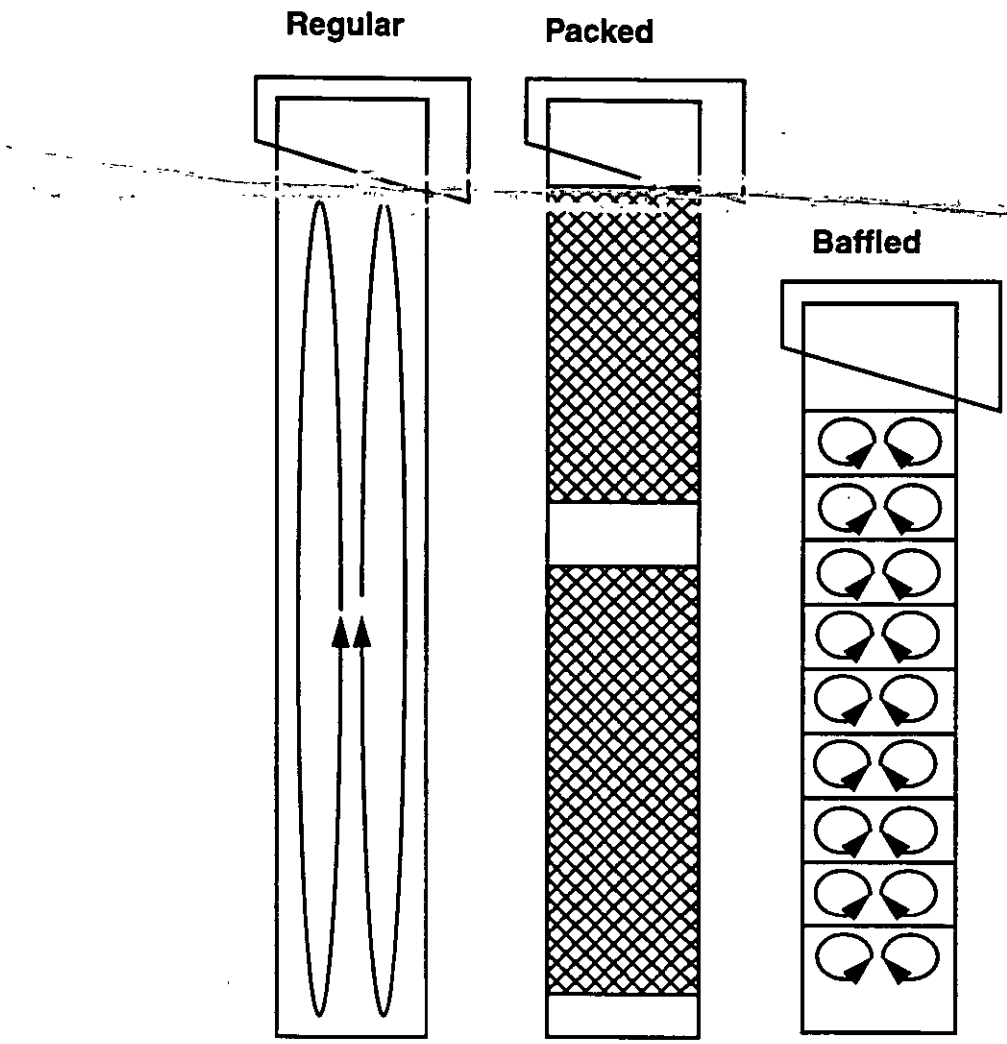

Figure 1. Comparison of mixing in regular, packed, and horizontally baffled columns.

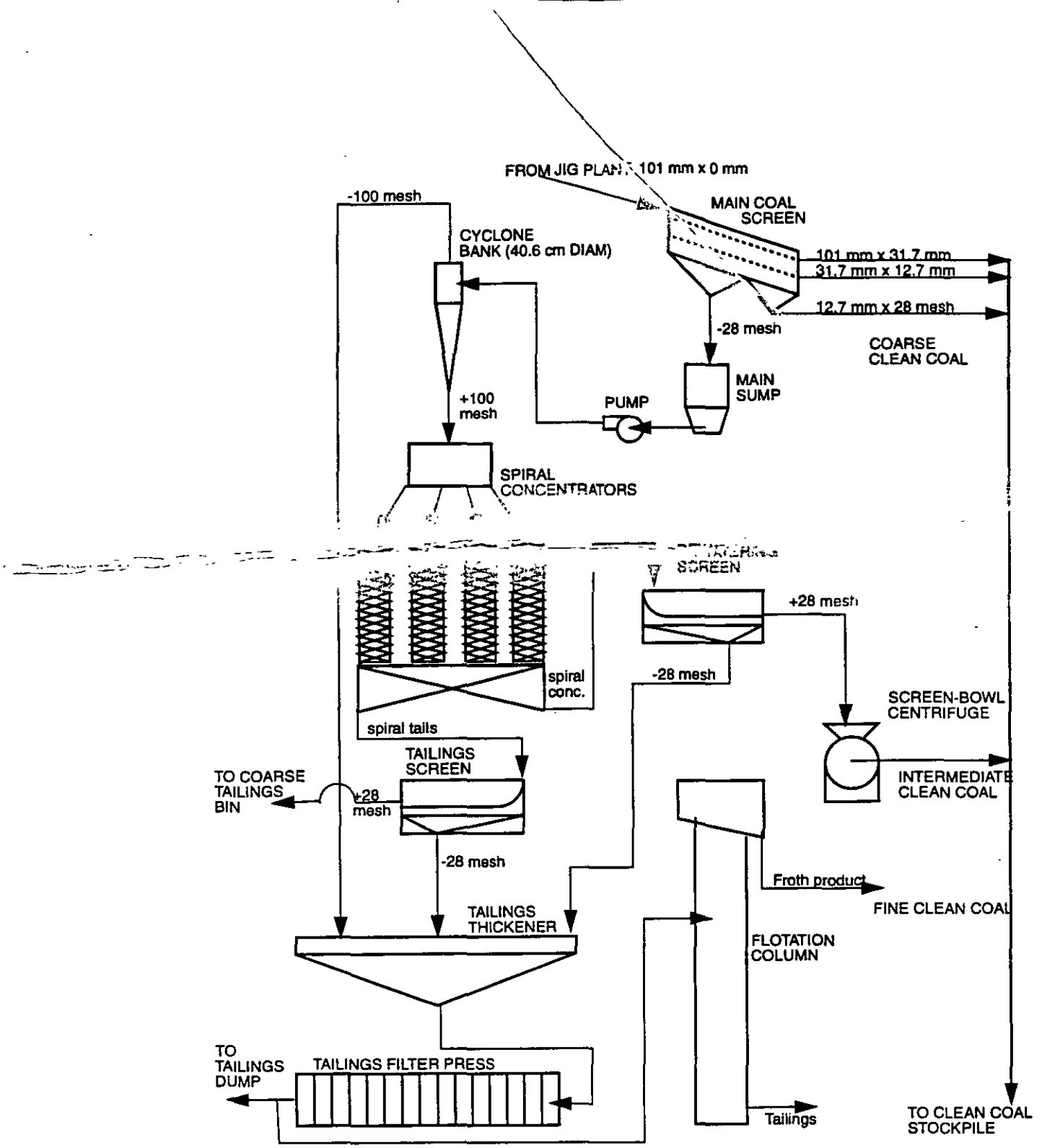

Figure 2. Flowsheet for the fine-coal processing circuit at the Empire coal processing plant. Column feed was taken from the filtered thickener product.

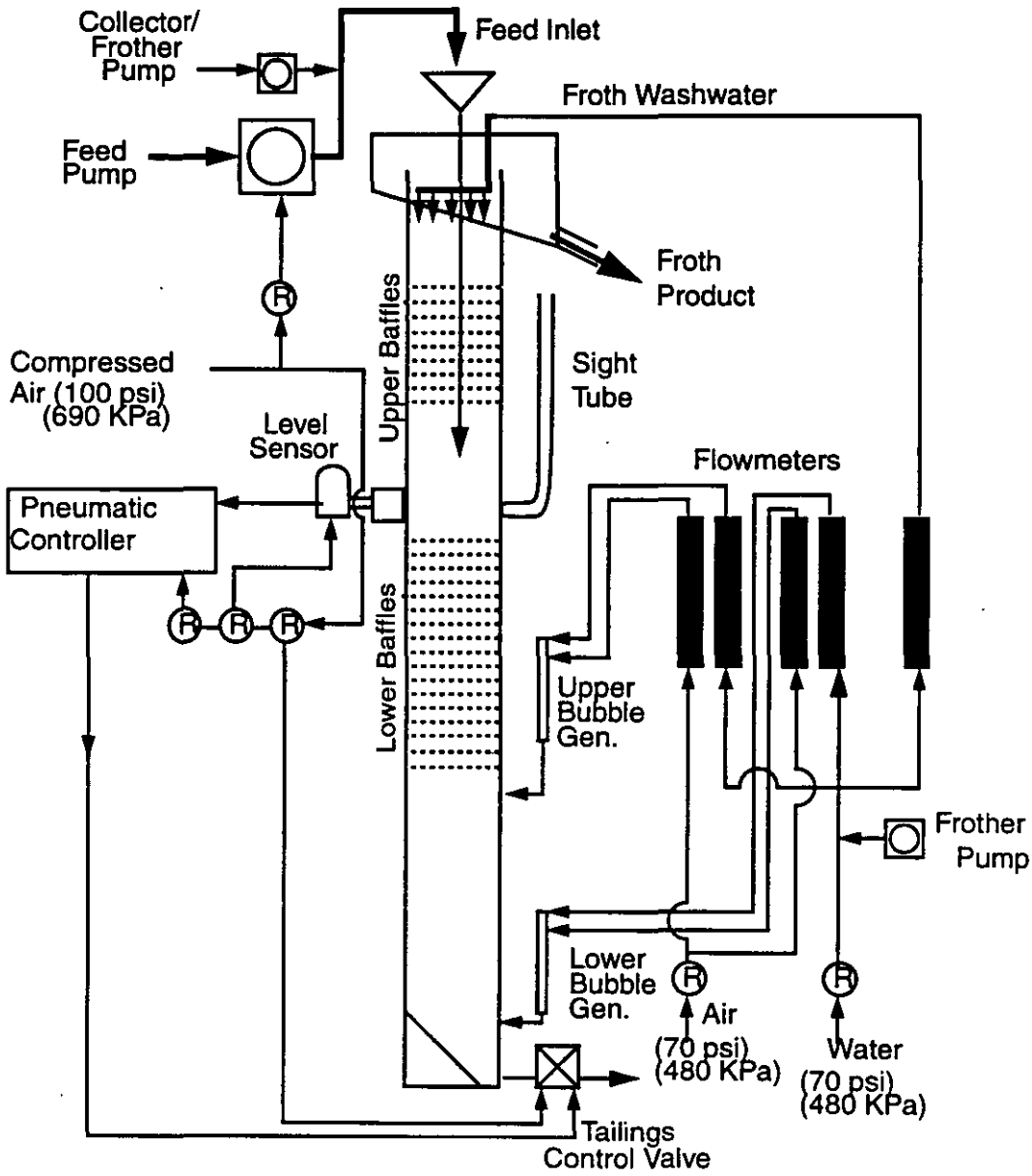

Figure 3. Schematic of the pilot-scale baffled flotation column.

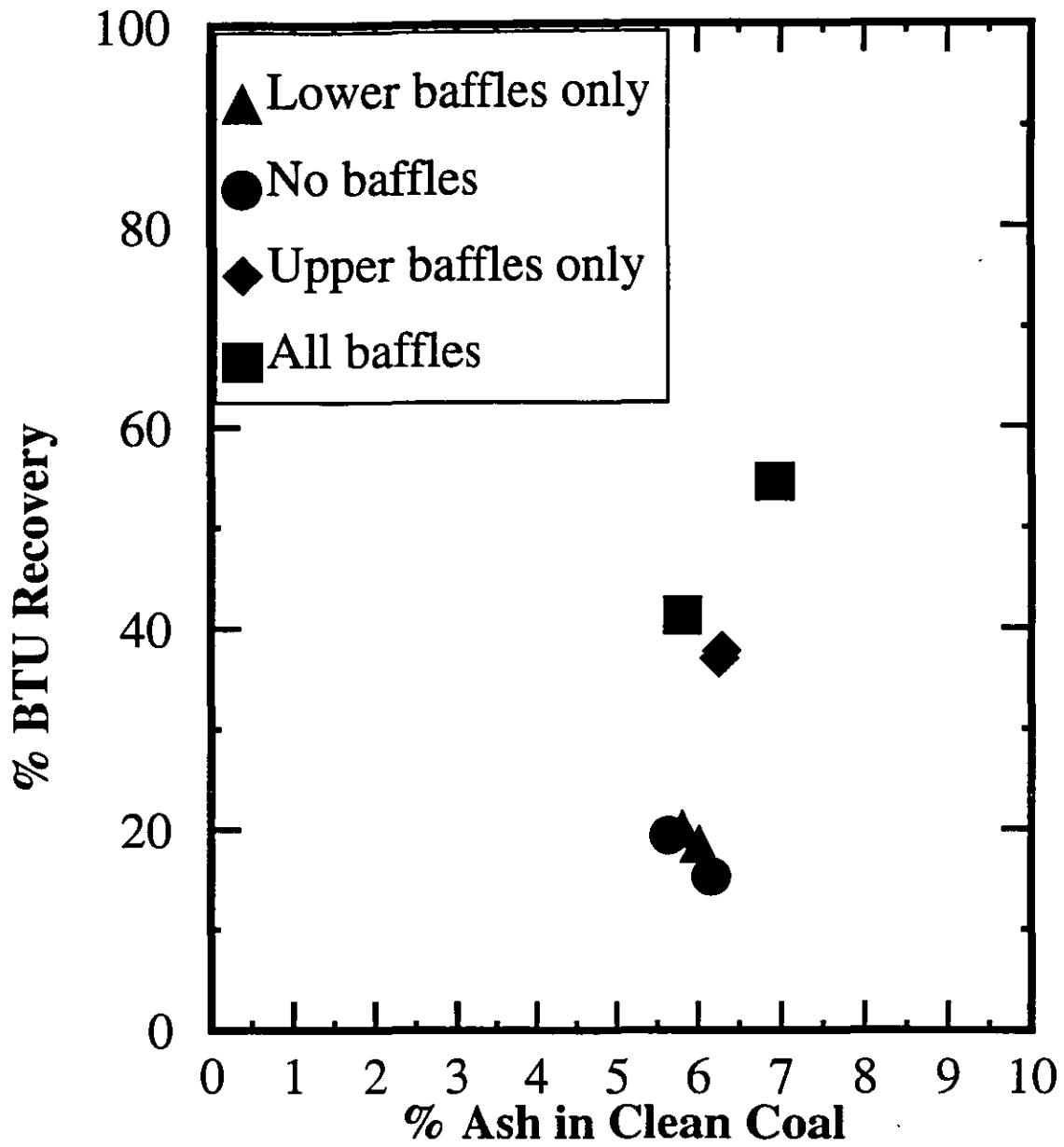

Figure 4. Effect of baffles above and below the feed inlet on the grade-recovery performance of a pilot-scale column with respect to ash. (Feed- 39.8% Ash; Collector- 80% #2 Fuel Oil, 20% Dow M210, 1.1 kg/mt; Frother- Dowfroth DF1012, 0.36 kg/mt

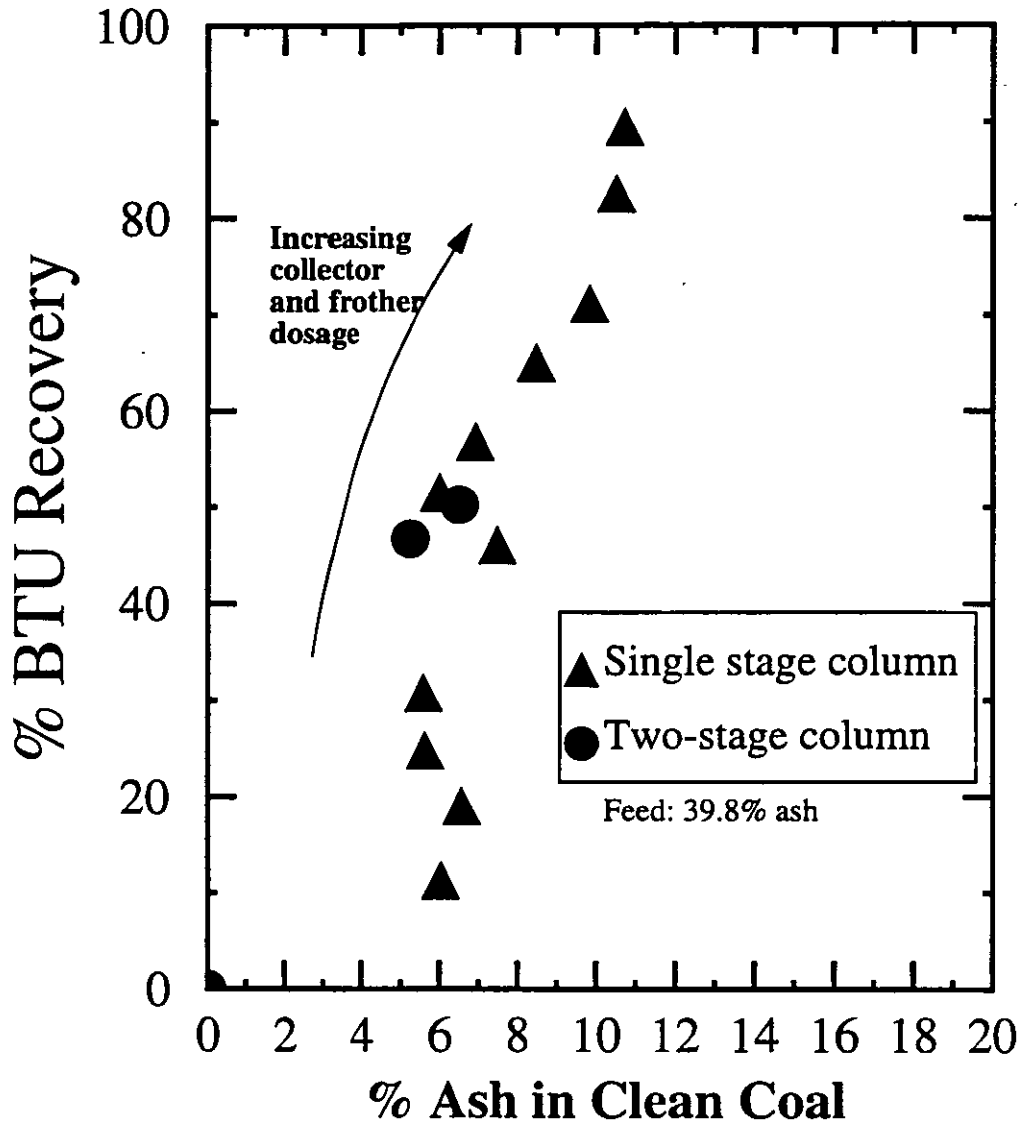

Figure 5. Grade-recovery performance of the pilot-scale column at the Empire Coal processing plant, with all baffles installed and using only the upper bubble generator.

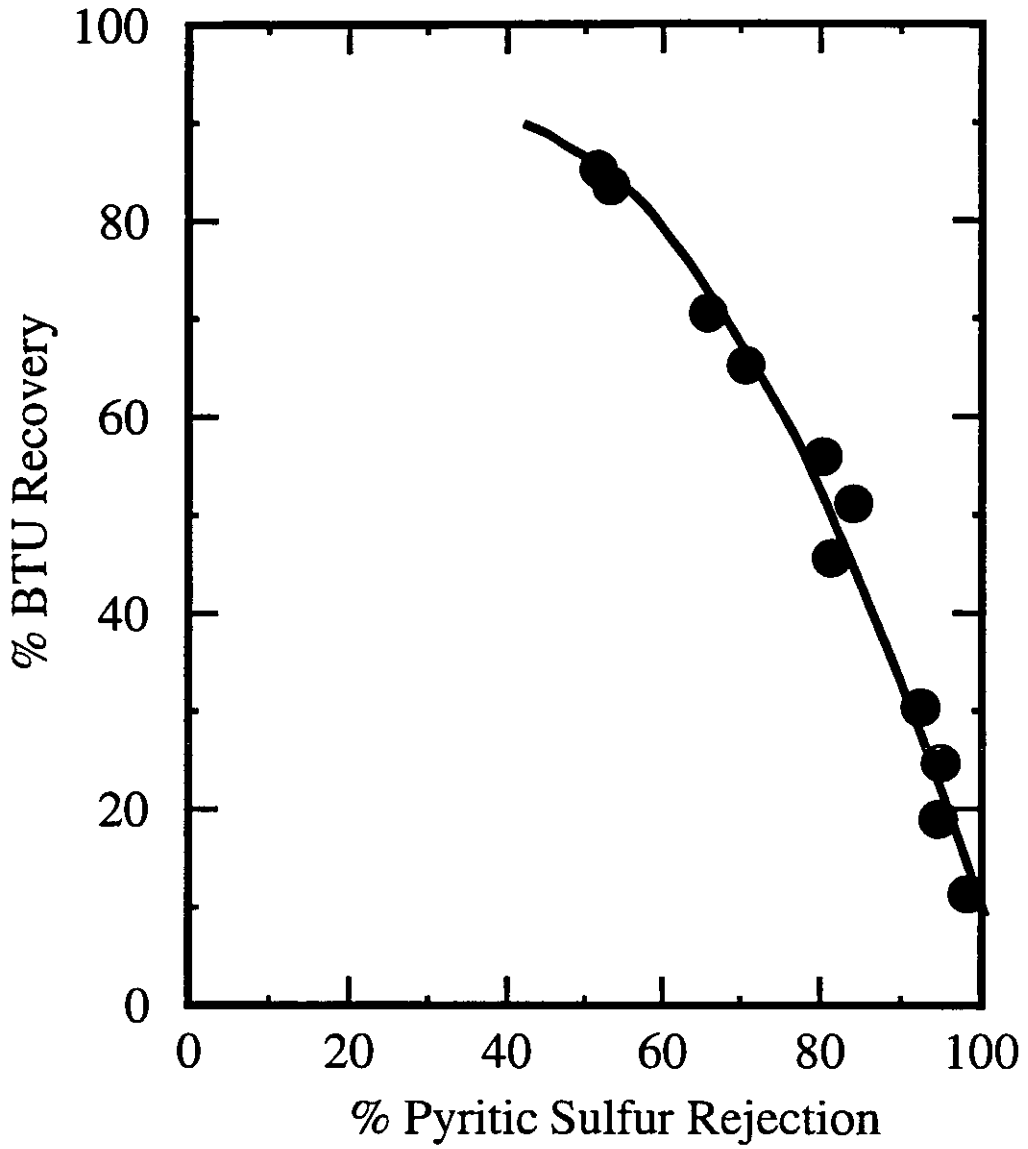

Figure 6. Comparison of BTU recovery and pyritic sulfur rejection in the pilot-scale column tests, with all baffles installed and using only the upper bubble generator.

FACULTAD DE INGENIERIA U.N.A.M.
DIVISION DE EDUCACION CONTINUA

CURSOS ABIERTOS

DESARROLLO Y OPERACIÓN DE SENSORES PARA CONTROL DIRECTO Y CONTINUO EN PLANTAS DE BENEFICIO DE MINERALES Y EN LA RESTAURACIÓN DEL MEDIO AMBIENTE

Del 18 al 23 de mayo de 1998

TEMA: LABORATORY BAFFLED - COLUMN FLOTATION OF MIXED LOWER/ MIDDLE KITTANNING SEAM BITUMINOUS COAL

EXPOSITOR :DR. KOMAR KAWATRA

1998

Volume 12, No. 2

Laboratory baffled-column flotation of mixed Lower/Middle Kittanning seam bituminous coal

S.K. Kawatra and T.C. Eisele

Abstract — *The separating efficiency of a flotation column is largely limited by the degree of back mixing of tailings into the froth zone, and the recovery is limited by the degree of short-circuiting of feed to the tailings. Current columns are typically constructed very tall (30 to 40 ft) to limit the effects of back mixing and short-circuiting. These effects can also be reduced in a much shorter column, provided that the flow in the column approaches plug-flow.*

In this work, horizontal baffles were shown to improve the performance of a 6-ft laboratory-scale flotation column treating a poorly floatable coal. Tests with variations in the baffle positions showed that baffles are needed both above and below the feed inlet to achieve the greatest benefit. Tracer tests with a fluorescent dye in water showed that baffles reduce the amount of feed water entrained in the froth at any given coal recovery.

Introduction

Because they are more efficient separators than conventional flotation machines, flotation columns are being increasingly used for many different applications. Columns are more effective because they establish a long concentration gradient between the froth product and the sinks product, so that several meters are available over which the separation can take place. This is in contrast to conventional flotation machines in which the separation mainly occurs at the pulp/froth interface. Froth washing in the columns, which reduces entrainment of gangue into the froth, further improves the separation.

In flotation columns, vertical mixing along the axis of the column (axial mixing) is generally harmful because it tends to reduce the product recovery and makes the separation less selective (Finch and Dobby, 1990). As columns are increased in size from laboratory- or pilot-scale to full-scale, the amount of axial mixing tends to increase, which not only harms the performance of larger-diameter columns, but also makes scale-up calculations more difficult (Finch and Dobby, 1990).

Previous work was performed using vertical baffles to subdivide the column in order to reduce the apparent diameter with the goal of reducing axial mixing, but this was found to introduce bubble-distribution problems (Finch and Dobby, 1990) and, in any case, was found to have only a small effect on performance (Alford, 1992). Other work attempted to use column packing similar to that used in chemical processing (Yang, 1988), but this has often introduced serious operating problems. In this paper, the use of horizontal baffles is described. These baffles reduce axial mixing by a method that is expected to be more suitable for larger columns.

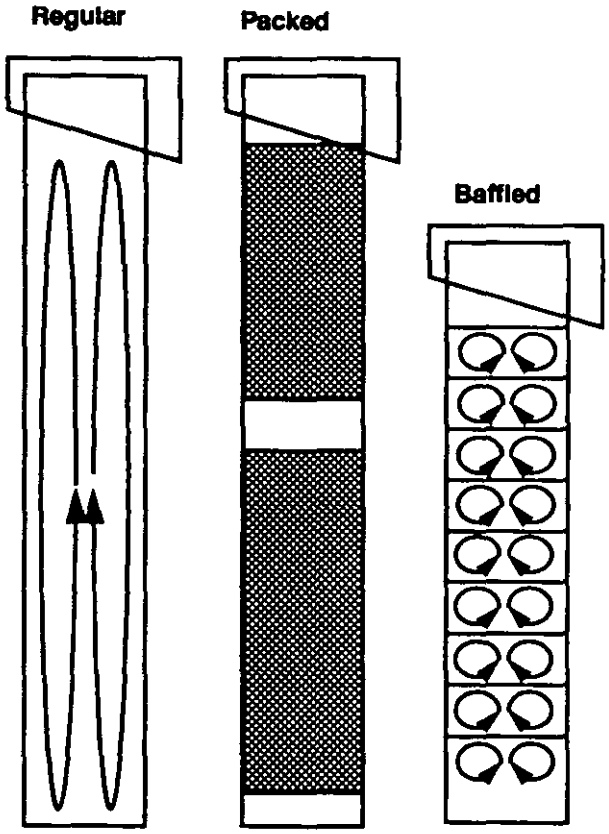

Fig 1 — Comparison of flow patterns in regular, packed and horizontally baffled columns.

Theoretical discussion

In the most common type of flotation column (shown in

S.K. Kawatra and **T.C. Eisele**, members SME, are professor and graduate student, respectively, with the Metals and Materials Engineering Department, Michigan Technological University, Houghton, MI SME Preprint 94–22, SME Annual Meeting, Feb. 14–17, 1994, Albuquerque, NM. Manuscript Feb., 1994. Discussion of this peer-reviewed and approved paper is invited and must be submitted, in duplicate, prior to Aug. 31, 1995.

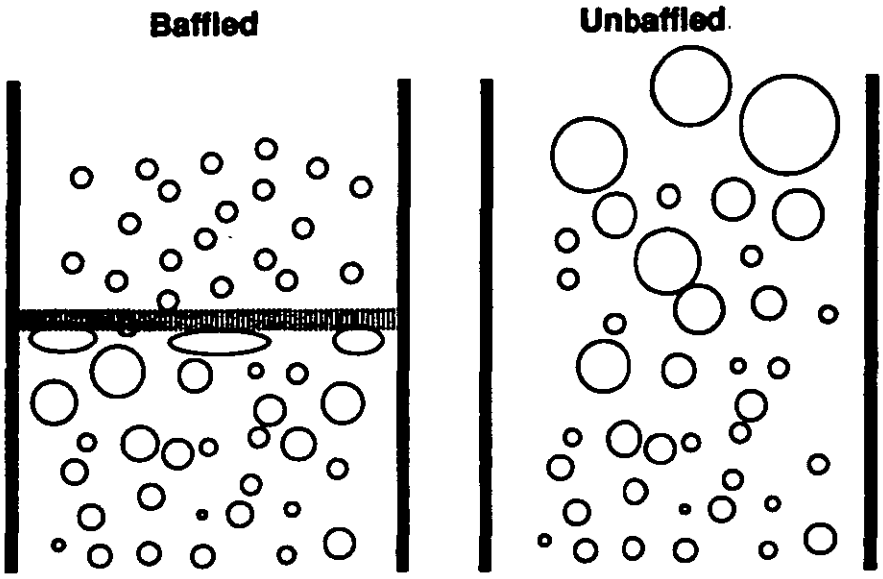

Fig. 2 — Effect of horizontal baffles on the maximum bubble size. Bubbles enlarge with time in unbaffled columns, due to both coalescence and decreasing hydrostatic pressure. Horizontal baffles break up the large bubbles, which keeps them from disrupting the froth layer.

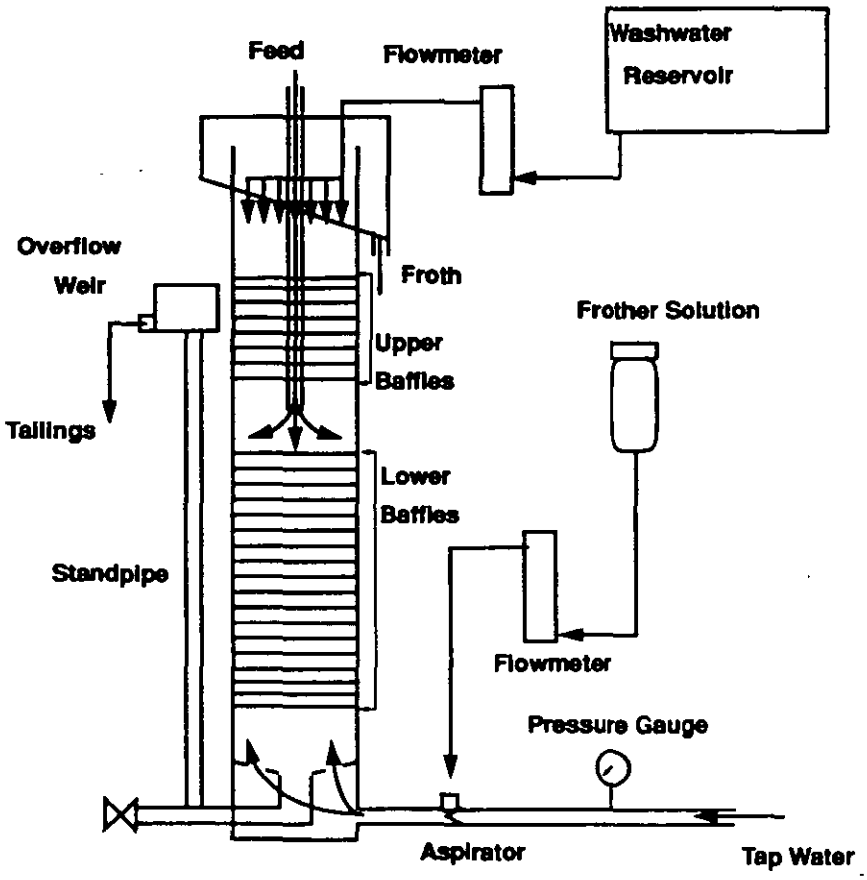

Fig. 3 — Schematic of laboratory-scale flotation column.

Fig. 1), there is no restriction to flow along the axis of the column. Rising air bubbles are therefore free to carry slurry up along the axis, which then returns to the bottom along the sides of the column, producing strong axial mixing.

In attempts to reduce this mixing, two different approaches were taken by Yang (1988) and Dell (1976). Yang (1988) used packing similar to that used in packed distillation columns. While this was effective for ultrafine particles (<20 μm), the packing was very prone to plugging by solids. In addition, the packing was heavily worn by the slurry after only a short time, which would result in high maintenance costs. In Dell's column, also known as the Leeds column (Dell, 1976; Degner and Sabey, 1988), a combination of fixed and movable rods in discrete racks were used to horizontally divide what was essentially a conventional flotation machine into a series of stacked chambers. The goal was to mimic the performance of a multistage flotation circuit with several stages of froth recleaning, and this was quite successful. Because the feed was introduced into the bottom chamber, this machine produced a considerably cleaner froth, although no attempt was made to improve recovery. Also, because the rod-racks are fairly thick, the machine is only sectioned into a few chambers. This column is not presently being used industrially, mainly because of corrosion and wear problems.

The horizontally-baffled column described in this paper has many of the advantages of both the regular column and the packed column. The horizontal baffles consist of simple perforated plates with openings large enough to keep them from being plugged by solid particles and small enough to break up the vertical mixing currents, so that slurry cannot be rapidly swept along the axis of the column. In addition, the baffles act to produce a uniform distribution of bubbles and particles and act to break up bubbles that become excessively large, as shown in Fig. 2. This provides for a much closer approximation of plug flow and improves the separation. The perforated-plate baffles are much simpler and take up less volume than the rod-racks developed by Dell (1976) and are much more resistant to plugging and wear than closely spaced packing material. Also, because they are simple to make and install, they are more suitable for retrofitting existing columns.

In previous work by the authors (Kawatra and Eisele, 1993), it was found that the best results were obtained when the baffles had an open area of 29% to 38% and when they were present both above and below the feed inlet. In the work described in this paper, the effects of the number of baffles and their position within the column were studied. In particular, the ability of the baffles positioned below the feed inlet to prevent short-circuiting of material to the tailings was determined.

Experimental procedures

Laboratory column design. A modified Deister Flotaire column, 7.6-cm-diam. and 1.83-m-tall, was used. This column is significantly shorter than a typical laboratory column of this diameter. Columns of this diameter are more com-

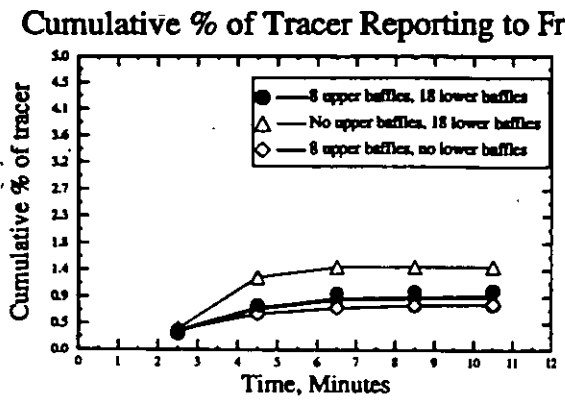

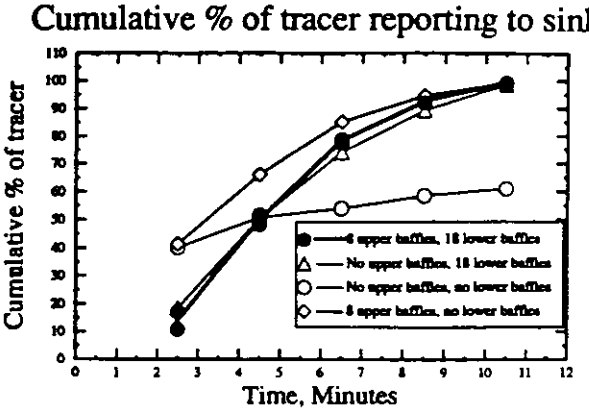

Fig. 4 — Results of selected solids-free tracer tests with the laboratory column. These results show that the upper baffles tend to improve the froth grade, and that the lower baffles increase the residence time. Also, the presence of any baffles at all prevents the type of operating instability that was seen in the no-baffles test, where over half of the tracer was carried off in the froth product

monly 4-to 5-m tall. The short column was used so that its height/diameter ratio would be similar to that of a plant-scale column. A similar height/diameter ratio insured that there was a similar degree of axial mixing. The column used an aspirator-type bubble generator and a wash-water spray ring that supplied water at a rate of 1.0 L/min. An overflow weir was used to control the pulp level in the column, and frother was metered directly into the aspirator, as shown in Fig. 3. Frother was also added to the wash-water reservoir, so that all of the water entering the column would have the same frother concentration. The froth depth was maintained at 0.5 m, and the feed was introduced at a depth of 1 m. To operate properly, the aspirator required 7 L/min of water at a pressure of 138 KPa.

The baffles were of two types: The first type consisted of three baffles that were bolted into place above the tailings outlet at heights of 0.3, 0.9 and 1.2 m, and the second type consisted of a large number of adjustable baffles that were threaded onto support rods at 3.5-cm intervals. The column was made from 30-cm-long sections of tubing. The bolt-in baffles were inserted at the flanges between the tubing sections. All of the baffles had had an open area of 29%, and all could be removed when desired. The adjustable baffles were installed as two sets, i.e., eight baffles above the feed inlet (upper baffles) and eighteen baffles below the feed inlet (lower baffles). The reason for having more lower baffles than upper baffles was that the upper baffles tended to restrict the flow to the froth, which forced more material into the tailings. To compensate for this effect and to provide additional improvements over an unbaffled column, it was considered necessary to use more lower baffles than upper baffles.

Solids-free tracer tests. A series of experiments was carried out to determine how the presence of baffles affected the water flows (without interference from solid particles) within the column. To track the water flow, a pulse of fluorescein dye was added as a tracer. Dowfroth 1012, a strong polypropylene glycol (PPG)-based frother, was used at a concentration of 0.03 g/L. The frother was selected to ensure that there would be a stable froth overflow in the absence of solid particles. The concentration of tracer dye in the products was determined using a spectrophotometer set to a wavelength of 492 nm to measure the absorbance. Tap water with a pH of 7 and a hardness of 150 ppm was used.

For each experiment, the column was first run for 5 min, so that the froth overflow is at a steady-state. The fluorescein pulse was then added, and the timer was started. All of the froth and tailings produced by the column were then collected over the following time intervals: 0.5 to 2.5 min, 2.5 to 4.5 min, 4.5 to 6.5 min, 6.5 to 8.5 min and 8.5 to 10.5 min. All 10 products collected were weighed, and the tracer concentration in each were determined, so that the fraction of the total tracer in each product could be calculated.

The baffle arrangement was changed for each test. The arrangements ranged from no baffles at all to a complete set of eight upper and 18 lower baffles.

Laboratory coal flotation tests. The coal used in these experiments was a blend of bituminous coals collected from the Empire Coal processing plant, Gnadenhutten, OH. The plant processes coal from the Lower Kittanning (#5) seam and the Middle Kittanning (#6) seam. The coal sample was prepared by stage-crushing to -850 µm. The sample was then stored at -20° C to prevent further oxidation. Column feed was prepared by grinding 900-g lots of the stage-crushed coal in a 20.3-cm-diam. rod mill. The samples were ground for 45 min with 1500 ml of distilled water. The assay and size distribution of the rod-milled coal was as follows: 13.5% ash; 3.41% total sulfur; 12,100 Btu/lb; 80% passing 40 µm and 10% passing 4.5 µm.

After grinding, the slurry was filtered, and the wet filter cake was split into three 250-g flotation charges and one 150-g head sample. The coal was found to be poorly floatable when #2 fuel oil was used as the only collector. Therefore, a mixture of 80% #2 fuel oil and 20% Dow M210 froth conditioner was used. The froth conditioner is an agent that improves the wetting of oxidized coals by neutral oils and, therefore, reduces the collector requirements for flotation of these coals. The dosage of the collector mixture was 3.4 kg/t, and the nominal frother dosage was 0.83 kg/t (0.03 g/L). The frother used for these experiments was Dowfroth 200, a moderate-strength PPG-based frother. The Dowfroth 200 was selected for these experiments because the presence of floatable solids stabilized the froth enough for it to overflow freely from the column. Also, a stronger frother, such as Dowfroth 1012, would have increased the tendency to entrain gangue in the clean-coal product.

For each test, a flotation charge was repulped with water to a volume of 1600 ml. After the addition of the desired reagents and the tracer dye, the pulp was conditioned by shaking vigorously for 1 min in a stoppered Erlenmeyer flask. The flow rates in the column were then adjusted to the desired level, the tailings valve was closed, so that filling of the column would begin, and the timer was started. Thirty seconds after closing the tailings valve, the feed was added to

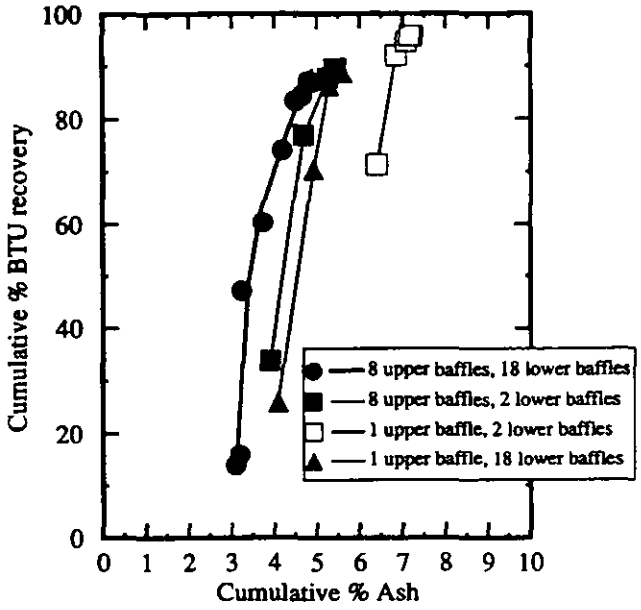

Fig. 5 — Grade-recovery performance of the laboratory column with varying numbers of baffles. The column showed the best results when the full set of baffles was installed. The feed was 13.5% ash and 12,100 BTU/lb.

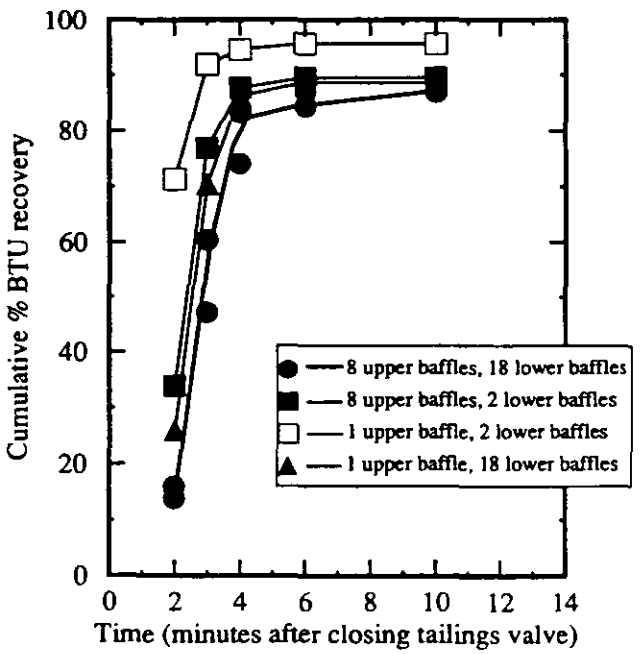

Fig. 6 — BTU recovery as a function of time for the laboratory column with varying numbers of baffles.

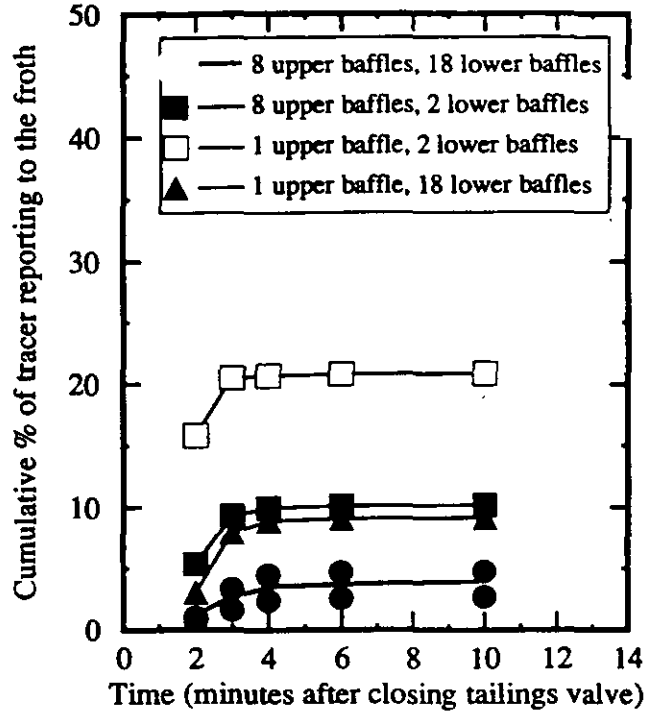

Fig. 7 — Recovery of tracer dye into the froth as a function of time during laboratory coal flotation tests. Increasing the number of baffles, and installing baffles both above and below the feed inlet, greatly reduced the amount of tracer reaching the froth, showing that entrainment is reduced.

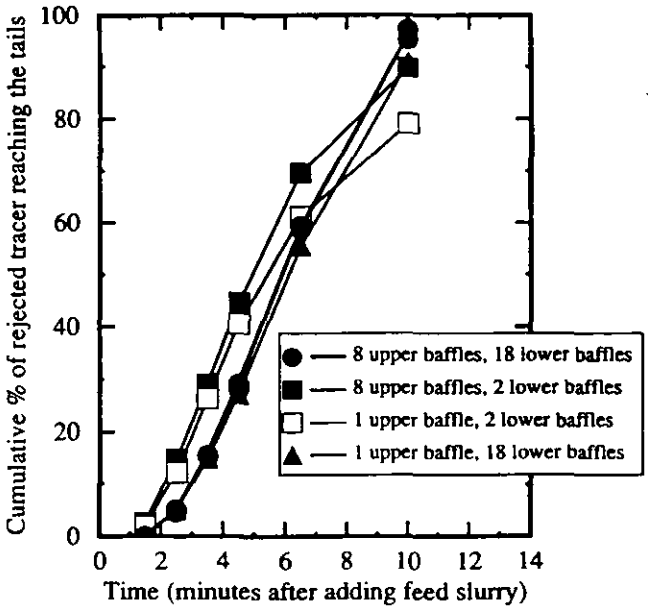

Fig. 8 — Quantity of tracer dye reaching the tailings product as a function of time in laboratory coal flotation tests. Greater numbers of lower baffles consistently cause the tracer to reach the tailings more slowly, regardless of the number of upper baffles. Therefore, addition of baffles below the feed inlet reduces short-circuiting to the tailings.

the column over a 15-sec interval. The froth overflow began at 1 min, and froth samples were collected over the following intervals: 0 to 1.5 min, 1.5 to 2 min, 2 to 3 min, 3 to 4 min, 4 to 6 min and 6 to 10 min. In addition, tailings samples were collected over the intervals of 0 to 3 min and 3 to 10 min. After 10 min of operation, the column was shut down. The material remaining in the column (the "holdup" product) was collected separately. Small samples of the tailings were collected at intervals for the determination of tracer concentrations. The filtrates from the froth samples were also collected, so that the tracer concentration in the froth water could be measured. Before determining the tracer concentration, the water samples were filtered through a micropore syringe filter to remove suspended solids that could interfere with the spectrophotometer reading. The weights, ash contents, total sulfur contents and calorific values of the solid products were also determined.

Experimental results and discussion

Solids-free tracer results. The results of these experiments are given in Fig. 4A and Fig. 4B. The test without

baffles showed a serious operating instability. The froth level gradually surged over a period of several minutes, and a considerable amount of water and nearly half of the tracer were carried into the froth. When even a single baffle was present in the column, this did not occur.

Figure 4A shows that the upper baffles are most effective in reducing the amount of tracer carried into the froth and are therefore able to reduce entrainment of gangue into the clean product. Figure 4B shows that the lower baffles have a significant effect on the time needed for the tracer to reach the sinks product. When all 18 lower baffles are present, the time needed for 50% of the tracer to reach the tailings is 4.5 min. This compares to only 3 min when no lower baffles are present. This increase in retention time will result in an improved recovery at any given grade.

Laboratory coal flotation results. Results of the coal flotation experiments are given in Fig. 5. All of these tests were conducted with at least one upper baffle and two lower baffles to prevent the operating instability that was seen in the solids-free tracer test with no baffles. These tests show that adding baffles to the column markedly improved the grade-recovery performance. The best results (i.e., a markedly higher grade with little loss of recovery) were reproducibly obtained when a complete set of baffles (eight upper and 18 lower) were present. The change in recovery rate due to the baffles is shown in Fig. 6. The complete set of baffles reduced the ultimate recovery by only a few percentage points, which was compensated for by an increase in froth grade, as seen in Fig. 5.

The amount of tracer reporting to the froth was greatly reduced by the baffles, as shown by Fig. 7. This indicates that entrainment is reduced by the baffles, which accounts for the improvement in the froth grade. The best results were achieved when the complete set of baffles was installed.

Figure 8 shows that the addition of lower baffles increased the residence time in the column, which is the same effect as was seen in the solids-free tracer tests. The effect of the upper baffles was to change the total amount of tracer that reached the tails. However, the upper baffles did not affect the residence time.

Conclusions

The performance of a coal flotation column can be markedly improved by the use of horizontal baffles. These baffles reduce axial mixing in the column, which improves both the column retention time and the grade-recovery performance. Another important benefit of the baffles is that they prevent the formation of large bubbles that could otherwise disrupt the froth layer.

Baffles below the feed inlet are mainly responsible for increasing the residence time in the column by preventing feed from short-circuiting directly to the tailings.

Baffles above the feed inlet are more effective in reducing entrainment into the froth. They are therefore useful in improving the product grade.

Acknowledgments

Support for this research was provided by the Empire Coal Co. and the Ohio Coal Development Office. Also, the authors would like to thank Ms. J. F. Bird and Dr. Howard Johnson of the Ohio Coal Development Office and Dr. R. R. Klimpel of Dow Chemical for their useful suggestions and critical discussion of this project.

References

Alford, R A., 1992, "Modeling of single flotation column stages and column circuits," *International Journal of Mineral Processing*, 36 pp 155-174

Degner, V.R , and Sabey, J B , 1988, "WEMCO/Leeds flotation column development," *Column Flotation '88*, K.V.S Sastry, ed , SME, Littleton, CO, pp 267-280

Dell, C C., 1976, *Froth Flotation*, British Patent No 1,519,075

Finch, J A., and Dobby, G S , 1990, *Column Flotation*, Pergamon Press, Oxford, England

Kawatra, S K., and Eisele, T C , 1993 "The use of horizontal baffles to improve the effectiveness of column flotation of coal," *XVIII International Mineral Processing Congress*, Sydney, Australia, May 23-28, pp 771-778

Yang, D C , 1988, "A new packed column flotation system," *Column Flotation '88*, K.V.S Sastry, ed , SME, Littleton, CO, pp. 257-266

FACULTAD DE INGENIERIA U.N.A.M.
DIVISION DE EDUCACION CONTINUA

CURSOS ABIERTOS

DESARROLLO Y OPERACIÓN DE SENSORES PARA CONTROL DIRECTO Y CONTINUO EN PLANTAS DE BENEFICIO DE MINERALES Y EN LA RESTAURACIÓN DEL MEDIO AMBIENTE

Del 18 al 23 de mayo de 1998

TEMA: REMOVAL OF PYRITE IN COALFLOTATION

EXPOSITOR :DR. KOMAR KAWATRA

1998

Mineral Processing and Extractive Metallurgy Review, 1992, Vol. 8, pp. 205–218
Reprints available directly from the publisher
Photocopying permitted by license only
© 1992 Gordon and Breach Science Publishers S.A.
Printed in the United States

Removal of Pyrite in Coal Flotation

S. K. KAWATRA and T. C. EISELE

Dept. of Metallurgical and Materials Engineering, Michigan Technological University, Houghton, MI 49931

In most operating coal-cleaning plants, a significant amount of pyrite is recovered in the froth during flotation of high-sulfur coal. Reducing the pyrite recovery first requires that the primary recovery mechanism should be identified, as different measures are required for reducing entrainment, locked-particle flotation, or true hydrophobic flotation. In this paper, evidence is presented which suggests that hydrophobic flotation is not an important mechanism for recovery of liberated pyrite when the collector is a neutral oil, and that the bulk of the floated pyrite occurs either as a result of simple entrainment or by mechanical locking with floatable coal particles. Column flotation results are also presented which show that significant sulfur reductions can be achieved by reducing levels of entrainment.

Key words: coal flotation, pyrite, entrainment, hydrophobicity, liberated pyrite

INTRODUCTION

In many coal flotation operations, a significant amount of apparently liberated pyrite is seen to report to the froth, thus raising the sulfur content of the clean product and reducing its economic value. Prevention of this unwanted recovery of pyrite is therefore desirable. It has frequently been indicated in laboratory studies[1,2] that depressants can reduce hydrophobic pyrite in coal flotation. Yet, these depressants are not found to be commonly used on an industrial scale, which raises the question of whether hydrophobic flotation of pyrite is really a significant source of contamination when compared to entrainment effects. Therefore, before the best means for preventing liberated coal pyrite recovery can be selected, it is necessary to determine which recovery mechanisms are actually dominant. Separation of particle entrainment and bubble attachment effects in a real experiment is very difficult, especially when locked particles are being floated as well. Since coal pyrite does not have the same properties as pure mineral pyrite,[3] and it is not practical to produce coal pyrite which is completely free of locked coal particles, experiments to demonstrate conclusively whether pyrite from a given coal either does or does not float by hydrophobic bubble attachment are impractical, and the best which can be done is to estimate the relative probable quantity of liberated pyrite which can be accounted for by the two mechanisms.

For this paper, a conventional flotation machine was used to compare the floatability of two different mineral pyrites and two coal pyrites, using only nonpolar

oil as collector. Experiments were also carried out to attempt to measure the floatability of liberated pyrite in coal using both a conventional cell and a laboratory-scale flotation column, and using reagents which are commonly selected in current industrial practice.

THEORETICAL DISCUSSION

It has long been known that mineral pyrite has some hydrophobic tendency, as do several other sulfide minerals. However, this tendency is normally very slight, and significant flotation of pyrite requires addition of a collector such as a xanthate. The natural floatability of pyrite is also strongly pH dependent, with the highest floatability in acidic solutions. Depression of mineral pyrite is quite easy, with a variety of highly effective depressants being available, and in most selective sulfide mineral flotation circuits the bulk of the floated pyrite occurs as a result of entrainment and locking to hydrophobic particles[4].

While the responses of mineral pyrite in flotation are fairly well known, the behavior of coal pyrite is poorly understood[3]. Due to its formation and long residence in the presence of a variety of organic compounds, it is often reported that coal pyrite exhibits surface chemistry radically different from that of mineral pyrite. In addition, the extreme heterogeneity of coal deposits apparently results in the properties of the associated pyrite also varying over a wide range. As a result, experiments with coal pyrite from a specific source may not be particularly relevant to pyrites from other sources.

Many investigators have attempted to use various chemicals as depressants for coal pyrite in order to reduce the sulfur content of the product, with some success[1,2]. However, in most reported experiments it has not been clear whether the decrease in pyrite flotation was due to reduced pyrite hydrophobicity or improved froth drainage, as the quantity of entrained water in the froth is often not measured. Also, since pyrite depressants reduce the floatability of coal slightly, it is reasonable to expect that fewer locked particles will float in the presence of these reagents, and the quantity of pyrite floating can be reduced by this means as well.

Determination of the quantity of entrained material is difficult, particularly when a small number of experiments is conducted, as the water recovery in the froth must be determined and correlated with the recovery of the entrained species. Since entrainment is, in theory, directly related to water recovery[5], the entrainment constant can be determined by linear regression when the data set available is sufficiently large. The floated material which is not accounted for by the regression line is then assumed to be floating either by hydrophobic bubble attachment or as part of locked particles. The slope of the regression line varies with particle size, becoming less steep as the particle size increases. Since a range of particles is present in flotation experiments, this tends to introduce a small amount of scatter and curvature to the data. However, the linear trend will still be evident.

EXPERIMENTAL PROCEDURES AND RESULTS

In order to determine whether the pyrite in a particular Pittsburgh Seam coal was floating by locking/entrainment or by true flotation, three sets of experiments were carried out. These experiments provided data on the extent to which coal pyrite flotation occurs during normal flotation of coal, and its correlation to the quantity of water entrained in the froth; the quantity of pyrite reporting to the froth in a flotation column designed to reduce entrainment, as shown in Figure 1; and the conditions under which pure mineral pyrite flotation could be expected with only #2 fuel oil as a collector.

Conventional Flotation: Pittsburgh Seam Coal

The first objective was to determine the relative proportions of sulfur reporting to a coal froth by entrainment and true flotation. To accomplish this, it was necessary to measure the recovery of coal, ash, water, and the various forms of sulfur as a function of time. Variations in collector dosage were intended to vary the coal flotation rate, and determine whether pyrite flotation was or was not sensitive to collector dosage.

These experiments used 250 gram charges of a Pittsburgh seam coal which had been stored at −20°C prior to use, to retard oxidation. For experiments, this coal was ground in a steel rod mill to the size distribution given in Table I. The freshly ground coal was then divided into 250 gm charges for flotation. Timed flotation

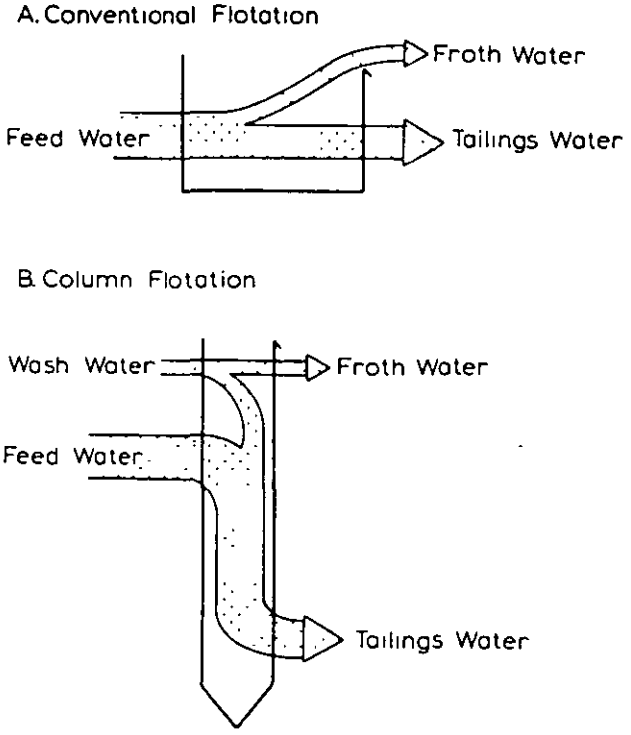

FIGURE 1 Mechanism of entrainment reduction in flotation columns.

TABLE I
Size distribution of Pittsburgh seam coal used in the coal flotation experiments, produced by grinding 900 *g* charges of coal at 40% solids in a steel rod mill for 45 minutes. Size distribution was measured using a Microtrac particle size analyzer.

Size, μm	Cumulative % Passing
88	100.0
62	96.0
44	87.5
31	74.7
22	61.7
16	49.2
11	37.6
7.8	28.4
5.5	20.3
3.9	13.7
2.8	8.1
1.9	3.1
1.4	1.1
0.9	0.0

experiments were carried out in a 4-liter flotation cell, with gravity-feed pulp level control and mechanical froth scrapers (Figure 2), under the conditions given in Table II. The frother was Dowfroth 200, added at a rate of 0.03g/liter. Froth was collected over the time intervals 0–30 sec, 30 sec–1 min, 1 min–2 min, 2 min–3 min, 3 min–5 min, and 5 min–9 min, filtered, dried, and weighed. All products were analyzed for ash content, and total sulfur content was determined using a LECO SC-132 sulfur determinator. The results for all six tests are given in Table III.

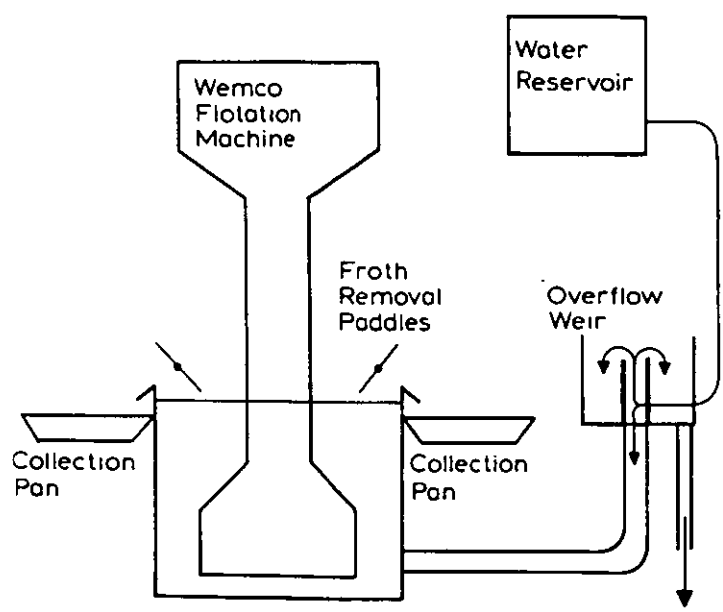

FIGURE 2 Schematic diagram of flotation cell with automatic pulp level control.

TABLE II
Flotation conditions for timed tests using conventional flotation and Pittsburgh seam coal.

Test #	pH	Collector (fuel oil)
1	7.6	0.0
2	7.7	0.0
3	7.7	0.0
4	7.5	0.18 kg/mt
5	7.5	0.35 kg/mt
6	7.6	0.70 kg/mt

Column Flotation Experiments

Experiments with column flotation were intended to determine the behavior of the coal components when entrainment was minimized by froth washing. Flotation experiments were carried out in a laboratory-scale coal flotation column, using coal prepared in the same manner as that used in the conventional coal flotation tests. A modified Deister 3″ diameter column 6′ high (Figure 3) was used for these experiments. A froth depth of 18″ was maintained, at a washwater flowrate of 1 liter/min. Aeration was provided by an aspirator, with a water pressure of 15 psi and a flowrate of 5 liters/minute. Frother was introduced with the aspirated air as a 1% solution. The frother concentration was the same as for the conventional tests, and no collector was added. Tracer experiments using sodium fluorescein dye showed that less than 4% of the feed water was entrained in the froth product using this column.

Timed flotation experiments were carried out by adding a 400 gm charge of the coal in slurry form as a single increment. After adding the feed, 30 seconds were required before coal began flowing into the overflow launder. Froth increments were then removed over the 0–30 sec, 30 sec–1 min, 1 min–2 min, 2 min–3 min, 3 min–5 min, and 5 min–9 min. These samples were analyzed in the same fashion as for the conventional flotation tests, and the results are given in Table IV.

Pure Pyrite Flotation

These experiments were intended to determine the conditions under which pyrite is floatable by a neutral oil collector such as #2 fuel oil. They also compared two different mineral pyrites to two different coal pyrites to determine whether mineral pyrite is at all suitable as a model for coal pyrite.

Relatively pure pyrite from four sources (Custer, SD, and Rico, CO, mineral pyrites obtained from Ward's Natural Science Establishment, and coal pyrites collected as large nodules from Panther Valley, PA, and Empire Coal, OH) were ground to the size distribution given in Table V, using a steel rod mill, at 60% solids and a pH adjusted to 12 with NaOH to prevent corrosion and subsequent dissolution of iron, which is reported to be a pyrite depressant[6]. The pyrite was then filtered, divided into charges of the desired weight, repulped in a Denver laboratory flotation cell (volume of 1.9 liters), and the pH was adjusted to the

TABLE III
Results from timed flotation experiments using a constant-level conventional flotation cell.

Product	% Wt	% Ash	% S	% Solids	% Pyritic S
Test 1 30 sec Froth	31.24	11.1	2.14	15.14	0.9
1 min	26.60	13.2	2.59	16.04	1.6
2 min	8.83	26.8	3.64	8.88	2.5
3 min	4.83	61.1	5.17	2.41	4.4
5 min	5.70	82.5	5.08	1.15	4.5
9 min	6.73	88.1	4.22	0.70	3.7
Final Tails	16.07	88.2	4.55		4.2
Test 2 30 sec Froth	44.37	12.7	2.37	15.70	1.1
1 min	18.19	17.5	2.86	13.73	1.7
2 min	8.47	42.5	4.33	4.01	3.3
3 min	3.88	79.5	5.27	1.37	4.7
5 min	4.70	87.4	4.56	0.90	4.0
9 min	4.66	89.0	3.91	0.59	3.7
Final Tails	15.72	84.2	4.54		4.2
Test 3 30 sec Froth	43.82	12.4	2.26	16.00	1.1
1 min	19.00	17.1	2.69	13.90	1.7
2 min	8.73	43.3	3.81	3.95	3.3
3 min	3.91	79.1	4.67	1.33	4.6
5 min	4.90	86.3	4.06	0.90	4.0
9 min	6.01	88.6	3.49	0.56	3.4
Final Tails	13.63	87.0	3.98		4.0
Measured Head		37.2	2.90		
Test 4 30 sec Froth	23.1	10.3	1.85	16.21	0.8
1 min	14.3	9.4	1.89	19.41	0.9
2 min	19.9	12.9	2.39	21.83	1.5
3 min	9.8	35.3	3.94	6.08	3.3
5 min	7.7	73.9	4.51	1.46	4.4
9 min	6.6	86.7	3.76	0.77	3.7
Final Tails	18.4	85.6	3.86		3.8
Test 5 30 sec Froth	55.4	14.0	2.24	14.73	1.3
1 min	10 9	27.1	3.13	7.78	2.3
2 min	7.2	58.2	4.20	2.09	3.7
3 min	4.1	72.3	3.84	1.16	3.7
5 min	4.9	84.2	3.63	0.73	3.7
9 min	5.2	87.5	3.30	0.47	3.3
Final Tails	12.3	84.4	4.10		4.1
Test 6 30 sec Froth	56.0	15.0	2.33	14.50	1.4
1 min	8.9	33.0	3.51	5.96	2.8
2 min	6.9	63.2	4.10	1.77	3.7
3 min	5.4	64.4	3.48	1.26	3.3
5 min	5.6	77.4	3.36	0.73	3.4
9 min	5.5	81.4	3.19	0.43	3.2
Final Tails	11.7	75.7	4.02		4.0
Measured Head		37.3	2.99		

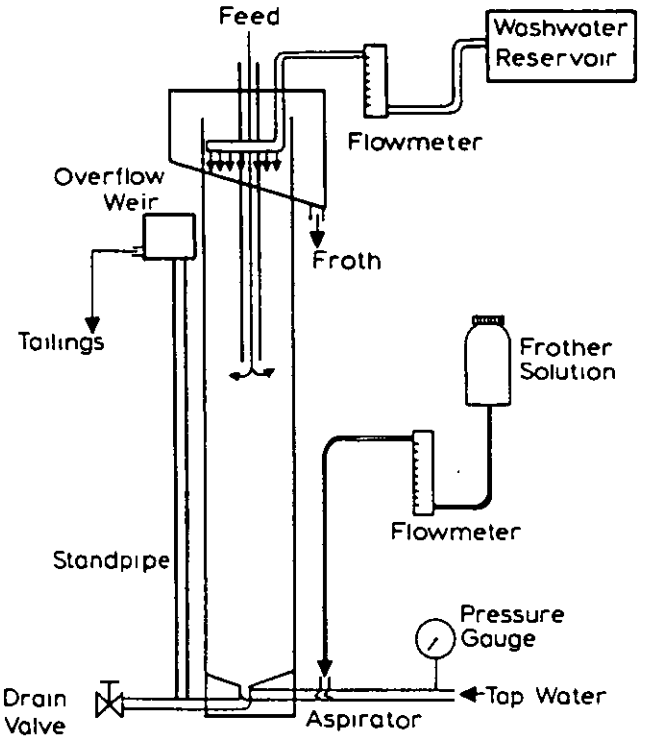

FIGURE 3 Schematic of the modified Deister flotation column.

TABLE IV
Timed column flotation results.

Product	% Wt	% Ash	% S
Test 1 30 sec Froth	0.61	7.78	2.35
1 min	1.07	2.91	1.72
2 min	3.42	2.85	1.67
3 min	6.05	3.13	1.74
5 min	24.11	4.52	1.96
9 min	22.29	11.74	2.73
Final Holdup	7.41	56.68	7.45
2 min Tails	12.79	76.38	4.32
9 min Tails	22.24	83.91	3.92
Test 2 30 sec Froth	0.00	0.00	0.00
1 min	0.86	3.42	1.71
2 min	3.57	3.11	1.66
3 min	7.97	3.38	1.73
5 min	21.59	4.51	1.93
9 min	23.29	11.54	2.68
Final Holdup	8.25	57.04	6.99
2 min Tails	11.39	75.02	4.17
9 min Tails	23.06	83.87	3.86
Measured Head		36.85	3.36

TABLE V
Size distributions for the samples used in the pyrite flotation experiments, determined by Microtrac particle size analyzer.

Size, μm	Cumulative % passing, mineral pyrite samples	Cumulative % passing, coal pyrite samples
62	100.0	100.0
44	97.4	100.0
31	88.3	97.3
22	73.5	89.6
16	56.5	75.8
11	42.2	59.6
7.8	31.7	45.2
5.5	23.0	32.7
3.9	16.1	22.1
2.8	10.0	13.1
1.9	4.3	5.4
1.4	1.8	2.2
0.9	0.3	0.4

desired level with sulfuric acid. Finally, 0.03 gm MIBC/liter and the noted quantities of #2 fuel oil were added as frother and collector, respectively. The pulp was then conditioned for 2 minutes, and floated for 5 minutes with froth removed manually. The results of these experiments are given in Table VI, along with two experiments using pure silica which had been prepared in the same manner as the pyrite. The pH values were selected on the basis of earlier tests, which showed that mineral pyrite floats well below pH = 4, and poorly at higher pH values.

The pyrite appeared strongly to buffer the pH at pH = 4, consuming approxi-

TABLE VI
Conditions and results for pure pyrite experiments.

Test	Pyrite	Charge wt.	#2 fuel oil, kg/mt	pH	% Floats
1A	Custer, S.D.	150	3.0	7.5	3.34
2A	"	150	3.0	7.5	4.34
3A	"	150	3.0	8.3	4.65
4A	"	150	3.0	2.0	98.57
5A	"	75	6.0	2.4	97.07
6A	"	75	6.0	3.6	43.10
7A	"	75	6.0	2.5	77.21
8A	"	75	6.0	2.5	67.27
1B	Panther Valley	150	3.0	8.8	31.64
2B	"	150	3.0	3.5	36.47
1C	Custer, S.D.	150	3.0	2.3	98.01
2C	"	150	3.0	2.2	97.57
3C	Panther Valley	150	3.0	2.2	43.00
4C	"	150	3.0	2.0	35.22
5C	Rico, CO	150	3.0	2.1	98.62
6C	"	150	3.0	5.0	9.56
1D	Silica	150	3.0	5.3	13.6
2D	"	150	3.0	5.3	15.3

mately 3 grams sulfuric acid per kilogram of pyrite to reduce pH below this level. As a result, intermediate pH values were difficult to achieve. Upon lowering the pH below 4, the pyrite became strongly floatable, simultaneously releasing a strong odor of H_2S. The charges for tests 7A and 8A were allowed to air-dry before repulping for flotation, and became warm to the touch while drying. The reduced recovery for these tests was most likely due to oxidation of the pyrite. Unlike the two mineral pyrites, the Panther Valley coal pyrite never became strongly floatable, and also never released the characteristic H_2S odor. The froth product from the coal pyrite appeared, from qualitative examination at 40× magnification of the loose powder, to be predominantly composed of locked coal-pyrite particles, floating as a result of the hydrophobicity of the coal portion.

Additional experiments were attempted using coal pyrite from a second source, the Empire Coal mine, Gnadenhutten, Ohio. However, it was found that even when apparently pure pyrite nodules were collected and cleaned by hand, the pyrite still contained 27% material which was insoluble in nitric acid, the residue being predominantly composed of coal and clay. As a result, it was not possible to conduct the desired experiments using coal pyrite which had been isolated from the associated organic inclusions, and the results obtained were similar to those for the Panther Valley coal for this reason. Since no conclusive technique was available for distinguishing liberated particles from locked particles in quantity, the role of locked coal/pyrite particles in pyrite flotation, relative to liberated pyrite, could not be confirmed.

Experiments with the Empire coal pyrite were conducted using the automatic flotation cell shown in Figure 2, using 300 gram charges ground for 10 minutes. Reagent dosages were 3.3 kg fuel oil/mt. and 1.7 kg Dowfroth 200/mt. Flotation was carried out for six minute intervals. Three tests were run, at pH = 2.5, 5.1, and 10.5 Results are given in Table VII. A slight increase in flotation rate and froth percent solids is seen with increasing pH, which is consistent with flotation being primarily of the carbonaceous component.

TABLE VII
Timed flotation results using the coal-pyrite samples

	Product	% Wt.	% Solids
Test 1, pH = 2.5	1 minute froth	34.09	11.7
	3 min froth	23.41	11.7
	6 min froth	13.90	10.5
	Tails	28.60	2.5
Test 2, pH = 5.1	1 minute froth	35.47	14.1
	3 min froth	18.92	12.2
	6 min froth	10.05	8.5
	Tails	35.57	3.4
Test 3, pH = 10.5	1 minute froth	45.06	23.7
	3 min froth	10.07	15 4
	6 min froth	4.21	7 1
	Tails	40.66	3.1

DISCUSSION

An approximate estimation of whether coal, mineral, and pyrite particles are being recovered by true flotation, locking, or entrainment can be achieved by correlating the recovery of a given component with the recovery of water in the froth. If the correlation with water recovery is nearly linear, then the component is being recovered predominantly by entrainment. Deviations from linearity are caused either by hydrophobic flotation of the component directly, or by mechanical attachment to another particle which is hydrophobic. The contribution due to locking can also be estimated by observing similarities in the water recovery/solids recovery curves. If the deviations from linearity for one component follow precisely those for another which is known to be hydrophobic, then the most likely explanation is a high degree of mechanical locking.

Correlations between solids recovery and water recovery for a constant-level batch cell are complicated somewhat by the fact that such cells are batch with respect to solids, but continuous with respect to water. This introduces a significant curvature in the water recovery/solids recovery plots, even in the case of pure entrainment. In order to correct for the continuous dilution by the makeup water addition, a corrected water recovery was calculated, based on the assumption that the pulp phase in the cell was nearly perfectly mixed. The proportion of the water originally present in the cell which is removed by time T can then be calculated according to a simple residence-time formula[7], $F(T) = 1 - e^{-R/V}$, where F(T) = fraction of the water originally present in the cell which is removed by time T; R = volume of water which has been removed, and replaced by fresh water, by time T; and V = total cell volume. This corrected water recovery will correlate linearly with recovery of solid particles by pure entrainment, making it much simpler to distinguish between the various recovery mechanisms.

When pyritic sulfur, ash, and combustible matter recovery are plotted against corrected water recovery as in Figure 4, it is immediately seen that the ash content follows the water recovery line very closely. Since the ash fraction of this coal is predominantly clay slimes, which are known to be hydrophilic and easily entrained, this corresponds well with the expected results. Likewise, the behavior of the combustible matter is as expected, with a recovery rate much faster than that of the water until the coal had been almost completely removed from the cell. This was followed by a sharp inflection in the curve as the remaining traces of combustibles were gradually recovered. It should be noted that these curves are composites of all six experiments, which showed a range of flotation rates due to changes in the collector dosage, but which nevertheless showed the same correlations with water recovery.

Examining the pyrite recovery curve shows that the pyrite was initially recovered faster than the water, although not as fast as the combustibles. The pyrite curve then shows a sharp inflection, and falls back to a slope consistent with recovery by entrainment. The point of most interest is that the inflection in the pyrite curve is at exactly the same water recovery as the inflection in the combustibles curve, to within the limits of accuracy of the data. This is what would be expected if the pyrite attached to air bubbles primarily due to locking with floatable coal. If the

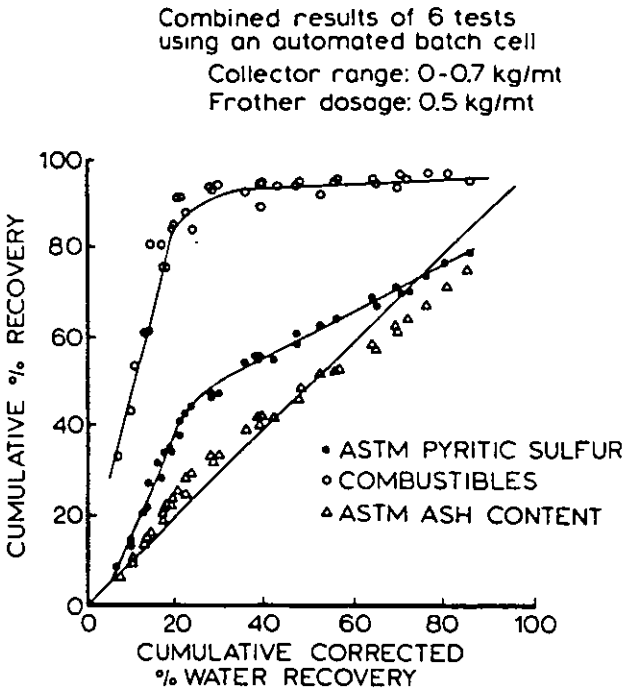

FIGURE 4 Correlation of ash, total pyritic sulfur, and combustibles recovery with corrected water recovery for the batch coal flotation experiments.

pyrite were hydrophobic in its own right, and floating with a different rate constant than the coal, then a second inflection would be expected to occur at a different water recovery, or the inflection in the pyrite curve would appear broader than the inflection in the combustibles curve. Since neither of these effects is seen, it appears most likely that pyrite recovery occurs almost entirely through a combination of locking and entrainment, with true hydrophobic flotation of liberated pyrite being minimal.

The column flotation results represent a flotation separation where entrainment is reduced to very low levels, and thus all pyrite which is recovered under these conditions does so as a result of either locking or true flotation[8,9]. Comparison of the results for conventional tests 1–3 and the column flotation tests are given in Figures 5 and 6, and the shift in the grade/recovery curves is most consistent with pyrite being recovered primarily by entrainment. As a result, it is probable that when this particular coal exhibits excessive pyrite recovery, it is more effective to switch to column flotation (thus minimizing entrainment) than to attempt to use chemical depressants to prevent hydrophobic flotation which does not appear to be occurring. A complete review of available column flotation can be found in the literature[10].

The results from the pyrite flotation experiments show very clearly that pure mineral pyrite loses its natural floatability nearly completely when the pH is greater than 5.0, and also that the floatability of silica, which is known to be hydrophilic, is very comparable to the floatability of pyrite at pH = 5 or greater. This indicates that under normal conditions for coal flotation (pH = 5 − 9), unmodified mineral pyrite is not noticeably recovered by true hydrophobic flotation. Even large dosages

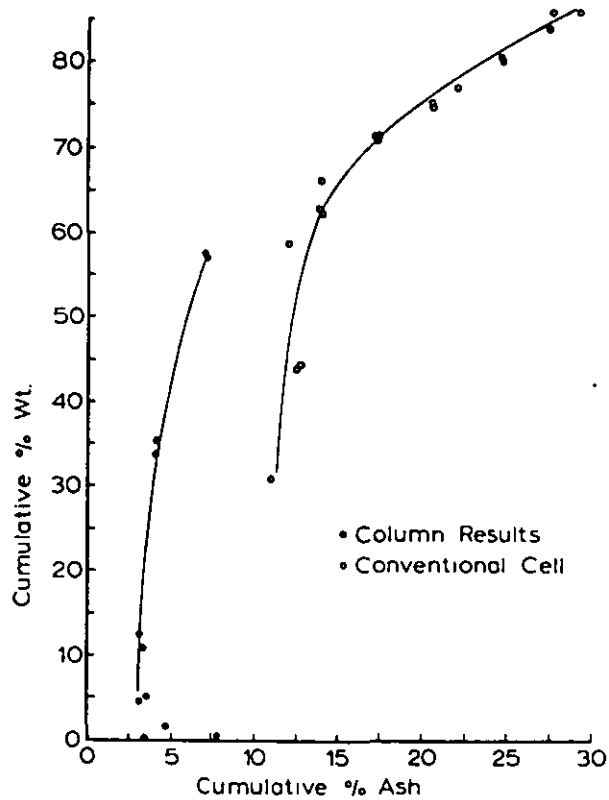

FIGURE 5 Comparison of column and conventional grade-recovery curves with respect to ash.

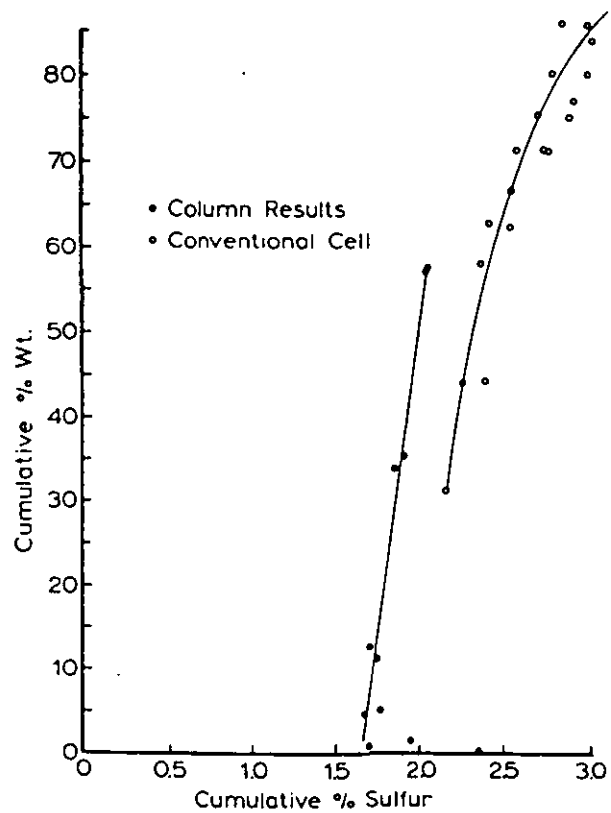

FIGURE 6 Comparison of column and conventional grade-recovery curves with respect to sulfur.

of neutral oil collectors do not render mineral pyrite floatable over this pH range, up to 3 kg collector/metric ton pyrite. This has been found to be true for pyrites from two distinct sources, and is likely to be generally true for all pyrites which are not associated with organic matter. Therefore, true hydrophobic flotation of coal pyrite should only be expected when the pyrite has been heavily modified by organic material, or when flotation is being carried out under acid conditions. The coal pyrite, although prepared in the same fashion as the mineral pyrites, did not exhibit similar behavior, as it maintained essentially constant levels of flotation recovery (31–43%) over the pH range from 2.2 to 8.8, while the mineral pyrite dropped from nearly 99% recovery to in some cases less than 4% over the same pH range. Qualitative microscopic examination of the coal pyrite flotation product indicated that much of the floating material was coal and locked coal/pyrite particles. It is therefore hypothesized that, in this case, the coal pyrite is floating due to attachment to coal. This hypothesis is supported by recent work by Chander and Aplan[11], where great care was taken to isolate liberated pyrite from seven coal sources for a variety of detailed analyses. Using a microflotation cell aerated with nitrogen gas, all of the purified pyrites were found to show very little inherent floatability (average = 1.9% wt. floating, range = 0–7% wt.). The procedure which Chander and Aplan describe for purifying the pyrites does provide opportunity for the pyrite to oxidize somewhat, which may conceivably destroy its inherent floatability. Nevertheless, it appears likely that coal pyrites have a very low inherent floatability, and are therefore floated primarily as either locked or entrained particles.

Unfortunately, there does not appear to be any practical method available for conclusively measuring the relative qualities of locked and liberated pyrite particles in coal flotation, nor is there an effective method for isolating coal-free pyrite from coal which does not also either contaminate or oxidize the pyrite surfaces. At the present time, it is therefore not possible to prove that coal pyrite either does or does not enter the froth as a result of true hydrophobic attachment. Based on the behavior of the pure mineral pyrite samples, it is hypothesized that coal pyrite is recovered in the froth by entrainment and by mechanical attachment to floatable coal particles. However, as a result of the fine scale of the organic contaminants in coal pyrite, it is clear that mineral pyrite is not a good model for the behavior of coal pyrite, and should not be treated as such.

CONCLUSIONS

From the results presented, the following conclusions are drawn:

1. Mineral pyrite is readily floatable by fuel oil alone at acid pH (<4), but this native floatability is entirely lost at the higher pH levels where coal flotation is most often carried out.
2. Determination of the floatability of coal pyrite in the absence of coal particles is not practical, due to the intimate intermixing of carbonaceous and pyritic components even in pyrite nodules which appear visually to be relatively pure. As a result, pyrite which floats by true hydrophobic bubble attachment cannot

readily be distinguished from that which floats due to mechanical attachment to coal particles. While it can be hypothesized that completely liberated coal-pyrite particles behave similarly to mineral pyrite, and are therefore not recovered by hydrophobic flotation at near neutral pH, this is very difficult to prove.

3. The results of timed flotation of a Pittsburgh seam coal using both conventional and column flotation are consistent with the pyrite being recovered in the froth predominantly by entrainment and locked particles, with any contribution from hydrophobic flotation of liberated pyrite being minimal.

Acknowledgments

The authors would like to thank Ms. Jacqueline F. Bird, Director of the Ohio Coal Development Office, for her useful suggestions and critical discussion; Mr. W. Kukura for providing the plant facilities, personnel, the valuable signatures and the engineering services; and Dr. R. R. Klimpel, Dow Chemical Company, for his repeated patience and for the chemical reagents used in this work.

References

1. R. J. Purcell, Circuitry Variations for the Rejection of Pyritic Sulfur during Coal Flotation, unpublished Master's thesis, Pennsylvania State University (1982).
2. W. C. Hirt, Separation of Pyrite from Coal by Froth Flotation unpublished Master's thesis, Pennsylvania State University (1973).
3. F. J. Chernosky and F. M. Lyon, AIME Transactions, **252**, 11–14 (1972).
4. SME-AIME, SME Mineral Processing Handbook, Section 5, (Society of Mining, Metallurgical, and Petroleum Engineers, Littleton, CO 1985).
5. A. J. Lynch, N. W. Johnson, E. V. Manlapig and C. G. Thorne, Mineral and Coal Flotation Circuits: Their Simulation and Control, (Elsevier, Amsterdam, 1981).
6. K. J. Miller and A. F. Baker, U.S. Bureau of Mines Technical Progress Report TPR51 (1972).
7. P. V. Dankwerts, *Chemical Engineering Science*, **2**, 1–13 (1953).
8. S. K. Kawatra and T. C. Eisele, *Column Flotation '88*, Chap. 22, 213–220, (Society of Mining, Metallurgy and Exploration, Littleton, CO 1988).
9. S. K. Kawatra and T. C. Eisele, *Processing and Utilization of High Sulfur Coals II*, Chap. 7, 61–70, (Elsevier, New York 1988).
10. S. K. Kawatra and T. C. Eisele, *Fine Coal Processing*, Chap. 16, 414–428, (Noyes Publications, NJ 1987).
11. S. Chander and F. F. Aplan, Final Report to the U.S. Department of Energy, DOE/PC/80523-T11 (DE 9000-7603) (1989).

FACULTAD DE INGENIERIA U.N.A.M.
DIVISION DE EDUCACION CONTINUA

CURSOS ABIERTOS

DESARROLLO Y OPERACIÓN DE SENSORES PARA CONTROL DIRECTO Y CONTINUO EN PLANTAS DE BENEFICIO DE MINERALES Y EN LA RESTAURACIÓN DEL MEDIO AMBIENTE

Del 18 al 23 de mayo de 1998

TEMA: ON - STREAM COMPOSITION ANALYSIS OF MINERAL SLURRIES

EXPOSITOR :DR. KOMAR KAWATRA
1998

Palacio de Minería Calle de Tacuba 5 Primer piso Deleg. Cuauhtemoc 06000 Mexico, D.F. APDO. Postal M-2285
Teletonos 512-8955 512-5121 521-7335 521-1987 Fax 510-0573 521-4020 AL 26

Chapter 41

ON-STREAM COMPOSITION ANALYSIS OF MINERAL SLURRIES

S. K. Kawatra* and Harrison R. Cooper**

Department of Metallurgical Engineering*
Michigan Technological University
Houghton, MI 49931

Harrison R. Cooper Systems, Inc.**
Salt Lake City, UT

ABSTRACT

In the last 30 years, on-stream slurry analyzers have proven to be of great use in the control of mineral processing circuits. This review discusses the two most popular methods, x-ray fluorescence and neutron activation analysis, and also considers techniques which are still under development.

INTRODUCTION

On-stream composition analysis of process streams in mineral processing operations has been proven to be a powerful tool for the adjustment of the process to variations in plant feed quality. The benefits derived from the use of on-stream analysis are now widely accepted in the base metal industry (Cooper, 1976, 1984 and Wells, 1983). The rapid feed back of the chemical assay drastically reduces the response time of control schemes, and thus helps to increase grade and recovery while reducing reagent consumption and operating costs. Also, the installation of an on-line analyzer frequently reveals that a process stream which has been considered to be stable actually undergoes sizable fluctuations, which may be detrimental to plant operation. For these reasons, a large number of on-stream analyzers have been installed throughout the world during the last 30 years.

An on-stream composition analyzer may operate in a number of ways, as discussed in the literature (Kawatra, 1984). The principles used by commercial units range from excitation by gamma-ray irradiation or neutron activation to measurement of radiation from naturally-occurring isotopes. Elemental analysis by use of fluorescent x-rays is commonly used. Several systems employing neutron activation have been installed for continuous analysis of silica in iron ore slurries. Natural isotope decay has been widely applied in the potash industry for determination of the potassium content of ore carried on conveyors (Cooper, 1976, 1984). Several analyzers employing non-radiometric technology are also in use. The following sections describe the various types of on-stream composition analyzers which have been used or are being developed for

use in mineral concentration operations.

X-RAY FLUORESCENCE ANALYZERS

Fundamental Principles

Conventional on-stream analysis is based on the principle of x-ray fluorescence (XRF) analysis. The basic principle of this method is illustrated in Figure 1. The sample may be excited either by low energy photons from radioisotope sources, or by electronically produced x-rays. The characteristic radiations emitted by the excited samples may be measured using either a wavelength-dispersive x-ray analyzer (WDX), or an energy-dispersive x-ray analyzer (EDX).

The WDX systems are based on the fact that the angle at which an x-ray photon is diffracted from a crystal is a function of its wavelength. Since the wavelength of a photon is a function of its energy, a WDX analyzer determines the energies of x-rays with great accuracy by geometric measurements. For on-stream analysis, the elements of interest are specified in advance, and individual diffracting crystal and detector units are provided to select and measure the characteristic x-rays of each element simultaneously.

Energy dispersive x-ray systems (EDX) use radiation detectors which produce electrical pulses with amplitudes proportional to the energy of the x-ray photons which were detected. The number of pulses produced with amplitudes corresponding to the energy of the characteristic x-rays of the elements of interest is then used to determine the concentrations of these elements.

The WDX systems have a much better energy resolution (20-25 eV) than do EDX systems, and therefore are less subject to error from peak overlap. However, a great deal of the x-ray intensity is lost in the diffraction crystal, with the result that WDX systems can only be used with an intense source of exciting x-rays, such as an x-ray tube. EDX systems are usable at much lower intensities, which may be produced by radioisotope sources. The energy resolution of an EDX system depends on the type of detector used. Solid-state detectors have the best energy resolution, but must operate at cryogenic temperatures. Proportional and scintillation counters can both operate at room temperature, but whereas the proportional counter has the superior energy resolution, the scintillation counter has a higher detection efficiency. A discussion of the advantages and disadvantages of these detectors was presented by Carr-Brion (1980). It may be noted that all three types of detector have been used in on-stream analyzers, with the selection depending on the number of elements to be determined, the energy resolution required to separate the characteristic x-rays, and the x-ray intensity which may be feasibly produced. The general principles of EDX and WDX systems are illustrated in Figure 1.

Excitation Sources

A mineral slurry may be excited into production of characteristic x-rays for quantitative analysis by use of either electronic x-ray tubes or by low-energy photons from radioisotope gamma-ray sources.

Radioisotope Excitation

Many radioisotope sources are available which are suitable for exciting characteristic x-rays for energy-dispersive x-ray analysis. Table 1 lists commonly

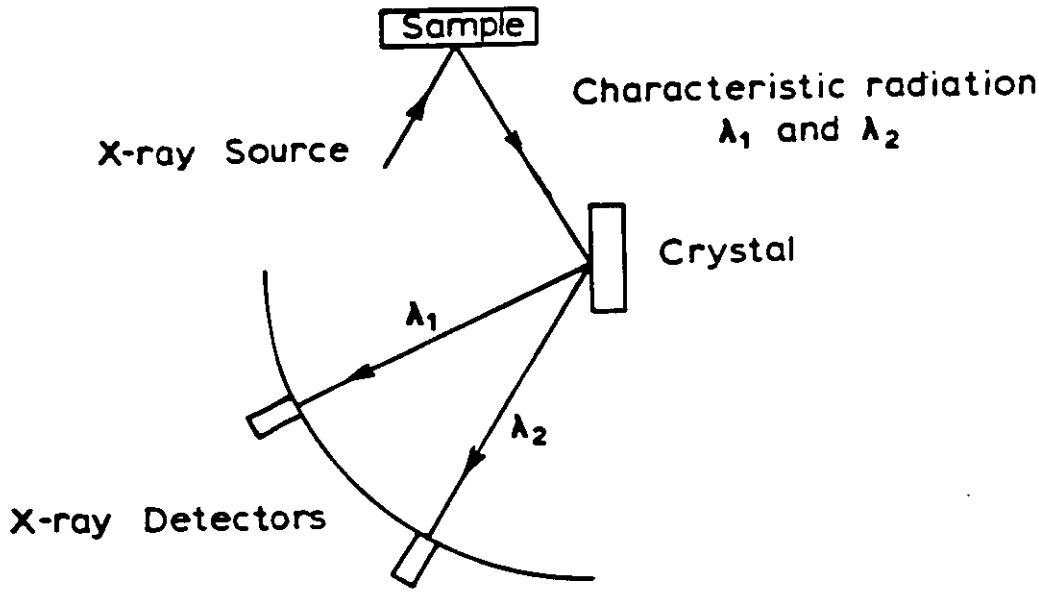

a) Wavelength - dispersive Spectrometer

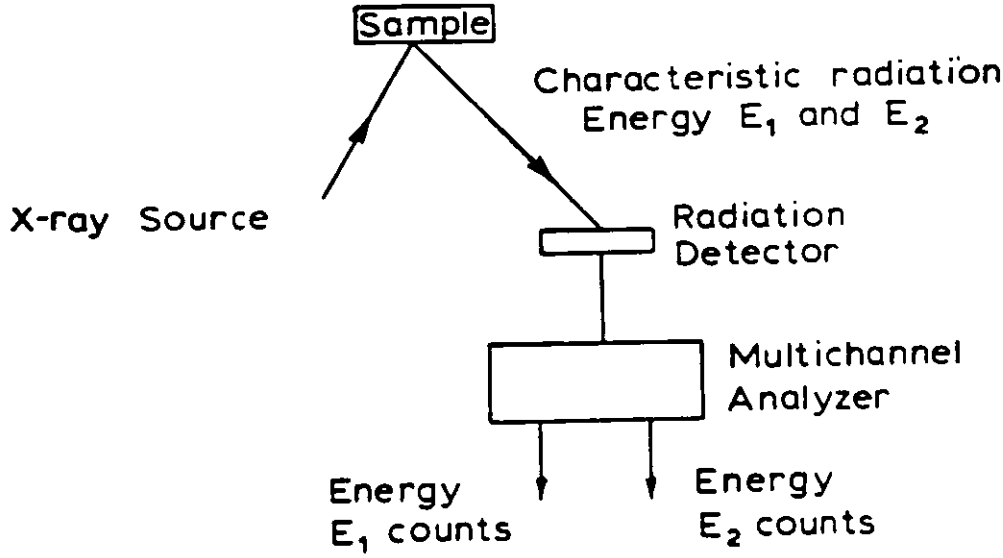

b) Energy - dispersive Spectrometer

Figure 1 X-ray Fluorescence Spectrometer Configurations. Wavelengths λ_1 and λ_2, and energies E_1 and E_2, are emitted by elements 1 and 2.

Table 1

Properties of x-ray and x-ray sources used in on-stream composition analysis.

Radioisotope	Half-life (yr)	Energy KeV	Relative Abundance*
Am-241	458	14-21 (Np L x-rays)	36
		59.6	37
Gd-153	0.65	41-47 (Eu K x-rays)	89
		70	2.6
		97	20
		103	30
Co-57	0.74	122	89
		136	9
Fe-55	2.7	5-9 (Mn K x-rays)	28.5
Pu-238	86.4	13-20 (U L x-rays)	10
Cm-244	18	14-21	8
Cd-109	1.3	22-25 (Ag K x-rays)	107
		88	
I-125	0.16	27-31 (Te K x-rays)	138
		35	7
Cs-137	30	662	82
Co-60	5.3	1170	100
		1330	100

*percent photons per disintegration

used low energy gamma and x-ray sources. Since optimum fluorescence efficiency is achieved when the excitation photon energy is close to, but greater than, the critical excitation potential required to produce the characteristic x-ray of interest, optimum source selection depends on the elements to be determined.

X-ray Tube Excitation

An x-ray tube provides a useful excitation source for either WDX or EDX systems. X-ray tubes provides a much higher x-ray intensity than is possible with radioisotope sources. As a result, small-area detectors may be used. Also, it is not as critical that the source and detector be in close proximity to the sample as is the case for radioisotope sources. X-ray tubes are sometimes used with a secondary source to reduce background radiation.

COMMERCIAL XRF ON-STREAM ANALYZERS

Commercially available on-stream analyzers can be divided into two categories; centralized and distributed systems.

Centralized Systems

In a centralized XRF system, samples of several slurry streams are transported to a common sensing unit. Such installations are generally of the wavelength-dispersive type, as this configuration allows the relatively expensive and bulky equipment required for WDX analysis to be shared among several streams. This system is particularly suited for large plants where more than five or six slurry streams are to be analyzed. A typical centralized analyzer is shown in Figure 2.

As it is usually not feasible to send entire slurry streams to a centralized analyzer, such systems require carefully designed

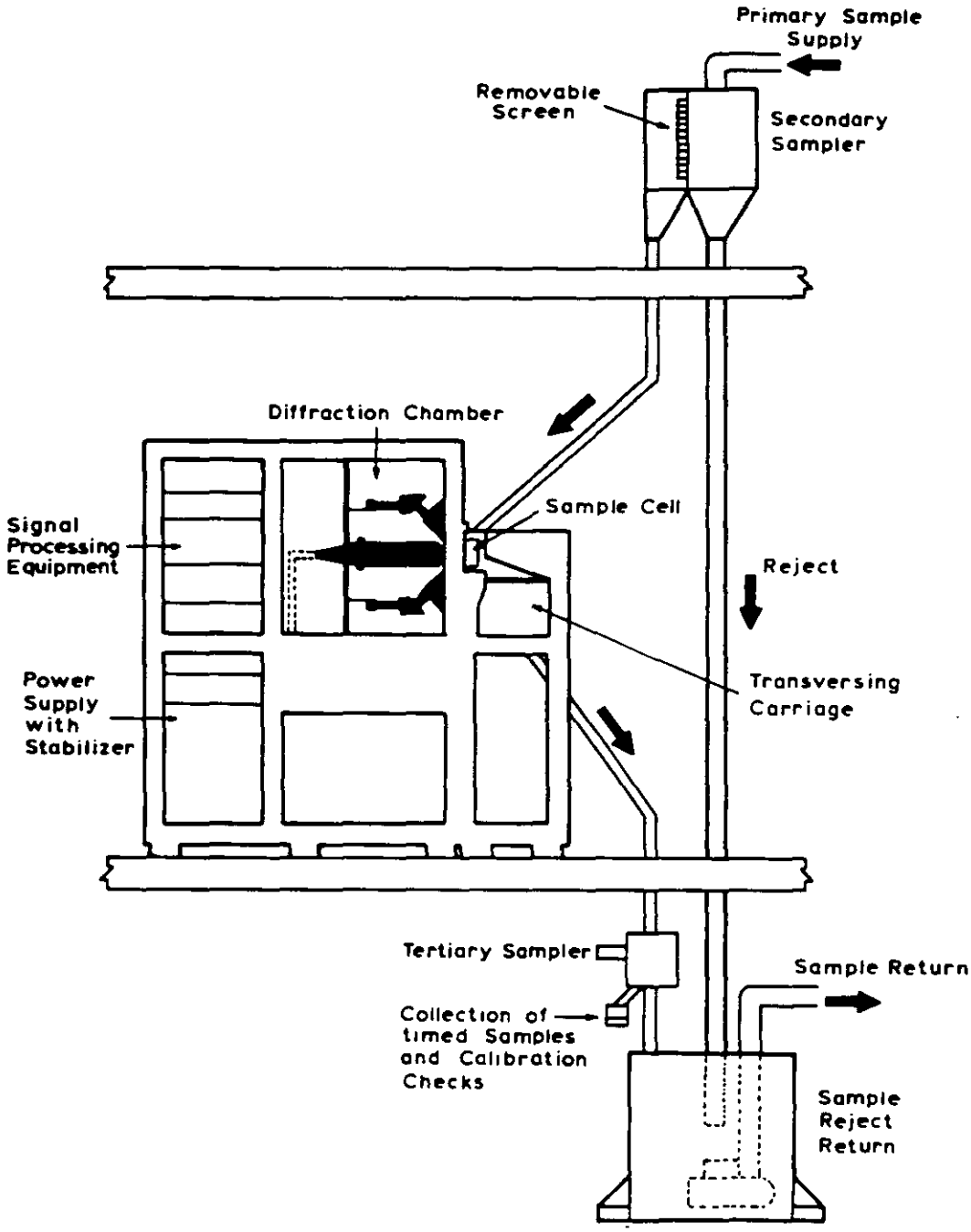

Figure 2 Centralized On-Stream Analyzer (Monitor System)

slurry sampling, pumping, and flow reducing equipment. The slurry is presented to the x-ray equipment through a flow cell having a plastic window (usually Mylar or Kapton) approximately 25 microns thick. Since the x-rays travel only a few millimeters into the flowcell, the layer of slurry in immediate proximity to the window has the greatest influence on assays. Hence, obtaining a representative sample for analysis is essential. Generally, a primary sample of 200-250 liter/min is taken, and is transmitted through two inch diameter pipes by pumping, pressure flow, or gravity flow to a secondary sampler, which removes 20 liters/min as a secondary sample, and returns the remainder to the main stream. Secondary sample streams are then presented to the x-ray analyzer unit.

Examples of centralized XRF systems are the Courier 300, manufactured by Outkumpu Oy, Finland, and the Monitor 1000 System, from Harrison R. Cooper Systems, U.S.A. The first commercial systems of Courier design were installed in 1967, and since then about fifty have been put into use. Several detailed descriptions are available in the literature (Lundan et al, 1977; Leskinen and Lundan, 1983). Elements of atomic number greater than titanium (no. 22) can be analyzed, often at assays of 0.01% by weight or below. Metals subjected to on-stream slurry analysis include copper, zinc, iron, silver, cobalt, nickel, lead, molybdenum, barium, and tungsten (Saarhelo, 1985).

The Courier system uses a series of fixed flow cells, with a movable x-ray head travelling on a precision guide rail. The system is modular, with fourteen cells in each. As many as six elements can be assayed, up to many as three modules can be used in a Courier configuration. This design enables a degree of expandability in the analyzer's capacity as requirements increase (Leppala et al, 1971).

On-stream XRF analyzer acceptance by industry has resulted from attention given to design of sampling, and other factors providing for all needs of turn-key installations. The systems incorporate built-in minicomputers with data processing including programs for assay computations, self monitoring, and other elements for fully developed operating capability.

The Monitor analyzers, from Harrison R. Cooper Systems, Inc. employ a fixed spectrometer unit with the multiple sample cell assembly positioned sequentially at the spectrometer head. Two designs are available: the Monitor 1000, with capability for measuring elements above titanium similar to the Courier 300, and Monitor 2000 systems for measurements of elements as low as aluminum (no. 13). Measurement of low order atomic species is made possible with a sealed spectrometer unit flushed with helium gas, enabling transmission of low energy photons from elements below titanium that otherwise would be absorbed by air in the spectrometer. Monitor analyzers are installed on a turn-key basis in units of 14, 28, and 42 flow cell modules. Primary sample streams are divided in secondary sampling to sequence flow of slurry sample streams to the measuring head. Figure 2 provides a schematic diagram of the system.

Other manufacturers offer similar equipment, of which the Boliden "Boxray" is an example (Sundvist and Sehlstedt, 1978). In this system, the samples are excited by radiation from secondary targets, which produce highly monochromatic excitation radiation to thus reduce background noise. EDX analysis is then carried out with a lithium-drifted-silicon

solid state detector. The spectrometer is held stationary, with slurry flowcells for each sample moved into analysis position by rotating the presentation system around a vertical axis. A similar sample presentation system has been described earlier in the literature (Kawatra, 1976a).

Distributed Systems

In a typical distributed system, several small on-line analyzers are provided, one for each slurry stream. The sensors are located on the mill floor at the points where analyses are desired. The analyzer may be either in-stream, which eliminates the need for sampling equipment, or near-stream, in which case the sampling requirements are greatly reduced compared to those of a centralized system. These systems are available using either WDX or EDX spectrometry.

Typical examples of distributed systems include the systems manufactured by Outokumpu Oy, Finland; Australian Mineral Development Laboratories (AMDEL), Australia; Austrian Research Center, Seibersdorf, Austria; Nuclear Equipment Corporation, U.S.A.; Autometrics, U.S.A.; and Harrison Cooper, U.S.A. The following sections discuss the sensor units for in-stream and near-stream analyzers.

In-stream X-ray Analyzers. This type of sensor consists of a radioisotope excitation source and a detector which are immersed directly in the process stream. Analyzers of this type are the result of excellent research work by the Australian Atomic Energy Commission (Watt, 1977), and several commercial units are available. The most commonly used units are those manufactured by AMDEL, Australia, and Outokumpu Oy, Finland. Another attractive unit for in-stream analysis, the Inscan System, has been developed by Texas Nuclear, U.S.A. These units differ primarily in the type of detector used, with the Inscan using a solid-state detector, the Outokumpu Oy Minexan-202 system using a proportional counter, and the AMDEL probe equipped with a scintillation counter. It may be reiterated that the energy resolution of solid-state detectors is superior to that of proportional counters, which in turn have better resolution than scintillation counters.

Since in-stream units utilize radioisotope excitation sources, the intensity of the excitation radiation is inherently stable, with only a slight correction for decay being needed. With radioisotope excitation sources, fluorescence response is of low intensity, making WDX spectrometry impractical, so in-stream analyzers are exclusively EDX systems. This severely limits the ability of in-stream probes to resolve fluorescent x-rays of similar energies. The background radiation levels are inherently high, particularly at low metal concentrations. These factors limit the ability of in-stream probes to produce accurate assays at low metal concentrations (Cooper, 1976). Serious accuracy problems arise in measuring low metal concentrations when elements with fluorescence spectra overlapping that of the element of interest are present in concentrations greater than one percent.

The AMDEL probe system requires a separate source-detector set for each element of interest at each measurement point. In addition, this system requires an additional probe for measuring pulp density. A difficulty with in-stream systems in general is the fact that repeatable measurements of pulse amplitude and number require high order electronic stability. Electronic drift

cannot be effectively evaluated unless the probe is tested after being removed from its sensing position in the slurry. Also, the fact that these probes must be immersed in a corrosive slurry introduces problems, as the detector will be destroyed if slurry leaks into the sensor head. In general, therefore, the in-stream systems require a high level of routine maintenance, and since they make use of radioisotopes, they may be a health hazard if handled improperly.

Even though the AMDEL and Outokumpu probes have been successfully used in in-stream analysis situations, there are many applications that do not lend themselves to systems of this type. For example, immersion of the probe in a large vessel, where slurry segregation is likely due to settling, flotation, or poor mixing, will produce poor results.

Near-stream X-ray Analyzers. Near-stream analyzers consist of an on-site unit through which a portion of a slurry stream is shunted for analysis, without traveling any great distance. There are several general types of excitation source/detector arrangements in use, which are described in the following sections.

1) X-ray Tube Diffraction Crystal. Excellent sensitivity and accuracy is achieved down to very low metal concentrations often in the parts per million range, as a result of the high primary x-ray intensity and high resolution capability of crystal spectrometers. Such devices are mechanically more complex, and thus more costly, than in-stream analyzers. Typical examples of this type of analyzer include the Courier-30 system, manufactured by Outokumpu Electronics, Finland, and the Monitor 500 system, manufactured by Harrison R. Cooper Systems, Inc., U.S.A.

The first application of on-stream x-ray fluorescence to an industrial mineral process was carried out with the Monitor 500 system. The Monitor 500 was used at a baryte mineral beneficiation facility where several process slurry streams in flotation were analyzed for barium sulphate. In this process, a critical requirement was providing information to a computer control system to maintain final product grade in the range of 90% baryte. The Monitor 500 system with two channels for rhodium backscatter radiation was installed to measure the Rayleigh and Compton scattering intensities. Preliminary tests conducted with process samples showed a correlation of impurity level in the concentrate with the difference (divergence) between inelastic scattering intensity and elastic scattering intensity. The Monitor 500 system was employed in this application because it has the capability for extension of measurement range to low atomic number elements, which allows for determination of silica if such should become necessary for impurity control in the future.

2) X-ray Tube/Solid State Detector. A system based on this combination has been described by Sundkvist and Sehlstedt (1978), and used in Boliden Metal's Aktiebolag Copper mine in Sweden. This System utilizes energy dispersive analysis in combination with secondary excitation. Secondary excitation consists of directing the tube output to a secondary target. The secondary target then emits nearly monochromatic fluorescent radiation, which is used to excite the sample. In the process, the continuous and characteristic spectra of the tube are largely eliminated. This allows both precise selection of excitation photon energy, and

reduction of background radiation. The line-to-background ratio for the energy-dispersive spectrometer is then nearly comparable to the line-to-background ratio of wavelength-dispersive systems.

Another example of this type of near-stream analyzer is the XRA-1500 system developed by Armco Autometrics, Boulder, Colorado. This system utilizes a germanium solid-state detector, rather than a lithium-drifted silicon detector (Ballard et al, 1983, and Kouns, 1985).

3) Radioisotope/Solid-State Detector. A by-line system based on Iodine-125 as an excitation source and a solid-state detector for energy-dispersive analysis has been developed by INAX, Ottawa; Bondar-Clegg, Ottawa; and Ramsey Rec. Ltd., Richmond Hill, Canada (Ereiser et al, 1980). Since solid-state detectors are capable of resolving x-rays of most elements of interest even when their atomic numbers are consecutive, simultaneous multi-element analysis is possible with this system. High resolution with solid-state detectors can be achieved only if the diameter is small, usually 4 mm. Since this is considerably less than the 25 mm typical for scintillation or proportional counters, an intense radioisotope source is required for solid-state detectors. This type of analyzer has been tested in plant trials at Noranda Mines Ltd., Ontario, Canada, for assaying copper, lead and zinc.

4) Radioisotope/Proportional Counter. An example of this type of analyzer is Outokumpu's Minexan 202 system, which is available in both in-stream and near-stream configurations. Each Minexan probe is capable of determining concentrations of as many as five elements plus pulp density. The probe employs a sealed proportional counter, and utilizes energy-dispersive analysis. While such detectors are relatively inexpensive and simple to use, resolution is inferior to both solid-state detectors and wavelength-dispersive systems, and thus elements with closely spaced fluorescent lines are difficult to distinguish (Barker and Saarhelo, 1984).

FACTORS AFFECTING MEASUREMENT ACCURACY

XRF analysis accuracy depends on several factors, some of which may be beyond the control of the instrumental technique such as mineralogical conditions, size distributions, interelement effects, and the level of assays which exist in the slurry being analyzed. Several fundamental sources of error inherent to x-ray fluorescent analyzers are discussed below. Within these limitations, the accuracy to be attained by XRF becomes dependent on the care and details put forth to the process of calibration.

A variety of methods for XRF calibration are available, ranging from simplistic multiple linear regression to more advanced methods employing mathematical models based on the x-ray fluorescence process. Calibration procedures are discussed in other tests (Cooper 1976). It is to be emphasized that effective use of on-stream x-ray fluorescence analysis depends on producing reliable assays which can be derived only from application of proper calibration technique.

Some factors such as particle size distribution, air content and pulp density can have significant effects on XRF accuracy. These factors are discussed below:

Atomic Number of Element. The higher the atomic number of the element being analyzed, the greater is the accuracy of

measurement.

Concentration of the Element. The higher the concentration of the element being analyzed, the greater is the accuracy of measurement. Expected relative accuracies to be attained are given for typical cases (relative accuracy is the standard error of measurement divided by the average concentration, multiplied by 100 percent).

Copper in concentrates (25% grade)	4-5%
Copper in tails (0.1%)	6-8%
Molybdenum in feed (0.2%)	4-6%
Lead in feed (5%)	7-9%
Zinc in tails (0.5%)	6-8%

Particle Size. The smaller the particle size the greater is the measurement accuracy. Variation in particle size distribution can give rise to errors. Berry et al (1969) have discussed particle size effects in detail. If a grinding circuit has a particle size control, variations in the particle size in the flotation section would be less, giving lower errors (Kawatra, 1975).

Mineralogy. Variations in the composition and variety of mineral types incorporating the element to be measured, as well as mineral grain size variation, cause reduced possibilities for accurate measurement.

Pulp Density. Measurement accuracy becomes greater for higher pulp densities and reduced variations in pulp densities, noting that the measurement result is the element content of the solids portion of the slurry.

Entrained Air. Since the intensity of the fluorescent x-rays depends on the amount of suspended solids, and hence on the slurry density, it is necessary to apply a density correction to the fluorescent intensity. This correction may be obtained through either of two methods; gamma-ray transmission, and x-ray backscatter. For example, AMDEL probes use a gamma-ray-transmission density gauge to correct for pulp density. Entrained air is always present in flotation slurries, and causes errors in the pulp density measurement, with the magnitude of the error being greater for transmission density corrections. In a study conducted for the measurement of percent copper in a chalcopyrite slurry using a transmission gauge for density compensation, it has been shown that an increase of entrained air from 0 to 30 percent resulted in a 40% error in the copper determination (Kawatra, 1976b).

NEUTRON ACTIVATION ANALYZERS

Fundamental Principles

Neutron techniques are attractive for analysis of elements with low atomic number such as silicon, aluminum, chlorine, sulfur, and fluorine. These elements may only be measured with difficulty by x-ray fluorescence analysis due to their low-energy characteristic x-rays. Thus, neutron activation may be considered as a viable method to carry out on-stream analysis when XRF methods cannot be used.

Neutron activation analysis is based on the interactions of neutrons with atomic nuclei, rather than on interactions with the electron shells. The results are therefore independent of the chemical state of the elements being measured. There are two types of neutron-nucleus interaction which may be applied for analytical techniques: 1) Radionuclide production, which results in delayed gamma-ray emissions as the unstable nucleus decays, and 2) prompt gamma emission, which

occurs immediately following the capture of a thermal neutron by the target nucleus.

Radionuclide production has been employed for on-line analysis of silica in iron ore, and silica and chromium in chromite. The nuclear reaction for silicon activation is as follows:

$$_{14}Si^{28} + n\ (fast) \rightarrow {}_{13}Al^{28} + p$$

$_{13}Al^{28}$ has a half-life of 2.3 minutes, and decays to the original stable silicon nucleus by emitting a beta particle accompanied by a 1.78 MeV gamma ray.

The neutron sources used are typically either Cf-252, or an α-n source. α-n sources consist of a source of alpha particles, such as Po-210 or Pu-239, and a target such as beryllium. The reaction of the alpha particles with the target causes neutrons to be emitted. These sources produce on the order of 10^8 neutrons per second.

Determination of Silica in Iron Ore Slurries

At present, only one type of neutron activation sensor is commercially available. This is the NOLA 1 system, produced by Texas Nuclear, Texas. This unit has been installed in at least eight operating iron ore processing plants with satisfactory results.

The NOLA unit consists of an analysis loop which recirculates a sample of slurry through the irradiator, detector, and density gauge units, as shown in Figure 3. The analysis loop holds approximately 500 milliliters of slurry, which must be at least 50% solid for a reasonable analysis. The loop is filled automatically from the slurry stream through a solenoid-operated 2-way valve. This technique, termed Recirculation Activation Analysis, has several advantages (Texas Nuclear, 1985):

1) increased sensitivity over single-pass analysis schemes;

2) lower dependence on fluctuations in slurry flowrate; and

3) minimal slurry sedimentation, due to the capability of maintaining a high flowrate in the analysis loop.

The NOLA system uses a Pu-Be α-n source (half-life 87.4 years) which emits 10^8 neutrons per second. At the Reserve Mining Co., Silver Bay, Minnesota, the NOLA system has been found to be capable of measuring silica content with an accuracy of $\pm$ 0.2% by weight (Allie, 1980). The NOLA analyzer at U.S. Steel's Minntac taconite plant measures the silica content in a slurry containing from 20 to 70% solids at 5 to 6% silica, with results within $\pm$ 0.2% of the silica content determined by wet chemical methods (Benner and Ludwig, 1984).

ON-LINE COMPOSITION ANALYZERS USING OTHER TECHNOLOGIES

The discussion in this chapter heretofore has dealt with the more established on-stream XRF and neutron activation analyzer systems, as these technologies have become of substantial importance to the metallurgical and mineral processing industries. Nevertheless, newer on-line composition analysis technologies have been introduced in recent years which offer the possibility of extending the range of analyzer methods which can be applied for improved process control. Several of the techniques are based on non-radiometric methodologies. Salient features

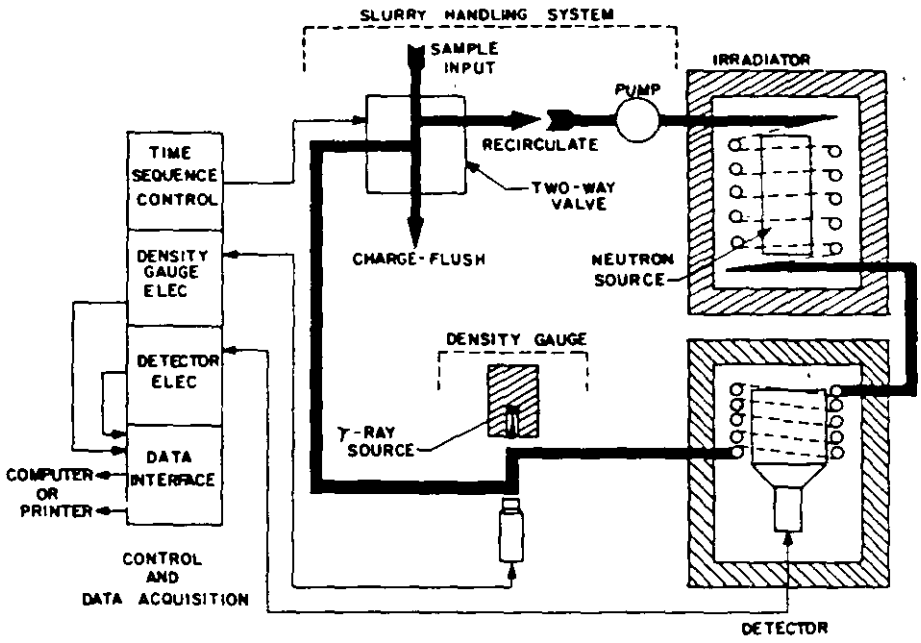

Figure 3. Schematic of NOLA analyzer (after Berry, 1978).

of the newer techniques are briefly described below.

Several methods for on-line analysis of gold in solutions and slurries are currently being developed. Witteck Development of Toronto, Canada, is currently developing an on-line gold analyzer based on the Direct Current Plasma (DCP) principle. Unlike the atomic absorption spectroscopy (AAS) method, which utilizes light absorption, DCP is based on light emission. The plasma yields a much higher operating temperature with resulting sensitivities of 5-10 ppb achievable from unconcentrated samples. This compares very favorably with the levels of .1 ppm (unconcentrated samples) and 20 ppb (concentrated samples) normally obtainable with AAS. Plant trials have been scheduled for the near future, however, no details are available at this time because of commercial interests. Robert and Ormrod (1982) have described an on-line gold analyser, the 'Tele-tale' which is based on solvent extraction and flame atomization and has a lower limit of determination of 0.005 mg/l. It is in use in a number of gold mines to monitor the gold content of barren solutions from filters. Recently, Mintek (1985) has improved upon this analyzer and developed a prototype system based on atomic absorption spectrophotometry and electrothermal atomization. It was designed to monitor the gold in solutions from the carbon-in-pulp process. Although the improved on-line analyzer is not commercially available as a package, all the separate components except the modified furnace autosampler are available. Bateman Process Instrumentation Ltd. (1985) has installed on-line gold sensors based on the principle of atomic absorption spectrometry.

Nuclear applications, Harwell, U.K., has recently built an on-line

monitoring system for a feldspar mill for Amberger Kaolinweke GmbH in West Germany (Wheeler, 1985). Tne details of this installation may soon be available.

The National Institute of Mining and Metallurgy, South Africa, has developed an on-line instrument in a feasibility study of the applicability of x-ray diffraction to the analysis of fluorspar-containing slurries. The instrument is shown to have adequate sensitivity and resolution and further test work is recommended (de Villiers, 1981). This method has been extended to on-stream analysis of apatite slurries as well.

On-stream analysis of coal slurries or of solid material flows has not been discussed in this chapter. A number of techniques such as prompt gamma neutron activation, nuclear magnetic resonance and electron spin resonance are described by Cooper (1984).

REFERENCES

Allie, C. L., 1980, "Reserve's Process Modifications Succeed at Silver Bay", Mining Engineering, vol. 32, no. 12, pp. 1695-1698.

Ballard, B. J., Dick, D. E., Barton, P. M. and Rathburn, R. H., 1983, "A New On-Stream X-ray Analyzer", Presented at the 11th Annual Meeting of the Instrument Society of America, Tucson, Arizona.

Barker, D. R. and Saarhelo, K., 1984, "A Recent Advance in On-Stream and Analysis Equipment for Mineral Concentrators and Metal Refineries", Paper Presented at the MINTEK 50 International Conference, Sandton, South Africa.

Bateman Instrumentation, 1985, "Olga Mark III Gold Analyzer", Bateman Industries Brochure, South Africa.

Benner, B. R. and Ludwig, J. R., 1984, "On-Line Silica, Size and Surface Area Measurements at U. S. Steel's Minntac Taconite Concentrator", Control '84, Published by the AIME, N.Y., pp. 21-28.

Berry, P. F., 1978, "On-stream Composition Analysis Using Neutron Activation", Report of a workshop on "On-Stream Characterization and Control of Particulate Processes", published by the Engineering Foundation, New York.

Berry, P. F., Furuta, T. and Rhodes, J. R., 1969, "Particle Size Effects in Radioisotope X-ray Spectrometry", vol. 12, pp. 612-632.

Carr-Brion, K. G., 1980, "Recent Developments in Detectors for Process Control X-ray Sensors", X-ray Spectrometry, vol. 9, no. 4, pp. 184-188.

Cooper, H. R., 1976, "On-Stream X-ray Analysis", Flotation, A. M. Gaudin Memorial, vol. 2, Fuerstenau, M. C., ed., AIME, New York, pp. 865-894.

Cooper, H. R., 1984, "Recent Development in On-Line Composition Analysis of Process Streams", Control '84, Herbst, J. A., ed., AIME, New York, pp. 28-38.

Cullity, B. D., 1978, "Elements of X-ray Diffraction", Second Edition, Addison-Wesley Publishing Co. Inc., U.S.A.

de Villiers, J.P.R., 1981, "On-Line Analysis by X-ray Diffraction of Fluorspar-Containing Slurries", NIM Report 2134D, Randburg, South Africa, pp. 1-3.

Dibbs, H. P., 1970, "The Application of Neutron Activation Analysis to the Determination of Copper in Minerals", CIM Bulletin, no. 4, pp. 493-499.

Dibbs, H. P. and Dalton, J. L., 1973, "Neutron Methods for On-Line Analysis, CIM Bulletin, no. 9, pp. 61-69.

Ereiser, J., Fran, K. G., Guy, J. W. and Litchinsky, D., 1980, "On-Stream X-ray Analysis of Float Process Slurries by XRF, "Advances in X-ray Analysis, vol. 24, Plenum Press, N.Y., pp. 297-302.

Kawatra, S. K., 1975, "On-Line Determination of Copper and Lead in Mineral Slurries", Ph.D. Thesis, University of Queensland, Brisbane.

Kawatra, S. K., 1976a, "The Design and Operational Characteristics of a Portable Multi-Stream On-Line Analyzer", International Journal of Mineral Processing, vol. 3, no. 1, pp. 41-50.

Kawatra, S. K., 1976b, "Effect of Variation of Entrained Air in Flotation Slurries on the On-Stream Determination of Copper by Radioisotope X-ray Fluorescent Analysis", Canadian Journal of Spectroscopy, vol. 21, no. 1, pp. 5-10.

Kawatra, S. K., 1984, "Methods of On-Stream Analysis", Presented at the SME-AIME Annual Meeting, Los Angeles, CA, Preprint no. 84-113.

Kouns, W., 1985, Personal Communication.

Leppala, A., Koskinen, J., Leskinen, T., and Vanninen, P., 1971, "Courier 300 On-Stream Analysis System", Trans. SME-AIME, vol. 250, pp. 261-268.

Leskinen, T. and Lundan, A., 1983, "Concentrator Process Control and Instrumentation", Presented at the Symposium on New Trends in Metallurgical Processing, October.

Lundan, A., Tarvainen, M., and Mattila, O., 1977, "Experience in Applying Computers for On-Stream Analyzing and Development of Automation in Mineral Flotation Processes", 15th APCOM Symposium, Brisbane, Australia, pp. 187-197.

MINTEK, 1985, "An Improved On-Line Gold Analyzer", 1985, MINTEK Research Digest Report, no. 11, March, pp. 4.

Robert, R.V.D. and Ormrod, G.T.W., 1982, "The Development of an On-Line Gold Analyzer", MINTEK Report no. M50, Randburg, South Africa, pp. 1-22.

Sundkvist, G. and Sehlstedt, H., 1978, "On-Stream Analysis System for Ore Dressing Plans Developed by Boliden Metall Aktiebolag", Presented at the Canadian Institute of Mining and Metallurgy Annual Meeting, Vancouver, 1978.

Taylor, M. C. and Rhodes, J. R., 1974, "Analyzing Process Streams by Neutrons", Instrumentation Technology, pp. 32-35.

Texas Nuclear, 1985, Product Bulletin for NOLA-1, Model NA79.

Tuttle, W. H., Williams, C. J. and Peterson, G. A., 1972, "A New Approach to Ore Grading Using On-Line Analysis", Mining Congress Journal, pp. 47-54.

Watt, J. S., 1977, "Nuclear Techniques for On-Line Measurement in the Control of Mineral Processing", Nuclear Techniques and Mineral Resources, I.A.E.A., Vienna, pp. 617-625.

Wells, A. P., 1983, "On-Stream Analysis at Wheal Jane", Mining Magazine, February, pp. 124-131.

Wheeler, V. J., 1985, Personal Communication.

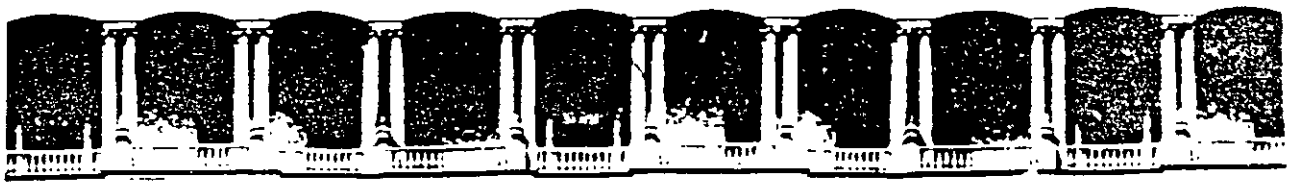

FACULTAD DE INGENIERIA U.N.A.M.
DIVISION DE EDUCACION CONTINUA

CURSOS ABIERTOS

DESARROLLO Y OPERACIÓN DE SENSORES PARA CONTROL DIRECTO Y CONTINUO EN PLANTAS DE BENEFICIO DE MINERALES Y EN LA RESTAURACIÓN DEL MEDIO AMBIENTE

Del 18 al 23 de mayo de 1998

TEMA: A PROCEDURE FOR EVALUATING EXISTING HEAVY - MEDIA COAL PREPARATION. CIRCUITS TO ENHANCE REMOVAL: A CASE STUDY

EXPOSITOR :DR. KOMAR KAWATRA

Palacio de Minería Calle de Tacuba 5 Primer piso Deleg. Cuauhtemoc 06000 Mexico, D.F. APDO Postal M-2285
Teléfonos: 512-8955 512-5121 521-7335 521-1987 Fax 510-0573 521-4020 AL 26

1998

Chapter 4

A PROCEDURE FOR EVALUATING EXISTING HEAVY-MEDIA COAL PREPARATION CIRCUITS TO ENHANCE SULFUR REMOVAL: A CASE STUDY

S. K. Kawatra[1], T. C. Eisele[1], and H. L. Dilley[2]

[1]Department of Metallurgical and Materials Engineering
Michigan Technological University
Houghton, MI 49931

[2]American Electric Power Service Co.
AEP Central Coal Laboratory
Albany, OH 45710

ABSTRACT

To improve the sulfur-rejection capability of a coal-cleaning plant, it is first necessary to evaluate the performance of the existing circuit. This information can then be used to decide whether there would be significant benefits from improving the operation and control of the existing circuit, or whether further improvements would require more radical process changes. This paper describes a simple model for evaluating heavy-media separation circuits, and presents a case-study of such an analysis of an operating heavy-media coal cleaning plant. Efficiency curves were calculated and modelled using Lynch's method, and a simplified expression was derived for calculating the Ecart Probability value from the model parameters.

INTRODUCTION

Since new environmental regulations are greatly restricting the emissions of sulfur oxides by coal-fired power plants, there is considerable interest in removing sulfur from coal before it is burned. The sulfur removal by coal-cleaning plants can be improved either by improving the effectiveness of existing equipment through better operation and control, or by the introduction of advanced processes and radical process changes. To select between these two choices, it is necessary to decide whether an existing circuit can be improved significantly, or whether it is already near its theoretical limit. In this paper, a method is illustrated for determining how closely a heavy-media circuit is approaching the theoretical optimum performance. This is useful for determining whether there is much further improvement that can be made in a particular heavy-media circuit without changing to a completely different process.

The theoretical limit of sulfur removal by heavy-media separation is mainly determined by the nature of the feed. Much of the sulfur in coal occurs as particles of pyrite (FeS_2) which typically accounts for between 15 and 80% of the total sulfur in the coal (Hower and Parekh, 1991). Since pyrite (specific gravity of about 5) is considerably denser than coal (specific gravity of approximately 1.2-1.6 for most

components of bituminous coal) (Dyrcacz et al., 1984), a density-based separation is ideal for separating pyrite from coal.

Two factors prevent heavy-media separation from removing all of the sulfur from coal:

1. Heavy-media separation is not very effective at particle sizes smaller than 200 micrometers (Wills, 1992). Since pyrite particles that are only a few micrometers in diameter are poorly liberated at this size, they are difficult to remove.

2. The second major form of sulfur in coal, the organic sulfur, consists of carbon-sulfur compounds that are an intimate part of the coal structure, and so cannot be removed by a purely physical separation.

Allowing for their basic particle size limitations, heavy-media separations can nevertheless remove a large fraction of the pyritic sulfur that is partially liberated from the coal at a fairly coarse size. In this paper, the performance of a commercial plant which uses heavy-media separation to clean coal was examined to determine its sulfur-removal capacity, and the observed performance was compared with the theoretical maximum performance.

THEORETICAL DISCUSSION

A very useful tool for evaluating the performance of a heavy-media separator is the partition curve, or Tromp curve (Wills, 1992). This curve is constructed by first carrying out sink-float analyses of the separator products. This data is then used to calculate the fraction of the total material in each density fraction that reports to the sinks product. This fraction is the partition coefficient for the given density, and when the partition coefficients are plotted versus density, they fall along the partition curve. The simplest method for creating these curves would be to plot the individual points and then to draw a smooth curve through them by hand. However, for many data sets the resulting curve is subjective, and will vary depending on the judgement of the person drawing it (Wizzard et al., 1983). In these cases, it is helpful to use a standard formula for the curve, using a curve-fitting computer program to calculate the adjustable parameters, so that the curve-fitting can be standardized and made reproducible. A number of such formulas have been developed over the years, which are each suited for particular types of separator (Peng and Luckie, 1991). It is generally best to use an equation with a small number of adjustable parameters when possible, since this makes the curve-fitting operation simpler, and the values for the adjustable parameters are tightly constrained, and therefore more likely to be physically meaningful.

The following equation, which was originally used for hydrocyclone efficiency curves (Lynch, 1977), can be curve-fitted to heavy-media partition curves, using a standard non-linear fitting algorithm:

$$y = \frac{e^{\alpha x} - 1}{e^{\alpha x} + e^{\alpha} - 2} \qquad (1)$$

where $x = \rho/\rho_{50}$

y = percent of material of the given density that reports to the sink product

ρ = particle density

ρ_{50} = density at which 50% of the particles report to the sink product

α = sharpness parameter

The values of α and ρ_{50} for each circuit provides a quantitative measure of the performance, where increasing values of α indicate an increasingly precise separation, and ρ_{50} is a measure of the density at which the separation is actually being made.

The standard measure of separation accuracy, which is widely used in the coal industry, is the Ecart Probability, or E_p (Wills, 1992). This is defined as:

$$E_p = \frac{\rho_{75} - \rho_{25}}{2} \tag{2}$$

where ρ_{75} and ρ_{25} are the densities on the partition curve where 75% and 25% of the particles, respectively, would report to the floats product. This is a measure of the slope of the efficiency curve in its middle region, where it is approximately linear, with the quality of the separation improving as the E_p value decreases. For a perfect separation, the value of E_p would be zero. The value of E_p can be calculated from Lynch's model, using a formula that was derived as follows. First, equation 1 was solved for x, to give:

$$x = \left(\frac{1}{\alpha}\right)\ln\left(\frac{y\left(2 - e^{\alpha}\right) - 1}{y - 1}\right) \tag{3}$$

By substituting y=0.75 and y=0.25 into equation 3, we obtained:

$$x_{75} = \left(\frac{1}{\alpha}\right)\ln\left(3e^{\alpha} - 2\right) \tag{4}$$

$$x_{25} = \left(\frac{1}{\alpha}\right)\ln\left(\frac{2 + e^{\alpha}}{3}\right) \tag{5}$$

Since $x=\rho/\rho_{50}$, and therefore $\rho=\rho_{50}x$:

$$E_p = \frac{x_{75}\rho_{50} - x_{25}\rho_{50}}{2} = \frac{\rho_{50}}{2}(x_{75} - x_{25}) \tag{6}$$

By substituting equations 4 and 5 into equation 6 and simplifying, we obtained the exact solution for the Ecart Probability:

$$E_p = \left(\frac{\rho_{50}}{2\alpha}\right)\ln\left(\frac{9e^{\alpha} - 6}{2 + e^{\alpha}}\right) \tag{7}$$

If the separation is efficient, the value of α from Lynch's equation will be large. For large α, the value of e^{α} becomes so large that the effects of subtracting 6 and adding 2 are negligible, and so equation 7 can greatly simplified to:

$$E_p = \left(\frac{\rho_{50}}{2\alpha}\right)\ln(9) = (1.0986)\frac{\rho_{50}}{\alpha} \tag{8}$$

Whenever α is greater than 5, the difference between equations 7 and 8 is less than 1%, and when $\alpha>27$, the difference between the two equations is less than the normal round-off error of most calculators. For comparison, the circuits described in this paper all had values of α greater than 40, as shown in Table 5, and so for these cases equation 8 is just as accurate as equation 7.

Using equations 1 and 8, it is straightforward to characterize the performance of a heavy-media separator. Given the sink-float analysis of a particular feed coal, they can be used to calculate the expected recovery and product quality. They can also be used to determine whether the separator would be more effective on a given feed if the separating density or separation sharpness were changed.

Using this method, the performance of an operating heavy-media circuit was examined to determine how closely the plant was approaching the maximum theoretical performance for the feed being processed.

PLANT DESCRIPTION

A simplified flowsheet of the plant is given in Figure 1. The plant used heavy-media separation to clean all of the coal coarser than 0.6 mm (28 mesh). The heavy-media was a slurry of finely ground magnetite in water. After being reduced to pass 152 mm (6") by a rotary breaker, the feed was screened to remove a 152 x 16 mm (6" x 5/8") coarse fraction. The material finer than 16 mm (5/8") was then further screened at 0.6 mm (28 mesh) using a sieve bend and vibrating screen, to produce a 16 x 0.6 mm (5/8"x28 mesh) intermediate product. The 0.6 mm (-28 mesh) material was then separated by a clas cyclone into 600 x 150 µm (28 mesh x 100 mesh) and 150 x 0 µm (-100 mesh) size fractions that were treated in two separate froth-flotation circuits, which are not discussed here.

The 152 x 16 mm (6"x5/8") material was cleaned using two Peters washers, which are heavy-media baths. The rated capacity of these units was 454 metric tons/hr (500 tph each), or 907 mt/hr (1000 tph) for the two units. The feedrate to the entire plant was 1868 mt/hr (2059 tph), of which approximately 40%, or 748 mt/hr (824 tph), reported to the Peters washers.

The 16 x 0.6 mm (5/8" x 28 mesh) coal accounted for approximately 45% of the plant feed, and was treated by heavy-media cyclones. Normally three of the four available cyclone circuits were operating at any given time. Each circuit consisted of two 61 cm (24") diameter heavy-media cyclones, rated at 136 mt/hr (150 tph) each. The six operating cyclones received 841 mt/hr (927 tph), or 141 mt/hr (155 tph) each. The specifications of the cyclones were as shown in Table 1:

Table 1: Specifications of Krebs 24" Heavy-Media Cyclone, Model 24b-20FA

Inlet area:	290 cm^2 (45 in^2)
Overflow diameter:	28 cm (11")
Underflow diameter:	15.9 cm (6.25")
Cone Angle:	0.174 radians (10°)
Flow Rating:	7570 liters/min @ 103 kilopascals (2000 gpm @ 15 psi)

The correct media specific gravity targets were 1.70 in the heavy-media baths, and 1.75 in the cyclones. Actual separating gravities were 1.75 in the baths, and 1.82-1.88 in the cyclones.

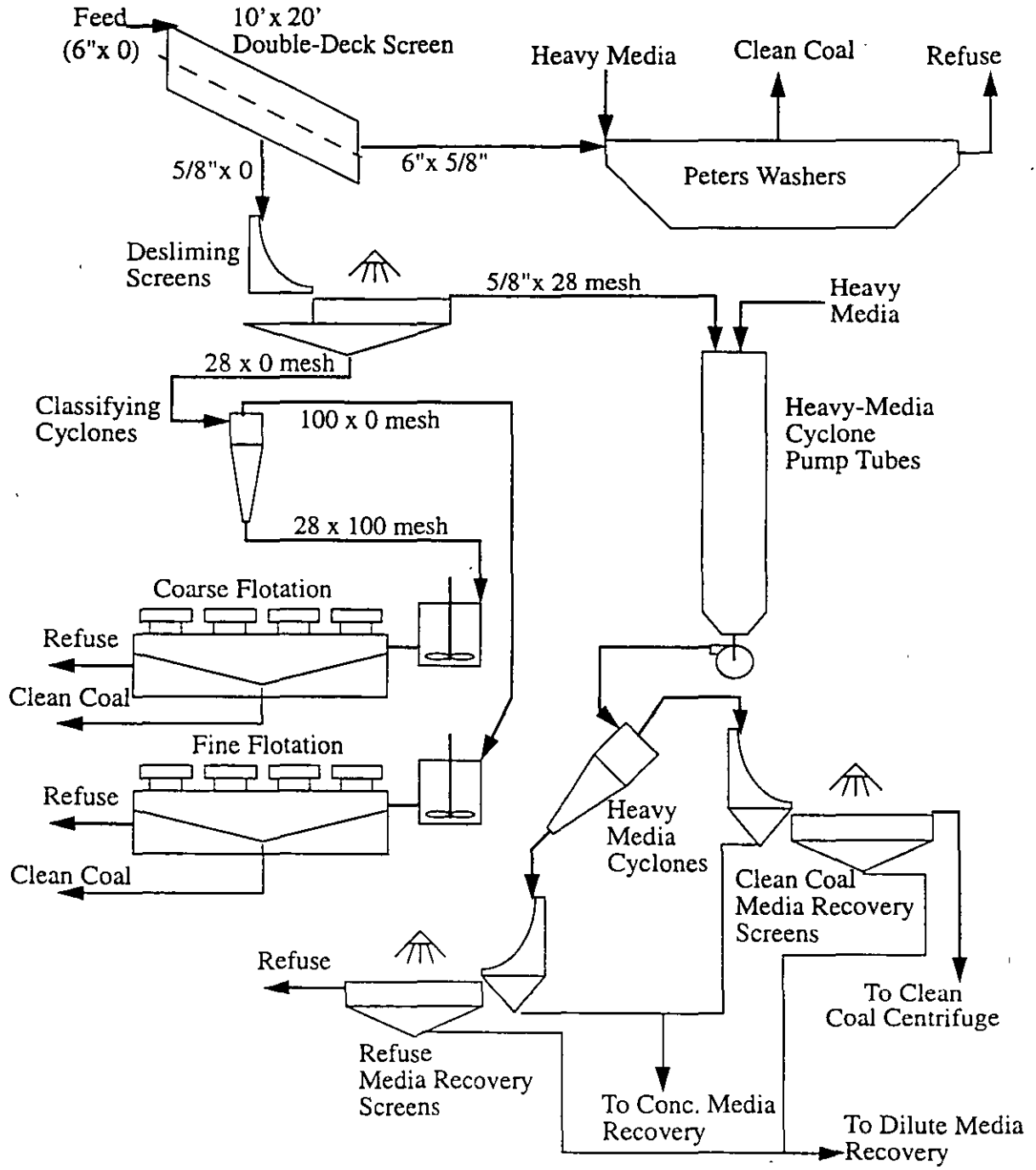

Figure 1. Simplified flow diagram of the Meigs coal cleaning plant, not including the reclamation circuits for heavy-media and water.

Feed Characteristics

The coal was mined from the Clarion 4A seam, and was a high-volatile bituminous coal containing approximately 1.05% organic sulfur and 0. 06% sulfate sulfur, with 3.5-4.6% pyritic sulfur. The composition of the feeds to the heavy-media bath and to the three cyclone circuits described is given in Table 2, with the feed size distributions given in Table 3. The washability of each of the feed-coal

streams was determined by heavy-liquid sink-float analysis, and the weight and sulfur content in each density fraction is given in Table 4. From this data, it is seen that it is possible to reject a greater proportion of the sulfur from the cyclone feeds than from the bath feed, because the cyclone feeds contain a greater amount of low-density, low-sulfur material. This is a result of the finer size distribution of the cyclone feeds, which allows better liberation of the pyrite from the coal.

Table 2: Heavy-media bath and heavy-media cyclone feed coal composition

	Feed Size Range	%Ash	%Sulfur	BTU/lb
Heavy-media bath	152 x 16 mm	46.27	5.63	6950
Cyclone Circuit B	16 x 0.6 mm	40.97	4.68	7801
Cyclone Circuit C	16 x 0.6 mm	45.56	4.54	7149
Cyclone Circuit D	16 x 0.6 mm	44.41	4.74	7271

Table 3: Heavy-media bath and heavy-media cyclone feed coal size distributions (cumulative percent passing each size). Since the cyclone feeds have a finer size distribution, the liberation of coal and pyrite is higher than for the bath feed, and so there is a larger quantity of low-sulfur, low-density coal that can be recovered.

Size	Heavy-Media Bath	Cyclone Circuit B	Cyclone Circuit C	Cyclone Circuit D
6" (152 mm)	100	100	100	100
5/8" (16 mm)	15.00	93.76	97.17	90.12
3/8" (9.5 mm)		69.56	75.07	64.38
1/4" (6.3 mm)	4.23	50.98	54.59	47.71
8 mesh (2.36 mm)		24.39	27.15	26.17
28 mesh (0.6 mm)		2.21	3.74	5.31

Table 4: Sink/Float washability results for the feeds to the heavy-media bath and cyclones.

S.G. Range	Heavy-Media Bath		Cyclone Circuit B		Cyclone Circuit C		Cyclone Circuit D	
	%wt	%S	%wt	%S	%wt	%S	%wt	%S
-1.3	15.81	2.70	33.19	2.55	29.86	2.58	28.34	2.65
+1.3/-1.4	17.65	3.99	13.73	3.52	12.04	3.56	14.34	3.37
+1.4/-1.5	4.89	5.60	4.79	5.48	4.62	4.74	4.39	4.95
+1.5/-1.6	2.35	6.72	2.12	6.08	2.45	5.83	2.34	5.91
+1.6/-1.65	0.78	5.65	0.57	5.88	0.73	6.12	0.94	5.66
+1.65/-1.7	1.08	6.02	0.71	5.31	0.79	5.56	0.91	5.14
+1.7/-1.75	2.00	8.82	0.92	6.71	1.02	7.93	1.12	7.53
+1.75/-1.8	5.79	9.13	2.51	8.31	2.43	8.96	2.42	8.91
+1.8/-1.85	3.03	8.83	2.12	9.84	1.51	8.66	2.00	9.42
+1.85/-1.9	1.45	9.09	1.78	8.07	1.31	8.25	1.20	8.41
+1.9	45.16	6.33	37.56	6.02	43.24	5.44	42.00	5.85
Total	99.99	5.63	100.00	4.68	100.00	4.54	100.00	4.74

RESULTS AND DISCUSSION

A summary of the separation results for the four circuits studied is given in Table 5. As would be expected from the sink/float results in Table 4, the cyclone products (Table 5) are all lower in sulfur than the product from the heavy-media bath, and the % weight yields and BTU recoveries are higher, due to better liberation at the finer particle sizes where the cyclones operate.

Table 5: Plant performance summary, clean coal products. The pyritic sulfur contents were estimated from the total sulfur contents, assuming that all products contained 1.05% organic sulfur.

	% Weight Recovery (Yield)	% BTU Recovery	%Ash	%S	% Pyritic Sulfur	% Pyritic Sulfur Rejection	BTU/lb
Heavy Media Bath	45.18	71.48	14.99	4.28	3.23	68.1	12090 (28102 J/gm)
Cyclone Circuit B	60.00	86.40	12.47	3.80	2.75	54.5	12429 (28890 J/gm)
Cyclone Circuit C	56.32	86.64	12.09	3.80	2.75	55.6	12533 (29132 J/gm)
Cyclone Circuit D	56.67	85.81	12.92	3.93	2.88	55.8	12361 (28732 J/gm)

While the data in Table 5 is useful for determining whether the product being produced is meeting specifications, it does not give any indication of whether the performance of the circuit can be improved significantly. To determine this, it is necessary to calculate the sharpness of the separation being made by the separator. This is most easily done by using the procedure outlined in the theoretical section.

Separation Efficiency

Partition curves for the plant being studied were calculated based on sink/float analyses of the separator products. The partition data calculated for these tests is plotted in Figure 2, along with the best-fit curves for each circuit, as determined by non-linear regression, using Equation 1. The values and the uncertainties of the calculated parameters are given in Table 6. Two general-purpose curve-fitting programs were used (Sherrod, 1992; Temple University, 1993), which gave identical results even though they used different curve-fitting algorithms (Dennis et al., 1981; Press et al., 1988). Lynch's model fits the central portion of the partition curve very well, and deviates only a small amount near the ends. If the deviations at the ends were large, this would be an indication that there were mechanical problems with the separator which were allowing either high-density or low-density particles to be misplaced into the wrong product.

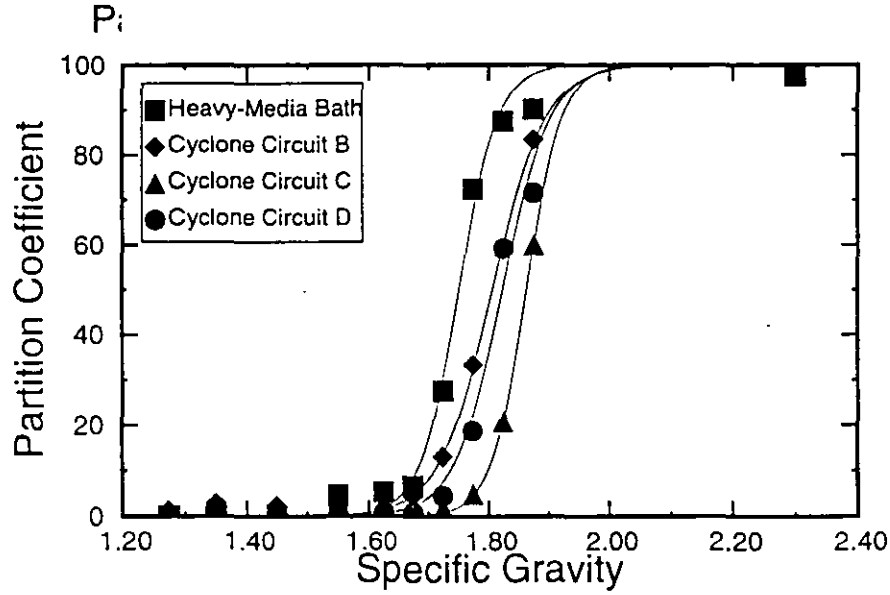

Figure 2. Partition curves for the heavy-media bath and the three hydrocyclone circuits studied. The partition coefficient is the percent of the feed material at a particular specific gravity that reports to the sink product.

Table 6: Results of fitting Lynch's equation to the plant partition data, and using the parameters α and ρ_{50} to calculate the Ecart Probability number, E_p, using Equation 8. Increasing values of α indicate an increasingly sharp separation, the ρ_{50} value increases as the separating density of the separator increases, and the value of E_p approaches zero as the separation becomes sharper.

	α	ρ_{50}	E_p
Heavy-Media Bath	54.87+/-5.93	1.752+/-.004	0.0351
Cyclone circuit B	41.28+/-1.66	1.807+/-.002	0.0480
Cyclone Circuit C	64.07+/-1.64	1.8633+/-.0007	0.0319
Cyclone Circuit D	46.25+/-5.12	1.824+/-.005	0.0433

To show the effect of changes in the density of separation (ρ_{50}) and the separation sharpness parameter (α), Equation 1 was used to calculate the % clean coal yield and the % pyritic sulfur that would be expected from the Peters Washer and Cyclone Circuit B feeds as ρ_{50} and α were varied. The results of these calculations are given in Table 7. The pyritic sulfur contents of the products were estimated from the total sulfur contents, assuming that all products contained 1.05% organic sulfur. The percent pyrite rejection was calculated from the expression:

$$\%\text{Rejection} = \frac{(\%\text{Wt. in Feed} \times \text{Feed Wt.}) - (\%\text{Wt in Floats} \times \text{Floats Wt})}{(\%\text{Wt. in Feed} \times \text{Feed Wt.})} \times 100 \qquad (9)$$

Comparing the actual plant results from Table 5 and Table 6 with the predicted results in Table 7, it is seen that the predicted results show lower sulfur contents and higher sulfur rejections than was actually seen in the plant. This difference is due to the small deviations of Lynch's model from the actual data near the ends of the partition curve. Since the ends of the curve represent either very low-ash coal or very high-ash reject, a very small deviation in the curve fit will result in a disproportionately large error in the predicted values. The predicted results are mainly suitable for determining whether a given change in separation sharpness or separating density will improve the plant performance. The difference between the predicted and the actual values are also useful for determining whether a significant amount of material is bypassing the separation because of mechanical problems.

From Table 7, it can be seen that increasing the ρ_{50} increases both the clean coal yield and the % sulfur in the clean coal, as would be expected, since a higher separating density will carry more locked coal/pyrite particles into the float product. There are also changes in yield and product quality when α is varied, but the changes are very small because these feeds do not contain a great deal of near-gravity material. This shows that in this plant, the separation performance is good enough that the product quality is determined more by the characteristics of the feed than by the performance of the plant, and that increasing the sharpness of the separation will have only a small effect on the plant performance for this feed.

Table 7: Calculation of the predicted performance of the Peters Washer (heavy-media bath) and Cyclone Circuit B, as the specific gravity of separation (ρ_{50}) and sharpness parameter (α) are varied. These values are calculated from the sink/float analyses in Table 3, using Equations 1 and 8.

ρ_{50}	α	E_p	Peters Washer			Cyclone Circuit B		
			% Yield	% Pyritic S	% Pyrite Rejection	%Yield	% Pyritic S	% Pyrite Rejection
1.70	60	0.031	42.31	2.89	73.30	54.82	2.20	73.67
	55	0.034	42.37	2.91	73.08	54.84	2.20	73.66
	45	0.042	42.54	2.94	72.69	54.87	2.20	73.64
	35	0.053	42.77	2.98	72.17	54.90	2.22	73.39
	20	0.093	42.77	3.11	70.96	54.33	2.26	73.19
1.75	60	0.032	44.34	3.09	70.09	55.89	2.27	72.30
	55	0.035	44.45	3.11	69.82	55.94	2.27	72.27
	45	0.043	44.71	3.14	69.35	56.05	2.29	71.98
	35	0.055	45.00	3.19	68.66	56.17	2.31	71.67
	20	0.096	44.99	3.28	67.78	55.84	2.36	71.23
1.80	60	0.033	47.62	3.42	64.44	57.50	2.40	69.87
	55	0.036	47.64	3.42	64.43	57.53	2.41	69.73
	45	0.044	47.67	3.43	64.30	57.60	2.42	69.57
	35	0.056	47.67	3.44	64.20	57.65	2.43	69.41
	20	0.099	47.13	3.45	64.50	57.24	2.45	69.38
1.85	60	0.034	51.06	3.72	58.53	59.44	2.57	66.65
	55	0.037	50.95	3.71	58.73	59.41	2.57	66.66
	45	0.045	50.67	3.69	59.18	59.33	2.57	66.71
	35	0.058	50.28	3.66	59.82	59.19	2.56	66.92
	20	0.102	49.07	3.60	61.43	58.50	2.54	67.56

Particle Size Effects

The variation in separation performance as a function of size was determined for all three of the cyclone circuits by screening and analyzing the feeds, clean coal products, and tailings. The BTU recoveries, pyritic sulfur rejections, and total sulfur rejections were determined for each circuit as the particle size was decreased.

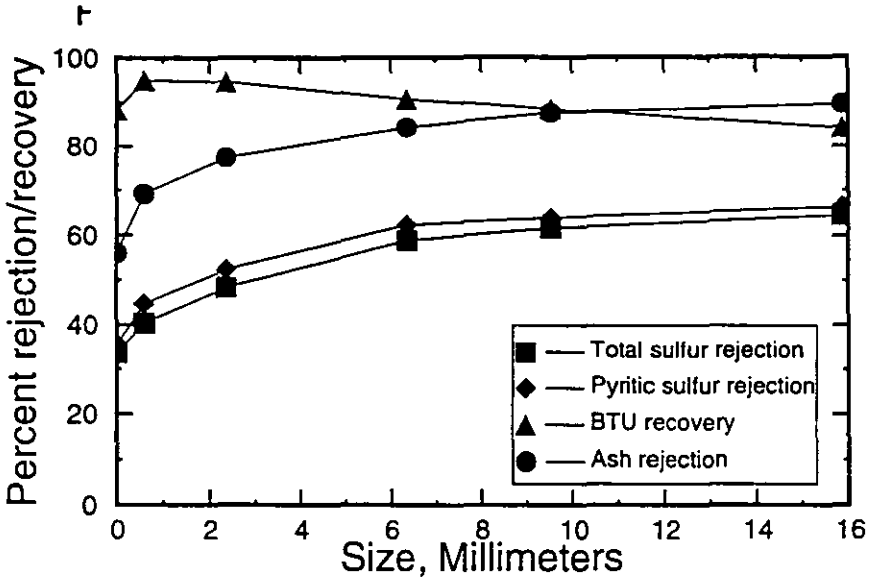

Figure 3. Variation in separation efficiency as a function of size for Cyclone Circuit B.

The results are shown in Figure 3 for Cyclone Circuit B, which was representative of all three units. For this circuit, we see that the BTU recovery slowly increases as the particle size decreases, due to improved liberation at finer sizes. However, the pyrite and sulfur rejections decrease at the finest particle sizes, particularly at sizes smaller than 6 millimeters. This is due to the decreased separation performance of heavy-media separators that results from the increased influence of hydrodynamic forces as particles become smaller. Therefore, grinding to a finer size to improve liberation of ash and pyrite would not be of particular benefit for this circuit.

CONCLUSIONS

Lynch's model expresses the sharpness of a separation in terms of the parameter α, which is not an intuitively obvious measure of the separation sharpness. The Ecart Probability value (E_p) is much more widely used in the coal industry, and its relevance is well understood, but no relationship was available in the literature for converting α to E_p. Therefore, a conversion formula was derived. For high-efficiency separators such as heavy-media baths and cyclones, the E_p can be closely approximated using the formula $E_p = (1.0986)\rho_{50}/\alpha$, where ρ_{50} is the specific gravity of separation.

Once a model of the partition curve has been determined, it is relatively straightforward to use it to predict the performance of the separator with various feeds. This helps to assess whether the product quality from the separator can be significantly improved by adjusting the separating density or improving the sharpness of the separation, or whether further improvements can only be made by radical changes in the process.

Using this method, an operating heavy-media plant was analyzed. It was found that the plant was producing a very sharp separation, and that for the coal being processed, increasing the sharpness of separation further would have a minimal effect on the product quality. To significantly increase the pyritic sulfur removal from this coal, it would be necessary to grind the coal to a finer size to improve

liberation. However, heavy-media separations become less effective at finer sizes, and so it would be necessary to switch to an advanced coal-cleaning process that could deal with finer coal.

REFERENCES

1 Dennis, J. E. Jr., D. M. Gay, and R. E. Welsch (1981) "An Adaptive Nonlinear Least-Squares Algorithm", ACM Transactions on Mathematical Software, Vol. 7, No. 3, pp 348-368

2 Dyrcacz, G. R., C. A. A. Bloomquist, L. Ruscic, and E. P. Horwitz (1984) "Variations in Properties of Coal Macerals Elucidated by Density Gradient Separation", *Chemistry and Characterization of Coal Macerals* (ACS Symposium Series No. 252), American Chemical Society, pp 65-78

3 Hower, J. C., and B. K. Parekh (1991) "Chemical/Physical Properties and Marketing," Coal Preparation, 5th edition (Leonard and Hardinge, eds), Society for Mining Metallurgy, and Exploration, Littleton, CO, Chapter 1

4 Lynch, A. J. (1977) Mineral Crushing and Grinding Circuits, Their Simulation, Optimisation, Design, and Control (Developments in Mineral Processing 1), Elsevier, Amsterdam, page 116

5 Peng, F. F., and P. T. Luckie (1991) "Process Control, Part 1: Separation Evaluation," Coal Preparation, 5th edition (Leonard and Hardinge, eds), Society for Mining Metallurgy, and Exploration, Littleton, CO, Chapter 10

6 Press, W. H., B. P. Flannery, S. A. Teukolsky, and W. T. Vetterling (1988) Numerical Recipe The Art of Scientific Computing, section 14.4, "Nonlinear Models," Cambridge University Cambridge, pp. 540-547

7 Sherrod, P. H. (1992) "Nonlin" (program for PC-compatible computers), available from P. H. Sherrod, 4410 Gerald Place, Nashville, TN 37205-3806

8 Temple University (1993) "TempleGraph" (program for Unix-based computers), available from Mihalisin Associates, 600 Honey Run Rd., Ambler, PA 19002

9 Wills, B. A. (1992) Mineral Processing Technology, 5th edition, Pergamon Press, Oxford

10 Wizzard, J. T., R. P. Killmeyer, and B. S. Gottfried (1983) "Computer Program for Evaluating Coal Washer Performance," Mining Engineering, March 1983, pp252-257

FACULTAD DE INGENIERIA U.N.A.M.
DIVISION DE EDUCACION CONTINUA

CURSOS ABIERTOS

DESARROLLO Y OPERACIÓN DE SENSORES PARA CONTROL DIRECTO Y CONTINUO EN PLANTAS DE BENEFICIO DE MINERALES Y EN LA RESTAURACIÓN DEL MEDIO AMBIENTE

Del 18 al 23 de mayo de 1998

TEMA: ON - LINE TESTING OF A HORIZONTALLY - BAFFLED FLOTATION COLUMN IN AN OPERATING COAL - CLEANING PLANT

EXPOSITOR :DR. KOMAR KAWATRA

1998

Chapter 20

ON-LINE TESTING OF A HORIZONTALLY-BAFFLED FLOTATION COLUMN IN AN OPERATING COAL-CLEANING PLANT

T. C. Eisele and S. K. Kawatra

Department of Metallurgical and Materials Engineering
Michigan Technological University
Houghton, Michigan 49931

ABSTRACT

A horizontal-baffle arrangement has been developed to prevent excessive axial mixing in flotation umns. These baffles have been shown in previous work to improve the grade/recovery performance of both a laboratory-scale column and a pilot-scale column (Kawatra and Eisele, 1993). In this paper, results are given for continuous on-line operation of the pilot-scale baffled column in a commercial coal-cleaning plant. These results show its ability to operate for extended periods without plugging, to produce a consistent-quality product even while the feed quality was fluctuating, and to remove much of the pyritic sulfur from the coal.

INTRODUCTION

Flotation columns have been widely adopted in many applications in recent years, because they are more efficient separators than conventional flotation machines. Columns are more effective because they establish a long concentration gradient between the froth product and the sinks product, so that several meters are available over which the separation can take place. This is in contrast to conventional flotation machines, where the separation mainly occurs at the pulp/froth interface. Froth washing in the columns, which reduces entrainment of gangue into the froth, further improves the separation. However, in order for the concentration gradient to be established properly and for froth washing to work well, the column should approach plug-flow, where the vertical velocity of the pulp is approximately constant across the entire cross-section of the column (Finch and Dobby, 1990).

In flotation columns, vertical mixing along the axis of the column (axial mixing) causes the slurry flow in the column to deviate from plug-flow. This is generally harmful, as it tends to reduce the product recovery and to make the separation less selective (Finch and Dobby, 1990). As columns are increased in : from laboratory or pilot scale to full scale, the amount of axial mixing tends to increase, as larger diameter columns generally have a smaller height/diameter ratio than smaller columns. This axial mixing not only harms the performance of larger-diameter columns, but also makes scale-up calculations more difficult. A related problem is the formation of large bubbles, which cause the froth to "churn" when they go through the froth layer. If it is severe, the churning caused by large bubbles can disrupt the froth layer, causing a loss of selectivity. These large bubbles will form when the bubble generators are not working

properly, when air is entrained into the feed stream, or when bubbles coalesce as they rise through the column.

Work has been done in the past using vertical baffles to subdivide the column and reduce the apparent diameter, with the goal of reducing axial mixing, but this has been found to introduce bubble-distribution problems (Finch and Dobby, 1990) and has been found to have only a small effect on performance in any case (Alford, 1992). In previous work by the authors (Eisele and Kawatra, 1994a,b), the use of horizontal baffles to reduce axial mixing was described. It was found that the best results were obtained in the laboratory when the baffles had between 29 and 38% open area and when they were present both above and below the feed inlet. A pilot-scale column of the same design as was developed in the laboratory was then built and tested off-line, to determine whether there were any serious scale-up problems (Eisele and Kawatra, 1994b). In this paper, the results of continuous on-line tests with the pilot-scale column in an operating coal-cleaning plant are discussed. These results demonstrate the ability of the column to operate stably and produce a consistent-quality froth with normal feed-quality variations (31-39% ash, 3.8-4.8% total sulfur, 2.2-3.6% pyritic sulfur).

THEORETICAL DISCUSSION

In the most common type of flotation column, there is no restriction to flow along the axis of the column. Rising air bubbles therefore are free to carry slurry up along the axis, which then returns to the bottom along the sides of the column, producing strong axial mixing. This can be controlled by using microbubble generators, by carefully aligning the column, and by closely controlling the column operation. However, if a disturbance forms for any reason, then there is nothing to prevent the disturbance from rapidly growing into a major disruption of the column operation. For example, if a malfunction of the bubble generators occurs that allows some large bubbles to form, these bubbles will tend to coalesce with other bubbles to grow still larger, and will expand further as they rise in the column due to the decreased water pressure. Because they rise very rapidly, such bubbles will contribute significantly to axial mixing, and if they are large enough they will disrupt the froth layer and degrade the column performance still further.

Horizontal baffles, such as those described in this paper, provide a simple method for suppressing such disturbances and preventing axial mixing, as shown in Figure 1. The horizontal baffles have openings large enough to keep them from being plugged by solid particles, but small enough to break up vertical mixing currents, so that slurry cannot be rapidly swept along the axis of the column. This provides a much closer approximation to plug flow, and therefore improves the separation. Horizontal baffles are suitable for retrofitting existing columns, as they are simple to make and install. They can also be made of wear-resistant and corrosion-resistant materials, so that they will be low-maintenance.

There are two important effects of horizontal baffling, as follows (Kawatra and Eisele, 1993): 1. Baffles that are installed below the feed entry point increase the minimum residence time of particles in the column. This ensures that all floatable particles will have a better chance of attaching to air bubbles, and so recovery will be improved. 2. Baffles installed above the feed inlet point keep the bubbles from becoming too large. This prevents churning and mixing of the froth layer by coarse bubbles, which is a common problem in unbaffled columns. Froth washing is more effective when the froth layer is not being churned, and so the product quality will be improved by baffles above the feed inlet.

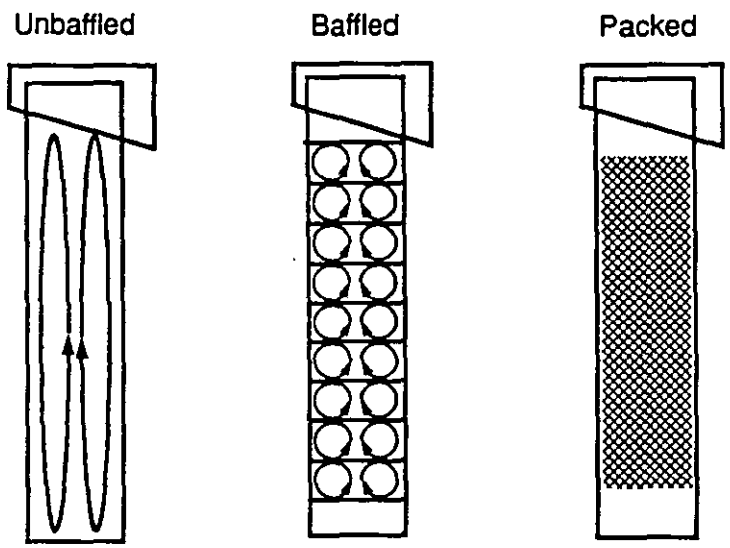

Figure 1. Comparison of flow patterns in regular and horizontally baffled columns. In the regular, unbaffled column, slurry can be carried up by the air bubbles in the center, which produces axial mixing along the entire height of the column. Horizontal baffles can break up the currents, so that axial mixing is limited to shorter distances. Packed columns can also prevent axial mixing (Yang, 1988), but in these columns the flow restriction is much greater than in the baffled column, and so they can be prone to plugging.

CONDITIONS AND PROCEDURES

Plant Characteristics

A pilot-scale Deister Flotaire column was modified and installed in the Empire Coal processing plant, Gnadenhutten, Ohio. The flowsheet of the Empire fine coal cleaning circuit is given in Figure 2, showing the location of the flotation column.

Feed Characteristics

This plant processed a mixture of bituminous coals from the Lower and Middle Kittanning seams, with the main gangue mineral in the -0.6 mm particles being fine clay. The feed used for the tests described in this paper was taken from the waste fines produced by the clean coal dewatering screens.

Pilot-Scale Column Design

The column was derived from a Deister Flotaire unit, 20.3 cm in diameter and 9.1 meters tall. A schematic of the column is given in Figure 3. Air bubbles were injected at 4.5 meters and 9.1 meters below the froth overflow lip. The column contained 9 upper baffles, and 17 lower baffles, as shown in Figure 3, each with 34% open area. The bubble generators were a design manufactured by the Deister Concentrator Co., which injected an air-water mixture at a volume ratio of 7.5/1. The units used each had maximum flowrates of 28.3 standard liters/min of air, and 3.78 liters/min of water.

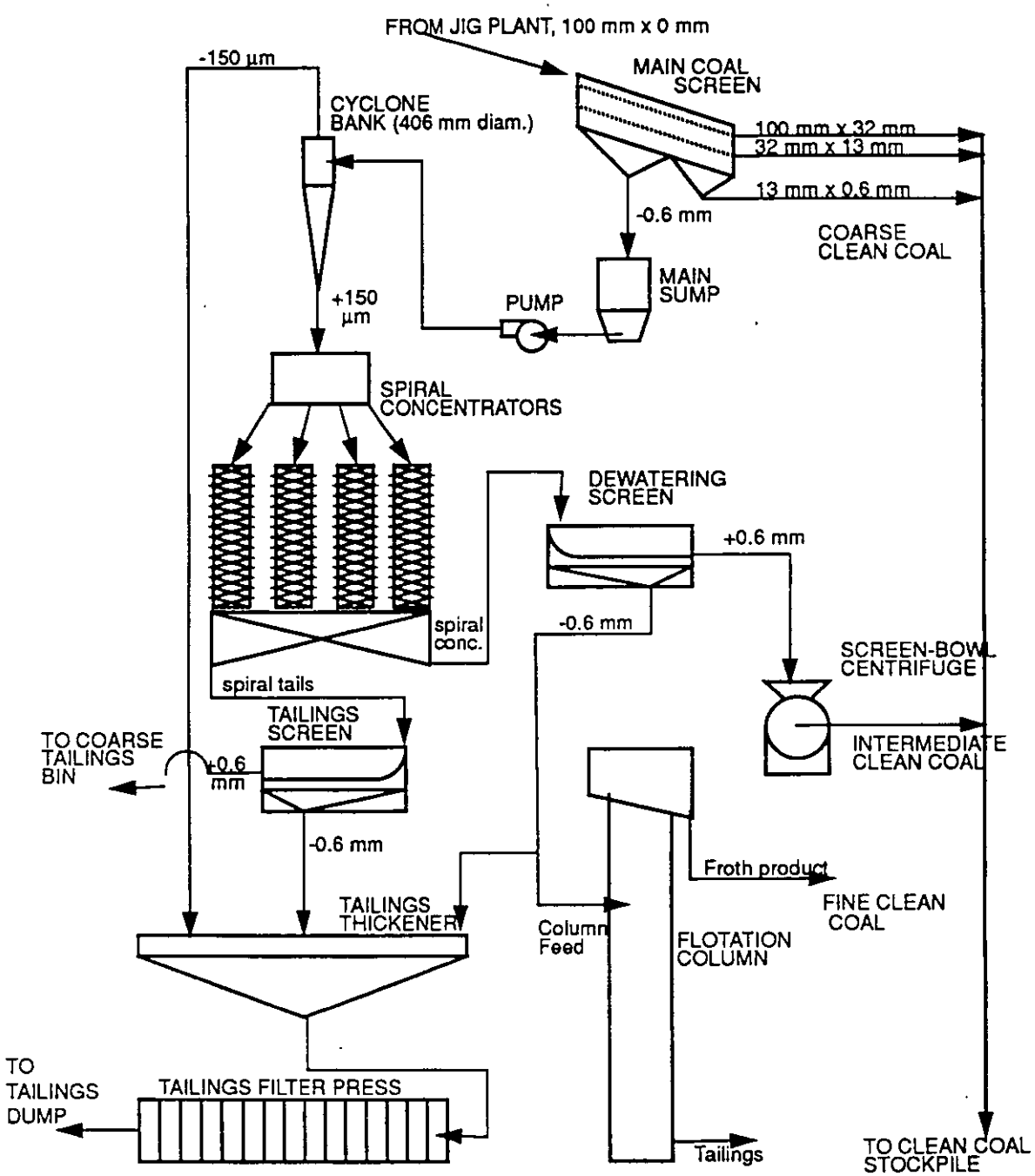

Figure 2. Flowsheet for the fine-coal processing circuit at Empire coal. Column feed was taken fro the dewatering screen waste fines, which had a nominal top size of 0.6 mm (28 mesh).

The column was operated with a froth depth of 61 cm. Measuring from the froth overflow lip, of the feed inlet tube was at a depth of 122 cm. This long feed tube was needed so that there would be enough room between the froth base and the feed inlet to install baffles. The upper baffles extended fro a depth of 71 cm to 117 cm, and the lower baffles extended from 147 cm to 234 cm. The washwater spra ring was immersed 5 cm below the froth surface, and the washwater flowrate was 7.57 liters/min. Froth

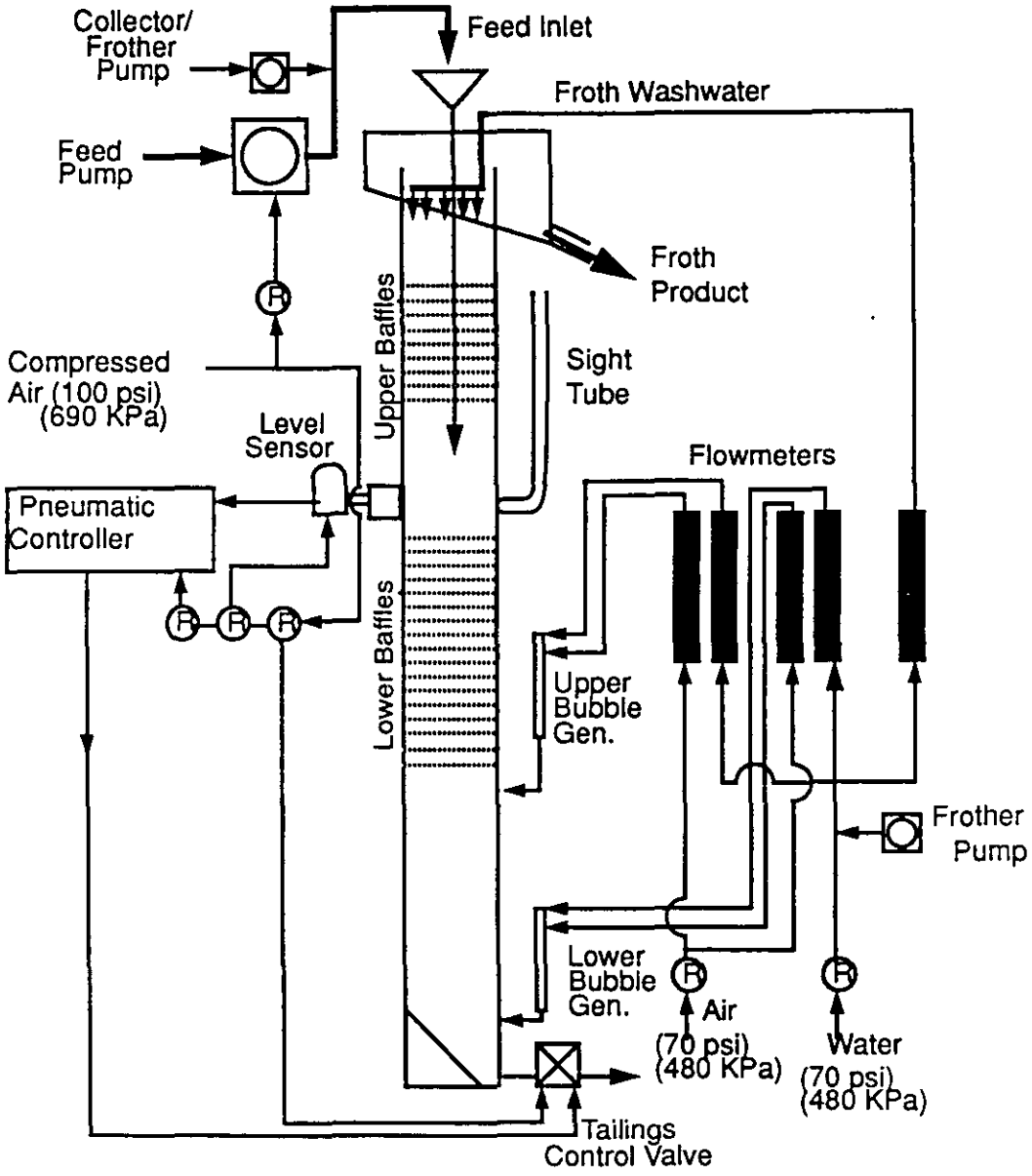

Figure 3. Schematic of the pilot-scale baffled flotation column. The column was 8" (20.3 cm) in diameter and 30' (9.1 meters) tall, with the upper bubble generator 15' (4.5 meters) down from the top. The ratio of air to water in the bubble generators was 7.5:1 by volume.

was added to the froth washwater at the same rate as it was added to the feed and to the bubble generator water, to ensure a stable froth.

The baffles caused the froth to be much more quiescent, because they broke up large bubbles into smaller bubbles, and made them rise more slowly. This was mostly beneficial, as it prevented the froth from churning. However, it also allowed parts of the top of the froth to dry slightly into a semisolid, sticky mass that adhered to the feed tube. Over time, this would form a cap and eventually plug the top of the column. This was corrected by installing spray nozzles above the froth, spraying a mist of water at 1

liter/min to keep the top of the froth moist and fluid. With the water sprays running, the froth overflowed cleanly without adhering to the feed tube.

Reagents and Analytical Methods

The frother used for these tests was Dow DF 1012, a strong polyglycol frother. This was selected to ensure a stable, consistent froth. The collector was composed of #2 fuel oil and Dow M210 froth conditioner. The froth conditioner was added because, in earlier laboratory tests, the coal was found to be poorly floatable with fuel oil alone.

The reagents were mixed in the following proportions before adding them to the column feed stream: Frother, 50%; Fuel oil, 40%; Froth conditioner, 10%. The reagents were combined both to emulsify the collector so that it would disperse more readily into the feed, and to simplify the reagent addition. The dosage rate for the complete reagent mixture was 0.5-0.75 ml/min (0.9-1.0 kilograms/metric ton total; 0.45-0.5 kg/mt frother; 0.36-0.4 kg/mt fuel oil; 0.09-0.1 kg/mt froth conditioner).

Analyses were carried out using ASTM standard methods (ASTM, 1989). Ash was measured using Method D3174, and pyritic sulfur was determined using Method D2492. Total sulfur was measured using a LECO SC-132 sulfur determinator, and calorific value was measured using a LECO AC-300 automatic calorimeter.

Ash and pyritic sulfur rejections were calculated using the following formula:

$$\%\text{Rejection} = \frac{(\%\text{Wt. in Tails} \times \text{Tails Wt.})}{(\%\text{Wt. in Feed} \times \text{Feed Wt.})} \times 100$$

RESULTS AND DISCUSSION

Continuous on-line experiments were conducted using the clean coal dewatering screen underflow, with the feed's particle size and composition varying as shown in Table 1.

TABLE 1: Average characteristics of the dewatering screen underflow during the final series of on-line experiments. This table is a composite of the assays of each feed sample for the on-line tests summarized in Table 2.

	Mean	Standard Deviation
80% passing size (μm)	306.7	3.8
20% passing size (μm)	42.0	0.6
% Ash	34.8	2.66
% Sulfur	4.41	0.34
% Pyritic Sulfur	3.1	0.50
BTU/lb	9275	365

TABLE 2: Summary of the froth product results for on-line tests, using the dewatering screen underflow product. Samples for each test were collected for a minimum of 45 seconds, sampling the entire stream. The feed quality was 31-39% ash, 3.8-4.8% total sulfur, and 2.2-3.6% pyritic sulfur.

Test #	%Pyritic S	%Ash	BTU/lb	%BTU Recovery	%Pyrite Rejection	%Ash Rejection
1	2.1	7.49	13236	83.9	61.8	87.6
2	2.4	8.18	13315	77.6	53.7	88.6
3	2.4	7.49	13308	86.6	56.2	89.0
4	2.2	7.22	13411	90.1	48.6	80.3
5	2.6	6.78	13460	87.9	51.1	87.8
6	2.6	6.96	13420	86.9	56.5	87.9
7A	2.9	7.62	13351	86.7	40.3	85.2
7B	2.7	6.70	13575	85.4	52.9	87.2
7C	2.9	7.19	13391	79.4	54.7	88.2
7D	2.8	7.84	13368	91.2	49.2	84.8
7E	2.4	6.71	13514	88.8	56.1	87.6
7F	2.7	6.90	13506	91.2	49.9	87.2

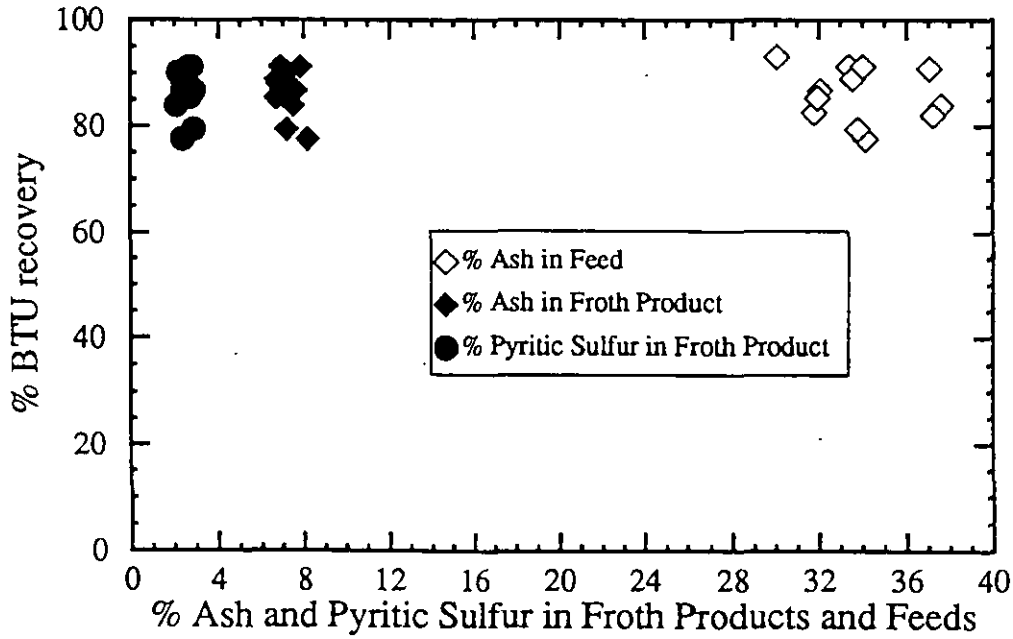

Figure 4. Grade-recovery results for the on-line continuous flotation tests, all baffles installed, with water sprays on the froth top. The ash content of the feed for each test is also given. In spite of the wide variation in feed ash contents, the ash content of the froth product is quite constant.

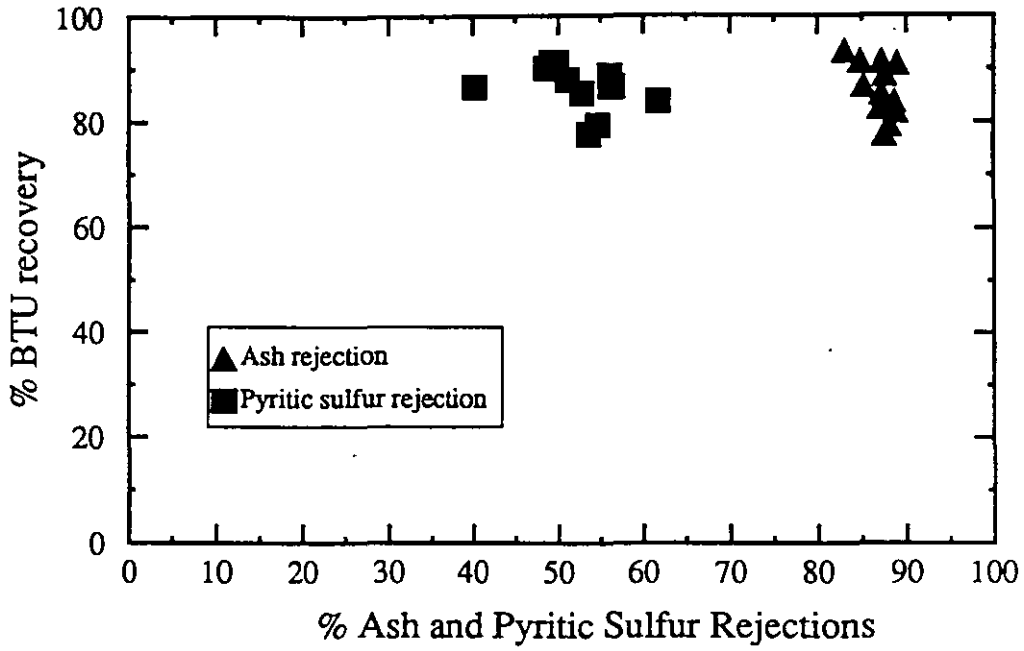

Figure 5. Pyritic sulfur and ash rejections as a function of BTU recovery in the on-line continuous tests with all baffles installed. This shows that between 40 and 65% of the pyritic sulfur being rejected by the column, even at high BTU recoveries, and that over 80% of the ash is consistently being rejected.

Slurry was pumped directly from the dewatering screen underflow at 10% solids and 0.5-0.8 kg of solids per minute. Samples of the froth, tails, and feed were collected after allowing a full hour for the column to stabilize. The samples were taken by collecting the entire froth, tailings, and feed streams for a minimum of 45 seconds. A summary of the results is given in Table 2.

Figure 4 shows the grade/recovery performance of the column on-line for removing both ash and pyritic sulfur. The % ash of the feed for each test is also plotted. From this graph, it can be seen that in spite of large variations in the feed quality, the grade of the froth product was very uniform regardless of recovery variations. The BTU recovery was consistently greater than 75% and all but two tests were above 80% BTU recovery, with a high of 91.2%. The ability of the column to remove pyritic sulfur is clearly shown by Figure 5, which plots pyrite and ash rejections against BTU recovery. The rejection values are the percentages of the weights of pyrite and ash originally in the feed which is rejected to the tailings. This figure shows that the column is rejecting between 40% and 62% of the pyritic sulfur from the coal, while simultaneously rejecting from 80% to 93% of the ash.

CONCLUSIONS

From the work with the baffled column, the following conclusions were reached:

1. In conventional, open-pipe flotation columns, there is little to prevent initially small disturbances from growing into major disruptions of the column performance. As a result, even slight problems with the column operation can be rapidly amplified to the point where they degrade the column performance. Fully packed columns can prevent this from occurring, but these are prone to plugging and excessive wear. Horizontal baffling has been found to be sufficient to prevent excessive axial mixing and to prevent

the formation of unusually large bubbles, and such baffles are sufficiently open and durable that plugging and rapid wear are not problems.

2. The capacity of a coal flotation column is limited by the rate at which the clean coal can be withdrawn from the froth. The horizontal baffles increase the residence time of the tailings, but they do not directly affect the froth layer, and so their effect on the capacity of coal flotation columns is minimal.

2. The column equipped with horizontal baffles could operate stably and produce a consistently high-quality product while encountering normal variations in plant feed characteristics.

3. The horizontally-baffled column produced a high-quality product in a single stage from a high-clay feed coal, rejecting up to 87% of the ash and 50% of the pyrite while recovering 91% of the heating value.

4. The baffles were designed for use with particles as coarse as 2 millimeters. As a result, they never plugged in operation, and upon disassembly after several months of testwork, no evidence of plugging or rapid baffle wear was found.

ACKNOWLEDGMENTS

Support for this research was provided by the Empire Coal Co. and the Ohio Coal Development Office. The authors would also like to thank Ms. J. F. Bird and Dr. Howard Johnson of the Ohio Coal Development Office, and Dr. R. R. Klimpel of the Dow Chemical Co., for their useful suggestions and critical discussion of this project.

REFERENCES

Alford, R. A., 1992, "Modelling of Single Flotation Column Stages and Column Circuits," International Journal of Mineral Processing, 36 pp 155-174

Degner, V. R. and Sabey, J. B., 1988, "WEMCO/Leeds Flotation Column Development," Column Flotation '88 (K. V. S. Sastry, editor) Society of Mining Engineers, Littleton, CO, pp 267-280

Dell, C. C., 1976, Froth Flotation, British Patent No. 1,519,075

Eisele, T. C., and Kawatra, S. K., 1994a, "Laboratory Baffled-Column Flotation of Mixed Lower/ Middle Kittanning Seam Bituminous Coal," 1994 SME annual meeting, Albuquerque, NM, preprint no. 94-22

Eisele, T. C., and Kawatra, S. K., 1994b, "Baffled-Column Flotation of a Coal Plant Fine Waste Stream," 1994 SME annual meeting, Albuquerque, NM, preprint no. 94-21

Finch, J. A., and Dobby, G. S., 1990, Column Flotation, Pergamon Press, Oxford

Kawatra, S. K., and Eisele, T. C., 1993 "The Use of Horizontal Baffles to Improve the Effectiveness of Column Flotation of Coal," XVIII International Mineral Processing Congress, Sydney, 23-28 May, pp 771-778

Yang, D. C., 1988, "A New Packed Column Flotation System," Column Flotation '88 (K. V. S. Sastry, editor) Society of Mining Engineers, Littleton, CO, pp 257-266

FACULTAD DE INGENIERIA U.N.A.M.
DIVISION DE EDUCACION CONTINUA

CURSOS ABIERTOS

DESARROLLO Y OPERACIÓN DE SENSORES PARA CONTROL DIRECTO Y CONTINUO EN PLANTAS DE BENEFICIO DE MINERALES Y EN LA RESTAURACIÓN DEL MEDIO AMBIENTE

Del 18 al 23 de mayo de 1998

TEMA: THE INFLUENCE OF LENGTH OF FLOW CELL AND STRENGTH OF SOURCE ON THE PERFORMANCE OF A GAMMA DENSITY GAUGE

EXPOSITOR :DR. KOMAR KAWATRA

1998

International Journal of Mineral Processing, 3 (1976) 167—174

© Elsevier Scientific Publishing Company — Printed in The Netherlands

THE INFLUENCE OF LENGTH OF FLOW CELL AND STRENGTH OF SOURCE ON THE PERFORMANCE OF A GAMMA DENSITY GAUGE*

S.K. KAWATRA

Canada Centre for Mineral and Energy Technology, Mineral Sciences Laboratories, Ottawa, Ont. (Canada)

(Received May 21, 1975; revision accepted November 28, 1975)

ABSTRACT

Kawatra, S.K., 1976. The influence of length of flow cell and strength of source on the performance of a gamma density gauge. Int. J. Miner. Process., 3: 167—174.

A mathematical equation has been derived from which the optimum length of flow cell of a gamma density gauge can be calculated. The equation has been experimentally verified by conducting experiments on two flow cells of different lengths.

The effect of strength of the source on the performance of a gamma density gauge is also discussed.

INTRODUCTION

Recently, there has been an increasing interest in the development of instruments for on-line analysis of mineral slurries (Lynch and Stanley, 1971; Carr-Brion and Williams, 1972; Kawatra, 1974). These instruments incorporate a gamma density gauge for the correction of percent solids in slurry. The aim of the present work has been confined to the optimisation of the characteristics of a gamma density gauge.

When gamma rays pass through matter, they lose in intensity. In a density gauge, the loss in intensity is related to the density of the material. Mathematically:

$$N_l = N_0 \, e^{-\rho m l} \tag{1}$$

where N_l = count rate with flow cell full of slurry;
N_0 = count rate with empty flow cell;
m = mass absorption coefficient of the slurry;
l = length of flow cell;
ρ = slurry density.

* National Research Mineral Program, Mineral Science Laboratories, Report MRP/MSL 75—205(J) — Crown copyrights reserved.

From the above equation, it may be inferred that the important variables for the suitable design of a density gauge are:
(1) length of the flow cell, l, and (2) count rate, N_0, which is dependent upon the strength of the source.

Stacey and Bolt (1971) maintain that for optimum sensitivity, length of the flow cell should be 15 cm, Wilkinson (1969) has also observed that a 15-cm long flow cell gives better sensitivity than a 23-cm long flow cell.

Platzek and Meyer (1965) have developed an optimising procedure for obtaining maximum sensitivity. This follows from the assumption that the ratio of relative signal variation over the noise level $\Delta N_x/\sqrt{N_x}$ to the relative variation of surface density (product of density ρ and length l) $\Delta x/x$, should be a maximum.

That is:

$\frac{\Delta N_x}{\sqrt{N_x}} \Big| \frac{\Delta x}{x}$ should be maximised, where:

$$N_x = N_0 e^{-mx} \tag{2}$$

$$\Delta N_x = N_x - N_{x+\Delta x} \tag{3}$$

$$x = \rho l \tag{4}$$

Using the above expressions Platzek and Meyer (1965) have shown that:

$$m\, x_{\text{opt}} = 2 \tag{5}$$

Thus, for the ^{137}Cs source, if water is used as an absorber, $m = 0.086$ cm^2/g, hence $x_{\text{opt}} = 23.3$ g/cm^2. Since $\rho = 1$, $l_{\text{opt}} = 23.3$ cm
where x_{opt} and l_{opt} are the optimum values of x and l respectively.

Fig.1 illustrates the variation of maximum sensitivity function $\frac{\Delta N}{\sqrt{N_x}} \Big| \frac{\Delta x}{x}$ (in arbitrary units), versus surface density, x, in g/cm^2. From the figure it is apparent that a 23-cm-long flow cell would give better sensitivity than a 15-cm-long flow cell. The above statement contradicts Wilkinson's (1969) observation.

From the foregoing discussion, it may be commented that diverse opinions exist regarding the effect of length of flow cell on the performance characteristics of density gauges.

MATHEMATICAL DEVELOPMENT

The output of a source (that is the count rate) is, in general, a random variable and in practice can be approximated by a Poisson distribution. Thus it is characterised by a mean value N_0 and a standard deviation $\sigma = \sqrt{N_0}$

For a given dimension of the flow cell (equivalent to the thickness of the absorber or length of the flow cell), the count rate N can also be a random variable with the mean given by:

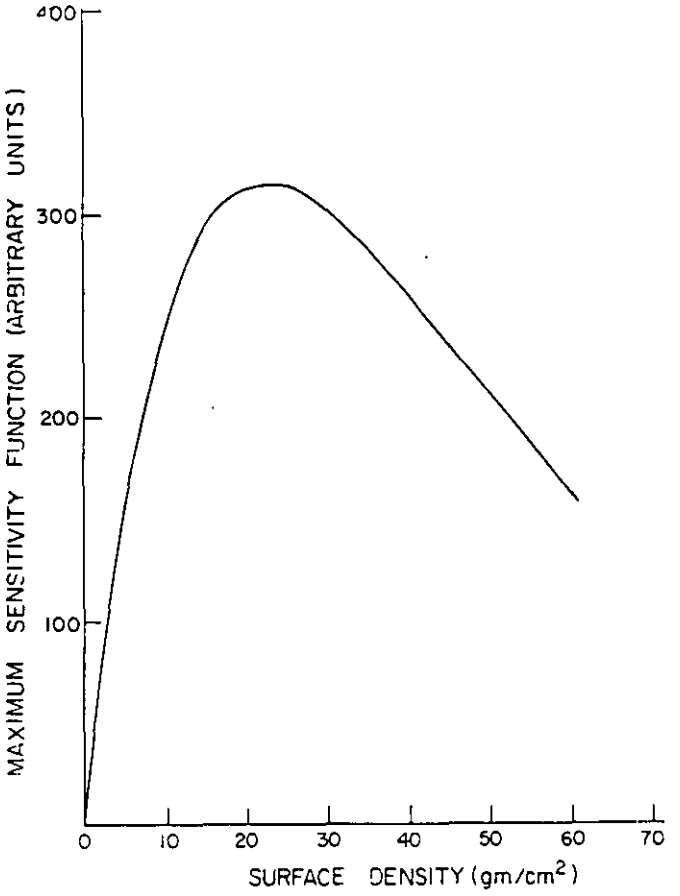

Fig.1. Relationship between maximum sensitivity function and surface density.

$N_l = N_0 e^{-\rho m l}$

where it is assumed that ρ, l and m are fixed. The observed count rate N can be assumed to lie between $N_l \pm \sqrt{N_l}$ with a probability of 68.3%. It may be noted that this involves a further approximation that N_l is approximately normal in distribution and the above statement corresponds to $1-\sigma$ confidence interval. The value of N can take the extremes $N_l + \sqrt{N_l}$ and $N_l - \sqrt{N_l}$. Thus the estimates of ρ obtained will have the following upper and lower bounds:

$$\rho_+ : N_l - \sqrt{N_l} = N_0 \, e^{-m\rho+l} \tag{6}$$

and:

$$\rho_- : N_l + \sqrt{N_l} = N_0 \, e^{-m\rho_- \, l} \tag{7}$$

(Note: m and l are fixed and ρ is estimated through observation of count rate.)

A good criteria to choose the length of the flow cell l is to minimise the difference between the upper and lower bound of ρ.

The necessary condition for this is given by:

$$\frac{d(\rho_+ - \rho_-)}{dl} = 0 \tag{8}$$

since:

$$\rho_+ - \rho_- = \frac{1}{ml} \ln\left(\frac{1+\alpha}{1-\alpha}\right) \tag{9}$$

where:

$$\alpha = 1/\sqrt{Nl} \tag{10}$$

It follows that:

$$\rho\, m\, l_{opt} = \alpha\, Nl\, (1-\alpha^2)\, \ln\left(\frac{1+\alpha}{1-\alpha}\right) \tag{11}$$

For large N, eq. 7 reduces to:

$$\rho\, m\, l_{opt} = 2 \tag{12}$$

This is Platzek and Meyer's (1965) equation which is a particular case of eq. 11.

A programme was written to calculate the errors for different lengths of the flow cell. The calculations were made using ^{137}Cs as a source of radiation and water flowing through the flow cell. The results are presented in Fig. 2. It may be noted that the nature of the curve is parabolic. An intuitive explanation of this is as follows:

When the length of the flow cell is small, the error is large because the change in count rate on introduction of the slurry in the flow cell is small.

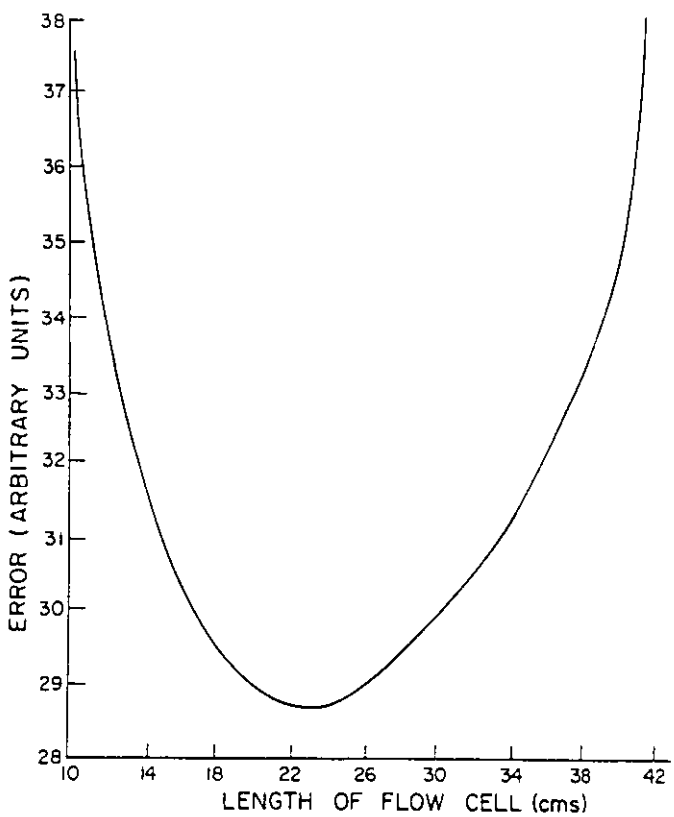

Fig. 2. Relationship between error and length of flow cell.

On the other hand, when the length of flow cell is large, the error is large because very few photons come out of the flow cell to be detected.

Variation of error with the strength of the source

Having chosen the optimum length of the flow cell, the next question arises as to what should be the strength of the source.

For a given slurry flowing through the flow cell:

$$N_l \propto N_O \tag{13}$$

$$\propto S \tag{14}$$

where S is the source strength.

Hence eq. 9 can be modified to:

$$\rho_+ - \rho_- = \frac{1}{ml_{\text{opt}}} \ln\left(\frac{1 + 1/K\sqrt{S}}{1 - 1/K\sqrt{S}}\right) \tag{15}$$

From eq. 15, it may be concluded that, as the strength of the source increases, the error in the measurement of slurry density reduces. The relationship between the error and strength of the source is shown in Fig.3.

However, in practice, error cannot be indefinitely reduced. The lower limit of the error will be determined by the drift errors in the counting equipment.

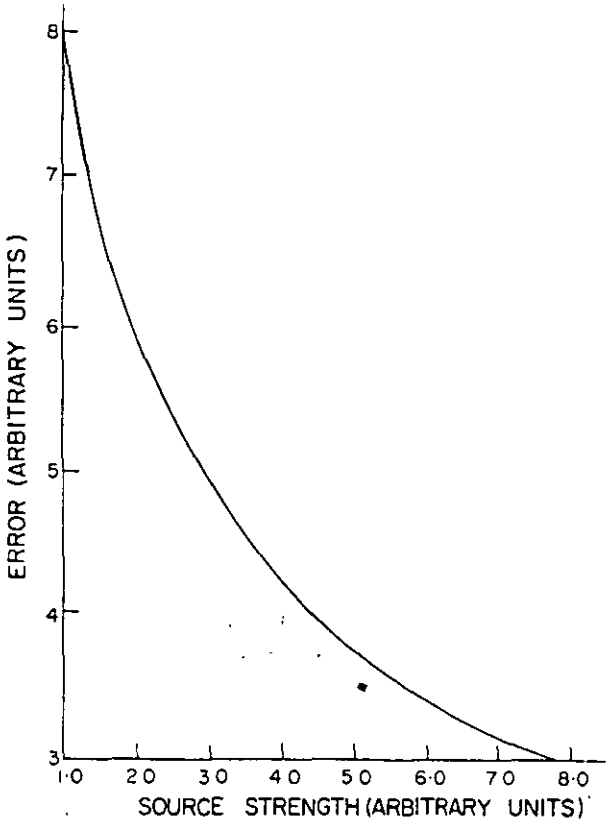

Fig.3. Relationship between error and source strength.

EXPERIMENTAL

Selection of the length of the flow cell

It was decided to verify the mathematical model on zinc sulphate slurries ($ZnSo_4.7H_2O$). For lead and zinc slurries, ^{60}Co has been recommended as a suitable source (Churchill et al., 1975). For the determination of the optimum length of flow cell, knowledge of the mass absorption coefficient of slurry and its specific gravity is required.

The mass absorption coefficient of the slurry was calculated, using the relationship:

$$m_{sl} = w_s m_s + w_w m_w \qquad (16)$$

where: m_{sl} = mass absorption coefficient of slurry;
m_w = mass absorption coefficient of water;
m_s = mass absorption coefficient of solids.

The value of the mass absorption coefficient of slurry with 15% solids was calculated to be 0.0595 cm^2/g and its specific gravity to be 1.079 g/cm^3. From equation 12, the optimum length of flow cell was calculated to be 29.2 cm. Two values of length of flow cell, 20 cm and 11 cm, both being less than the optimum length, were selected.

Test circuit

A schematic diagram of the test circuit is shown in Fig.4. It consisted essentially of a variable speed peristaltic pump, head and receiving tanks and a flow cell for the density gauge. A 2" × 2" NaI (T) detector was used as a detector of the radiation.

Experimental procedure

The experimental procedure was to add 3 l of water to the receiving tank, start the peristaltic pump, and then add known quantities of $ZnSO_4.7H_2O$ in the receiving tank. For each increment, five 100-sec counts were taken on the Baird-Atomic Spectrometer.

RESULTS AND DISCUSSION

The relationship between slurry counts to the water counts and percent solids in the slurry is shown in Fig. 5. A regression analysis, carried out on the data, gave the following results:

For 20-cm-long flow cell;

$$\% \text{ solids} = -164.41 \text{ (slurry counts/water counts)} + 163.87 \qquad (17)$$

with a standard error of 0.416 and a correlation coefficient of −0.999.

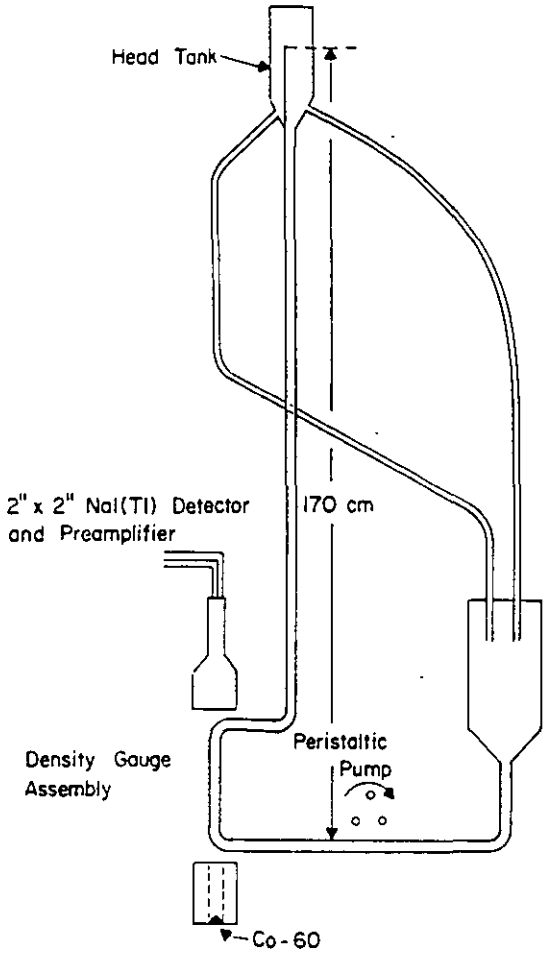

Fig.4. Schematic diagram of the test slurry circuit.

For 11-cm-long flow cell:

$$\% \text{ solids} = -255.08 \text{ (slurry counts/water counts)} + 255.18 \qquad (18)$$

with a standard error of 1.14 and a correlation coefficient of −0.992.

Thus the standard error for the percent solids determination with a flow cell 20 cm long is less than with a flow cell 11 cm long. Moreover, the slope of the curve, in Fig.5, is higher for a flow cell 20 cm long than for 11 cm long, giving higher sensitivity or higher resolution for percent solids determination.

CONCLUSIONS

It has been shown that there is an optimum length of flow cell at which the error in the determination of percent solids in slurry is a minimum. However this error can further be reduced by increasing the strength of the source. The lower limit of the error will be determined by the drift errors in the counting equipment.

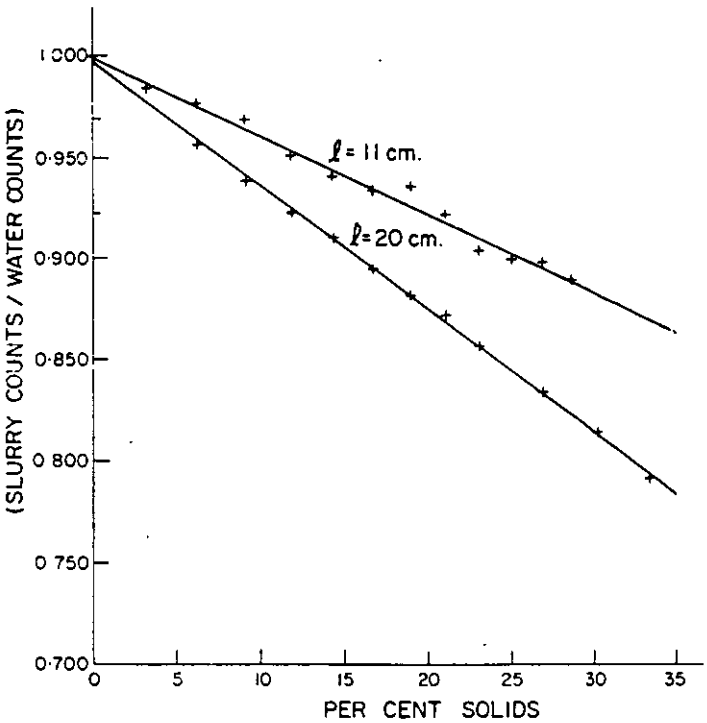

Fig. 5. Relationship between slurry counts/water counts and the percent solids.

ACKNOWLEDGEMENTS

The author would like to thank Mr. G.L. Mason, Head; Mr. J.L. Dalton, Chemist; Spectrochemistry Section, Canada Centre for Mineral and Energy Technology, Canada and Dr. A.J. Lynch, Director, Dr. W.J. Whiten, Research Fellow; Mr. C.W. Bailey, Research Officer; Julius Kruttschnitt Mineral Research Centre, Brisbane, Australia for useful discussions when the project was in progress.

REFERENCES

Carr-Brion, K.G. and Williams, A.W., 1972. On-stream determination of copper — a new concept in control analysis. Mining Mag., 127.

Churchill, T.R., Dalton, J.L. and Dibbs, H.P., 1975. The determination of lead in ore slurries by gamma-ray attenuation. Canada Centre for Mineral and Energy Technol., Sci. Bull., CM 75-3.

Kawatra, S.K., 1974. On-Line Determination of Copper and Lead in Mineral Slurries. Thesis, Univ. of Queensland, Brisbane, Qld.

Lynch, A.J. and Stanley, G.G., 1971. Automatic control in Australian mineral processing plants. World Mining, 24.

Platzek, P. and Meyer, A.C., 1965. Choice of most suitable radiation characteristics for any given gauging problem. Int. Conf. on Peaceful Uses of Atomic Energy, EUR 2221. e (U.N., Geneva).

Stacey, G.S. and Bolt, W.A., 1973. Multi-stream X-ray fluorescence analysis of mineral slurries in No.1 copper concentrator at Mount Isa. Proc. of the Review of on-stream analysis practice, (Publ. by AMIRA Ltd., Australia).

Wilkinson, L.R., 1969. Application of radioisotope X-ray sources to on-stream process control and analysis. Aust. Mineral Industries Res. Assoc. Ltd., Rep. 651.

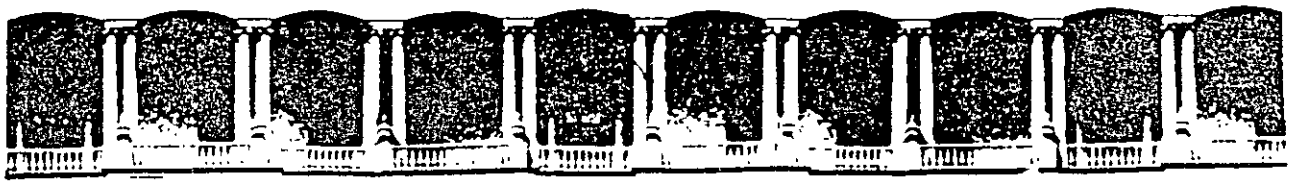

FACULTAD DE INGENIERIA U.N.A.M.
DIVISION DE EDUCACION CONTINUA

CURSOS ABIERTOS

DESARROLLO Y OPERACIÓN DE SENSORES PARA CONTROL DIRECTO Y CONTINUO EN PLANTAS DE BENEFICIO DE MINERALES Y EN LA RESTAURACIÓN DEL MEDIO AMBIENTE

Del 18 al 23 de mayo de 1998

TEMA: ON - LINE SENSORS AND PROCESS CONTROL FOR COAL PREPARATION PLANTS

EXPOSITOR :DR. KOMAR KAWATRA

1998

Chapter 25

On-Line Sensors and Process Control for Coal Preparation Plants

S. K. Kawatra and K. A. DeLa'O

Department of Metallurgical Engineering
Michigan Technological University
Houghton, MI 49931

ABSTRACT

On-line sensors and process controls are important for efficient operation of coal preparation plants. The objective of this paper is to describe the current practice in on-line measurement of composition, density, moisture, level, flow and weight. This paper also discusses how on-line sensors can be implemented in process control, and how sensors which are currently being developed can be utilized.

INTRODUCTION

Careful process control is becoming increasingly necessary for the efficient operation of a coal preparation plant. The conventional analysis practice of collecting a sample in a preparation plant and analyzing it in a laboratory is expensive and does not provide information fast enough for quality control purposes. To implement an effective process control loop, it is necessary to use on-line sensors which can measure products accurately and rapidly. With the advent of accurate and rugged on-line instrumentation, it has become economically advantageous to install control systems to optimize performance. The following sections describe various on-line instruments which are being used or are currently being developed. Their use in process control loops is also discussed.

ON-LINE ELEMENTAL COMPOSITION SENSORS

Neutron Activation Analysis

On-line analysis of sulphur and other elements found in coal can be carried out by prompt-gamma-neutron activation analysis (PGNAA). This technique was developed by Stewart et al (1974), at the Morgantown Energy Technology Center, WV. PGNAA is based on the capture of fast neutrons by the nuclei of the various elements comprising a coal sample. A source of fast neutrons is placed on one side of a gravity chute or beneath a conveyor belt, with a detector on the other. As the coal sample is bombarded with fast neutrons, elastic and inelastic collisions occur between the neutrons and the medium nuclei. These collisions cause the neutrons to lose much of their kinetic energy. Ultimately, their average kinetic energy will equal that of the atoms and molecules comprising the coal sample. As this equilibrium kinetic energy is temperature dependent, the slowed neutrons are called "thermal" neutrons. Thermal neutrons have a vastly greater probability of being captured by a nucleus than do fast neutrons. The probability of neutron capture by a specific nucleus depends on its capture cross-section and weight percent. The majority of the captures (85 to 95%) occur by the hydrogen nuclei, with only 0.1 to 3% of the captures by the sulphur nuclei.

Once a capture has occurred, the next higher isotope (atomic weight + 1) of the target nucleus is formed. Relaxation from this excited state causes the target nucleus to emit gamma rays whose energy and intensities are unique to the element. The gamma ray spectrum is then measured by a gamma ray detector (usually NaI(Tl)) to provide an elemental analysis of the coal sample. Analysis of the resulting spectrum is extremely complicated due mainly to some elements, such as chlorine, which is capable of capturing large quantities of neutrons in relation to its relative wt.%, and calcium, which produces gamma radiation with several different energies. Analysis is further complicated by the fact that the radioactive source (Cf 252 is the standard choice) emits gamma radiation as well as neutrons. Figure 1 shows how MDH-Motherwell, Inc. (Zumberge, 1987) alleviated this problem. The Cf 252 source is encased in a Pb-Bi alloy, which effectively attentuates the emitted gamma rays while remaining virtually transparent to emitted fast neutrons. The other source of "noise" is the Na and I nuclei contained in the scintillation crystal of the detector, which may capture neutrons and emit characteristic gamma radiation. To prevent this from occurring, a patented LiH window is placed in front of the detector. Li is very effective for capturing neutrons, while it lets gamma rays pass unattenuated, thus cutting down on excess detector "noise".

The complicated spectrum data is interpreted by one of two methods in commercially available

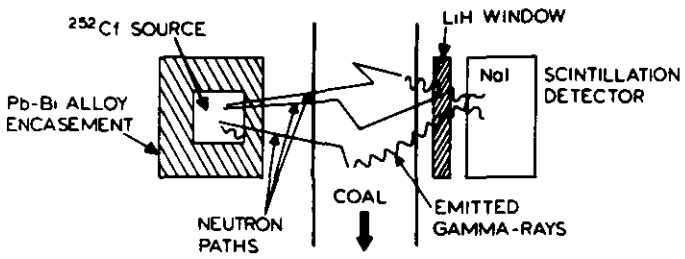

Figure 1. Principle of elemental analyzer (Zumberge, 1987).

analyzers. The first method involves empirical correlation of ASTM standard chemical analyses and PGNAA measurements of a large number of actual field samples to calculate the composition which produces the measured spectrum. This method is time consuming and extremely sensitive to variations in coal composition, due to the small sample size required for the ASTM analyses. The other method, utilized in the Elemental Analyzer (ELAN), manufactured by MDH-Motherwell, Inc. (Marshall and Zumberge, 1987), uses the measured spectrum areas of artificially produced coal samples of known composition being stored in the instruments memory. The unknown amount of a given element is determined by comparing the shapes and spectrums stored in memory with the spectrum measured.

All of the commercially available instruments which utilize the PGNAA method have a common problem. None of these instruments are capable of distinguishing chemical forms from one another. They are also incapable of determining quantities of oxygen or magnesium because these elements have a low cross sectional area available for neutron capture. This lack of discrimination results in the hydrogen content of the dry coal being overestimated when water is present. This problem can be alleviated for coal analysis by incorporating a moisture meter with the PGNAA instrument.

Moisture measurements are utilized in three ways in coal elemental analyzer measurements. The first, and most obvious, is the actual moisture measurement itself, which is necessary for sales and water balances. Secondly, the measurement can determine the water component of oxygen. This value and the amounts of other elements present can be used to infer the quantity of oxygen in the dry coal. Lastly, the hydrogen in water is accounted for, thus allowing organic hydrogen to be determined. This value is necessary for calculation of the estimated calorific value of the coal sample.

MEASUREMENT OF ASH CONTENT OF SLURRIES

Coal ash is the oxidized residue remaining after coal has been burnt and consists primarily of alumina, silica, iron compounds, and small quantities of the oxides of potassium, calcium, titanium, and so on. Typically, coal has an effective atomic number of approximately 6, while that of the various ash-forming minerals is approximately 10. The effective atomic number is therefore a good indicator of the ash content. Several methods which utilize the differences in these effective atomic numbers have been proposed. These methods are based on the interaction of x-rays and low energy γ-rays with coal (Watt and Sowerby, 1983; Kawatra, 1976b, 1980; Clayton and Wormald, 1983; Fauth, 1980, 1984; Cutmore et al 1986). Also, gauges based on pair production γ-ray interactions have been developed (Cutmore et al 1986; Millen et al, 1984).

Ash Analyzers Based Upon the Backscattering of X-rays and γ-rays

Two measurements are necessary for the determination of ash content in coal slurries, one to obtain the ash content of the slurry and the other to obtain the solids content of the slurry. The solids content can be obtained by the use of a gamma density gauge (Kawatra, 1976a,b), to be discussed later, while the determination of coal ash content is based on the scattering of radiation energy that is less than 100 KeV. The intensity of this scattered radiation is proportional to the ratio of probability of a scattering incident occurring to the probability of an absorption interaction. Two types of radiation scattering may occur: Compton (incoherent) scattering and Rayleigh (coherent) scattering. Compton scattering involves an x-ray photon colliding with a loosely bound electron. During this elastic collision, the photon loses some of its energy to the electron and is deflected from its original path of travel. The energy loss suffered increases as the angle of scatter increases. In Rayleigh scattering, the photon collides with a tightly bound electron, which is neither excited nor ionized. Thus, the scattered photon has the same energy as the primary photon.

Compton scattering relationships are given by the Klein-Nishina formula (Hubbel, 1977; Hubbel and Overbo, 1979),

$$\sigma_c = 3.92 \times 10^{-26} (E'/E)^2 (E/E' + E'/E - \sin^2\theta)$$

where σ_c is the Compton differential cross section per sq. cm. per electron per steradian, E is the energy of the primary photons, E' is the energy of the scattered photons and θ is the scattering angle. The relationship between E' and E is given by (Evans, 1955, 1958)

$$E' = E/(1 + (E/mc^2)(1-\cos\theta))$$

where m is the electron rest mass, and c is the speed of light. For a mixture of elements, the

probability of Compton scattering per unit path length traversed in the medium into the elemental solid angle $d\Omega$ in the direction θ is given by (Evans, 1955, 1958)

$$P(\theta,E)_c = N\rho\sigma_c(\theta,E)d\Omega\Sigma_i\alpha_i(Z/A)_i$$

where N is Avogadro's number, ρ is the density of the material, α_i is the fraction of the total weight comprised by the ith type atoms, and Z and A are respectively the atomic number and atomic weight of the ith type atoms.

The Rayleigh scattering can be approximated by the relationship (Evans, 1955, 1958)

$$\sigma_R = K\pi/4(e/mc^2)^2\ f(\theta)\ Z^3/E^3$$

where σ_R is the Rayleigh cross section per sq. cm. per electron per steradian, e is the electronic charge, K a constant and $f(\theta)$ is a function of scattering angle. For a mixture, the probability of Rayleigh scattering per unit path length traversed in the medium into the elemental solid angle $d\Omega$ in the direction θ is given by (Evans, 1958)

$$P(\theta,E)_R = KN\rho d\Omega\Sigma_i((\alpha_i Z_i^3)/(A_i))$$

where ρ is the density, N is Avogadro's number and α_i is the fraction of the total weight comprised by the ith type atoms.

The above theory states that the cross section of Compton scattering is proportional to the atomic number (Z) of the scattering atoms, while Rayleigh scattering cross section is closely proportional to Z^3. Therefore, as the higher atomic number material varies within a lower atomic number matrix, the Compton and Rayleigh scattering will vary accordingly. Since the effective atomic number of coal increases with ash content, the ash content can theoretically be determined by measuring the intensity of the scattered low energy photons.

Large changes in scattered intensity are produced by relatively small variations in the amount of iron-sulphur minerals, such as pyrite and pyrrhotite, in the coal. This is due to the fact that iron sulphur minerals, which may account for as much as 5-10 wt.% of the material, have an effective atomic number of about 20, while alumina and silica minerals have an effective atomic number of about 10. Therefore, iron content must be compensated for if accurate ash measurements are to be made when iron minerals are present. If a radioisotope is selected so that FeKα x-rays (6.4 KeV) are excited and measured, a quantitative measurement of the iron-sulphur mineral content in the slurry can be made. This measurement provides a correction for the additional scattering due to the iron-sulphur minerals. Use of this procedure allows an accurate determination of ash content to be made.

A schematic of a test rig developed at Michigan Technological University is shown in Figure 2. It consisted of a variable speed centrifugal pump, head and collecting tanks, a flow cell for the x-ray fluorescence and backscatter measurements and a lucite assembly with a 20 cm. radiation path for a density gauge. A gamma density gauge employing a Gd-153 source was used. This isotope was selected over Co-57 because of its sensitivity, and over Ir-192 and Ce-139 because of sensitivity and half-life considerations. Commercially available gauges generally use a Cs-137 or a Co-60 source. The characteristics of common sources for the measurement of percent solids of coal slurries are discussed in the literature (Kawatra, 1980).

A Cd-109 source was selected for the determination of ash content in coal slurries. This source decays by emitting AgK x-rays with energies of 24.9 and 22.1 KeV. A correction for pyrite was provided by measuring the FeK x-rays with a gas filled proportional counter. Plant results for the ash analyzer can be found in Figure 3, an extensive discussion of these results are available in the literature (Laurila and Kawatra, 1984). In the plant, it was necessary for a deaerating device, manufactured by Armco Autometrics, to be used in conjunction with the ash analyzer to remove air bubbles from concentrate slurries. Vibrational problems encountered were solved by using flexible connections between the pump and the sensor, and by mounting the sensor separate from the pump support frame.

The on-line measurement of ash by scattered radiation has many advantages; the method is simple, the sensor is rugged and the system provides corrections for the varying quantities of iron-sulphur minerals. Similar systems have been designed by others, for example, the OSCAA system by Flintoff et al (1984), and the MRDE by Boyce (1983). The results from these instruments and others are found in Table I from the work of Cooper (1984).

Watt (1983) has used the same backscattering technique for measuring coal ash. However, in place of a mechanical deaerating device, he proposed a method which depends on the measurement of neutron moderation and gamma-ray transmission to determine the hydrogen (wt/wt) in the slurry, and combines these with ash sensitive measurements. As neutron sources are a much greater radiation hazard than x or gamma-ray sources, it is safer and less expensive to employ mechanical deaerating devices. Mechanical deaerating devices have been used all around the world and have proven to be successful. The results of Watt's (1983) work at CSIRO is presented in Table I (Cooper, 1984).

Ash Analyzers Based Upon the Absorption of Gamma Rays

The basis of the measurement is similar to that of the backscattering method except that the effective atomic number of coal is determined by the absorption of gamma rays rather than a ratio of absorption to scattering (Kawatra, 1976b). Ash

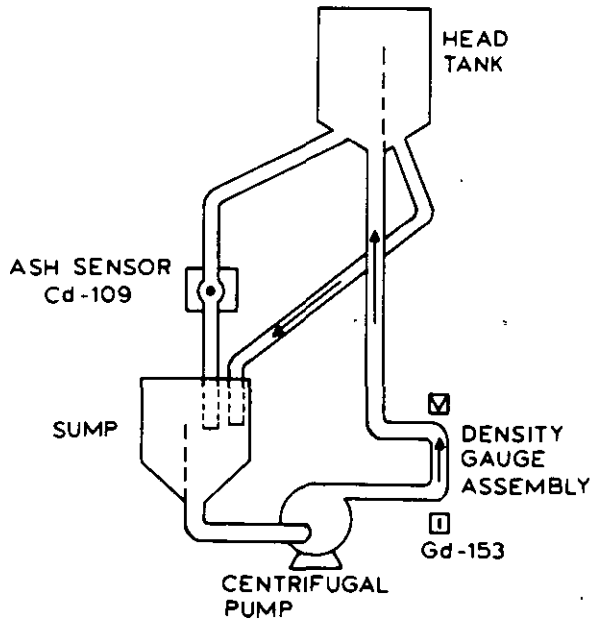

Figure 2. Ash analyzer test rig.

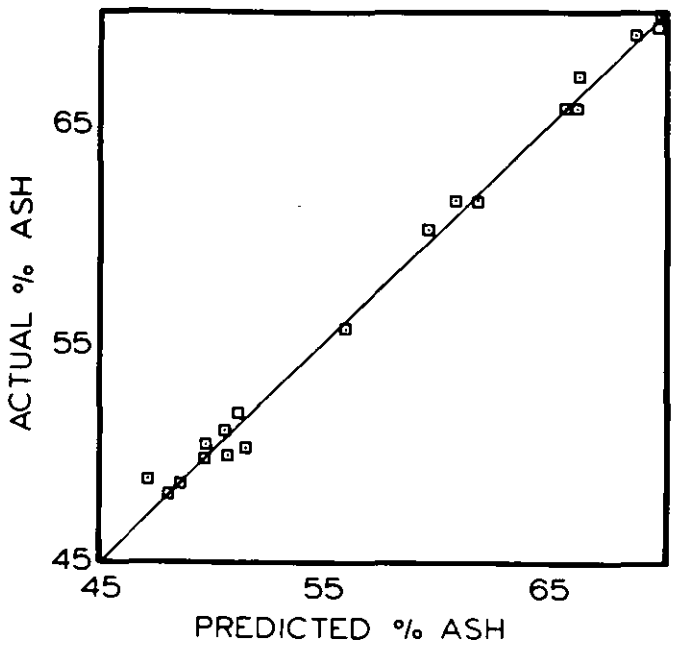

Figure 3. Relationship between ash observed and calculated ash.

Table I. Accuracy of Coal-Slurry Measurements

Name and Type		% Ash			% Solids		
		Standard Error	Range/ Average	Rel. Error	Standard Error	Range/ Average	Rel. Error
ASHSCAN	Feed	2.5	12-30/21	11.9	0.6	5-20/12.5	4.8
Absorption	Conc	0.3	5-11/8	3.8	0.7	15-35/25	2.8
	Tails	4.4	40-80/60	7.3	0.6	3-10/6.5	9.2
Bergbau Absorption	Tails	1.6	5-65/35	4.6	0.4	5-18/11.5	3.5
CSIRO	Tails	0.8	20-30/25	3.2	0.5	5-22/13.5	3.7
Backscattered	Feed	0.9	10-24/17	5.3	1.0	5-19/12	8.3
MTU	Tails	0.7	56-78/67	1.1	-	15-40/27.5	2.7
Backscattered	Feed	0.32	12-26/19	1.7	-	13-17/15	-
MRDE Backscattered	Tails	2.0	50-80/65	3.1	0.3	2-17/9.5	3.1
OSCAA	Conc.	0.4	6-13/10	4.0	0.7	15-35/25	2.8
Backscattered	Tails	4.4	40-80/60	40.5	0.6	3-10/6.5	9.2

content is determined by absorption of low energy gamma rays, which are sensitive to the elemental composition and, therefore, ash content as well as to the density of the slurry. This method was developed by Fauth et al (1984) at Bergbau-Forschung, Germany. Variation of percent solids is corrected with a gamma density gauge. Fauth et al (1984) used a Am-241 source for the Bergbau gauge and a Cs-137 source for the gamma density gauge. Results for this ash analyzer and similar types (ASHSCAN developed by Lyman et al (1980)) are summarized in Table I by Cooper (1984). For slurries containing entrained air, this type of sensor requires deaeration. Fauth (1984) achieved this by subjecting the slurry to high pressures before presentation to the sensor. Clarkson et al (1983) have described a similar arrangement. All of the above methods require correction for slurry pyrite content. If pyrite content does not vary considerably, these methods will provide excellent results, but errors will be introduced if the pyrite content varies.

MEASUREMENT OF ASH CONTENT OF BULK SOLIDS

Backscattered low energy photons or gamma ray intensities can also be utilized to measure the ash content of bulk solids, as it overcomes the need to measure the thickness and density of the material. Figure 4 shows a typical system manufactured by Tema Systems Inc., a Siebtechnik Co. (Berthold, 1987). In this system the radiation source (Am-241) is mounted a fixed distance from the detector and the leveled material surface. The detector, a NaI(Tl) crystal, is protected against direct radiation and only measures backscattered intensity. The scattering factor is essentially independent of atomic number, though an increase in ash will increase the radiation absorption as it traverses the stream (Berthold, 1987).

This ash monitor requires an elaborate sample preparation scheme to ensure a uniform material size and packing (shown in Figure 4). A correction for pyrite is not provided for, rendering this gauge unsuitable for coals with widely varying amounts of pyrite.

A gauge manufactured by Gunson's Sortex Ltd. (Cammack, 1973; Cammack and Balint, 1976) is capable of measuring and compensating for the amount of pyrite present in the coal. This gauge consists of a low energy source (Pu-238) and a gas filled proportional counter equipped with an aluminum filter (Figure 5). The low energy photons (15 to 17 KeV) emitted from the source cause the iron in the sample to become excited and produce fluorescent x-rays which can be filtered and measured. The proportional detector simultaneously detects the backscattered and fluorescent x-rays, after they have passed through an aluminum filter. This filter absorbs the fluorescent x-rays preferentially, its thickness being preselected to suit the iron content and its variations. These two detected quantities are then used to determine the ash content, with the iron content being compensated for by the amount of x-ray fluorescence measured.

The accuracy of ash measurement at the 95% confidence level was in the range of 0.3 to 2.2%.

Determination of Ash Content of Coal on Conveyor Belts

Two types of gauges for on-line determination of ash content of coal on conveyor belts are available. The first are gauges based on the absorption of gamma rays, the second type are gauges based on pair production gamma ray interactions.

Gamma Ray Absorption. Watt and Sowerby (1983) have developed a gauge which measures ash on conveyor belts. It is called a Low Energy Transmission (LET) gauge. It operates by measuring the intensities of a narrow beam transmission of low and high energy gamma rays through coal on a conveyor (Figure 6). Both intensities depend on the weight/unit area of coal in the gamma ray beam. The low energy beam also depends on the effective atomic number of coal. As this gauge does not provide a correction for the variation of iron sulphur minerals, its accuracy is dependent on the type of coal.

Pair Production. This method measures the intensities of backscattered gamma rays, due to pair production and Compton interactions (Watt and Sowerby, 1983). Both interactions depend on the bulk density of coal, although pair production alone depends on the effective atomic number of coal. This gauge is suitable for low ash and high ash coals, but is nearly twice as expensive as the Low Energy Transmission gauge.

SLURRY DENSITY MEASUREMENT

On-line slurry density measurements can be carried out by differential pressure (DP) cells or by nuclear density gauges. With the advent of nuclear density gauges, DP cells have lost their exclusive status, as the nuclear gauges are external to the process stream, produce an electronic signal that is more useful for computerized controllers, and are generally more accurate than DP cells.

Nuclear density gauges are based on the principle of radiation absorption. As radiation is passed through a slurry, the loss of radiation intensity can be related to the density or percent solids of that slurry. Gamma ray attenuation is dependent on both atomic number and photon energy, care must be taken to match the source to the application. Customarily, gamma ray energies of 0.7 MeV are used for material free of high atomic number elements, such as lead, while energies of 1.2 MeV are used if high atomic number elements are present (Kawatra, 1976c; Evans, 1955, 1958). For solids content measurements of low atomic number aqueous slurries of coal, energies of 0.6 - 1.2 MeV are not sufficiently sensitive over the radiation path lengths typically encountered ($\sim$25 cm). Larger path lengths or lower energy isotopes are required for a measurable amount of attenuation to be detected.

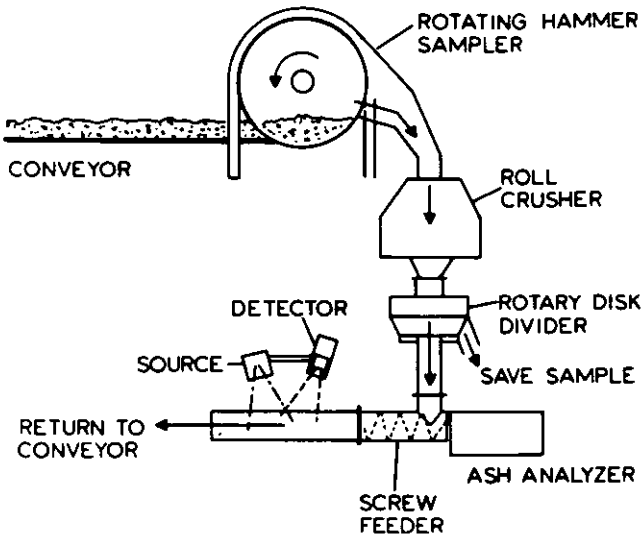

Figure 4. Ash analyzer and sample preparation for bulk solids (Berthold, 1987).

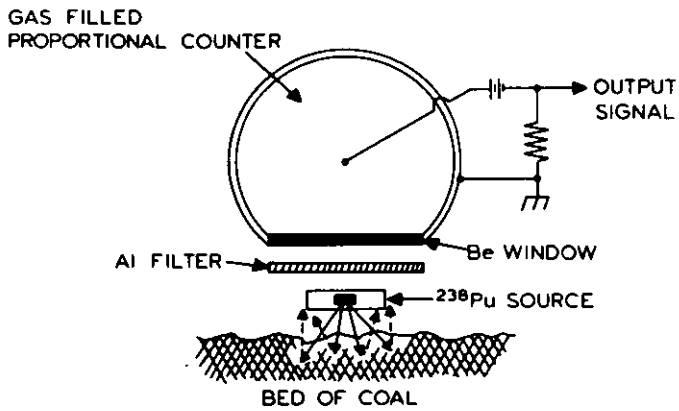

Figure 5. Principle of ash monitor for bulk solids (Cammack and Balint, 1976).

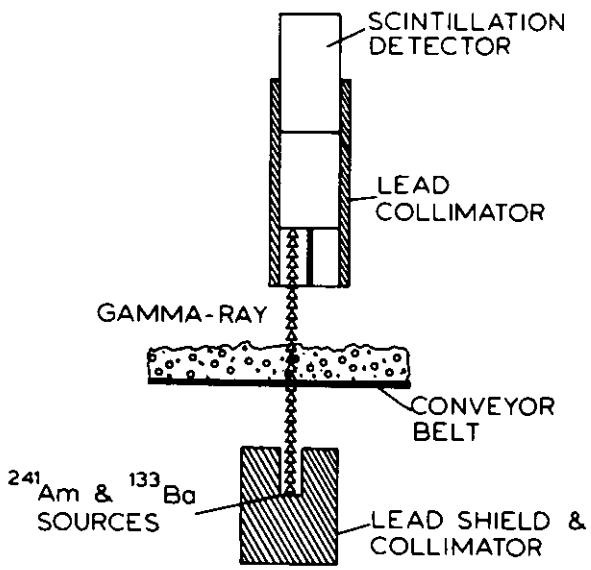

Figure 6. Low energy transmission gauge.

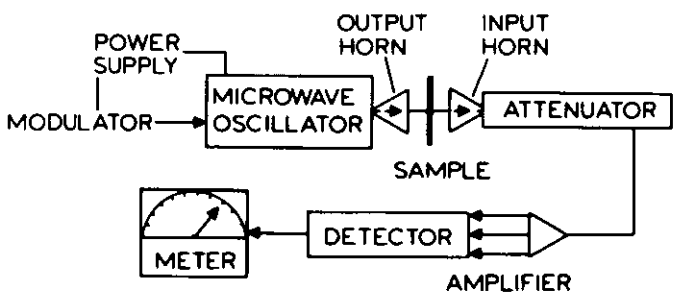

Figure 7. Microwave attenuation type moisture gauge.

Characteristics of some useful low energy isotopes are found in Table II. The use of nuclear density gauges in the coal industry is extensively discussed by Sigal (1981).

MOISTURE CONTENT

In the combustion of fine coal, a high coal moisture content has the effect of reducing the calorific value of the coal. This is due to the substantial quantity of heat required to vaporize water. Also, moisture increases the weight of the coal, which increases transport costs and causes the fine coal to freeze in the winter. For these reasons, it is necessary to continuously monitor and control the moisture content of the final fine coal product.

A large number of commercially available moisture meters have been developed for the chemical industry (Liptak, 1969; Considine, 1974). Unfortunately, these instruments cannot readily be applied in the coal industry, as all applied measurements are affected by such variables as coal rank, particle size distribution, bulk density and chemical and petrographic composition. Accordingly, a moisture meter that can be used at every location in every coal plant does not exist. A moisture meter cannot be selected in isolation from its process, rather, each situation must be studied to determine the sensor that will meet the processes particular needs. A summary of some of the techniques used for on-line determination of moisture content are presented in Table III. As capacitance and microwave methods are the most widely used, they will be discussed in detail.

Capacitance Method

This method is based on the fact that the dielectric constant of water is much greater than that of coal and its constituents. For example, the dielectric constant of water is 80, while that of quartz is 4, and the average dielectric constant of coal ranges from 3 to 5. Therefore, there will be a noticeable rise in capacitance as the moisture of the coal between the plates of the capacitor increases.

Under laboratory conditions, this technique has worked well. At Ewald Mine, Germany, accuracies of ±0.8% with one standard deviation have been reported (Fauth, 1984). Relatively homogeneous metallurgical coal was being produced, an ideal condition for capacitance sensors. The sensors are prone to errors if dissolved salts are present, if the particle size varies greatly, if a nonuniform layer is presented to the meter and if the dielectric constant of the material varies.

Microwave Methods

When a coal sample is exposed to a microwave field, some of the microwave energy is transferred to the coal. If the sample is moist, water, which is a polar molecule, absorbs more energy from the microwaves than does the coal, due to dipole relaxation. In addition to the attenuation, microwaves undergo a phase shift when traveling through coal. Almost all commercially available transmission microwave moisture meters are based only on the measurement of attenuation of the microwaves (Fauth, 1984). A common microwave moisture meter assembly is shown in Figure 7. Currently, a moisture meter based on phase shift and attenuation is being put to plant trials (Klein, 1987).

Error Inducing Factors in Microwave Methods

Particle Size. Work by Hall (1970) at the National Coal Board has indicated that the changes in coal particle size influence the moisture measurements made by attenuation methods. Klein (1987) has also found particle size to be an influential factor in attenuation/phase shift methods.

Temperature and Bulk Density of Coal. The influence of these parameters were studied by Hall et al (1970, 1972). They observed that a 15°C change in temperature or a 12% change in mass/unit area on the belt caused moisture measurement error of 1%.

Coal Rank. There are conflicting opinions that are yet to be resolved concerning this factor. The work of Hall (1970) reported no effect of coal rank upon moisture measurements. Fauth (1980) contradicts this, he indicates that rank is influential in coal moisture measurements.

Microwave Frequency. Water is a more efficient absorber of high frequency microwaves than it is of low frequency microwaves. Therefore, it is common practice to use frequencies of 1 to 10 GHz. At 1 GHz the attenuation by 150 cm of coal is equivalent to the attenuation by 13 cm of coal at 10 GHz (Brown et al 1980).

The microwave system manufactured by Kay-Ray monitors the bulk density and temperature of the coal stream and continuously compensates for the variations encountered (Brown et al, 1980).

The method of utilizing the ratio of microwave attenuation to phase shift was suggested by Klein (1987) as a better method of measuring coal moisture then attenuation of microwave energy alone. At Ewald Mine, W. Germany, moisture measurements by use of attenuation/phase shift demonstrated a standard deviation of 0.27 wt.%. By attenuation alone, the standard deviation was 0.44 wt.%, and phase shift alone had a standard deviation of 0.30 wt.% (Klein, 1987). These results were obtained on metallurgical coal.

LEVEL MEASUREMENT

Instrumentation for on-line measurement of level is well developed and readily implemented into a coal processing plant. Typical applications would include; solids level in surge bins, slurry level in sumps and flotation cells, and froth depth measurement in flotation cells.

Table II. Isotopes Commonly Used in Density Gauges

Isotope	Half-Life	Radiation Used for Gauging (MeV)
Cs 137	30 years	0.662
Co 60	5.2 years	1.173
		1.332
Isotopes suited for coal slurries:		
Gd 153	239 days	0.099
Co 57	270 days	0.122
		0.136
Ce 139	140 days	0.165
Ir 192	74 days	0.062
		0.066
		0.296
		0.308
		0.317

Table III. Moisture Measurement-Techniques Applied to Coal

Type	Principle	Source of Error
Neutron Thermalization	Moderation of fast neutrons by hydrogen atoms	Coal contains organic hydrogen in varying amounts
Capacitance	Dielectric measurement	Salt content, particle size distribution, changes in electrolytic constant and layer thickness
Electrical	Measures DC resistance and correlates to moisture content	Dissolved salts, packing density, variations in electrolytic constant, layer thickness variations and particle size changes
Nuclear Magnetic Resonance	Measures nuclear magnetic resonance of the hydrogen nuclei in water	Small sample size, ferromagnetic impurities in the coal
Microwave	Power loss and phase shift due to moisture in coal	Particle size distribution, change in bulk density and temperature; methods are available to diminish these effects
Infrared	Absorption of infrared by water	Small sample size, very susceptible to changes in particle size, layer thickness sensitive

Slurry Level Measurement

Three types of slurry level gauges are commonly used; capacitance gauges, differential pressure (DP) gauges and ultrasonic gauges. All three are robust and fairly accurate. Their selection depends more on the application at hand than the accuracies they can attain.

Capacitance Level Gauges. These gauges generally consist of two vertical, insulated electrodes inserted within a tank. If the tank wall is conductive, the second electrode can be dispensed with, as the tank wall will serve in its place. The capacitance is continually measured with an A.C. bridge circuit.

When the tank is empty, the electrodes are separated by air, which has a dielectric constant nearly equal to unity. As the tank fills with slurry, which typically has a dielectric constant greater than 80, the electrodes are exposed to a higher dielectric constant. This increase in dielectric constant with level of slurry will cause a corresponding increase in capacitance. Provided that the distance between the electrodes is a constant, the capacitance will increase essentially linearly with increasing slurry level.

The major error in this assembly arises from the assumption that the dielectric constant of a slurry is a constant value. While this assumption is generally true, drastic changes in solids content, solids particle size, solids electrical characteristics or the amount of entrained air in the slurry will cause substantial changes in the dielectric constant. If the slurry characteristics are known to fluctuate wildly, capacitance level gauges should not be used.

Differential Pressure Gauges. These gauges monitor the slurry level simply by measuring the pressure at two different depths. The type of DP gauge most widely used in coal preparation plants is the bubble tube, although other types are extensively discussed in textbooks (Liptak, 1969).

Bubble tubes consist of a vertically submerged tube connected to a source of pressurized air and a flow meter. The air pressure is adjusted until the flowmeter indicates that air is just bubbling from the bottom of the tube. At this point, the pressure in the tube is equal to the hydrostatic head of the slurry. To convert hydrostatic head to depth, the slurry density must be known. This can be determined after measuring the difference in pressure between two points at different depths in a tank. Such an arrangement allows for the determination of both slurry level and density.

Several drawbacks are encountered with bubble tubes, the first being that their pneumatic signal must be converted before it can be implemented into an electronic control scheme. Another is that it is more suited for manual operation than for automated control. Third, it is subject to errors if the slurry is overly turbulent or if its density varies with depth. Since the advent of capacitance and ultrasonic gauges, the bubble gauge is not as applicable as it once was.

Ultrasonic Level Gauges. These gauges function by producing ultrasonic pulses, which are reflected from the material surface. The echoes are detected by the instrument, and the distance from the transducer to the surface is calculated from the pulse travel time. This allows a level measurement to be made without contacting the slurry, which prevents wear and corrosion of the instrument. The ultrasound frequency used varies depending on the distance from the transducer to the slurry surface. Frequencies of about 20 kilohertz can be used at distances of up to 30 meters without difficulty. However, for a distance of a few meters, higher frequencies produce more accurate results due to the faster transducer response times and shorter pulse durations possible.

Froth Level Measurement

Measurement of froth level is always a difficult problem due to the high variability of the froth level and physical characteristics. Currently, there are only two types of gauges which will perform adequately, a series of conductivity probes and a neutron level system.

The series of conductivity probes (Figure 8) monitors the resistance of each probe, with the lower resistance probes being considered submerged in the froth. As the froth layer coalesces and bursts, each probe spends a varying amount of time submerged. The resistances of the probes are constantly interfaced to a small computer which can calculate the average time each probe is submerged, and thus the mean froth level.

Neutron source systems are generally only used when all other methods have failed. This is not due to a lack of reliability, but rather to their high costs and the regulations and dangers involved with a neutron source.

Solids Level Measurement

Of the level gauges aforementioned, only the ultrasonic gauge will provide adequate measurement of bulk solids in bins or silos. For the best results from a fairly rough surface, low-frequency ultrasonic pulses would be used. If the surface is too rough and the container cannot be supported on load cells to determine the weight of the contained solids, a variety of on-off level switches are available for level measurement (Liptak, 1969).

FLOWMETERS

Many flowmeters which utilize flow restrictions for the flow measurement of clean liquids are available, and are extensively discussed in instrumentation handbooks. (Liptak, 1969). Unfortunately, fine coal processing plants are mainly concerned with monitoring coal slurries, which would rapidly plug or erode restricted flow flowmeters. More suited for such hostile

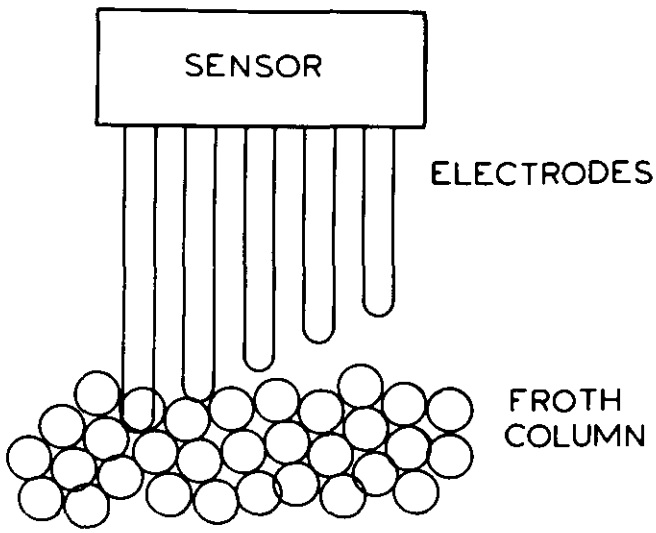

Figure 8. Conductivity Probe

environments are non-restricting volume flowmeters and non-restricting mass flowmeters.

Non-restricting Mass Flowmeters

This type of flowmeter measures mass directly by using only Coriolis force for mass determinations. In one instrument, manufactured by Micro Motion (1985), the fluid flow is directed through a vibrating U-shaped tube. The vibrational force on the tube causes the fluid to accelerate on the inlet side of the U and decelerate on the outlet side. The resultant twist force at the tube's axis of rotation is caused by the two opposing forces of the fluid flow. The amount of twist is proportional to mass flow rate, which is proportional only to the time interval and geometric constants. Mass is independent of temperature and pressure, therefore, variations in these fluid variables will not affect mass flow rate.

Non-Restricting Volume Flowmeters

Magnetic flowmeters are based upon a principle of Faraday's Law, which states that a conductor passed at right angles through a magnetic field will generate a voltage. Coils produce a magnetic field throughout a region of a pipe with a known length and diameter which is positioned perpendicular to slurry flow. As a minimum conductivity slurry flows through the pipe, electrodes on the pipe monitor the potential difference across the moving slurry. Since the magnetic field is uniform, this potential is proportional to the average slurry velocity.

Caution must be exercised in the application of magnetic flowmeters, as some physical conditions can lead to reduction of accuracy. One such condition is the presence of ferromagnetic particles, which will alter the magnetic flux in the pipe, thus causing substantial error. Another is temperature changes, because magnetic flux density, produced by the field coils, will vary with changing temperature. Severe environmental vibrations must also be avoided unless the meter is specially designed to meet this application.

High frequency sound waves (typically 10^7 Hz) are used by ultrasonic flowmeters for determining fluid velocity. There are three general methods for wave transmission and detection;

The frequency method of wave transmission and detection measures the difference between upstream and downstream frequencies with diagonally directed waves. The measurements are independent of the velocity of sound, thus eliminating errors introduced by fluid temperature, composition and density.

The beam deflection method involves an acoustic beam being transmitted perpendicular to fluid flow. The deflection distance is monitored and used to compute flow. Since the measurements are dependent on the speed of sound, accurate measurements require fluid temperature, composition and density to be compensated for.

The doppler shift method transmits ultrasonic pulses into the slurry pipeline. The frequency at which they are reflected back from air bubbles and particulates is a function of the slurry flowrate.

In general, the doppler shift method is preferred for coal slurries because its accuracy is not affected by variation in the amount of entrained air in the slurry.

A series of tests were executed at Michigan Technological University to compare the performance of a magnetic flowmeter and a "Doppler Shift" type of ultrasonic flowmeter (Kawatra et al, 1980). Densities of the various coal slurries ranged from 5-50% solids and flowrates ranged from 5-30 gpm. Such ranges on any given stream would rarely be encountered in operating plants, but the high accuracy shown by the meters even when subjected to such conditions illustrates the versatility and dependability of the instruments.

PRESSURE MEASUREMENTS

A wide range of pressure measuring devices are used in the coal industry. All types fall into the category of devices which are designed to respond to a change in pressure by deforming or moving an external device in a manner proportional to the change in pressure. The most commonly used pressure monitors are Bourdon tubes, pressure bellows and strain gauges. All of these transducers are discussed in detail in standard instrumentation handbooks, and are not discussed here.

WEIGHT MEASUREMENTS

A wide range of static load cells are available to the mineral industry, and are most often used when accuracy is an absolute necessity, such as for sales. Implementation of

control schemes has caused an increase in continuous weight monitors, e.g. belt scales.

Belt weigh feeders are simple devices that present a fixed volume of coal to a moving conveyor belt. This fixed volume is accomplished by feeding coal from a hopper to a conveyor belt, and shearing the coal to a fixed height and width on the belt with a gate. If coal had a fixed density, the speed of the belt would be the only other information to be measured. Since coal density varies, a better method is to weigh the material on the moving belt with a belt scale. Belt scales consist of one or more conveyor idlers mounted on a weigh bridge, which can be hydraulically, mechanically, pneumatically or electrically activated. Weight per unit belt length measurements are combined with speed to provide a continuous weight/unit time readout. The more idlers mounted to the weigh bridge, the greater the length of belt involved and thus, the greater the accuracy of measurement.

One significant problem with belt scales is their physical attachment to the conveyor. Any detrimental factors acting on the conveyor will affect the accuracy of the weight measurements. Placement of the belt scale is also crucial, with the best results being obtained on horizontal belt sections provided with a smooth, continuous flow of material.

CONTROL IN FINE COAL PROCESSING

There are two basic objectives for any control scheme for coal processing. The first is to minimize the effects of feed disturbances on the grade-recovery performance, and the other is to operate at the optimum on the grade-recovery curve for a particular coal. Coal processing methods do not give a perfect separation and recovery is always less than is theoretically possible. The implementation of process control is one method of reducing the difference between theoretical and actual by reducing much of the wild fluctuations that occur. In spite of the proven gains of process control, most coal processing plants in the United States have only the most rudimentary instrumentation for process control. This is mainly due to the historically low value of coal, which has made it more economical in the past to construct a simple tipple and discard the coal which did not meet standards.

Basic Characteristics of Automatic Control

Initial attempts towards automatic controls used proportional, integral and derivative controllers. These controllers were used to automate simple control loops, such as sump level, mill feed rate and flowrate of water. Once these control schemes were successfully implemented, the next logical step was to develop model-based control systems (Burdett et al, 1986). There are three types of model-based systems available; Empirical Systems (Lynch et al, 1981), Phenomenological-based systems (Nieme and Maijanen, 1973; Klimpel, 1984; Mika and Fuerstenau, 1969; Herbst and Bascur, 1983), and Artificial Intelligence/Expert systems (Moore et al, 1984). A schematic diagram of the general elements of control systems is shown in Figure 9.

Empirical Models. This method involves a large amount of experimental data from an operating plant of interest being collected. The empirical relationships between various variables are typically developed using techniques which define the regression relationships between the measured and controlled parameters. Care should be exercised while using these models, as they are only good for the range and conditions under which the original data was collected.

Phenomenological Models. These models are based on first principles and involve the use of physical laws to develop relationships between the measured and controlled variables. These models are difficult to develop but have a much wider application than empirical models.

Artificial Intelligence/Expert Systems. The development of computers that are capable of carrying out commands in parallel rather than sequentially has created interest in the possibilities of expert systems. This development has allowed computers to mimic, at a much slower rate, the human thought process to some extent. This technique holds great promise for certain areas of process control, areas which do not lend themselves to mathematical modelling and involve too many variables for phenomenological modelling. Presently, these processes are controlled by humans with expertise in their operation; they can combine judgmental capabilities with knowledge gained from previous experience (Sutton, 1984). Commercially viable expert systems would incorporate human expertise into a set of rules which would form the basis of a knowledge-based automatic system of control. The economic viability of expert systems in automatic process control will be governed by both the time and cost involved in their generation and the necessary interpreting software for compatibility with existing controllers.

Blending Control

A typical system for the blending of coal involves raw coal and clean coal being fed simultaneously to meet some specified blend. The raw coal feed is maintained at a constant rate, while the clean coal feed rate is varied such that the final product meets the buyers specifications. This system must be conservatively lower than the specifications to allow for the fluctuations in combustible coal composition, thus essentially giving away a fair proportion of coal. Zumberge (1987) has shown that this scenario can be improved by using a ash or elemental analyzer to monitor the blended product in real time and control the rate at which clean coal is fed. This method allows for a product that is nearer to the specifications because the results are immediately available, thus keeping the saleable product much closer to specifications. A third approach may

Table IV. Variables and Sensors for Flotation Control

Measurable Variables	Sensing Device
composition	slurry ash analyzer
water flow rate	orifice plate
pulp density	gamma density gauge
pH	pH probe
reagent addition rates	flowmeter
froth depth/level	bubbler tubes, sonic detectors, nuclear gauge, conductivity probes
slurry flow rate	magnetic flow meter, doppler flow meter
power draw	watt meter

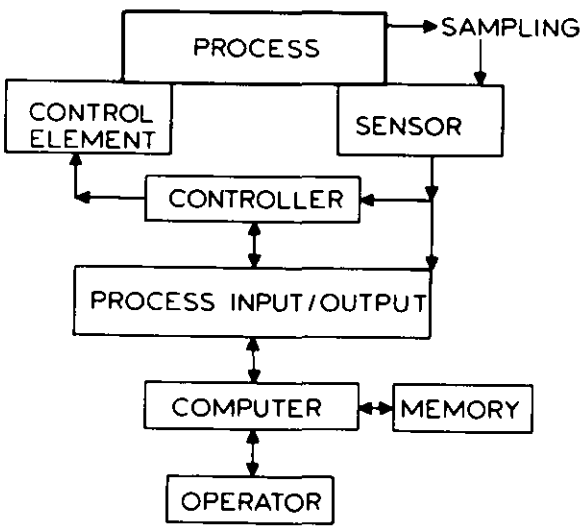

Figure 9. General elements of a control system (arrows indicate direction of information flow).

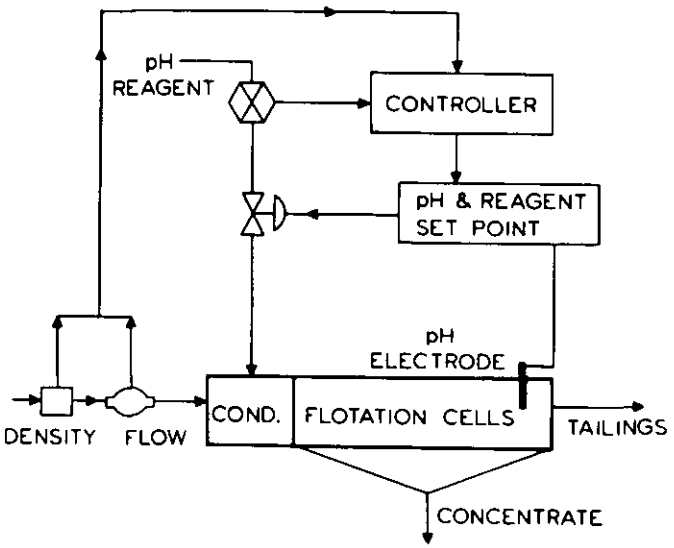

Figure 10. pH control in flotation circuit.

also be taken, it involves feeding forward analyses to both the raw and clean coal feed controllers (Zumberge, 1987). With this system an ash or elemental analyzer is placed on both the raw coal and clean coal streams. Their real time measurements are processed by a computer and used to blend the coals closely to buyer specifications. This system, though more expensive than the feed back type, has distinct advantages when the combustible coal varies greatly in a short period of time.

Flotation Control

Coal flotation differs drastically from metallic mineral flotation in operation, design and control. The main differences are that the coal is not ground to liberation size, and only a small fraction of the plant feed is processed by flotation. These factors and upstream disturbances lead to rather large fluctuations in the characteristics of the flotation feed. An additional difference is that coal is light, readily flotable and the majority of the feed is recovered in the concentrate, as opposed to metallic flotation where the bulk of the weight reports to the tailings. Thus coal flotation circuits are usually run in an overloaded froth condition.

Control is desirable for coal flotation circuits because it serves to calm the short term fluctuations caused by feed variability and prior upstream disturbances. The coal concentrate variations can be controlled by controlling reagent addition, froth depth, aeration rate and water additions. The more stable these variables remain for a given type of coal, the fewer fine coal losses to the tailings circuit. Additionally the flowrates and compositions of concentrates and tailings streams can have significant effects on dewatering processes (Kawatra and Seitz, 1984).

The objective of any control strategy in fine coal processing is to minimize the effects of feed disturbances on circuit grade-recovery performance, and to operate on the optimal grade-recovery curve for a particular coal. Unfortunately, a universal control scheme cannot be developed because of the wide variability of coal characteristics and their individual responses to processing circuits.

Two levels of control must be considered when developing fine coal processing control strategies. The first level, stabilizing control, is intended to minimize the effect of feed and prior processing disturbances, and the second, optimizing control, is to operate on the optimal grade-recovery curve for the circuit. Obviously, the stabilizing of a circuit is necessary before the optimization can be effective. The effects of circuit design and operating practice are very important factors in maintaining stable and optimal circuit operation. The use of circuit design and operating practice to obtain some stability and optimization can drastically reduce the burden of any control strategy (Seitz and Kawatra, 1985; Kawatra et al, 1984).

For effective process control of a flotation circuit it is necessary to measure several variables, which are listed in Table IV. Using the sensors listed in Table IV several control loops can be developed. Figure 10 shows a pH control loop, as pH control is often necessary to maintain optimum recovery. A variation of two pH units will cause an increase in ash to 10% and a 4% reduction of recovery in a flotation circuit (Lynch et al, 1978, Wells 1981). The intention of the control loop is to ensure that the ratio of pH reagents varies according to the flowrate of solids to the float cells. Similarly, pulp level is used to control grade. Higher grade is accomplished by increasing the froth depth, thus increasing the particle residence time in the froth and allowing greater ash drainage. After sampling three plants in Pennsylvania and one in West Virginia, a control scheme for reagent additions was developed at Michigan Technological University (Seitz and Kawatra, 1987; Kawatra and Waters, 1982; Kawatra and Seitz, 1984). In this strategy, a coal flotation circuit could be monitored to ensure that the MIBC addition was maintained at starvation level (i.e. adequate additions to prevent froth overloading) and then the collector addition rate could be monitored to obtain the optimal grade and recovery. This strategy is particularly useful in plants treating coal with large amounts of clay and slimes. The results obtained in the circuit when MIBC additions were below starvation levels are presented in Figure 11. The nearly instantaneous results obtained when the MIBC addition to the circuit was cut off (point 3), then restored (point 11) to its original level prove the inherently short retention times encountered in coal flotation circuits. As expected, when the MIBC addition is reduced, the % ash in the tailings is decreased and the % solids increased, as the circuit was operating below optimum MIBC additions. The process was quick to stabilize and established a new equilibrium until an increase in feed rate again disrupted the system (point 8), sending the % ash in the tailings even lower. Shortly after MIBC addition was restored, the plant prepared for shutdown and the feed was slowed quickly and sporadically.

Thickeners

A conventional thickener generally involves a hydraulic retention time of one-half to four hours, whereas a high capacity thickener involves a hydraulic retention time of 15 minutes to 1 hour. High capacity thickening is accomplished by introducing the feed slurry under the slime layer, hence effecting a more rapid settling rate which reduces the required thickening area. Because of the shorter retention time and greater operational instability, these thickeners require close control of solids inventory to ensure that the slime layer does not drop below the slurry inlet (Yingst, 1986; Wells, 1981).

Of the independent variables of thickening, only polymer addition rate and underflow pumping rate are considered useful for control. Feed rate and composition are not useful as they are

Table V. Variable and Sensors for Thickener Control

Measurable Variables	Sensing Device
solids level	ultrasonic level gauge
feed flow rate	ultrasonic flow meter
feed percent solids	gamma density gauge
reagent flow rate	metering pump
pH	pH electrodes
underflow rate	ultrasonic flowmeter
underflow percent solids	gamma density gauge
overflow turbidity	clarometer turbidity sensor

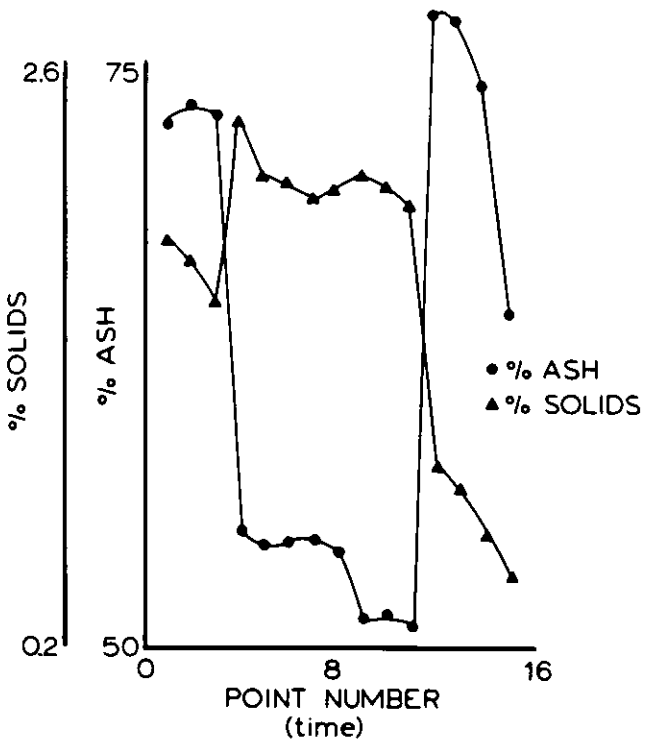

Figure 11. Flotation respone to MIBC.

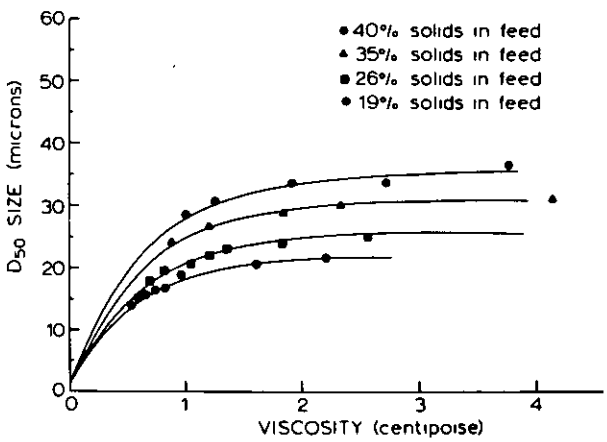

Figure 12. Viscosity effect on cyclone d_{50} size. Test work carried out with a 4" Krebs cyclone and pure silica (80% - 62 microns). Viscosity determined with a Nametre vibrating sphere viscometer in a sampling system developed at MTU (Kawatra and Eisele, 1988).

dependent on prior processing. Controllable dependent variables are overflow turbidity, sludge bed level and underflow density, though underflow density is somewhat dependent on sludge bed level (Yingst, 1986). Appropriate sensors for measuring these variables are listed in Table V.

Several different strategies for controlling thickeners have been proposed and tried. Generally, flocculant addition is controlled to reduce the costs involved. This can be accomplished by utilizing both underflow density and solids feed rate to determine flocculant addition. A level measurement of the slime blanket is used to control the rate at which variable speed pumps remove the underflow. The sludge bed level must be maintained between specific set points to ensure both efficient clarification of the overflow and adequate thickening of the underflow. Conventionally, flocculant addition rates are balanced with overflow turbidity. However, there are problems associated with this method. Turbidity sensors are known for their tendency to foul quickly and being difficult to clean. Also, nearing optimal flocculant dosage causes the overflow turbidity to change rapidly, as do the large cyclic "dead times" inherent to thickener operation. The resulting non-linear response tends to be difficult to implement into control.

A new technique for flocculant dosage control has been attained by Ramsey Engineering in St. Paul, Minnesota (Maehling, 1985). It involves periodic sampling of a thickener feedwell to determine the flocculated material's settling rate. It is well known that the rate of settling of a solid liquid interface is a function of the flocculant dosage. In the Ramsey Clarometer, a desired settling time is used as a set point, and the flocculant dosage is controlled to maintain that set point. This scheme has been tested at several U.S. coal plants with an average flocculant saving of 16% being the result (Maehling, 1986).

In most coal applications underflow density is not critical. Thus, sludge bed level is controlled preferentially for operational stability, with underflow rate being used to maintain a given sludge bed level. The biggest problem with level control is achieving an accurate level measurement. The interface in a refuse thickener is not a well defined line, but a gradient. The most successful instruments are sonic devices and ball floats. A new device by Krohne involves a moveable sonic sensor which seeks a certain sludge consistency, then transmits that level information to a controller (Yingst, 1986).

Filtration Devices. The most commonly used filtration devices in fine coal processing are belt presses, vacuum drum filters and vacuum disk filters. Generally, little control of these devices has been attempted, due to their relative stability and lack of suitable instrumentation.

As the feed to the filters is uncontrolled, the only reasonable place for control is flocculant dosage and, in the case of the vacuum filters, rotational speed. Polymer costs can be minimized as well as energy requirements for dewatering if dosage is carefully matched to mass flow rate. Operation of a belt press generally involves flocculation of a thickened sludge, gravity dewatering or drainage of that flocculated sludge, and subsequent final dewatering via roll compression. Control is accomplished by measuring the flow rate and solids content (using a nuclear density gauge) of the feed to the belt press, calculating the total dry solids throughput, and controlling the polymer feed rate at a constant dosage. This does not work well when the characteristics of the solid material change with time (Yingst, 1986). For vacuum filters, a level of control can be obtained by using a level gauge to control the speed of rotation. When the rate of feed increases, the drive speed can increase in proportion with rising level, thereby increasing solids removal.

HEAVY MEDIA CYCLONES

The objective of heavy media cycloning is to maximize clean coal yield for a given specific ash content and to reduce ash variability in the final product. A typical control scheme would involve accurate control of the cyclone feed gravity and cyclone velocity (Wells, 1981). To accomplish these objectives, feed velocity and feed density control will be required. The level in the heavy media sumps can be measured by ultrasonic, capacitance or bubble tubes, thus controlling velocity fluctuations. Density measurement can be made with a nuclear density gauge to maintain the density of the heavy media cyclone feed stream.

Presently, viscosity in a heavy media plant is not controlled. The importance of this control loop was first suggested by Valentyik (1971) after extensive experimental work at Michigan Technological University. Kawatra and Eisele (1988) have found that viscosity has a decided effect on cyclone d_{50} size as shown in Figure 12. The problem in implementing such a control loop has been the lack of on-line instrumentation which could deliver reliable results. Recent work at Michigan Technological University suggests that some of the recently available on-line instruments are suitable for this application.

CONCLUSION

The technology for on-line elemental and ash measurements is well established. Sensors for the on-line measurement of density, flow, level and weight are well developed and are being extensively used in industry. The technology for on-line measurement of pyrite and macerals should be developed, though very little work has been done in these areas.

ACKNOWLEDGMENTS

The work conducted was supported by the Department of Interior Mineral Institute program administered by the USBM under Grant G1184126.

REFERENCES

Armstrong, M. P., Gray, W. A., Haynes, J. and Page D., 1984, "On-Line Ash, Sulphur and Moisture Monitoring of Coking Coal, Mining Engineering, September, pp. 181-184.

Berthold, "Ash Content Determining in Coal Fines with Analyzer LB 360-AS", Tema Systems Inc.

Brown, D. R., Gozani, T., Elias, E., Bozorgmanesh, H., Bevan, R. and Luckie, P., 1980, "Nuclear Assay of Coal", Vol. 4, Moisture Determination in Coal Survey of Electromagnetic Techniques", EPRI Report No. CS-989, Vol. 4, FP 989.

Boyce, I.S., Clayton, C. G., and Page, D., 1977, "Some Considerations Relating to the Accuracy of Measuring the Ash Content of Coal by X-ray Backscattering", Nuclear Techniques and Mineral Resources, International, Atomic Energy Agency, Vienna, pp. 135-165.

Boyce, I. S., 1983, "A Technique for Measuring the Ash Content of Coal in a Tailing Stream", Int. J. Appl. Radiat. Isot., 34, pp. 45-54.

Burdette, B. W., Hales, L. B., Probert, T. I., 1986, "Selection of Control Systems for Concentrator Operations," Chapter 33, Design and Installation of Concentration and Dewatering Circuits, (eds. A. Mular and M. Anderson) SME, Littleton, CO, pp. 509-518.

Cammack, P., 1973, "Ash Monitor for On-Stream Coal Analysis", presented to the Institution of Mechanical Engineers, London.

Cammack, P. and Balint, A., 1976, "On-Stream Ash in Coal Monitoring for Profit", Transactions SME, 260, pp. 361-366.

Cekorich, A., Deich, H., Harrington, T., Marshall, J. H. III, 1979, "Development of an Elemental Analyzer for Coal, Oil and Similar Bulk Streams - A Status Report", Proceedings 1979 Symposium Instrumentation and Control Fossil Energy Processes, ANL-79-62, pp. 297-313.

Clarkson, C., Fiedler, V. A. and Tonkim, D. A., 1983, "Use of On-Stream Ash Analysis", Proc. of 3rd Austrailian Coal Preparation Conference, (R. L. Whitmore Ed.) pp. 310-333.

Clayton, C., Wormald, M., 1983, "Coal Analysis by Nuclear Methods, Int. J. Appl. Radiat. Isot., 34(1), pp. 3-22.

Clarkson, C., Hornsby, D. and Walker, D., 1985, "Automatic Flotation Control Using On-Stream Analysis", presented at the Third Australian Coal Preparation Conference, Wollongong, Australia.

Considine, D. (ed.), 1969, Instrument Engineers Handbook-Process Measurements, vol. 1, Chilton Book Company, NY.

Cooper, H., 1984, "On-Line Analysis of Coal Slurries for Improved Control in Coal Processing", Journal of Coal Quality, January, pp. 14-19.

Cutmor, N., Holmes, R., Sowerby, B. and Watt, J., 1986, "Nuclear Techniques for On-Line Analysis in Mineral and Coal Processing", Paper to be presented at the 13th Congress of the Council of Mining and Metallurgical Institutions, Singapore.

Evans, R., 1955, The Atomic Nucleus, McGraw-Hill Book Co., Inc., New York.

Evans, R., 1958, "Compton Effect", Handbuch Der Physik, S. Flugge, (ed.), Springer-Verlag, Berlin.

Dartnell, J. and Berry P., 1974, "On-Line Analysis of Moisture Content of Bulk Solids in Transit", Institute of Mechanical Engineers, London, pp. 99-109.

Fauth, G., 1980, "On-Stream Determination of Ash and Moisture Content in West German Coal Preparation Plants", Proc. 1980 Symp. Instr. and Control for Fossil Energy Processes Report ANL080-62, pp. 428-445.

Fauth, G., Bachmann, C. and Klein, A., 1984, "Instrumentation for the On-Stream Analysis of Ash Content and Moisture Content in Coal Cleaning Plants", AIME Annual Meeting, Preprint Number 84-171.

Flintoff, B., Plitt, L. and Konzuk, R., 1984, "On-Stream Analysis of Fine Coal Slurries", presented at the CIM Annual Meeting, Quebec, Canada.

Fuller, E., Jr. (ed.) 1982, Coal and Coal Products: Analytical Characterization Techniques, ACS Symposium Series 205, American Chemical Society, Washington, D.C.

Goxsni, T., Bozorgmaresh, H., Brown, D., Elias, E., Tassicker, O. and Bevan, R., 1979, "Advanced Techniques and Instrumentation for Real Time On-Line and Laboratory Analysis of Coal, Proc. 1979 Symp. Instrum. and Control Fossil Energy Processes, ANL-79-62, pp. 266-296.

Hall, D., Morris, G. and Scott, C., 1969, "The Continuous Determination of Moisture in Coal", Mining and Minerals Engineering, 5(11), pp. 30-40.

Hass, D., Sporson, J. and Gray, W., 1970, "The Rapid Determination of Moisture in Coal Using Microwaves, Part I: Laboratory Investigations", Journal of the Institute of Fuels, September, pp. 350.

Hall, D., Sporson, J. and Gray, W., 1972. "The Rapid Determination of Moisture in Coal Using Microwaves, Part 2: Plant Trials", Journal of the Institute of Fuels, March, pp. 163.

Harmon, P. and King, D., 1985, "Expert Systems: Artificial Intelligence in Business", John Wiley and Sons, Inc., 1984.

Herbst, J. and Bascur, O., 1983, "Evaluation of Alternate Control Strategies for Coal Flotation", presented at the AIME Annual Meeting, Atlanta.

Hills, W., 1987, "The Connection Machine", Scientific American, June, pp. 108-115.

Hubbel, J., 1977, "Photon Mass Attenuation and Mass-Energy-Absorption Coefficients for H, C, N, O, Ar and Seven Mixtures from 0.1 KeV to 20 MeV", Radiation Research, 70, pp. 58-81.

Hubbel, J. and Overbo, I., 1979, "Relativistic Atomic Form Factors and Photon Scattering Cross Sections", J. Phys. Chem. Ref. Data, 8(1), pp. 69-105.

Kawatra, S., 1976a, "The Design and Operational Characteristics of a Portable Multi-Stream-On-Line Analyzer", International Journal of Mineral Processing, 3(1), pp. 41-50.

Kawatra, S. and Dalton, J., 1976b, "The On-Line Determination of Ash in Coal Slurries", Can. J. Spectroscopy, 21(2), pp. 58-60.

Kawatra, S., 1976e, "Use of Scattered Radiation in the Determination of Copper in Mineral Slurries", Canadian Mining and Metallurgical Bulletin, vol. 69 (772).

Kawatra, S., 1976d, "The Use of a Gd-153 Gamma Ray Density Gauge for Coal Slurries in an On-Line-X-ray Fluorescence System", Canadian Journal of Spectroscopy, 21, (3).

Kawatra, S., 1976c, "The Influence of Length of Flow Cell and Strength of a Source on the Performance of a Gamma Density Gauge", International Journal of Mineral Processing, 3(2), pp. 167-174.

Kawatra, S., 1980, "A Coal Ash Monitor for Coal Cleaning Processes", Chapter 30, Fine Particle Processing, P. Somasundaran (ed.) AIME, New York, pp. 583-593.

Kawatra, S., Laurila, M. and Keck, J., 1980, "On-Line Characterization of Coal Slurries", Proc. of 1980 Symposium on Instrumentation and Control for Fossil Energy Processes, Argonne National Laboratory, Report N. 80-62, pp. 133-149.

Kawatra, S. and Water, J., 1982, "An Investigation of the Effect of Reagent Addition on the Response of a Fine Coal Flotation Circuit", Proc. of the 14th IMPC, Toronto.

Kawatra, S., 1984, "Methods of On-stream Analysis", presented at the SME-AIME Annual Meeting, preprint No. 84-113.

Kawatra, S. and Seitz, R., 1984, "The Effect of Froth Structure on Coal Flotation and Its Use in Process Control", Proc. of 18th APCOM, IMM, London, pp. 139-147.

Kawatra, S., Seitz, R. and Suardini, P., 1984, "The Control of Coal Flotation Circuits" Control '84 Mineral/Metallurgical Processing, J. Herbst (ed.), AIME, pp. 225-233.

Kawatra, S. and Eisele, T. C., 1988, "Rheology Effects in Grinding Circuits", International Mineral Processing Congress, Forssberg, K.S.E., ed., Elsevier, Amsterdam, pp. 195-207.

Kawatra, S. K. and DeLa'O, K. A., 1987, "Auxiliary Measurements in Particulate Processes, Submitted for Publication.

Kitzinger, F., Rosenblum, F. and Spira, P., 1979, "Continuous Monitoring and Control of Froth Level and Pulp Density" Mining Engineering, April, pp. 390-394.

Klein, A., 1987, "Comparison of Rapid Moisture Meters", Mineral Processing, January, pp. 1-8.

Klein, A., 1981, "Microwave Determination of Moisture in Coal: Comparison of Attenuation and Phase Measurement", Journal of Microwave Power, 16(314), pp. 289-304.

Klimpel, R., 1984, "Froth Flotation: The Kinetic Approach", Proceedings of Mintek(50), L. Haughton, (ed.), Council for Mineral and Energy Technology, Johannesburg, pp. 385-392.

Kohler, J., Sottile, J. and Placha, D., 1987, "Process Control of Heavy-Media Systems for Coal-Preparation Plants, IEEE Transactions on Industry Applications, vol. IA-23(2), March/April, pp. 382-388.

Kouns, W., 1986, Personal Communication, Armco Autometrics, Co.

Krugers, J. (ed), 1973, Instrumentation in Applied Nuclear Chemistry, Plenum Press, New York-London.

Laurila, M. and Kawatra, S., 1984, "Plant Trials of an Ash Analyzer for Control of a Coal Flotation Circuit", presented at Canadian Institute of Mining and Metallurgy Annual Meeting, August.

Liptak, B., (ed.), 1969, Instrument Engineers Handbook - Process Measurements, vol. 1, Chilton Book Company, NY.

Lyman, G. and Chester, R., 1980, "On-Stream Analysis for Ash in Coal Slurries, Proc. 5th Int. Conf. on Coal Research, Dusseldorf, DFR, pp. 145-163.

Lynch, A., Johnson, N., Manlapig, E. and Thorne, C., 1981, Mineral and Coal Flotation Circuits, D. Fuerstenau (ed.), Elsevier Scientific Publishing Company, Amsterdam.

Maehling, L., 1985, "The Clarometer: A System for Controlling Flocculant Feed to Process Thickners", presented at the 2nd Annual Coal Preparation Exhibition and Conference, Lexington.

Maehling, K., 1986, Personal Communication.

Micro Motion, Inc., 1985. Micro Motion Instruction Manual.

Mika, T. and Fuerstenau, D., 1969, "A Microscopic Model of the Flotation Process", VIII International Mineral Processing Congress, vol. 2, Mechanobr, Leningrad, pp. 249-269.

Millen, J., Sowerby, B., Rafter, P., Ellis, W., Gravitis, V., Howells, E., McLennan, T. and Muldoon L., 1984, "Field Trial of a Pair Production Gauge for the On-Line Determination of Ash in Coal on a Conveyor Belt", Int. J. Appl. Radiat. Isot., 35(11), pp. 1009-1021.

Moore, R., Hawkinson, L. and Knickerbocker, C., 1984, "Expert Systems Application in Industry", Advances in Instrumentation, vol. 3-9, Part 2, Instrument Society of America, Research Triangle Park, NC, pp. 1081-1094.

Mular, A., 1986, "Automatic Control of Mineral Processing Circuits", Advances in Mineral Processing, P. Somasundaran (ed.), SME-AIME, Littleton, CO., pp. 663-681.

Niemi, A. and Maijanen, J., 1973, "Computation of Optimal Feed Forward Control for Flotation Cell", Proceedings of Symposium on Dynamic Modeling and Computer Control of Technological Processes, Tbilisi, pp. 352-368.

Robertson, S., Cunliffe, F., Fowler, C. and Richmond, I., 1979, "Rapid Measure of Moisture in Coal and Total Solids in Coal Slurries by Low-Resolution Proton Nuclear Magnetic Resonance", Fuel, 58, pp. 770-774.

Seitz, R., 1983, "General Elements of Control Systems", unpublished results.

Seitz, R. and Kawatra, S., 1985, "Control Strageties for Coal Flotation Circuits", IFAC Symp. on Automation for Mineral Resource Development, Brisbane.

Seitz, R. and Kawatra, S., 1987, "The Role of Frothers in Coal Flotation", to be presented at the AIME Annual Meeting, Denver, Co.

Shaw, W., 1984, "Process Control of Coal Preparation Plants", Mining Engineer, vol. 144, pp. 323-325.

Sigal, P., 1981, "The Use of Nuclear Gauges in Coal Preparation", Proc. of 1st Australian Coal Preparation Conference, A. Swanson (ed.), pp. 298-316.

Sigal, P., 1986, Personal Communication.

Stewart, R., Hall, A. and Konchesky, J., 1970, "Plant Tests of a Neutron Moisture Meter for Coal", Mining Congress Journal, November, pp. 44-48.

Stewart, R., Hall, A., Martin, J., Farrior, W. and Poston, A., 1974, "Nuclear Meter for Monitoring the Sulfur Content of Coal Streams" U. S. Bureau of Mines Technical Report, No. TPR 74, January.

Sutton, R., 1984, "Expert Systems for Process Control", Real Time Computer Control, S. Bennett and D. Linkens (eds.) Peter Perigrinus Ltd., U.K.

Valentyik, L., 1971, "Instrumentation and Control of the Specific Gravity and Rheology of Heavy Media Suspensions", Minerals Science and Engineering, 3(1), pp. 38-44.

Watt, J. and Sowerby, B., 1983, "On-Line Determination of Ash in Coal Using "SIROASH" Gauges", Proceedings of the 2nd Austrailian Coal Preparation Conference, R. Whitmore (ed.), pp. 263-298.

Watt, J., 1984, "Determination of Ash Content of Coal On-Line on Conveyors and In-Stream Coal Slurries", IAEA Advisory Group Meeting on Gamma, X-ray and Neutron Techniques in the Coal Industry, Vienna.

Weiss, E. and Frock, H., 1976, "Rapid Analysis of Particle Size Distribution by Laser Light Scattering", Powder Technology, 14, pp. 287-293.

Wells, C., 1981, "Control Systems in Coal Preparation Plants", EPRI Report No. CS-1880.

Wertheimer, A. and Wilcock, W., 1976, "Light Scattering Measurements of Particle Size Distribution", Applied Optics, 15(6), pp. 1616-1620.

Yingst, J., 1986, Personal Communication.

Zumberge, J., 1987, "On-Line Rapid Coal Analysis Offers Processing and Marketing Opportunities", Coal Mining, November, pp. 37-39.

Zumberge, J., 1987, "On-Line Analysis Can Boost Profits from Blending", Coal Age, June, pp. 48-51.

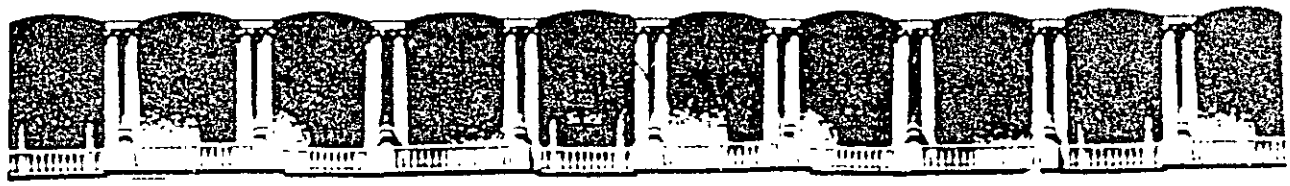

FACULTAD DE INGENIERIA U.N.A.M.
DIVISION DE EDUCACION CONTINUA

CURSOS ABIERTOS

DESARROLLO Y OPERACIÓN DE SENSORES PARA CONTROL DIRECTO Y CONTINUO EN PLANTAS DE BENEFICIO DE MINERALES Y EN LA RESTAURACIÓN DEL MEDIO AMBIENTE

Del 18 al 23 de mayo de 1998

TEMA: DEVELOMENT OF AN IMPROVED ON STREAM COAL SLURRY ASH ANALYZER

EXPOSITOR :DR. KOMAR KAWATRA

1998

Kawatra, S.K. and Eisele, T.C., "Development of an Improved On-Stream Coal Slurry Ash Analyzer," Ch. 18, Control 90, publ. by the Society of Mining, Metallurgy and Exploration, 1990, pp. 151-162.

Chapter 18

Development of an Improved On-Stream Coal Slurry Ash Analyzer

S. K. Kawatra and T. C. Eisele

Department of Metallurgical Engineering
Michigan Technological University
Houghton, MI 49931

ABSTRACT

Production of highly-cleaned coal for advanced utilization schemes requires close control of the coal ash content at very low levels. For this purpose, a sensitive, low-cost, robust on-stream ash analyzer is needed. The development of such an instrument based on x-ray backscatter and fluorescence is described, including features to improve its sensitivity at low ash levels. The performance of the resulting device in testing a real coal sample is discussed.

INTRODUCTION

Coal cleaning plants have traditionally been operated to achieve high coal recovery with little concern being given to quality control. This is because the price of coal had been low compared to the cost of upgrading it. Developments in world energy supplies have directed the coal cleaning industry towards a more sophisticated approach. Increased demand, coupled with environmental concerns, dictate that more productive and efficient coal cleaning processes be used to meet industrial requirements.

Present day coal preparation operations give less than the theoretical maximum recovery for a given ash content. Instrumentation and control is essential to all coal preparation processes to obtain maximum recovery at a consistent quality.

The conventional analysis procedure of collecting a sample in a preparation plant and analyzing it in a laboratory is expensive and does not provide information fast enough for quality control. To implement an effective process control loop, it is necessary to use on-line sensors which can measure product quality effectively and rapidly. Also, the instruments must be rugged enough to withstand the plant environment, straightforward to use, and inexpensive enough to be applied wherever they are needed.

Coal ash is the oxidized residue remaining after coal has been burnt and consists essentially of alumina, silica, iron compounds, and small quantities of the oxides of potassium, calcium, titanium, etc. Since coal has a lower effective atomic number than do the various ash-forming minerals, the effective atomic number is a good indicator of the ash content. Several ash measurement methods which utilize the differences in these effective atomic numbers have been proposed. These methods are based on the interaction of x-rays and low energy γ-rays with coal (Watt and Sowerby, 1983; Kawatra, 1976b; 80; Clayton and Wormald, 1983; Fauth, 1980, 84; Cutmore, et al 1986). In addition gauges based on pair production γ-ray interactions have been developed (Cutmore et al, 1986; Millen et al, 1984).

Ash Analyzers Based Upon the Backscattering of X-rays and γ-rays

The determination of ash content in coal slurries requires at least two measurements, one to obtain the solids content of the slurry and the other to obtain the ash content of the solids. The solids content of the slurry can be determined by a gamma density gauge (Kawatra, 1976a,b,c,d). The gauge is based on the principle of radiation absorption. As the radiation passes through matter, the loss in intensity of gamma rays is related to the density of the material. Because gamma ray mass attenuation coefficients are both atomic number and energy dependent (Kawatra, 1976c, Evans, 1955, 1958) it is customary to use a gamma ray energy of about 0.7 MeV for applications free of high atomic number elements, and a gamma ray energy of about 1.2 MeV when high atomic-number elements are present. For solids content measurement of low density slurries, such as an aqueous coal slurry, gamma-ray energies in the range 0.6 MeV to 1.3 MeV are not sufficiently sensitive for practical path lengths (25 cm) and it is necessary to use an isotope which has a lower energy gamma ray. The characteristics of isotopes commonly used in density gauges are shown in Table 1 as well as the characteristics of isotopes that could be used to measure solids content of coal slurries. Gd-153 is selected for this application over Co-57 because of sensitivity, and over Ir-192 and Ce-139 because of both half-life considerations and sensitivity.

Table 1A

Isotopes Commonly Used in Density Gauges

Isotope	Half-Life	Radiation Used for gauging (MeV)
Cs 137	30.0 years	0.662
Co 60	5.2 years	1.173
		1.332

Table 1B

Useful Isotopes for Gauging Low Density Material

Isotope	Half-Life	Radiation Used for gauging (MeV)
Gd 153	239 days	0.099
Co 57	270 days	0.122
		0.136
Ce 139	140 days	0.165
Ir 192	74 days	0.062
		0.066
		0.296
		0.308
		0.317

The coal ash content determination is based on the scattering of radiation energy less than 100 KeV, the intensity of scattered radiation being proportional to the ratio of the probability of a scattering interaction occurring opposed to an absorption interaction. Two types of radiation scattering may occur: incoherent or Compton scattering and coherent or Rayleigh scattering. In Compton scattering, a photon collides with an electron, loses some of its energy and is deflected from its original direction of travel. In Rayleigh scattering, photons are scattered by bound atomic electrons under conditions such that the atom is neither ionized nor excited. The scattering from different parts of the atomic charge distribution is then "coherent". Compton scattered low energy gamma rays suffer an energy loss which grows larger as the angle of scatter increases. Rayleigh scattered photons have the same energy as the primary photons regardless of scattering angle. In addition, the cross section of Compton scattering is proportional to the Atomic Number (Z) of the scattering atoms while the Rayleigh scattering cross section is closely proportional to Z^3. Compton scattering relationships are given by the Klein-Nishina formula (Hubbel, 1977; Hubbel and Overbo, 1979)

$$\sigma_c = 3.92 \times 10^{-26} \left(\frac{E'}{E}\right)^2 \left(\frac{E}{E'} + \frac{E'}{E} - \sin^2\theta\right) \qquad (1)$$

where σ_c is the Compton differential cross section per sq. cm. per electron per steradian, E is the energy of the primary photons, E' is the energy of the scattered photons and θ is the scattering angle. The relationship between E' and E is given by (Evans, 1955, 1958)

$$E' = \frac{E}{1 + \frac{E}{mc^2}(1-\cos\theta)} \qquad (2)$$

where m is the electron rest mass, and c is the speed of light. For a mixture of elements, the probability of Compton scattering per unit path length traversed in the medium into the elemental solid angle $d\Omega$ in the direction θ is given by (Evans, 1955, 1958)

$$P(\theta,E)_c = N\rho\sigma_c(\theta,E)\,d\Omega \sum_i \alpha_i \left(\frac{Z}{A}\right)_i \qquad (3)$$

where N is Avogadro's number, ρ is the density of the material, α_i is the fraction of the total weight comprised by the ith type atoms, and Z and A are respectively the atomic number and atomic weight of the i'th type atoms.

The Rayleigh scattering can be approximated by the relationship (Evans, 1955, 1958)

$$\sigma_R = K\frac{\pi}{4}\left(\frac{e}{mc^2}\right)^2 f(\theta)\,\frac{Z^3}{E^3} \qquad (4)$$

where σ_R is the Rayleigh cross section per sq. cm. per electron per steradian, e is the electronic charge, K a constant and $f(\theta)$ is a function of scattering angle. For a mixture, the probability of Rayleigh scattering per unit path length traversed in the medium into the elemental solid angle $d\Omega$ in the direction θ is given by (Evans, 1958)

$$P(\theta,E)_R = KN\rho d\Omega \sum_i \frac{\alpha_i Z_i^3}{A_i} \qquad (5)$$

where ρ is the density, N is Avogadro's number, and α_i is the fraction of the total weight comprised by the i'th type atoms.

The theory outlined suggests the application of Rayleigh and Compton scattering to the chemical analysis. If the amount of high atomic number material varies in a low atomic number matrix, the Compton and Rayleigh scattered intensities would also vary accordingly.

Coal ash is the oxidized residue remaining after coal has been burnt and consists essentially of alumina, silica, iron minerals and compounds and small quantities of the oxides of potassium, calcium, titanium, etc. In coal, the effective atomic number of ash is about 10, while that of combustible carbonaceous material is about 6. Thus, since the effective atomic number of coal increases with increasing ash content, the ash content can be theoretically determined by measuring the intensity of scattered low energy photons. The effect of photon energy on the sensitivity of ash measurement is shown in Fig. 1 (Boyce, et al 1977).

The presence of iron-sulphur minerals in coals, such as pyrite and pyrrhotite, which may be present in concentrations as high as 5-10 weight percent and which have an effective atomic number of about 20, will cause greater changes in scattering intensity than alumina and silica with their effective atomic number of about 10. Therefore, compensation should be made for the

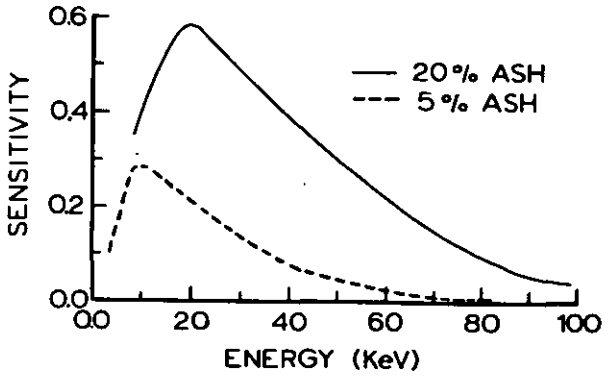

Figure 1. Relationship between sensitivity of an ash analyzer and the energy of the excitation source for various ash levels.

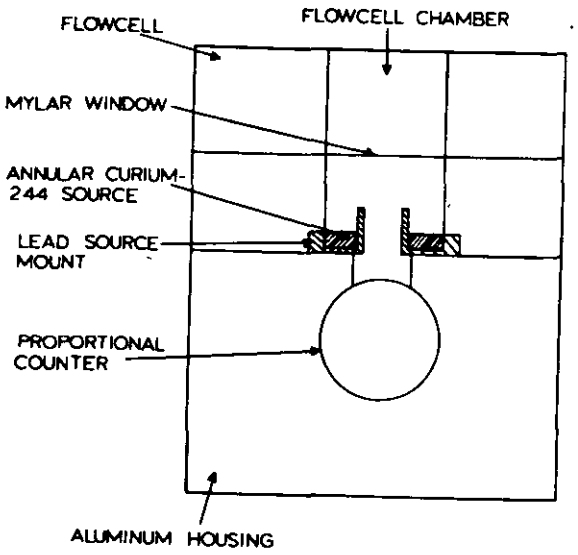

Figure 3. Horizontal cross section of the annular-source x-ray irradiation configuration.

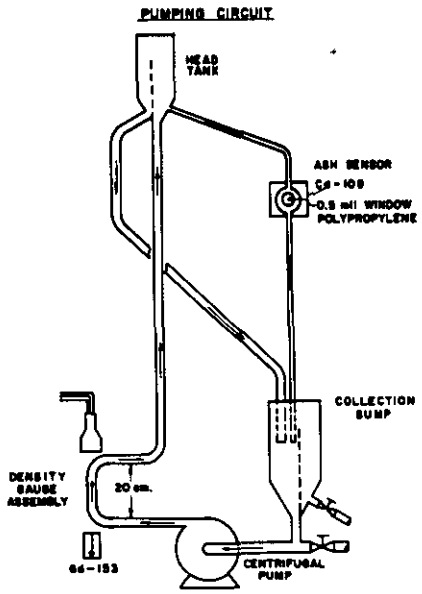

Figure 2. Configuration of the first MTU ash analyzer test rig.

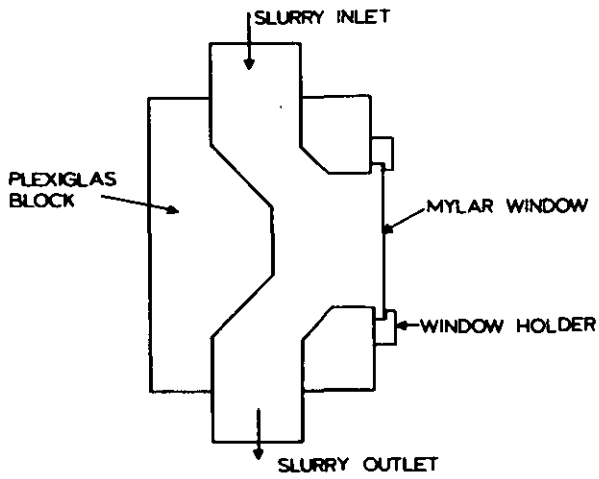

Figure 4. Vertical cross section of the high-throughput flowcell for the backscatter sensor.

iron content in order to accurately determine the ash content. If a radioisotope is selected so that Fe K_α fluorescent x-rays (6.4 KeV) are excited and measured a quantitative measurement of the iron-sulphur mineral content in the slurry can be made. This measurement provides a correction for the additional scattering due to the iron-sulphur minerals. With this procedure an accurate determination of ash content can be made. A schematic of an early test rig developed at Michigan Tech is shown in Fig. 2, which illustrates the basic principles of this technique. This device used a single flow cell for backscatter and XRF measurements and a lucite assembly with a 20 cm radiation path for a density gauge. A gamma density gauge employing a Gd-153 source was used. Generally, commercially available gauges use a Cs-137 or a Co-60 source. The characteristics of these sources for the measurement of percent solids of coal slurries are discussed in the literature (Kawatra, 1980).

For the determination of ash in coal slurries a Cd-109 source was selected. This source emits AgK x-rays of 24.9 and 22.1 KeV. The Rayleigh scattered radiations and Fe K_α x-rays were measured by a gas-filled proportional counter. The Fe K_α x-rays provided a correction for the variation of pyrite in coal. The ash analyzer was installed in an operating plant and the results are extensively discussed in the literature (Laurila and Kawatra, 1984; Kawatra, 1984; Kawatra et al, 1980; Kawatra and Waters, 1984). In the plant operation a deaerating device manufactured by Armco Autometrics was used along with the ash analyzer to analyze concentrate slurries.

The on-line measurement of ash by scattered radiation has several advantages. The method is simple, provides corrections for the variation of pyrite, and is rugged. Systems of this general type have been reported by several investigators, for instance, the OSCAA system by Flintoff, et al (1984), and the MRDE method by Boyce (1983). The results of these systems and others are presented in Table 2 from the work of Cooper (1984).

Watt (1983) has also used the technique of backscattered γ-rays for the measurement of ash in coal slurries. However, instead of using mechanical deaerating devices, he proposed a technique which depends on the measurements of neutron moderation and gamma-ray transmission to determine hydrogen (wt/wt) in the slurry, and combining these with ash-sensitive measurements e.g. x-ray backscatter and iron K_α x-ray excitation. It is much better to use a mechanical deaerating device than to use neutrons to provide a correction for air, as neutron sources are a greater radiation hazard than x or gamma-ray sources. Mechanical deaerating devices have been used all around the world and have proven to be successful. The results of Watt's (1983) work at CSIRO are presented in Table 2 (Cooper, 1984).

The primary use of these instruments has been to measure the ash content of slurry streams which are fairly high in ash, such as the feed and tailings streams. In normal coal cleaning

Table 2. Accuracy of Coal-Slurry Measurements

	Ash			% Solids		
	St. Error	Range/ Avg.	Rel. Error	St. Error	Range/ Avg.	Rel. Error
ASHSCAN						
Feed	2.5	12-30/21	11.9	0.6	5-20/12.5	4.5
Conc	0.3	5-11/8	3.8	0.7	15-35/25	2.8
Tails	4.4	40-80/60	7.3	0.6	3-10/65	8.6
Michigan Tech						
Tails	0.7	56-78/67	1.2	-	15-40	2.7
Bergbau						
Tails	1.6	5-65/35	4.4	0.4	5-18/12.5	2.8
MRDE						
Tails	2.0	50-80/65	3.1	0.3	2-17/9.5	3.1
CSIRO						
Tails	0.8	20-30/25	3.2	0.5	5-22/13.5	3.7
Feed	0.9	10-24/17	5.3	1.0	5-19/12	8.7
OSCAA						
Conc	0.4	6-13/10	3.6	0.7	15-35/25	2.7
Tails	4.4	40-80/60	40.5	0.6	3-10/6.5	16.4

circuits, this is sufficient for maintaining coal quality. However, greater sensitivity is needed if the ash content of the clean coal is to be measured and tightly controlled, as would be necessary in a plant for producing highly-cleaned coal at less than 2% ash. With this goal in mind, a new x-ray backscatter ash sensor was designed, built, and tested at Michigan Technological University.

DESIGN CONSIDERATIONS

Ash Sensor

The original Michigan Tech ash analyzer used, in the ash sensor, a point source mounted in a lead cup emitting a collimated x-ray beam. This narrow beam was directed at the center of the flowcell window providing a narrow range of scattering angles centered about 135°, with radiation outside this range being absorbed in the aluminum housing or in the flowcell material.

Specifically designed for use in coal preparation plants where product ash content is at least six percent, the point source configuration is of inadequate sensitivity for monitoring coal-water fuel slurries, which can be less than 1% ash.

The sensitivity of the backscatter sensor could be improved by increasing the size of the flowcell window, and redesigning the source configuration to provide more even illumination of the flowcell, thus exposing a greater quantity of slurry to the radiation.

An annular source situated squarely facing the flowcell window is a configuration which readily provides a high irradiation area and uniform flow cell irradiation, while still

permitting the transmission of backscattered radiation to the detector. Such an arrangement, shown in Fig. 3, was selected for this project. A xenon-filled gas proportional counter was used to detect backscattered radiation and Fe K_α x-rays. This type of detector was used because it is cheaper and easier to maintain than solid-state detectors, and its energy resolution is sufficient for the purpose.

The flowcell designed for the ash sensor uses a 0.5 mil mylar window to separate the slurry from the source and the detector. A sensor which uses backscattered radiation is most sensitive to material which is very near to the window. It was therefore necessary to design the flowcell to ensure that the slurry contacting the window was representative of the entire slurry. This was achieved by arranging the inlet to force incoming material to impinge directly on the window, and by situating the outlet to ensure that coarse material did not accumulate anywhere in the cell. The resulting flowcell design is shown in Fig. 4. Initially, it was considered possible that this arrangement might cause rapid wear of the window, but this proved not to be a problem.

When the backscatter sensor was first used, a large x-ray peak was noted at 8.4 KeV, as shown in Fig. 5A. This was found to be due to fluorescent x-rays excited by the Cm-244 from the tungsten shielding in the source housing. The presence of this peak could not be tolerated, as it largely obscured the iron fluorescence peak, and therefore made accurate pyrite compensation impossible.

An aluminum collimator was first used to screen out the W-L_α x-rays, as shown in Fig. 5B. Aluminum was used so that any fluorescent x-rays from the collimator would differ greatly in energy from the Fe K_α peak. However, the aluminum was unable to completely absorb the tungsten x-rays, even when made thick enough to seriously constrict the opening of the source annulus. For this reason, a lead collimator was substituted, as shown in Fig. 5C. Although a small quantity of lead fluorescent x-rays were excited by the source, the intensity of these x-rays was only one-half that of the radiation which leaked through the aluminum, and of sufficiently high energy not to interfere with the iron fluorescence measurement.

Test Rig

In order to produce the best results, the test rig was designed to meet the following conditions:

1. The ash sensor and density gauge are monitoring identical streams.
2. The slurry is provided at a low, constant pressure to prevent shape changes of the ash sensor window.
3. Air is removed from the slurry before it reaches the density gauge, which is sensitive to air bubbles.
4. The slurry is kept thoroughly mixed to prevent errors due to settling in the system.
5. The ash sensor and density gauge are isolated from the vibration of the centrifugal pump.

To accomplish this, the rig was designed as shown in Fig. 6. Slurry is added to the sump, and is pumped to a constant-head tank, which is designed to remove air as well as maintain a constant pressure. The head tank overflow is recirculated to the sump. The head tank supplies slurry to both the ash sensor and density gauge via a 1" diameter line, and the slurry is then returned to the sump. A sampling port is provided immediately following the density gauge.

The constant head tank contains an arrangement of baffles which allow a high throughput of slurry without splashing or level fluctuations. This arrangement is shown in Fig. 7. The anti-splash plate shown also serves as a surface which encourages the coalescence of air bubbles, and hence deaerates the slurry. The high throughput rate prevents particle settling in the tank, and ensures that the composition of the underflow stream is representative of the entire sample.

Slurry is supplied to the head tank by a flexible line, and the head tank, ash sensor, and density gauge are mounted on a support structure which is not attached to the centrifugal pump. This effectively isolates the sensors from the pump vibration, thus eliminating the possibility of error from this source.

The main slurry stream, which flows through the sensors, is returned to the sump through flexible piping. A vertical plate installed in the sump prevents the formation of a vortex, which would cause classification of the slurry solids. Since the head tank overflow is quite turbulent and entrains a large amount of air, it is returned to the head tank via a side-mounted feed box. This provides an opportunity for the bulk of the air to be removed, and causes the material to enter the sump with a minimum of turbulence. The slurry from the density gauge is caused to flow down the sump wall, thus minimizing air entrainment.

EXPERIMENTAL PROCEDURE

Sample Preparation

Coal samples were obtained from the Kitt Energy Co. coal washery, in West Virginia. All samples were dried, and if necessary crushed to 100%-20 mesh by stage crushing to allow suspension in a slurry.

Each sample was split into increments of approximately 200 grams with a riffle splitter. A total of 80 increments of coal were prepared in this manner. In addition, a single 2270 gram increment was prepared for use as the first coal to be added to the test rig.

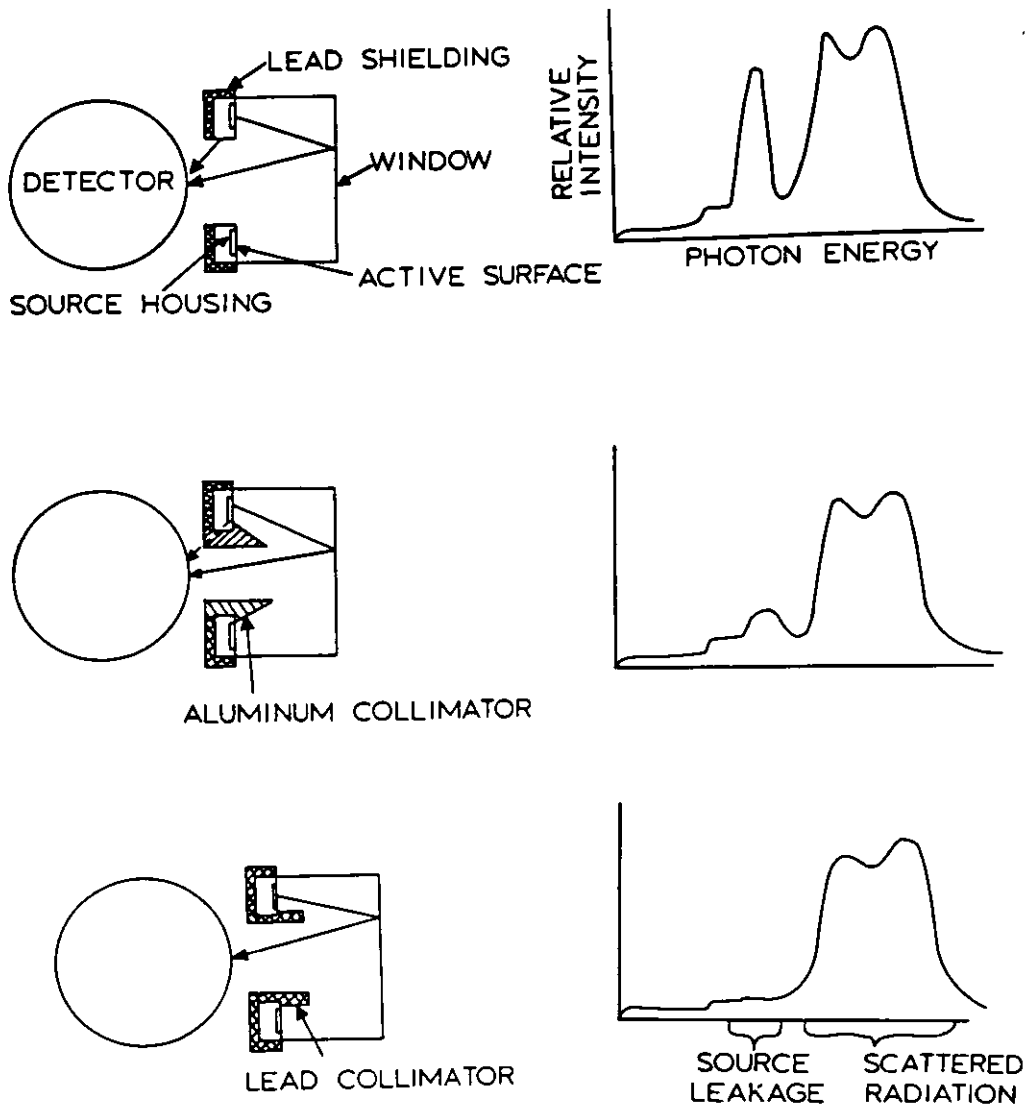

Figure 5. Effect of various collimators on the spectra produced by the backscatter sensor.

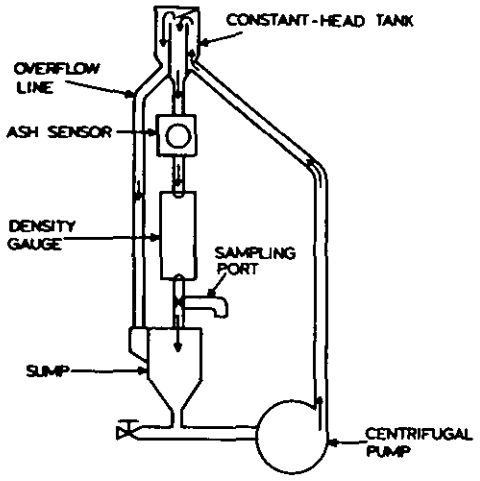

Figure 6. Configuration of the improved MTU ash analyzer test rig.

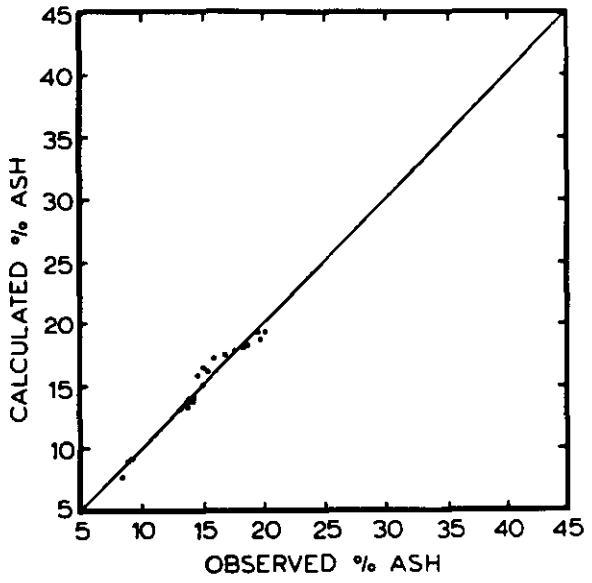

Figure 8. True ash content versus ash content calculated by ash analyzer, sampling campaign #1. Ash range: 8.4-20.2% ash Standard error: 0.68% ash

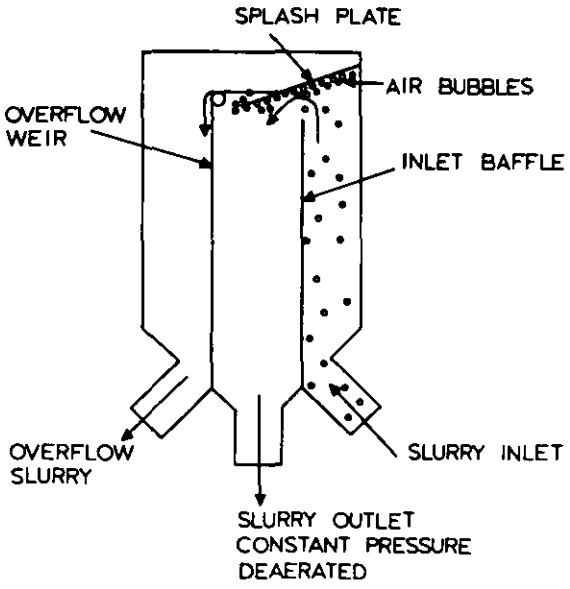

Figure 7. High-throughput head tank/ deaerator for improved test rig.

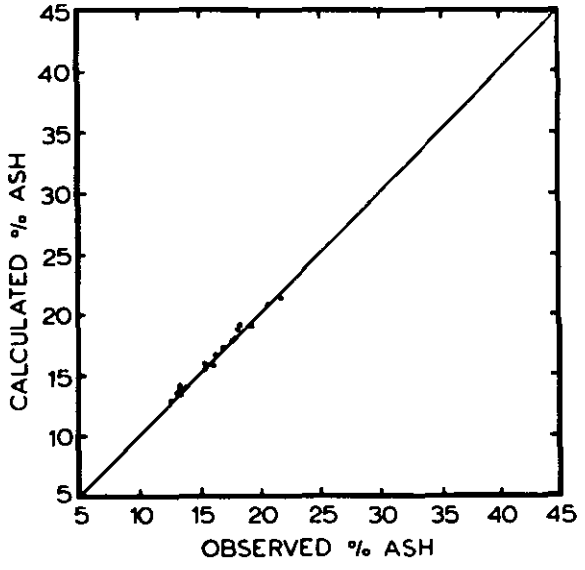

Figure 9. True ash content versus ash content calculated by ash analyzer, sampling campaign #2; Ash range 12.8-21.8% ash Standard error: 0.27% ash

Test Rig Stability Determination

The analyzer electronics were turned on, and allowed to stabilize for several hours. Following this, the test rig was filled with 15 liters of tap water, and the pump was started. The water was then circulated through the rig continuously for 18 hours. Radiation readings were taken with a counting time of 800 seconds, and were recorded continuously by the computer.

This counting time is a function of the source intensity, and can be easily decreased merely by using a higher activity curium-244 source.

At the end of 18 hours, the results were examined for signs of electronic drift.

After stability with water was confirmed, the 2270 gram coal increment was added, to produce a slurry containing 13% solids by weight. The stability was then monitored for an additional 24 hours, to determine whether the presence of solid particles produced any increase in the variation in the readings.

Ash Content Variation

After stability testing, the ash content of the coal in the rig was varied in order to provide data for calibration, according to the following procedure:

1. A reading was taken using the ash sensor, with a counting time of 800 seconds.
2. A one-liter slurry sample was removed from the test loop, using the sampling valve immediately following the density gauge. The entire stream was diverted to the sampling container during sample removal.
3. One of the 200 gram increments of Kitt Energy Co. Coal was selected at random, slurried with one liter of water, and added to the ash analyzer sump.
4. The slurry sample was weighed, filtered, and dried at 75°C.
5. The test rig was allowed to stabilize for a period of time, and the cycle was repeated.

Using this procedure, a series of four sampling campaigns were carried out at 48 hour intervals. Each campaign consisted of 20 data points, taken at half-hour intervals, for a total of 80 points collected over a period of seven days. Between sampling campaigns, the test rig was left operating continuously while the computer monitored the system for stability.

After the samples had been dried the coal was ground to -65 mesh, and ash content was determined in duplicate according to the method set forth in ASTM Standard D 3174.

Calibration

Due to the fairly short half life of the Gadolinium-153 gamma-ray source used in the density gauge (242 days), a decay correction was applied to the density gauge readings. This correction was applied according to the formula

$$I_c = I \cdot \exp(t \cdot k)$$

where I = uncorrected density gauge reading
I_c = corrected density gauge reading
k = Gd-153 decay constant, .000119 hr^{-1}
t = time since the reference reading was taken, hours

The result of this correction is to predict the reading which the density gauge would have provided if the source had possessed the same strength as it did when the reference reading was taken. The time spans over which each campaign was carried out are as follows: Campaign #1: t = 0 to 10 hours; Campaign #2: t = 51.5 to 61.5 hours; Campaign #3: t = 96 to 106 hours; Campaign #4: t = 144.5 to 154.5 hours. No correction for decay of the curium-244 source was necessary, as its half-life of 17.8 years makes the loss of strength over a period of seven days negligible.

Calibration equations were determined using standard multiple linear regression. Due to the difficulty of theoretically deriving a relationship between ash content and backscatter, Fe K_α, and transmitted gamma ray intensities, a simple empirical equation was used, as follows:

$$A = K_1(B.S.) + K_2(FeK_\alpha) + K_3(DG) + C$$

where A = weight % ash
BS = backscattered x-ray intensity
FeK_α = iron K_α fluorescence intensity
DG^α = gamma-ray transmission intensity
K_1, K_2, K_3, C = arbitrary constants

Equations of this form have been found to give good results in this application, provided that the ash content does not vary over a range much wider than 20 weight % Ash. If the ash range is greater than this value, errors will begin to mount noticeably.

Experimental Results

The calibration data collected in the four sampling campaigns is presented in tables 3 through 6, along with the regression equation constants for each campaign, the ash values calculated from the regression equation, and the expected uncertainty in the calculated ash valued due to statistical variations in the radiation counts.

In Figs 8-11, the ash values calculated using the regression equations are plotted against the corresponding measured ash values for each sampling campaign. These figures show that the variation between the actual and predicted ash values is greatest in campaigns #1 and #4. In the case of campaign 1, this variation is due to errors made in removing slurry samples, and apparently not to any machine flaws, as no other possible evidence of equipment failure or electronic drift was found in the course of experimentation. This is borne out by the consistentl,

Table 3. Ash analyzer test results for sampling campaign 1. Density counts are corrected for source decay. The regression equation is of the form: Wt.% Ash = K1 (Backscatter)+K2(FeK)+K3(Density)+C

Wt.% Ash	Backscatter Counts	FeK Counts	Density Counts	Calculated Wt.% Ash
8.4	1255619	93637	241096	7.43
9.1	1241459	93433	240134	9.01
8.8	1243141	93359	239461	8.83
14.4	1197747	95986	233303	14.12
13.9	1202118	97944	234213	13.71
15.0	1193432	104022	232563	15.00
14.3	1200171	94953	233107	13.81
13.8	1203340	94308	235236	13.38
13.2	1205730	94996	234901	13.16
18.7	1160342	96245	231607	18.32
19.8	1154906	96204	231634	18.93
20.2	1151305	96884	230830	19.37
19.7	1151878	96363	231414	19.27
18.5	1160795	96126	231359	18.27
17.8	1164370	96092	232061	17.86
16.9	1168427	96012	231903	17.41
16.0	1170176	96586	231553	17.25
15.5	1178425	96727	232797	16.32
15.2	1176816	96279	233382	16.46
14.6	1182496	96329	233425	15.83

Regression Equation Constants:
K1 = -.0001110850 K2 = .0000477558
K3 = -.0000196438 C = 147.1744
Mean Ash Value = 15.19000 Standard Error = .68420
Expected uncertainty calculated ash values = ± 0.15% ash.

Table 4. Ash analyzer test results for sampling campaign 2.

Wt.% Ash	Backscatter Counts	FeK Counts	Density Counts	Calculated Wt.% Ash
13.6	1178552	100353	231389	14.01
13.5	1181270	100336	232668	13.64
12.8	1186190	99445	232568	12.97
13.3	1183854	100355	232465	13.29
12.8	1187354	99636	233738	12.81
14.0	1179417	99598	231273	13.89
13.6	1183792	98890	232875	13.30
18.6	1141562	101098	229010	19.03
17.8	1151269	100723	230365	17.71
16.6	1159951	100072	231188	16.54
16.3	1165239	99677	232474	15.82
15.7	1168228	99710	232221	15.41
17.1	1155780	99773	231852	17.10
21.8	1123949	99809	228654	21.42
20.6	1128042	100449	229591	20.87
19.4	1141108	99845	229184	19.09
18.2	1144284	99228	230326	18.66
18.1	1149691	100532	231002	17.93
16.5	1159452	98948	231971	16.60
15.6	1165453	98620	231792	15.79

Regression Equation Constants:
K1 = -.0001357976 K2 = .0000004379
K3 = -.0000001902 C = 174.0541
Mean Ash Value = 16.29500 Standard Error = .27457
Expected uncertainty of calculated ash values = ± 0.15% ash.

Table 5. Ash analyzer test results for sampling campaign 3.

Wt.% Ash	Backscatter Counts	FeK Counts	Density Counts	Calculated Wt.% Ash
15.8	1171341	102341	229302	15.30
20.4	1125739	102594	226616	20.92
21.2	1117790	102365	226648	21.90
25.9	1085772	103494	223066	25.85
26.4	1084200	102976	222553	26.04
25.8	1086533	103654	223747	25.76
24.3	1099081	103662	225363	24.21
23.2	1106376	103175	225653	23.31
22.3	1113133	102990	226307	22.47
22.0	1116860	102010	227272	22.00
21.0	1123772	101846	228537	21.15
20.5	1130509	102487	228643	20.33
19.4	1139841	101401	229261	19.17
18.7	1146051	100283	228819	18.40
17.7	1152223	100823	230852	17.64
17.5	1154879	101004	230948	17.31
16.6	1162790	100137	232045	16.33
15.7	1167354	100602	233435	15.76
15.1	1171428	99973	232131	15.26
14.7	1172822	100058	232150	15.09

Regression Equation Constants:
K1 = -.0001229317 K2 = .0000077743
K3 = -.0000034722 C = 159.2980
Mean Ash Value = 20.21000 Standard Error = .29739
Expected uncertainty of calculated ash values = ± 0.14% ash.

Table 6. Ash analyzer test results for sampling campaign 4.

Wt.% Ash	Backscatter Counts	FeK Counts	Density Counts	Calculated Wt.% Ash
14.5	1165451	101962	232181	14.36
14.0	1173111	101488	232388	13.38
19.0	1132347	102039	227756	19.57
23.2	1098564	103245	226140	24.24
21.8	1114097	102972	226947	22.00
26.0	1083462	103235	224569	26.58
32.1	1054396	103374	220258	31.18
29.0	1066797	103322	222147	29.21
34.8	1032075	103818	218076	34.49
31.9	1044695	103158	220035	32.67
32.7	1051769	103223	220691	31.56
30.4	1063334	103152	224093	29.56
33.8	1030011	103683	221570	34.46
38.6	1002700	105036	217660	38.40
43.7	983886	106902	193341	43.13
39.7	1002624	105608	196762	40.46
42.9	982953	105842	192378	43.69
40.9	1004468	105288	193717	40.62
39.2	1014459	105607	195530	38.89
37.4	1024715	105843	197454	37.14

Regression Equation Constants:
K1 = -.0001439180 K2 = -.0003038374
K3 = -.0001066754 C = 237.8353
Mean Ash Value = 31.28000 Standard Error = .64974
Expected uncertainty of calculated ash values = ± 0.30% ash.

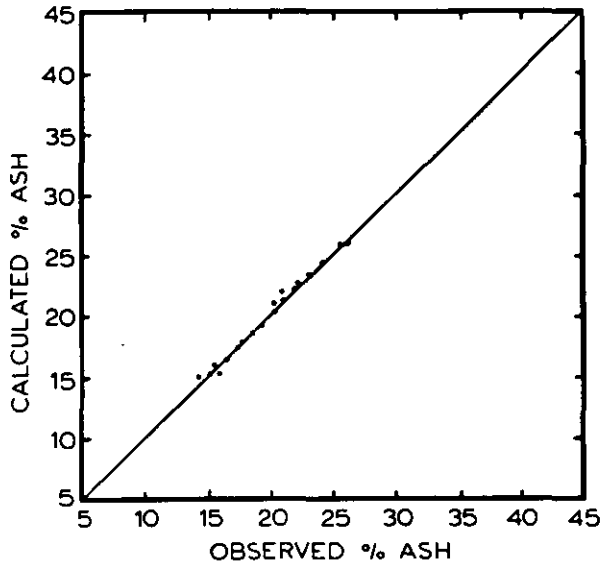

Figure 10. True ash content versus ash content calculated by ash analyzer, sampling campaign #3.
Ash range: 14.7-26.4% ash
Standard error: 0.30% ash

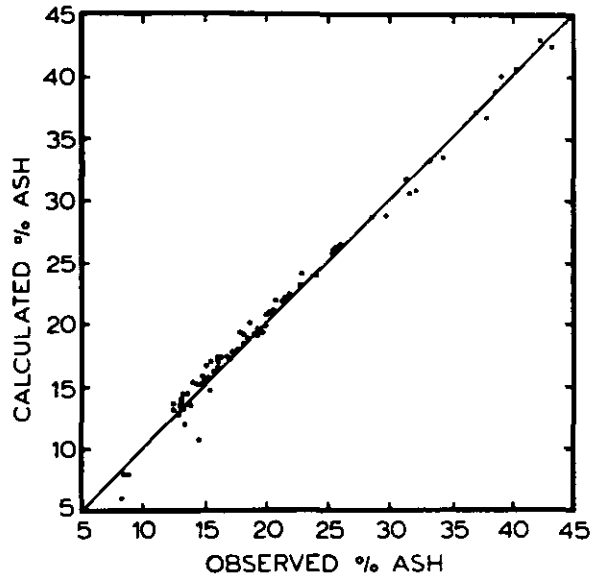

Figure 12. True ash content versus ash content calculated by ash analyzer, combined results.
Ash range: 8.4-43.7% ash
Standard error: 0.88% ash

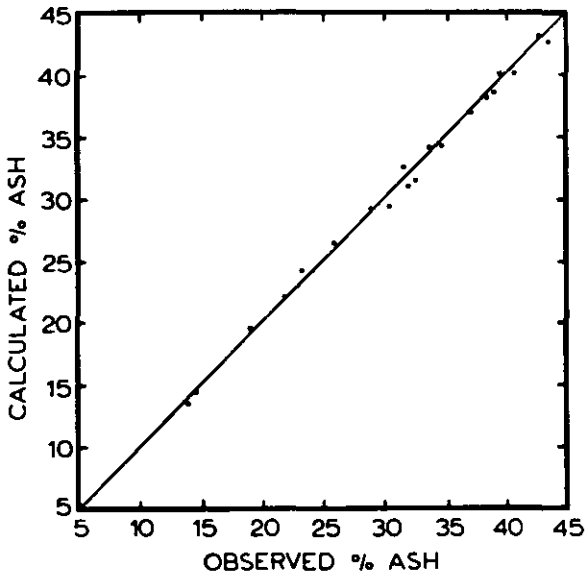

Figure 11. True ash content versus ash content calculated by ash analyzer, sampling campaign #4.
Ash range: 14.0-43.7%
Standard error: 0.65% ash

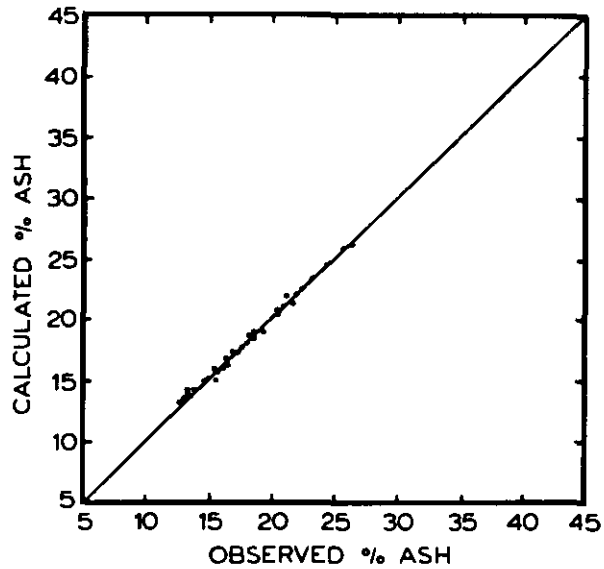

Figure 13. True ash content versus ash content calculated by ash analyzer, campaigns #2 and #3 combined.
Ash range: 12.8-26.4% ash
Standard error: 0.32% ash

low variations seen subsequently for campaigns 2 and 3. The increase in variation for campaign #4 is to be expected, due to the extremely wide range of ash values (14% to 43.7%, difference of 29.7).

Combining all of the data and finding a single overall regression equation results in the plot shown in Fig. 12. This illustrates that the results are quite stable over time and over a wide ash range. If campaigns 1 and 4 are ignored, the plot of Fig. 13 is produced, which is more representative of conditions which are likely to occur in practice, and shows very good agreement between the measured and the calculated ash contents.

The ability of the ash analyzer to operate continuously for nine days without breaking down or showing signs of electronic drift indicates that the design is sufficiently robust to be used in an operating plant without difficulty. The accuracy of the system, and its stability with time, is indicated by the combined results of sampling campaigns 2 and 3, which show a standard error of the predicted ash content of ±0.32% ash at 15 wt% solids and 12% to 26% ash.

For ash measurement of coals cleaned to less than 3% ash, it is only necessary to increase the solids content of the slurry in order to achieve higher accuracy. Increasing the percentage solids will increase the fraction of the slurry which is mineral matter, and will therefore increase the change in the slurry atomic number corresponding to changing ash content of the coal. If the standard error at 15% solids is ± 0.32% ash, it would then be expected to have roughly one quarter the value, or ± 0.08% ash, at 60% solids.

CONCLUSIONS

The ash analyzer described has been shown to be capable of measuring the ash content of coal in slurries to within ± 0.32% ash at 15 wt.% solids. This is primarily due to the annular CM-244 x-ray source used for backscatter measurements, and to the high flowrate configuration which provides for good sampling and a uniform slurry. The resulting instrument performance is superior to that obtained by other on-stream ash analyzers.

Extended operation has shown that the instrument is not prone to frequent electronic or mechanical failure, and produces stable results over period of at least one week. It is therefore suitable for plant use without further modification.

REFERENCES

Boyce, I. S., Clayton, C. G., and Page D., 1977. Some Considerations Relating to the Accuracy of Measuring the Ash Content of Coal by X-ray Backscattering. Nuclear Techniques and Mineral Resources, International, Atomic Energy Agency, Vienna, pp. 135-165.

Boyce, I.S., 1983. A Technique for Measuring the Ash Content of Coal in a Tailing Stream, Int. J. Appl. Radiat. Isot. 34, pp. 45-54.

Clayton, C. G., Wormald, M. R., 1983. Coal Analysis by Nuclear Methods, Int. J. Appl. Radiat. Isot. 34(1), pp. 3-22.

Cooper, H. R., 1984. On-Line Analysis of Coal Slurries for Improved Control in Coal Processing, Journal of Coal Quality, January, pp. 14-19.

Cutmore, N. G., Holmes, R. J., Sowerby, B. D. and Watt, J. S., 1986. Nuclear Techniques for On-Line Analysis in Mineral and Coal Processing, Paper to be presented at the 13th Congress of the Council of Mining and Metallurgical Institutions, Singapore.

Evans, R. D., 1955. The Atomic Nucleus, McGraw-Hill Book Co., Inc., New York.

Evans, R.D., 1958. Compton Effect, Handbuch Der Physik, S. Flugge, (ed.), Springer-Verlag, Berlin.

Fauth, G., 1980. On-Stream Determination of Ash and Moisutre Content in West German Coal Preparation Plants, Proc. 1980 Symp. Instr. and Control for Fossil Energy Processes Report ANL-80-62, pp. 428-445.

Fauth, G., Bachmann, C. and Klein, A., 1984. Instrumentation for the On-Stream Analysis of Ash Content and Moisture Content in Coal Cleaning Plants, AIME Annual Meeting, Preprint Number 84-171.

Flintoff, B.C., Plitt, L. R. and Konzuk, R. A., 1984. On-Stream Analysis of Fine Coal Slurries, Presented at the CIM Annual Meeting, Quebec, Canada.

Hubbel, J. H., 1977. Photon Mass Attenuation and Mass-Energy-Absorption Coefficients for H, C, N, O, Ar and Seven Mixtures from 0.1 KeV to 20 MeV, Radiation Research, 70, pp. 58-81.

Hubbel, J. H. and Overbo, I., 1979. Relativistic Atomic Form Factors and Photon Scattering Cross Sections, J. Phys. Chem. Ref. Data, 8(1), pp. 69-105.

Kawatra, S. K., 1976a. The Design and Operational Characteristics of a Portable Multi-Stream On-Line Analyzer, International Journal of Mineral Processing, 3(1), pp. 41-50.

Kawatra, S. K. and Dalton, J. L., 1976b. The On-Line Determination of Ash in Coal Slurries, Can. J. Spectroscopy, 21(2), pp. 58-60.

Kawatra, S. K. 1976d. The Use of a Gd-153 Gamma Ray Density Gauge for Coal Slurries in an On-Line X-ray Florescence System, Canadian Journal of Spectroscopy, 21, (3).

Kawatra, S. K., 1976c. The Influence of Length of Flow Cell and Strength of a Source on the Performance of a Gamma Density Gauge, International Journal of Mineral Processing, 3(2), pp. 167-174.

Kawatra, S. K., 1980. A Coal Ash Monitor for Coal Cleaning Processes, Chapter 30, Fine Particles Processing, p. Somasundaran (ed.) AIME, New York, pp. 583-593.

Kawatra, S. K., Laurila, J. J. and Keck, J., 1980. On-Line Characterization of Coal Slurries, Proc. of 1980 Symposium on Instrumentation and Control for Fossil Energy Processes, Argonne National Laboratory Report No. 80-62, pp. 133-149.

Kawatra, S. K., and Waters, J. L., 1982. An Investigation of the Effect of Reagent Addition on the Response of a Fine Coal Flotation Circuit, Proc. of the 14th IMPC, Toronto, pp. I.

Kawatra, S. K., 1984. Methods of On-Stream Analysis, Presented at the SME-AIME Annual Meeting, Preprint No. 84-113.

Laurila, M. J. and Kawatra, S. K., 1984. Plant Trials of an Ash Analyzer for Control of a Coal Flotation Circuit, Presented at Canadian Institute of Mining and Metallurgy Annual Meeting, August.

Millen, J. J., Sowerby, B. D., Rafter, P. T., Ellis W. K., Gravitis, V. L. Howells, E., McLennan, T. D. and Muldoon, L. J., 1984. Field Trial of a Pair Production Gauge for the On-Line Determination of Ash in Coal on a Conveyor Belt, Int. J. Appl. Radiat. Isot., 35(11), pp. 1009-1021.

Sigal, P. M., 1981. The Use of Nuclear Gauges in Coal Preparation, Proc. of 1st Australian Coal Preparation Conference, (A. R. Swanson, ed.) pp. 298-316.

Watt, J. S. and Sowerby, B. D., 1983. On-Line Determination of Ash in Coal Using "SIROASH" Gauges, in Whitmore, R. L. (ed.), Proceedings of the Second Australian Coal Preparation Conference, pp. 263-298.

Watt, J. S., 1984. Determination of Ash content of Coal On-Line on Conveyors and In-Stream Coal Slurries, IAEA Advisory Group Meeting on Gamma, X-ray and Neutron Techniques in the Coal Industry, Vienna.

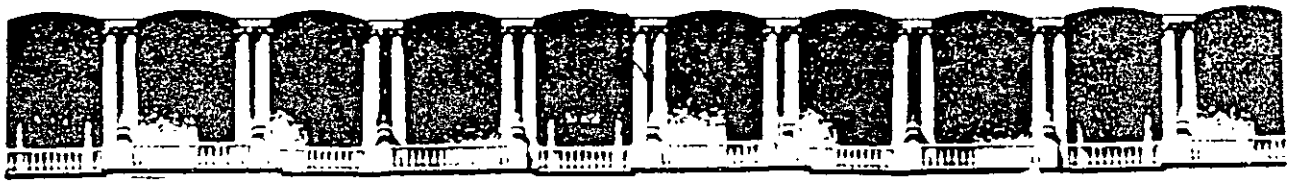

FACULTAD DE INGENIERIA U.N.A.M.
DIVISION DE EDUCACION CONTINUA

CURSOS ABIERTOS

DESARROLLO Y OPERACIÓN DE SENSORES PARA CONTROL DIRECTO Y CONTINUO EN PLANTAS DE BENEFICIO DE MINERALES Y EN LA RESTAURACIÓN DEL MEDIO AMBIENTE

Del 18 al 23 de mayo de 1998

TEMA: STUDIES RELATING TO REMOVAL OF PYRITC SULFUR FROM COAL BY FLOTATION

EXPOSITOR :DR. KOMAR KAWATRA

1998

Chapter 22

Studies Relating to Removal of Pyritic Sulfur from Coal by Column Flotation

S. K. Kawatra and T. C. Eisele

Department of Metallurgical Engineering
Michigan Technological University
Houghton, MI 49931

ABSTRACT

Although column flotation is known to be more effective than conventional flotation for cleaning fine coal, little attention has been paid to the considerable sulfur removal potential of this process. Whereas conventional flotation can only with difficulty remove pyritic sulfur from coal, flotation columns can make this separation readily due to their greater selectivity. This project has used a modified flotation column to remove pyrite from fine coal. This column has been shown to be capable of removing 70 to 85 percent of the pyritic sulfur from coal while recovering 80 to 85 percent of the total calorific value. However, the remaining pyrite is too finely disseminated to be readily removed by physical means. Currently, experimentation is in progress using bacterially-catalyzed dissolution of pyrite in acid solution to remove ultrafine pyrite and aid in the removal of coarser pyrite inclusions.

INTRODUCTION

Due to the severe environmental effects resulting from release of sulfur oxides into the atmosphere, it is necessary to limit the emissions of sulfur resulting from coal combustion. Since the majority of eastern and midwestern coals exceed the federal emission standards, these coals cannot be utilized without some form of sulfur removal before, during, or after combustion. A cost-effective method for removing sulfur prior to combustion would therefore have considerable utility.

The bulk of the sulfur present in coal is in the form of either inclusions of pyrite, or is covalently bonded into the coal structure as organic compounds such as thiophenes and mercaptans. The sulfur is typically distributed between the pyritic and organic forms in roughly equal amounts. Since the organic sulfur is an intimate part of the coal molecular structure, it cannot be effectively removed without extensive chemical processing, which is presently prohibitively expensive. However, since the pyrite is present as discrete inclusions it is amenable to removal by a physical separation of the pyrite particles from the coal. Since physical separations are less expensive than chemical techniques in most cases, and many coals can be made to meet emission standards by complete removal of the pyritic sulfur, a physical pyrite removal process is the preferred technique.

A major difficulty in the removal of pyrite by physical means is the size of the pyrite particles, a substantial quantity of which are finer than 25 micrometers. Liberation of the pyrite inclusions from the coal matrix therefore requires that the coal be ground to a fine particle size. The most effective processes for separation of very fine particles are those based on differences in surface chemistry.

Froth flotation is normally the most effective and efficient of the surface chemistry based separation technologies. It is particularly applicable to coal, as coal particles are naturally hydrophobic and therefore attach to air bubbles readily after addition of small amounts of a neutral oil. However, pyrite is also slightly hydrophobic, and conventional flotation is insufficiently selective to prevent flotation of much of the fine pyrite along with the coal. The use of various agents to depress pyrite flotation has generally not produced satisfactory results, and so column flotation has been adopted in order to improve flotation selectivity.

COLUMN FLOTATION PRINCIPLES

The basic principle of column flotation is the use of countercurrent flow of air bubbles and solid particles. This is achieved by injecting air at the base of the column, and allowing the bubbles to rise through a downward-flowing slurry. Countercurrent flow is accentuated in most columns by the addition of washwater at the top of the column, which forces all of the water which entered with the feed downward. This flow pattern is in direct contrast to that found in conventional cells, where air, water, and solids are all driven in the same directions. The result

is that columns exhibit improved hydrodynamic conditions for flotation, and thus produce a cleaner product at higher recoveries and lower power consumption. The performance differences between columns and conventional cells may best be described in terms of the collection zone size, particle-bubble contact efficiency, and fines entrainment.

Collection Zone Size

A major difference between conventional and column flotation is the size of the collection zone. Whereas in a conventional cell the particle-bubble contact occurs primarily in the high-shear region around the impeller, in a column contact occurs throughout the entire volume. A flotation column therefore provides a greater number of opportunities for particle collection, and thus provides an increased flotation rate.

Particle-Bubble Contact Efficiency

The efficiency of particle-bubble contact in a column is greater than that in a conventional machine due to the difference in the type of collisions. In column flotation, particles and bubbles travel in opposite directions, and so while the absolute velocities are low, the relative velocities are quite high. In contrast, conventional cells drive particles and bubbles in approximately the same direction, providing for high absolute velocities but with collision velocities on the same order as those found in columns. Since less energy is wasted in the column, these machines are less turbulent than conventional cells and are therefore less energy-intensive to operate.

Several flotation columns presently in use are capable of producing finer air bubbles than is possible with conventional mechanical air dispersers. This reduction in bubble size allows for improved flotation rate and selectivity, particularly for very coarse or very fine particles (Yoon and Luttrell, 1986). In the case of coarse particles, this is due to the fact that a greater number of bubbles attach to the surface, rather than only one or two (Fig. 1a). This prevents turbulence from tearing loose all of the air bubbles, and hence increases the flotation rate. For fine particles, the flotation rate increase is due to an improved contact probability. If an air bubble is very much larger than a particle, then the liquid flow around the bubble is likely to sweep the particle around, without contact every occurring. The use of smaller bubbles decreases the probability of this, and also increases the bubble surface area available for contact (Fig. 1b).

Fines Entrainment

In conventional flotation cells, a substantial amount of waste is carried into the froth by the water contained in the froth layer, thus degrading the separation. Most column flotation machines prevent this through the use of

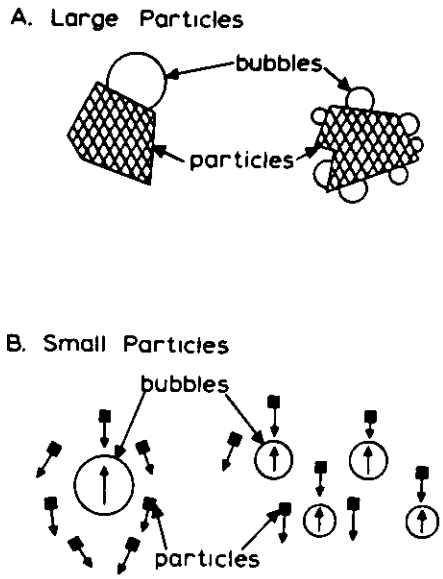

Figure 1: Effect of air bubble size on collection of A) large particles, and B) small particles.

a deep froth layer which is washed by clean water. The washwater forces all of the water entering with the feed down to the tailings outlet, largel eliminating entrainment, as shown in Figure 2. In addition to preventing feed water from entering the froth, the wash water reduces the quantity of waste material in the upper region of the column, thus establishing a concentration gradient and reducing the probability of waste material entering the froth layer. The net effect of this is that the column froth is as clean as the product obtained by several stages of conventional flotation, while the operation costs are similar to those of a single conventional stage.

The improvement in selectivity obtained with column flotation is of particular importance for the removal of pyritic sulfur from coal. This is due to the slight hydrophobicity of pyrite particles, which causes fine pyrite to tend to float with the clean coal. Addition of fuel oil aggravates this effect, as it increases the floatability of the pyrite in the same fashion as it improves the flotation of coal. The higher selectivity and lower reagent requirements of column flotation were therefore expected to allow removal of pyrite with higher efficiency than is possible with conventional flotation processes.

EXPERIMENTAL PROCEDURE

Materials

Coal samples for this project were collected from the three seams comprising the greatest

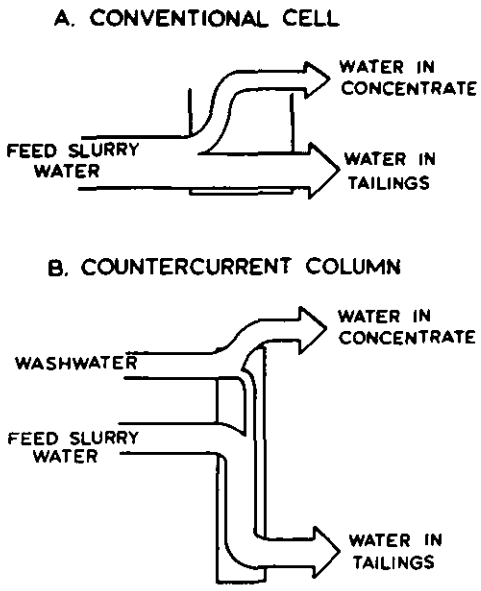

Figure 2: Distribution of water flow in a countercurrent flotation column.

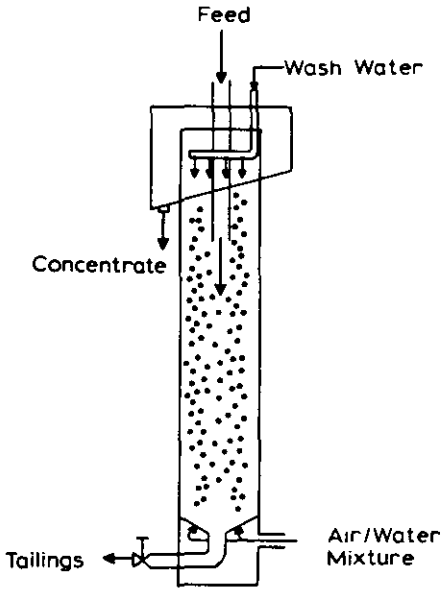

Figure 3: Schematic Diagram of a laboratory column.

reserves in Ohio (Wizzard et al, 1983): The Pittsburgh, or No. 8 seam; the Middle Kittaning, or No. 6 seam; and the Meigs Creek, or No. 9 seam. Of these coals, the Meigs Creek is generally considered to be the lowest quality, and the Middle Kittaning is considered to be the highest quality. The coal samples used were collected from the raw coal storage piles of mines operating on these seams, and stored at -20°C until needed. Washability data for the coals used is presented in Table 1.

Analyses were carried out using the methods of ASTM standards D3174-82 and D2492-8 for determination of ash content and pyritic sulfur content, respectively, a LECO SC-132 sulfur analyzer for determination of total sulfur, and a LECO Automatic calorimeter for determination of calorific value.

The column used for this work was a 3" diameter laboratory column, as shown in Figure 3. The height of this column was increased from two feet to seven feet in order to increase the residence time sufficiently for high-efficiency flotation of fines.

Initial experiments showed that, at the size required for liberation of fine pyrite, excessive quantities of ash minerals caused BTU recovery to be low. To reduce this problem a two-stage process was used, consisting of coarse flotation to remove the bulk of the ash followed by fine flotation to remove the remaining ash and the fine pyrite. A flow diagram for the process is given in Figure 4.

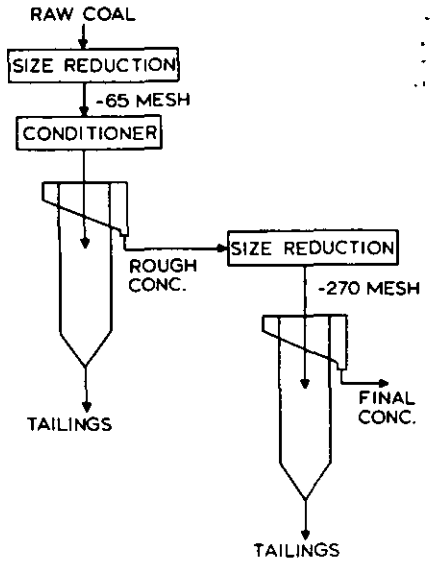

Figure 4: Flow diagram for experimental pyrite removal process. First stage feed was 90% passing 100 mesh (65 mesh top size), and second stage feed was 90% passing 400 mesh (270 mesh top size).

TABLE 1. Washability data for coals used in this project. All coals were stage crushed to pass 20 mesh for the washability determination.

A) Meigs Creek Seam

	% wt.	% Ash	% Pyritic S	% Total S	BTU/ lb.	Lb.SO_2 MM BTU
Float - 1.30	21.1	3.9	0.5	4.1	13838	5.9
Float - 1.40	61.7	7.7	0.9	4.2	13236	6.3
Float - 1.60	81.0	10.8	1.3	4.3	12786	6.7
Total	100.0	18.0	2.0	4.8	11406	8.4

B) Pittsburgh Seam

	% wt.	% Ash	% Pyritic S	% Total S	BTU/ lb.	Lb.SO_2 MM BTU
Float - 1.30	14.6	5.8	0.5	2.4	14957	3.2
Float - 1.40	43.3	8.3	0.9	2.6	14775	3.5
Float - 1.60	58.7	12.4	1.5	3.0	14086	4.3
Total	100.0	29.1	2.8	4.3	10059	8.5

C) Middle Kittaning Seam

	% wt.	% Ash	% Pyritic S	% Total S	BTU/ lb.	Lb.SO_2 MM BTU
Float - 1.30	71.2	3.0	0.2	1.9	13253	2.9
Float - 1.40	92.4	3.9	0.3	2.0	13120	3.0
Float - 1.60	95.8	4.4	0.4	2.1	13040	3.2
Total	100.0	7.9	1.1	2.2	12734	3.5

1. Raw coal was reduced to 100% -20 mesh by stage crushing with a roll crusher, mixed, split into uniform portions, and frozen.

2. Coal was ground 2.5 minutes at 40% solids in a rod mill to reduce the particle size to 90% passing 100 mesh.

3. Reagents were added as necessary, and the pulp was agitated for 1 minute at 25% solids by weight.

4. The flotation column was started and operated until the water level was uniform.

5. Coal was added to the column at the rate of 200 grams/minute, at 25% solids by weight, for a period of 20 minutes. Froth, tailings, and holdup material were collected and filtered.

6. The froth product was ground in the rod mill at 40% solids for an additional 15 minutes to achieve a particle size of 90% passing 400 mesh.

7. When necessary, additional reagent was added to the reground coal, which was then floated in the column in the manner previously stated.

8. Froth, tailings, and holdup material from each stage were dried, weighed, and analyzed to determine ash content, total sulfur, pyritic sulfur, and calorific value. Mass balances were carried out from this information to determine the precise performance characteristics.

EXPERIMENTAL RESULTS

Results for the flotation of each type of coal are presented in Table 2. Recoveries and sulfur rejections are expressed in terms of the initial feed of the first stage.

From the Stage 1 results, it is readily seen that the flotation column is extremely effective for removing ash minerals from all three coals at a fairly coarse size with excellent BTU recovery rates. In addition, 45 to 65 percent of the total pyrite is also rejected under these flotation conditions. The Stage 2 results show that grinding the coarse flotation froth and refloating allows a substantial increase in pyritic sulfur rejection, while, for the cases of the Pittsburgh and Middle Kittaning coals, maintaining a good BTU recovery rate.

Of the three coals, the Pittsburgh and Middle Kittaning seams show the greatest benefits from column flotation, with substantial ash and sulfur reductions in both stages of flotation and overall BTU recoveries for the entire process of 85-87%. The Meigs Creek sample shows a lesser change in its overall sulfur content due to its large fraction of organic sulfur and low native floatability, which also results in a lower BTU recovery in fine-particle flotation. Nevertheless, it shows acceptable results in coarse-particle flotation from the standpoint of ash removal, with a rejection of 56% of the ash while recovering 96% of the calorific value.

Although the bulk of the pyrite can be removed from the coal by the preceeding method, a fairly substantial amount remains in the clean coal. This remaining pyrite is very finely disseminated, and would require grinding to unreasonable particle sizes before liberation could be achieved. Physical separation processes are therefore not suitable for removing this ultrafine pyrite, and some sort of chemical processing is required.

While most chemical techniques are prohibitively expensive for use in coal depyritization, bacterially-catalyzed dissolution of pyrite is promising due to its low reagent costs and ability to proceed under ambient temperature and pressure conditions. However, the process is fairly slow, requiring a period of some weeks for pyrite dissolution, as is illustrated by the preliminary results shown in Figure 5. Since the dissolution rate increases as the particle size decreases, a promising approach is to use column flotation to remove the coarser pyrite particles, and bacterial leaching to remove the ultrafine, unliberated pyrite. This would result in more complete pyrite removal in a shorter time than is presently possible with either process alone. Investigation of this technique is presently in progress.

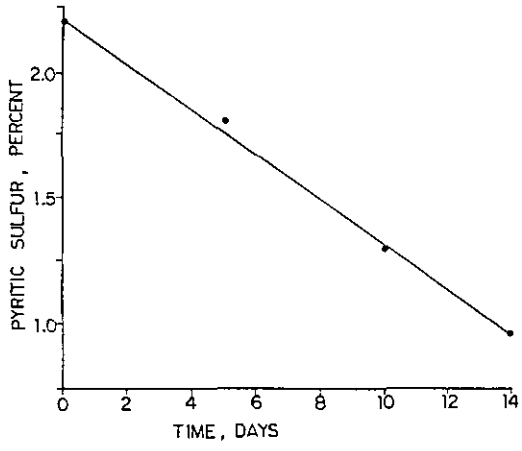

Figure 5: Removal of pyrite from Meigs Creek coal by bacterially-catalyzed pyrite dissolution.

TABLE 2. Two-Stage Column Desulfurization Results

Recoveries and sulfur rejections are expressed in terms of initial feed to first stage.

A. Pittsburgh Seam

Stage 1: 1.0 lb PPG/Ton
Stage 2: 1.0 lb PPG/Ton

	% Wt.	% Ash	% S	BTU/lb	% Pyritic Sulfur	% Organic Sulfur	Lb. SO_2 MM BTU
Feed	100	29.1	4.3	10059	2.8	1.5	8.5
Stage 1 Froth	71.0	6.6	3.4	13730	1.4	2.0	4.9
Stage 1 Tails	29.0	84.7	6.5	1009	6.3	0.2	-
Stage 2 Froth	59.8	3.6	2.7	14246	0.6	2.1	3.8
Stage 2 Tails	11.2	22.3	7.2	11180	5.5	1.7	-

Stage 1: BTU recovery = 97%, % Pyritic Sulfur rejection = 65%
Weight recovery = 71%
Stage 2: BTU recovery = 85%, % Pyritic Sulfur rejection = 87%
Weight recovery = 59.8%
Sulfur emission reduction = 55%

B. Middle Kittaning Seam

Stage 1: 1.0 lb PPG/Ton, 0.4 lb #2 Fuel Oil/Ton
Stage 2: 1.0 lb PPG/Ton, 0.1 lb #2 Fuel Oil/Ton

	% Wt.	% Ash	% S	BTU/lb	% Pyritic Sulfur	% Organic Sulfur	Lb. SO_2 MM BTU
Feed	100	7.9	2.2	12734	1.1	1.1	3.5
Stage 1 Froth	92.1	4.7	1.8	13309	0.6	1.2	2.7
Stage 1 Tails	7.9	49.7	6.9	5982	6.3	0.6	-
Stage 2 Froth	81.0	2.7	1.5	13717	0.3	1.2	2.2
Stage 2 Tails	11.1	23.5	4.0	10355	3.1	0.9	-

Stage 1: BTU recovery = 96%, % Pyritic Sulfur rejection = 45%
Weight recovery = 92.1%
Stage 2: BTU recovery = 87%, % Pyritic Sulfur rejection = 76%
Weight recovery = 81.0%
Sulfur emission reduction = 37%

C. Meigs Creek Seam

Stage 1: 1.0 lb PPG/Ton, 0.4 lb #2 Fuel Oil/Ton
Stage 2: 1.0 lb PPG/Ton, 0.1 lb #2 Fuel Oil/Ton

	% Wt.	% Ash	% S	BTU/lb	% Pyritic Sulfur	% Organic Sulfur	Lb. SO_2 MM BTU
Feed	100.0	18.0	4.8	11406	2.0	2.8	8.4
Stage 1 Froth	85.0	9.6	4.4	12896	1.2	3.2	6.8
Stage 1 Tails	15.0	67.4	7.1	3287	6.4	0.7	-
Stage 2 Froth	56.0	4.9	3.7	13670	0.4	3.3	5.4
Stage 2 Tails	29.0	18.9	5.7	11434	2.9	2.8	-

Stage 1: BTU recovery = 96%, % Pyritic Sulfur rejection = 48%
Weight recovery = 85%
Stage 2: BTU recovery = 67%, % Pyritic Sulfur rejection = 89%
Weight recovery = 56%
Sulfur emission reduction = 36%

SUMMARY

Removal of pyritic sulfur from coal by froth flotation is in general not satisfactory. This is due to the low capability of conventional flotation to distinguish between coal and pyrite particles at the fine sizes commonly necessary for pyrite liberation.

Column flotation exhibits considerably greater selectivity for fine particles than conventional cells, particularly when fine bubbles are used, and therefore has much greater capability for removing pyritic sulfur from coal.

A flotation column was constructed to maximize its ability to reject pyrite particles from coal. The column uses fine air bubbles to produce a deep washed froth while minimizing channeling and turbulence, resulting in high selectivity and the ability to operate on a wide particle size range.

The highest BTU recoveries and pyrite rejections were obtained using a two-stage process. The first stage, carried out at a top size of 90% passing 100 mesh, removed the bulk of the ash minerals, which had been found to interfere with combustibles recovery while attempting to maximize pyrite removal. The second stage was carried out at 90% passing 400 mesh and removed the bulk of the very fine pyrite particles.

Of the three coals tested, the Pittsburgh and Middle Kittaning coals derived the greatest benefits from column flotation, with pyrite rejections of 76-78% and BTU recoveries of 85-87%. Further reduction of the pyrite content by the column is limited by the liberation characteristics of the coal. For complete pyrite removal column flotation must be assisted by a chemical process, such as bacterially catalyzed pyrite dissolution.

ACKNOWLEDGMENTS

The authors gratefully acknowledge the financial support provided for this project by the Ohio Coal Development Office. The cooperation of Norton-Hambleton, Inc. in the collection of coal samples, the assistance of Deister Concentrator Co. in the construction of the flotation column, and the analytical equipment provided by Michigan Technological University are also acknowledged.

REFERENCES

Boutin, P. and Wheeler, D. A. (1967); "Column Flotation Development Using an 18 Inch Pilot Unit", Canadian Mining Journal, March 1967.

Chemical Engineering (1986); "Improved Flotation Routes Get Separations Tryouts", March 31, pp. 27-31.

Cienski, T. and Coffin, V. (1981); "Column Flotation Operation at Mines Gaspe Molybdenum Circuit", Canadian Mining Journal, March, pp. 28-33.

Clarke, A. N. and Wilson, D. J. (1983); Foam Flotation, Theory, and Applications, Marcel Dekker, Inc., New York.

Coffin, V. L. (1982); "Column Flotation at Mines Gaspe", 14th International Mineral Processing Congress, Toronto, Canada, Section 4, Paper No. 21.

Dell, C. C. (1976a); Froth Flotation, British Patent No. 1,519,075.

Dell, C. C. (1985); "The Leeds Flotation column, How it Works and What it Does", Leeds University Mining Assn. Magazine.

Dell, C. C. (1978); "Column Flotation of Coal - The Way to Easier Filtration", Mine and Quarry, 7 March, pp. 36-40.

Dell, C. C. and Jenkins, B. W. (1976b); "The Leeds Flotation Column", Seventh International Coal Preparation Congress, Sydney, paper J3.

Dobby, G. S. and Finch, J. A. (1986); "Flotation Column Scale-Up and Modelling", CIM Bulletin, May, pp. 89-96.

Dobby, G. S., Amelunxen, R., Finch, J. A. (1985); "Column Flotation: Some Plant Experience and Model Development", International Federation of Automatic Control (IFAC).

Eberts, D. H. (1986); "Flotation-Choose the Right Equipment for Your Needs", Canadian Mining Journal, March, pp. 25-33.

Hollingsworth, C. A. (1981); "The Flotaire Flotation Cell:, AIME Annual Meeting Chicago, February 22-26.

Holt, E. C., Jr. (1981); "An Engineering/Economic Analysis of the Coal-Pyrite Flotation Process", U. S. Dept. of Energy, Report DOE/PC/30149-1.

Im, C. J. and Wolfe, R. A. (1986); "Application of Flotaire Flotation Cell in Coal Preparation Plant", SME Annual Meeting, New Orleans, March 2-6, SME-AIME Preprint No. 86-36.

Mathieu, G. I. (1972); "Comparison of Flotation Column with Conventional Flotation for Concentration of a Molybdenum Ore", CIM Bulletin, May, pp. 41-45.

Mauro, F. L. and Grundy, M. R (1984); "The Application of Flotation Columns at Lornex Mining Corporation Ltd.", presented at the CIM District Six Meeting, Kamloops, B. C., October.

Miller, K. J. and Baker, A. F. (1972); Flotation of Pyrite from Coal", Bureau of Mines Technical Progress Report #51.

Moon, K. S. and Sirois, L. L. (1983); "Column Flotation", 15th Canadian Mineral Processors Annual Meeting, Ottawa, Ontario, paper no. 18.

Rubinshtein, Y. B., Dymko, N. I., Markarushina, N. I. (1976); New Apparatus for Coal Flotation", Koks i khimiya, no. 6, pp. 43-45.

Shah, Y. T., Kelkar, B. G., Godbole, S. P., Deckwer, W. D. (1982); "Design Parameters EStimations for Bubble Column Reactors", AICHE Journal, vol. 28, no. 3, pp. 353-357.

Sorokin, A. F., Filippov, A. I., Shelyakin, L. E., Medvedev, A. V., Suslow, V. I. (1978); "Cleaning Coal Slurries in Column-type Flotation Machines", Koks Khim, no. 5, pp. 6-9.

Wizzard, J. T., Cavallaro, J. A., and Deurbrouck, A. W. (1983) Sulfur Reduction Potential of the Coals of Ohio, DOE/PETC/TR-83/7 (De83012219).

Yang, D. C. (1984); "Static Tube Flotation for Fine Coal Cleaning", Proceedings of the 6th International Symposium on Coal Slurry Combustion and Technology, Orlando, FL. (PETC-DOE), pp. 582-597.

Yianatos, J. B., Laplante, A. R., Finch, J. A. (1985); "Estimation of Local Holdup in the Bubbling and Froth Zones of a Gas-Liquid Column", Chem. Eng. Sci., accepted for publication, January 1985.

Yoon, R. H. and Luttrell, G. H. (1986); "The Effect of Bubble Size on Fine Coal Flotation", Coal Preparation, vol. 2, pp. 174-192.

Zimmerman, R. E. (1979); "Froth Flotation" in Coal Preparation, J. W. Leonard (Ed.), AIME, New York, pp. 1075-, 10-104.

Zipperian, D. E. (1984); "Characteristics of Column Flotation Utilizing Aspirated Aeration", AIME Fall Meeting, Denver, October 24-26.

Zipperian, D. E. and Christophersen, J. A. (1985); "Plant Operation of The Deister Flotaire Column Flotation Cell", AIME Annual Meeting, New York, February 24-28.

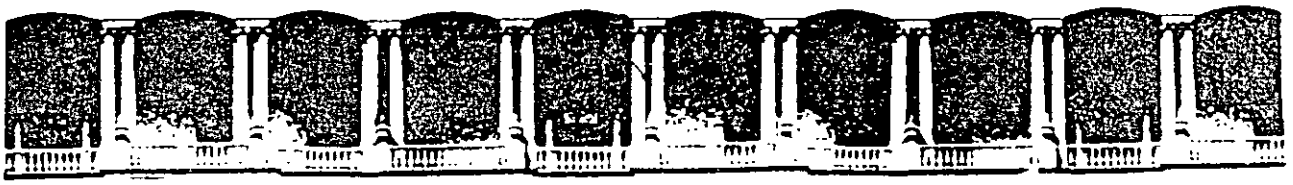

FACULTAD DE INGENIERIA U.N.A.M.
DIVISION DE EDUCACION CONTINUA

CURSOS ABIERTOS

DESARROLLO Y OPERACIÓN DE SENSORES PARA CONTROL DIRECTO Y CONTINUO EN PLANTAS DE BENEFICIO DE MINERALES Y EN LA RESTAURACIÓN DEL MEDIO AMBIENTE

Del 18 al 23 de mayo de 1998

TEMA: INFLUENCE OF TEMPERATURE ON THE ENERGY EFFICIENCY OF AN INDUSTRIAL CIRCUIT PROCESSING IRON ORE

EXPOSITOR :DR. KOMAR KAWATRA

1998

Palacio de Mineria Calle de Tacuba 5 Primer piso Deleg Cuauhtemoc 06000 México. D.F. APDO. Postal M-2285
Teléfonos. 512-8955 512-5121 521-7335 521-1987 Fax 510-0573 521-4020 AL 26

Influence of temperature on the energy efficiency of an industrial circuit processing iron ore

S.K. Kawatra and T.C. Eisele

Abstract—*In many mining operations, particularly northern open-pit mines, large seasonal variations in grinding slurry temperature can occur. It is shown in this paper that this temperature shift can cause a winter-time loss in autogenous grinding efficiency of as much as 20% if it is not controlled. Laboratory experimentation indicates that much of this effect is due to increases in slurry viscosity as the temperature is decreased. An additional effect may result from changes in rock strength upon freezing, for which possible mechanisms are discussed. However, no effect clearly resulting from rock strength changes has been definitely confirmed.*

Introduction

A great many excellent studies of the autogenous grinding process have been conducted since its development (Digre, 1979a and 1979b; Forssberg and Ekblom, 1979; Manlapig, Seitz and Spottiswood, 1979; Turner, 1979; Mokken, 1978; Stanley, 1974; Moys and Loveday, 1979; Rowland, 1981; Tangsathitkulchai and Austin, 1985; Austin, Klimpel and Luckie, 1984), allowing substantial improvements in autogenous milling performance. Nevertheless, the influence of temperature, viscosity and rheology on grinding circuit performance has largely been ignored, due both to the belief that it is of no consequence and to the expense of controlling the temperature of the mill feed. However, when the temperature approaches the freezing point of water, substantial changes in slurry rheology occur, and these changes would be expected to alter mill and hydrocyclone performance. This has been confirmed in the case of hydrocyclones (Kawatra et al., 1988 and 1989) and would be expected to be true for rod and ball mills as well (Austin, Klimpel and Luckie, 1984; Kawatra and Eisele, 1988). However, the rheology of mineral suspensions is difficult to measure (Cheng, 1984; Jinescu, 1974; Klimpel, 1982a and 1982b), particularly in real time and is therefore not used as a grinding circuit control parameter.

In addition to the rheological effects, any changes in the mechanical properties of the rock being ground, such as the hardness and fracture toughness, would also have an effect (Vitton, 1978). Mechanical changes in the rock would have the greatest effect on autogenous mill performance, as the grinding competency of the media-sized rock particles could be altered (Rowland, 1988). In extremely cold conditions, ice forms on the surface of the rock as it enters the mill, substantially changing the performance of the mill.

To understand the relative importance of each of these factors, and thus allow improved operating efficiency for grinding circuits, a study is being conducted at MTU of the effects of temperature on autogenous grinding. This study includes analysis of operating plant data, laboratory-scale experiments and pilot-scale grinding tests.

S.K. Kawatra and **T.C. Eisele**, members SME, are professor and graduate student, respectively, with Michigan Technical University, Metallurgy Dept., Houghton, MI. SME preprint 90-8, SME Annual Meeting, Salt Lake City, UT, Feb. 26-March 1,1990. M&MP paper 90-606. Manuscript July 24, 1989. M&MP paper 90-606. Discussion of this paper must be submitted, in duplicate, prior to June 1, 1991.

Theory

The effects of temperature on autogenous grinding can be immediately divided into rheological effects and mechanical effects. The rheological effects are a result of the substantial increase in the viscosity of water as the freezing point is approached. The change in apparent slurry viscosity that results from changing temperature is shown in Fig. 1. As can be seen, the effect at high percent solids is very pronounced, particularly when the temperature is quite low. This increased viscosity acts to cushion the impact of the media-sized particles, impede transport of slurry and in extreme cases cause the media to centrifuge at speeds well below the critical speed. The net result is decreased grinding rate and increased specific power consumption.

Effects resulting from changes in the mechanical properties of the rock are considerably more complicated, as they depend strongly on the specific characteristics of the rock. The major effect is a change in the mechanical strength, which alters the competency of the ore as grinding media.

One possible mechanism for strength changes with temperature is shown in Fig. 2. Here, the change is a result of water freezing in the pores and cracks of the rock, with the result depending on the degree of interconnections of the openings (Vitton, 1978). If the rock is very porous, as is the case with sandstone, the water can percolate freely through it and upon freezing form a continuous matrix that holds the rock together. This increases the fracture toughness of the rock and its competency as grinding media.

However, a hard, dense rock such as chert has relatively few, unconnected pores, which only collect water with difficulty. When the water in these pores freezes, frost cracking is likely to

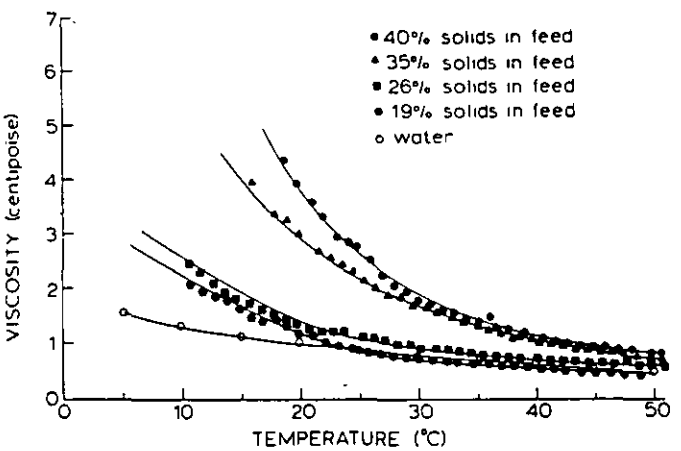

Fig. 1—Changes in apparent viscosity of fine silica slurries as a function of temperature. The viscosity was measured using a Nametre vibrating-sphere viscometer at an average shear rate of 4700 sec^{-1}, and the silica was 80% passing 270 mesh. The effect of temperature on apparent viscosity is most pronounced at high slurry solids contents and low temperatures.

Table 7—Effect of the hypochlorite concentration on hypochlorite consumption and gold extraction.*

leaching time (days)	NaOCl conc. (g/L)	NaOCl consumption (lbs/ton)	percent gold extraction
5	20.0	44.6	35.7
15	10.0	56.2	56.4
24	5.0	50.8	47.6

* pH was increased in all tests.

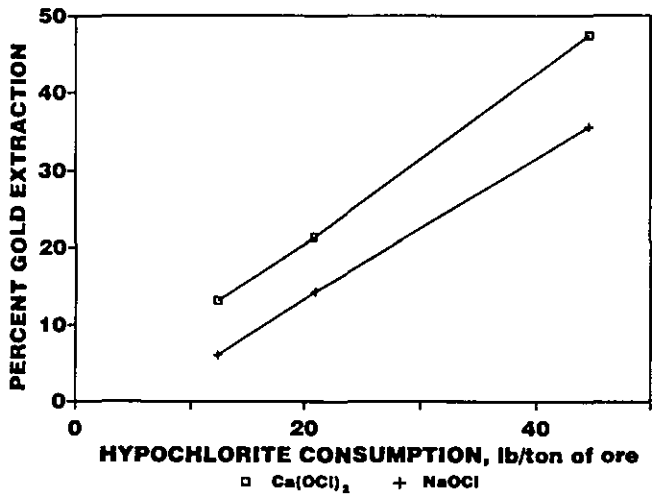

Fig. 7—Percent gold extraction as a function of sodium and calcium hypochlorite consumption. (pH was increased with 10 lb/ton of lime).

$Ca(OCl)_2$ vs. NaOCl

The effectiveness of $Ca(OCl)_2$ in comparison to NaOCl on total gold extraction is demonstrated in Fig. 7. Calcium and sodium hypochlorite concentrations were 20.0 g/L. For the same consumption, pretreatment with calcium hypochlorite resulted in higher gold extraction than with sodium hypochlorite. The reason for this behavior is not clear. Sodium and calcium hypochlorite are both ionic salts. $Ca(OCl)_2$ is a 2:1 electrolyte, while NaOCl is 1:1. Hence, the ionic strength of the former is greater than the latter for solutions of a given concentration. However, the calculated OCl^- activities for 20.0 g/L of $Ca(OCl)_2$ and NaOCl, using the extended Debye-Huckel law, are nearly the same (0.176 and 0.180, respectively). It has been found that the carbon activity is inhibited by adsorption of inorganic foulant such as $CaCO_3$ at high pH (Muir, 1987). This behavior might be partially responsible for effectiveness of $Ca(OCl)_2$ on overall gold extraction. However, $Ca(OCl)_2$ solutions usually contain an excessive amount of undissolved lime, which can cause percolation problems during pretreatment. Percolation can be improved by agglomerating the ore.

Conclusions

The following conclusions may be drawn from this investigation.

- Hypochlorite pretreatment is a promising approach for processing low grade carbonaceous gold ores.
- Gold recovery as high as 80% is achieved for 160 lbs./ton NaOCl consumption with no modifications.
- Hypochlorite consumption can be decreased by increasing pH.
- Hypochlorite is consumed by gangue materials as it percolates through the column.
- For crushed ore, calcium hypochlorite yields a 10% higher gold extraction than sodium hypochlorite for a given consumption.
- The rate of oxidation is dependent on hypochlorite concentration. However, higher concentrations could result in higher consumption.

Acknowledgement

The authors wish to thank Newmont Mining Corp. for its financial support.

References

Guay, W.J., 1980, "How Carlin Treats Gold Ores by Double Oxidation," *World Mining*, March, pp. 47-49.

Guay, W.J., 1981, "The Treatment of Refractory Gold Ores Containing Carbonaceous Material and Sulfides," *Gold and Silver Leaching—Recovery and Economics*, W.J. Schlitt, W.C. Larson and J.B. Hiskey, eds., SME-AIME, pp. 17.

Habashi, F., 1967, "Kinetics and Mechanism of Gold and Silver Dissolution in Cya Solution," Bulletin 59, Montana Bureau of Mines and Geology, pp 25

Hausen, D.M., 1981, "Process Mineralogy of Auriferous Pyritic Ores at Carlin, NV," *Process Mineralogy*, D.M. Hausen and W.C. Park, eds., TMS-AIME, Warrendale, PA, pp 271-289.

Hedley, N., and Tabachmick, H., 1958, "Chemistry of Cyanidation," *Mineral Dressing Notes*, No. 33, American Cyanamid Co., New York, pp. 31-34.

Muir, D., 1987, *Recent Advances in Gold Metallurgy*, Research and Development in Extractive Metallurgy, AusIMM, Adelaide Branch, May pp 4

Nagy, I., Markusic, P., and McCulloch, H.W., 1966, "Chemical Treatment of Refractory Gold Ores," National Institute for Metallurgy, No 38, pp 5.

Nice, R W., 1971, "Recovery of Gold from Active Carbonaceous Ores at McIntyre," *Canadian Mining Journal*, June, pp 41.

Osseo-Asare, K., Afenya, P.M., and Abotsi, G M.K, 1984, "Carbonaceous Matter in Gold Ores. Isolation, Characterization and Adsorption Behavior in Aurocyanide Solutions," *Precious Metals*, V. Kudryk, D.A. Corrigan and W W. Liang, eds.,TMS-AIME, Warrendale, PA, pp. 125-144

Radtke, A.S., and Scheiner, B.J., 1970, "Studies on Hydrothermal Gold Deposition I. Carlin Gold Deposit, Nevada. The Role of Carbonaceous Materials in Gold Deposition," *Economic Geology*, Vol 65, pp.87-102.

Sawyer, F P., and Hendrix, J L.,1988, "Sodium Hypochlorite Pretreatment for Heap Leaching Gold Ores," *Proceedings of the First International Conference on Hydrometallurgy*, (Zheng Yuhan and Xu Jiazhong, eds.), Beijing, International Academic Publishers, pp 452-456, Oct. 9-13.

Scheiner, B J., 1987, "Relation of Mineralogy to Treatment Methods for Carbonaceous Gold Ores," SME-AIME preprint No. 87-96

Scheiner, B J., Lindstrom, R E., and Henrie, T A., 1971, "Processing Refractory Carbonaceous Ores for Gold Recovery," *Journal of Metals*, March, pp 37-40.

Wells, J D., and Mullen, T E., 1973, "Gold-Bearing Arsenian Pyrite Determined by Microprobe Analysis, Cortez and Carlin Gold Mines, NV," *Economic Geology*, Vol. 68, pp. 187-201.

Wu, J-K., 1987, "Kinetics of the Reduction of Hypochlorite Ion," *Journal of the Electrochemical Society*, Vol. 134, p 1462

occur around them, resulting in a slight weakening of the rock and a loss of grinding competency.

The effect of temperature on autogenous grinding is therefore highly variable and difficult to predict. No large effect is seen unless the water in the ore freezes, and this only occurs when the ore is exposed for some time before processing, as is the case in open-pit mines. An additional effect that can occur if the ore is seriously chilled is the formation of ice on the surface of the rock when it is added to the mill. The ice must then either melt or be ground away before grinding of the ore particle can commence, resulting in a reduced grinding rate. However, this requires both severely chilled ore and a near-freezing mill slurry, and should therefore not be a frequent problem.

For non-porous ores, each of these factors will result in a loss of autogenous milling efficiency. However, it has not been determined which of these phenomena is most important, or to what extent they reduce efficiency in real situations. In order to determine this, quantitative data are needed for both overall plant operation and for laboratory experiments designed to suppress all but one effect.

Plant studies

An iron ore processing plant that is subjected to large seasonal temperature variations was studied. This plant uses a fully autogenous grinding circuit, as shown in Fig. 3. Initially, plant personnel observed a significant seasonal variation in feed rate, as is illustrated in Fig. 4. This trend was observed for four years and so is unlikely to be entirely due to normal variations in ore characteristics. When com-

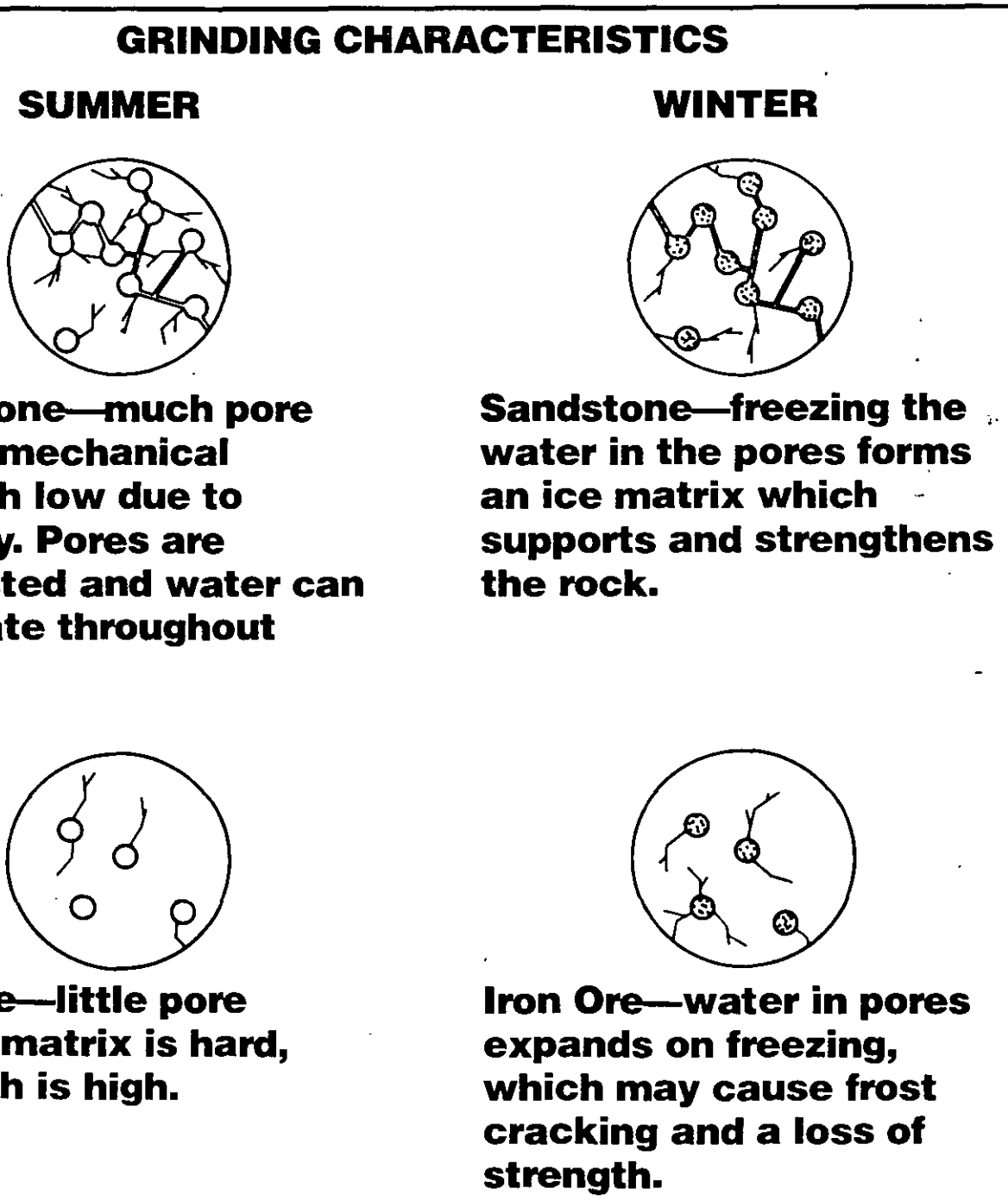

Fig. 2—Mechanism for changes in rock strength resulting from freezing of pore water. This effect is more important than changes in the hardness of the rock proper.

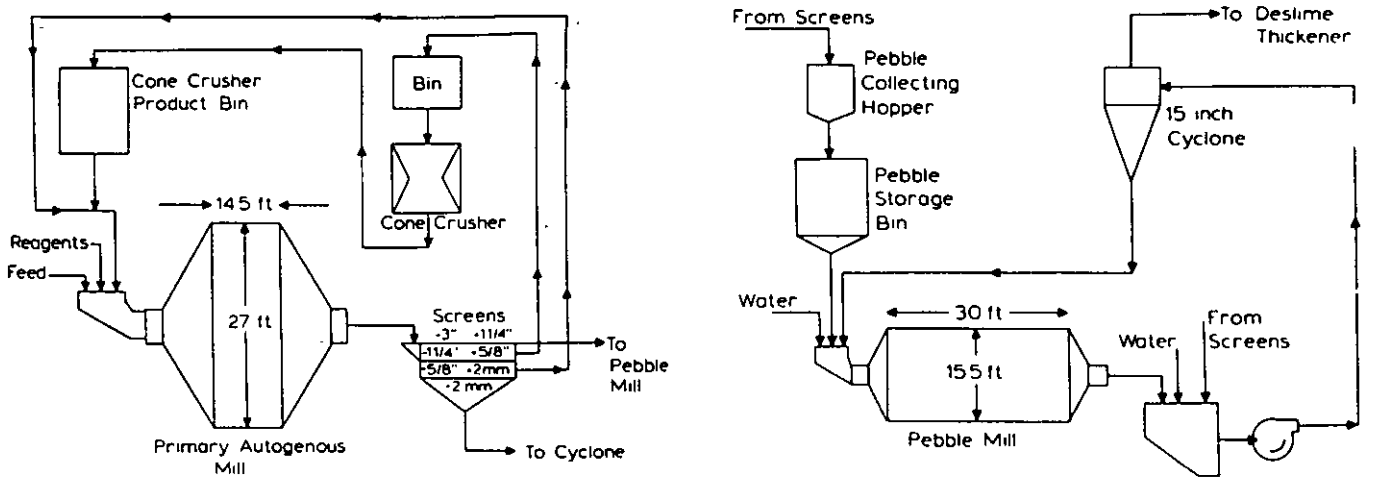

Fig. 3—Schematic of the grinding circuit discussed in this paper. The circuit is fully autogenous, with critical-size material crushed by a cone crusher to prevent buildup.

pared with measurements of the feed water temperature, which are also plotted in Fig. 4, it appears that the temperature effect is relatively slight until temperatures fall below 10° C. At temperatures below this value, the drop in throughput becomes quite pronounced.

Subsequently, the specific power consumption was computed for the primary, secondary and overall grinding circuits and plotted against the feed water temperature. Monthly averages were used to minimize the effects of variation in ore quality. The results for the primary autogenous mill are given in Fig. 5, where a pronounced decrease in specific energy consumption occurred as the temperature increased. A similar effect is shown in Fig. 6 for the pebble mill, although the trend is less pronounced. This is due to the warming of the pulp in the primary mill, which reduces the temperature fluctuation seen by the pebble mill. The overall result for the circuit is as shown in Fig. 7, which shows a total seasonal efficiency variation of 18% in the course of a year.

In addition to the efficiency measurements, plant personnel observed that the quantity of critical-size material circulated to the crusher increased in the winter, as indicated by Fig. 8 (Rowland, 1988; Kampe, 1988). This indicates that coarse rock may be more readily shattered at lower temperatures. Since large rocks are needed for effective autogenous grinding, the increased rate at which they are shattered into relatively ineffective critical-size material when the temperature is lowered results in reduced grinding efficiency. However, it is not clear whether this is due to changes in rock strength or to changes in the transport characteristics in the mill arising from rheological effects.

Laboratory studies

Laboratory tests were carried out primarily to determine the extent to which rheology alone would be expected to affect autogenous grinding. These experiments used a 20-cm-diam x 30-cm-long mill, rotating at 64 rpm with four 0.5-cm lifter bars. The mill and ore charge were heated in a forced-air drying oven for elevated temperature experiments and chilled using a freezer and an ice-water bath for low-temperature experiments. Polyurethane foam insulation was used to help keep the mill at a uniform temperature.

The results of initial experiments using Jacobsville sandstone have been previously reported (Kawatra et al., 1989). Further experiments were conducted using an iron ore sample from a local mine. The ore was crushed and mulled to the size

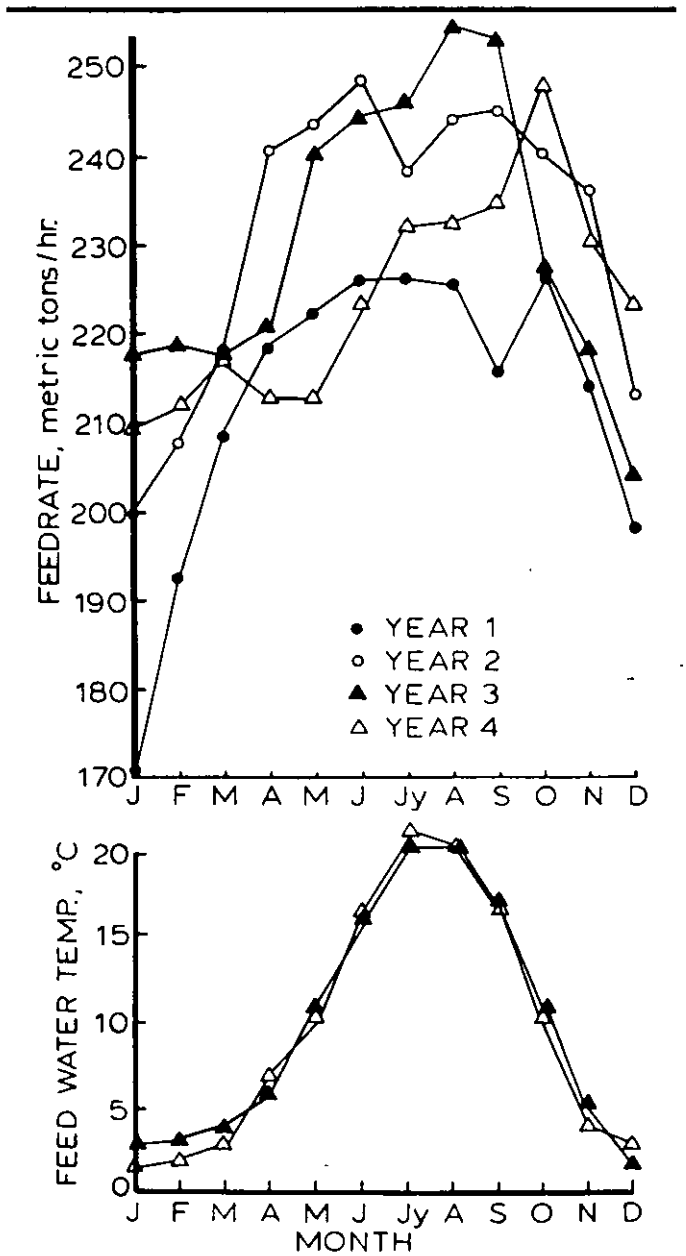

Fig 4—Seasonal variations in grinding circuit throughput rate as compared to average monthly feed water temperatures. A consistant seasonal trend is shown, with the greatest change in throughput exhibited during those months when the water temperature drops below approximately 10° C.

Table 1—Size Distribution of Charges for Laboratory Grinding Experiments	
Size, millimeters	**wt.%**
50.8x38.1	41.5
38.1x25.4	25.2
25.4x19.0	15.1
19.0x12.7	13.1
12.7x 9.5	5.1
−9.5	0.0
	100.0

distribution given in Table 1, and each experiment used a 5.0-kg charge in 2 L of water. Six experiments were conducted consisting of three sets of duplicate tests at 2°-9° C, 24°-26° C, and 84°-62° C. For each experiment, the ore, water and mill were adjusted to temperature, and the ore was ground for 30 min. The slurry viscosity and quantity of -100 mesh material were then determined, the -100 mesh material was returned to the mill, the temperature was readjusted and the cycle was repeated. Viscosity was measured using a Brookfield viscometer fitted with a UL adapter for low viscosity measurements. Results of these experiments are given in Table 2.

Plotting these data as in Fig. 9 again shows a definite dependence of fines production on temperature. However, when grinding rate is plotted against viscosity, as in Fig. 10, it is evident that some factor other than viscosity is responsible for a portion of the change in grinding rate.

Discussion

In a plant situation, uncontrolled temperature changes can produce sizable changes in milling efficiency. The plant

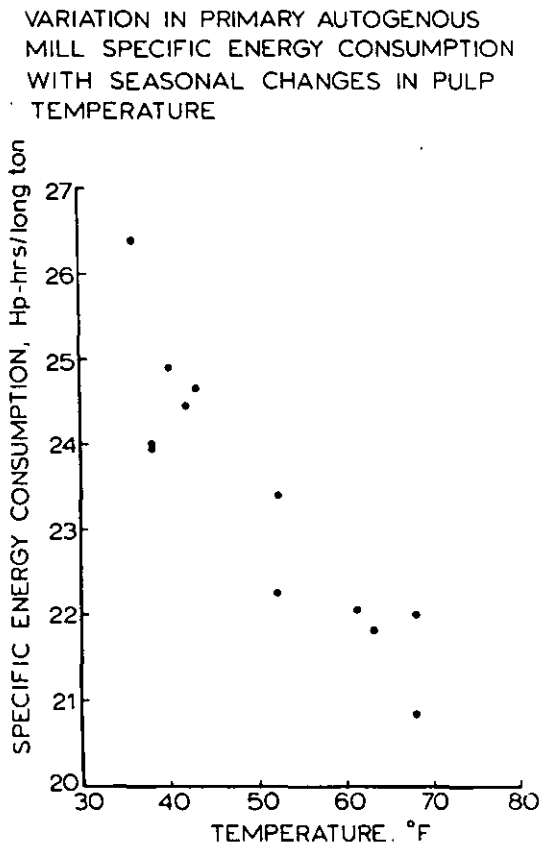

Fig. 5—Monthly change in specific energy consumption of the primary autogenous mill as a function of feed water temperature.

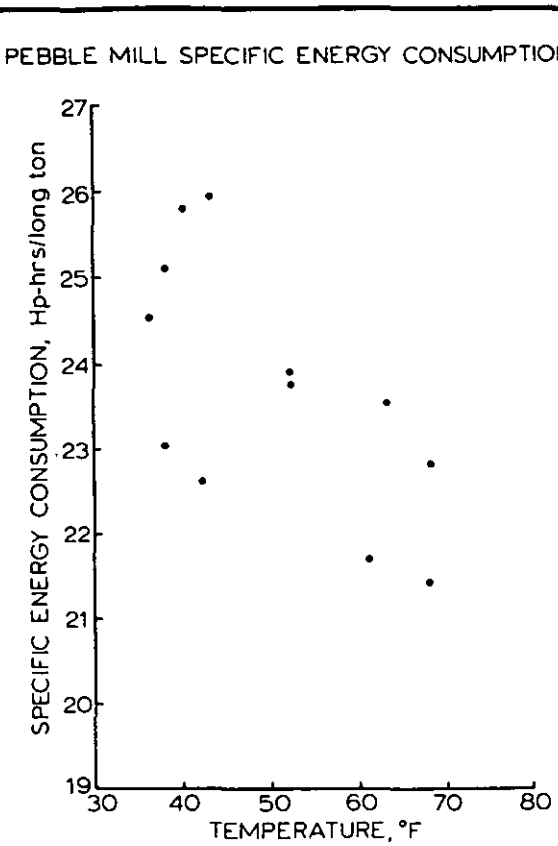

Fig. 6—Monthly change in specific energy consumpion of the pebble mill as a function of feed water temperature.

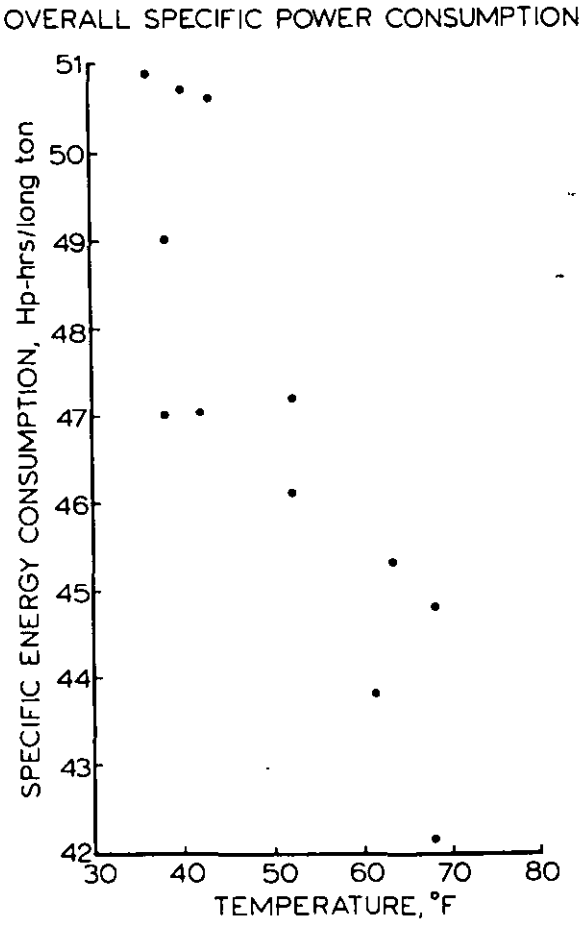

Fig. 7—Monthly change in specific energy consumption of the overall grinding circuit as a function of feed water temperature.

Table 2—Results for Laboratory Grinding Experiements of Hematite Ore

	Grinding time (min.)	Temp. (°C)	Viscosity (cp)	Shear Rate (sec^{-1})	-100 mesh product (grams)
	30	4-9	1.57	73.42	69
	60	2-7	1.74	73.42	126
Test	90	2-9	1.82	73.42	178
1-1	120	2-7	1.93	73.42	206
	150	2-7	1.99	73.42	230
	180	2-6	2.18	73.42	248
	30	24-25	1.05	73.42	76
	60	26	1.23	73.42	145
Test	90	25	1.42	73.42	197
1-2	120	25	1.61	73.42	249
	150	25	1.78	73.42	289
	180	25	1.92	73.42	327
	30	83-64	0.83	73.42	85
	60	84-64	0.90	73.42	155
Test	90	84-64	0.97	73.42	218
1-3	120	84-64	1.02	73.42	281
	150	84-62	1.17	73.42	327
	180	84-63	1.28	73.42	366
	30	2-7	1.66	73.42	67
	60	2-8	1.72	73.42	122
Test	90	2-10	1.78	73.42	176
2-1	120	2-7	1.90	73.42	200
	150	2-6	2.02	73.42	227
	180	2-7	2.15	73.42	255
	30	24-25	1.06	73.42	79
	60	24-25	1.24	73.42	144
Test	90	25	1.43	73.42	195
2-2	120	25	1.62	73.42	248
	150	25	1.80	73.42	290
	180	25	1.94	73.42	329
	30	84-65	0.85	73.42	86
	60	84-65	0.90	73.42	157
Test	90	84-64	0.96	73.42	219
2-3	120	84-64	1.02	73.42	280
	150	84-63	1.15	73.42	325
	180	84-64	1.27	73.42	364

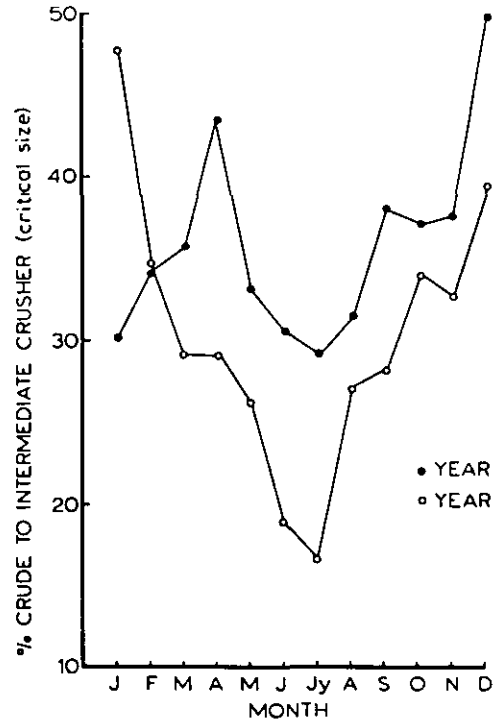

Fig. 8—Monthly variation in critical-size production as measured by the tonnage of material circulated to the crusher.

data presented here show a seasonal efficiency shift of approximately 18% for the overall circuit and more for the primary autogenous mill alone. It is difficult to be completely certain of the precise mechanism, but it is likely that most of the effect is due to viscosity changes. It is seen th the temperature effect is much less pronounced in the peb mill, but this is almost certainly due to the warming that occurs in the primary mill and not to inherently lower temperature sensitivity in the pebble mill. The change in production of critical-size material in the primary mill may be a result of changing rock strength, but it is possible that increasing viscosity forces the media-size particles to migrate to those portions of the charge where the impacts are most severe, causing them to break up more rapidly (Rowland, 1988). The seasonal shifts of mill throughput show clearly that the greatest change occurs at temperatures below about 10° C. It is therefore evident that simply maintaining the temperature above this point will greatly reduce the seasonal throughput variation. This may be accomplished by prevent-

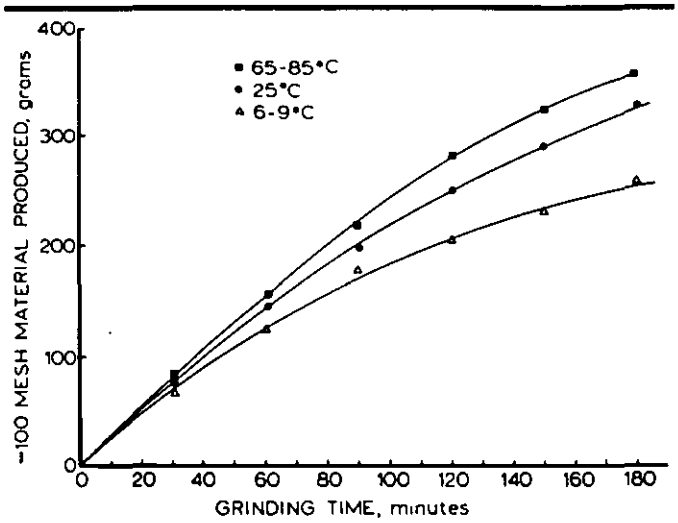

Fig. 9—Variation in laboratory-scale fines production as a function of time and temperature for an iron ore. The behavior of the non-porous iron ore is very similar to that of the porous sandstone.

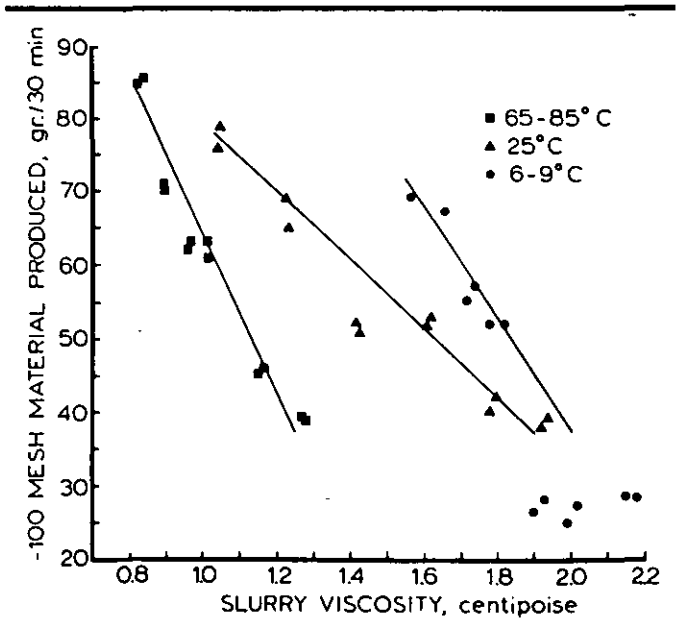

Fig. 10—Grinding rate vs. viscosity for the six laboratory-scale iron ore grinding experiments. While decreasing the viscosity produces an increase in the grinding rate, this is obviously not the only effect occurring in these experiments.

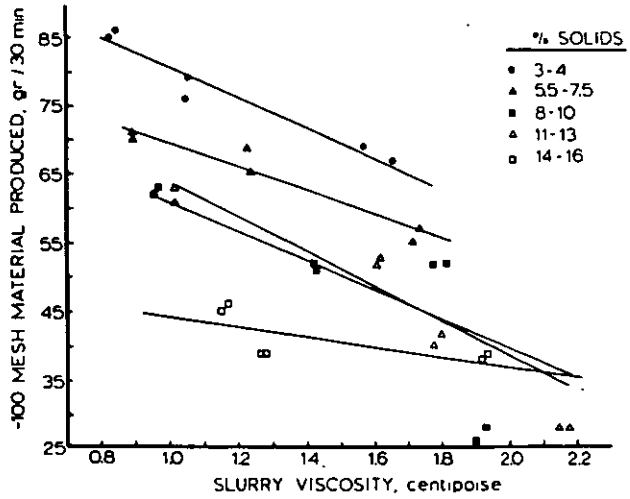

Fig. 11—Viscosity vs. grinding rate for the six laboratory-scale grinding experiments, correlating those measurements that contained similar amounts of -100 mesh fines. The listed percent solids ranges represent the ratio of -100 mesh material to water. The resulting lines are roughly parallel, indicating that buildup of fines is responsible for the drop in grinding rate with time.

ing the recycle water from being chilled and by thawing the ore before grinding.

From the laboratory experiments, it is readily seen that the changes in grinding rate are closely tied to slurry viscosity. However, in these experiments the viscosity was not the only factor influencing fines production, as shown in Fig. 10. If viscosity were the only relevant factor, tests for all three temperatures should have followed the identical grinding rate vs. viscosity curve. The second factor appears to be the quantity of fines in the suspension, as plotting grinding rate vs. viscosity for only those tests with similar quantities of fines generates a series of roughly parallel lines as in Fig. 11. It is likely that as the fines are accumulating, work is being expended to make the fines finer rather than generating additional fines. It is also possible that the increasing slurry density is cushioning the impacts due to increased buoyancy, thus further retarding the grinding rate.

Conclusions

From this investigation, the following conclusions are drawn:

1. In autogenous milling, temperature can significantly influence the grinding efficiency, particularly if the temperature falls below about 10° C. These efficiency changes can be reduced by preventing recycle water from becoming chilled, and by thawing frozen rock before grinding. Since the magnitude of the efficiency change is reduced at higher temperatures, heating the mill slurry to higher temperatures is unlikely to provide significant benefits.

2. Laboratory experiments indicate that the effect of slurry rheology changes with temperature is a significant factor in the grinding rate for both porous and non-porous rock types, with higher temperatures resulting in reduced viscosity and hence increased grinding rate.

Acknowledgements

This research has been supported by the Department of the Interior's Mineral Institute Program administered by the Bureau of Mines through the Generic Mineral Technology Center for Comminution under grant number G1175149.

References

Austin, L.G., Klimpel, R.R., and Luckie, P.T., 1984, *Process Engineering of Size Reduction: Ball Milling*, SME-AIME, New York, pp. 385-406.

Cheng, D C-H., 1984, "Further Observations on the Rheological Behavior of Dense Suspensions," *Powder Technology*, Vol. 37, pp 255-273.

Digre, M., 1979a, "Autogenous Grinding in Relation to Abrasion Conditions and Mineralogical Factors," *Proceedings of the Autogenous Grinding Seminar*, Trondheim, Norway, Session A—Fundamentals, paper A1

Digre, M., 1979b, "Autogenous Grinding Testing and Scale-Up," *Proceedings of the Autogenous Grinding Seminar*, Trondheim, Norway, paper F5.

Forssberg, E., and Ekblom, K., 1979, "Experience of Autogenous Grinding in Sweden," *Proceedings of the Autogenous Grinding Seminar*, Trondheim, Norway, Session A—Fundamentals, paper A2.

Jinescu, V.V., 1974, "The Rheology of Suspensions," *International Chemical Engineering*, Vol. 14, No. 3, pp 397-420.

Kampe, H., 1988, personal communication.

Kawatra, S.K., and Eisele, T.C., 1988, "Rheological Effects in Grinding Circuits," *International Journal of Mineral Processing*, Vol 22, pp. 251-259

Kawatra, S.K., Eisele, T.C., Zhang, D.X., and Rusesky, M.T., 1988, "Effects of Temperature on Hydrocyclone Efficiency," *International Journal of Mineral Processing*, Vol. 23, pp 205-211.

Kawatra, S.K., Eisele, T.C., Zhang, D X., and Rusesky, M T., 1989, "Effects of Seasonal Temperature Changes on Autogenous Milling Performance," SME-AIME Meeting, Las Vegas, Nevada, Feb. 27-March 2, 1989.

Klimpel, R.R., 1982a, "Slurry Rheology: Influence on the Performance of Mineral/Coal Grinding Circuits," *Mining Engineering*, December 1982, pp 1665-1668, and January 1983, pp. 21-26.

Klimpel, R.R., 1982b, "Laboratory Studies of the Grinding and Rheology of Coal-Water Slurries," *Powder Technology*, Vol 32, pp 267-277.

Manlapig, E V., Seitz, R A., and Spottiswood, D J., 1979, "Analysis of the Breaking Mechanism in Autogenous Grinding," *Proceedings of the Autogenous Grinding Seminar*, Trondheim, Norway, Session A—Fundamentals, paper A3.

Mokken, A H., 1978, "Progress in Run-of-Mine (Autogenous) Milling as Originally Introduced and Subsequently Developed in the Gold Mines of the Union Corporation Group," *Eleventh Commonwealth Mining and Metallurgical Congress*, Hong Kong, Institution of Mining and Metallurgy.

Moys, M.H., and Loveday, B.K., 1979, "Autogenous Milling Research at the South African National Institute for Metallurgy," *Proceedings of the Autogenous Grinding Seminar*, Trondheim, Norway, paper F2.

Rowland, C.A., 1981, "Pilot Plant Data for the Design of Primary Autogenous and SemiAutogenous Mills," *CIM Bulletin*, November 1981.

Rowland, C A., 1988, personal communication.

Stanley, G G., 1974, "Mechanisms in the Autogenous Mill and Their Mathematical Representation," *Journal of the South African Institute of Mining and Metallurgy*, November 1974.

Tangsathitkulchai, C., and Austin, L.G., 1985, "The Effect of Slurry Design on Breakage Parameters of Quartz, Coal, and Copper Ore in a Laboratory Ball Mill," *Powder Technology*, Vol 42, pp. 287-296

Turner, R.R., 1979, "Primary Autogenous Grinding—A Study of Ball Charge Effects," *Proceedings of the Autogenous Grinding Seminar*, Trondheim, Norway, Session B—Mill and Mill Circuit Design, paper A4.

Vitton, S J., 1978, "An Experimental Study of the Effects of Low Temperature on the Mechanical Properties of Iron Ore," unpublished M.S. thesis, Michigan Technological University.

Investigation to control mine dust using surfactants and a new approach for eliminating their negative effect on flotation

M.A. Cristovici

Abstract—*The use of surfactants as wetting agents to suppress sulfide ore dust has been investigated. Numerous surfactants were examined to determine their characteristics and to investigate their ability to improve the wetting of the sulfide ore dust. However, the surfactants selected as suitable dust suppressors proved to have a negative effect on the flotation of ore contaminated with such reagents. A method was developed to eliminate the detrimental influence of dust-suppressing surfactants. It consisted of surfactant adsorption on activated carbon and separation of loaded carbon prior to flotation. The technique is simple and requires minimal changes in the plant flowsheet.*

Introduction

Dust measurements in mines clearly indicate that the major mineral dust exposure is due to loading and transport of ore from mining areas (Knight, 1980; Hamilton and Knight, 1963). One approach to the solution of this dust problem is the application of water sprays to reduce dust dispersion. Wetting of broken rock is very effective in preventing fine dust from becoming airborne because the water binds the dust to the larger lumps. Experiments have shown that most common rocks are readily wetted by water. However, the dust originating from sulfide minerals exhibits an inherent hydrophobicity that makes water spreading on the surface of the particles more difficult, creating problems in dust suppression.

Surfactants are known to be able to reduce the surface tension of water, facilitating the wetting and suppression of sulfide ore dust, but, on the other hand, flotation of sulfide ore is susceptible to interference by surfactants.

A laboratory study was initiated to examine the effects of surfactants on the wetting of sulfide ore dust Numerous surfactants were investigated for their properties and their ability to suppress dust, and some were selected as suitable dust suppressors.

However, further testwork indicated that the presence of the wetting agents in the ore adversely affected the efficiency of minerals separation in the flotation process. A research program was started to investigate the possibility of eliminating the detrimental effect of the surfactants on flotation results.

Several possibilities were explored, and a technique was developed by which the surfactants used as dust suppressors were adsorbed on activated carbon and removed from the slurry prior to the flotation process. This paper covers the results of the investigation carried out to select suitable surfactants as potential dust suppressors and to annihilate their negative effect on flotation.

M.A Cristovici, member SME, is a research scientist with the Dept. of Energy, Mines and Resources, CANMET, Ottawa, Ontario, Canada.
SME preprint 90-56, SME Annual Meeting, Salt Lake City, UT, Feb. 26-March 1, 1990. M&MP paper 90-612. Manuscript Nov. 8, 1990. Discussion of this paper must be submitted, in duplicate, prior to June 1, 1991.

Experimental materials

Ore sample

A sample of copper sulfide ore from Opemiska Division of Falconbridge Co. was used for selecting suitable wetting agents as potential sulfide dust suppressors. The sample also served to investigate the surfactant's influence on copper flotation and to develop the technique for surfactant removal prior to the mineral extraction process. Table 1 gives the head assay of the sample.

Table 1—Head Assay

Element:	Pb	Cu	Zn	S	Fe	SiO_2
Assay %:	0.02	4.39	0.08	5.27	15.98	41.83

The sample was crushed to minus 12 mm and then split into two portions. One portion was screened through a 37-μm sieve. The minus 37-μm fraction represented the dust product that was used to test the surfactants' wetting properties. The other pa the minus 12-mm sample was further crushed to minus 1.7 ι. and was employed for flotation experiments.

Wetting agents

A large number of surfactants were examined. Following are briefly described some that were investigated in more detail:

Coherex, a dust control agent, was developed by the Golden Bear Division of Witco Chemical Corp. It is a stable, nonvolatile emulsion consisting of 60% petroleum resins and 40% wetting solution.

Tergitol 08, also known as Niaproof anionic surfactant 08, is available in an aqueous solution containing 40% of sodium 2 ethylhexyl sulfate. It is manufactured by Bate Chemical.

Sterling NP - 10 is a nonyl phenol polyglycol ether condensate, a surfactant of non-ionic type. Sterling Snow White 750 is a cationic fabric softener product containing 75% active substance. Both surfactants are produced by Canada Packers.

Aerosol OT surfactants provided by Cyanamid are sodium dioctyl sulphosuccinamates of anionic type.

The surfactants offered by Armak (presently AKZO) were: CES 372, a monooleate ester of a polyethylene glycol; CES - 265, also called ethofat T/25, a polyethylene glycol ester; and Ethomeen C/15, a polyoxyethylene cocoamine.

Silicone glycol copolymers of non-ionic type (ex. E-5753- 11-1) the X2-8063, a cationic aminofunctional silicon emulsi and Q43667, a silicone polycarbinol were provided by D Corning.

Antarox BL are non-ionic, modified linear aliphatic polyethers manufactured by G.A.F.

Wetting agents supplied by Alchem Inc. included Dust-Ban 8A04, a specially formulated organic activating agent, 8A07, an

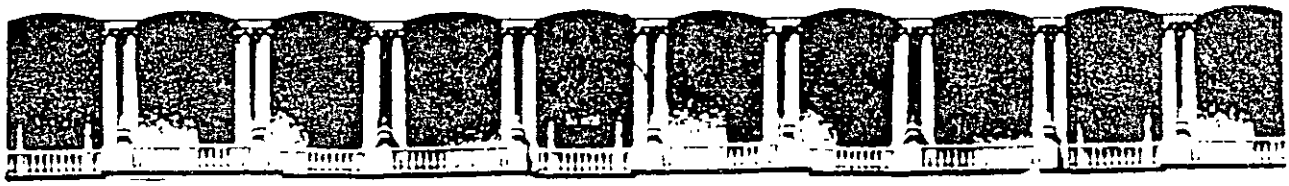

FACULTAD DE INGENIERIA U.N.A.M.
DIVISION DE EDUCACION CONTINUA

CURSOS ABIERTOS

DESARROLLO Y OPERACIÓN DE SENSORES PARA CONTROL DIRECTO Y CONTINUO EN PLANTAS DE BENEFICIO DE MINERALES Y EN LA RESTAURACIÓN DEL MEDIO AMBIENTE

Del 18 al 23 de mayo de 1998

TEMA: TEMPERATURE EFFECT ON GRINDING CIRCUIT PERFORMANCE

EXPOSITOR :DR. KOMAR KAWATRA

1998

Temperature effect on grinding circuit performance

S. K. Kawatra, T. C. Eisele, D. X. Zhang, and M. T. Rusesky

Abstract—*It has been observed in some mineral processing plants that grinding circuit efficiency varies seasonally, such as in some plants which are located in the northern US and Canada and undergo large seasonal temperature changes, with the grinding circuit efficiency different between summer and winter. This indicates that the temperature of grinding circuit slurry has a noticeable effect on grinding performance. The effect has rarely been studied. To this end, an investigation to examine the effects of changing temperature on efficiency and determination of the mechanism responsible has been carried out. Plant investigations and laboratory experiments have been conducted in order to study hydrocyclones. It was demonstrated that when the pressure drop is held constant, the $d_{50(c)}$ size decreased approximately linearly with increasing temperature, while the shape of the reduced efficiency curve remained nearly constant. This effect was determined to be due to changes in slurry viscosity with temperature.*

Introduction

As is well known, the single most energy intensive unit operation in mineral processing is comminution. Size reduction consumes approximately 25% of the total energy used in mineral concentrators, while typically less than 5% of this energy is consumed in the production of new mineral surface (NMAB, 1981). Thus, there is much room for improvement in grinding operations, and even a slight increase in efficiency would produce substantial energy savings. Such improvements are most readily obtainable by optimization and control of mill operating conditions.

A number of investigators (Austin, et al., 1984; El-Shall and Somasundaran, 1984; Klimpel, 1982, 1982a, 1983, 1984; Fuerstenau, et al., 1985) have determined that rheology has a large effect on the efficiency of grinding mills. Four parameters influence the rheology of slurry in a grinding mill: solids content, particle size distribution, chemical environment, and temperature. The effect of temperature is particularly significant in areas with large seasonal temperature variations such as the northern United States and Canada (Kampf, 1985). However, due to the unavailability of suitable viscometers and measurement techniques for mineral slurries, the control of mill rheology, especially the effects of temperature on efficiency of grinding mill and hydrocyclones, has been neglected or rarely studied. The investigation described here was therefore carried out to determine the magnitude and nature of temperature effects on hydrocyclone operation.

S.K. Kawatra, T.C. Eisele, members SME, **D.X. Zhang**, and **M.T. Rusesky**, member SME, are with Dept. of Metallurgical Engineering, Michigan Technologicval University, Houghton, MI. SME preprint 88-1, SME Annual Meeting, Phoenix, AZ, January. M&MP paper 88-639. Manuscript June 12, 1987. Discussion of this paper must be submitted, in duplicate, prior to July 31, 1989.

Experimental Work

Plant Studies

The plant site that was chosen for obtaining the samples was an iron ore processing plant, which experiences substantial seasonal temperature variations. The plant has primary autogenous and secondary pebble mill grinding. The cyclones are operated in parallel banks of nine, with seven of the classifiers in use at any one time. The cyclones are Krebs model D15B-852-M271. This plant processes a very finely disseminated iron ore which requires grinding to -25 μm for liberation.

Sampling was carried out in the summer and in the winter in order to achieve the greatest temperature variation. Pulp temperature ranged from a high of 20°C (68°F) in the summer to a low of 3.3°C (38°F) in the winter. The resulting corrected efficiency curves for these conditions are shown in Fig. 1.

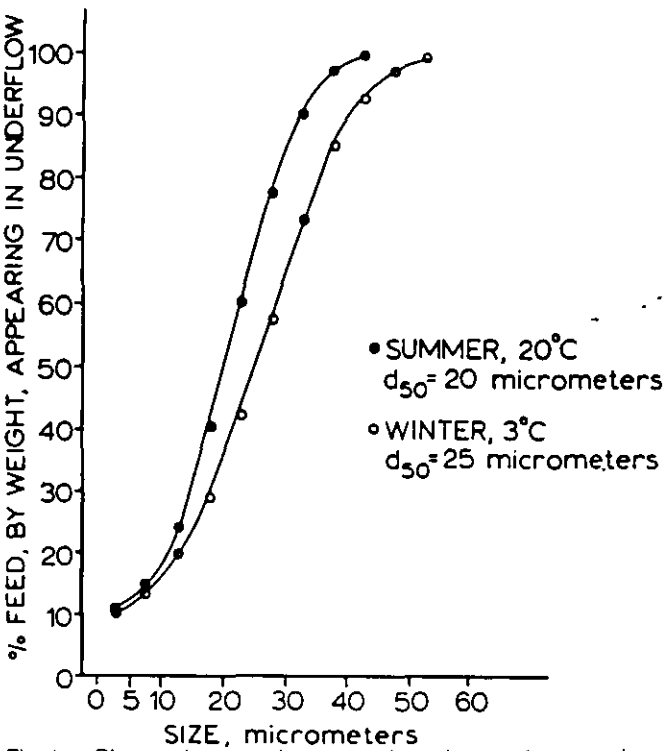

Fig. 1 — Observed seasonal variations in cyclone performance in an iron ore processing plant.

Laboratory Studies

Laboratory experiments were carried out using a Krebs hydrocyclone. The cyclone parameters were as follows: feed inlet diameter, 1.2 in. (3 cm); vortex finder diameter, 1 1/2 in. (3.8 cm); apex diameter, 7/8 in. (2.2 cm); cyclone diameter, 4 in. (10.2 cm); and pressure drop, 10 psi (69 kPa).

The cyclone was mounted on a laboratory test rig in closed circuit with a Warman centrifugal pump and a slurry tank. The cyclone overflow and underflow streams discharged freely into separate launders, which were used to either remove simultaneous samples from two streams or to recombine the streams before returning them to the slurry tank. The slurry temperature sensor was mounted in the feed sump, and a diaphragm-type pressure gage and an ultrasonic doppler flowmeter were both mounted on the cyclone inlet line. Apparent slurry viscosity was also measured at the cyclone feed inlet using a Namotre Model 810 vibrating sphere viscometer. Flowrate, viscosity, and temperature data were continuously collected and logged by a HP-85 computer.

The mineral used for these experiments was pure silica obtained from Ottawa Sand Co., Ottawa, IL. The particle size distribution was obtained using a Leeds and Northrup Microtrac particle size analyzer and is shown in Table 1. The temperature range was from 50 to 11°C.

Table 1 — Size Distribution of Ground Ottowa Sand

Size, μm	Cumulative Wt % Passing
176	100
125	97
88	93.6
62	75 5
44	49.8
31	34.9
22	24.0
16	17.5
11	12.7
7.8	8 1
5.5	5.1
3.9	3.9
2.8	2.0

Results and Discussion

A summary of the data collected in the laboratory cyclone experiments is presented in Table 2. The Rf is the water split, and α is the shape parameter from Lynch's equation,

$$y = \frac{e^{\alpha x} - 1}{e^{\alpha x} + e^{\alpha} - 2} \quad \text{where } x = \frac{d}{d_{50(c)}}.$$

Table 2 — Summary of Laboratory Cyclone Test Results

Test	Temperature °C	R_f, %	$d_{50(c)}$, μm	α	Viscosity Centipose
1	48.8	22.0	21 0	2 83	8.9
2	40.4	23.3	23 6	2 85	10 4
3	35.2	24 3	25 0	2 54	10 6
4	30.0	23.2	26.8	2.74	10 3
5	25.0	24.7	29.1	2.44	10 8
6	20.0	23 5	30 0	2.12	12.0
7	15 1	23.9	31 4	2 69	14 2
8	11.1	24 4	32 4	2.54	13 8

The values for α and $d_{50(c)}$ were determined by simplex optimization after the data was corrected for *Rf*.

It is clear from both plant and laboratory data that $d_{50(c)}$ does indeed decrease with increasing temperature in Figures 1 and 2. When $d_{50(c)}$ is plotted against temperature it is further observed that the relationship is essentially linear, as is illustrated by Fig. 3. From Fig. 2 it is clearly shown that increasing temperature shifts the efficiency curve towards finer sizes. However, the sharpness of the reduced efficiency curve for all of the temperatures is essentially unchanged, as shown by the curve in Fig. 4. This result is in agreement with the results of Lynch (1977), who stated that the reduced efficiency curve is a function only of cyclone geometry and particle characteristics in slurry and is largely unchanged by alternations in operating conditions.

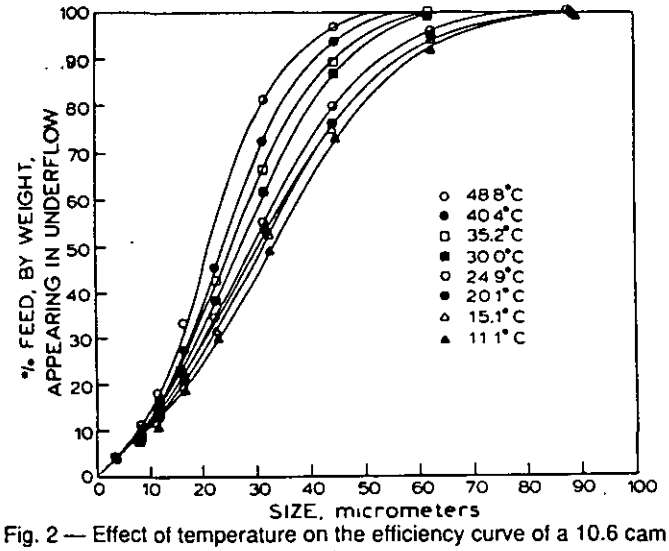

Fig. 2 — Effect of temperature on the efficiency curve of a 10.6 cam (4 in) hydrocyclone processing silica.

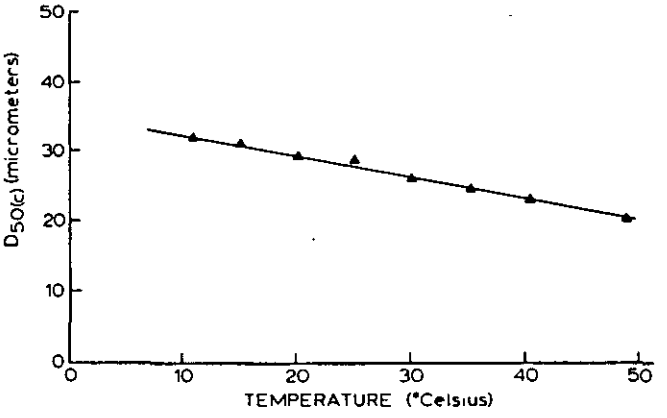

Fig. 3 — Relationship of hydrocyclone corrected d_{50} size and slurry temperature for a 10.16 cm (4 in) hydrocyclone processing silica.

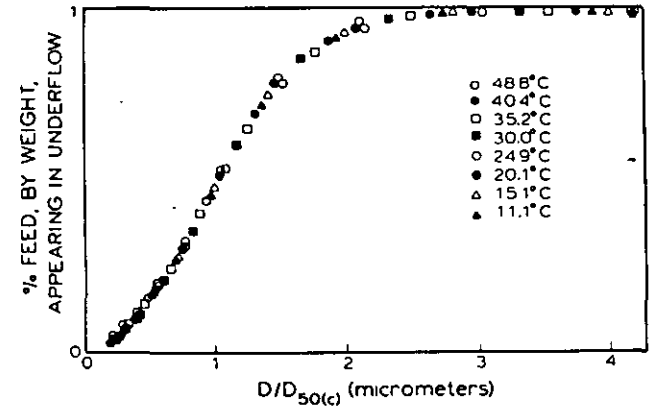

Fig. 4 — Reduced efficiency curve for varying percent solids and temperature for a 10.16 cm (4 in) hydrocyclone processing silica.

From Table 2 it is shown that apparent slurry viscosity varies significantly with temperature.

The behavior of hydrocyclones as classifiers of mill output is dependent on slurry rheology (Austin et al, 1984, Agar and Herbst, 1966).

If the cyclone returns excessive amounts of fine material to feed, over-grinding will reduce mill efficiency and may cause difficulties in later separation processes as well.

Variations in temperature affect slurry viscosity by reducing the viscosity of the carrier water. A major effect of this is

on hydrocyclone performance. The observed shift of the cyclone efficiency curve and reduction in $d_{50(c)}$ size arises from the reduced viscosity of water at elevated temperatures. Reduction of viscosity increases the settling velocity of the particles, which causes them to segregate more rapidly with fewer misplaced particles, thus improving efficiency. The increase in settling velocity also causes the apparent size of any given particle to increase which reduces the $d_{50(c)}$ size. This effect is amplified by an increase in flowrate at constant pressure as the viscosity is lowered, which increases centrifugal effects and hence raises the settling velocity. Similar conclusions can be drawn by analyzing the data obtained by Agar and Herbst (1966) where the water viscosity was altered with sucrose. It may be noted that viscosity reduction by increasing temperature, which reduces $d_{50(c)}$ size in cyclones, appears to conflict with Klimpel's data (1982), which predicts an increase in $d_{50(c)}$ size with a decrease in viscosity. This discrepancy may be explained by the difference in the mechanism of viscosity reduction. However, it should be kept in mind that direct comparisons of hydrocyclone results may be misleading due to the difficulty of ensuring that the same variables are held constant. For example, the results reported here are for constant pressure and varying throughput, while Klimpel's results may well have been for constant throughput and varying pressure.

Temperature changes have little effect on the interaction of water and solids, but produce a great alteration in the viscosity of water. It is the viscosity of the carrier liquid which controls the viscosity of the slurry under high shear conditions such as those encountered in the cyclone separating zone (Bradley, 1965), while the slurry viscosity at lower shear rates control the slurry flowrate and hence the magnitude of the centrifugal forces. Thus, increasing the temperature strongly influences both the centrifugal forces and the particle settling velocity, while viscosity reduction by chemical addition, which most strongly effects particle interactions and therefore the low-shear-rate apparent viscosity, has its greatest influence on centrifugal forces.

Conclusion

It has been shown that in both plant and laboratory environments, the temperature of the grinding circuit slurry has a noticeable effect on grinding and cyclone efficiency. The $d_{50(c)}$ size of a hydrocyclone is a function of the viscosity of the carrier liquid, which in turn is a function of temperature. The $d_{50(c)}$ size therefore decreases nearly linearly with increasing temperature. The sharpness of the separation is largely unaffected by temperature changes, as illustrated by the constant nature of the reduced efficiency curve.

Acknowledgments

The authors gratefully acknowledge the financial support for this project provided by the US Bureau of Mines through the Generic Center for Comminution at the University of Utah, and by the Dow Chemical Company. The authors also thank Krebs Engineers, Inc. for providing the hydrocyclone used in this project.

References

Agar, G. E. and Herbst, J. A., 1966, "The Effect of Fluid Viscosity on Cyclone Classification", *Trans SME-AIME*, vol. 235, pp 145-149

Austin, L. G., Klimpel, R. R., and Luckie, P. T., 1984, *Process Engineering of Size Reduction. Ball Milling*, AIME, New York.

Bradley, D , 1965, *The Hydrocyclone*, Pergamon Press Ltd , London.

El-Shall, H , Somasundaran, P., 1984, "Mechanisms of Grinding Modification by Chemical Additives: Organic Reagents", *Powder Technology*, Vol 38, pp 267-273.

Fuerstenau, D. W., Venkataraman, K. S., and Velamakanni, B V , 1985, "Effect of Chemical Additives on the Dynamics of Grinding Media in Wet Ball Mill Grinding", *International Journal of Mineral Processing*, Vol. 15, no. 4, pp. 251-268

Herbst, J. A., and Rajamani, K, 1979, "Control of Grinding Circuits", in *Computer Methods for the 80's*, A. Weiss, ed , AIME, New York, pp 770-786.

Kampl, H J , 1985, personal communication.

Klimpel, R. R., 1982, "The Influence of a Chemical Dispersant on the Sizing Performance of a 24-inch Hydrocyclone," *Powder Technology*, Vol. 31, pp. 255-262

Klimpel, R. R , 1984, "Influence of Material Breakage Properties and Associated Slurry Rheology on Breakage Rates in Wet Grinding of Coal and Ores in Tumbling Media Mills," in *Reagents in the Minerals Industry*, M J Jones and R. Oblatt, eds , Institution of Mining and Metallurgy, London, pp 265-270

National Materials Advisory Board (NMAB), 1981, *Comminution and Energy Consumption.*, NMAB-364

Selective flotation of fossil resin from Wasatch Plateau high-volatile bituminous coal

J. D. Miller and Y. Ye

Abstract — *Certain bituminous coals are known to contain appreciable quantities of natural fossil or subfossil resin. Such resinous coals are found in the western US, particularly the Wasatch Plateau coalfield of UT. Some of the seams in this field contain an average of 5% resin. This fossil resin has been recovered by gravity and/or flotation processes since 1929. Resin concentrates thus produced are of low quality and are usually refined by solvent extraction. The purified resins are of commercial importance in the adhesive, coating, rubber, and ink industries, etc. An improved flotation technique has been developed which involves ozone conditioning to selectively float resin from high-volatile bituminous coal. With this flotation process, a concentrate product which contains 95%*

Y. Ye, and **J.D. Miller**, member SME are with Dept. of Metallurgy and Metallurgical Engineering, University of Utah, Salt Lake City, UT.

SME preprint 88-198. SME Annual Meeting, Phoenix, AZ, January 1988. M&MP paper 88-614. Manuscript January 1988. Discussion of this paper must be submitted, in duplicate, prior to July 31, 1989.

resin at a recovery of 80% can be obtained in single-stage flotation. By comparison, conventional flotation at 80% recovery produces a concentrate having a resin content of 30 to 40%.

Introduction

Many bituminous coals are known to contain small quantities of natural (fossil or subfossil) resin. In the US, highly resinous coals are found in western coalfields, particularly the Wasatch Plateau coalfield in UT (Spieker and Baker, 1928; Tomlinson, 1932; Thiessen and Sprunk, 1937; Crawford and Buranek, 1952). The geographic location of the Wasatch Plateau coalfield together with mine locations is presented in Fig. 1. Some of the seams in this field average even more than 5% resin. Such resinous coals are also found in Colorado, New Mexico, and Wyoming.

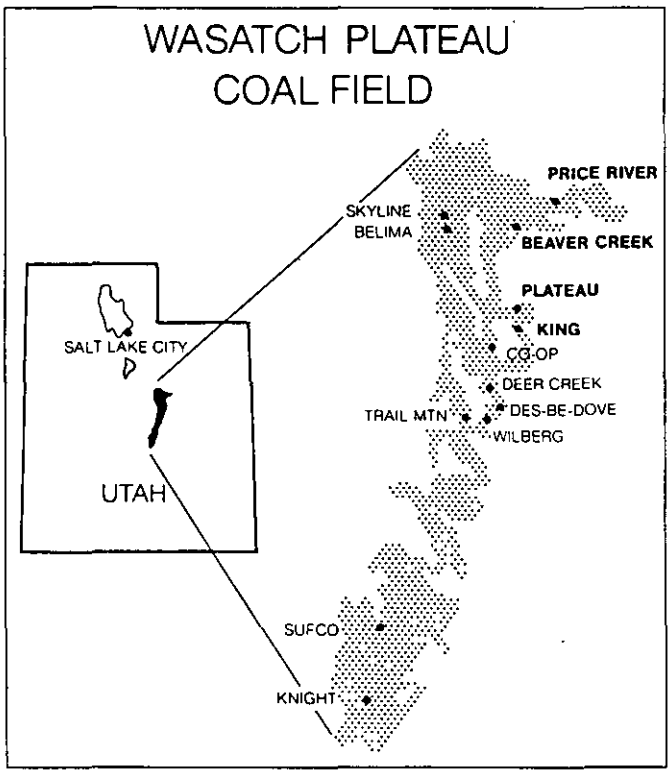

Fig. 1 — Mine locations in the Wasatch Plateau coalfield. Preparation plants located at Price River, Beaver Creek, King, and Plateau.

Fossil resin has been recovered from the Wasatch Plateau coalfield intermittently since 1929 by gravity and/or flotation processes. Resin production nevertheless has been on a very small scale. Of the four coal preparation plants in the Wasatch Plateau coalfield (US Fuel, Plateau, Beaver Creek, and Price River), only one plant (US Fuel) recovers this valuable resource at a rather low level of production.

Resin concentrates thus produced are usually refined by solvent extraction and precipitation. Such purified resins typically have a molecular weight of about 730, a melting point of about 170°C, and an iodine number of about 145. The product, at the present time, has a market value of approximately $1.00/kg and is used in the adhesive, rubber, varnish, enamel, paint and coatings, thermoplastics, and ink industries. Most recently, it has been suggested that these resins could have a special value as feedstock for high density jet fuels.

In the recovery of resin from coal, most of the resin phase is liberated at a relatively coarse size, approximately 20 mesh, and has a variable shade of resinous yellow/brown color. In addition to its color, the resin is distinguished by a specific gravity of about 1.00 to 1.08 g/cm³. From a chemical standpoint, the resin is characterized as being considerably less aromatic than other coal macerals with an aromaticity of 0.16 to 0.23, compared to more than 0.60 for other coal macerals as determined by nuclear magnetic resonance (Wender, e 1981). Recent thermogravimetric and spectrometric NMR) analysis suggests that the fossil resins from the Wasatch Plateau region consist of macromolecular aggregates composed of polymerized sesquiterpenoids (Crelling, et al., 1987); see Fig. 2. Further, the structural difference between resin and other coal macerals manifests itself by a slight difference in the respective hydrophobicities of the two components as revealed in Table 1.

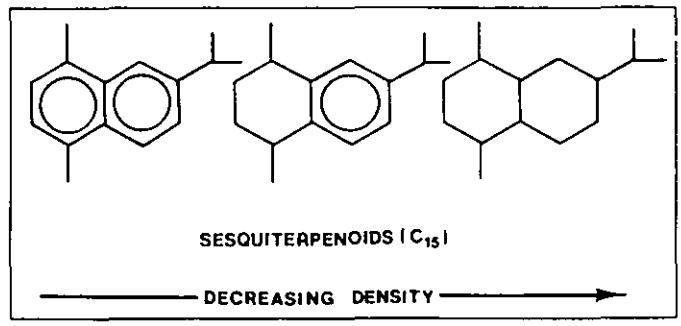

Fig. 2 — Sesquiterpenoid structures similar to the fossil resin structure found in Utah coals.

Table 1 — Bubble Attachment-Time Measurements for Resin and Coal Particles from the Hiawatha Seam, Utah (Particle Size 212x300µm, pH 6.5) and Contact-Angle Measurements for Polished Samples (Miller and Ye, 1988).

Component	Bubble Attachment Time, ms	Contact Angle, degrees
Resin	5.0	58-59
Coal	15 0	48-51

From this small difference in the respective hydrophobicities, it might be expected that a flotation separation would be possible as has been reported (Green, 1930; Klepetko, et al., 1947, 1950, 1952). However, because the difference in the respective hydrophobicities of coal and resin is not great, the flotation separation of resin from coal is poor, and a multistage flotation circuit is needed even to produce a resin concentrate of modest quality. In this regard, efforts have been made to improve resin flotation from coal by controlled reagent addition (Laros and Pick, 1983) and by using coal depressants/oxidants (Arabidze, et al., 1980). Only modest success has been realized.

Also, it has been found that the high-capacity air-sparged hydrocyclone is effective for the flotation of fine resin from coal using a traditional reagent schedule. Resin concentrates containing about 50% resin can be produced in a single stage of flotation at a dry solids specific capacity of about 91 t/d/m³ (100 tpd per cubic ft) of cell volume (Miller, et al., 1986).

Research efforts at the University of UT have been devoted to finding a more effective coal depressant in order to increase the difference in hydrophobicity between resin and coal and hence make a more selective flotation separation. The results from this research program are reported herein, and, most significantly, it has been found that ozone conditioning for coal depression is particularly effective (Miller and Ye, 1989).

Evaluation of flotation reagents

The first effort made in this study was to evaluate flotation strategies to improve the separation efficiency for resin concentration. The resin/coal slurry samples were taken from a

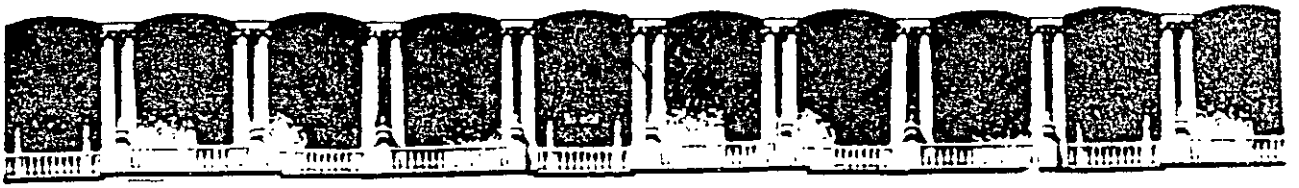

FACULTAD DE INGENIERIA U.N.A.M.
DIVISION DE EDUCACION CONTINUA

CURSOS ABIERTOS

DESARROLLO Y OPERACIÓN DE SENSORES PARA CONTROL DIRECTO Y CONTINUO EN PLANTAS DE BENEFICIO DE MINERALES Y EN LA RESTAURACIÓN DEL MEDIO AMBIENTE

Del 18 al 23 de mayo de 1998

TEMA: BIOTECHNOLOGY APPLIED TO RAW MATERIALS PROCESSING

EXPOSITOR :DR. KOMAR KAWATRA

1998

Palacio de Minería Calle de Tacuba 5 Primer piso Deleg. Cuauhtemoc 06000 México, D.F. APDO. Postal M-2285
Teléfonos. 512-8955 512-5121 521-7335 521-1987 Fax 510-0573 521-4020 AL 26

53. A. J. Rubin, "Removal and Use of Hydrolyzable Metals in Foam Fractionations," in: Adsorptive Bubble Separation Techniques, ed. R. Lemlich, Academic Press (1972) 199-217.

54. E.A. Cassell, E. Matijevic, F.J. Mangravite, Jr., T.M. Buzzell and S.B. Blabac, "Removal of Colloidal Pollutants by Microflotation," AIChE Journ., 17 (1971) 1486-1492.

55. W.F.R. Bare, N.B. Jones and E.J. Middlebrooks, "Algae Removal Using Dissolved Air Flotation," Journ. Water Pollut. Control Federation, 47 (1975) 153-169.

56. E.J. Middlebrooks, D.B. Porcella, R.A. Gearheart, G.R. Marshall, J.H. Reynolds and W.J. Grenney, "Techniques for Algae Removal from Wastewater Stabilization Ponds," Journ. Water Pollut. Control Federation, 46 (1974) 2676-2695.

57. M.E. Tittlebaum and S. Holtman, "Algae Removal by Induced Air Flotation," Completion Report for Office of Water Research and Technology, U.S. Dept. of the Interior, (1982) 33 pp.

58. J. Arbelaez, B. Koopman and E.P. Lincoln, "Effects of Dissolved Oxygen and Mixing on Algal Autoflotation," Journ. WPCF, 55 (1983) 1075-1079.

59. S.S. Huneycutt, D.A. Wallis and F. Sebba, "A Technique for Harvesting Unicellular Algae Using Colloidal Gas Aphrons," in: Biotech. Bioeng. Symp. No. 13, John Wiley and Sons, (1983) 567-575

60. R. Klute and U. Neis, "Coagulation of Algae and Subsequent Removal by Filtration or Flotation," Water Supply, (1983) 157-162.

61. E.S. Sharpe, A.I. Herman and S.C. Toolan, "Separation of Spores and Parasporal Crystals of Bacillus thuringiensis by Flotation," Journ. of Invertebrate Path., 34 (1979) 315-316.

62. C.A. Hansen and H.B. Gotaas, "Sewage Treatment by Flotation," Sewage Works J., 15 (1943) 212-252.

63. Z. Gotab, Private communication with R.W. Smith, Technical University of Wroclaw, Poland, 13 June 1988.

BIOTECHNOLOGY APPLIED TO RAW MATERIALS PROCESSING

S. K. Kawatra and T. C. Eisele
Department of Metallurgical Engineering
Michigan Technological University
Houghton, MI 49931

Abstract

Recent advances in microbiology have made the application of biotechnology to metallurgical processes possible. Hydrometallurgy stands to gain the most from the use of microorganisms, as they are useful for both dissolution aids and for removing metals from solution. The development of genetic engineering techniques promises to greatly increase the importance of bioprocessing of metals and minerals by the year 2000.

In this paper, the basic effects of microorganisms on metallurgical processes are reviewed, and the applications which are currently either in use or near being used are presented. Representative data collected at Michigan Technological University is also given.

Metallurgical Processes for the Year 2000 and Beyond
Edited by H.Y. Sohn and E.S. Geskin
The Minerals, Metals & Materials Society, 1988

Introduction

Many hydrometallurgical operations exist which are thermodynamically possible, but which are industrially impractical due to slow kinetics, high reagent costs, or the need for a highly corrosive environment. However, recent discoveries in microbiology indicate that in many cases these difficulties can be reduced greatly by the action of bacteria and other microorganisms (1-8).

A major advantage of using living organisms in hydrometallurgy is that once the culture is established the microorganisms produce their own reagents either from the material being processed or from low-cost nutrient supplements. They thus allow extremely complex chemical reactions to be carried out at reasonable cost. The major drawback of using microorganisms is their inability to tolerate extremely high temperatures, excessive concentrations of toxic metals, or very highly acidic, alkaline, or corrosive conditions. However, the complex reactions which bacteria make possible frequently eliminate the need for such extreme conditions. Also, in recent years a number of organisms have been isolated from such exotic environments as hot springs and deep-ocean vents which can tolerate temperatures higher than was previously thought possible for any organism, and can catalyze a number of metallurgically important reactions (8).

Of the numerous potential applications for microbial processing, only a few, notably the dump leaching of copper and uranium, are currently used industrially (8). In their present fairly primitive level of development, many biohydrometallurgical processes are too slow to be economical. However, work is underway at Michigan Technological University and elsewhere to develop methods for speeding up these processes. This will result in biohydrometallurgy being well developed and widely used by the beginning of the next century.

Microorganism Characteristics

Microorganisms can be conveniently classified according to what they "eat", as given in Table 1. The two most familiar types of organisms are the chemoheterotrophs, which extract energy from chemical reactions and construct cellular material from organic compounds, and the photoautotrophs, which extract energy from light and construct cellular material from carbon dioxide and water. However, the impact of these organisms on minerals and dissolved metals is typically minimal. The lithotrophs are much more important for hydrometallurgical applications, as these organisms extract their metabolic energy from inorganic chemical reactions, such as the oxidation of metals to more soluble forms. Such organisms are therefore often useful for accelerating oxidative leaching reactions (9).

Table 1: Classification of Microorganisms

	Energy Source	Carbon Source	Examples
Lithotrophs	inorganic chemical reactions	CO_2	*Thiobacillus ferrooxidans*, *Sulfolobus* species
Chemoheterotrophs	chemical reactions	organic chemicals	most bacteria, all fungi, and protozoans
Photoautotrophs	sunlight	CO_2	photosynthetic bacteria, algae
Photoheterotrophs	sunlight	organic chemicals	purple and green sulfur bacteria

A major consideration in any type of bioprocessing is that, unlike chemical reagents, the cells can reproduce when conditions are favorable, and die when they are not. It is therefore necessary to more carefully control the conditions in a bioreactor than in a reactor which uses only chemical reagents. In general, a bacterial population in a batch process will behave as shown in Figure 1, assuming that the initial conditions are suitable for growth. For a short period after addition, the microorganisms will not reproduce, as they are adjusting their metabolisms to the prevailing conditions. Following this "lag phase", the organisms will enter the exponential growth phase, where cells are actively reproducing and few or none are dying. Eventually, however, some factor such as limited nutrient supply, toxin accumulation, or a shortage of living space causes the microorganisms to die as fast as they reproduce, and the cell numbers become roughly constant. Ultimately, conditions become such that the culture can no longer maintain its numbers, and wholesale death of cells results. The activity of a culture of cells is greatest when they are in the exponential growth phase, and this condition is therefore preferred for biohydrometallurgical applications. Since high cell numbers are also desirable, the optimum condition is exponential growth with the culture just short of entering the stationary phase. The cell concentration at which this occurs can be increased by reducing the influences of limiting factors, such as by increasing the concentrations of critical nutrients and by increasing the tolerance of the microorganisms to the toxins produced by their activity.

Basic Biometallurgical Processes

There are three general ways in which microbes can be useful in metallurgy: 1) as aids in the dissolution of minerals in water solutions; 2) as agents for altering the surface chemistry of mineral particles, and 3) as selective accumulators of metal ions from dilute solutions. Each of these applications depend on completely different properties of the cells used, and therefore the microorganisms best suited for each differ greatly from one another.

Bioleaching

Mineral leaching is the only type of biometallurgical process which is currently used on an industrial scale. The organisms which have been most intensively used are bacteria of the genus *Thiobacillus*, which get their metabolic energy from the oxidation of sulfur compounds to sulfates. Since sulfates are typically much more soluble than the corresponding sulfides, these bacteria are very useful for sulfide mineral leaching. The two most important of these organisms are *Thiobacillus ferrooxidans* and *Thiobacillus thiooxidans*, which frequently occur in a natural mixed culture which oxidizes sulfides more rapidly than can be done by either organism alone. A number of other sulfur-oxidizing bacteria have also been discovered, and their full capabilities are currently being explored (10,11). However, the *Thiobacillus* cultures will naturally arise in heap and dump leaching operations without the need for specific inoculation, which is a powerful argument in their favor (12).

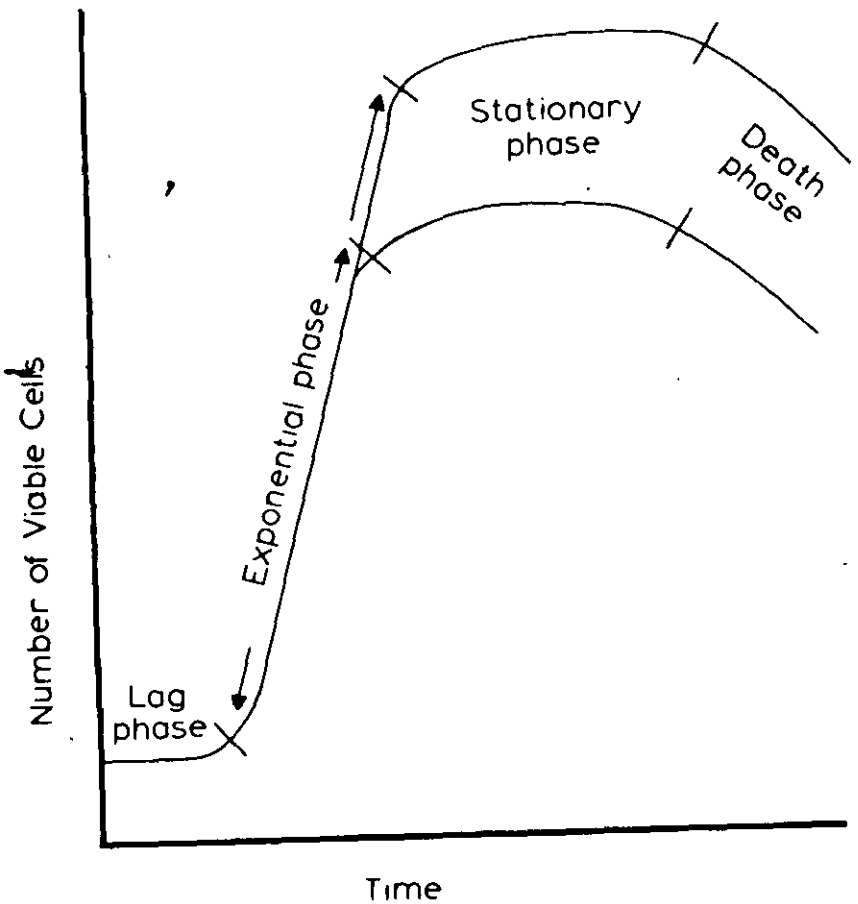

Figure 1. Variation of bacterial numbers over time in a batch culture. The time scale varies from hours for certain chemoheterotrophic bacteria to weeks for lithotrophs such as T. ferrooxidans. The addition of supplemental nutrients will often be able to increase the maximum cell concentration as shown. In a continuous reaction, it is possible to maintain a culture in the expontential growth phase by controlled removal of cells.

The mechanisms through which T. ferrooxidans and T. thiooxidans oxidize sulfide minerals are not fully understood, as many of the biochemical reactions involved require that the bacteria be either contacting or in close proximity to the mineral surface. However, the primary mechanism used by T. ferrooxidans, termed indirect oxidation, can proceed even when the bacteria are completely dissociated from any particular mineral particle, and can therefore be examined fairly easily. In this pathway, the bacteria generate ferric iron from ferrous iron, according to the reaction:

$$4\ Fe^{+2} + O_2 + 4H^+ \xrightarrow{\text{Bacteria}} 4\ Fe^{+3} + 2H_2O$$

Since this is an exothermic reaction, the bacteria can gain metabolic energy from the process. The ferric iron generated can then attack sulfide minerals, pyrite for example:

$$FeS_2 + 14\ Fe^{+3} + 8H_2O \rightarrow 15\ Fe^{+2} + 2SO_4^{-4} + 16H^+$$

with the ferrous iron produced then being reoxidized by the bacteria (13-16). While this reaction will occur even in the absence of bacteria, the regeneration of ferric iron is accelerated several hundred fold by T. ferrooxidans. Since the solubility of ferric iron is very low when the pH is higher than about 4, indirect oxidation can obviously only be important in acid solutions (13). For this reason sulfide-oxidizing bacteria which can use this pathway are specifically adapted to solutions with a pH between 1.5 and 3 and will be killed if the pH exceeds 4.

Although bacteria greatly increase the oxidation rate of sulfide minerals, the reactions are still frequently too slow to be industrially practical. Often the reaction rate could be increased by simply increasing the temperature, but the maximum temperature is limited by the heat tolerance of the organisms used. In the case of the Thiobacilli, this maximum is around 35-40°C. However, numerous examples of bacteria have been isolated from sulfurous hot springs worldwide which live at temperatures from 60-98°C. Some of these bacteria, such as the Sulfolobus genus, oxidize and reduce sulfur and iron compounds (11). Bacteria have also been isolated from undersea hydrothermal vents which grow at high pressure and at temperatures somewhat above 100°C, and may therefore be useful for exotic applications such as in-situ leaching of extremely deep mineral deposits. Unlike the Thiobacillus genus, these high-temperature organisms typically require organic nutrient supplements. Also, as a result of their adaptation to high temperatures the cells are somewhat fragile, and may be torn apart in high-shear applications (11).

Mineral Surface Alteration

Many microorganisms have the ability to attach themselves to solid surfaces, either because the surface supplies some nutrient to the cell or simply to keep the cell from being randomly swept away by flowing water (9). This attachment occurs rapidly, typically in times shorter than 15 minutes, and can be very selective. Lithotrophic bacteria in particular will often specifically attach to those minerals which they can most effectively degrade, and will be attracted to crystalline imperfections where dissolution will occur most rapidly (17). Since the surface chemistry of a bacterial cell is quite different from that of the mineral surface, this would be expected to strongly influence the behavior of the mineral in processes such as froth flotation or oil agglomeration. A typical application would be the use of bacteria to depress pyrite during coal flotation. Since attachment is far more rapid than dissolution, bacterially-aided flotation may very well be preferable to bacterial leaching for certain mineral systems.

Bioaccumulation

It has been found that many microorganisms are capable of specifically adsorbing metal ions from dilute solution (8). This is particularly useful for treatment of mining and processing effluents, with low-cost biomass being used to remove and concentrate heavy metals. Depending on the metal adsorbed, it may be possible to use dead biomass instead of living cells,

thus reducing the control problems which result from maintaining live cultures (18).

The microorganisms useful for bioaccumulation can be of any type, and need not be specifically lithotrophic. Often, the accumulation of metals is a side effect of the cell metabolism, with the metals accumulated poisoning the cell. Since the microorganisms are not gaining useful material from the adsorbed ions, and indeed may be killed by them, it is preferable to grow the microbes in a separate vessel, and only add them to the process when they are in the optimum condition for metal adsorption.

Current Applications

A number of promising applications of bacteria to metallurgy have been identified in the laboratory, particularly in the last few years (8). However, very few are currently applied industrially. This limited application is due more to a lack of development than to any insurmountable failing of bacterial processing. The most common problem with bioprocessing, and particularly for leaching processes, is the long leaching time frequently required. The primary thrust of research in bioleaching is therefore to improve its kinetics. Until the dissolution rate can be increased, only leaching processes where speed is not essential, such as dump and in-situ leaching, will be practical.

Copper Leaching

Bioleaching of copper minerals has been carried out since at least the 17th century, although the necessity for bacterial action in acid dump leaching was not discovered until the early 1940's. The bacteria responsible for copper leaching are generally Thiobacillus species, particularly T. ferrooxidans. Most important copper minerals, including oxides, carbonates, and silicates as well as sulfides, are either naturally soluble in sulfuric acid or become soluble after being indirectly oxidized by bacteria. Bacterial leaching of copper is particularly useful when pyrite is present in the ore, as it can then generate both its own acid and the dissolved iron needed for indirect oxidation. This obviously keeps reagent costs low (19). If insufficient pyrite is present, the necessary iron can be dissolved during cementation of the copper from solution with metallic iron.

Current copper leaching practice is restricted to heap and dump leaching (19). However, in-situ bacterial leaching is also a strong possibility. The major hurdle is the difficulty of uniformly supplying well-oxygenated leaching solutions to the ore body. One method being investigated is to carry out bacterial iron oxidation in reactors on the surface, and then to pump the ferric iron/sulfuric acid solution through the ore body, leaving the bacteria behind, as shown in Figure 2. While this improves the aeration situation, it also eliminates most of the contribution of bacteria which directly oxidize sulfur, and need to be in contact with the mineral surface. In addition to leaching using Thiobacillus species, there is potential for using organisms from hot springs and deep-sea hydrothermal vents for in-situ leaching of very deep, high temperature deposits which cannot be economically mined by any other means (8,11).

Coal

Although bioprocessing has not been applied to coal on an industrial scale, a number of possible applications have been examined in the laboratory. The primary thrust has been in coal desulfurization (21-32),

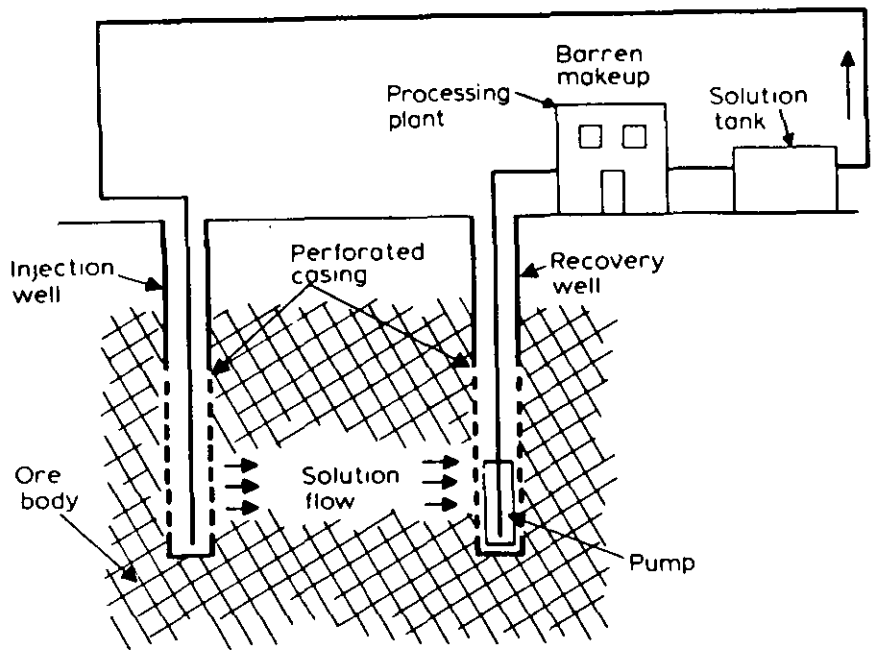

Figure 2. General in-situ leaching arrangement. For leaching of copper by Fe^{+3} in acid solution, the bacterial oxidation of Fe^{+2} to Fe^{+3} can be carried out above-ground. The oxidized solution is then pumped through the permeable ore body. This allows for thorough aeration of the solution during the iron reoxidation, which would be difficult underground.

although some work has also been done recently in biological liquefication (20).

Since a major portion of the sulfur in coal is in the form of pyrite, most research has focused on bacterial dissolution of pyritic sulfur. The reactions are therefore similar to those encountered in copper leaching, and can be carried out by Thiobacillus species. However, heap and dump leaching of coal are not generally suitable for desulfurization, as removal of pyrite is not sufficiently complete. More expensive methods, such as stirred tank reactors, are therefore required, and the one to three week residence times necessary make capital costs prohibitive (30). Thorough oxygenation, such as by the use of pachuca tank reactors, produces a significant increase in leaching rate over simple stirred reactors, as shown in results collected at Michigan Technological University (Figure 3). These results show that for an Ohio coal, pachuca tanks reduce the lag period by about three days, or 25%, and increase the ultimate pyrite removal. However, equipment design has not yet improved leaching performance sufficiently to make this means of coal desulfurization economical.

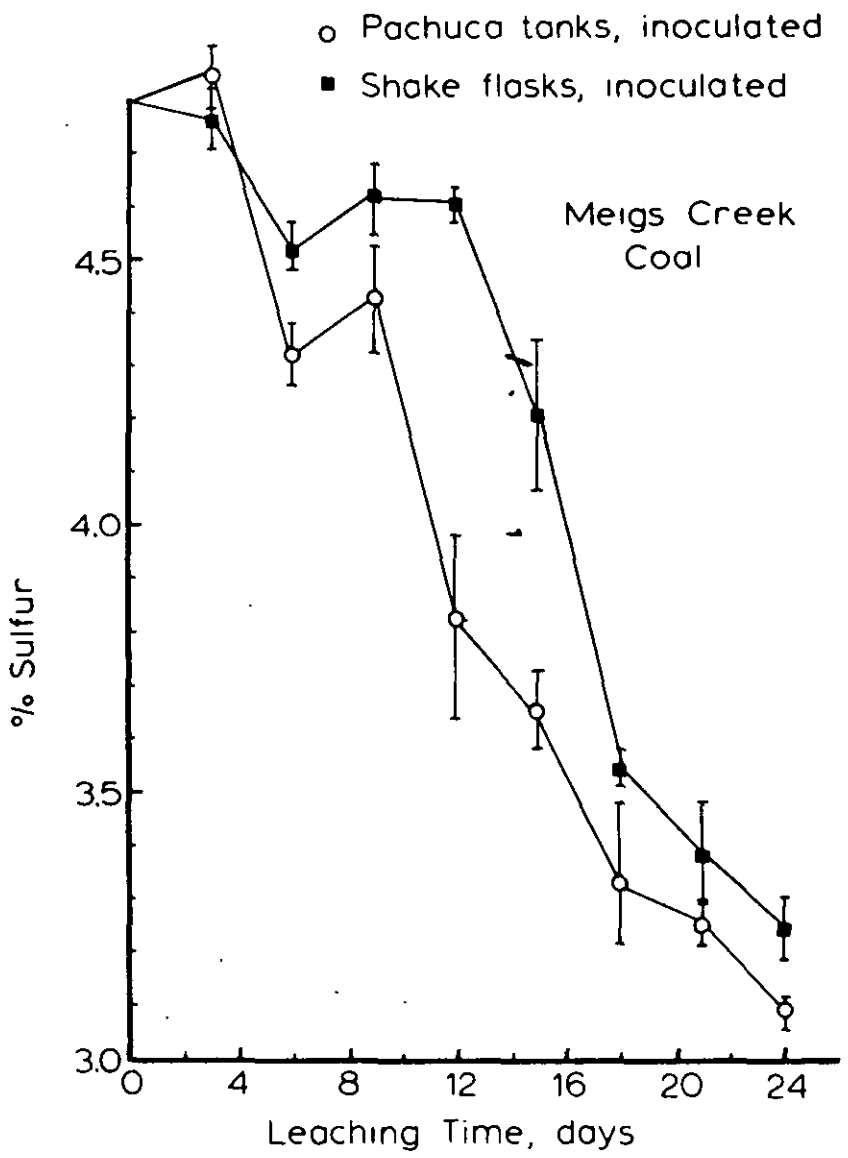

Figure 3. Comparision of the bacterial leaching of pyrite from coal in pachuca tanks and shake flasks. The superior aeration of the pachuca tanks produces a significant increase in the leaching rate, and also results in a greater ultimate removal of pyrite from the coal.

The use of high-temperature bacteria of the Sulfolobus genus is also being investigated for pyrite removal (24) as the increas mperatures produce a corresponding increase in leaching rate. While decreases the equipment volume needed, the operating cost is increased due to the higher energy consumption. It has been suggested that the leaching operation be installed at the power plant, so that the process can be heated by the waste heat from the generators, thus obtaining the heat for free.

An alternate, much more rapid means of using bacteria to remove pyrite depends on selective attachment of bacteria to the pyrite surface (33-38). The bacteria coating the pyrite particles make the particles strongly hydrophilic, and thus increase the ability of processes such as froth flotation and oil agglomeration to distinguish between coal and pyrite. A number of investigators have used Thiobacillus ferrooxidans for this purpose, with reasonable success. Recent work at Michigan Technological University has shown that many, and perhaps all, other microorganisms are also capable of preventing pyrite flotation, regardless of whether or not they are lithotrophic. Indeed, these other organisms may well be superior to Thiobacillus species for this purpose. Further investigation in this area is currently underway. The major limitation, as with any physical separation, is the need for nearly complete liberation of the pyrite from the coal. This technique will therefore only be practical when the coal is very fine, and will therefore be most beneficial for such processes as column flotation and selective flocculation.

In addition to the sulfur contained in pyrite inclusions, coal contains a substantial amount of organically bound sulfur which is very difficult to remove. There have been some indications, however, that certain bacteria may be able to remove much of this organic sulfur without completely destroying the coal structure. While no organisms have yet shown an unequivocal ability to do this, a number of bacteria are known which can degrade specific sulfur-carbon compounds similar to those found in coal. Further mutation and selection of these bacteria may make possible the low-cost removal of all sulfur from coal (8).

Quite recently, it has been discovered that certain wood-decomposing fungi can partially or completely liquefy some low-rank coals, particularly highly-oxidized lignites (20). The coals are converted into a complex mixture of water-soluble organic liquids, which may be useful in a variety of chemical applications. Initial results are reported to be highly variable, and so the value of this technique is not yet known.

Gold

Probably the most important application of biotechnology to gold recovery will be the treatment of refractory ores to increase gold dissolution during cyanide leaching (39,40). In many such ores, finely divided gold is encapsulated in pyrite particles and cannot be reached by the cyanide solutions unless the ore is very finely ground. An alternative to grinding is to use bacteria to selectively dissolve enough of the pyrite to expose the gold, and then to leach with cyanide in the normal fashion. It is of course necessary to do this in two steps, both because cyanide will kill the bacteria and because pyrite dissolution must be carried out in acid solution while cyanide leaching requires alkaline conditions. The use of bacteria keeps the cost of pyrite dissolution at a reasonable level, and since it is only necessary to dissolve a fraction of the pyrite to expose the gold, the leaching time can be kept to a few days.

Uranium

The dissolution of uranium in acid solution is greatly increased by the presence of Thiobacillus ferrooxidans, as the ferric iron produced by this bacteria oxidizes the uranium from UO_2 to the much more soluble UO_2^{+2} (41,42,19). A typical application has been to use acidic mine water containing these bacteria to wash down the stopes and pillars in the mine, and then to extract the dissolved uranium from the water (41). Microbial leaching will also be useful for in-situ mining of uranium, using techniques similar to those being investigated for copper. In addition, uranium concentration by adsorption in biomass is possible (43).

Nickel and Cobalt

Economical dissolution of nickel and cobalt from low-grade laterites requires the addition of complexing agents to increase their solubility. It has been found that the metabolic products which many organisms produce from glucose, such as citric, tartaric, and pyruvic acids, are useful for this purpose (44). Unlike leaching with lithotrophic bacteria, a nutrient sources other than the ore is needed, usually in the form of a low-cost organic additive such as glucose. It may be practical to provide nutrients through the use of photoautotrophic organisms such as algae (45), and thus use sunlight to provide the necessary energy to the process.

The adsorption of nickel from solution by a Pseudomonas species has been reported, which may be useful for treating wastewater. The nickel adsorption appears to be a simple exchange for magnesium in the outer membrane. However, nickel tolerance of existing strains is not sufficient for greatly concentrating the nickel (46).

Selenium

Recent work by the Bureau of Mines has been concerned with reducing the amount of selenium in process waste waters and in agricultural runoff. It has been discovered that certain bacteria isolated from brackish-water marshes are capable of reducing soluble selenate ions to selenite and ultimately to insoluble elemental selenium. The organisms which do this are heterotrophic, and therefore require organic nutrients. Approximately 95% of the dissolved selenium is removed by this means, and since the selenium is not adsorbed permanently by the cells they are not killed in the process (47).

Radium

For the adsorption of metals such as radium from wastewater streams, the microorganisms used need not be alive or of a particular species. Work with killed sludge from sewage treatment plants has shown that this material is useful for removing radium from uranium mine runoff, which can then be disposed of properly. The primary difficulty has been that the biomass particles were too small to be easily removed from the runoff stream after loading with radium. This problem has been reduced by the development of a technique for forming biomass pellets which are large enough to be easily removed, and sufficiently porous to be effective adsorbers. Since the material used as adsorbent is itself a waste product, the cost of this technology is quite low (43).

Conclusions

Biological processing of minerals and metals is a rapidly growing, diverse field whose importance will become considerable in the next century. Using naturally occurring microorganisms, [illegible] techniques are already possible which will reduce the cost of recovering and purifying raw materials. The use of genetic engineering techniques will allow organisms to be precisely tailored to their applications, and thus improve their effectiveness. Also, the utilization of organisms which live in extreme environments will allow biometallurgical processes to be carried out at higher temperatures and under conditions which were once believed to be impossible for living organisms.

The major factor limiting the application of biohydrometallurgy is the short time since most of the applications were first discovered. Implementation of this technology therefore requires a great deal of work in areas such as reactor design and process scaleup.

References

1. D. S. Holmes, "Biotechnology in the Mining and and Metal Processing Industries: Challenges and Opportunities", Minerals and Metallurgical Processing (May, 1988) 49-56.

2. V. I. Lakshmanan, "Industrial Views and Applications: Advantages and Limitations of Biotechnology", Biotechnology and Bioengineering Symposium No. 16, John Wiley & Sons (1986) 351-361.

3. G. J. Olson and R. M. Kelly, "Microbiological Metal Transformations: Biotechnological Applications and Potential", Biotechnology Progress, vol. 2, no. 1 (1986) 1-15.

4. P. L. Wichlacz, "Practical Aspects of Genetic Engineering for the Mining and Mineral Industries", Biotechnology and Bioengineering Symposium No. 16, John Wiley & Sons (1986) 319-326.

5. J. F. Spisak, "Biotechnology and the Extractive Metallurgical Industries: Perspectives for Success", Biotechnology and Bioengineering Symposium No. 16, John Wiley & Sons (1986) 331-341.

6. A. Bruynesteyn, "Biotechnology: Its Potential Impact on the Mining Industry", Biotechnology and Bioengineering Symposium No. 16, John Wiley and Sons (1986) 343-350.

7. M. C. Campbell, H. W. Parsons, A. Jongejan, V. Senmugasunderam, M. Silver, "Biotechnology for the Mineral Industry", Canadian Metallurgical Quarterly, vol 24, no. 2 (1985) 115-120.

8. B. J. Ralph, "Biotechnology Applied to Raw Minerals Processing", Comprehensive Biotechnology, (Murray Moo-Young, ed.), vol. 4, Pergamon Press, NY (1985) 201-234.

9. T. D., Brock, D. W. Smith and M. T. Madigan, Biology of Microorganisms, Prentice-Hall; Englewood Cliffs, New Jersey (1984).

10. G. Huber, H. Huber, K. O. Stetter, "Isolation and Characterization of New Metal-Mobilizing Bacteria", Biotechnology and Bioengineering Symposium No. 16, John Wiley and Sons (1986) 239-251.

11. R. M. Kelly and J. W. Deming, "Extremely Thermophilic Archaebacteria: Biological and Engineering Considerations", Biotechnology Progress, vol. 4, no. 2 (1988) 47-62.

12. J. R. Yat[illegible] and D. S. Holmes, "Molecular Probes for the Identification and Quar[illegible]n of Microorganisms Found in Mines and Mine Tailings", Biotechn[illegible] and Bioengineering Symposium No. 16, John Wiley and Sons (1986) 301-309.

13. M. P. Silverman, "Mechanism of Bacterial Pyrite Oxidation", Journal of Bacteriology, vol. 94, no. 4 (1967) 1046-1051.

14. S. B. Yunker and J. M. Radovich, "Enchancement of Growth and Ferrous Iron Oxidation Rates of T. ferrooxidans by Electrochemical Reduction of Ferric Iron", Biotechnology and Bioengineering, vol. 28 (1986) 1867-1875.

15. L. Toro, B. Paponetti, C. Cantalini, "Precipitate formation in the Oxidation of Ferrous Ions in the Presence of Thiobacillus ferrooxidans", Hydrometallurgy, vol. 20 (1988) 1-9.

16. N. LaZaroff, "Sulfate Requirement for Iron Oxidation by Thiobacillus ferrooxidans", J. Bacteriology, vol. 85 (1963) 78-83.

17. G. F. Andrews, "The Selective Adsorption of Thiobacilli to Dislocation Sites on Pyrite Surfaces", Biotechnology and Bioengineering, vol. 31 (1988) 378-381.

18. M. TseZos, "The Selective Extraction of Metals from Solution by Micro-organisms: A Brief Overview", vol. 24 no. 2 (1985) 141-144.

19. L. E. Murr, A. E. Torma, J. A. Brierley (eds.), Metallurgical Applications of Bacterial Leaching and Related Microbiological Phenomena, Academic Press, New York (1978).

20. C. D. Scott, G. W. Strandberg, S. N. Lewis, "Microbial Solubilization of Coal", Biotechnology Progress, vol. 2, no. 3 (1986) 131-139.

21. M. R. Hoffmann, B. C. Faust, F. A. Panda, H. H. Koo, H. M. Tsuchiya, "Kinetics of the Removal of Iron Pyrite from coal by Microbial Catalysis", Applied and Environmental Microbiology, vol. 42, no. 2, (1981) 259-271.

22. J. D. Isbister and E. A. Kobylinski, "Microbial Desulfurization of Coal", Processing and Utilization of High-Sulfur Coals (Y. A. Attia, ed.) Elsevier, New York (1985) 627-641.

23. J. Murphy, E. Riestenberg, R. Mohler, D. Marek, B. Beck, D. Skidmore, "Coal Desulfurization by Microbial Processing", Processing and Utilization of High-Sulfur Coals (Y. A. Attia, ed.) Elsevier, New York (1985) 643-652.

24. F. Kargi and J. M. Robinson, "Microbial Desulfurization of Coal by Thermophilic Microorganism Sulfolobus acidocaldarius", Biotechnology and Bioengineering, vol. 24 (1982) 2115-2121.

25. F. Kargi, "Enhancement of Microbial Removal of Pyritic Sulfur from Coal Using Concentrated Cell Suspension of T. ferrooxidans and an External Carbon Dioxide Supply", Biotechnology and Bioengineering, vol. 24, (1982) 749-752.

26. P. R. Dugan, "Microbiological Desulfurization of Coal and Its Increased Monetary Value", Biotechnology and Bioengineering Symposium No. 16, John Wiley & Sons (1986) 185-203.

8

27. F. Kargi and J. M. Robinson, "Biological Removal of Pyritic Sulfur from Coal by the Thermophilic Organism Sulfolobus acido[illegible]darius", Biotechnology and Bioengineering, vol. 27 (1985) 41-4[illegible]

28. F. Kargi and J. M. Robinson, "Removal of Organic Sulphur from Bituminous Coal: Use of the Thermophilic Organism Sulfolobus acidocaldarius", Fuel, vol. 65 (1986) 397-399.

29. R.G.L. McCready and M. Zentilli, "Beneficiation of Coal by Bacterial Leaching", Canadian Metallurgical Quarterly, vol. 24, no. 2 (1985) 135-139.

30. C. Rai, "Microbial Desulfurization of Coals in a Slurry Pipeline Reactor Using Thiobacillus ferrooxidans", Biotechnology Progress, vol. 1, no. 3 (1985) 200-204.

31. F. Kargi and J. M. Robinson, "Removal of Sulfur Compounds from Coal by the Thermophilic Organism Sulfolobus acidocaldarius", Applied and Environmental Microbiology, vol. 44, no. 4 (1982) 878-883.

32. S. K. Kawatra, T. C. Eisele and S. Bagley, "Coal Desulfurization by Bacteria", Minerals and Metallurgical Processing, (November 1987) 189-192.

33. C. C. Townsley, A. S. Atkins, A. J. Davis, "Suppression of Pyritic Sulphur During Flotation Tests Using the Bacterium Thiobacillus ferrooxidans", Biotechnology and Bioengineering, vol. 30 (1987) 1-8.

34. A. S. Atkins, E. W. Bridgwood, A. J. Davis, F. D. Pooley, "A Study of the Suppression of Pyritic Sulphur in Coal Froth Flotation by Thiobacillus ferrooxidans", Coal Preparation, vol. 5, (1987) pp. 1-13.

35. M. Elzeky and Y. A. Attia, "Coal Slurries Desulfurization by Flotation Using Thiophilic Bacteria for Pyrite Depression", Coal Preparation, vol. 5 (1987) 15-37.

36. B. J. Butler, A. G. Kempton, R. D. Coleman, C. E. Capes, "The Effect of Particle Size and pH on the Removal of Pyrite from Coal by Conditioning with Bacteria Followed by Oil Agglomeration", Hydrometallurgy, vol. 15 (1986) 325-336.

37. C. E. Capes, A. E. McIlhinney, A. F. Sirianni, I. E. Puddington, "Bacterial Oxidation in Upgrading Pyritic Coals", CIM Bulletin, (November 1973) 88-91.

38. A. G. Kempton, N. Moneib, R.G.L. McCready, C. E. Capes, "Removal of Pyrite from Coal by Conditioning with Thiobacillus ferrooxidans Followed by Oil Agglomeration", Hydrometallurgy, vol. 5 (1980) 117-125.

39. Y. Attia, J. Litchfield, L. Vaaler, "Applications of Biotechnology in the Recovery of Gold", Microbiological Effects on Metallurgical Processes, TMS-AIME (1985) 111-120.

40. A. Bruynesteyn, R. P. Hackl, "The Biotankleach Process for the Treatment of Refractory Gold/Silver Concentrates", Microbiological Effects on Metallurgical Processes, TMS-AIME (1985) 121-127.

41. R.G.L. McCready, D. Wadden, A. Marchbank, "Nutrient Requirements for the In-Place Leaching of Uranium by Thiobacillus ferrooxidans", Hydrometallurgy, vol. 17 (1986) 61-71.

42. L. G. Leduc, G. D. Ferroni, D. Belcourt, "Liquid Scintillation Counting as a Means of Measuring Uranium Leached from Low-Grade Ores by Thiobacillus ferrooxidans", Hydrometallurgy, vol. 18 (1987) 255-263.

43. M. Tsezos, M.H.I. Baird, L. W. Shemilt, "The Use of Immobilized Biomass to Remove and Recover Radium from Elliot Lake Uranium Tailing Streams", Hydrometallurgy, vol. 17 (1987) 357-368.

44. D. I. McKenzie, L. Denys, A. Buchanan, "The Solubilization of Nickel, Cobalt and Iron from Laterites by Means of Organic Chelating Acids at Low pH", International Journal of Mineral Processing, vol. 21 (1987) 275-292.

45. M. J. Hart and J. L. Madgwick, "Utilization of Algae as a Sole Nutrient for Microorganisms Biodegrading Manganese Dioxide", Bull. Proc. Australasian Institute of Mining and Metallurgy, vol. 292, no. 1 (1987) 61-63.

46. A. Bordons and J. Jofre, "Extracellular Adsorption of Nickel by a Strain of Pseudomonas Sp.", Enzyme Microb. Technol., vol. 9 (1987) 709-713.

47. D. M. Larsen, K. R. Gardner, and P. B. Altringer, "Biologically Assisted Control of Selenium in Process Waste Waters", in press (1988).

48. A. D. Agate, "Isolation and Preservation of Bacterial Cultures with Special Reference to Leaching of Indian Copper Ores", Minerals and Metallurgical Processing, (May 1988) 66-68.

49. R. M. Bagdigian and A. S. Myerson, "The Adsorption of Thiobacillus ferrooxidans on Coal Surfaces", Biotechnology and Bioengineering, vol. 28 (1986) 467-479.

50. C.-Y. Chen and D. R. Skidmore, "Attachment of Sulfolobus acidocaldarius cells on Coal Particles", Biotechnology Progress, vol. 4, no. 1 (1988) 25-30.

51. Z. M. Dogan, C. F. Gokcay, and E. Atabey, "Bacterial Leaching of Turkish Pyrite Cinders", Progress in Biohydrometallurgy, Cagliari, Italy, (May 1983) 693-703.

52. H. L. Ehrlich, "Recent Advances in Microbial Leaching of Ores", Minerals and Metallurgical Processing, (May 1988) 57-60.

53. S. E. Follin, M. V. Yates, J. A. Brierley and C. L. Brierley, "Microbial Effects on In-Situ Leaching" Microbiological Effects on Metallurgical Processes, TMS-AIME (1985) 129-144.

54. S. Ford, S. C. Simpson, D. Condliffe, and B. H. Olson, "Distribution of Mercury Resistance Genes Among Resistance Determinants in Contaminated Soils in the U.K.", SME Annual Meeting, Phoenix, Arizona, preprint no. 88-25 (1988).

55. A. M. Johnson, D. G. Carlson, S. T. Baley, D. L. Johnson, "In-Situ Bioleaching Investigations of Michigan Chalcocite Ores", SME-AIME Annual Meeting, Phoenix, Arizona, Preprint No. 88-96 (1988).

56. B. H. Kaye, "Fine Particle Characterization Aspects of Predictions Affecting the Efficiency of Microbiological Mining Techniques", Powder Technology, vol. 50, (1987) 177-191.

57. A. B. King, A.W.L. Dudeney, "Bioleaching of Nepheline", Hydrometallurgy, vol. 19, (1987) 69-81.

58. R. W. Lawrence, A. Vizsolvi and R. J. Vos, "The Silver Catalyzed Bioleach Process for Copper Concentrate", Microbiological Effects on Metallurgical Processes, TMS-AIME, Warrendale, PA (1985) 65-82.

59. K. A. Natarajan, "Electrochemical Aspects of Bioleaching Multisulfide Minerals", Minerals and Metallurgical Processing (May 1988) 61-65.

60. D. E. Rawlings, I-M. Pretorius, and D. R. Woods, "Expression of Thiobacillus ferrooxidans Plasmid Functions and the Development of Genetic Systems for the Thiobacilli" Biotechnology and Bioengineering Symposium No. 16, John Wiley & Sons (1986) 281-287.

61. S. E. Shumate and G. W. Strandberg, "Accumulation of Metals by Microbial Cells", Comprehensive Biotechnology, vol. 4 (Murray Moo-Young, ed.) Pergamon Press (1985) 235-247.

62. M. J. Southwood, "Bacterial Leaching: Some Mineralogical Constraints in the Selection of Low-grade Nickel Ores", Mintek Review, no. 1 (1985) 25-30.

63. A. O. Summers, P. Roy, and M. S. Davidson, "Current Techniques for the Genetic Manipulation of Bacteria and their Application to the study of Sulfur-Based Autotrophy in Thiobacillus", Biotechnology and Bioengineering Symposium No. 16, John Wiley & Sons, (1986) 267-279.

64. M.C.M. Van Loosdrecht, J. Lylema, W. Norde, G. Schraa and A.J.B. Zehnder, "Electrophoretic Mobility and Hydrophobicity as a Measure to Predict the Initial Steps of Bacterial Adhesion", Applied and Environmental Microbiology, vol. 53, no. 8 (1987) 1898-1901.

65. M.C.M. Van Loosdrecht, J. Lyklema, W. Norde, G. Schraa, and A.J.B. Zehnder, "The Role of Bacterial Cell Wall Hydrophobicity in Adhesion", Applied and Environmental Microbiology, vol. 53, no. 8, (1987) 1893-1897.

Acknowledgment

The work conducted was supported by the Department of Interior Mineral Institute program administered by the USBM under Grant G1184126.

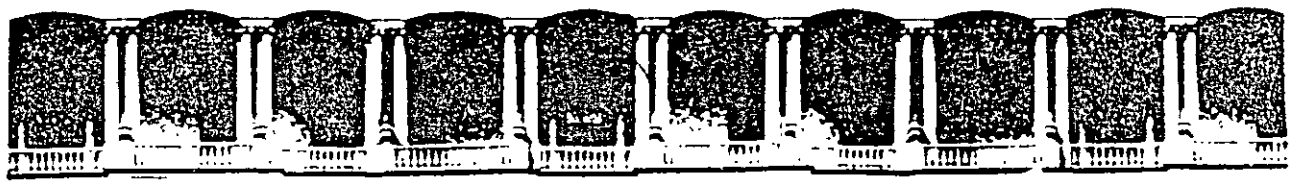

FACULTAD DE INGENIERIA U.N.A.M.
DIVISION DE EDUCACION CONTINUA

CURSOS ABIERTOS

DESARROLLO Y OPERACIÓN DE SENSORES PARA CONTROL DIRECTO Y CONTINUO EN PLANTAS DE BENEFICIO DE MINERALES Y EN LA RESTAURACIÓN DEL MEDIO AMBIENTE

Del 18 al 23 de mayo de 1998

TEMA: ANALYSIS OF WET GRINDING CIRCUIT CONTROL USING INFERENTIAL PARTICLE SIZE MEASUREMENT

EXPOSITOR :DR. KOMAR KAWATRA

1998

Prestridge, F.L., 1973, U.S. Patent 3,772,180.

Prestridge, F.L., 1974, U.S. Patent 3,847,775.

Prestridge, F.L., 1978, U.S. Patent 4,126,537.

Prestridge, F.L. and Longwell, R.L., 1981, U.S. Patent 4,308,127.

Sadek, S.E. and Hendricks, C.D., 1974, "Electrical Coalescence of Water Droplets in Low-Conductivity Oils," *I&EC Fund.*, 13, 139-142.

Warren, K.W., Prestridge, F.L., Sinclair, B.A., 1978, "Electrostatic Separators May Supplant Mixer-Settlers," *Mining Engineering, 30* (4), 355-357.

Waterman, L.C., 1965, "Electrical Coalescers," *Chem. Eng. Prog., 61* (10), 51-57.

Analysis of Wet Grinding Circuit Control Using Inferential Particle Size Measurement

S.K. Kawatra and R.A. Seitz

Abtract—*The use of inferential particle sizing for closed wet grinding circuit control has been practiced for several years. This paper presents a review of some inferential sizing equations developed for pilot and industrial plants using regression analysis. An analytical development is then presented showing how the general inferential sizing model arises from the nature of the classifier model. The relation between the general sizing model and the individual equations is then discussed.*

Introduction

The development of mathematical models capable of describing classifier performance and relating it to circuit operating variables permits the classifier to be used as an on-line sizing instrument. This use provides two additional benefits over the use of alternative methods of on-line size analysis (Hinde and Lloyd, 1975; Kawatra et al., 1979):

- Data from the instrumentation used for inferring particle size provides significant information on the performance of the grinding circuit, and
- Problems associated with the sampling of high-volume slurry streams are avoided along with their errors.

A number of concentrators have implemented grinding circuit control using inferential sizing, for forward and reverse closed wet circuits with spiral, rake, and cyclone classifiers. This approach is based on an experimental analysis by Rao (1966) of the effect of changes in operating variables on the performance of cyclones. The following is a review of the sizing equations developed at some of these mills.

- Asarco's Silver Bell ball mill cyclone circuit (Lynch, 1977):

$$\ln(\% + 65 \text{ mesh}) = K_O + K_1 \text{MFO} - K_2 \text{MFW} - K_3 \text{FF} + K_4 \text{TW} \quad (1)$$

- Climax Molybdenum Co. ball mill cyclone circuit (Manning and Chang, 1977):

$$\log(\% + 100 \text{ mesh}) = 1.554 + 0.00004 \text{MFO} - 0.0001 \text{MFW} + 0.0002 \text{FF} \quad (2)$$

After additional data collection, this equation was reevaluated and became

$$\log(\% + 100 \text{ mesh}) = 1.294 + .00263 \text{FF} - .00033 \text{MFW} \quad (3)$$

ball mill/spiral classifier circuit (Manning, 1978):

$$\% + 100 \text{ m} = -8.622 + .875 \text{ Density} + 0.0297 \text{FF} + 3.0285 \text{CLR} - 0.00323 \text{CL} \quad (4)$$

- Mount Isa Mines Number 1 concentrator, ball mill/cyclone circuit (Lynch, 1977):

$$\log(\% - 200 \text{ mesh}) = 1.8995 - 0.00299 \text{FF} + 0.002638 \text{MFW} - 0.01475 \text{P} \quad (5)$$

Due to difficulties in measuring pressure, the pressure term was removed and this equation was developed:

$$\log(\% - 200 \text{ mesh}) = K_1 \text{MFW} - K_2 \text{MFO} - K_3 \text{FF} + K_4 \quad (6)$$

Control of the Number 4 concentrator has been instituted using an even simpler equation (Fewings et al., 1979):

$$\% - 200 \text{ mesh} = K_1 - K_2 \text{FF} + K_3 \text{BMW} \quad (7)$$

- Pinto Valley ball mill/cyclone circuit (Watts et al., 1978)

$$\% + 65 \text{ mesh} = K_1 + K_2 \text{LN(CFV.CFD)} + K_3 \text{LN CPP} \quad (8)$$

- New Broken Hill Consolidated Ltd. ball mill/rake classifier (Lynch, 1977):

$$\% + 63\mu = 0.067 \text{FF} + 26.7 \text{ density} \quad (9)$$

- Pilot circuits:

Ball mill/cyclone (Watson et al., 1970):

$$\% - 200 \text{ mesh} = 66.38 - 2.74 \text{FF} + .33 \text{BMW} - .50 \text{MWA} \quad (10)$$

Ball mill/cyclone (Wiegal, 1973):

$$\% - 325 \text{ mesh} = 154.07 - .4944 \text{MFO} - .2259/\text{MFW} \quad (11)$$

Later, using additional data, this model was reevaluated and changed to

$$\% - 325 \text{ mesh} = 70.34 + 1.043 \text{MFW} - .724 \text{MFO} \quad (12)$$

S.K. Kawatra, member SME, associate professor, and **R.A. Seitz**, member SME, graduate student, are with Michigan Technological University, Houghton, MI. SME preprint 82-18, SME-AIME Annual Meeting, Dallas, TX, Feb. 1982. Manuscript Oct. 1982. Discussion of this paper must be submitted, in duplicate, prior to Aug. 31, 1984.

emulsion formation was due to increased mixing intensity in the eductors at this higher feed rate or to insufficient residence time in the coalescing vessel.

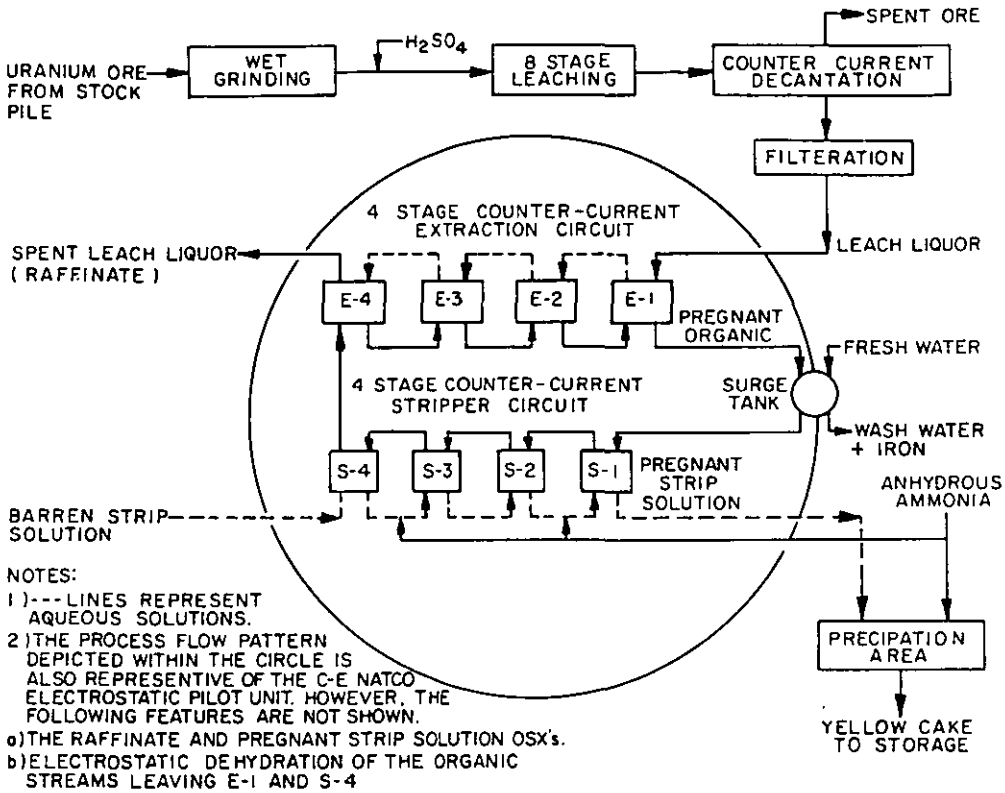

Fig. 1—A flow diagram of the United Nuclear Church Rock Mill and C-E Natco SX pilot plant

Table 1*—Operating Log for United Nuclear and C-E Natco SX Systems

Date	Feed Rate (l/min)	Organic Rate (l/min)	Strip Rate (l/min)	Feed Conc (g/l U_3O_8)	Raffinate (g/l U_3O_8)	Pregnant Organic (g/l U_3O_8)	Barren Organic (g/l U_3O_8)	Strip. Effic. %	Pregnant Strip (g/l U_3O_8)	Extr. Effic. %
UNITED NUCLEAR SX SYSTEM										
10-28-80	6050	2460	76	0.370	0.0111	1.218	0.0732	94.0	42.3	97.0
10-29-80	6050	2460	76	0.422	0.0030	1.195	0.0558	95.3	37.1	99.3
10-30-80	5300	2460	95	0.438	0.0038	1.193	0.0398	96.7	39.0	99.1
C-E NATCO ELECTROSTATIC SX PILOT SYSTEM										
10-28-80	370	150	5.7	0.408	0.0059	1.119	0.0976	91.3	39.7	98.6
10-29-80	460	160	6.2	0.441	0.0038	1.382	0.1125	91.9	32.0	99.1
10-30-80	590	230	7.8	0.453	0.0109	N.A.	N.A.	--	39.5	97.6

*All analyses performed by United Nuclear

Summary

Electrostatic coalescers have been shown to offer two advantages over conventional mixer-settlers in a uranium SX system. First, electrostatic coalescers operate at much higher liquid loading rates than gravity settlers, thereby reducing plant size and reagent inventories. At a feed rate of 8 L/s (125 gpm) the C-E Natco SX system operated at six times the liquid loading rate of conventional mixer-settlers. Secondly, the use of electrostatic coalescence reduced aqueous communication between extraction and stripping circuits. ■

References

Allan, R.S. and Mason, S.G., 1961, "Effects of Electric Fields on Coalescence in Liquid-Liquid Systems," *Trans. Far. Soc., 57,* 2027-2040.

Bailes, P.J. and Larkai, S.K.L., 1981, "An Experimental Investigation into the Use of High Voltage D.C. Fields for Liquid Phase Separation," *Trans. IChemE., 59,* 229-237.

Pearce, C.A.R., 1954, "The Mechanism of the Resol of Water-In-Oil Emulsions by Electrical Treatment," *J. Appl. Phys., 5,* 136-143.

Pohl, H.A., 1951, "The Motion and Precipitation of Suspensoids in Divergent Electric Fields," *J. Appl. Phys., 22* (7), 869-871.

Development of General Inferential Sizing Model

The development of mathematical models reported by Lynch (1977) and Plitt (1971, 1973) that are capable of simulating classifier performance, permits the classifier to be used as an on-line sizing sensor. This use of the classifier in the inference of particle size is based on the reduced efficiency curve, relating d/d_{50c} to $E_c(d)$, and relationships between d_{50c} and circuit operating variables.

If f(d) is the fraction of particles of size d in the feed, and R_f is the fractional recovery of water to the underflow, the fraction of particles of size d subject to classification is

$$f(d)\,(1-R_f) \tag{13}$$

The recovery of this fraction to the classifier fine product is

$$f(d)\,(1-R_f)\,[1-E_c(d)] \tag{14}$$

The total recovery of particles to the overflow is

$$\sum_{d=0}^{d_{max}} f(d)\,(1-R_f)\,[1-E_c(d)] \tag{15}$$

Hence, the size distribution of the overflow can be calculated

$$f_{o/f}(d) = \frac{f(d)\,[1-E_c(d)]}{\sum_{d=0}^{d_{max}} f(d)\,[1-E_c(d)]} \tag{16}$$

Thus, the percentage of particles in the classifier overflow finer than size D, i.e. PMD, is

$$PMD = 100\left(\frac{\sum_{d=0}^{D} f(d)\,[1-E_c(d)]}{\sum_{d=0}^{d_{max}} f(d)\,[1-E_c(d)]}\right) \tag{17}$$

Note that the size distribution of the overflow can be determined without knowledge of R_f.

Plitt (1971, 1973) modeled the relationship between $E_c(d)$ and d/d_{50c} using

$$E_c(d) = 1 - \exp[-.6931(d/d_{50c})^m] \tag{18}$$

The Schuhmann equation can be used to represent the cumulative size distribution of ore particles

$$P_f = 0.5[d/f(50)]^{\alpha} \tag{19}$$

Lowrison (1974) stated that the exponent α is dependent on the comminution process and gave typical values for crusher/rod mill products and ball mill products. The exponent m is dependent on the classification behavior of the ore particles and, according to Lynch (1977), remains constant. Typical values of m for silica and copper ore were given by Plitt (1973) and for taconite ore by Lynch (1972).

It should be understood that m is an ore-grinding circuit characteristic and should be determined specifically for each system of interest, since considerable differences can exist for the same ore in different circuits. From equation (17) and the above discussion, it is apparent that the PMD is a function of the classifiers feed size distribution and reduced efficiency curve, which can be characterized by f(50) and d_{50c}, respectively

$$PMD = g[f(50), d_{50c}] \tag{20}$$

To quantify this relationship between PMD and d_{50c}, a computer simulation of a classifier was carried out.

Since the classification equations are point functions with respect to size, the feed was subdivided into 100 equal parts to minimize the error associated with obtaining an average particle size for the particle size fractions. Classifier behavior has then simulated by using equations (18) and (19) with equation (17), a range of values of α and m, and by varying the ratio: $d_{50c}/f(50)$. From these simulations, a family of curves showing the relationship between PMD and d_{50c} were developed. Figure 1 shows the general relationship between PMD and $d_{50c}/f(50)$ for m = 2.0 and α = 0.5, 0.625, 0.75, 0.875, 1.0.

Analysis of all these families of curves over the region of major interest shows that the relationship between PMD and d_{50c} is

$$\log PMD = K_0 - K_1 \log d_{50c} \tag{21}$$

where the parameters K_0 and K_1 are functions of m and α. This equation, based only on the nature of the classifier performance curve and the size distribution of particles, is essentially the same equation that Rao (1966) developed by regression analysis of data from an extensive experimental study of the behavior of silica in a closed-circuit test rig.

In a closed loop grinding circuit, variations in α, which is dependent on ore breakage characteristics and feed rate, may be accounted for by using some directly related variable such as the circulating load or new feed rate.

Using equation (21) and the relationships between d_{50c} and operating variables reported by Lynch (1977) and Plitt (1973), various forms of an inferential sizing equation for grinding circuit control can be postulated.

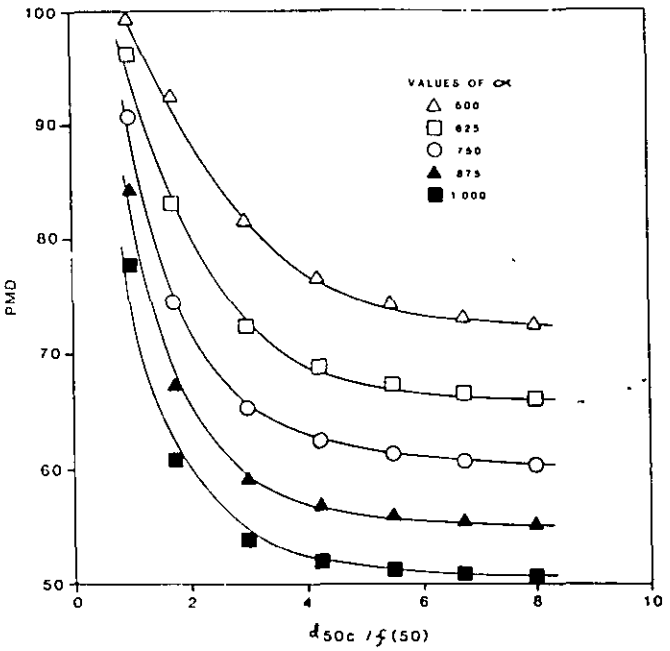

Fig. 1—Analytical relationship between percent passing size D in the cyclone overflow and the ratio of d_{50c}/cyclone feed 50% passing size for selected values of m, α, and D

Discussion

Equations relating d_{50c} to operating variables have been developed using regression analysis (Lynch, 1977; Plitt, 1973). The predicted effects of changing operating variables can be determined by combining equation (21) with some of these equations relating d_{50c} to operating variables. This analysis also provides information on the types of variables and equation forms that should be found in inferential sizing equations. The exact nature of the sizing equation will be site specific.

Cyclones are often selected and operated over the range of equation (21) where a linear relationship between PMD and d_{50c} exists

$$PMD = K_0 - K_1 d_{50c} \quad (22)$$

Again, using the reported relations between d_{50c} and operating variables, a group of equations relating PMD to operating variables could be developed. The effect of grinding circuit operating philosophy must also be considered in this analysis, since it will affect the nature and range of variations in the operating variables.

The work of Hinde and Lloyd (1975) indicates the parameters and possibly even the form of the equation will require constant updating due to short- and long-term variations. Such factors as the relationship between the mineralogy of the ore and its grinding characteristics, or the effect of wear and d_{50c} of the cyclone, can be of critical importance. The required frequency of updating will depend on individual concentrator characteristics.

The factors discussed above should give some idea of the multitude of different inferential sizing equations that could arise.

Conclusion

This analysis provides a fundamental basis for developing inferential sizing equations that should be better than the random use of regression analysis on plant data. Also, this method of analysis permits the simulation of classifier behavior without requiring knowledge of R_f. Even though the water entrainment mechanism is probably size-dependent, the resulting error should be minimal. If this mechanism can be modeled, then even this error source can be eliminated. ■

Definitions of Terms and Symbols

BMW — Water added to ball mill sump, TPH
CFD — Cyclone feed density, SGU
CFV — Cyclone feed volume, GPM
CL — Circulating load, TPH
CLR — Circulating load ratio
CPP — Cyclone pump power, SGU
d_{50c} or
d_{50} corrected — Size of particle in the feed pulp that is equally distributed between the overflow and underflow streams due soley to classification
Density — Mass/volume in appropriate units
$E_c(d)$ — The fraction of particles in the feed of size d that appear in the underflow due to classification
f(d) — The fraction of particles of size d in the feed
f(50) — Mass median particle size, the size at which $P_f = 0.5$
$f_{o/f}(d)$ — The size distribution of the overflow
FF — Mass flow of fresh feed to mill, TPH
FPS — Weight percent solids of cyclone feed
GPM — Gallons per minute
LPM — Flow rate of cyclone feed
LPM — Liters per minute
m — Classifier performance curve parameter
MFO — Mass flow of solids to cyclone, TPH
MFW — Mass flow of water to cyclone, TPH
MWA — Water addition to mill feed, LPM
P_f — The mass fraction of particles smaller than size d
P — lb/in^2, gauge pressure of cyclone feed
PMD — The percentage of particles in the overflow that are finer than size D
K_j — Model parameters
R_f — The fractional recovery of water to the underflow
TW — Total water addition to circuit, TPH
TPH — Tons per hour
α — Gaudin-Schuhmann distribution modulus
β — Volume percent solids of cyclone feed
ρ_p — Density of cyclone feed, g/ml
ρ_s — Density of ore particles, g/ml

Acknowedgments

The authors thank the US Bureau of Mines for support of this work. This paper is based on a presentation given by the authors at the 1982 AIME Annual Meeting and subseq work performed with funding from the US Bureau Mines.

References

Fewings, J.H., Wickham, P., and Wiseman, D., 1979, "Centralized Control of a Mineral Processing Plant Using a Digital Computer," 16th APCOM, Tucson, AZ, pp. 579-593.

Hinde, A.L., and Lloyd, P.J.D., 1975, "Real Time Particle Size Analysis in Wet Closed Circuit Milling," Powder Tech., 12, pp. 37-50.

Kawatra, S.K., and Thayer, D.M., 1979, "Particle Size Control in a Wet Grinding Circuit," 16th APCOM, Tucson, AZ, pp. 595-603.

Lowrison, G.C., 1974, *Crushing and Grinding*, CRC Press, Cleveland, OH, p. 286.

Lynch, A.J., 1972, "Preliminary Study of the Classification of Taconite in Hydrocyclones," Univ. Minn. MRRC progress report No. 27, Aug., pp. 43-54.

Lynch, A.J., 1977, *Mineral Crushing and Grinding Circuits*, Elsevier, New York, p. 342.

Manning, K.L., and Chang, J.W., 1977, "Computer Control of a Cyclone Grinding Circuit at Climax Molybdenum Company," paper 77-B-373, SME fall meeting.

Manning, K.L., 1978, "Computer Control of Grinding Climax," *Mining Congress Journal*, Nov., pp. 47-50.

Plitt, L.R., 1971, "The Analysis of Solid-Solid Separations in Classifiers," *CIM Bulletin*, Apr., pp. 42-47.

Plitt, L.R., 1973, "A mathematical Model of the Hydrocyclones Classifier," *CIM Bulletin*, Dec., pp. 114-123.

Rao, T.C., 1966, "The Characteristics of Hydrocyclones and Their Application as Control Units in Comminution Circuits, Ph.D. thesis, Univ. of Queensland, Brisbane.

Watson, D., Cropton, R.W.G., and Brookes, G.F., 1970, "Modeling Methods for a Grinding Classification Circuit and the Problems of Plant Control," *Trans. Inst. Min. Metall.*, section C, pp. 112-119.

Watts, J.C., Thompson, P.E., and White, J.W., 1978, "Hierarchial Computer Monitoring and Grinding Control at Pinto Valley, paper 78-B-60, AIME meeting, Denver, CO.

Wiegal, R.L., 1973, "The Direct Digital Control of Cyclone Overflow Size in Taconite Processing," Univ. of Minn. MRRC progress report No. 29, Apr., pp. 1-41.

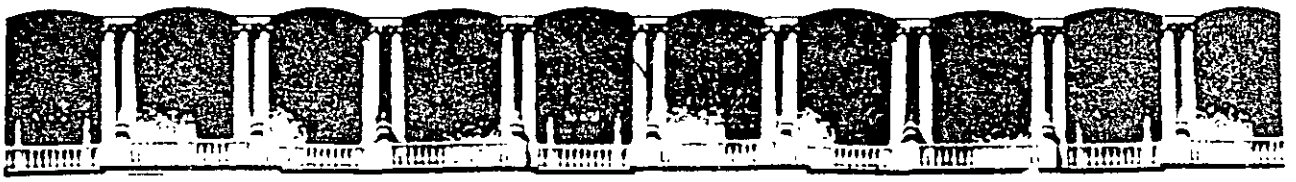

FACULTAD DE INGENIERIA U.N.A.M.
DIVISION DE EDUCACION CONTINUA

CURSOS ABIERTOS

DESARROLLO Y OPERACIÓN DE SENSORES PARA CONTROL DIRECTO Y CONTINUO EN PLANTAS DE BENEFICIO DE MINERALES Y EN LA RESTAURACIÓN DEL MEDIO AMBIENTE

Del 18 al 23 de mayo de 1998

TEMA: COAL DESULFURIZATION BY BACTERIA

EXPOSITOR :DR. KOMAR KAWATRA
1998

Palacio de Minería Calle de Tacuba 5 Primer piso Deleg. Cuauhtemoc 06000 México, D.F. APDO. Postal M-2285
Telefonos. 512-8955 512-5121 521-7335 521-1987 Fax 510-0573 521-4020 AL 26

being conducted in the following areas: determinations of the types of fracture-hosted minerals and their behavior during leaching, permeability enhancement, mineral solubility, rate of leach solution diffusion and how it relates to fluid viscosity, and geochemical computer modeling. ■

References

Lewis, W.E., and Tandanand, S., 1974, "Bureau of Mines Test Procedures for Rocks," IC 8628, US Bureau of Mines, 223 pp.

Mallio, W.J., Park, W.C., Pojasek, W.J., and Rainville, G.D., 1981, "Parameters and Petrographic Interpretation of In Situ Copper Leaching," *Process Mineralogy*, TMS-AIME, pp. 339-352.

Coal desulfurization by bacteria

S.K. Kawatra, T.C. Eisele, and S. Bagley

Abstract – *To meet federal air pollution guidelines, it is necessary to remove a considerable quantity of sulfur from many North American coals. This may be accomplished by oxidizing the sulfur to water soluble forms, followed by washing the coal. Selective oxidation of the various sulfur forms can be accomplished through the use of a variety of types of bacteria. In this paper, the various bacteria and their requirements are described, and processes using bacteria to remove coal sulfur are discussed.*

Introduction

Perhaps the single most important pollutant produced during the combustion of coal is sulfur dioxide, the primary cause of acid precipitation (Dugan, 1986). This is a particular problem with high-sulfur eastern and midwestern coals. Although sulfur emissions may be greatly reduced by simply burning low-sulfur western coal, this is frequently not a practical option for eastern utilities, due to high transportation costs. Also, while sulfur oxides can be removed from the stack gases by scrubbers, these devices are quite expensive to install and operate. An economical, effective technique for removing sulfur from coal prior to combustion is therefore desired.

Microbial coal desulfurization makes use of the abilities of certain bacteria to metabolize the sulfur forms contained in the coal and, in the process, convert it to a form that can be more easily removed (Dugan, 1986). A variety of bacteria can be used for this purpose, to remove particular types of sulfur under various sets of conditions (Ehrlich, 1986). This paper presents a review of the techniques and the bacterial species being used for coal desulfurization.

Forms of sulfur

Sulfur in coal is typically present in three primary forms: sulfate, sulfide, and organic compounds (Wizzard et al., 1983). Sulfate sulfur is in the form of various sulfate salts that can be fairly easily removed and contribute only a minor portion of the total sulfur. Sulfide minerals, on the other hand, typically account for 50% of the total sulfur. Sulfides are generally either pyrite or marcasite and occur as particles ranging from submicron sizes to sizable lumps. While large pyrite particles are readily removed by a variety of gravity separation techniques, the finest pyrite cannot be effectively liberated from coal and, therefore, must be caused to dissolve if it is to be removed. Organic sulfur compounds make up the remainder of coal sulfur. A wide variety of such compounds occur, but the most prevalent are the thiophenes (Isbister and Kobylinski, 1985).

In general, pyrite and organic sulfur require differing types of bacteria for their removal. Bacteria for pyrite dissolution use pyrite oxidation as their primary energy source, whereas bacteria that remove organic sulfur typically do so as a secondary portion of their metabolism.

Bacteria useful in coal desulfurization

The most important bacteria in desulfurizing coal fall into three general classes: (1) acidophilic bacteria growing at ambient or slightly elevated temperatures, such as certain *Thiobacillus* species (Hoffmann et al., 1981); (2) acidophilic bacteria growing at extremely elevated temperatures, such as the various *Sulfolobus* species (Murphy et al., 1985); and (3) altered soil bacteria, which grow at ambient temperatures and approximately neutral pH, such as the mutant strain CB1 of the Atlantic Research Corp. (Isbister and Kobylinski, 1985).

Thiobacillus

The most frequently used bacteria of this genus is the species *T. ferrooxidans,* which oxidizes pyrite to soluble sulfates. This species has no confirmed ability to remove organic sulfur compounds. The dissolution of pyrite by *T. ferrooxidans* proceeds by both an indirect and a direct mechanism, of which the indirect is better understood (Silverman, 1967). In indirect oxidation, pyrite oxidation occurs as a result of the action of the Fe^{+3} ion, according to the equation (Hoffmann et al., 1981)

$$FeS_2 + 14Fe^{+3} + 8H_2O \rightarrow 15Fe^{+2} + 2SO_4^{-2} + 16H^+ \quad (1)$$

S.K. **Kawatra** and T.C. **Eisele**, members SME, are professor and graduate research assistant, respectively, Department of Metallurgical Engineering, and S. **Bagley** is an associate professor, Department of Biological Sciences, Michigan Technological University, Houghton, MI.

SME preprint 87-133, SME-AIME Annual Meeting, Denver, CO, February 1987. MMP paper 87-623. Manuscript March 1987. Discussion of this paper must be submitted, in duplicate, prior to Jan. 31, 1988.

which proceeds spontaneously when the Fe^{+3}/Fe^{+2} ratio is greater than 2:1 (Singer and Stumm, 1970). While Fe^{+2} can be oxidized to Fe^{+3} by free oxygen, the uncatalyzed reaction is extremely slow. However, if *T. ferrooxidans* is present, the rate of the regeneration reaction (Hoffmann et al., 1981)

$$4Fe^{+2} + O_2 + 4H^+ \xrightarrow{Bacteria} 4Fe^{+3} + 2H_2O \quad (2)$$

can be accelerated by a factor of as much as 10^6 (Singer and Stumm, 1970). So, in the presence of these bacteria, the overall reaction for indirect oxidation of pyrite is

$$FeS_2 + \tfrac{1}{2}O_2 + H_2O \xrightarrow{Bacteria} Fe^{+2} + 2SO_4^{-2} + 2H^+ \quad (3)$$

Since the actual pyrite oxidation is carried out by the Fe^{+3} ion, the bacteria need not be in intimate contact with the pyrite, as long as transport of ions to and from the pyrite surface is fairly unobstructed. Indirect oxidation can only occur at pH values less than 4, as at higher pH values the Fe^{+3} ions will precipitate as insoluble iron hydroxides (Baker and Miller, 1971).

The direct oxidation mechanism requires intimate contact between pyrite and bacteria, as in this case the disulfide is being oxidized without a soluble intermediate. Direct oxidation by *T. ferrooxidans* proceeds at only about one-seventh the rate of indirect oxidation, provided that sufficient Fe^{+3} is present for the indirect process to occur. However, when little dissolved iron is present, only direct oxidation is possible. It is then the dominant process until oxidation of pyrite has released sufficient iron into solution for indirect oxidation to be practical (Singer and Stumm, 1970).

Another acidophilic *Thiobacillus* species, *T. thiooxidans,* is also capable of dissolving pyrite, although not as rapidly as *T. ferrooxidans*. However, mixed cultures of these two species dissolve pyrite at a substantially greater rate than either bacteria alone. This is apparently due to the ability of *T. thiooxidans* to catalyze the oxidation of pyrite by Fe^{+3}, while *T. ferrooxidans* regenerates the oxidizing agent (Hoffmann et al., 1981). Other bacterial species may also be used to regenerate Fe^{+3}, although they may lack the capability of *T. ferrooxidans* for direct sulfur oxidation and, hence, may not be as effective for this purpose (Norris et al., 1986).

Sulfolobus

Bacteria of the *Sulfolobus* genus are acidophiles and extreme thermophiles, requiring pH in the range of 1.5 to 4 and temperatures in the range of 50° to 80°C. These bacteria are native to sulfurous hot springs worldwide (Brock, 1978). Their primary advantage is their ability to catalyze pyrite oxidation at elevated temperatures, shortening the time required for oxidation to occur.

Unlike *T. ferrooxidans* and *T. thiooxidans, Sulfolobus* species are capable of extracting metabolic energy from sources other than oxidation of inorganic material. For this reason, it has been considered possible that removal of organic sulfur may be accomplished using *Sulfolobus*. While some researchers have reported that *S. acidocaldarius* is indeed capable of removing a portion of the organic sulfur (Kargi and Robinson, 1986), this has not yet been proven (Dugan, 1986). This uncertainty is due to the difficulties involved in accurately determining the organic sulfur content of coal, and to the possibility that some organic sulfur dissolves naturally at elevated temperatures.

At present, little meaningful comparative data for sulfur removal by *T. ferrooxidans* and *S. acidocaldarius* exists. This lack is due to the extreme heterogeneity of coal, which ensures that unless investigators ha taken care to use identical coal samples for bo bacteria, results are not directly comparable. However, it appears that *S. acidocaldarius* can remove pyrite approximately twice as fast as *T. ferrooxidans*.

Mutated soil bacteria

Atlantic Research Corp. has developed a mutant bacteria strain from certain soil bacteria that were originally minimally capable of oxidizing organic sulfur compounds, particularly thiophenes. The mutant, labeled CB1, has considerably enhanced thiophene-oxidizing capabilities over its parent culture (Isbister and Kobylinski, 1985). Experimentation with radioisotope-labeled dibenzothiophene showed that CB1 oxidizes sulfur from thiophene compounds without breaking the carbon ring structure. This is in contrast with other thiophene-oxidizing microbes that break the rings but do not release the sulfur.

The strain CB1 oxidizes thiophenes over a temperature range of 25° to 40°C and at approximately neutral pH. This strain is capable of removing up to 47% of the organic sulfur from certain coals. However, it has not been effective in dissolution of pyritic sulfur (Isbister and Kobylinski, 1985) and, therefore, requires that pyrite be removed by some other means. Since CB1 cannot survive at the low pH values required by *T. ferrooxidans* and *S. acidocaldarius,* it cannot be used in mixed cultures with pyrite-removing bacteria.

Bacterial processing techniques

Microbial leaching

Sulfur removal by bacterially catalyzed oxidation imposes the following requirements on any process that makes use of it: (1) the leaching unit must have sufficient residence time for dissolution to be carried out, generally a period ranging from several days to over a week; (2) the solution temperature and pH must be closely controlled at the optimum values for bacterial growth; (3) supplemental nutrients and oxygen must be supplied to the bacteria; and (4) the coal must be reduced to a fine size, as leaching rates increase rapidly with decreasing particle size (Beier, 1985). In addition, means must be provided for removing and neutralizing the sulfate produced by the leaching process and for supplying seed bacteria to the beginning of the process.

Handling of the bacteria is of critical importance in maintaining the bacteria in the proper growth phase for optimum pyrite removal. The various growth phases are illustrated in Fig. 1 (Murphy et al., 1985). The lag phase is the time required for the bacteria to acclimate themselves to conditions, while the stationary and death phases result from depletion of nutrients or accumulation of toxins. For best results in continuous processing, bacteria should be maintained as much as possible in the exponential phase, as they are then multiplying and metabolizing sulfur at thei maximum rate (Murphy et al., 1985). Since maintaining bacteria at the exponential growth phase may be difficult, bioleaching processes frequently maintain a seed culture in a separate fermenter. This supplies bacteria to the desulfurization process as needed.

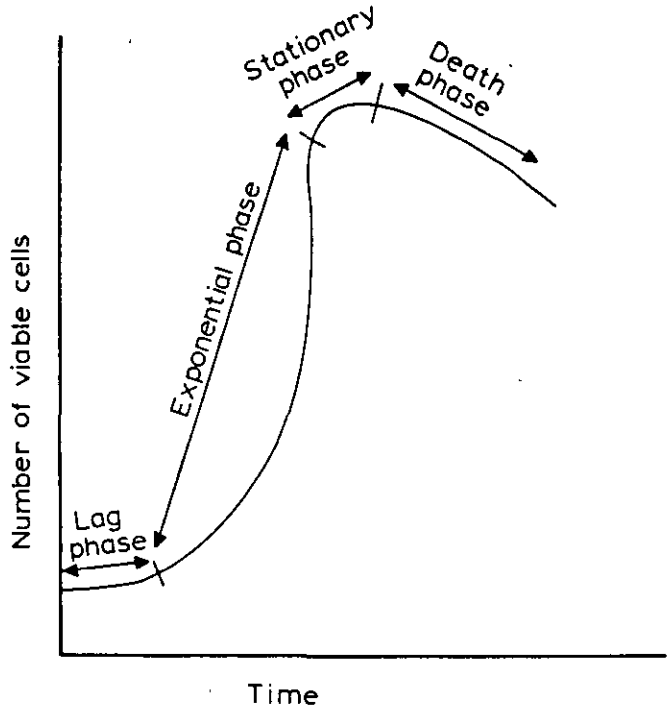

Fig. 1 — Generalized growth curve of a bacterial culture in a batch process

A typical process flowsheet for continuous microbial coal desulfurization is illustrated in Fig. 2 (Murphy et al., 1985). Ground coal, air, bacteria, and heat (if required) are added to any of a variety of reactor types. Treated coal slurry is withdrawn from the reactor and thickened, with the solids filtered, washed, and dried to produce a desulfurized product. Also, the exhaust air from the reactor is scrubbed to remove acid fumes that would otherwise be released in the immediate vicinity of the process. The solutions from the thickener, filter, and exhaust gas scrubber, which contain the products of the sulfur oxidation, are then sent to the precipitator, where the sulfates are removed by addition of lime and occasionally aluminum salts. The resulting sulfate precipitate is then disposed of, and the cleaned water is returned to the reactor. The major variation in bioleaching circuits is in the design of the reactor. The reactor used must provide long residence times at reasonable cost, should approach plug flow to maximize kinetics, and yet should have sufficient backmixing to prevent "washout" of the bacteria. In the case of pyrite dissolution, the reactor should also be resistant to corrosion by acidic slurries and, hence, use a minimum number of moving parts.

There are three basic configurations for practical bioleaching reactors: cascades of continuously stirred tanks, pipelines, and horizontal rotating drums (Vaseen, 1985).

Cascades of stirred tanks have the advantage of being highly controllable, with leaching being carried out in discrete steps. Either mechanically or pneumatically agitated tanks may be used, as air must be supplied to the bacteria in any case. However, the requirement of long residence times ensures that plants of this type must be extremely large (Vaseen, 1985).

Bioleaching in a coal-slurry transport pipeline has the major advantage that coal is being transported to the end user while leaching is being carried out, and that the transportation and reactor time costs are combined (Beier, 1985). However, such a system provides little control of residence time, which is primarily determined by the distance to the end user. Also, addition of air to the slurry is somewhat difficult, and the lifetime of the pipeline is reduced by the corrosive nature of the slurry.

The horizontal rotating drum reactor consists of a very long horizontal drum, equipped with slurry lifters and means for supplying air to the slurry all along the drum length. The drum is rotated at from 1 to 20 rpm to provide agitation. Such a reactor provides a compromise between plug flow and backmixing suitable for maintaining a good bacterial distribution (Vaseen, 1985). Again, a reactor of this type must be very large, requiring a 20:1 length to diameter ratio to provide sufficient residence time for leaching by *T. ferrooxidans* (Vaseen, 1985).

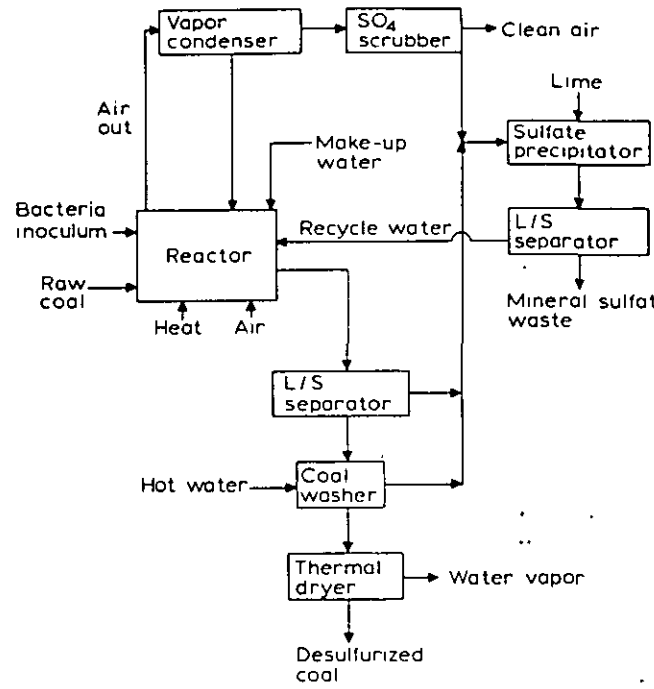

Fig. 2 — Typical process flowsheet for biological desulfurization of coal

A bioleaching system could either be located at the plant where the coal will be burned or at the mine, depending on the circumstances. Locating the leaching operation at the plant allows the use of waste heat for maintaining the slurry at the proper temperature and for drying the cleaned coal (Murphy et al., 1985). However, if the plant receives coal from a variety of suppliers, the need to adjust the process for great variations in feed character may make this arrangement impractical. Locating the operation at the mine will ensure a fairly consistent coal quality, but, here, heating and drying costs will be greater. These costs may be reduced if a coal-water fuel (60% to 75% by weight coal) is produced because thermal drying is then unnecessary. The bioleaching process is therefore most suitable either (1) located at the power plant when coal is received from a single source, or (2) located at the mine if a coal-water fuel is the desired product.

Bacterially assisted coal cleaning

The primary disadvantage of microbially catalyzed sulfur oxidation is the long residence time required for sulfur removal to be completed, which makes for large installations and high capital costs. If bacterial treatment times can be reduced, processing will obviously become much more cost-effective. One method for reducing treatment time is to use bacteria to assist more conventional, physical separation processes.

Separation techniques that depend on differences in surface chemistry, such as froth flotation and oil agglomeration, have a limited ability to remove pyrite particles from coal (Baker and Miller, 1971). This is due to the slight hydrophobic character of pyrite, which causes it to attach to air bubbles and oil droplets to a greater extent than other common minerals contained in coal. Improving the pyrite-rejection capability of these processes therefore rests on rendering the surfaces of the pyrite particles hydrophilic.

While complete oxidation of pyrite by *S. acidocaldarius* or *T. ferrooxidans* is very time-consuming, the bacteria effectively alter the pyrite surface within a short time, on the order of 30 minutes. This is a result both of oxidation of the pyrite surface and of the direct attachment of the bacteria to the pyrite. Since the bacteria have a hydrophilic surface and the oxidation products of pyrite are also hydrophilic, the net result of the short-term bacterial action is to destroy the hydrophobicity of the pyrite surface.

The effect of bacterial treatment on physical pyrite removal was first noted for the oil agglomeration process (Kempton et al., 1980; Capes et al., 1973), where conditioning with bacteria produced a 50% decrease in product sulfur content (Kempton et al., 1980). Since oil agglomeration is itself not a particularly economical process due to the cost of the oil, attention has shifted to bacterially assisted froth flotation. Work by Attia and Elzeky, 1985, and Dogan et al., 1985, has indicated that this technique does improve pyrite rejection, without producing notable decreases in coal recovery. This is a failing of many chemical pyrite depressants (Baker and Miller, 1971).

Conclusions

Bacterial desulfurization of coal provides a method for oxidizing sulfur to water-soluble forms without the extreme conditions of temperature and pressure required for completely chemical desulfurization. Bacteria have been discovered or developed that are capable of oxidizing either inorganic or organic sulfur, but to date it has not been shown conclusively that any one bacteria is capable of oxidizing both. Also, presently available bacteria known to be capable of removing organic sulfur cannot survive in the extremely acidic conditions required by pyrite oxidizers, and, hence, the two types of bacteria cannot be used as a mixed culture.

Bacterial leaching is most effective in reactors that provide sufficient backmixing for good bacteria distribution, but otherwise approximate plug flow. This can be most readily achieved with cascades of stirred tanks, slurry transport pipelines, or horizontal rotating drum reactors. Due to the long treatment time required for sulfur oxidation to be completed (3 to 5 days for *S. acidocaldarius*, and 9 to 16 days for *T. ferrooxidans*), such installations must be extremely large.

In addition to their usefulness in catalyzing sulfur dissolution, pyrite-oxidizing bacteria are also capable of improving the pyrite rejection capability of oil agglomeration and froth flotation. This is accomplished by using the bacteria to coat and slightly oxidize the pyrite surface, thus destroying its normally slightly hydrophobic character. ■

References

Attia, Y.A., and Elzeky, M.A., 1985, "Biosurface Modification in the Separation of Pyrite from Coal by Froth Flotation," *Processing and Utilization of High-Sulfur Coals*, Coal Science and Technology #9, Elsevier, pp. 673-682.

Baker, A.F., and Miller, K.J., 1971, "Hydrolized Metal Ions as Pyrite Depressants in Coal Flotation: A Laboratory Study," Report of Investigation 7518, US Bureau of Mines.

Beler, E., 1985, "Removal of Pyrite from Coal Using Bacteria," *Processing and Utilization of High-Sulfur Coals*, Coal Science and Technology #9, Elsevier, pp. 653-672.

Brock, T.D., 1978, *Thermophilic Microorganisms and Life at High Temperatures*, Springer Verlag, New York.

Capes, C.E., McIlhinney, A.E., Sirianni, A.F., Puddington, I.E., 1973, "Bacterial Oxidation in Upgrading Pyritic Coals," *CIM Bulletin*, November, pp 88-91.

Dogan, M.Z., Ozbayoglu, G., Hicyilmax, C., Sarikaya, M., and Ozcengiz, G., 1985, "Bacterial Leaching Versus Bacterial Conditioning and Flotation in Desulfurization of Coal," *Proceedings*, 15th International Mineral Processing Congress, Cannes, France, Vol. 2, pp. 304-313.

Dugan, P.R., 1986, "Microbiological Desulfurization of Coal and Its Increased Monetary Value," *Biotechnology and Bioengineering Symposium No. 16*, John Wiley & Sons, pp. 185-203.

Ehrlich, H.L., 1986, "What Types of Microorganisms are Effective in Bioleachi Bioaccumulation of Metals, Ore Beneficiation, and Desulfurization of Foss Fuels," *Biotechnology and Bioengineering Symposium No. 16*, John Wiley & Sons, pp 227-237.

Hoffmann, M.R., Faust, B.C., Panda, F.A., Koo, H.H., Tsuchiya, H.M., 1981, "Kinetics of the Removal of Iron Pyrite from Coal by Microbial Catalysis," *Applied and Environmental Microbiology*, Vol. 42, pp 259-271.

Isbister, J.D., and Kobylinski, E.A., 1985, "Microbial and Desulfurization of Coal," *Processing and Utilization of High-Sulfur Coals*, Coal Science and Technology #9, Elsevier, pp. 627-641.

Kargi, F., and Robinson, J.M., 1986, "Removal of Organic Sulphur from Bituminous Coal," *Fuel*, Vol. 65, March, pp. 397-399.

Kempton, A.G., Monelb, N., McCready, R.G L., and Capes, C.E., 1980, "Removal of Pyrite from Coal by Conditioning with *Thiobacillus Ferrooxidans* Followed by Oil Agglomeration," *Hydrometallurgy*, Vol. 5, pp. 117-125.

Murphy, J., Riestenberg, E., Mohler, R., Marek, D., Beck, B., and Suidmore, D., 1985, "Coal Desulfurization by Microbial Processing," *Processing and Utilization of High-Sulfur Coals*, Coal Science and Technology #9, Elsevier, pp 643-652

Norris, P.R., Parrott, L., and Marsh, R.M., 1986, "Moderately Thermophilic Mineral-Oxidizing Bacteria," *Biotechnology and Bioengineering Symposium No 16*, John Wiley & Sons, pp. 253-262.

Silverman, M.P., 1967, "Mechanism of Bacterial Pyrite Oxidation," *Journal of Bacteriology*, Vol. 94, pp. 1046-1051.

Singer, P.L., and Stumm, W., 1970, "Acidic Mine Drainage: The Rate Determining Step," *Science*, Vol. 167, p. 1121.

Vaseen, V.A., 1985, "Commercial Microbial Desulfurization of Coal," *Processing and Utilization of High-Sulfur Coals*, Coal Science and Technology #9, Elsevier, pp 699-715

Wizzard, J.T., Cavallaro, J.A., and Duerbrouck, A.W., 1983, "Sulfur Reduction Potential of the Coals of Ohio," DOE/PETC/TR-83/7 (DE 83012219), Pittsburgh Energy Technology Center.

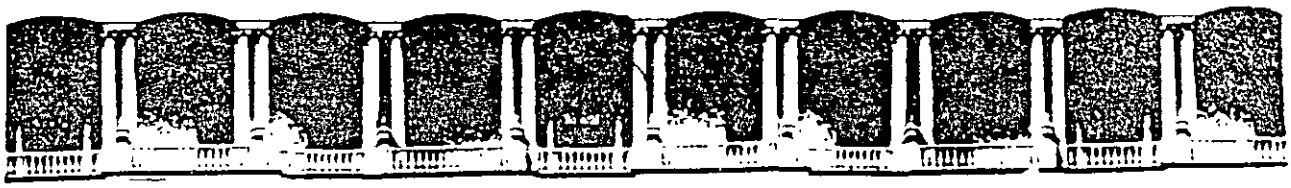

FACULTAD DE INGENIERIA U.N.A.M.
DIVISION DE EDUCACION CONTINUA

CURSOS ABIERTOS

DESARROLLO Y OPERACIÓN DE SENSORES PARA CONTROL DIRECTO Y CONTINUO EN PLANTAS DE BENEFICIO DE MINERALES Y EN LA RESTAURACIÓN DEL MEDIO AMBIENTE

Del 18 al 23 de mayo de 1998

TEMA: METHODS OF ON STREAM ANALYSIS

EXPOSITOR :DR. KOMAR KAWATRA
1998

Palacio de Mineria Calle de Tacuba 5 Primer piso Deleg Cuauhtémoc 06000 Mexico. D.F. APDO Postal M-2285
Teléfonos: 512-8955 512-5121 521-7335 521-1987 Fax 510-0573 521-4020 AL 26

SOCIETY OF MINING ENGINEERS OF AIME
CALLER NO. D, LITTLETON, COLORADO 80127

PREPRINT NUMBER
84-113

METHODS OF ON-STREAM ANALYSIS

S. K. Kawatra

Michigan Technological University
Houghton, Michigan

For presentation at the SME-AIME Annual Meeting
Los Angeles, California - February 26-March 1, 1984

Permission is hereby given to publish with appropriate acknowledgments, excerpts or summaries not to exceed one-fourth of the entire text of the paper. Permission to print in more extended form subsequent to publication by the Institute must be obtained from the Executive Director of the Society of Mining Engineers of AIME.

If and when this paper is published by the Society of Mining Engineers of AIME, it may embody certain changes made by agreement between the Technical Publications Committee and the author, so that the form in which it appears here is not necessarily that in which it may be published later.

These preprints are available for sale. Mail orders to PREPRINTS, Society of Mining Engineers, Caller No. D, Littleton, Colorado 80127.

PREPRINT AVAILABILITY LIST IS PUBLISHED PERIODICALLY IN MINING ENGINEERING

Methods of On-Stream Analysis

Abstract. In this paper three methods of on-stream analysis 1) Radiometric techniques, 2) X-ray tube techniques and 3) Neutron activation method are reviewed. Advantages and disadvantages of each method are discussed.

Introduction

An on-stream analyser cannot be considered in isolation from the mineral process where it is to be ultimately installed. Depending upon the requirements of the process, an on-stream analyser can be designed in several ways. If a feasibility study done on the process shows that several elements in a multi-channel stream are to be analysed with high precision, a very sophisticated on-stream analyser, which would take into account matrix effects etc., would be desirable. On the other hand, where moderate precision is required, a simple portable on-stream analyser can be designed. Despite the fact that sophisticated techniques are available for determining percentage of solids in a slurry, the Marcy Direct Reading pulp density scale finds extensive use in mineral processing plants.

The techniques currently being developed for on-stream analysis can be broadly classified into three categories:

1) Radiometric techniques
2) X-ray tube techniques
3) Neutron activation techniques

Radiometric Techniques

Radiometric analysis is well known in nearly all branches of science and technology. Such analysis has helped industry to achieve objectives which could not otherwise have been attained. A radioisotope gauge based upon the principle of backscattering of alpha particles was incorporated in the Surveyor V mission to analyse the surface of the moon (Turkevich, Franzgrote and Patterson, 1967). Now, radiometric techniques are finding extensive applications in mineral processing plants. Some of the main advantages and disadvantages of the radiometric techniques are discussed below.

1) Every radioisotope emits radiations which are subjected to statistical fluctuations. When an instrument is designed to measure some parameter of an object, care should be taken to ensure that the statistical error in the measurement is considerably less than the required precision.

2) Every radioactive isotope disintegrates at a characteristic rate that is defined by its half life, that is, the time required for a radioactive material to lose 50 percent of its activity by decay. Each radionuclide has a unique half life. A radioisotope selected for applications in gauging should normally have a half life of several years so that the daily rate of change of intensity is small and can be compensated for readily. For tracing purposes, radioisotopes with short half life can be selected. This is because the radioactivity will practically disappear in a short time after the completion of the test.

3) The intensity of the radiation can be measured with great precision and recorded.

4) The ability of the radiations to penetrate matter and to make measurements on the contents without contacting them is an important advantage.

5) An instrument using radioisotopes is normally small in size and relatively portable.

A radiometric analyser can be designed to operate as:

1) an adsorption system
2) a scatter system, and
3) a fluorescent system.

An Adsorption System

When radiation passes through matter, it loses intensity due to adsorption by the material. Based upon this principle, two types of gauges can be designed, that is, a density gauge or an element analysis probe. In the density gauge the loss in intensity is related to the density of the material. This property of the radiation is discussed in greater detail in subsequent sections. In the element analysis probe, the loss in intensity is related to the percentage of some specific element in the slurry. This technique is well known in the petroleum industry and increased use is being made in the mineral industry.

Hinckfuss and Stump (1971) and Stump (1973) used the preferential adsorption technique for the determination of lead content in slurries. Lead, with atomic number 82, is present in the Broken Hill ores in the mineral galena (PbS) and is associated with a matrix of elements of relatively low atomic number. A 100 KeV radiation (close to the adsorption edge of lead) obtained by filtering the radiation emitted by gadolinium-153 through 0.20 inches of tin was used to determine lead in flotation feed slurries.

Synman (1971) has determined the uranium content of slurries using 0.166 KeV radiation obtained from Ce-139. This radiation is preferentially adsorbed by the uranium.

Figure 1 is a schematic diagram of the adsorption type of system.

A Scatter System

In the scatter system, source and detector are placed on the same side of the material being examined. When the radiation strikes the material it is partly adsorbed and partly scattered. Again, as with the adsorption system, two types of gauges can be designed. In the density gauge some property of the scattered radiation is related to the density of the material (or the slurry). In the elemental analysis probe some property of the scattered radiation is related to a 'wanted' element in the material (or the slurry).

The scatter technique is very useful for density or thickness measurement when only one side of the material is available for examination. The technique is also useful for bulk density measurements of material such as coal (Semmler, Brugger and Rieke, 1961).

Czubek et al (1972) have described a gamma ray scattering method, using an americium-241 source for the field determination of iron in iron-bearing sands. They also used a fluorescent method which employed a 3H/Zr source together with an argon filled proportional counter

covered by a 20 um thick iron foil. They have reported an accuracy of 2% by both the methods.

Czubek et al (1972) have also described a method for determining lead and zinc in multimetallic ores. Two gamma ray sources, americium-241 and selenium-75 with energies on both sides of the lead K adsorption edge were used. They measured the scattered intensities from artificially prepared ore samples and determined the equivalent concentration of one element that produced the same decrease in scattered radiation as 1% of the other element. Using the information gained, a field probe was designed for simultaneous determination of lead and zinc.

Gorski and Lubecki (1965) used a beta backscatter technique for determining tungsten in the range 16 to 20 percent in the tool industry. The accuracy reported is $\pm$0.9% with a measurement time between 1 and 5 minutes.

Figure 2 is a schematic diagram of the scatter type of system.

A Fluorescent System

Any method that causes removal of an electron from one of the inner orbits of an atom and subsequent readjustment of the remaining electrons results in the emission of characteristic X-rays. The emission caused by filling vacancies in the innermost shell is called K X-rays while that caused by filling vacancies in the next shell is called L X-rays. Every element, when excited, emits X-rays at certain characteristic energies that are equal to the energies of the corresponding electron transitions. Thus, if a substance is suitably excited, the elements composing it can be determined as the X-ray intensity at each characteristic level depends upon the weight fraction of the elements emitting it. The basic components of a radioisotope X-ray fluorescence spectrometer are the radioisotope source for excitation and the X-ray detection system which isolates and records the intensity of the desired X-rays.

Different methods for excitation of X-rays from matter are discussed below.

1) Excitation by Alpha Particles. An alpha particle is a charged particle emitted from the nucleus of an atom having a mass equal in magnitude to that of a helium nucleus, that is, two protons and two neutrons. Excitation by alpha particles cause emission of low energy X-rays with high efficiency and is particularly suited for light elements from carbon to calcium (Carr-Brion and Payne, 1970). Excitation with alpha particles has a special advantage over beta particles in that less bremsstrahlung is produced. However, the hazard due to alpha particle is very high. Kohl et al (1961) classify alpha emitters among the most toxic poisons.

Robert and Martinelli (1964) have demonstrated the excitation of K X-rays of elements from carbon to chlorine by using a 6 mCi polonium-210 alpha source (Half life 138 days; α energy = 5.3 MeV), with a one mg per cm^2 mica window and for the detector a windowless flow proportional counter.

Uchida et al (1966) have developed a practical X-ray emission analyzer, using radioisotope sources, for control of the mixing of raw materials in the manufacture of cement where light elements are determined in a sample matrix of higher atomic number elements. For light elements polonium-210 sources and for higher elements especially iron, two 3 Ci 3H-Zr bremsstrahlung sources were used.

2) Excitation by Beta Particles. A beta particle is a charged particle emitted from the nucleus of an atom with a charge and mass equal in magnitude to that of the electron. When a beta particle strikes a target, it emits characteristic X-rays and bremsstrahlung (beta excited X-rays). Consequently, characteristic X-rays can be excited by beta particles or indirectly by beta excited X-rays.

Enomoto and Tanemura (1966) claim that a beta particle can excite characteristic X-rays of much higher intensity than that excited by beta excited X-rays of equal activity. However, when a beta source was used, a magnet was placed between the specimen and the X-ray detector to deflect beta particles scattered towards the detector. The use of a beta source also has the disadvantage that the X-ray spectrum is accompanied by background radiation due to bremsstrahlung.

X-ray spectra analysis by beta particles has been discussed in detail by Crompton (1955); Leveque, Martinelli and Chauvin (1955); Muller (1962); Cameron and Rhodes (1963a) and Enomoto and Tanemura (1966).

Florkowski et al (1965) have described a method of analyzing iron, zinc and copper ores in the field and in the laboratory by fluorescence excited by 3H/Zr bremsstrahlung. In both zinc and copper ores, interference due to iron was overcome by independent measurement of zinc and iron, or copper and iron concentrations. An accuracy of $\pm$0.25% iron or zinc in zinc ores in the concentration range of 0 to 10% is reported. For copper ores, an accuracy of $\pm$0.1% in the range 0 to 2% and $\pm$0.3% copper at concentrates up to 15% copper is reported. Lower accuracies are reported for field measurements where an X-ray Geiger counter was used in place of the proportional counter used in the laboratory.

Siebel and Le Traon (1963) have described the use of tritium bremsstrahlung for the laboratory determination of magnesium, aluminium, silicon, calcium and iron in cement and iron ores.

3) Excitation by Primary X-ray and Gamma Ray Sources. Commonly available radioisotope sources for this purpose are americium-241, cadmium-109, cobalt-57, iron-55, plutonium-238, gadolinium-153, iridium-192 and curium-244. The choice of source is made by selecting exciting energies just about the K absorption edge of the elements under analysis.

Watt and Gravitis (1973) have suggested the use of plutonium-238 and curium-244 for determination of elements from manganese to arsenic, and americium-241 from zirconium to barium. They have determined copper, tin and zinc in slurries. The reported accuracy (Rms error * 100/mean element concentration) for different slurries is between 1.2 and 15.5 percent.

Watt (1972a) has developed a technique for analysis of an element in samples containing high concentrations of another element of slightly lower atomic number. The sensitivity of the analysis was achieved by use of a radiator foil whose fluorescent X-rays can be excited only by the higher of the two close-in-energy X-ray components from the sample. The principle

this arrangement is illustrated in Figure 3. Using this arrangement, Watt (1972a) measured copper in the range of 0.1 to 0.44 percent in the presence of iron in the range of 46-52 percent with an accuracy of 13.6.

Synman (1971) has used Ge(Li) detector and cobalt-57 source to determine uranium in solid samples and slurries. The reported lower limit of detection is 11 ppm.

4) Excitation by Secondary X-ray and Gamma Ray Sources. When a radioisotope emitting a desired energy is not available, use can be made of a source-target assembly (Rhodes, 1966; Watt, 1964; Giauque, 1968).

In this method, a radioactive source is used to excite the K X-rays of a selected target material, and these in turn excite X-rays from the specimen. The geometrical arrangement (Figure 4) is such that the specimen 'sees' the X-rays from the sample under analysis. Detection limits in the range 50 to 200 ppm can be attained. The system is also flexible because targets can be changed easily. For analytical work, such secondary sources have significant advantages such as efficiency, purity over beta excited X-ray sources.

Secondary X-ray or gamma ray sources have been used by the mineral industry. Fookes et al (1971) have used plutonium-238 with gallium (Ga_2O_3) for the copper determination and germanium for the zinc determination. The X-ray filters used were nickel for copper determinations (22 mg/cm^2 thick for concentrates and feeds, 33 mg/cm^2 for tailings) and (23 mg/sq cm) for all zinc determinations. Errors (percent by weight of wanted element) for above mentioned slurries lie between 0.06 to 0.16.

Carr-Brion (1967), Carr-Brion and Rhodes (1965) have determined molybdenum, niobium, tin, barium and zinc in slurries using different source-target assemblies. Tin, in the range of 0.01 to 0.1% in the slurry was measured with an accuracy of $\pm$10% at 0.1% tin.

5) Proton Excitation. Excitation of soft X-rays with protons is a very efficient process and is accompanied by an extremely high signal to background ratio. At present the main applications are restricted to the determination of X-ray yields and ionization cross sections etc. Brady and Cahil (1973) have discussed this mode of excitation in detail. They have observed several similarities between excitation by protons and by alpha particles.

Remarks on the Different Modes of Excitation

From the literature it may be inferred that primary and secondary X-or gamma ray mode of excitation is the more common method. In this technique it is possible to isolate the wanted characteristic X-ray from the unwanted radiation. When a suitable source for excitation is not available, a γ-x source can be used. Thus the selection can be made from a wide variety of sources. When excited with beta particles, samples can be examined through relatively thick windows, such as 0.3 cm thick polythene. Such windows contribute to a very small extent to bremsstrahlung. Photon sources are scattered heavily from thick windows. However, beta particle excitation has several disadvantages. It has lower efficiency and has higher background count rate due to bremsstrahlung. Alpha particle excitation is very useful when the wanted element is of low atomic number. When excited with alpha particles, the window should be very thin because of the limited range of alpha particles.

After exciting the 'wanted' element, it is necessary to isolate the characteristic X-ray of the wanted element from the unwanted radiation. This is done by energy selection.

Energy Selection

On account of the relatively low activity of the radionuclides (especially with secondary radiation sources), wave length dispersive methods where energy losses are high, are not very suitable. Radiometric method of quantitative analysis commonly employs the following methods of energy selection.

1) Pulse Height Selection. Radiation is received by a detector with response proportional to the energy of the incident radiation, e.g., gas-filled proportional counter, the scintillation counter and the semi-conductor detector. The signal from the detector is amplified and passed into a discriminator which selects a specified range of pulse amplitude from a spectrum. The resolution power of the proportional counter is better than the scintillation counter. For example, percent resolution for FeKα equals approximately 51 percent for a scintillation counter compared to about 15 percent for the gas flow proportional counter (Jenkins and De Vries, 1970). Although the scintillation counter has the advantage of having an almost constant spectral response over a wide range, its working range is limited at low energies. As such a scintillation counter is not normally used for K radiations from elements of lower atomic number than titanium or for L radiations from elements of lower atomic number less than 53 (Jenkins and De Vries, 1970).

The high intrinsic X-ray resolution systems employing Si(Li) and Ge(Li) detectors are becoming increasingly important. The separation of the Kα X-rays of adjacent elements varies from about 200 eV for sodium to about 600 eV for copper. The limitation of these detectors are:

(i) their small area; currently available detectors have areas between 12 mm^2 and 25 mm^2. The small areas result in reduced count rates;

(ii) need for cryogenic cooling;

(iii) these detectors are expensive.

A comparison of the resolution of various detectors as a function of the energy is given in Figure 5. Langheinrich, Forster and Linn (1972) have reviewed in detail the advantages and disadvantages of these detectors.

2) Balance Filters. Two filters with adsorption edges on either side of the characteristic X-ray energy of the wanted element are selected. These filters are mounted between the sample and the detectors. One filter is selected to transmit all the background radiation plus the wanted signal. The other transmits background only. Difference between the signals obtained from the counters is proportional to the concentration of the wanted element. The measurements can be made with the same detector by changing or rotating the two filters. In order to isolate CuKα X-rays (8.05 KeV), for example,

from unwanted radiation of energy less than 7.5 KeV and greater than 8.3 KeV balanced filters of nickel and cobolt are placed successively on the detector window.

Filters can be made from metallic foils, powdered element or from the oxide of the metal. Cameron and Rhodes 1963b; Berman and Eroun, 1970 and Rhodes, 1971, have discussed in detail the criterion for balancing filters and selecting their optimum mass, etc.

3) Source Target Assemblies. Carr-Brion and Jenkinson (1966) have isolated characteristic X-ray line of the 'wanted' element by using two targets emitting close X-ray energies. One excited the required fluorescence while the second, with its energy below the absorption edge of the element being excited, provided backscattered X-rays for correction of interelement effects. The ratio of the two detector outputs was found to be independent of the matrix adsorption effects. Carr-Brion and Jenkinson (1966) concluded that the analytical sensitivity obtained by this method was of the same order as that of balanced filters.

X-Ray Tube Techniques

An X-ray tube provides a useful source of excitation - a much more intense source than a radioactive isotope can provide. A commonly available X-ray tube is the Coolidge tube. Basically, it is a highly evacuated tube inside which are mounted a tungsten filament cathode and an anode made of tungsten or chromium. The tungsten anode is useful for low energy lines.

In the fluorescent system (the principle of which is the same as the radioisotope X-ray fluorescence), the spectral distribution of characteristic X-rays can be ascertained by a wavelength dispersive spectrometer utilizing a crystal monochromator (for example, LiF or NaCl crystal) or else by energy dispersive system, utilizing a semiconductor detector, coupled to a multi-channel analyzer (Birks, 1969; Skogg and West, 1971; Wittkop, 1971; Porter, 1973; Porter and Woldseth, 1973; Frankel and Woldseth, 1973; Carr-Brion, 1973). The wave-length dispersive spectrometer (Figure 6) has low overall efficiency due to several intensity losses through the restriction of solid angle, the low reflectivity of the analyzing crystal. Also such a spectrometer is very sensitive to surface finish of the crystal monochromator, to changes in its position relative to the X-ray system. On the other hand, the energy dispersive spectrometer offers better efficiency but poorer resolving power compared to the wavelength dispersive system. Another disadvantage of energy dispersive spectrometer is its inability to operate at high count rates.

The wave-length dispersive spectrometer has been extensively used for on-stream composition analysis of mineral slurries (Fuller, McGarry and Pellett, 1967; Lewis et al, 1968; Penttı Vanninen and Seppor Kreula, 1973; Seppo Kreula, 1973; Stacey and Bolt, 1971, 1973). Lewis et al (1968) have determined copper and zinc with standard deviations of 0.025 and 0.15 respectively.

Recently, Clayton, Packer and Fisher (1972) have described an X-ray fluorescence analysis system. The system incorporates an X-ray tube and energy selector capable of generating virtually monochromatic X-rays, and also provides some variation in the energy of the exciting radiation. The equipment is essentially an x-ray tube and a high voltage supply in an oil filled enclosure which is coupled to an energy selector.

Another recent development in excitation is the use of pulsed X-ray tubes as reported by Jaklevic, Goulding and Landis (1972). As soon as a pulse is detected, the X-ray tube turns off for the duration of the pulse processing time. This approach eliminates the need for pulse pile up rejection and permits high count rates without significant degradation in system resolution.

For analytical work, X-ray adsorption techniques are analogous to radiometric adsorption techniques.

Neutron Activation

The neutron is an uncharged particle with very nearly the same mass as the proton. When an element is bombarded with neutrons, it becomes radioactive and decays with the emission of beta or gamma radiations with characteristic energies and half lives. Neutron activation is independent of the electron distribution around the nucleus and is based upon the interaction between a neutron and the target material.

Neutrons can be produced by bombardment of a material of suitable threshold and cross-section with high energy particles, for example, protons, deutrons, neutrons and even photons. Alternatively, the spontaneous fission neutron source californium-252 can be used. Californium-252 decays for 97 percent by alpha emission and by 3 percent by spontaneous fission. One mg of californium gives 10^9 neutrons per second.

Atomic Energy of Canada, Ltd. has developed a small reactor known as SLOWPIKE (Tolmie, 1972). This is a water moderated reactor with a beryllium reflector and produces a thermal neutron flux of 2.5×10^{11} neutrons/cm^2 second from 800 grams of uranium-235 when running at a power level of 5 kW and at this level the core life is expected to be five years.

Ricci and Handley (1970) have discussed in detail the use of californium-252 source for activation analysis. The main objection against the radioisotope sources in neutron activation is the lack of sensititivity for several applications. This drawback can be overcome in certain cases, particularly for determination of metal content in slurries. When a slurry is circulated in a closed loop, recirculation activation analysis improves the sensitivity.

Kussi (1971) has determined silicon, aluminium and chromium in chromium ores by using 5 curie Am-Be source giving 1.25×10^7 neutrons/second. Precisions reported are 0.1% for SiO_2, 0.3% for Al_2O_3 and 0.5% for Cr_2O_3. Clayton (1972) has described a commercial activation analysis system to measure silicon in iron ore slurries with an accuracy of $\pm 0.2\%$. A 50 curie Pu-Be source giving 10^6 neutrons/second was used. Possible interference from aluminium was eliminated by means of a cadmium shield placed around the activation cell.

Resonance Scattering

Sowerby (1971) has described a technique for elemental analysis using nuclear reasonance scattering of gamma radiation. It is claimed that the system can be incorporated in a borehold probe and has potential for on-stream process control. The sample to be analyzed is irradiated with gamma rays of energy just above the energy of the nuclear level being excited in the wanted element. The concentration of the element is determined by measuring the intensity of the resonantly scattered radiation.

A Comparison Between Radiometric and X-Ray Tube Techniques

1) An on-stream analyzer using radioisotopes is normally small in size and relatively portable. It is possible to take the analyzer to the flowing stream rather than taking the pulp streams to the sampler. On the other hand, an on-stream analyzer using an X-ray tube is bulky, expensive and requires a central control room. This also necessitates the use of long sampling lines, which add to the cost of the system. Therefore the use of an analyzer for assay or process control work cannot always be justified. Nevertheless, when multielements in a multi-stream are to be analyzed, the cost difference narrows down. However, entry into the field of on-stream analysis can be made at lower cost with the radioisotope system. Initially, the system can be used to analyze one or two elements in a single important stream and then extended at a later stage.

2) A radioisotope source can be made for any specific requirement. This is not true for the X-ray tube. Moreover, sometimes it is difficult to replace the X-ray tube.

3) The output of a radioactive material is stable and does not require power supply which is necessary for an X-ray tube. Consequently, it was decided to look into the commercial availability of probes in greater detail.

Comment on Radiometric and Neutron Activation Technique

Although radioisotope techniques are more developed, neutron techniques have gained importance in recent years. This is because smaller neutron tubes and neutron source californium-252 are now available at low cost. Neutron techniques are more readily suitable for lighter elements. Radiometric techniques are not suited for this purpose. In this respect, it is expected that the neutron techniques would be complementary and not competitive with the radiometric techniques.

Conclusion

The aim of this review has been to develop a logical sequence of information relevant to the design and development of an on-stream analyzer, using radioisotopes. X-ray tube and neutron activation techniques are competitive to the radioisotope systems and as such they have been reviewed briefly.

References

1. Birks, L. S., 1969, "Current trends in X-ray fluorescence spectroscopy", Applied Spectroscopy, Vol. 23.
2. Brady, F. P. and Cahil, T. A., 1973, "Development of X-ray fluorescence analysis and application", Crocker Nuclear Laboratory, University of California, Davis Report UCD-CNL 166.
3. Cameron, J. F. and Rhodes, J. R., 1963a, Radioisotope X-ray sources", The Encyclopedia of X-rays and Gamma Rays, edited by G. L. Clark.
4. Carr-Brion, K. G., 1967, "Performance of an on-stream radioisotope X-ray fluorescence analyser", Transactions/Section C of the Institute of Min. and Met., Vol. 76.
5. Carr-Brion, 1973, "On-stream energy dispersive X-ray analyzers", X-ray Spectrometry, Vol. 2.
6. Carr-Brion, K. G. and Jenkinson, D. A., 1966, "A selective non-dispersive X-ray fluorescence analyzer without balanced filter", Brit. J. Appl. Phys., Vol. 17.
7. Carr-Brion, K. G. and Rhodes, J. R., 1965, "On-stream X-ray fluorescence analysis of ore slurries with a radioisotope X-ray source", Inst. Prac., Vol. 19.
8. Carr-Brion, K. G. and Payne, K. W., 1970. "X-ray fluorescence analysis - A review", The Analyst, Vol. 95.
9. Clayton, C. G., 1972, "Recent developments and applications of nuclear techniques in the exploitation of mineral resources", Conference on the Technological Applications of Nuclear Techniques, Pelindaba.
10. Clayton, C. G., Packer, T. W. and Fisher, J. C., 1972, "Primary energy selection in non-dispersive X-ray fluorescence spectrometry for alloy analysis and coating thickness measurement", Symposium on the use of Nuclear Techniques in the Basic Metal Industry, Helsinki, Finland.
11. Crompton, C. E., 1955. The versatility of radiation applications involving penetration or reflection", Internat. Conf. of Peaceful Uses of Atomic Energy, Paper 164, Vol. 15.
12. Czubek, J. A., Florkowski, T., Niewodniczanski, J. and Przewlocki, K., 1972, "Progress in the application of nuclear techniques in Geophysics, Mining and Hydrology in Poland", Internat. Conf. on Peaceful Uses of Atomic Energy, Paper A/Conf. 49/P/334, Vol. 14.
13. Enomoto, S. and Tanemura, T., 1966, "X-ray spectroanalysis using a promethium-147 beta source", Proceedings of Symposium on Radioisotopes, Vol. 1, International Atomic Energy Agency, Vienna.
14. Florkowski, T., Dziunikowski, D., Kosiara, A. and Wasilewska, M., 1965, "Analysis of iron, zinc and copper ores in the field and in the laboratory by X-ray fluorescence excited by H^3/Zr bremsstrahlung", Radiochemical Methods of Analysis, Vol. II, IAEA, Vienna.
15. Fookes, R. A., Gravitis, V. L., Watt, J. S., Wenk, G. J., Wilkinson, L. R., McColl, I. G. and Bougnen, H. J., 1971, "Plant trials of radioisotope X-ray methods for the on-stream determination of copper, lead and zinc in mineral slurries at Cobar Mines Pty. Ltd.", Proc. Aust. Inst. Min. Met., No. 239.

16. Frankel, R. and Woldseth, R., 1973, "Applications of non-dispersive X-ray techniques", Research/Development, Vol. 24, No. 6.
17. Fuller, M. L., McGarry, P. E. and Pellett, J. R., 1967, "X-ray assaying and reagent control at Friedensville", Mining Congr. J., Vol. 53, No. 108.
18. Glauque, R. D., 1966, "A radioisotope source-target assembly for X-ray spectrometry", Anal. Chem., Vol. 40, No. 13.
19. Gorski, L., Lubecki, A., 1965, "Two radiometric methods for rapid tungsten determination in tool steel", Radiochemical Methods of Analysis II, IAEA, Vienna.
20. Hinckfuss, D. A. and Stump, N. W., 1971, "System design for on-stream analysis at New Broken Hill Consolidated Ltd.", Symposium on Automatic Control Systems in Mineral Processing Plants, Technical papers, pp. 85-95 (Brisbane:Aust. Inst. Min. and Met.).
21. Jaklevic, J. M., Goulding, F. S. and Landis, D. A., 1972. High rate X-ray fluorescence analysis by pulsed excitation", IEEE Trans. Nucl. Sci., Vol. 19, No. 3.
22. Jenkins, R. and DeVries, J. L., 1970, "Practical X-ray Spectrometry, Second Edition (MacMillan and Co. Ltd., New York).
23. Kohl, J., Zentner, R. D. and Lukens, H. R., 1961, Radioisotope Applications Engineering, (D. Van Nostrand Company Inc., New York).
24. Kussi, J., 1971, "Use of radioisotopic neutron sources for process-control activation analysis", Isotope and Radiation Technology, Vol. 9, No. 1.
25. Langheinrich, A. P., Forster, J. W. and Linn, T. A., 1972, "Current status and potential of solid state detectors in industrial and field applications", Paper SM-159/21, I.A.E.A. Symp. on the Use of Nuclear Techniques in the Basic Metal Industry, Helsinki.
26. Leveque, P., Martinelli, P. and Chauvin, R., 1955, "Studies and industrial applications of bremsstrahlung from the beta rays of Yttrium-90, Internat. Conf. on Peaceful Uses of Atomic Energy, Paper P/383.
27. Lewis, C. L., Hall, R. A., Anderson, J. W. and Timm, W. H. A., 1968, "The on-stream X-ray analysis installation at the Lake Dufault Mine, Can. Inst. Min. Bull., Vol. 61.
28. Muller, R. H., 1962, "Research applications of beta-particle techniques:back-scattering and X-ray excitation", Proc. of the Radioisotopes in the Physical Sciences and Industry, I.A.E.A., Vienna.
29. Pentti Vanninen and Seppor Kreula, 1973, "Plant experience from Courier-300 on-stream analysis system", Proc. of the Review of On-Stream Analysis Practice, (published by AMIRA Ltd., Australia).
30. Porter, D. E., 1973, "High intensity excitation sources for X-ray energy spectroscopy", X-ray Spectrometry, Vol. 2.
31. Porter, D. E. and Woldseth, R., 1973, "X-ray energy spectrometry", Anal. Chem., Vol. 45, No. 7.
32. Robert, A. and Martinelli, P., 1964, "Methode radioactive d'analyse par fluorescence X des elements legers", Radiochemical Methods of Analysis, Proc. Symp. Salzburg, Vol. II, I.A.E.A., Vienna.
33. Rhodes, J., 1966, "Radioisotope X-ray spectrometry", The Analyst, Vol. 91.
34. Ricci, E. and Handley, T. H., 1960, "Activation analysis with Cf-252", Analytical Chemistry, Vol. 42.
35. Semmler, J. E., Brugger, J. E., Rieke, F. F., 1961, "Gamma-scattering density meters: Analysis and design with applications to coal and soil laboratories for applied sciences", The University of Chicago, Report No. TID-14178.
36. Seppo Kreula, 1973, "Courier 300 on-stream X-ray analysis system", Proc. of the Review of On-stream Analysis Practice, (published by AMIRA Ltd., Australia).
37. Siebel, G. and Letron, J. Y., 1963, "Mesure d'intensite de rayonnements X d'energie voisine en spectrometrie non-dispersive", Int. J. Appl. Radiat. and Isotopes, Vol. 14.
38. Skoog, D. A. and West, D. M., 1971, Principles of instrumental analysis (published by Holt, Rinehart and Winston, Inc., New York).
39. Synman, G. C., 1971, "On-stream analysis of uranium solutions and slurries using nuclear techniques", "Symposium on Automatic Control Systems in Mineral Processing Plants: Technical papers (Brisbane: Aust. Inst. Min. and Met.).
40. Sowerby, B. D., 1971, "A new method of element analysis using nuclear resonance scattering of gamma rays", Nuclear Instruments and Methods, Vol. 94.
41. Stacey, G. S. and Bolt, W. A., 1971, "Developments in instrument design and calibration procedures for X-ray fluorescent 'on stream' analysis of mineral processing streams", Symposium on Automatic Control Systems in Mineral Processing Plants: Technical papers (Brisbane:Aust. Inst. Min. and Met.).
42. Stacey, G. S. and Bolt, W. A., 1973, "Multi-stream X-ray fluorescence analysis of mineral slurries in No. 1 copper concentrator at Mount Isa", Proc. of the Review of On-Stream Analysis Practice, (published by AMIRA Ltd., Australia).
43. Stump, N. W., 1973, "The application of probe systems for radioisotope on-stream analysis at the New Broken Hill Consolidated Ltd.," Proc. of the Review of On-Stream Analysis Practice, (published by AMIRA Ltd., Australia).
44. Tolmie, R. W., 1972, "Applications of isotopes for industrial measurements and control" Peaceful Uses of Atomic Energy, Vol. 14, (published by the United Nations and the International Atomic Energy Agency).
45. Turkevich, A. L., Franzgrote, E. J. and Patterson, J. H., 1967, "Chemical analysis of the moon at the Surveyor V landing site", Science, Vol. 158, No. 635.
46. Uchida, K., Tominaga, H. and Imamura, H., 1966, "Light-elements simultaneous analyser by the X-ray emission method using alpha- and X-ray sources, for cement raw control", Proceedings of the Symposium on Radioisotope Instruments in Industry and Geophysics, Vol.I, International Atomic Energy Agency, Vienna.
47. Watt, J. S., 1964, "Gamma-ray excited X-ray sources", International Journal of Applied Radiation and Isotopes, Vol. 15.

48. Watt, J. S., 1972a, "Radioisotope detector-radiator assemblies in X-ray fluorescence analysis for copper and zinc in iron rich minerals", International Journal of Applied Radiation and Isotopes, Vol. 23.
49. Watt, J. S. and Gravitis, V. L., 1973, "Radioisotope X-ray fluorescence techniques applied to on-stream analysis of mineral process streams", IFAC Symposium on Automatic Control in Mining, Mineral and Metal Processing, Sydney.
50. Wittkopp, R. W., 1971, "Energy dispersive X-ray analysis", Minerals Science and Engineering, Vol. 3, No. 4.

Illustrations

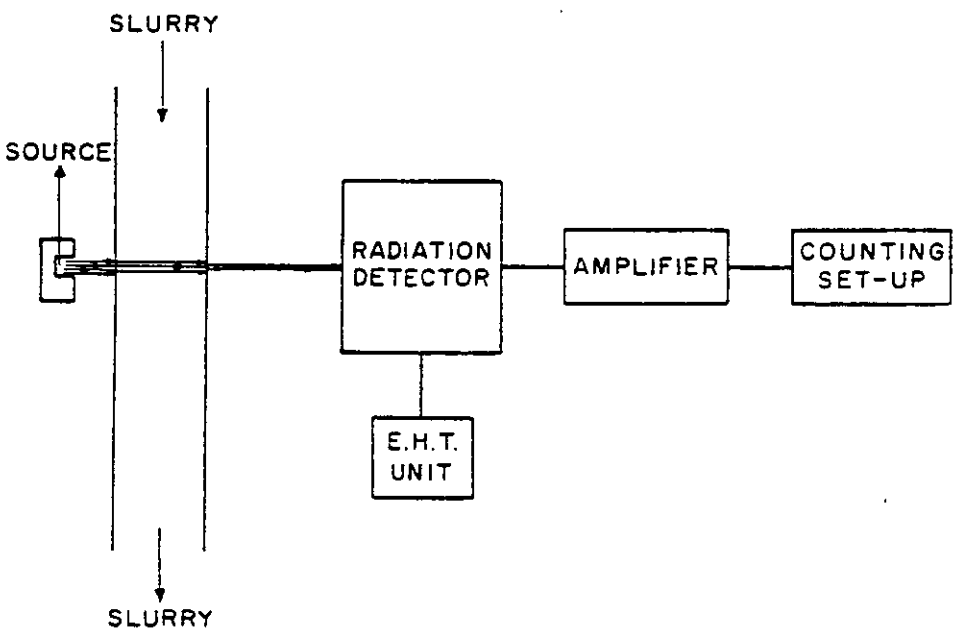

Figure 1. Schematic diagram of transmission type of system.

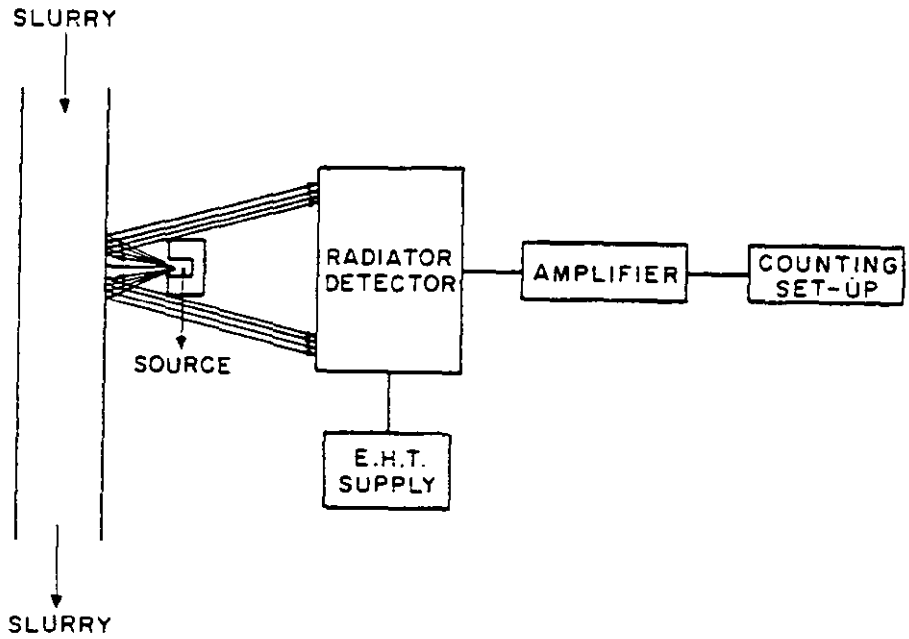

Figure 2. Schematic diagram of scatter type of system.

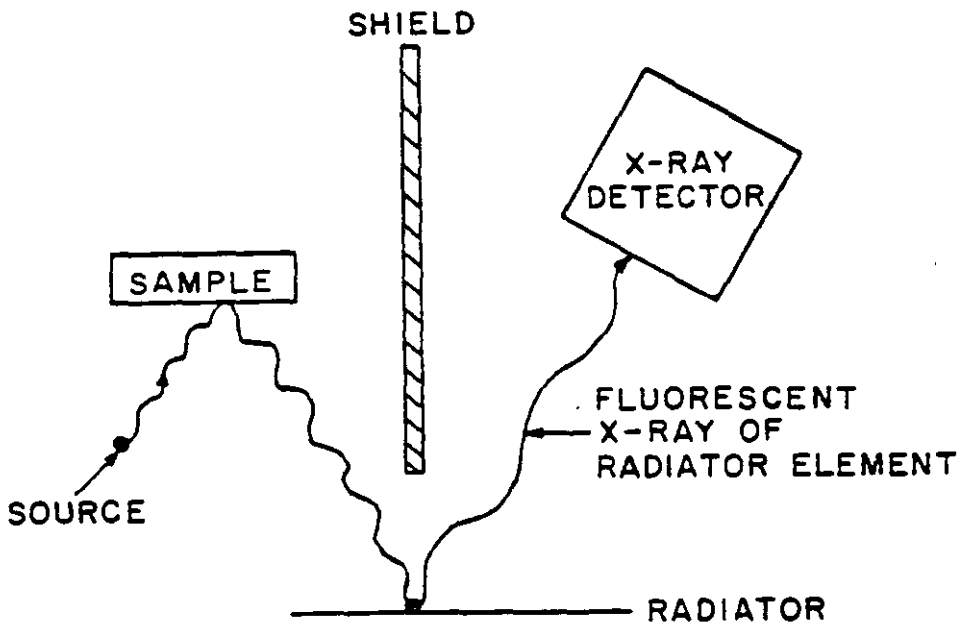

Figure 3. Use of a radiator material to isolate the higher of two close-in-energy X-ray components from a sample.

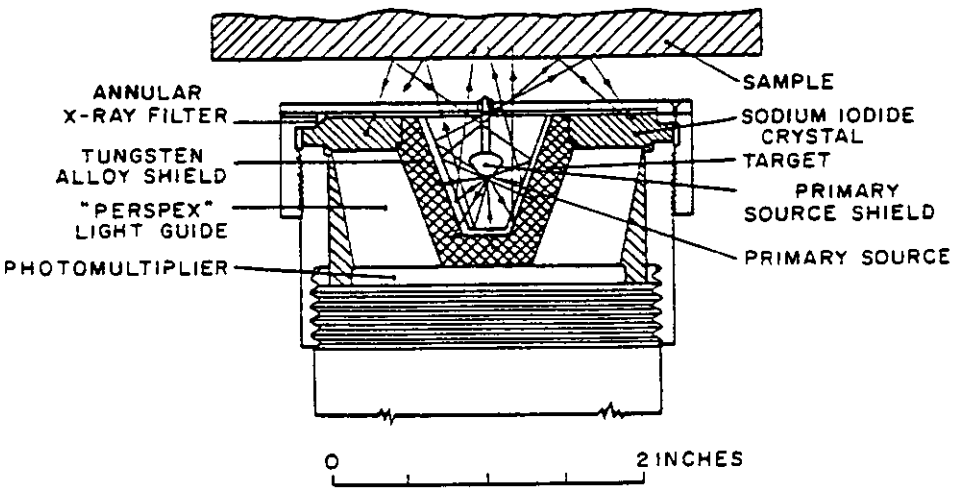

Figure 4. Excitation by secondary X-ray and gamma ray sources.

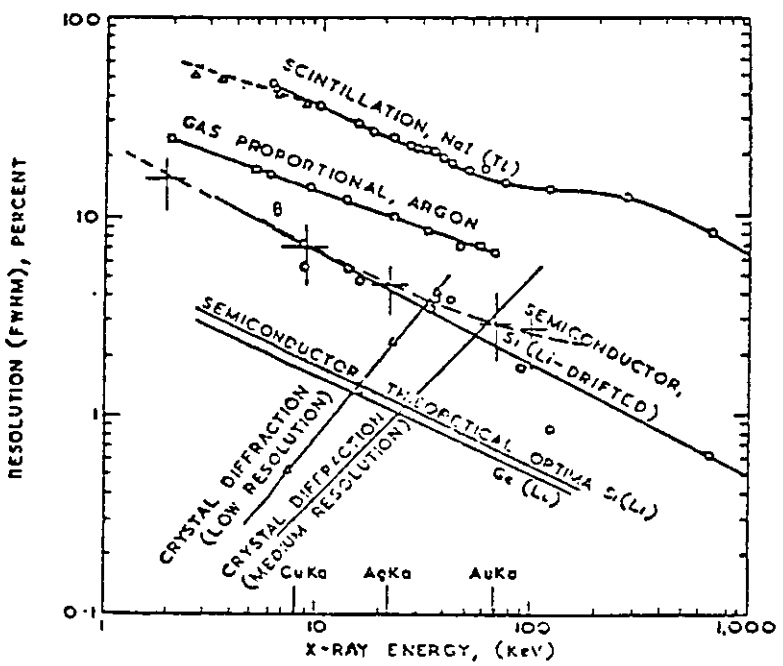

Figure 5. A comparison of the resolution of various detectors as a function of energy.

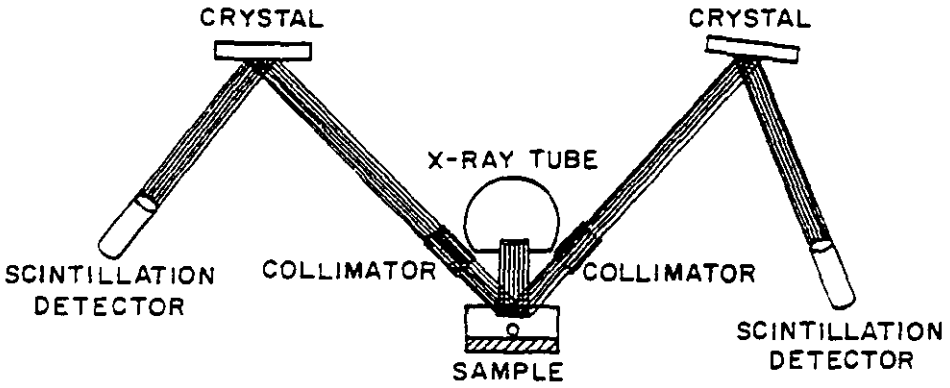

Figure 6. Principle of wave-length dispersive system.

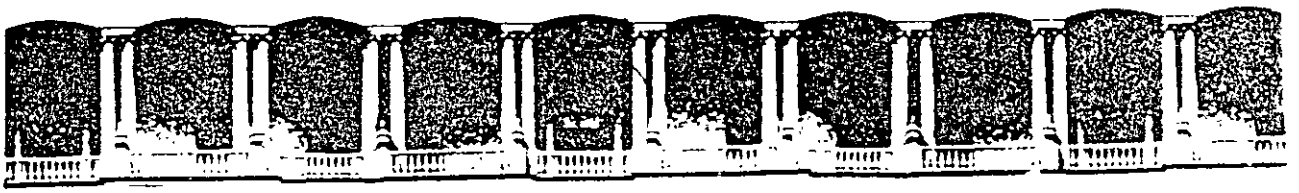

FACULTAD DE INGENIERIA U.N.A.M.
DIVISION DE EDUCACION CONTINUA

CURSOS ABIERTOS

DESARROLLO Y OPERACIÓN DE SENSORES PARA CONTROL DIRECTO Y CONTINUO EN PLANTAS DE BENEFICIO DE MINERALES Y EN LA RESTAURACIÓN DEL MEDIO AMBIENTE

Del 18 al 23 de mayo de 1998

TEMA: ON STREAM COMPOSITION ANALYSIS OF MINERAL SLURRIES

EXPOSITOR :DR. KOMAR KAWATRA

1998

Kawatra, S. K. and Cooper, H. R., 1986, "On-Stream Composition Analysis of Mineral Slurries," Design and Installation of Concentration and Dewatering Circuits," Mular, A. L. and Anderson, M. A., ed., AIME, New York, pp. 641-654.

Chapter 41

ON-STREAM COMPOSITION ANALYSIS OF MINERAL SLURRIES

S. K. Kawatra* and Harrison R. Cooper**

Department of Metallurgical Engineering*
Michigan Technological University
Houghton, MI 49931

Harrison R. Cooper Systems, Inc.**
Salt Lake City, UT

ABSTRACT

In the last 30 years, on-stream slurry analyzers have proven to be of great use in the control of mineral processing circuits. This review discusses the two most popular methods, x-ray fluorescence and neutron activation analysis, and also considers techniques which are still under development.

INTRODUCTION

On-stream composition analysis of process streams in mineral processing operations has been proven to be a powerful tool for the adjustment of the process to variations in plant feed quality. The benefits derived from the use of on-stream analysis are now widely accepted in the base metal industry (Cooper, 1976, 1984 and Wells, 1983). The rapid feed back of the chemical assay drastically reduces the response time of control schemes, and thus helps to increase grade and recovery while reducing reagent consumption and operating costs. Also, the installation of an on-line analyzer frequently reveals that a process stream which has been considered to be stable actually undergoes sizable fluctuations, which may be detrimental to plant operation. For these reasons, a large number of on-stream analyzers have been installed throughout the world during the last 30 years.

An on-stream composition analyzer may operate in a number of ways, as discussed in the literature (Kawatra, 1984). The principles used by commercial units range from excitation by gamma-ray irradiation or neutron activation to measurement of radiation from naturally-occurring isotopes. Elemental analysis by use of fluorescent x-rays is commonly used. Several systems employing neutron activation have been installed for continuous analysis of silica in iron ore slurries. Natural isotope decay has been widely applied in the potash industry for determination of the potassium content of ore carried on conveyors (Cooper, 1976, 1984). Several analyzers employing non-radiometric technology are also in use. The following sections describe the various types of on-stream composition analyzers which have been used or are being developed for

use in mineral concentration operations.

X-RAY FLUORESCENCE ANALYZERS

Fundamental Principles

Conventional on-stream analysis is based on the principle of x-ray fluorescence (XRF) analysis. The basic principle of this method is illustrated in Figure 1. The sample may be excited either by low energy photons from radioisotope sources, or by electronically produced x-rays. The characteristic radiations emitted by the excited samples may be measured using either a wavelength-dispersive x-ray analyzer (WDX), or an energy-dispersive x-ray analyzer (EDX).

The WDX systems are based on the fact that the angle at which an x-ray photon is diffracted from a crystal is a function of its wavelength. Since the wavelength of a photon is a function of its energy, a WDX analyzer determines the energies of x-rays with great accuracy by geometric measurements. For on-stream analysis, the elements of interest are specified in advance, and individual diffracting crystal and detector units are provided to select and measure the characteristic x-rays of each element simultaneously.

Energy dispersive x-ray systems (EDX) use radiation detectors which produce electrical pulses with amplitudes proportional to the energy of the x-ray photons which were detected. The number of pulses produced with amplitudes corresponding to the energy of the characteristic x-rays of the elements of interest is then used to determine the concentrations of these elements.

The WDX systems have a much better energy resolution (20-25 eV) than do EDX systems, and therefore are less subject to error from peak overlap. However, a great deal of the x-ray intensity is lost in the diffraction crystal, with the result that WDX systems can only be used with an intense source of exciting x-rays, such as an x-ray tube. EDX systems are usable at much lower intensities, which may be produced by radioisotope sources. The energy resolution of an EDX system depends on the type of detector used. Solid-state detectors have the best energy resolution, but must operate at cryogenic temperatures. Proportional and scintillation counters can both operate at room temperature, but whereas the proportional counter has the superior energy resolution, the scintillation counter has a higher detection efficiency. A discussion of the advantages and disadvantages of these detectors was presented by Carr-Brion (1980). It may be noted that all three types of detector have been used in on-stream analyzers, with the selection depending on the number of elements to be determined, the energy resolution required to separate the characteristic x-rays, and the x-ray intensity which may be feasibly produced. The general principles of EDX and WDX systems are illustrated in Figure 1.

Excitation Sources

A mineral slurry may be excited into production of characteristic x-rays for quantitative analysis by use of either electronic x-ray tubes or by low-energy photons from radioisotope gamma-ray sources.

Radioisotope Excitation

Many radioisotope sources are available which are suitable for exciting characteristic x-rays for energy-dispersive x-ray analysis. Table 1 lists commonly

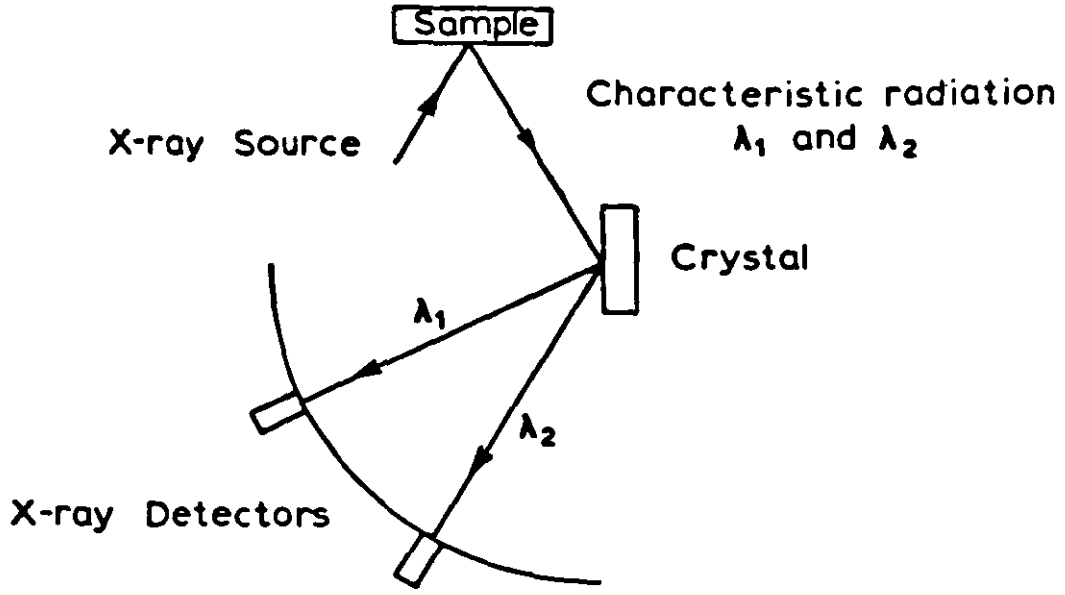

a) Wavelength - dispersive Spectrometer

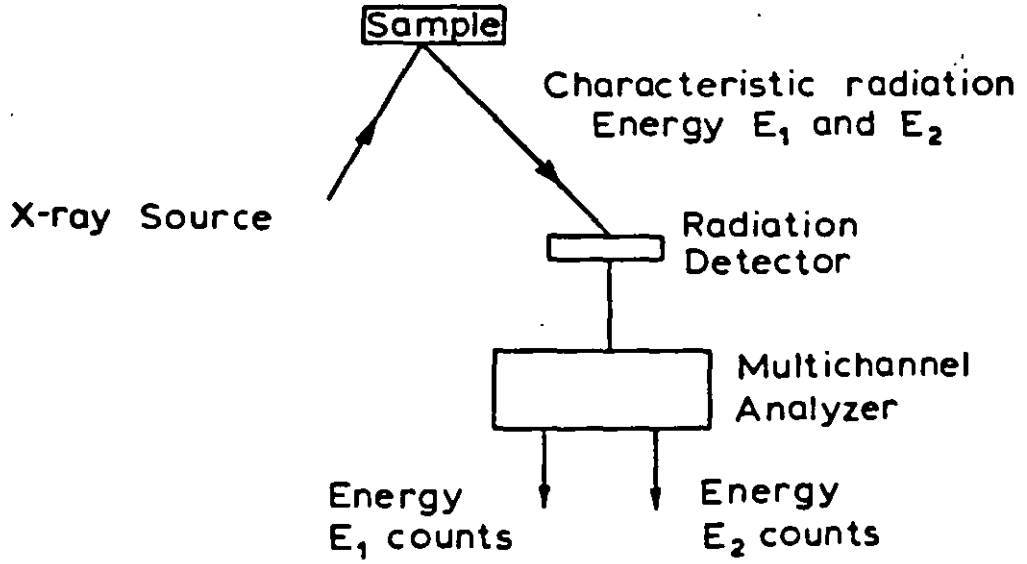

b) Energy - dispersive Spectrometer

Figure 1 X-ray Fluorescence Spectrometer Configurations. Wavelengths λ_1 and λ_2, and energies E_1 and E_2, are emitted by elements 1 and 2.

Table 1

Properties of x-ray and x-ray sources used in on-stream composition analysis.

Radioisotope	Half-life (yr)	Energy KeV	Relative Abundance*
Am-241	458	14-21 (Np L x-rays)	36
		59.6	37
Gd-153	0.65	41-47 (Eu K x-rays)	89
		70	2.6
		97	20
		103	30
Co-57	0.74	122	89
		136	9
Fe-55	2.7	5-9 (Mn K x-rays)	28.5
Pu-238	86.4	13-20 (U L x-rays)	10
Cm-244	18	14-21	8
Cd-109	1.3	22-25 (Ag K x-rays)	107
		88	
I-125	0.16	27-31 (Te K x-rays)	138
		35	7
Cs-137	30	662	82
Co-60	5.3	1170	100
		1330	100

*percent photons per disintegration

used low energy gamma and x-ray sources. Since optimum fluorescence efficiency is achieved when the excitation photon energy is close to, but greater than, the critical excitation potential required to produce the characteristic x-ray of interest, optimum source selection depends on the elements to be determined.

X-ray Tube Excitation

An x-ray tube provides a useful excitation source for either WDX or EDX systems. X-ray tubes provides a much higher x-ray intensity than is possible with radioisotope sources. As a result, small-area detectors may be used. Also, it is not as critical that the source and detector be in close proximity to the sample as is the case for radioisotope sources. X-ray tubes are sometimes used with a secondary source to reduce background radiation.

COMMERCIAL XRF ON-STREAM ANALYZERS

Commercially available on-stream analyzers can be divided into two categories; centralized and distributed systems.

Centralized Systems

In a centralized XRF system, samples of several slurry streams are transported to a common sensing unit. Such installations are generally of the wavelength-dispersive type, as this configuration allows the relatively expensive and bulky equipment required for WDX analysis to be shared among several streams. This system is particularly suited for large plants where more than five or six slurry streams are to be analyzed. A typical centralized analyzer is shown in Figure 2.

As it is usually not feasible to send entire slurry streams to a centralized analyzer, such systems require carefully designed

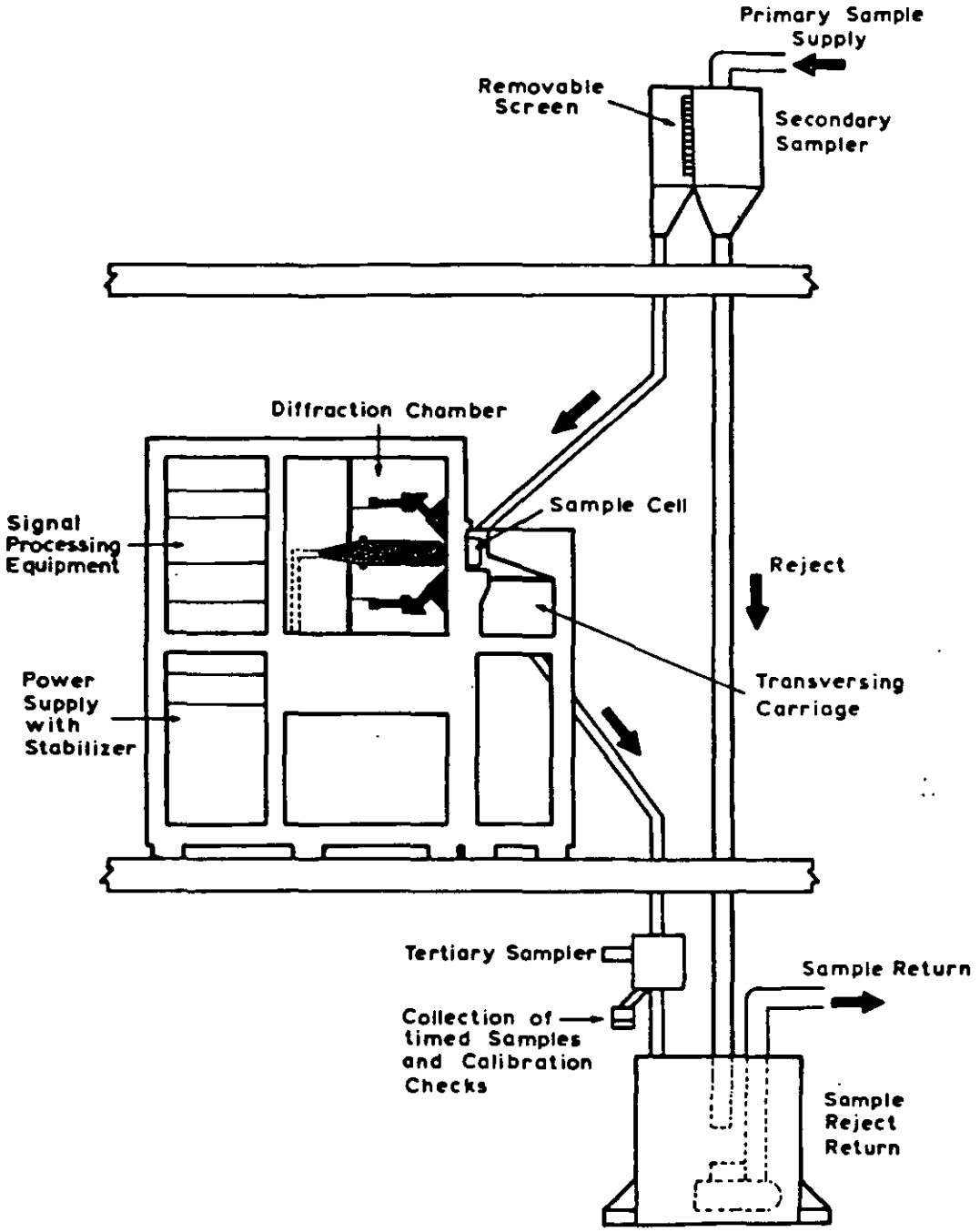

Figure 2 Centralized On-Stream Analyzer (Monitor System)

slurry sampling, pumping, and flow reducing equipment. The slurry is presented to the x-ray equipment through a flow cell having a plastic window (usually Mylar or Kapton) approximately 25 microns thick. Since the x-rays travel only a few millimeters into the flowcell, the layer of slurry in immediate proximity to the window has the greatest influence on assays. Hence, obtaining a representative sample for analysis is essential. Generally, a primary sample of 200-250 liter/min is taken, and is transmitted through two inch diameter pipes by pumping, pressure flow, or gravity flow to a secondary sampler, which removes 20 liters/min as a secondary sample, and returns the remainder to the main stream. Secondary sample streams are then presented to the x-ray analyzer unit.

Examples of centralized XRF systems are the Courier 300, manufactured by Outkumpu Oy, Finland, and the Monitor 1000 System, from Harrison R. Cooper Systems, U.S.A. The first commercial systems of Courier design were installed in 1967, and since then about fifty have been put into use. Several detailed descriptions are available in the literature (Lundan et al, 1977; Leskinen and Lundan, 1983). Elements of atomic number greater than titanium (no. 22) can be analyzed, often at assays of 0.01% by weight or below. Metals subjected to on-stream slurry analysis include copper, zinc, iron, silver, cobalt, nickel, lead, molybdenum, barium, and tungsten (Saarhelo, 1985).

The Courier system uses a series of fixed flow cells, with a movable x-ray head travelling on a precision guide rail. The system is modular, with fourteen cells in each. As many as six elements can be assayed, up to many as three modules can be used in a Courier configuration. This design enables a degree of expandability in the analyzer's capacity as requirements increase (Leppala et al, 1971).

On-stream XRF analyzer acceptance by industry has resulted from attention given to design of sampling, and other factors providing for all needs of turn-key installations. The systems incorporate built-in minicomputers with data processing including programs for assay computations, self monitoring, and other elements for fully developed operating capability.

The Monitor analyzers, from Harrison R. Cooper Systems, Inc. employ a fixed spectrometer unit with the multiple sample cell assembly positioned sequentially at the spectrometer head. Two designs are available: the Monitor 1000, with capability for measuring elements above titanium similar to the Courier 300, and Monitor 2000 systems for measurements of elements as low as aluminum (no. 13). Measurement of low order atomic species is made possible with a sealed spectrometer unit flushed with helium gas, enabling transmission of low energy photons from elements below titanium that otherwise would be absorbed by air in the spectrometer. Monitor analyzers are installed on a turn-key basis in units of 14, 28, and 42 flow cell modules. Primary sample streams are divided in secondary sampling to sequence flow of slurry sample streams to the measuring head. Figure 2 provides a schematic diagram of the system.

Other manufacturers offer similar equipment, of which the Boliden "Boxray" is an example (Sundvist and Sehlstedt, 1978). In this system, the samples are excited by radiation from secondary targets, which produce highly monochromatic excitation radiation to thus reduce background noise. EDX analysis is then carried out with a lithium-drifted-silicon

solid state detector. The spectrometer is held stationary, with slurry flowcells for each sample moved into analysis position by rotating the presentation system around a vertical axis. A similar sample presentation system has been described earlier in the literature (Kawatra, 1976a).

Distributed Systems

In a typical distributed system, several small on-line analyzers are provided, one for each slurry stream. The sensors are located on the mill floor at the points where analyses are desired. The analyzer may be either in-stream, which eliminates the need for sampling equipment, or near-stream, in which case the sampling requirements are greatly reduced compared to those of a centralized system. These systems are available using either WDX or EDX spectrometry.

Typical examples of distributed systems include the systems manufactured by Outokumpu Oy, Finland; Australian Mineral Development Laboratories (AMDEL), Australia; Austrian Research Center, Seibersdorf, Austria; Nuclear Equipment Corporation, U.S.A.; Autometrics, U.S.A.; and Harrison Cooper, U.S.A. The following sections discuss the sensor units for in-stream and near-stream analyzers.

In-stream X-ray Analyzers. This type of sensor consists of a radioisotope excitation source and a detector which are immersed directly in the process stream. Analyzers of this type are the result of excellent research work by the Australian Atomic Energy Commission (Watt, 1977), and several commercial units are available. The most commonly used units are those manufactured by AMDEL, Australia, and Outokumpu Oy, Finland. Another attractive unit for in-stream analysis, the Inscan System, has been developed by Texas Nuclear, U.S.A. These units differ primarily in the type of detector used, with the Inscan using a solid-state detector, the Outokumpu Oy Minexan-202 system using a proportional counter, and the AMDEL probe equipped with a scintillation counter. It may be reiterated that the energy resolution of solid-state detectors is superior to that of proportional counters, which in turn have better resolution than scintillation counters.

Since in-stream units utilize radioisotope excitation sources, the intensity of the excitation radiation is inherently stable, with only a slight correction for decay being needed. With radioisotope excitation sources, fluorescence response is of low intensity, making WDX spectrometry impractical, so in-stream analyzers are exclusively EDX systems. This severely limits the ability of in-stream probes to resolve fluorescent x-rays of similar energies. The background radiation levels are inherently high, particularly at low metal concentrations. These factors limit the ability of in-stream probes to produce accurate assays at low metal concentrations (Cooper, 1976). Serious accuracy problems arise in measuring low metal concentrations when elements with fluorescence spectra overlapping that of the element of interest are present in concentrations greater than one percent.

The AMDEL probe system requires a separate source-detector set for each element of interest at each measurement point. In addition, this system requires an additional probe for measuring pulp density. A difficulty with in-stream systems in general is the fact that repeatable measurements of pulse amplitude and number requires high order electronic stability. Electronic drift

cannot be effectively evaluated unless the probe is tested after being removed from its sensing position in the slurry. Also, the fact that these probes must be immersed in a corrosive slurry introduces problems, as the detector will be destroyed if slurry leaks into the sensor head. In general, therefore, the in-stream systems require a high level of routine maintenance, and since they make use of radioisotopes, they may be a health hazard if handled improperly.

Even though the AMDEL and Outokumpu probes have been successfully used in in-stream analysis situations, there are many applications that do not lend themselves to systems of this type. For example, immersion of the probe in a large vessel, where slurry segregation is likely due to settling, flotation, or poor mixing, will produce poor results.

Near-stream X-ray Analyzers. Near-stream analyzers consist of an on-site unit through which a portion of a slurry stream is shunted for analysis, without traveling any great distance. There are several general types of excitation source/detector arrangements in use, which are described in the following sections.

1) X-ray Tube Diffraction Crystal. Excellent sensitivity and accuracy is achieved down to very low metal concentrations often in the parts per million range, as a result of the high primary x-ray intensity and high resolution capability of crystal spectrometers. Such devices are mechanically more complex, and thus more costly, than in-stream analyzers. Typical examples of this type of analyzer include the Courier-30 system, manufactured by Outokumpu Electronics, Finland, and the Monitor 500 system, manufactured by Harrison R. Cooper Systems, Inc., U.S.A.

The first application of on-stream x-ray fluorescence to an industrial mineral process was carried out with the Monitor 500 system. The Monitor 500 was used at a baryte mineral beneficiation facility where several process slurry streams in flotation were analyzed for barium sulphate. In this process, a critical requirement was providing information to a computer control system to maintain final product grade in the range of 90% baryte. The Monitor 500 system with two channels for rhodium backscatter radiation was installed to measure the Rayleigh and Compton scattering intensities. Preliminary tests conducted with process samples showed a correlation of impurity level in the concentrate with the difference (divergence) between inelastic scattering intensity and elastic scattering intensity. The Monitor 500 system was employed in this application because it has the capability for extension of measurement range to low atomic number elements, which allows for determination of silica if such should become necessary for impurity control in the future.

2) X-ray Tube/Solid State Detector. A system based on this combination has been described by Sundkvist and Sehlstedt (1978), and used in Boliden Metal's Aktiebolag Copper mine in Sweden. This System utilizes energy dispersive analysis in combination with secondary excitation. Secondary excitation consists of directing the tube output to a secondary target. The secondary target then emits nearly monochromatic fluorescent radiation, which is used to excite the sample. In the process, the continuous and characteristic spectra of the tube are largely eliminated. This allows both precise selection of excitation photon energy, and

reduction of background radiation. The line-to-background ratio for the energy-dispersive spectrometer is then nearly comparable to the line-to-background ratio of wavelength-dispersive systems.

Another example of this type of near-stream analyzer is the XRA-1500 system developed by Armco Autometrics, Boulder, Colorado. This system utilizes a germanium solid-state detector, rather than a lithium-drifted silicon detector (Ballard et al, 1983, and Kouns, 1985).

3) Radioisotope/Solid-State Detector. A by-line system based on Iodine-125 as an excitation source and a solid-state detector for energy-dispersive analysis has been developed by INAX, Ottawa; Bondar-Clegg, Ottawa; and Ramsey Rec. Ltd., Richmond Hill, Canada (Ereiser et al, 1980). Since solid-state detectors are capable of resolving x-rays of most elements of interest even when their atomic numbers are consecutive, simultaneous multi-element analysis is possible with this system. High resolution with solid-state detectors can be achieved only if the diameter is small, usually 4 mm. Since this is considerably less than the 25 mm typical for scintillation or proportional counters, an intense radioisotope source is required for solid-state detectors. This type of analyzer has been tested in plant trials at Noranda Mines Ltd., Ontario, Canada, for assaying copper, lead and zinc.

4) Radioisotope/Proportional Counter. An example of this type of analyzer is Outokumpu's Minexan 202 system, which is available in both in-stream and near-stream configurations. Each Minexan probe is capable of determining concentrations of as many as five elements plus pulp density. The probe employs a sealed proportional counter, and utilizes energy-dispersive analysis. While such detectors are relatively inexpensive and simple to use, resolution is inferior to both solid-state detectors and wavelength-dispersive systems, and thus elements with closely spaced fluorescent lines are difficult to distinguish (Barker and Saarhelo, 1984).

FACTORS AFFECTING MEASUREMENT ACCURACY

XRF analysis accuracy depends on several factors, some of which may be beyond the control of the instrumental technique such as mineralogical conditions, size distributions, interelement effects, and the level of assays which exist in the slurry being analyzed. Several fundamental sources of error inherent to x-ray fluorescent analyzers are discussed below. Within these limitations, the accuracy to be attained by XRF becomes dependent on the care and details put forth to the process of calibration.

A variety of methods for XRF calibration are available, ranging from simplistic multiple linear regression to more advanced methods employing mathematical models based on the x-ray fluorescence process. Calibration procedures are discussed in other tests (Cooper 1976). It is to be emphasized that effective use of on-stream x-ray fluorescence analysis depends on producing reliable assays which can be derived only from application of proper calibration technique.

Some factors such as particle size distribution, air content and pulp density can have significant effects on XRF accuracy. These factors are discussed below:

Atomic Number of Element. The higher the atomic number of the element being analyzed, the greater is the accuracy of

measurement.

Concentration of the Element. The higher the concentration of the element being analyzed, the greater is the accuracy of measurement. Expected relative accuracies to be attained are given for typical cases (relative accuracy is the standard error of measurement divided by the average concentration, multiplied by 100 percent).

Copper in concentrates (25% grade)	4-5%
Copper in tails (0.1%)	6-8%
Molybdenum in feed (0.2%)	4-6%
Lead in feed (5%)	7-9%
Zinc in tails (0.5%)	6-8%

Particle Size. The smaller the particle size the greater is the measurement accuracy. Variation in particle size distribution can give rise to errors. Berry et al (1969) have discussed particle size effects in detail. If a grinding circuit has a particle size control, variations in the particle size in the flotation section would be less, giving lower errors (Kawatra, 1975).

Mineralogy. Variations in the composition and variety of mineral types incorporating the element to be measured, as well as mineral grain size variation, cause reduced possibilities for accurate measurement.

Pulp Density. Measurement accuracy becomes greater for higher pulp densities and reduced variations in pulp densities, noting that the measurement result is the element content of the solids portion of the slurry.

Entrained Air. Since the intensity of the fluorescent x-rays depends on the amount of suspended solids, and hence on the slurry density, it is necessary to apply a density correction to the fluorescent intensity. This correction may be obtained through either of two methods; gamma-ray transmission, and x-ray backscatter. For example, AMDEL probes use a gamma-ray-transmission density gauge to correct for pulp density. Entrained air is always present in flotation slurries, and causes errors in the pulp density measurement, with the magnitude of the error being greater for transmission density corrections. In a study conducted for the measurement of percent copper in a chalcopyrite slurry using a transmission gauge for density compensation, it has been shown that an increase of entrained air from 0 to 30 percent resulted in a 40% error in the copper determination (Kawatra, 1976b).

NEUTRON ACTIVATION ANALYZERS

Fundamental Principles

Neutron techniques are attractive for analysis of elements with low atomic number such as silicon, aluminum, chlorine, sulfur, and fluorine. These elements may only be measured with difficulty by x-ray fluorescence analysis due to their low-energy characteristic x-rays. Thus, neutron activation may be considered as a viable method to carry out on-stream analysis when XRF methods cannot be used.

Neutron activation analysis is based on the interactions of neutrons with atomic nuclei, rather than on interactions with the electron shells. The results are therefore independent of the chemical state of the elements being measured. There are two types of neutron-nucleus interaction which may be applied for analytical techniques: 1) Radionuclide production, which results in delayed gamma-ray emissions as the unstable nucleus decays, and 2) prompt gamma emission, which

occurs immediately following the capture of a thermal neutron by the target nucleus.

Radionuclide production has been employed for on-line analysis of silica in iron ore, and silica and chromium in chromite. The nuclear reaction for silicon activation is as follows:

$$_{14}Si^{28} + n\ (fast) \rightarrow {}_{13}Al^{28} + p$$

$_{13}Al^{28}$ has a half-life of 2.3 minutes, and decays to the original stable silicon nucleus by emitting a beta particle accompanied by a 1.78 MeV gamma ray.

The neutron sources used are typically either Cf-252, or an α-n source. α-n sources consist of a source of alpha particles, such as Po-210 or Pu-239, and a target such as beryllium. The reaction of the alpha particles with the target causes neutrons to be emitted. These sources produce on the order of 10^8 neutrons per second.

Determination of Silica in Iron Ore Slurries

At present, only one type of neutron activation sensor is commercially available. This is the NOLA 1 system, produced by Texas Nuclear, Texas. This unit has been installed in at least eight operating iron ore processing plants with satisfactory results.

The NOLA unit consists of an analysis loop which recirculates a sample of slurry through the irradiator, detector, and density gauge units, as shown in Figure 3. The analysis loop holds approximately 500 milliliters of slurry, which must be at least 50% solid for a reasonable analysis. The loop is filled automatically from the slurry stream through a solenoid-operated 2-way valve. This technique, termed Recirculation Activation Analysis, has several advantages (Texas Nuclear, 1985):

1) increased sensitivity over single-pass analysis schemes;

2) lower dependence on fluctuations in slurry flowrate; and

3) minimal slurry sedimentation, due to the capability of maintaining a high flowrate in the analysis loop.

The NOLA system uses a Pu-Be α-n source (half-life 87.4 years) which emits 10^8 neutrons per second. At the Reserve Mining Co., Silver Bay, Minnesota, the NOLA system has been found to be capable of measuring silica content with an accuracy of $\pm$ 0.2% by weight (Allie, 1980). The NOLA analyzer at U.S. Steel's Minntac taconite plant measures the silica content in a slurry containing from 20 to 70% solids at 5 to 6% silica, with results within $\pm$ 0.2% of the silica content determined by wet chemical methods (Benner and Ludwig, 1984).

ON-LINE COMPOSITION ANALYZERS USING OTHER TECHNOLOGIES

The discussion in this chapter heretofore has dealt with the more established on-stream XRF and neutron activation analyzer systems, as these technologies have become of substantial importance to the metallurgical and mineral processing industries. Nevertheless, newer on-line composition analysis technologies have been introduced in recent years which offer the possibility of extending the range of analyzer methods which can be applied for improved process control. Several of the techniques are based on non-radiometric methodologies. Salient features

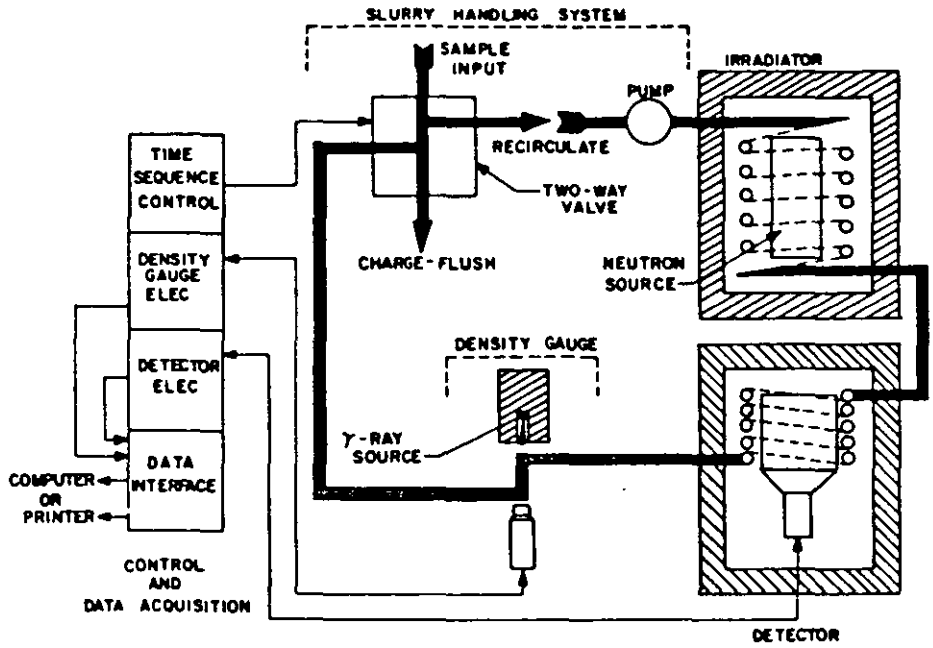

Figure 3. Schematic of NOLA analyzer (after Berry, 1978).

of the newer techniques are briefly described below.

Several methods for on-line analysis of gold in solutions and slurries are currently being developed. Witteck Development of Toronto, Canada, is currently developing an on-line gold analyzer based on the Direct Current Plasma (DCP) principle. Unlike the atomic absorption spectroscopy (AAS) method, which utilizes light absorption, DCP is based on light emission. The plasma yields a much higher operating temperature with resulting sensitivities of 5-10 ppb achievable from unconcentrated samples. This compares very favorably with the levels of .1 ppm (unconcentrated samples) and 20 ppb (concentrated samples) normally obtainable with AAS. Plant trials have been scheduled for the near future, however, no details are available at this time because of commercial interests. Robert and Ormrod (1982) have described an on-line gold analyser, the 'Tele-tale' which is based on solvent extraction and flame atomization and has a lower limit of determination of 0.005 mg/l. It is in use in a number of gold mines to monitor the gold content of barren solutions from filters. Recently, Mintek (1985) has improved upon this analyzer and developed a prototype system based on atomic absorption spectrophotometry and electrothermal atomization. It was designed to monitor the gold in solutions from the carbon-in-pulp process. Although the improved on-line analyzer is not commercially available as a package, all the separate components except the modified furnace autosampler are available. Bateman Process Instrumentation Ltd. (1985) has installed on-line gold sensors based on the principle of atomic absorption spectrometry.

Nuclear applications, Harwell, U.K., has recently built an on-line

monitoring system for a feldspar mill for Amberger Kaolinweke GmbH in West Germany (Wheeler, 1985). The details of this installation may soon be available.

The National Institute of Mining and Metallurgy, South Africa, has developed an on-line instrument in a feasibility study of the applicability of x-ray diffraction to the analysis of fluorspar-containing slurries. The instrument is shown to have adequate sensitivity and resolution and further test work is recommended (de Villiers, 1981). This method has been extended to on-stream analysis of apatite slurries as well.

On-stream analysis of coal slurries or of solid material flows has not been discussed in this chapter. A number of techniques such as prompt gamma neutron activation, nuclear magnetic resonance and electron spin resonance are described by Cooper (1984).

REFERENCES

Allie, C. L., 1980, "Reserve's Process Modifications Succeed at Silver Bay", Mining Engineering, vol. 32, no. 12, pp. 1695-1698.

Ballard, B. J., Dick, D. E., Barton, P. M. and Rathburn, R. H., 1983, "A New On-Stream X-ray Analyzer", Presented at the 11th Annual Meeting of the Instrument Society of America, Tucson, Arizona.

Barker, D. R. and Saarhelo, K., 1984, "A Recent Advance in On-Stream and Analysis Equipment for Mineral Concentrators and Metal Refineries", Paper Presented at the MINTEK 50 International Conference, Sandton, South Africa.

Bateman Instrumentation, 1985, "Olga Mark III Gold Analyzer", Bateman Industries Brochure, South Africa.

Benner, B. R. and Ludwig, J. R., 1984, "On-Line Silica, Size and Surface Area Measurements at U. S. Steel's Minntac Taconite Concentrator", Control '84, Published by the AIME, N.Y., pp. 21-28.

Berry, P. F., 1978, "On-stream Composition Analysis Using Neutron Activation", Report of a workshop on "On-Stream Characterization and Control of Particulate Processes", published by the Engineering Foundation, New York.

Berry, P. F., Furuta, T. and Rhodes, J. R., 1969, "Particle Size Effects in Radioisotope X-ray Spectrometry", vol. 12, pp. 612-632.

Carr-Brion, K. G., 1980, "Recent Developments in Detectors for Process Control X-ray Sensors", X-ray Spectrometry, vol. 9, no. 4, pp. 184-188.

Cooper, H. R., 1976, "On-Stream X-ray Analysis", Flotation, A. M. Gaudin Memorial, vol. 2, Fuerstenau, M. C., ed., AIME, New York, pp. 865-894.

Cooper, H. R., 1984, "Recent Development in On-Line Composition Analysis of Process Streams", Control '84, Herbst, J. A., ed., AIME, New York, pp. 28-38.

Cullity, B. D., 1978, "Elements of X-ray Diffraction", Second Edition, Addison-Wesley Publishing Co. Inc., U.S.A.

de Villiers, J.P.R., 1981, "On-Line Analysis by X-ray Diffraction of Fluorspar-Containing Slurries", NIM Report 2134D, Randburg, South Africa, pp. 1-3.

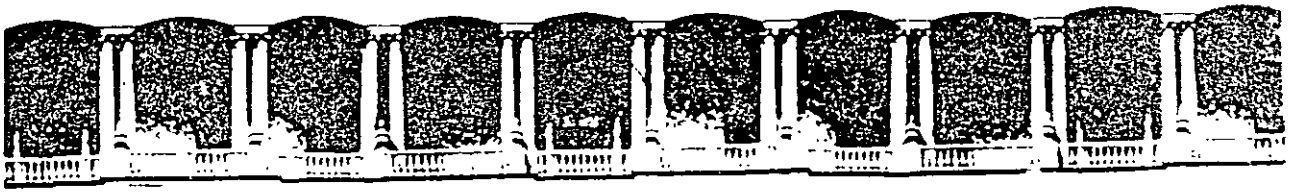

FACULTAD DE INGENIERIA U.N.A.M.
DIVISION DE EDUCACION CONTINUA

CURSOS ABIERTOS

DESARROLLO Y OPERACIÓN DE SENSORES PARA CONTROL DIRECTO Y CONTINUO EN PLANTAS DE BENEFICIO DE MINERALES Y EN LA RESTAURACIÓN DEL MEDIO AMBIENTE

Del 18 al 23 de mayo de 1998

TEMA: A COAL ASH MONITOR FOR COAL CLEANING PROCESSES

EXPOSITOR :DR. KOMAR KAWATRA

1998

Kawatra, S. K., "A Coal Ash Monitor for Coal Cleaning Processes", Chapter 30, Fine Particles Processing, Published by Society of Mining Engineers, Vol. 1, 1980.

Chapter 30

A COAL ASH MONITOR FOR COAL CLEANING PROCESSES

S. K. Kawatra

Department of Metallurgical Engineering
Michigan Technological University
Houghton, Michigan 49931

ABSTRACT

The paper describes a system for on-line analysis of ash in solids in coal slurries for coal cleaning operations. The system consists of two sensors: 1) gamma density gauge, and 2) ash sensor. The operational characteristics of each sensor are discussed.

INTRODUCTION

Traditionally coal has been considered to be a mineral with a low intrinsic value. Being a cheap mineral, only the simplest of processing methods could be economically applied to reduce the inorganic matter content (ash forming constituents) prior to utilization. With the price of coal now several times its value five years ago, the picture has changed such that more advanced processing methods can be justified. In recent years most companies have placed the highest priority on the development and expansion of mining systems and have only spent as little as possible on coal beneficiation. The bulk of the current coal oriented research and development, particularly in North America, seems to be focussed on coal utilization (i.e., coal gasification, carbonization, liquifaction) with very little devoted to coal beneficiation.

The area in coal beneficiation which seems to offer the greatest potential for improvement is process control. At the present time, coal preparation plants have crude control methods compared to the chemical and metallurgical process industries. In these industries, it was found that closer control resulted in greater productivity and/or improved average process efficiencies. It is reasonable to assume

that similar benefits could be achieved in the coal industry through implementation of similar process control methods. One of the key elements required to develop an effective method of controlling a coal cleaning plant is a method to continually monitor the ash content of the coal, so that the processing conditions may be changed in accordance with the compositional changes of the coal entering the plant. It is also important to determine the sulphur content of the coal and the goal of such a project is to determine on-line both the sulphur and ash content. This report is an account of the development of a system for on-line analysis of ash in coal slurries.

THEORETICAL DEVELOPMENT

The determination of ash content in coal slurries requires at least two measurements, one to obtain the solids content of the slurry and the other to obtain the ash content of the solids (1-5).

The solids content of the slurry can be determined by a gamma density gauge (1-5). The gauge is based on the principle of radiation absorption. As the radiation passes through matter, the loss in intensity of gamma rays is related to the density of the material. Because gamma ray mass attenuation coefficients are both atomic number and energy dependent (6-7), it is customary to use a gamma ray energy of about 0.7 MeV for applications free of high atomic number elements, and a gamma ray energy of about 1.2 MeV when high atomic-number elements are present (14). For solids content measurement of low density slurries, such as an aqueous coal slurry, gamma-ray energies in the range 0.6 MeV to 1.3 MeV are not sufficiently sensitive for practical path lengths (25 cm) and it is necessary to use an isotope which has a low energy gamma ray. The characteristics of isotopes commonly used in density gauges are shown in Table 1 as well as the characteristics of isotopes that could be used to measure solids content of coal slurries (13). Gd-153 is selected for this application over Co-57 because of sensitivity, and over Ir-192 and Ce-139 because of both half-life consideration and sensitivity.

The coal ash content determination is based on the scattering of radiation energy less than 100 KeV, the intensity of scattered radiation being proportional to the ratio of the probability of a scattering interaction occurring opposed to an absorption interaction. Two types of radiation scattering may occur: incoherent or Compton scattering and coherent or Rayleigh scattering (7,8). In Compton scattering, a photon collides with an electron, loses some of its energy and is deflected from its original direction of travel. In Rayleigh scattering, photons are scattered by bound atomic electrons under conditions such that the atom is neither ionized nor excited. The scattering from different parts of the atomic charge distribution is then "coherent." Compton scattered low energy gamma rays suffer an energy loss which grows larger as the angle of scatter increases. Rayleigh scattered photons have the same energy as the primary photons regard-

TABLE 1(A). - Isotopes commonly used in density gauges

Isotope	Half-Life	Radiation used for gauging (MeV)
Cs 137	30 years	0.662
Co 60	5.2 years	1.173
		1.332

TABLE 1(B). - Useful isotopes for gauging low density material

Isotope	Half-Life	Radiation used for gauging (MeV)
Gd 153	239 days	0.099
Co 57	270 days	0.122
		0.136
Ce 139	140 days	0.165
Ir 192	74 days	0.062
		0.066
		0.296
		0.308
		0.317

less of scattering angle. In addition, the cross section of Compton scattering is proportional to the "Z" of the scattering atoms while the Rayleigh scattering cross section is closely proportional to Z^3. Compton scattering relationships are given by the Klein-Nishna formula (9,10,11):

$$\sigma_c = 3.92 \times 10^{-26} \left(\frac{E'}{E}\right)^2 \left(\frac{E}{E'} + \frac{E'}{E} - \sin^2\theta\right) \quad (1)$$

where σ_c is the Compton differential cross section per sq. cm. per electron per steradian, E is the energy of the primary photons, E' is the energy of the scattered photons and θ is the scattering angle. The relationship between E' and E is given by (7,8):

$$E' = \frac{E}{1 + \frac{E}{mc^2}(1-\cos\theta)} \quad (2)$$

For a mixture of elements, the probability of scattering per unit path length traversed in the medium into the elemental solid angle $d\Omega$ in the direction θ is given by (9,10,11):

$$P(\theta,E)_c = N\rho\sigma_c(\theta,E)d\Omega \sum_i \alpha_i \left(\frac{Z}{A}\right)_i \quad (3)$$

where N is the Avogadro's number, ρ is the density of the material, α_i is the fraction of the total weight comprised by the ith type atoms, Z and A are respectively the atomic number and atomic weight of the ith type atoms.

The Rayleigh scattering can be approximated by the relationship (9,10,11):

$$\sigma_R = K \frac{\pi}{4} \left(\frac{e}{mc^2}\right)^2 f(\theta) \frac{Z^3}{E^3} \quad (4)$$

where σ_R is the Rayleigh cross section per sq. cm. per electron per steradian, e is the electronic charge, K a constant and $f(\theta)$ is a function of scattering angle. For a mixture, the probability of scattering per unit path length traversed in the medium into the elemental solid angle $d\Omega$ in the direction θ is given by (9,10,11):

$$P(\theta,E)_R = KN\rho d\Omega \sum_i \frac{\alpha_i Z_i^3}{A_i} \quad (5)$$

where ρ is the density, N is the Avogadro's number, α_i is the fraction of the total weight comprised by the ith type atoms.

The theory outlined suggests the application of Rayleigh and Compton scattering to the chemical analysis. If the amount of high atomic number material varies in a low atomic number matrix, the Compton and Rayleigh scattered intensities would also vary accordingly.

Coal ash is the oxidized residue remaining after coal has been burnt and consists essentially of alumina, silica, iron minerals and compounds and small quantities of the oxides of potassium, calcium, titanium, etc. In coal, the effective atomic number of ash is about 10, while that of combustible carbonaceous material is about 6. Thus, since the effective atomic number of coal increases with increasing ash content, the ash content can be theoretically determined by measuring the intensity of scattered low energy photons.

The presence of iron-sulphur minerals in coal, such as pyrite and pyrrhotite, which may be as high as 5-10 weight percent, with an effective atomic number of about 20, will cause greater changes in

scattering intensity than alumina and silica with their effective atomic number of about 10. Therefore, compensation should be made for the iron content in order to accurately determine the ash content. If a radioisotope is selected so that Fe K_α (6.4 KeV) is excited and measured, a quantitative measurement of the iron-sulphur mineral content in the slurry can be made. This measurement provides a correction for the additional scattering due to the iron-sulphur minerals. With this procedure an accurate determination of ash content can be made.

EXPERIMENTAL

A schematic diagram of the test rig is shown in Fig. 1. It consisted of a variable speed peristaltic pump, head and receiving tanks, a flow cell for the XRF measurements and a lucite assembly with a 20 cm. radiation path for a density gauge. The head tank provided a constant flow rate of slurry through the flow cell. The experimental procedure was to add 3 litres of water at the receiving tank, start the peristaltic pump, and then add varying quantities of coal. The chemical composition as well as the weight of each increment was varied, as far as was practical, by using various coal samples, of which the chemical composition of the two samples used is listed in Table 2.

A 5 mCi Gd-153 point source was placed in a brass fitting located at the bottom of the lead plates forming the base of the density gauge assembly. A 2 in. x 2 in. NaI (Tℓ) activated detector with a gamma-ray spectrometer was used to integrate the radiation intensity between 40 and 100 KeV. Commercially available density gauges employ a Cs-137 or a Co-60 source. To insure that the Gd-153 source gave better results than a Cs-137 source, experimental work was repeated with a Cs-137 source.

The radioisotope used for the scattering measurement was Cd-109. It emits AgK x-rays of energy 24.9 and 22.1 KeV. The scattered AgK radiation and the fluorescent FeK radiation were detected and resolved by a xenon-filled sealed proportional counter. Thus three sets of counts for different slurries were taken. These counts were density gauge counts, FeK_α and scattered counts.

ANALYSIS OF RESULTS

The experimental results for the density gauge are shown in Figures 2 and 3. From these plots, it is obvious that the low-energy radiation from Gd-153 is more sensitive to mass variation than the high energy radiation from Cs-137. Furthermore, the two curves shown for the Gd-153 isotope, which were obtained from slurries of samples 1 and 2, are almost coincident: the difference in chemical composition, particularly the factor of two in iron content (Table 2), has no practical effect on the radiation attenuation.

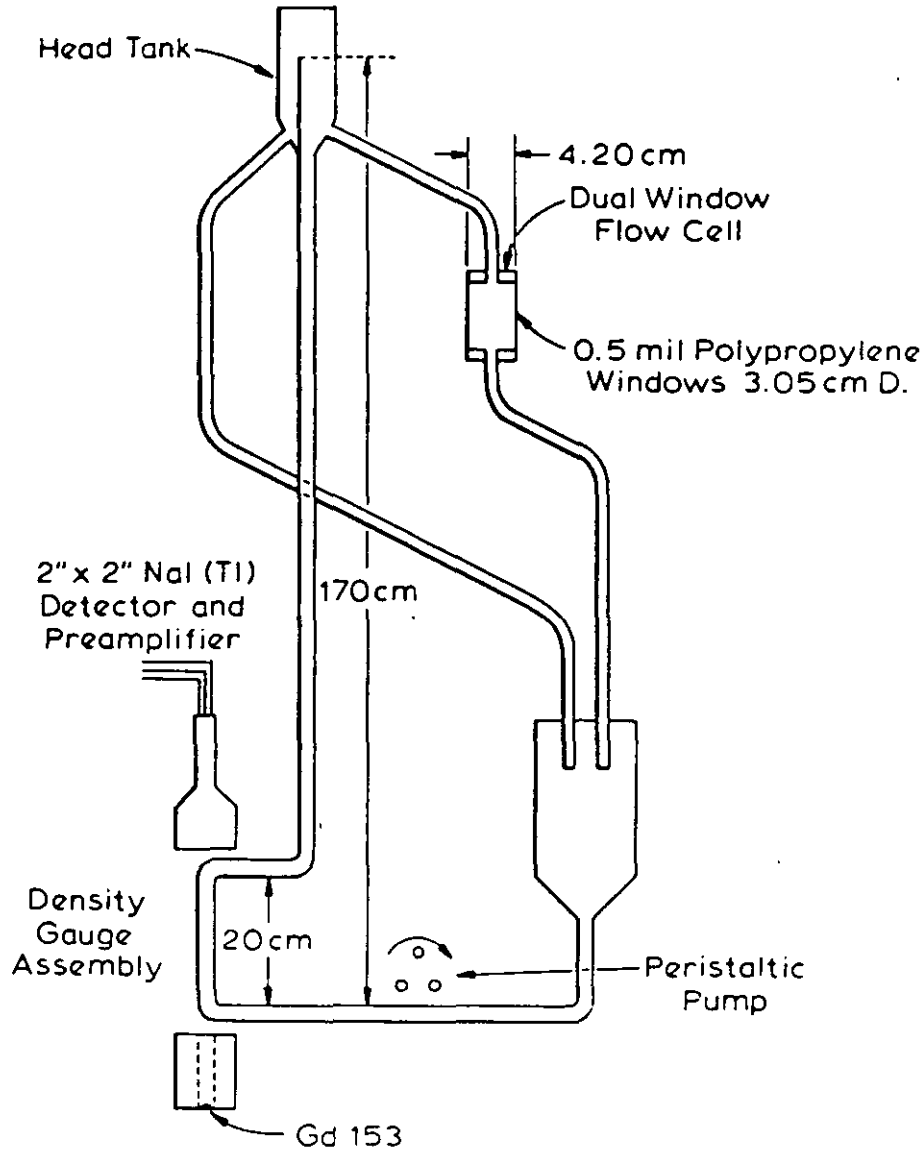

FIG. 1. - Schematic Diagram of the Test Slurry Circuit

TABLE 2. - Values of mass absorption coefficients of constituent elements of a coal sample

Element	Assay (%) Sample 1	Sample 2	$\frac{\mu}{\rho}$ (.662 MeV) (cm^2/g)	$\frac{\mu}{\rho}$ (100 KeV) (cm^2/g)
S	5.30	2.43	0.0779	0.202
Fe	4.01	2.19	0.0739	0.370
Ca	0.64	0.13	0.0783	0.256
K	0.11	0.36	0.0762	0.233
Ti	0.069	0.078	0.0732	0.240
Si	2.44	3.02	0.077	0.184
C	68.30	70.27	0.0774	0.152
O	3.00	3.50	0.0787	0.156
H	-	-	0.0863	0.169

Theoretical plots for sample No. 1 are also shown in Figs. 2 and 3. These plots were obtained by using the relationship (12):

$$\frac{I_{s\ell}}{I_{water}} = \exp - \frac{[m_s r_s + m_w (1-r_s)]}{(1 - r_s(1 - \rho_s^{-1})} \ell, \qquad (6)$$

where $I_{s\ell}$, I_{water} are the count rates with the flow cell full of slurry and water, respectively, m_s and m_w are the mass absorption coefficients of solids and water, respectively, ℓ is the length of flow cell, ρ_s is the specific gravity of solids, and r_s is the fraction of solids in the slurry.

It is apparent that the values of $I_{s\ell}/I_{water}$ as predicted by Eq. (6) are slightly lower than the experimental values. This is because of the "buildup factors" (7). Equation (6) does not take into account the secondary photons produced in the slurry that reach the detector. From the present studies, it may be concluded that for coal slurries, where the iron content varies from one to five percent, a Gd-153 source is more efficient than a Cs-137 source. However, in the present studies Fe K_α is also being excited, therefore for on-line analysis of ash in coal slurries, variation of pyrite has no effect.

With this technique, percent ash in coal was determined as a function of scatter counts, iron fluorescent counts and the gamma density gauge counts. For this purpose a simple mathematical model was tested, viz,

$$\% \text{ Ash} = K1 \frac{\text{Pd ct}}{\text{Sc ct}} + K_2 \text{ Fe ct. Pd ct} + K3 \qquad (7)$$

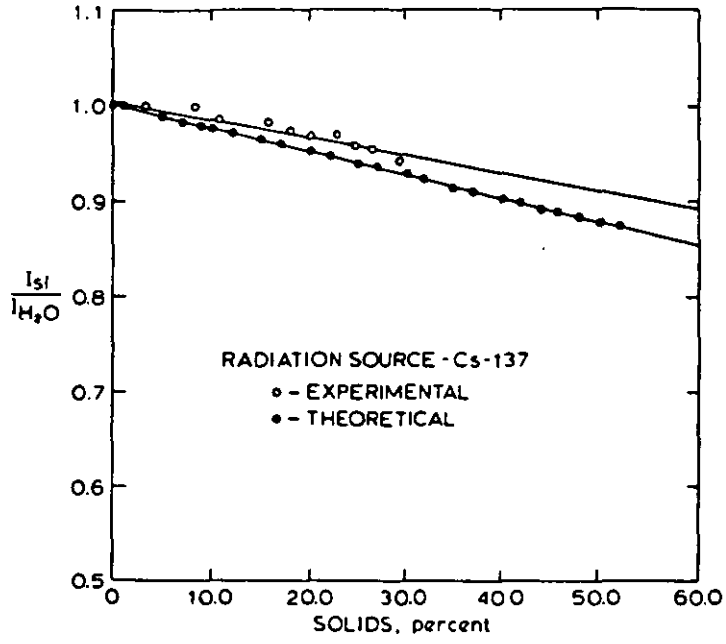

FIG. 2. - Relationship Between $\frac{I_{sl}}{I_{H_2O}}$ and percent solids in slurry for a Cs-137 source.

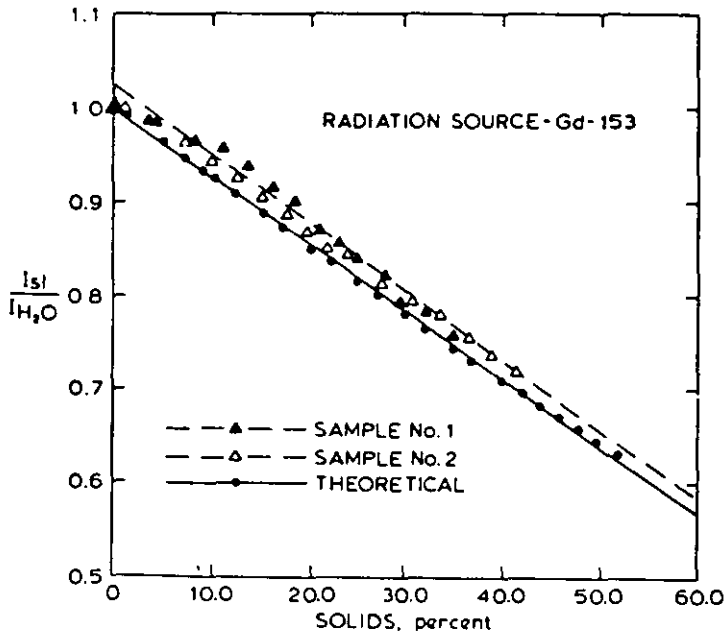

FIG. 3. - Relationship Between $\frac{I_{sl}}{I_{H_2O}}$ and percent solids in slurry for a Gd-153 source.

where K1 to K3 are calibration constants and Sc ct, Fe ct and Pd ct are scatter counts, iron counts and density gauge counts respectively. In this equation Fe ct and Pd ct provide the corrections due to the variation of iron and solids in the slurry.

Constants in equation (7) were determined by using a "simplex" program. The ash content was determined with a precision of 4% in the range of ash in coal samples from 13% ash to 23% ash. Figure 4 shows the relationship between ash observed and ash calculated by equation (7).

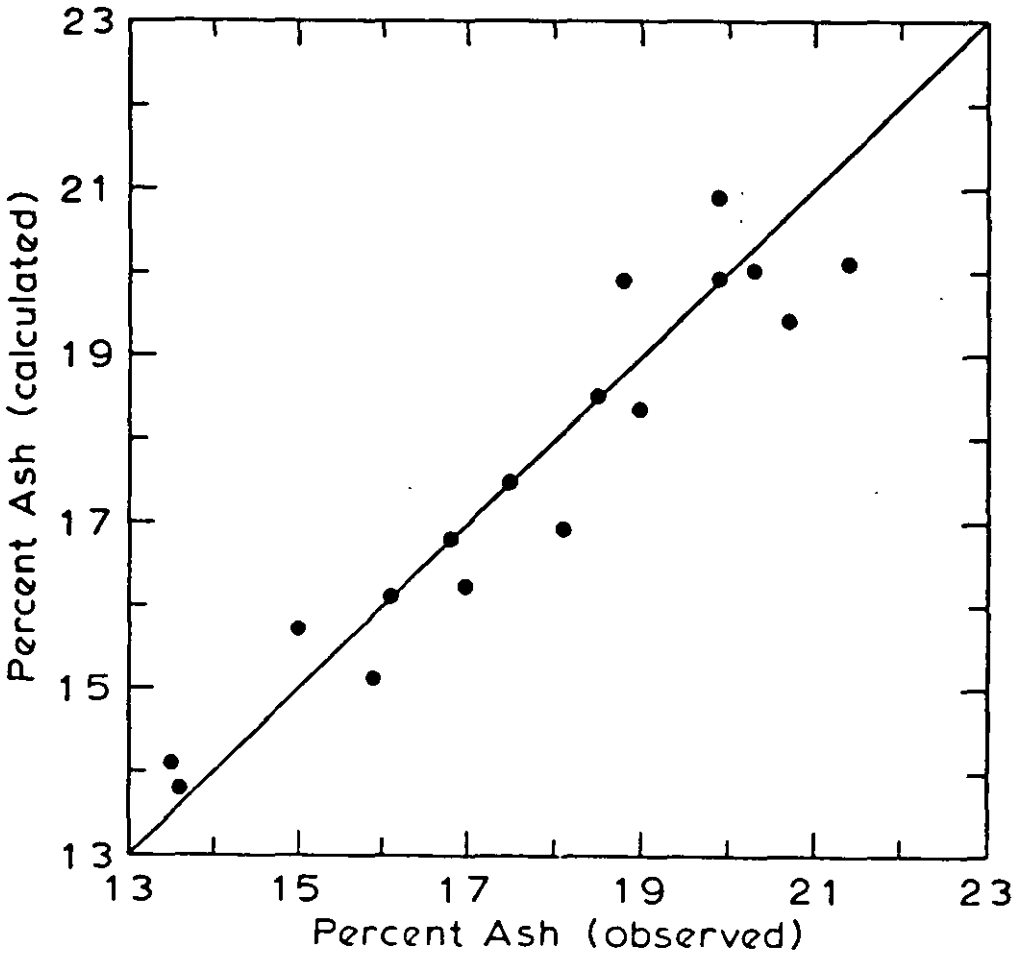

FIG. 4. - Relationship Between Ash Observed and Ash Calculated

CONCLUSIONS

The ash content of coal can be determined in an aqueous slurry by the measurement of scattered Ag K radiation provided correction for the variation of percent solids and the iron content is provided. The technique is simple and efficient.

REFERENCES

1. Kawatra, S. K., "Effect of Variation of Entrained Air in Flotation Slurries on the On-Stream Determination of Copper by Radio-Isotope X-ray Fluorescent Analysis," Canadian Journal of Spectroscopy, Vol. 21, No. 1, 1976.

2. Kawatra, S. K., "The Design and Operational Characteristics of a Portable Multi-Stream On-Line Analyser," International Journal of Mineral Processing, Vol. 3, No. 1, 1976.

3. Kawatra, S. K. and Dalton, J. L., "The On-Line Measurement of Ash in Coal Slurries," Canadian Journal of Spectroscopy, Vol. 21, No. 2, 1976.

4. Kawatra, S. K., "Use of Scattered Radiation in the Determination of Copper in Mineral Slurries," Canadian Mining and Metallurgical Bulletin, Vol. 69, No. 772, 1976.

5. Kawatra, S. K., "The Influence of Length of Flow Cell and Strength of a Source on the Performance of a Gamma Density Gauge," International Journal of Mineral Processing, Vol. 3, No. 2, 1976.

6. Kawatra, S. K., "Feasibility Studies of the On-Stream Analysis of Lead in Mineral Slurries," Journal of the South African Institute of Mining and Metallurgy, No. 1, Vol. 77, 1976.

7. Evans, R. D., The Atomic Nucleus,McGraw-Hill Book Co., Inc., New York, (1955)

8. Evans, R. D., "Compton Effect," Handbuch Der Physik, S. Flugge, Ed., Springer-Verlag, Berlin, 1958.

9. Hubbel, J. H., "Photon Mass Attenuation and Mass-Energy-Absorption Coefficients for H, C, N, O, Ar and Seven Mixtures from 0.1 KeV to 20 MeV," Rad. Res., 70, 58 (1977).

10. Hubbel, J. H. and Overbo, I., "Relativistic Atomic Form Factors and Photon Coherent Scattering Cross Sections," J. Phys. Chem. Ref. Data, Vol. 8, No. 1, (1979).

11. Semmler, R. A., "Gamma-Scattering Density Meters," Report No. LAS-TR-161-35, The University of Chicago, (1961).

12. Kawatra, S. K., "On-Line Determination of Copper and Lead in Mineral Slurries," Ph.D. Thesis, Univ. of Queensland, Brisbane, (1975).

13. U.S. Department of Health, Education and Welfare, "Radiological Health Handbook," (1970).

14. Churchill, T. R., Dalton, J. L., and Dibbs, H.P., "The Determination of Lead in Ore Slurries by Gamma-Ray Attenuation," Canada Centre for Mineral and Energy Technology, Scientific Bulletin CM 75-3, (1975).

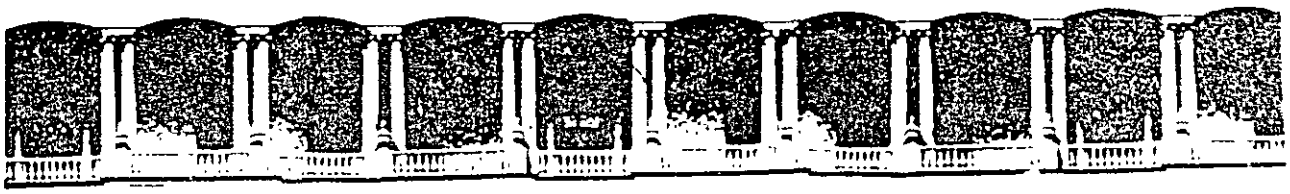

FACULTAD DE INGENIERIA U.N.A.M.
DIVISION DE EDUCACION CONTINUA

CURSOS ABIERTOS

DESARROLLO Y OPERACIÓN DE SENSORES PARA CONTROL DIRECTO Y CONTINUO EN PLANTAS DE BENEFICIO DE MINERALES Y EN LA RESTAURACIÓN DEL MEDIO AMBIENTE

Del 18 al 23 de mayo de 1998

TEMA: ESTIMATING THE CUT (dso) SIZE OF CLASSIFIERS WITHOUT PRODUCT PARTICLE - SIZE MEASUREMENT

EXPOSITOR :DR. KOMAR KAWATRA

1998

International Journal of Mineral Processing, 5 (1979) 369—378
© Elsevier Scientific Publishing Company, Amsterdam — Printed in The Netherlands

ESTIMATING THE CUT (d_{50}) SIZE OF CLASSIFIERS WITHOUT PRODUCT PARTICLE-SIZE MEASUREMENT

L.R. PLITT and S.K. KAWATRA*

Department of Mineral Engineering, University of Alberta, Edmonton, Alta. (Canada)

(Received September 28, 1977; accepted October 11, 1978)

ABSTRACT

Plitt, L.R. and Kawatra, S.K., 1979. Estimating the cut (d_{50}) size of classifiers without product particle-size measurement. Int. J. Miner. Process., 5: 369—378.

A technique is presented by which the cut size of a classifier can be estimated without size analyses of the coarse and fine products. Using the corrected solids recovery and the classifier feed size distribution, an indicated d_{50} size can be determined which is usually within ± 10% of the actual cut size.

By computer simulation of the classification process, actual/indicated cut size ratios were determined for a variety of operating conditions. Through the application of these ratios, it has been demonstrated that the d_{50} of a classifier can be estimated with an accuracy comparable to that obtained through the use of classification curves. The main limitations of this technique are that accurate measurement of the solids content in the slurry streams is required and that no information is obtained concerning the sharpness of separation.

INTRODUCTION

In most industrial situations the performance of a classifier is determined from the particle size distributions of the feed, and coarse and fine products. The methodology for carrying out the mass flow split in classifiers using particle-size distributions is well established (Mular and Bates, 1971; Luckie and Austin, 1973). There are some situations, such as when well-instrumented classifiers are used, where the mass flow splits can be accurately measured. In these cases, the cut size (d_{50}) can be estimated directly from the solids split and the feed size distribution, thus eliminating the need to obtain samples and size analyses of the coarse and fine products.

This procedure has been practiced in our laboratory for several years for preliminary adjustment of variables. The object of this work was to determine how close these estimates are to the true cut size and to develop correction factors to expand the limits of applicability of this estimating technique.

*Present address: Michigan Technological University, Houghton, Mich. (U.S.A.)

THE CLASSIFICATION PROCESS

In mineral processing, classification usually refers to a separation of particles according to their differing settling velocities in a suspending fluid. If the material is of uniform density, then the separation would be based entirely upon particle size and/or shape. A typical classification curve of a uniform density material in a wet classifier is represented as Curve y in Fig.1. The point at which $y = 0.5$ is usually selected as the characteristic cut size and is designated d_{50}.

In wet classifiers, such as hydrocyclones and rake classifiers, it is generally assumed that solids of all sizes are entrained by the coarse product liquid. It is possible to 'correct' the observed classification curve for this bypassing effect caused by the coarse product liquid according to the equation:

$$y' = \frac{y - R_f}{1 - R_f} \tag{1}$$

where y' is the mass fraction of particles of a particular size and density which will be directed to the coarse product as a result of the classifying action;

y is the mass fraction of particles of a given size and density which actually report to the coarse product, and

R_f is the fraction of feed liquid which is recovered in the coarse product stream

As shown on Fig.1, the size at which $y' = 0.5$ is the corrected d_{50} (d_{50c}).

Various mathematical functions have been proposed to represent the corrected classification curve. Two of the most widely used equations are:

$$y' = 1 - \exp\left[-0.693\left(\frac{d}{d_{50c}}\right)^m\right] \tag{2}$$

and:

$$y' = \frac{\exp[ad/d_{50c}] - 1.0}{\exp[ad/d_{50c}] + \exp[a] - 2.0} \tag{3}$$

where d_{50c} is the size of particle in the portion of the feed subjected to classification which has equal (50%) probability of reporting to the coarse and fine products, and

a and m are both measures of the sharpness of separation and are approximately interrelated as follows:

$a = 1.54m - 0.47$.

In an earlier paper (Plitt, 1971) it was shown that both equations represent classification with equal effectiveness.

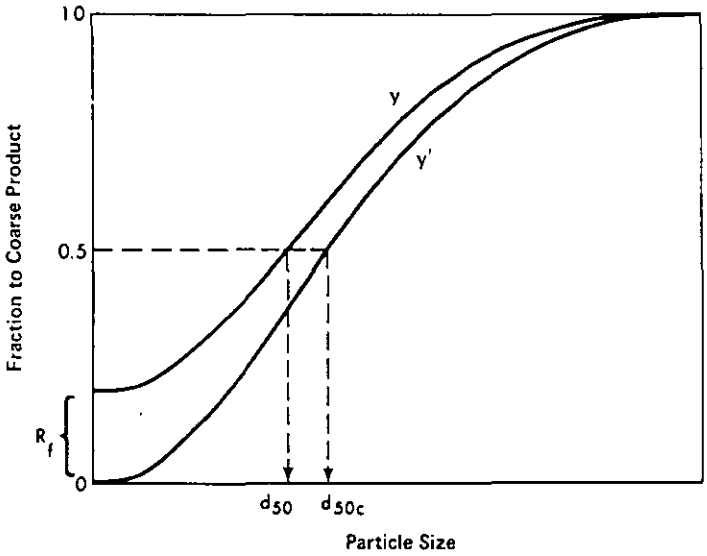

Fig.1. Typical uncorrected and corrected classification curve.

ESTIMATION OF CLASSIFIER CUT SIZE

One may rewrite eq. 1 in terms of the total solids recovery to the coarse product as follows:

$$R_c = \frac{R_s - R_f}{1 - R_f} \tag{4}$$

where R_c is the total fraction of solids of all sizes recovered by the coarse product as a result of the classification action, i.e. corrected for by-passing of coarse product liquid, and

R_s is the total observed solids recovery in the coarse product.

It is evident that if perfect classification occurs on the portion of the feed subjected to classification, the corrected cut size (d_{50c}) is equivalent to the $f(1-R_c)$ size where $f(x)$ is equal to the particle size in the feed which has a cumulative weight fraction finer than x. The relationship between corrected recovery and indicated cut size is illustrated in Fig.2. Since classifiers are not perfect (i.e., they do not have infinite values of m or a), the indicated cut size determined from the feed size distribution (id_{50c}) may differ from the actual cut size.

Fig.3 illustrates a typical corrected classification curve. The hatched areas indicate the misplaced material: fines in coarse product and coarse in fine product. It follows that if an equal amount of feed material is distributed on either side of the cut size the relative amounts of misplaced material will tend to compensate each other, and the indicated cut size determined from the feed size distribution will correspond to the actual cut size. On the other hand if the major part of the size distribution lies above the cut point, the amount of misplaced coarse in the fine product will exceed the misplaced fines in the coarse product and the indicated cut size (id_{50c}) will be higher than the actual

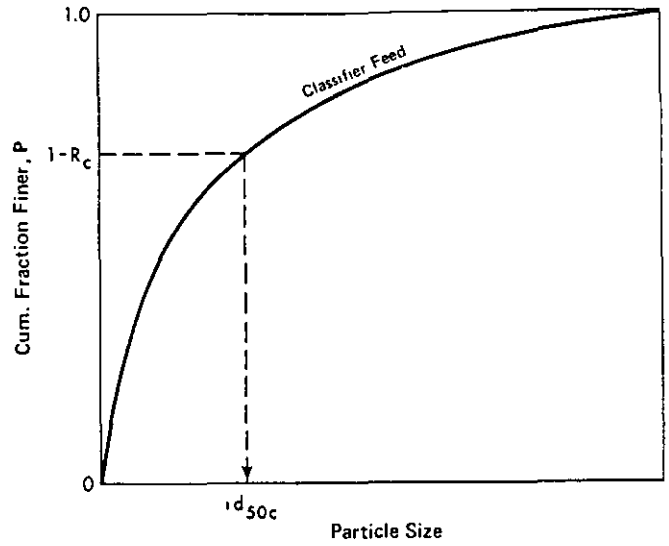

Fig. 2. Illustration of how the indicated cut size is obtained from the particle-size analysis of the feed.

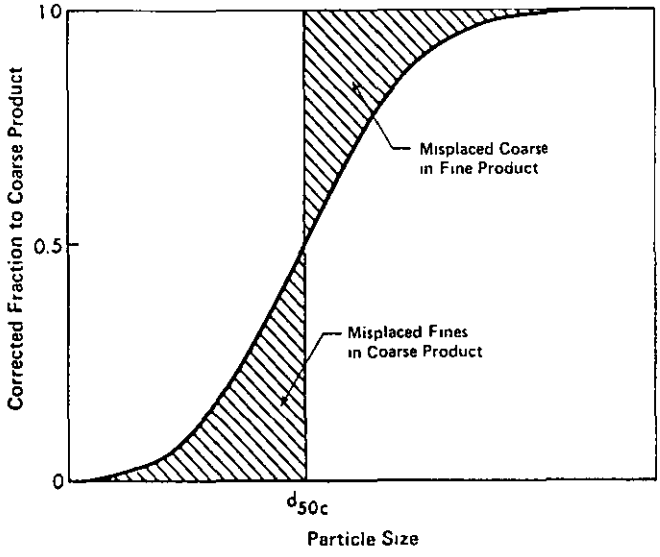

Fig. 3. Typical corrected classification curve illustrating the misplaced material concept.

cut size. Conversely, if the classifier cut point lies above the mode of the particle size distribution the indicated d_{50} size should be below the actual cut size. Applying the above logic to symmetrical feed size distributions the following relationships between actual and indicated cut sizes should exist:

$d_{50c} = f(50)$ (i.e. $R_c = 50\%$), $id_{50c} = d_{50c}$.
$d_{50c} < f(50)$ (i.e. $R_c > 50\%$), $id_{50c} > d_{50c}$
$d_{50c} > f(50)$ (i.e. $R_c < 50\%$), $id_{50c} < d_{50c}$

COMPUTER SIMULATION

To quantify the difference between the indicated and actual cut sizes a

computer simulation of a classifier was carried out. The simulation assumed that the classifier functioned according to either eqs. 2 or 3. Assumed feed size distributions using both Gaudin—Schuhmann and Rosin—Rammler distribution functions were generated in the simulation and compared. These functions are:

Gaudin—Schuhmann $P = 0.5[d/f(50)]^{\alpha}$ (5)

Rosin—Rammler $P = 1-\exp[-0.693\{d/f(50)\}^{n}]$ (6)

where P = mass fraction of classifier feed with a particle size less than d,
$f(50)$ = mass median particle size,
α = Gaudin—Schuhmann distribution modulus, and
n = Rosin—Rammler distribution modulus.

As the classification equations are point functions with respect to size, the feed was subdivided into 100 equal parts to eliminate any substantial error in obtaining an average size for the particle size fractions. The classifier cut size was varied over a wide range using various sharpness of separation coefficients and various size distribution constants.

RESULTS

The results shown in Figs.4, 6 and 7 are plotted in terms of the ratio between actual and indicated cut size versus the corrected solids recovery. The curves all display the same general form: rising sharply at low recoveries and levelling off at a constant value near 1 at high recoveries.

As would be expected the difference between the actual and indicated cut size is least when the sharpness of separation is the greatest (high values of m or a).

Fig.4a, b and c show the comparison of the cut size ratios with a variation of feed size distributions. For a narrow feed size distribution ($\alpha = 1.0$) the sharp rise in the cut size ratio occurs at a higher recovery then for flat feed size distributions. Fig.5 shows the constant values of the d_{50c}/id_{50c} ratios and the point where the ratios begin to deviate substantially from the constant values both plotted as a function of the distribution modulus. Below a distribution modulus of 0.7 the d_{50c}/id_{50c} ratios level off at values above 1.0. This somewhat unexpected result is due to the highly negative skew of Gaudin—Schuhmann distributions with low distribution moduli. The result of the negative skew is that even when the cut size is in the finer size region of the feed (i.e. high values of R_c) more fines are misplaced to the coarse product then vice versa. Fig.5 was prepared using a sharpness of separation, m, of 2.5, which represents average conditions for hydrocyclone classifiers.

Fig.6 shows the actual/indicated cut size ratios for an assumed Rosin—Rammler feed size distribution. With a different feed distribution the curves are only slightly different from those using a Gaudin—Schuhmann distribution. This similarity suggests that all natural feed size distributions will give a similar relationship between the actual and indicated cut size. To check that the assumed classification function did not produce unique results, Fig.7 shows the

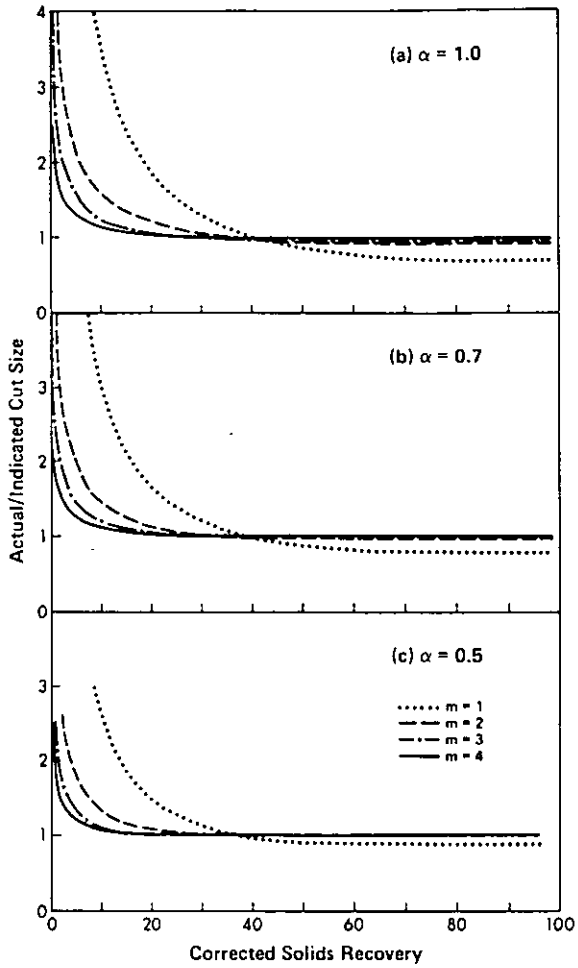

Fig. 4. Actual/indicated cut size ratios for the Rosin—Rammler classification function with Gaudin—Schuhmann feed size distributions.

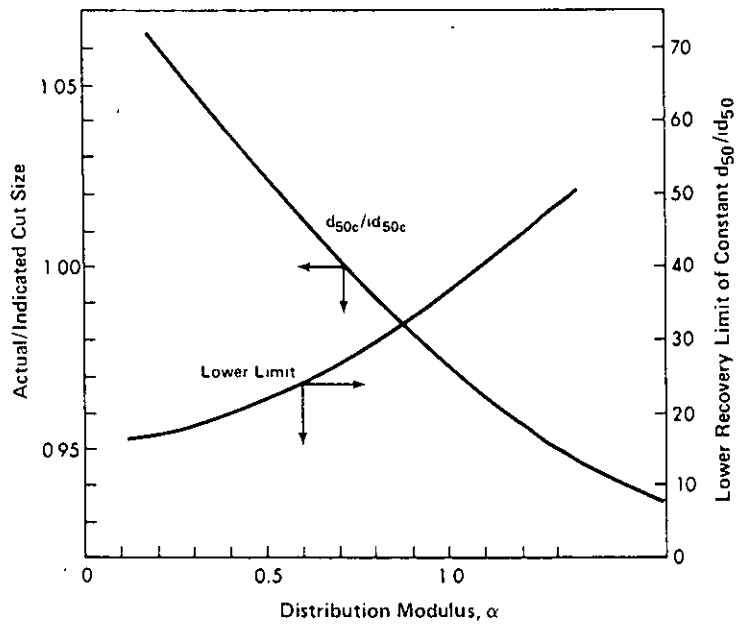

Fig. 5. Values of constant actual/indicated cut size ratios and lower limit of applicability as a function of the Gaudin—Schuhmann distribution modulus (all for m = 2.5).

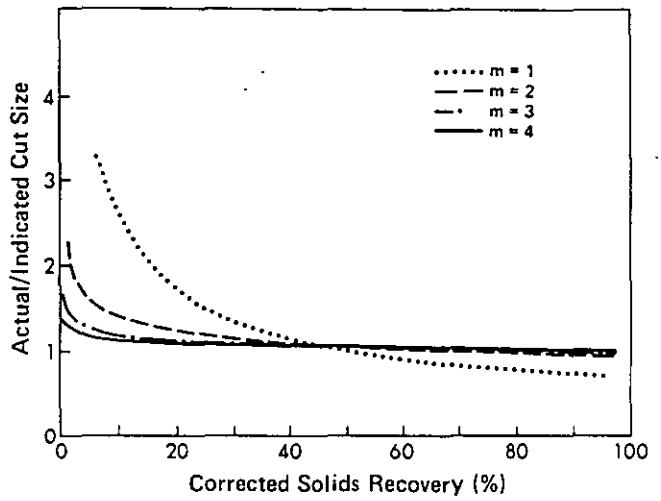

Fig.6. Actual/indicated cut size ratios for the Rosin—Rammler classification function with a Rosin—Rammler feed size distribution. Distribution modulus n = 1.0.

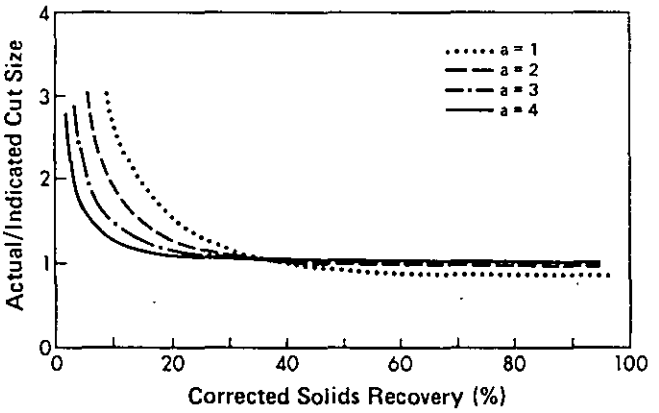

Fig.7. Actual/indicated cut size ratios using the Lynch classification function with a Gaudin—Schuhmann feed size distribution (α = 0.7).

actual/indicated ratios using the Lynch equation (No. 3). The form of the curves is again very similar to those in Fig.4. From these results it can be concluded that with reasonable sharpness of separation (i.e. $m > 2$) the indicated d_{50c} size will provide an estimate within ± 10% of the actual d_{50c} size providing the solids corrected recovery is over 30%.

APPLICATIONS

d_{50}-size estimation

This technique is restricted to instances when reliable data is available which will permit calculation of the solid and liquid recoveries. With this information the cut size of the classifier can be quickly estimated without carrying out a size analysis of the coarse and fine products. This method is particularly useful to monitor changes in the cut size or to check that it is within the proper

range before coarse and fine product size analyses are carried out.

As an example, if the data from the cyclone test shown in Appendix A were available except for the underflow and overflow size analyses, it would be possible to determine the values of d_{50} and d_{50c}. The feed size analysis is plotted as shown in Fig.8. The distribution follows the Gaudin—Schuhmann equation remarkably well with a rather low distribution modulus of 0.23. From the mass balance the corrected solids recovery (R_c) is 24.6% such that the indicated d_{50c} size is equal to 280 μm and corresponds to the 75.4% passing size. With reference to Fig.5 the d_{50c}/id_{50c} ratio for an $\alpha = 0.23$ is 1.057. As the R_c of 24.6 is above the lower limit of 17% the ratio applies. Thus the estimated d_{50c} is:

$$1.057 \times 280 = 296\ \mu m$$

The estimate of d_{50} using an assumed $m = 2.5$ is:

$$y' \text{ (at } d_{50}) = \frac{0.50-0.179}{1-0.179}$$

$$= 0.391$$

$$d_{50} = 296\left[\frac{1}{0.693} \ln \left(\frac{1}{1-0.391}\right)\right]^{1/2.5}$$

$$= 258\ \mu m$$

The estimated corrected and uncorrected cut sizes compare to the actual values of 298 μm and 259 μm respectively. Although agreement within 2% is most acceptable the reasons for the apparent decrepancy in the estimated d_{50c} may be:

(1) The sharpness of separation value of m assumed in Fig.5 is 2.5, the actual value for this test was 3.06 which would lower the d_{50c}/id_{50c} ratio.

(2) The geometric mean was employed as the average size for the size intervals in the d_{50c} size determination. If the arithmetic mean had been used, the d_{50c} would have been 294 μm.

Although this method of estimating the cut size is a useful analytical tool

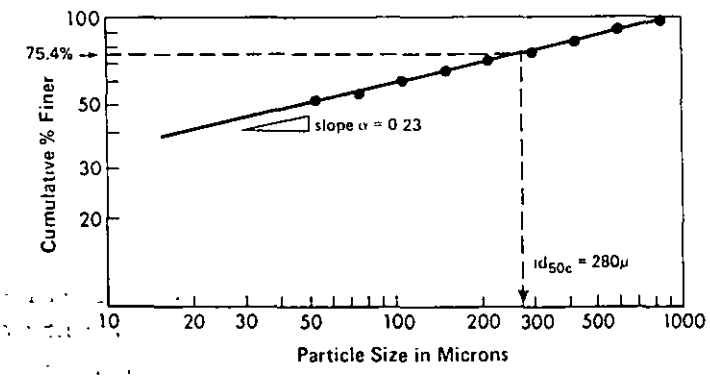

Fig.8. Gaudin—Schuhmann plot of feed size analysis illustrating the determination of the indicated cut size (data from Appendix A).

it does not replace the value of classification curves. The estimate is of limited usefulness because it provides no information regarding the sharpness of separation or the shape of the classification curve.

Particle size measurement

This technique also suggests the possibility of using a classifier as a particle size measuring device. A classifier with a known cut size, if instrumented to provide a mass balance, could be calibrated to determine the particle size of the feed. To illustrate, let us assume that the hydrocyclone in Appendix A was known to have a d_{50c} of 289 μm. Then by simply using an assumed d_{50c}/id_{50} of 1.0 it could be determined that the feed contained 75.4% material finer than 289 μm. This size compares to the actual value of about 280 μm. This principle is, in fact, the basis behind the London School of Mines on-stream particle size analyser (Osborne, 1972).

CONCLUSIONS

When accurate solids and liquid mass flow data are available the cut size of a classifier can be estimated from the feed size analysis with an accuracy comparable to that obtained from classification curves. This technique provides a rapid means of checking the cut size of a classifier without the need of carrying out size analyses of the coarse and fine products.

APPENDIX A

Calculation of d_{50c} from a classification test (Lynch, 1974)

Data: Percent solids by weight: feed 70.4
overflow 64.2
underflow 83.5

Size Analyses

Mesh B.S.S.	Feed	Overflow	Underflow
+14	0.1	0	0.3
14/18	1.5	0	3.6
18/25	7.8	0.1	20.7
25/36	8.6	0.6	21.3
36/52	6.1	2.2	13.1
52/72	5.6	4.7	7.0
72/100	5.0	5.9	3.7
100/150	5.3	6.7	3.4
150/200	5.4	7.0	2.7
200/300	3.4	4.7	1.7
−300	51.2	68.1	22.5

Calculated parameters: R_s = 38.1%, R_f = 17.9%, and R_c = 24.6%.

Calculation of classifier functions (Efficiencies)

Geometric mean size (μm)	% to U.F. y	Corrected % to U.F. y'	Predicted $\hat{y}'$ (eq.2, m = 3.06, d_{50c} = 289 μm)
—	100.0	100.0	—
1010	100.0	100.0	100.0
714	99.3	99.1	100.0
502	95.6	94.7	97.7
355	78.6	73.9	72.9
251	47.9	36.5	36.2
177	27.9	12.1	14.3
126	23.9	7.2	5.3
89	19.2	1.6	1.9
63	18.3	0.4	0.6
—	16.9	— 1.2	—

Lynch equation (No. 3) best fit parameters α = 4.57, d_{50c} = 289 μm.
Uncorrected cut size d_{50} = 259 μm.

REFERENCES

Luckie, P.T. and Austin, L.G., 1973. Technique for derivation of selectivity functions from experimental data. In: Proceedings of 10th International Mineral Processing Congress, IMM 1974, pp. 773—790.

Lynch, A.J., Rao, T.C. and Prisbrey, K.A., 1974. The influence of hydrocyclone diameter on reduced efficiency curves. Int. J. Miner Process., 1: 173—181.

Mular, A.L. and Bates, M.W., 1971. Modelling of parallel cyclones in the absence of flow measurement. CIM Bull., 64: 51—56.

Plitt, L.R., 1971. The analysis of solid—solid separations in classifiers. CIM Bull., 64: 42—48.

Osborne, B.F., 1972. A complete system for on-stream particle size analysis. CIM Bull., 65: 97—107.

International Journal of Mineral Processing, 23 (1988) 205–211
Elsevier Science Publishers B.V., Amsterdam — Printed in The Netherlands

Effects of Temperature on Hydrocyclone Efficiency

S.K. KAWATRA, T.C. EISELE, D. ZHANG and M. RUSESKY

Metallurgical Engineering, Michigan Technological University, Houghton, MI 49931 (U.S.A.)

(Received December 9, 1986; accepted after revision September 15, 1987)

ABSTRACT

Kawatra, S.K., Eisele, T.C., Zhang, D. and Rusesky, M., 1988. Effects of temperature on hydrocyclone efficiency. Int. J. Miner. Process, 23: 205–211.

Plant investigations and laboratory experiments have been conducted in order to study the effects of temperature on the classification efficiency of a cyclone. It was demonstrated that, under otherwise constant operating conditions, alterations in temperature produced a nearly linear change in $d_{50(c)}$ size. However, the sharpness of the separation, as defined by the reduced efficiency curve, showed no dependence on temperature.

INTRODUCTION

The hydrocyclone has become a very popular classification device in mineral processing circuits, primarily due to its simplicity, high capacity, and small size. However, control of hydrocyclones is complicated by the numerous variables affecting their performance, the sometimes counterintuitive results of altering these variables, and the general lack of certainty of the true results of changing a given variable. In order to improve this state of affairs, a number of investigators (Plitt, 1976; Lynch, 1977; Klimpel et al., 1984) have intensively studied such variables as feed solids content, particle size, inlet pressure, inlet diameter, vortex finder diameter, spigot diameter, throughput, and particle specific gravity. However, little work has been reported which determines the effect of temperature on cyclone performance, in spite of the fact that many mineral processing operations are subject to large seasonal temperature variations, and have in several cases observed seasonal changes in grinding efficiency which appear to be due to temperature. The investigation described here was therefore carried out to determine the magnitude and nature of temperature effects in hydrocyclone operation.

0301-7516/88/$03.50 © 1988 Elsevier Science Publishers B.V.

EXPERIMENTAL WORK

Laboratory studies

Laboratory experiments were carried out using a 10.2-cm (4-inch) diameter Krebs hydrocyclone. The cyclone was mounted on a laboratory test rig, in closed circuit with a Warman centrifugal pump and a slurry tank. The cyclone overflow and underflow streams discharged freely into separate launders, which were used to either remove simultaneous samples from the two streams or to recombine the streams before returning them to the slurry tank. The slurry temperature sensor was mounted in the feed tank, and a diaphragm-type pressure gauge and an ultrasonic Doppler flowmeter were both mounted on the cyclone inlet line. Apparent slurry viscosity was also monitored at the cyclone inlet, using a vibrating-sphere viscometer. Flowrate, viscosity, and temperature data were collected and logged by an Hp-85 computer. The slurry temperature was controlled with an immersion heater and an immersion chiller.

Test material. The mineral used for these experiments was pure silica, with specific gravity of 2.65, obtained from the Ottawa Sand Co., Ottawa, Illinois. The silica was ground in a dry ball mill until the size distribution given in Table I was achieved.

Experimental procedure. The slurry tank was initially filled with hot water and sufficient silica to produce a slurry of 33% solids. The cyclone inlet pressure was then set to 6.9 N/cm^2 (10 psi), and the immersion heater was used to maintain the slurry at an elevated temperature. The system was allowed to

TABLE I

Size distribution of ground Ottawa Sand

Size (μm)	Cumulative wt.% passing
176	100
125	97
88	93.6
62	75.5
44	49.8
31	34.9
22	24.0
16	17.5
11	12.7
7.8	8.1
5.5	5.1
3.9	3.9
2.8	2.0

stabilize for 10 min before the first overflow and underflow samples were taken, after which the slurry temperature was gradually decreased, with samples taken at approximately 5°C intervals. The use of the chiller allowed experiments over a temperature range of 50°C to 12°C.

The overflow and underflow samples were weighed, filtered, and dried. The dried samples were then weighed to allow the calculation of pulp densities, and the particle size distributions were determined with a Leeds and Northrop Microtrac particle size analyzer. The particle bypass fraction, R_f, was calculated from the fraction of the feed water which reported to the underflow, and cyclone efficiency values were corrected for R_f.

Plant studies

Investigations were carried out in an iron ore processing plant located in the northern U.S. which experiences substantial seasonal temperature variations, in order to determine whether normal temperature fluctuations produce a notable change in cyclone performance. This plant processes a very fine-grained iron ore which requires grinding to -75 μm for liberation. The grinding circuit is closed with 38-cm (15-inch) diameter hydrocyclones.

Sampling was carried out in the summer and in the winter in order to achieve the greatest temperature variation. Pulp temperatures ranged from 20°C (68°F) in the summer to 3.3°C (38°F) in the winter. The resulting corrected efficiency curves for these conditions are shown in Fig. 1.

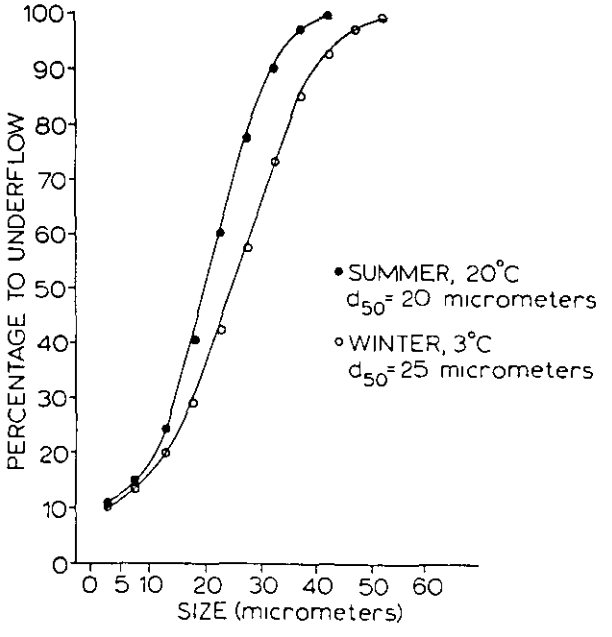

Fig. 1. Seasonal variations of cyclone performance in an iron ore processing plant.

RESULTS AND DISCUSSION

A summary of the data collected in the laboratory cyclone experiments is presented in Table II. The values of α and $d_{50(c)}$ in this table were determined from the equation (Lynch, 1977):

$$y' = \frac{e^{\alpha x} - 1}{e^{\alpha x} + e^{\alpha} - 2}$$

where $x = d/d_{50(c)}$; y' = corrected fraction of feed to the coarse product; $d_{50(c)}$ = corrected 50% separation size; d = particle size; α = a measure of the sharpness of the separation, sharpness increases with increasing values of α.

A simplex optimization program was used to find the best-fit values of α and $d_{50(c)}$, and the corrected efficiency curves at various temperatures are plotted in Fig. 2.

It is clear from these data that $d_{50(c)}$ does indeed decrease with increasing temperature. When $d_{50(c)}$ is plotted against temperature, it is further observed that the relationship is nearly linear, as is illustrated by Fig. 3. While the relationship of cut size to temperature is definite, the parameter α exhibits little dependence on temperature, which indicates that changing temperature has little if any effect on the sharpness of the separation. This is clearly shown by the reduced efficiency curve of Fig. 4, which is essentially identical for all of the tests. This result is in agreement with the results of Lynch (1977), which show that the reduced efficiency curve is a function only of cyclone geometry and particle characteristics, and is largely unchanged by alterations in operating conditions.

It is known that increasing the fluid viscosity affects the cyclone performance both by slowing the settling rate of particles and by suppressing the tangential velocity of the fluid in the cyclone (Bradley, 1965). The net result

TABLE II

Summary of experimental results

Test	Temperature (°C)	R_f (%)	$d_{50(c)}$ (μm)	α	Viscosity (cp)
1	48.8	22.0	21.0	2.83	8.9
2	40.4	23.3	23.6	2.85	10.4
3	35.2	24.3	25.0	2.54	10.6
4	30.0	23.2	26.8	2.74	10.3
5	25.0	24.7	29.1	2.44	10.8
6	20.0	23.5	30.0	2.12	12.0
7	15.1	23.9	31.4	2.69	14.2
8	11.1	24.4	32.4	2.54	13.8

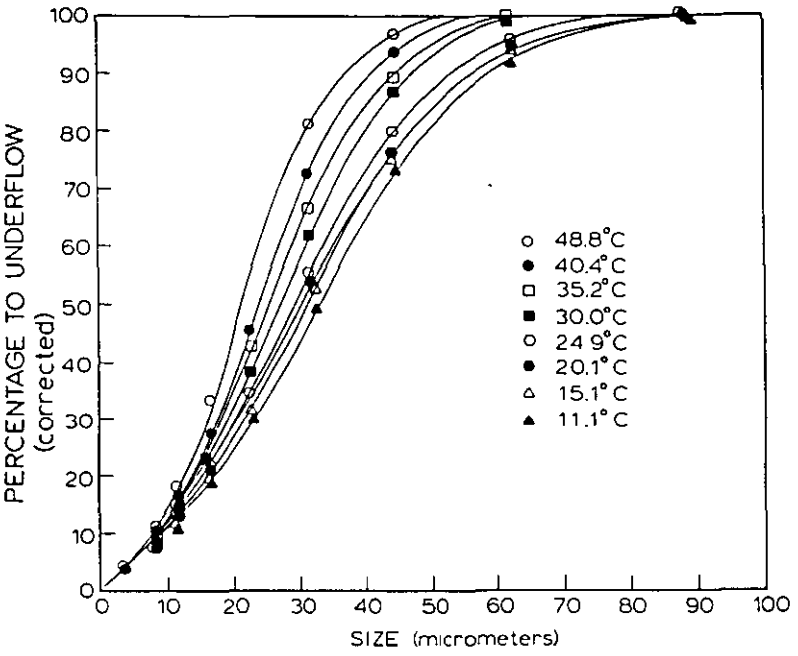

Fig. 2. Corrected efficiency curves showing dependence of hydrocyclone performance on slurry temperature.

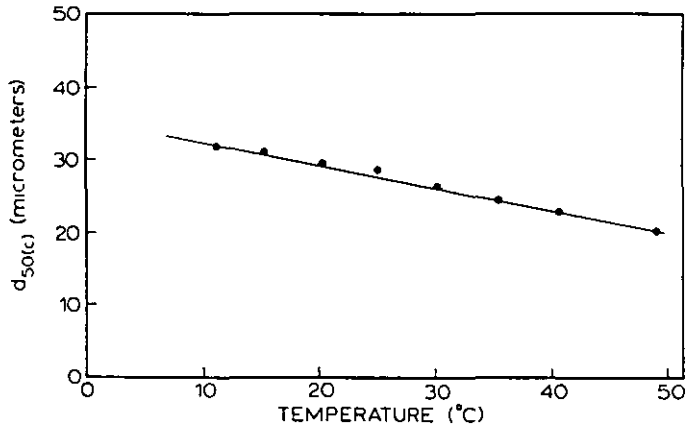

Fig. 3. Dependence of corrected d_{50} size on slurry temperature.

is that increasing the viscosity of the slurry increases the cyclone $d_{50(c)}$ size. Since the viscosity of a fluid typically increases with decreasing temperature, the observed temperature-dependence of $d_{50(c)}$ appears to be primarily a result of changes in slurry viscosity. Repeatable measurement of the viscosity of mineral slurries has proven to be very difficult, although workers in South Africa have achieved this with heavy-media slurries (Reeves, 1985; Napier-Munn et al., 1985). For our work, a vibrating-sphere viscometer was used, which produced the results shown in Table II. Although pump vibration produced a high background viscosity reading, the apparent slurry viscosity showed a temper-

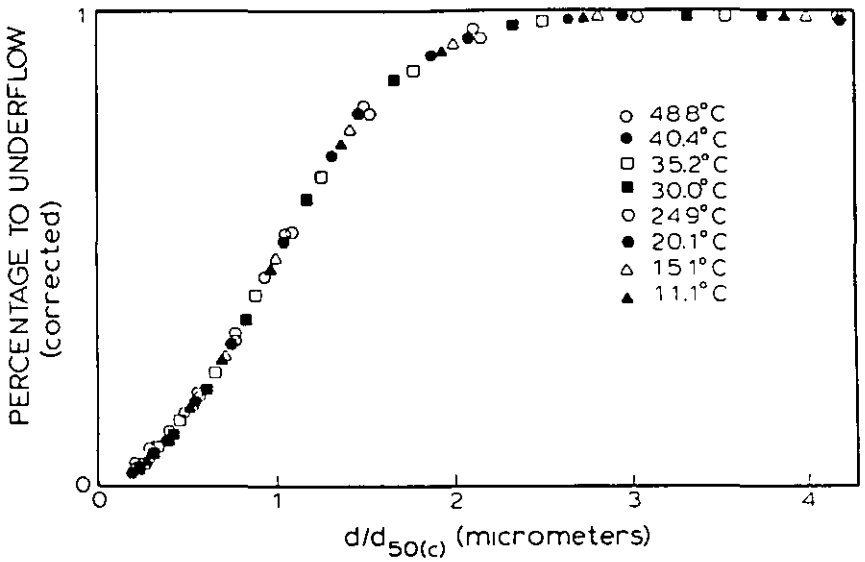

Fig. 4. Reduced efficiency curve for laboratory experiments.

ature variation of sufficient magnitude to account for the observed shift in $d_{50(c)}$.

CONCLUSIONS

It has been shown that, in both plant and laboratory environments, the $d_{50(c)}$ size of a hydrocyclone is temperature-dependent, with the cut size decreasing with increasing temperature. This effect is primarily due to the decreased slurry viscosity at elevated temperatures. The sharpness of the separation is largely unaffected by temperature changes, as illustrated by the constant nature of the reduced efficiency curve.

These results show the necessity for monitoring slurry viscosity in order to improve cyclone efficiency, and moreover that the control strategies based on inferential sizing techniques (Seitz and Kawatra, 1984) must be modified to allow for the observed behavior. Further work must be done to improve the quality of on-line viscosity measurements of mineral slurries.

ACKNOWLEDGEMENTS

This research has been supported by the Department of the Interior's Mineral Institute program administered by the Bureau of Mines through the Generic Mineral Technology Center for Comminution under grant number G1125149. Additional support was provided by the Dow Chemical Co., Midland, Michigan.

REFERENCES

Bradley, D., 1965. The Hydrocyclone. Pergamon Press, New York, N.Y.

Equipment Testing Procedures Committee, 1980. Particle Size Classifiers: A Guide to Performance Evaluation. American Institute of Chemical Engineers, New York, N.Y.

Klimpel, R.R., Austin, L. and Luckie, P.T., 1984. Process Engineering of Size Reduction; Ball Milling. Society of Mining Engineers, AIME, New York, N.Y.

Lilge, E.O., 1962. Hydrocyclone Fundamentals. Trans. IMM, Vol. 71, Part 6.

Lynch, A.J., 1977. Mineral Crushing and Grinding Circuits. Elsevier, New York, N.Y.

Lynch, A.J., Rao, T.C. and Bailey, C.W., 1975. The influence of design and operating variables on the capacities of hydrocyclone classifiers. Int. Miner. Process., 2: 29-37.

Napier-Munn, T.J., Reeves, T.J. and Hansen, J.O., 1985. The monitoring of medium rheology in dense medium cyclone plants. 2nd Samancor Symp. Dense Medium Separation, Perth, July, 1985.

Plitt, L.R., 1976. A mathematical model of the hydrocyclone classifier. Can. Inst. Min. Metall. Bull., 66: 114-123.

Reeves, T.J., 1985. On-line viscometer for mineral slurries. Trans. IMM, 94: C201-C208.

Seitz, R.A. and Kawatra, S.K., 1984. Further studies on the use of classifiers for control of wet grinding circuits. Int. Miner. Process., 12: 239-249.

Mineral Processing and Extractive Metallurgy Review,
1995, Vol. 14, pp. 249–273
Reprints available directly from the publisher
Photocopying permitted by license only

© 1995 OPA (Overseas Publishers Association)
Amsterdam B.V. Published under license by
Gordon and Breach Science Publishers SA
Printed in Malaysia

On-Line Viscometry in Particulate Processing

S. K. KAWATRA and A. K. BAKSHI

Department of Metallurgical and Materials Engineering, Michigan Technological University, Houghton, MI 49931

(Received 23 Jun 1995; in final form 11 September 1995)

On-line viscometry of suspensions is very difficult compared to viscometry of pure liquids. The problem arises because of the unstable nature of the suspensions, particularly when coarse and fast settling particulates are present. Several attempts have been made in the past in which special mixing chambers have been designed to maintain slurry homogeneity while measuring viscosity. However, the credibility of these instruments are questioned by many authors, as quite often the same systems measure different rheological behavior for similar suspensions. In most of the designs suggested in the past, solving one of the problems of suspension viscometry introduces new problems. For example, agitation can keep the solids suspended, but it can also seriously affect the sensitivity of the viscometer. In this article the problems involved with three different types of viscometers (rotational, capillary, and vibrational), which have been used for measuring viscosity of suspensions, are discussed.

BACKGROUND

Unlike non-particulate fluids, rheological measurements of particulate fluids (suspensions) are very difficult. Since a suspension is a multi-phase system, its rheology depends upon the properties of both the liquid and the solids which constitute the suspension. During rheological measurement, the stability of the suspension must be maintained, so that the properties of the suspension will not change while they are being measured. Suspension stability is influenced by several interdependent parameters, such as: (i) Settling velocity of the particles, which depends upon the liquid viscosity, particle size, and particle density; and (ii) Coagulation and flocculation, which depend upon the surface properties of the particles, which in turn are influenced by the chemistry of the carrier liquid. Other parameters, such as particle concentration and particle packing, also influence interparticle interaction, and hence the rheology. The forces arising from all these parameters affect the movement of the fluid, and changes in these will change the rheology of the suspension. Unfortunately, most of the viscometers available to-day are not capable of keeping up with these complex mechanisms of suspension rheology.

Nevertheless, the importance of suspension rheology is widely felt in various industries. In the food industry, more and more attention is given to rheological properties to utilize modern technology for food production, handling, storage, and

quality improvement[1]. In injection molding (ceramic and metal casting) lower viscosities are needed to facilitate mixing, transportation, and enhance solids loading (to reduce shrinkage during sintering)[2]. In paint manufacturing, optimum rheology is needed for quality control. Similarly in the coal and mineral industries, a complete knowledge of rheology is necessary for optimum grinding[3-5,38,39] and efficient separations[6,7,40]. Slurry rheology is also important in the emerging coal slurry utilization technologies. A suitable yield value is needed to store the slurry without allowing the solids to settle, while lower viscosities are needed at intermediate and high shear rates for easier transportation and better atomization[8,9]. Similarly, examples of the importance of slurry rheology can be seen in many other industries, such as in paper and pulp making, waste treatment, cement manufacturing, and so on. Therefore, the need for a suitable rheometer for process control in these industry is always felt. The search for such an instrument was reported as early as 1940[10] and researchers are still working towards it in the 1990's[11-13]. This shows that until today a satisfactory on-line rheometer for suspensions has not been developed. In this article, a survey of viscometry systems for particulate fluids is provided. Since measurement of coarse suspensions is more difficult than measurement of suspensions containing submicron particles, emphasis is given to research work conducted on systems containing coarse, fast settling particles. Three different types of viscometers, the rotational type, the capillary type, and the vibrational type, are discussed whose use have been reported widely for suspensions.

ROTATIONAL VISCOMETERS

Operating Principle

Because of their control over shear rate, rotational viscometers are widely used among researchers. Most rotational viscometers used for suspensions are of the co-axial cylinder type. A line diagram of a simple co-axial cylinder viscometer is given in Figure 1. In this type of viscometer, the fluid is placed in the gap between two concentric cylinders for measurement. Then one of the cylinders is rotated by a motor at a particular r.p.m. while the other is kept stationary, and the torque required to rotate the cylinder is measured. As the viscosity of the fluid increases, the drag force on the surface of the rotating cylinder increases. This in turn increases the torque reading, from which viscosity of the fluid is determined.

Thus the only parameters which are measured by the instrument are the torque (T) and angular velocity (Ω) of the rotating cylinder. Then shear stress is calculated from torque, and shear rate is calculated from angular velocity. Viscosity is calculated by taking the ratio of shear stress and shear rate. The rheological type of the fluid is determined based on the variation of shear stress as a function of shear rate, as shown in Figure 2. A Newtonian fluid has the same viscosity at all shear rates, while the viscosity of a non-Newtonian fluid varies as the shear rate changes. Unless proper equations are used to calculate shear stress and shear rates from torque and angular velocity, an incorrect value of fluid viscosity will result. Calculation of shear stress from torque is straightforward and can be expressed by the following equation, which is valid for both Newtonian and non-Newtonian fluids:

$$\tau = T/(2\pi r^2 L) \qquad (1)$$

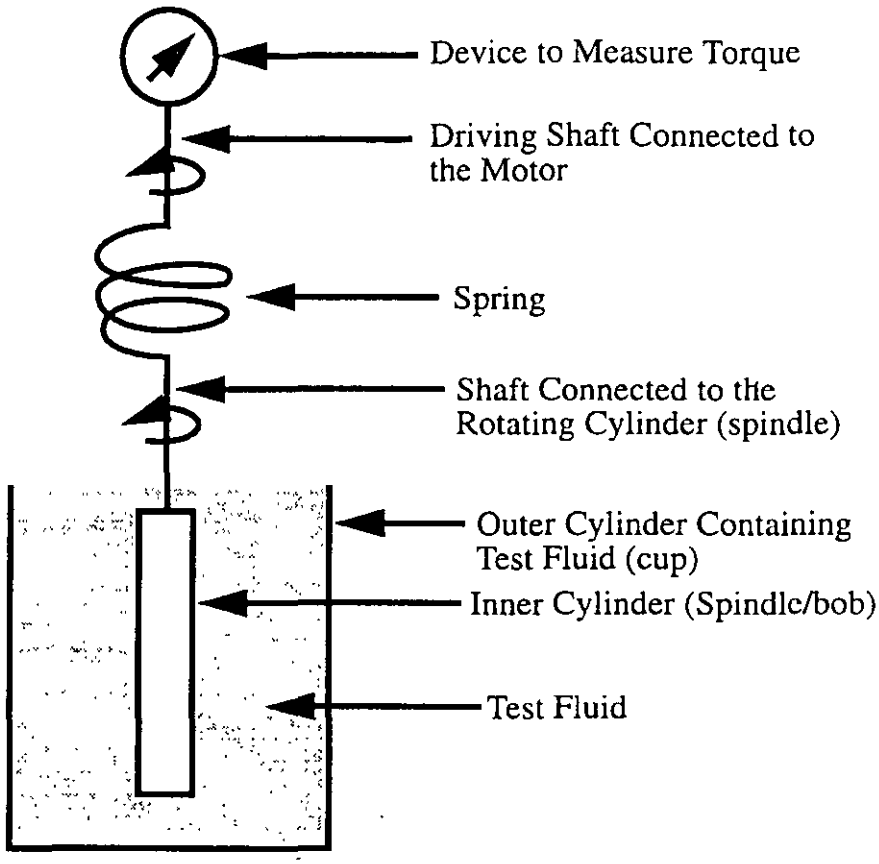

FIGURE 1 Line diagram showing the mechanism of a typical co-axial cylinder viscometer. The change in torque due to the drag force of the fluid on the rotating surface of the cylinder is the measure of viscosity.

Where, τ = shear stress
r = radial distance of the fluid from the axis of the inner cylinder
T = torque
L = length of the inner cylinder.

From this, it can be seen that the shear stress in the viscometer is not a constant, but decreases as one moves from the wall of the inner cylinder to the wall of the outer cylinder.

Calculation of the shear rate from the angular velocity is more complex, and depends upon both the type of fluid and the gap between the two cylinders. For Newtonian fluids:

$$\tau = \eta\dot{\gamma} \tag{2}$$

Where, τ = shear stress
$\dot{\gamma}$ = shear rate
η = viscosity

From this flow model it can be shown that[15],

$$\dot{\gamma} = [2R_2^2/(R_2^2-R_1^2)]\Omega \tag{3}$$

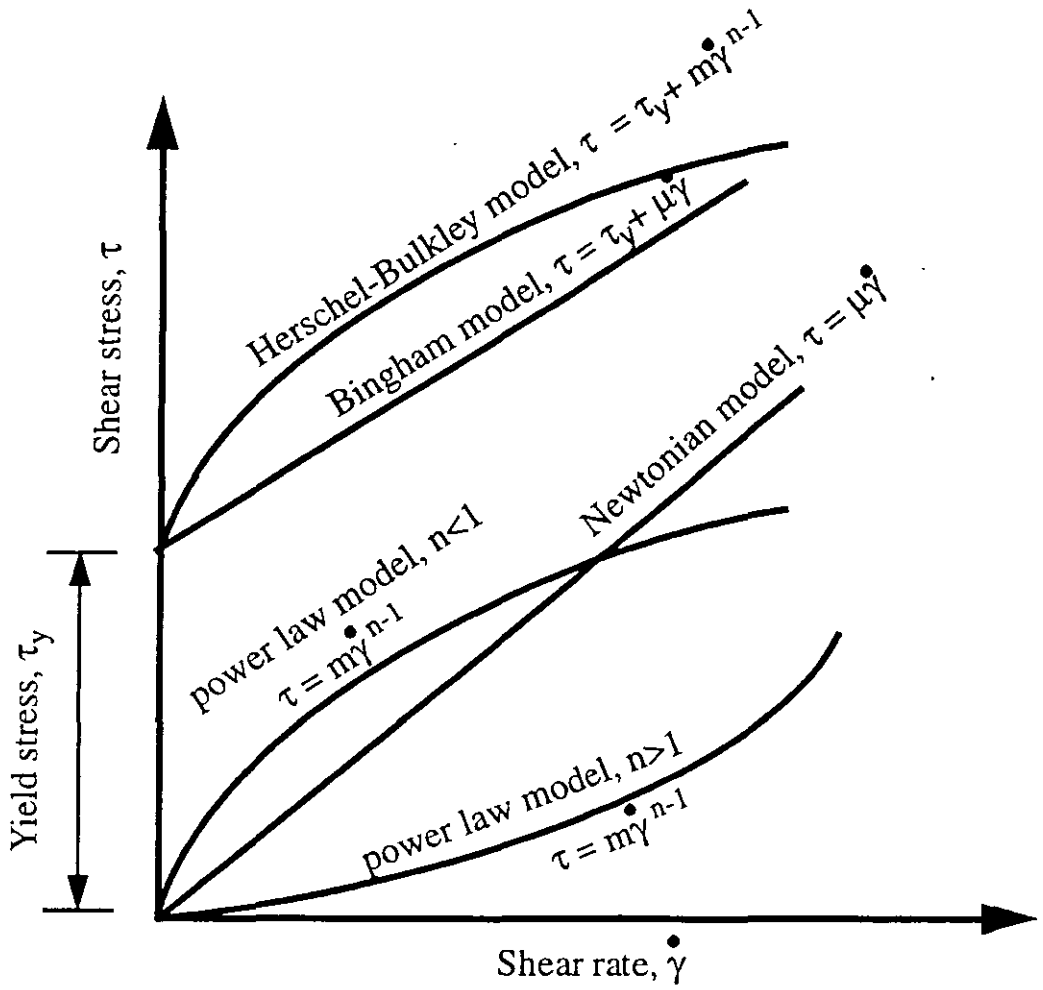

FIGURE 2 Flow curve models reported for suspensions.

where, $\dot{\gamma}$ = shear rate at the surface of the inner cylinder
R_1 = radius of the inner cylinder
R_2 = radius of the outer cylinder
Ω = angular velocity of the inner cylinder.

Quite often, Newtonian solutions of known viscosity are used to calibrate the torque scale of the viscometer to determine viscosity of non-Newtonian fluids. This is not correct because with different flow models different expression for shear rate will be obtained. For example, for a non-Newtonian fluid that obeys the power law (see Figure 2), the shear rate is given by the following equation:

$$\dot{\gamma} = 2\Omega/n[1-(R_2/R_1)^{-2/n}] \quad (4)$$

where, $\dot{\gamma}$ = shear rate at the surface of the inner cylinder
R_i = radius of the inner cylinder
R_2= radius of the outer cylinder
Ω = angular velocity of the inner cylinder
n = flow index, from the power law equation.

From equations 3 and 4 it is seen that unless the appropriate equation is used to calculate shear rates of a particular fluid the viscosity measured by the viscometer will be wrong.

The measurement of the viscosity of a fluid with unknown flow behavior can be greatly simplified by using a coaxial cylinder viscometer whose annular gap is very narrow. If this gap is less than 1% of the diameter of the inner cylinder, then the velocity gradient of the fluid inside the annular gap will very closely approximate linearity for fluids of all types (Newtonian as well as non-Newtonian). In this case, the equation of the shear stress can be written as[15]:

$$\tau = T/(2\pi R_a^2 L) \tag{5}$$

Where, τ = shear stress at all points in the gap
R_a = average radial distance of the fluid from the axis of the inner cylinder
T = torque
L = length of the inner cylinder.

and the equation for shear rate can be simplified to[15]:

$$\dot{\gamma} = [R_a\Omega/(R_2-R_1)] \tag{6}$$

where, $\dot{\gamma}$ = shear rate at all points in the gap

From these values of shear stress and shear rates, flow curves of unknown fluid types can be determined.

While the narrow-gap coaxial-cylinder viscometers work well for liquids, they are unfortunately not suitable for coarse suspensions. This is because the narrow gap is prone to jamming and plugging by solid particles.

Critical Discussion of the Rotational Viscometers

Constant shear operation Rotational viscometers can be operated at a steady shear rate for a long time. This helps in taking precise measurements of viscosity at any particular shear rate, especially at low shear rates where yield stress can be calculated. By changing the rpm of the rotating spindle (or cylinder), the shear rate can be changed, thus a flow curve for non-Newtonian fluids can be determined with these instruments.

Wall slip The equations for shear stress and shear rates described in Equations 1 through 6 are derived under the assumption that the velocity of the fluid at the surface of each cylinder is the same as the velocity of the cylinder surface. This is the no slip condition or shear-flow condition. However, quite often slip occurs at the wall, and correct viscosity of a suspension cannot be obtained by using standard formulas. One of the reasons for such slippage in suspensions is believed to be migration of particles away from the cylinder wall[15,27]. This leaves a dilute suspension at the wall compared to the bulk of the fluids. This is often termed "apparent slippage," and it must be addressed while measuring suspension rheology. Corrections for slippage can be obtained experimentally by varying spindle dimensions, or theoretically by using correction factors suggested by various authors[15,37]. Some investigators have used cylinders with roughened surfaces (e.g., by cutting grooves on the surface) to avoid wall slip[10].

End effects Ideally the length of the cylinder in a co-axial cylinder viscometer should be infinite, to eliminate end effects. End effects are seen, because the fluid below the inner cylinder (and above the inner cylinder if it is submerged) will exert an additional torque on the spindle that is not included in Equations 1 through 6. End corrections are further complicated when different spindle shapes are used, such as the design shown in Figure 3(b) which has been used for eliminating solids build up on top of the spindle[11–13,20]. By changing this geometry, the direction of the velocity gradients will no longer be radially outwards at the ends. In some high precision laboratory viscometers, the bottom surface of the inner cylinder is made cup shaped to trap a layer of air below it, and so minimize the end effects. Also, by keeping the top surface of the inner cylinder above the fluid, torque exerted by the fluid on this surface can be eliminated. However, both these options cannot be practical in a flowing slurry line, and so cannot be used in on-line instruments. As far as end effects are concerned, the double gap design shown in Figure 3(c) is most suitable for suspensions, because it minimizes the end surfaces of the spindle.

Sensitivity Rotational viscometers are very sensitive and any disturbances associated with sample flow will offset the torque reading. In order to avoid settling of solids, many researchers have suggested top to bottom flow of slurry in the annular space. This arrangement will work if the flow is strictly vertical and has no component acting in the r (radial to spindle) or θ (tangential to spindle) directions. Otherwise the change in torque experienced by the spindle will not be solely from the molecular forces (shear) within the fluid, but will be supplemented by the fluid flow (see Figure 4). This also changes the shear rate experienced at the surface of the spindle because the flow interferes with its rotation[11,12].

Solids settling and centrifuging The most difficult suspensions for viscometers to deal with are those which contain fast settling particles. The solids settle during measurement, which not only destroys the homogeneity of the sample but also interferes with spindle

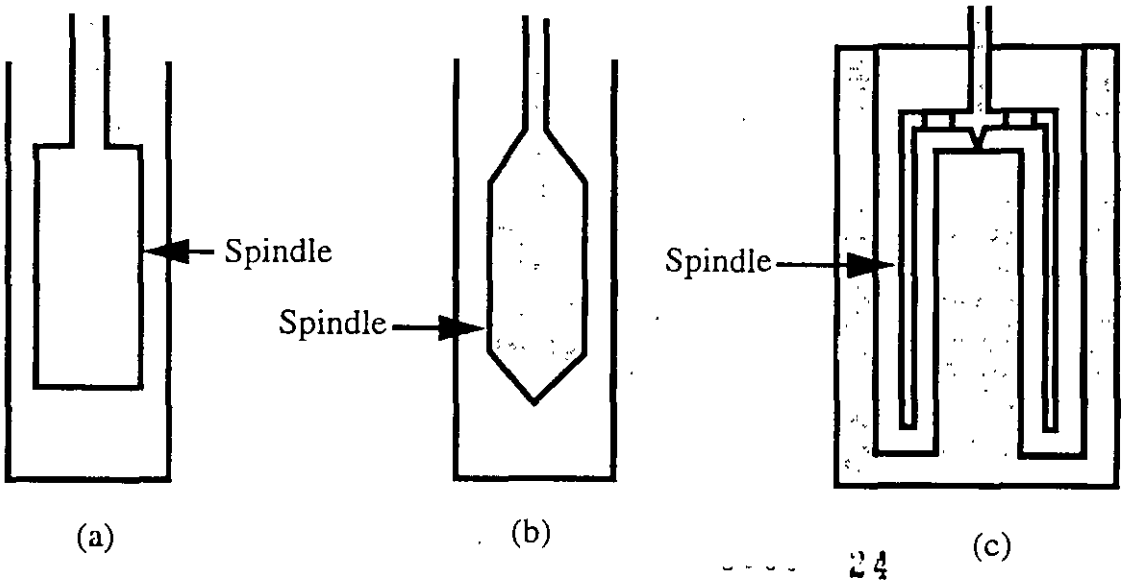

FIGURE 3 Different spindle designs adopted for suspension use.

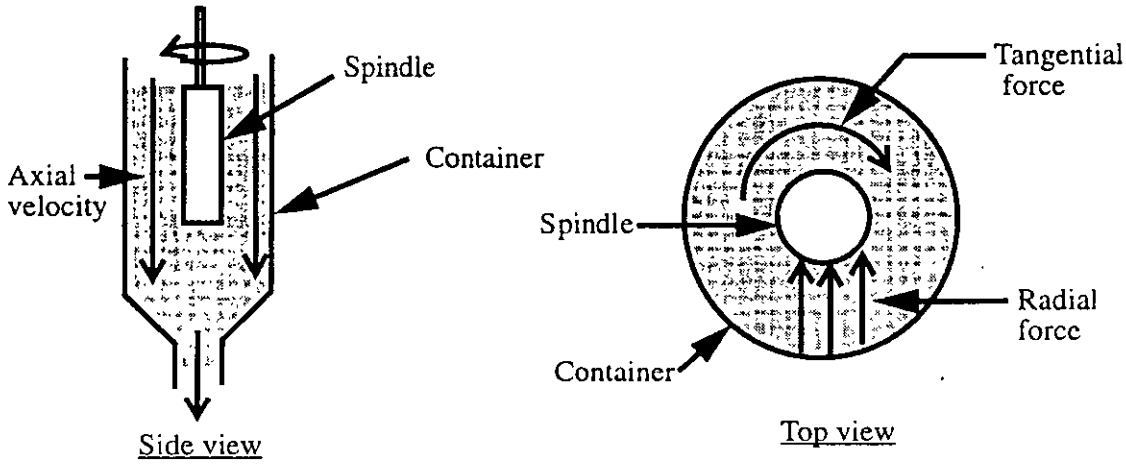

FIGURE 4 The axial flow (side view) prevents the solids from settling by continuously sweeping fresh slurry past the spindle. This component of the flowing slurry stream does not affect the rotation of the spindle. But any radial or tangential forces (Top view), arising from the flow, may put additional strain on the spindle resulting in erroneous viscosity readings. Unbalanced radial flows push the spindle to one side so that it does not spin uniformly and results in erratic readings. Tangential flows increase or decrease the torque on the spindle, making the fluid appear to be either more or less viscous then it really is.

rotation. For example, when the sample is taken in a beaker, solids start settling and slurry at the top of the beaker becomes dilute compared to the slurry at the bottom. Therefore, the spindle is no longer in contact with a representative sample. In this situation, the viscometer will read low viscosity if the compacted solids are below the spindle as shown in Figure 5(a) and a high viscosity if the compacted solids are touching the spindle as shown in Figure 5(b). Furthermore, when the rotational speed of the cylinder is increased to take measurements at high shear, the solids centrifuge outward towards the outer wall resulting in a poor measurement. These problems have been addressed by many past designs, and are discussed in the following section.

Solids plugging and the effect of annular gap For suspensions, the annular gap (the gap between the spindle and the sample holder) is usually large to avoid solids plugging. As a rule of thumb, this gap should be at least 10 times the largest particle size in the suspension[14]. Quite often liquids of known viscosity (Newtonian fluids like silicon oil or sucrose solution) are used to calibrate the torque scales which are then applied to calculate viscosity of non-Newtonian fluids. This is acceptable only when the annular gap is small (< 1% of the cylinder radius), and may not be correct when the gap is large. Therefore, for non-Newtonian suspensions, depending upon the flow model, proper equations (such as Equation 4) should be used to calculate the correct viscosity. Otherwise, the measurements will result in erroneous rheological characterization of the suspension.

Slurry Presentation Systems for Rotational Viscometers

Solids settling has been the major concern for most of the researchers who have used rotational viscometers for suspension viscometry. This has resulted in various designs of

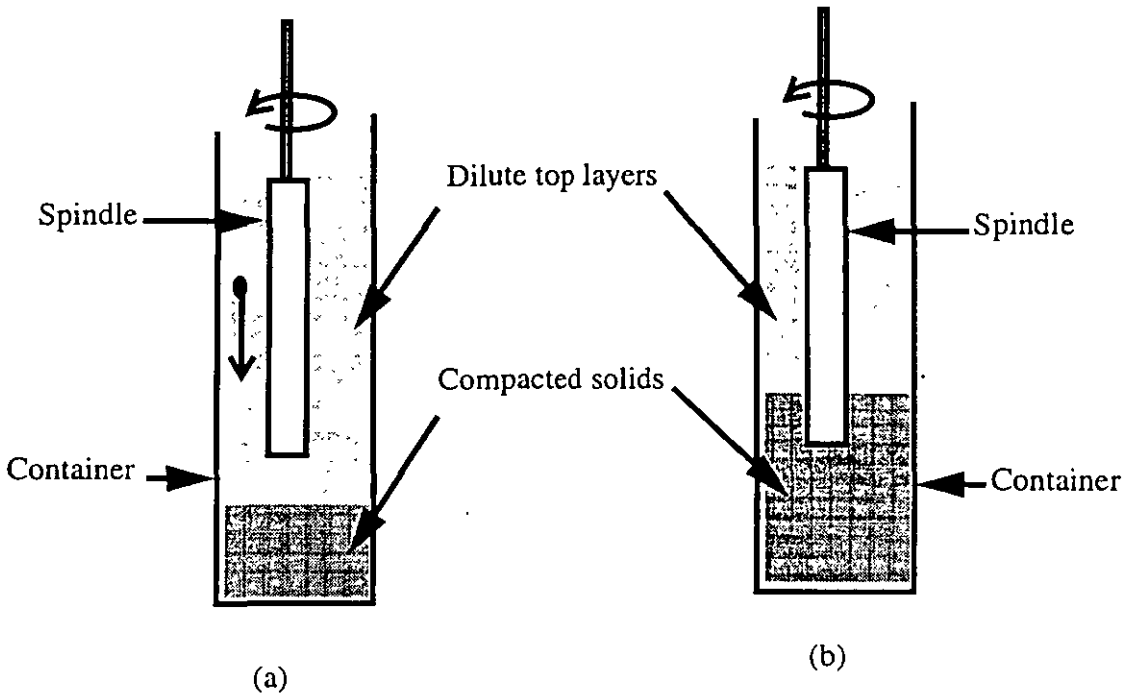

FIGURE 5 Solids settling leaves a dilute suspension on the top layers of the container. When the solids content is low (a) the solids gradually settle and are compacted below the spindle and the viscometer reads progressively lower viscosity as the solids settle. At higher concentration of solids, the compacted solids can touch the spindle (b) resulting in higher readings.

sample presentation systems to prevent solids settling during viscosity measurement. Some of these designs are discussed in this section.

Presentation systems in stirred tanks If proper precautions are taken, slurry viscosity can be measured by placing a rotational viscometer inside a stirred tank. One such arrangement has been reported by Clarke[16]. A line diagram of this measuring system is provided in Figure 6. He used a co-axial cylinder viscometer (Ferranti, Model VL), which could be operated between shear rates of 43 to 950 sec^{-1} with interchangeable spindles. The sample holder consisted of a 450 ml vessel with an eight bladed impeller at the bottom to keep the solids in dispersion. The impeller operated at 400 revolutions per minute. In order to prevent rotation of the sample inside the vessel, vertical baffles were fitted above the impeller. The whole arrangement was intended to encourage top to bottom flow of the solids so that the viscosity could be measured without obstructing the flow. Clarke tested suspensions of quartz, glass, and polymethacrylate in water with particle sizes up to 211 microns and concentrations up to 50% solids by volume. He measured apparent viscosity up to a shear rate of 350 sec^{-1}.

Clarke reported centrifuging of coarse particles (above 150 μm) because of the high speed of the impeller required to keep the solids in suspension. This offset the homogeneity of the suspension for many samples. In order to avoid centrifuging of solids, he took instantaneous measurements before the solids started outward movement. Clarke reported dilatancy of quartz suspensions at very low percent solids (10% by volume) which may have resulted from trapping of particles in the grooves which were made on the spindle surface to prevent slippage of the sample.

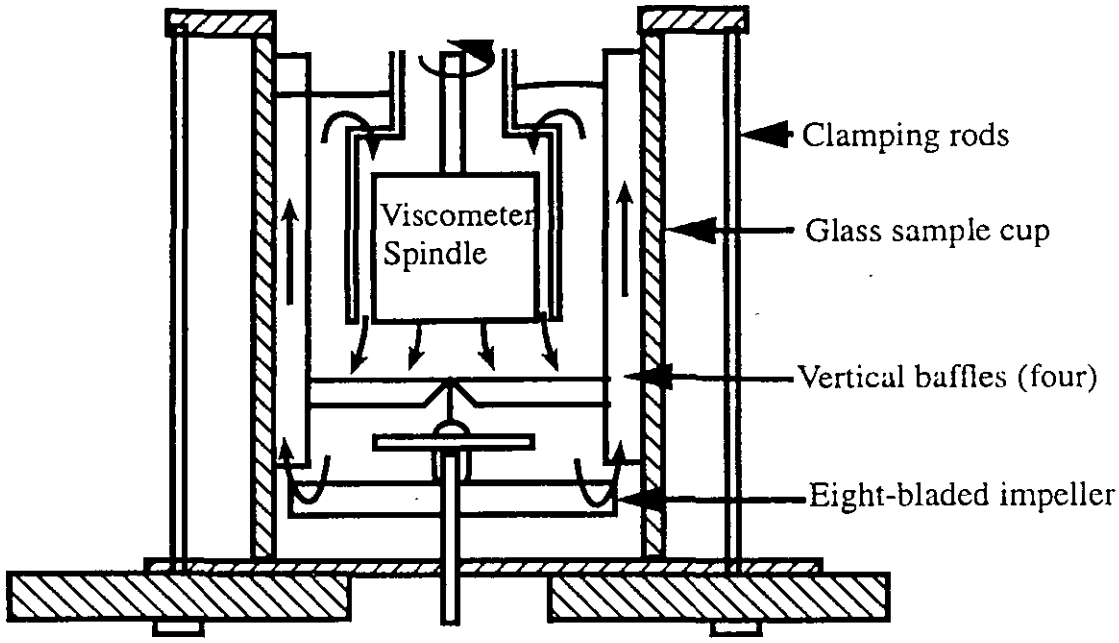

FIGURE 6 Sectional view of sample cup and measuring cylinders showing flow pattern (from Clarke 1967).

Similar designs were later reported by Lapasin[17] and Underwood[18] (Figure 7). In the Underwood design, a modified T-bar spindle (standard Brookfield spindles) was used. The modified spindle had twelve cylindrical bars extending from a vertical shaft. The spindle was connected to a Brookfield model RVT viscometer. The sample was placed in a beaker which had an annular sleeve. A honeycomb of small diameter vertical cylinders was placed at the bottom. Below this honeycomb arrangement, a Teflon coated magnetic stir bar was placed. When the stir bar rotated, slurry ascended through the annular space, entered the beaker, flowed down past the spindle, and then drained through the honeycomb. The swirls and eddies created by the stirrer were prevented from reaching the spindle by this honeycomb arrangement.

Presentation systems in tanks with top to bottom flow Hemmings and Boyes[19] used a Brabender-Messtechnik Convimeter viscometer to measure apparent viscosity on the discharge line of a ball mill. The convimeter was mounted inside a column (Figure 8) and rotated in a gyratory motion at 120 revolutions per minute. Slurry from the ball mill flowed through this column. The level of slurry within the column was controlled by sensing the hydrostatic pressure and automatically controlling the slurry flow through the valve (by expanding or contracting an elastomeric flow restrictor). The operating range of the instrument was governed by the flowability of the slurry. This viscometer arrangement will not work for high solids concentrations when the slurry does not flow under gravity. Also, since the sensor moved in a gyratory motion, it did not have a well-defined shear rate. Therefore, at high percent solids when the slurry behaves in a non-Newtonian manner, the viscosity measured by the viscometer may not be the same as the viscosity experienced inside the mill.

Reeves[13,20] reported a rotational type viscometer for on-line use with slurries. He installed a specially designed spindle in a sample preparation and presentation system as

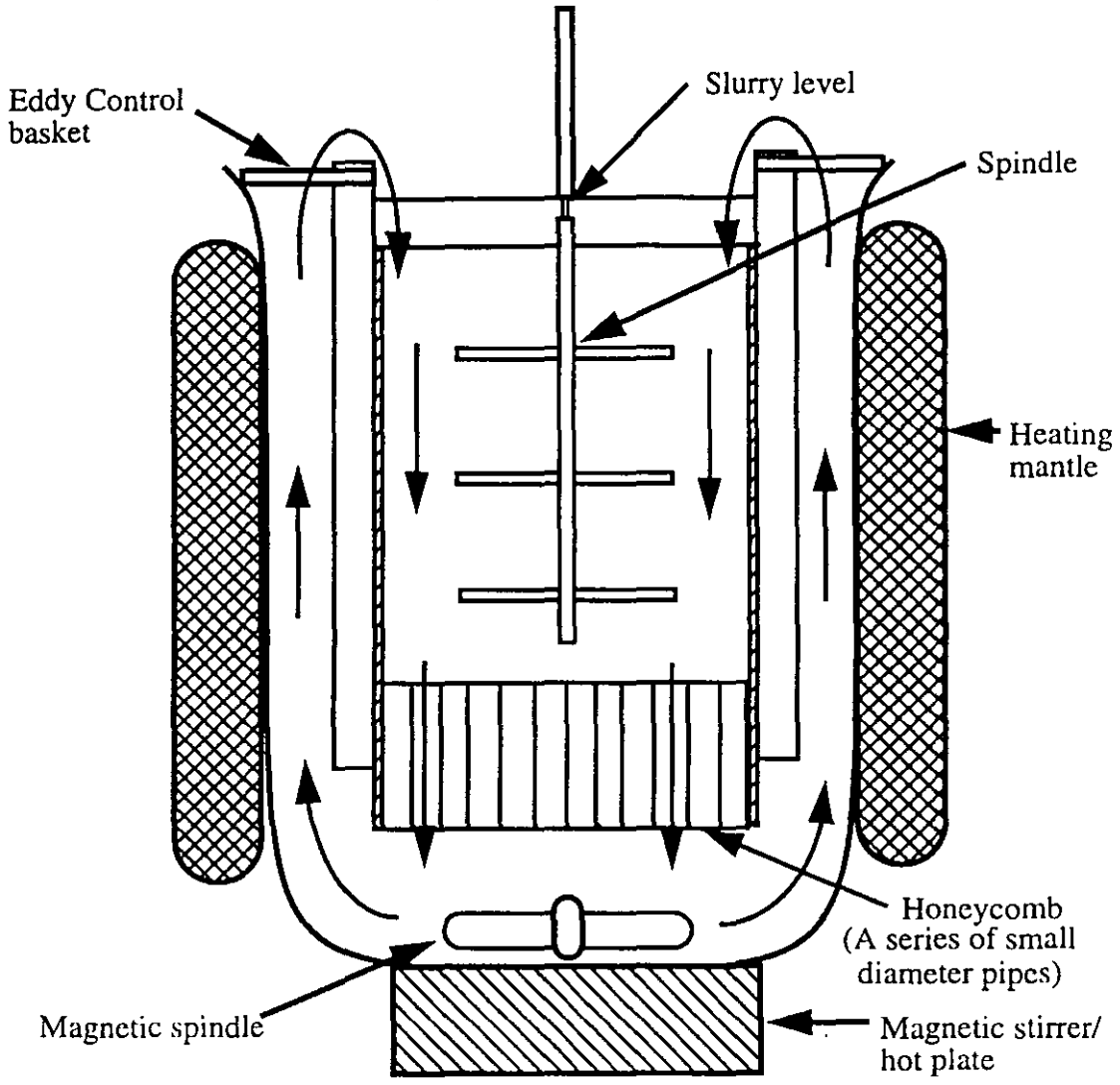

FIGURE 7 Viscometric assembly showing the spindle and eddy current basket (from Underwood 1976).

shown in Figure 9. The feed sample from the plant passed over a stationary screen (10–12 mm opening) to remove large particles and tramp materials. The instrument was capable of measuring viscosity within a shear rate range of 0 to 200 sec^{-1}, with the shear rate adjusted by changing the rotational speed of the bobbin. The viscometer operated at a constant shear rate by choosing a single rotational speed for the spindle. Reeves made on-line rheological measurements of ferro-silicon suspensions with 14–16% solid concentrations. In this design, baffles were installed in the measuring chamber to eliminate rotation of the sample in the container. Still he reported fluctuations in viscometer reading for fluids below 10 centipoise.

The Hemmings and Boyes design and the Reeves design were the only two rotational viscometer systems tried on-line for mineral slurries. These viscometers depend upon the flowability of the slurry[19], i.e. as long as the slurry flows under gravity through the sample presentation system, the associated viscometers can measure the viscosity. This may not be the case in many concentrated suspensions, where yield stresses are seen,

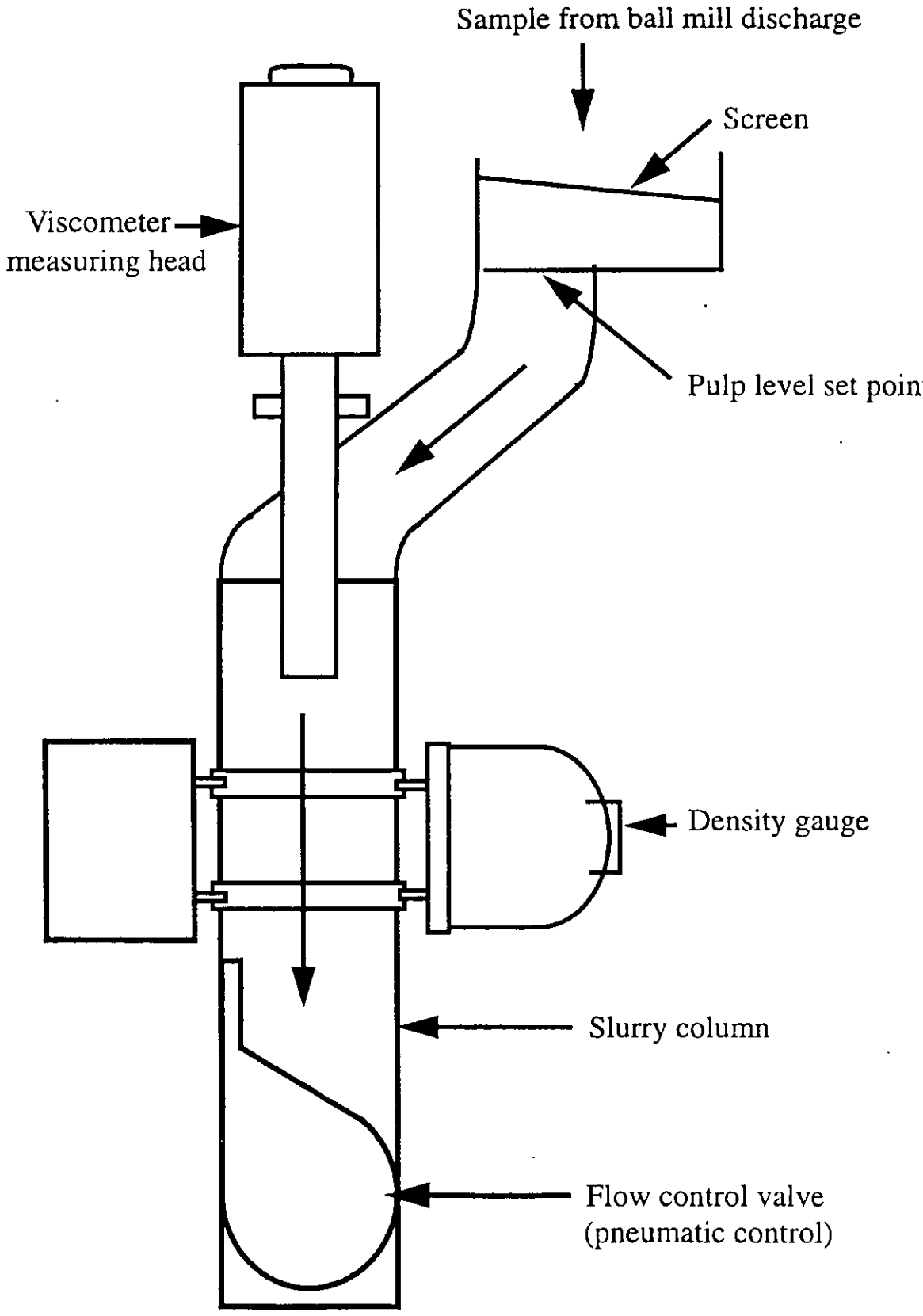

FIGURE 8 Viscosity sensing system designed by Hemmings and Boyes (from Hemmings and Boyes 1977).

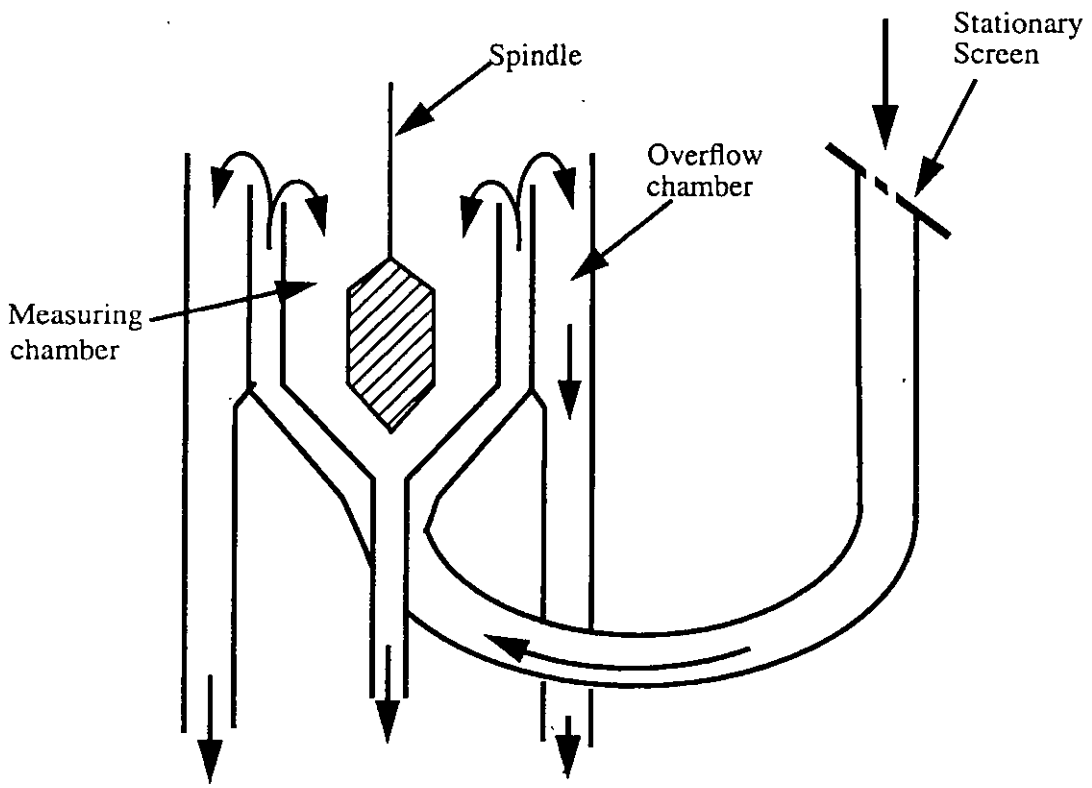

FIGURE 9 Viscometer arrangement developed by Reeves, 1984. The spindle, is made conical at the top and bottom surfaces to avoid solids deposition on top of it. (from Reeves 1984)

e.g., in grinding mills and concentrated coal slurries[4]. These slurries will be too viscous to flow properly through the gravity flow sample presentation systems.

Unless precautions are taken, the annular space in rotational viscometers can be plugged by coarse particles or tramp materials. In both the systems described above, it has been suggested that this problem be solved by pre-screening the sample before it entered the measurement chamber.

In general, the use of rotational viscometers in gravity fed sample presentation systems are questionable because the viscometer measures the drag from the fluid, and any tangential or radial forces on the spindle will affect this measurement (Figure 4). Most rotational viscometers are very sensitive to these forces, and the problem becomes severe when the instruments are used on-line. The use of baffles is aimed at reducing these effects. While evaluating the use of an eddy control basket[18] for measuring viscosity with a Brookfield viscometer, we realized that completely avoiding tangential or radial forces from fluid flow is a very difficult task. This is especially true for low viscosity fluids (such as water). Because of these concerns, Klien *et al.*[11] designed a different technique for measuring the rheology of unstable mineral suspensions which took advantage of the zone settling properties of some suspensions. They assumed that after the sample is placed in a container, solids settle and a constant density zone is created in the container. Then they constructed a double gap bob and cup arrangement. This bob and cup fixture was attached to a Haake Rotovisco RV 20 viscometer. They tried to place the bob in the constant density zone for shear stress and shear rate measurement (Figure 10). They measured rheograms of magnetite suspensions at solid

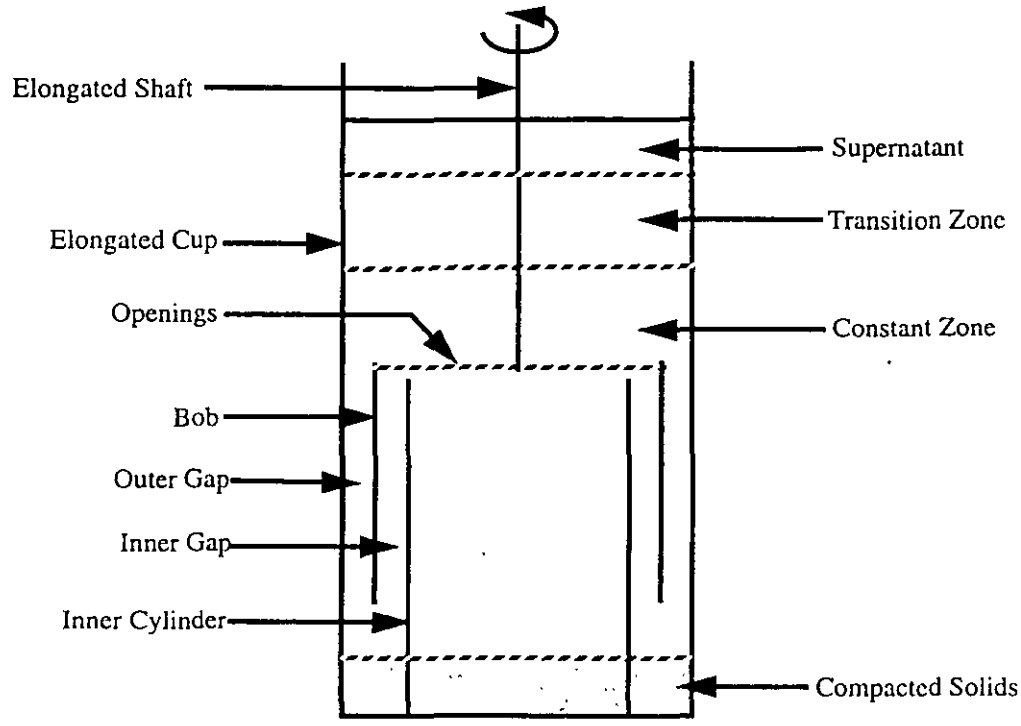

FIGURE 10 Line diagram of the double gap cup and bob arrangement for measuring the zone settling properties of suspensions (from Klien *et al.*, 1990).

concentrations of 11 to 25% by volume. In this way the undefined forces (tangential and radial) that could be generated by mixing arrangements were eliminated. However, since the coarse and fast settling particles were allowed to settle at the bottom of the container, the solids contents in the constant density zone must be different from the initial sample. Thus this arrangement cannot maintain a representative sample. Since solids concentration greatly influences the slurry rheology, this arrangement cannot be accepted for rheological measurements of suspensions.

The influence of undetermined forces generated by slurry flow (across the viscometer) is further reported by Kiljanski[12]. He too used a double gap coaxial fixture attached to the driving and measuring unit of a commercial rheometer (Figure 11). The viscometer operated at shear rates between 0.26 sec^{-1} and 870 sec^{-1}. The sample was pumped through the viscometer by a centrifugal pump, making a top to bottom flow (axial flow) of the fluid sample inside the viscometer. He used two samples of magnetite dense media, one at 34.5 vol% collected from the bottom of a drum separator which was contaminated with processed coal and the other was a 12.5 vol% suspension made out of pure magnetite dense medium. In his experiments, Kiljanski measured shear stress and viscosity at different shear rates at two different conditions, (i) while the sample was flowing through the instrument and (ii) after the flow was stopped. He noticed clear difference in readings between measurements made with circulation (when the suspension was flowing) and without circulation (when the flow was stopped). He argued that these differences in readings were (i) because of the additional shear rates imposed due to axial flow of sample, and (ii) because of an additional torque developed due to the inertia of the fresh, non-rotating fluid entering the viscometer, to which the rotation has to be imparted by the spindle (resulting in a higher shear stress). Kiljanski

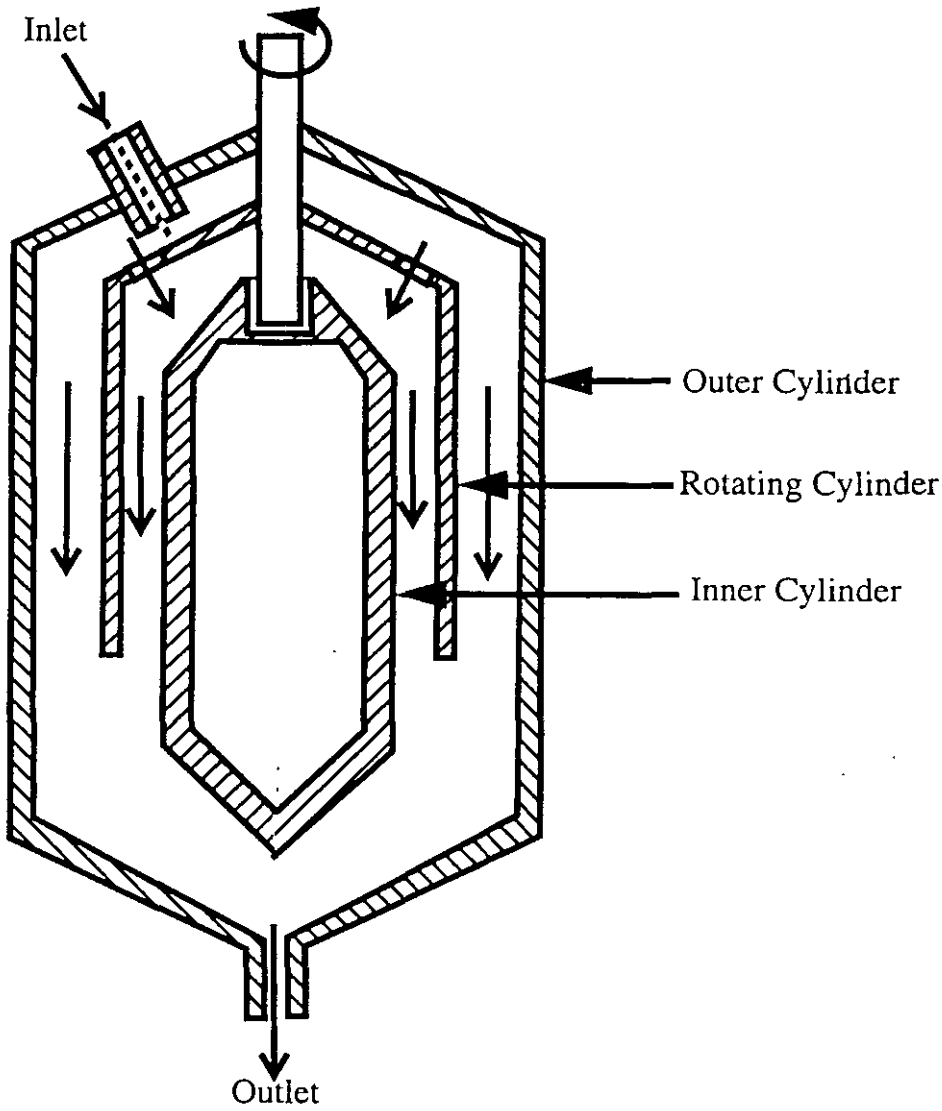

FIGURE 11 Simplified diagram of double gap rotational viscometer designed by Kiljansski, 1993. Both the outer and inner cylinders were held stationary. The diameters of the gaps outside and inside of the rotating cylinder (spindle) were designed such that the shear rates on both outer and inner surfaces were constant (from Kiljanski 1993).

also noticed differences in viscosity readings when the annular gap was increased. He argued that for smaller gap the axial shear rate originating from axial flow (top to bottom flow of the fluid) of fluid is higher than the axial shear rate for a wider gap, therefore viscosity measured at similar shear rates (calculated from the rotational speed of the spindle) were different. This shows how the undetermined forces from the sample circulation in the viscometer can generate misleading results.

Summary Solids settling has been the primary focus area for researchers working on rotational viscometers. Continuous agitation or top to bottom flow seems to be the answer to this problem. However, rotational viscometers are very sensitive and both these methods for keeping the solids in suspension create undue forces which seriously affects the viscometer readings.

Control of shear rate is the strongest point of rotational viscometers. This helps in measuring the rheology of non-Newtonian fluids, specially at low and medium shear rates. However, at higher shear rates (above 300 sec^{-1}) rotational viscometers are not suitable for suspensions because high rotational speed of the spindle produces a centrifugal force that segregates the solids.

The annular gap between the cylinders must be at least 10 times larger than the largest particle in the suspension to avoid solids plugging. The sample must also be screened to remove any oversize and tramp material. Other problems which must be considered for rotational viscometers are wall slip and end effects.

CAPILLARY VISCOMETER

Operating Principle

In a capillary viscometer the fluid is passed through a tube under pressure. By measuring the flow rate and pressure drop across the tube shear stress and shear rate can be calculated. Although capillary viscometers are normally designed for Newtonian fluids, they are also extensively used for non-Newtonian fluids. These viscometers provide a simple and inexpensive method for rheological measurement, and when suitable for an application, capillary viscometers are more precise than rotational viscometers[15]. Specifically, these viscometers operate better at higher shear rates[22] which are common in many processing and manufacturing units.

For a fluid flowing through a tube (Figure 12) the shear stress at the wall can be calculated from the pressure difference across the tube by using the following formula:

$$\tau = R(P_1 - P_2)/(2L) \tag{7}$$

Where, τ = shear stress at the wall
P_1 = Pressure at the entry of the tube
P_2 = Pressure at the exit of the tube
L = Length of the tube
R = radius of the tube.

Shear rate at the wall for Newtonian fluids can be calculated by measuring the flow rate, Q through the tube by applying the following formula:

$$\dot{\gamma} = 32Q/\pi R^3 \tag{8}$$

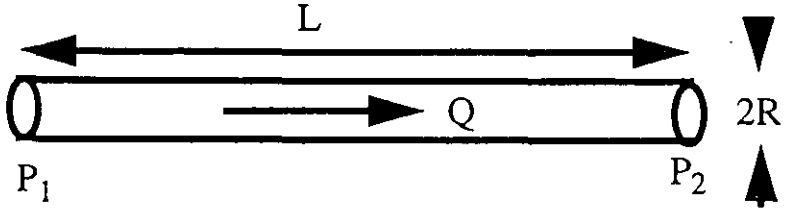

FIGURE 12 Line diagram of a capillary tube.

Where, $\dot{\gamma}$ = shear rate at the wall
Q = flow rate

Thus by using the measured pressure difference across the tube and the flow rate through the tube, shear stress, shear rate, and viscosity can be calculated. Equation 8 is derived from the Newtonian flow model. Therefore, for such fluids Equation 8 gives the true shear rate of the fluid. For non-Newtonian fluids the shear rate obtained from Equation 8 is called the apparent shear rate. True shear rate of non-Newtonian fluids can be obtained from $32Q/\pi R^3$(Equation 8) by the following formula which is derived by Metzner and Reed[23] after modifying the Rabinowitsch[24] equation:

$$\dot{\gamma} = (3n' + 1/4n'). (32Q/\pi R^3) \quad (9)$$

Where, $\dot{\gamma}$ = shear rate at the wall
n' = flow index given by the following formula

$$n' = \frac{d\log (\Delta P/4L)}{d\log (4Q/\pi R^3)} \quad (10)$$

Where, n' = flow index
ΔP = pressure difference across the tube = $P_1 - P_2$

n' can be determined graphically by plotting $\Delta P/4L$ vs. $32Q/\pi R^3$ on a log-log scale and measuring the slope of the resulting line. Equations 9 and 10 are valid for fluids with or without yield stress[23].

Necessary Conditions for Capillary Viscometers

The necessary conditions[25] (Bird *et al.*, 1960), which must be satisfied in a capillary viscometer measurements are:

a) Laminar flow (Reynolds number < 2100)
b) Constant fluid density
e) Steady flow
d) End effects are negligible
e) No slip between the wall and the fluid
f) The fluid must be incompressible.

Common Capillary Viscometer Types

Common capillary viscometers are either constant flow type or constant pressure type viscometers. Piston viscometers are examples of the constant flow type. In these viscometers, fluid is pushed through the tube by a piston moving at a constant speed. Thus the flow rate through the tube remains constant. By measuring the pressure difference across the tube, viscometric functions can be calculated. In constant pressure

capillary viscometers a constant pressure is applied at the entry of the tube and the flow rate is measured by collecting the fluid flowing through the tube[15].

Discussion of the Capillary Viscometers

Capillary viscometers have several advantages as listed below.

- Since the flow is continuous and the sample stays inside the tube for a very short time, solid settling inside the viscometer is not a problem. However, the suspension should be kept well mixed before it enters the tube. This is usually done in an agitated system immediately before the sample enters the tube[28,29].
- Capillary viscometers are suitable for making measurements at high shear rates, where industrial operations such as pumping and spraying are carried out.
- They are simple to construct, and if they can be suitably used with a given fluid, can generate more accurate data than a rotational viscometer.

Many of the problems encountered in rotational viscometer are also common in capillary viscometers. Some of the examples are listed below.

- Similar to rotational viscometers, the diameter of the capillary viscometer should be at least 10 times larger than the top particle size of the suspended particles. Therefore, the sample must be screened to remove unusually coarse material before it is allowed to pass through the tube.
- Slippage at the wall is still a problem with capillary viscometers. This is mainly because of particle migration away from the wall[15,21]. As a result, a more dilute fluid is left in contact with the wall. The presence of wall slip can be detected by comparing flow curves of the same sample generated by tubes of different diameters[27]. This problem is minimized by selecting tubes with larger diameters with respect to the top particle size in the suspension, or by using any of several suggested correction factors[15,37].
- End effects are noticed in capillary tube viscometers, because of pinching of the slurry stream at the entry and exit of the tube[21]. Therefore, flow profiles at the ends are different than in the rest of the tube. This problem is eliminated by using tubes with high length to diameter ratio (above 300).
- Tubes must be calibrated at suitable intervals to compensate for any diameter changes resulting from abrasion or scaling.

Despite these problems, capillary viscometers are widely used by many investigators[15,21,23,27,28].

Selected Designs

Examples of the use of capillary viscometers for suspensions are abundant in the literature. Antonini *et al.*[28] measured rheological properties of a coal water slurry with 70 wt% solids content by using different dimension tubes. Their apparatus consisted of a 10 liter reservoir equipped with interchangeable tubes of different lengths and diameters.

The slurry was agitated by a pneumatic stirrer. For each pressure applied, they measured the flow rates by continuously weighing the slurry flowing through the tubes. Then from pressure gradient and flowrate, they generated flow curves for the coal slurry samples.

Turian *et al.*[29] reported a new design of capillary viscometer for measuring shear stress, shear rate, and yield stress of suspensions. The main body of the instrument consisted of a stainless steel container to hold the sample. The solids were kept in suspension by stirring the sample in the container. They used different dimension stainless steel tubes (with diameters from 2.4 to 8.8 mm) which could be connected to the bottom of the container. The sample flowing through the capillary tube was collected by a bucket placed on top of a electronic balance. The whole system was covered by a water jacket to maintain a constant temperature. Flow rate through the tube was determined by the balance whose signal was recorded by a computer. Shear stress (τ) and shear rate $\dot{\gamma}$ were calculated from pressure drop ΔP and flow rate Q.

Turian *et al.* determined yield stress by extrapolating the shear stress-shear rate curve to a shear rate of zero. They used pulverized Pittsburgh Seam (No. 8) coal to make the measurements over a shear rate range of 1 to 10^4 sec^{-1}. They also determined the yield stress of the slurry by the vane method[30] to verify the result obtained from the capillary tube, and reported that the yield stresses obtained by both the methods were similar.

Another way of measuring viscosity of a slurry is to drain a measured volume of slurry from an overhead container through a capillary tube and to measure the time taken for the material to drain completely. The slurry is kept in suspension in the tank by constant stirring. This method was first tried by DeVaney and Shelton[10], later it was reported by other authors[7,26]. The model used by Schack *et al.*[26] is shown in Figure 13. The authors measured the viscosity by measuring the time required for 100 ml. of

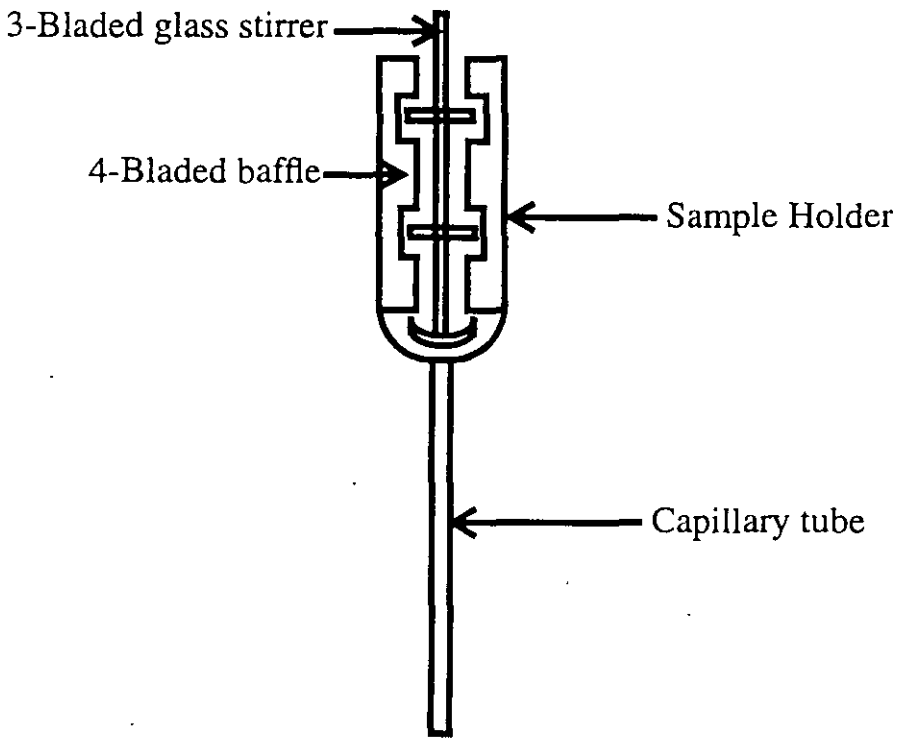

FIGURE 13 Diagram of consistometer chamber and capillary discharge tube used by Shack *et al.*, (from Schack *et al.*, 1957).

suspension to flow through the discharge tube. The major drawback of this instrument is that it does not determine whether the suspension is Newtonian or non-Newtonian. Also, it makes measurements at low shear rates, making it impossible to extrapolate to high shear rates (for hydrocyclone or pumping)[7].

Capillary viscometers are also used in plants to measure effective viscosity of fluids. This can be accomplished by measuring the pressure drop across a straight stretch of pipe. Shear stress and shear rate at the pipe wall can be calculated from pressure difference, flow rate and pipe dimensions. Apparent viscosity can be determined from the ratio of shear stress and shear rate at the wall. In this measurement, the fluid flow in the pipe must be laminar. In order for this method to work with suspensions, the suspension must be very stable (a high yield value), otherwise under laminar conditions a slow sedimentation process will take place at the bottom of the pipe[31].

Summary Compared to rotational viscometers, avoiding solids settling is relatively simpler in capillary viscometers, because the residence time of the sample inside the tube is very small. Measurements of non-Newtonian fluids can be made by changing different dimension tubes or by changing flow rates, which may not be an easy task in plants. For such measurements proper correction factors such as that suggested by Rabinowitsch[23,24] should be considered to obtain true viscosity of non-Newtonian fluids. As with rotational viscometers, wall slip and end effects must be considered while using capillary viscometers. Also, the sample must be pre-screened before allowing it to flow through the tube.

VIBRATING VISCOMETERS

Working Principle

Unlike rotational and capillary viscometers which are volume loading instruments, vibrating or oscillating viscometers are surface loading instruments, because they react only to a thin layer of fluid adjacent to the probe. The probe or sensor of the viscometer can be spherical (Figure 14), rod or plate shaped, or like a fork which vibrates in the fluid. The sinusoidal shear wave from the immersed probe is damped by the fluid, and

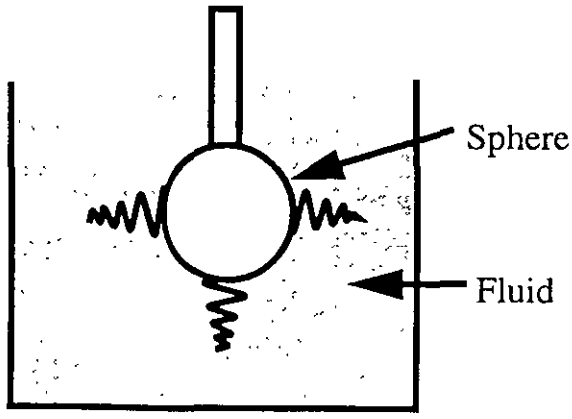

FIGURE 14 Vibrating sphere viscometer. The probe oscillates in the fluid, and the power required to maintain a constant amplitude of oscillation is the measure of viscosity.

the damping is a function of the product of the viscosity and the density of the fluid. Usually the probe is oscillated at a constant amplitude and the force or power required to maintain this amplitude is measured. Rachman[33] derived the following formula for a vibrating rod viscometer to determine viscosity.

$$\eta = R_0^2/A^2\omega_0\rho[F_0x_{00}\omega_{00}/F_{00}x_0\omega_{00})-1]^2 \quad (11)$$

where, η = viscosity of the liquid
ρ = density of the fluid
ω_0 = resonant frequency
ω_{00} = free resonant frequency
x_0 = amplitude at resonance
x_{00} = amplitude in vacuum
F_0 = force at resonance
$F_{(x)}$ = force required to maintain x_{00}
A = area of the surface in contact with the fluid
R_0 = transducer loss in the vacuum.

Thus by measuring the force F_0 which is required to maintain a constant amplitude x_0, and knowing the density ρ of the fluid one can measure the viscosity η. The remainder of the terms in Equation 13 will be constants for a particular instrument.

Discussion of the Vibrating Viscometers

Some of the advantages of vibrating viscometers over rotational and capillary viscometers are:

- Since the gap of fluid between the sensor and the container wall does not affect the reading, suspensions with coarse particles can be tested without the danger of plugging.
- Unlike rotational viscometers, oscillating viscometers are not affected by minor turbulences associated with slurry flow. Therefore, forces associated with slurry flow (see Figure 4) will not affect its readings.

The major disadvantage of this type of instrument is that the operator does not have any control over the shear rate. It is also difficult to measure the true viscosity of non-Newtonian fluid whose viscosity changes with shear rate. The shear rate $\dot{\gamma}$ will be a sinusoidal function of time. For a spherical probe, its peak value will be maximum at the equator and will be smaller by a factor cos ϕ at a sphere latitude of ϕ. Perry[34] derived the following equation for determining the maximum shear rate for the vibrating sphere viscometers:

$$\dot{\gamma} = k(\rho/\eta)^{1/2} \quad (12)$$

where, $\dot{\gamma}$ = maximum shear are
k = an instrument constant

From this equation we see that the maximum shear rate decreases as viscosity of the fluid increases. For a Newtonian fluid viscosity η is a constant, so maximum shear rate will remain constant. However, for viscoelastic fluids, the viscosity varies with shear rate, and computation of shear rate becomes complicated. Some investigators have suggested measuring the amplitude of vibration[33] and oscillating frequency as a means of measuring the apparent viscosity of viscoelastic fluids (non-Newtonian fluids)[35]. However, the reasoning provided for such measurements apply only to limited polymeric fluids, and the method does not work for suspensions[33,34].

Vibrating viscometers are sensitive to vibrations from supporting structures32,35. Unless precautions are taken to dampen these vibrations the instrument will pick up erroneous signals.

Selected Designs of Vibrating Viscometers

Vibrating rod viscometer for viscosity measurement Rachman[34] reported an assessment of vibrating viscometers in slurries. He utilized a vibrating plate transducer and a flexurally vibrating rod transducer in his research. However, for the suspension studies (with quartz slurries) only the flexurally vibrating rod transducer was used. In his initial experiment with 0.065 volume fraction solids in the slurry, Rachman experienced difficulty in measuring the viscosity because the solids settled quickly. In subsequent tests, the slurry was stirred vigorously by a motor driven pump to keep the solids in suspension. Then the stirrer was stopped and after 15 seconds, measurements were taken with the viscometer. In this way the investigator assumed that the slurry would have been in a similar state when each reading was taken. Similar measurements were taken with quartz-water slurries at 0.24 and 0.36 volume fraction solids. By changing the amplitude of vibration and transducer loading they showed that the denser slurries showed non-Newtonian flow whereas the dilute slurry with 0.065 volume fraction solids had Newtonian flow. However because of uncertain results, Rachman suggested use of this method only if no other simpler viscometer is obtained for measuring non-Newtonian slurry rheology.

Vibrating sphere viscometer for viscosity measurement Kawatra *et al.*[32] used a vibrating sphere viscometer manufactured by Nametre Co. along with a gravity flow sample presentation vessel as shown in Figure 15. Because of the basic design of the spherical oscillating probe (which oscillates at a high frequency and low amplitude rather than rotate in a single direction) and its durable construction, the flow of the slurry did not influence its reading. The solids settling problem was also eliminated because of the gravity flow arrangement of the slurry around the probe. Using this system Kawatra *et al.* were able to continuously measure viscosity of silica slurry at varying concentrations and temperatures in the feed line of a hydrocyclone.

However, the major difficulty in this type of instrument is that the operator has no control over the shear rate. The shear rate is a function of viscosity, higher in low viscosity fluids and lower in high viscosity fluids. Since most of the suspensions at higher solids contents show non-Newtonian flow their viscosity is highly dependent on shear rate. Thus for such suspensions, no logical conclusion can be drawn from viscosity measurements by these instruments unless they operate at the same shear rate as the process itself. Another problem with this type of instrument is that if the fluid velocity is very low, solids tend to settle in small layers over the top of the sphere (Figure 16)

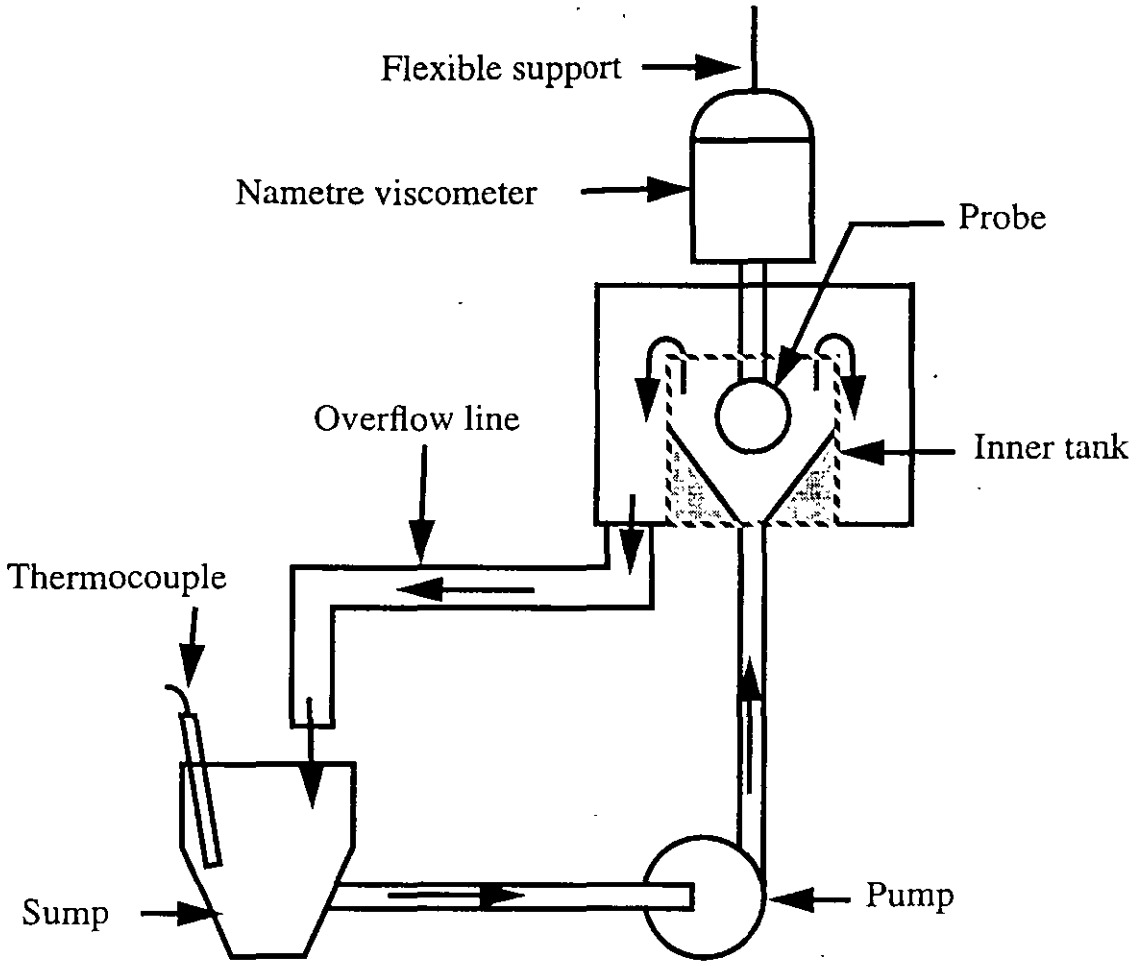

FIGURE 15 Nametre viscometer set-up. Sample is circulated through the system by a pump to keep the solids in suspension.

resulting in higher readings. These instruments are also affected by vibration from their surroundings, and special design is required to isolate from vibration. However, due to their ability to work in hostile plant environment, so far they are the most suitable instrument for making on-line viscosity measurements of Newtonian mineral slurries. The slurry used by Kawatra *et al.*[32] was Newtonian and therefore, good correlation could be established between the viscosity measured by this instrument and the hydrocyclone performance.

Vibrating sphere viscometer for distinguishing Newtonian and non-Newtonian suspensions Recently Kawatra and Bakshi[36] reported a system for classifying Newtonian and non-Newtonian suspensions in slurry streams. They used a vibrating sphere viscometer to measure apparent viscosity of slurries at high shear rates and a rotational viscometer to measure apparent viscosity of the same slurry at low shear rates. Since the shear rates were widely different, comparison of the apparent viscosities from the vibrating viscometer and the rotational viscometer allowed classification of the suspensions as either Newtonian or non-Newtonian flow types.

Summary The main advantages of vibrating viscometers over rotational and capillary

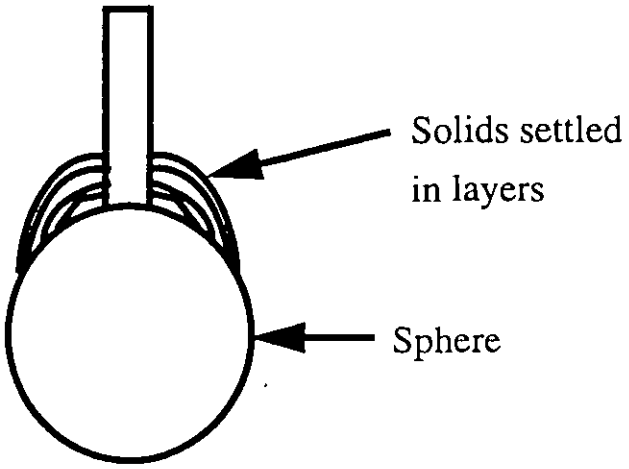

FIGURE 16 Vibrating sphere viscometer showing layers of solids settling on top of the sphere when the fluid velocity passing the spherical probe is small.

viscometers are, (i) these are less sensitive to plant disturbances, (ii) plugging is less of a problem, because these are surface loading instruments and the gap between the sensor and the container wall can be kept as large as required.

Vibrating viscometers still require some sort of agitation system to avoid solids settling. Since these viscometers are highly sensitive to vibrations from surrounding structures, steps must be taken to damp these vibrations. The main disadvantage of these instruments is their poorly defined shear rates which makes them highly unsuitable for measuring true viscosity of non-Newtonian suspensions.

CONCLUSIONS

Rotational and capillary viscometers are the most common viscometers which have been tried for measuring suspension rheology. Rotational viscometers have better control over shear rate which is essential for measuring the full rheology of non-Newtonian fluids. However, these instruments are very sensitive to disturbances in slurry flow. Because of this, many of the special designs studied in this report had baffle arrangements to inhibit unwanted forces like swirling and turbulence in the region of the measuring device. In capillary rheometers this problem is felt to a lesser extent because of the shorter residence time of the suspension inside the tube. However, the sample must be thoroughly mixed prior to its entry into the tube. Plugging is more of a problem in capillary tubes than in rotational viscometers. Slip at the walls is another problem felt by both the capillary and the rotational viscometers. In vibrating viscometers both plugging and wall slip can be eliminated easily, because vibrating viscometers are surface loading and the gap between the sensor and the container wall does not affect the measurement. Also, the vibrating viscometer can tolerate slight disturbance from slurry flow and is rugged enough for on-line use in suspensions. The main disadvantage of a vibrating viscometer is its inability to operate in a steady shear, which makes it unsuitable for non-Newtonian fluids. Otherwise, for Newtonian suspensions and for operations where a relative viscosity is needed vibrating viscometers are best suited for on-line use.

Although in the past many authors have claimed success in measuring on-line

rheology of suspensions, their claims have been refuted later by other authors, because the instruments were not capable of repeating their performance. This shows that the particulate processing industry still needs a reliable viscometer which can work on-line under plant conditions.

References

1. R. Lu and V. M. Puri, *J. Rheol.*, **36**(2), 303 (1992).
2. M. K. Agarwala, B. R. Patterson and P. E. Clark, *J. Rheol.*, **36**(2), 319 (1992).
3. D. W. Fuerstenau, K. S. Venkataramana, B. V. Velamakanni, *Inter. J. of Miner. Process.*, **15**, 251 (1984).
4. R. R. Klimpel, Part I, *Mining Engineering*, **34**(12), 1665 (1982), Part II, *Mining Engineering*, **35**(1), 21 (1983).
5. P. Tucker, *Trans. of Instn. Min. Metall.*, Section C, Mineral Processing and Extractive Metallurgy, **91**, C117 (1982).
6. S. K. Kawatra, T. C. Eisele, Proceedings of the Sixteenth International Mineral Processing, Congress, Elsevier Science Publishers B. V., *Amsterdam*, 1988, pp. 195–207.
7. F. F. Aplan and H. R. Spedden, Seventh International Mineral Congress, New York (Ed.) N. Arbiter, Gordon and Breach, New York, 1965, pp. 103–113.
8. R. B. Klose, Proceedings of the Sixth International Symposium on Coal Combustion and Technology, June 25–27, Orlando, Florida, 1984, pp. 791–805.
9. S. C. Tsai and E. W. Knell, FUEL, **65**, 566 (1986).
10. F. D. DeVaney, S. M. Shelton, Rep. Invest. U. S. Bur. *Mines*, **3469R.**, 24 (1940).
11. B. Klien, S. J. Partrigdge, J. S. Laskowski, *Coal Preparation*, **8**, 123 (1990).
12. T. Kiljanski, *Coal Preparation*, **13**, 107 (1993).
13. T. J. Reeves, *Coal Preparation*, **8**, 135 (1990).
14. J. Orban and P. Pacevaux, *Oil and Gas Journal*, **84**(26), 94 (1986).
15. R. W. Whorlow, Rheological Techniques, Chapter 2 and 3, Halsted Press, New York, 1980, pp. 57–191.
16. B. Clarke, *Trans. Inst. Chem. Engrs.*, **45**, T251 (1967).
17. R. Lapasin, *Coal Preparation*, **5**, 167 (1988).
18. W. M. Underwood, *Rev. Sci. Instrum.*, **47**(9), 1079 (1976).
19. C. E. Hemmings and J. M. Boyes, Twelfth International Mineral Processing Congress, Sao Paulo, 1977, pp. 46–64.
20. T. J. Reeves, *Trans. Instn. Min. Metall.*, Section C, Mineral Processing and Extractive Metallurgy, **94**, C201 (1985).
21. E. I. Shaheen and D. C. Bogue, Rheological Study of Viscosities and Pipeline Flow of Concentrated Slurries, Selected Papers, Part 1, No. 58d, Sixty-Second Annual Meeting, AIChE, Washington, D.C., 1969, pp. 1–47.
22. S. C. Tsai and E. W. Knell, *FUEL*, **65**, 566 (1986).
23. A. B. Metzner and J. C. Reed, *AIChE Journal*, **1**(4), 434 (1955).
24. B. Rabinowitsch, *Physik. Chem.*, **1415A**, 1 (1929).
25. R. B. Bird, W. E. Stewart and E. N. Lightfoot, Transport Phenomena, Chapter 1 and 2, John Wiley & Sons Publication, Wiley International Edition, Singapore, 1960, pp. 3–70.
26. C. H. Schack, K. C. Dean and S. M. Molloy, Report of Investigations **5334**, U. S. Bureau of Mines, 1957, pp. 1–16.
27. R. J. Mannheimer, J. T. Park, T. A. Grimley and T. B. Morrow, Fluids Engineering (Eds.) John Hyun Kim, Jae Min Hyun, Chung-Oh Lee, Hemisphere Pub. Corp., New York, 1991, pp. 513–535.
28. G. Antonini, O. Francois, P. Gislais and A Touret, Proceedings of the Sixth International Symposium on Coal Combustion and Technology, June 25–27, Orlando, Florida 1984, pp. 266–281.
29. R. M. Turian, F. Hsu, K. S. Avramidis, D. Sung and R. K. Allerndorfer, *AIChE Journal*, **38**(7), 969 (1992).
30. K. S. Avramidis and R. M, Turian, *Journal of Colloidal Interf. Science.*, **143**(1), 54 (1991)
31. E. E. Cone, E/MJ, **169**(120), 82 (1968).
32. S. K. Kawatra, T. C. Eisele and M. T. Rusesky, Chapter 6, Comminution-Theory and Practice,

(Ed.) S. K. Kawatra, Society of Mining, Metallurgy, and Exploration, Littleton, 1992, pp. 529–545.
33. Y. A. Rachman, An Assessment of Vibrating Viscometers in Slurries, Report No. 2001, National Institute for Metallurgy, Private Bag X3015, Randburg, 2125 South Africa, 1979, pp. 1–20.
34. J. D. Perry, *Measurement and Control*, **143**(89), 89 (1977).
35. J. V. Fitzerald, F. J. Matusik and T. M. Walsh, *Measurement and Control*, December (1987).
36. S. K. Kawatra and A. K. Bakshi, *Coal Preparation*, **24**, 123 (1995).
37. M. Mooney, *J. Rheol.*, **2**(2), 210 (1931).
38. S. K. Kawatra, S. A. Moffat and K. A. DeLa'O, The effects of Freezing Conditions on Rock Breakage, Society of Mining, Metallurgy, and Exploration, Inc., Preprint Number 93–17, 1993.
39. K. J. Shoop and S. K. Kawatra, Effect of Rock Breakage Characteristics and Fines/Clay Content on the Autogenous Grinding of Iron Ore, Society of Mining, Metallurgy, and Exploration, Inc., Preprint Number 93–17, 1995.
40. A. K. Bakshi, K. J. Shoop and S. K. Kawatra, Changes in Autogenous Grinding and Classification Performance due to Variation in Slurry Rheology, paper to be presented at the Society of Mining, Metallurgy, and Exploration, Inc. annual meeting 1996.

Reprinted from

INTERNATIONAL JOURNAL OF MINERAL PROCESSING

Int. J. Miner. Process. 44–45 (1996) 155–165

Rheological characterization of mineral suspensions using a vibrating sphere and a rotational viscometer

S.K. Kawatra [a], A.K. Bakshi [a], T.E. Miller Jr. [b]

[a] *Michigan Technological University, Department of Metallurgical and Materials Engineering, Houghton, MI 49931, USA*

[b] *The Dow Chemical Company, Dow Central Research, Midland, MI, USA*

41

ELSEVIER

Int. J. Miner. Process. 44–45 (1996) 155–165

INTERNATIONAL JOURNAL OF MINERAL PROCESSING

Rheological characterization of mineral suspensions using a vibrating sphere and a rotational viscometer

S.K. Kawatra [a], A.K. Bakshi [a], T.E. Miller Jr. [b]

[a] *Michigan Technological University, Department of Metallurgical and Materials Engineering, Houghton, MI 49931, USA*

[b] *The Dow Chemical Company, Dow Central Research, Midland, MI, USA*

Abstract

A new technique has been developed for the characterization of the rheology of mineral slurries into Newtonian and non-Newtonian flows. It utilizes a rotating type viscometer to measure apparent viscosity at a low shear rate, and a vibrating sphere type viscometer to measure the apparent viscosity at a high shear rate. Special precautions were taken to allow measurements of apparent viscosity of rapidly settling mineral suspensions. Both the viscometers are able to measure apparent viscosity as low as one mPa · s (millipascal-seconds) (1 mPa · s = 1 centipoise), which is the approximate room temperature viscosity of water. Because the vibrating sphere viscometer operates at a much high shear rate than the rotating viscometer, the two instruments together can determine the shear-rate dependency of the viscosity. Ground silica of −65 mesh size was used to prepare slurries in water at different percent solids. The apparent viscosity of each slurry sample was measured simultaneously by both viscometers, and the results were compared with each other. In this way, it was determined that silica slurries, for a given particle size distribution, between 0–70% solids by weight in distilled water have Newtonian flow behavior.

1. Introduction

It has long been observed that performance of grinding mills depends upon the rheological properties of the slurry (Klimpel, 1982). Several investigators (Klimpel, 1982; Fuerstenau et al., 1984; Tucker, 1982) have claimed improvement in grinding performance by altering the slurry rheology with grinding aids. These works suggest that by controlling the rheology of the slurry, the efficiency of a grinding mill can be improved. However, to accomplish this, it is first necessary to be able to monitor the slurry rheology.

0301-7516/96/$15.00 © 1996 Elsevier Science B.V. All rights reserved
SSDI 0301-7516(95)00026-7

Rheology of mineral suspensions is highly complex and difficult to predict. It depends upon several parameters, such as solids concentration, particle size and shape, chemical environment, and temperature (Schack et al., 1957). The flow behavior of these suspensions can be divided into different general categories depending upon the relationship between the shear stress developed in the fluid and its rate of shear (Fig. 1). The ratio of shear stress and shear rate is the viscosity. For a Newtonian fluid, the viscosity remains constant as the rate varies. But, for non-Newtonian fluids this ratio changes with shear rate, and is called the apparent viscosity of the fluid at any particular shear rate. The apparent viscosity increases with increase in shear rate for a dilatant fluid, and decreases with increase in shear rate for a pseudoplastic fluid. Dilatant and pseudoplastic fluids are also called shear thickening and shear thinning fluids respectively. Bingham plastics exhibit a yield stress, that is, they do not begin to flow until a critical shear stress is reached. Some suspensions also show yield stress with pseudoplastic flow. Among all the parameters, percent solids has the most visible effect on slurry rheology. At lower percent solids most slurries show Newtonian flow properties, but as the solids content increases, particle–particle interactions become important and the slurry changes to a non-Newtonian flow regime.

The importance of these rheological properties in mineral processing operations have been long realized (Klimpel, 1982). However, measuring slurry rheology is difficult with existing apparatus. The main difficulty of this measurement is rapid settling of the solid particles during measurement. The settling constantly changes the percent solids in the sample holder before the instrument can display a steady reading. This settling effect can be eliminated by measuring the viscosity of a constantly moving slurry in contact with the measuring device. Specially designed baffles (Clarke, 1967) and eddy control baskets (Underwood, 1976) have been used by several investigators to maintain a uniform suspension of solids and reduce the effect of fluid motion on viscometer readings. One of the promising designs for on-line application for slurry viscometry is the gravity flow system, in which the slurry flows through a conduit or a vessel under gravity (Hemmings and Boyes, 1977; Reeves, 1985). By constricting the out flow of slurry from this conduit, a constant hold-up of slurry can be maintained. Then the viscometer can be placed in this slurry to take viscosity measurements. In this way,

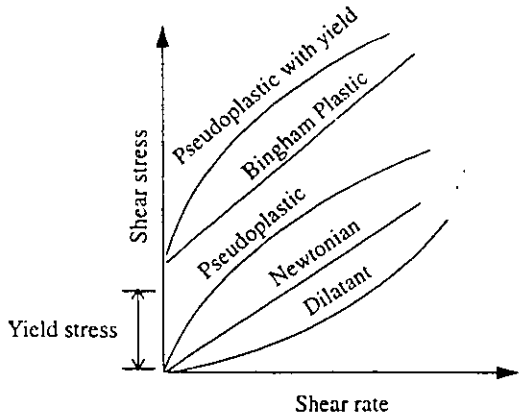

Fig. 1. Generalized time-independent rheology curves for mineral slurries.

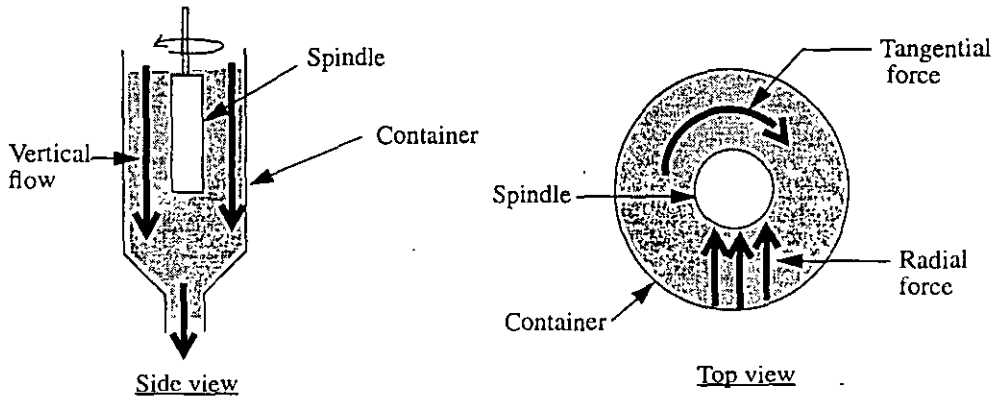

Fig. 2. The vertical flow (side view) prevents the solids from settling by continously sweeping fresh slurry past the spindle. This component of the flowing slurry stream does not affect the rotation of the spindle. But, any radial or tangenial forces (top view), arising from the flow, may put additional strain on the spindle resulting in erroneous viscosity readings. Unbalanced radial flows push the spindle to one side so that it does not spin uniformly and results in erratic readings. Tangential flows increase or decrease the torque on the spindle, making the fluid appear to be either more or less viscous then it really is.

solids settling can be avoided to obtain a homogeneous slurry sample. However, the problem with this method is to obtain a smooth laminar flow of slurry without causing any disturbances in the sample holder. This is particularly true for rotating viscometers, which measure viscosity by measuring the torque generated by the rotation of the spindle (see Fig. 2). The flow of the sample should be strictly vertical, because forces in any other direction will interfere in the rotation of the spindle. In this way, a small turbulence originating from the mixing or flow of slurry can produce a shift in the viscometer reading. Klien et al. (1990) and Kiljanski (1993) have discussed separately how the slurry flow in recirculation systems can change the effective shear rate, which results in different viscosity figures. Also, when one of these techniques (the Underwood design) was tried by the investigators with a Brookfield viscometer, erratic viscosity readings were obtained for suspensions, because the effect of eddies from fluid flow could not be eliminated. In the system described in this paper, suitable slurry handling systems have been designed to eliminate these problems. The details are discussed in the following sections.

2. Methods and materials

2.1. System development

Viscosity of a Newtonian fluid is not affected by shear rates, but for non-Newtonian fluids it changes with change in shear rate. Thus, by measuring the viscosity at two different shear rates sufficiently apart from each other, and comparing the two viscosity values, the fluid can be designated as Newtonian if both the viscosities are similar, and non-Newtonian if the viscosities are different. Based on this concept, a new system has been developed to determine the flow regimes of mineral slurries. Two viscometers were

used for this purpose: the first one was a Brookfield (rotating type) viscometer and the other was a Nametre (vibrating sphere type) viscometer. In this system the Brookfield viscometer operated at a much lower shear rate than the Nametre viscometer. Thus for Newtonian fluids readings from both the viscometers were the same; For pseudoplastic fluids the Brookfield reading was higher than the Nametre reading; and for dilatant fluids it was lower than the Nametre reading. The details of the Brookfield set-up and the Nametre set-up are discussed in the following sections.

2.2. *The Brookfield set-up*

A Brookfield viscometer (DV-I model) was used to measure apparent viscosity at low shear rates. It was a rotational viscometer (coaxial cylinder) and could operate at different shear rates. But, all of its spindles, except for the UL adaptor, were designed for high viscosity solutions and are not suitable for many mineral slurries. The UL adaptor consisted of a cylindrical spindle and a tube which housed the spindle. Sample was placed in the annular space between the spindle and the tube. Then, the viscosity was measured by measuring the torque required to rotate the spindle at a constant rotational speed. Although this arrangement could measure viscosity as low as 1 mPa · s, it failed to operate with slurry, because the solids settled quickly before the instrument could display a steady reading. Therefore, it was necessary to develop a system where the solids would be kept in suspension while the reading was taken. This was accomplished by the slurry presentation system described in Fig. 3. Slurry was mixed in a overhead tank and passed continuously through the annular space between the UL adapter and the tube. After a steady state reading was displayed, flow was stopped by both the pinch valves (to eliminate any swirling motion caused by the flow at the inlet) and the reading was taken immediately. This assembly operated at different shear rates depending upon the viscosity of the slurry. The range of viscosities which could be

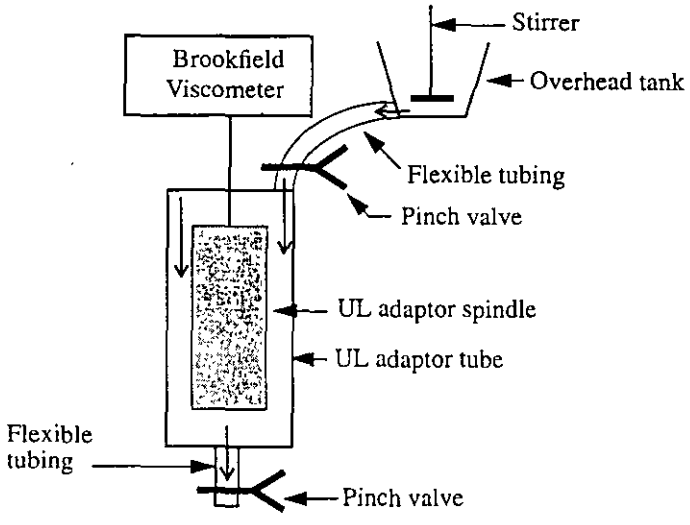

Fig. 3. Brookfield viscometer set-up showing the UL adaptor assembly and the slurry presentation system. This arrangement is very suitable for dilute suspensions, and could measure viscosities of silica slurries up to 70% solids by weight in water without any difficulty.

Table 1
Range of apparent viscosities at any rate for the UL adaptor (Brookfield Engineering Laboratories, 1985)

R.P.M. of the spindle	Shear rate, sec^{-1}	Viscosity range, mPa·s	
		Minimum	Maximum
60.0	73.42	1	9.9
30.0	36.75	2	19.8
12.0	14.68	5	49.5
6.0	7.34	10	99
3.0	3.67	20	198
1.5	1.83	40	396
0.6	0.73	100	990
0.3	0.36	200	1980

measured at any shear rate are given in Table 1. Although the Brookfield viscometer could operate at different shear rates, it was not sufficient by itself to determine the rheological type, because for most of the slurries, readings could be taken only at a single shear rate. When the shear rate was changed by changing the r.p.m. of the spindle, the instrument went out of its operating range. Therefore, a Nametre viscometer was used to measure the viscosity of the fluid at another shear rate. The set-up for the Nametre viscometer is discussed in the next section.

2.3. The Nametre set-up

The Nametre viscometer consisted of a spherical probe, which oscillated along a vertical shaft at its resonant frequency of 750 Hz and a constant amplitude of 1 micron. This viscometer was selected because it operated at a much higher shear rate than the Brookfield viscometer and could measure viscosity as low as 1 mPa · s. When immersed in a fluid, the probe created a shear wave in the fluid, and the fluid dampened the oscillatory motion. The damping, or the power to restore constant amplitude, is a measure of the apparent viscosity of the fluid. Since the probe was vibrating rather than rotating in a single direction, the shear rate was a sinusoidal function of time. Also, the probe was spherical in shape, therefore its vibration had its maximum amplitude at the equator and gradually dropped to zero at the poles (Ferry, 1977). For these reasons, the Nametre viscometer did not operate at a specific shear rate but averaged the shear rates from zero to the maximum value. The maximum shear rate was not a definite constant for the instrument and it varied according to the velocity of propagation of the shear wave in the fluid, which in turn depended upon the fluid viscosity. Therefore, it was necessary to get an idea of its operating shear rate for fluids at different viscosities. This was done by measuring the apparent viscosity of non-Newtonian Methocel A4M (methylcellulose) solutions at different concentrations with the Nametre viscometer, and comparing these figures with the readings of a Bohlin viscometer (details of this test are discussed in the following sections). The shear rates for the Nametre viscometer obtained by this procedure are listed in Table 2. From Tables 1 and 2 it is seen that the Nametre viscometer operates at a much higher shear rate than the Brookfield viscometer with its UL adaptor.

Table 2
Apparent viscosities of Methocel solutions at different concentrations from the Nametre viscometer and their shear rates

Concentrations of Methocel A4M in water	Apparent viscosity from the Nametre viscometer, mPa·s	Shear rate, sec^{-1}
2.0%	212	1500
1.0%	49	3000
0.5%	13	3500

In earlier experiments, an attempt was made to install the Nametre viscometer on a T-joint and fit it to a pipe-line through which the sample was flowing (Kawatra et al., 1992). When the viscometer was bolted to the flange in this manner its response characteristics changed. The major problems encountered involved maintaining a constant tension on the mounting bolts, and dealing with vibration acting upon the instrument from the surrounding structure. The pumping system transmitted excessive vibration through the pipeline, loosening one or the other mounting bolts, which caused a drifting of the zero setting. This problem was eliminated by designing a special slurry presentation system as shown in Fig. 4. This was comprised of a vessel of two concentric cylinders made out of plexiglass. The bottom of the inner cylinder was made conical to avoid solids settling and had an inlet opening through which slurry from the pump entered the vessel. The outer cylinder was one inch taller than the inner cylinder and had a discharge opening on its side. Slurry overflowed from the inner cylinder and returned to the sump through this outlet. The viscometer was suspended from the top by a cable and the probe of the viscometer was immersed inside the inner cylinder. In this way the cable dampened any vibration from the surrounding structures. The weight of the viscometer kept the cable stretched, and the position of the viscometer was kept quite constant. A thermocouple was also placed inside the sump, so that both viscosity and temperature of the sample were recorded simultaneously.

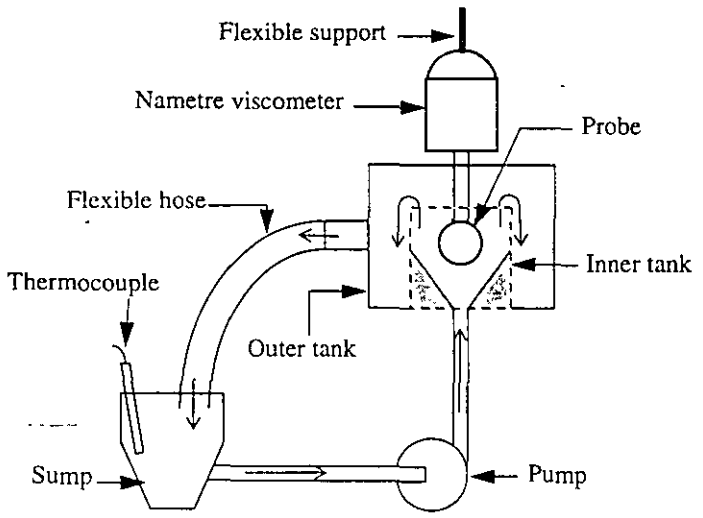

Fig. 4. Nametre viscometer set-up. Sample is placed in the sump and is circulated through the system by a centrifugal pump. Thus the probe of the viscometer comes in contact with a continously flowing slurry.

Table 3
Viscosity of sucrose solutions at different concentrations in water at room temperature (Weast, 1984)

Sucrose content, % by weight	10	20	30	40	50	60
Viscosity, mPa·s	1.33	1.94	3.18	6.15	15.40	58.37

2.4. Bohlin viscometer

A Bohlin viscometer was used to determine the shear rates of the Nametre viscometer for fluids of different viscosities. The Bohlin was a rotational viscometer, in which the spindle was held stationary and the outer cup, surrounding the spindle, rotated. The sample was placed in the annular space between the spindle and the cup, and measurements were taken at different rotational speeds of the cup. With this instrument, measurements of viscosity and shear stress could be taken at different shear rates within a range of 0–1450 sec^{-1}. However, this viscometer could not be used for slurries, because solids settled at the bottom and also on the wall of the cup because of gravity and centrifugal forces. Apparent viscosity vs. shear rate plots of three solutions of Methocel A4M were obtained from this instrument. From these plots, shear rates for the Nametre viscometer were determined.

2.5. Materials used

2.5.1. Sucrose solutions

Sucrose solutions show Newtonian flow properties, and were used to verify the system's ability to work with Newtonian fluids. Six different solutions at different sucrose concentrations were used, with the theoretical viscosities (Weast, 1984) of these solutions listed in Table 3.

2.5.2. Methocel A4M solutions

The molecular structure of Methocel A4M (methylcellulose), a water soluble polymer manufactured by The Dow Chemical Company, Midland, Michigan is given in Fig. 5. Four solutions of this product at 0.5%, 1.0%, 1.5% and 2.0% concentrations by weight in water were prepared. These solutions display pseudoplastic flow behavior (The Dow Chemical Company, 1988) and were used for the following purposes:

(1) To determine the shear rates for the Nametre viscometer for fluids at different viscosities. This was done by first obtaining the apparent viscosity vs. shear rate graph

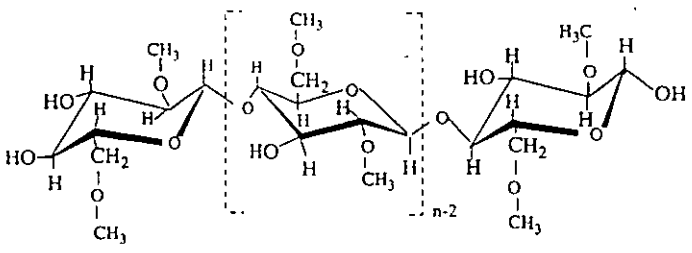

Fig. 5. Molecular structure of methylcellulose (The Dow Chemical Company, 1988).

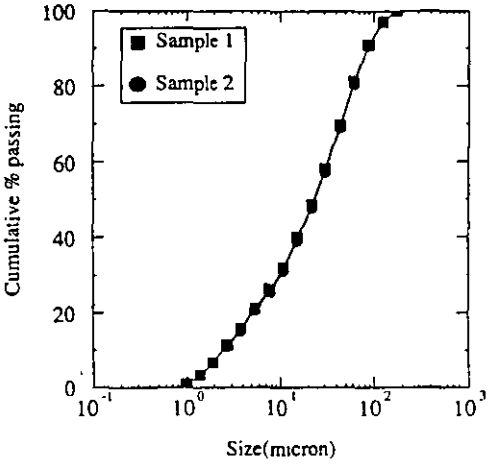

Fig. 6. Size distribution of the silica sample as determined by a Microtrac size analyzer. The sample was analyzed in duplicate, with excellent reproducibility.

for these solutions from the Bohlin viscometer and then finding the shear rates corresponding to the apparent viscosity values obtained from the Nametre viscometer.

(2) To verify the system's ability to detect non-Newtonian characteristics of fluids. This was accomplished by measuring the apparent viscosities of these solutions with the Nametre and the Brookfield viscometers respectively and then comparing the two apparent viscosity values.

2.5.3. Silica slurries

Ground silica at 99.9% purity was obtained from Ottawa Sands Company of Ottawa, Illinois. The size distribution as determined by a Microtrac size analyzer is given in Fig. 6. Several slurry samples were prepared, ranging from 0 to 70% silica by weight in distilled water.

3. Results and discussion

3.1. Determination of shear rates for the Nametre viscometer

Apparent Viscosity vs. shear rate plots obtained from the Bohlin viscometer were extrapolated to include the apparent viscosity values from the Nametre viscometer (Fig. 7). Then the shear rate corresponding to the apparent viscosity from the Nametre viscometer was obtained. As it can be seen from Fig. 7, this shear rate increases with a decrease in apparent viscosity. In this case the minimum shear rate corresponding to 2.0% Methocel solution (212 mPa · s) was 1500 sec^{-1}.This shows that even for high viscosity fluids, the Nametre viscometer operated at a very high shear rate compared to the Brookfield viscometer. Thus, readings from both the viscometers will give the viscosity values of any fluid at two extreme shear rates.

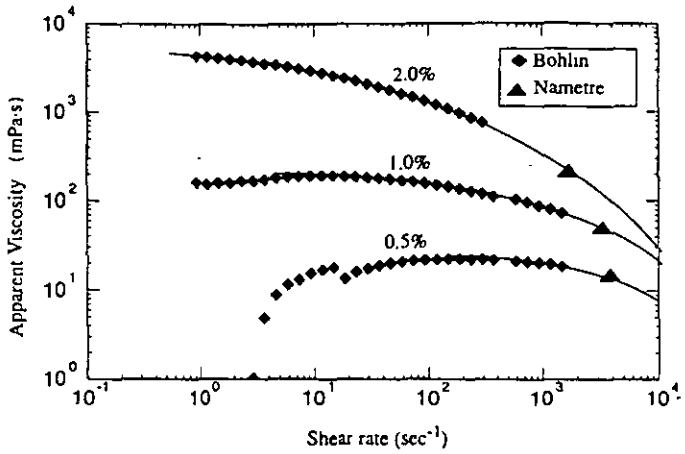

Fig. 7. Apparent viscosity vs. shear rate curves for Methocel A4M solutions at different concentrations, generated by the Bohlin viscometer. Apparent viscosity values from the Nametre viscometer plotted on these curves show that at higher viscosity the Nametre operates at lower shear rate. At very low shear rates, these solutions do not show pseudoplasticity (The Dow Chemical Company, 1988) and for solutions with lower concentrations, this shear rate above which the solutions show pseudoplasticity increases. That is why Methocel solution at a concentration of 0.5% and 1.0% did not show pseudoplasticity at low shear rates.

3.2. Calibration of the system with known solutions

Apparent viscosities of sucrose solutions at concentrations of 10–60 wt% in water and Methocel A4M Solutions at 0.5, 1.0, 1.5, and 2.0 wt% concentrations in water were measured first by the Nametre viscometer and then by the Brookfield viscometer. While measuring the apparent viscosity of Methocel at 2.0% concentration with the Brookfield viscometer, a different spindle (LV #1) was used. This was necessary because the apparent viscosity of 2% Methocel was above 2000 mPa · s, which is too high to be measured by the UL adaptor. For the rest of the samples, the UL adaptor was used. The viscosity readings from the Nametre viscometer were plotted against the viscosity readings from the Brookfield viscometer (Fig. 8). Since sucrose solutions are Newtonian, viscosity readings from both the Nametre (high shear rate) and the Brookfield (low shear rate) viscometers are similar for these solutions, as shown by the line drawn at a slope of 45° and passing through the origin, which coincides with these points. But, the points obtained from tests with Methocel solutions lie below this line, which shows that for these solutions, apparent viscosity values obtained from the Nametre (high shear rate) viscometer are less than their corresponding values from the Brookfield (low shear rate) viscometer. This is expected from Methocel solutions, because these are pseudoplastic fluids (The Dow Chemical Company, 1988). This proves that the system could distinguish between Newtonian and non-Newtonian fluids.

3.3. Viscosity measurements for silica slurries

After calibrating the system with known Newtonian (sucrose) and non-Newtonian (Methocel) solutions, tests were conducted with silica–water slurries at different percent solids ranging from 10–70% by weight in water. Apparent viscosities of these slurries

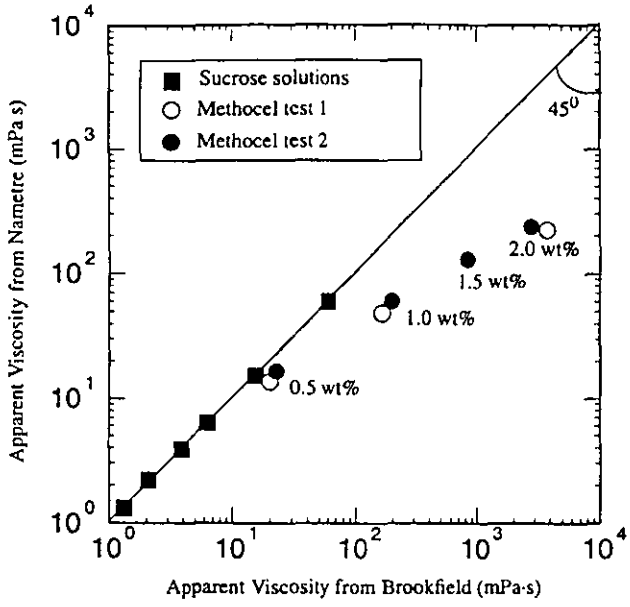

Fig. 8. Reading from Nametre viscometer vs. reading from Brookfield viscometer for sucrose solutions from 10 to 60 wt% and Methocel solutions from 0.5 to 2.0 wt% in water. Since sugar solutions have Newtonian flow properties, the points lie over a line drawn through the origin at a slope of 45°. Duplicate tests (test 1 and test 2) were conducted with Methocel solutions. These solutions are pseudoplastic and the points corresponding to these solutions lie below the line.

were measured by both the Nametre and Brookfield viscometers. The results are shown in Fig. 9. For all these slurries, viscosities obtained from both the viscometers are similar and a line drawn at a slope of 45° passes through these points. This shows that between 0–70% solids by weight the above slurries must have Newtonian flow properties.

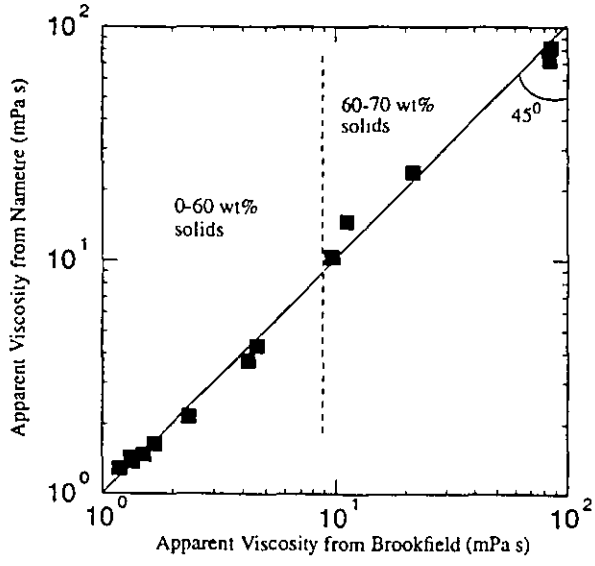

Fig. 9. Apparent viscosities of silica slurries at different % solids from Brookfield and Nametre viscometers. Since all the points lie over a line drawn through the origin at a slope of 45°, these slurries must have Newtonian flow properties.

4. Conclusions

The following conclusions were drawn from these tests:

(1) The system described in this article provides a simple method for characterizing mineral suspensions and liquids into Newtonian and non-Newtonian flow regions while also determining their viscosities.

(2) Between 0–70% solids by weight the slurry of ground silica (with the given size distribution) displayed Newtonian flow behavior.

Acknowledgements

Part of the funding for this project was obtained from the Dow Chemical Company, Midland, Michigan and the Department of the Interior's Mineral Institute program administered by the Bureau of Mines through the Generic Mineral Technology Center for Comminution under grant number G1125149. This paper was published without prior review by the Bureau of Mines.

References

Brookfield Engineering Laboratories, 1985. Assembly and Operating Instructions, UL Adaptor. Stoughton, MA 02072.

Clarke, B., 1967. Rheology of Coarse Settling Suspensions. Trans. Inst. Chem. Eng., 45: 7251–7256.

Fuerstenau, D.W., Venkataramana, K.S. and Velamakanni, B.V., 1984. Effect of chemical additives on the dynamics of grinding media in wet ball mill grinding. Int. J. Miner. Process., 15: 251–267.

Ferry, J.D., 1977. Oscillation viscometry — effects of shear rate and frequency. Meas. Control, 11(5): 89–91.

Hemmings, C.E. and Boyes, J.M., 1977. An on-line viscometry technique for improved operation and control of wet grinding circuits. In: 12th International Mineral Processing Congress, Sao Paulo, pp. 46–64.

Kawatra, S.K., Eisele, T.C. and Rusesky, M.T., 1992. Development of an on-line slurry viscosity monitoring system. In: S.K. Kawatra (Editor), Comminution—Theory and practice. Society of Mining, Metallurgy, and Exploration, Littleton, CO, Ch. 6, pp. 529–545.

Klimpel, R.R., 1982. Slurry rheology influence on the performance of mineral/coal grinding circuits. Parts I and II. Min. Eng., 34(12): 1665–1688; 35(1): 21–26.

Klien, B., Partrigdge, S.J. and Laskowski, J.S., 1990. Rheology of unstable mineral suspensions. Coal Prep., 8: 123–134.

Kiljanski, T., 1993. On the measurement of the rheological properties of unstable mineral suspensions. Coal Prep., 13: 107–112.

Reeves, T.J., 1985. On-line viscometer for mineral slurries. Trans. Inst. Min. Metall. Sect. C. Miner. Process. Extract. Metall., 94: C201–C208.

Schack, C.H., Dean, K.C. and Molly, S.M., 1957. Measurement and Nature of the Apparent Viscosity of Water Suspensions of Some Common Minerals. Report of Investigation 5334, U.S. Bureau of Mines.

The Dow Chemical Company, 1988. Technical Handbook, Methocel Cellulose Ether. The Dow Chemical Company, Midland, MI 48674.

Tucker, P., 1982. Rhelogical factors that affect the wet grinding of ores. Trans. Inst. Min. Metall., 91: 117–122.

Underwood, W.M., 1976. Viscometer for slurries and suspensions. Rev. Sci. Instrum., 47(9): 1079–1082.

Weast, R.C. (Editor), 1984. CRC Handbook of Chemistry and Physics. 65th Edition, CRC Press, Boca Raton, FL.

Australia, Brazil, Canada, Hong Kong, India, Israel, Japan, Malaysia, Mexico, New Zealand, Pakistan, PR China, Singapore, South Africa, South Korea, Taiwan, Thailand, USA. For all other countries airmail rates are available upon request. Claims for missing issues must be made within six months of our publication (mailing) date. Please address all your requests regarding orders and subscription queries to: Elsevier Science B.V., Journal Department, P.O. Box 211, 1000 AE Amsterdam, The Netherlands. Tel.: +31-20-4853642, fax: +31-20-4853598.

US mailing info – *International Journal of Mineral Processing* (ISSN 0301-7516) is published bimonthly by Elsevier Science B.V. (Molenwerf 1, P.O. Box 211, 1000 AE Amsterdam). Annual suscription price in the USA US$ 671.00 (valid in North, Central and South America), including air speed delivery. Application to mail at second class postage rate is pending at Jamaica, NY 11431.
USA POSTMASTERS: Send address changes to. *International Journal of Mineral Processing,* Publications Expediting, Inc., 200 Meacham Avenue, Elmont, NY 11003.
AIRFREIGHT AND MAILING IN THE USA by Publications Expediting. Inc., 200 Meacham Avenue, Elmont, NY 11003.

Advertising information
Advertising orders and enquiries may be sent to: Elsevier Science B.V., Advertising Department, P.O. Box 211, 1000 AE Amsterdam, The Netherlands, tel.: +31-20-4853796, fax: +31-20-4853810. Courier shipments to street address: Molenwerf 1, 1014 AG Amsterdam, The Netherlands. *In the UK*: TG Scott & Son Ltd., attn. Vanessa Bird, Portland House, 21 Narborough Road, Cosby, Leicestershire, LE9 5TA, UK, tel: 0116-2750521/2753333, fax: 0116-2750522. *In the USA and Canada*: Weston Media Associates, attn. Daniel Lipner, P.O. Box 1110, Greens Farms, CT 06436-1110, USA, tel: 203-2612500, fax: 203-2610101.

NOTE TO CONTRIBUTORS

A detailed Guide for Authors is available upon request. Please pay special attention to the following notes:

Language
The official language of the journal is English.

Preparation of the text
(a) The manuscript should preferably be prepared on a word processor and printed with double spacing and wide margins and include an abstract of not more than 500 words.
(b) Authors should use IUGS terminology. The use of S.I. units is also recommended.
(c) The title page should include the name(s) of the author(s), their affiliations, fax and e-mail numbers. In case of more than one author, please indicate to whom the correspondence should be addressed.

References
(a) References in the text consist of the surname of the author(s), followed by the year of publication in parentheses. All references cited in the text should be given in the reference list and vice versa.
(b) The reference list should be in alphabetical order.

Tables
Tables should be compiled on separate sheets and should be numbered according to their sequence in the text. Tables can also be sent as glossy prints to avoid errors in typesetting.

Illustrations
(a) All illustrations should be numbered consecutively and referred to in the text.
(b) Colour figures can be accepted providing the reproduction costs are met by the author. Please consult the publisher for further information.

Page proofs
One set of page proofs will be sent to the corresponding author, to be checked for typesetting/editing. The author is not expected to make changes or corrections that constitute departures from the article in its accepted form. To avoid postal delay, authors are requested to return corrections to the desk-editor, Mr. Herman E. Engelen, by FAX (+31-20-4852696) or e-mail (h.engelen@elsevier.nl), preferably within 3 days.

Reprints
Fifty reprints of each article are supplied free of charge. Additional reprints can be ordered on a reprint order form which will be sent to the corresponding author upon receipt of the accepted article by the publisher.

Submission of electronic text
Authors are requested to submit the final text on a 3.5" or 5.25" diskette. It is essential that the name and version of the word processing program, the type of computer on which the text was prepared, and the format of the text files are clearly indicated. Authors are requested to ensure that the contents of the diskette correspond exactly to the contents of the hard copy manuscript. If available, electronic files of the figures should also be included on a separate floppy disk.

Submission of manuscripts
Authors are requested to submit, with their manuscripts, the names and addresses of *four* potential referees. Manuscripts should be submitted in triplicate; those originating in North and South America should be sent to D.W. Fuerstenau, and all other manuscripts should be submitted to J. Cases (addresses are given on the inside front cover). Illustrations: Please note that upon submission of a manuscript that three sets of all photographic material printed sharply on glossy paper or high-definition laser prints must be provided to enable meaningful review. Photocopies and other low-quality prints will not be accepted for review.
The inclusion of a fax and e-mail number on submission of the manuscript could assist in speeding

Mineral Deposits of the World

Ores, industrial minerals and rocks

Edited by **M. Vaneček**

Developments in Economic Geology Volume 28

Distributed in the East European Countries, China, Cuba, Mongolia, North Korea and Vietnam by ARTIA VERLAG

This overview of the world's mineral deposits lists the metallic and non-metallic mineral deposits according to continents, subdividing the latter with respect to regional metallogenic zones. The introductory chapters summarize present knowledge of the basic concepts of the geologic structure and the evolution of the continents and oceans. The description of the essential metallogenic units has been complemented by main aspects of the development of global metallogeny in time and space. The characteristics of the world's mineral wealth have been supplemented with basic data on the amount, extent and manner of using these mineral resources. Economic geologists will find this volume of interest.

1994 520 pages
Dfl. 375.00
(US $ 214.25)
ISBN 0-444-98667-7

Elsevier Science B.V.
P.O. Box 1930
1000 BX Amsterdam
The Netherlands

P.O. Box 945
Madison Square Station
New York
NY 10160-0757

The Dutch Guilder (Dfl.) prices quoted apply worldwide. US $ prices quoted may be subject to exchange rate fluctuations. Customers in the European Community should add the appropriate VAT rate applicable in their country to the price.

ELSEVIER SCIENCE B.V.

Comminution Theory & Practice,
Published by the Society for Mining,
Metallurgy and Exploration
Editor: S. K. Kawatra

Chapter 39

DEVELOPMENT OF AN ON-LINE SLURRY VISCOSITY MONITORING SYSTEM

S. K. Kawatra[1], T. C. Eisele[1], and M. T. Rusesky[2]

Department of Metallurgical and Materials Engineering[1]
Michigan Technological University
Houghton, MI 49931
Copper Range Company[2]
White Pine, MI 49971

ABSTRACT

An on-line monitoring system for apparent slurry viscosity has been developed at Michigan Technological University. It utilizes a vibrating sphere viscometer in conjunction with a special slurry presentation system to reduce particle settling and turbulence effects. It has proven to give accurate, reproducible results in an on-line hydrocyclone installation. Its performance shows that it can be an effective instrument on an industrial scale, particularly in grinding circuits. Development of the sensor and the importance of rheology in grinding are also discussed.

INTRODUCTION

Comminution is the single most energy intensive unit operation in mineral processing. Although it has been known for some time that the efficiency of a wet grinding circuit is dependent on the rheology of the mineral slurry, no grinding circuits use rheological measurement for direct control (Kawatra and Eisele, 1988). This is primarily because a reliable sensing system has not been developed which can handle the industrial environment. A Michigan Technological University research group is working on the development of a monitoring system for measuring apparent viscosity of mineral slurries.

RHEOLOGICAL EFFECTS IN GRINDING CIRCUITS

The rheology of mineral slurries is highly complex and difficult to predict. It contains both time-dependent and time-independent components, along with a number of variations from ideal behavior. Due to the high shear environment in a grinding mill only the time-independent components are of particular importance in comminution circuits (Bradley, 1965).

Time-independent behavior can be divided into four categories; Newtonian, pseudoplastic, dilatent and Bingham plastic. These classifications are based on how the shear stress developed in the fluid varies with shear rate. A schematic of this behavior is illustrated in Figure 1, with the shear rate being the velocity gradient in a flowing fluid (expressed as sec^{-1}) and the shear stress being the force transmitted to a surface parallel to the fluid flow (expressed as $dynes/cm^2$). For a Newtonian fluid, the shear rate-shear stress relationship is a straight line and the viscosity of the fluid is the slope of this line.

For dilatent or pseudoplastic fluids, the viscosity as such is not defined. Instead, two related parameters are used, the consistency and the apparent viscosity. The consistency is the constant K in the empirical Ostwald-de Waele power-law equation (Tsai and Knell, 1986):

$$\tau = K \dot{\gamma}^{n} \qquad (1)$$

where τ = shear stress in $dynes/cm^2$

$\dot{\gamma}$ = shear rate in sec^{-1}

n = flow behavior index

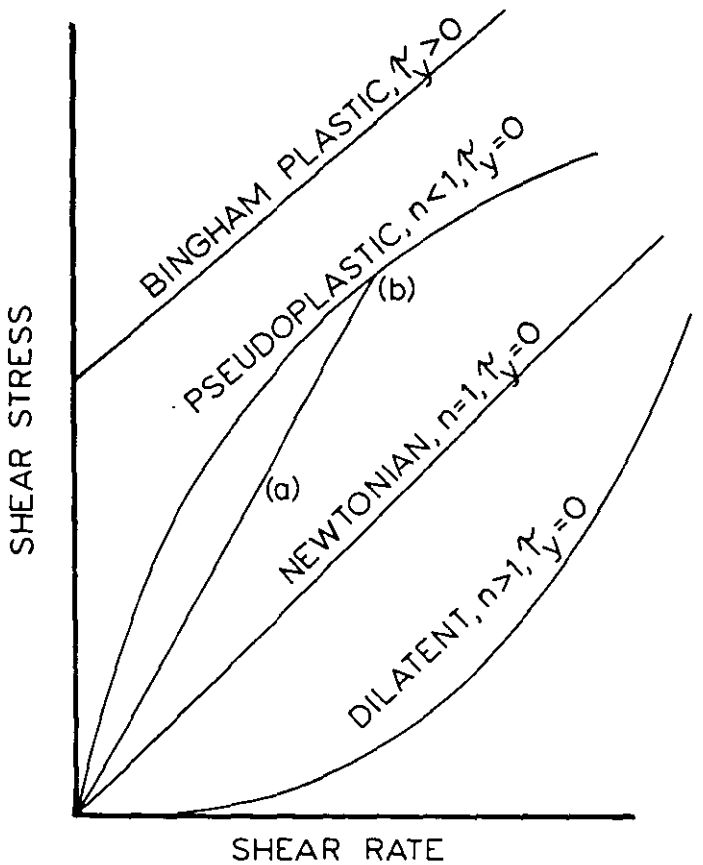

Figure 1. Shear-stress versus shear-rate curves illustrating the various forms of time-independent rheology. The slope of the line (a) is the apparent viscosity of point (b). These curves can be described using the power-law equation, $\tau = \tau_y + K\dot{\gamma}^n$, where τ is shear stress, τ_y is yield stress, K is the consistency, $\dot{\gamma}$ is the shear rate, and n is a parameter for the deviation from newtonian behavior.

Using this equation, a fluid is Newtonian if $n = 1$, pseudoplastic if $n < 1$, and dilatent if $n > 1$, and the consistency K is a constant for all shear rates for a given fluid. However, the consistency can only be calculated if the shear stress is determined at a number of shear rates. This determination is time-consuming, and is not well suited for on-line applications. The apparent viscosity is much easier to determine, as it requires only a single shear stress measurement. It is defined as shown in Figure 1, as the slope of a line (a) drawn between the origin and the measured shear stress value at a particular shear rate (b). The apparent viscosity η_α can therefore be simply calculated by dividing the measured shear stress by the corresponding shear rate:

$$\eta_\alpha = \tau/\dot{\gamma} \qquad (2)$$

For a Newtonian fluid, the viscosity, apparent viscosity, and consistency are all equivalent. In a dilatent fluid, the apparent viscosity increases with increasing shear rate, while in a pseudoplastic fluid it decreases with increasing shear rate. In certain fluids another parameter, the yield stress, is required to describe the time-independent rheology. This parameter is illustrated by the curve for a Bingham plastic shown in Figure 1. Here, the material behaves as if it were a solid until some critical shear stress (τ_y) is reached, after which it begins to flow as a fluid. For a true Bingham plastic, the consistency remains constant at all shear rates once flow has begun, while the apparent viscosity decreases with increasing shear rate.

Mineral slurries can be Newtonian, pseudoplastic, dilatent, or Bingham plastic, depending on factors such as solids concentration, particle size and shape, chemical environment, and temperature. In general, very dilute slurries in water are Newtonian, becoming slightly dilatent as the particle concentration becomes high enough for particle-particle interactions to begin to occur. Once particle interactions become the dominant mechanism for energy transfer in the slurry, it typically becomes pseudoplastic, and develops a yield value as the percent solids increases further. The yield value ultimately becomes very pronounced, producing a fluid which is essentially Bingham plastic just before it ceases to flow at all.

Rheology affects the efficiency of both the mill and the classifier in a closed grinding circuit. The effect of rheology on mill performance has been extensively studied, mostly in conjunction with grinding aids (El-Shall and Somasundaran, 1984, Fuerstenau et al, 1985, Klimpel, 1984, Austin et al, 1984). It is well known that increasing the percent solids increases the mill throughput. However, ultimately the slurry becomes so concentrated as to develop a yield stress. Once this occurs, the breakage rate in the mill decreases due to adhesion of the grinding media to the mill wall (Fuerstenau et al, 1985). Decreasing the slurry viscosity, through the use of grinding aids, at a constant solids concentration, was found to result in an increased fines production rate. These effects are due to changes in the motion of the mill charge resulting from elimination or reduction of the slurry yield value, and to a decrease in the energy dissipated by fluid flow at lower viscosities.

The rheological effects on classifier performance are quite pronounced and fairly complex (Bradley, 1965). These effects have not been well studied, due to the lack of suitable instrumentation. Some data are available using various methods to alter medium viscosity, such as sugar solutions (Agar and Herbst, 1966), viscosity-modifying reagents (Austin et al, 1984) and temperature variations (Kawatra et al, 1988). From the published results, two effects are noted. As the viscosity of the slurry increases, the corrected d50 size for the

hydrocyclone increases, which is primarily a result of the lower settling velocity of particles in a higher-viscosity medium. The second effect is that the fluid speed in the hydrocyclone is reduced due to increased viscous drag at higher viscosities, and therefore the amount of material which exits with the coarse fraction without being subjected to classification is increased. These effects have been shown on both a laboratory and a plant scale in temperature-variation experiments conducted by MTU researchers (Kawatra et al, 1988).

Several theoretical treatments of hydrocyclones include a viscosity term. In theory it is possible to divide this term into two categories; the effect on overall fluid flow patterns, and the effect on individual particle movement. In practice these two effects are inseparable (Bradley, 1965).

EXISTING ON-LINE VISCOMETERS

Currently, three systems for on-line measurements of viscosity exist which would conceivably be used for slurries. The first system, developed by Hemmings and Boyes (1977), used a Brabender Convimeter as the viscometer. The Brabender Convimeter consists of a drive motor which imparts a gyratory movement through a bent shaft to a conical sensor that rotates eccentrically within a cylindrical protective sheath, shown in Figure 2. It utilizes the change in energy required to keep the sensor rotating at a constant rate as a measure of the viscosity. Hemmings and Boyes mounted the viscometer as shown in Figure 3. This system's major drawback was that coarse material and trash in the processing stream tends to get lodged between the spindle and the sheath, causing an unpredictable loss o. stability.

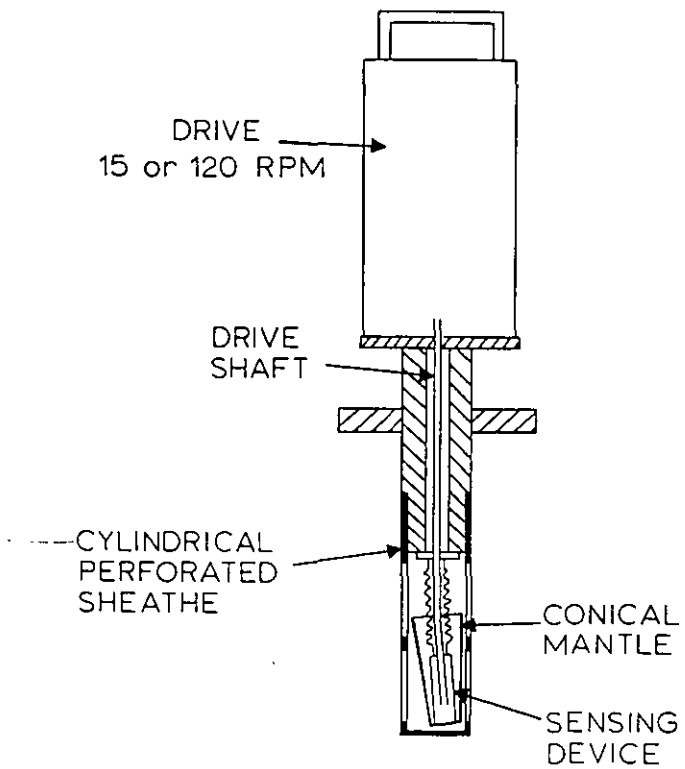

Figure 2. Configuration of the Brabender Convimeter. As the eccentric conical mantle rotates, fluid is forced through the perforations in the cylindrical sheath. Apparent viscosity is determined by measuring the drag force on the rotating mantle.

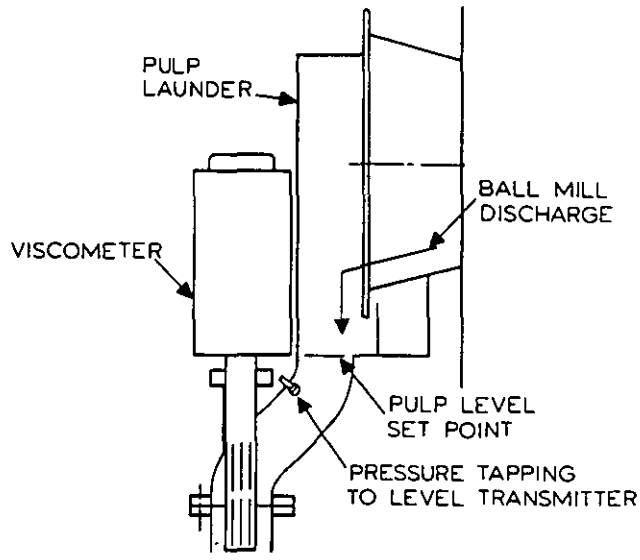

Figure 3. Hemming's and Boyes' (1977) method of mounting the Brabender convimeter.

The second method, described by Reeves (1984), utilizes a viscometer manufactured by the Debex corporation. This rotational type viscometer was driven at a fixed rate by a torque sensitive motor. Viscosity was measured by the amount of torque required to keep the spindle rotating at a constant rate. It was mounted, as shown in Figure 4, to reduce the effects of rapid particle settling. It has been frequently reported that rotating viscometers do not work well in a slurry environment (Clarke, 1967). They are highly sensitive to fluid turbulence,

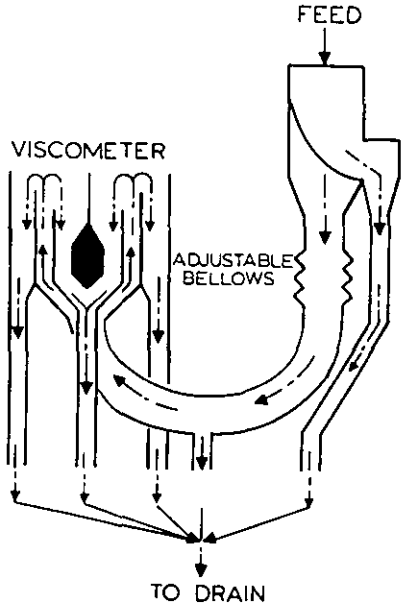

Figure 4. Schematic demonstrating the slurry presentation system used by Reeves (1984).

their moving parts are generally too delicate to tolerate a plant environment, and the rotational motion can cause particle concentration gradients which produce erratic results.

The third method suggested in the literature (Opplinger, Matusik, and Fitzgerald, 1975) utilized a Nametre vibrating sphere viscometer mounted in a T-fitting as shown in Figure 5. The principle of the Nametre viscometer is that the sphere is vibrated around the axis of the shaft to produce shear waves traveling into the fluid at the probe's resonant frequency about 700 Hz, with energy being supplied to maintain the vibration at a constant amplitude of 1 micron. The energy supplied to keep a constant amplitude is indicative of the apparent viscosity of the fluid. Since the probe is vibrating rather than constantly traveling in a single direction, the shear rate is a sinusoidal function of time. Also, the spherical shape of the probe tip results in the vibration having its maximum amplitude at the sphere equator, dropping to zero amplitude at the sphere poles (Ferry, 1977). As a result, the Nametre viscometer cannot be said to operate at a specific shear rate, but rather averages the results from shear rates ranging from zero to the maximum value. This maximum shear rate is not a definite constant for the instrument, as it varies depending on the propagation velocity of shear waves in the fluid, which in turn is a function of several factors, such as the viscosity, and is consequently difficult to determine precisely. The maximum shear rate in water has been calculated to be approximately 6000 sec^{-1} in water at 1 centipoise, but would be a factor of 10 lower at 100 centipoise (Ferry, 1977). In a Newtonian fluid this does not affect the reading, as such fluids exhibit a constant viscosity at all shear rates. Non-Newtonian fluids are more complicated to deal with, both due to viscoelastic effects and to the dependence of the apparent viscosity of these fluids on shear rates. A reading obtained with the Nametre viscometer with a non-Newtonian mineral slurry may best be considered to be obtained at a mean shear rate of approximately 4000-5000 sec^{-1}.

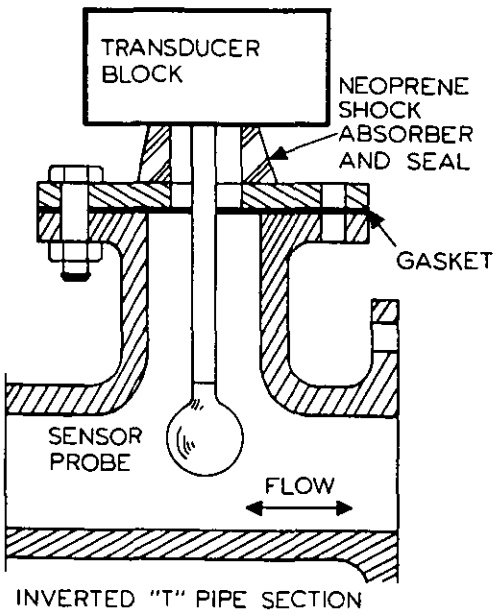

C3

Figure 5. Normal method of mounting the Nametre viscometer in non-slurry service.

Viscometer Selection

After reviewing the three available systems it was decided to start with a commercially available viscometer and to adapt it as necessary for mineral slurry service. The Debex system was not available at the time of this study, and so was not considered further. To determine the ability of the viscometers to function using real materials, samples of finely ground iron ore were sent to both Nametre and Brabender. The Brabender viscometer could not be tested as their laboratory test apparatus was not designed to handle fast-settling slurries, and so no data could be obtained. The results obtained with the Nametre viscometer are shown in Figure 6, and agree with results obtained by other investigators using different techniques (DeVaney and Shelton, 1939, Clarke, 1967, Jeffery and Acrivos, 1965). Based on these results, the Nametre viscometer was selected as the starting point for further work. The viscometer selected had a resonance frequency ranging from 708.0 Hz in air to 701.0 when loaded at 23000 centipoise.

Advantages of the Nametre Viscometer

The high average shear rate and rapid oscillation of the Nametre viscometer allows the instrument to remain insensitive to moderate levels of slurry turbulence. Due to the rapid sampling, fast response time and noise filtering electronics, large particles striking the probe have a very transitory effect on the measurement.

The Nametre viscometer is also ruggedly designed and capable of withstanding the abuse of a plant environment. The design consists of a sensor enclosed in a sealed housing which prevents corrosive or abrasive materials from reaching the delicate moving parts.

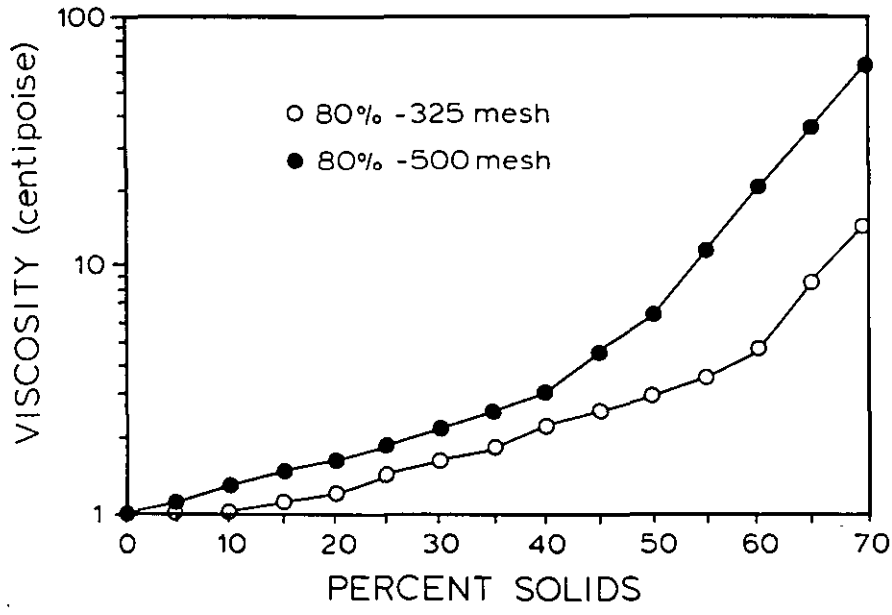

Figure 6. Measurements performed by Nametre viscometer.

SYSTEM DEVELOPMENT

The first step in the development of the on-line system was to calibrate the viscometer by a series of static bench tests. This calibration was then verified and the stability checked on an in-line installation.

The first attempt at installing the instrument was per manufacturer recommendations. This was accomplished by mounting the viscometer into a straight section of pipe using a heavy duty T-fitting, as shown in Figure 7. When the viscometer was bolted to the flange its response characteristics changed, making the rezeroing of the instrument necessary. The major problems encountered involved both maintaining a constant tension on the mounting bolts, and dealing with the very high levels of fluid drag and vibration acting upon the probe.

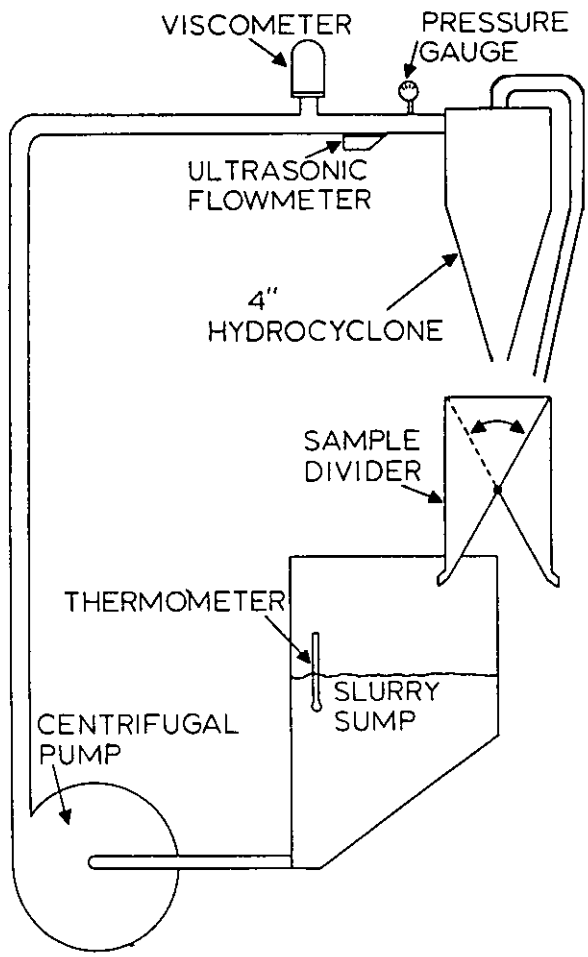

Figure 7. Initial test set up with the Nametre viscometer.

As the tension on the bolts changed, the zero setting tended to drift. The pumping system transmitted excessive vibrations through the pipeline, and over several hours one or more of the bolts would tend to loosen. Lock washers and jam nuts were tried, but they had little effect. As the tension on the bolts varied the zero setting drifted, causing unpredictable changes in the viscosity reading. Even when the zero setting was adjusted before each test to compensate for changes in bolt tension, the measured viscosity of water was unacceptably high (3.7-3.8 cP). This was due to the high levels of pump vibration and turbulence.

The second problem encountered was the strong dependency of measured viscosity on the flow rate, shown in Figure 8. This was probably due to the probe producing a severe restriction in the pipe, which caused substantial drag forces to act on the probe. This stress apparently slightly deformed the probe and changed its vibrational characteristics, producing the observed flow rate dependence. This necessitated further measures to improve the setup, by reducing the effects of both mechanical stresses on the sensor and interferences from vibrations and turbulence.

The stability of the readings were improved by isolating the pump from the viscometer by mounting it on a separate platform and connecting the pump to the viscometer with flexible pipe. Lead blocks were bolted to the pipeline on either side of the viscometer to damp vibrations and thus reduce the instrument noise. However this did not address the mechanical stress problems which were causing the zero drift and flow rate dependence.

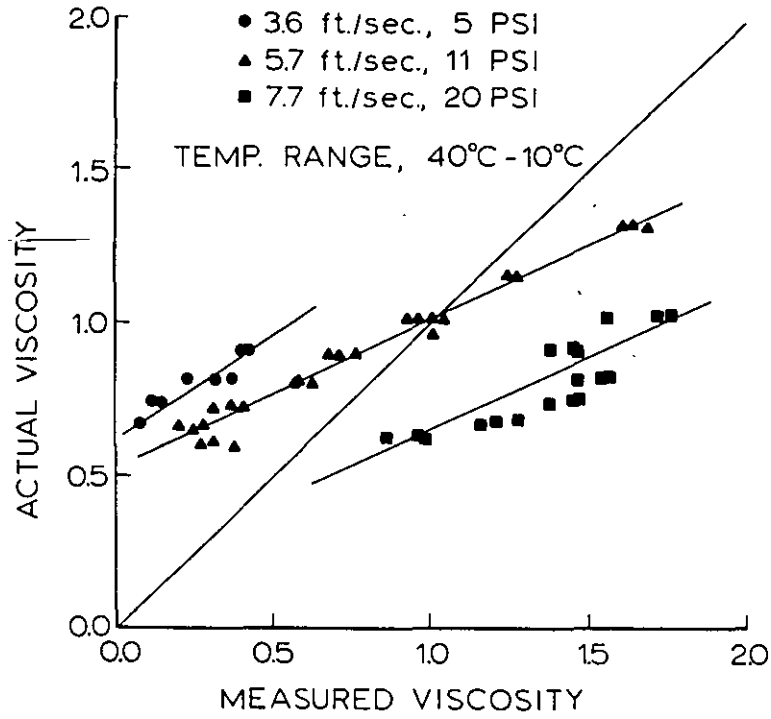

Figure 8. Apparent dependence of measured water viscosity on flow rate before making installation modifications.

It was decided to develop a slurry presentation system to eliminate the effects of vibration and turbulence on the Nametre viscometer. Figure 9 illustrates how a slurry stream is allowed to flow upwards and over an annulus which acted as a weir. A constant level of one inch over the top of the measurement chamber was maintained by the overflow lip of the annulus. Slurry which overflowed this barrier was returned to the sump by the overflow launder.

The sensing unit was suspended with rubber straps and was allowed to hang free of any contact with the mounting bolts, as shown in Figure 9. This minimized the stresses acting on the sensor, and provided nearly complete isolation from

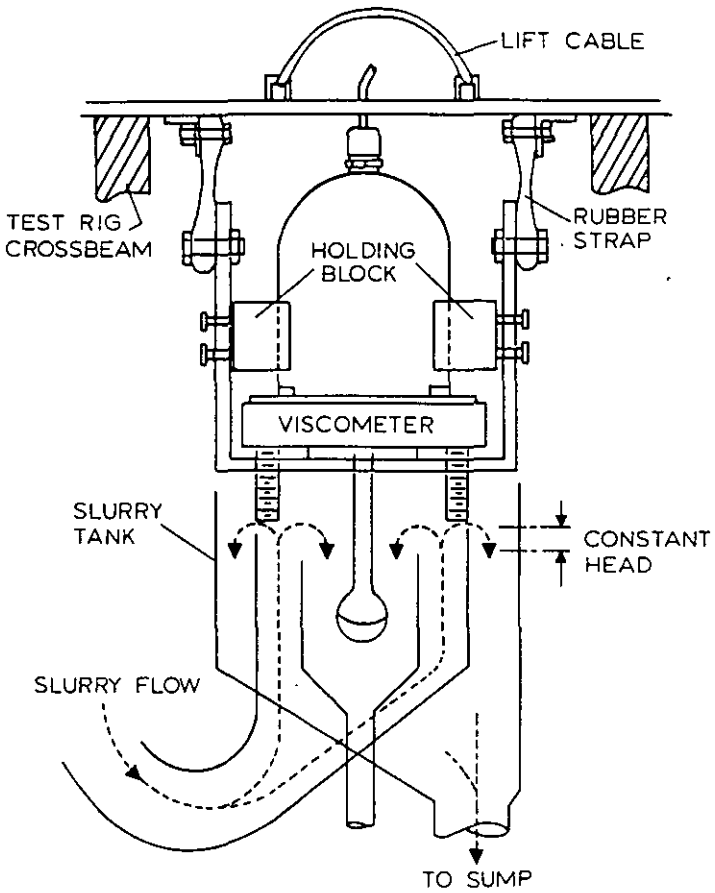

Figure 9. A method of mounting Nametre viscometer over an open slurry tank to eliminate problems with drifting zero setting and turbulence.

vibrations. This method of mounting has the additional advantage of easy removal of the sensor from the slurry presentation system via an overhead cable attached to the sensor. This feature was useful for cleaning or drying the sensor as well as checking the zero setting. A temperature sensor was inserted next to the viscometer probe to ensure that the slurry temperature was known accurately.

EXPERIMENTAL PROCEDURE

Equipment Description

The equipment used in this project consisted of a hydrocyclone test rig with a 4" diameter Krebs hydrocyclone. The viscometer was mounted to measure the viscosity of the recombined cyclone overflow and underflow products, which were kept well-mixed and had a consistent solids content in the course of each test. Data was collected by an HP-85 microcomputer with an HP-3497A data acquisition/ control unit. The computer was used to collect single data points, to collect data at specific time intervals, or to collect data after a specified change in slurry temperature had occurred.

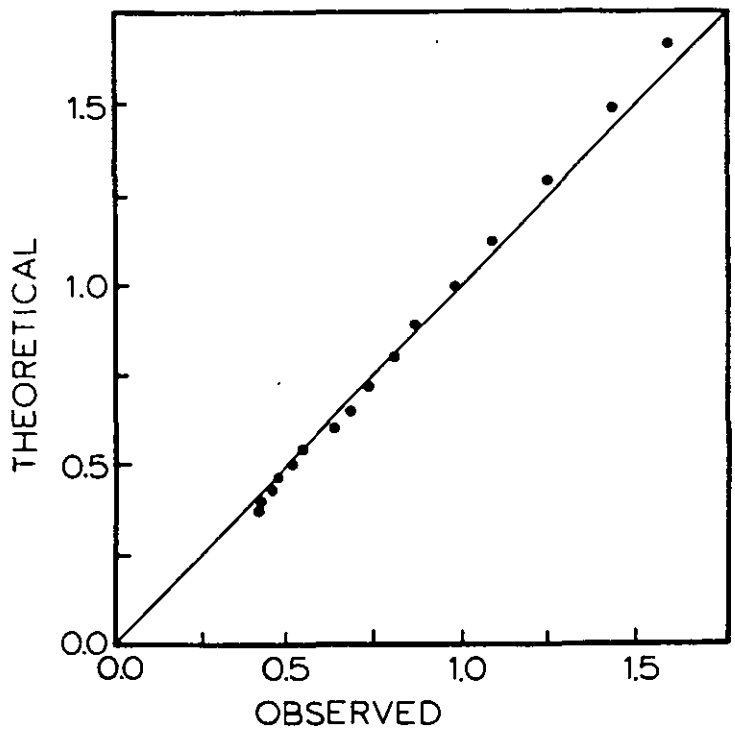

Figure 10. On-line test of viscometer installation on water viscosity after making improvements in the mounting arrangement. The viscosity of water is being varied by changing its temperature.

Experiments with Water

Initial tests with the slurry presentation system were run using water to compare measured values to those calculated from the formulas in the Handbook of Chemistry and Physics (CRC 1984)

$\log_{10}\eta = 1301/[998.333+8.1855(T-20)+0.00585(T-20)^2]-1.30233$ for 0°C to 20°C and

$\log_{10}\eta/\eta_{20} = [1.3272(20-T)-0.001053(T-20)^2]/(T+105)$ for 20°C to 100°C, where

η = viscosity, centipoise
T = Temperature, °C
η_{20} = Viscosity at 20°C, which is 1.002 centipoise

Tap water was circulated through the system while the temperature was varied between 10°C and 50°C. The results are shown in Figure 10. The stability of the slurry presentation system was then determined by allowing the system to measure the viscosity of water for 15 hours, while maintaining the temperature at 22.5°C to ± 0.3°C. Figure 11 shows the improvement between tests run on the initial installation as opposed to the improved system.

Experiments with Mineral Slurries

Following the initial tests with water, work was begun to determine the capabilities of the system with mineral slurries. A 99.9% pure silica provided by the Ottawa Sand Co. of Ottawa Illinois, with the size distribution shown in Table 1, was used in the mineral slurry experiments.

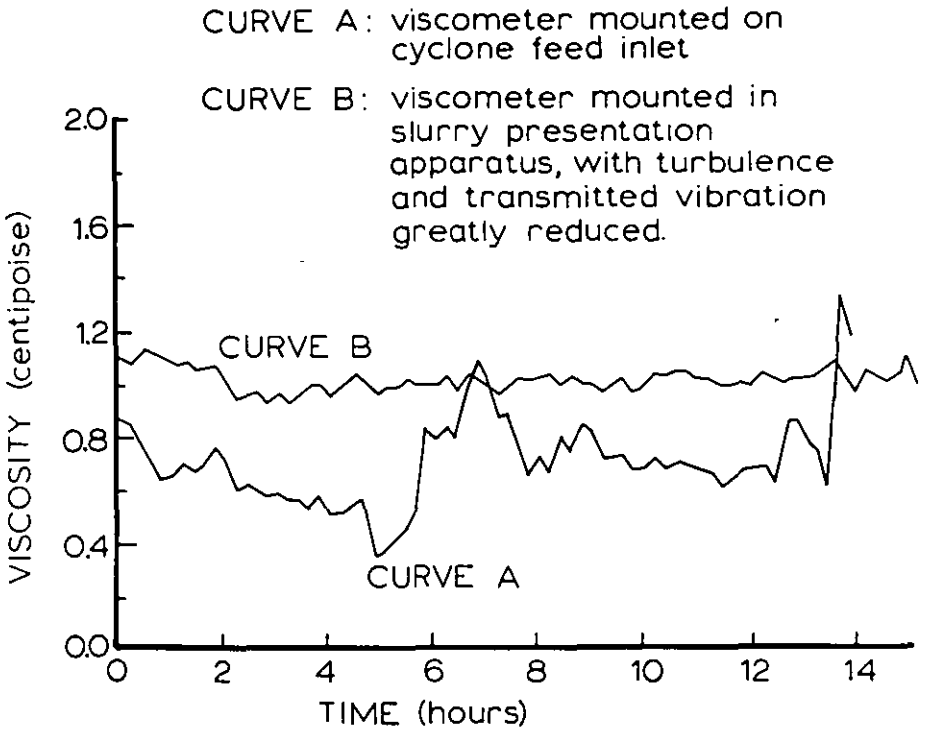

Figure 11. Stability check of on-line water viscosity measurements before and after making improvement in the mounting of the sensor with temperature controlled to 22.2°C ± 0.2°C.

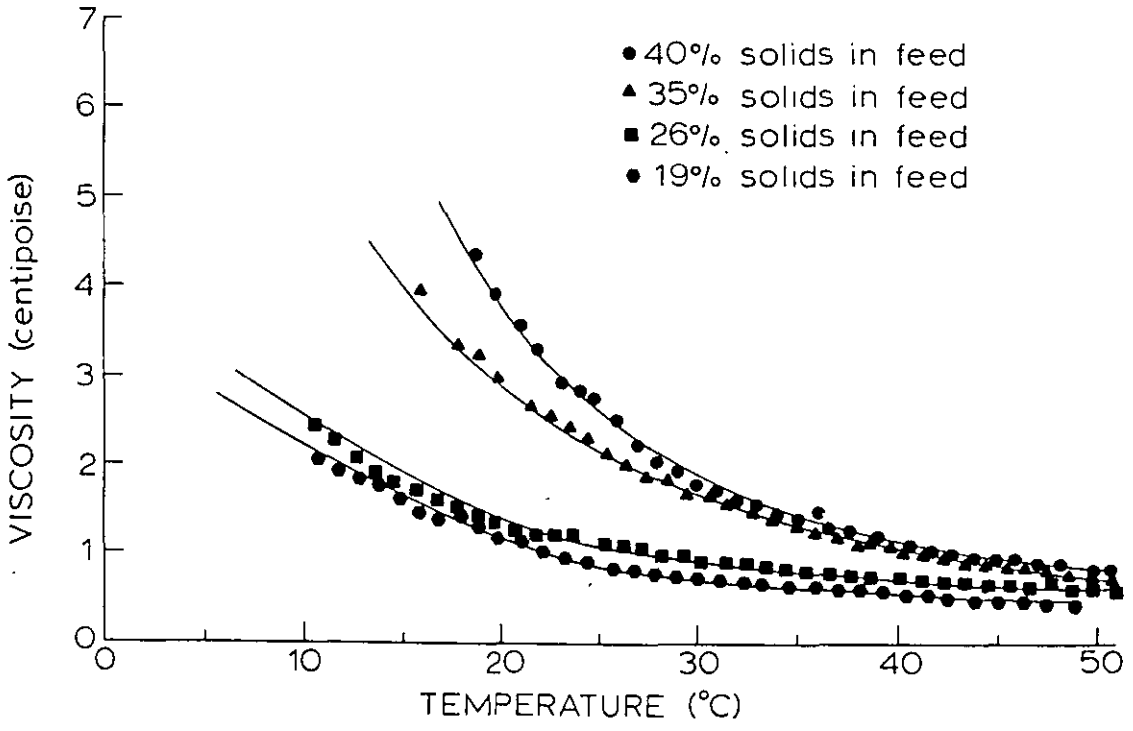

Figure 12. On-line viscosity measurements of silica/water slurries as a function of temperature at various solids concentrations.

Table 1. Size distribution of silica used for on-line tests of the viscometer system, as determined using a Leeds and Northrup Microtrac particle size analyzer.

Size, Micrometers	Cumulative % Passing
176	100
125	97.0
88	93.6
62	75.5
44	49.8
31	34.9
22	24.0
16	17.5
11	12.7
7.8	8.1
5.5	5.1
3.9	3.9
2.8	2.0

The experimental work was conducted at temperatures ranging from 10°C to 50°C, and percent solids ranging from 19% to 40%. For each experiment the cyclone test rig was filled with a known volume of water, the pump was started, and silica was added to the desired percent solids. Solids concentrations were checked by taking wet and dried sample weights after each test run. The temperature was controlled by the use of heating and refrigeration coils in the sump.

For initial experiments viscosity values were measured over a 40°C temperature range for solids concentrations of 19%, 26%, 35% and 40% solids. Figure 12 illustrates the dependence of viscosity on percent solids over this temperature range. The curves above 26% solids are noticeably steeper, which shows that increased interaction between particles is taking place.

To test the reproducibility of the system a second set of experiments at 15%, 25% and 40% solids were carried out. Samples to check percent solids were not removed until the completion of the experiments. This allowed the tests to be continued for an extended time through several temperature cycles without sampling introducing changes in the slurry composition or test rig operation. Each slurry was cycled through the temperature range from 50°C to 15°C. Viscosity measurements were made at 1°C intervals above 25°C, and 1/2°C intervals below 25°C. Each measurement is an average from 30 seconds of data acquisition.

RESULTS

Figures 13 through 15 show the temperature vs. viscosity data for three slurry solids concentrations. The second order polynomial curve fit was calculated from the total number of available points from the individual temperature runs, with the fitted polynomial equations, correlation coefficients, and standard errors for each percent solids given in Table 2.

From the results shown in Table 2, it is seen that the performance of the instrument is highly reproducible, with standard deviations less than 0.05 centipoise for all three percent solids. The average error, which is the standard deviation divided by the mean viscosity, is consistently under 4%, which, considering the difficulties with measuring slurry viscosity is completely acceptable for the goal of on-line control of grinding classification circuits.

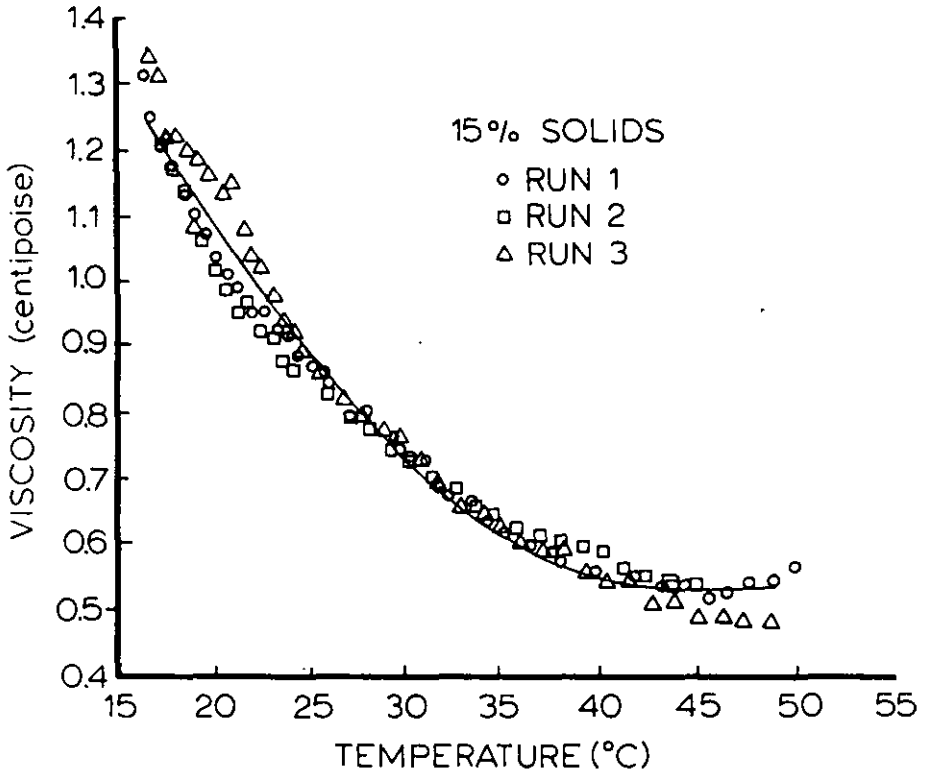

Figure 13. Viscosity measurements made during three runs of temperature between 50°C and 10°C on a 15 wt.% silica/water slurry.

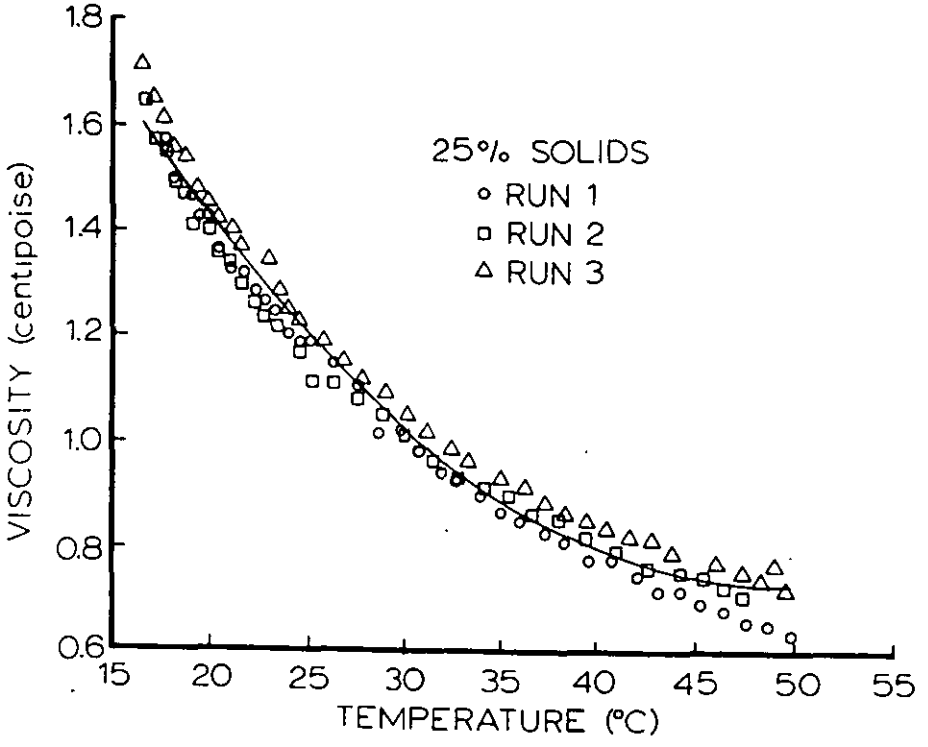

Figure 14. Viscosity measurements during three runs of temperature between 50°C and 10°C on a 25 wt.% silica/water slurry.

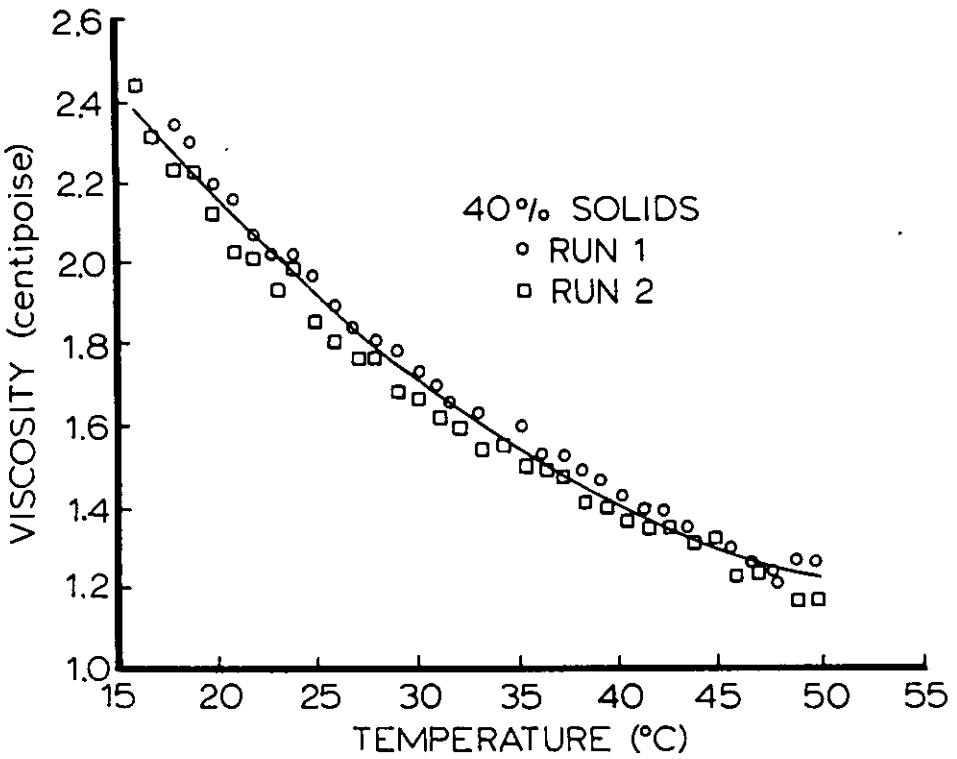

Figure 15. Viscosity measurements made during two runs of temperature between 50°C and 10°C on a 40 wt.% SiO_2/water slurry.

Table 2. Polynomial equations, correlation coefficients, and standard errors at 15% solids, 25% solids, and 40% solids. η = measured viscosity, centipoise; T = temperature, °C, and $\eta = A + BT + CT^2$.

%Solids	A	B	C	Mean η	Correlation Coefficient	Standard Deviation	Average % Error
15%	2.325	-0.079	0.001	0.81	0.979	0.03	3.70%
25%	2.725	-0.079	0.0008	1.09	0.981	0.04	3.67
45%	3.485	-0.079	0.001	1.66	0.986	0.04	2.41

CONCLUSION

It is well established that rheological control is important in the improvement of grinding efficiency in an operating plant. Such control has not been implemented primarily due to the lack of instrumentation. However an on-line apparent viscosity measuring system has been develped at Michigan Technological University which is capable of reproducible measurement of this parameter in mineral slurries. It is robust enough to be used on-line in grinding circuits, while still being precise enough to provide useful control data.

ACKNOWLEDGMENTS

This research has been supported by the Department of the Interior's Mineral Institute program administered by the Bureau of Mines through the Generic Mineral Technology Center for Comminution under grant number G1125149. Additional support was provided by Dow Chemical Co., Midland, Michigan.

REFERENCES

Agar, G. E. and Herbst, J. A., "The Effect of Fluid Viscosity on Cyclone Classification", Trans. AIME, vol. 235, 1966, pp. 145-149.

Austin, L. G., Klimpel, R. R., and Luckie, P.T., Process Engineering of Size Reduction: Ball Milling, SME-AIME, 1984.

Bradley, D., The Hydrocyclone, Pergamon Press, 1965.

Clarke, B., "Rheology of Coarse Settling Suspensions", Trans. of the Institution of Chem. Eng., vol. 45, pp. 251-256, 1967.

CRC Handbook of Chemistry and Physics 64th Ed., Weast, R. C., Chief Ed., Astle, M. J., and Beyer, W. A., Asst. Ed., CRC Press, Inc., Boca Raton, Fl., 1984.

DeVany, F. D. and Shelton, S. M., "Properties of Suspension Media for Float and Sink Concentration", U.S.B.M. Report of Investigations 3469, September 1939.

El-Shall, H., Somasundaran, P. "Physico-Chemical Aspects of Grinding: A Review of Use of Additives", Powder Technology, vol. 38, pp. 275-293, 1984.

Ferry, J. D., "Oscillation Viscometry-Effects of Shear Rate and Frequency", Measurements and Control, Sept.-Oct., vol. 11, no. 5, 1977.

Fuerstenau, D. W., Venkataraman, K. S. and Velamakanni, B. V., "Effect of Chemical Additives on the Dynamics of Grinding Media in Wet Ball Mill Grinding", Int. J. of Mineral Processing, vol. 15, no. 4, 1985, pp. 251-268.

Hemmings, C. E., and Boyes, J. M., "Plant Trial Evaluation of On-Stream Measurement System for Wet Grinding Mills", Int. Chem. Eng. Symposium Series, no. 63, 1977, pp. D4/EE/1-13.

Jeffery, D. J., and Acrivos, A., "The Rheological Properties of Suspensions of Rigid Particles", AiChE J., vol. 20, 1965, pp. 267-277.

Jinescu, V. V., "The Rheology of Suspension", Int. Chem. Eng., vol. 14, 1974, pp. 397-420.

Kawatra, S. K. and Eisele, T. C., "Rheology Effects in Grinding Circuits", Proceedings of the XVI International Mineral Processing Congress, Elsevier, New York, Part A, 1988, pp. 195-207.

Kawatra, S. K., Eisele, T. C., Zhang, D., and Rusesky, M. T., "Effects of Temperature on Hydrocyclone Efficiency", Int. J. of Min. Processing, vol. 23, 1988, pp. 205-211.

Klimpel, R. R., "Influence of Material Breakage Properties and Associated Slurry Rheology on Breakage Rates in Wet Grinding of Coal and Ores in Tumbling Media Mills", Reagents in the Minerals Industry, (M. J. Jones and R. Oblatt, eds.), Institution of Mining and Metallurgy, London, 1984, 265-270.

Oppliger, H. R., Matusik, F. J. and Fitzgerald, J. V., "New Technique Accurately Measures Low Viscosity On-Line", Control Eng., vol. 22, no. 7, 1975, pp. 39-40.

Reeves, T. J., "On-Line Viscometer for Mineral Slurries", Transactions of the Institution of Mining and Metallurgy: Section C: Mineral Processing and Extractive Metallurgy, vol. 94, 1984, pp. C201-C208.

Tadros, T., "Rheology of Concentrated Suspensions", Chem. and Industry, April 1985, pp. 210-219.

Tsai, S. C. and Knell, E. W., "Viscometry and Rheology of Coal-Water Slurry", Fuel, vol. 65, April 1986, pp. 566-571.

Pergamon

Minerals Engineering, Vol. 9, No. 8, pp 881–891, 1996
Copyright © 1996 Published by Elsevier Science Ltd
Printed in Great Britain. All rights reserved
PII:S0892–6875(96)00079–9
0892–6875/96 $15.00+0.00

EFFECT OF VISCOSITY ON THE CUT (d_{50}) SIZE OF HYDROCYCLONE CLASSIFIERS

S.K. KAWATRA§, A.K. BAKSHI§ and M.T. RUSESKY†

§ Department of Metallurgical and Materials Engineering, Michigan Technological University, Houghton, MI 49931, USA
† Copper Range Company, White Pine, MI 49971, USA
(Received 15 February 1996; accepted 1 May 1996)

ABSTRACT

On-line measurement of slurry viscosity was carried out to study the effect of viscosity on the cut (d_{50}) size of hydrocyclone classifiers. As slurry viscosity increases, the settling rate of particle decreases, causing the d_{50} size to become coarser. The viscometer set-up used a vibrating sphere viscometer and a specially designed slurry presentation device to avoid settling of solids during viscosity measurement. This set-up was mounted on a test rig for a 10.2 cm diameter hydrocyclone. Test samples were prepared from ground silica (80% passing 65 microns) and water. Both the solids content and temperature of the samples were varied to change their viscosities. Samples from overflow and underflow streams were collected at regular intervals, and data from these samples were used to calculate the $d_{50}(c)$ size. Temperature and viscosity were recorded simultaneously during these tests.

From these data it was observed that $d_{50}(c)$ was proportional to the 0.35th power of the slurry viscosity. This relationship was then introduced in the existing Lynch and Rao model for siliceous material, to develop a modified model for hydrocyclone classification. This modified Lynch and Rao model incorporated a viscosity parameter from direct measurement, and predicted the cut size precisely when the viscosities of the slurries were altered by factors other than changing percent solids, such as temperature variation. This was not possible with the original Lynch and Rao model, which did not include any viscosity term. It was also determined that increasing slurry viscosity produced an increase in the bypass fraction, R_f. This effect was due to increased fluid drag in the hydrocyclone as the viscosity increased.
Copyright © 1996 Published by Elsevier Science Ltd

Keywords
Hydrocyclones; modelling; on-line analysis

INTRODUCTION

Fluid viscosity has a profound effect on the separation characteristics of hydrocyclones [1, 2]. Changing viscosity alters the particle settling rates and the slurry velocities in the hydrocyclone, and so alters the performance. When the viscosity increases, the settling speed of particles is decreased. Particles in the hydrocyclone must therefore be coarser in order to reach the underflow when the viscosity is high, and increasing viscosity causes the d_{50} size to increase. Therefore, viscosity must be included while developing mathematical models for cut size prediction. Although many models for classifier cut size developed in the

past have viscosity terms, most of these equations were developed for dilute suspensions and smaller diameter hydrocyclones, which are not comparable to normal plant conditions [3, 4]. In later years, Lynch and Rao [5], and Plitt [3] used data from large diameter hydrocyclones and slurries with higher percent solids to develop more versatile models to predict separation size in actual plant situations. However, neither of these equations have explicit slurry viscosity terms in them. Instead, both of these equations depended on solids content as an indicator of slurry rheology. Lynch and Rao used weight percent solids for their model, whereas Plitt used volume percent solids. However, it is well known that solid content is not the only parameter which affects slurry rheology. Besides solids content, the temperature, size distribution of the solids, and chemical environment can also alter rheology [6]. This suggests the need for direct measurement of rheology to determine its effect on classifier performance.

One of the major reasons for not including a viscosity term in the hydrocyclone models is the difficulty in measuring slurry rheology on-line [7]. In this work, an on-line viscometer along with a specially designed sample presentation system made it possible to measure the hydrocyclone feed slurry viscosity in real time, and then develop a model for predicting separation size from the measured value of slurry viscosity.

THEORETICAL BACKGROUND

The dependency of viscosity on cut (d_{50}) size of a hydrocyclone can be explained by the equilibrium orbit theory [3, 8], which assumes laminar flow conditions, and states that each particle in the hydrocyclone tends to be in equilibrium between two opposing forces, (i) centrifugal force acting towards the wall of the hydrocyclone, and (ii) drag force from the liquid acting towards the axis (Figure 1). From this theory, the diameter of a particle that is in equilibrium at a particular orbit is given by:

$$d = \sqrt{\frac{18\eta \cdot W \cdot r}{(\rho_s - \rho_l) \cdot V_t^2}} \qquad (1)$$

Where:

d	= diameter of the particle
ρ_s	= density of the solid particles
ρ_l	= density of the liquid
V_t	= tangential velocity of the particle
r	= radius of the equilibrium orbit
η	= fluid viscosity
W	= radial velocity

For the d_{50} size, the equilibrium orbit overlaps with the envelope of zero vertical velocity (Figure 1) and so for this size the particles have equal chances of reporting to the overflow and the underflow. Thus, from Equation 1 we see that cut (d_{50}) size is proportional to the 0.5th power of viscosity. However, when the flow conditions inside the hydrocyclone changes from laminar flow the exponent of viscosity also changes [8]. In many empirical and semi-empirical models for hydrocyclone classification this exponent of viscosity has been assigned different values which vary between 0.50 to 0.60 [1]. However, most of these tests were done at lower percent solids where hindered settling is not important. At higher solids content, hinderance from surrounding particles increases, which causes the settling behavior of particles to deviate from the laminar flow condition where Stoke's law (based on which the equilibrium orbit theory is designed) is valid. Deviation from Stoke's law also occurs if the terminal velocity is excessive in relation to the size of the particle. High velocity with large particles can cause a transition to flow around the particles that is intermediate between laminar and turbulent flow [8]. Due to these reasons the cut size no longer remains proportional to the 0.5th power of viscosity.

Another important factor which should be considered for determining the effect of viscosity is the rate of shear inside the hydrocyclone. Movement of concentric layers of fluids at increasing tangential velocities with decrease in radius produces intense shear forces inside the hydrocyclone [9]. For Newtonian fluids,

viscosity is independent of shear rate, but for non-Newtonian fluids it changes with changes in shear rate. This makes the viscosity effects on separation size more complex for non-Newtonian suspensions. Luckily, most mineral suspensions are Newtonian below 50% by volume [10] and their viscosities will not be affected by changes in shear rate. Recently in other work [11], it was found that the silica slurries in our experiments, with an 80% passing size of 65 micron, were in the Newtonian flow regime up to a solids concentrations of 70% by weight. Of course, this will also depend upon the size distribution of the solids. Finer solids may begin to show non-Newtonian behavior at lower concentrations than coarser solids.

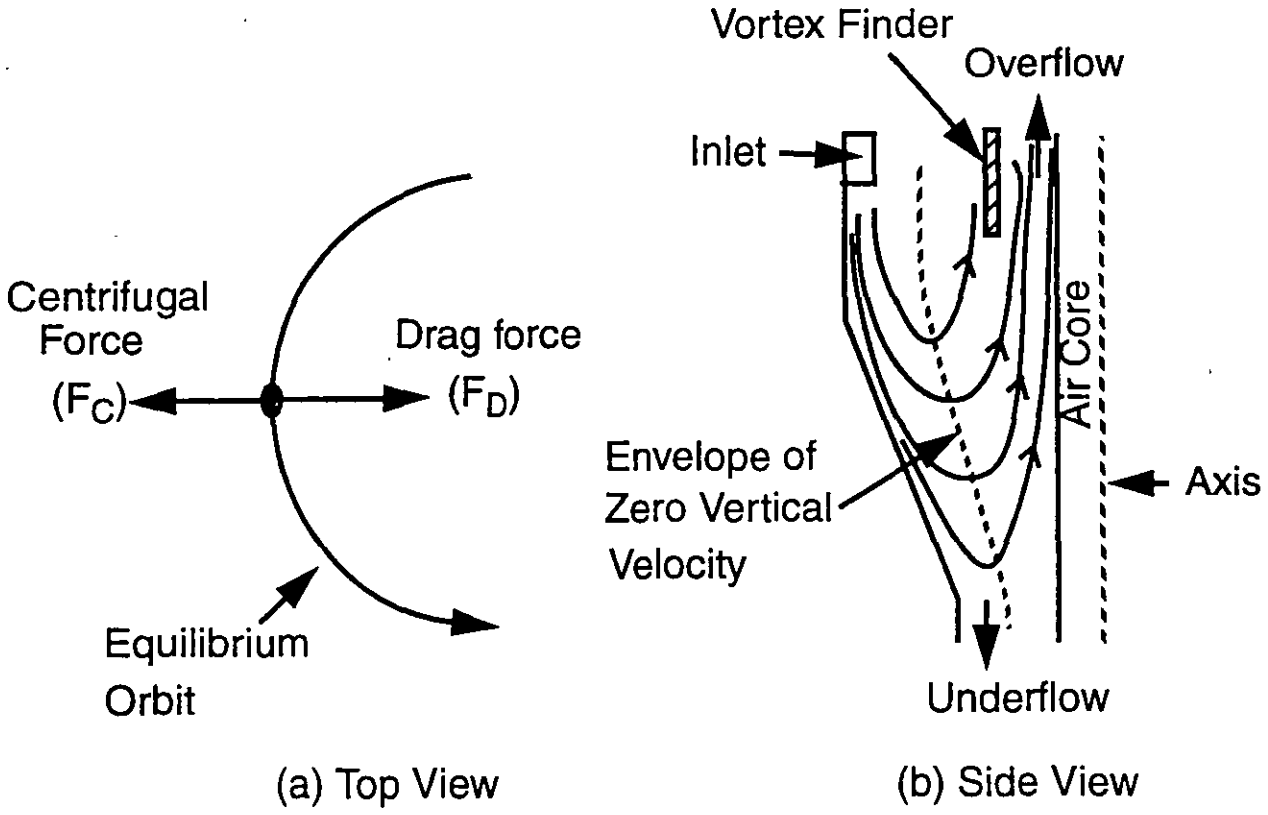

Fig.1 Diagrams to explain the equilibrium orbit theory of hydrocyclone mechanism. The equilibrium orbit (a) is reached when the centrifugal force on the particle is equal to the fluid drag force. d_{50} size particles lie on the envelope of zero vertical velocity (b), and have equal chance of going to the overflow or to the underflow.

Viscosity also changes the water-to-underflow term, R_f, of the hydrocyclone. R_f is the fraction of feed liquid reporting to the underflow. The particles associated with this portion of the liquid travel downwards near the conical wall of the hydrocyclone, and are not centrifugally separated. Therefore, a fraction R_f of all particles irrespective of shape and size report to the underflow of the hydrocyclone. The fluid speed in the hydrocyclone is reduced due to increased viscous drag at higher viscosities, and this causes an increase in R_f.

Viscosity of the suspension certainly influences the separation mechanism of the hydrocyclone and should be addressed in the formulation of models depicting d_{50} size. The purpose of the test plan was to collect the data needed to modify the Lynch and Rao hydrocyclone model, which was developed under plant condition, to predict cut size not only from changes in percent solids, but also due to changes in slurry viscosity originating from factors other than percent solids (such as temperature, chemical environment, etc.). During all the tests conducted the slurry rheology was Newtonian.

EXPERIMENTAL WORK

Hydrocyclone Test Rig

A line diagram of the hydrocyclone test rig is shown in Figure 2. A Krebs hydrocyclone of the following dimensions was used for all the experiments:

Hydrocyclone diameter:	10.2 cm (4")
Feed inlet diameter:	3.0 cm
Vortex finder diameter:	3.8 cm
Apex diameter:	2.2 cm

The hydrocyclone overflow and underflow discharged freely into a sample cutter designed to remove both samples for precisely the same time interval. When sampling was not being carried out the products were recombined and returned to the slurry tank. Temperature was monitored by a thermocouple in the slurry tank, and feed inlet pressure was monitored with a diaphragm-type pressure gauge. A vibrating sphere viscometer along with a specially designed sample holder to avoid slurry settling was installed in the circuit to monitor slurry viscosity.

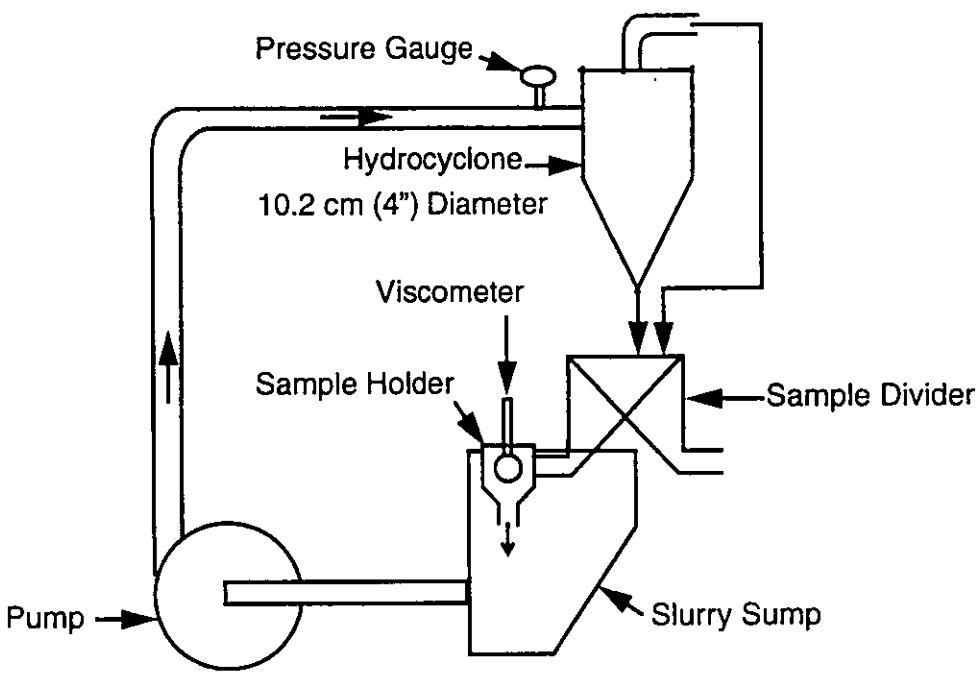

Fig.2 Line diagram of the hydrocyclone test rig. A 10.2 cm Krebs hydrocyclone was used. The vibrating sphere viscometer was used on-line to measure slurry viscosity.

Test Material

Silica sand from the Ottawa Sand Co., Ottawa, Illinois, was procured for this experiment. Particle size distribution of this sample is shown in Figure 3. The sample had an 80% passing size of 65μm.

Test Procedure

The test rig was filled with slurry of the desired solids content, and the hydrocyclone was operated at a constant inlet pressure of 69KPa (10 psi). Between samples, several minutes were allowed for the system to stabilize. Slurry temperature was continuously varied from 55°C to 10°C, with samples taken at 10°C intervals. Tests were conducted with slurries of 19%, 26%, 35%, and 40% solids by weight. Samples were weighed, filtered, dried, and size distributions were determined using a Leeds and Northrup Microtrac particle size analyzer.

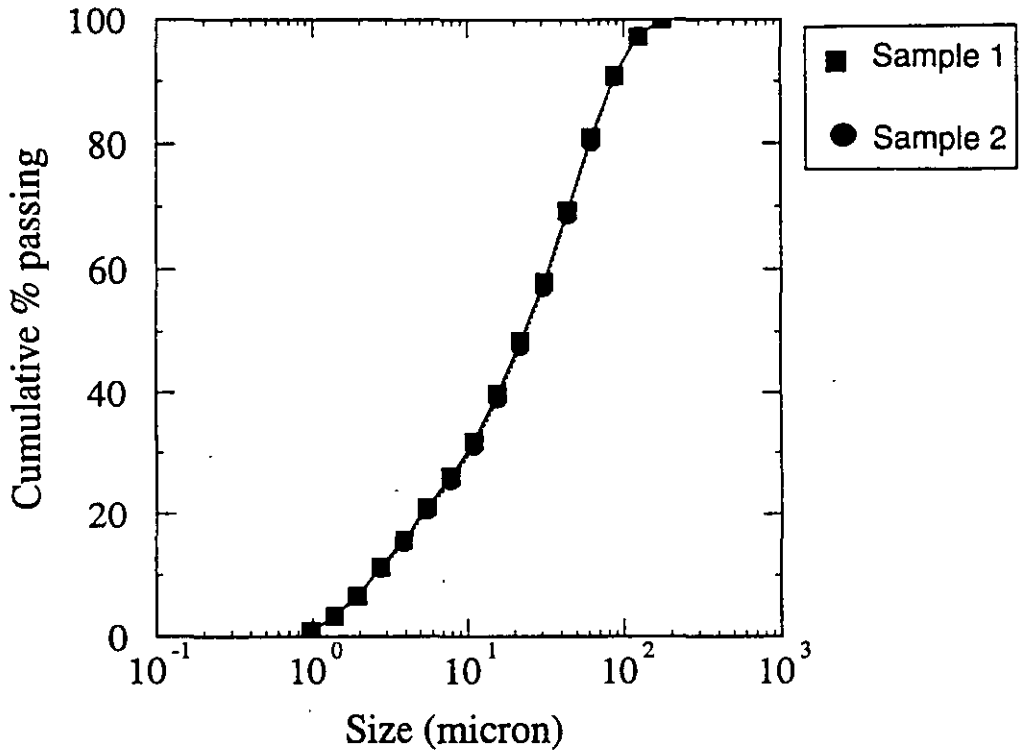

Fig.3 Size distribution of duplicate silica sample. The sample had a d_{80} passing size of 65 μm.

RESULTS AND DISCUSSION

Development of the Mathematical Model to Predict $d_{50}(c)$ Size

A modified model for $d_{50}(c)$ size was formulated by first introducing a viscosity term and then changing the percent solids term in the Lynch and Rao model [5, 12]. The viscosity term for the modified Lynch and Rao model was determined by plotting $d_{50}(c)$ vs. viscosity in a log-log scale (Figure 4). From this graph it was determined that the $d_{50}(c)$ size is proportional to the 0.35th power of the slurry viscosity, i.e.

$$d_{50}(c) \propto \eta^{0.35} \tag{2}$$

In the modified Lynch and Rao model a different percent solids term was used. This was necessary because higher percent solids not only increases the slurry viscosity but also causes hindered settling, and underflow crowding. These in turn increases the d_{50} size. In the original Lynch and Rao model this term was given as "$0.0173 \cdot \phi_w$." In the modified Lynch and Rao equation the percent solid term was found to be "$0.41 \log 10\ \phi_v$." The models before and after these corrections are given below.

(A) Lynch and Rao model before viscosity and percent solids correction:

$$\log_{10} d_{50}(c) = 0.0173 \cdot \phi_w - 0.0695 \cdot Spig + 0.0130 \cdot VF + 0.0048 \cdot Q + K_1 \tag{3}$$

Where,

K_1 = a constant
VF = inside diameter of the overflow or vortex finder, cm
Spig = inside diameter of underflow or spigot of the hydrocyclone, cm
Q = feed flow rate of slurry, liter/min
$d_{50}(c)$ = corrected cut size of the hydrocyclone, micron
ϕ_w = weight percent solids in the feed slurry

The flow rate Q in the above equation can be measured by a flowmeter or can be determined by the following equation [12]:

$$Q = K_2 \cdot VF^{0.73} \cdot Inlet^{0.86} \cdot P^{0.42} \quad (4)$$

Where,
K_2 = a constant
Inlet = Inlet diameter, cm
P = pressure at the inlet of the hydrocyclone, kilopascal

(B) Modified Lynch and Rao model after introducing the viscosity term:

$$\log_{10} d_{50}(c) = 0.41 \log_{10} \phi_v - 0.0695 \cdot Spig + 0.0130 \cdot VF + 0.0048 \cdot Q + 0.35 \log_{10} \eta + K_3 \quad (5)$$

Where,
K_3 = a constant
ϕ_v = volume percent solids in the feed slurry
η = viscosity of the feed slurry, centipoise

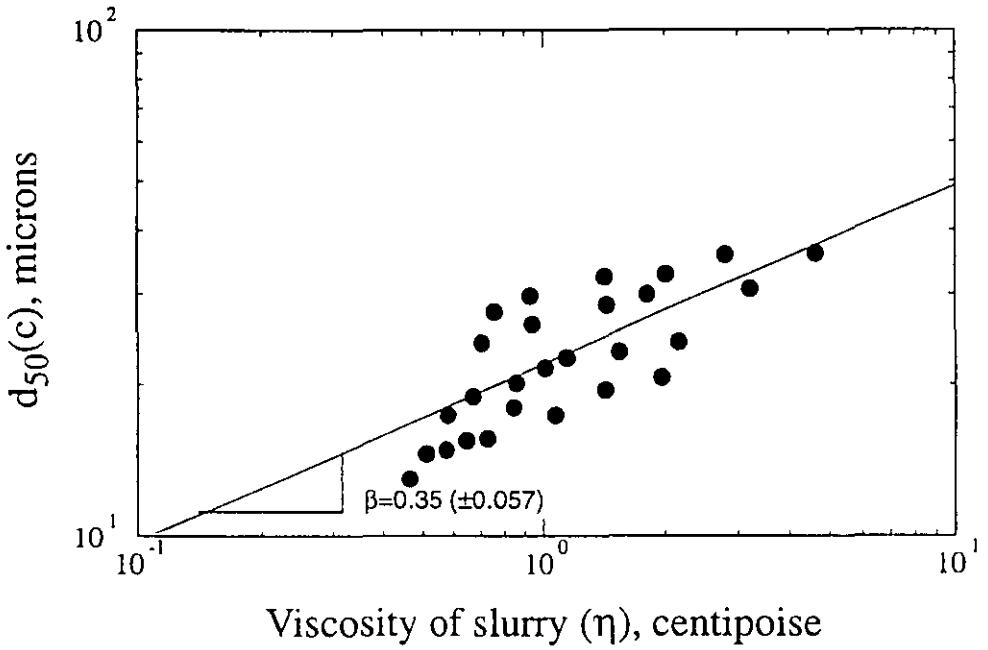

Fig.4 Observed $d_{50}(c)$ size vs. viscosity (η) to determine the exponent of viscosity in the modified Lynch and Rao model. Since $d_{50}(c) \propto \eta^{\beta}$, a linear relationship between the two is obtained by plotting them in a log-log scale (i.e $\log d_{50}(c) = \beta \log \eta + C$). The slope ($\beta$) of the regression line drawn through the above points shows that $d_{50}(c)$ is proportional to the 0.35th power of the viscosity of slurry. The standard error of β is 0.057.

Predicted $d_{50}(c)$ vs. observed $d_{50}(c)$ sizes for silica-water slurry from both the models (given by Eqs 3 and 5) are shown in Figures 5 and 6 respectively. As can be seen from Figure 5, the observed $d_{50}(c)$ size increased in each percent solids range due to the change in viscosity resulting from changing temperature. This was not predicted by the Lynch and Rao model. The reason for this is that the Lynch and Rao model accounts only for slurry viscosity changes from changes in solids percentage, and it does not take into account the viscosity changes from other sources (in this case temperature). In Figure 6, the change in $d_{50}(c)$ from both temperature and percent solids is predicted by using the modified Lynch and Rao model (Eq 10).

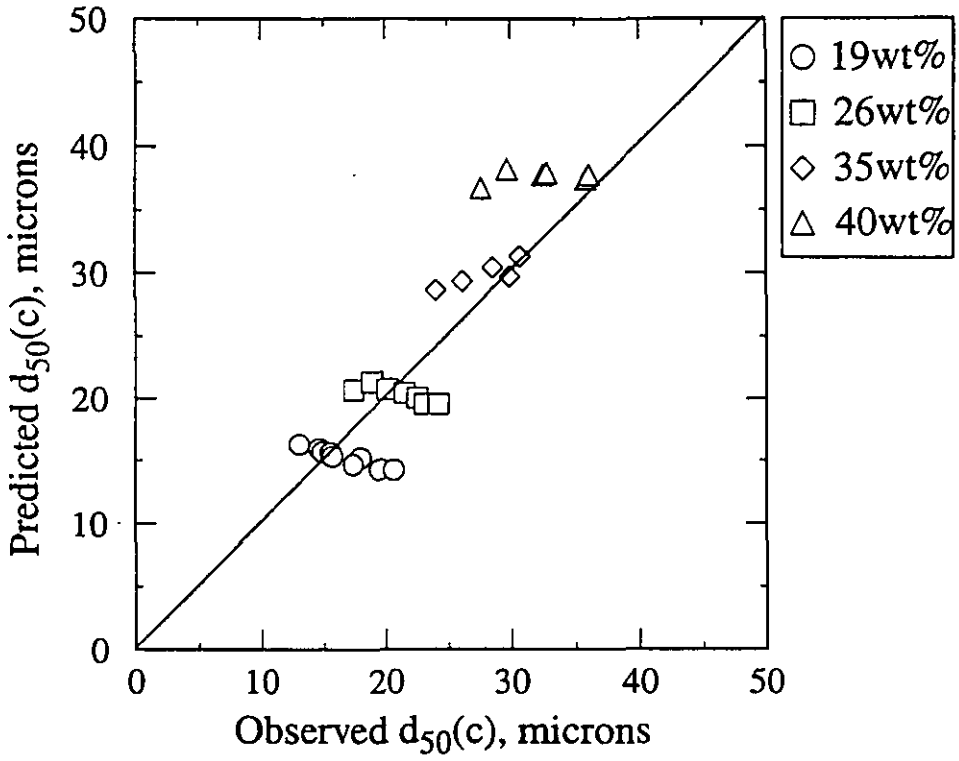

Fig.5 Predicted $d_{50}(c)$ size from Lynch and Rao equation vs. observed $d_{50}(c)$ size. The change in observed $d_{50}(c)$ size within each solids percentage range is due to viscosity changes from changes in temperature. Since Lynch and Rao model does not include a separate viscosity term, the predicted $d_{50}(c)$ size in individual percent solids range did not change.

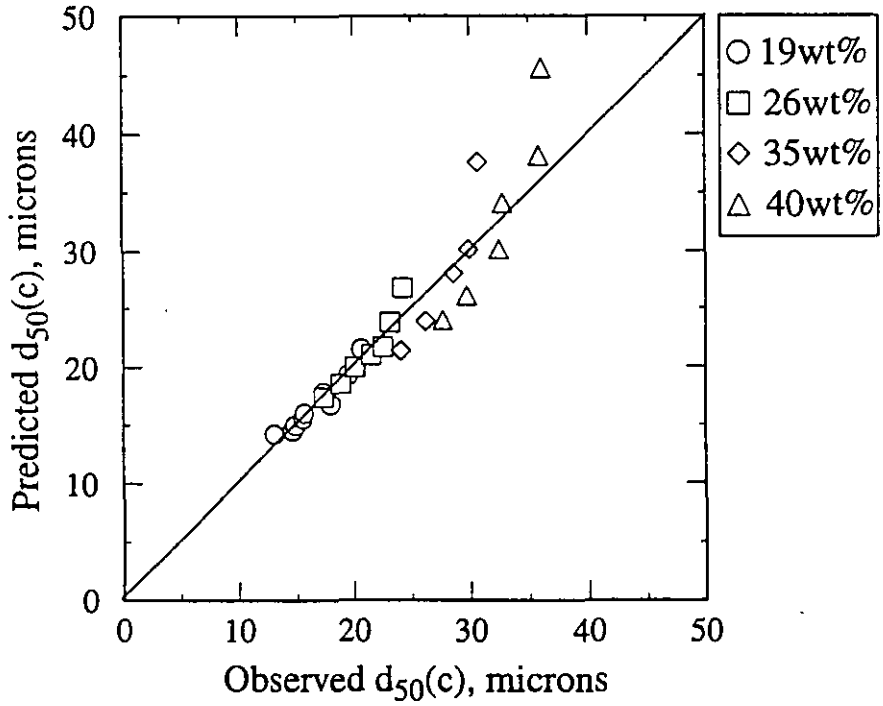

Fig.6 Predicted $d_{50}(c)$ size from the new equation vs. observed $d_{50}(c)$ size. Since this equation utilizes the viscosity data obtained by direct measurement, the increase in $d_{50}(c)$ size due to viscosity changes from both increase in solids content and changes in temperature (10°C to 50°C at individual percent solids range) is reflected.

The importance of direct measurement of viscosity is again seen from Figure 7. The data for this graph were obtained from tests conducted by Agar and Herbst [1]. They changed the viscosity of the liquid by sucrose addition. Agar and Herbst did not provide the dimensions of the vortex finder (VF) and the spigot (Spig), but these were known to be held constant. Therefore, Eqs 3 and 5 were condensed to the following forms respectively:

From Lynch and Rao model:

$$\log_{10} d_{50}(c) = 0.0173 \cdot \phi_w + 0.0048 \cdot Q + K_4 \tag{6}$$

From the modified Lynch and Rao model:

$$\log_{10} d_{50}(c) = 0.41 \log_{10} \phi_v + 0.0048 \cdot Q + 0.35 \log_{10} \eta + K_5 \tag{7}$$

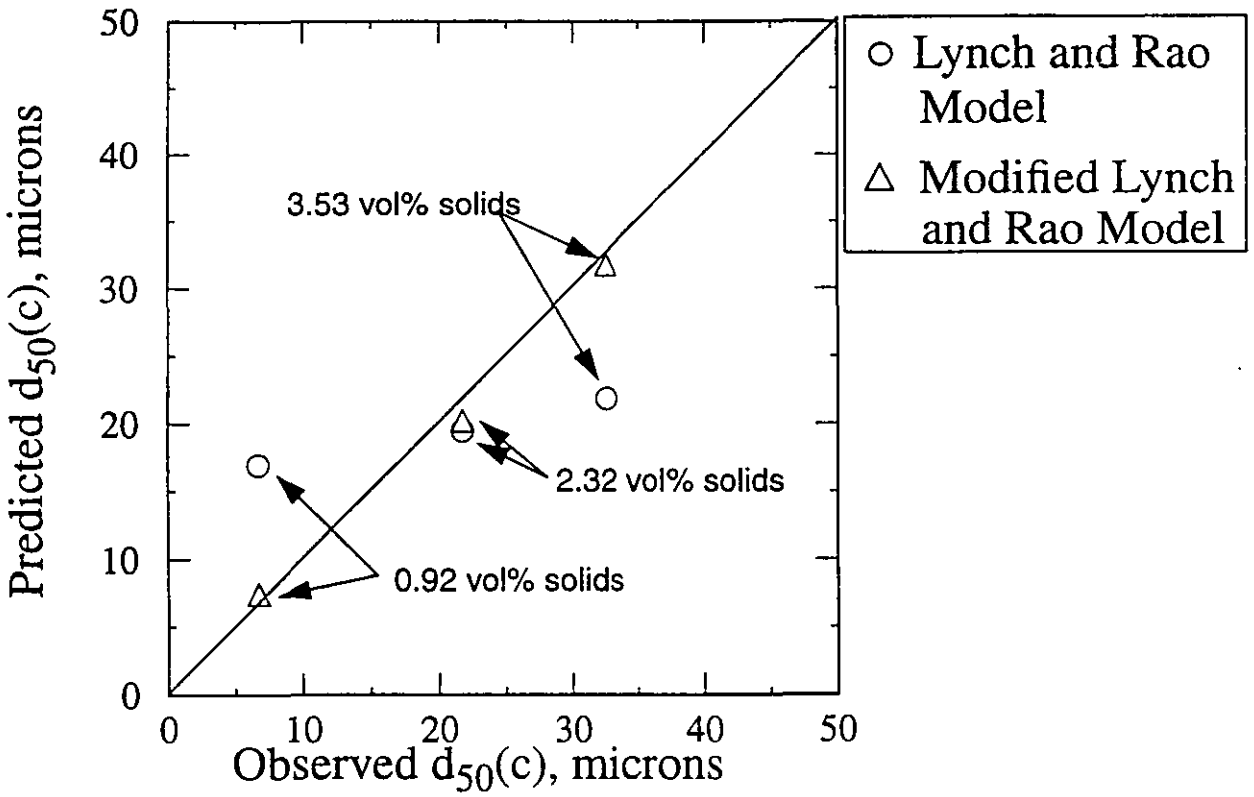

Fig.7 Predicted $d_{50}(c)$ sizes from both Lynch and Rao original model and the new modified model vs. observed $d_{50}(c)$ sizes for silica-sugar solution mixtures. These data were obtained from tests conducted by Agar and Herbst (1966). The increase in viscosity in these tests are primarily due to increase in sugar concentrations in the pulp. Since the modified Lynch and Rao model is based on direct measurement of viscosity, predicted values from this model agree well with the observed values. However, Lynch and Rao model infers viscosity from percent solids and so the changes in viscosity due to sugar addition did not reflect in his equation.

In their study, Agar and Herbst [1] measured the liquid viscosity instead of the pulp-viscosity. Since the solids concentrations were very low (< 4vol%), liquid viscosity did not differ much from the pulp viscosity, and these values were used to predict $d_{50}(c)$ size from the modified Lynch and Rao model. Here again the cut size could not be predicted by using the Lynch and Rao model which uses solids content alone. But by using the viscosity term in the modified Lynch and Rao model the $d_{50}(c)$ size could be calculated precisely, and predicted values and observed values are in close agreement to each other.

Effect of viscosity on water-to-underflow term, R_f

As can be seen from Figure 8, for slurries with 19, 26, and 35 wt% solids, R_f increased by as much as six percent when the viscosity of the slurry was increased by 2-3 centipoise. For the slurry with 40 wt% solids the change was rather less noticeable, at less than three percent for a 6 centipoise change in viscosity.

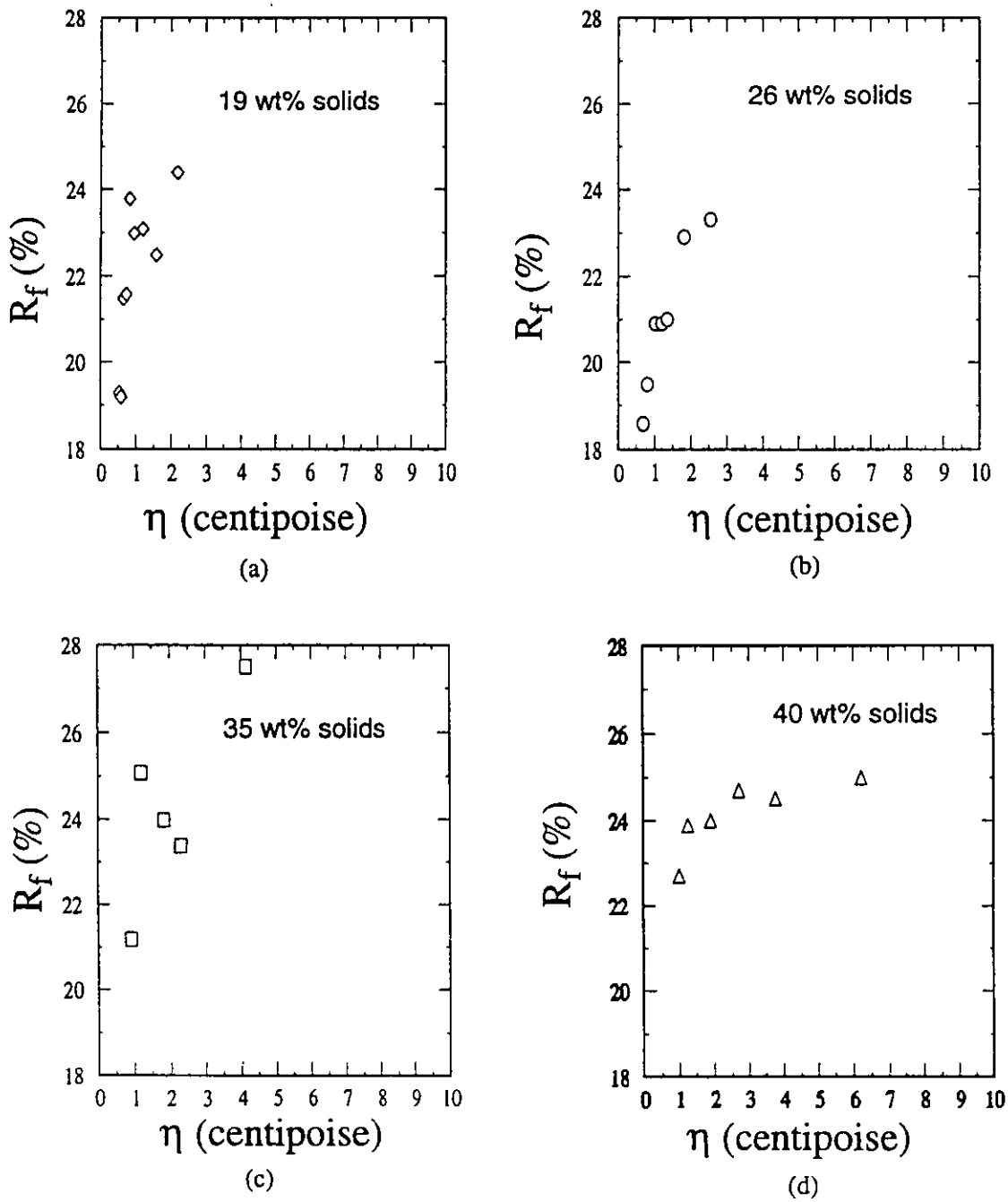

Fig.8 Effect of viscosity (η) on the water-to-underflow ratio (R_f). In each percent solids range, R_f increased with increase in η.

Effect of viscosity on classification index

Figure 9 gives the reduced efficiency curve for all the tests at 4 different concentrations and varied viscosities. The slope of this curve, called the classification index (α) is given by the following equation [12]:

$$y = \frac{e^{\alpha x} - 1}{e^{\alpha x} + e^{\alpha} - 2} \tag{8}$$

Where,

y = size fraction reporting to underflow
x = $d/d_{50}(c)$
α = classification index

From Figure 9 it is seen that viscosity has limited effect on the shape of the reduced efficiency curve. It is noted that there is some scattering of data in this graph.

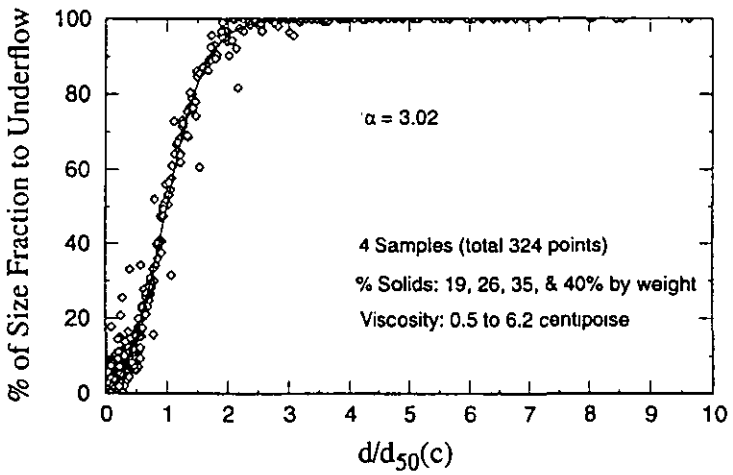

Fig.9 Reduced efficiency curve from all the tests. This graph shows that slurry viscosity has no significant effect on the sharpness of classification.

CONCLUSIONS

The following conclusions were drawn from this study:

(1) Viscosity of the slurry can change due to reasons other than changes in percent solids, such as temperature, size distribution, chemical environment, etc. Therefore, in addition to the percent solids term, a viscosity term must be considered when formulating models for hydrocyclone cut size.

(2) The following model, which was developed by modifying the Lynch and Rao model, can be used to predict $d_{50}(c)$ size more precisely:

$$\log_{10} d_{50}(c) = 0.41 \log_{10}\phi_v - 0.0695 \cdot Spig + 0.0130 \cdot VF + 0.0048 \cdot Q + 0.35 \log_{10}\eta + K_3$$

This model developed was verified by the experimental results obtained at Michigan Technological University where viscosity was varied by changes in both temperature and solids content. The modified Lynch and Rao model was also confirmed to predict $d_{50}(c)$ very well for data available in the literature where viscosity was varied by addition of sucrose. The model is therefore well suited for the many situations where factors other than slurry solids content are affecting the slurry viscosity.

(3) Slurry viscosity has no significant effect on the reduced efficiency curve of the hydrocyclone. However, water to underflow ratio increased with increase in slurry viscosity. This was a result of increasing drag forces acting on particles as the slurry viscosity increased.

REFERENCES

1. Agar, G.E. & Herbst, J.A., The Effect of Fluid Viscosity on Cyclone Classification. *Trans. AIME*, **235**, 145–149 (1966).
2. Kawatra, S.K. & Eisele, T.C., Rheology effects in Grinding Circuits. *XVI International Mineral Processing Congress*, Elsevier Science Publishers B. V., Amsterdam, 195–207 (1988).
3. Plitt, L.R., A Mathematical Modelling of the Hydrocyclone Classifier. *CIM Bulletin 69*, **776**, 114–123 (1976).
4. Plitt, L.R. & Kawatra, S.K., Estimating the Cut (d_{50}) Size of Classifiers Without Product Particle—Size Measurement. *International Journal of Mineral Processing*, **5**, 364–378 (1979).
5. Lynch, A.J. & Rao, T.C., Modelling and Scale-Up of Hydrocyclone Classifiers. *The XI International Mineral Processing Congress*, Cagliari, 245–269 (1975).
6. Schack, C.H., Dean, K.C. & Molly, S.M., Measurement and Nature of the Apparent Viscosity of Water Suspensions of Some Common Minerals. *Report of Investigation 5334, U. S. Bureau of Mines*, (1957).
7. Kawatra, S.K. & Bakshi, A.K., On-Line Viscometry in Particulate Processing. *Mineral Processing and Extractive Metallurgy Review*, **14**, 249–273 (1995).
8. Bradley, D., *The Hydrocyclone*, Pergamon Press, New York, NY (1965).
9. Lilge, E.O., Fundamentals of Hydrocyclone. *Trans. Inst. Min. and Metll.*, **71** 285–337 (1962).
10. Klimpel, R.R., Slurry Rheology Influence on the Performance of Mineral/Coal Grinding Circuits. *Mining Engineering*, **34**(12), 1665–1668 (1982).
11. Kawatra, S.K. & Bakshi, A.K., Determination of Flow Behavior Changes in Mineral Suspensions, in the annual meeting of the *Society for Mining, Metallurgy, and Exploration*, Inc., Denver, CO, Preprint No. 95-33 (1995).
12. Lynch, A.J., *Mineral Crushing and Grinding Circuits*, Vol. 1, Elsevier/North-Holland Inc., New York, NY 10017 (1977).

NOMENCLATURE

Inlet	inside diameter of the hydrocyclone inlet, cm
VF	inside diameter of the overflow or vortex finder, cm
Spig	inside diameter of underflow or apex of the hydrocyclone,
ϕ_w	weight percent solids in feed
ϕ_v	volume percent solids in feed
D_c	inside diameter of the hydrocyclone at the bottom of the vortex finder, cm
R_c	radius of the hydrocyclone, cm
F_C	centrifugal force
F_D	drag force
S	shear rate, sec^{-1}
V_t	tangential velocity of the fluid
W	radial velocity of the fluid
Q	feed flow rate of slurry, liters/minute
P	feed pressure, kilopascal
R_f	water-to-underflow ratio
K_1, K_2, K_3, K_4, K_5,	constants
d	diameter of the particle, micron
ρ_s	density of solid, gm/cm^3
ρ_l	density of liquid, gm/cm^3
η	viscosity of slurry, centipoise
β	exponent of slurry viscosity
α	classification index

Influence of temperature on the energy efficiency of an industrial circuit processing iron ore

S.K. Kawatra and T.C. Eisele

Abstract—*In many mining operations, particularly northern open-pit mines, large seasonal variations in grinding slurry temperature can occur. It is shown in this paper that this temperature shift can cause a winter-time loss in autogenous grinding efficiency of as much as 20% if it is not controlled. Laboratory experimentation indicates that much of this effect is due to increases in slurry viscosity as the temperature is decreased. An additional effect may result from changes in rock strength upon freezing, for which possible mechanisms are discussed. However, no effect clearly resulting from rock strength changes has been definitely confirmed.*

Introduction

A great many excellent studies of the autogenous grinding process have been conducted since its development (Digre, 1979a and 1979b; Forssberg and Ekblom, 1979; Manlapig, Seitz and Spottiswood, 1979; Turner, 1979; Mokken, 1978; Stanley, 1974; Moys and Loveday, 1979; Rowland, 1981; Tangsathitkulchai and Austin, 1985; Austin, Klimpel and Luckie, 1984), allowing substantial improvements in autogenous milling performance. Nevertheless, the influence of temperature, viscosity and rheology on grinding circuit performance has largely been ignored, due both to the belief that it is of no consequence and to the expense of controlling the temperature of the mill feed. However, when the temperature approaches the freezing point of water, substantial changes in slurry rheology occur, and these changes would be expected to alter mill and hydrocyclone performance. This has been confirmed in the case of hydrocyclones (Kawatra et al., 1988 and 1989) and would be expected to be true for rod and ball mills as well (Austin, Klimpel and Luckie, 1984; Kawatra and Eisele, 1988). However, the rheology of mineral suspensions is difficult to measure (Cheng, 1984, Jinescu, 1974; Klimpel, 1982a and 1982b), particularly in real time and is therefore not used as a grinding circuit control parameter.

In addition to the rheological effects, any changes in the mechanical properties of the rock being ground, such as the hardness and fracture toughness, would also have an effect (Vitton, 1978). Mechanical changes in the rock would have the greatest effect on autogenous mill performance, as the grinding competency of the media-sized rock particles could be altered (Rowland, 1988). In extremely cold conditions, ice forms on the surface of the rock as it enters the mill, substantially changing the performance of the mill.

To understand the relative importance of each of these factors, and thus allow improved operating efficiency for grinding circuits, a study is being conducted at MTU of the effects of temperature on autogenous grinding. This study includes analysis of operating plant data, laboratory-scale experiments and pilot-scale grinding tests.

S.K. Kawatra and **T.C. Eisele**, members SME, are professor and graduate student, respectively, with Michigan Technical University, Metallurgy Dept., Houghton, MI. SME preprint 90-8, SME Annual Meeting, Salt Lake City, UT, Feb 26-March 1, 1990. M&MP paper 90-606. Manuscript July 24, 1989. M&MP paper 90-606. Discussion of this paper must be submitted, in duplicate, prior to June 1, 1991.

Theory

The effects of temperature on autogenous grinding can be immediately divided into rheological effects and mechanical effects. The rheological effects are a result of the substantial increase in the viscosity of water as the freezing point is approached. The change in apparent slurry viscosity that results from changing temperature is shown in Fig. 1. As can be seen, the effect at high percent solids is very pronounced, particularly when the temperature is quite low. This increased viscosity acts to cushion the impact of the media-sized particles, impede transport of slurry and in extreme cases cause the media to centrifuge at speeds well below the critical speed. The net result is decreased grinding rate and increased specific power consumption.

Effects resulting from changes in the mechanical properties of the rock are considerably more complicated, as they depend strongly on the specific characteristics of the rock. The major effect is a change in the mechanical strength, which alters the competency of the ore as grinding media.

One possible mechanism for strength changes with temperature is shown in Fig. 2. Here, the change is a result of water freezing in the pores and cracks of the rock, with the result depending on the degree of interconnections of the openings (Vitton, 1978). If the rock is very porous, as is the case with sandstone, the water can percolate freely through it and upon freezing form a continuous matrix that holds the rock together. This increases the fracture toughness of the rock and its competency as grinding media.

However, a hard, dense rock such as chert has relatively few, unconnected pores, which only collect water with difficulty. When the water in these pores freezes, frost cracking is likely to

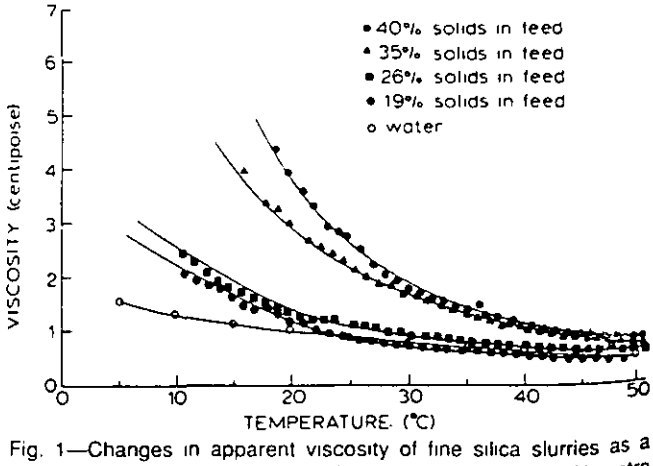

Fig. 1—Changes in apparent viscosity of fine silica slurries as a function of temperature. The viscosity was measured using a Nametre vibrating-sphere viscometer at an average shear rate of 4700 sec^{-1}, and the silica was 80% passing 270 mesh. The effect of temperature on apparent viscosity is most pronounced at high slurry solids contents and low temperatures.

occur around them, resulting in a slight weakening of the rock and a loss of grinding competency.

The effect of temperature on autogenous grinding is therefore highly variable and difficult to predict. No large effect is seen unless the water in the ore freezes, and this only occurs when the ore is exposed for some time before processing, as is the case in open-pit mines. An additional effect that can occur if the ore is seriously chilled is the formation of ice on the surface of the rock when it is added to the mill. The ice must then either melt or be ground away before grinding of the ore particle can commence, resulting in a reduced grinding rate. However, this requires both severely chilled ore and a near-freezing mill slurry, and should therefore not be a frequent problem.

For non-porous ores, each of these factors will result in a loss of autogenous milling efficiency. However, it has not been determined which of these phenomena is most important, or to what extent they reduce efficiency in real situations. In order to determine this, quantitative data are needed for both overall plant operation and for laboratory experiments designed to suppress all but one effect.

Plant studies

An iron ore processing plant that is subjected to large seasonal temperature variations was studied. This plant uses a fully autogenous grinding circuit, as shown in Fig. 3. Initially, plant personnel observed a significant seasonal variation in feed rate, as is illustrated in Fig. 4. This trend was observed for four years and so is unlikely to be entirely due to normal variations in ore characteristics. When com-

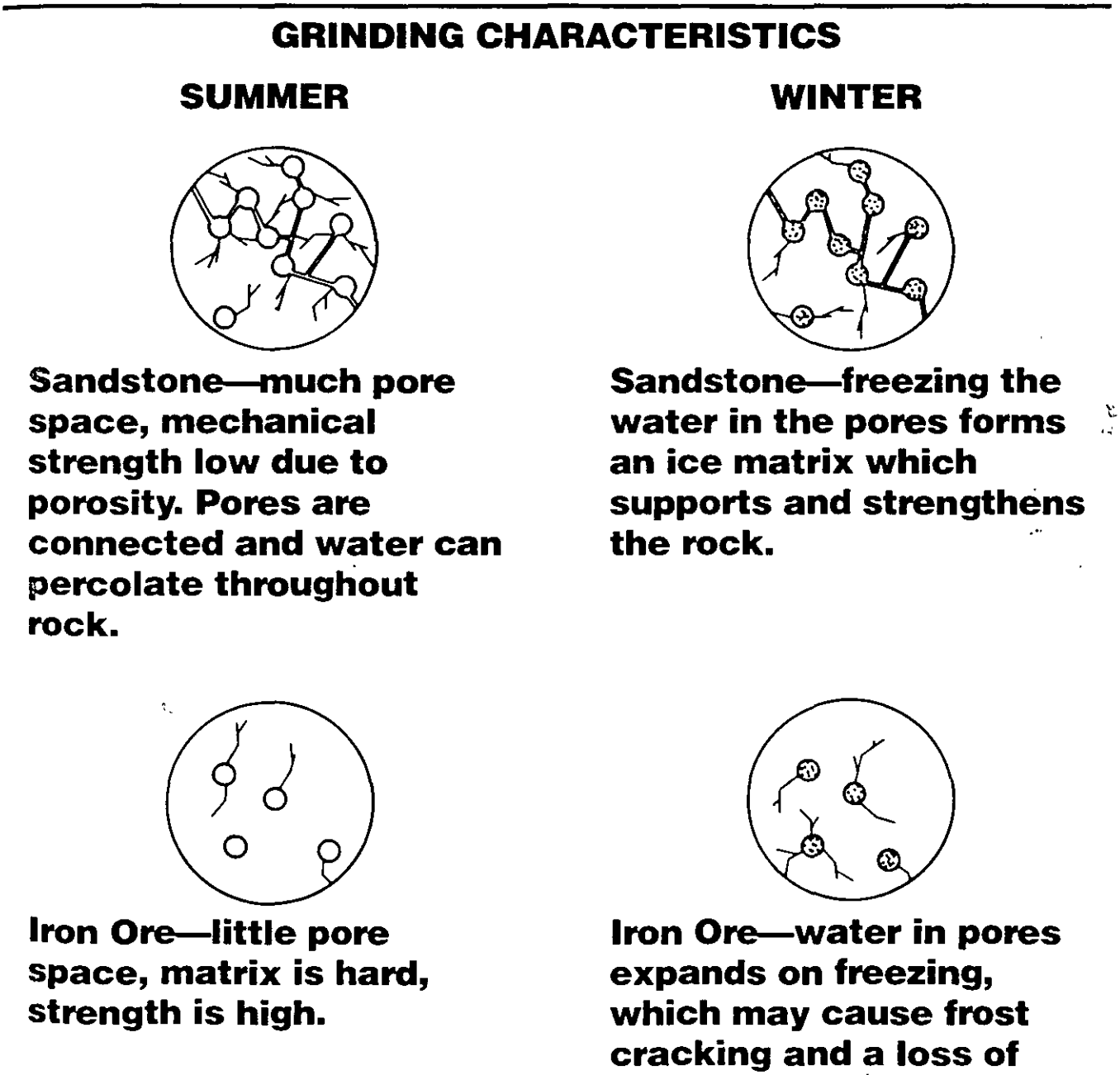

Fig. 2—Mechanism for changes in rock strength resulting from freezing of pore water. This effect is more important than changes in the hardness of the rock proper.

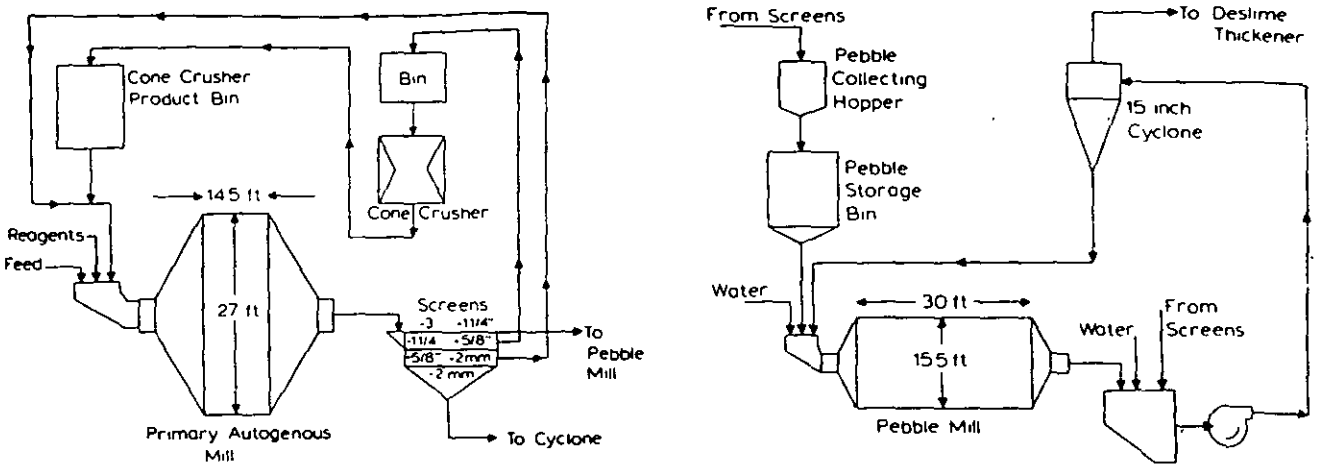

Fig. 3—Schematic of the grinding circuit discussed in this paper. The circuit is fully autogenous, with critical-size material crushed by a cone crushe to prevent buildup.

pared with measurements of the feed water temperature, which are also plotted in Fig. 4, it appears that the temperature effect is relatively slight until temperatures fall below 10° C. At temperatures below this value, the drop in throughput becomes quite pronounced.

Subsequently, the specific power consumption was computed for the primary, secondary and overall grinding circuits and plotted against the feed water temperature. Monthly averages were used to minimize the effects of variation in ore quality. The results for the primary autogenous mill are given in Fig. 5, where a pronounced decrease in specific energy consumption occurred as the temperature increased. A similar effect is shown in Fig. 6 for the pebble mill, although the trend is less pronounced. This is due to the warming of the pulp in the primary mill, which reduces the temperature fluctuation seen by the pebble mill. The overall result for the circuit is as shown in Fig. 7, which shows a total seasonal efficiency variation of 18% in the course of a year.

In addition to the efficiency measurements, plant personnel observed that the quantity of critical-size material circulated to the crusher increased in the winter, as indicated by Fig. 8 (Rowland, 1988; Kampe, 1988). This indicates that coarse rock may be more readily shattered at lower temperatures. Since large rocks are needed for effective autogenous grinding, the increased rate at which they are shattered into relatively ineffective critical-size material when the temperature is lowered results in reduced grinding efficiency. However, it is not clear whether this is due to changes in rock strength or to changes in the transport characteristics in the mill arising from rheological effects.

Laboratory studies

Laboratory tests were carried out primarily to determine the extent to which rheology alone would be expected to affect autogenous grinding. These experiments used a 20-cm-diam x 30-cm-long mill, rotating at 64 rpm with four 0.5-cm lifter bars. The mill and ore charge were heated in a forced-air drying oven for elevated temperature experiments and chilled using a freezer and an ice-water bath for low-temperature experiments. Polyurethane foam insulation was used to help keep the mill at a uniform temperature.

The results of initial experiments using Jacobsville sandstone have been previously reported (Kawatra et al., 1989). Further experiments were conducted using an iron ore sample from a local mine. The ore was crushed and mulled to the size

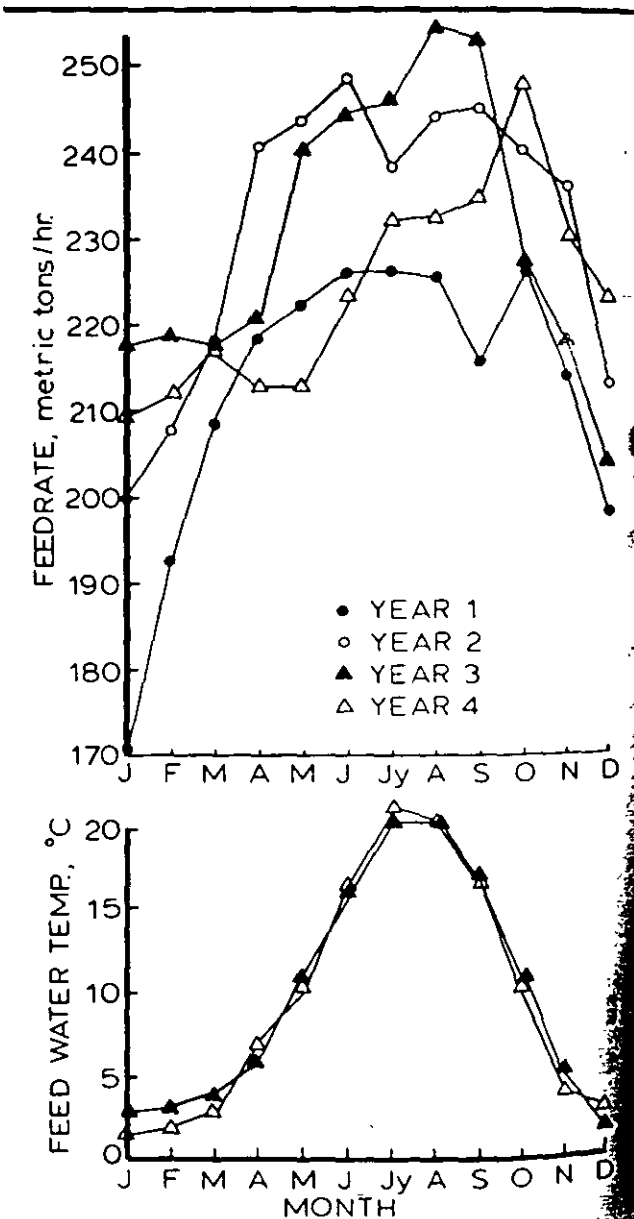

Fig 4—Seasonal variations in grinding circuit throughput rate compared to average monthly feed water temperatures. A consist seasonal trend is shown, with the greatest change in throug exhibited during those months when the water temperature dro below approximately 10° C.

Table 1—Size Distribution of Charges for Laboratory Grinding Experiments

Size, millimeters	wt.%
50.8x38.1	41.5
38.1x25.4	25.2
25.4x19.0	15.1
19.0x12.7	13.1
12.7x 9.5	5.1
−9.5	0.0
	100.0

distribution given in Table 1, and each experiment used a 5.0-kg charge in 2 L of water. Six experiments were conducted consisting of three sets of duplicate tests at 2°-9° C, 24°-26° C, and 84°-62° C. For each experiment, the ore, water and mill were adjusted to temperature, and the ore was ground for 30 min. The slurry viscosity and quantity of -100 mesh material were then determined, the -100 mesh material was returned to the mill, the temperature was readjusted and the cycle was repeated. Viscosity was measured using a Brookfield viscometer fitted with a UL adapter for low viscosity measurements. Results of these experiments are given in Table 2.

Plotting these data as in Fig. 9 again shows a definite dependence of fines production on temperature. However, when grinding rate is plotted against viscosity, as in Fig. 10, it is evident that some factor other than viscosity is responsible for a portion of the change in grinding rate.

Discussion

In a plant situation, uncontrolled temperature changes can produce sizable changes in milling efficiency. The plant

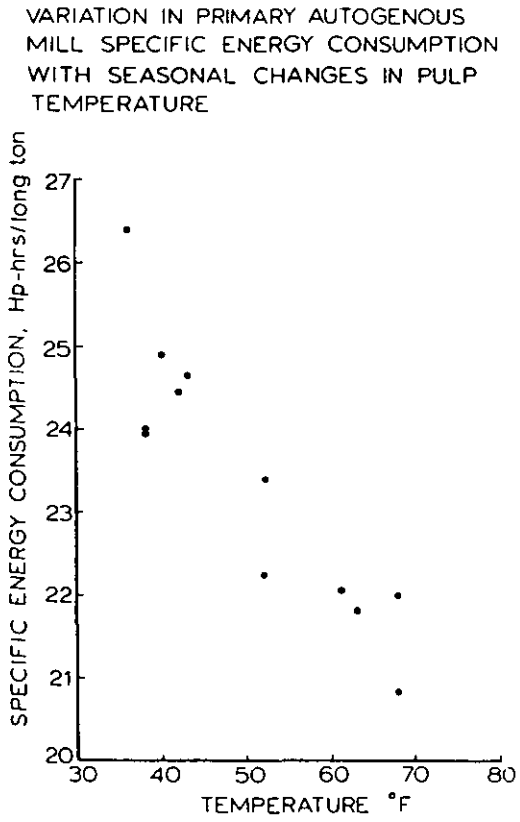

Fig. 5—Monthly change in specific energy consumption of the primary autogenous mill as a function of feed water temperature.

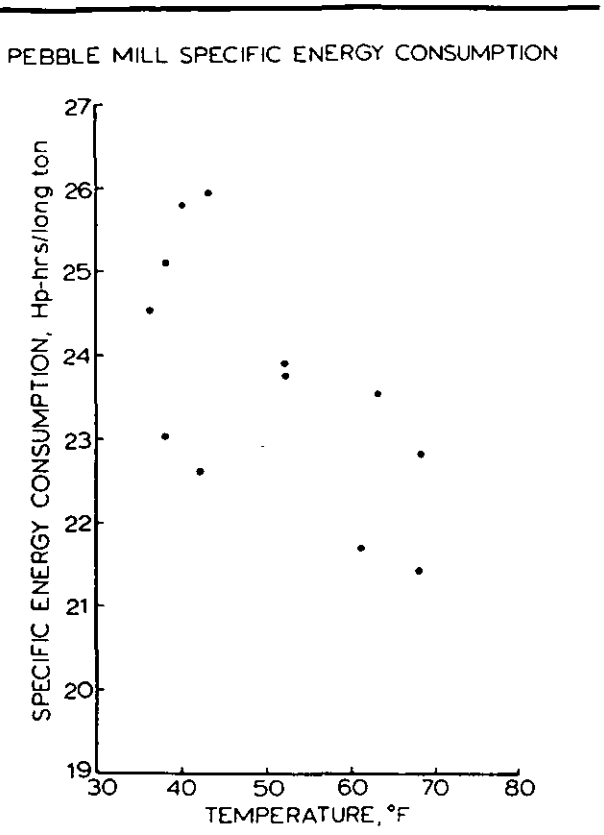

Fig 6—Monthly change in specific energy consumption of the pebble mill as a function of feed water temperature.

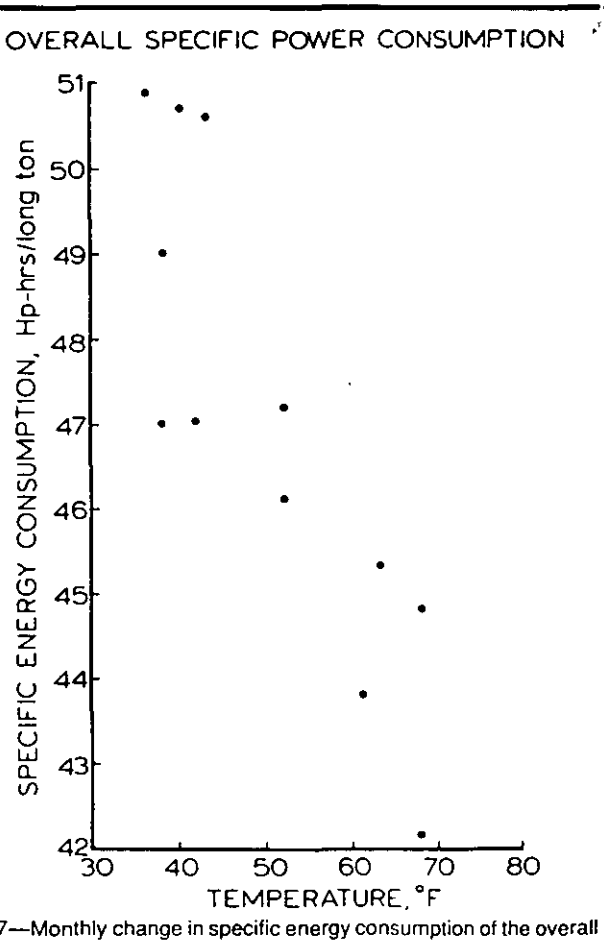

Fig. 7—Monthly change in specific energy consumption of the overall grinding circuit as a function of feed water temperature

Table 2—Results for Laboratory Grinding Experiements of Hematite Ore

	Grinding time (min.)	Temp. (°C)	Viscosity (cp)	Shear Rate (sec^{-1})	-100 mesh product (grams)
	30	4-9	1.57	73.42	69
	60	2-7	1.74	73.42	126
Test	90	2-9	1 82	73.42	178
1-1	120	2-7	1.93	73.42	206
	150	2-7	1 99	73 42	230
	180	2-6	2.18	73.42	248
	30	24-25	1.05	73.42	76
	60	26	1 23	73 42	145
Test	90	25	1 42	73.42	197
1-2	120	25	1.61	73.42	249
	150	25	1.78	73 42	289
	180	25	1.92	73.42	327
	30	83-64	0.83	73.42	85
	60	84-64	0.90	73.42	155
Test	90	84-64	0.97	73.42	218
1-3	120	84-64	1 02	73 42	281
	150	84-62	1 17	73.42	327
	180	84-63	1.28	73.42	366
	30	2-7	1 66	73 42	67
	60	2-8	1.72	73 42	122
Test	90	2-10	1.78	73.42	176
2-1	120	2-7	1.90	73.42	200
	150	2-6	2.02	73.42	227
	180	2-7	2.15	73.42	255
	30	24-25	1.06	73.42	79
	60	24-25	1.24	73.42	144
Test	90	25	1.43	73 42	195
2-2	120	25	1 62	73 42	248
	150	25	1.80	73.42	290
	180	25	1 94	73 42	329
	30	84-65	0.85	73.42	86
	60	84-65	0.90	73.42	157
Test	90	84-64	0 96	73 42	219
2-3	120	84-64	1 02	73 42	280
	150	84-63	1 15	73.42	325
	180	84-64	1.27	73 42	364

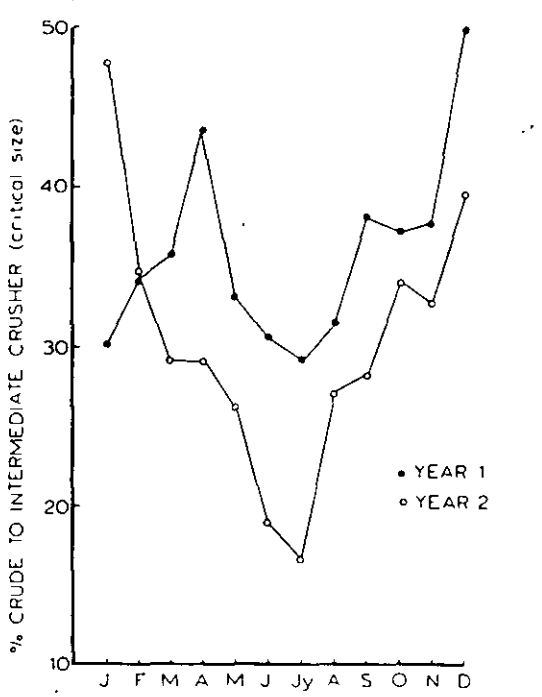

Fig 8—Monthly variation in critical-size production as measured by the tonnage of material circulated to the crusher

data presented here show a seasonal efficiency shift of approximately 18% for the overall circuit and more for the primary autogenous mill alone. It is difficult to be completely certain of the precise mechanism, but it is likely that most of the effect is due to viscosity changes It is seen that the temperature effect is much less pronounced in the pebble mill, but this is almost certainly due to the warming that occurs in the primary mill and not to inherently lower temperature sensitivity in the pebble mill. The change in production of critical-size material in the primary mill may be a result of changing rock strength, but it is possible that increasing viscosity forces the media-size particles to migrate to those portions of the charge where the impacts are most severe, causing them to break up more rapidly (Rowland, 1988). The seasonal shifts of mill throughput show clearly that the greatest change occurs at temperatures below about 10° C. It is therefore evident that simply maintaining the temperature above this point will greatly reduce the seasonal throughput variation. This may be accomplished by prevent-

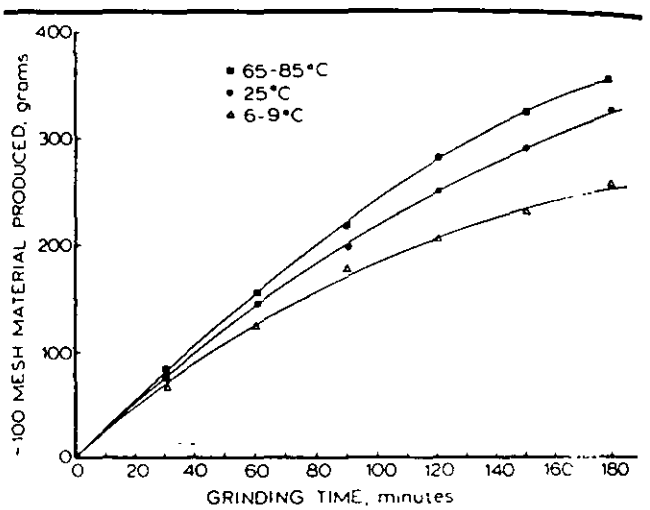

Fig 9—Variation in laboratory-scale fines production as a function of time and temperature for an iron ore The behavior of the non-porous iron ore is very similar to that of the porous sandstone.

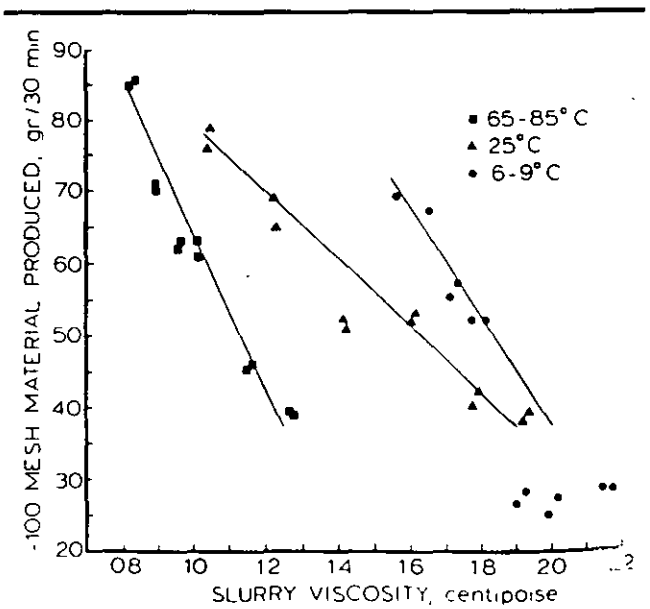

Fig. 10—Grinding rate vs viscosity for the six laboratory-scale iron ore grinding experiments. While decreasing the viscosity produces an increase in the grinding rate, this is obviously not the only effect occurring in these experiments.

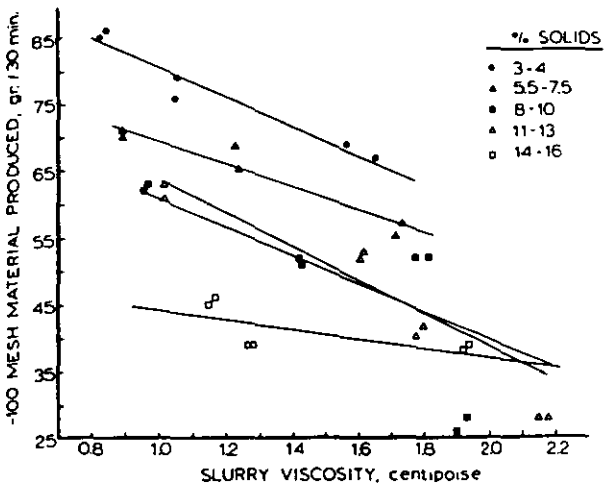

Fig. 11—Viscosity vs. grinding rate for the six laboratory-scale grinding experiments, correlating those measurements that contained similar amounts of -100 mesh fines. The listed percent solids ranges represent the ratio of -100 mesh material to water. The resulting lines are roughly parallel, indicating that buildup of fines is responsible for the drop in grinding rate with time.

ing the recycle water from being chilled and by thawing the ore before grinding.

From the laboratory experiments, it is readily seen that the changes in grinding rate are closely tied to slurry viscosity. However, in these experiments the viscosity was not the only factor influencing fines production, as shown in Fig. 10. If viscosity were the only relevant factor, tests for all three temperatures should have followed the identical grinding rate vs. viscosity curve. The second factor appears to be the quantity of fines in the suspension, as plotting grinding rate vs. viscosity for only those tests with similar quantities of fines generates a series of roughly parallel lines as in Fig. 11. It is likely that as the fines are accumulating, work is being expended to make the fines finer rather than generating additional fines. It is also possible that the increasing slurry density is cushioning the impacts due to increased buoyancy, thus further retarding the grinding rate.

Conclusions

From this investigation, the following conclusions are drawn:

1. In autogenous milling, temperature can significantly influence the grinding efficiency, particularly if the temperature falls below about 10° C. These efficiency changes can be reduced by preventing recycle water from becoming chilled, and by thawing frozen rock before grinding. Since the magnitude of the efficiency change is reduced at higher temperatures, heating the mill slurry to higher temperatures is unlikely to provide significant benefits.

2. Laboratory experiments indicate that the effect of slurry rheology changes with temperature is a significant factor in the grinding rate for both porous and non-porous rock types, with higher temperatures resulting in reduced viscosity and hence increased grinding rate.

Acknowledgements

This research has been supported by the Department of the Interior's Mineral Institute Program administered by the Bureau of Mines through the Generic Mineral Technology Center for Comminution under grant number G1175149.

References

Austin, L.G., Klimpel, R.R., and Luckie, P T , 1984, *Process Engineering of Size Reduction: Ball Milling*, SME-AIME, New York, pp 385-406

Cheng, D. C-H , 1984, "Further Observations on the Rheological Behavior of Dense Suspensions," *Powder Technology*, Vol 37, pp. 255-273

Digre, M , 1979a, "Autogenous Grinding in Relation to Abrasion Conditions and Mineralogical Factors," *Proceedings of the Autogenous Grinding Seminar*, Trondheim, Norway, Session A—Fundamentals, paper A1.

Digre, M , 1979b, "Autogenous Grinding Testing and Scale-Up," *Proceedings of the Autogenous Grinding Seminar*, Trondheim, Norway, paper F5

Forssberg, E., and Ekblom, K , 1979, "Experience of Autogenous Grinding in Sweden," *Proceedings of the Autogenous Grinding Seminar*, Trondheim, Norway, Session A—Fundamentals, paper A2

Jinescu, V V., 1974, "The Rheology of Suspensions," *International Chemical Engineering*, Vol 14, No 3, pp 397-420.

Kampe, H., 1988, personal communication

Kawatra, S K , and Eisele, T.C , 1988, "Rheological Effects in Grinding Circuits," *International Journal of Mineral Processing*, Vol. 22, pp 251-259

Kawatra, S.K., Eisele, T.C , Zhang, D X., and Rusesky, M T , 1988, "Effects of Temperature on Hydrocyclone Efficiency," *International Journal of Mineral Processing*, Vol 23, pp 205-211

Kawatra, S K., Eisele, T.C., Zhang, D.X., and Rusesky, M T , 1989, "Effects of Seasonal Temperature Changes on Autogenous Milling Performance," SME-AIME Meeting, Las Vegas, Nevada, Feb 27-March 2, 1989

Klimpel, R R , 1982a, "Slurry Rheology: Influence on the Performance of Mineral/Coal Grinding Circuits," *Mining Engineering*, December 1982, pp 1665-1668, and January 1983, pp 21-26.

Klimpel, R R , 1982b, "Laboratory Studies of the Grinding and Rheology of Coal-Water Slurries," *Powder Technology*, Vol 32, pp 267-277.

Mantapg, E.V., Seitz, R A , and Spottiswood, D.J., 1979, "Analysis of the Breaking Mechanism in Autogenous Grinding," *Proceedings of the Autogenous Grinding Seminar*, Trondheim, Norway, Session A—Fundamentals, paper A3

Mokken, A H., 1978, "Progress in Run-of-Mine (Autogenous) Milling as Originally Introduced and Subsequently Developed in the Gold Mines of the Union Corporation Group," *Eleventh Commonwealth Mining and Metallurgical Congress*, Hong Kong, Institution of Mining and Metallurgy.

Moys, M H , and Loveday, B K , 1979, "Autogenous Milling Research at the South African National Institute for Metallurgy," *Proceedings of the Autogenous Grinding Seminar*, Trondheim, Norway, paper F2.

Rowland, C A., 1981, "Pilot Plant Data for the Design of Primary Autogenous and SemiAutogenous Mills," *CIM Bulletin*, November 1981

Rowland, C A., 1988, personal communication.

Stanley, G G , 1974, "Mechanisms in the Autogenous Mill and Their Mathematical Representation," *Journal of the South African Institute of Mining and Metallurgy*, November 1974.

Tangsathitkulchai, C., and Austin, L G , 1985, "The Effect of Slurry Design on Breakage Parameters of Quartz, Coal, and Copper Ore in a Laboratory Ball Mill," *Powder Technology*, Vol 42, pp. 287-296

Turner, R R , 1979, "Primary Autogenous Grinding—A Study of Ball Charge Effects," *Proceedings of the Autogenous Grinding Seminar*, Trondheim, Norway, Session B—Mill and Mill Circuit Design, paper A4.

Vitton, S.J , 1978, "An Experimental Study of the Effects of Low Temperature on the Mechanical Properties of Iron Ore," unpublished M S thesis, Michigan Technological University.

SOCIETY FOR MINING, METALLURGY, AND EXPLORATION, INC.

P.O. BOX 625002 • LITTLETON, COLORADO • 80162-5002

PREPRINT

96-144

CHANGES IN AUTOGENOUS GRINDING PERFORMANCE DUE TO VARIATION IN SLURRY RHEOLOGY

A.K. Bakshi
K. J. Shoop
S. K. Kawatra

Michigan Technological University
Houghton, Michigan

For presentation at the SME Annual Meeting
Phoenix, Arizona — March 11-14, 1996

Permission is hereby given to publish with appropriate acknowledgments, excerpts or summaries not to exceed one-fourth of the entire text of the paper. Permission to print in more extended form subsequent to publication by the Society for Mining, Metallurgy, and Exploration (SME), Inc. must be obtained from the Executive Director of the Society.

If and when this paper is published by the SME, it may embody certain changes made by agreement between the Technical Publications Committee and the author so that the form in which it appears is not necessarily that in which it may be published later.

Current year preprints are available for sale from the SME, Preprints, P.O. Box 625002, Littleton, CO 80162-5002 (303-973-9550). Prior year preprints may be obtained from the Linda Hall Library, 5109 Cherry Street, Kansas City, MO 64110-2498 (800)662-1545.

PREPRINT AVAILABILITY LIST IS PUBLISHED PERIODICALLY IN MINING ENGINEERING

ABSTRACT

Slurry rheology affects autogenous grinding performance by changing the rock's breakage characteristics. In this study pilot scale batch autogenous grinding was carried out to observe the effect of viscosity on the breakage characteristics of the rocks (the media), and on the overall specific energy consumption. Clay/fines content, and temperature of the initial charge, were varied to alter the viscosity of the slurry. Results showed that at higher slurry viscosity, rocks became more difficult to break, resulting in an overall increase in the specific energy consumption of the mill. Also, it was observed that viscosity had a significant effect on the amount of critical size material present in the grinding circuit, where the critical size material is the material which is too large to be effectively ground in the mill, and too fine to act as grinding media.

INTRODUCTION

Slurry rheology has a significant effect on the performance of autogenous grinding. The rheology in an autogenous mill can change due to several factors. Percent solids has the most prominent effect on slurry rheology. As solids content increases, the viscosity of the slurry increases gradually to a point beyond which a small increase in solids content can cause a drastic increase in viscosity. Other factors, such as size distribution, slimes content, clay content, temperature change, and chemical additives also significantly change the slurry rheology.

The mechanism by which slurry rheology affects grinding has been discussed in the literature by many investigators (Hemmings and Boyes, 1977, Tucker 1982, Klimpel, 1982 and 1983, Fuerstenau et al., 1984, Austun et al., 1984, Moys, 1989, Kawatra and Eisele, 1988). These studies explain the effect of rheology on the load behavior, slurry hold-up, and grinding rates in a mill. At a given flow rate and grate design, viscosity is the most prominent factor which affect slurry hold-up (Moys, 1989). At low viscosity, the grinding media is not adequately covered with pulp, and results in a loss of the impact energy. On the other hand, at very high viscosity there is excess pulp in the interstitial spaces of the media. This restricts the free movement of the media and cushions the impacts (Hemmings and Boyes, 1977). Higher viscosity also increases the chances of centrifuging by binding the media to the wall, which reduces the mill volume and reduces the throughput (Fuerstenau et al., 1984). The effect of slurry rheology on the rate of grinding is investigated in depth by Klimpel (1982, 1983). His study showed that higher yield stress (which is a rheological property defined as the minimum stress to initiate fluid flow) leads to a decrease in grinding rate.

Most of the above studies were done for ball mills, where the grinding media are metal balls. However, in autogenous grinding, the media is the ore itself. Therefore, the efficiency of autogenous grinding also depends upon the way the media (larger size rocks) break inside the mill. Although the effect of rheology has been studied for various aspects of autogenous grinding (Moys, 1989), its effect on the breakage characteristics of the media is not discussed in the literature. This is an important problem, because small changes in the break-up rate of the media-sized rock will significantly affect the grinding efficiency of the mill.

A related problem is the production of critical size material. These are particles that are too small to efficiently grind other particles, but too large to be easily ground themselves. These critical size particles tend to accumulate in the mill, and have to be removed and crushed separately. Any changes in the slurry viscosity that result in a change in the rate of media break-up will also tend to change the amount of critical size material that is produced. This effect has been observed in an operating plant (Kawatra and Eisele, 1988). The plant personnel noted that the grinding efficiency was reduced in the winter, and that the amount of critical-size material produced was increased. These changes were linked to the seasonal temperature variations of the mill slurry. Two possible mechanisms were considered that could have been causing these effects: 1. The rock may have been becoming more brittle at low temperatures; or 2. The increasing slurry viscosity at low temperatures could have been affecting how the charge was lifted and tumbled in the mill. Past work by the authors has shown that the rocks were not becoming more brittle over the temperature range of interest (Kawatra et al., 1993), and so subsequent studies concentrated on the viscosity effects.

Studies of the effects of rheology on autogenous grinding media competency have not previously been carried out, because such studies cannot be carried out using small laboratory-scale mills. Small mills do not impart enough energy to the media particles to cause them to break up in the same way as they would in a full-scale mill. Because of this, studies of the media break-up rate require an autogenous mill that is pilot-scale or larger.

This article investigates the impact of rheology on the breakage characteristics of the rock, using a pilot-scale mill so that the results would be relevant to what happens in a full-scale autogenous mill. The effect of viscosity on size stability, and critical size material production has been examined.

EXPERIMENTAL

Experimental set-up

Pilot scale autogenous mill: The pilot plant tests were done in a 1.8 meter diameter by 0.6 meter long Hardinge Cascade Mill. The mill contained sixteen, 2.5 cm high lifter bars. It was converted from continuous operation to batch operation by removing the grates on the discharge end of the mill and replacing them with liners made at Michigan Technological University. This mill was also insulated to maintain the initial charge temperatures, using 20 cm of Corning fiberglass insulation applied to the circumference of the mill and 2.54 cm thick polystyrene foam insulation on the ends. Energy consumption during each test was measured by a standard watt-hour meter.

Viscometer set-up: A Brookfield viscometer (DV-I model) was used to measure viscosity of the slurry collected immediately after each test. It was necessary to modify the viscometer so that the solids would be kept in suspension while the reading was being taken. This was accomplished by the slurry presentation system shown in Figure 1. The slurry was mixed in an overhead tank and passed continuously through the annular space between a steel tube and the spindle. After a steady state reading was displayed, flow was momentarily interrupted (to eliminate any swirling motion caused by the flow at the inlet) and the reading was taken immediately. This set-up is very suitable for measuring viscosity of slurries containing fast settling solids, and has been successfully used to characterize different slurries on the basis of their rheology (Kawatra and Bakshi, 1995).

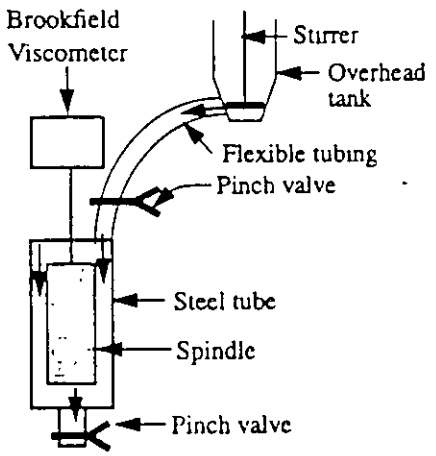

Figure 1. Brookfield set-up showing the special arrangement for measuring viscosity of slurries containing rapidly settling solids.

Sample preparation

A 6500 kg iron ore sample was collected from a local iron ore deposit. Each rock was sized and washed to (i) remove any fines that might be in the pores or fractures of the sample, and (ii) remove the visually detectable clay material present in the sample. The washed ore was then dried. From the above material, six samples were reconstituted according to the size distribution shown in Table 1. This was the original size distribution of the rocks in the pit from where the sample was collected. Samples prepared for cold tests were stored in a freezer at -25°C, and samples prepared for tests at room temperature were stored in 55 gallon drums.

Table 1: Size distribution of the reconstituted feed sample for the pilot scale autogenous tests.

Size Distribution (mm)	Weight (kg)	% Weight
-152.4 + 127.0	63.12	14.93
-127.0 + 101.6	65.83	15.59
-101.6 + 76.2	79.45	18.80
-76.2 + 50.8	82.17	19.47
-50.8 + 25.4	92.16	21 83
-25.4 + 12.7	39.50	9.38
Total	422.22	100.00

Test procedure

Six tests were carried out in the pilot scale autogenous mill. The viscosity of the mill slurry in these tests was changed by changing the clay/fines content in the initial feed and by changing the temperature of both iron ore and water. The mill was chilled prior to the tests conducted at low temperatures. The conditions for each test are given in Table 2.

The mill was run empty for 30 minutes before each test to allow the bearings to warm-up. Then the mill was stopped, and solids charge was added to the mill. A total of 423 kg solids were added for each test. Then, 182 kg of water was added to keep the total solids content at 70% by weight. The mill volume occupied by the charge was 26%. The initial temperature of water for the cold tests was maintained at 4°C (for test # 2, 4, and 6), and for other tests the water was at room temperature. The slurry temperature was measured both at the beginning and the end of each test, to be sure that the mill did not warm significantly during the test.

Table 2: Test conditions for each test conducted with the pilot scale autogenous mill.

Test No.	Initial Ore Temperature	Clay or Fines Content in the Feed
1	25°C	No clay No fines
2	-25°C	No clay No fines
3	25°C	10% clay No fines.
4	-25°C	10% clay No fines
5	25°C	No clay 50% fines
6	-25°C	No clay 50% fines

Once the mill was charged with solids and water, it was run for 15 minutes. A slurry sample for viscosity measurement was collected from the mill as soon as it stopped rotating. Energy consumption during the 15 minute grinding was measured by the watt-hour meter. The material from the mill was removed manually, and screened for size analysis.

The clay material added was the same metamorphic clay which was washed from the initial ore collected from the mine pit. During tests 5 and 6, 50% fines were added in the mill. This was done to simulate the plant conditions, where due to the continuous operation a certain amount of fine (ground ore) is always present inside the mill. Since we conducted batch tests, the loads in the mill for tests 1-4 were initially devoid of these fines, which gave a low viscosity at the beginning. Thus by adding 50% iron ore fines, it was expected that the viscosity of the pulp would be comparable to the continuous operation in a plant. The size distribution of these fines is shown in Table 3.

Table 3: Size distribution of the fines which were added during tests 5 and 6 to simulate plant conditions.

Size Distribution (mm)	Weight (kg)	Weight Percent
-1.40 + 0.850	0.11	0.05
-0.850 + 0.600	8.88	4.20
-0.600 + 0.500	14.37	6.80
-0.500 + 0.425	21.85	10.34
-0.425 + 0.212	21.55	10.19
-0.212 + 0.150	18.77	8.88
-0.150	125.85	59.54
Total	211.38	100.00

RESULTS AND DISCUSSION

The effect of the viscosity of the slurry on size stability, critical size material production, and specific energy consumption were studied, and are discussed below.

Size stability

The resistance of the media to impact breakage was measured in terms of size stability. Size stability is expressed as (ASTM, 1991):

$$\% \text{ Size stability} = \frac{\Sigma(\text{initial wt\%}) \times (\text{avg. sieve size})}{\Sigma(\text{final wt\%}) \times (\text{avg. sieve size})} \times 100$$

Therefore, a size stability of 100% corresponds to a rock that did not break during grinding, and a size stability of 0% corresponds to a rock that broke completely below the finest size measured (-12.5 mm in these tests).

As it can be seen from Figure 2, size stability increased with increase in slurry viscosity, showing that at high viscosity the rocks had a higher resistance to breakage. This could be due to the fact that at higher viscosity the impact force between rocks was retarded by the viscous slurry which acted as a cushion, resulting in less breakage in the rock.

Critical size material

Critical size material is the material which is too large to be effectively ground in the mill, and too fine to be effective for grinding other particles. In our tests, the change in the amount of material in the - 25.4mm + 12.7mm size fraction in the course of each test was small. Therefore, particles of this size were considered to be the critical size material. In a

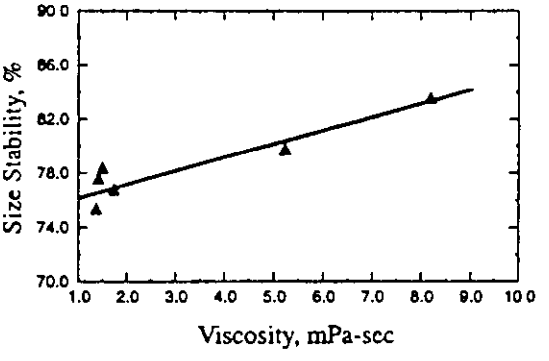

Figure 2. Size stability vs. viscosity. The increased size stability shows that at higher viscosity the ore is less likely to be broken. These are results of all six of the tests conducted.

plant situation, the critical size material would typically be crushed in a cone crusher before it was recycled to the autogenous mill, as shown in Figure 3.

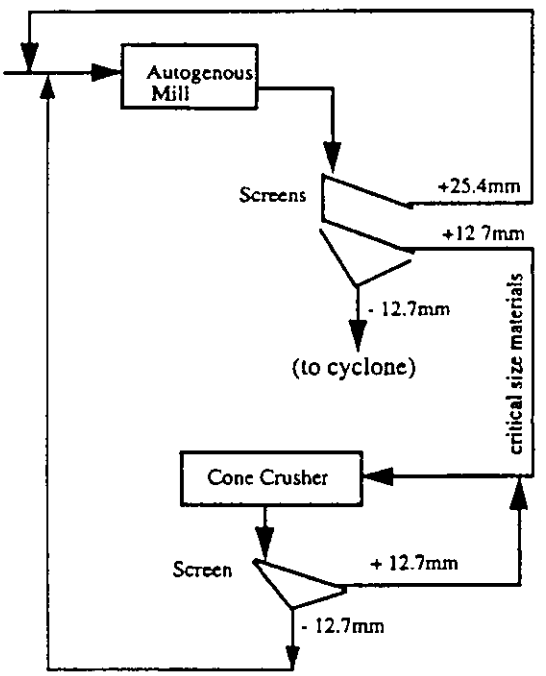

Figure 3. An autogenous grinding mill circuit, showing the treatment for critical size materials.

The feed for each test contained 9.38% critical size material (see Table 1). The percentage of the critical size material was determined again after each test. As it can be seen in Figure 4, at low slurry viscosity the amount of critical size material in the mill after grinding was less than the amount of critical size material present before grinding. At higher viscosity there was an increase in critical size material after grinding. This is primarily due to the fact that higher viscosity reduces the energy of the impact collisions, which reduces the chances that a critical size particle will be broken up in the mill. Therefore, at a higher slurry viscosity an increase in critical size material production is expected.

During test No.6, when the viscosity was 8.2 mPa-sec, the critical size content in the product was found to be 10.75%, which is 1.37% higher than the amount of critical size material originally present in the feed. Under these conditions, if a mill is processing 1000 tones of ore per hour, then 107.5 tones of critical size material will need to be recycled through the cone crusher, which will make the circuit more energy consuming.

In the local iron ore plant which provided the material for this work, data collected over a period of two years showed that critical size material production was at a minimum between April and September, and increased significantly during December and January months when the temperature was low (Kawatra and Eisele, 1992). It was originally believed that this change in critical size production was due to increased brittleness of the rock at low temperatures. However, drop tests conducted at Michigan Technological University showed that rocks did not become brittle over the temperature range of interest (+25°C to -25°C) (Kawatra et al., 1993). These changes in critical size material production can instead be attributed to viscosity changes, because viscosity of slurry increases at lower temperature.

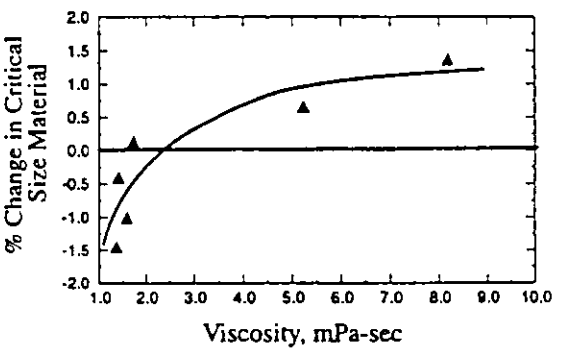

Figure 4. % change in critical size material vs. viscosity. There was a net decrease in critical size material during grinding when slurry viscosity was low. At higher slurry viscosity amount of critical size material in the product was more than the amount of critical size material initially present in the feed

Specific energy consumption

Specific energy consumption was measured by calculating the energy required to produce one kilogram of material finer than 150 microns. As can be seen from Figure 5, the specific energy consumption of the mill increased with increasing slurry viscosity. The increase in specific energy from test 1 to test 4 was not significant because the viscosity changes during these tests were very small. However, during tests 5 and 6 specific energy consumption increased significantly. While comparing the specific energy consumption between tests, the following observations were made:

(i) When the viscosity increased from 1.37 mPa-sec (test no. 1) to 5.24 mPa-sec (test no. 5) due to fines addition, specific energy consumption increased from 0.63 kwhr/kg to 1.11 kwhr/kg.

(ii) When the viscosity increased from 5.24 mPa-sec (test no. 5) to 8.19 mPa-sec (test no. 6) due to decrease in temperature, specific energy consumption increased again, going from 1.11 kwhr/kg to 5.0 kwhr/kg. This trend agrees with the observations made in the local iron ore plant, where specific energy consumption increased by ~20% during winter months when the slurry temperature was very low (Kawatra and Eisele, 1992).

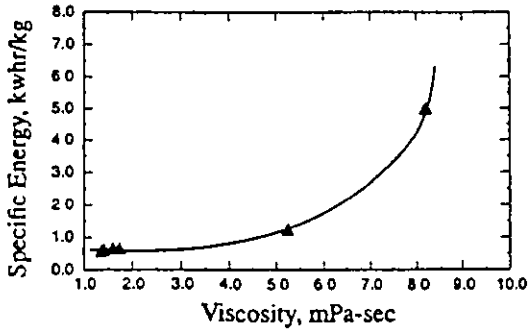

Figure 5. Specific energy vs. viscosity. The increase in specific energy consumption is significant at higher viscosity values.

CONCLUSIONS

Viscosity of the pulp in the mill increased with addition of clay and fines content and also by decreasing the temperature. With each increase in viscosity there was a consistent increase in all three parameters measured during the tests; size stability values increased with viscosity, production of critical size material increased with viscosity, and specific energy consumption increased with viscosity. Therefore, we can say that viscosity had a definite influence during grinding and can conclude the following from this study;

1. The resistance of the media-sized ore to breakage increased when the slurry viscosity was increased. This effect was prominent at higher viscosities.

2. At lower slurry viscosity, there was a net decrease in the amount of critical size material present in the mill during grinding. However, as the viscosity increased, the amount of critical size material became higher than the amount of critical size material initially present in the feed. These results agree with plant observations reported by Kawatra and Eisele (1992), where specific energy consumption and critical size material production increased during winter months. It has already been determined that the breakage characteristics of the individual rocks do not change with temperature (Kawatra et al., 1993), and so the change must be due to changes in the behavior of the mill slurry as a whole. Since pulp viscosity increases at lower temperatures during winter months, such changes can be attributed to changes in pulp viscosity.

3. The specific energy consumption in the mill increased as the viscosity increased. This was a result of the increased viscosity reducing the grinding rate by cushioning of impacts, and by changing the motion of the charge in the mill.

ACKNOWLEDGEMENTS

This research has been supported by the Department of Interior's Mineral Institute program administered by the Bureau of Mines through the Generic Mineral Technology Center for Comminution under grant number G1115149.

REFERENCES

ASTM, 1991, Standard Method of Drop Shatter Tests for Coal, D440-86, Annual book of ASTM standards, Vol. 5.05, pp. 214.

Austin, L. G., Klimpel, R. R., and Luckie, P. T., 1984, "What Laboratory Tests Tell Us About Breakage in Ball Mills," Chapter 5, Process engineering of Size Reduction: Ball Milling, Society of Mining Engineers, American Institute of Mining, Metallurgical, and Petroleum Engineers, Inc., New York, pp. 79-176.

Fuerstenau, D. W., Venkataramana, K. S., Velamakanni, B. V., 1984, "Effect of Chemical Additives on the Dynamics of Grinding Media in Wet Ball Mill Grinding," Inter. J. of Miner. Process., Vol. 15, pp. 251-267.

Hemmings, C. E., and Boyes, J. M., 1977, "An On-Line Viscometry Technique for Improved Operation and Control of Wet Grinding Circuits," Twelfth International Mineral Processing Congress, Sao Paulo, pp 46-64.

Klimpel, R. R., 1982 & 1983, "Slurry Rheology Influence on the Performance of Mineral/Coal Grinding Circuits," Part I, Mining Engineering, 34 (12), (1982), pp. 1665-1668, Part II, Mining Engineering, Vol. 35, No. 1, (1983), pp. 21-26.

Kawatra, S. K. and A. K. Bakshi, 1995, "Determination of Changes in Rheological Properties of Coal Slurries in Process Streams," Coal Preparation, Vol. 15, pp. 165-175.

Kawatra, S. K., Moffat, S. A., DeLa'O, K. A., 1993, "The Effect of Freezing Conditions on Rock Breakage," Society for Mining, Metallurgy, and Exploration, Inc., Preprint Number 93-17.

Kawatra, S. K., and Eisele, T. C., 1992, "Influence of Temperature on the Energy Efficiency of an Industrial Circuit Processing Iron Ore," Minerals and Metallurgical Processing, Vol. 8, No. 1, pp 32-37.

Kawatra, S. K. and Eisele, T. C., 1988, "Rheology effects in Grinding Circuits," XVI International Mineral Processing Congress, Elsevier Science Publishers B. V., Amsterdam, pp. 195-207.

Moys, M. H., 1989, "Advances in Autogenous and Semi-autogenous Grinding Technology," Vol. 2, (Editors) A. L. Mular and G. E. Agar, Mining and Mineral Processing Engineering, University of British columbia, Vancouver, Canada, pp 713-728.

Tucker, P., 1982, "Rheological Factors that Affect the Wet Grinding of Ores," Trans. of Instn. Min. Metall., Section C, Mineral Processing and Extractive Metallurgy, Vol. 91, pp. 117-122.

XVI International Mineral Processing Congress, edited by E. Forssberg
Elsevier Science Publishers B.V., Amsterdam, 1988 — Printed in The Netherlands

RHEOLOGY EFFECTS IN GRINDING CIRCUITS

S. K. KAWATRA and T. C. EISELE

Department of Metallurgical Engineering, Michigan Technological University, Houghton, Michigan 49931, U.S.A.

SUMMARY

A discussion of the effects of rheology on the performance of grinding circuits is presented, as well as a description of the major factors which influence the rheology of mineral slurries. One of these factors, slurry temperature, has long been discounted as unimportant to mill efficiency. The results of plant and laboratory investigations of the effects of temperature on grinding circuit performance are presented.

INTRODUCTION

Comminution is the single most energy-intensive and least efficient unit operation in mineral processing (Ref. 1). Although it has been known for some time that the efficiency of a wet grinding circuit is dependent on the rheological character of the mineral slurry (Ref. 2), no grinding circuits presently exist which use direct rheology control. This state of affairs is primarily due to the lack of a suitable sensor arrangement for on-line monitoring of mineral slurry rheology. For the same reason, there is a high degree of uncertainty concerning the responses of components such as mills and classifiers to changes in slurry rheology. As a result of the difficulties involved in actual rheology measurement, attention has been limited to readily measurable quantities such as pulp density, and to a lesser extent, particle size, which have a strong influence on rheology.

In general, it is unfortunately not feasible to assume that rheology can be predicted solely from the value of a single parameter such as percent solids. This is due to the strong influence of variables such as particle surface chemistry, particle size and shape, and temperature on rheology (Ref. 3). Of these factors, consideration of surface chemistry has been limited by the difficulty of determining the relevant parameters, and temperature has been largely ignored due to the common assumption that temperature effects are negligible.

THEORETICAL DISCUSSION

The rheology of mineral suspensions is highly complex and difficult to predict, with both time-dependent and time-independent components and a range

99

of possible variations from ideal behavior. Since time-dependent phenomena such as thixotropy and rheopexy depend on the development of a structure in a quiescent fluid (Ref. 4), the high-shear environment of the grinding circuits prevents such phenomena from occurring and only time-independent behavior need be considered (Ref. 5).

Time-independent behavior can be divided into four general categories, depending on how the shear stress developed in the fluid varies with shear rate, as shown in Figure 1. The slope of each of these curves represents the viscosity at a given shear rate. Thus, a Newtonian fluid exhibits a constant viscosity for all shear rates, the apparent viscosity of a dilatent fluid increases with shear rate, the apparent viscosity of a pseudoplastic fluid decreases with shear rate, and a Bingham plastic requires a minimum shear stress, or yield stress, before flow can begin. The empirical mathematical expressions for each type of behavior may be expressed as follows:

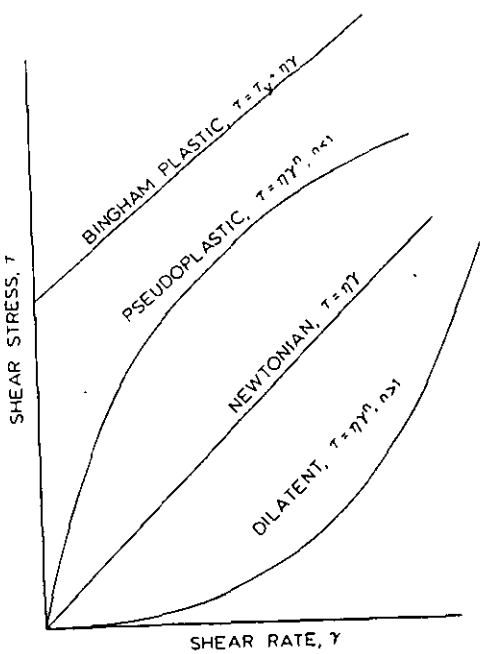

Figure 1. eralized time-independent rheology curves. The minimum shear ss required for flow of a Bingham plastic, τ_y, is the yield ess.

Newtonian: $\tau = \mu\gamma$

Dilatent: $\tau = \mu\gamma^n$, where $n>1$

Pseudoplastic: $\tau = \mu\gamma^n$, where $n<1$

Bingham plastic: $\tau = \tau_y + \mu\gamma$

where τ is the shear stress, γ is the shear rate, μ is the apparent viscosity, n is a dimensionless constant, and τ_y is the yield stress (Ref. 6). Although a slurry may exhibit any of these behaviors, very concentrated slurries are generally pseudoplastic or Bingham plastic. Indeed, in some cases it is very difficult to determine whether a slurry is pseudoplastic or Bingham plastic without very careful measurements at very low shear rates, as the curves obtained may be very similar otherwise (Ref. 6).

Known Effects in Grinding Circuits

The efficiency of closed circuit grinding is dependent on rheological effects both in the mill proper and in the classifiers used to close the circuit. Effects on mill performance have been extensively studied, largely in connection with studies of polymeric grinding aids (Refs. 2,7-10). The most notable result was that increasing the solids concentration of the slurry increased the fines production rate provided that the product slurry did not exhibit a non zero yield stress. Once a yield stress was exhibited, the breakage rate in the mill fell off (Ref. 8). In addition, decreasing the slurry viscosity frequently produced an increase in the fines production rate at a constant percent solids (Ref. 10). These effects are due to changes in the motion of the mill charge upon development of a non zero yield stress (Ref. 8), and to a decrease in the energy absorbed by the fluid at lower viscosities.

The effects of rheology on the performance of classifiers such as hydrocyclones is quite pronounced and fairly complex (Ref. 5). Although these effects have not been well studied due to the lack of suitable instrumentation, some data is available using sugar solutions to alter the medium viscosity. Also, several theoretical treatments of hydrocyclones include an explicit viscosity term. It is possible to divide the rheological influences into two categories for theoretical consideration; the effect on particle movement through the fluid, and the effect on flow patterns and velocities. However, it is not possible in practice to dissociate the two influences (Ref. 5).

At a constant cyclone inlet pressure, increasing the viscosity first decreases the centrifugal velocity, which results in a higher flowrate due to the lowered centrifugal force at the inlet. At viscosities greater than 50 centipoise, viscous drag causes the inlet flowrate to decrease again (Ref. 5). The decrease in centrifugal velocity will decrease the particle settling rate and the result will therefore be to increase the 50% cyclone cut size, d_{50}, and the particle by pass fraction, R_f, as the viscosity increases. In general, the effect of viscous drag will cause the cyclone to be ineffective as a classifier when the viscosity exceeds approximately 30 centipoise (Ref. 5).

Virtually no work has been done to determine the actual effect of slurry viscosity on the real performance of a hydrocyclone under plausible industrial conditions. In many cases, rheological effects have not been separated from the effects of percent solids, which is the most commonly used factor for controlling slurry viscosity (Ref. 10). The few experiments which have been carried out in the past, which have varied viscosity without varying percent solids, have produced contradictory results (Refs. 10,11), with the d_{50} size increasing with increasing viscosity in one case, and decreasing with increasing viscosity in the other. Additional, more carefully controlled experimentation is therefore needed to determine the true effect.

Factors Influencing Rheology

The rheology of a mineral suspension, consisting of particles fine enough to remain in suspension for more than a few seconds, is strongly influenced by the following four factors; solids concentration, particle size and shape, chemical environment, and temperature. Each factor has a characteristic effect on slurry rheology, which is described below:

(i) Solids Concentration. Solids concentration has a powerful effect on the apparent viscosity of a slurry, as shown by Figure 2. The effect is particularly strong at high percent solids, with slight changes in concentration producing large shifts in viscosity. In addition to affecting the viscosity, increasing the percent solids causes changes in the rheological curve for the slurry. In general, the rheology at very high solids content will shift from dilatent to pseudoplastic to Bingham plastic as the percent solids increases (Ref. 9), which will alter grinding mill operation.

(ii) Particle Size and Shape. For any given percent solids, a reduction in particle size will produce an increase in slurry viscosity. This is considered to be largely a result of increased particle surface area, which

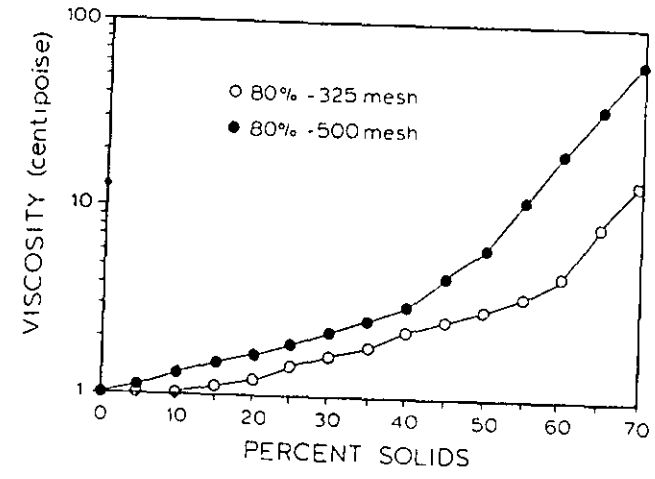

Figure 2. Effect of percent solids and particle size on slurry viscosity. Work described in this paper was carried out in the range of 20 to 40% solids by weight.

causes a greater proportion of the fluid phase to be bound up in particle boundary layers. The amount of free fluid is thus decreased, and the effective percent solids becomes greater. In addition to this effect, the manner in which the particles interact with the fluid changes with decreasing particle size. This causes an increase in viscosity through complex effects on both the manner in which the fluid flows and on interparticle friction. The net result is as shown by the two curves of Figure 2, with the finer particle size producing a substantially higher viscosity. Increasing the angularity of particles will also increase the viscosity, for reasons similar to those previously stated.

(iii) Chemical Environment. The chemical environment of the slurry includes a wide variety of factors such as particle surface chemistry and chemical effects on the viscosity of the fluid phase. These effects are highly complex and poorly understood, although the effects of surface-active agents on suspension rheology have been extensively studied empirically (Refs. 2,7-10). Chemical effects have been particularly studied in mill circuits in connection with the use of grinding aids, which are basically viscosity-reducing agents.

(iv) Temperature. The effect of temperature on slurry viscosity differs from that of the other three factors in that the slurry viscosity change results entirely from changes in the viscosity of the carrier fluid. The

viscosity of water varies with temperature as shown in Figure 3 (Ref. 12). Changes in slurry viscosity with temperature obviously have a similar form, modified by the presence of particles.

While the effects of percent solids and particle size on mill and cyclone performance have been intensively studied, and chemical effects have been studied to a lesser extent, the influence of temperature on performance has been largely ignored. This is due to the widely held belief that temperature is of little consequence for the efficiency of grinding circuits. Nevertheless, it has been reported in several mills in Canada and the northern United States that seasonal shifts in grinding efficiency occur which are apparently due to the sizable temperature variation in these areas. This is borne out by the fact that when the mills take precautions to prevent chilling of the recycled water in the winter, the seasonal efficiency changes become less pronounced (Ref. 13). For this reason, an investigation was carried out to determine the effect of temperature on grinding circuit efficiency, particularly the effect on hydrocyclone performance.

PLANT STUDIES

An extensive campaign of plant sampling was carried out in an iron ore concentrator located in northern Michigan to monitor the effect of seasonal temperature changes on the performance of the grinding circuit.

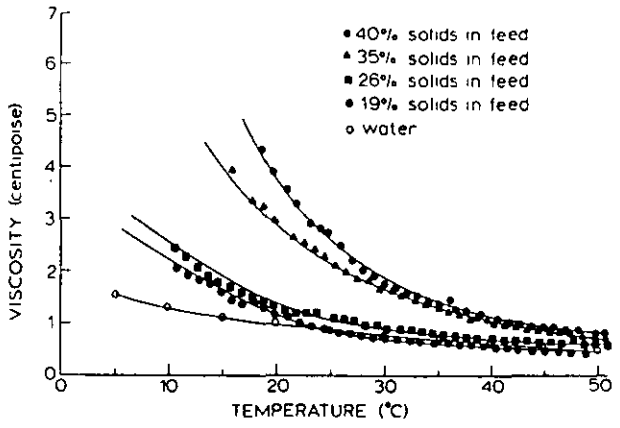

Figure 3. fect of temperature variation on the viscosity of pure water and of fine silica slurries at four solids concentrations.

The plant selected for this investigation was specifically chosen due to its need to grind to a very fine particle size (80% passing 500 mesh) in order to achieve liberation. This ensured that the effects of seasonal temperature change would be most pronounced, as finer particles are more readily affected by rheology change than are coarser particles. In addition, since the plant used reverse flotation to remove quartz from hematite, downstream processing was highly sensitive to the size of grind. This ensured that the operation of the entire plant would be influenced by small changes in grinding performance, and that the temperature effect would be more likely to be of importance to plant operations.

The most notable seasonal effect observed in the grinding circuit was the change in the hydrocyclone efficiency curve. The representative data given in Figure 4 show that an increase in temperature from 4°C to 20°C produced a 20% decrease in the d_{50} size from 25 micrometers to 20 micrometers. Other data confirmed this trend. While the plant sampling was sufficient to show that an important effect exists, laboratory experimentation was necessary to properly measure the effect.

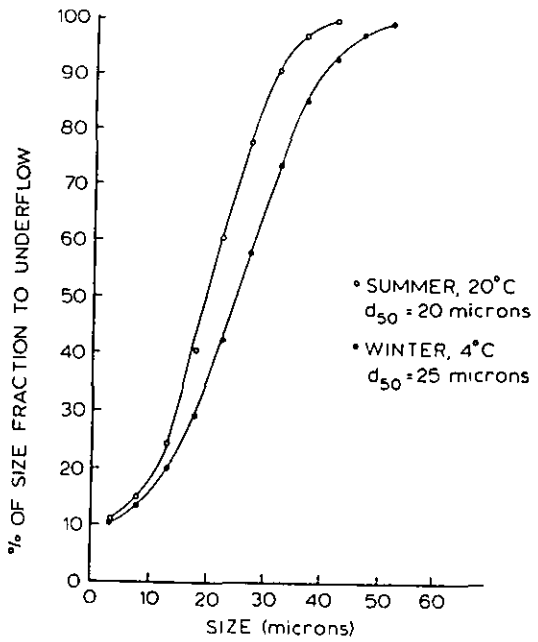

Figure 4. Effect of seasonal temperature changes on hydrocyclone performance in an operating iron ore concentrator.

LABORATORY STUDIES

Laboratory experiments were carried out using a 10.2 cm (4 inch) diameter Krebs hydrocyclone. The cyclone was mounted on a laboratory test rig, in closed circuit with a Warman centrifugal pump and a slurry tank. The cyclone overflow and underflow streams discharged freely into separate launders, which were used to either remove simultaneous samples from the two streams, or to recombine the streams before returning them to the slurry tank. Temperature was measured by a thermocouple mounted in the feed tank, and a diaphragm-type pressure gauge and an ultrasonic doppler flowmeter were mounted on the cyclone inlet line. Slurry viscosity was measured by a vibrating-sphere viscometer equipped with a specially designed sample presentation arrangement and receiving the recombined overflow and underflow slurries from the discharge launders when sampling was not being carried out. This instrument allowed the continuous monitoring of the viscosity, which had not previously been possible for mineral slurries in this size range. Data was collected and logged by an HP-85 computer and slurry temperature was controlled using an immersion heater and an immersion chiller.

Test Material

The mineral used for these experiments was pure silica, specific gravity = 2.65, obtained from the Ottawa Sand Co., Ottawa, Illinois. The size distribution of the silica is given in Table 1.

TABLE 1
Size distribution of ground Ottawa sand

Size (microns)	Cumulative wt. % passing
176	100
125	100
88	94
62	79
44	61
31	47
22	35
16	26
11	19
7.8	12
5.5	8
3.9	5
2.8	0.3

Experimental Procedures

The slurry tank was initially filled with hot water and sufficient silica to produce a slurry of the desired percentage solids. The cyclone inlet pressure was then set to 10 psi, and the immersion heater was used to maintain the slurry at 50°C. The system was allowed to stabilize for 10 minutes before the first overflow and underflow samples were taken, after which the slurry temperature was gradually decreased, with samples taken at approximately 5°C intervals. The use of the chiller allowed experiments over a temperature range of 50°C to 12°C.

The overflow and underflow samples were weighed, filtered, and dried. The dried samples were then weighed to allow the calculation of pulp densities, and the particle size distributions were determined with a Leeds and Northrup Microtrac particle size analyzer. The particle bypass fraction, R_f, was calculated from the fraction of the feed water which reported to the underflow, and cyclone efficiency values were corrected for R_f.

RESULTS AND DISCUSSION

A summary of the data collected in the laboratory cyclone experiments is presented in Table 2. The values of α and $d_{50(c)}$ in this table were determined from the equation (Ref. 14)

$$y' = (e^{\alpha x}-1)/(e^{\alpha x}+e^{\alpha}-1) \qquad (1)$$

where $x = d/d_{50(c)}$

y' = corrected fraction of feed to the coarse product

$d_{50(c)}$ = corrected 50% separation size

d = particle size

α = a measure of the sharpness of the separation, sharpness increases with increasing values of α.

A simplex optimization program was used to find the best-fit values of α and $d_{50(c)}$.

Plotting the corrected efficiency curves obtained at each temperature, as shown in the representative plot of Figure 5, shows the systematic shift in the curves towards finer sizes with increasing temperature.

It is clear from this data that $d_{50(c)}$ does indeed decrease with increasing temperature. When $d_{50(c)}$ is plotted against temperature, it is further observed that the relationship is nearly linear, as is illustrated by Figure 6. When the solids content of the slurry is increased, the line relating d_{50} to temperature is shifted upward, but the slope of the line remains constant over the range investigated. While the relationship of cut size to temperature is definite, the parameter α exhibits little dependence on temperature, which indicates that changing temperature has little if any effect on the sharpness of the separation. This is clearly shown by the reduced efficiency curve of Figure 7, which is essentially identical for all of the tests. This result is in agreement with the results of Lynch

TABLE 2

Summary of experimental results

Wt.% Solids	Temperature °C	Viscosity Centipoise	$D_{50(c)}$ Micrometers	R_f(%)	α
19.80	49.93	.53	13.02	19.30	2.80
19.30	44.85	.58	14.61	19.20	3.77
18.90	40.14	.65	14.87	21.50	3.87
18.80	35.72	.73	15.52	21.60	3.28
18.30	29.82	.82	15.65	23.80	2.89
18.10	25.42	.95	18.01	23.00	3.03
17.20	20.83	1.20	17.40	23.10	2.70
16.50	15.67	1.58	19.52	22.50	3.78
16.40	10.60	2.18	20.63	24.40	3.02
25.80	50.70	.69	17.40	18.60	3.48
26.60	41.00	.80	18.90	19.50	3.51
25.90	30.14	1.02	20.10	20.90	3.42
25.50	25.00	1.20	21.50	20.90	3.84
25.00	20.46	1.35	22.50	21.00	3.46
24.40	15.44	1.81	23.10	22.90	3.82
24.40	10.41	2.54	24.20	22.30	3.04
34.00	50.64	.89	24.04	21.20	3.26
34.60	40.01	1.20	26.15	25.10	3.48
35.50	30.61	1.84	28.56	24.00	3.09
34.90	25.31	2.31	29.91	23.40	2.88
36.20	14.75	4.15	30.71	27.50	2.47
40.20	50.62	1.01	27.62	22.70	2.62
41.20	40.54	1.25	29.69	23.90	2.36
40.90	30.85	1.90	32.46	24.00	2.78
41.00	25.75	2.70	32.76	24.70	2.69
40.70	20.84	3.75	35.83	24.50	2.87
40.90	14.38	6.22	36.06	25.00	3.03

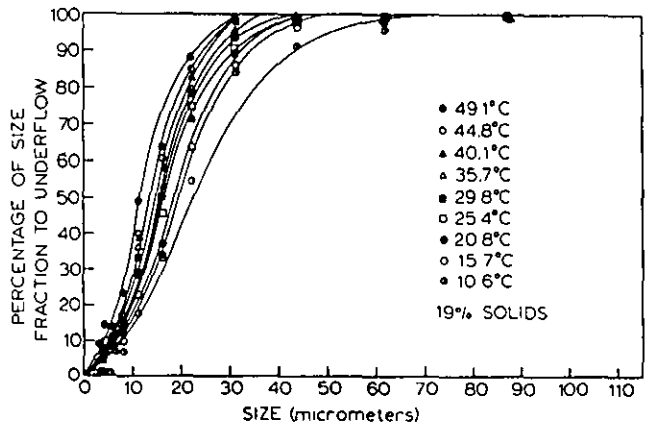

Figure 5. ct of changing temperature on the corrected hydrocyclone efficiency curve for pure silica, as determined in laboratory experiments.

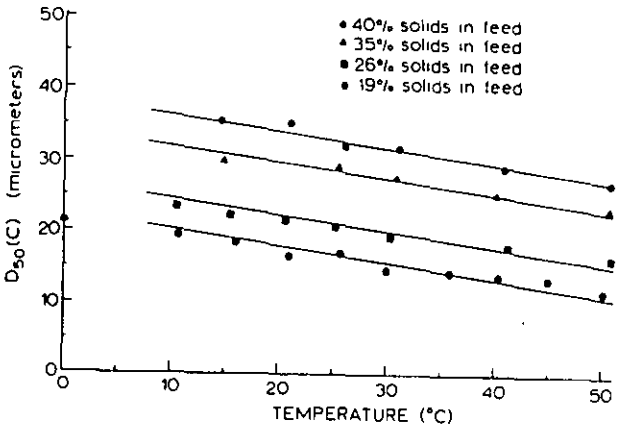

Figure 6. Experimentally determined relationship of corrected cyclone d_{50} size and slurry temperature for a 4" diameter hydrocyclone.

(Ref. 14), which show that the reduced efficiency curve is a function only of cyclone geometry and particle characteristics, and is largely unchanged by alterations in operating conditions.

It is known that increasing the fluid viscosity affects the cyclone performance both by slowing the settling rate of particles and by suppressing the tangential velocity of the fluid in the cyclone (Ref. 5). The net result is that increasing the viscosity of the slurry increases the cyclone $d_{50(c)}$ size. Since the viscosity of a fluid typically increases with decreasing temperature, the observed temperature dependence of $d_{50(c)}$ is primarily a result of changes in slurry viscosity.

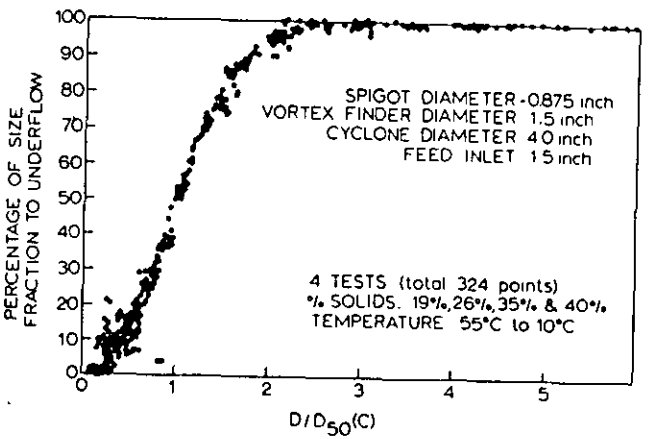

Figure 7. Reduced efficiency curve obtained for the classification of fine silica in a 4" diameter hydrocyclone at 10 psi for all tests.

CONCLUSIONS

From the available information concerning the effects of slurry rheology on mineral grinding circuits, it can be concluded that:

(i) The efficiency of the mill proper is maximized when the percent solids is held just below the level which will produce a yield value in the output slurry, and the viscosity is reduced as far as possible.

(ii) The d_{50} size for a hydrocyclone is expected to increase as the slurry viscosity increases, with d_{50} being roughly proportional to the square root of the viscosity.

(iii) In both plant and laboratory environments, the $d_{50(c)}$ size of a hydrocyclone is temperature dependent, with the cut size decreasing with increasing temperature. This effect is primarily due to the decreased slurry viscosity at elevated temperatures.

(iv) The dependence of $d_{50(c)}$ on temperature is very nearly linear, and the line is shifted to coarser $d_{50(c)}$ sizes with increasing percent solids, although the slope remains unchanged over the range investigated. The reduced efficiency curve for a given cyclone remains unchanged with changes in temperature or percent solids.

These results show the necessity for monitoring slurry viscosity in order to improve cyclone efficiency, and moreover, that the control strategies based on inferential sizing techniques (Ref. 15) must be modified to allow for the observed behavior. Further work must be done to improve the quality of on-line viscosity measurements of mineral slurries.

ACKNOWLEDGMENTS

The authors gratefully acknowledge the financial support for this project provided by the U. S. Bureau of Mines (through the Generic Centre for Comminution at the University of Utah), and the industrial support provided by the Dow Chemical Co., Midland, Michigan. The authors also thank Krebs Engineers, Inc. for providing the hydrocyclone used in this project.

REFERENCES

1. National Materials Advisory Board, Comminution and Energy Consumption, NMAB-364, 1981.

2. H. El-Shall, P. Somasundaran, "Mechanisms of Grinding Modification by Chemical Additives: Organic Reagents", Powder Technology, vol. 38, pp. 267-273, 1984.

3. C. H. Schack, K. C. Dean, S. M. Molloy, "Measurement and Nature of the Apparent Viscosity of Water Suspensions of Some Common Minerals", Report of Investigations 5334, U. S. Bureau of Mines, May 1957.

4. D. C.-H. Cheng, "Further Observations on the Rheological Behavior of Dense Suspensions", Powder Technology, vol. 37, pp. 255-273, 1984.

5. D. Bradley, The Hydrocyclone, Pergamon Press, 1965.

6. Parviz Shamlou, "Fine Solids Suspension and Rheology", The Chemical Engineer, May, 1984, pp. 31-34.

7. H. El-Shall and P. Somasundaran, "Mechanisms of Grinding Modification by Chemical Additives: Organic Reagents," Powder Technology, vol. 38, pp. 267-273, 1984.

8. D. W. Fuerstenau, K. S. Venkataraman, and B. V. Velamakanni, "Effect of Chemical Additives on the Dynamics of Grinding Media in Wet Ball Mill Grinding," Int. J. of Mineral Processing, vol. 15, no. 4, pp. 251-268, 1985.

9. R. R. Klimpel, "Influence of Material Breakage Properties and Associated Slurry Rheology on Breakage Rates in Wet Grinding of Coal and Ores in Tumbling Media Mills", in Reagents in the Minerals Industry, (M. J. Jones and R. Oblatt, eds.), Institution of Mining and Metallurgy, London, pp. 265-270, 1984.

10. L. G. Austin, R. R. Klimpel, and P. T. Luckie, Process Engineering of Size Reduction: Ball Milling, AIME, 1984.

11. G. E. Agar and J. A. Herbst, "The Effect of Fluid Viscosity on Cyclone Classification", Trans. AIME, vol. 235, pp. 145-149, 1966.

12. Handbook of Chemistry and Physics, 65th edition, CRC Press, 1984.

13. H. J. Kampf, Personal Communication, 1985.

14. A. J. Lynch, Mineral Crushing and Grinding Circuits, Elsevier, New York, 1977.

15. R. A. Seitz and S. K. Kawatra, "Further Studies on the Use of Classifiers for Control of Wet Grinding Circuits", International Journal of Mineral Processing, vol. 12, pp. 239-249, 1984.

Temperature effect on grinding circuit performance

S. K. Kawatra, T. C. Eisele, D. X. Zhang, and M. T. Rusesky

Abstract — *It has been observed in some mineral processing plants that grinding circuit efficiency varies seasonally, such as in some plants which are located in the northern US and Canada and undergo large seasonal temperature changes, with the grinding circuit efficiency different between summer and winter. This indicates that the temperature of grinding circuit slurry has a noticeable effect on grinding performance. The effect has rarely been studied. To this end, an investigation to examine the effects of changing temperature on efficiency and determination of the mechanism responsible has been carried out. Plant investigations and laboratory experiments have been conducted in order to study hydrocyclones. It was demonstrated that when the pressure drop is held constant, the $d_{50(c)}$ size decreased approximately linearly with increasing temperature, while the shape of the reduced efficiency curve remained nearly constant. This effect was determined to be due to changes in slurry viscosity with temperature.*

Introduction

As is well known, the single most energy intensive unit operation in mineral processing is comminution. Size reduction consumes approximately 25% of the total energy used in mineral concentrators, while typically less than 5% of this energy is consumed in the production of new mineral surface (NMAB, 1981). Thus, there is much room for improvement in grinding operations, and even a slight increase in efficiency would produce substantial energy savings. Such improvements are most readily obtainable by optimization and control of mill operating conditions.

A number of investigators (Austin, et al., 1984; El-Shall and Somasundaran, 1984; Klimpel, 1982, 1982a, 1983, 1984; Fuerstenau, et al., 1985) have determined that rheology has a large effect on the efficiency of grinding mills. Four parameters influence the rheology of slurry in a grinding mill: solids content, particle size distribution, chemical environment, and temperature. The effect of temperature is particularly significant in areas with large seasonal temperature variations such as the northern United States and Canada (Kampf, 1985). However, due to the unavailability of suitable viscometers and measurement techniques for mineral slurries, the control of mill rheology, especially the effects of temperature on efficiency of grinding mill and hydrocyclones, has been neglected or rarely studied. The investigation described here was therefore carried out to determine the magnitude and nature of temperature effects on hydrocyclone operation.

S.K. **Kawatra**, **T.C. Eisele**, members SME, **D.X. Zhang**, and **M.T. Rusesky**, member SME, are with Dept. of Metallurgical Engineering, Michigan Technological University, Houghton, MI. SME preprint 88-1, SME Annual Meeting, Phoenix, AZ, January M&MP paper 88-639. Manuscript June 12, 1987. Discussion of this paper must be submitted, in duplicate, prior to July 31, 1989.

Experimental Work

Plant Studies

The plant site that was chosen for obtaining the samples was an iron ore processing plant, which experiences substantial seasonal temperature variations. The plant has primary autogenous and secondary pebble mill grinding. The cyclones are operated in parallel banks of nine, with seven of the classifiers in use at any one time. The cyclones are Krebs model D15B-852-M271. This plant processes a very finely disseminated iron ore which requires grinding to -25 μm for liberation.

Sampling was carried out in the summer and in the winter in order to achieve the greatest temperature variation. Pulp temperature ranged from a high of 20°C (68°F) in the summer to a low of 3.3°C (38°F) in the winter. The resulting corrected efficiency curves for these conditions are shown in Fig. 1.

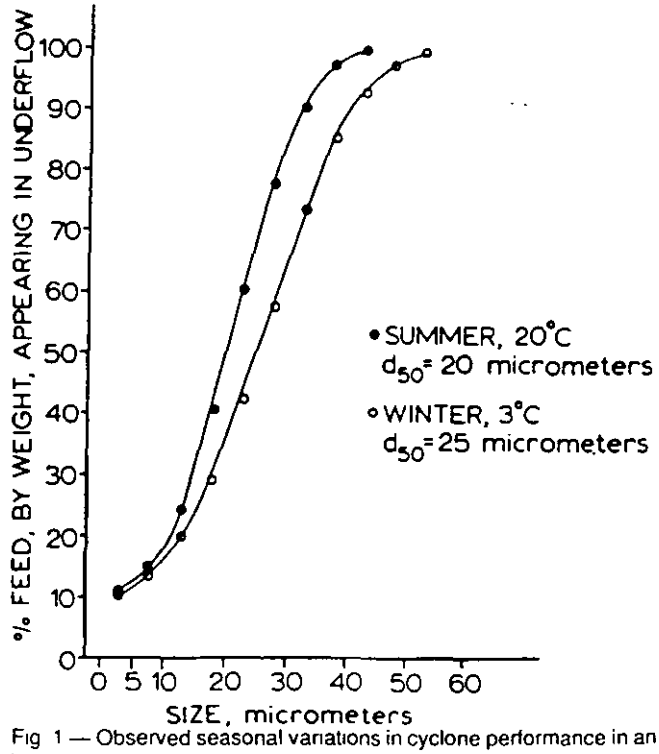

Fig 1 — Observed seasonal variations in cyclone performance in an iron ore processing plant.

Laboratory Studies

Laboratory experiments were carried out using a 15 hydrocyclone. The cyclone parameters were as follows: feed inlet diameter, 1.2 in. (3 cm); vortex finder diameter, 1 1/2 in. (3.8 cm); apex diameter, 7/8 in. (2.2 cm); cyclone diameter, 4 in. (10.2 cm); and pressure drop, 10 psi (69 kPa).

The cyclone was mounted on a laboratory test rig in closed circuit with a Warman centrifugal pump and a slurry tank. The cyclone overflow and underflow streams discharged freely into separate launders, which were used to either remove simultaneous samples from two streams or to recombine the streams before returning them to the slurry tank. The slurry temperature sensor was mounted in the feed sump, and a diaphragm-type pressure gage and an ultrasonic doppler flowmeter were both mounted on the cyclone inlet line. Apparent slurry viscosity was also measured at the cyclone feed inlet using a Namotre Model 810 vibrating sphere viscometer. Flowrate, viscosity, and temperature data were continuously collected and logged by a HP-85 computer.

The mineral used for these experiments was pure silica obtained from Ottawa Sand Co., Ottawa, IL. The particle size distribution was obtained using a Leeds and Northrup Microtrac particle size analyzer and is shown in Table 1. The temperature range was from 50 to 11°C.

Table 1 — Size Distribution of Ground Ottowa Sand

Size, μm	Cumulative Wt % Passing
176	100
125	97
88	93 6
62	75 5
44	49 8
31	34 9
22	24 0
16	17 5
11	12 7
7.8	8 1
5 5	5 1
3.9	3 9
2 8	2 0

Results and Discussion

A summary of the data collected in the laboratory cyclone experiments is presented in Table 2. The Rf is the water split, and α is the shape parameter from Lynch's equation,

$$y = \frac{e^{\alpha x} - 1}{e^{\alpha x} + e^{\alpha} - 2} \quad \text{where } x = \frac{d}{d_{50(c)}}.$$

Table 2 — Summary of Laboratory Cyclone Test Results

Test	Temperature °C	R_f, %	$d_{50(c)}$, μm	α	Viscosity Centipose
1	48 8	22 0	21 0	2 83	8 9
2	40 4	23 3	23 6	2 85	10 4
3	35 2	24 3	25 0	2 54	10 6
4	30 0	23 2	26 8	2 74	10 3
5	25 0	24 7	29 1	2 44	10 8
6	20 0	23 5	30 0	2 12	12 0
7	15 1	23 9	31 4	2 69	14 2
8	11 1	24 4	32 4	2 54	13 8

The values for α and $d_{50(c)}$ were determined by simplex optimization after the data was corrected for *Rf*.

It is clear from both plant and laboratory data that $d_{50(c)}$ does indeed decrease with increasing temperature in Figures 1 and 2. When $d_{50(c)}$ is plotted against temperature it is further observed that the relationship is essentially linear, as is illustrated by Fig. 3. From Fig. 2 it is clearly shown that increasing temperature shifts the efficiency curve towards finer sizes. However, the sharpness of the reduced efficiency curve for all of the temperatures is essentially unchanged, as shown by the curve in Fig. 4. This result is in agreement with the results of Lynch (1977), who stated that the reduced efficiency curve is a function only of cyclone geometry and particle characteristics in slurry and is largely unchanged by alternations in operating conditions.

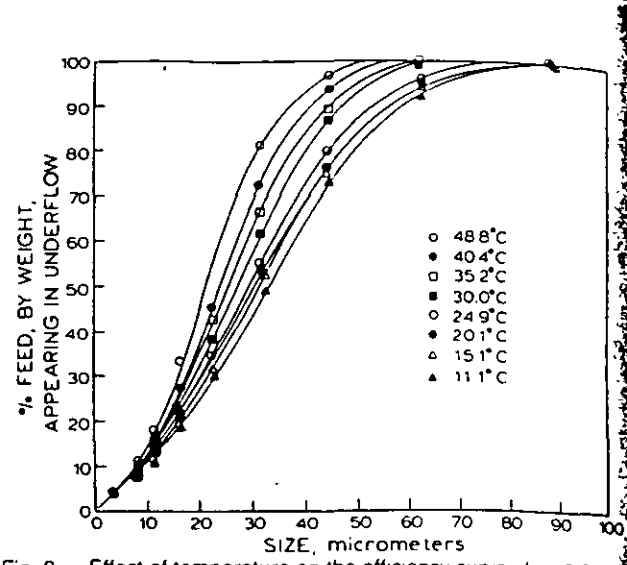

Fig. 2 — Effect of temperature on the efficiency curve of a 10.6 cm (4 in) hydrocyclone processing silica.

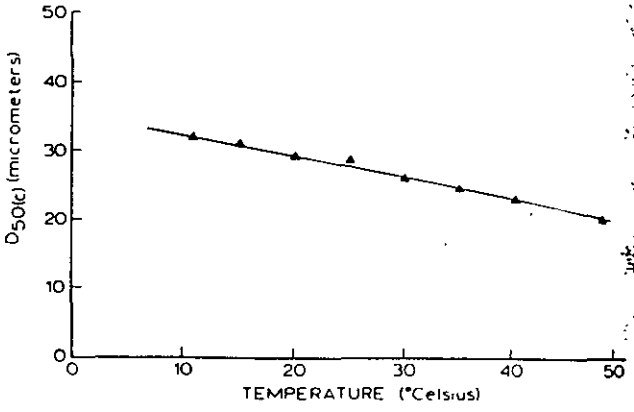

Fig. 3 — Relationship of hydrocyclone corrected d_{50} size and slurry temperature for a 10.16 cm (4 in) hydrocyclone processing silica.

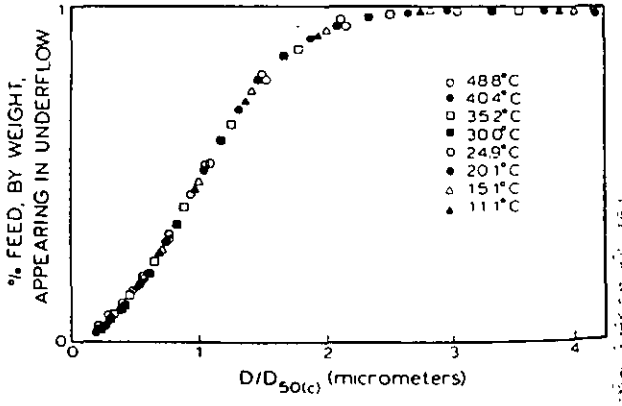

Fig. 4 — Reduced efficiency curve for varying percent solids and temperature for a 10.16 cm (4 in) hydrocyclone processing silica.

From Table 2 it is shown that apparent slurry viscosity varies significantly with temperature.

The behavior of hydrocyclones as classifiers of mill output is dependent on slurry rheology (Austin et al. 1984, Agar and Herbst, 1966).

If the cyclone returns excessive amounts of fine material to feed, over-grinding will reduce mill efficiency and may cause difficulties in later separation processes as well.

Variations in temperature affect slurry viscosity by reducing the viscosity of the carrier water. A major effect of this is

on hydrocyclone performance. The observed shift of the cyclone efficiency curve and reduction in $d_{50(c)}$ size arises from the reduced viscosity of water at elevated temperatures. Reduction of viscosity increases the settling velocity of the particles, which causes them to segregate more rapidly with fewer misplaced particles, thus improving efficiency. The increase in settling velocity also causes the apparent size of any given particle to increase which reduces the $d_{50(c)}$ size. This effect is amplified by an increase in flowrate at constant pressure as the viscosity is lowered, which increases centrifugal effects and hence raises the settling velocity. Similar conclusions can be drawn by analyzing the data obtained by Agar and Herbst (1966) where the water viscosity was altered with sucrose. It may be noted that viscosity reduction by increasing temperature, which reduces $d_{50(c)}$ size in cyclones, appears to conflict with Klimpel's data (1982), which predicts an increase in $d_{50(c)}$ size with a decrease in viscosity. This discrepancy may be explained by the difference in the mechanism of viscosity reduction. However, it should be kept in mind that direct comparisons of hydrocyclone results may be misleading due to the difficulty of ensuring that the same variables are held constant For example, the results reported here are for constant pressure and varying throughput, while Klimpel's results may well have been for constant throughput and varying pressure.

Temperature changes have little effect on the interaction of water and solids, but produce a great alteration in the viscosity of water. It is the viscosity of the carrier liquid which controls the viscosity of the slurry under high shear conditions such as those encountered in the cyclone separating zone (Bradley, 1965), while the slurry viscosity at lower shear rates control the slurry flowrate and hence the magnitude of the centrifugal forces. Thus, increasing the temperature strongly influences both the centrifugal forces and the particle settling velocity, while viscosity reduction by chemical addition, which most strongly effects particle interactions and therefore the low-shear-rate apparent viscosity, has its greatest influence on centrifugal forces.

Conclusion

It has been shown that in both plant and laboratory environments, the temperature of the grinding circuit slurry has a noticeable effect on grinding and cyclone efficiency. The $d_{50(c)}$ size of a hydrocyclone is a function of the viscosity of carrier liquid, which in turn is a function of temperature. $d_{50(c)}$ size therefore decreases nearly linearly with increasing temperature. The sharpness of the separation is largely unaffected by temperature changes, as illustrated by the constant nature of the reduced efficiency curve.

Acknowledgments

The authors gratefully acknowledge the financial support for this project provided by the US Bureau of Mines through the Generic Center for Comminution at the University of Utah, and by the Dow Chemical Company. The authors also thank Krebs Engineers, Inc. for providing the hydrocyclone used in this project.

References

Agar, G. E. and Herbst, J. A., 1966. "The Effect of Fluid Viscosity on Cyclone Classification", *Trans. SME-AIME*, vol. 235, pp. 145-149.

Austin, L. G., Klimpel, R. R., and Luckie, P. T., 1984, *Process Engineering of Size Reduction: Ball Milling*, AIME, New York.

Bradley, D., 1965, *The Hydrocyclone*, Pergamon Press Ltd., London.

El-Shall, H., Somasundaran, P., 1984, "Mechanisms of Grinding Modification by Chemical Additives: Organic Reagents", *Powder Technology*, Vol. 38, pp. 267-273.

Fuerstenau, D. W., Venkataraman, K. S., and Velamakanni, B. V., 1985, "Effect of Chemical Additives on the Dynamics of Grinding Media in Wet Ball Mill Grinding", *International Journal of Mineral Processing*, Vol. 15, no. 4, pp. 251-268.

Herbst, J. A., and Rajamani, K., 1979, "Control of Grinding Circuits", in *Computer Methods for the 80's*, A. Weiss, ed., AIME, New York, pp. 770-786.

Kampf, H. J., 1985, personal communication.

Klimpel, R. R., 1982, "The Influence of a Chemical Dispersant on the Sizing Performance of a 24-inch Hydrocyclone," *Powder Technology*, Vol. 31, pp. 255-262.

Klimpel, R. R., 1984, "Influence of Material Breakage Properties and Associated Rheology on Breakage Rates in Wet Grinding of Coal and Ores in Tumbling Media Mills," in *Reagents in the Minerals Industry*, M. J. Jones and R. Oblatt, eds., Institution of Mining and Metallurgy, London, pp. 265-270.

National Materials Advisory Board (NMAB), 1981, *Comminution and Energy Consumption*, NMAB 364.

Selective flotation of fossil resin from Wasatch Plateau high-volatile bituminous coal

J. D. Miller and Y. Ye

Abstract — *Certain bituminous coals are known to contain appreciable quantities of natural fossil or subfossil resin. Such resinous coals are found in the western US, particularly the Wasatch Plateau coalfield of UT. Some of the seams in this field contain an average of 5% resin. This fossil resin has been recovered by gravity and/or flotation processes since 1929. Resin concentrates thus produced are of low quality and are usually refined by solvent extraction. The purified resins are of commercial importance in the adhesive, coating, rub' and ink industries, etc. An improved flotation technique been developed which involves ozone conditioning to selec· tively float resin from high-volatile bituminous coal. With this flotation process, a concentrate product which contains 95%*

Y. Ye, and J.D. Miller, member SME are with Dept. of Metallurgy and Metallurgical Engineering, University of Utah, Salt Lake City, UT.

SME preprint 88-198. SME Annual Meeting, Phoenix, AZ, January 1988. M&MP paper 88-614. Manuscript January 1988. Discussion of this paper must be submitted, in duplicate, prior to July 31, 1989.

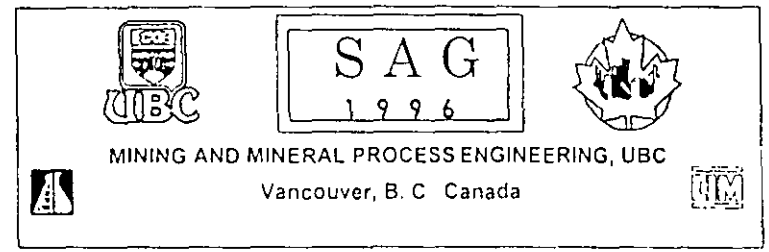

EFFECT OF PULP RHEOLOGY ON AUTOGENOUS GRINDING PERFORMANCE

A. K. Bakshi, K J. Shoop and S. K. Kawatra
Department of Metallurgical and Materials Engineering
Michigan Technological University
Houghton, MI 49931 U. S A.

ABSTRACT

Autogenous grinding mill efficiency is affected by pulp rheology, which can change due to several factors such as ore composition, temperature, or chemical additions. In this study the effect of slurry viscosity on rock breakage characteristics and specific energy consumption were studied in a pilot scale autogenous mill Rock breakage inside the mill was studied quantitatively by measuring the size stability of rocks on a scale of 0 to 100%, where a 100% size stability corresponds to zero rock breakage . Also, the effect of slurry viscosity on the production of critical size material was studied, where the "critical size" is material which is too large to be effectively ground in the mill, and too small to be effective for grinding other particles The pulp rheology was altered by changing the initial clay/fines content of the feed and also by changing the initial temperature of both ore and water It was observed that size stability, critical size material production, and specific energy consumption all increased as the slurry viscosity increased.

INTRODUCTION

The effect of slurry rheology on the performance of grinding ciruits has been well discussed in the literature (Hemmings and Boyes, 1977, Tucker 1982, Klimpel, 1982 and 1983, Fuerstenau

,G testing of core samples, however, will require y samples because the core itself gives the proper types.

ist offers the potential to implement mine planning roduction on a routine basis.

RECOMMENDATIONS

Power Index Test can be used to determine the to grind to 10 mesh. Additional power to give a ild be added according to Bond ball mill grinding . If Bond ball mill work index data is not available, Figure 2 as a first estimate of SAG power required idicated natural grain size

Test for new projects to determine hardness vari- ing the various rock types in several continuous ersections through an ore body. By knowing the in hardness, needed adjustments to pilot plant nade at the design stage. The SPI Test can be cations for mining pilot plant bulk samples for pilot g.

can be used as a problem solving tool at any op- pecially where ore hardness variance is causing ems due to lack of blending or other reasons.

ACKNOWLEDGMENTS

edgment is given to the six MITEC study spon- their support of the work described herein, but mission to publish this paper. Our thanks are Miramar Mining who have given permission to ing to the Delita Gold Project Feasibility Study eparation.

REFERENCE

y, G. and Kosick, G., "A New Tool For SAG , Proc. Canadian Mineral Processor's Confer-

et al., 1984, Austin et al , 1984, Moys, 1989, Kawatra and Eisele, 1988, Kawatra and Bakshi, 1996). However, most of these studies dealt with ball mill grinding, where the grinding media are metal balls. In autogenous grinding, the media is the ore itself. Therefore, the efficiency of autogenous grinding also depends upon the way the media (larger size rocks) break inside the mill. Although the effect of rheology has been studied for various aspects of autogenous grinding (Moys, 1989), its effect on the breakage characteristics of the media is not discussed in the literature. This is an important problem, because small changes in the break-up rate of the media-sized rock will significantly affect the grinding efficiency of the mill.

Another problem in autogenous grinding is the production of critical size material. These are the particles that are too small to efficiently grind other particles, but too large to be easily ground themselves. Critical size particles tend to accumulate in the mill, and have to be removed and crushed separately as shown in Figure 1.

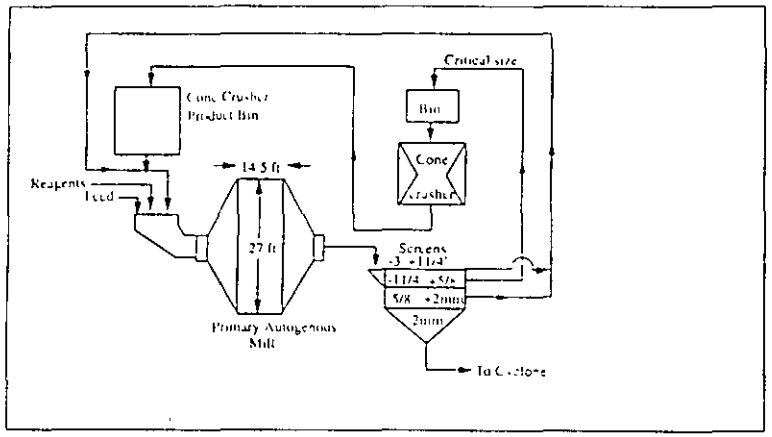

Figure 1: Typical autogenous circuit. Critical size is crushed before feeding back to the autogenous mill

Therefore, production of critical size must be minimized to further save in energy consumption. Any changes in the slurry viscosity that result in a change in the rate of media break-up will also tend to change the amount of critical size material that is produced. This effect has been observed in an operating plant (Kawatra and Eisele, 1988). The plant personnel noted that in the winter the grinding efficiency was reduced, and the amount of critical size of

material produced was increased. These changes were linked to the seasonal temperature variations of the mill slurry. Two possible mechanisms were considered that could have been causing these effects: (1) The rock may have been becoming more brittle at low temperatures or (2) The increasing slurry viscosity at low temperatures could have been affecting how the charge was lifted and tumbled in the mill. Past work by the authors has shown that the rocks were not becoming more brittle over the temperature range of interest (Kawatra et al., 1993), and so subsequent studies concentrated on the viscosity effects. In this article the impact of slurry rheology on the breakage characteristics of the rock and the overall energy consumption during autogenous grinding have been discussed. All tests were carried out using a pilot-scale mill so that the results would be relevant to what happens in a full-scale autogenous mill.

EXPERIMENTAL

Experimental Set-Up

Pilot Scale Autogenous Mill. Pilot plant tests were carried out in a 1.8 meter diameter by 0 6 meter long Hardinge cascade mill. The mill contained sixteen 2.5 cm high lifter bars. It was converted from continuous operation to batch operation by removing the grates on the discharge end of the mill and replacing them with liners made at Michigan Technological University. This mill was also insulated to maintain the initial charge temperatures, using 20 cm of fiberglass insulation applied to the circumference of the mill and 2.54 cm thick polystyrene foam insulation on the ends Energy consumption during each test was measured by a standard watt-hour meter

Viscometer Set-Up. Slurry viscosity was measured by a Brookfield viscometer. Since the slurry contained fast settling solids, it was necessary to modify the viscometer so that the solids would be kept in suspension while the reading was being taken. This was accomplished by the slurry presentation system shown in Figure 2. The slurry was mixed in an overhead tank and passed continuously through the annular space between a steel tube andthe spindle. After a steady state reading was displayed, flow was momentarily interrupted to eliminate any swirling motion caused by flow at the inlet and a reading was taken immediately.

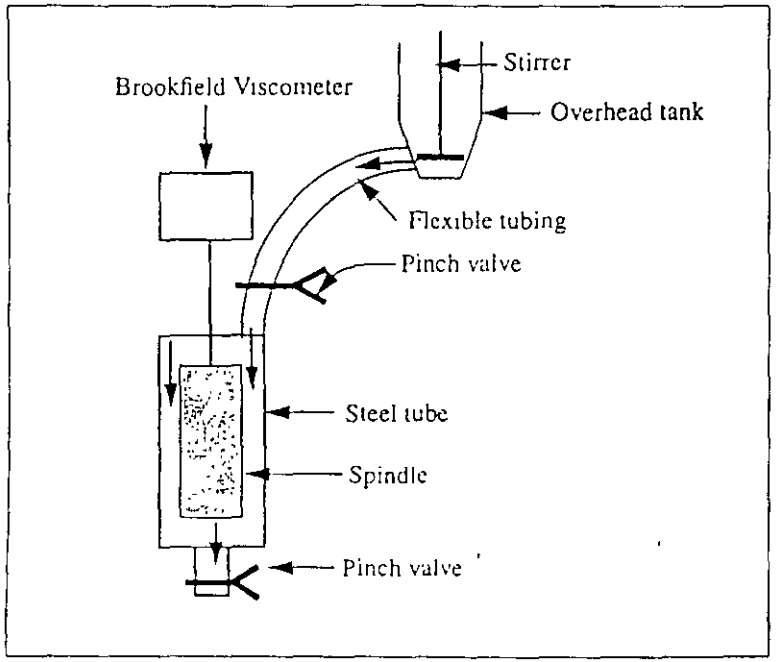

Figure 2: Brookfield set-up showing arrangement for measuring viscosities of rapidly-settling solids in slurries

This set-up is very suitable for measuring viscosity of slurries containing fast settling solids, and has been successfully used to characterize different slurries on the basis of their rheology (Kawatra and Bakshi, 1995)

Sample Preparation

An iron ore sample was collected from a local iron ore deposit. Each rock was sized and washed to (i) remove any fines that might be in the pores or fractures of the sample, and (ii) remove the visually detectable metamorphic clay material present in the sample The washed ore was then dried From this material, six samples were reconstituted according to the size distribution shown in Table 1 This was the original size distribution of the rocks in the pit from where the sample was collected. Samples prepared for cold tests were stored in a freezer at -25 °C, and samples prepared for tests at room temperature were stored in 55 gallon drums.

Table 1: Size distribution of reconstituted feed sample for pilot scale AG tests.

Size Distribution, mm	Weight, kg	% Weight
-152.4 + 127 0	63.12	14.93
-127 0 + 101.6	65.83	15.59
-101.6 + 76.2	79.45	18.80
-76.2 + 50 8	82.17	19.47
-50.8 + 25.4	92.16	21.83
-25.4 + 12.7	39.50	9.38
Total	422.22	100.00

Test Procedure

Six tests were carried out in the pilot scale autogenous mill. The viscosity of the mill slurry in these tests was changed by changing the clay/fines content in the initial feed and by changing the temperature of both iron ore and water as shown in Table 2.

Table 2: Conditions for tests with pilot scale AG mill.

Test no.	Initial ore temp, °C	Feed composition	Slurry viscosity at end of test, mPa-sec
1	+25	Ore only	1 37
2	-25	Ore only	1.60
3	+25	Ore with 10% clay	1.42
4	-25	Ore with 10% clay	1.74
5	+25	Ore with 50% fines	5 24
6	-25	Ore with 50% fines	8 19

The clay material added during tests 3 and 4 was the same metamorphic clay which was washed from the initial ore collected from the mine pit. During tests 5 and 6, 50% fines were added in the mill. The fines were prepared by grinding iron ore to pass 425 mm, and 59 5% of the resulting fines were finer than 150 mm. This was done because under plant conditions, a certain amount of fines (ground ore) is always present inside the mill due to

continuous operation. Since the tests were conducted as batch tests, the loads in the mill for tests 1-4 were initially devoid of these fines, and therefore had low slurry viscosities. The addition of a large amount of fine iron ore in tests 5 and 6 was expected to strongly show the effects that would occur in a plant situation due to the presence of fines.

The mill was chilled prior to the tests conducted at low temperatures. It was run empty for 30 minutes before each test to allow the bearings to warm up, so that bearing friction would be constant during the test. Then the mill was stopped, and solids charge was added to the mill. A total of 423 kg solids were added for each test. Then, 182 kg of water was added to keep the total solids content at 70% by weight The mill volume occupied by the charge was 26% The initial temperature of water for the cold tests was maintained at 4 °C for test # 2, 4, and 6, and for other tests the water was at room temperature The slurry temperature was measured both at the beginning and the end of each test, to be sure that the mill did not warm significantly during the test.

Once the mill was charged with solids and water, it was run for 15 minutes. A slurry sample for viscosity measurement was collected from the mill as soon as it stopped rotating. Energy consumption during the 15 minute grinding was measured using a watt-hour meter. The material from the mill was removed manually, and screened for size analysis.

RESULTS AND DISCUSSION

Size Stability

Size stability vs. slurry viscosity is shown in Figure 3 Size stability is a measure of the resistance of the media to impact breakage, and is expressed as follows (ASTM, 1991)

$$\% \text{ Size Stability} = \frac{\Sigma[(initialWt\%)x(avg\ sievesize)]}{\Sigma[(finalWt\%)x(avg.sievesize)]} \times 100$$

Therefore, a size stability of 100% corresponds to a rock that did not break during grinding, and a size stability of 0% corresponds

to a rock that broke completely below the finest size measured (-12.5 mm in these tests).

As can be seen from Figure 3, size stability increased with increase in slurry viscosity, showing that at high viscosity the rocks had a higher resistance to breakage. This could be due to the fact that at higher viscosity the impact force between rocks was retarded by the viscous slurry which acted as a cushion, resulting in less breakage of the rock.

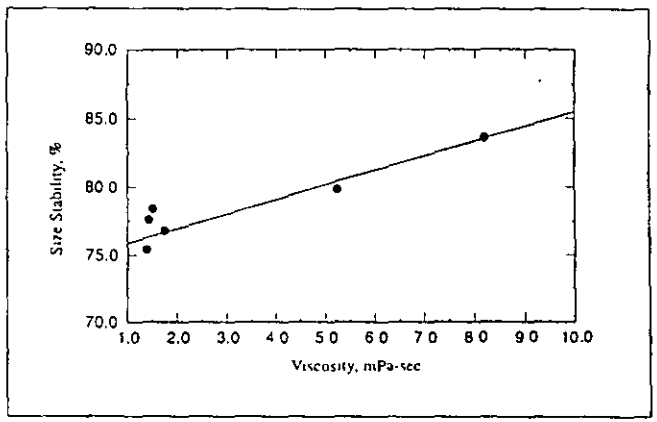

Figure 3: Size stability vs viscosity. At higher viscosity ore is less likely to be broken for all results.

Critical Size Material

The effect of slurry viscosity on critical size material is shown in Figure 4. Critical size material is the material which is too large to be effectively ground in the mill, and too fine to be effective for grinding other particles. This material is usually crushed outside the grinding mill (for example in a cone crusher as shown in Figure 1) before it can be sent back to the mill. In our tests, the change in the amount of material in the -25.4mm +12.7mm size fraction in the course of each test was small. Therefore, particles of this size were considered to be the critical size material.

The feed for each test initially contained 9.38% critical size material (see Table 1) The percentage of the critical size material was determined again at the end of each test. As can be seen in

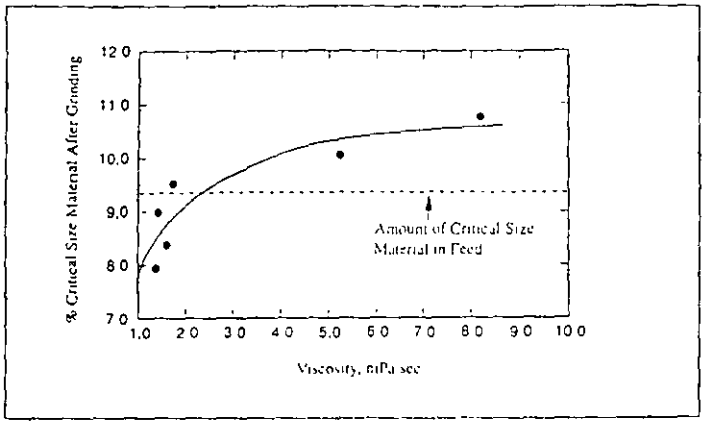

Figure 4: % critical size in mill after grinding vs viscosity. At high viscosity amount of critical was larger than at the start.

Figure 4, at low slurry viscosity the amount of critical size material in the mill after grinding was less than the amount of critical size material present before grinding. However, at higher viscosity there was an increase in critical size material after grinding. During the first four tests, when the viscosity was low the slurry was more like water. Therefore, in this condition the slurry did not leave a thick coating on the surfaces of both the media and the critical size particles. This allowed some critical size material to be crushed upon impact At higher viscosity, there was a thick coat of slurry on the media (large rocks). This retarded the energy of the impact collisions, and reduced the chances of a critical size particle to be broken up in the mill. Therefore, during test No 6, when the viscosity was increased to 8 19 mPa-sec by adding fines and decreasing the temperature, the critical size content in the product increased by 1 37% to 10 8%

The results with added fines are most similar to the situation in full size plants, because due to continuous operation considerable amounts of fines are always present inside the mill which will keep the slurry viscosity in a higher range. For example Figure 5, shows the critical size material in a full-scale plant as a percentage of total feed during each month The data were collected over a period of two years from the local iron ore plant that provided the iron ore for the work reported herein. As seen from the figure, critical size material production was at a minimum between April and September, and increased significantly duringDecember and January when the temperature was low (Kawatra and Eisele, 1992). It was originally believed that this change in

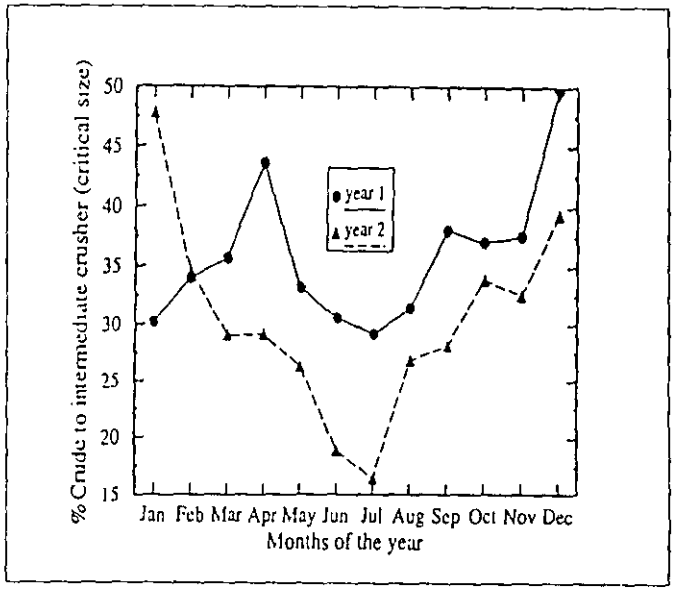

Figure 5: Critical size production in 8.2m x 4.4m primary AG mill for iron ore over 2 years.

critical size production was due to increased brittleness of the rock at low temperatures. However, drop tests conducted at Michigan Technological University showed that rocks did not become brittle over the temperature range of interest (+25 °C to -25 °C) (Kawatra et al., 1993). Therefore, these changes in critical size material production are due to viscosity changes caused by temperature variation.

Specific Energy Consumption

Specific energy consumptions at different slurry viscosities are shown in Figure 6 Specific energy consumption was calculated as the energy required to produce one kilogram of -150 micron material

As can be seen from Figure 6, the specific energy consumption of the mill increased with increasing slurry viscosity. The increase in specific energy from test 1 to test 4 was small, because the viscosity changes during these tests were also very small. However, during tests 5 and 6 specific energy consumption increased significantly While comparing the specific energy con-

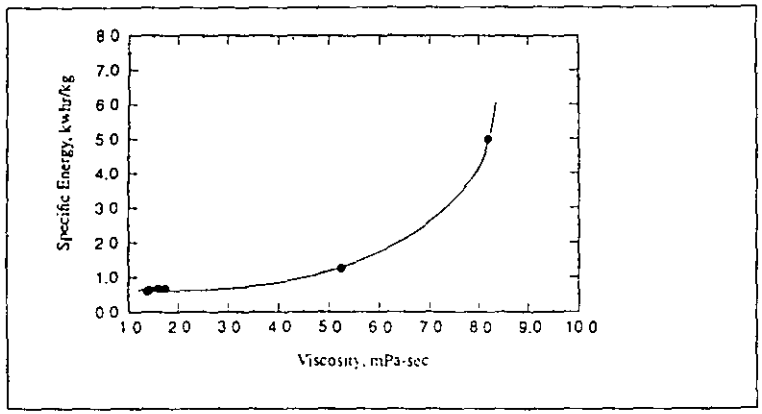

Figure 6: Specific energy vs viscosity. Noteincrease at high viscosities.

creased significantly While comparing the specific energy consumption between tests, the following observations were made:

(i) When the viscosity increased from 1.37 mPa-sec (test no.1) to 5.24 mPa-sec (test no. 5) due to fines addition, specific energy consumption increased from 0.63 kwhr/kg to 1.11 kwhr/kg.

(ii) When the viscosity increased from 5.24 mPa-sec (test no. 5) to 8.19 mPa-sec (test no. 6) due to decrease in temperature, specific energy consumption increased again, going from 1.11 kwhr/kg to 5.0 kwhr/kg. This trend agreed with the observations made in the local iron ore plant (Figure 7), where specific energy consumption increased by ~20% during winter months when the slurry temperature was very low (Kawatra and Eisele, 1992).

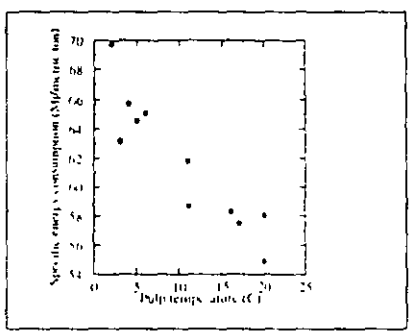

Figure 7: Specific energy consumption for 8.2m x 4.4m primary iron ore AG mill as function of temperature (see Kawatra and Eisele, 1992).

CONCLUSIONS

From our tests the following conclusions were made:

1. The resistance of the media-sized ore to breakage increased when the slurry viscosity was increased. This effect was prominent at higher viscosities.

2. Production of critical size material increased at higher slurry viscosity These results agreed with plant observations reported by Kawatra and Eisele (1992), where critical size material production increased during winter months. It has already been determined that brittleness of the individual rocks does not change with temperature (Kawatra et al., 1993), and so the change must be due to changes in the behavior of the mill slurry as a whole. Since pulp viscosity increases at lower temperatures during winter months, such changes can be attributed to changes in pulp viscosity.

3. The specific energy consumption in the mill increased as the viscosity increased. This was a result of the increased viscosity reducing the grinding rate by cushioning of impacts, and by changing the motion of the charge in the mill. This explains the increased specific energy consumption in northern U.S. operations during winter months, when the temperature is very low.

ACKNOWLEDGEMENTS

This research has been supported by the Department of Interior's Mineral Institute program administered by the Bureau of Mines through the Generic Mineral Technology Center for Comminution under grant number G1115149.

REFERENCES

ASTM, 1991, Standard Method of Drop Shatter Tests for Coal, D440-86, Annual book of ASTM standards, Vol. 5.05, pp. 214.

Austin, L. G., Klimpel, R. R., and Luckie, P. T., 1984, "What Laboratory Tests Tell Us About Breakage in Ball Mills," Chapter 5, Process engineering of Size Reduction: Ball Milling, Society of Mining Engineers, American Institute of Mining, Metallurgical , and Petroleum Engineers, Inc , New York, pp. 79-176.

Fuerstenau, D. W., Venkataramana, K. S., Velamakanni, B. V., 1984, "Effect of Chemical Additives on the Dynamics of Grinding Media in Wet Ball Mill Grinding," Inter. J. of Miner. Process., Vol. 15, pp 251-267.

Hemmings, C E , and Boyes, J M., 1977, "An On-Line Viscometry Technique for Improved Operation and Control of Wet Grinding Circuits," Twelfth International Mineral Processing Congress, Sao Paulo, pp 46-64

Klimpel, R. R., 1982 & 1983, "Slurry Rheology Influence on the Performance of Mineral/Coal Grinding Circuits," Part I, Mining Engineering, 34 (12), (1982), pp. 1665-1668, Part II, Mining Engineering, Vol. 35, No 1, (1983), pp. 21-26.

Kawatra, S. K. and A. K Bakshi, 1996, "The Effect of Slurry Viscosity on Hydrocyclone Classification," Inter. J. of Miner. Process., paper accepted for publication.

Kawatra, S. K. and A. K. Bakshi, 1995, "Determination of Changes in Rheological Properties of Coal Slurries in Process Streams," Coal Preparation, Vol 15, pp 165-175

Kawatra, S. K , Moffat, S. A , DeLa'O, K. A., 1993, "The Effect of Freezing Conditions on Rock Breakage," Society for Mining, Metallurgy, and Exploration, Inc , Preprint Number 93-17.

SAG 1996

MINING AND MINERAL PROCESS ENGINEERI

Vancouver, B. C. Canada

THE INFLUENCE OF SLURRY TRANSPORT OI DRAW OF AUTOGENOUS AND SEMI-AUTOGI

Dr. S. Morrell[1] and Dr. T. Kojovic[2]

1- Manager - Comminution Research, 2- Senior R
Julius Kruttschnitt Mineral Research Ce
Isles Road, Indooroopilly, Brisbane, Aus

ABSTRACT

In recent years there has been a trend in Australia circuiting autogenous and semi-autogenous mills clones. This has resulted in attention being focus relating to the ability of the grates and pulp lifters tc move slurry from the mill. This paper describes the fects on power draw and mill performance tha observed to occur due to poor slurry transport. which explain these phenomena are described. Tl to develop mathematical models which link grate fl slurry hold-up and power draw. The model's ability capacity and its effect on power draw is illustrated u data.

INTRODUCTION

Recent experience with a number of autogenous (a autogenous (sag) mills in Australia has highlighted th of efficient slurry transport related to power draw and

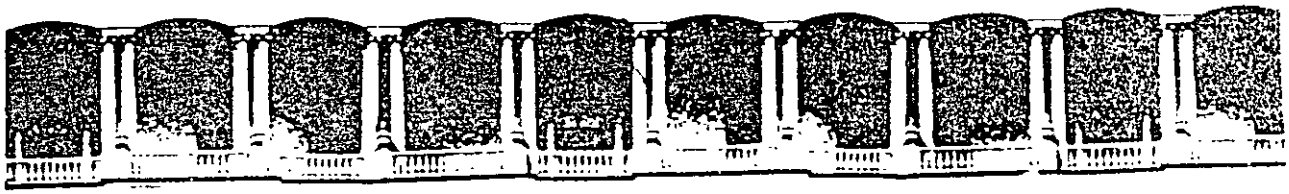

FACULTAD DE INGENIERIA U.N.A.M.
DIVISION DE EDUCACION CONTINUA

CURSOS ABIERTOS

DESARROLLO Y OPERACIÓN DE SENSORES PARA CONTROL DIRECTO Y CONTINUO EN PLANTAS DE BENEFICIO DE MINERALES Y EN LA RESTAURACIÓN DEL MEDIO AMBIENTE

Del 18 al 23 de mayo de 1998

TEMA: COMBINTATION TECHNIQUES

EXPOSITOR :DR. KOMAR KAWATRA

1998

OKKawatra

CHAPTER 12 Combination Techniques

12.1 Advantages of Combined Processes for Desulfurization

It has often been found that a combination of two different processes gives better desulfurization results than multiple stages of a single type of desulfurization process. This is because different types of separators will be most effective for removing particular kinds of sulfur-bearing particles. For example, if a pyrite particle has a thin coating of coal on its surface, it will behave as a coal particle in column flotation, and will report to the clean coal product. The same particle will be removed by a density-based separation, because its high pyrite content will cause it to have a high density. Conversely, a very fine particle of pure pyrite is likely to be too fine to be removed by a density-based separator, but will be easily rejected by froth flotation. It should also be remembered that fine pyrite particles without coal inclusions can also become hydrophobic upon oxidation.

Column flotation is now in commercial use for removing ash-forming minerals from fine coal, and has been studied for pyrite removal as well. According to release analysis tests that have been carried out on many high-sulfur coals, the maximum possible sulfur removal by column flotation is substantially less than the sulfur removal predicted from float/sink washability tests. It is generally accepted that release analysis represents the best possible flotation separation, while float/sink washability results are the best possible using density-based separations.

There are many possible combinations of desulfurization processes that would perform better than either process alone. The most basic approach is to divide the feed coal stream into size fractions, and then to process each stream by the most efficient process for that size. For example, Pittston Coal Management Company (USA) has constructed the Pittston Moss 3 preparation plant, which has a capacity of 800 tph and replaces a previous 35 year old facility. This plant incorporates a heavy-media cyclone/spiral/froth flotation circuit, which produces a product that is two percent lower in ash than was produced by the old heavy-media bath/Deister table/froth flotation plant,

without a loss in yield. Adjacent to this plant is the Middle Fork Pond Recovery operation, which replaced conventional flotation with Microcel column flotation in order to meet coal quality requirements. The Microcel columns are combined with improved desliming of the spiral product, which has reduced product ash and improved overall recovery (Stanley and Bethell, 1993).

While many plants utilize combinations of several different desulfurization processes, relatively few use these processes in series, with the same coal passing through two different types of separation. This is the type of combined operation which is most capable of producing a synergetic effect, where the product quality is higher than is possible with either process alone. Many of the possible process combinations have not yet been attempted. Others, such as the combination of selective comminution/classification with electrostatic separation, have been used in the laboratory but have not been used on a larger scale. There are many examples of such combinations, which are too numerous to be within the scope of this book. The combinations discussed will be those which are currently used in industrial practice, or which have significant potential for commercialization.

12.2 Flotation and Gravity

12.2.1 Gravity Separator followed by Flotation

Several examples of gravity separators followed by froth flotation have been described in the literature. A selection of case studies is presented here:

12.2.1.1 Case Study #1: Heavy Media/Water Only Cyclone, followed by Column Flotation with Regrind

A circuit was set up at the Ohio Coal Testing and Development center (OCTAD) as shown in Figure 12.1. This circuit used heavy cyclones and water-only cyclones to pre-clean the feed to an advanced column flotation cell. The circuit was operated at a feedrate of 2-3 tph, and was used to process coals from the Pittsburgh No. 8, Upper Freeport, and Illinois No. 6 seams (ICF Kaiser, 1993,1994; Ferris and Bencho, 1995).

The flowsheet was configured so that the raw coal was crushed to pass 1/4 inch, and then screened on a deslime sieve at 48 mesh. The material coarser than 48 mesh was fed to a 15-inch diameter heavy-media cyclone. The heavy-media refuse was dewatered and disposed of, while the heavy-media cleaned coal was crushed to pass 48 mesh. This re-crushed coal was combined with the minus 48 mesh material from the deslime screen, and pumped to two 6-inch diameter water-only cyclones. The water-only cyclone refuse was sent to the refuse thickener, while the clean coal overflow was directed to classifying cyclones. The classifying cyclone underflow (48 x 200 mesh) was reground in a 6-foot diameter ball mill, which was operated in closed circuit with the classifying cyclones. The classifying cyclone overflow, consisting of coal which had been pre-cleaned, crushed, and ground to pass 200 mesh, was used as feed to a 6-foot diameter advanced flotation cell. The column produced a final clean coal product which was thickened and dewatered using a solid-bowl centrifuge.

The performance of this circuit in processing a Pittsburgh No. 8 seam coal is given in Table 12.1, which shows the distribution of total weight, BTU content, and total pyrite among the reject products.

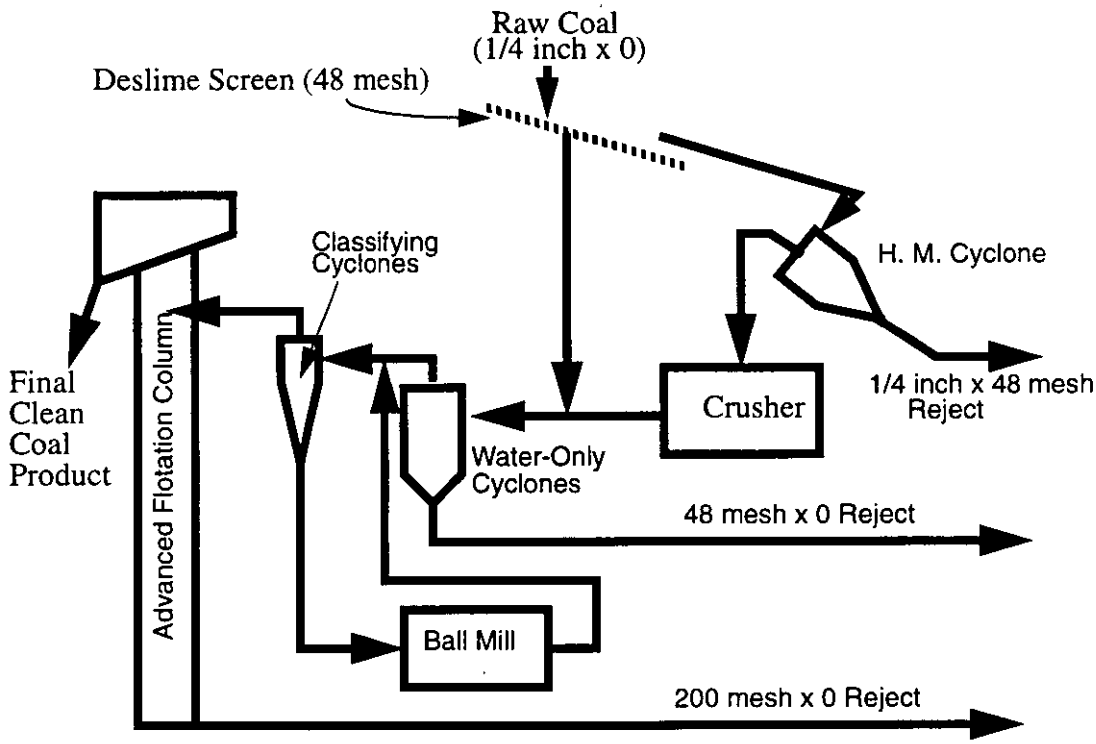

FIGURE 12.1 Flow diagram for the combined gravity/column flotation circuit tested at the OCTAD facility

TABLE 12.1 Summary of the results of processing a Pittsburgh No. 8 seam coal, using the OCTAD process flowsheet shown in Figure 12.1

Circuit Product	% Weight	%Ash	% Pyritic S	% of Feed BTU Content	% of Feed Pyrite Content
Raw Feed	100.00	46.05	2.04	100.0	---
1/4 inch x 48 mesh reject	31.1	---	---	3.8	44.3
48 mesh x 0 reject	4.5	---	---	4.0	16.6
200 mesh x 0 reject	16.2	---	---	2.7	12.7
Total Refuse	51.8	81.77	2.90	10.5	73.6
Final Clean Coal	48.2	7.65	1.12	89.5	26.4

Overall, the circuit showed a 48% yield at 89.5% BTU recovery, while removing 73.6% of the pyrite. A summary of the results obtained for all three coal seams processed is given in Table 12.2.These results indicate that for all three coals, it was possible to reject over 73% of the pyritic sulfur while

recovering over 85% of the total calorific value. This separation is largely due to the ability of the flotation column to reject the fine pyrite which was liberated during the crushing and grinding operations. This pyrite could not have been removed by the heavy-media cyclone or the water-only cyclones, because it was too fine for these units to process.

TABLE 12.2 Summary of the results of 24-hour demonstration runs of the OCTAD circuit shown in Figure 12.1, for coal from three different seams.

Coal Seam Processed	% BTU Recovery	% Pyrite Removal
Pittsburgh No. 8 seam	89.5	73.6
Upper Freeport seam	87.5	76.2
Illinois No. 6 seam	85.8	79.4

12.2.1.2 Case Study No. 2: Column Flotation followed by multigravity separator

The Mozley multigravity separator (MGS) is adversely affected by large quantities of ultrafine minerals (such as clays) in the feed, and so pilot-scale studies were carried out using a Microcel flotation column to pre-clean coal before using the multigravity separator (Venkatraman et al., 1995). When the MGS was used alone to treat Pittsburgh No. 8 seam coal, it could remove 70% of the pyritic sulfur but only 40% of the ash at 95% BTU recovery. When the flotation column was used to pre-treat the MGS feed, the overall removals of both ash and pyritic sulfur were 75-85%, at BTU recoveries of 85-90%.

12.2.2 Air-Sparged Hydrocyclone

The air-sparged hydrocyclone is an attempt to combine the hydrocyclone with froth flotation. It can therefore be considered as a combination of a density separation and a flotation separation being carried out simultaneously (Miller and Van Camp, 1981). A schematic of an air-sparged hydrocyclone is shown in Figure 12.2.

In air-sparged hydrocyclone flotation, the slurry is fed into the device through a standard hydrocyclone header. The swirling slurry enters a porous tube, where air bubbles are sparged into the slurry. The slurry is then discharged through an annular opening at the base of the cyclone. The feedrate and the diameter of the annular opening are adjusted to maintain a particular thickness of slurry on the cyclone wall (called the swirl-layer thickness). The air that is sparged into the cyclone is sheared into small bubbles at the cyclone wall, and the bubbles then migrate towards the center axis. As the bubbles travel, they attach to hydrophobic particles and carry them to the froth phase. The froth phase forms on the axis of the cyclone, and is supported by the froth pedestal, which forces the froth to discharge through the vortex finder. As in conventional flotation, the hydrophilic particles remain in suspension, and are discharged with the slurry phase. The flow patterns that occur in an air-sparged hydrocyclone are shown in Figure 12.3.

Conventional flotation separations becomes less effective as the particle size is reduced, because of the lower probability of collision between particles and air bubbles at fine particle sizes. In the air-

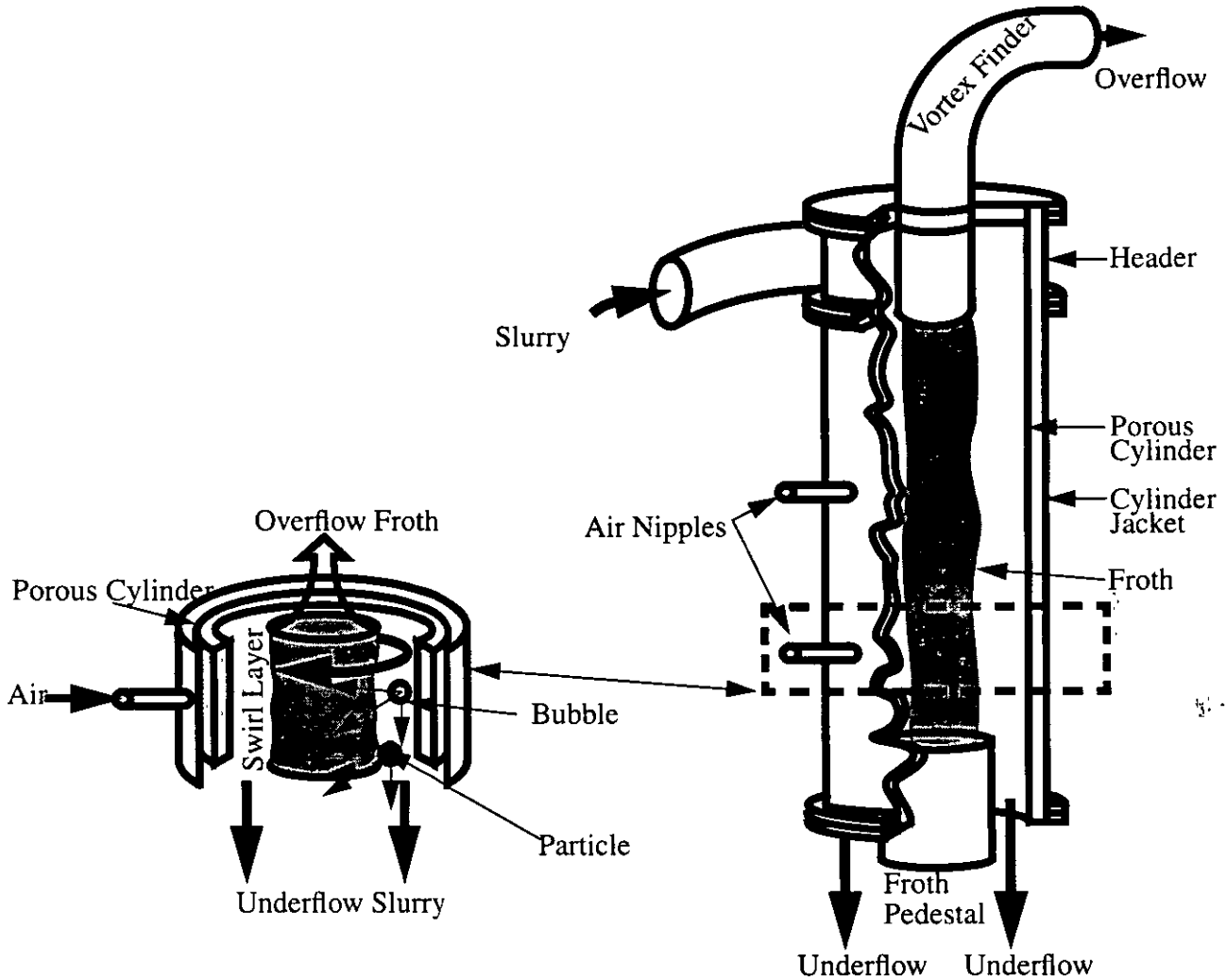

FIGURE 12.2 Cutaway diagram of an air-sparged hydrocyclone.

sparged cyclone, the application of a centrifugal force increases the probability that fine particles will interact with coal particles.

Miller and Kinneberg (1984) studied the effects of frother dosage on the bubble size in the air-sparged cyclone. As the level of MIBC frother was increased from 0 to 120 ppm, the bubble size remained essentially constant. Frother addition in the air-sparged cyclone is therefore required only to stabilize the froth phase.

The primary advantage of the air-sparged hydrocyclone is that it has a higher capacity per unit volume than conventional froth flotation machines. The high capacity is a direct result of the short residence time of slurry in the cyclone, which is only a few seconds.

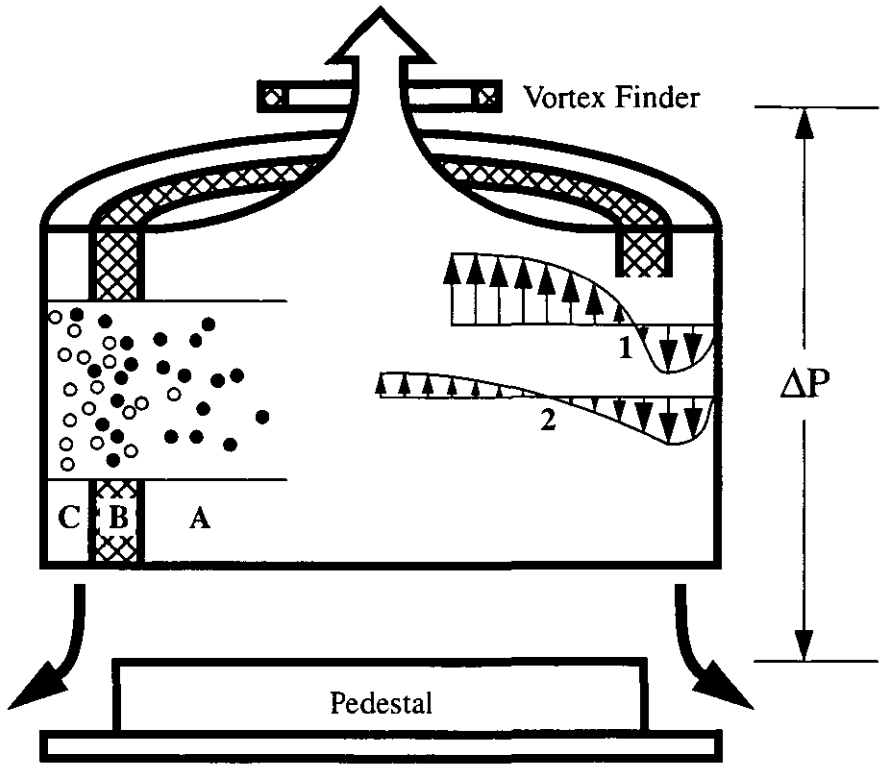

Region A	Froth Phase
Region B	Transition Phase
Region C	Slurry Phase
Region 1	Velocity Profile with Small Underflow Opening
Region 2	Velocity Profile with Large Underflow Opening

FIGURE 12.3 Flow profiles in an air-sparged hydrocyclone. As the diameter of the underflow opening is decreased, the magnitude of the vertical flows in the cyclone are altered as shown.

12.2.2.1 Froth Structure

In the air-sparged hydrocyclone, the air bubbles and attached hydrophobic particles lose their rotational velocity and move radially to the center of the cylinder, forming the froth core. The size of the froth core and its motion are dependent on the cyclone operating conditions and feed characteristics. The froth core is constrained on the sides by the swirl-layer, and is prevented from dropping out of the bottom of the cyclone by the froth pedestal. The froth is therefore forced to move upwards, discharging through the vortex finder (Stoessner, 1990).

12.2.2.2 Particle Size Effects

Since it is a modified hydrocyclone, the particles move through the air-sparged hydrocyclone in a manner similar to their motion in a conventional hydrocyclone. The coarser and denser particles tend to report to the underflow, where they discharge through the annular opening. The fine particles and low-density particles tend to be removed through the vortex finder, along with the froth product (Stoessner, 1990).

12.2.2.3 Operating Variables

A number of variables which are important for conventional hydrocyclones also influence the performance of air-sparged hydrocyclones. These include cyclone length, vortex finder diameter, size of underflow discharge, slurry inlet pressure, and feed percent solids. The operation of the air-sparged cyclone is also affected by the variables that influence flotation, including collector and frother type and dosages, particle size, and water quality. In addition, there are variables which are specific to they air-sparged cyclone, such as the pore diameter of the porous wall, and the air flowrate. These numerous variables make the operation of the air-sparged cyclone very complex, and its operation in a plant environment can be very difficult.

Stoessner (1990) has discussed the effects of these variables on the operation of 2 inch and 5 inch diameter air-sparged cyclones. Even in laboratory studies, the "fine" and "medium" grade porous tubes which sparge the air into the cyclones had to be replaced every 5 to 6 hours of operation, because of plugging. The "coarse" grade of porous tubes had a longer lifetime, in excess of 120 hours.

12.2.2.4 Processing Results

A 2 inch diameter air-sparged cyclone was tested at the EPRI/CQDC test facility, processing coals from the Upper Freeport, Pittsburgh No. 8, and Illinois No. 6 seams. Each coal was sized to pass 100 mesh. Testing of the Pittsburgh No. 8 and Illinois No. 6 coals at this facility was not successful, with the failure attributed to water quality (Stoessner, 1990). However, successful flotation of these coals was reported by the University of Utah. The reported results are given in Table 12.3.

TABLE 12.3 Pyrite removal results reported for a 2 inch diameter air-sparged hydrocyclone (Stoessner, 1990)

Feed Coal	Feed % Py. S.	Feed Pressure, PSI	Air Flowrate, slpm	Clean Coal % Py. S	Yield	% Py. S Removal	% Coal Recovery
Upper Freeport Seam	0.31	5	150	0.21	74.6	49.2	83.2
	0.33	20	450	0.28	57.2	51.9	65.4
Pittsburgh No. 8 Seam	1.57	5	150	0.59	58.4	77.9	73.1
	1.84	20	450	0.52	35.5	90.1	46.7
Illinois No. 6 Seam	1.11	5	150	1.08	37.0	64.2	63.1
	1.94	20	450	1.60	34.0	71.4	56.0

Tests have been carried out using larger-diameter air-sparged hydrocyclones (5 inches and 15 inches in diameter), but pyrite removal results for these units are not available.

12.3 Flotation and Agglomeration

12.4 Gravity and Magnetic Separation

Gravity separation processes, such as heavy-media separation, can be used in combination with magnetic separation (Liu, 1982). The advantage of this process is that fine grinding to liberate the smallest pyrite inclusions could be delayed until after the gravity separation, which saves the cost of grinding large amounts of gangue minerals that can be rejected at a coarse size. The removal of the bulk of the mineral matter before it reaches the magnetic separator also decreases the demands on this separator, allowing it to operate more efficiently. One of the potential disadvantages of this technique is that the magnetite heavy media which is commonly used in heavy-media separators can be carried over into the magnetic separator, interfering with its performance.

High-gradient magnetic separation has been studied in conjunction with heavy-media separation, using a pulverized Pennsylvania coal from the Sewickley seam (Weschler et al., 1980). The coal was ground to 90% finer than 200 mesh, and a portion of it was cleaned by heavy-media separation, using zinc chloride solution at a specific gravity of 1.6 as the dense medium. Using a magnetic field intensity of 17.1 Kilo-Oersteds and a slurry velocity of 18 to 20 mm/sec, the combined process could produce a product with a total sulfur content of 1.03%, compared to 1.33% sulfur when the magnetic separator was used alone, and 1.63% sulfur when the heavy-media separation was used alone.

12.5 Flotation and Magnetic Separation

Flotation can be readily used in conjunction with high-gradient magnetic separation, because both processes work well for fine coal particles (Liu, 1982). Flotation can remove the bulk of the impurities, including the clays with low magnetic susceptibilities, and the magnetic separator can then readily remove the residual pyrite.

Experiments were conducted by the U. S. Department of Energy to compare the performance of a combination of flotation and high-gradient magnetic separation (HGMS) with the performance of two-stage coal-pyrite flotation (Hucko, 1979). The magnetic field used was 21.6 kilogauss, and coals ground to pass 35 mesh and 200 mesh were studied. For the -35 mesh coal, the flotation/HGMS combination could remove 76% of the pyritic sulfur at a clean product yield of 65%. When the coal was ground to pass 200 mesh, 77% of the pyritic sulfur was removed at a product yield of 69%. The performance was approximately equal to the performance of two-stage coal-pyrite flotation at -35 mesh, and was superior to the coal-pyrite flotation at -200 mesh.

Pilot-scale tests of combined froth flotation/HGMS have been carried out for pulverized Pittsburgh No. 8 and Illinois No. 6 coals (Freyberger et al., 1979). A rod-mill/ball-mill/cyclone circuit was used to grind the coals to 75% passing 325 mesh, and they were then treated by rougher-

effects (such as froth flotation or oil agglomeration) with processes based on volume effects (such as density separators or magnetic separators). The main drawback to such combinations is that it is necessary to pay for installing and operating two different separation processes instead of only a single one.

12.8 References

Ferris, D. D., and Bencho, J. R. (1995) "Engineering Development of Advanced Physical Fine Coal Cleaning Technologies," *Proceedings of the 11th Annual Coal Preparation, Utilization and Environmental Control Conference*, U. S. Department of Energy, Pittsburgh Energy Technology Center, pp. 9-16

Freyberger, W. L., Keck, J. W., Spottiswood, D. J., Solem, N. D., and Doane, V. L. (1979) "Cleaning of Eastern Bituminous Coals by Fine Grinding, Froth Flotation, and High Gradient Magnetic Separation," *Proceedings of the Symposium on Coal Cleaning to Achieve Energy and Environmental Goals* (Rodgers and Lemmon, eds.) U. S. Environmental Protection Agency, EPA-600/7-79-098a, pp. 534-567

Hucko, R. E. (1979) "DOE Research in High Gradient Magnetic Separation Applied to Coal Beneficiation," *Industrial Applications of Magnetic Separation* (Liu, ed.), IEEE publication no. 78CH1447-2MAG, Institute of Electrical and Electronic Engineers, New York, pp. 62063

ICF Kaiser (1993) "Engineering Development of Advanced Physical Fine Coal Cleaning Technologies," 18th Quarterly Progress Report, U. S. Department of Energy, Pittsburgh Energy Technology Center, Project No. DE-AC22-88-PC88881

ICF Kaiser (1994) "Engineering Development of Advanced Physical Fine Coal Cleaning Technologies," 25th Quarterly Progress Report, U. S. Department of Energy, Pittsburgh Energy Technology Center, Project No. DE-AC22-88-PC88881

Liu, Y. A. (1982), "High-Gradient Magnetic Separation for Coal Desulfurization", *Physical Cleaning of Coal,* (Liu, ed.) Marcel Dekker, Inc.: New York, Basel

Miller, J. D., and Van Camp, M. C. (1981) "Fine Coal Flotation in a Centrifugal Force Field with an Air Sparged Hydrocyclone," SME-AIME Fall Meeting, Preprint No. 81-360

Miller, J. D., and Kinneberg, D. J. (1984) "Fast Flotation in an Air-Sparged Hydrocyclone," *Proceedings of MINTEK 50*, South Africa, Vol. 1, pp. 353

Oder, R. R. (1991) "Separation of Pyrites by Combined Agglomeration and High Field Magnetic Separation," *Processing and Utilization of High Sulfur Coals IV* (Dugan, Quigley, and Attia, eds.) Elsevier, Amsterdam, pp. 491-502

Stanley, F. L., and Bethell, P. J. (1993) "Process Modifications at Moss 3 Preparation Plant," *Proceedings of the 6th Australian Coal Preparation Conference* (Davis and MacKay, eds.), pp. 20-31, paper A2

cleaner froth flotation. The cleaner froth was then screened at 200 mesh to remove coarse particles that could plug the magnetic separator. The objective was to demonstrate the performance of the process during continuous operation in 15-hour operating shifts. With the Illinois No. 6 coal, pyrite removal was 73-76% at a clean coal yield of 85%.

12.6 Agglomeration and Magnetic Separation

The combination of agglomeration and high intensity magnetic separation has been studied on a bench scale. Agglomeration is used first to remove the bulk of the (largely non-magnetic) mineral matter, and is then followed by high-gradient magnetic separation to remove the pyrite particles not fully removed by the agglomeration stage.

This approach has been studied by Oder (1991) in bench-scale experiments, using Pittsburgh and Lower Freeport seam coals ground to particle sizes on the order of 1 micron. The agglomerant used was perchloroethylene (PCE), added at dosages ranging from 10% to 150% of the coal weight. Agglomeration was carried out in a 14 speed Hamilton Beach blender, with the shear rate varied by adjusting the blender speed. Agglomerates were screened at 200 mesh to separate them from the water and dispersed mineral matter. The aggomerated material was then treated in a high intensity magnetic separator at magnetic field strengths up to 15 Tesla (150,000 Gauss).

Using the above process, a Lower Freeport middling coal was treated, producing the results given in Table 12.4. These results show that by using this combination of processes, it is possible to produce a super-clean coal. The excellent ash and pyrite removal is made possible by the ability of the agglomeration stage to process very finely-ground and well-liberated coal, and of the magnetic stage to remove the remaining locked coal/pyrite particles.

TABLE 12.4 Results from processing a micronized Lower Freeport middling coal using agglomeration followed by froth flotation (Oder, 1991)

Product	% Combustibles Recovery	% Ash	% Total Sulfur	% Pyritic Sulfur
Feed Coal	100.0	15.37	1.78	1.11
Agglomeration Clean Coal Product	99.1	4.69	0.98	0.35
Agglomeration + Magnetic Separation Clean Coal Product	76.5	1.65	0.76	0.18

12.7 Summary

It has been shown that in many cases, treating a coal using two different processes in series provides better desulfurization results than can be achieved with either process alone. This is possible because the types of sulfur-bearing particle that are poorly removed by one type of separator can be readily removed by another. This is particularly true of combinations of processes based on surface

Stoessner, R. D. (1990) "Air-Sparged Hydrocyclone/Advanced Froth Flotation Fine Coal Cleaning," Final Report, U. S. Department of Energy, Pittsburgh Energy Technology Center, Report No. DOE/PC/88853-T2 (DE90016410)

Venkatraman, P., Luttrell, G. H., and Yoon, R.-H. (1995) "Fine Coal Cleaning Using the Multi-Gravity Separator,"*High-Efficiency Coal Preparation* (Kawatra, ed.), Society for Mining, Metallurgy, and Exploration, Littleton, CO, pp. 109-117

Weschler, I., Doulin, J., and Eddy, R. (1980) "Coal Preparation using Magnetic Separation," EPRI Report No. CS1517, Vol. 3, Electric Power Research Institute, Palo Alto, CA

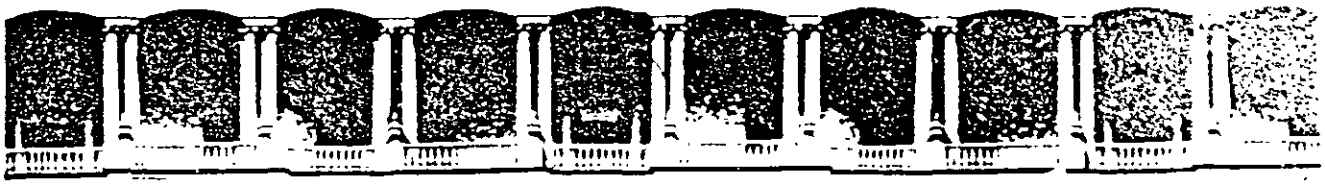

FACULTAD DE INGENIERIA U.N.A.M.
DIVISION DE EDUCACION CONTINUA

CURSOS ABIERTOS

DESARROLLO Y OPERACIÓN DE SENSORES PARA CONTROL DIRECTO Y CONTINUO EN PLANTAS DE BENEFICIO DE MINERALES Y EN LA RESTAURACIÓN DEL MEDIO AMBIENTE

Del 18 al 23 de mayo de 1998

**TEMA: EFFECTS OF VISCOSITY ON THE CUT (d 50)
SIZE OF HYDROCYCLONE CLASSIFIERS**

EXPOSITOR :DR. KOMAR KAWATRA

1998

Palacio de Minería Calle de Tacuba 5 Primer piso Delog. Cuauhtémoc 06000 Mexico D.F. A.P. Postal M-2285
Telefonos 512-8955 512-5121 521-7335 521-4021 Fax 512-8955 521-4020 AL 22

REFERENCES

Bradley, D., 1965. The Hydrocyclone. Pergamon Press, New York, N.Y.

Equipment Testing Procedures Committee, 1980. Particle Size Classifiers: A Guide to Performance Evaluation. American Institute of Chemical Engineers, New York, N.Y.

Klimpel, R.R., Austin, L. and Luckie, P.T., 1984. Process Engineering of Size Reduction: Ball Milling. Society of Mining Engineers, AIME, New York, N.Y.

Lilge, E.O., 1962. Hydrocyclone Fundamentals. Trans. IMM, Vol. 71, Part 6.

Lynch, A.J., 1977. Mineral Crushing and Grinding Circuits. Elsevier, New York, N.Y.

Lynch, A.J., Rao, T.C. and Bailey, C.W., 1975. The influence of design and operating variables on the capacities of hydrocyclone classifiers. Int. Miner. Process., 2: 29–37.

Napier-Munn, T.J., Reeves, T.J. and Hansen, J.O., 1985. The monitoring of medium rheology in dense medium cyclone plants. 2nd Samancor Symp. Dense Medium Separation, Perth, July, 1985.

Plitt, L.R., 1976. A mathematical model of the hydrocyclone classifier. Can. Inst. Min. Metall. Bull., 66: 114–123.

Reeves, T.J., 1985. On-line viscometer for mineral slurries. Trans. IMM, 94: C201–C208.

Seitz, R.A. and Kawatra, S.K., 1984. Further studies on the use of classifiers for control of wet grinding circuits. Int. Miner. Process., 12: 239–249.

FACULTAD DE INGENIERIA U.N.A.M.
DIVISION DE EDUCACION CONTINUA

CURSOS ABIERTOS

DESARROLLO Y OPERACIÓN DE SENSORES PARA CONTROL DIRECTO Y CONTINUO EN PLANTAS DE BENEFICIO DE MINERALES Y EN LA RESTAURACIÓN DEL MEDIO AMBIENTE

Del 18 al 23 de mayo de 1998

TEMA: EFFECTS OF VISCOSITY ON THE CUT (d 50) SIZE OF HYDROCYCLONE CLASSIFIERS

EXPOSITOR :DR. KOMAR KAWATRA

1998

Pergamon

PII:S0892-6875(96)00079-9

Minerals Engineering, Vol 9, No 8 pp 881-891 1996
Copyright © 1996 Published by Elsevier Science Ltd
Printed in Great Britain All rights reserved
0892-6875/96 $15.00+0.00

EFFECT OF VISCOSITY ON THE CUT (d_{50}) SIZE OF HYDROCYCLONE CLASSIFIERS

S.K. KAWATRA§, A.K. BAKSHI§ and M.T. RUSESKY†

§ Department of Metallurgical and Materials Engineering, Michigan Technological University, Houghton, MI 49931, USA

† Copper Range Company, White Pine, MI 49971, USA

(Received 15 February 1996; accepted 1 May 1996)

ABSTRACT

On-line measurement of slurry viscosity was carried out to study the effect of viscosity on the cut (d_{50}) size of hydrocyclone classifiers. As slurry viscosity increases, the settling rate of particle decreases, causing the d_{50} size to become coarser. The viscometer set-up used a vibrating sphere viscometer and a specially designed slurry presentation device to avoid settling of solids during viscosity measurement. This set-up was mounted on a test rig for a 10.2 cm diameter hydrocyclone. Test samples were prepared from ground silica (80% passing 65 microns) and water. Both the solids content and temperature of the samples were varied to change their viscosities. Samples from overflow and underflow streams were collected at regular intervals, and data from these samples were used to calculate the $d_{50}(c)$ size. Temperature and viscosity were recorded simultaneously during these tests.

From these data it was observed that $d_{50}(c)$ was proportional to the 0.35th power of the slurry viscosity. This relationship was then introduced in the existing Lynch and Rao model for siliceous material, to develop a modified model for hydrocyclone classification. This modified Lynch and Rao model incorporated a viscosity parameter from direct measurement, and predicted the cut size precisely when the viscosities of the slurries were altered by factors other than changing percent solids, such as temperature variation. This was not possible with the original Lynch and Rao model, which did not include any viscosity term. It was also determined that increasing slurry viscosity produced an increase in the bypass fraction, R_f. This effect was due to increased fluid drag in the hydrocyclone as the viscosity increased.
Copyright © 1996 Published by Elsevier Science Ltd

Keywords
Hydrocyclones; modelling; on-line analysis

INTRODUCTION

Fluid viscosity has a profound effect on the separation characteristics of hydrocyclones [1, 2]. Changing viscosity alters the particle settling rates and the slurry velocities in the hydrocyclone, and so alters the performance. When the viscosity increases, the settling speed of particles is decreased. Particles in the hydrocyclone must therefore be coarser in order to reach the underflow when the viscosity is high, and increasing viscosity causes the d_{50} size to increase. Therefore, viscosity must be included while developing mathematical models for cut size prediction. Although many models for classifier cut size developed in the

viscosity is independent of shear rate, but for non-Newtonian fluids it changes with changes in shear rate. This makes the viscosity effects on separation size more complex for non-Newtonian suspensions. Lucki[1] most mineral suspensions are Newtonian below 50% by volume [10] and their viscosities will not affected by changes in shear rate. Recently in other work [11], it was found that the silica slurries in our experiments, with an 80% passing size of 65 micron, were in the Newtonian flow regime up to a solids concentrations of 70% by weight. Of course, this will also depend upon the size distribution of the solids. Finer solids may begin to show non-Newtonian behavior at lower concentrations than coarser solids.

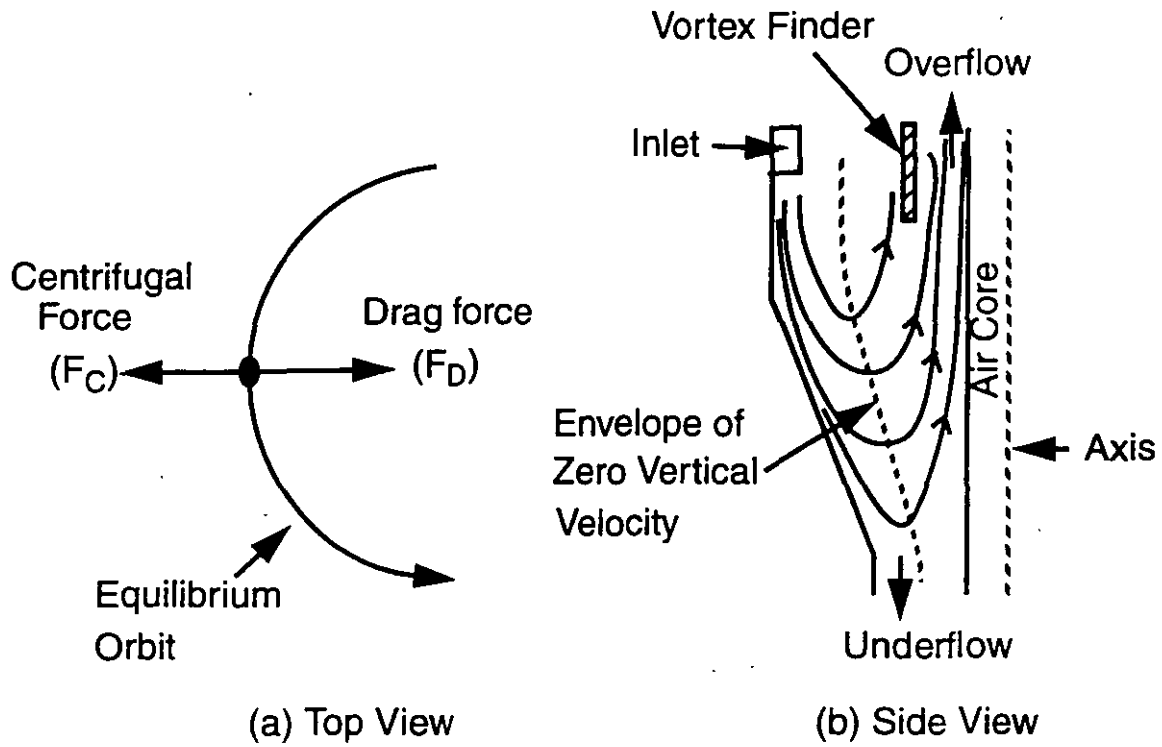

Fig. 1 Diagrams to explain the equilibrium orbit theory of hydrocyclone mechanism. The equilibrium orbit (a) is reached when the centrifugal force on the particle is equal to the fluid drag force. d_{50} size particles lie on the envelope of zero vertical velocity (b), and have equal chance of going to the overflow or to the underflow.

Viscosity also changes the water-to-underflow term, R_f, of the hydrocyclone. R_f is the fraction of feed liquid reporting to the underflow. The particles associated with this portion of the liquid travel downwards near the conical wall of the hydrocyclone, and are not centrifugally separated. Therefore, a fraction R_f of all particles irrespective of shape and size report to the underflow of the hydrocyclone. The fluid speed in the hydrocyclone is reduced due to increased viscous drag at higher viscosities, and this causes an increase in R_f.

Viscosity of the suspension certainly influences the separation mechanism of the hydrocyclone and should be addressed in the formulation of models depicting d_{50} size. The purpose of the test plan was to collect the data needed to modify the Lynch and Rao hydrocyclone model, which was developed under plant condition, to predict cut size not only from changes in percent solids, but also due to changes in slurry viscosity originating from factors other than percent solids (such as temperature, chemical environment, etc.). During all the tests conducted the slurry rheology was Newtonian.

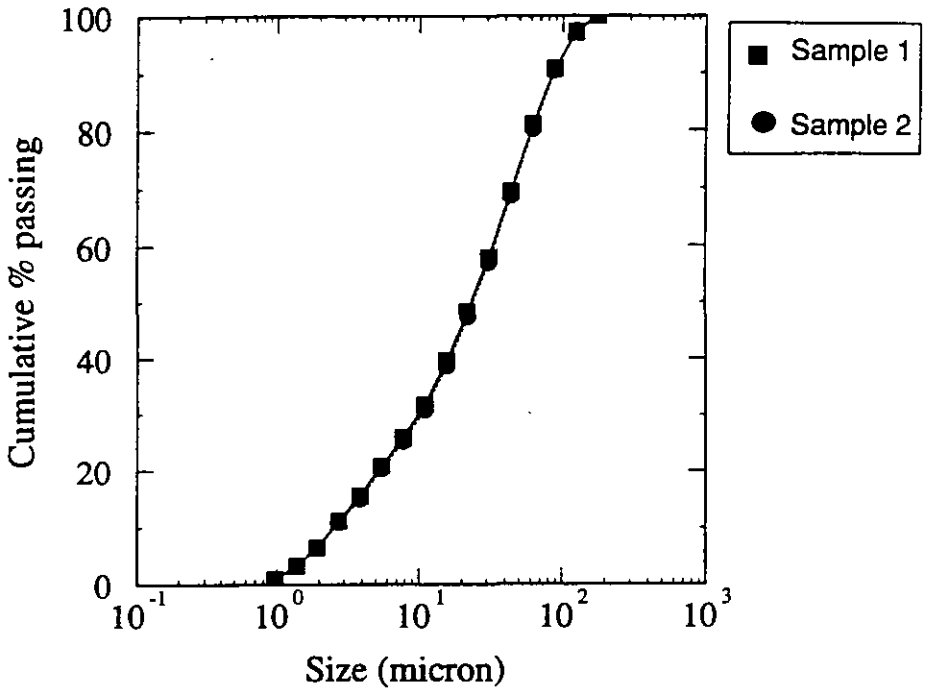

Fig.3 Size distribution of duplicate silica sample. The sample had a d_{80} passing size of 65 μm.

RESULTS AND DISCUSSION

Development of the Mathematical Model to Predict $d_{50}(c)$ Size

A modified model for $d_{50}(c)$ size was formulated by first introducing a viscosity term and then changing the percent solids term in the Lynch and Rao model [5, 12]. The viscosity term for the modified Lynch and Rao model was determined by plotting $d_{50}(c)$ vs. viscosity in a log-log scale (Figure 4). From this graph it was determined that the $d_{50}(c)$ size is proportional to the 0.35th power of the slurry viscosity, i.e.

$$d_{50}(c) \propto \eta^{0.35} \tag{2}$$

In the modified Lynch and Rao model a different percent solids term was used. This was necessary because higher percent solids not only increases the slurry viscosity but also causes hindered settling, and underflow crowding. These in turn increases the d_{50} size. In the original Lynch and Rao model this term was given as "$0.0173 \cdot \phi_w$." In the modified Lynch and Rao equation the percent solid term was found to be "0.41 log10 ϕ_v." The models before and after these corrections are given below.

(A) Lynch and Rao model before viscosity and percent solids correction:

$$\log_{10} d_{50}(c) = 0.0173 \cdot \phi_w - 0.0695 \cdot Spig + 0.0130 \cdot VF + 0.0048 \cdot Q + K_1 \tag{3}$$

Where,

K_1 = a constant
VF = inside diameter of the overflow or vortex finder, cm
Spig = inside diameter of underflow or spigot of the hydrocyclone, cm
Q = feed flow rate of slurry, liter/min
$d_{50}(c)$ = corrected cut size of the hydrocyclone, micron
ϕ_w = weight percent solids in the feed slurry

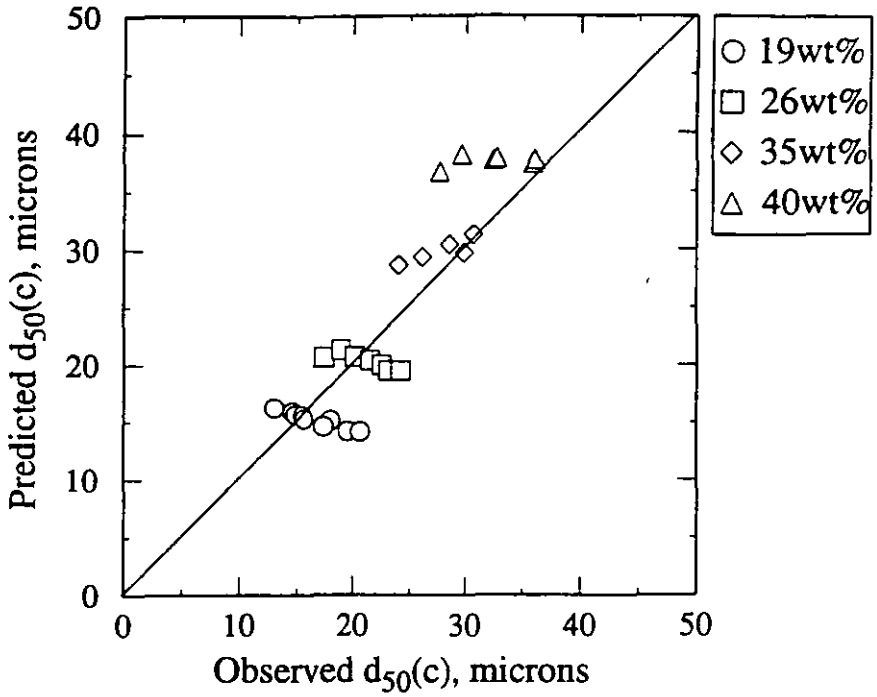

Fig.5 Predicted d_{50}(c) size from Lynch and Rao equation vs. observed d_{50}(c) size. The change in observed d_{50}(c) size within each solids percentage range is due to viscosity changes from changes in temperature. Since Lynch and Rao model does not include a separate viscosity term, the predicted d_{50}(c) size in individual percent solids range did not change.

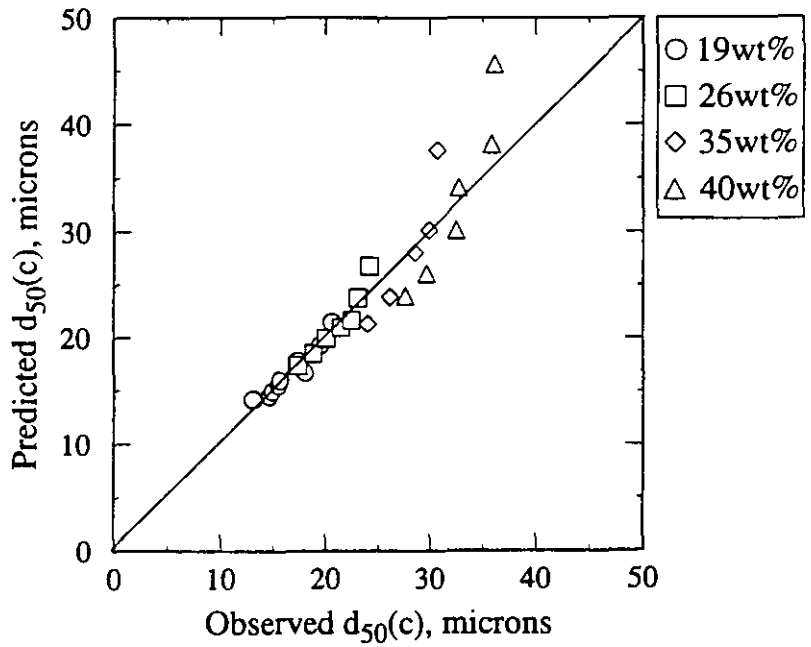

Fig.6 Predicted d_{50}(c) size from the new equation vs. observed d_{50}(c) size. Since this equation utilizes the viscosity data obtained by direct measurement, the increase in d_{50}(c) size due to viscosity changes from both increase in solids content and changes in temperature (10°C to 50°C at individual percent solids range) is reflected.

Effect of viscosity on water-to-underflow term, R_f

As can be seen from Figure 8, for slurries with 19, 26, and 35 wt% solids, R_f increased by as much as six percent when the viscosity of the slurry was increased by 2-3 centipoise. For the slurry with 40 wt% solids the change was rather less noticeable, at less than three percent for a 6 centipoise change in viscosity.

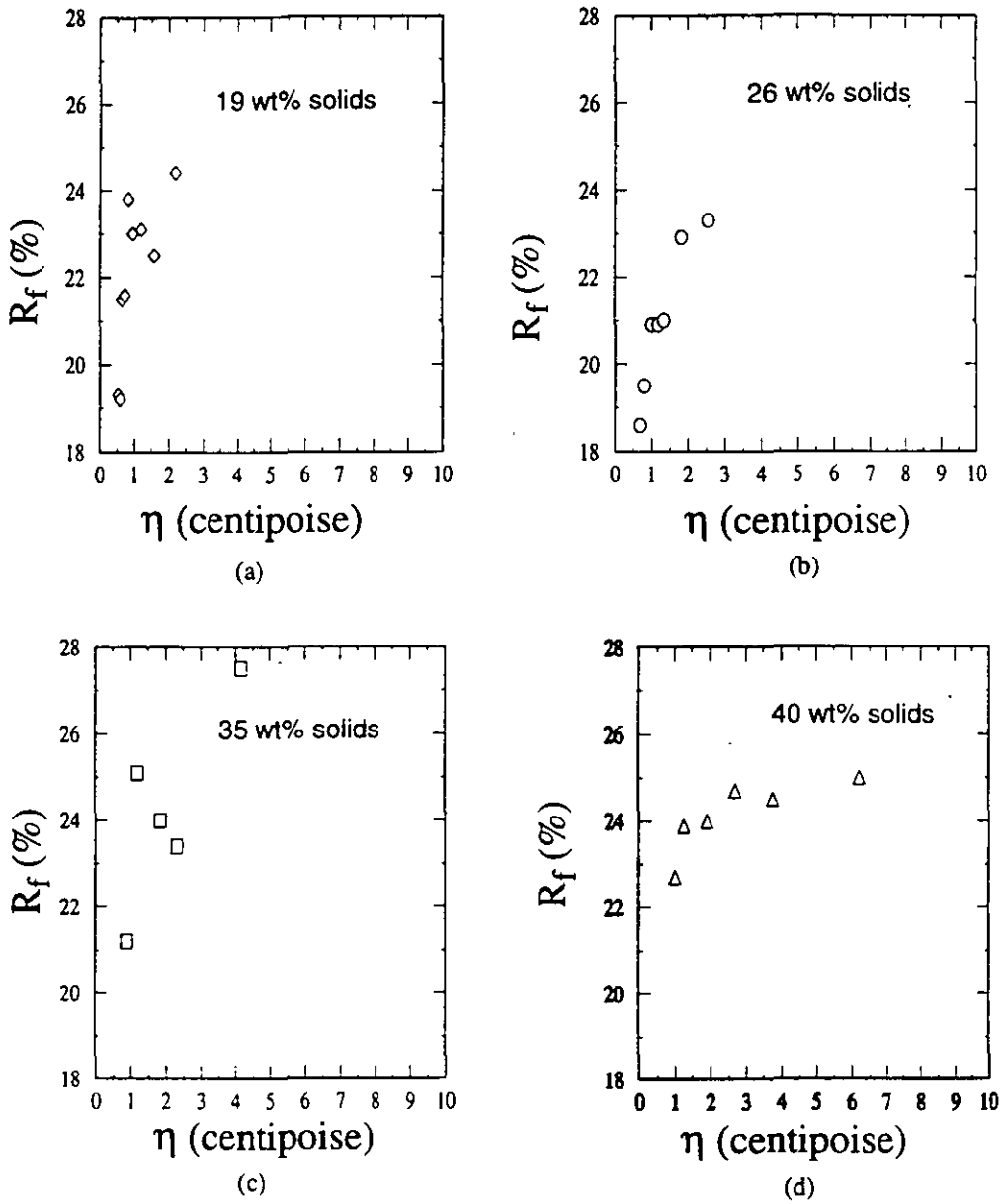

Fig.8 Effect of viscosity (η) on the water-to-underflow ratio (R_f). In each percent solids range, R_f increased with increase in η.

Effect of viscosity on classification index

Figure 9 gives the reduced efficiency curve for all the tests at 4 different concentrations and varied viscosities. The slope of this curve, called the classification index (α) is given by the following equation [12]:

REFERENCES

1. Agar, G.E. & Herbst, J.A., The Effect of Fluid Viscosity on Cyclone Classification. *Trans. AIME*, **235**, 145–149 (1966).
2. Kawatra, S.K. & Eisele, T.C., Rheology effects in Grinding Circuits. *XVI International Mineral Processing Congress*, Elsevier Science Publishers B. V., Amsterdam, 195–207 (1988).
3. Plitt, L.R., A Mathematical Modelling of the Hydrocyclone Classifier. *CIM Bulletin* 69, **776**, 114–123 (1976).
4. Plitt, L.R. & Kawatra, S.K., Estimating the Cut (d_{50}) Size of Classifiers Without Product Particle—Size Measurement. *International Journal of Mineral Processing*, 5, 364–378 (1979).
5. Lynch, A.J. & Rao, T.C., Modelling and Scale-Up of Hydrocyclone Classifiers. *The XI International Mineral Processing Congress*, Cagliari, 245–269 (1975).
6. Schack, C.H., Dean, K.C. & Molly, S.M., Measurement and Nature of the Apparent Viscosity of Water Suspensions of Some Common Minerals. *Report of Investigation 5334, U. S. Bureau of Mines*, (1957).
7. Kawatra, S.K. & Bakshi, A.K., On-Line Viscometry in Particulate Processing. *Mineral Processing and Extractive Metallurgy Review*, **14**, 249–273 (1995).
8. Bradley, D., *The Hydrocyclone*, Pergamon Press, New York, NY (1965).
9. Lilge, E.O., Fundamentals of Hydrocyclone. *Trans. Inst. Min. and Metll.*, 71 285–337 (1962).
10. Klimpel, R.R., Slurry Rheology Influence on the Performance of Mineral/Coal Grinding Circuits. *Mining Engineering*, **34**(12), 1665–1668 (1982).
11. Kawatra, S.K. & Bakshi, A.K., Determination of Flow Behavior Changes in Mineral Suspensions, in the annual meeting of the *Society for Mining, Metallurgy, and Exploration*, Inc., Denver, CO, Preprint No. 95–33 (1995).
12. Lynch, A.J., *Mineral Crushing and Grinding Circuits*, Vol. 1, Elsevier/North-Holland Inc., New York, NY 10017 (1977).

NOMENCLATURE

Inlet	inside diameter of the hydrocyclone inlet, cm
VF	inside diameter of the overflow or vortex finder, cm
Spig	inside diameter of underflow or apex of the hydrocyclone,
ϕ_w	weight percent solids in feed
ϕ_v	volume percent solids in feed
D_c	inside diameter of the hydrocyclone at the bottom of the vortex finder, cm
R_c	radius of the hydrocyclone, cm
F_C	centrifugal force
F_D	drag force
S	shear rate, sec^{-1}
V_t	tangential velocity of the fluid
W	radial velocity of the fluid
Q	feed flow rate of slurry, liters/minute
P	feed pressure, kilopascal
R_f	water-to-underflow ratio
K_1, K_2, K_3, K_4, K_5,	constants
d	diameter of the particle, micron
ρ_s	density of solid, gm/cm^3
ρ_l	density of liquid, gm/cm^3
η	viscosity of slurry, centipoise
β	exponent of slurry viscosity
α	classification index

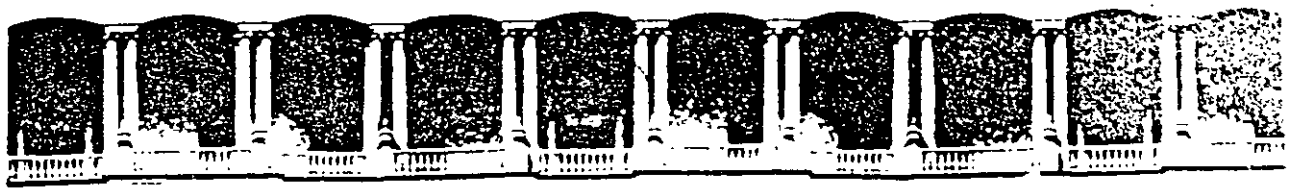

FACULTAD DE INGENIERIA U.N.A.M.
DIVISION DE EDUCACION CONTINUA

CURSOS ABIERTOS

DESARROLLO Y OPERACIÓN DE SENSORES PARA CONTROL DIRECTO Y CONTINUO EN PLANTAS DE BENEFICIO DE MINERALES Y EN LA RESTAURACIÓN DEL MEDIO AMBIENTE

Del 18 al 23 de mayo de 1998

TEMA: EFFECTS OF TEMPERATURE ON HYDROCYCLONE EFFICIENCY

EXPOSITOR :DR. KOMAR KAWATRA

1998

International Journal of Mineral Processing, 23 (1988) 205–211
Elsevier Science Publishers B.V., Amsterdam — Printed in The Netherlands

Effects of Temperature on Hydrocyclone Efficiency

S.K. KAWATRA, T.C. EISELE, D. ZHANG and M. RUSESKY

Metallurgical Engineering, Michigan Technological University, Houghton, MI 49931 (U.S.A.)

(Received December 9, 1986; accepted after revision September 15, 1987)

ABSTRACT

Kawatra, S.K., Eisele, T.C., Zhang, D. and Rusesky, M., 1988. Effects of temperature on hydrocyclone efficiency. Int. J. Miner. Process, 23: 205–211.

Plant investigations and laboratory experiments have been conducted in order to study the effects of temperature on the classification efficiency of a cyclone. It was demonstrated that, under otherwise constant operating conditions, alterations in temperature produced a nearly linear change in $d_{50(c)}$ size. However, the sharpness of the separation, as defined by the reduced efficiency curve, showed no dependence on temperature.

INTRODUCTION

The hydrocyclone has become a very popular classification device in mineral processing circuits, primarily due to its simplicity, high capacity, and small size. However, control of hydrocyclones is complicated by the numerous variables affecting their performance, the sometimes counterintuitive results of altering these variables, and the general lack of certainty of the true results of changing a given variable. In order to improve this state of affairs, a number of investigators (Plitt, 1976; Lynch, 1977; Klimpel et al., 1984) have intensively studied such variables as feed solids content, particle size, inlet pressure, inlet diameter, vortex finder diameter, spigot diameter, throughput, and particle specific gravity. However, little work has been reported which determines the effect of temperature on cyclone performance, in spite of the fact that many mineral processing operations are subject to large seasonal temperature variations, and have in several cases observed seasonal changes in grinding efficiency which appear to be due to temperature. The investigation described here was therefore carried out to determine the magnitude and nature of temperature effects in hydrocyclone operation.

0301-7516/88/$03.50 © 1988 Elsevier Science Publishers B.V.

stabilize for 10 min before the first overflow and underflow samples were taken, after which the slurry temperature was gradually decreased, with samples taken at approximately 5°C intervals. The use of the chiller allowed experiments over a temperature range of 50°C to 12°C.

The overflow and underflow samples were weighed, filtered, and dried. The dried samples were then weighed to allow the calculation of pulp densities, and the particle size distributions were determined with a Leeds and Northrop Microtrac particle size analyzer. The particle bypass fraction, R_f, was calculated from the fraction of the feed water which reported to the underflow, and cyclone efficiency values were corrected for R_f.

Plant studies

Investigations were carried out in an iron ore processing plant located in the northern U.S. which experiences substantial seasonal temperature variations, in order to determine whether normal temperature fluctuations produce a notable change in cyclone performance. This plant processes a very fine-grained iron ore which requires grinding to $-75\ \mu m$ for liberation. The grinding circuit is closed with 38-cm (15-inch) diameter hydrocyclones.

Sampling was carried out in the summer and in the winter in order to achieve the greatest temperature variation. Pulp temperatures ranged from 20°C (68°F) in the summer to 3.3°C (38°F) in the winter. The resulting corrected efficiency curves for these conditions are shown in Fig. 1.

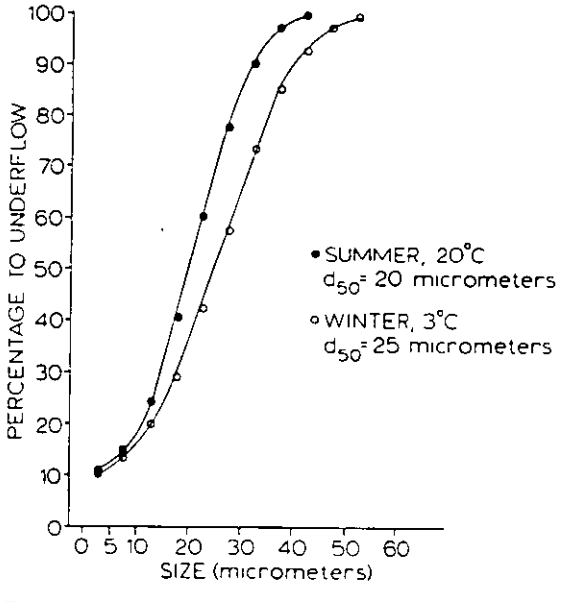

Fig. 1. Seasonal variations of cyclone performance in an iron ore processing plant.

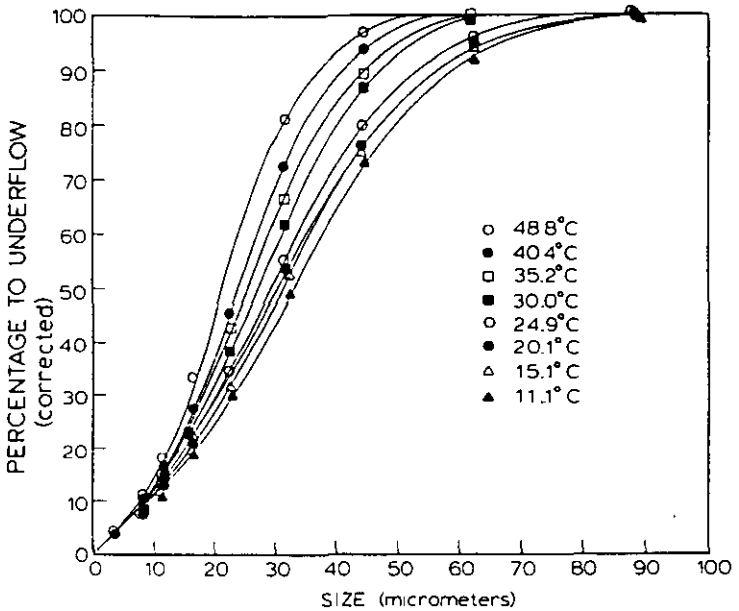

Fig. 2. Corrected efficiency curves showing dependence of hydrocyclone performance on slurry temperature.

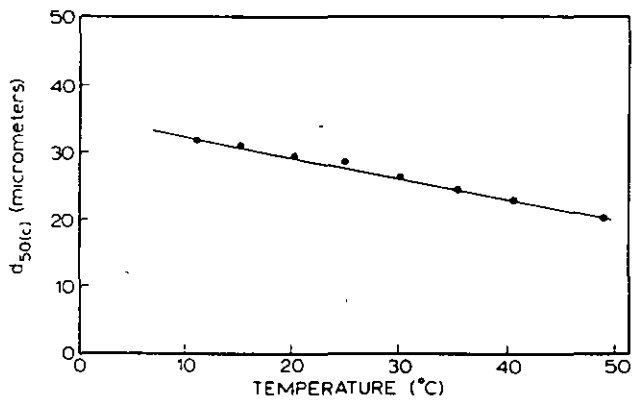

Fig. 3. Dependence of corrected d_{50} size on slurry temperature.

is that increasing the viscosity of the slurry increases the cyclone $d_{50(c)}$ size. Since the viscosity of a fluid typically increases with decreasing temperature, the observed temperature-dependence of $d_{50(c)}$ appears to be primarily a result of changes in slurry viscosity. Repeatable measurement of the viscosity of mineral slurries has proven to be very difficult, although workers in South Africa have achieved this with heavy-media slurries (Reeves, 1985; Napier-Munn et al., 1985). For our work, a vibrating-sphere viscometer was used, which produced the results shown in Table II. Although pump vibration produced a high background viscosity reading, the apparent slurry viscosity showed a temper-

REFERENCES

Bradley, D., 1965. The Hydrocyclone. Pergamon Press, New York, N.Y.

Equipment Testing Procedures Committee, 1980. Particle Size Classifiers: A Guide to Performance Evaluation. American Institute of Chemical Engineers, New York, N.Y.

Klimpel, R.R., Austin, L. and Luckie, P.T., 1984. Process Engineering of Size Reduction; Ball Milling. Society of Mining Engineers, AIME, New York, N.Y.

Lilge, E.O., 1962. Hydrocyclone Fundamentals. Trans. IMM, Vol. 71, Part 6.

Lynch, A.J., 1977. Mineral Crushing and Grinding Circuits. Elsevier, New York, N.Y.

Lynch, A.J., Rao, T.C. and Bailey, C.W., 1975. The influence of design and operating variables on the capacities of hydrocyclone classifiers. Int. Miner. Process., 2: 29-37.

Napier-Munn, T.J., Reeves, T.J. and Hansen, J.O., 1985. The monitoring of medium rheology in dense medium cyclone plants. 2nd Samancor Symp. Dense Medium Separation, Perth, July, 1985.

Plitt, L.R., 1976. A mathematical model of the hydrocyclone classifier. Can. Inst. Min. Metall. Bull., 66: 114-123.

Reeves, T.J., 1985. On-line viscometer for mineral slurries. Trans. IMM, 94: C201-C208.

Seitz, R.A. and Kawatra, S.K., 1984. Further studies on the use of classifiers for control of wet grinding circuits. Int. Miner. Process., 12: 239-249.

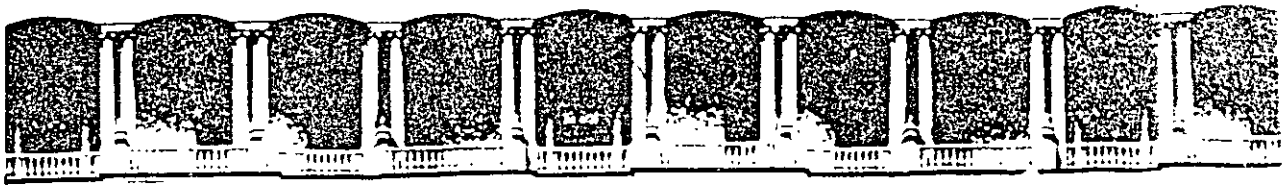

FACULTAD DE INGENIERIA U.N.A.M.
DIVISION DE EDUCACION CONTINUA

CURSOS ABIERTOS

DESARROLLO Y OPERACIÓN DE SENSORES PARA CONTROL DIRECTO Y CONTINUO EN PLANTAS DE BENEFICIO DE MINERALES Y EN LA RESTAURACIÓN DEL MEDIO AMBIENTE

Del 18 al 23 de mayo de 1998

TEMA: USE OF FUNGI AND BACTERIA FOR THE DEPRESSION OF MINERAL AND COAL PYRITE

EXPOSITOR :DR. KOMAR KAWATRA

1998

Palacio de Minería Calle de Tacuba 5 Primer piso Deleg. Cuauhtemoc 06000 México, D.F. APDO. Postal M-2285
Teléfonos 512-8955 512-5121 521-7335 521-1987 Fax 510-0573 521-4020 AL 26

Reagents in Better Metallurgy
Chapter 11, SME

Chapter 11

USE OF FUNGI AND BACTERIA FOR THE DEPRESSION OF MINERAL AND COAL PYRITE

T. C. Eisele and S. K. Kawatra

Department of Metallurgical and Materials Engineering
Michigan Technological University
Houghton, Michigan

ABSTRACT

Pyrite depression is of great interest in sulfide mineral flotation, where pyrite is a common gangue mineral. Since the floatability of pyrite is a function of the pH and a variety of other chemical factors, pH control is a critical part of sulfide flotation circuits. A wide variety of pyrite-depressing chemicals have been studied and used in sulfide-mineral processing, with considerable success. However, there are certain applications where there are still no satisfactory pyrite depressants, and even when suitable depressants are available, there is always a need for less-expensive reagents.

Microorganisms, such as the bacteria *Thiobacillus ferrooxidans*, are known to depress pyrite flotation. However, the dependence of the depression on the type of organism or on suspension pH is still being determined. In this study, the relative effectiveness of various microorganisms, and the effect of pH, has been examined. Screening tests using microflotation showed that every microorganism tested was capable of depressing naturally hydrophobic pyrite at acidic pH. Larger-scale experiments with two of the screened organisms and two different pyrites showed that microorganisms are very effective depressants at acid pH, but are largely ineffective at neutral and alkaline pH where the pyrite surface is not naturally hydrophobic.

INTRODUCTION

Since pyrite is usually an undesirable gangue mineral, it is of great interest to prevent it from reporting to the concentrate in sulfide flotation. Currently, this is done using various chemical depressants. However, there are some applications where existing pyrite depressants do not work well, and even when effective depressants are available, there is always a need to minimize reagent costs.

One condition where pyrite depression is very difficult is when the material being treated has a high hydrocarbon content, with an extreme example being coal flotation (Baker and Miller, 1971; Yancey and Taylor, 1935; Raleigh and Aplan, 1991). The main difficulty with chemical pyrite depressants in coal flotation has been that their benefits are small to nonexistent in industrial-scale coal flotation operations (Kawatra et al., 1991). Several investigators have therefore turned to the study of microorganisms,

particularly the bacteria *Thiobacillus ferrooxidans*, as pyrite depressants (Elzeky and Attia, 1987; Atkins et al., 1987; Ohmura et al., 1993; Townsley and Atkins, 1986; Stainthorpe, 1989; Atkins, 1990; Capes et al., 1973). The basis for this is that certain microorganisms are reported to have a specific affinity for pyrite surfaces, and it is therefore hoped that they can be made to attach to the pyrite in large numbers with a higher degree of selectivity than is possible with chemical depressants. Most microorganisms are hydrophobic, and so once the pyrite surface is completely covered by microorganisms, its recovery by froth flotation would then be depressed.

In this paper, the ability of several different microorganisms to depress pyrite flotation is evaluated, using two carbon-free mineral pyrites and a coal pyrite under a range of pH conditions. The goal of this work was to determine what microorganism types are most effective for this type of work, and whether the effect varies significantly with changes in pH or with pyrite type.

THEORETICAL DISCUSSION

There are three ways in which a pyrite particle can reach the froth product in flotation: true flotation, entrainment, and locking (or "induced floatability") (Lynch et al., 1981). For true flotation to occur, the pyrite surfaces must become hydrophobic, so that they can attach directly to the air bubbles. Entrainment occurs when fine particles are suspended in the water making up the bubble films, and are not actually attached to the bubbles. Locking of pyrite particles to floatable particles will allow even large pyrite particles to be carried into the froth.

Of the three mechanisms of pyrite flotation, only the true flotation can be significantly affected by chemical depressants, which work by altering the pyrite surface chemistry to make it less hydrophobic. Both entrainment and locking are mechanical effects which have little to do with the hydrophobicity of the particles involved. Entrainment can only be reduced by reducing the amount of water carried into the froth or by increasing the settling rate of the particles, and the effects of locking can only be reduced if the ore is either ground to a finer size to improve liberation, or some recovery is sacrificed to avoid floating all of the locked particles (Kawatra et al., 1991; Lynch et al., 1981).

The true flotation of pyrite from both synthetic coal/pyrite mixtures and high-sulfur coals has been reported to be depressed by the bacterium *Thiobacillus ferrooxidans* (Elzeky and Attia, 1987). This organism has been extensively studied for its ability to dissolve pyrite by using it as a food source. It was therefore originally investigated as a pyrite depressant because it has a biological reason for having a specific affinity for pyrite surfaces. It is believed that this bacteria specifically and selectively attaches to pyrite within a matter of minutes. Early work (Elzeky and Attia, 1987) was carried out by conditioning coal/pyrite slurries with bacteria at a pH of 2, followed by flotation over the pH range of 7-9. The rationale was that *T. ferrooxidans* would be most active at a pH of 2, while it is well known that coal is most floatable at near-neutral pH (Zimmerman, 1979). Other investigators have generally used a pH near 2 for both bacterial conditioning and for the flotation step (Atkins et al., 1987; Ohmura et al., 1993; Townsley and Atkins, 1986; Stainthorpe, 1989; Atkins, 1990). It has also been reported

that organisms other than *T. ferrooxidans* are effective pyrite depressants, as are a number of miscellaneous proteins, such as those found in whey (a by-product of cheesemaking) (Stainthorpe, 1989; Atkins, 1990).

The research described in this paper was intended to address the following points, which have not been completely answered by the studies reported in the literature; 1. What microorganisms are most effective for pyrite depression; and 2. What is the effect of pH on the depression of pyrite flotation by microorganisms? The answers to these questions will determine whether microbial pyrite depression is a potentially useful industrial technique, or simply a laboratory curiosity.

EXPERIMENTAL PROCEDURE

Materials

Three materials were used in the froth flotation studies; a high-purity mineral pyrite, a lower-purity mineral-pyrite from a different source, and a coal-pyrite.

The mineral-pyrites were purchased from Wards Natural Science Establishment. The high-purity pyrite was collected from a deposit in Rico, Colorado, and the low-purity pyrite had been collected from a deposit in Custer, South Dakota. Both pyrites were stage-ground and screened to maximize the amount in the 105x74 micrometer size fraction. This size fraction was used in all experiments with these materials, because it was fine enough to be floatable but coarse enough to minimize entrainment effects. It was then stored at -20° C until needed. The Rico pyrite in this size fraction was over 95% pyrite by weight, and the Custer pyrite in this size fraction consisted of 52% pyrite by weight, with the remainder being calcium carbonate and silicates.

The coal-pyrite was hand-collected as coarse nodules from the jig refuse belt at the Empire Coal Mine, Gnadenhutten, Ohio, which processes a mixture of bituminous coals from the Lower Kittanning (#5), Middle Kittanning (#6), and Upper Freeport (#7) seams. The hand-picked pyrite was then stage-ground, screened, and stored in the same manner as the mineral-pyrite. The 105x74 micrometer size fraction of the coal-pyrite contained 70% pyrite, with the remainder being mainly coal and clay.

Organisms

A wide range of species of microorganism were used in the microflotation screening tests; *Pseudomonas fluorescens, Lactobacillus acidophilus, Staphylococcus epidermis, Klebsiella terrigena,* two strains of *Thiobacillus ferrooxidans*, and *Saccharomyces cerevisiae*. These organisms were taken from standard stock cultures maintained by the Biological Sciences department at Michigan Tech., except for the *Thiobacillus ferrooxidans* culture, which was originally obtained from EG&G Idaho (culture DSM-83) and was subsequently adapted to grow on pyrite to create strain PA-1 (Eisele, 1992). The *Thiobacillus* strains were grown in a nutrient medium with the composition given in Table 1 (Tuovinen and Kelly, 1973).

TABLE 1. Composition of nutrient media used for growing *Thiobacillus ferrooxidans*

Chemical	Quantity
Ammonium Sulfate, $(NH_4)_2SO_4$	0.4 grams
Potassium Phosphate, K_2HPO_4	0.4 grams
Magnesium Sulfate, $MgSO_4$-$7H_2O$	0.4 grams
Ferrous Sulfate, $FeSO_4$-$7H_2O$	33.3 grams
Distilled, Sterilized Water	1000 ml
Sulfuric Acid, H_2SO_4	To pH=2.0

The other organisms were grown in a standard nutrient broth, and all organisms were cultured on an orbital flask shaker at 200 RPM and 30° C. After growing to a sufficiently high cell density, the various microorganisms were all washed and rinsed twice by centrifuging 20 minutes at 15,000 gravities and resuspending in distilled water at 4° C. Following the second rinse, the cells were diluted to 2 x 10^8 cells/ml, based on cell counts using a Petroff-Hauser counting chamber under a phase-contrast microscope at 400x magnification. Since the Thiobacillus strains lyse and die due to breakdown of their cell walls if the pH is much higher than 4, the washwater for these bacteria was adjusted to a pH of 2 with sulfuric acid.

For the larger-scale flotation tests with impure mineral-pyrite and coal-pyrite, only *Thiobacillus ferrooxidans* culture DSM-83 and *Saccharomyces cerevisiae* were used. The *Thiobacillus* were cultured in the above medium using an orbital flask shaker at 200 RPM and a temperature of 30° C for approximately one week. The cell density of the culture used for pyrite flotation tests was $3.4x10^8$ cells/ml, as determined with a Petroff-Hauser cell-counting chamber. These microorganisms were not washed, so that results would be more comparable to likely industrial practice. The *Saccharomyces cerevisiae* used in these larger-scale experiments was a commercially available active dry yeast, which contained no additives (Red Star, Inc., 1992). Dosages of *S. cerevisiae* in flotation experiments were determined by weighing the dry yeast with a standard 4-place analytical balance.

Microflotation Procedure

Each microflotation test used 5 grams of 105x74 micrometer Rico pyrite, suspended in 80 ml of washed bacterial suspension with the pH adjusted to 2 with sulfuric acid, and mixed for 15 minutes. Controls were mixed with pH 2 distilled water for the same length of time. Each charge was then mixed for an additional minute with 0.005 ml (0.86 kg/mt) of a 50/50 mixture of #1 and #2 fuel oil, and 0.003 ml (0.60 kg/mt) of MIBC, and added to a glass microflotation cell with a working volume of 80 ml, and an air flowrate of 100 ml/min. The pyrite was then floated for one minute.

Mineral-pyrite and Coal-pyrite Flotation Procedure

Each test used 150 grams of either Custer or Empire pyrite sized to 105x74 micrometer. This size fraction was selected so that the pyrite would be fine enough to be flotatable by true flotation, but coarse enough to minimize the effects of entrainment. Each charge was suspended in 1.9 liters of distilled water (7.3% solids) in a Denver flotation machine, and treated as follows:

1. The pH was adjusted as desired with either sulfuric acid or sodium hydroxide solution, and conditioned until the pH stabilized (about 5 minutes).
2. The desired microorganisms were added, and conditioned for 10 minutes.
3. The collector (#2 fuel oil, 3.0 kg/mt) was added, and conditioned for 2 minutes. A large dosage of collector was used to ensure that all particles that were even slightly hydrophobic would float.
4. The frother (MIBC, 0.2 kg/mt) was added, and conditioned for 30 seconds.
5. The pyrite was floated for 5 minutes, scraping the froth from the flotation cell by hand.

Analyses and Calculations

All flotation products were dried at 75° C, the microflotation products were weighed to the nearest milligram, and the larger-scale test products were weighed to the nearest 0.1 gram. Since the Rico pyrite used was essentially pure, the pyrite recovery in the microflotation tests was equal to the total weight recovery. Because of the very high pyrite levels in the impure mineral-pyrite and coal-pyrite samples, a simplified procedure for measuring the pyrite content could be used. For each sample, two portions of 1 gram each were weighed out. The first portion was leached by adding 50 ml of 4.8 N hydrochloric acid solution, and boiling gently for 30 minutes. The second portion was leached by adding 75 ml of 1.0 N nitric acid solution, and boiling gently for 30 minutes. The residues from each leach were then filtered, dried, and weighed to determine the percentage weight loss. Since pyrite does not dissolve in hydrochloric acid, but dissolves completely in nitric acid (Hurlbut and Klein, 1977), the pyrite content of the sample is taken to be:

$$\%\text{Pyrite} = (\%\text{wt. loss in } HNO_3) - (\%\text{wt. loss in HCl})$$

Total weight % recovery to the froth product is calculated as:

$$\text{Recovery},\%\text{Wt.} = \frac{\text{Froth Wt.}}{\text{Feed Wt.}} \times 100$$

Recovery of pyrite is calculated as:

$$\%\text{Recovery} = \frac{(\%\text{Wt. in Froth} \times \text{Froth Wt.})}{(\%\text{Wt. in Feed} \times \text{Feed Wt.})} \times 100$$

RESULTS AND DISCUSSION

Microflotation Tests

From the microflotation results shown in Table 2, it is seen that all of the microorganisms tested are capable of effectively depressing the flotation of pure Rico mineral pyrite at a pH of 2. This then is a general property of microorganisms, and not a specific action of lithotrophic bacteria such as *Thiobacillus ferrooxidans*. In fact, the two strains of *Thiobacillus* are the least effective of all of the microorganisms tested, and the pyrite-adapted strain is even less effective than the parent strain. Of the other organisms, the yeast *Saccharomyces cerevisiae* was the most effective, and also gave the most reproducible results

TABLE 2. Results of flotation of the pure Rico pyrite with various microorganisms at a pH of 2. The two *Thiobacillus ferrooxidans* strains were obtained from EG&G Idaho, and the other organisms were taken from stock cultures maintained by the Biological Sciences department at MTU. Tests were run in triplicate and the results averaged. The range of uncertainty is equal to the difference between the highest and lowest values for each set of three tests. The microorganism dosage for each test was held constant at 3.2 x 10^9 cells/gram of pyrite, at 5.88% solids. The microorganisms for each test were centrifuged, washed, and resuspended to prevent side-effects from the growth medium.

Organisms	Percentage of pyrite reporting to the froth
Pseudomonas fluorescens	2.0 +/- 0.25
Lactobacillus acidophilus	2.4 +/- 1.40
Staphylococcus epidermis	2.3 +/- 0.60
Klebsiella terrigena	4.4 +/- 0.40
Saccharomyces cerevisiae	1.8 +/- 0.02
Thiobacillus ferrooxidans	9.4 +/- 1.80
T. ferrooxidans strain PA-1	39.9 +/- 2.70
Distilled water controls	76.5 +/- 2.50

Mineral-Pyrite Flotation.

In the results shown in Figure 1, it is seen that the mineral-pyrite is very floatable under acidic conditions, but that its floatability becomes negligible at neutral and alkaline pH. This effect is believed to be due to the changes in solubility of iron hydroxides on the pyrite surface as the pH changes. These hydroxides form as a result of partial oxidation of the pyrite, which appears to occur almost immediately and make the pyrite surface hydrophilic and prevent its flotation (Baker and Miller, 1971). Under acid conditions, this coating dissolves, leaving a hydrophobic pyrite surface (Kawatra et al.,1991)

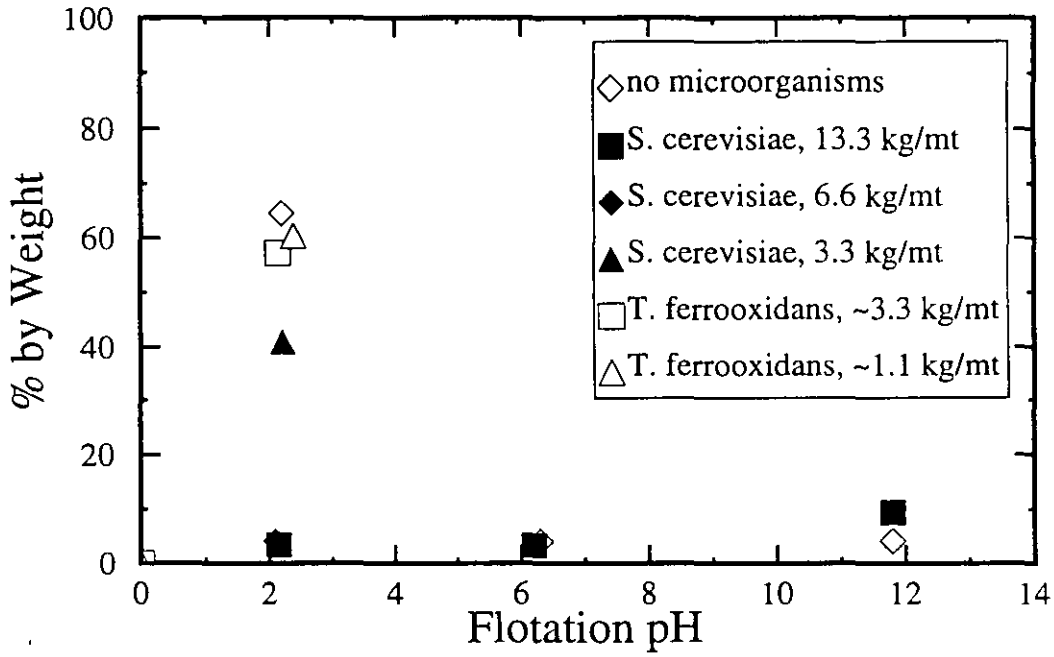

FIGURE 1. Flotation of 150 x 200 mesh mineral-pyrite over a wide pH range, with varying dosages of both *Thiobacillus ferrooxidans* and *Saccharomyces cerevisiae.* The *T. ferrooxidans* dosage was estimated from cell counts, and is only approximate. A large dosage of microorganisms is required to depress flotation at a pH of 2. At higher pH, the floatability of this pyrite is lost and little effect is seen from microorganisms.

The froth product at a pH of 2 contains virtually all of the pyrite, with the non-floating cell product being silicates and carbonates with less than 1% pyrite remaining. Since flotation is normally carried out at near-neutral pH to prevent equipment corrosion, pyrite with surface chemistry similar to mineral-pyrite will not be a problem in coal flotation because it will only float in acid solution. At a pH of 2, the *T. ferrooxidans* was only able to slightly reduce the pyrite floatability, but the effectiveness of the *S. cerevisiae* was much greater, mainly because it could be added in much higher quantities. However, to achieve complete pyrite depression at a pH of 2, it was necessary to add 6.6 kg of *S. cerevisiae* per metric ton of pyrite, a level that is likely to cause problems such as excessive foaming in other parts of the processing circuit. At neutral pH, the effect of *S. cerevisiae* was negligible, simply because there was no hydrophobic pyrite to be depressed at this pH. Under alkaline conditions, the *S. cerevisiae* actually caused a slight increase in the pyrite flotation, because the microorganism acts as a mild foaming agent under these conditions. Because the *T. ferrooxidans* was largely ineffective at the acid pH where it was expected to work best,

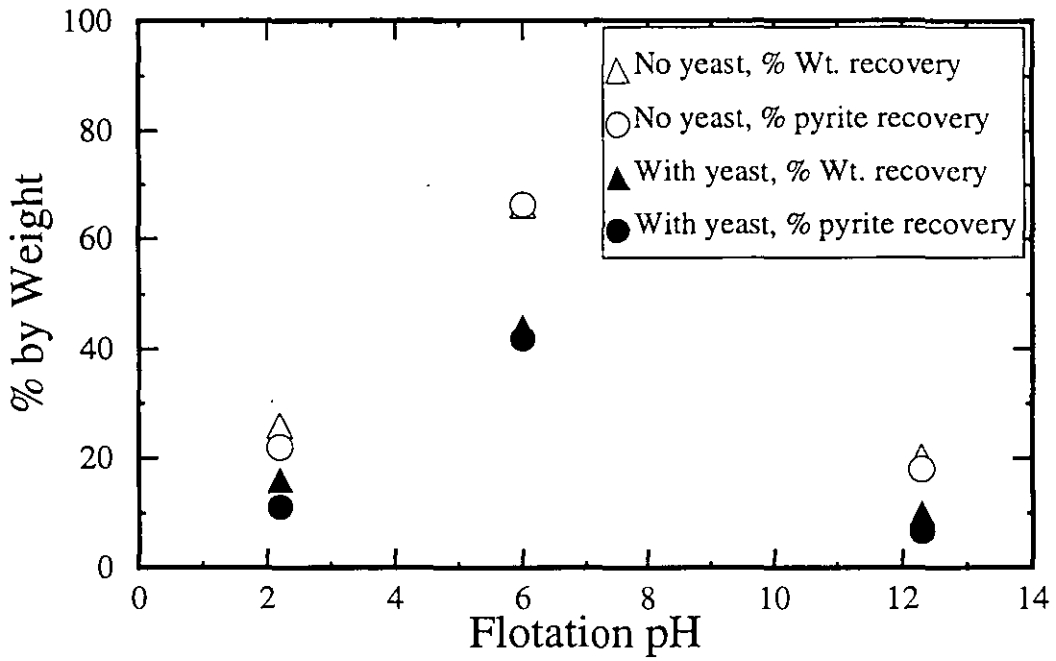

FIGURE 2. Flotation of 150 x 200 mesh Empire coal-pyrite, with and without added yeast (*Saccharomyces cerevisiae*). The yeast dosage was 13.3 kg/mt. The yeast produces a general depression of all components, and is not selective towards pyrite, as is shown by the close similarity of the values for total weight recovery and pyrite recovery.

it was not used in the neutral and alkaline pH flotation experiments because it is much more difficult to grow and handle than the *S. cerevisiae*.

Coal-Pyrite Flotation

The coal-pyrite was hand-collected as coarse nodules from the jig refuse belt at the Empire Coal Mine, Gnadenhutten, Ohio. The behavior of the coal-pyrite was completely different from the mineral-pyrite, as shown in Figure 2. First, the coal-pyrite was most floatable at near-neutral pH, with over 60% of the total weight floating at a pH of 6 in the absence of microorganisms, but less than 25% floating at either a pH of 2 or a pH of 12. This behavior is very similar to that reported for coal (Zimmerman, 1979), but very unlike that seen for the mineral-pyrite. Second, there was no pH where the pyrite floated preferentially. The recovery of pyrite was always very close to the total weight recovery, which shows that the pyrite particles were being recovered at the same rate as the coal particles. When *S. cerevisiae* was added to the coal-pyrite, it did depress the pyrite recovery. However, it also depressed the total weight recovery to the same degree, showing that it was a general flotation depressant, and not a highly selective one. The behavior of the coal-pyrite is consistent with the pyrite floating because the particles have surfaces which are at least partially made up of hydrophobic coal, and not because

the pyrite itself is hydrophobic. If the actual pyrite surfaces were contributing to the hydrophobicity, then the flotation of pyrite should have been considerably enhanced at a pH of 2, as was seen for the mineral pyrite.

CONCLUSIONS

In microflotation experiments with a wide range of microorganisms, every organism tested was found to be able to depress pyrite flotation. In larger-scale experiments, both *Saccharomyces cerevisiae* and *Thiobacillus ferrooxidans* can depress the flotation of mineral-pyrite at acidic pH, but only at high dosage levels. However, *T. ferrooxidans* has been found to be the least effective organism for pyrite depression, and not the most effective as was originally expected, although it is still possible that it is more selective than other organisms. At neutral pH, *S. cerevisiae* does depress coal-pyrite flotation, but the depression is unselective between pyrite and coal particles and therefore unlikely to be industrially useful.

ACKNOWLEDGEMENTS

Support for this research was provided by the State of Michigan Research Excellence Fund, Consumers Power Co., Detroit Edison Co., and the Ohio Coal Development Office. The *Thiobacillus ferrooxidans* culture was kindly provided by Dr. D. R. Lueking, and the other organisms were provided by Dr. S. T. Bagley, both of the MTU Department of Biological Sciences. The authors would also like to thank Ms. J. F. Bird and Dr. Howard Johnson of the Ohio Coal Development Office, and Dr. R. R. Klimpel of the Dow Chemical Co., for their useful suggestions and critical discussion of this project.

REFERENCES

Atkins, A. S., 1990, "Developments in the Biological Suppression of Pyritic Sulfur in Coal Flotation," Bioprocessing and Biotreatment of Coal (ed. D. L. Wise) Marcel Dekker, NY, pp. 507-548.

Atkins, A. S., Bridgewood, E. W., Davis, A. J., and Pooley, F. D., 1987, "A Study of the Suppression of Pyritic Sulfur in Coal Froth Flotation by *Thiobacillus ferrooxidans*," Coal Preparation, vol. 5, pp. 1-13.

Baker, A. F., and Miller, K. J., 1971, "Hydrolyzed Metal Ions as Pyrite Depressants in Coal Flotation: A Laboratory Study," Bureau of Mines Report of Investigations RI 7518, U.S. Bureau of Mines.

Capes, C. E., McIlhinney, A. E., Sirianni, A. F., and Puddington, I. E., 1973, "Bacterial Oxidation in Upgrading Pyritic Coals," CIM Bulletin, November, pp. 88-91.

Chander, S., and Aplan, F. F., 1990, Surface and Electrochemical Studies in Coal Cleaning, Final Report, U.S. Department of Energy, DOE/PC/80523-T11 (DE 9000-7603).

Eisele, T. C., 1992, Unpublished results.

Elzeky, M., and Attia, Y. A., 1987, "Coal Slurry Desulfurization by Flotation Using Thiophilic Bacteria for Pyrite Depression," Coal Preparation, vol. 5, pp 15-37.

Hurlbut, C. S. and Klein, C., 1977, Manual of Mineralogy, 19th edition, John Wiley & Sons, N.Y.

Kawatra, S. K., Eisele, T. C., and Bagley, S., 1987, "Coal Desulfurization by Bacteria," Mineral and Metallurgical Processing, vol. 4(4) pp.189-192.

Kawatra, S. K., Eisele, T. C., and Johnson, H., 1991, "Recovery of Liberated Pyrite in Coal Flotation: Entrainment or Hydrophobicity?," Processing and Utilization of High-Sulfur Coals IV (ed. Dugan, Quigley, and Attia), Elsevier, Amsterdam pp. 255-277.

Lynch, A. J., Johnson, N. W., Manlapig, E. V., and Thorne, C. G., 1981, Mineral and Coal Flotation Circuits: Their Simulation and Control, Elsevier, Amsterdam.

Ohmura, N., Kitamura, K., and Saiki, H., 1993, "Mechanism of Microbial Flotation Using *Thiobacillus ferrooxidans* for pyrite suppression," Biotechnology and Bioengineering, vol. 14, pp. 671-76.

Raleigh, C. E., and Aplan, F. F., 1991, "Effect of Feed Particle Size and Reagents on Coal-mineral matter selectivity during the flotation of bituminous coals," Minerals and Metallurgical Processing, vol. 8(2) pp. 82-90.

Red Star, Inc., 1992, Personal Communication, February.

Stainthorpe, A. C., 1989, "An Investigation of the Efficacy of Biological Additives for the Suppression of Pyritic Sulfur during simulated Froth Flotation of Coal," Biotechnology and Bioengineering, vol. 33, pp. 694-98.

Townsley, C. C., and Atkins, A. S., 1986,"Comparative Coal Fines Desulphurization Using the Iron Oxidising Bacterium *Thiobacillus ferrooxidans* and the Yeast *Saccharomyces cerevisiae* During Simulated Froth Flotation," Process Biochemistry, vol. 21(6) pp. 188-91.

Townsley, C. C., Atkins, A. S., and Davis, A. J., 1987, "Suppression of Pyritic Sulfur During Flotation Tests Using the Bacterium *Thiobacillus ferrooxidans*," Biotechnology and Bioengineering, vol. 30, p. 108.

Tuovinen, O. H., and Kelly, D. P., 1973, "Studies of the Growth of *Thiobacillus ferrooxidans*," Arch. Mikrobiol., vol. 88, pp. 285-298.

Yancey, H. F., and Taylor, J. A., 1935, "Froth Flotation of Coal--Sulfur and Ash Reduction," Bureau of Mines Report of Investigations RI 3263, U.S. Bureau of Mines.

Zimmerman, R. E., 1979, "Froth Flotation," Coal Preparation (J. W. Leonard, ed.), AIME, New York, Chapter 10 part 3.

Comminution Practices, SME, 1997
Editor S. K. Kawatra

Chapter 21

SLURRY RHEOLOGY IN AUTOGENOUS GRINDING AND CLASSIFICATION

S.K. Kawatra, A.K. Bakshi, K.J. Shoop, and T.C. Eisele
Department of Metallurgical and Materials Engineering, Michigan Technological University, Houghton, MI

ABSTRACT

Slurry rheology can have significant impact on the performance of autogenous grinding circuits. A viscous slurry can act as a cushion and retard impact forces between the media and the ore, which reduces grinding efficiency. On the other hand, a dilute slurry will not be viscous enough to hold slurry in the impact zone of the media, which will lead to inefficient use of impact energy. An unfavorable rheology can also lead to overgrinding or centrifuging of the slurry inside the mill. Slurry rheology also affect classification, with higher viscosity increasing the cut size.

In this article, the causes of the rheological effects on autogenous grinding and hydrocyclone classification have been discussed Both plant and pilot scale data from autogenous grinding have been provided to show the effects of viscosity on specific energy consumption and other breakage characteristics of the ore. It is shown that: (1) high viscosity, produced by low temperature and high fines content, significantly increases the specific energy consumption and the production of critical size material in an autogenous mill; (2) In hydrocyclone operation, increasing the viscosity causes the $d_{50}(c)$ size to become coarser.

INTRODUCTION

Slurry rheology has been shown to significantly affect the performance of grinding and classification circuits (Hemmings and Boyes,1977; Tucker, 1982; Klimpel, 1982; Fuerstenau et al., 1984; Austin et al., 1984; Moys, 1989; Kawatra and Eisele, 1988; Shoop and Kawatra, 1995; Kawatra et al , 1996; Kawatra and Bakshi, 1996). Variation in slurry rheology can occur due to changes in solids content, particle size distribution, clay content, temperature, and chemical environment (Shack et al., 1957). As will be shown later, the specific energy consumption of autogenous grinding in some northern US iron ore mines increased in winter as the temperature dropped, which caused the viscosity of the slurry to increase. It has also been shown by many researchers that mill efficiency can be improved significantly by adding chemical reagents which change the slurry rheology (Klimpel, 1982; Tucker 1982). From such observations it has been realized for some time that on-line monitoring of slurry rheology can be used to produce better control strategies for grinding and classification circuits. The main barrier to the use of viscosity as a control parameter in comminution has been the lack of a suitable on-line viscosity sensor. The slurries encountered in grinding circuits are composed of rapidly-settling, highly abrasive particles which give very erratic viscosity readings with the available on-line instruments. Nevertheless, there is no satisfactory substitute for direct measurement of slurry viscosity, and so these problems must be overcome if the control of comminution circuits is to be improved.

Although the effect of slurry rheology on grinding is discussed in the literature, past studies are primarily done with ball mill grinding, where the media is distinct from the feed material. In contrast, in autogenous grinding, the media is the ore itself. Therefore, the efficiency of autogenous grinding also depends upon the added variable of media competency (the way the media-size rocks break inside the mill). In this article, besides specific energy consumption, the effect of rheology on the breakage characteristics of the ore is discussed Since the overall efficiency of the autogenous grinding is partly dependent on the classifier performance, the effect of rheology on classification efficiency is also discussed.

EFFECT OF SLURRY RHEOLOGY ON AUTOGENOUS GRINDING

Rheology affects grinding in two ways: (i) it influences the breakage mechanism of the ore, and (ii) it influences the transportation of particles both inside and outside the mill. During grinding, an optimum viscosity of the slurry is needed to obtain an efficient performance of the mill. When the slurry viscosity is very low, energy is wasted because of the following reasons:

(1) The grinding media is not adequately covered with particles. Therefore, during impact not all the energy is utilized to grind the particles
(2) At low viscosity, water content of the slurry is usually high, and energy is wasted in tumbling this excess water.
(3) Low viscosity results in poor transfer of momentum from the rotating shell to the charge, because of slippage. As a result, the energy available for grinding is reduced.

On the other hand, at very high slurry viscosity energy is also wasted because:

(1) More slurry is drawn into the void zones in the load than is needed to fill the voids, and the media is partially suspended ... the viscous slurry causing the charge to become expanded. As a result less lift is imparted to the load resulting in a substantial loss of energy.

(2) At high viscosity, the slurry forms a thick coating on the surfaces of the media-sized pieces, which cushions the impact between rocks and reduces the impact energy available for grinding small particles (Fuerstenau et al., 1984).

(3) At higher mill speed, when the viscosity is high some rocks stick to the mill liner and centrifuge (Moys, 1989; Fuerstenau et al., 1984). This also reduces efficiency by decreasing the overall mill diameter and volume.

Although most of the postulates mentioned here are reported for ball mill grinding, they are also valid for autogenous grinding In autogenous grinding the media size rocks are expected to be hard enough so that they do not crumble while breaking small ore particles. and later unlike ball mills, they are also expected to break in order to initiate ore breakage. In other words rocks inside an autogenous mill are expected to grind and get ground simultaneously This is not the case in a ball mill where the balls must grind ore particles only However, the large rocks in an autogenous mill must break in a useful manner. Sometimes they break down to sizes which are not big enough to grind small particles and are not small enough to be ground by large rocks. These particles are called the critical size material and are treated outside the autogenous mill.

The behavior of the rocks inside an autogenous mill is definitely governed by slurry rheology. For example, at low viscosity the transfer of momentum from the mill shell is lowest, and so the media is not lifted to as great a height as it would be at higher viscosity. As a result, increasing viscosity causes the media to undergo more energetic impacts, which is more likely to crack into several critical size pieces than to gradually chip and abrade in the most efficient way.

Since slurry rheology is influenced by various factors such as solids content, particle size distribution, clay content, temperature changes, etc., any change in these parameters will change the breakage characteristics of the rocks. Different breakage characteristics such as resistance to breakage, critical size production, and their effects on specific energy consumption are discussed in the following sections

Effect of Viscosity on Size Stability

The rock's resistance to breakage can be quantitatively measured by size stability. Size stability is expressed as (ASTM, 1991)

$$\% \text{ Size stability} = \frac{\Sigma(\text{final wt\%}) \times (\text{avg. sieve size})}{\Sigma(\text{initial wt\%}) \times (\text{avg. sieve size})} \times 100 \quad (1)$$

Therefore, a size stability of 100% corresponds to a rock that did not break during grinding, and a size stability of 0% corresponds to a rock that broke completely below the finest size measured.

In Figure 1, the effect of viscosity on size stability is demonstrated. These tests were carried out in a 1.83 meter (6 feet) diameter pilot scale autogenous mill with iron ore samples collected from a local mine. The viscosity of the slurry during these tests was changed by changing the clay/fines content in the initial feed and by changing the temperature of both iron ore and water (Shoop and Kawatra, 1995) Tests were carried out at two rock temperatures of 25°C and -25°C to simulate the summer and winter conditions in the northern US operations. As can be seen from Figure 1, size stability increased with increase in slurry viscosity, showing that at high viscosity the rocks had a higher resistance to breakage This could be due to the fact that at higher viscosity the impact force between rocks

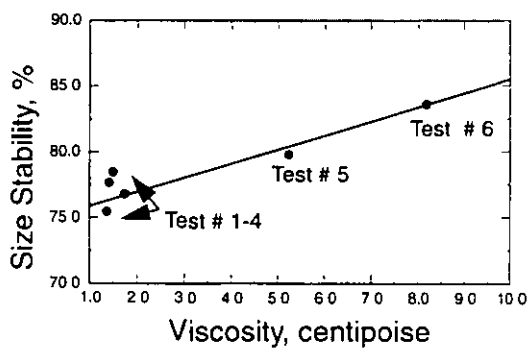

Figure 1. Size stability vs viscosity from the pilot scale 1.83 meter (6 feet) diameter batch autogenous grinding test The increased size stability shows that at higher viscosity the ore is less likely to be broken

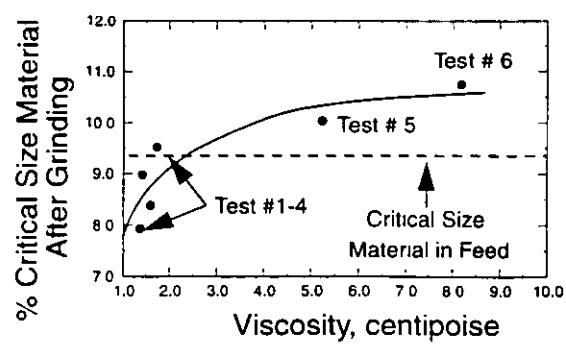

Figure 2 % critical size material in mill after grinding as a function of viscosity At higher slurry viscosity amount of critical size material in the product was more than the amount of critical size material initially present in the feed

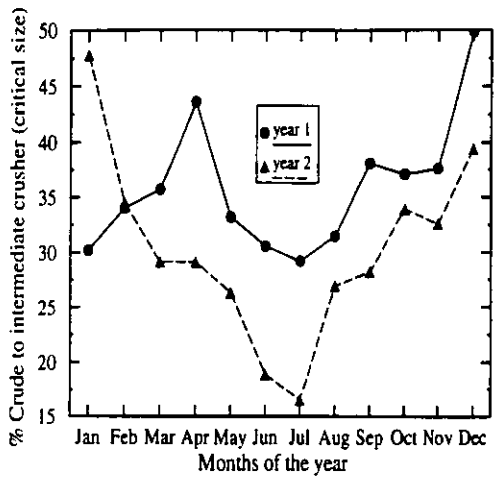

Figure 3 Critical size production for an 8.2 meter diameter by 4.4 meter long primary autogenous mill processing iron ore over a two year period (Kawatra and Eisele, 1992).

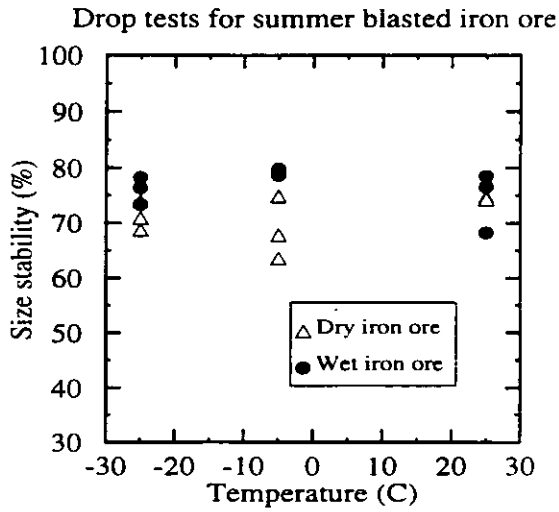

Figure 4. Dry tests have little change in size stability indicating brittleness was not changing. Wet frozen tests showed a slight increase in size stability compared to dry frozen tests This slight increase was due to the low apparent porosity of iron ore (Kawatra et al , 1993).

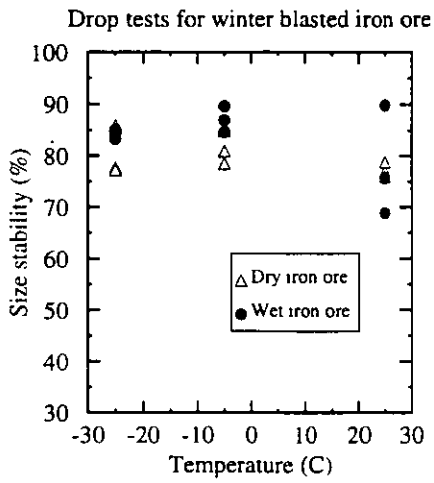

Figure 5. Dry samples show no changes in brittleness upon freezing. Size stability of wet frozen samples did change slightly, again due to low apparent porosity The difference between wet and dry frozen samples showed the same trend as for summer blasted iron ore (Figure 4) This indicated winter blasted ore was not fractured more than samples from summer blasted ore (Kawatra et al., 1993)

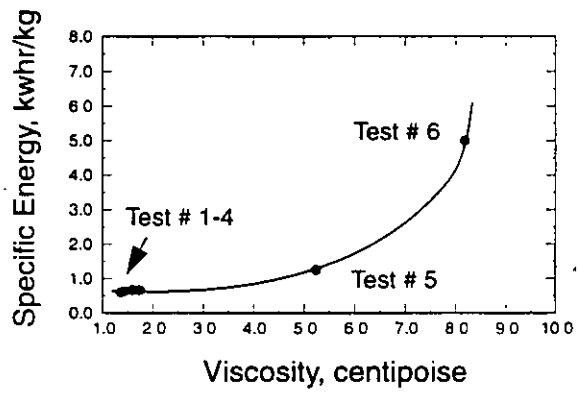

Figure 6. Specific energy vs viscosity from the pilot scale autogenous grinding test The increase in specific energy consumption is significant at higher viscosity values

was retarded by the viscous slurry which acted as a cushion, resulting in less breakage of the rock. Therefore, at higher viscosity (originating from causes such as high clay content, high fines, low temperature, etc.) more energy will be needed to break rocks in the mill.

Relationship Between Critical Size Material and Viscosity

Critical size material is the material which is too large to be effectively ground in the mill, and too fine to be effective for grinding other particles This material is usually crushed outside the grinding mill before it can be sent back to the mill. The effect of slurry viscosity on critical size material from pilot scale autogenous grinding of iron ore is shown in Figure 2. The feed for each test initially contained 9.38% critical size material. The percentage of the critical size material was determined again at the end of each test. As can be seen in Figure 2, at low slurry viscosity the amount of critical size material in the mill after grinding was less than the amount of critical size material present before grinding. However, at higher viscosity there was an increase in critical size material after grinding. During the first four tests, when the viscosity was low the slurry was more like water. Therefore, in this condition the slurry did not leave a thick coating on the surfaces of both the media and the critical size particles. This allowed some critical size material to be crushed upon

impact. At higher viscosity, there was a thick coat of slurry on the media (large rocks). This retarded the energy of the impact collis within the grinding charge, and reduced the chances of breakage of the critical size particles. At the same time, increased viscosity tended to lift the media pieces to a greater height, so that the largest pieces underwent more violent impacts on the surface of the charge. This increased the tendency of large pieces to be cracked into critical size particles. Therefore, during test No.6, when the viscosity was increased to 8.19 centipoise by adding fines and decreasing the temperature, the critical size content in the product increased to 10.8% (a 1.37% increase).

This data agrees with plant observations made by Kawatra and Eisele (1992) shown in Figure 3, which gives the critical size material in a full-scale plant as a percentage of total feed during each month. The data was collected over a period of two years from the local iron ore plant which provided the iron ore for the work reported above. As it can be seen from this figure, critical size material production was at a minimum between April and September, and increased significantly during December and January when the temperature was low. It was originally believed that this change in critical size production was due to increased brittleness of the rock at low temperatures This was disproved by drop test studies conducted at Michigan Technological University (Kawatra et al., 1993) shown in Figures 4 and Figure 5. Figure 4 shows drop test results of summer blasted ores, and Figure 5 shows results from winter blasted ores Both the tests were carried out wet and dry at 25°C and -25°C to simulate actual plant scenario. As can be seen from these figures the size stability of both summer and winter blasted ore at different temperatures are unchanged This shows that within the above range of temperature rocks did not become brittle. Therefore, these changes in critical size material production are due to viscosity changes caused by temperature variation, and are not because of changes in brittleness of the rock.

Specific Energy Consumption

Specific energy consumptions at different slurry viscosities from the pilot scale autogenous grinding of iron ore are shown in Figure 6. The conditions for these experiments have been described elsewhere (Bakshi et al., 1996). Specific energy consumption was calculated as the energy required to produce one kilogram of -150 micron material.

As can be seen from Figure 6, the specific energy consumption of the mill increased with increasing slurry viscosity. The increase in specific energy from test 1 to test 4 was small, because the viscosity changes during these tests were also very small. However, during tests 5 and 6 specific energy consumption increased significantly This trend agreed with the observations made in the local iron ore plant (Figure 7), where specific energy consumption increased by as much as 20% during winter months when the slurry temperature was very low (Kawatra and Eisele, 1992).

EFFECT OF SLURRY RHEOLOGY ON HYDROCYCLONE CLASSIFICATION

Fluid viscosity has a profound effect on the separation characteristics of hydrocyclones (Agar and Herbst, 1966; Kawatra and Eisele, 1988). Changing viscosity alters the particle settling rates and the slurry velocities in the hydrocyclone, and so alters the performance. The mechanism of the change in d_{50} size are as follows:

(a) As the slurry becomes more viscous, the settling speed of the particles becomes slower due to the increase in viscous drag. Increasing the slurry viscosity therefore allows coarser particles to be swept out the hydrocyclone overflow, and so the d_{50}(c) size becomes coarser.

(b) Increasing slurry viscosity causes the swirling slurry to lose its energy and slow down more rapidly, due to increased interac-

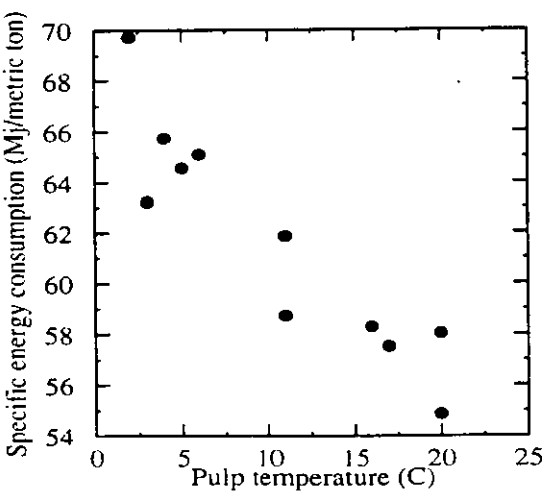

Figure 7. Specific energy consumption for a 8.2 meter diameter by 4.4 meter long primary autogenous mill processing iron ore as a function of temperature. Energy increases as pulp temperature decreases (Kawatra and Eisele 1992)

tion with the hydrocyclone wall. The decreased rotational speed results in a reduction in the centrifugal force, which reduces the particle settling velocity and again increases the $d_{50}(c)$ size.

Rheology also affects the R_f factor of a hydrocyclone. These effects are discussed in more detail in the following paragraphs.

Effect of viscosity on the d_{50} size

The effect of viscosity on d_{50} size can be explained by the following equation which is derived from the equilibrium orbit theory using Stoke's law and gives the diameter of any particle (including d_{50} size) at equilibrium at a particular radius inside the hydrocyclone:

$$d = \sqrt{\frac{18\eta \cdot W \cdot r}{(\rho_s - \rho_l) \cdot V_t^2}} \qquad (2)$$

Where

d	=	diameter of the particle
ρ_s	=	density of the solid particles
ρ_l	=	density of the liquid
V_t	=	tangential velocity of the particle
r	=	radius of the equilibrium orbit
η	=	fluid viscosity
W	=	radial velocity

From the above equation it is seen that d_{50} size increases with increase in slurry viscosity. This can be seen from Figure 8, which shows data from a classification study carried out with a 10.2 cm (4") diameter hydrocyclone using ground silica.

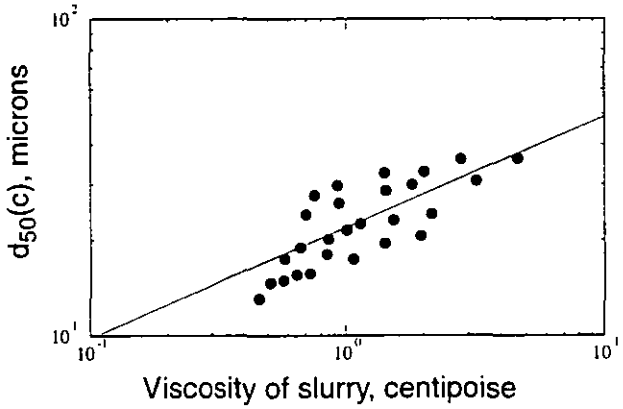

Figure 8 $d_{50}(c)$ size vs viscosity for silica slurry As seen from this figure $d_{50}(c)$ size increased with increase in slurry viscosity.

Although, theoretically d_{50} size is proportional to the 0.5th power of viscosity (Equation 1), experimental and numerical values of the viscosity exponent have been reported between 0.3 and 0.6 by various researchers (Kawatra et al., 1996, Agar and Herbst, 1966). Using these values many empirical models for d_{50} size prediction have been reported in the literature (Bradley, 1965). However, most of these equations were developed for dilute suspensions and small diameter hydrocyclones, which are not comparable to normal plant conditions (Plitt, 1976, Plitt and Kawatra, 1979) In later years, Lynch and Rao (1975), and Plitt (1976) used data from large diameter hydrocyclones and slurries with higher percent solids to develop more versatile models to predict separation size in actual plant situations However, neither of these equations have explicit slurry viscosity terms in them. Instead, both of these equations depend on solids content as an indicator of slurry rheology. It is well known that solids content is not the only parameter which affects slurry rheology. Besides solids content, the temperature, size distribution of the solids, and chemical environment can also alter rheology (Schack et al , 1957). Therefore, these models cannot predict the correct cut size when the viscosity changes due to factors other than changes in solids content. For example, consider the following two equations, one developed by Plitt (1976) which does not contain an explicit viscosity term, and the other developed by the authors which contains an explicit viscosity term.

(a) Plitt's model, estimating the viscosity from the percent solids·

$$d_{50}(c) = \frac{K_1 \; D_c^{0.46} \cdot D_i^{0.6} \cdot D_o^{1.21} \cdot \exp(0.063\Phi)}{D_u^{0.71} \cdot h^{0.38} \cdot Q^{0.45} \cdot (\rho_s - \rho_l)^{0.5}} \qquad (3)$$

(b) The authors' model, incorporating an explicit viscosity term:

$$d_{50}(c) = \frac{K_2 \cdot D_c^{0.46} \cdot D_i^{0.6} \cdot D_o^{1.21} \cdot \Phi^{0.41} \cdot \eta^{0.35}}{D_u^{0.71} \cdot h^{0.38} \cdot Q^{0.45} \cdot (\rho_s - \rho_l)^{0.5}} \quad (4)$$

Where

K_1, K_2	=	constants
D_c	=	inside diameter of the hydrocyclone at the bottom of the vortex finder, cm
D_i	=	inside diameter of the hydrocyclone inlet, cm
D_o	=	inside diameter of the overflow or vortex finder, cm
D_u	=	inside diameter of underflow or apex of the hydrocyclone, cm
Q	=	feed flowrate of slurry, liters/minute
$d_{50}(c)$	=	corrected cut size of the hydrocyclone, micron
h	=	distance between the bottom of the vortex finder to the top of the underflow orifice, cm
Φ	=	volume percent solids in the pulp
η	=	viscosity, centipoise
ρ_s	=	density of solid, gm/cm^3
ρ_l	=	density of liquid, gm/cm^3

Using the two previous models, predicted and measured cut sizes from a classification study of ground silica (d_{80} size = 65 micron) using a 10 2 cm (4") hydrocyclone are shown in Figure 9 and 10 respectively. Viscosity of the slurries was varied by changing both solids content and temperature. As can be seen from Figure 9, which was drawn by using Plitt's model, the observed $d_{50}(c)$ size varied within each percent solids range, while Plitt's model predicted a constant $d_{50}(c)$. The reason for this is that Plitt's model (Equation 2) accounts for slurry viscosity effects based on changes in solids percentage only, and does not take into account the viscosity changes from other sources (in this case, temperature). In Figure 10, which was drawn by using the authors' model, the change in $d_{50}(c)$ from both temperature and percent solids is accurately predicted. This is possible because in the authors' model (Equation 3) an explicit viscosity term is included, and the viscosities of slurries during their experiments were measured on-line.

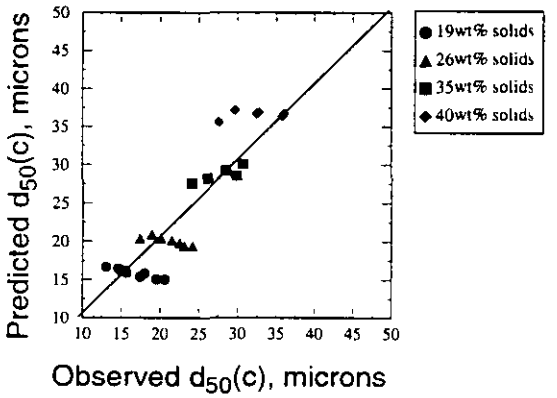

Figure 9 Predicted $d_{50}(c)$ size from Plitt's equation vs observed $d_{50}(c)$ size. The change in observed $d_{50}(c)$ size within each solids percentage range is due to viscosity changes produced by changing the temperature. Since Plitt's model accounts for viscosity changes from solids content alone, the predicted $d_{50}(c)$ size in individual percent solids range did not change

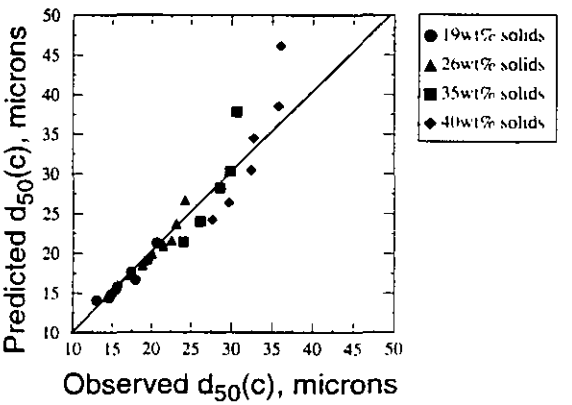

Figure 10 Predicted $d_{50}(c)$ size from the new modified equation vs observed $d_{50}(c)$ size. Since this equation utilizes the viscosity data obtained by direct measurement, the increase in $d_{50}(c)$ size due to viscosity changes from both increase in solids content (at different solids percent) and changes in temperature (10°C to 50°C at individual percent solids range) is reflected

Effect of viscosity on Rf

Viscosity also changes the water-to-underflow term, R_f, of the hydrocyclone. R_f is the fraction of feed liquid reporting to the underflow. The particles associated with this portion of the liquid travel downwards near the conical wall of the hydrocyclone, and are not centrifugally separated. Therefore, a fraction R_f of all particles irrespective of shape and size report to the underflow of the hydrocyclone. The fluid speed in the hydrocyclone is reduced due to increased viscous drag at higher viscosities, and this causes an increase in R_f. As can be seen from Figure 11, for slurries with 19, 26, and 35wt% solids, R_f increased by as much as six percent when the viscosity of the slurry was increased by 2-3 centipoise. For the slurry with 40wt% solids the change was rather less noticeable, with the observed change being less than 3% for a 6 centipoise change in viscosity.

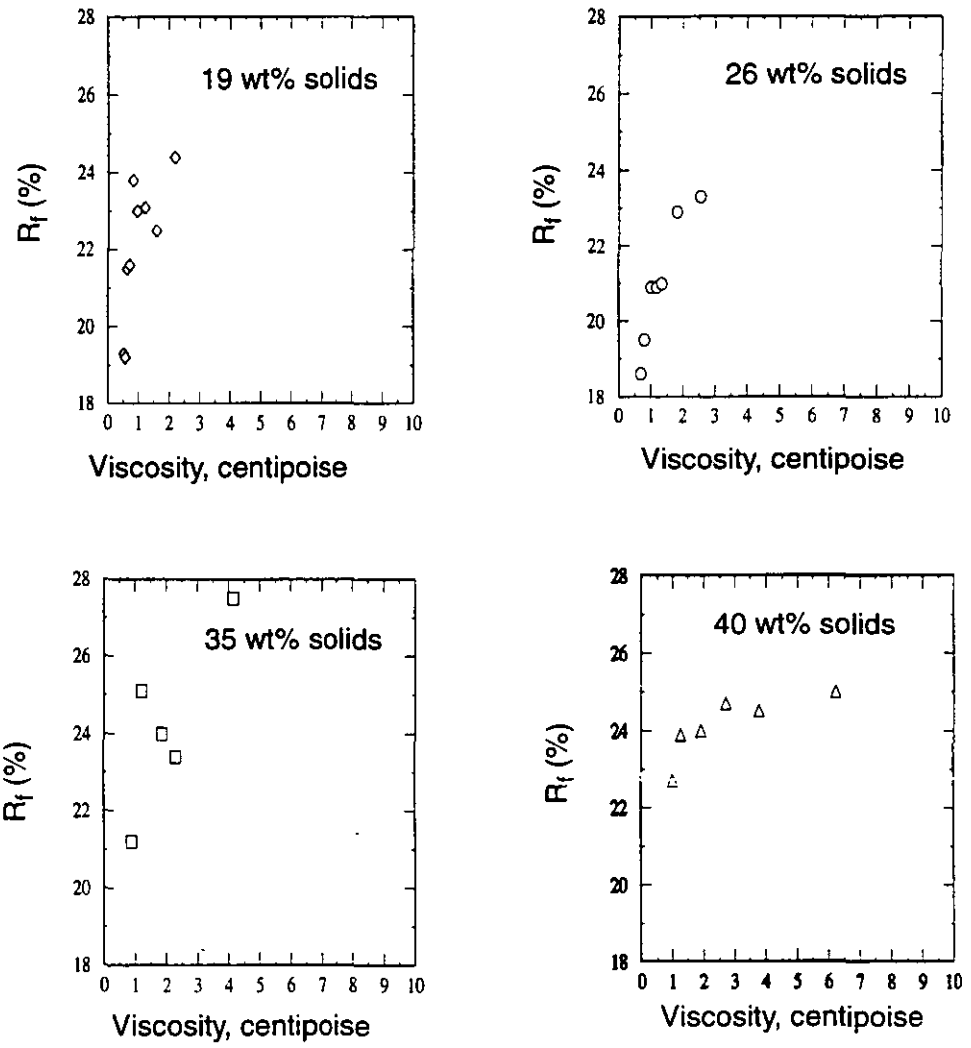

Figure 11 Effect of viscosity on the water-to-underflow ratio (R_f) In each percent solids range, R_f increased with increase in viscosity

Effect of viscosity on classification index

Figure 12 gives the reduced efficiency curve for all the tests carried out with the 10.2 cm hydrocyclone using ground silica. The slope of this curve, called the classification index (a) is given by the following equation (Lynch, 1977):

$$y = \frac{e^{\alpha x} - 1}{e^{\alpha x} + e^{\alpha} - 2}. \quad (5)$$

Where

y	=	size fraction reporting to underflow
x	=	$d/d_{50}(C)$
α	=	classification index

From Figure 12 it is seen that viscosity has limited effect on the shape of the reduced efficiency curve. It is noted that there is some scattering of data in this graph.

CONCLUSIONS

From the results presented in this paper, the following conclusions were reached:

(1) The efficiency of an autogenous mill is reduced if the slurry viscosity is either too low, or too high. Low viscosity reduces the

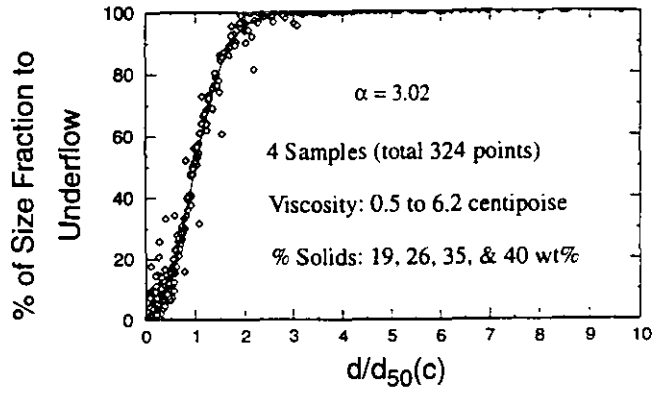

Figure 12 Reduced efficiency curve from all the tests This graph shows that slurry viscosity has no significant effect on the sharpness of classification

mill efficiency by reducing the energy transfer into the charge, and by poor positioning of the particles for grinding High viscosity reduces the efficiency by cushioning of impacts within the grinding charge

(2) Increasing viscosity tends to increase the amount of critical size material produced in an autogenous mill This is a result of an increased tendency to crack the largest pieces into critical size particles, and reduce ability to chip and abrade the critical size into finished product.

(3) In hydrocyclones, increasing viscosity produces an increase in the $d_{50}(c)$ size. This is a result of reduced particle settling speeds at higher viscosity. The lower settling rates are caused by increased viscous drag on the velocity of the fluid in the hydrocyclone.

(4) The numerous direct effects of viscosity changes in grinding circuits illustrate the need for reliable on-line viscosity measurement methods. Unfortunately there are no commercially-available viscosity sensors that can make reliable measurements on the unstable, highly abrasive slurries encountered in grinding circuits.

ACKNOWLEDGEMENTS

This research has been supported by the Department of the Interior's Mineral Institute program administered by the Bureau of Mines through the Generic Mineral Technology Center for Comminution under grant number G 1115149.

REFERENCES

Agar, G.E., and Herbst, J. A., 1966, "The Effect of Fluid Viscosity on Cyclone Classification," Trans. AIME, Vol. 235, pp. 145-149

Austin, L. G , Klimpel, R. R., and Luckie, P. T., 1984, "What Laboratory Tests Tell Us About Breakage in Ball Mills," Chapter 5, Process engineering of Size Reduction: Ball Milling, Society of Mining Engineers, American Institute of Mining, Metallurgical, and Petroleum Engineers, Inc., New York, pp. 79-176.

ASTM, 1991, Standard Method of Drop Shatter Tests for Coal, D440-86, Annual book of ASTM standards, Vol. 5.05, pp. 214.

Bakshi, A K , Shoop, K J., and Kawatra, S. K , 1996, "C langes in Autogenous Grinding and Classification Performance due to Variation in Slurry Rheology," Society of Mining, Metallurgy, and Exploration, preprint no. 96144

Bradley, D , 1965, The Hydrocyclone, Pergamon Press, New York, NY

Fuerstenau, D. W., Venkataramana, K. S., Velamakanni, B V., 1984, UEffect of Chemical Additives on the Dynamics of Grinding Media in Wet Ball Mill Grinding," International Journal of Mineral Processing, Vol. 15, pp 251-267.

Hemmings, C E , and Boyes, J. M , 1977, "An On-Line Viscometry Technique for Improved Operation and Control of Wet Grinding Circuits," Twelfth International Mineral Processing Congress, Sao Paulo, pp 46-64.

Kawatra, S. K , Bakshi, A. K., and Rusesky, M T., 1996, UThe effect of Slurry Viscosity on Hydrocyclone Classification," International Journal of Mineral Processing, in press.

Kawatra, S. K., and Bakshi, A. K., 1996, "On-line Viscometry in Particulate Processing," Mineral Processing and Extractive Metallurgy Review, Vol 14, pp. 249-273.

Kawatra, S K., Moffat, S. A., and DeLa'O, K A., 1993, gThe effects of Freezing Conditions on Rock Breakage," Society of Mining, Metallurgy, and Exploration, Inc., preprint no 93-17.

Kawatra, S K , and Eisele, T. C , 1992, "Influence of Temperature on the Energy Efficiency of an Industrial Circuit Processing Iron Ore," Minerals and Metallurgical Processing, Vol. 8, No. 1, pp 32-37.

Kawatra, S K , and Eisele, T. C , 1988, "Rheology Effects in Grinding Circuits," XVI International Mineral Processing Congress, Elsevier Science Publishers B. V., Amsterdam, pp 195-207.

Klimpel, R. R , 1982-1983, "Slurry Rheology Influence on the Performance of MineraVCoal Grinding Circuits," Part I, Mining Engineering, Vol 34, No. 12, pp 1665-1668, December 1982, Part II, Mining Engineering, January 1983, Vol. 35, No. 1, pp 21-26

Lynch, A. J., and Rao, T C., 1975, SModeling and Scale-Up of Hydrocyclone Classifiers," The XI International Mineral Processing Congress, Cagliari, pp 245-269.

Moys, M. H., 1989, "Slurry Rheology-The Key to a Future Advance in Grinding Mill Control," Advances in Autogenous and Semi-autogenous Grinding Technology. Vol. 2, (Editors) A. L. Mular and G. E. Agar, Mining and Mineral Processing Engineering, University of British columb a, Vancouver, Canada, pp 713-728.

Plitt, L. R., 1976, "A Mathematical Modeling of the Hydrocyclone Classifier," CIM Bulletin, Vol. 69, No. 776, pp 114123

Plitt, L. R., and Kawatra, S. K., 1979, gEstimating the Cut (d_{50}) Size of Classifiers Without Product Particle-Size Measurement," International Journal of Mineral Processing, Vol. 5, pp 364-378

Schack, C. H., Dean, K. C., and Moliy, S M., 1957, aMeasurement and Nature of the Apparent Viscosity of Water Suspensions of Some Common Minerals," Report of Investigation 5334, U S Bureau of Mines.

Shoop, K. J , and Kawatra, S, K., 1995, UEffect of Rock Breakage Characteristics and Fines/Clay Content on the Autogenous Grinding of Iron Ore," Society of Mining, Metallurgy, and Exploration, Inc., preprint no. 93-17.

Tucker, P., 1982, gRheological Factors that Affect the Wet Grinding of Ores," Trans. of Instn. Min. Metall., Section C, Mineral Processing and Extractive Metallurgy. Vol. 91, pp. C117-C122

Comminution Practices, SME, 1997
Editor S. K. Kawatra

Chapter 10

PLANT TRIAL OF A NEW ON-LINE PRESSURE VESSEL RHEOMETER FOR SLURRIES

A.K. Bakshi and S.K. Kawatra
Department of Metallurgical and Materials Engineering, Michigan Technological University, Houghton, MI

ABSTRACT

A plant trial of a new on-line pressure vessel rheometer for slurries, developed at Michigan Technological University, was carried out at a nearby copper concentrator. The rheometer measured the flow curves (shear stress vs. shear rate) of chalcocite slurries. Viscosity of non-Newtonian slurries changes with shear rate and so, for such slurries viscosity measurement at a single shear rate (often seen in the literature for grinding and classification studies) cannot be correlated to process performance. For these slurries, viscosity at various shear rates can be measured from flow curves generated by the pressure vessel rheometer. Other rheological properties, such as flow type and yield stress can be determined by this rheometer to better characterize the slurries.

The slurry at the copper concentrator consisted of ground chalcocite ore. The solids content in the slurry varied between 30-60 % by weight. Top size of the particles was 125 micron, and 80% passing size was 34 micron. Measurements by the pressure vessel rheometer showed that most of the slurries had pseudoplastic flow at shear rates below ~3000 sec^{-1}, where the viscosity of the slurry decreased with increase in shear rate. Above ~3000 sec^{-1}, like a Newtonian fluid, the viscosity of the slurry remained steady. Flow curves and viscosity from the pressure vessel rheometer were verified with a Brookfield viscometer and a vibrating sphere viscometer, and the results were found to be accurate.

INTRODUCTION

Suspension rheology plays an important role in comminution, both during grinding and classification (Klimpel, 1982; Fuerstenau et al., 1984, Hemmings and Boyes, 1977; Kawatra and Bakshi, 1996). Therefore, on-line monitoring of rheology can lead to a better control of these operations. However, due to measurement difficulties, a suitable rheometer for in-stream rheological measurement of slurries has not yet been available. One of the major difficulties in suspension rheometry is the unstable nature of the suspension The solids quite often settle before any measurement can be taken. Several sample presentation devices, such as agitation tanks and gravity flow vessels have been used along with rotational viscometers in attempts to over come this probl em (Reeves, 1990; Underwood, 1976; Clarke, 1967) However, rotational viscometers are very sensitive to plant disturbances, and even the slightest amount of swirling of slurry inside these containers can cause false readings (Kiljanski, 1993). Other viscometers which have been reported in the past such as the capillary tube viscometers and vibrating viscometers measure viscosity only at a single shear rate, and so they cannot be used for non-Newtonian slurries whose viscosity changes with shear rate (Aplan and Spedden, 1965; Rachman, 1979).

In this article a new on-line pressure vessel rheometer is presented which was recently tested in a copper plant. It measures the flow curves (Figure 1) of samples on a continuous basis. Different rheological parameters such as flow types, viscosity at different shear rates, and yield stresses can be measured These measurements are important for non-Newtonian slurries whose viscosity changes with rate of shear

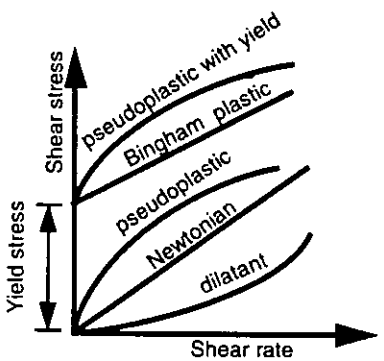

Figure 1. Generalized flow curves of suspensions

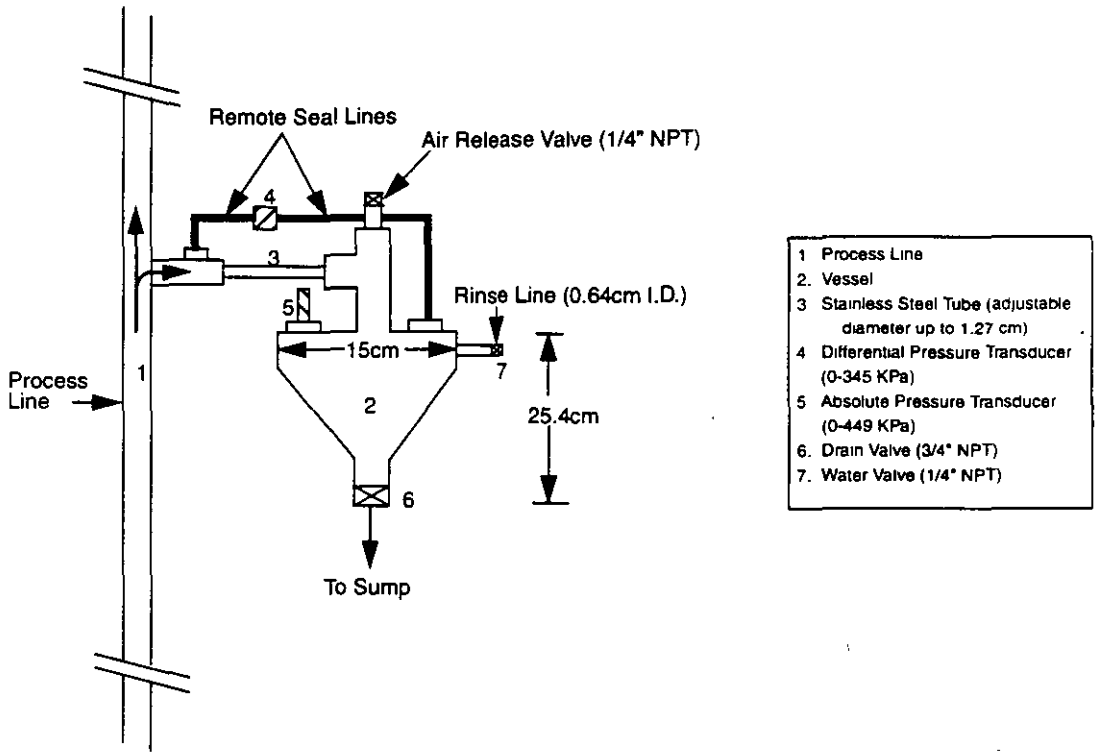

Figure 2 Schematic of the pressure vessel rheometer The instrument is directly connected to the process line to tap a sample for measurement

INSTRUMENT DESCRIPTION

A schematic of the on-line pressure vessel rheometer is shown in Figure 2. In this rheometer, slurry sample from the process stream passes through an interchangeable stainless steel tube (up to a diameter of 1.27 cm) into a sealed vessel. The pressure changes across the tube and inside the vessel are measured by two pressure transducers, as shown in Figure 2. Shear stress and shear rate are calculated by applying Poiseuille's law, in which shear rate is calculated from the flow rate of slurry through the tube and shear stress is calculated by measuring the pressure difference across the tube (measured by the differential pressure transducer) Flow rate is calculated from the pressure changes in the vessel (measured by the absolute pressure transducer) by applying Boyle's law. After the end of the test the drain valve is opened to empty the vessel. Since slurry inside the vessel during the test is preserved under pressure, most of the material is forced out as soon as this valv e is opened. Then the water valve is opened to wash out any solids sticking to the vessel wall. The air valve helps in draining the remaining water from the vessel after the water rinsing stage. All the operations are automated by a computer

PLANT SET-UP

The pressure vessel rheometer was installed in a slurry line carrying ground chalcocite ore at the Copper Range Company, White Pine, Michigan A flow diagram showing the rheometer set-up and sampling procedure is given in Figure 3. Sample from the slurry line (a 7.62 cm (3") diameter vertical pipe) was collected continuously by a 2.54 cm (1") diameter PVC pipe. The sampling line was connected directly to a 20 mesh Y-strainer. The strainer removed tramp material which would otherwise plug the tube of the rheometer. The screened material from the strainer went to the rheometer through a 0.3330 cm diameter stainless steel tube. The remainder of the sample passed through a sample holder. Comparative on-line results were measured by a vibrating sphere viscometer placed in the sample holder. The vibrating sphere viscometer was manufactured by the Nametre Company, NJ, and measured viscosity at a single shear rate Material from both the pressure vessel rheometer and the Nametre viscometer were discharged to a drain, from where it was pumped to the filter Arrangements were made to clean the entire system with water when necessary. Sample from the Nametre and the pressure vessel rheometer discharge streams were collected periodically to measure density with a Marcy density gauge.

SLURRY CHARACTERISTICS

The slurry fed to the rheometer consisted of ground chalcocite ore. Solids content in the slurry varied between 30-60% by weight during this trial period The solids had a top size of 125 microns and a 80% passing size of 34 microns. pH remained around 10.5, while

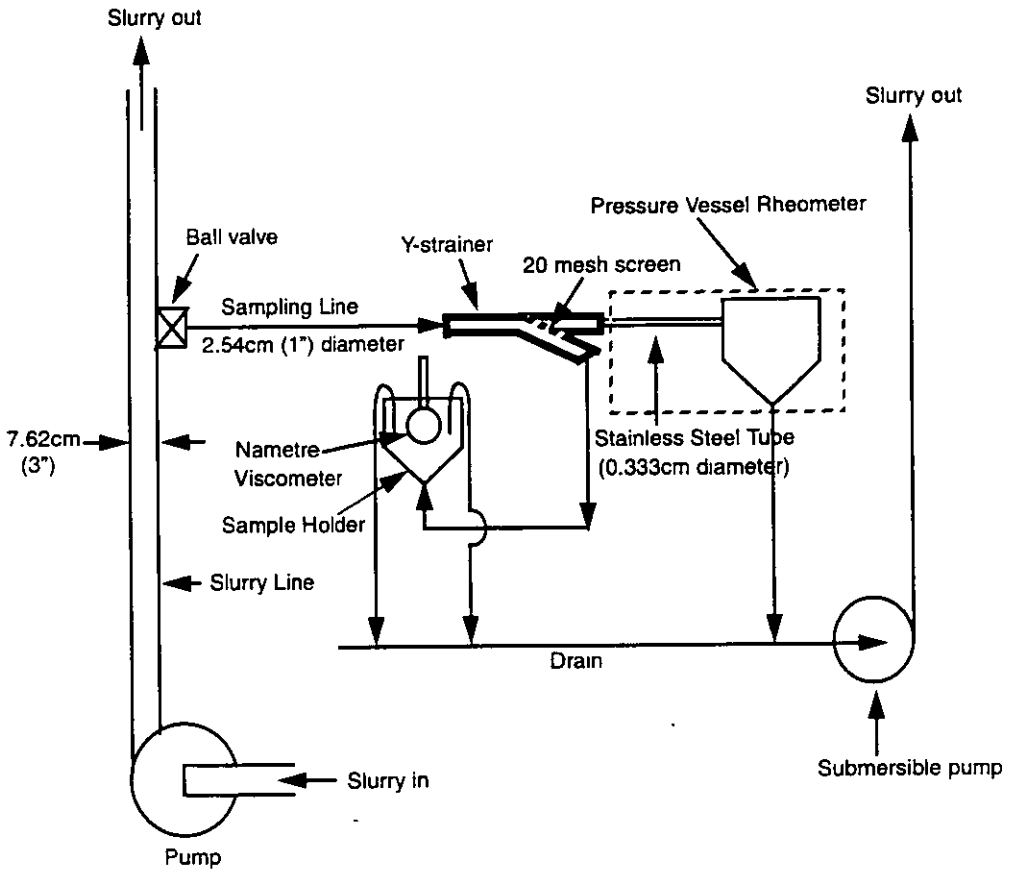

Figure 3 Flow diagram of the rheometer set-up in the plant The Y-strainer with a 20 mesh screen was installed to prevent tramp material from entering the capillary tube. A Nametre vibrating sphere viscometer was also installed to measure viscosity at a high shear rate

temperature varied between 25 and 30°C

RHEOLOGICAL MEASUREMENTS

The following rheological parameters were measured during this trial period.

Flow Curves

Flow curves (Shear stress vs. shear rate and viscosity vs. shear rate) were continuously plotted by the pressure vessel rheometer. For a typical slurry in this plant the pressure vessel rheometer took approximately 2 minutes to measure a complete flow curve. However, flow curves were measured at a 15 minute interval to allow sufficient time for cleaning the vessel of the rheometer. Each point (shear stress vs. shear rate) in the flow curve was measured at a 1/10 second interval. Data for these curves were being stored in the computer after each consecutive measurement.

Viscosity by Nametre and Brookfield Viscometers

Both these instruments were used to measure slurry viscosity to compare with the pressure vessel rheometer. The Nametre viscometer is an on-line vibrating sphere viscometer, and makes viscosity measurements at a single shear rate. Although not suitable for non-Newtonian fluids, its measurements could be used as an on-line cross-check for the viscosity readings from the pressure vessel rheometer with Newtonian fluids The Brookfield viscometer is a rotational viscometer. With proper sample handling de sign (Kawatra and Bakshi, 1995) viscosity of slurries at low shear rates can be measured in the laboratory with this viscometer. It is a laboratory viscometer and is not suitable for in-plant installations This viscometer was used to measure viscosity at low shear rates of the chalcosite slurry sample collected from the plant. From the readings of the Brookfield and Nametre, the shape of the flow curve generated by the pressure vessel rheometer were verified. For example, if the viscosity measured by Brookfield (low shear rate) was more than that measured by the Nametre (high shear), than the fluid is shear thinning or pseudoplastic

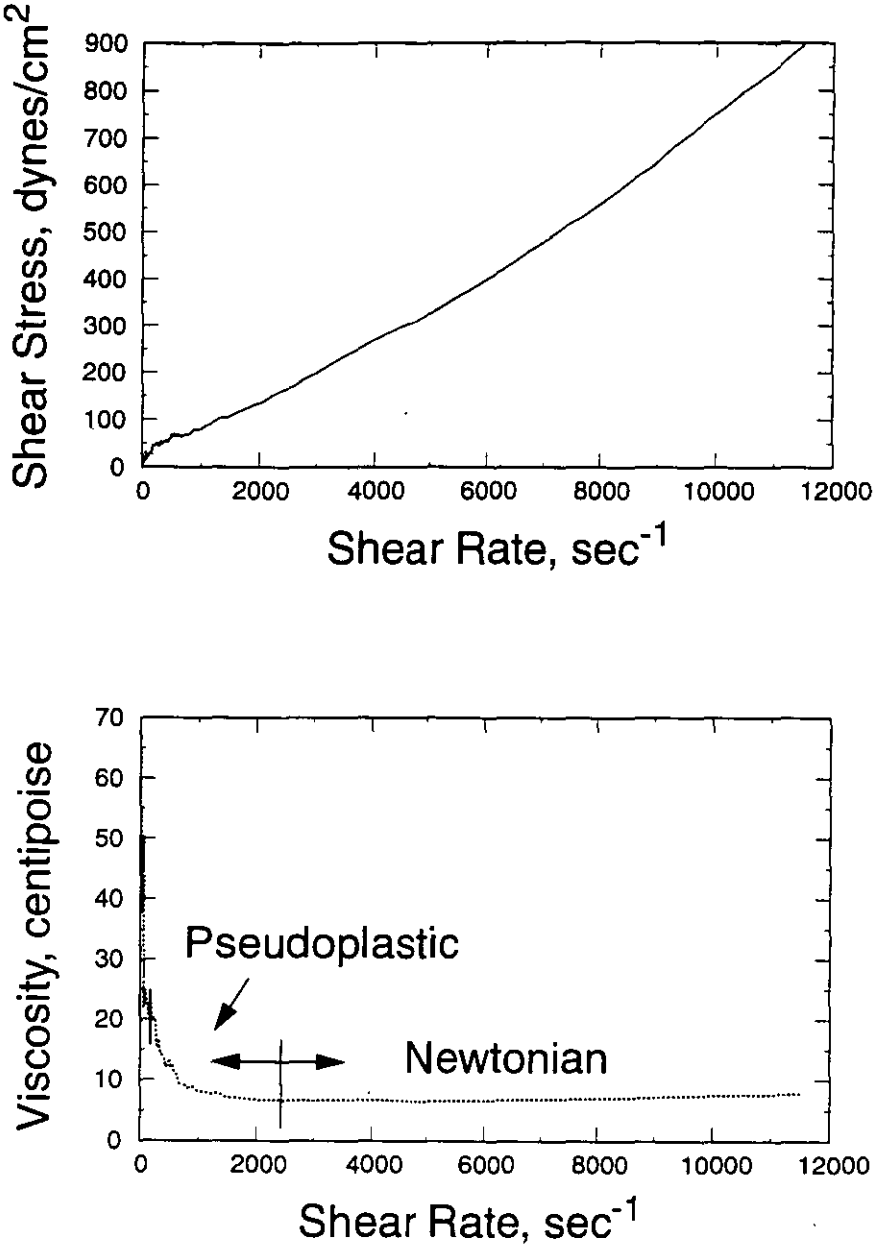

Figure 4 Typical flow characteristics of a slurry as measured by the on-line pressure vessel rheometer. The slurries show pseudoplasticity to a certain shear rate, during which the viscosity decreases with shear rate Then the slurry showed constant viscosity similar to a Newtonian fluid.

RESULTS AND DISCUSSION

Flow curves (shear stress vs. shear rate) of the slurry were measured continuously by the pressure vessel rheometer and were stored in the computer. Due to fluctuations in plant operation, solids content in the slurry varied over a wide range, but the reagents addition rates were not changed proportionally, which frequently changed the slurry characteristics. Detail rheological measurements are discussed below.

General Shape of Flow curves

The general shape of the flow curves were as shown in Figures 4 and 5. Most of the slurries showed pseudoplastic flow (viscosity decreased with shear rate) at lower shear rates. After a certain shear rate, the slurries appeared Newtonian, i.e. their viscosities re-

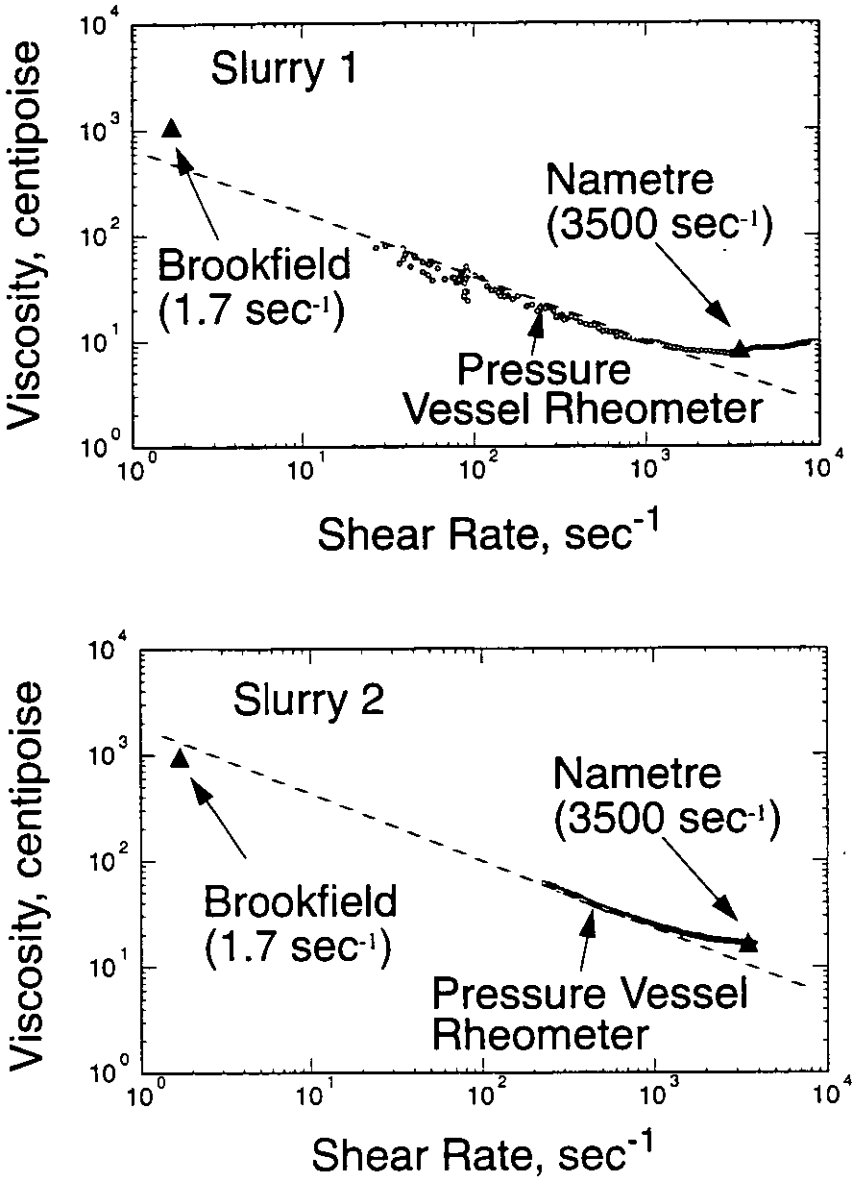

Figure 5 Viscosity of two typical slurries from the thickener underflow in White Pine. Since viscosity decreases with shear rate, the slurries have pseudoplastic flow behavior This is also confirmed by the readings taken by the Brookfield and the Nametre viscometers of the same slurry samples as shown above

mained constant (see Figure 4). This shape of flow curves was verified by measuring the viscosity of samples by a Brookfield viscometer and a Nametre viscometer. The Brookfield viscometer measured viscosity at low shear rates (1 to 34 sec^{-1}) and the Nametre measured viscosity at high shear rates (3000 to 4000 sec^{-1}). As shown in Figure 5, Brookfield measured high viscosity and the Nametre viscometer measured low viscosity, which followed the shape of the flow curve as determined by the pressure vessel rheometer. This showed that the shapes of the flow curves determined by the pressure vessel rheometer were correct.

The pseudoplasticity can be attributed to lime and flocculant addition in the slurry. The calcium ions from the lime compresses the double layer leaving a neutral surface on the individual particles. As a result individual particles are held together by Van der Waals forces to generate bigger flocs This results in an apparent increase in the particle size in the slurry. Also, these flocs trap water inside, which leave less water to transport the solids. All these leads to a higher viscosity at low shear. However, at higher shear rates these flocs are broken and viscosity decreases. That is why we see shear thinning or psuedoplastic properties of the slurries in our study. The addition of flocculant also acts in a similar way. At higher shear rate when the shear force become high the flocs are broken and viscosity decreases. Thus both lime and flocculant made the slurry pseudoplastic.

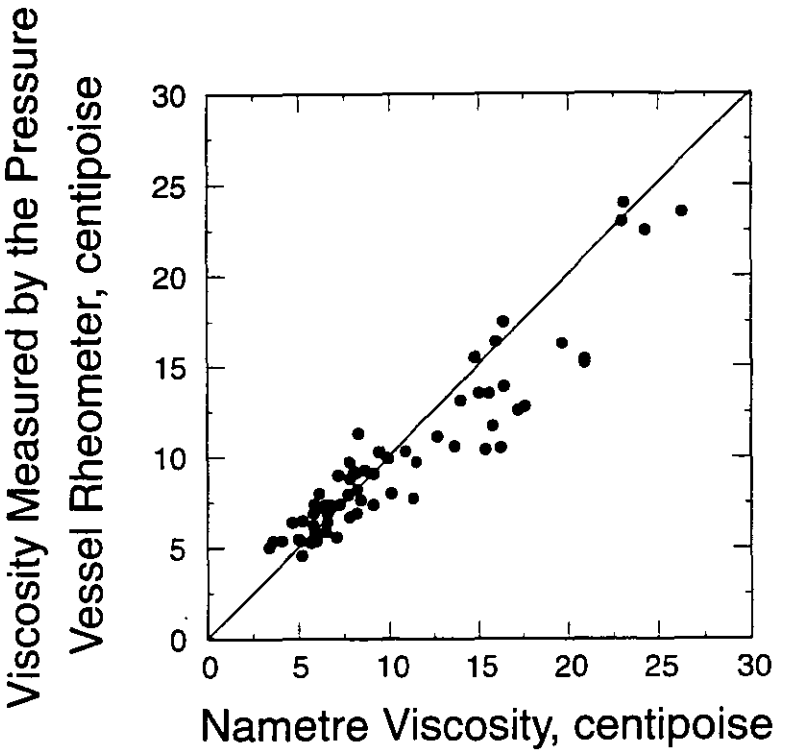

Figure 6 Comparison of viscosity measured with the pressure vessel rheometer with viscosity measured with the Nametre viscometer at 3500 sec^{-1} shear rate.

Viscosity Comparison with Nametre Viscometer

The Nametre viscometer measured viscosity of the slurry on-line. However, this viscometer measures viscosity only at a single shear rate, which is useful only if the slurry is Newtonian Since most of the slurries in the copper plant showed constant viscosity (similar to Newtonian flow) above 3000 sec^{-1}, viscosity from the pressure vessel rheometer at 3500 sec^{-1} was compared with the viscosity from the Nametre viscometer. The results are shown in Figure 6.

While measuring viscosity with the Nametre viscometer, it was observed that solids gradually adhered to the probe. This sharply increased the viscosity reading on the viscometer. Therefore, it was necessary to clean the probe before each reading was taken. Also, when flow through the sample holder of the Nametre increased, the slurry level increased. As a result the probe was often submerged more than the manufacturer's suggested depth. This also caused an increase in viscosity reading. This was partially overcome by controlling the flow of slurry by a ball valve before it entered the sample holder. The deviations of Nametre readings from the pressure vessel rheometer for some points shown in Figure 6 are due to these factors

Effect of Solids Content on Viscosity at the Newtonian Zone (> 3000 sec^{-1})

Solids content is a major factor influencing slurry rheology, and it is often assumed that the viscosity can be inferred from the percent solids The viscosity trend of the chalcocite slurries as a function of solids content is shown in Figure 7. As it can be seen from this figure, viscosity at the Newtonian zone (above ~3000 sec^{-1}) appears to follow the % solids in the slurry. However, from Figure 8 it is seen that the correlation between percent solids and slurry viscosity is not very close, especially at higher percent solids. Thus, for this slurry viscosity cannot be inferred from percent solids measurement.

CONCLUSIONS

An on-line pressure vessel rheometer for suspensions has been developed at Michigan Technological University. This rheometer was successfully installed in a local copper plant to measure the rheology of chalcocite slurry. The slurries showed pseudoplastic flow behavior up to a certain shear rate (around 3000 sec^{-1}), beyond which the viscosity of the slurry remained unchanged like a Newtonian fluid. This was verified by two other viscometers, a Brookfield rotational viscometer which measured viscosity at a low shear rate, and a Nametre vibrating sphere viscometer which measured viscosity at a high shear rate. While comparing the viscosities at the Newtonian range measured by the pressure vessel rheometer and the Nametre viscometer, similar results were observed.

Since the rheometer is capable of measuring flow curves of suspensions of both Newtonian and non-Newtonian flow properties, it can be used on-line to generate a more detailed rheology of suspensions which is not possible by most of the rheometers available today.

Clarke, B., 1967, "Rheology of Coarse Settling Suspensions," Trans. Inst. Chem. Engrs., Vol. 45, pp. T251-T266.

Fuerstenau, D. W., Venkataramana, K. S., Velamakanni, B. V., 1984, "Effect of Chemical Additives on the Dynamics of Grinding Media in Wet Ball Mill Grinding," International Journal of Mineral Processing, Vol. 15, pp. 251-267

Hemmings, C E., and Boyes, J. M., 1977, "An On-Line Viscometry Technique for Improved Operation and Control of Wet Grinding Circuits," Twelfth International Mineral Processing Congress, Sao Paulo, pp. 46-64.

Kawatra, S. K., and Bakshi, A. K., 1996, "On-line Viscometry in Particulate Processing," Mineral Processing and Extractive Metallurgy Review, Vol. 14, pp. 249-173.

Kawatra, S. K., and Bakshi, A. K., 1995, "Determination of Changes in Rheological Properties of Coal Slurries in Process Streams," Coal Preparation, Vol 15, No 3-4, pp. 165-175.

Kiljanski, T., 1993, "On the Measurement of the Rheological Properties of Unstable Mineral Suspensions," Coal Preparation, Vol 13, pp. 107-112.

Klimpel, R. R., 1982-1983, "Slurry Rheology Influence on the Performance of Mineral/Coal Grinding Circuits," Part I, Mining Engineering, Vol. 34, No. 12, pp 1665-1668, December 1982, Part II, Mining Engineering, January 1983, Vol. 35, No 1, pp. 21-26.

Rachman, Y A., 1979, "An Assessment of Vibrating Viscometers in Slurries," Report No. 2001, National Institute for Metallurgy, Private Bag X3015, Randburg, 2125 South Africa.

Reeves, T J 1990, "On-line Viscosity Measurement Under Industrial Conditions," Coal Preparation, Vol. 8, pp. 135-144.

Underwood, W. M , 1976, "Viscometer for Slurries and Suspensions," Rev. Sci Instrum., Vo 47, No. 9, pp. 1079-1082

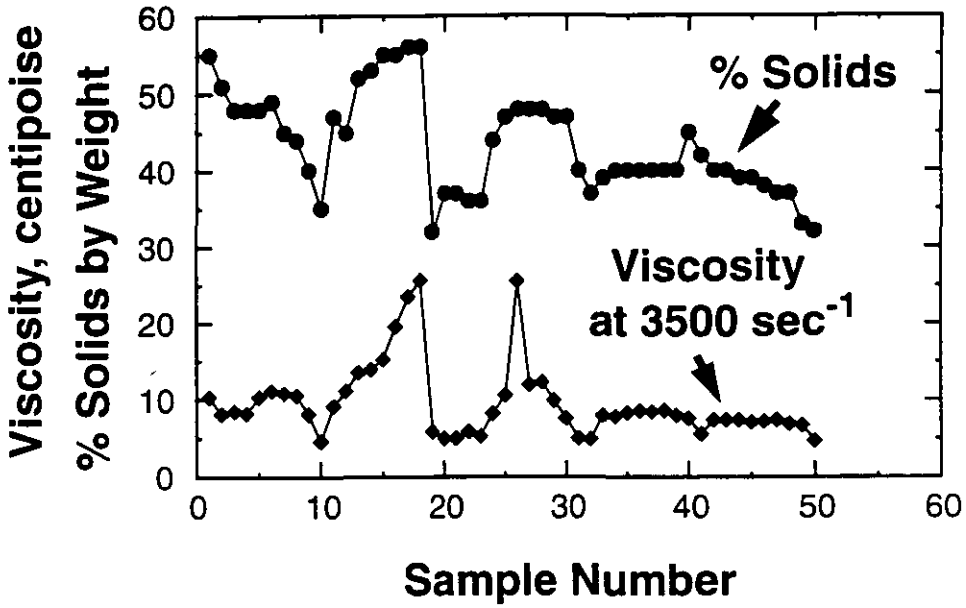

Figure 7 Comparison of viscosity and % solids of chalcocite slurries Viscosity at the Newtonian zone (above ~3000 sec^{-1}) appears to follow the % solids in the slurry.

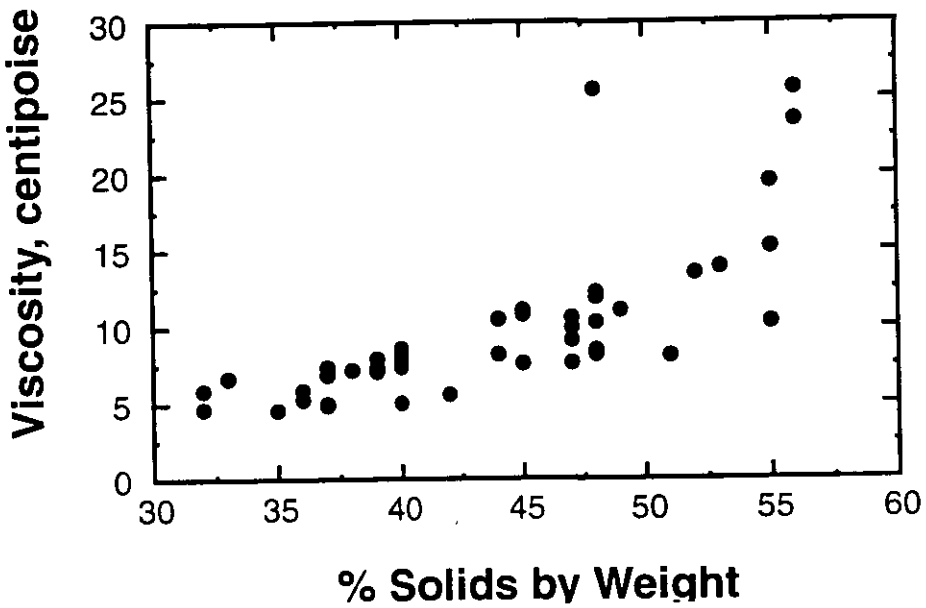

Figure 8 Viscosity vs solids content, Viscosity at the Newtonian zone (above ~3000 sec^{-1}) does not show a linear relationship with percent solids and there is a considerable amount of scatter in the data which tells that % solids monitoring alone can not predict slurry rheology

ACKNOWLEDGMENT

The authors gratefully acknowledge the funding for this project provided by the Dow Chemical Company, Midland, Michigan, and the Copper Range Company at White Pine, Michigan

REFERENCES

Aplan, F. F., and Spedden, H. R., 1965," Viscosity Control in Heavy Media Suspensions," Seventh International Mineral Congress, New York (Ed.) N. Arbiter, Gordon and Breach, New York, pp. 103-113.

FACULTAD DE INGENIERIA U.N.A.M.
DIVISION DE EDUCACION CONTINUA

CURSOS ABIERTOS

DESARROLLO Y OPERACIÓN DE SENSORES PARA CONTROL DIRECTO Y CONTINUO EN PLANTAS DE BENEFICIO DE MINERALES Y EN LA RESTAURACIÓN DEL MEDIO AMBIENTE

Del 18 al 23 de mayo de 1998

TEMA: ON - LINE VISCOMETRY IN PARTICULATE PROCESSING

EXPOSITOR :DR. KOMAR KAWATRA

1998

Palacio de Minería Calle de Tacuba 5 Primer piso Deleg. Cuauhtemoc 06000 Mexico, D.F. APDO. Postal M-2285
Telefonos. 512-8955 512-5121 521-7335 521-1987 Fax 510-0573 521-4020 AL 26

Mineral Processing and Extractive Metallurgy Review,
1995, Vol 14, pp 249–273
Reprints available directly from the publisher
Photocopying permitted by license only

© 1995 OPA (Overseas Publishers Association)
Amsterdam B V Published under license by
Gordon and Breach Science Publishers SA
Printed in Malaysia

On-Line Viscometry in Particulate Processing

S. K. KAWATRA and A. K. BAKSHI

Department of Metallurgical and Materials Engineering, Michigan Technological University, Houghton, MI 49931

(Received 23 Jun 1995, in final form 11 September 1995)

On-line viscometry of suspensions is very difficult compared to viscometry of pure liquids The problem arises because of the unstable nature of the suspensions, particularly when coarse and fast settling particulates are present Several attempts have been made in the past in which special mixing chambers have been designed to maintain slurry homogeneity while measuring viscosity. However, the credibility of these instruments are questioned by many authors, as quite often the same systems measure different rheological behavior for similar suspensions In most of the designs suggested in the past, solving one of the problems of suspension viscometry introduces new problems. For example, agitation can keep the solids suspended, but it can also seriously affect the sensitivity of the viscometer. In this article the problems involved with three different types of viscometers (rotational, capillary, and vibrational), which have been used for measuring viscosity of suspensions, are discussed

BACKGROUND

Unlike non-particulate fluids, rheological measurements of particulate fluids (suspensions) are very difficult. Since a suspension is a multi-phase system, its rheology depends upon the properties of both the liquid and the solids which constitute the suspension. During rheological measurement, the stability of the suspension must be maintained, so that the properties of the suspension will not change while they are being measured Suspension stability is influenced by several interdependent parameters, such as, (i) Settling velocity of the particles, which depends upon the liquid viscosity, particle size, and particle density; and (ii) Coagulation and flocculation, which depend upon the surface properties of the particles, which in turn are influenced by the chemistry of the carrier liquid Other parameters, such as particle concentration and particle packing, also influence interparticle interaction, and hence the rheology. The forces arising from all these parameters affect the movement of the fluid, and changes in these will change the rheology of the suspension Unfortunately, most of the viscometers available to-day are not capable of keeping up with these complex mechanisms of suspension rheology.

Nevertheless, the importance of suspension rheology is widely felt in various industries. In the food industry, more and more attention is given to rheological properties to utilize modern technology for food production, handling, storage, and

quality improvement[1] In injection molding (ceramic and metal casting) lower viscosities are needed to facilitate mixing, transportation, and enhance solids loading (to reduce shrinkage during sintering)[2]. In paint manufacturing, optimum rheology is needed for quality control. Similarly in the coal and mineral industries, a complete knowledge of rheology is necessary for optimum grinding[1-5,38,39] and efficient separations[6,7,40]. Slurry rheology is also important in the emerging coal slurry utilization technologies. A suitable yield value is needed to store the slurry without allowing the solids to settle, while lower viscosities are needed at intermediate and high shear rates for easier transportation and better atomization[8,9]. Similarly, examples of the importance of slurry rheology can be seen in many other industries, such as in paper and pulp making, waste treatment, cement manufacturing, and so on. Therefore, the need for a suitable rheometer for process control in these industry is always felt. The search for such an instrument was reported as early as 1940[10] and researchers are still working towards it in the 1990's[11-13]. This shows that until today a satisfactory on-line rheometer for suspensions has not been developed. In this article, a survey of viscometry systems for particulate fluids is provided. Since measurement of coarse suspensions is more difficult than measurement of suspensions containing submicron particles, emphasis is given to research work conducted on systems containing coarse, fast settling particles Three different types of viscometers, the rotational type, the capillary type, and the vibrational type, are discussed whose use have been reported widely for suspensions.

ROTATIONAL VISCOMETERS

Operating Principle

Because of their control over shear rate, rotational viscometers are widely used among researchers. Most rotational viscometers used for suspensions are of the co-axial cylinder type A line diagram of a simple co-axial cylinder viscometer is given in Figure 1. In this type of viscometer, the fluid is placed in the gap between two concentric cylinders for measurement. Then one of the cylinders is rotated by a motor at a particular r p.m. while the other is kept stationary, and the torque required to rotate the cylinder is measured. As the viscosity of the fluid increases, the drag force on the surface of the rotating cylinder increases. This in turn increases the torque reading, from which viscosity of the fluid is determined.

Thus the only parameters which are measured by the instrument are the torque (T) and angular velocity (Ω) of the rotating cylinder. Then shear stress is calculated from torque, and shear rate is calculated from angular velocity. Viscosity is calculated by taking the ratio of shear stress and shear rate The rheological type of the fluid is determined based on the variation of shear stress as a function of shear rate, as shown in Figure 2. A Newtonian fluid has the same viscosity at all shear rates, while the viscosity of a non-Newtonian fluid varies as the shear rate changes. Unless proper equations are used to calculate shear stress and shear rates from torque and angular velocity, an incorrect value of fluid viscosity will result. Calculation of shear stress from torque is straightforward and can be expressed by the following equation, which is valid for both Newtonian and non-Newtonian fluids:

$$\tau = T/(2\pi r^2 L) \qquad (1)$$

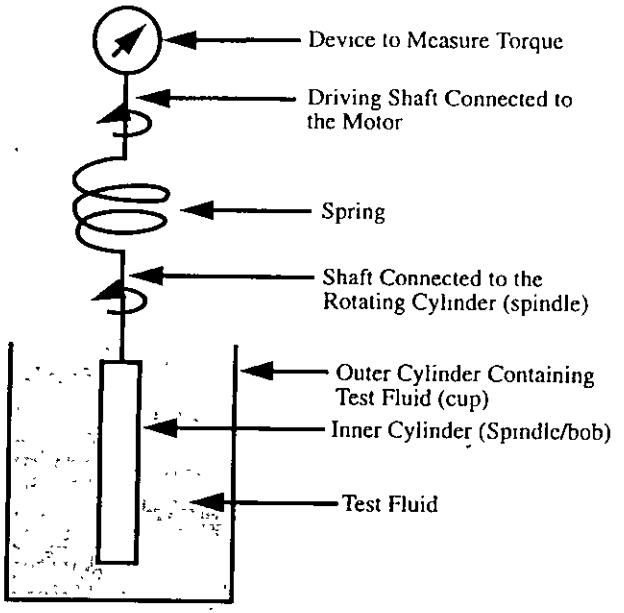

FIGURE 1 Line diagram showing the mechanism of a typical co-axial cylinder viscometer. The change in torque due to the drag force of the fluid on the rotating surface of the cylinder is the measure of viscosity.

Where, τ = shear stress
r = radial distance of the fluid from the axis of the inner cylinder
T = torque
L = length of the inner cylinder.

From this, it can be seen that the shear stress in the viscometer is not a constant, but decreases as one moves from the wall of the inner cylinder to the wall of the outer cylinder.

Calculation of the shear rate from the angular velocity is more complex, and depends upon both the type of fluid and the gap between the two cylinders For Newtonian fluids:

$$\tau = \eta\gamma \qquad (2)$$

Where, τ = shear stress
γ = shear rate
η = viscosity

From this flow model it can be shown that[15],

$$\gamma = [2R_2^2/(R_2^2-R_1^2)]\Omega \qquad (3)$$

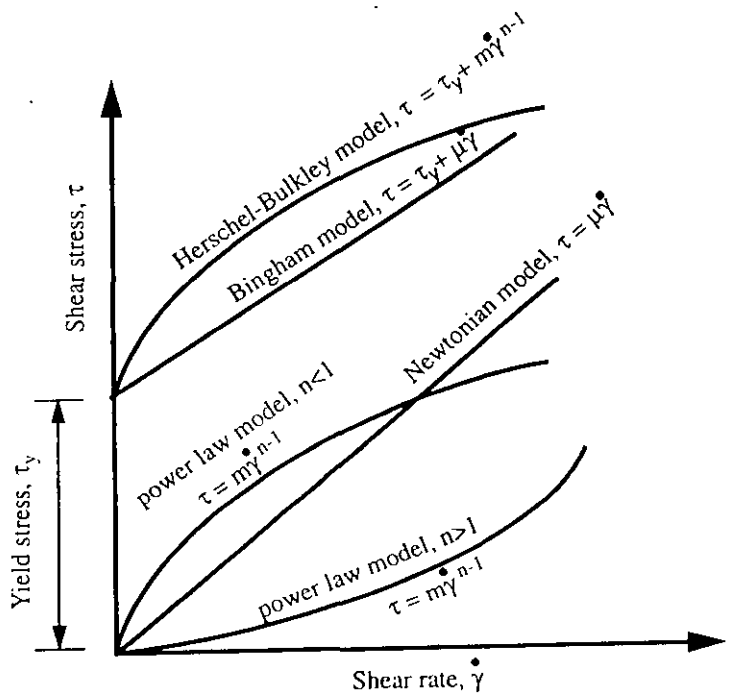

FIGURE 2 Flow curve models reported for suspensions

where, $\dot{\gamma}$ = shear rate at the surface of the inner cylinder
R_1 = radius of the inner cylinder
R_2 = radius of the outer cylinder
Ω = angular velocity of the inner cylinder.

Quite often, Newtonian solutions of known viscosity are used to calibrate the torque scale of the viscometer to determine viscosity of non-Newtonian fluids. This is not correct because with different flow models different expression for shear rate will be obtained. For example, for a non-Newtonian fluid that obeys the power law (see Figure 2), the shear rate is given by the following equation:

$$\dot{\gamma} = 2\Omega/n[1-(R_1/R_2)^{-2/n}] \quad (4)$$

where, $\dot{\gamma}$ = shear rate at the surface of the inner cylinder
R_1 = radius of the inner cylinder
R_2 = radius of the outer cylinder
Ω = angular velocity of the inner cylinder
n = flow index, from the power law equation

From equations 3 and 4 it is seen that unless the appropriate equation is used to calculate shear rates of a particular fluid the viscosity measured by the viscometer will be wrong.

The measurement of the viscosity of a fluid with unknown flow behavior can be greatly simplified by using a coaxial cylinder viscometer whose annular gap is very narrow. If this gap is less than 1% of the diameter of the inner cylinder, then the velocity gradient of the fluid inside the annular gap will very closely approximate linearity for fluids of all types (Newtonian as well as non-Newtonian). In this case, the equation of the shear stress can be written as[15]

$$\tau = T/(2\pi R_a^2 L) \quad (5)$$

Where, τ = shear stress at all points in the gap
R_a = average radial distance of the fluid from the axis of the inner cylinder
T = torque
L = length of the inner cylinder.
and the equation for shear rate can be simplified to[15]:

$$\dot{\gamma} = [R_a\Omega/(R_2-R_1)] \quad (6)$$

where, $\dot{\gamma}$ = shear rate at all points in the gap

From these values of shear stress and shear rates, flow curves of unknown fluid types can be determined.

While the narrow-gap coaxial-cylinder viscometers work well for liquids, they are unfortunately not suitable for coarse suspensions. This is because the narrow gap is prone to jamming and plugging by solid particles.

Critical Discussion of the Rotational Viscometers

Constant shear operation Rotational viscometers can be operated at a steady shear rate for a long time. This helps in taking precise measurements of viscosity at any particular shear rate, especially at low shear rates where yield stress can be calculated. By changing the rpm of the rotating spindle (or cylinder), the shear rate can be changed, thus a flow curve for non-Newtonian fluids can be determined with these instruments.

Wall slip The equations for shear stress and shear rates described in Equations 1 through 6 are derived under the assumption that the velocity of the fluid at the surface of each cylinder is the same as the velocity of the cylinder surface. This is the no slip condition or shear-flow condition. However, quite often slip occurs at the wall, and correct viscosity of a suspension cannot be obtained by using standard formulas. One of the reasons for such slippage in suspensions is believed to be migration of particles away from the cylinder wall[15,27]. This leaves a dilute suspension at the wall compared to the bulk of the fluids. This is often termed "apparent slippage," and it must be addressed while measuring suspension rheology. Corrections for slippage can be obtained experimentally by varying spindle dimensions or theoretically by using correction factors suggested by various authors[15,17]. Some investigators have used cylinders with roughened surfaces (e.g., by cutting grooves on the surface) to avoid wall slip[16].

End effects Ideally the length of the cylinder in a co-axial cylinder viscometer should be infinite, to eliminate end effects. End effects are seen, because the fluid below the inner cylinder (and above the inner cylinder if it is submerged) will exert an additional torque on the spindle that is not included in Equations 1 through 6. End corrections are further complicated when different spindle shapes are used, such as the design shown in Figure 3(b) which has been used for eliminating solids build up on top of the spindle[11-13,20]. By changing this geometry, the direction of the velocity gradients will no longer be radially outwards at the ends. In some high precision laboratory viscometers, the bottom surface of the inner cylinder is made cup shaped to trap a layer of air below it, and so minimize the end effects. Also, by keeping the top surface of the inner cylinder above the fluid, torque exerted by the fluid on this surface can be eliminated. However, both these options cannot be practical in a flowing slurry line, and so cannot be used in on-line instruments. As far as end effects are concerned, the double gap design shown in Figure 3(c) is most suitable for suspensions, because it minimizes the end surfaces of the spindle.

Sensitivity Rotational viscometers are very sensitive and any disturbances associated with sample flow will offset the torque reading. In order to avoid settling of solids, many researchers have suggested top to bottom flow of slurry in the annular space. This arrangement will work if the flow is strictly vertical and has no component acting in the r (radial to spindle) or θ (tangential to spindle) directions. Otherwise the change in torque experienced by the spindle will not be solely from the molecular forces (shear) within the fluid, but will be supplemented by the fluid flow (see Figure 4). This also changes the shear rate experienced at the surface of the spindle because the flow interferes with its rotation[11,12].

Solids settling and centrifuging The most difficult suspensions for viscometers to deal with are those which contain fast settling particles. The solids settle during measurement, which not only destroys the homogeneity of the sample but also interferes with spindle

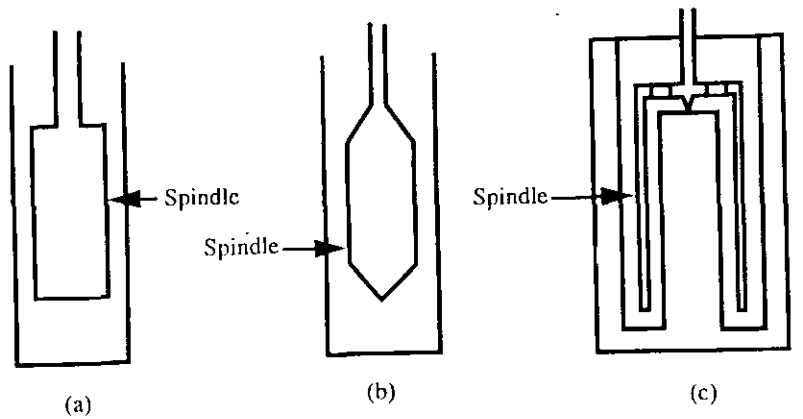

FIGURE 3 Different spindle designs adopted for suspension use.

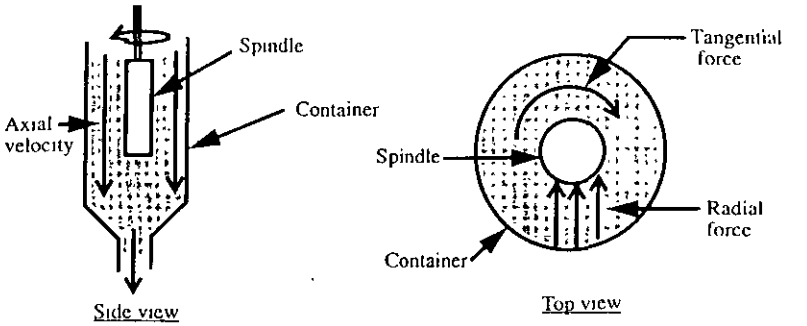

FIGURE 4 The axial flow (side view) prevents the solids from settling by continuously sweeping fresh slurry past the spindle. This component of the flowing slurry stream does not affect the rotation of the spindle. But any radial or tangential forces (Top view), arising from the flow, may put additional strain on the spindle resulting in erroneous viscosity readings. Unbalanced radial flows push the spindle to one side so that it does not spin uniformly and results in erratic readings. Tangential flows increase or decrease the torque on the spindle, making the fluid appear to be either more or less viscous then it really is.

rotation. For example, when the sample is taken in a beaker, solids start settling and slurry at the top of the beaker becomes dilute compared to the slurry at the bottom. Therefore, the spindle is no longer in contact with a representative sample. In this situation, the viscometer will read low viscosity if the compacted solids are below the spindle as shown in Figure 5(a) and a high viscosity if the compacted solids are touching the spindle as shown in Figure 5(b). Furthermore, when the rotational speed of the cylinder is increased to take measurements at high shear, the solids centrifuge outward towards the outer wall resulting in a poor measurement. These problems have been addressed by many past designs, and are discussed in the following section.

Solids plugging and the effect of annular gap For suspensions, the annular gap (the gap between the spindle and the sample holder) is usually large to avoid solids plugging. As a rule of thumb, this gap should be at least 10 times the largest particle size in the suspension[14]. Quite often liquids of known viscosity (Newtonian fluids like silicon oil or sucrose solution) are used to calibrate the torque scales which are then applied to calculate viscosity of non-Newtonian fluids. This is acceptable only when the annular gap is small (< 1% of the cylinder radius), and may not be correct when the gap is large. Therefore, for non-Newtonian suspensions, depending upon the flow model, proper equations (such as Equation 4) should be used to calculate the correct viscosity. Otherwise, the measurements will result in erroneous rheological characterization of the suspension.

Slurry Presentation Systems for Rotational Viscometers

Solids settling has been the major concern for most of the researchers who have used rotational viscometers for suspension viscometry. This has resulted in various designs of

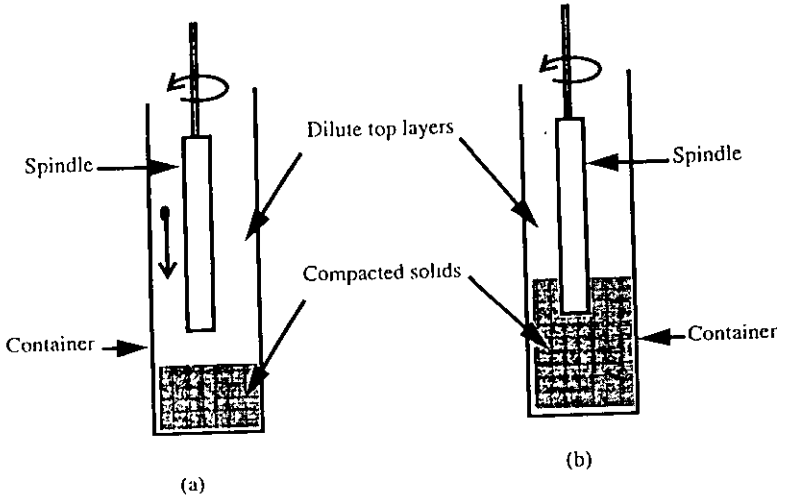

FIGURE 5 Solids settling leaves a dilute suspension on the top layers of the container. When the solids content is low (a) the solids gradually settle and are compacted below the spindle and the viscometer reads progressively lower viscosity as the solids settle At higher concentration of solids, the compacted solids can touch the spindle (b) resulting in higher readings

sample presentation systems to prevent solids settling during viscosity measurement. Some of these designs are discussed in this section.

Presentation systems in stirred tanks If proper precautions are taken, slurry viscosity can be measured by placing a rotational viscometer inside a stirred tank. One such arrangement has been reported by Clarke[16] A line diagram of this measuring system is provided in Figure 6 He used a co-axial cylinder viscometer (Ferranti, Model VL), which could be operated between shear rates of 43 to 950 sec^{-1} with interchangeable spindles The sample holder consisted of a 450 ml vessel with an eight bladed impeller at the bottom to keep the solids in dispersion The impeller operated at 400 revolutions per minute. In order to prevent rotation of the sample inside the vessel, vertical baffles were fitted above the impeller The whole arrangement was intended to encourage top to bottom flow of the solids so that the viscosity could be measured without obstructing the flow Clarke tested suspensions of quartz, glass, and polymethacrylate in water with particle sizes up to 211 microns and concentrations up to 50% solids by volume He measured apparent viscosity up to a shear rate of 350 sec^{-1}.

Clarke reported centrifuging of coarse particles (above 150 μm) because of the high speed of the impeller required to keep the solids in suspension This offset the homogeneity of the suspension for many samples In order to avoid centrifuging of solids, he took instantaneous measurements before the solids started outward movement. Clarke reported dilatancy of quartz suspensions at very low percent solids (10% by volume) which may have resulted from trapping of particles in the grooves which were made on the spindle surface to prevent slippage of the sample

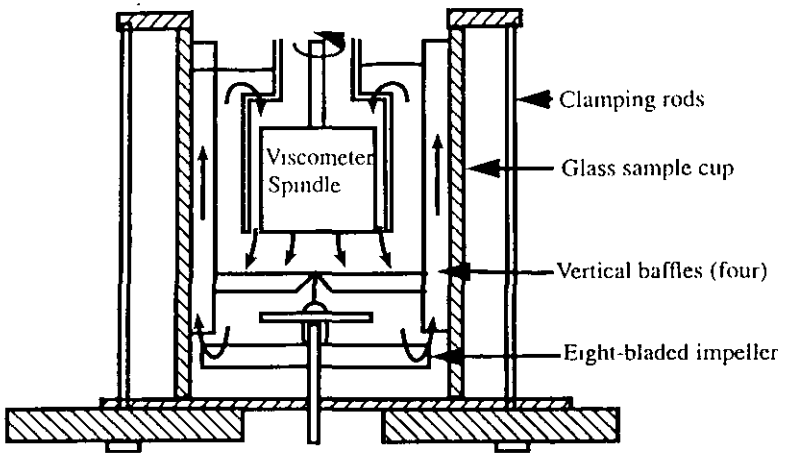

FIGURE 6 Sectional view of sample cup and measuring cylinders showing flow pattern (from Clarke 1967)

Similar designs were later reported by Lapasin[17] and Underwood[18] (Figure 7) In the Underwood design, a modified T-bar spindle (standard Brookfield spindles) was used The modified spindle had twelve cylindrical bars extending from a vertical shaft The spindle was connected to a Brookfield model RVT viscometer. The sample was placed in a beaker which had an annular sleeve A honeycomb of small diameter vertical cylinders was placed at the bottom Below this honeycomb arrangement, a Teflon coated magnetic stir bar was placed. When the stir bar rotated, slurry ascended through the annular space, entered the beaker, flowed down past the spindle, and then drained through the honeycomb The swirls and eddies created by the stirrer were prevented from reaching the spindle by this honeycomb arrangement.

Presentation systems in tanks with top to bottom flow Hemmings and Boyes[19] used a Brabender-Messtechnik Convimeter viscometer to measure apparent viscosity on the discharge line of a ball mill The convimeter was mounted inside a column (Figure 8) and rotated in a gyratory motion at 120 revolutions per minute Slurry from the ball mill flowed through this column. The level of slurry within the column was controlled by sensing the hydrostatic pressure and automatically controlling the slurry flow through the valve (by expanding or contracting an elastomeric flow restrictor) The operating range of the instrument was governed by the flowability of the slurry This viscometer arrangement will not work for high solids concentrations when the slurry does not flow under gravity Also, since the sensor moved in a gyratory motion, it did not have a well-defined shear rate Therefore, at high percent solids when the slurry behaves in a non-Newtonian manner, the viscosity measured by the viscometer may not be the same as the viscosity experienced inside the mill.

Reeves[11,20] reported a rotational type viscometer for on-line use with slurries He installed a specially designed spindle in a sample preparation and presentation system as

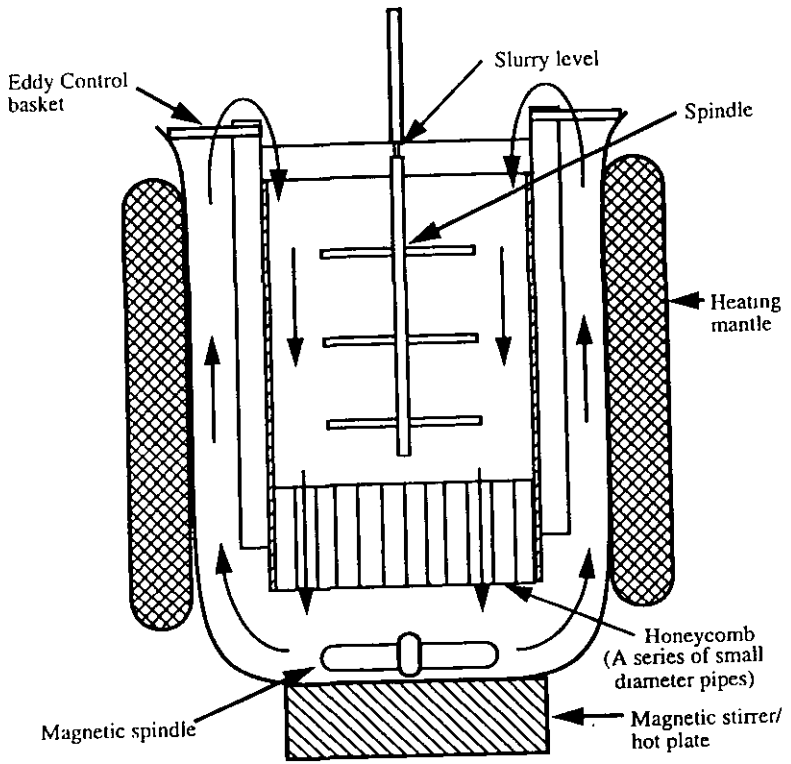

FIGURE 7 Viscometric assembly showing the spindle and eddy current basket (from Underwood 1976)

shown in Figure 9. The feed sample from the plant passed over a stationary screen (10–12 mm opening) to remove large particles and tramp materials. The instrument was capable of measuring viscosity within a shear rate range of 0 to 200 sec^{-1}, with the shear rate adjusted by changing the rotational speed of the bobbin. The viscometer operated at a constant shear rate by choosing a single rotational speed for the spindle Reeves made on-line rheological measurements of ferro-silicon suspensions with 14–16% solid concentrations. In this design, baffles were installed in the measuring chamber to eliminate rotation of the sample in the container. Still he reported fluctuations in viscometer reading for fluids below 10 centipoise

The Hemmings and Boyes design and the Reeves design were the only two rotational viscometer systems tried on-line for mineral slurries. These viscometers depend upon the flowability of the slurry[19], i.e. as long as the slurry flows under gravity through the sample presentation system, the associated viscometers can measure the viscosity This may not be the case in many concentrated suspensions, where yield stresses are seen.

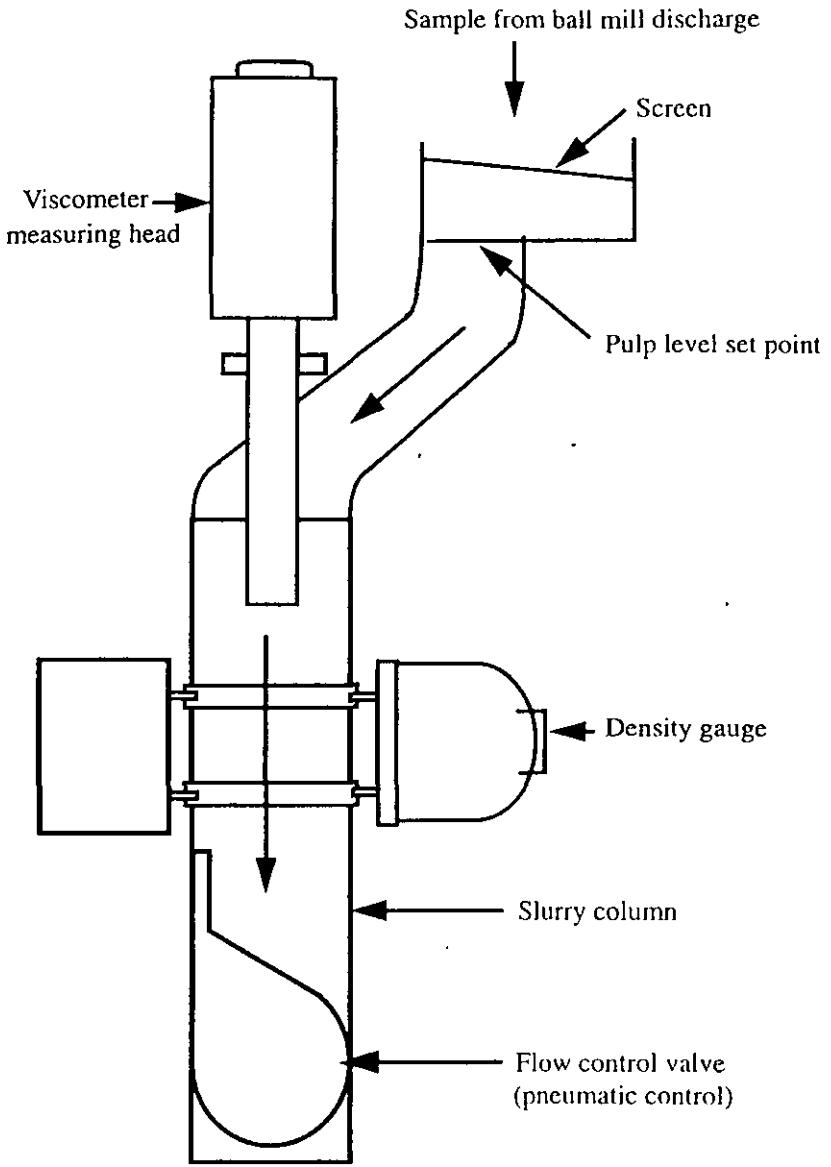

FIGURE 8 Viscosity sensing system designed by Hemmings and Boyes (from Hemmings and Boyes 1977)

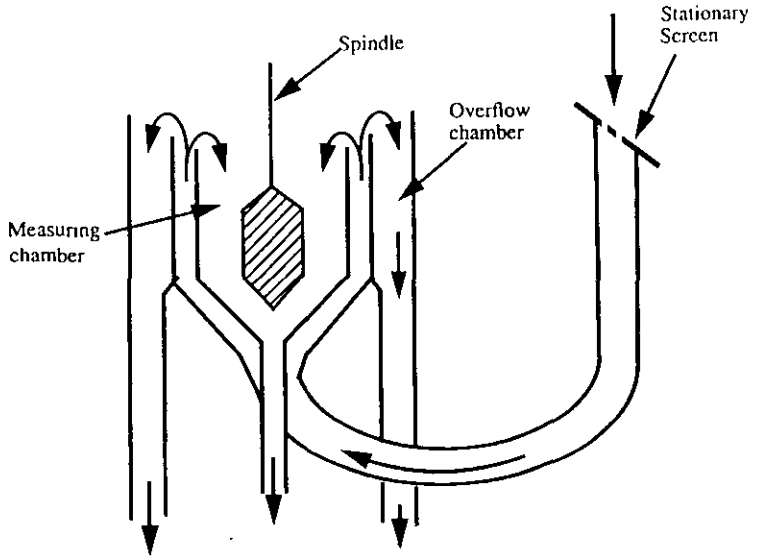

FIGURE 9 Viscometer arrangement developed by Reeves, 1984. The spindle, is made conical at the top and bottom surfaces to avoid solids deposition on top of it. (from Reeves 1984)

e.g., in grinding mills and concentrated coal slurries[4]. These slurries will be too viscous to flow properly through the gravity flow sample presentation systems.

Unless precautions are taken, the annular space in rotational viscometers can be plugged by coarse particles or tramp materials. In both the systems described above, it has been suggested that this problem be solved by pre-screening the sample before it entered the measurement chamber.

In general, the use of rotational viscometers in gravity fed sample presentation systems are questionable because the viscometer measures the drag from the fluid, and any tangential or radial forces on the spindle will affect this measurement (Figure 4). Most rotational viscometers are very sensitive to these forces, and the problem becomes severe when the instruments are used on-line. The use of baffles is aimed at reducing these effects. While evaluating the use of an eddy control basket[18] for measuring viscosity with a Brookfield viscometer, we realized that completely avoiding tangential or radial forces from fluid flow is a very difficult task. This is especially true for low viscosity fluids (such as water). Because of these concerns, Klien *et al.*[11] designed a different technique for measuring the rheology of unstable mineral suspensions which took advantage of the zone settling properties of some suspensions. They assumed that after the sample is placed in a container, solids settle and a constant density zone is created in the container. Then they constructed a double gap bob and cup arrangement. This bob and cup fixture was attached to a Haake Rotovisco RV 20 viscometer. They tried to place the bob in the constant density zone for shear stress and shear rate measurement (Figure 10). They measured rheograms of magnetite suspensions at solid

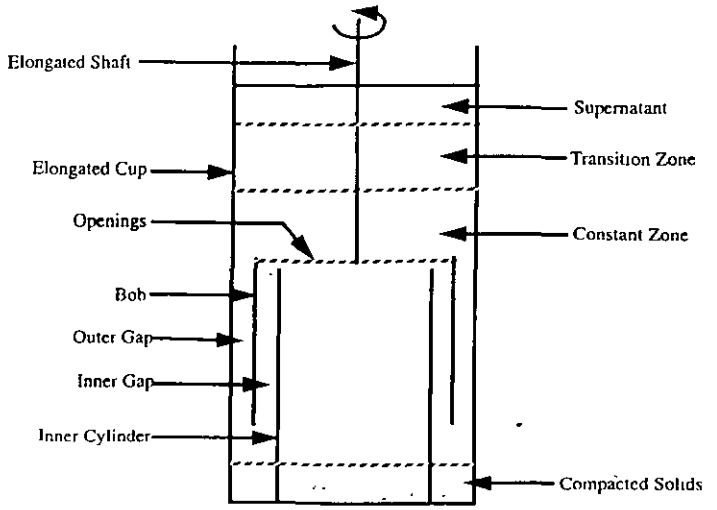

FIGURE 10 Line diagram of the double gap cup and bob arrangement for measuring the zone settling properties of suspensions (from Klien *et al.*, 1990)

concentrations of 11 to 25% by volume. In this way the undefined forces (tangential and radial) that could be generated by mixing arrangements were eliminated. However, since the coarse and fast settling particles were allowed to settle at the bottom of the container, the solids contents in the constant density zone must be different from the initial sample. Thus this arrangement cannot maintain a representative sample. Since solids concentration greatly influences the slurry rheology, this arrangement cannot be accepted for rheological measurements of suspensions.

The influence of undetermined forces generated by slurry flow (across the viscometer) is further reported by Kiljanski[12]. He too used a double gap coaxial fixture attached to the driving and measuring unit of a commercial rheometer (Figure 11). The viscometer operated at shear rates between 0.26 sec^{-1} and 870 sec^{-1}. The sample was pumped through the viscometer by a centrifugal pump, making a top to bottom flow (axial flow) of the fluid sample inside the viscometer. He used two samples of magnetite dense media, one at 34.5 vol% collected from the bottom of a drum separator which was contaminated with processed coal and the other was a 12.5 vol% suspension made out of pure magnetite dense medium. In his experiments, Kiljanski measured shear stress and viscosity at different shear rates at two different conditions, (i) while the sample was flowing through the instrument and (ii) after the flow was stopped. He noticed clear difference in readings between measurements made with circulation (when the suspension was flowing) and without circulation (when the flow was stopped). He argued that these differences in readings were (i) because of the additional shear rates imposed due to axial flow of sample, and (ii) because of an additional torque developed due to the inertia of the fresh, non-rotating fluid entering the viscometer, to which the rotation has to be imparted by the spindle (resulting in a higher shear stress). Kiljanski

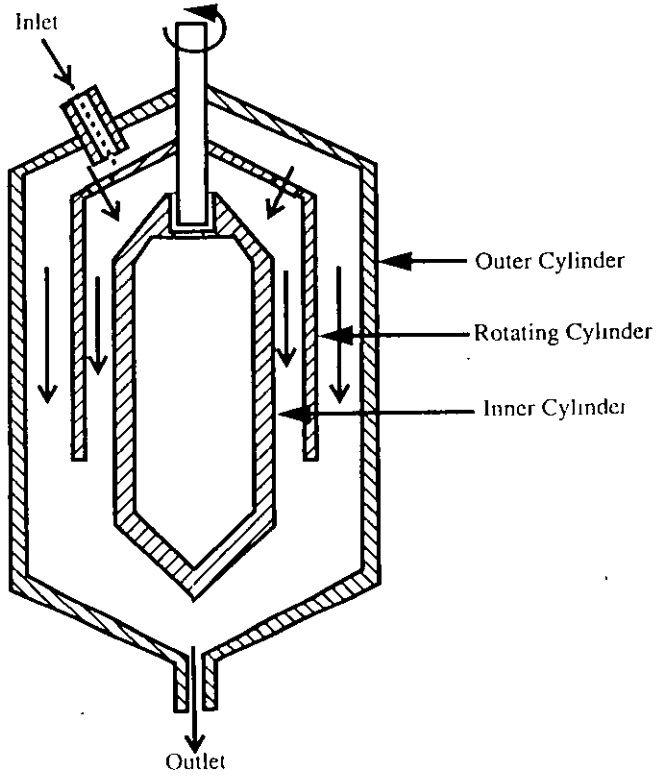

FIGURE 11 Simplified diagram of double gap rotational viscometer designed by Kiljanski, 1993 Both the outer and inner cylinders were held stationary The diameters of the gaps outside and inside of the rotating cylinder (spindle) were designed such that the shear rates on both outer and inner surfaces were constant (from Kiljanski 1993)

also noticed differences in viscosity readings when the annular gap was increased. He argued that for smaller gap the axial shear rate originating from axial flow (top to bottom flow of the fluid) of fluid is higher than the axial shear rate for a wider gap, therefore viscosity measured at similar shear rates (calculated from the rotational speed of the spindle) were different This shows how the undetermined forces from the sample circulation in the viscometer can generate misleading results

Summary Solids settling has been the primary focus area for researchers working on rotational viscometers Continuous agitation or top to bottom flow seems to be the answer to this problem. However, rotational viscometers are very sensitive and both these methods for keeping the solids in suspension create undue forces which seriously affects the viscometer readings

Control of shear rate is the strongest point of rotational viscometers This helps in measuring the rheology of non-Newtonian fluids, specially at low and medium shear rates However, at higher shear rates (above 300 sec^{-1}) rotational viscometers are not suitable for suspensions because high rotational speed of the spindle produces a centrifugal force that segregates the solids

The annular gap between the cylinders must be at least 10 times larger than the largest particle in the suspension to avoid solids plugging. The sample must also be screened to remove any oversize and tramp material. Other problems which must be considered for rotational viscometers are wall slip and end effects.

CAPILLARY VISCOMETER

Operating Principle

In a capillary viscometer the fluid is passed through a tube under pressure By measuring the flow rate and pressure drop across the tube shear stress and shear rate can be calculated. Although capillary viscometers are normally designed for Newtonian fluids, they are also extensively used for non-Newtonian fluids. These viscometers provide a simple and inexpensive method for rheological measurement, and when suitable for an application, capillary viscometers are more precise than rotational viscometers[15] Specifically, these viscometers operate better at higher shear rates[22] which are common in many processing and manufacturing units.

For a fluid flowing through a tube (Figure 12) the shear stress at the wall can be calculated from the pressure difference across the tube by using the following formula

$$\tau = R(P_1-P_2)/(2L) \tag{7}$$

Where, τ = shear stress at the wall
P_1 = Pressure at the entry of the tube
P_2 = Pressure at the exit of the tube
L = Length of the tube
R = radius of the tube

Shear rate at the wall for Newtonian fluids can be calculated by measuring the flow rate, Q through the tube by applying the following formula

$$\dot{\gamma} = 32Q/\pi R^3 \tag{8}$$

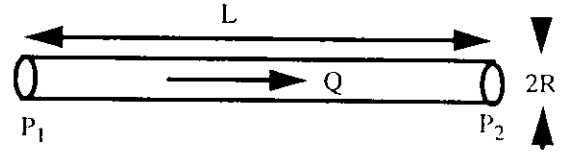

FIGURE 12 Line diagram of a capillary tube

Where, γ = shear rate at the wall
Q = flow rate

Thus by using the measured pressure difference across the tube and the flow rate through the tube, shear stress, shear rate, and viscosity can be calculated. Equation 8 is derived from the Newtonian flow model Therefore, for such fluids Equation 8 gives the true shear rate of the fluid. For non-Newtonian fluids the shear rate obtained from Equation 8 is called the apparent shear rate. True shear rate of non-Newtonian fluids can be obtained from $32Q/\pi R^3$ (Equation 8) by the following formula which is derived by Metzner and Reed[23] after modifying the Rabinowitsch[24] equation·

$$\dot{\gamma} = (3n' + 1/4n'). (32Q/\pi R^3) \quad (9)$$

Where, $\dot{\gamma}$ = shear rate at the wall
n' = flow index given by the following formula

$$n' = \frac{d\log(\Delta P/4L)}{d\log(4Q/\pi R^3)} \quad (10)$$

Where, n'= flow index
ΔP = pressure difference across the tube = $P_1 - P_2$

n' can be determined graphically by plotting $\Delta P/4L$ vs $32Q/\pi R^3$ on a log-log scale and measuring the slope of the resulting line Equations 9 and 10 are valid for fluids with or without yield stress[23].

Necessary Conditions for Capillary Viscometers

The necessary conditions[25] (Bird *et al*, 1960), which must be satisfied in a capillary viscometer measurements are.

a) Laminar flow (Reynolds number < 2100)
b) Constant fluid density
e) Steady flow
d) End effects are negligible
e) No slip between the wall and the fluid
f) The fluid must be incompressible

Common Capillary Viscometer Types

Common capillary viscometers are either constant flow type or constant pressure type viscometers. Piston viscometers are examples of the constant flow type In these viscometers, fluid is pushed through the tube by a piston moving at a constant speed Thus the flow rate through the tube remains constant By measuring the pressure difference across the tube, viscometric functions can be calculated In constant pressure

capillary viscometers a constant pressure is applied at the entry of the tube and the flow rate is measured by collecting the fluid flowing through the tube[15]

Discussion of the Capillary Viscometers

Capillary viscometers have several advantages as listed below

- Since the flow is continuous and the sample stays inside the tube for a very short time, solid settling inside the viscometer is not a problem However, the suspension should be kept well mixed before it enters the tube. This is usually done in an agitated system immediately before the sample enters the tube[28,29]
- Capillary viscometers are suitable for making measurements at high shear rates, where industrial operations such as pumping and spraying are carried out.
- They are simple to construct, and if they can be suitably used with a given fluid, can generate more accurate data than a rotational viscometer.

Many of the problems encountered in rotational viscometer are also common in capillary viscometers Some of the examples are listed below.

- Similar to rotational viscometers, the diameter of the capillary viscometer should be at least 10 times larger than the top particle size of the suspended particles. Therefore, the sample must be screened to remove unusually coarse material before it is allowed to pass through the tube
- Slippage at the wall is still a problem with capillary viscometers This is mainly because of particle migration away from the wall[15,21]. As a result, a more dilute fluid is left in contact with the wall. The presence of wall slip can be detected by comparing flow curves of the same sample generated by tubes of different diameters[27]. This problem is minimized by selecting tubes with larger diameters with respect to the top particle size in the suspension, or by using any of several suggested correction factors[15,17]
- End effects are noticed in capillary tube viscometers, because of pinching of the slurry stream at the entry and exit of the tube[21]. Therefore, flow profiles at the ends are different than in the rest of the tube This problem is eliminated by using tubes with high length to diameter ratio (above 300).
- Tubes must be calibrated at suitable intervals to compensate for any diameter changes resulting from abrasion or scaling.

Despite these problems, capillary viscometers are widely used by many investigators[15,21,23,27,28]

Selected Designs

Examples of the use of capillary viscometers for suspensions are abundant in the literature Antonini *et al*[28] measured rheological properties of a coal water slurry with 70 wt% solids content by using different dimension tubes Their apparatus consisted of a 10 liter reservoir equipped with interchangeable tubes of different lengths and diameters

The slurry was agitated by a pneumatic stirrer. For each pressure applied, they measured the flow rates by continuously weighing the slurry flowing through the tubes. Then from pressure gradient and flowrate, they generated flow curves for the coal slurry samples.

Turian *et al*.[29] reported a new design of capillary viscometer for measuring shear stress, shear rate, and yield stress of suspensions. The main body of the instrument consisted of a stainless steel container to hold the sample. The solids were kept in suspension by stirring the sample in the container. They used different dimension stainless steel tubes (with diameters from 2.4 to 8.8 mm) which could be connected to the bottom of the container. The sample flowing through the capillary tube was collected by a bucket placed on top of a electronic balance. The whole system was covered by a water jacket to maintain a constant temperature. Flow rate through the tube was determined by the balance whose signal was recorded by a computer. Shear stress (τ) and shear rate γ were calculated from pressure drop ΔP and flow rate Q.

Turian *et al*. determined yield stress by extrapolating the shear stress-shear rate curve to a shear rate of zero. They used pulverized Pittsburgh Seam (No. 8) coal to make the measurements over a shear rate range of 1 to 10^4 sec^{-1}. They also determined the yield stress of the slurry by the vane method[30] to verify the result obtained from the capillary tube, and reported that the yield stresses obtained by both the methods were similar.

Another way of measuring viscosity of a slurry is to drain a measured volume of slurry from an overhead container through a capillary tube and to measure the time taken for the material to drain completely. The slurry is kept in suspension in the tank by constant stirring. This method was first tried by DeVaney and Shelton[10], later it was reported by other authors[7,26]. The model used by Schack *et al*.[26] is shown in Figure 13. The authors measured the viscosity by measuring the time required for 100 ml. of

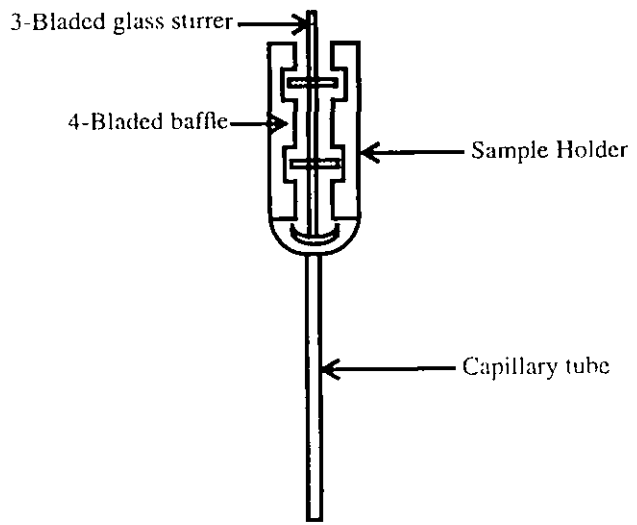

FIGURE 13 Diagram of consistometer chamber and capillary discharge tube used by Shack *et al* (from Schack *et al*., 1957).

suspension to flow through the discharge tube. The major drawback of this instrument is that it does not determine whether the suspension is Newtonian or non-Newtonian. Also, it makes measurements at low shear rates, making it impossible to extrapolate to high shear rates (for hydrocyclone or pumping)[7].

Capillary viscometers are also used in plants to measure effective viscosity of fluids. This can be accomplished by measuring the pressure drop across a straight stretch of pipe. Shear stress and shear rate at the pipe wall can be calculated from pressure difference, flow rate and pipe dimensions. Apparent viscosity can be determined from the ratio of shear stress and shear rate at the wall. In this measurement, the fluid flow in the pipe must be laminar. In order for this method to work with suspensions, the suspension must be very stable (a high yield value), otherwise under laminar conditions a slow sedimentation process will take place at the bottom of the pipe[31].

Summary Compared to rotational viscometers, avoiding solids settling is relatively simpler in capillary viscometers, because the residence time of the sample inside the tube is very small. Measurements of non-Newtonian fluids can be made by changing different dimension tubes or by changing flow rates, which may not be an easy task in plants. For such measurements proper correction factors such as that suggested by Rabinowitsch[23,32] should be considered to obtain true viscosity of non-Newtonian fluids. As with rotational viscometers, wall slip and end effects must be considered while using capillary viscometers. Also, the sample must be pre-screened before allowing it to flow through the tube.

VIBRATING VISCOMETERS

Working Principle

Unlike rotational and capillary viscometers which are volume loading instruments, vibrating or oscillating viscometers are surface loading instruments, because they react only to a thin layer of fluid adjacent to the probe. The probe or sensor of the viscometer can be spherical (Figure 14), rod or plate shaped, or like a fork which vibrates in the fluid. The sinusoidal shear wave from the immersed probe is damped by the fluid, and

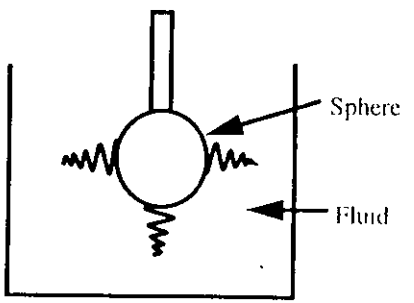

FIGURE 14 Vibrating sphere viscometer. The probe oscillates in the fluid, and the power required to maintain a constant amplitude of oscillation is the measure of viscosity.

the damping is a function of the product of the viscosity and the density of the fluid. Usually the probe is oscillated at a constant amplitude and the force or power required to maintain this amplitude is measured. Rachman[33] derived the following formula for a vibrating rod viscometer to determine viscosity.

$$\eta = R_0^2/A^2\omega_0\rho[F_0x_{00}\omega_{00}/F_{00}x_0\omega_{00})-1]^2 \qquad (11)$$

where, η = viscosity of the liquid
ρ = density of the fluid
ω_0 = resonant frequency
ω_{00} = free resonant frequency
x_0 = amplitude at resonance
x_{00} = amplitude in vacuum
F_0 = force at resonance
F_{00} = force required to maintain x_{00}
A = area of the surface in contact with the fluid
R_0 = transducer loss in the vacuum

Thus by measuring the force F_0 which is required to maintain a constant amplitude x_0, and knowing the density ρ of the fluid one can measure the viscosity η. The remainder of the terms in Equation 13 will be constants for a particular instrument.

Discussion of the Vibrating Viscometers

Some of the advantages of vibrating viscometers over rotational and capillary viscometers are.

- Since the gap of fluid between the sensor and the container wall does not affect the reading, suspensions with coarse particles can be tested without the danger of plugging
- Unlike rotational viscometers, oscillating viscometers are not affected by minor turbulences associated with slurry flow. Therefore, forces associated with slurry flow (see Figure 4) will not affect its readings.

The major disadvantage of this type of instrument is that the operator does not have any control over the shear rate. It is also difficult to measure the true viscosity of non-Newtonian fluid whose viscosity changes with shear rate. The shear rate γ will be a sinusoidal function of time. For a spherical probe, its peak value will be maximum at the equator and will be smaller by a factor cos ϕ at a sphere latitude of ϕ. Perry[34] derived the following equation for determining the maximum shear rate for the vibrating sphere viscometers:

$$\dot{\gamma} = k(\rho/\eta)^{1/2} \qquad (12)$$

where, $\dot{\gamma}$ = maximum shear are
k = an instrument constant

From this equation we see that the maximum shear rate decreases as viscosity of the fluid increases. For a Newtonian fluid viscosity η is a constant, so maximum shear rate will remain constant. However, for viscoelastic fluids, the viscosity varies with shear rate, and computation of shear rate becomes complicated. Some investigators have suggested measuring the amplitude of vibration[33] and oscillating frequency as a means of measuring the apparent viscosity of viscoelastic fluids (non-Newtonian fluids)[35]. However, the reasoning provided for such measurements apply only to limited polymeric fluids, and the method does not work for suspensions[33,34].

Vibrating viscometers are sensitive to vibrations from supporting structures32,35. Unless precautions are taken to dampen these vibrations the instrument will pick up erroneous signals.

Selected Designs of Vibrating Viscometers

Vibrating rod viscometer for viscosity measurement Rachman[33] reported an assessment of vibrating viscometers in slurries. He utilized a vibrating plate transducer and a flexurally vibrating rod transducer in his research. However, for the suspension studies (with quartz slurries) only the flexurally vibrating rod transducer was used. In his initial experiment with 0.065 volume fraction solids in the slurry, Rachman experienced difficulty in measuring the viscosity because the solids settled quickly. In subsequent tests, the slurry was stirred vigorously by a motor driven pump to keep the solids in suspension. Then the stirrer was stopped and after 15 seconds, measurements were taken with the viscometer. In this way the investigator assumed that the slurry would have been in a similar state when each reading was taken. Similar measurements were taken with quartz-water slurries at 0.24 and 0.36 volume fraction solids. By changing the amplitude of vibration and transducer loading they showed that the denser slurries showed non-Newtonian flow whereas the dilute slurry with 0.065 volume fraction solids had Newtonian flow. However because of uncertain results, Rachman suggested use of this method only if no other simpler viscometer is obtained for measuring non-Newtonian slurry rheology.

Vibrating sphere viscometer for viscosity measurement Kawatra *et al.*[32] used a vibrating sphere viscometer manufactured by Nametre Co. along with a gravity flow sample presentation vessel as shown in Figure 15. Because of the basic design of the spherical oscillating probe (which oscillates at a high frequency and low amplitude rather than rotate in a single direction) and its durable construction, the flow of the slurry did not influence its reading. The solids settling problem was also eliminated because of the gravity flow arrangement of the slurry around the probe. Using this system Kawatra *et al.* were able to continuously measure viscosity of silica slurry at varying concentrations and temperatures in the feed line of a hydrocyclone.

However, the major difficulty in this type of instrument is that the operator has no control over the shear rate. The shear rate is a function of viscosity, higher in low viscosity fluids and lower in high viscosity fluids. Since most of the suspensions at higher solids contents show non-Newtonian flow their viscosity is highly dependent on shear rate. Thus for such suspensions, no logical conclusion can be drawn from viscosity measurements by these instruments unless they operate at the same shear rate as the process itself. Another problem with this type of instrument is that if the fluid velocity is very low, solids tend to settle in small layers over the top of the sphere (Figure 16)

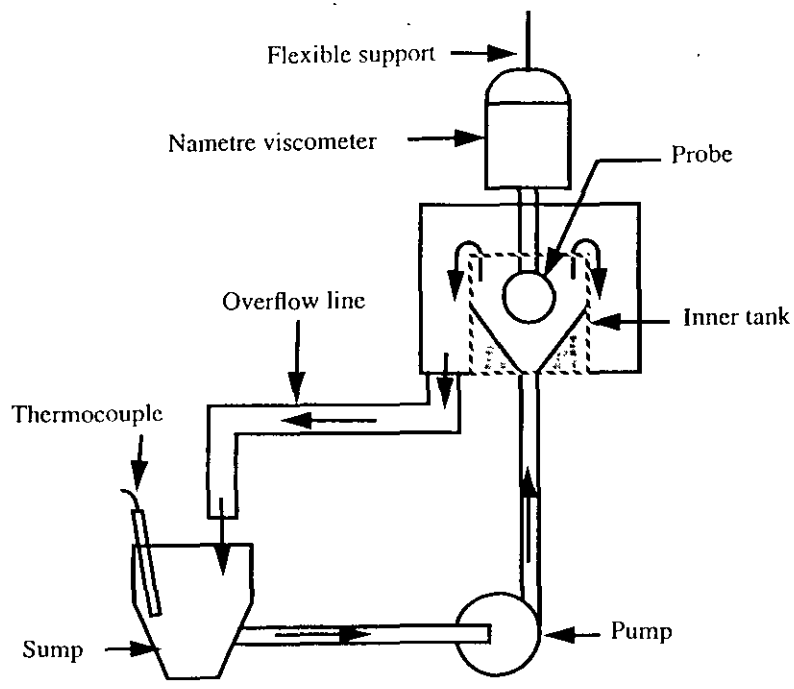

FIGURE 15 Nametre viscometer set-up Sample is circulated through the system by a pump to keep the solids in suspension

resulting in higher readings. These instruments are also affected by vibration from their surroundings, and special design is required to isolate from vibration. However, due to their ability to work in hostile plant environment, so far they are the most suitable instrument for making on-line viscosity measurements of Newtonian mineral slurries. The slurry used by Kawatra *et al.*[12] was Newtonian and therefore, good correlation could be established between the viscosity measured by this instrument and the hydrocyclone performance.

Vibrating sphere viscometer for distinguishing Newtonian and non-Newtonian suspensions Recently Kawatra and Bakshi[16] reported a system for classifying Newtonian and non-Newtonian suspensions in slurry streams. They used a vibrating sphere viscometer to measure apparent viscosity of slurries at high shear rates and a rotational viscometer to measure apparent viscosity of the same slurry at low shear rates. Since the shear rates were widely different, comparison of the apparent viscosities from the vibrating viscometer and the rotational viscometer allowed classification of the suspensions as either Newtonian or non-Newtonian flow types.

Summary The main advantages of vibrating viscometers over rotational and capillary

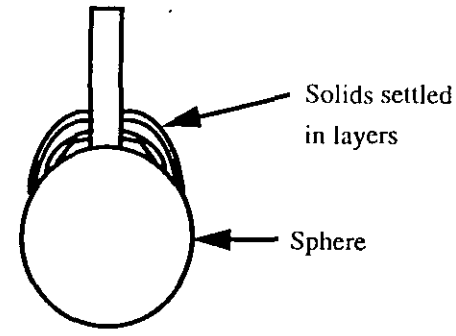

FIGURE 16 Vibrating sphere viscometer showing layers of solids settling on top of the sphere when the fluid velocity passing the spherical probe is small

viscometers are, (i) these are less sensitive to plant disturbances, (ii) plugging is less of a problem, because these are surface loading instruments and the gap between the sensor and the container wall can be kept as large as required.

Vibrating viscometers still require some sort of agitation system to avoid solids settling. Since these viscometers are highly sensitive to vibrations from surrounding structures, steps must be taken to damp these vibrations. The main disadvantage of these instruments is their poorly defined shear rates which makes them highly unsuitable for measuring true viscosity of non-Newtonian suspensions.

CONCLUSIONS

Rotational and capillary viscometers are the most common viscometers which have been tried for measuring suspension rheology Rotational viscometers have better control over shear rate which is essential for measuring the full rheology of non-Newtonian fluids. However, these instruments are very sensitive to disturbances in slurry flow. Because of this, many of the special designs studied in this report had baffle arrangements to inhibit unwanted forces like swirling and turbulence in the region of the measuring device. In capillary rheometers this problem is felt to a lesser extent because of the shorter residence time of the suspension inside the tube. However, the sample must be thoroughly mixed prior to its entry into the tube. Plugging is more of a problem in capillary tubes than in rotational viscometers. Slip at the walls is another problem felt by both the capillary and the rotational viscometers In vibrating viscometers both plugging and wall slip can be eliminated easily, because vibrating viscometers are surface loading and the gap between the sensor and the container wall does not affect the measurement. Also, the vibrating viscometer can tolerate slight disturbance from slurry flow and is rugged enough for on-line use in suspensions The main disadvantage of a vibrating viscometer is its inability to operate in a steady shear, which makes it unsuitable for non-Newtonian fluids Otherwise, for Newtonian suspensions and for operations where a relative viscosity is needed vibrating viscometers are best suited for on-line use

Although in the past many authors have claimed success in measuring on-line

rheology of suspensions, their claims have been refuted later by other authors, because the instruments were not capable of repeating their performance. This shows that the particulate processing industry still needs a reliable viscometer which can work on-line under plant conditions.

References

1. R. Lu and V. M. Puri, *J. Rheol.*, **36**(2), 303 (1992).
2. M. K. Agarwala, B. R. Patterson and P. E. Clark, *J. Rheol.*, **36**(2), 319 (1992).
3. D. W. Fuerstenau, K. S. Venkataramana, B. V. Velamakanni, *Inter. J. of Miner. Process.*, **15**, 251 (1984).
4. R. R. Klimpel, Part I, *Mining Engineering*, **34**(12), 1665 (1982), Part II, *Mining Engineering*, **35**(1), 21 (1983).
5. P. Tucker, *Trans. of Instn. Min. Metall.*, Section C, Mineral Processing and Extractive Metallurgy, **91**, C117 (1982).
6. S. K. Kawatra, T. C. Eisele, Proceedings of the Sixteenth International Mineral Processing Congress, Elsevier Science Publishers B. V., *Amsterdam*, 1988, pp. 195–207.
7. F. F. Aplan and H. R. Spedden, Seventh International Mineral Congress, New York (Ed.) N. Arbiter, Gordon and Breach, New York, 1965, pp. 103–113.
8. R. B. Klose, Proceedings of the Sixth International Symposium on Coal Combustion and Technology, June 25–27, Orlando, Florida, 1984, pp. 791–805.
9. S. C. Tsai and E. W. Knell, FUEL, **65**, 566 (1986).
10. F. D. DeVaney, S. M. Shelton, Rep. Invest. U. S. Bur. *Mines*, **3469R**, 24 (1940).
11. B. Klien, S. J. Partrigdge, J. S. Laskowski, *Coal Preparation*, **8**, 123 (1990).
12. T. Kiljanski, *Coal Preparation*, **13**, 107 (1993).
13. T. J. Reeves, *Coal Preparation*, **8**, 135 (1990).
14. J. Orban and P. Pacevaux, *Oil and Gas Journal*, **84**(26), 94 (1986).
15. R. W. Whorlow, Rheological Techniques, Chapter 2 and 3, Halsted Press, New York, 1980, pp. 57–191.
16. B. Clarke, *Trans. Inst. Chem. Engrs.*, **45**, T251 (1967).
17. R. Lapasin, *Coal Preparation*, **5**, 167 (1988).
18. W. M. Underwood, *Rev. Sci. Instrum.*, **47**(9), 1079 (1976).
19. C. E. Hemmings and J. M. Boyes, Twelfth International Mineral Processing Congress, Sao Paulo, 1977, pp. 46–64.
20. T. J. Reeves, *Trans. Instn. Min. Metall.*, Section C, Mineral Processing and Extractive Metallurgy, **94**, C201 (1985).
21. E. I. Shaheen and D. C. Bogue, Rheological Study of Viscosities and Pipeline Flow of Concentrated Slurries, Selected Papers, Part I, No. 58d, Sixty-Second Annual Meeting, AIChE, Washington, D.C., 1969, pp. 1–47.
22. S. C. Tsai and E. W. Knell, *FUEL*, **65**, 566 (1986).
23. A. B. Metzner and J. C. Reed, *AIChE Journal*, **1**(4), 434 (1955).
24. B. Rabinowitsch, *Physik. Chem.*, **1415A**, 1 (1929).
25. R. B. Bird, W. E. Stewart and E. N. Lightfoot, Transport Phenomena, Chapter 1 and 2, John Wiley & Sons Publication, Wiley International Edition, Singapore, 1960, pp. 3–70.
26. C. H. Schack, K. C. Dean and S. M. Molloy, Report of Investigations **5334**, U. S. Bureau of Mines, 1957, pp. 1–16.
27. R. J. Mannheimer, J. T. Park, T. A. Grimley and T. B. Morrow, Fluids Engineering (Eds.) John Hyun Kim, Jae Min Hyun, Chung-Oh Lee, Hemisphere Pub. Corp., New York, 1991, pp. 513–535.
28. G. Antonini, O. Francois, P. Gislais and A. Touret, Proceedings of the Sixth International Symposium on Coal Combustion and Technology, June 25–27, Orlando, Florida, 1984, pp. 266–281.
29. R. M. Turian, F. Hsu, K. S. Avramidis, D. Sung and R. K. Allerndorfer, *AIChE Journal*, **38**(7), 969 (1992).
30. K. S. Avramidis and R. M. Turian, *Journal of Colloidal Interf. Science*, **143**(1), 54 (1991).
31. E. E. Cone, E/MJ, **169**(120), 82 (1968).
32. S. K. Kawatra, T. C. Eisele and M. T. Rusesky, Chapter 6, Comminution-Theory and Practice (Ed.) S. K. Kawatra, Society of Mining, Metallurgy, and Exploration, Littleton, 1992, pp. 529–545.
33. Y. A. Rachman, An Assessment of Vibrating Viscometers in Slurries, Report No. 2001, National Institute for Metallurgy, Private Bag X3015, Randburg, 2125 South Africa, 1979, pp. 1–20.
34. J. D. Perry, *Measurement and Control*, **143**(89), 89 (1977).
35. J. V. Fitzerald, F. J. Matusik and T. M. Walsh, *Measurement and Control*, December (1987).
36. S. K. Kawatra and A. K. Bakshi, *Coal Preparation*, **24**, 123 (1995).
37. M. Mooney, *J. Rheol.*, **2**(2), 210 (1931).
38. S. K. Kawatra, S. A. Moffat and K. A. DeLa'O, The effects of Freezing Conditions on Rock Breakage, Society of Mining, Metallurgy, and Exploration, Inc., Preprint Number 93–17, 1993.
39. K. J. Shoop and S. K. Kawatra, Effect of Rock Breakage Characteristics and Fines/Clay Content on the Autogenous Grinding of Iron Ore, Society of Mining, Metallurgy, and Exploration, Inc., Preprint Number 93–17, 1995.
40. A. K. Bakshi, K. J. Shoop and S. K. Kawatra, Changes in Autogenous Grinding and Classification Performance due to Variation in Slurry Rheology, paper to be presented at the Society of Mining, Metallurgy, and Exploration, Inc. annual meeting 1996

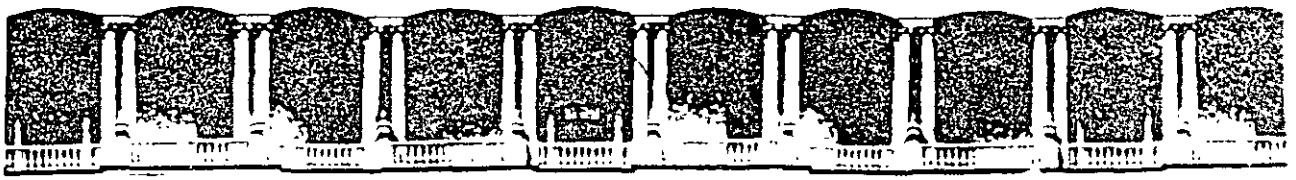

FACULTAD DE INGENIERIA U.N.A.M.
DIVISION DE EDUCACION CONTINUA

CURSOS ABIERTOS

DESARROLLO Y OPERACIÓN DE SENSORES PARA CONTROL DIRECTO Y CONTINUO EN PLANTAS DE BENEFICIO DE MINERALES Y EN LA RESTAURACIÓN DEL MEDIO AMBIENTE

Del 18 al 23 de mayo de 1998

TEMA: RECOVERY OF PYRITE IN COAL FLOTATION: ENTRAINMENT OR HYDROPHOBICITY

EXPOSITOR :DR. KOMAR KAWATRA

1998

Recovery of pyrite in coal flotation: Entrainment or hydrophobicity?

S.K. Kawatra and T.C. Eisele

Abstract — *Under normal conditions, a significant amount of pyrite is recovered in the froth during flotation of high-sulfur coal. To reduce this pyrite recovery, it is first necessary to determine the primary recovery mechanism, because different measures are required for reducing entrainment, locked-particle flotation or true hydrophobic flotation. In this paper, evidence is presented that suggests that hydrophobic flotation is not the major mechanism for recovery of liberated pyrite; instead, the bulk of the recovered pyrite results either from simple entrainment or from being physically locked with floatable coal particles.*

Introduction

In many coal flotation operations, a significant amount of apparently liberated pyrite is seen to report to the froth, thereby raising the inorganic sulfur content of the clean product and reducing its economic value. Obviously, a method of preventing this unwanted recovery of pyrite is desirable. The best means for preventing liberated coal pyrite recovery will be primarily controlled by the recovery mechanism for these particles; therefore, this recovery mechanism should be determined before selecting a particular method for removing or suppressing pyrite.

In general, there are two ways for a liberated particle to enter the froth phase:

- particle entrainment, and/or
- bubble attachment.

The separation of these two effects in a real experiment is very difficult due to the presence of locked particles. Coal pyrite does not have the same properties as pure mineral pyrite (Chernosky and Lyon, 1972), and it is not practical to produce coal pyrite that is completely free of locked coal particles. Therefore, experiments to demonstrate conclusively whether pyrite from a given coal does or does not float by hydrophobic bubble attachment are impractical. The best that can be done is to estimate the relative probable quantity of liberated pyrite that can be accounted for by the two mechanisms.

For this paper, a conventional flotation machine was used to compare the floatability of three different mineral pyrites and two coal pyrites, using only non-polar oil as a collector. Experiments were also carried out to attempt to measure the floatability of liberated pyrite in coal using a conventional flotation cell.

Theoretical discussion

It has long been known that mineral pyrite has some hydrophobic tendency. However, this tendency is normally very slight, and significant flotation of pyrite requires addition of a collector of some type. The natural floatability of pyrite is also strongly pH dependent, with the highest floatability in acidic solutions. Depression of mineral pyrite is quite easy, with a variety of highly effective depressants being available. In most selective sulfide mineral flotation circuits, the bulk of the floated pyrite results from entrainment and locking to hydrophobic particles (*Mineral Processing Handbook*, 1985).

While the responses of mineral pyrite in flotation are fairly well known, the behavior of coal pyrite is poorly understood (Chernosky and Lyon, 1972), because of its formation and long residence in the presence of a variety of organic compounds. It is often reported that coal pyrite exhibits surface chemistry radically different from that of mineral pyrite. Some investigators also claim that experiments with coal pyrite from a specific source may not be particularly relevant to coal pyrites from other sources, due to the heterogeneity of coal.

Many investigators have, with some success, attempted to use various chemicals as depressants for coal pyrite to reduce the sulfur content of the product (Purcell, 1982; Hirt, 1973). However, in most reported experiments, it has been unclear whether the decrease in pyrite flotation was due to reduced pyrite hydrophobicity or to improved froth drainage, because the quantity of entrained water in the froth is often not measured. Also, since pyrite depressants reduce the floatability of coal slightly, it is reasonable to expect that fewer locked particles will float in the presence of these reagents. Thus, the quantity of pyrite floating by this means is reduced as well.

Determination of the quantity of entrained material is difficult, particularly when a small number of experiments are conducted, because the water recovery in the froth must be determined and correlated with the recovery of the entrained species. Since entrainment is, in theory, linearly related to water recovery, the entrainment constant can be determined by linear regression when the data set available is sufficiently large. If the particles are sufficiently fine, then their weight percent recovery by entrainment will be equal to the weight percent recovery of water. The floated material that is not accounted for by the regression line is then assumed to be floating either by hydrophobic bubble attachment or as part of locked particles. Since the entrainment constant varies with particle size, any changes in this variable for the entrained species will tend to significantly change the results (Lynch, et al., 1981).

Experimental procedures and results

To determine whether the pyrite in a particular Pittsburgh seam coal was floating by locking/entrainment or by true flotation, two sets of experiments were conducted. These experiments provided data for conditions in which pure mineral pyrite flotation could be expected with only #2 fuel oil as a collector, the extent to which coal pyrite flotation occurs during normal flotation of coal, and the quantity of water entrained in the froth.

Pure pyrite flotation

Relatively pure pyrite was obtained from five sources:

S.K. Kawatra and **T.C. Eisele**, members SME, are professor and graduate student, respectively, Department of Metallurgical and Materials Engineering, Michigan Technological University, Houghton, MI.
SME preprint 91-89, SME Annual Meeting, Feb. 25-28, 1991, Denver, CO. M&MP paper 91-624. Manuscript Nov. 19, 1990. Discussion of this paper must be submitted, in duplicate, prior to Aug. 31, 1992

Table 1 — Size distributions for the samples used in the pyrite flotation experiments, determined by Microtrac particle size analyzer.

Size, μm	Cumulative % passing, mineral pyrite samples	Cumulative % passing, coal pyrite samples
62	100.0	100.0
44	97.4	100.0
31	88.3	97.3
22	73.5	89.6
16	56.5	75.8
11	42.2	59.6
7.8	31.7	45.2
5.5	23.0	32.7
3.9	16.1	22.1
2.8	10.0	13.1
1.9	4.3	5.4
1.4	1.8	2.2
0.9	0.3	0.4

two lots of mineral pyrite from Custer, SD and one lot from Rico, CO (all three lots obtained from Ward's Natural Science Establishment) and coal pyrites collected as large nodules from Panther Valley, PA and Empire Coal, OH. Using a steel rod mill, the pyrite was ground to the size distribution given in Table 1, at 60% solids and a pH adjusted to 12 with NaOH. The pH adjustment was necessary to prevent corrosion and subsequent dissolution of iron, which is reported to be a pyrite depressant (Miller and Baker, 1972). The pyrite was then filtered, divided into charges of the desired weight, repulped in a Denver laboratory flotation cell (volume of 1.9 L), and pH adjusted to the desired level with sulfuric acid.

Finally, MIBC (0.3 kg/t) and the noted quantities of #2 fuel oil were added as frother and collector, respectively. The pulp was then conditioned for two minutes and floated for five minutes, with the froth removed manually. The results of these experiments are given in Table 2, along with results from two control runs using pure silica that had been prepared in the same manner as the pyrite. The pH values were selected on the basis of earlier tests, which showed that mineral pyrite floats well below pH 4 and poorly at higher pH values.

The pyrites strongly appeared to buffer the pH at pH 4, consuming approximately 3 g sulfuric acid per kg of pyrite to reduce pH below this level. Upon lowering the pH below 4, the pyrite became strongly floatable, simultaneously releasing a strong odor of H_2S. Additional experiments were conducted with the first lot of Custer pyrite as shown in Table 3, after it had aged at -15° C for over a year. After aging, this pyrite was floatable at neutral pH, showing that the flotation properties of pyrites can vary widely depending on their past oxidation history. When the aged pyrite was oxidized at 100° C for 44 days, the neutral-pH floatability was lost. These changes in hydrophobicity are likely due to the formation of a species such as elemental sulfur on the pyrite surface when the oxidation conditions are favorable. Since elemental sulfur is naturally hydrophobic, it will act as a pyrite collector when it forms.

Unlike the two mineral pyrites, the Panther Valley coal pyrite never became strongly floatable and never released the characteristic H_2S odor. The froth product from the coal pyrite appeared, from qualitative examination at 40x magnification of the loose powder, to be predominantly composed of locked coal-pyrite particles, floating as a result of the hydrophobicity of the coal portion.

Table 2 — Conditions and results for pure pyrite experiments.

Test	Pyrite	Charge wt., g	#2 fuel oil,kg/t	pH	% Floats
1	Rico, CO	150	3.0	2.1	98.62
2	Rico, CO	150	3.0	5.0	9.56
3	Rico, CO	150	0.0	8.4	3.9
4	Rico, CO	150	0.0	2.1	14.2
5	Silica	150	3.0	5.3	13.6
6	Silica	150	3.0	5.3	15.3
7	Custer, SD	150	3.0	7.5	3.34
8	Custer, SD	150	3.0	7.5	4.34
9	Custer, SD	150	3.0	8.3	4.65
10	Custer, SD	150	3.0	2.0	98.57
11	Custer, SD	150	3.0	2.3	98.01
12	Custer, SD	150	3.0	2.2	97.57
13	Panther Valley	150	3.0	8.8	31.64
14	Panther Valley	150	3.0	3.5	36.47
15	Panther Valley	150	3.0	2.2	43.00
16	Panther Valley	150	3.0	2.0	35.22
17	Empire	150	0.0	5.1	15.6
18	Empire	150	3.0	12.3	20.6
19	Empire	150	3.0	10.4	36.8
20	Empire	150	3.0	8.2	40.0
21	Empire	150	3.0	6.2	40.8
22	Empire	150	3.0	5.3	44.8
23	Empire	150	3.0	4.7	52.7
24	Empire	150	3.0	2.6	56.7
25	Custer Lot #2	150	0.0	9.8	7.6
26	Custer Lot #2	150	0.6	6.8	10.0
27	Custer Lot #2	150	3.0	11.7	20.7
28	Custer Lot #2	150	3.0	9.7	11.4
29	Custer Lot #2	150	3.0	5.7	14.9
30	Custer Lot #2	150	3 0	2.3	68.3
31	Custer Lot #2	150	3.0	1.8	69.7

The Custer and Rico pyrites are mineral pyrites and the Panther Valley and Empire pyrites are from coal. The Rico and the first lot of Custer pyrite were nearly pure, while the second lot of Custer pyrite contained 30% silicates and carbonates. The mineral pyrites show a strong pH dependence and do not float well at near-neutral pH. The coal pyrites are hypothesized to be much less pH sensitive because their floatability is largely due to locked coal particles.

Table 3 — Results of floating the first lot of Custer pyrite after aging at -50° C for over one year and after oxidizing at 100° C for 44 days.

Treatment	pH	% Floats
Aged at – 15° C	9.0	46
Aged at – 15° C	6.8	37
Aged at – 15° C	6.0	35
Aged at – 15° C	1.9	92
Oxidized at 100° C	6.2	7
Oxidized at 100° C	2.0	82

Additional experiments were attempted using coal pyrite from a second source, the Empire Coal mine, Gnadenhutten, Ohio. However, it was found that even when apparently pure pyrite nodules were collected and cleaned by hand, the pyrite still contained a residue (27% by wt.), composed predominantly of coal and clay, which was insoluble in nitric acid.

Table 4 — Size distribution of Pittsburgh seam coal used in the coal flotation experiments, produced by grinding 900-g charges of coal at 40% solids in a steel rod mill for 45 mins. Size distribution was measured using a Microtrac particle size analyzer.

Size, μm	Cumulative % Passing
88	100.0
62	96.0
44	87.5
31	74.7
22	61.7
16	49.2
11	37.6
7.8	28.4
5.5	20.3
3.9	13.7
2.8	8.1
1.9	3.1
1.4	1.1
0.9	0.0

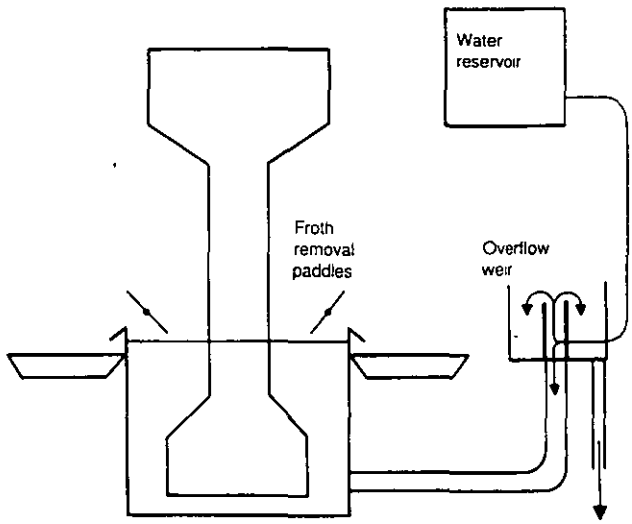

Fig. 1 — Schematic diagram of flotation cell with automatic pulp level control.

Therefore, it was impossible to conduct the desired experiments using coal pyrite that had been isolated from the associated organic inclusions, and the results obtained were similar to those for the Panther Valley coal for this reason.

Pittsburgh coal conventional flotation

For experiments, this coal was ground in a steel rod mill to the size distribution given in Table 4. The freshly ground coal was then divided into 250-g charges for flotation, which were stored at -20° C to retard oxidation. Timed flotation experiments were conducted in a 4-liter flotation cell, with gravity-feed pulp level control and mechanical froth scrapers (Fig. 1), under the conditions given in Table 5. The frother was Dowfroth 200, added at a rate of 0.03 g/L (0.5 kg/t). Froth was collected over the time intervals 0-30 sec, 30 sec-1 min., 1 min.-2 min., 2 min.-3 min., 3 min.-5 min. and 5 min.-9 min. The products were weighed, filtered, dried, and reweighed. All products were analyzed for ash content, and total sulfur content was determined using a LECO SC-132 sulfur determinator. The results for all six tests are given in Table 5.

Table 5 — Results from timed flotation experiments using a constant-level conventional flotation cell. The measured heads were determined from incremental samples taken from the feeds for the three tests preceding each. The % Pyritic Sulfur was determined by the ASTM nitric-acid-leach method.

Product	% Wt	% Ash	% S	% Py. S	% Solids
pH = 7.6 Collector Dosage (fuel oil) = 0.0 kg/t					
Test 1 — 30 sec Froth	31.24	11.1	2.14	0.9	15.14
1 min.	26.60	13.2	2.59	1.6	16.04
2 min.	8.83	26.8	3.64	2.5	8.88
3 min.	4.83	61.1	5.17	4.4	2.41
5 min.	5.70	82.5	5.08	4.5	1.15
9 min.	6.73	88.1	4.22	3.7	0.70
Final tails	16.07	88.2	4.55	4.2	
pH = 7.7 Collector = 0.0 kg/t					
Test 2 — 30 sec Froth	44.37	12.7	2.37	1.1	15.70
1 min.	18 19	17.5	2.86	1.7	13.73
2 min.	8.47	42.5	4.33	3.3	4.01
3 min.	3.88	79.5	5.27	4.7	1.37
5 min.	4.70	87.4	4.56	4.0	0.90
9 min.	4.66	89.0	3.91	3.7	0.59
Final tails	15.72	84.2	4.54	4.2	
pH = 7.7 Collector = 0.0 kg/t					
Test 3 — 30 sec Froth	43.82	12.4	2.26	1.1	16.00
1 min.	19.00	17.1	2.69	1.7	13.90
2 min.	8.73	43.3	3.81	3.3	3.95
3 min.	3.91	79.1	4.67	4.6	1.33
5 min.	4.90	86.3	4.06	4.0	0.90
9 min.	6.01	88.6	3.49	3.4	0.56
Final tails	13.63	87.0	3.98	4.0	
Measured head		37.2	2.90		
pH = 7.5 Collector = 0.18 kg/t					
Test 4 — 30 sec Froth	23.1	10.3	1.85	0.8	16.21
1 min.	14.3	9.4	1.89	0.9	19.41
2 min.	19.9	12.9	2.39	1.5	21.83
3 min.	9.8	35.3	3.94	3.3	6.08
5 min.	7.7	73.9	4.51	4.4	1.46
9 min.	6.6	86.7	3.76	3.7	0.77
Final tails	18.4	85.6	3.86	3.8	
pH = 7.5 Collector = 0.35 kg/t					
Test 5 — 30 sec Froth	55.4	14.0	2.24	2.3	14.73
1 min.	10.9	27.1	3.13	2.3	7.78
2 min.	7.2	58.2	4.20	3.7	2.09
3 min.	4.1	72.3	3.84	3.7	1.16
5 min.	4.9	84.2	3.63	3.7	0.73
9 min.	5.2	87.5	3.30	3.3	0.47
Final tails	12.3	84.4	4.10	4.1	
pH = 7.6 Collector = 0.70 kg/t					
Test 6 — 30 sec Froth	56.0	15.0	2.33	1.4	14.50
1 min.	8.9	33.0	3.51	2.8	5.96
2 min.	6.9	63.2	4.10	3.7	1.77
3 min.	5.4	64.4	3.48	3.3	1.26
5 min.	5.6	77.4	3.36	3.4	0.73
9 min.	5.5	81.4	3.19	3.2	0.43
Final tails	11.7	75.7	4.02	4.0	
Measured head (tests 4 - 6)		37.3	2.99		

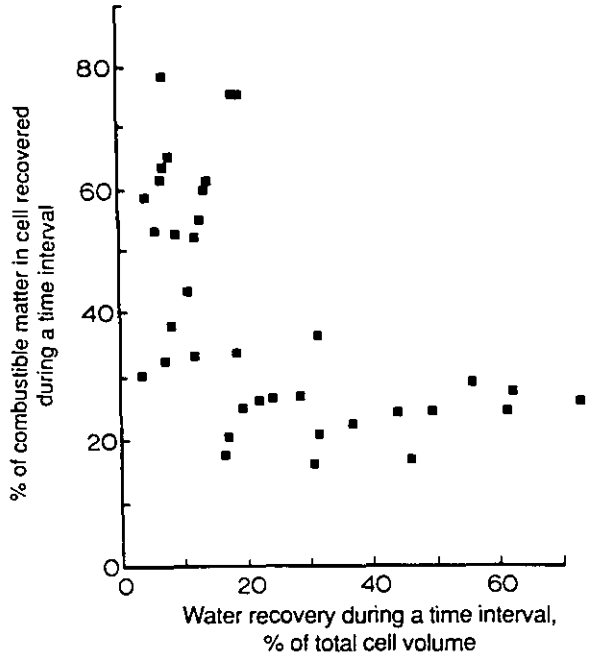

Fig. 2 — Comparison of ash-free combustible matter recovery with water recovery during timed, constant-level, conventional flotation experiments. These points were determined by first calculating how much combustible matter was present in the cell and calculating the percentage recovered in the first time interval. The amount remaining in the cell was then calculated, and the percentage of the remaining material recovered during the next time interval was determined. This was repeated for each subsequent time interval.

Discussion

The results from the pyrite flotation experiments show very clearly that pure mineral pyrite loses its natural floatability nearly completely when the pH exceeds 5.0. At near-neutral pH, its floatability is comparable to the floatability of silica, which is known to be hydrophilic. This indicates that, under normal conditions for coal flotation (pH 5-9), unmodified mineral pyrite is not noticeably recovered by true hydrophobic flotation. Even large dosages of neutral oil collectors (up to 3 kg collector/t pyrite) do not render mineral pyrite floatable over this pH range. This has been found true for pyrites from two distinct sources and is likely to be generally true for all pyrites not associated with organic matter. Therefore, true hydrophobic flotation of coal pyrite should only be expected when the pyrite has been heavily modified by organic material or when flotation is carried out under acid conditions.

Although prepared identically to the mineral pyrites, the coal pyrite did not exhibit similar behavior. It maintained essentially constant levels of flotation recovery (31%-43%) over the pH range from 2.2 to 8.8. Conversely, the mineral pyrite dropped from nearly 99% recovery to, in some cases, less than 4% over the same pH range.

Qualitative microscopic examination of the coal pyrite flotation product indicated that much of the floating material was coal and locked coal-pyrite particles. Therefore, in this case, it is hypothesized that the coal pyrite is floating due to attachment to coal. This hypothesis is supported by recent work by Chander and Aplan (1989), where they claim to have isolated liberated pyrite from seven coal sources for a variety of detailed analyses. Using a microflotation cell aerated with nitrogen gas, all of the purified pyrites were found to show very little inherent floatability (average = 1.9% wt. floating; range = 0-7% wt.). The procedure that Chander and Aplan describe for purifying the pyrites does provide opportunity for the pyrite to oxidize somewhat, which may conceivably destroy its inherent floatability. Nevertheless,

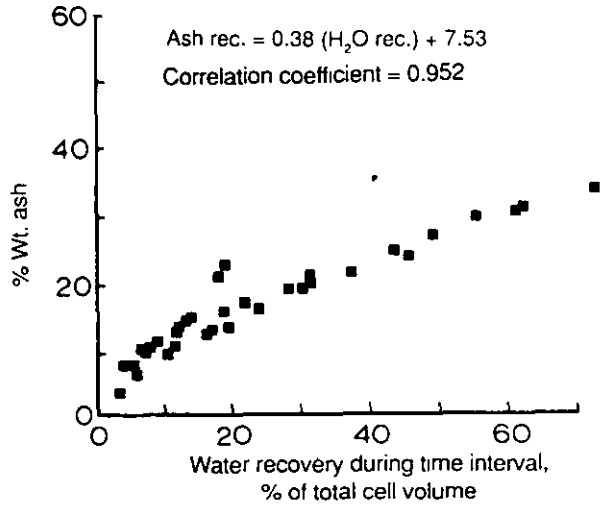

Fig. 3 — Correlation of ash recovery with water recovery in timed conventional flotation experiments.

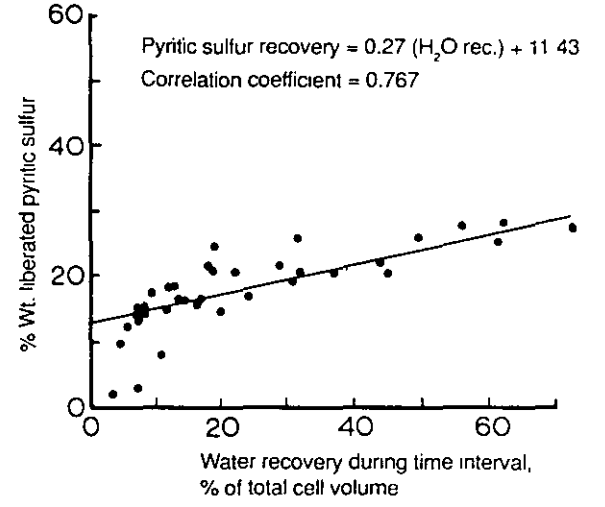

Fig. 4 — Correlation of liberated pyritic sulfur recovery with water recovery in timed conventional flotation experiments.

it appears likely that coal pyrites have a very low inherent floatability and are, therefore, floated primarily as either locked or entrained particles.

Unfortunately, there does not appear to be any available method for conclusively measuring the relative quantities of locked and liberated pyrite particles in coal flotation; nor is there a rapid, effective method for isolating coal-free pyrite from coal which does not also either contaminate or oxidize the pyrite surfaces. Therefore, it is presently impossible to prove that coal pyrite either does or does not enter the froth as a result of true hydrophobic attachment. Based on the behavior of the pure mineral pyrite samples, it is hypothesized that coal pyrite is recovered in the froth by entrainment and by mechanical attachment to floatable coal particles. However, due to the fine scale of the organic contaminants in coal pyrite, mineral pyrite is clearly not a good model for the behavior of coal pyrite and should not be treated as such.

An approximate estimation of whether coal, mineral and pyrite particles are being recovered by true flotation, locking or entrainment can be achieved by correlating the recovery of a given component with the recovery of water in the froth. This correlation is shown in Figs. 2, 3 and 4 for ash, liberated pyritic sulfur and ash-free coal for the Pittsburgh seam coal sample.

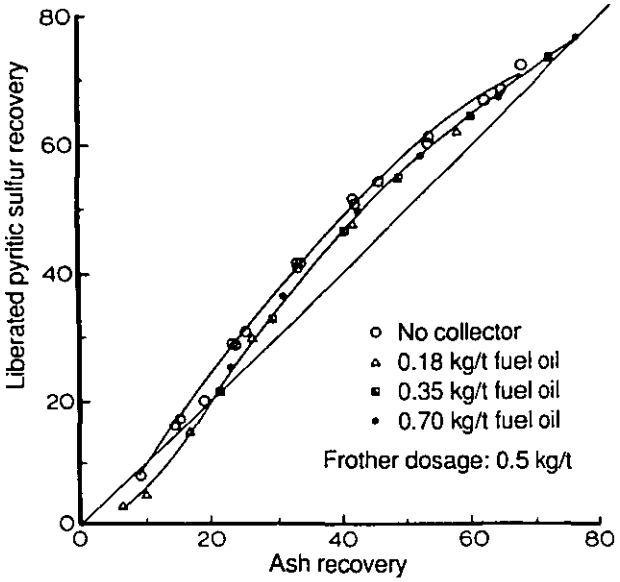

Fig. 5 — Correlation of liberated pyritic sulfur recovery with ash recovery in timed flotation tests. The ash is well-liberated fine clay, which is known to be hydrophilic and will, therefore, be recovered mainly by entrainment. Since the liberated pyrite recovery tracks the ash recovery very closely, it is being recovered by the same mechanism.

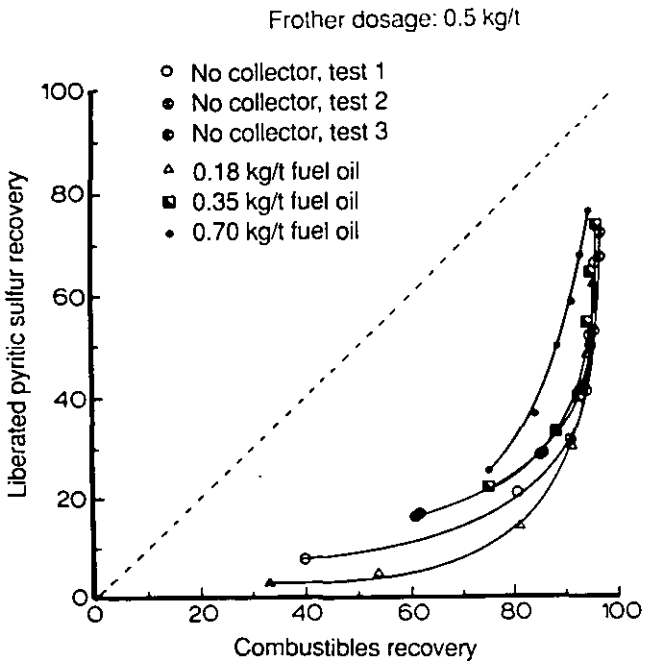

Fig. 6 — Correlation of liberated pyritic sulfur recovery with combustible matter recovery in timed flotation tests

Liberated pyritic sulfur (S_{LP}) was obtained from the formula $\%S_{LP} = \%S - 1.7(\%\text{wt. ash-free coal})$, where 1.7% sulfur is the lowest sulfur content obtained for this coal by flotation.

While Fig. 2 shows that ash-free coal recovery does not correlate with water recovery, Figs. 3 and 4 demonstrate that ash and liberated sulfur correlate linearly with the water recovery, with correlation coefficients of 0.952 and 0.767, respectively. It is immediately seen that the correlation of liberated pyrite and water recoveries are unaffected by the collector dosage over the range studied, which confirms that the liberated pyrite is being recovered by entrainment and not true flotation.

This is further borne out by the correlations of liberated pyrite recovery with ash (Fig. 5) and ash-free coal (Fig. 6) recoveries. The behavior of the liberated pyrite is nearly indistinguishable from that of the strongly hydrophilic ash (predominantly clay slimes known to float by entrainment), but it is wildly variant from the behavior of the ash-free coal. Since the relationship of pyrite recovery to ash recovery is virtually unaffected by fuel oil dosage, the most reasonable assumption is that the liberated pyrite is floating by entrainment and has no particular hydrophobic character (Kawatra and Eisele, 1988). Furthermore, if any liberated pyrite is floating by true hydrophobic flotation, increasing the fuel oil dosage does not increase the quantity of pyrite that floats in this fashion.

Conclusions

From the results presented, the following conclusions may be drawn:

- Some investigators have claimed that pyrite depressants sometimes work and sometimes do not. In the authors' opinion, it is most important to determine whether pyrite is being recovered by entrainment or hydrophobic flotation before attempting to use depressants.
- Mineral pyrite is readily floatable by fuel oil alone at acid pH (<4), but this native floatability is entirely lost at the usually higher pH levels occurring during coal flotation.
- Determination of the floatability of coal pyrite in the absence of coal particles is not practical, due to the intimate intermixing of carbonaceous and pyritic components even in pyrite nodules that appear, visually, to be relatively pure. As a result, pyrite that floats by true, hydrophobic bubble attachment cannot be readily distinguished from that which floats due to mechanical attachment to coal particles. It can be hypothesized that completely liberated coal-pyrite particles behave similarly to mineral pyrite and are, therefore, not recovered by flotation at near-neutral pH. However, this hypothesis is very difficult to prove.
- The results of timed flotation of a Pittsburgh seam coal using conventional flotation are consistent. The pyrite is being recovered in the froth predominantly by entrainment and locked particles, with any contribution from hydrophobic flotation of liberated pyrite being minimal.♦

Acknowledgments

The authors would like to thank Ms. Jacqueline F. Bird, Director of the Ohio Coal Development Office, for her useful suggestions and critical discussion; Mr. W. Kukura for providing the plant facilities, personnel, the valuable signatures and the engineering services; and Dr. R.R. Klimpel, Dow Chemical Company, for his repeated patience and for the chemical reagents to operate the flotation circuit at Empire Coal.

References

Anon., 1985, "Flotation," Section 5, *SME Mineral Processing Handbook*, Society for Mining, Metallurgy and Exploration, Littleton, CO

Chander, S., and Aplan, F.F., 1989, "Surface and electrochemical studies in coal cleaning," Final Report to the US Department of Energy, DOE/PC/ 80523-T11 (DE 9000-7603)

Chernosky, F.J., and Lyon, F.M., 1972, "Comparison of the flotation and adsorption characteristics of ore and coal-pyrite with ethyl xanthate," *Trans. SME-AIME*, Vol. 252, pp. 11-14.

Hirt, W.C., 1973, *Separation of Pyrite from Coal by Froth Flotation*, unpublished MS thesis, Pennsylvania State University.

Kawatra, S.K., and Eisele, T.C., 1988, "Studies relating to removal of pyritic sulfur from coal by column flotation," Chapter 22, *Column Flotation '88*, K.V.S. Sastry, ed., SME, Littleton, CO, pp. 213-222

Lynch, A.J., et al., 1981, *Mineral and Coal Flotation Circuits: Their Simulation and Control*, Elsevier, Amsterdam

Miller, K.J., and Baker, A.F., 1972, "Flotation of pyrite from coal," USBM Technical Progress Report, TPR51

Purcell, R.J., 1982, *Circuitry Variations for the Rejection of Pyritic Sulfur during Coal Flotation*, unpublished MS thesis, Pennsylvania State University

Getting the most salable product from gravity-based coal/mineral preparation plants

J.W. Leonard

Introduction

Gravity-based coal/mineral preparation plants must be operated to yield products of a quality satisfactory to existing markets. However, because of historic control problems, recovery is frequently sacrificed to achieve quality, resulting in losses of valuable product. Plant control has ranged from intuitive in-plant spot quality judgments made by various operators to gross methods involving such devices as density gauges, floats, grab-sample on-the-spot sink/float tests, etc.

Millions of tons of quality coal/minerals are lost to refuse each year, because of the historic lack of a continuous and dependable control system. The result is serious economic, as well as environmental, losses. While the economic losses are obvious, the less obvious environmental ones, in the case of coal, result from the misplacement of more ignitable quality fuel to refuse banks. Until recently, a control system capable of supplying a market-grade coal/mineral product, while continuously minimizing product losses to refuse, has been technologically unavailable.

Coal/Mineral Washing Tracer System Performance Monitor (CMWTSPM)

The first Coal/Mineral Washing Tracer System Performance Monitor (CMWTSPM) originated in the late 1970s as an innovative idea and ultimately resulted in Leonard Patent No. 4,345,994 issued on August 24, 1982. In a classic example of successful university basic research, the patent was followed by two US Department of Energy (DOE) merit awards for fundamental optimization research at the University of Kentucky, a number of publications, a successful applied research program (underwritten by SENTREX at Irvine, CA) and field tests at the Rochester and Pittsburgh Coal Company Keystone Mine near Indiana, PA.

The system is now operational and is marketed by SENTREX as the SENTREX Performance Monitor. A diagram of the system is shown in Fig. 1. This system relies on metal detection as the basic tracing medium. Since it is capable of tracing particles as fine as 0.19-in., the system is ideal for coarse coal/mineral cleaning processes.

Basically, the CMWTSPM records the distribution of synthetic coal/mineral particles, of known size and specific gravity, between product and refuse output streams of coal/mineral washing, gravity-concentrating processes. For any given particle size, surface area and shape are constant. The particles are designed to find their way into the center of their respective in-process specific gravity/size streamlines.

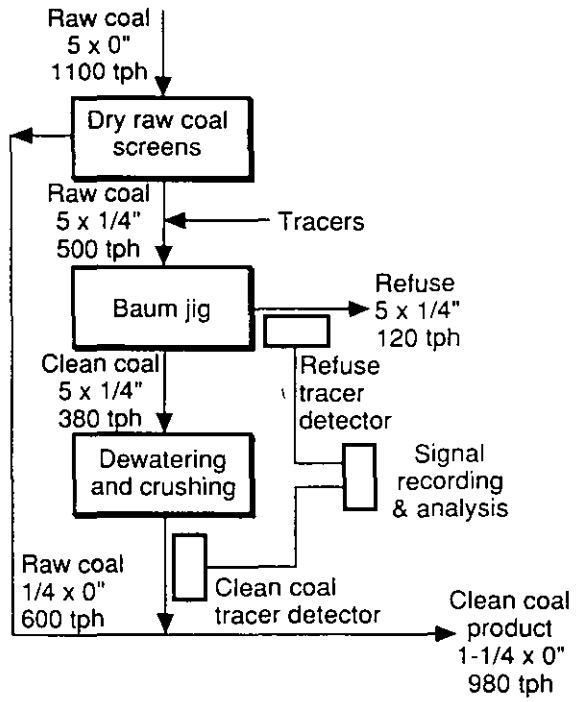

Fig. 1 — A simplified schematic highlighting major coal process equipment and CWTSPM components.

The system will yield a complete partition curve to show the percentage of misplacement for any selected size/specific-gravity particle fraction, thereby providing a point-to-point insight into process failure. When used to evaluate operational processes, this full partition curve is far more diagnostic than the simplifying, derivative, single index number known as the Ep value. The Ep value is commonly used for convenience to represent symmetrical partition curves, but, if the actual partition curve is non-symmetrical, use of the Ep value can result in serious diagnostic error. While the Ep is useful in design and for rapid performance evaluation and process adjustment, the full partition curve is by far the more diagnostic. It will provide insight into the behavior of particulate flow, through non-symmetry, as a means to highlight potential systemic failures.

Performance of the process is measured and improved by determining the extent of particle misplacement and by making timely adjustments to the unit to reduce the misplacement. Used in this manner, the CMWTSPM is not only a long needed processing control monitor, but it is also a very powerful diagnostic tool which, in the hands of skilled operators, has

J.W. Leonard, member SME, is professor of mining engineering, University of Kentucky, Lexington, KY. SME preprint 91-5, SME Annual Meeting, Feb. 25-28, 1991, Denver, CO. M&MP paper 91-607. Manuscript Oct. 1, 1990. Discussion of this paper must be submitted, in duplicate, prior to Aug. 31, 1992.

ELSEVIER

Int. J. Miner. Process. 47 (1996) 275–283

INTERNATIONAL JOURNAL OF MINERAL PROCESSING

On-line measurement of viscosity and determination of flow types for mineral suspensions

S.K. Kawatra, A.K. Bakshi

Department of Metallurgical and Materials Engineering, Michigan Technological University Houghton, MI 49931, USA

Received 19 July 1994; accepted 27 July 1995

Abstract

A viscometry system involving a vibrating sphere viscometer and a rotational viscometer has been developed for on-line measurement of viscosity, and for rheological characterization of mineral slurries into either Newtonian or non-Newtonian flows. Special precautions were taken to allow measurements of viscosity of rapidly settling mineral suspensions. Both the viscometers were able to measure viscosity as low as one centipoise, which is the approximate room temperature viscosity of water. Because the vibrating sphere viscometer operated at a much higher shear rate than the rotating viscometer, the two instruments together could determine the shear-rate dependency of the viscosity. Ground silica of 80% passing 65 μm size was suspended in water, and was used to prepare slurries at different percent solids. Viscosity of each slurry sample was measured simultaneously by both the viscometers, and the results were compared to determine the rheological characters of the slurries. With this technique, it was found that all the silica slurry samples (up to 70 wt% solids) at the given size distribution were in the Newtonian flow regime.

1. Introduction

It is known that suspension rheology affects many mineral processing operations, such as grinding and classification. However, measurement of slurry rheology using common viscometers is difficult mainly because mineral slurries contain rapidly-settling particles. If proper precautions are not taken, observations from standard instruments can lead to mistaken determinations of the fluid characteristics, and correlations between rheology and process performance will be impossible to determine (Kawatra and Bakshi, 1995).

Among the available viscometers, three basic types have been tried for slurry

0301-7516/96/$15.00 Copyright © 1996 Published by Elsevier Science B.V.
PII S0301-7516(96)00009-9

applications: (1) co-axial cylinder; (2) capillary tube; and (3) vibrating sphere type viscometers. Co-axial cylinder viscometers can measure viscosity at a particular shear rate, which can be varied by changing the rotational speed of the spindle. Because of this control in shear rate, co-axial cylinder viscometers have been very popular for many applications. However, settling of solid particles causes serious problems in these instruments, and special slurry presentation systems are needed to allow them to reliably measure slurry viscosity (Clarke, 1967; Underwood, 1976; Klien et al., 1990).

In a standard co-axial cylinder viscometer, the sample is stationary and particles can rapidly settle out of a slurry as shown in Fig. 1. Once the solids start settling, the slurry at the top becomes dilute compared to the slurry at the bottom. Then, the instrument sees a continuously changing solids content. Because of the changing viscosity arising from change in solids content, the user will wrongly interpret this as time dependency of the slurry rheology.

Several attempts have been made to prevent solids settling so that a co-axial cylinder instrument could reliably measure the viscosity of rapidly-settling slurries. These attempts generally used designs which moved slurry parallel to the rotational axis of the sensor, rapidly enough that the particles would be kept in suspension (Clarke, 1967; Underwood, 1976; Hemmings and Boyes, 1977; Reeves, 1990). However, the problem with this method is to obtain a smooth laminar flow of slurry without causing any disturbances in the sample holder (see Fig. 2). The flow of the sample should be strictly vertical, because forces in any other direction will interfere in the rotation of the spindle. In this way, a small turbulence originating from the mixing or flow of slurry will produce a shift in the viscometer reading. Klien et al. (1990) and Kiljanski (1993) have discussed separately how these disturbances (undetermined forces) from slurry mixing or recirculation will affect viscosity measurements.

Besides viscosity, another rheological parameter which is important for slurry handling is the flow type. Flow types for time independent fluids are shown in Fig. 3. Mineral suspensions show Newtonian flow behavior at dilute suspensions and non-Newtonian behavior at higher solids content. Other factors which affect the flow behavior are: (1) particle size; and (2) chemical nature, such as presence of dispersants (Schack et

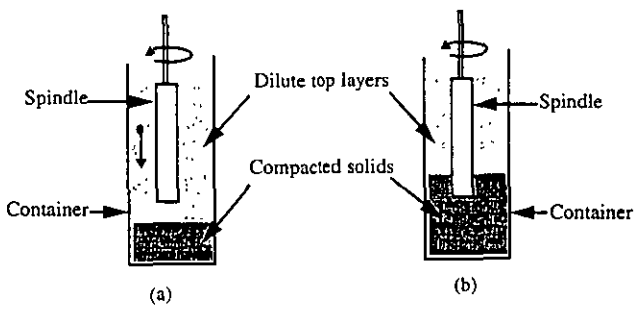

Fig. 1. Solids settling leaves a dilute suspension on the top layers of the container. When the solids content is low (a) the solids gradually settle and are compacted below the spindle and the viscometer reads progressively lower viscosity over time. At higher concentration of solids, the compacted solids can touch the spindle (b) resulting in progressive higher readings over time.

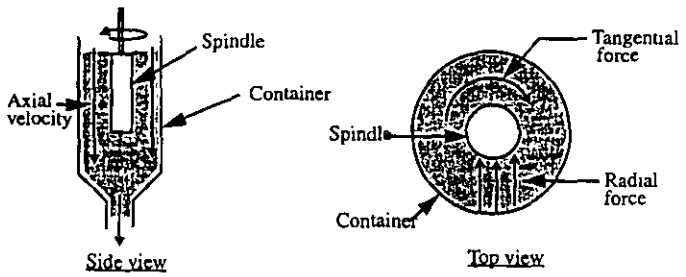

Fig. 2. The axial flow (side view) prevents the solids from settling by continuously sweeping fresh slurry past the spindle. This component of the flowing slurry stream does not affect the rotation of the spindle. But, any radial or tangential forces (top view), arising from the flow, will place additional forces on the spindle resulting in erroneous viscosity readings.

al., 1957). The knowledge of this flow type is essential in many mineral processing operations. For example, some suspensions show dilatancy and their viscosity increases with shear rate (Klose, 1984), which will result in plugging of pumps and pipelines. In grinding mills, it has been observed that optimum grinding is achieved when the slurry is pseudoplastic and does not have any yield stress (Klimpel, 1982, 1983). In hydrocyclone classifiers, it has been shown that the cut size changes with viscosity (Kawatra and Eisele, 1988).

Another important reason to know the flow type is that viscometers generally do not measure the viscosity at the shear rate that prevails in operations such as grinding, pumping, or classification. Since viscosity of non-Newtonian fluids depends upon the shear rate, viscosity cannot be correlated to equipment performance when the shear rates are different. Thus, the flow type must be measured before making correlations between viscosity and equipment performance. For example, in an hydrocyclone experiment with a 10.2 cm (4″) cyclone in the MTU laboratories, the maximum shear rate inside the cyclone was calculated to be 508 s^{-1}, while the Brookfield viscometer operated at shear rates below 74 s^{-1}. The viscosities measured by the Brookfield instrument therefore can only apply to the cyclone performance if the slurry is Newtonian. Also, the shear rate

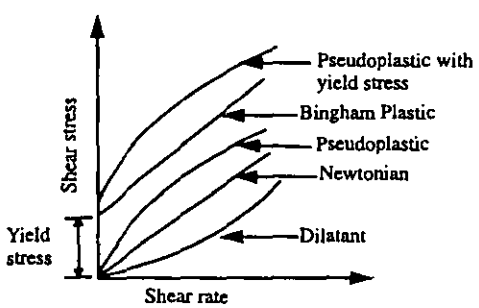

Fig. 3. Generalized time-independent rheology curves for mineral slurries. The ratio of shear stress and shear rate is the apparent viscosity. This ratio is constant for Newtonian fluids. The apparent viscosity decreases with increase in shear rates for pseudoplastic fluids and increases with increase in shear rates for dilatant fluids.

inside a cyclone varies a great deal from point to point (Bradley, 1965), and so no measurement of viscosity at a single shear rate can accurately reflect the conditions in a hydrocyclone when a slurry is non-Newtonian.

In this article a viscometry system is described, composed of a vibrating sphere viscometer used in combination with a rotational viscometer. The vibrating-sphere viscometer operates at a very high shear rate. This viscometer is insensitive to most turbulence, and can easily measure the viscosity of well-mixed slurries. The rotational viscometer used was modified to allow it to reliably measure the viscosity of slurries at low shear rates.

2. Methods and materials

2.1. System development

As pointed out earlier, viscosity of a Newtonian fluid is not affected by shear rates, but for non-Newtonian fluids the viscosity changes when the shear rate changes. Thus, by measuring the viscosity at two different shear rates sufficiently apart from each other and comparing the two values, the fluid can be designated as Newtonian if both the measured viscosities are similar, and non-Newtonian if the viscosities are different. Based on this concept, a new system was developed to determine the flow characteras-tics of mineral slurries. The two viscometers used for this purpose were a Brookfield (co-axial cylinder) viscometer and a Nametre (vibrating sphere) viscometer. In this system the Brookfield viscometer operated at a much lower shear rate than the Nametre viscometer. Thus, for Newtonian fluids readings from both the viscometers remained the same, and for non-Newtonian fluid the two instruments produced different readings.

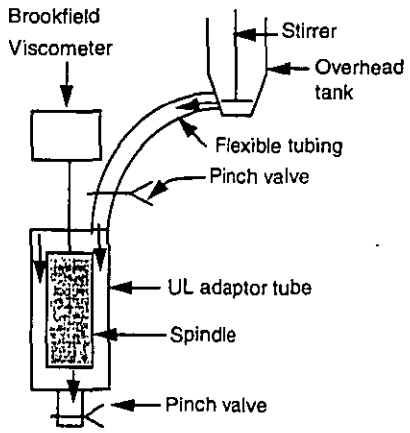

Fig. 4. Brookfield viscometer set-up showing the UL adaptor assembly and the slurry presentation system. This arrangement is very suitable for dilute suspensions, and could measure apparent viscosities of silica slurries up to 70% solids by weight in water without any difficulty.

2.1.1. The rotational viscometer

A Brookfield viscometer (DV-I model) was used to measure apparent viscosity at low shear rates (below 74 s^{-1}). The UL adaptor spindle was used for suspensions with a viscosity less than 10 centipoise, and the LV # 1 spindle was used for samples with viscosities above 10 centipoise. The UL adaptor consisted of a cylindrical spindle, and a tube which houses the spindle. The sample was placed in the annular space between the spindle and the tube to measure its viscosity. Solids were kept in suspension while the reading was taken by using the slurry presentation system shown schematically in Fig. 4. Slurry was mixed in an overhead tank, and passed continuously through the annular space between the UL spindle and the tube. After a steady state reading was displayed, flow was momentarily interrupted to eliminate any swirling motion caused by the flow at the inlet, and the reading was taken immediately. For denser suspensions (above 10 centipoise), the UL spindle was replaced by a LV # 1 spindle and rest of the parts in the setup were not changed. Although the Brookfield viscometer could operate at different shear rates, it was not sufficient by itself to determine the rheological type, because the instrument range was only sufficient for making one or two readings over closely-spaced shear rates.

2.2. The vibrating sphere viscometer

The vibrating sphere viscometer used for this study was manufactured by the Nametre Corporation, Metuchen, NJ. It consisted of a spherical probe, which oscillated along a vertical shaft at its resonant frequency of 750 Hz and a constant amplitude of 1 micron. When immersed in a fluid, the probe created a shear wave, and the fluid dampened the oscillatory motion. The damping, or the power to restore constant amplitude was a measure of the apparent viscosity of the fluid. Since the probe vibrated rather than rotating in a single direction, the shear rate was a sinusoidal function of time.

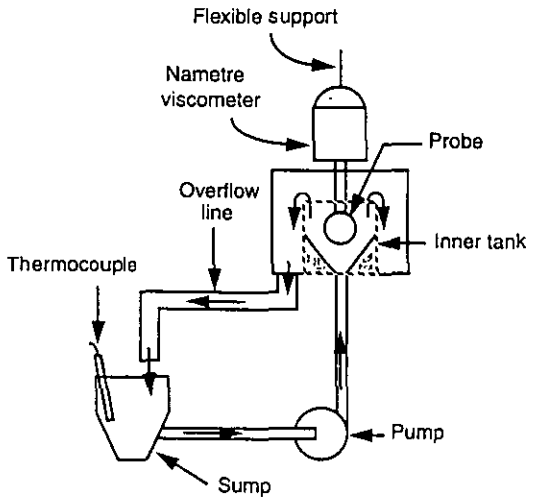

Fig. 5. Nametre set-up showing the special arrangement for slurry presentation. This arrangement is very suitable for suspensions with rapidly settling particles.

Also, the probe was spherical in shape, therefore its vibration had its maximum amplitude at the equator and gradually dropped to zero at the poles (Ferry, 1977). For these reasons, the Nametre viscometer did not operate at a specific shear rate, but averaged the shear rates from zero to the maximum value. The maximum shear rate was not a definite constant for the instrument because it was a function of the velocity of propagation of the shear wave in the fluid, which in turn depended upon the fluid viscosity (Ferry, 1977; Kawatra and Bakshi, 1995). A special slurry presentation system was built for this instrument as shown in Fig. 5. This was comprised of a vessel of two concentric cylinders, with the bottom of the inner cylinder made conical to avoid solids settling. The outer cylinder was one inch taller than the inner cylinder to prevent spillage of fluid. Slurry overflowed from the inner cylinder to the outer cylinder and then returned to the sump. The viscometer was suspended from the top by a cable, and the probe of the viscometer was immersed inside the inner cylinder. This arrangement prevented problems with vibration and excessive fluid drag on the sensor. A thermocouple was placed inside the sump, and both viscosity and temperature of the sample were recorded simultaneously.

2.3. Materials used

2.3.1. Sucrose solutions

Sucrose solutions show Newtonian flow properties. Six different solutions with 10 to 60 wt% sucrose in distilled water were used to confirm that both of the viscometers would register the same viscosity with Newtonian fluids.

2.3.2. Methylcellulose solutions

Methylcellulose is a water soluble polymer. Four solutions of methylcellulose at 0.5%, 1.0%, 1.5% and 2.0% concentrations by weight in water were prepared. These solutions display pseudoplastic flow behavior and were used to verify the system's ability detect non-Newtonian behavior.

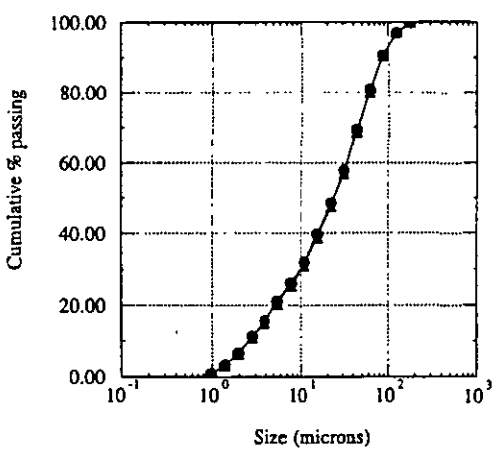

Fig. 6. Particle size distribution of the silica samples. Multiple samples in each category were measured with a Microtrac size analyzer with excellent reproducibility.

2.3.3. Silica slurries

Silica from the Ottawa Sand Co., IL, with the size distribution given in Fig. 6 was used to prepare slurry samples ranging from 0 to 70% solids by weight in distilled water. The d_{80} size of the silica sample was 65 μm.

3. Results and discussion

3.1. Calibration of the system with known solutions

Readings from the Nametre viscometer for sugar (sucrose) solutions and methylcellulose solutions were plotted against the readings from the Brookfield viscometer (Fig. 7). Since sucrose solutions were Newtonian, viscosity readings from both the Nametre (high shear rate) and the Brookfield (low shear rate) viscometers were similar for these solutions. For methylcellulose solutions, apparent viscosity values obtained from the Nametre viscometer were less than their corresponding values from the Brookfield viscometer showing that apparent viscosity decreased with increasing shear rate. This was expected from methylcellulose solutions, because these are known to be pseudoplastic fluids. This shows that the system could distinguish between Newtonian and non-Newtonian fluids.

3.2. Viscosity measurements for silica suspensions

After calibrating the system with known Newtonian (sucrose) and non-Newtonian (methylcellulose) solutions, tests were conducted with silica–water slurries at different percent solids. Viscosities of these slurries were measured by both the Nametre and

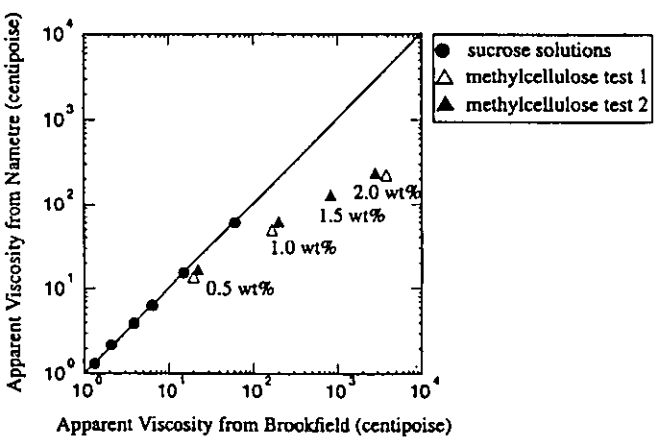

Fig. 7. Reading from the Nametre viscometer vs. reading from the Brookfield viscometer for sucrose solutions (from 10 to 60 wt% sucrose) and methylcellulose solutions (from 0.5 to 2.0 wt% methylcellulose) in water.

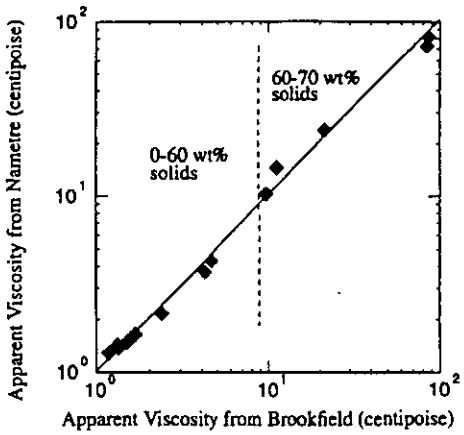

Fig. 8. Comparison of apparent viscosities of silica slurries at different percent solids, as measured by the Brookfield and the Nametre viscometers. For all the slurries (10–70 wt% solids) the readings from both instruments are similar, therefore these slurries are Newtonian.

Brookfield viscometers, with the results as shown in Fig. 8. For all the silica slurries, measurements from both the viscometers were in close agreement with each other, indicating that these slurries were Newtonian up to at least 70% solids by weight.

4. Conclusion

The following conclusions were drawn from these tests:

(1) The system suggested in this article eliminated the solids settling problem, and produced reproducible measurements of slurry viscosities in the laboratory.

(2) This system could measure the viscosities of silica slurries up to 70 wt% solids, and simultaneously provided a simple method to distinguish between Newtonian and non-Newtonian flow types. The flow type of all the silica slurries used in this study was found to be Newtonian.

(3) While the system does not give extreme details about the rheological type of the slurry, the measurement is quite rapid and reproducible, and so it is suitable for routine plant monitoring to detect changes in rheological type. Since such changes can have profound effects on plant operations, this technique has many potential applications.

Acknowledgements

Part of the funding for this project was obtained from the Dow Chemical Company, Midland, Michigan and the Department of the Interior's Mineral Institute program administered by the United States Bureau of Mines through the Generic Mineral Technology Center for Comminution under grant number G1125149. This paper was published without prior review by the Bureau of Mines.

References

Bradley, D., 1965. The Hydrocyclone Pergamon Press, New York, NY.

Clarke, B., 1967. Rheology of coarse settling suspensions. Trans. Inst. Chem. Eng., 45: T251–T256.

Ferry, J.D., 1977. Oscillation viscometry — effects of shear rate and frequency. Meas. Control, 11(5): 89–91.

Hemmings, C.E. and Boyes, J.M., 1977. An on-line viscometry technique for improved operation and control of wet grinding circuits. In: Twelfth International Mineral Processing Congress, Sao Paulo, pp. 46–64.

Kawatra, S.K. and Bakshi, A.K., 1995. On-line viscometry in particulate processing. Miner. Process. Extract. Metall. Rev., 14: 249–273.

Kawatra, S.K. and Eisele, T.C., 1988. Rheology effects in grinding circuits. In: XVI International Mineral Processing Congress. Elsevier, Amsterdam, pp. 195–207.

Kiljanski, T., 1993. On the measurement of the rheological properties of unstable mineral suspensions. Coal Prep., 13: 107–112.

Klien, B., Partridge, S.J. and Laskowski, J.S., 1990. Rheology of unstable mineral suspensions. Coal Prep., 8(3–4): 123–134.

Klimpel, R.R., 1982. Slurry rheology influence on the performance of mineral/coal grinding circuits. Part I. Min. Eng., 34(12): 1665–1668.

Klimpel, R.R., 1983. Slurry rheology influence on the performance of mineral/coal grinding circuits. Part II. Min. Eng., 35(1): 21–26.

Klose, R.B., 1984. Densecoal — an alternative to gas and oil. In: Proceedings of the Sixth International Symposium on Coal Combustion and Technology, Orlando, FL, pp. 791–805.

Reeves, T.J., 1990. On-line viscosity measurement under industrial conditions. Coal Prep , 8: 135–144.

Schack, C.H., Dean, K.C. and Molly, S.M., 1957. Measurement and Nature of the Apparent Viscosity of Water Suspensions of Some Common Minerals. Report of Investigations, U.S. Bureau of Mines, 5334, pp. 1–16.

Underwood, W.M., 1976. Viscometer for slurries and suspensions. Rev. Sci. Instrum., 47(9): 1079–1082.

Australia, Brazil, Canada, Hong Kong, India, Israel, Japan, Malaysia, Mexico, New Zealand, Pakistan, PR China, Singapore, South Africa, South Korea, Taiwan, Thailand, USA. For all other countries airmail rates are available upon request. Claims for missing issues must be made within six months of our publication (mailing) date. Please address all your requests regarding orders and subscription queries to: Elsevier Science B.V., Customer Support Department, P.O. Box 211, 1000 AE Amsterdam, The Netherlands. Tel.: +31-20-4853642, fax: +31-20-4853598.

US mailing info – *International Journal of Mineral Processing* (ISSN 0301-7516) is published bimonthly by Elsevier Science B.V. (Molenwerf 1, P.O. Box 211, 1000 AE Amsterdam). Annual suscription price in the USA US$ 671.00 (valid in North, Central and South America), including air speed delivery. Application to mail at second class postage rate is pending at Jamaica, NY 11431.
USA POSTMASTERS: Send address changes to. *International Journal of Mineral Processing,* Publications Expediting, Inc., 200 Meacham Avenue, Elmont, NY 11003.
AIRFREIGHT AND MAILING IN THE USA by Publications Expediting. Inc., 200 Meacham Avenue, Elmont, NY 11003.

Advertising information
Advertising orders and enquiries may be sent to:
International: Elsevier Science, Advertising Department, The Boulevard, Langford Lane, Kidlington, Oxford, OX5 1GB, UK; Tel: +44 (0)1865 843565; Fax: +44 (0)1865 843976.
USA and Canada: Weston Media Associates, attn. Daniel Lipner, P.O. Box 1110, Green Farms, CT 06436-1110, USA; Tel: +1 (203) 261 2500; Fax: +1 (203) 261 0101.
Japan: Elsevier Science Japan, Marketing Services, 1-9-15 Higashi-Azabu, Minato-ku, Tokyo 106, Japan; Tel: +81 3 5561 5033; Fax: +81 3 5561 5047

NOTE TO CONTRIBUTORS

A detailed Guide for Authors is available upon request. Please pay special attention to the following notes:

Language
The official language of the journal is English.

Preparation of the text
(a) The manuscript should preferably be prepared on a word processor and printed with double spacing and wide margins and include an abstract of not more than 500 words.
(b) Authors should use IUGS terminology. The use of S.I. units is also recommended.
(c) The title page should include the name(s) of the author(s), their affiliations, fax and e-mail numbers. In case of more than one author, please indicate to whom the correspondence should be addressed.

References
(a) References in the text consist of the surname of the author(s), followed by the year of publication in parentheses. All references cited in the text should be given in the reference list and vice versa.
(b) The reference list should be in alphabetical order.

Tables
Tables should be compiled on separate sheets and should be numbered according to their sequence in the text. Tables can also be sent as glossy prints to avoid errors in typesetting.

Illustrations
(a) All illustrations should be numbered consecutively and referred to in the text.
(b) Colour figures can be accepted providing the reproduction costs are met by the author. Please consult the publisher for further information.

Page proofs
One set of page proofs will be sent to the corresponding author, to be checked for typesetting/editing. The author is not expected to make changes or corrections that constitute departures from the article in its accepted form. To avoid postal delay, authors are requested to return corrections to the desk-editor, Mr. Herman E. Engelen, by FAX (+31-20-4852459) or e-mail (h.engelen@elsevier.nl), preferably within 3 days.

Reprints
Fifty reprints of each article are supplied free of charge. Additional reprints can be ordered on a reprint order form which will be sent to the corresponding author upon receipt of the accepted article by the publisher.

Submission of electronic text
Authors are requested to submit the final text on a 3.5" or 5.25" diskette. It is essential that the name and version of the word processing program, the type of computer on which the text was prepared, and the format of the text files are clearly indicated. Authors are requested to ensure that the contents of the diskette correspond exactly to the contents of the hard copy manuscript. If available, electronic files of the figures should also be included on a separate floppy disk.

Submission of manuscripts
Authors are requested to submit, with their manuscripts, the names and addresses of *four* potential referees. Manuscripts should be submitted in triplicate; those originating in North and South America should be sent to D.W. Fuerstenau, and all other manuscripts should be submitted to J. Cases (addresses are given on the inside front cover). Illustrations: Please note that upon submission of a manuscript that three sets of all photographic material printed sharply on glossy paper or high-definition laser prints must be provided to enable meaningful review. Photocopies and other low-quality prints will not be accepted for review.
The indication of a fax and e-mail number on submission of the manuscript could assist in speeding communications. The fax number for the Amsterdam office is +31-20-4852696.
Submission of an article is understood to imply that the article is original and unpublished and is not being considered for publication elsewhere.

Mineral Deposits of the World

Ores, industrial minerals and rocks

Edited by **M. Vaneček**

Developments in Economic Geology Volume 28

Distributed in the East European Countries, China, Cuba, Mongolia, North Korea and Vietnam by ARTIA VERLAG

This overview of the world's mineral deposits lists the metallic and non-metallic mineral deposits according to continents, subdividing the latter with respect to regional metallogenic zones. The introductory chapters summarize present knowledge of the basic concepts of the geologic structure and the evolution of the continents and oceans. The description of the essential metallogenic units has been complemented by main aspects of the development of global metallogeny in time and space. The characteristics of the world's mineral wealth have been supplemented with basic data on the amount, extent and manner of using these mineral resources. Economic geologists will find this volume of interest.

Contents: Preface. 1. Introduction. 2. Structure and Evolution of Continents and Oceans. 3. Mineral Deposits of Eurasia. A. Mineral Deposits of Europe. B. Mineral Deposits of North Asia. C. Mineral Deposits of the Gondwanian Asia. 4. Mineral Deposits of North America. 5. Mineral Deposits of Central America 6. Mineral Deposits of South America. 7. Mineral Deposits of Africa. 8. Mineral Deposits of Australasia. 9. Mineral Resources of Antarctica. 10. Mineral Resources of Oceanic Regions. 11. Main Features of the Metallogenic Development of Continents and Oceans. 12. Principal Trends in Exploiting the World's Mineral Wealth. Literature. Subject Index. Locality Index.

ELSEVIER SCIENCE B.V.

1994 520 pages
Dfl. 375.00
(US $ 214.25)
ISBN 0-444-98667-7

Elsevier Science B.V.
P.O. Box 1930
1000 BX Amsterdam
The Netherlands

P.O. Box 945
Madison Square Station
New York
NY 10160-0757

The Dutch Guilder (Dfl.) prices quoted apply worldwide. US $ prices quoted may be subject to exchange rate fluctuations. Customers in the European Community should add the appropriate VAT rate applicable in their country to the price.

ELSEVIER

Int. J. Miner. Process. 50 (1997) 187–201

INTERNATIONAL JOURNAL OF MINERAL PROCESSING

Pyrite recovery mechanisms in coal flotation

S.K. Kawatra *, T.C. Eisele

Department of Metallurgical and Materials Engineering, Michigan Technological University, 1400 Townsend Drive, Houghton, MI 49931-1295, USA

Received 26 June 1995; accepted 24 May 1996

Abstract

In most operating coal-cleaning plants, a significant amount of pyrite is recovered in the froth during flotation of high-sulfur coal. This pyrite recovery is commonly believed to be a result of pyrite particles floating due to hydrophobicity. However, even though a wide range of pyrite depressants have been reported over the years, there is no use of these depressants for industrial coal flotation, which suggests that the mechanism of pyrite flotation is not properly understood. In order to reduce the pyrite recovery during flotation, it is first necessary to identify the primary recovery mechanism, so that the appropriate method for correcting the problem can be selected. In this paper, it is shown that flotation of liberated pyrite due to its intrinsic hydrophobicity is not an important mechanism for recovery of pyrite from freshly ground coal, and that the bulk of the floated pyrite reaches the froth either as a result of simple entrainment or by mechanical locking with floatable coal particles. The experiments were carried out using both a conventional flotation cell, and a horizontally baffled flotation column. © 1997 Elsevier Science B.V.

Keywords: pyrite hydrophobicity; coal flotation; sulfur removal; pyrite removal

1. Introduction

In many coal flotation operations, a significant amount of apparently liberated pyrite is seen to report to the froth, thus raising the sulfur content of the clean product and reducing its economic value. This unwanted recovery of pyrite should therefore be prevented. This need has encouraged many investigators to develop a large number of depressants. However, there is no literature on the use of these depressants on an industrial scale. The purpose of the study described here was to determine why

* Corresponding author.

0301-7516/97/$17.00 © 1997 Elsevier Science B.V. All rights reserved.
PII S0301-7516(97)00012-4

depressants had not been industrially successful, which required determination of whether the pyrite was floating due to hydrophobicity in the first place.

Before the best means for preventing liberated coal pyrite recovery can be selected, it is necessary to determine how the coal pyrite is actually being recovered. There are three ways that a pyrite particle can reach the froth product: (1) the pyrite surface could be truly hydrophobic, and attach to air bubbles directly; (2) a pyrite particle could be entrained into the froth, without ever attaching to a bubble; or (3) the pyrite could be mechanically locked to a floatable coal particle. Pyrite has complex surface chemistry, making it possible for it to be either hydrophobic or hydrophilic (depending on conditions, and the past history of the pyrite). This makes it possible for pyrite to reach the froth by any of the above mechanisms. Unfortunately, once a pyrite particle has reached the froth, it can be difficult to determine why it went there. A partial solution was to conduct flotation tests where there are no locked coal/pyrite particles, by using pyrite collected from mineral deposits that were not associated with coal. The pure mineral pyrite used in this type of testing does not have the same properties as pure coal pyrite (Chernosky and Lyon, 1972), but the use of fully liberated coal pyrite is not feasible because there is no simple established method to produce unoxidized coal pyrite which is completely free of locked coal. In some past studies, the hydrophobicity of mineral pyrite has been artificially enhanced by addition of xanthates (Whelan and Brown, 1956) or sulfurizing agents such as sodium sulfide (Drzymala et al., 1991), but such treatments are not representative of the conditions that occur naturally in coal and so were not considered in this study.

The floatability of liberated coal pyrite can be indirectly estimated from coal flotation studies, provided that estimates are made of the recoveries of entrained coal pyrite and locked coal pyrite. The pyrite in the froth that is not accounted for by either locked particles or entrainment can then be considered to be the pyrite recovered due to intrinsic hydrophobicity.

The experiments described in this paper were carried out to attempt to measure the floatability of liberated coal pyrite in coal using both a conventional cell and a laboratory-scale horizontally baffled flotation column, with reagents which are commonly selected in current industrial practice. The objective was to determine why pyrite depressants were not found to be useful on an industrial scale, by demonstrating how pyrite particles were reaching the froth phase, and to determine which class of pyrite particles (locked particles, entrained particles, or particles floating due to their intrinsic hydrophobicity) were the most important contributors to pyritic sulfur recovery in froth flotation.

2. Theoretical discussion

While flotation is generally acceptable for ash removal, it often is not highly effective for removing the pyritic sulfur from the coal. It has been hypothesized that this is due to the pyrite being naturally hydrophobic, and therefore floated along with the coal (Yancey and Taylor, 1935; Baker and Miller, 1971; Raleigh and Aplan, 1993). A great number of chemical and biological pyrite depressants have been proposed by several

Table 1
Some representative depressants for coal pyrite which have been reported in the literature; none of these are widely used as pyrite depressants in industrial coal flotation

Reagent	Action	Reference
Alkali	pH	Liu et al., 1993
Lime, CaO	pH, hydrolyzed ion adsorption	Chander and Aplan, 1989
Potassium dichromate, $K_2Cr_2O_7$	Oxidizing agent	Chander and Aplan, 1989
Sodium hypochlorite, NaClO	Oxidizing agent	Chander and Aplan, 1989
Sodium sulfide, Na_2S	Reducing agent	Chander and Aplan, 1989
Sodium sulfite, Na_2SO_3	Reducing agent	Chander and Aplan, 1989
Corn starch	Physically adsorbed colloid	Chander and Aplan, 1989
High-amylose starch	Physically adsorbed colloid	Chander and Aplan, 1989
Cationic starch	Physically adsorbed colloid	Chander and Aplan, 1989
Xanthated cationic starch	Physically adsorbed colloid	Chander and Aplan, 1989
Congo red	Dye	Chander and Aplan, 1989
Nigrosine	Dye, chelating agent	Raleigh and Aplan, 1993
Sodium silicate	Dispersing agent	Raleigh and Aplan, 1993
Aerosol MA-80	Dispersing agent	Raleigh and Aplan, 1993
Citric acid	pH, complexing agent	Raleigh and Aplan, 1993
Marasperse CB	Dispersing agent	Raleigh and Aplan, 1993
Potassium hypochlorite, KClO	Oxidation	Raleigh and Aplan, 1993
Ferric chloride, $FeCl_3$	Hydrolyzed ion adsorption	Baker and Miller, 1971
Aluminum chloride, $AlCl_3$	Hydrolyzed ion adsorption	Baker and Miller, 1971
Chromium chloride, $CrCl_3$	Hydrolyzed ion adsorption	Baker and Miller, 1971
Copper sulfate, $CuSO_4$	Hydrolyzed ion adsorption	Baker and Miller, 1971
Calcium chloride, $CaCl_2$	Hydrolyzed ion adsorption	Baker and Miller, 1971
Sodium cyanide, NaCN	Complexing agent	Yancey and Taylor, 1935
Ferrous sulfate, $FeSO_4$	Hydrolyzed ion adsorption	Yancey and Taylor, 1935
Ferric sulfate, $Fe_2(SO_4)_3$	Hydrolyzed ion adsorption	Yancey and Taylor, 1935
Para-aminophenol	Complexing agent	Yancey and Taylor, 1935
Carboxymethyl cellulose	Physically adsorbed colloid	Laskowski et al., 1985
Thiobacillus ferrooxidans	Oxidation, surface attachment	Elzeky and Attia, 1987
Other microorganisms	Surface attachment	Townsley and Atkins, 1986
Potassium monopersulfate, KSO_5	Oxidation	Miller et al., 1989; Ye et al., 1990
Cato 2	Dispersing agent	Arnold and Aplan, 1990
Hylon VII	Dispersing agent	Arnold and Aplan, 1990
Aerosol OT	Dispersing agent	Arnold and Aplan, 1990
Quebracho	Dispersing agent	Arnold and Aplan, 1990
Daxad II KLS	Dispersing agent	Arnold and Aplan, 1990
Tergitol NPX	Dispersing agent	Arnold and Aplan, 1990
Sodium thiosulfate, $Na_2S_2O_4$	Reducing agent	Arnold and Aplan, 1990
Thioglycolic acid, $HSCH_2COOH$	Complexing agent	Chmielewski and Wheelock, 1991; Luo et al., 1993
Methanol	Surface tension modifier	Feeley, 1991
Ethanol	Surface tension modifier	Feeley, 1991
Butylbenzaldehyde	Surface tension modifier	Feeley, 1991

investigators, with a few representative examples shown in Table 1. However, while they have often been claimed to be effective in laboratory experiments, none have been adopted on a plant scale. No benefits have been reported for pyrite depressants in full-scale coal flotation plants, apparently because any natural hydrophobicity of pyrite

varies a great deal, and the variations are difficult to predict. Also, pyrite depressants require good control of the slurry pH in order to work properly (Baker and Miller, 1971) and existing coal flotation circuits typically are not equipped for more than the coarsest control of this parameter.

The most probable cause of the variation in pyrite hydrophobicity is the formation of elemental sulfur. Elemental sulfur is naturally hydrophobic (Fuerstenau et al., 1990), and so, if it forms on the surface of pyrite, it can act as a collector for the pyrite. Since 1942, it has been reported several times that elemental sulfur is not present in fresh coal, but is often found in weathered coal, and that it forms by oxidation of pyrite under the proper conditions (Chou, 1990; Stock and Wolny, 1990). There are two basic reactions that lead to elemental sulfur formation from pyrite. The simplest is:

$$2Fe^{+3}(aq) + FeS_2(s) \Rightarrow 3Fe^{+2}(aq) + 2S(s)$$

This reaction occurs during microbial oxidation of pyrite, and so elemental sulfur will be formed when pyrite oxidizes in the moist, acidic conditions that are needed for pyrite-oxidizing bacteria to grow (Kawatra et al., 1991; Kawatra and Eisele, 1992a,b).

The second reaction that can produce elemental sulfur from pyrite is a reaction with water (Ahlberg et al., 1990; Wadsworth et al., 1992) of the form:

$$FeS_2 + 3H_2O \Rightarrow Fe(OH)_3 + 2S^0 + 3H^+ + 3e^-$$

In both cases, the elemental sulfur is normally an intermediate product in a series of reactions that ultimately produce sulfate (SO_4^{2-}). However, if conditions are suitable, detectable amounts of elemental sulfur can form on the pyrite surfaces.

If the elemental sulfur is the main cause of pyrite hydrophobicity, then it would be expected that pristine, unoxidized pyrites would not be hydrophobic, while pyrites which had oxidized under the proper conditions would be hydrophobic.

At the particle sizes where pyrite recovery into the froth is reported (finer than 100 μm), entrainment is also an important effect. Determination of the quantity of entrained material in a flotation froth is based on correlation of the amount of water in the froth with the quantity of the entrained species in the froth. Since entrainment is directly related to water recovery (Lynch et al., 1981; Kawatra and Eisele, 1992a,b), a correlation between percent recovery of purely hydrophilic particles and of water will be linear. Deviations from linearity, or a solids recovery rate which is faster than the water recovery rate, are due to particles which are either recovered by direct bubble attachment due to their intrinsic hydrophobicity, or by mechanical locking with hydrophobic particles.

3. Experimental materials and procedures

Three sets of experiments were carried out for this work. The first set consisted of a series of flotation experiments with mineral pyrite, which determined whether the natural hydrophobicity of a mineral pyrite would vary upon aging under various conditions. The second set was a series of timed conventional flotation experiments with a particular Pittsburgh #8 Seam coal, which were conducted so that the degree of

entrainment could be determined based on the correlations of the recovery rates of solid particles with the recovery rate of water. The third set of experiments consisted of column flotation tests with the Pittsburgh #8 Seam coal. The column tests produced coal that was essentially free of entrained particles and liberated pyrite, and provided a measure of the organic sulfur and locked pyritic sulfur in the coal.

These experiments provided data on the extent to which coal pyrite flotation occurs during normal flotation of coal, and the types of conditions that are likely to result in natural hydrophobicity of pyrite.

3.1. Mineral pyrite conventional flotation

Purpose of the experiments. These experiments were intended to determine the conditions where mineral pyrite was floatable when fuel oil was used as a collector in the absence of pyrite depressants. Since it is not practical to liberate coal pyrite completely from the coal that is locked to its surface, experiments were conducted using mineral pyrite which had not been associated with coal. Although mineral pyrite does not necessarily have the same surface properties as coal pyrite, it is much easier to obtain in a reasonably pure form.

Materials. The pyrite used was obtained from Wards Natural Science Establishment, and was mined in Custer, South Dakota. It was stage-crushed by roll-milling to pass 28 mesh, and was stored in a freezer at −15°C to retard oxidation until the pyrite could be used. A portion of the pyrite was used within one week of stage-crushing, while the remainder was allowed to age in the freezer for one year.

Procedure. Immediately before the flotation experiments, the pyrite was ground in a steel rod mill at 60% solids and a pH of 12, to the final size distribution given in Table 2. The pH was adjusted with sodium hydroxide. Lime was not used for pH control,

Table 2
Size distributions of Pittsburgh seam coal and Custer mineral pyrite used in the flotation experiments

Size (μm)	Pittsburgh coal, cumulative % passing	Custer mineral pyrite, cumulative % passing
88	100.0	100.0
62	96.0	100.0
44	87.5	97.4
31	74.7	88.3
22	61.7	73.5
16	49.2	56.5
11	37.6	42.2
7.8	28.4	31.7
5.5	20.3	23.0
3.9	13.7	16.1
2.8	8.1	10.0
1.9	3.1	4.3
1.4	1.1	1.8
0.9	0.0	0.3

The coal was ground at 37.5% solids, and the pyrite was ground at 60% solids. Size distribution was measured using a Microtrac particle size analyzer

because it has been reported to be a pyrite depressant and could have led to misleading results. This pH was selected for grinding to prevent the steel grinding mill from corroding, and possibly contributing ferrous or ferric ions which would have altered the pyrite surface chemistry. The ground pyrite was then filtered, rinsed on the filter with distilled water, and divided into flotation charges of 150 g each. These were re-suspended in distilled water in a Denver laboratory flotation cell (cell volume of 1.9 liters). The tests were conducted with MIBC as the frothing agent. The pH was adjusted to the desired level with sulfuric acid. Once the pH had been adjusted, #2 fuel oil and MIBC were added to the cell at dosages of 3.0 kg/mt and 0.4 kg/mt, respectively. The pulp and reagents were then conditioned in the Denver cell for 2 min at 1200 rpm. The conditioned pulp was then floated for 5 min while continuously removing the froth.

Three sets of experiments were carried out with this pyrite. The first set used the pyrite which was freshly stage-crushed to pass 28 mesh; the second set used pyrite which had been stage-crushed, and then allowed to age in a freezer at −15°C for one year; and the third set used pyrite which had been aged for one year in the freezer, followed by heating to 100°C in a forced-air drying oven for one month to oxidize it.

3.2. Pittsburgh coal conventional flotation

Purpose of the experiments. These experiments were carried out to determine the quantity of pyrite reporting to a coal froth by entrainment. These tests used Dowfroth 200 (a polypropylene glycol methyl ether, molecular weight 200) as the frother. Entrainment was determined by correlating the water recovery with the recoveries of coal, ash, water, and the various forms of sulfur as a function of time. The dosage of collector (#2 fuel oil) was varied to change the coal flotation rate. The dosage of frother was held constant for these tests.

Material. These experiments used 250-g charges of Pittsburgh seam coal. The coal contained 37.2% ash, 2.2% pyritic sulfur, and 2.9% total sulfur, and had previously been stage-crushed to pass 20 mesh. The coal was prepared for flotation by grinding 900 g of coal in 1.5 liter of distilled water (37.5% solids) at its natural pH in a steel rod mill to the size distribution given in Table 2. The freshly ground coal was then filtered, and the cake was divided into three 250-g charges for flotation, with the remaining material used as a head sample. The coal was then floated immediately.

Procedure. Timed flotation experiments were carried out in a 4.25-liter flotation cell, agitated at 1200 rpm with a Wemco agitator. The cell was equipped with gravity-feed pulp level control and mechanical froth scrapers (Fig. 1). The frother was Dowfroth 200, and was added to all of the water used in the flotation tests at a rate of 0.03 g/l (corresponding to a frother dosage of 0.5 kg/mt). Distilled water was used throughout, and the tests were carried out at a pH of 7.6 (which was the natural pH for this coal). Frother was added to all of the water before adding the coal. For tests using collector, the fuel oil was added to the pulp in the cell, and conditioned at 1200 rpm for 5 min before beginning flotation. The air flow was then started, and froth was collected over the time intervals 0–30 s, 30 s–1 min, 1–2 min, 2–3 min, 3–5 min, and 5–9 min. The froth products were weighed, filtered, dried, and re-weighed to measure the water content of each. All products were analyzed for ash content, using ASTM method

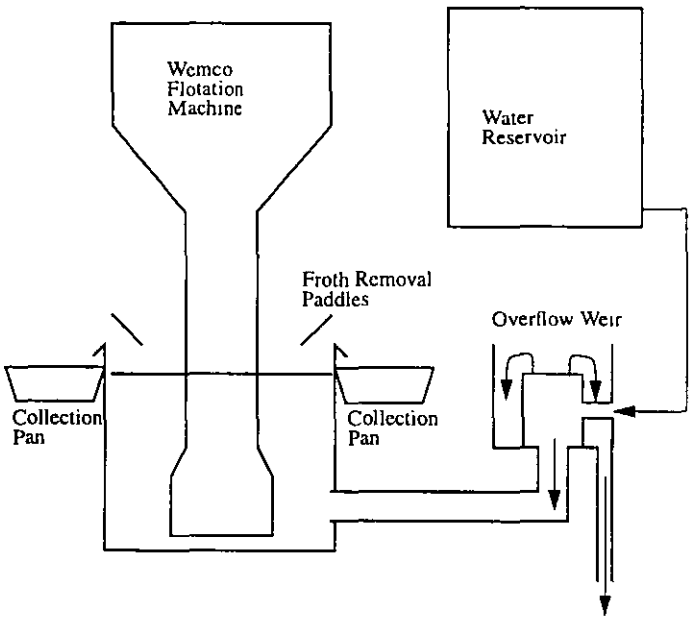

Fig. 1. Schematic diagram of the conventional flotation cell used in the timed flotation experiments, showing the motorized froth scrapers and the pulp level control. Froth paddle speed 18.75 rpm. Cell volume 4.25 l. Air flowrate to cell 15.7 l/min. Impeller speed 1200 rpm.

D3174 (ASTM, 1988a), and total sulfur content was determined using a LECO SC-132 sulfur determinator. Pyritic sulfur was measured using ASTM method D 2492 (ASTM, 1988b), with the nitric acid dissolution step carried out by leaching at room temperature overnight (16 h), followed by boiling for 30 min to ensure complete dissolution.

3.3. Pittsburgh coal column flotation

Purpose of the experiments. These experiments were intended to produce a coal that was as free as possible of entrained particles, so that the quantity of locked pyritic and organic sulfur in the coal could be determined. Flotation experiments were carried out in a laboratory-scale horizontally baffled flotation column, using coal prepared in the same manner as that used in the conventional coal flotation tests. The column had been modified by the introduction of horizontal baffles, which had been found to improve the performance of the column in earlier work. Tracer experiments previously conducted using sodium fluorescein dye showed that less than 4% of the feed water was entrained in the froth product using this column (Eisele and Kawatra, 1993; Kawatra and Eisele, 1995a,b).

Procedure. A 3-inch (7.62 cm) diameter horizontally baffled column, 6ft. (1.83 m) tall, was used for these experiments. A froth depth of 18 inches (45.7 cm) was maintained, with 1 l/min of wash-water. Aeration was provided by an aspirator, with a water pressure of 15 psi (103 kPa) and a flowrate of 5 l/min. The water injected into the column through the bubble generator and the wash-water ring was tap water, with a

nominal pH of 7.0 and a nominal hardness of 150 ppm. The frother was Dowfroth 200, introduced with the aspirated air as a 1% solution to give a concentration of 0.03 g/l (0.5 kg/mt coal), and also added to the wash-water at the same concentration. No collector was added in the column flotation tests.

The column flotation experiments were batch tests. Feed coal was prepared as for the conventional flotation experiments, except that each 900 g of ground coal was divided into two flotation feed charges of 400 g each, with the remaining 100 g reserved as a head sample. Timed flotation experiments were carried out by suspending the coal in distilled water at 25% solids, and adding the coal slurry as a single increment over a 30-s time interval while the column was being filled at the beginning of the test. After adding the feed, 30 s were required before coal began flowing into the overflow launder. From this time, froth increments were removed over the time intervals 0–30 s, 30 s–1 min, 1–2 min, 2–3 min, 3–5 min, and 5–9 min. These samples were analyzed in the same manner as the samples from the conventional flotation tests.

4. Results and discussion

4.1. Mineral pyrite flotation

It can be seen from the mineral-pyrite flotation results presented in Table 3 that the freshly prepared pyrite was not highly floatable at a pH between 7.5 and 8.3, but that it became very floatable (98–99% of the total weight floating) when the pH dropped to 2.3. When the mineral pyrite was aged for one year at −15°C, however, it became moderately floatable at neutral pH, with 35 to 37% of the total weight floating. When the aged pyrite was further oxidized at 100°C for 1 month, it was no longer floatable at neutral pH, but it could still be made very floatable by lowering the pH to 2.0.

Table 3
Flotation results for the Custer pyrite, after various pretreatments and over a wide pH range. Reagents were #2 fuel oil (3.0 kg/mt) and MIBC (0.4 kg/mt)

Pyrite pretreatment	Flotation pH	Wt.% reporting to froth
Fresh	8.3	5
Fresh	7.5	3
Fresh	7.5	4
Fresh	2.3	98
Fresh	2.2	98
Fresh	2.0	99
Aged 1 year at −15°C	9.0	46
Aged 1 year at −15°C	6.8	37
Aged 1 year at −15°C	6.0	35
Aged 1 year at −15°C	1.9	92
Aged 1 year at −15°C, then oxidized 1 month at 100°C	6.2	7
Aged 1 year at −15°C, then oxidized 1 month at 100°C	2.0	82

It has been reported (Chou, 1990; Stock and Wolny, 1990) that elemental sulfur can be formed as an oxidation product of pyrite, and that at times the quantity of elemental sulfur formed in oxidized coals can be considerable. Elemental sulfur is naturally hydrophobic, and so when it forms on the surface of pyrite it can act as a collector for the pyrite, making it floatable. However, iron sulfates are also formed during pyrite oxidation, and these salts are known to be flotation depressants (Baker and Miller, 1971). This accounts for the increase in floatability of the pyrite at low pH, as acidic conditions cause the iron salts to dissolve, but allow any elemental sulfur to remain. Whether or not a pyrite particle will be naturally floatable will depend on the flotation pH and on its oxidation history. If the oxidation favors elemental sulfur formation, the pyrite will be floatable at neutral pH, while oxidation that favors sulfate formation will result in pyrite that is not floatable at neutral pH. From the pyrite flotation experiments described, floatability at near-neutral pH is favored by slow, mild oxidation. If it is assumed that the reaction of coal-pyrite to oxidation is similar to the reaction of mineral-pyrite to oxidation, then: (1) moderately oxidized coals are the coals that are most likely to contain naturally hydrophobic pyrite; and (2) carrying out coal flotation in acidic solutions will cause the pyrite to become hydrophobic.

4.2. Conventional and column flotation of coal

From the timed-flotation data for the coal flotation it was possible to correlate the recovery of a given component (coal, ash, etc.) with the recovery of water in the froth, and to use this correlation to estimate the amount of entrainment that occurred. First, a method was needed to distinguish liberated pyrite particles from other sulfur forms. Sulfur in coal is predominantly in the form of organic sulfur and pyritic sulfur. The various microstructural forms of pyrite have been divided into the following three categories by Miller and Lin (1986): (1) liberated crystalline pyrite, consisting of single crystals with little or no attached carbonaceous material; (2) granular assemblies, consisting of aggregates of pyrite crystals, mineral matter, and carbonaceous matter in irregular masses; and (3) framboid clusters, consisting of spherical aggregates of pyrite microcrystals embedded in the coal. These can be distinguished microscopically, but for the sake of simplicity this paper will treat pyritic sulfur as being of two types: (1) liberated pyritic sulfur (liberated crystalline pyrite); and (2) unliberated pyritic sulfur (granular assemblies, and framboid clusters). The sulfur in coal can now be categorized as shown in Eq. (1):

$$\text{Total sulfur} = \text{organic sulfur} + \text{liberated pyritic sulfur} + \text{unliberated pyritic sulfur} \quad (1)$$

This equation does not account for sulfate sulfur and elemental sulfur, which are typically present only in trace amounts as oxidation products of the pyrite. For purposes of this discussion, sulfates and elemental sulfur will be considered to be part of the total pyritic sulfur.

Standard analysis techniques allow for quantitative measurement of total sulfur and pyritic sulfur, but it is difficult to differentiate between liberated and unliberated pyritic sulfur for large numbers of particles. By making the following simplifying assumptions,

it is possible to use Eq. (1) to develop a method of determining a numerical value for organic sulfur plus unliberated pyritic sulfur for a particular coal:

(1) The liberated pyrite is always less floatable than the most floatable coal particles when no collector is added. Therefore, the fastest-floating coal in the absence of collector will be free of liberated pyrite if entrainment is minimized.

(2) The locked (unliberated) pyrite and organic sulfur are distributed throughout the combustible fraction of the coal.

Given these assumptions, a value for organic sulfur plus unliberated pyritic sulfur in the combustible fraction of the coal sample can be determined by three different methods: (1) the coal can be successively refloated several times by conventional flotation to recover only the fastest floating particles; (2) the coal can be floated using column flotation, using care to eliminate entrainment, with the initial, fastest-floating, lowest-sulfur product being considered free of liberated pyritic sulfur; or (3) a heavy-liquid sink/float test can be carried out at the lowest density that will provide enough coal for analysis, with the float fraction being considered free of liberated pyrite.

Once the value for locked and organic sulfur has been determined for a sample by one of these three methods, it is possible to use Eq. (2) (derived from Hirt, 1973) to calculate the liberated pyritic sulfur content:

$$\%S_{LP} = \%S_T - \%S_{LO}(W_C) \tag{2}$$

where $\%S_{LP}$ = liberated pyritic sulfur content of the sample; S_T = total sulfur content of the sample; W_C = weight fraction of combustible matter in the sample; and $\%S_{LO}$ = locked and organic sulfur content of the combustible fraction.

From analysis of the column flotation results, the locked and organic sulfur content for this coal was found to be 1.7%. This was determined by collecting the initial, fastest-floating froth product from the flotation column, with wash-water used to minimize the entrainment. This was then analyzed to determine the sulfur content. When compared to the other froth products from the column flotation test, this initial froth was found to have the lowest sulfur content. This value was checked by a heavy-liquid separation of the feed, using a Certigrav® heavy liquid at a specific gravity of 1.35. The float product at this density was found to have a total sulfur content of 1.79% S, at a recovery of 20%wt.

A second correction was made necessary by the constant-level feature of the conventional cell. A constant froth depth is needed to keep the drainage characteristics of the froth from changing during the test. However, the addition of make-up water continuously changes the ratio of water to solids. If the cell is assumed to be a well-mixed system, a simple residence-time calculation can be used to correct for make-up water dilution, as follows (Dankwerts, 1953):

$$F(T) = 1 - e^{-R/V} \tag{3}$$

where $F(T)$ = the volume fraction of the water originally in the cell which is recovered by time T; R = total volume of water which is removed and replaced by make-up water by time T; and V = total cell volume.

Using this formula to correct for make-up water dilution, the cumulative percent recovery of the water originally in the cell can be calculated. This corrected water recovery can now be used to distinguish between entrainment and true flotation.

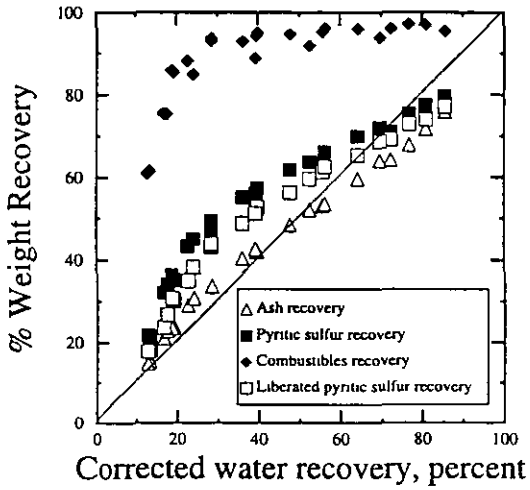

Fig. 2. Conventional timed flotation cell results, with a fixed frother dosage (0.5 kg/mt) and a varying collector dosage (0.0, 0.35, and 0.7 kg/mt). The feed coal contained 37.2% ash, 2.2% pyritic sulfur, 2.9% total sulfur, and 1.7% locked/organic sulfur. Correlations of combustible matter, ash, total pyritic sulfur, and liberated pyritic sulfur recoveries with water recovery are shown (corrected for make-up water addition using Equ. 2). Perfect entrainment would follow the 45° line.

Fig. 2 shows the correlations of combustible matter, ash, total pyritic sulfur, and liberated pyritic sulfur with the corrected water recovery for all six conventional tests. It is immediately evident that the ash shows a behavior strongly characteristic of entrainment, while the combustible matter behaves as a strongly floatable species. The pyritic sulfur behaves in an intermediate fashion, with recovery being initially slightly faster than that of water, then becoming slightly slower. When the liberated pyritic sulfur, calculated using Eq. (2), is plotted, the curve is similar to that of the pyritic sulfur (as determined using the ASTM nitric-acid leach method), and lies between the ash recovery curve and the pyritic sulfur curve. When the liberated pyritic sulfur recovery is plotted against the ash recovery (Fig. 3), it is seen that there is a good correlation between the two recoveries, and that they follow very closely the 45° line. This indicates that the recovery mechanisms for the liberated pyrite and the ash are similar.

The ash is primarily composed of fine clay particles which are expected to be strongly hydrophilic, and are well-liberated due to the high feed ash content (37.2% ash). Therefore, the ash is mainly recovered by entrainment. Since the behavior of the liberated pyrite is very similar to the behavior of the ash, this strongly implies that entrainment is the most important recovery mechanism for the liberated pyrite, as well.

Based on the data given here, it is hypothesized that, for this coal, the coal pyrite is floating due to being locked in floatable coal (incomplete liberation) and to entrainment, and not due to natural hydrophobicity of the pyrite. It appears that coal pyrites have a very low inherent floatability, and are therefore floated primarily as either locked or entrained particles, or due to formation of elemental sulfur on the pyrite surface.

Results have been reported for image analysis of coal products which were floated using release analysis to minimize entrainment (Wang et al., 1993). The image analysis of the release analysis products showed that completely liberated pyrite particles were

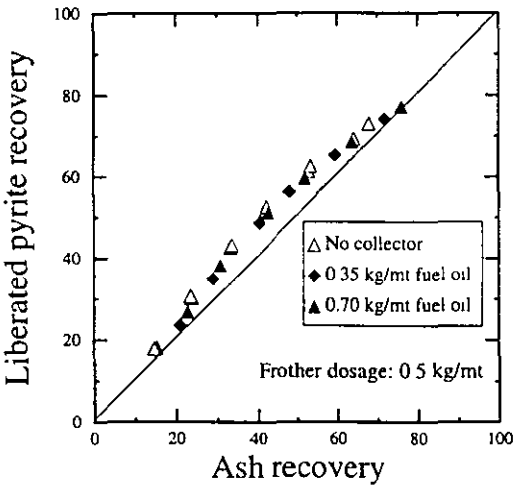

Fig. 3. Conventional timed flotation results, showing the correlation of liberated pyritic sulfur recovery with ash recovery, at a fixed frother dosage and a varying collector dosage.

scarce in the feed, and almost non-existent in the froth products. The majority of pyrite was seen to contain small inclusions of carbonaceous material, and flotation of the pyrite was attributed to the presence of these inclusions. Similarly, Miller and Lin (1986) found little liberated pyrite in their froth products, but liberated pyrite grains were the predominant form in the flotation tailings.

Referring to Table 1, it can be seen that a number of the chemicals claimed to be pyrite depressants are actually dispersants. Since dispersants act to reduce entrainment by preventing flocculation and improving froth drainage (Leja, 1982), this implies that the pyrite which is rejected more efficiently when dispersants are added is entrained pyrite, and not pyrite floating due to intrinsic hydrophobicity.

Although pyrite depressants have often been shown in the laboratory to reduce pyrite recovery, this may be a result of factors other than depression of floatable liberated pyrite particles. Pyrite depressants sometimes also act as mild coal depressants (Purcell and Aplan, 1991), and the coal particles which will be depressed first are the locked particles which include the greatest amount of gangue, since these particles have the least available hydrophobic surface area for bubble attachment. As a result, the last few percents of coal recovered during flotation carry a disproportionate amount of the total sulfur. Small decreases in the combustibles recovery will therefore produce significant reductions in the amount of pyritic sulfur which floats.

5. Conclusions

From the results presented, the following conclusions may be drawn:

(1) Freshly ground mineral pyrite is not readily floatable at neutral pH, although it becomes highly floatable at acidic pH. Pyrite oxidation normally results in the formation of sulfate sulfur, which is hydrophilic. However, if the conditions are right, it is possible

for pyrite oxidation to form elemental sulfur, which is hydrophobic. This suggests that pyrite can become naturally hydrophobic at neutral pH under certain conditions, but that this is not its normal state.

(2) Timed flotation of a freshly ground Pittsburgh seam coal in a conventional cell at near-neutral pH produced results consistent with the pyrite being recovered in the froth predominantly by entrainment and by mechanical locking with floatable coal particles. Any contribution from hydrophobic flotation of liberated pyrite appears to be minimal. This is why, even though numerous pyrite depressants have been developed, none have been accepted by the coal industry. Pyrite is not depressed in the full-scale plants, because in most cases it was not floating due to hydrophobicity in the first place.

(3) It is known that chemical pyrite depressants can only reduce the froth sulfur content in coal flotation if a significant amount of pyrite is floating due to hydrophobic bubble attachment. Since pyrite is not always naturally hydrophobic, investigators should first be certain that pyrite is being recovered by this mechanism (and not simply being entrained) before using such reagents. The contribution of entrainment can be estimated, but only if the water recovery is measured as carefully as the recovery of the other species. Such water recovery measurements should therefore be a routine part of coal flotation studies.

References

Ahlberg, E., Forssberg, K.S.E., Wang, X., 1990. The surface oxidation of pyrite in alkaline solution. J. Appl. Electrochem. 20, 1033–1039.

Arnold, B.J. and Aplan, F.F., 1990. The use of pyrite depressants to reduce the sulfur content of Upper Freeport Seam coal. In: R. Markuszewski and T.D. Wheelock (Editors), Processing and Utilization of High-Sulfur Coals, III. Elsevier, Amsterdam, pp. 171–186.

ASTM, 1988a. Standard Test Method for Ash in the Analysis Sample of Coal and Coke from Coal. 1988 Annual Book of ASTM Standards, Vol. 5.05 (gaseous fuels; coal and coke). American Society for Testing and Materials, Standard No. D3174-82.

ASTM, 1988b. Standard Test Method for Forms of Sulfur in Coal. 1988 Annual Book of ASTM Standards, Vol. 5.05 (gaseous fuels; coal and coke). American Society for Testing and Materials, Standard No. D2492-84.

Baker, A.F. and Miller, K.J., 1971. Hydrolyzed Metal Ions as Pyrite Depressants in Coal Flotation: A Laboratory Study. U.S. Bureau of Mines, Report of Investigations RI 7518.

Chander, S. and Aplan, F.F., 1989. Surface and Electrochemical Studies in Coal Cleaning. Final Report to the U.S. Department of Energy, DOE?PC/80523-T11 (DE 90007603).

Chernosky, F.J., Lyon, F.M., 1972. Comparison of the flotation and adsorption characteristics of ore and coal-pyrite with ethyl xanthate. AIME Trans. 252, 11–14.

Chmielewski, T. and Wheelock, T.D., 1991. Thioglycolic acid as a flotation depressant for pyrite. In: P.R. Dugan, D.R. Quigley and Y.A. Attia (Editors), Processing and Utilization of High-Sulfur Coals, IV. Elsevier, Amsterdam, pp. 295–308.

Chou, C.-L., 1990. Geochemistry of Sulfur in Coal, Geochemistry of Sulfur in Fossil Fuels. ACS Symposium Series No. 429, American Chemical Society.

Dankwerts, P.V., 1953. Continuous flow systems: distribution of residence times. Chem. Eng. Sci. 2, 11–14.

Drzymala, J., Markuszewski, R., Wheelock, T.D., 1991. Oil agglomeration of sulfurized pyrite. Miner. Eng. 4 (2), 161–172.

Eisele, T.C. and Kawatra, S.K., 1993. The use of horizontal baffles to improve the effectiveness of column

flotation of coal. Proc. XVIII International Mineral Processing Congress, Sydney, 23–28 May, pp. 771–778.

Elzeky, M., Attia, Y.A., 1987. Coal slurry desulfurization by flotation using thiophilic bacteria for pyrite depression. Coal Prep. 5, 15–37.

Feeley, T.J., 1991. Coal surface control for advanced physical beneficiation. In: P.R. Dugan, D.R. Quigley and Y.A. Attia (Editors), Processing and Utilization of High-Sulfur Coals, IV. Elsevier, Amsterdam, pp. 195–204

Fuerstenau, D.W , Diao, J., Hanson, J.S., 1990. Estimation of the distribution of surface sites and contact angles on coal particles from film flotation data. Energy Fuels 4, 34–37.

Hirt, W.C., 1973. Separation of Pyrite from Coal by Froth Flotation. Unpublished Master's thesis, Pennsylvania State University.

Kawatra, S.K., Eisele, T.C., 1992a. Removal of pyrite in coal flotation. Miner. Process. Extract. Metall. Rev. 8, 205–218.

Kawatra, S.K. and Eisele, T.C., 1992b. Pyrite recovery mechanisms in coal flotation. Presented at the SME Annual Meeting, Phoenix, Ariz., Feb. 24–27, Preprint No. 92–64.

Kawatra, S.K., Eisele, T.C., 1995a. Laboratory baffled-column flotation of mixed lower/middle Kittanning Seam bituminous coal. Miner. Metall. Process. 2 (2), 103–107.

Kawatra, S.K., and Eisele, T.C., 1995b. Baffled-column flotation of a coal plant fine-waste stream. Miner. Metall. Process., 12(3: 138–142.

Kawatra, S.K., Eisele, T.C. and Johnson, H., 1991. Recovery of liberated pyrite in coal flotation: entrainment or hydrophobicity? In: P.R. Dugan, D.R. Quigley and Y.A. Attia (Editors), Processing and Utilization of High-Sulfur Coals, IV. Elsevier, Amsterdam, pp. 255–277.

Laskowski, J., Bastin, M., Moon, K.S. and Sirois, L.L. 1985. Desulfurizing flotation of eastern Canada high-sulfur coal. In: Y.A. Attia (Editor), Coal Science and Technology, 9. Processing and Utilization of High-Sulfur Coals. Elsevier, Amsterdam, pp. 247–266.

Leja, J., 1982. Surface Chemistry of Froth Flotation. Plenum Press, New York.

Liu, D., Somasundaran, P. and Duby, P.F., 1993. Electrochemical equilibria in coal flotation systems and their role in determining the interfacial properties of pyrite and its separation from coal. In: B.K. Parekh and J.G. Groppo (Editors), Processing and Utilization of High-Sulfur Coals, V. Elsevier, Amsterdam, pp. 47–54.

Luo, S., McClelland, J.F. and Wheelock, T.D. 1993. The interaction of thioglycolic acid and pyrite. In: Parekh and Groppo (Editors), Processing and Utilization of High-Sulfur Coals, V. Elsevier, Amsterdam, pp. 55–70.

Lynch, A.J., Johnson, N.W., Manlapig, E.V. and Thorne, C.G., 1981. Mineral and coal flotation circuits: their simulation and control. Elsevier, Amsterdam.

Miller, J.D , Lin, C.L., 1986. Characterization of pyrite in products from the reverse flotation of coal,. Coal Prep. 2, 243–261.

Miller, J.D., Ye, Y., Jin, R., 1989. Improved pyrite rejection by chemically-modified fine coal flotation. Coal Prep. 6, 151–166.

Purcell, R.J.Jr. and Aplan, F.F., 1991. Pyrite and ash depression during coal flotation by flotation rate, recovery, and reagent control. In: P.R. Dugan, D.R. Quigley and Y.A. Attia (Editors), Processing and Utilization of High-Sulfur Coals, IV. Elsevier, Amsterdam, pp. 279–293.

Raleigh, C.E. and Aplan, F.F., 1993. The use of mineral matter dispersants and depressants during the flotation of bituminous coals. In: B.K. Parekh and J.G. Groppo (Editors), Processing and Utilization of High-Sulfur Coals, V. Elsevier, Amsterdam, pp. 71–90.

Stock, L.M. and Wolny, R., 1990. Elemental sulfur in bituminous coals. Geochemistry of Sulfur in Fossil Fuels, ACS Symposium Series No. 429, American Chemical Society.

Townsley, C.C., Atkins, A.S., 1986. Comparative coal fines desulphurization using the iron oxidising bacterium *Thiobacillus ferrooxidans* and the yeast *Saccharomyces cerevisiae* during simulated froth flotation. Process Biochem. 21 (6), 188–191.

Wadsworth, M.E., Zhu, X., Li, J., Zhong, T., Hu, W. and Bodily, D.M., 1992. Surface electrochemical control for fine coal and pyrite separation. Proc. 8th Annual Pittsburgh Coal Conference, Pittsburgh, Penn., pp. 404–411.

Wang, D., Adel, G.T., Yoon, R.-H., 1993. Image analysis characterization of pyrite in fine coal flotation. Miner. Metall. Process. 10 (3), 154–159.

Whelan, P.F., Brown, D.J., 1956. Particle–bubble attachment in froth flotation. Bull. Inst. Min. Metall. 591, 181–192.

Yancey, H.F. and Taylor, J.A., 1935. Froth Flotation of Coal: Sulphur and Ash Reduction. U.S. Bureau of Mines, Report of Investigations, RI 3263.

Ye, Y., Liu, Y., Miller, J.D. and Fuerstenau, C.D., 1990. Preliminary analysis of pyrite rejection during chemically modified fine coal flotation by conditioning with monopersulfate. In. R. Markuszewski and T.D. Wheelock (Editors), Processing and Utilization of High-Sulfur Coals, III. Elsevier, Amsterdam, pp. 159–170.

ELSEVIER

Int. J. Miner. Process. 47 (1996) 275–283

INTERNATIONAL JOURNAL OF MINERAL PROCESSING

On-line measurement of viscosity and determination of flow types for mineral suspensions

S.K. Kawatra, A.K. Bakshi

Department of Metallurgical and Materials Engineering, Michigan Technological University Houghton, MI 49931, USA

Received 19 July 1994; accepted 27 July 1995

Abstract

A viscometry system involving a vibrating sphere viscometer and a rotational viscometer has been developed for on-line measurement of viscosity, and for rheological characterization of mineral slurries into either Newtonian or non-Newtonian flows. Special precautions were taken to allow measurements of viscosity of rapidly settling mineral suspensions. Both the viscometers were able to measure viscosity as low as one centipoise, which is the approximate room temperature viscosity of water. Because the vibrating sphere viscometer operated at a much higher shear rate than the rotating viscometer, the two instruments together could determine the shear-rate dependency of the viscosity. Ground silica of 80% passing 65 μm size was suspended in water, and was used to prepare slurries at different percent solids. Viscosity of each slurry sample was measured simultaneously by both the viscometers, and the results were compared to determine the rheological characters of the slurries. With this technique, it was found that all the silica slurry samples (up to 70 wt% solids) at the given size distribution were in the Newtonian flow regime.

1. Introduction

It is known that suspension rheology affects many mineral processing operations, such as grinding and classification. However, measurement of slurry rheology using common viscometers is difficult mainly because mineral slurries contain rapidly-settling particles. If proper precautions are not taken, observations from standard instruments can lead to mistaken determinations of the fluid characteristics, and correlations between rheology and process performance will be impossible to determine (Kawatra and Bakshi, 1995).

Among the available viscometers, three basic types have been tried for slurry

0301-7516/96/$15.00 Copyright © 1996 Published by Elsevier Science B.V.
PII S0301-7516(96)00009-9

applications: (1) co-axial cylinder; (2) capillary tube; and (3) vibrating sphere type viscometers. Co-axial cylinder viscometers can measure viscosity at a particular shear rate, which can be varied by changing the rotational speed of the spindle. Because of this control in shear rate, co-axial cylinder viscometers have been very popular for many applications. However, settling of solid particles causes serious problems in these instruments, and special slurry presentation systems are needed to allow them to reliably measure slurry viscosity (Clarke, 1967; Underwood, 1976; Klien et al., 1990).

In a standard co-axial cylinder viscometer, the sample is stationary and particles can rapidly settle out of a slurry as shown in Fig. 1. Once the solids start settling, the slurry at the top becomes dilute compared to the slurry at the bottom. Then, the instrument sees a continuously changing solids content. Because of the changing viscosity arising from change in solids content, the user will wrongly interpret this as time dependency of the slurry rheology.

Several attempts have been made to prevent solids settling so that a co-axial cylinder instrument could reliably measure the viscosity of rapidly-settling slurries. These attempts generally used designs which moved slurry parallel to the rotational axis of the sensor, rapidly enough that the particles would be kept in suspension (Clarke, 1967; Underwood, 1976; Hemmings and Boyes, 1977; Reeves, 1990). However, the problem with this method is to obtain a smooth laminar flow of slurry without causing any disturbances in the sample holder (see Fig. 2). The flow of the sample should be strictly vertical, because forces in any other direction will interfere in the rotation of the spindle. In this way, a small turbulence originating from the mixing or flow of slurry will produce a shift in the viscometer reading. Klien et al. (1990) and Kiljanski (1993) have discussed separately how these disturbances (undetermined forces) from slurry mixing or recirculation will affect viscosity measurements.

Besides viscosity, another rheological parameter which is important for slurry handling is the flow type. Flow types for time independent fluids are shown in Fig. 3. Mineral suspensions show Newtonian flow behavior at dilute suspensions and non-Newtonian behavior at higher solids content. Other factors which affect the flow behavior are: (1) particle size; and (2) chemical nature, such as presence of dispersants (Schack et

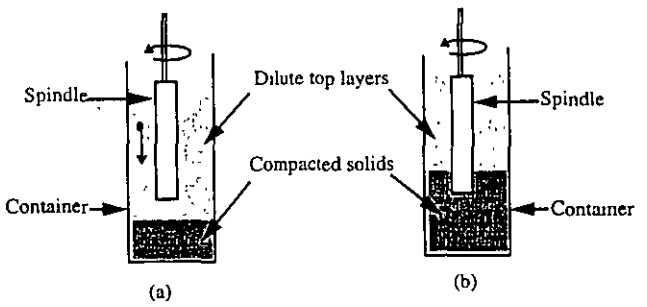

Fig. 1. Solids settling leaves a dilute suspension on the top layers of the container. When the solids content is low (a) the solids gradually settle and are compacted below the spindle and the viscometer reads progressively lower viscosity over time. At higher concentration of solids, the compacted solids can touch the spindle (b) resulting in progressive higher readings over time.

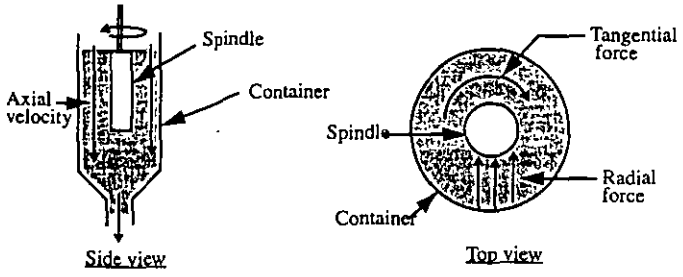

Fig. 2. The axial flow (side view) prevents the solids from settling by continuously sweeping fresh slurry past the spindle. This component of the flowing slurry stream does not affect the rotation of the spindle. But, any radial or tangential forces (top view), arising from the flow, will place additional forces on the spindle resulting in erroneous viscosity readings.

al., 1957). The knowledge of this flow type is essential in many mineral processing operations. For example, some suspensions show dilatancy and their viscosity increases with shear rate (Klose, 1984), which will result in plugging of pumps and pipelines. In grinding mills, it has been observed that optimum grinding is achieved when the slurry is pseudoplastic and does not have any yield stress (Klimpel, 1982, 1983). In hydrocyclone classifiers, it has been shown that the cut size changes with viscosity (Kawatra and Eisele, 1988).

Another important reason to know the flow type is that viscometers generally do not measure the viscosity at the shear rate that prevails in operations such as grinding, pumping, or classification. Since viscosity of non-Newtonian fluids depends upon the shear rate, viscosity cannot be correlated to equipment performance when the shear rates are different. Thus, the flow type must be measured before making correlations between viscosity and equipment performance. For example, in an hydrocyclone experiment with a 10.2 cm (4″) cyclone in the MTU laboratories, the maximum shear rate inside the cyclone was calculated to be 508 s^{-1}, while the Brookfield viscometer operated at shear rates below 74 s^{-1}. The viscosities measured by the Brookfield instrument therefore can only apply to the cyclone performance if the slurry is Newtonian. Also, the shear rate

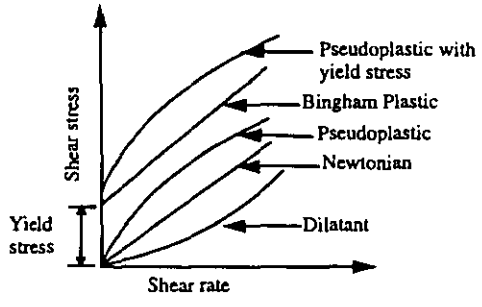

Fig. 3. Generalized time-independent rheology curves for mineral slurries. The ratio of shear stress and shear rate is the apparent viscosity. This ratio is constant for Newtonian fluids. The apparent viscosity decreases with increase in shear rates for pseudoplastic fluids and increases with increase in shear rates for dilatant fluids.

inside a cyclone varies a great deal from point to point (Bradley, 1965), and so no measurement of viscosity at a single shear rate can accurately reflect the conditions in a hydrocyclone when a slurry is non-Newtonian.

In this article a viscometry system is described, composed of a vibrating sphere viscometer used in combination with a rotational viscometer. The vibrating-sphere viscometer operates at a very high shear rate. This viscometer is insensitive to most turbulence, and can easily measure the viscosity of well-mixed slurries. The rotational viscometer used was modified to allow it to reliably measure the viscosity of slurries at low shear rates.

2. Methods and materials

2.1. System development

As pointed out earlier, viscosity of a Newtonian fluid is not affected by shear rates, but for non-Newtonian fluids the viscosity changes when the shear rate changes. Thus, by measuring the viscosity at two different shear rates sufficiently apart from each other and comparing the two values, the fluid can be designated as Newtonian if both the measured viscosities are similar, and non-Newtonian if the viscosities are different. Based on this concept, a new system was developed to determine the flow characteras-tics of mineral slurries. The two viscometers used for this purpose were a Brookfield (co-axial cylinder) viscometer and a Nametre (vibrating sphere) viscometer. In this system the Brookfield viscometer operated at a much lower shear rate than the Nametre viscometer. Thus, for Newtonian fluids readings from both the viscometers remained the same, and for non-Newtonian fluid the two instruments produced different readings.

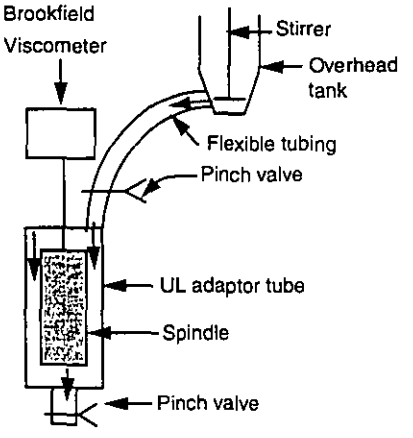

Fig. 4. Brookfield viscometer set-up showing the UL adaptor assembly and the slurry presentation system. This arrangement is very suitable for dilute suspensions, and could measure apparent viscosities of silica slurries up to 70% solids by weight in water without any difficulty.

2.1.1. The rotational viscometer

A Brookfield viscometer (DV-I model) was used to measure apparent viscosity at low shear rates (below 74 s^{-1}). The UL adaptor spindle was used for suspensions with a viscosity less than 10 centipoise, and the LV # 1 spindle was used for samples with viscosities above 10 centipoise. The UL adaptor consisted of a cylindrical spindle, and a tube which houses the spindle. The sample was placed in the annular space between the spindle and the tube to measure its viscosity. Solids were kept in suspension while the reading was taken by using the slurry presentation system shown schematically in Fig. 4. Slurry was mixed in an overhead tank, and passed continuously through the annular space between the UL spindle and the tube. After a steady state reading was displayed, flow was momentarily interrupted to eliminate any swirling motion caused by the flow at the inlet, and the reading was taken immediately. For denser suspensions (above 10 centipoise), the UL spindle was replaced by a LV # 1 spindle and rest of the parts in the setup were not changed. Although the Brookfield viscometer could operate at different shear rates, it was not sufficient by itself to determine the rheological type, because the instrument range was only sufficient for making one or two readings over closely-spaced shear rates.

2.2. The vibrating sphere viscometer

The vibrating sphere viscometer used for this study was manufactured by the Nametre Corporation, Metuchen, NJ. It consisted of a spherical probe, which oscillated along a vertical shaft at its resonant frequency of 750 Hz and a constant amplitude of 1 micron. When immersed in a fluid, the probe created a shear wave, and the fluid dampened the oscillatory motion. The damping, or the power to restore constant amplitude was a measure of the apparent viscosity of the fluid. Since the probe vibrated rather than rotating in a single direction, the shear rate was a sinusoidal function of time.

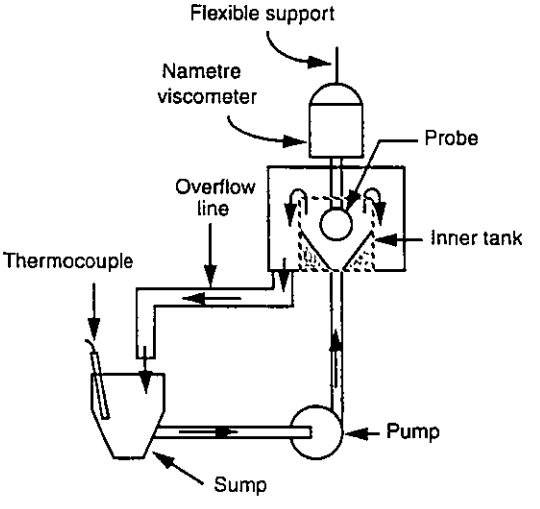

Fig. 5. Nametre set-up showing the special arrangement for slurry presentation. This arrangement is very suitable for suspensions with rapidly settling particles.

Also, the probe was spherical in shape, therefore its vibration had its maximum amplitude at the equator and gradually dropped to zero at the poles (Ferry, 1977). For these reasons, the Nametre viscometer did not operate at a specific shear rate, but averaged the shear rates from zero to the maximum value. The maximum shear rate was not a definite constant for the instrument because it was a function of the velocity of propagation of the shear wave in the fluid, which in turn depended upon the fluid viscosity (Ferry, 1977; Kawatra and Bakshi, 1995). A special slurry presentation system was built for this instrument as shown in Fig. 5. This was comprised of a vessel of two concentric cylinders, with the bottom of the inner cylinder made conical to avoid solids settling. The outer cylinder was one inch taller than the inner cylinder to prevent spillage of fluid. Slurry overflowed from the inner cylinder to the outer cylinder and then returned to the sump. The viscometer was suspended from the top by a cable, and the probe of the viscometer was immersed inside the inner cylinder. This arrangement prevented problems with vibration and excessive fluid drag on the sensor. A thermocouple was placed inside the sump, and both viscosity and temperature of the sample were recorded simultaneously.

2.3. Materials used

2.3.1. Sucrose solutions

Sucrose solutions show Newtonian flow properties. Six different solutions with 10 to 60 wt% sucrose in distilled water were used to confirm that both of the viscometers would register the same viscosity with Newtonian fluids.

2.3.2. Methylcellulose solutions

Methylcellulose is a water soluble polymer. Four solutions of methylcellulose at 0.5%, 1.0%, 1.5% and 2.0% concentrations by weight in water were prepared. These solutions display pseudoplastic flow behavior and were used to verify the system's ability detect non-Newtonian behavior.

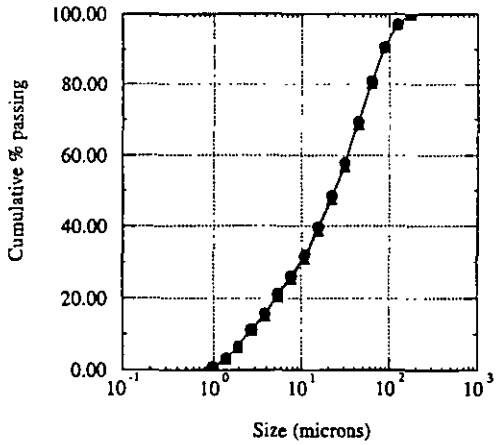

Fig. 6. Particle size distribution of the silica samples. Multiple samples in each category were measured with a Microtrac size analyzer with excellent reproducibility.

2.3.3. Silica slurries

Silica from the Ottawa Sand Co., IL, with the size distribution given in Fig. 6 was used to prepare slurry samples ranging from 0 to 70% solids by weight in distilled water. The d_{80} size of the silica sample was 65 μm.

3. Results and discussion

3.1. Calibration of the system with known solutions

Readings from the Nametre viscometer for sugar (sucrose) solutions and methylcellulose solutions were plotted against the readings from the Brookfield viscometer (Fig. 7). Since sucrose solutions were Newtonian, viscosity readings from both the Nametre (high shear rate) and the Brookfield (low shear rate) viscometers were similar for these solutions. For methylcellulose solutions, apparent viscosity values obtained from the Nametre viscometer were less than their corresponding values from the Brookfield viscometer showing that apparent viscosity decreased with increasing shear rate. This was expected from methylcellulose solutions, because these are known to be pseudoplastic fluids. This shows that the system could distinguish between Newtonian and non-Newtonian fluids.

3.2. Viscosity measurements for silica suspensions

After calibrating the system with known Newtonian (sucrose) and non-Newtonian (methylcellulose) solutions, tests were conducted with silica–water slurries at different percent solids. Viscosities of these slurries were measured by both the Nametre and

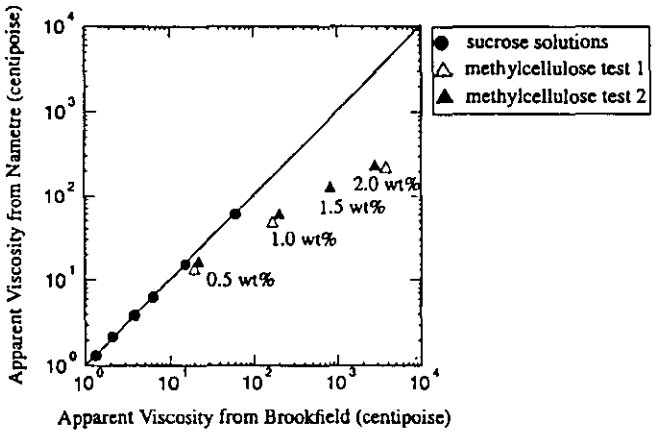

Fig. 7. Reading from the Nametre viscometer vs. reading from the Brookfield viscometer for sucrose solutions (from 10 to 60 wt% sucrose) and methylcellulose solutions (from 0.5 to 2.0 wt% methylcellulose) in water.

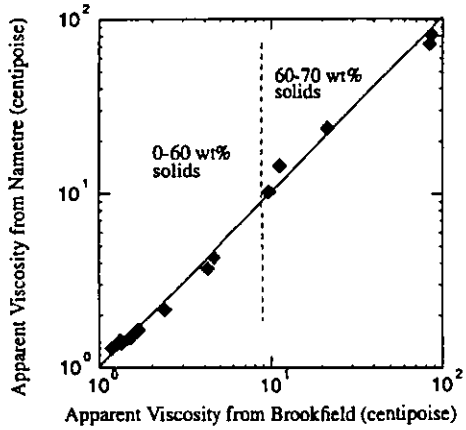

Fig. 8. Comparison of apparent viscosities of silica slurries at different percent solids, as measured by the Brookfield and the Nametre viscometers. For all the slurries (10–70 wt% solids) the readings from both instruments are similar, therefore these slurries are Newtonian.

Brookfield viscometers, with the results as shown in Fig. 8. For all the silica slurries, measurements from both the viscometers were in close agreement with each other, indicating that these slurries were Newtonian up to at least 70% solids by weight.

4. Conclusion

The following conclusions were drawn from these tests:

(1) The system suggested in this article eliminated the solids settling problem, and produced reproducible measurements of slurry viscosities in the laboratory.

(2) This system could measure the viscosities of silica slurries up to 70 wt% solids, and simultaneously provided a simple method to distinguish between Newtonian and non-Newtonian flow types. The flow type of all the silica slurries used in this study was found to be Newtonian.

(3) While the system does not give extreme details about the rheological type of the slurry, the measurement is quite rapid and reproducible, and so it is suitable for routine plant monitoring to detect changes in rheological type. Since such changes can have profound effects on plant operations, this technique has many potential applications.

Acknowledgements

Part of the funding for this project was obtained from the Dow Chemical Company, Midland, Michigan and the Department of the Interior's Mineral Institute program administered by the United States Bureau of Mines through the Generic Mineral Technology Center for Comminution under grant number G1125149. This paper was published without prior review by the Bureau of Mines.

References

Bradley, D., 1965. The Hydrocyclone. Pergamon Press, New York, NY.

Clarke, B., 1967. Rheology of coarse settling suspensions. Trans. Inst. Chem. Eng., 45: T251–T256.

Ferry, J.D., 1977. Oscillation viscometry — effects of shear rate and frequency. Meas. Control, 11(5): 89–91.

Hemmings, C.E. and Boyes, J.M , 1977. An on-line viscometry technique for improved operation and control of wet grinding circuits. In: Twelfth International Mineral Processing Congress, Sao Paulo, pp. 46–64.

Kawatra, S.K. and Bakshi, A.K., 1995. On-line viscometry in particulate processing. Miner. Process. Extract. Metall. Rev., 14: 249–273.

Kawatra, S.K. and Eisele, T.C., 1988. Rheology effects in grinding circuits. In: XVI International Mineral Processing Congress. Elsevier, Amsterdam, pp. 195–207.

Kiljanski, T., 1993. On the measurement of the rheological properties of unstable mineral suspensions. Coal Prep., 13: 107–112.

Klien, B., Partridge, S.J. and Laskowski, J.S., 1990. Rheology of unstable mineral suspensions. Coal Prep., 8(3–4): 123–134.

Klimpel, R.R., 1982. Slurry rheology influence on the performance of mineral/coal grinding circuits. Part I. Min. Eng., 34(12): 1665–1668.

Klimpel, R.R., 1983. Slurry rheology influence on the performance of mineral/coal grinding circuits. Part II Min. Eng., 35(1): 21–26.

Klose, R.B., 1984. Densecoal — an alternative to gas and oil. In: Proceedings of the Sixth International Symposium on Coal Combustion and Technology, Orlando, FL, pp. 791–805.

Reeves, T.J., 1990. On-line viscosity measurement under industrial conditions. Coal Prep., 8: 135–144.

Schack, C.H., Dean, K.C. and Molly, S.M., 1957. Measurement and Nature of the Apparent Viscosity of Water Suspensions of Some Common Minerals. Report of Investigations, U.S. Bureau of Mines, 5334, pp. 1–16.

Underwood, W.M., 1976. Viscometer for slurries and suspensions. Rev. Sci. Instrum., 47(9): 1079–1082.

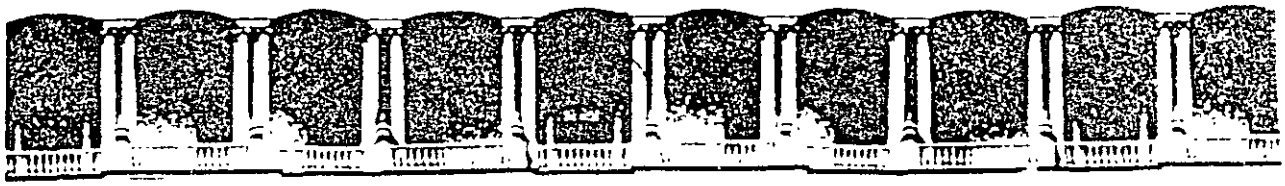

FACULTAD DE INGENIERIA U.N.A.M.
DIVISION DE EDUCACION CONTINUA

CURSOS ABIERTOS

DESARROLLO Y OPERACIÓN DE SENSORES PARA CONTROL DIRECTO Y CONTINUO EN PLANTAS DE BENEFICIO DE MINERALES Y EN LA RESTAURACIÓN DEL MEDIO AMBIENTE

Del 18 al 23 de mayo de 1998

TEMA: PARTICLE SIZE MEASUREMENT

EXPOSITOR :DR. KOMAR KAWATRA

1998

Particle Size Measurement

In industrial particulate processing, characterization of the particle sizes over the range from 1000 microns to 0.5 microns is of critical importance, as the particle size distribution controls the flow and packing characteristics, and strongly affects the surface area and chemical reactivity. The selection of an appropriate method for measuring the particle size depends upon both the particle size range of interest, and on the characteristics of the particles. A technique for the measurement therefore cannot be considered in isolation, but must take into account the form of the particles in the process. For example, to monitor the particle size of particles in an aqueous slurry which has a high volume flowrate, a method such as ultrasonic absorption would be selected. If, on the other hand, the powder is a water-reactive solid such as cement, a technique is needed which does not require the particles to be suspended in water.

Particle size measurement techniques also differ greatly in their speed, and their degree of shear. Methods which require very long times to complete a measurement, and have a low level of shear, allow particles to agglomerate. This results in a larger apparent particle size than would be measured by a rapid, high-shear-rate measurement technique.

Particle Size of Irregularly Shaped Particles

The size of a spherical particle can be uniquely defined by its diameter, and so it is easy to state its size unambiguously. The size of a cube can also be readily defined as the length of an edge. However, such ideal particles are rarely encountered in particulate processing, and so an unambiguous definition of "particle size" becomes difficult. There are numerous methods for assigning a particular size to an irregularly shaped particle, with the method selected depending both on the size measurement technique used, and on the application of the information. Several of the most important methods for defining size are as follows:

- Projected area. This can be considered as the area of the shadow that would be cast by the particle. For irregular particles, the value of the projected area will vary, depending on the orientation of the particle. This is of particular importance for particles that will be used for paint pigments, as it will determine their "hiding power" on a surface.
- Total surface area. This is the total area that the particle surface would have if it could be flattened out into a plane surface. This is of particular importance for determining the chemical reactivity of the particles, and is critical for catalysts and for powders to be used for making cement.
- Stokes diameter. This is used for size measurement methods which determine particle sizes based on their settling rate in a fluid. The terminal settling velocity of an irregularly-shaped particle is compared with the settling rates for spheres of the same density, and the Stokes diameter is the diameter of the sphere that has the same settling rate as the particle being measured.
- Sieve diameter. This is the size of the smallest opening that the particle can go through without deforming or fracturing, and is related to the minimum projected area for the particle.

Sieve Analysis

Sieving is an obvious, straightforward method form measuring particle size, and is discussed extensively in *Mineral Processing Technology*, by B. A. Wills. The simplest sieves are made by

weaving wire into a square grid, leaving openings of a precise size. Sieves are often referred to by their *mesh size*, which is the number of openings per linear inch, as shown in Figure 3.1:

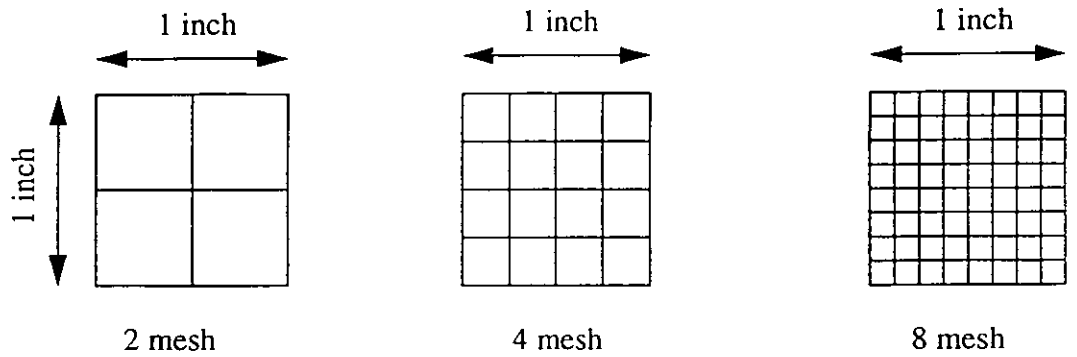

Figure 3.1: Definition of "mesh size."

However, the size of the opening for a given mesh size will obviously depend on the diameter of the wire used to weave the sieve, and so a number of different sieve series have been defined that use different wire thicknesses. In recent years, there has been a trend to express sieve size as the width of the opening in micrometers, to avoid ambiguity.

The *Tyler sieve series* is one of the common sieve series in use. It is defined based on a standard of 200 mesh = 74 micrometers. Coarser and finer sieve sizes are defined so that the ratio of the sizes of screens is the square root of 2. A Tyler fine sieve series is also defined that sets the ratio of subsequent screens at the fourth root of 2, which gives closer resolution of the particle size distribution because the sieve sizes are more closely spaced.

The results from a sieve test are generally presented in a tabular form, as shown in Table 3.1:

Table 3.1: Example of a sieve analysis

Sieve Size (Tyler Mesh)	Sieve Size (microns)	Nominal Size (microns)	Weight Retained (grams)	% Weight Retained	Cumulative %Wt. Passing
+48	296		0.02	0.1	99.9
48x65	209	250	1.32	2.9	97.0
65x100	148	180	4.23	9.5	87.5
100x150	105	125	9.44	21.2	66.3
150x200	74	90	13.10	29.4	39.9
200x270	52	63	11.56	26.0	10.9
-270	-52	26	4.87	10.9	

Once the particle sizes have been determined, there are several methods of presenting the complete size distribution as a graph. The type of plot selected depends on the information that is wanted, and the most common plots are discussed below:

- **Histogram:** The most straightforward plot is a histogram of the percent weight retained for each size fraction, as shown in Figure 3.2. Such a plot most clearly shows the physical significance of the data, and makes it simple to find the modal size (most common size). However, it is difficult to make an easily-expressed, meaningful comparison of the histograms for two different size distributions.

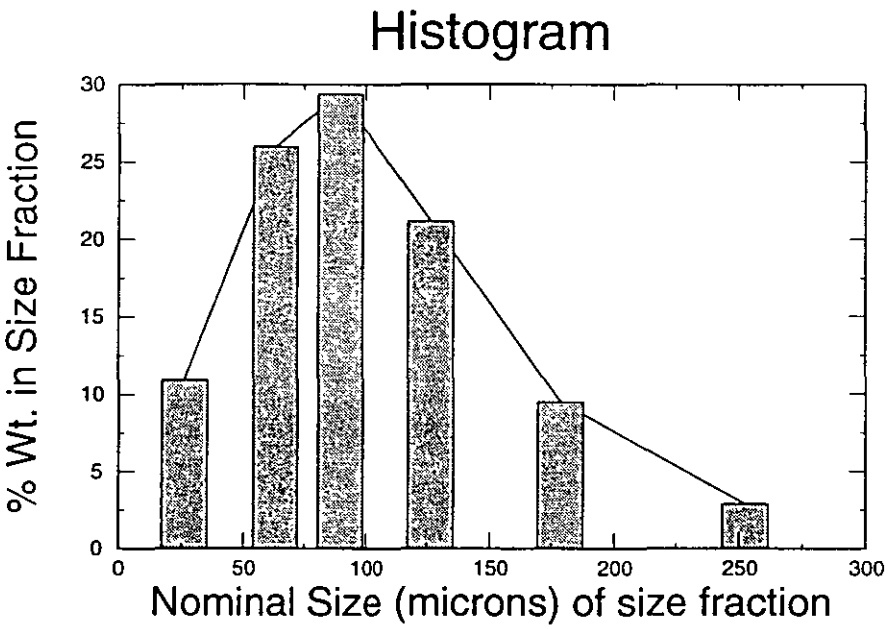

Figure 3.2: Histogram of data from Table 3.1

- **Rosin-Rammler Distribution:** The Rosin-Rammler Distribution is obtained from the equation

$$100 - P = 100 \cdot exp(-(b \cdot d^n)) \tag{3.1}$$

or

$$ln(ln(\frac{100}{100 - P})) = ln(b) + n \cdot ln(d) \tag{3.2}$$

where n= constant
b= constant
d= nominal sieve size, and
P= cumulative percent weight passing the size d

Special Rosin-Rammler graph paper is available, where the above equation becomes a straight line with a slope of n and a y-intercept of ln(b). Such a plot can also be made using standard rectangular or semi-log graph paper as shown in Figure 3.3, by plotting the parameters:

$$x = ln(d)$$

$$y = ln(ln(\frac{100}{100 - P})) \tag{3.3}$$

The parameters b and n can then be used to compare different size distributions, and to provide a compact description of the complete size distribution.

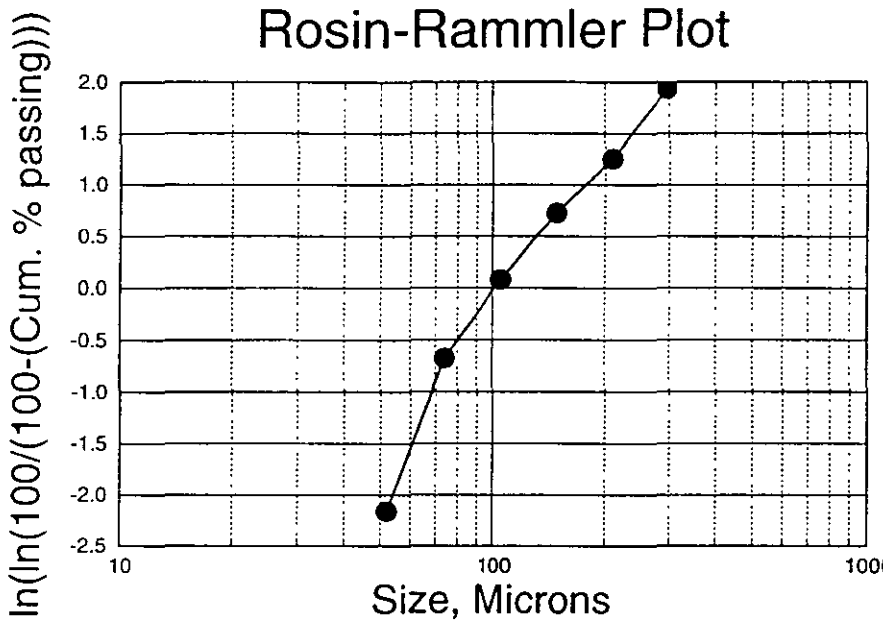

Figure 3.3: Rosin-Rammler Plot of data from Table 3.1

- Gates-Gaudin-Schumann Distribution: This is also a method for causing the plot of cumulative percent passing versus size to approximate a straight line. The cumulative percent weight passing each sieve is plotted versus the nominal sieve size on log-log graph paper, as in Figure 3.4, or the logarithms of these values are plotted on rectangular graph paper. The plot can then be approximated by a line with the equation:

$$y = 100\,(\frac{x}{k})^{\alpha} \tag{3.4}$$

where x= sieve size
y= cumulative percent passing
α= distribution modulus
k= size modulus

If the logarithm is taken of this equation, it is seen that it reduces to a linear form;

$$ln(y) = (ln(100) - (\alpha \cdot ln(k)) + \alpha \cdot ln(x)) \tag{3.5}$$

with α being the slope of the line. Further, when y=100, we find that

$$1 = \frac{x^{\alpha}}{k} \tag{3.6}$$

and that therefore x=k. So, the size modulus k corresponds to the x-intercept of the line.

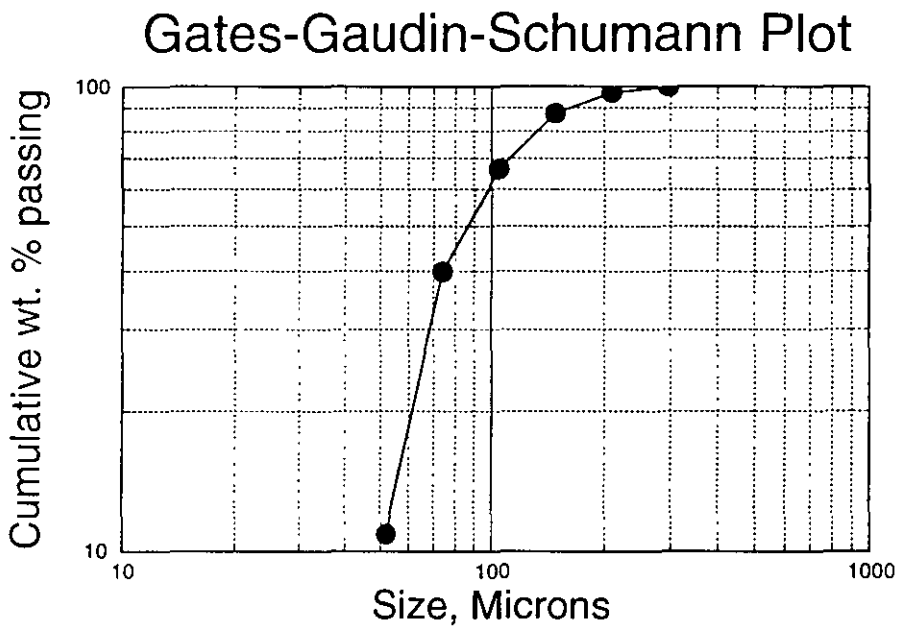

Figure 3.4: Gates-Gaudin-Schumann Plot of data from Table 3.1

Wet Screening versus Dry Screening

If a powder contains a significant fraction of material finer than approximately 74 microns, it is likely to cake badly during dry screening, and will not pass through the screen. In this situation, a liquid (usually water) is used to suspend the solids and prevent caking, and to wash the finest particles through a screen finer than 74 microns. The coarse material retained on the screen can then be dried, and screened easily without interference from the fine particles. Some materials, such as coal, are poorly wetted by water, and a wetting agent such as alcohol is needed to effectively wet-screen these materials using water as the dispersing liquid. Water-reactive powders, such as cement, can only be wet-screened using non-aqueous liquids such as kerosine.

Industrial Screening

Many types of industrial screen are available for various applications, and are discussed extensively by Wills (1994). A general classification of the various screen types is given in Figure 3.5.

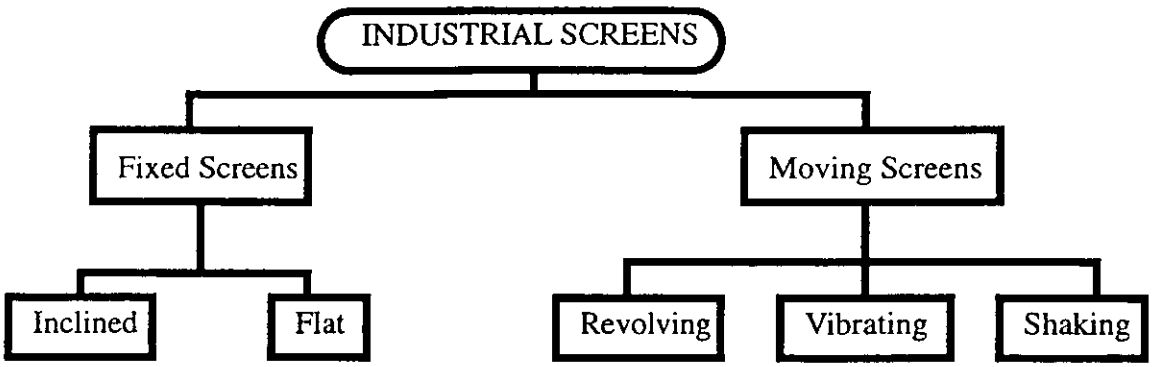

Figure 3.5: Basic types of industrial screens.

Screen Surfaces

Three basic types of screen surfaces are used in industrial screens, depending on the degree of durability and open area required:

- Parallel Rod: Mainly used for coarse scalping screens ("Grizzlies")
- Punched Plate: Used for coarse screening, where greater accuracy than the parallel rod design is desired.
- Woven Wire: Used in finer screening, where minimum open area and low cost per opening are desired.

Revolving Screens

These screens have the following characteristics:

- Low capacity (0.3-2 tons/sq.ft/hr), because most of the screen surface is not in contact with the material being screened at any given time.
- Low efficiency
- Large size
- Most useful for removing elongated tramp material and trash from the ore.

Vibrating Screens

The characteristics of these screens are:

- Capacity of 5-20 tons/sq. ft./hr
- Small vibration amplitude (1/8" to 3/8")
- High vibration frequency (800-3600 /min)
- Good material-flow characteristics, even with thick slurries
- Low slope
- Less screen blinding than other types.

Shaking Screens

- Capacity of 2-8 tons/sq.ft/hr
- Large shaking amplitude (2" to 8")
- Low shaking frequency (100-200 /min)
- Most useful for soft materials

Industrial Screening Performance

The performance of an industrial screen depends on many factors, not all of which can be controlled. Some of the most important factors are listed below:

- Relative sizes of particles and screen openings
- % open area of screen
- Incidence angle of fresh feed relative to the screen
- Rate of travel of material across screen
- Thickness of particle layer on screen
- Tautness of screen surface
- Kinetic energy of particles
- Shape of screen apertures
- Nature of particle motion on screen
- Corrosion of screen
- Moisture content of feed
- Stickiness of feed
- Tendency of particles to blind sieve openings
- Fraction of particles with size near that of the screen openings
- Electrostatic charge

Microscopy

Microscopy is a powerful tool to determine size and shape of particles. It is the only technique where various particles are observed and measured individually. The primary limitation of particle characterization by microscopy is that only a limited number of particles can be observed, which introduces difficulties in making measurements that are closely representative of the entire powder sample. The useful size ranges for several microscopic techniques are shown in Table 3.2

Table 3.2: Size ranges for various types of microscopy.

Method	Nominal Size Range (microns)
Visible Light	0.4 - 150
Ultraviolet Light	0.1 - 100
Transmission Electron Microscopy	0.001 - 5
Scanning Electron Microscopy	0.02 - 1000

The applications of microscopy will be covered in some detail in later courses.

Sedimentation Techniques

Sedimentation is one of the most commonly used techniques for analysis of mineral processing products that fall into the sub-sieve size range (less than approximately 50 micrometers). The particle sizes are calculated based on their terminal settling velocities in a liquid, based on Stokes Law:

$$v = \frac{g d^2 (\rho_s - \rho_l)}{18\mu} \tag{3.7}$$

where v= terminal velocity of particle (cm/sec)
g= acceleration due to gravity (cm/sec^2)
d= particle diameter (Stokes diameter) (cm)
μ= coefficient of absolute viscosity for the fluid (poise)
(water viscosity at 23°C is 0.01 poise)
ρ_s = density of solid particle
ρ_l= density of liquid

Stokes' Law is valid for non-interacting spherical particles settling through a fluid at their terminal velocity under laminar flow conditions. For the flow around the particle to be laminar, the Reynolds Number, R_e, as calculated from the expression

$$R_e = \frac{\rho d v}{\mu} \tag{3.8}$$

must be less than 0.2.

The need for laminar flow makes this technique most suitable for particles finer than 50 microns. Particle size measurements by sedimentation can be quite time-consuming if there are significant amounts of particles finer than 1 micron. For example, alumina particles 10 microns in diameter will settle 1 cm in about 1 minute, while a 1 micron diameter particle will settle 1 cm in about 2 hours.

Example Calculations:

A. Calculating settling velocity from size

Given:

Particle Size = 50 μm
$\rho_s = 2.65$ gm/cm^3
$g = 980$ cm/sec^2
$\mu = 0.01$ poise (water, 23°C)
$\rho_l = 1.0$ (water)

Calculate the terminal velocity of the particle by Stokes' Law, assuming the particle is essentially spherical. Calculate the Reynolds number to determine whether Stokes' Law is valid in this case.

Solution:

$$v = \frac{gd^2(\rho_s - \rho_l)}{18\mu} = \frac{980 \times (0.005)^2 \times (2.65 - 1)}{18 \times 0.01}$$

$$= 0.225 \text{ cm/sec}$$

$$R_e = \frac{\rho d v}{\mu} = \frac{1 \times 0.005 \times 0.225}{0.01}$$

$$= 0.113$$

Since the Reynolds number is less than 0.2, the calculated terminal velocity of 0.225 cm/sec for this particle is valid.

B. Calculating size from settling velocity

Given:

Terminal Velocity = 11 cm in 37 sec
Other conditions as in Example A, above

$$v = \frac{gd^2(\rho_s - \rho_l)}{18\mu} = \frac{980 \times d^2 \times (2.65 - 1)}{18 \times 0.01} = \frac{11}{37}$$

$$d = 0.00575 \text{ cm} = 57.5 \text{ microns}$$

$$R_e = \frac{\rho d v}{\mu} = 1 \times \frac{(0.00575)}{0.01} \times \frac{11}{37}$$

$$= 0.1710$$

So, Stokes' Law is valid for this case, and the calculated Stokes Diameter is correct.

C. Calculating size relative to a reference size

Given that the settling velocity of a 50 μm quartz particle in water is 0.225 cm/sec, what will be the settling velocity of a 100 μm quartz particle?

Solution: From Stokes' Law,

$$\frac{v_1}{d_1^2} = \frac{v_2}{d_2^2}$$

$$v_1=(100^2)(0.225/(50^2)) = 0.9 \text{ cm/sec}$$

$$R_e = \frac{\rho d v}{\mu} = \frac{1 \times 0.01 \times 0.9}{0.01}$$

$$= 0.90$$

The Reynolds number is now greater than 0.2, so the calculated settling velocity will not be correct.

Considerations For Using Stokes Law to Determine Particle Size

- Stokes Law is valid for free settling only. It is not valid for concentrated suspensions where the particles interact with each other when they settle.
- Sedimentation can be used for measuring the size of coarser particles by using a more viscous fluid. This reduces the settling velocity, and makes the Reynolds number smaller.
- Sedimentation cannot be used when particles are so fine that Brownian motion is significant.
- Masses of flocculated particles will behave as if they were single large particles. These floccules can be broken up with dispersing agents. Several common examples are given in Table 3.3:

Table 3.3: Dispersing agents used for various solid particle/fluid combinations

Type of Solid Particles	Suspending Liquid	Dispersing Agent
Alumina (alpha)	Water	Sodium Hexametaphosphate (0.1% by weight)
Alumina (beta)	N-propanol	Citric Acid (0.1% by weight)
Cement	Kerosine	Oleic Acid
Kaolin	Water	Sodium Silicate
Titanium Dioxide	Water	Sodium Pyrophosphate

- When using a sieve, the particle is classified by size and shape *alone*. When using fluid classification, the particle is classified by size, shape, *and density*. Since denser particles settle faster than less dense particles, small-diameter high-density particles will behave the same in a fluid classifier as larger-diameter, low-density particles. This leads to the definition of the *Free Settling Ratio: the ratio of the radii or diameters of particles of different densities that achieve the same terminal velocity under free settling conditions*. Mathematically, this is expressed as:

$$\sqrt{\left(\frac{\rho_{s1}-\rho_l}{\rho_{s2}-\rho_l}\right)} = \frac{d_2}{d_1} \qquad (3.9)$$

The normal convention is that these ratios are written to give a value greater than 1.

Sedimentation Methods

There are several types of apparatus that measure particle size based on the settling rate of the particles in a fluid. These vary widely in their cost and ease of use.

Andreason Pipette

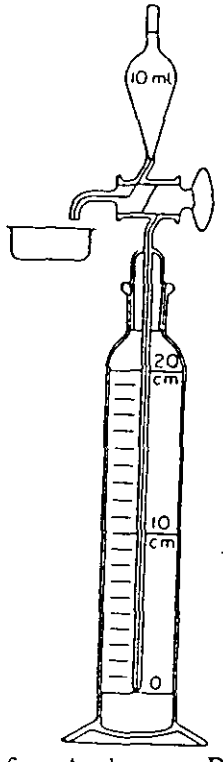

Figure 3.6: Schematic of an Andreason Pipette

This device was developed by Andreason and his colleagues in 1930. The apparatus is shown in Figure 3.6. The following procedure is used to measure particle size with this device;

- Add the solids and water to the pipette, and mix the particles thoroughly with the liquid by shaking. This will make a homogenous suspension.
- Immediately withdraw 10 ml of the suspension, from a depth of 20 cm.
- At selected time intervals, remove additional 10 ml samples of suspension.
- Evaporate the liquid from each sample, and weigh the solid residue. Standard tables are available, which are then used to determine the particle size distribution from this data.

The advantages of this method are that the apparatus is very simple, and is low cost compared to other particle size measurement methods. The main disadvantages are that it is very time consuming, and that the suspension is disturbed whenever a sample is removed, which distorts the results (Herbst and Sepulveda, 1985)

Automatic Sedimentometers

Several types of automated sedimentometer are available. These units automatically disperse the particles in the desired liquid, and then measure the density of the suspension as a function of time at some point in the settling chamber. The unit determines the suspension density by shining an X-ray beam through the settling chamber, and measuring the absorption of the X-rays by the suspension. A schematic of such a unit is shown in Figure 3.7

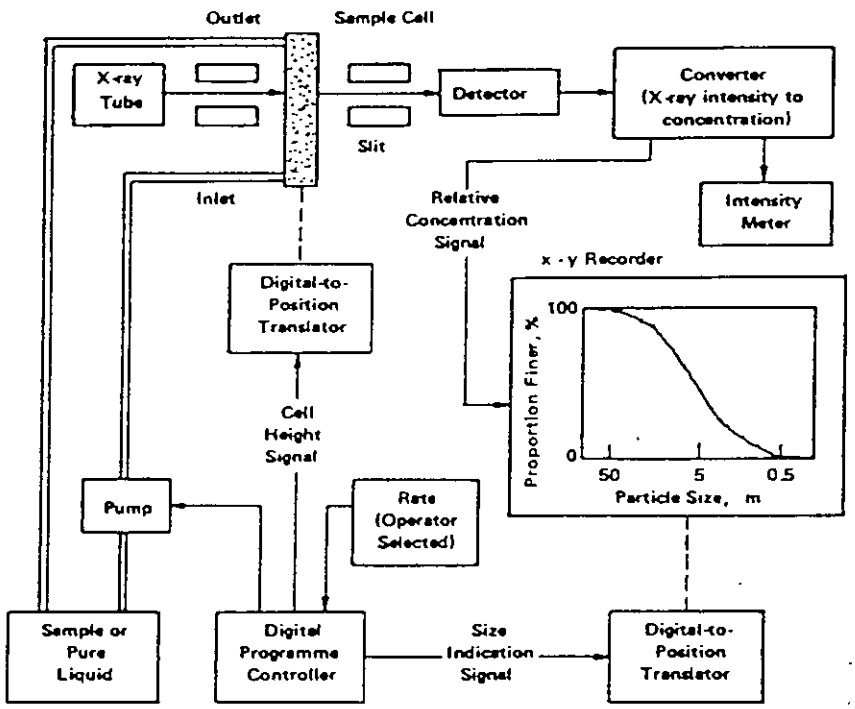

Figure 3.7: Schematic of an automatic sedimentometer

Elutriation Methods

Elutriation is very similar to sedimentation, except that in elutriation the particles remain stationary while the fluid moves, while in sedimentation the fluid remains stationary while the particles move. The main benefit of elutriation is that it can be used to divide a size distribution into clean, single-size fractions. The main disadvantage is that it uses a tremendous amount of fluid.

Teeter Tubes

The most basic elutriation device is the teeter tube. This is a vertical tube, which steadily increases in cross-section, as shown in Figure 3.8. Water is injected at the base of the tube at a

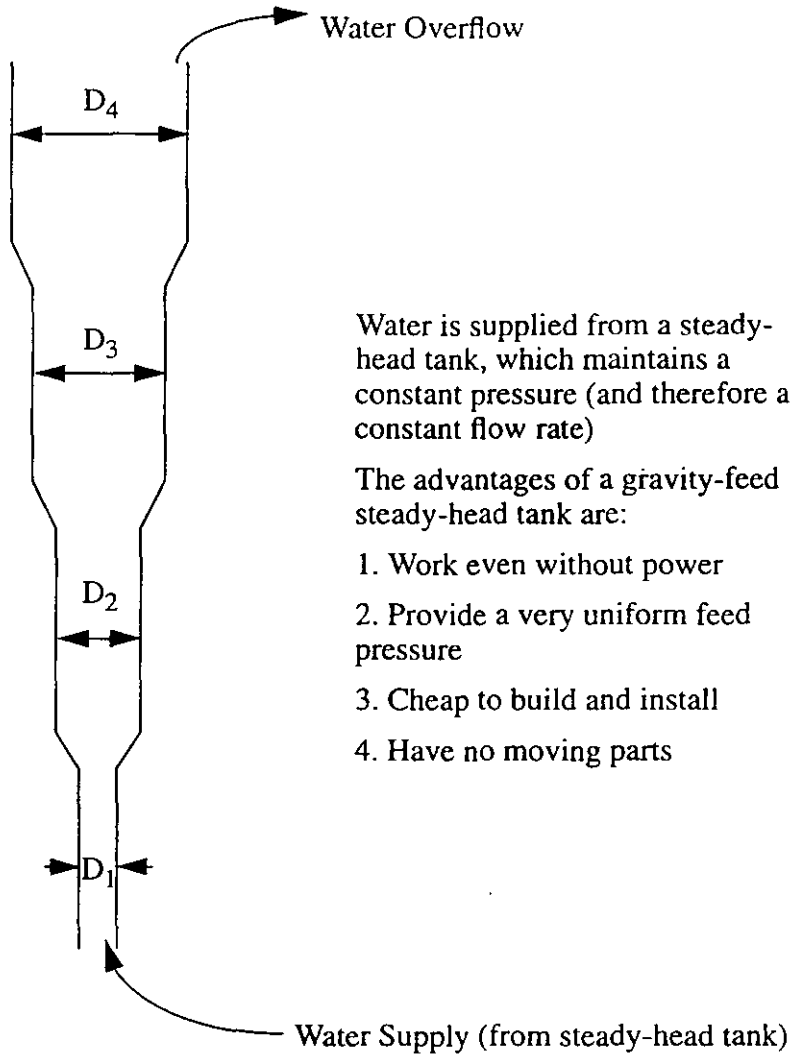

Figure 3.8: Schematic of a basic Teeter Tube

steady pressure and flow rate. As the liquid flows upward in the tube, its flowrate decreases as the tube diameter increases. The coarsest particles, with the highest settling rates, accumulate in the bottom sections of the tube, while the finest particles accumulate in the upper sections.

The upward velocity of the water in the tube at any given point can be calculated as follows:

$$V = \frac{Q}{A} \tag{3.10}$$

where V= fluid velocity
Q= total volume flowrate
A= cross-sectional area

Since Q must be constant throughout the entire tube, this means that $A \propto \frac{1}{V}$, and so $\frac{D^2}{4} \propto \frac{1}{V}$

Using this, it is straightforward to calculate what the diameters of the tube sections must be to produce size fractions in a standard $\sqrt{2}$ size series.

Let d be the particle diameters, and $d_1 = \sqrt{2} \times d_2$. From Stokes Law, we know that

$$V = \frac{d^2 g (\rho_s - \rho_l)}{18\mu} \tag{3.11}$$

Since $d^2 \propto V$, or $\sqrt{V} \propto d$, we can calculate that when $\frac{d_1}{d_2} = \sqrt{2}$, it must be true that $\frac{V_1}{V_2} = 2$

Since the volume flowrate, Q, is constant, we know that $A_1 V_1 = A_2 V_2$, and that therefore $D_1^2 V_1 = D_2^2 V_2$. Substituting $2V_2$ for V_1 and simplifying, we find that $2D_1^2 = D_2^2$, which reduces to $\sqrt{2} \times D_1 = D_2$. So, the ratios of the tube diameters must also be in a $\sqrt{2}$ series, with the tube diameters increasing to separate decreasing particle sizes.

Roller Analyzer

The Roller Analyzer uses air as the elutriating fluid instead of water. A single elutriation tube is used, with the flow velocity adjusted using the blower mechanism. A similar device, the Haultain Infrasizer, uses a series of tubes of progressively increasing diameters. However, the Haultain Infrasizer is now rarely used, because it is more awkward and less flexible.

This device has several advantages: 1. Large quantities of air are easier to handle than large quantities of water; 2. Water-reactive solids can be analyzed; and 3. The low viscosity of air, as shown in Table 3.4, makes it possible to classify finer particles.

Table 3.4: Comparison of density and viscosity for water and air

	Water	Air
Density (gm/cm^3)	1.0	0.0012
Viscosity (poise	0.01	180×10^{-6}

The disadvantages of the Roller Analyzer are that the air humidity has to be very closely controlled to prevent clumping, and that it is more difficult to closely control the air flowrate than to closely control a water flowrate.

Warman Cyclosizer

The Warman Cyclosizer is also a fluid classification device, but it uses centrifugal forces to separate the particles instead of using gravity. The effective particle size range is between 8 and 50 micrometers for silica particles, and the time required for the separation is between 10 and 30 minutes. The limiting sizes for materials of various densities are given in Table 3.5.

Table 3.5: Limiting particle sizes for the Warman Cyclosizer, for particles of various densities.

Cyclone No.	Equivalent Stokes Diameter, micrometers, of particles collected by each cyclone unit		
	S. G. = 2.7	S. G. = 5.2	S.G. = 7.5
1	44	27	22
2	35	22	18
3	23	14	11
4	15	9	8
5	9	6	5

This device was developed by CSIRO, Melbourne, Australia, and is capable of separating finer particles than is possible by using gravity sedimentation or elutriation.

The Cyclosizer consists of five 3-inch diameter inverted hydrocyclones and ancillary equipment mounted in a cabinet (Figure 3.9). The undersize from each cyclone becomes the feed for the next in the series. The oversize product is collected in a closed container at the apex of each cyclone.

An operating schematic of the entire unit is given in Figure 3.10. The flow pattern in a single cyclone unit is shown in Figure 3.11,and an operating cyclone is shown in Figure 3.12.

The Cyclosizer is very effective, and produces clean monosized products much more rapidly than sedimentation or elutriation techniques. It is one of the few commercially-available devices which can rapidly separate particles finer than 25 micrometers. The results of separating a typical silica sand with the cyclosizer are shown in Figure 3.13.

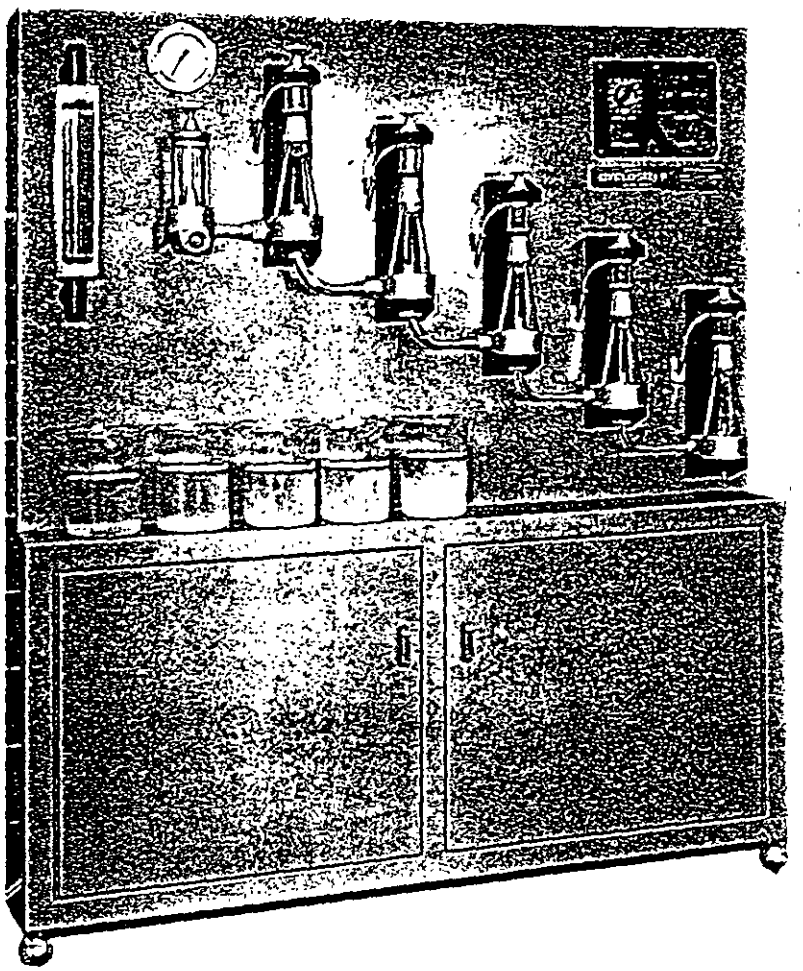

Figure 3.9: Warman Cyclosizer

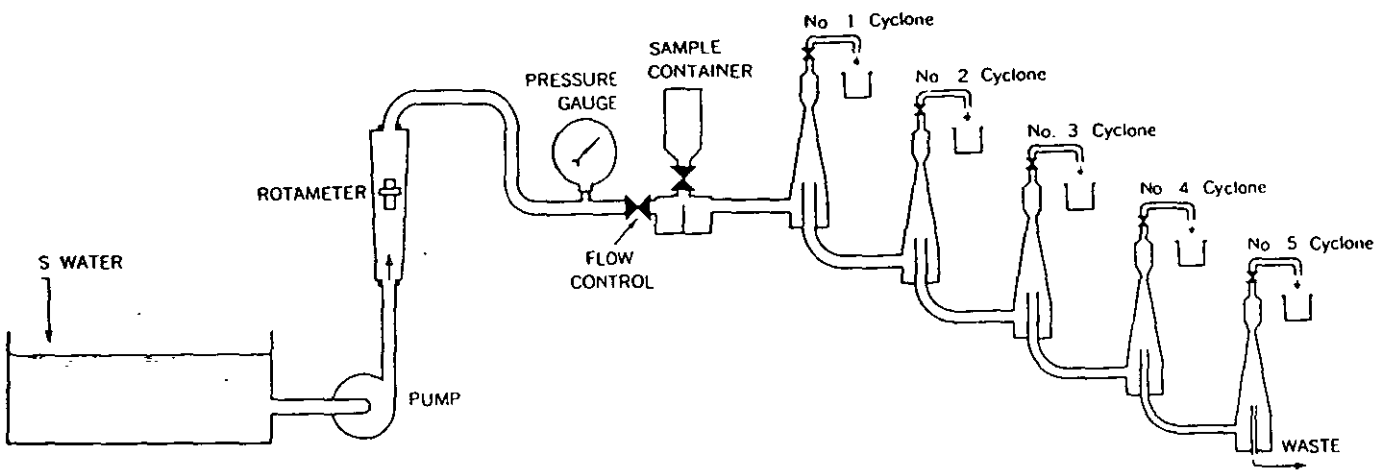

Figure 3.10: Operating principle of the Warman Cyclosizer

Figure 3.11: Schematic of a single cyclone unit in the Warman Cyclosizer.

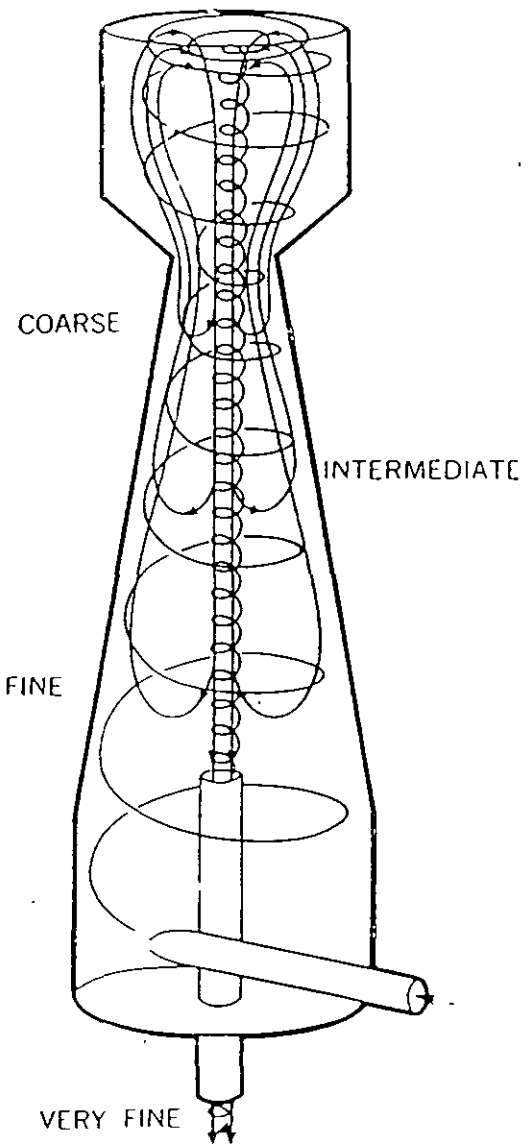

Figure 3.12: An operating hydrocyclone.

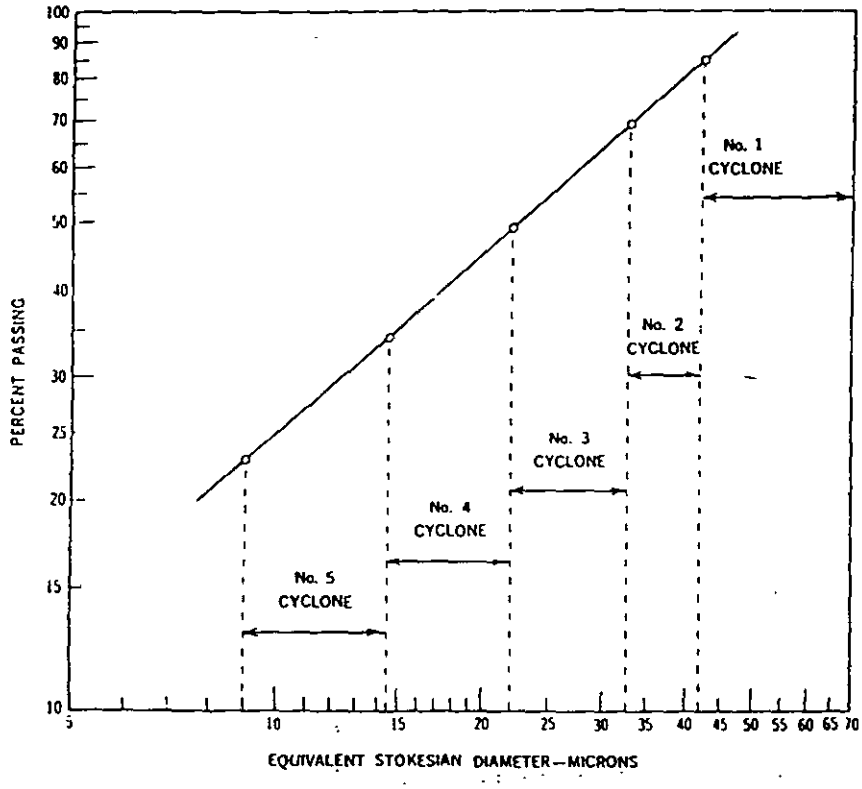

Figure 3.13: Results of separating a silica sand sample using the Warman Cyclosizer.

Electrical Sensing (Coulter Counter)

The principle of the coulter counter is illustrated by Figure 3.14. When an electrical potential is

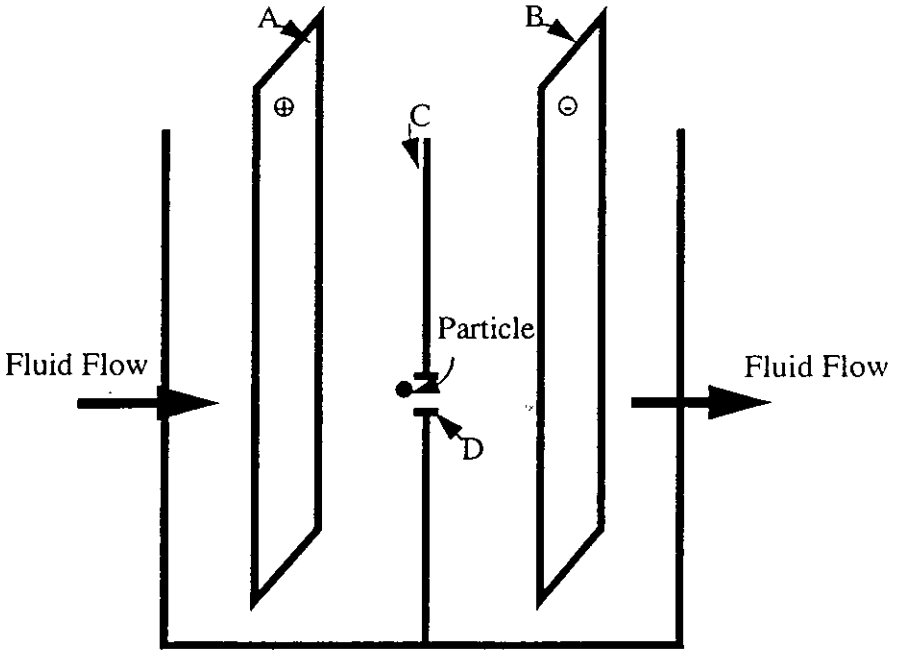

Figure 3.14: Operating principle of the Coulter Counter

established across electrodes A and B, a small current will flow through the hole D in insulator C. When a particle goes through the hole, it momentarily reduces the available area of the hole, and so briefly reduces the current flow. From the size and duration of the drop in electrical current, the size of the particle is determined. Unlike most of the particle size analysis methods discussed, the Coulter Counter measures single particles rather than groups of particles. It is most suited for extremely fine particle sizes which do not settle rapidly enough to be measured by sedimentation or elutriation techniques.

The working particle size range of the Coulter Counter is approximately 0.4 - 1200 microns (Coulter Instruments, 1994). This range is obtained by changing the aperture sizes. The results from a Coulter Counter are highly reproducible. However, if a suspension contains particles that are too coarse or too fine for the aperture in use, they will not be detected and so there will be a bias in the results. A detailed diagram of the Coulter Counter is given in Figure 3.15.

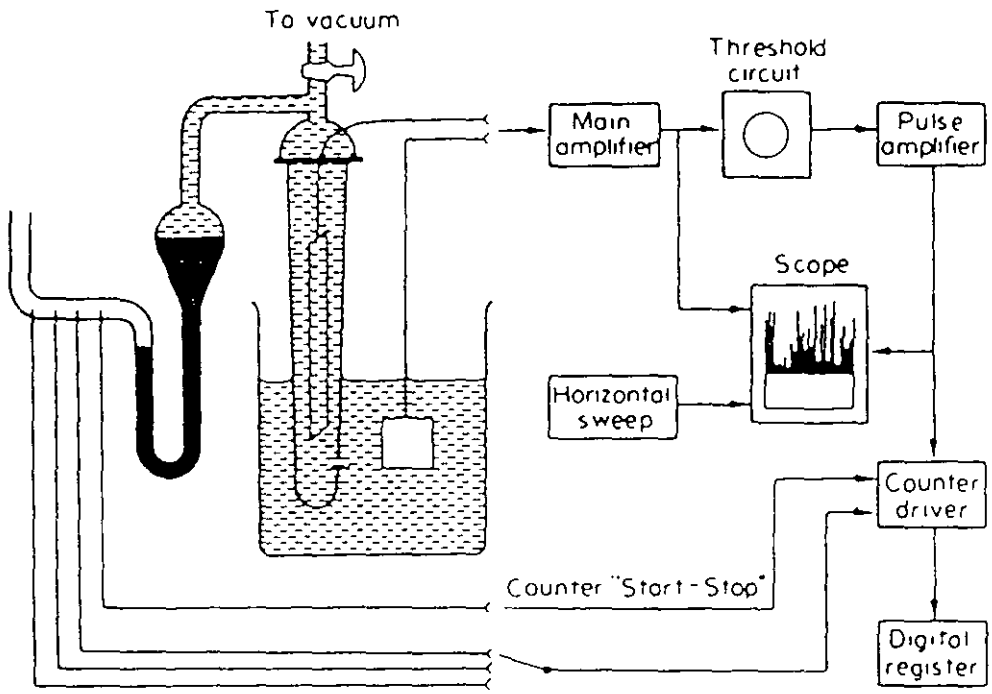

Figure 3.15: Detailed schematic of the Coulter Counter.

Laser Diffraction (Microtrac)

This type of unit is based on the Fraunhofer diffraction of a laser beam as it passes through a suspension of particles. This causes the beam to spread, with the angle of spreading related to the fineness of the diffracting particles. A schematic of the system is given in Figure 3.16, and typical diffraction patterns that are obtained from small and large particles are shown in Figure 3.17.

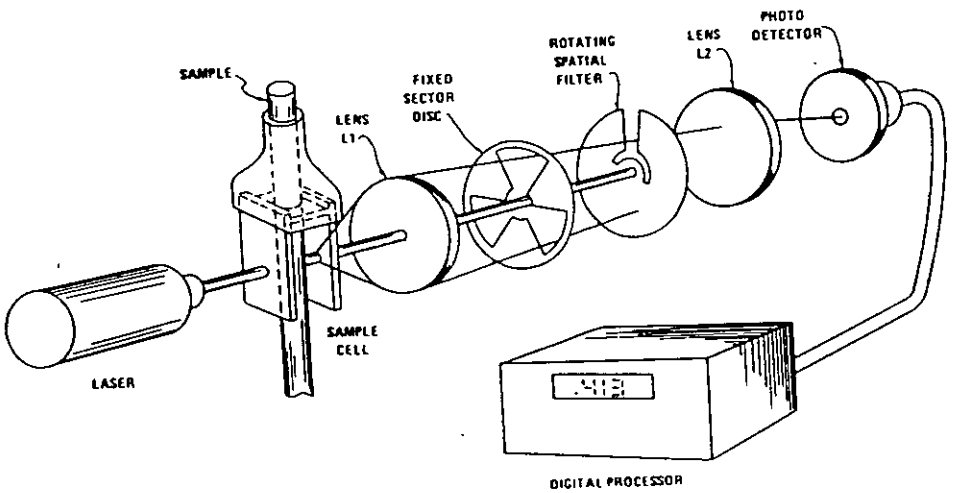

Figure 3.16: Operating principle of the Microtrac

In the Microtrac system manufactured by Leeds and Northrup, a Helium-Neon laser is used as the light source. The sample to be analyzed is suspended in air or water, and passed between two parallel, optically-flat glass plates. The light intensity is then measured as a function of the diffraction angle, and this is used to calculate the size distribution that would have to be present to produce the observed diffraction effects. The method is accurate and very rapid, and provides a size distribution down to a size of approximately 1 micron. It is suitable for laboratory use, or for on-line measurements in processing plants. It should be kept in mind that the size distributions from laser diffraction will not be the same as those obtained by screening or fluid classification, because the measurement method is based on a completely different principle.

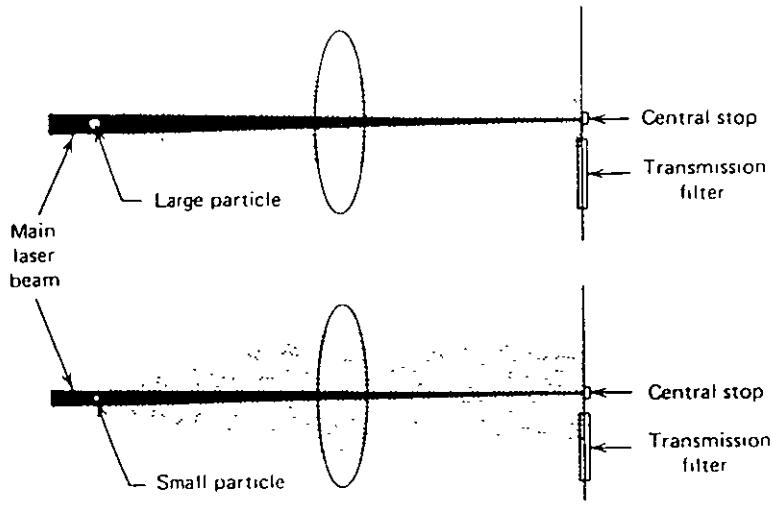

Figure 3.17: Microtrac diffraction patterns for particles of different sizes. The central stop blocks light proportional to the fourth power of the particle diameter. The transmission filter permits scattering light proportional to the third power of the particle diameter

Ultrasonic Absorption

The absorption of ultrasonic waves by particulate suspensions has been extensively studied by Flammer (1958). When ultrasonic waves pass through matter, their energy is gradually absorbed by the medium and their intensity decreases. The intensity of an ultrasonic emission passing through a suspension of particles is given by the relationship

$$I = I_0 e^{(-2\alpha x)} \tag{3.12}$$

where: I_0= Initial intensity of the ultrasonic wave
2α= Absorption Coefficient
x= Distance travelled into the medium
I= Intensity at distance x.

There is a complex relationship between the wavelength, the particle size, and the absorption coefficient. Ultrasonic absorption by slurries of monosized particles is shown in Figure 3.18.

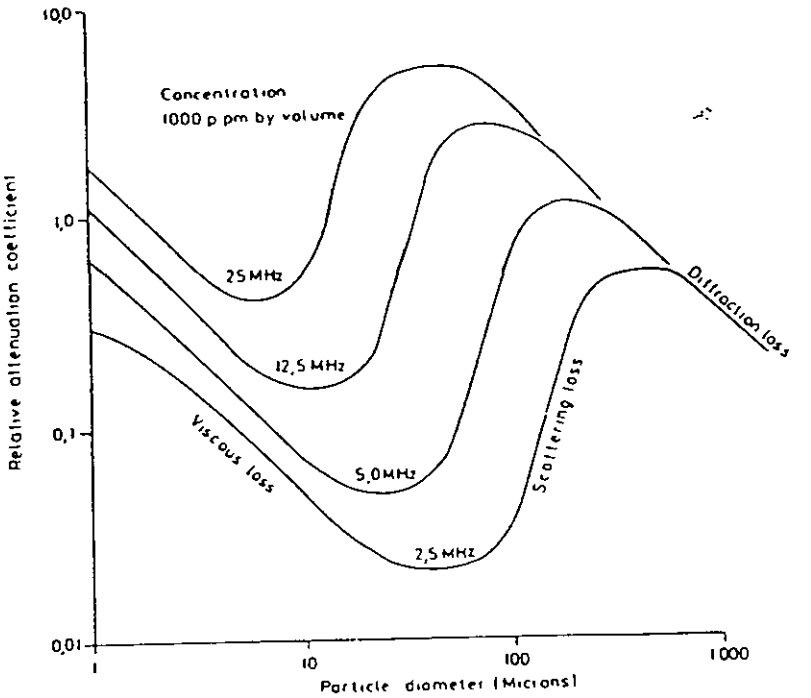

Figure 3.18: Attenuation of ultrasonic waves by slurries of uniform-size particles.

When $\lambda << 2\pi r$, where λ=wavelength and r = particle radius, the absorption coefficient for ultrasonic waves is given by

$$2\alpha = \frac{3c}{2r} \tag{3.13}$$

where r= particle radius
c= Volume concentration of solids

which shows that the absorption coefficient is inversely proportional to the particle size.

However, when $\lambda = 2\pi r$, then the value of 2α is essentially independent of the particle size. This can be exploited for simultaneous measurement of particle size and percent solids in a slurry, as is done in an instrument manufactured by Armco Autometrics.

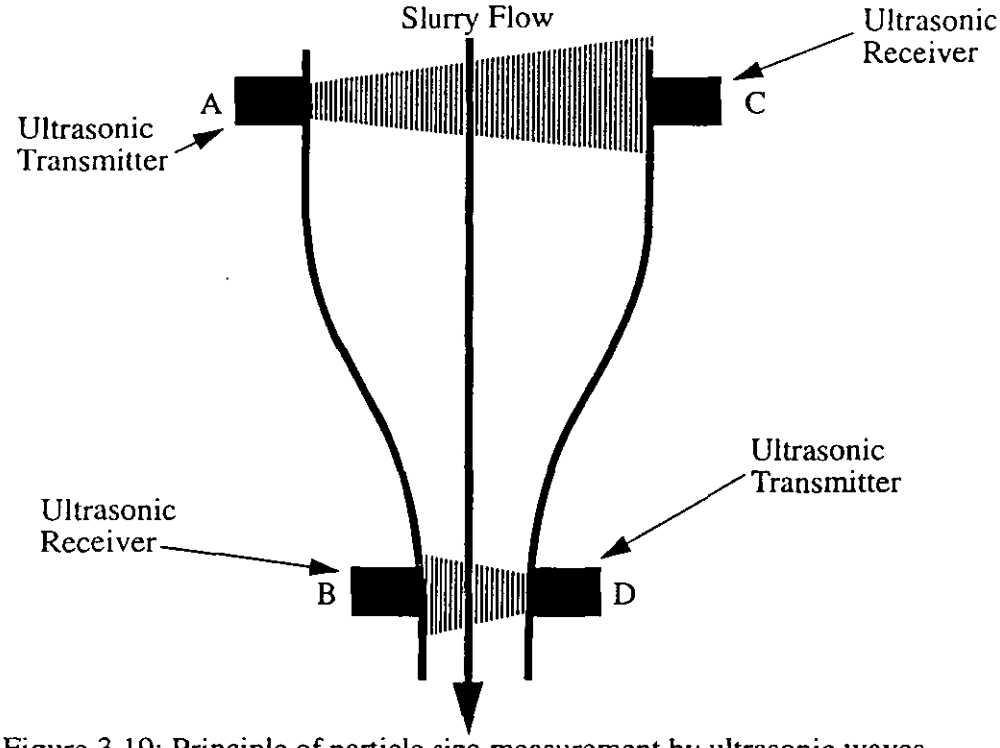

Figure 3.19: Principle of particle size measurement by ultrasonic waves.

In the Armco Autometrics system, two sets of ultrasonic transmitters and receivers are used, as shown in Figure 3.19. The frequency of Transmitter A is selected so that the absorption will be a function of both particle size and percent solids, while the frequency of Transmitter B is selected so that it will only depend on the percent solids. By combining the signals detected by receivers C and D, both the particle size and the slurry percent solids are determined. Since entrained air bubbles will cause the readings to be seriously in error, the Autometrics machine is equipped with an air eliminator system, as shown in Figure 3.20

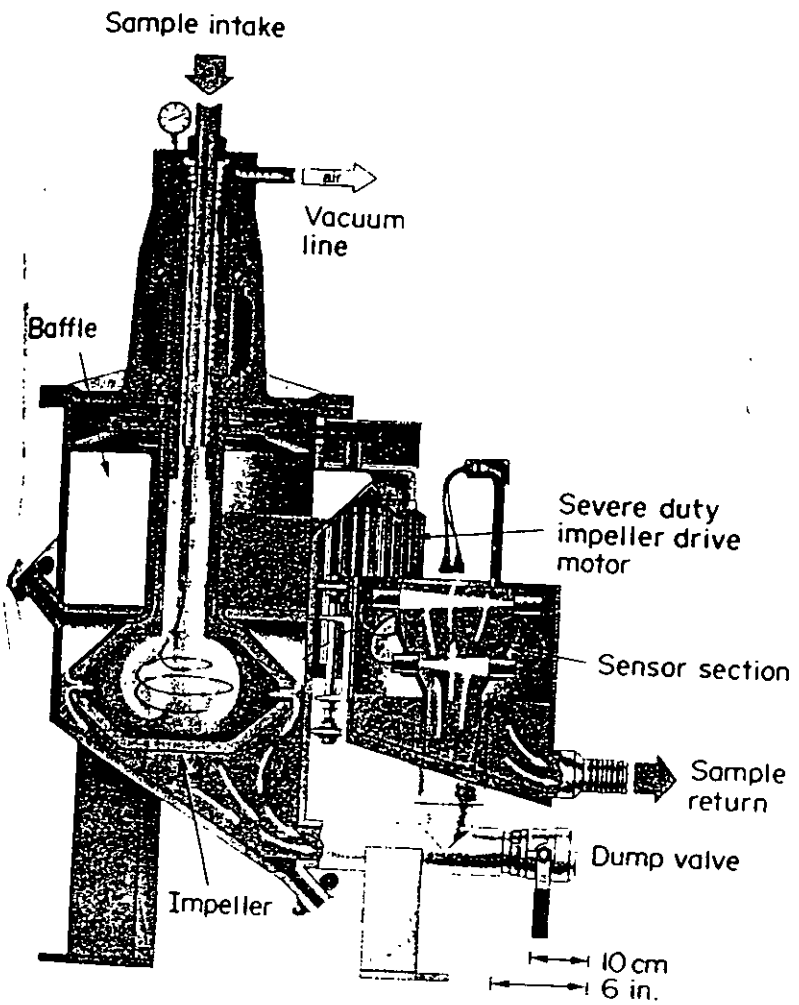

Figure 3.20: The Armco Autometrics PSM-400 system. This unit uses a combination of centrifugal forces and reduced pressure to remove all air bubbles from the slurry.

Outokumpu Particle Size Indicator

The principle of this device is illustrated in Figure 3.21. It is essentially a piston which moves up

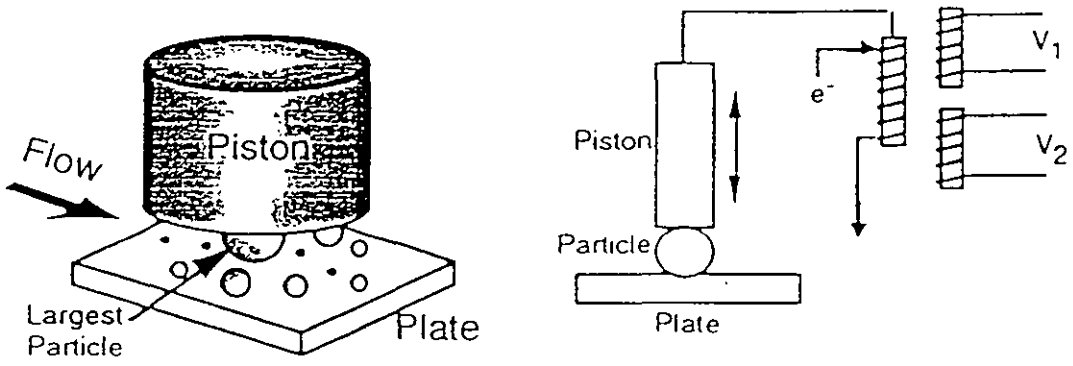

Figure 3.21: Operating principle of the Outokumpu Particle Size Indicator.

and down with a set frequency, while slurry flows between it and a fixed anvil. At the bottom of its stroke, particles are trapped by the piston. The displacement of the piston from the anvil is equal to the diameter of the largest trapped particle, and so a precise measurement of the piston position is a measure of the particle size. The results from each piston cycle are stored in a computer, which performs a statistical analysis on all of the measurements to produce a particle size distribution. In on-line implementations, the instrument is calibrated with up to two sets of data, so that it can continuously display the percentage of material that passes two different particle sizes. Some of the technical specifications are given in Table 3.6.

This unit does not require air eliminators, and is reported to be insensitive to variations in percent solids. The unit is rugged, reliable, and easy to install.

Table 3.6: Technical specifications and requirements for the Outokumpu Particle Size Indicator.

Absolute Accuracy	1 to 2 %
Particle Size Range	28 to 500 mesh
Power Requirements	120/222 VAC, +/- 10%
Output Signal	Two signals, 4-20 mA each
Water Supply	600 Kilopascals (87 psi)

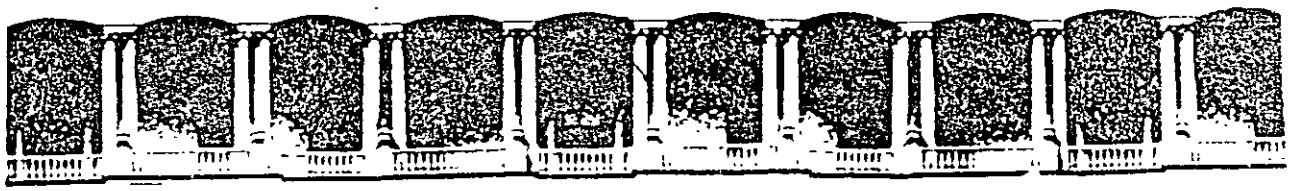

FACULTAD DE INGENIERIA U.N.A.M.
DIVISION DE EDUCACION CONTINUA

CURSOS ABIERTOS

DESARROLLO Y OPERACIÓN DE SENSORES PARA CONTROL DIRECTO Y CONTINUO EN PLANTAS DE BENEFICIO DE MINERALES Y EN LA RESTAURACIÓN DEL MEDIO AMBIENTE

Del 18 al 23 de mayo de 1998

TEMA: DEVELOPMENT OF AN ON - LINE SLURRY VISCOSITY MONITORING SYSTEM

EXPOSITOR :DR. KOMAR KAWATRA

1998

Comminution Theory & Practice,
Published by the Society for Mining,
Metallurgy and Exploration
Editor: S. K. Kawatra

Chapter 39

DEVELOPMENT OF AN ON-LINE SLURRY VISCOSITY MONITORING SYSTEM

S. K. Kawatra[1], T. C. Eisele[1], and M. T. Rusesky[2]

Department of Metallurgical and Materials Engineering[1]
Michigan Technological University
Houghton, MI 49931
Copper Range Company[2]
White Pine, MI 49971

ABSTRACT

An on-line monitoring system for apparent slurry viscosity has been developed at Michigan Technological University. It utilizes a vibrating sphere viscometer in conjunction with a special slurry presentation system to reduce particle settling and turbulence effects. It has proven to give accurate, reproducible results in an on-line hydrocyclone installation. Its performance shows that it can be an effective instrument on an industrial scale, particularly in grinding circuits. Development of the sensor and the importance of rheology in grinding are also discussed.

INTRODUCTION

Comminution is the single most energy intensive unit operation in mineral processing. Although it has been known for some time that the efficiency of a wet grinding circuit is dependent on the rheology of the mineral slurry, no grinding circuits use rheological measurement for direct control (Kawatra and Eisele, 1988). This is primarily because a reliable sensing system has not been developed which can handle the industrial environment. A Michigan Technological University research group is working on the development of a monitoring system for measuring apparent viscosity of mineral slurries.

RHEOLOGICAL EFFECTS IN GRINDING CIRCUITS

The rheology of mineral slurries is highly complex and difficult to predict. It contains both time-dependent and time-independent components, along with a number of variations from ideal behavior. Due to the high shear environment in a grinding mill only the time-independent components are of particular importance in comminution circuits (Bradley, 1965).

Time-independent behavior can be divided into four categories; Newtonian, pseudoplastic, dilatent and Bingham plastic. These classifications are based on how the shear stress developed in the fluid varies with shear rate. A schematic of this behavior is illustrated in Figure 1, with the shear rate being the velocity gradient in a flowing fluid (expressed as sec^{-1}) and the shear stress being the force transmitted to a surface parallel to the fluid flow (expressed as $dynes/cm^2$). For a Newtonian fluid, the shear rate-shear stress relationship is a straight line and the viscosity of the fluid is the slope of this line.

For dilatent or pseudoplastic fluids, the viscosity as such is not defined. Instead, two related parameters are used, the consistency and the apparent viscosity. The consistency is the constant K in the empirical Ostwald-de Waele power-law equation (Tsai and Knell, 1986):

$$\tau = K \dot{\gamma}^{n} \qquad (1)$$

where τ = shear stress in $dynes/cm^2$

$\dot{\gamma}$ = shear rate in sec^{-1}

n = flow behavior index

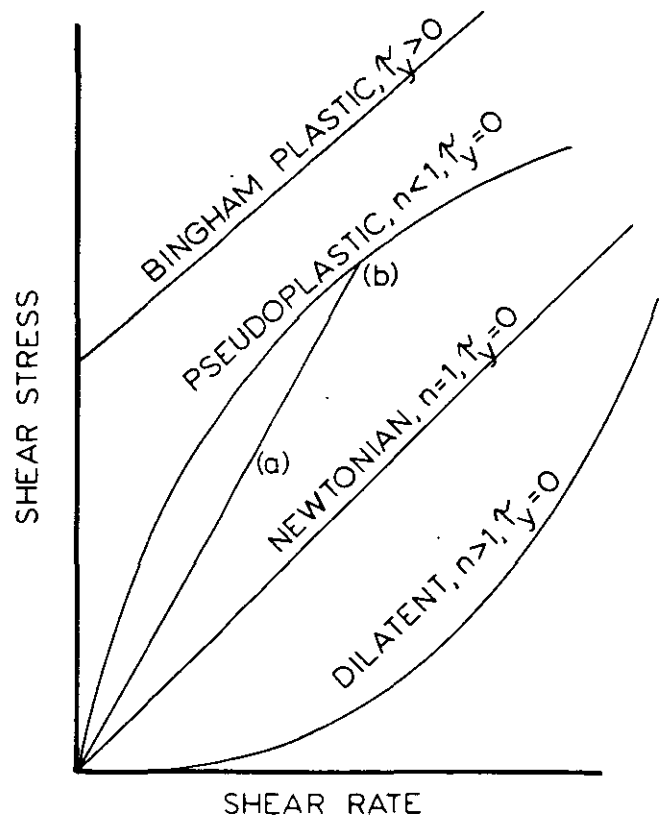

Figure 1. Shear-stress versus shear-rate curves illustrating the various forms of time-independent rheology. The slope of the line (a) is the apparent viscosity of point (b). These curves can be described using the power-law equation, $\tau = \tau_y + K\dot{\gamma}^n$, where τ is shear stress, τ_y is yield stress, K is the consistency, $\dot{\gamma}$ is the shear rate, and n is a parameter for the deviation from newtonian behavior.

Using this equation, a fluid is Newtonian if $n = 1$, pseudoplastic if $n < 1$, and dilatent if $n > 1$, and the consistency K is a constant for all shear rates for a given fluid. However, the consistency can only be calculated if the shear stress is determined at a number of shear rates. This determination is time-consuming, and is not well suited for on-line applications. The apparent viscosity is much easier to determine, as it requires only a single shear stress measurement. It is defined as shown in Figure 1, as the slope of a line (a) drawn between the origin and the measured shear stress value at a particular shear rate (b). The apparent viscosity η_α can therefore be simply calculated by dividing the measured shear stress by the corresponding shear rate:

$$\eta_\alpha = \tau/\dot{\gamma} \qquad (2)$$

For a Newtonian fluid, the viscosity, apparent viscosity, and consistency are all equivalent. In a dilatent fluid, the apparent viscosity increases with increasing shear rate, while in a pseudoplastic fluid it decreases with increasing shear rate. In certain fluids another parameter, the yield stress, is required to describe the time-independent rheology. This parameter is illustrated by the curve for a Bingham plastic shown in Figure 1. Here, the material behaves as if it were a solid until some critical shear stress (τ_y) is reached, after which it begins to flow as a fluid. For a true Bingham plastic, the consistency remains constant at all shear rates once flow has begun, while the apparent viscosity decreases with increasing shear rate.

Mineral slurries can be Newtonian, pseudoplastic, dilatent, or Bingham plastic, depending on factors such as solids concentration, particle size and shape, chemical environment, and temperature. In general, very dilute slurries in water are Newtonian, becoming slightly dilatent as the particle concentration becomes high enough for particle-particle interactions to begin to occur. Once particle interactions become the dominant mechanism for energy transfer in the slurry, it typically becomes pseudoplastic, and develops a yield value as the percent solids increases further. The yield value ultimately becomes very pronounced, producing a fluid which is essentially Bingham plastic just before it ceases to flow at all.

Rheology affects the efficiency of both the mill and the classifier in a closed grinding circuit. The effect of rheology on mill performance has been extensively studied, mostly in conjunction with grinding aids (El-Shall and Somasundaran, 1984, Fuerstenau et al, 1985, Klimpel, 1984, Austin et al, 1984). It is well known that increasing the percent solids increases the mill throughput. However, ultimately the slurry becomes so concentrated as to develop a yield stress. Once this occurs, the breakage rate in the mill decreases due to adhesion of the grinding media to the mill wall (Fuerstenau et al, 1985). Decreasing the slurry viscosity, through the use of grinding aids, at a constant solids concentration, was found to result in an increased fines production rate. These effects are due to changes in the motion of the mill charge resulting from elimination or reduction of the slurry yield value, and to a decrease in the energy dissipated by fluid flow at lower viscosities.

The rheological effects on classifier performance are quite pronounced and fairly complex (Bradley, 1965). These effects have not been well studied, due to the lack of suitable instrumentation. Some data are available using various methods to alter medium viscosity, such as sugar solutions (Agar and Herbst, 1966), viscosity-modifying reagents (Austin et al, 1984) and temperature variations (Kawatra et al, 1988). From the published results, two effects are noted. As the viscosity of the slurry increases, the corrected d50 size for the

hydrocyclone increases, which is primarily a result of the lower settling velocity of particles in a higher-viscosity medium. The second effect is that the fluid speed in the hydrocyclone is reduced due to increased viscous drag at higher viscosities, and therefore the amount of material which exits with the coarse fraction without being subjected to classification is increased. These effects have been shown on both a laboratory and a plant scale in temperature-variation experiments conducted by MTU researchers (Kawatra et al, 1988).

Several theoretical treatments of hydrocyclones include a viscosity term. In theory it is possible to divide this term into two categories; the effect on overall fluid flow patterns, and the effect on individual particle movement. In practice these two effects are inseparable (Bradley, 1965).

EXISTING ON-LINE VISCOMETERS

Currently, three systems for on-line measurements of viscosity exist which would conceivably be used for slurries. The first system, developed by Hemmings and Boyes (1977), used a Brabender Convimeter as the viscometer. The Brabender Convimeter consists of a drive motor which imparts a gyratory movement through a bent shaft to a conical sensor that rotates eccentrically within a cylindrical protective sheath, shown in Figure 2. It utilizes the change in energy required to keep the sensor rotating at a constant rate as a measure of the viscosity. Hemmings and Boyes mounted the viscometer as shown in Figure 3. This system's major drawback was that coarse material and trash in the processing stream tends to get lodged between the spindle and the sheath, causing an unpredictable loss stability.

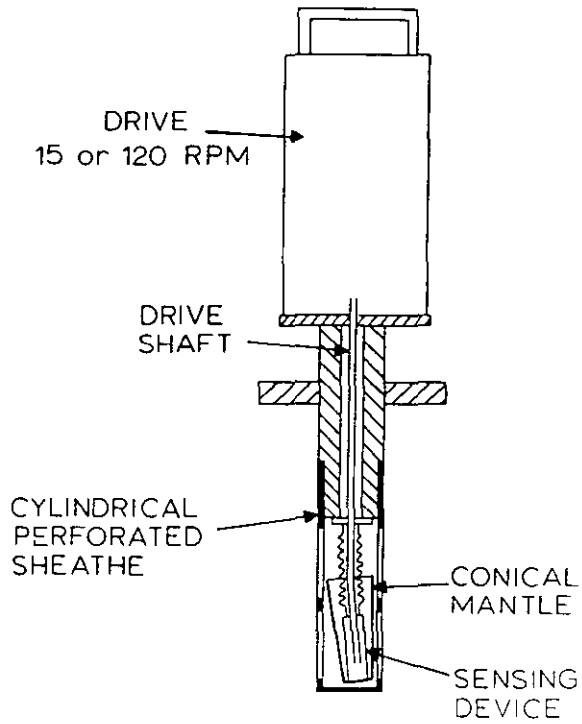

Figure 2. Configuration of the Brabender Convimeter. As the eccentric conical mantle rotates, fluid is forced through the perforations in the cylindrical sheath. Apparent viscosity is determined by measuring the drag force on the rotating mantle.

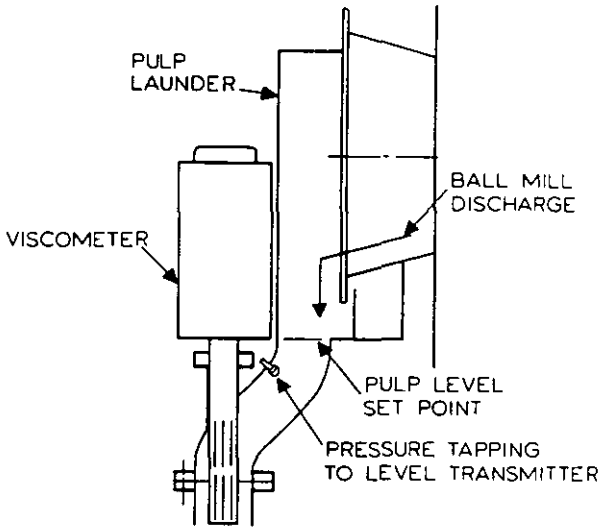

Figure 3. Hemming's and Boyes' (1977) method of mounting the Brabender convimeter.

The second method, described by Reeves (1984), utilizes a viscometer manufactured by the Debex corporation. This rotational type viscometer was driven at a fixed rate by a torque sensitive motor. Viscosity was measured by the amount of torque required to keep the spindle rotating at a constant rate. It was mounted, as shown in Figure 4, to reduce the effects of rapid particle settling. It has been frequently reported that rotating viscometers do not work well in a slurry environment (Clarke, 1967). They are highly sensitive to fluid turbulence,

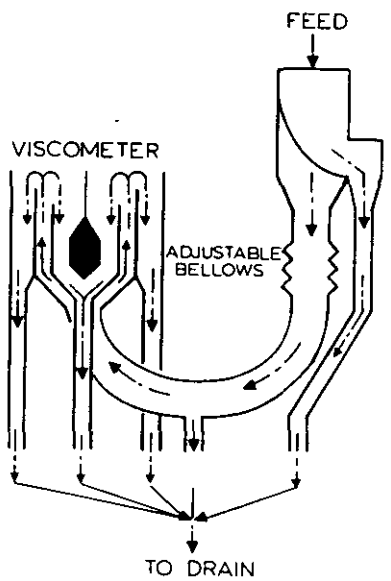

Figure 4. Schematic demonstrating the slurry presentation system used by Reeves (1984).

their moving parts are generally too delicate to tolerate a plant environment, and the rotational motion can cause particle concentration gradients which produce erratic results.

The third method suggested in the literature (Opplinger, Matusik, and Fitzgerald, 1975) utilized a Nametre vibrating sphere viscometer mounted in a T-fitting as shown in Figure 5. The principle of the Nametre viscometer is that the sphere is vibrated around the axis of the shaft to produce shear waves traveling into the fluid at the probe's resonant frequency about 700 Hz, with energy being supplied to maintain the vibration at a constant amplitude of 1 micron. The energy supplied to keep a constant amplitude is indicative of the apparent viscosity of the fluid. Since the probe is vibrating rather than constantly traveling in a single direction, the shear rate is a sinusoidal function of time. Also, the spherical shape of the probe tip results in the vibration having its maximum amplitude at the sphere equator, dropping to zero amplitude at the sphere poles (Ferry, 1977). As a result, the Nametre viscometer cannot be said to operate at a specific shear rate, but rather averages the results from shear rates ranging from zero to the maximum value. This maximum shear rate is not a definite constant for the instrument, as it varies depending on the propagation velocity of shear waves in the fluid, which in turn is a function of several factors, such as the viscosity, and is consequently difficult to determine precisely. The maximum shear rate in water has been calculated to be approximately 6000 sec^{-1} in water at 1 centipoise, but would be a factor of 10 lower at 100 centipoise (Ferry, 1977). In a Newtonian fluid this does not affect the reading, as such fluids exhibit a constant viscosity at all shear rates. Non-Newtonian fluids are more complicated to deal with, both due to viscoelasti effects and to the dependence of the apparent viscosity of these fluids on shea rates. A reading obtained with the Nametre viscometer with a non-Newtonian mineral slurry may best be considered to be obtained at a mean shear rate of approximately 4000-5000 sec^{-1}.

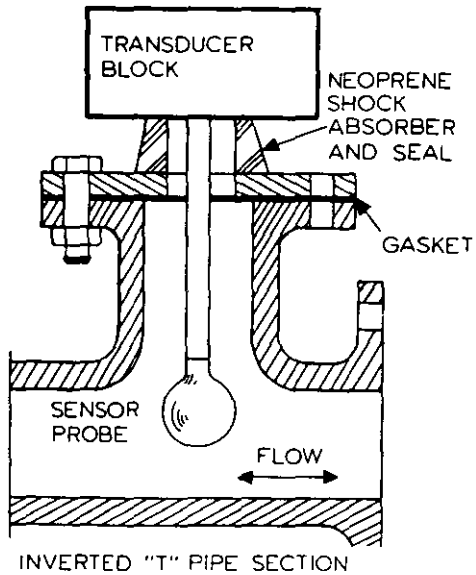

Figure 5. Normal method of mounting the Nametre viscometer in non-slurry service.

Viscometer Selection

After reviewing the three available systems it was decided to start with a commercially available viscometer and to adapt it as necessary for mineral slurry service. The Debex system was not available at the time of this study, and so was not considered further. To determine the ability of the viscometers to function using real materials, samples of finely ground iron ore were sent to both Nametre and Brabender. The Brabender viscometer could not be tested as their laboratory test apparatus was not designed to handle fast-settling slurries, and so no data could be obtained. The results obtained with the Nametre viscometer are shown in Figure 6, and agree with results obtained by other investigators using different techniques (DeVaney and Shelton, 1939, Clarke, 1967, Jeffery and Acrivos, 1965). Based on these results, the Nametre viscometer was selected as the starting point for further work. The viscometer selected had a resonance frequency ranging from 708.0 Hz in air to 701.0 when loaded at 23000 centipoise.

Advantages of the Nametre Viscometer

The high average shear rate and rapid oscillation of the Nametre viscometer allows the instrument to remain insensitive to moderate levels of slurry turbulence. Due to the rapid sampling, fast response time and noise filtering electronics, large particles striking the probe have a very transitory effect on the measurement.

The Nametre viscometer is also ruggedly designed and capable of withstanding the abuse of a plant environment. The design consists of a sensor enclosed in a sealed housing which prevents corrosive or abrasive materials from reaching the delicate moving parts.

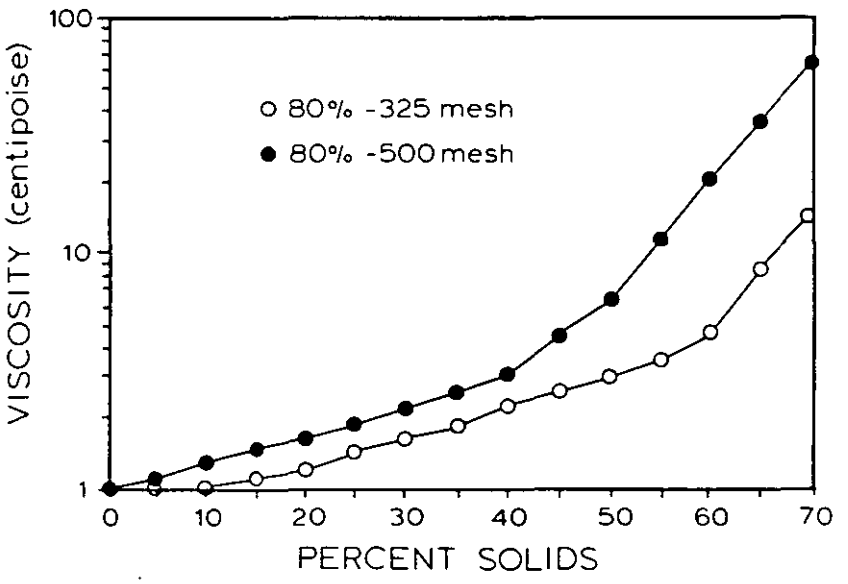

Figure 6. Measurements performed by Nametre viscometer.

SYSTEM DEVELOPMENT

The first step in the development of the on-line system was to calibrate the viscometer by a series of static bench tests. This calibration was then verified and the stability checked on an in-line installation.

The first attempt at installing the instrument was per manufacturer recommendations. This was accomplished by mounting the viscometer into a straight section of pipe using a heavy duty T-fitting, as shown in Figure 7. When the viscometer was bolted to the flange its response characteristics changed, making the rezeroing of the instrument necessary. The major problems encountered involved both maintaining a constant tension on the mounting bolts, and dealing with the very high levels of fluid drag and vibration acting upon the probe.

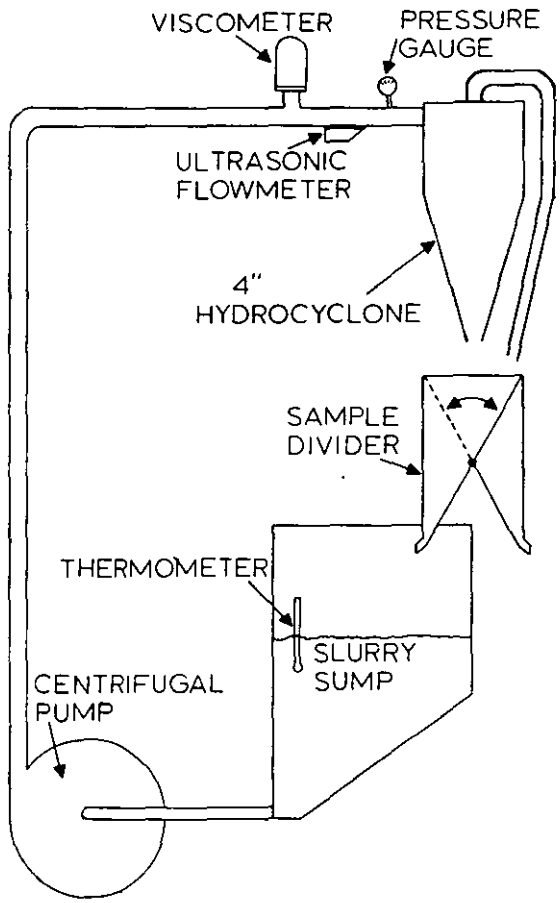

Figure 7. Initial test set up with the Nametre viscometer.

As the tension on the bolts changed, the zero setting tended to drift. The pumping system transmitted excessive vibrations through the pipeline, and over several hours one or more of the bolts would tend to loosen. Lock washers and jam nuts were tried, but they had little effect. As the tension on the bolts vari the zero setting drifted, causing unpredictable changes in the viscosity readi Even when the zero setting was adjusted before each test to compensate for changes in bolt tension, the measured viscosity of water was unacceptably high (3.7-3.8 cP). This was due to the high levels of pump vibration and turbulence.

The second problem encountered was the strong dependency of measured viscosity on the flow rate, shown in Figure 8. This was probably due to the probe producing a severe restriction in the pipe, which caused substantial drag forces to act on the probe. This stress apparently slightly deformed the probe and changed its vibrational characteristics, producing the observed flow rate dependence. This necessitated further measures to improve the setup, by reducing the effects of both mechanical stresses on the sensor and interferences from vibrations and turbulence.

The stability of the readings were improved by isolating the pump from the viscometer by mounting it on a separate platform and connecting the pump to the viscometer with flexible pipe. Lead blocks were bolted to the pipeline on either side of the viscometer to damp vibrations and thus reduce the instrument noise. However this did not address the mechanical stress problems which were causing the zero drift and flow rate dependence.

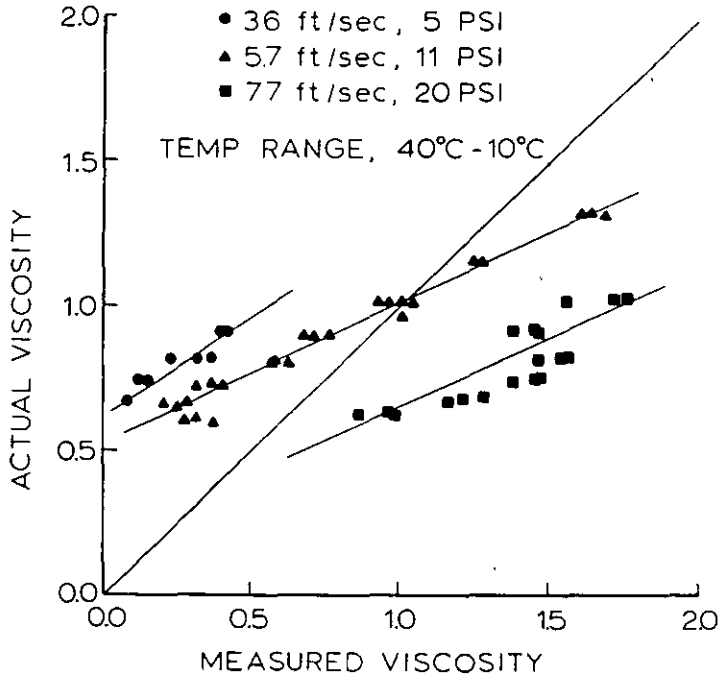

Figure 8. Apparent dependence of measured water viscosity on flow rate before making installation modifications.

It was decided to develop a slurry presentation system to eliminate the effects of vibration and turbulence on the Nametre viscometer. Figure 9 illustrates how a slurry stream is allowed to flow upwards and over an annulus which acted as a weir. A constant level of one inch over the top of the measurement chamber was maintained by the overflow lip of the annulus. Slurry which overflowed this barrier was returned to the sump by the overflow launder.

The sensing unit was suspended with rubber straps and was allowed to hang free of any contact with the mounting bolts, as shown in Figure 9. This minimized the stresses acting on the sensor, and provided nearly complete isolation from

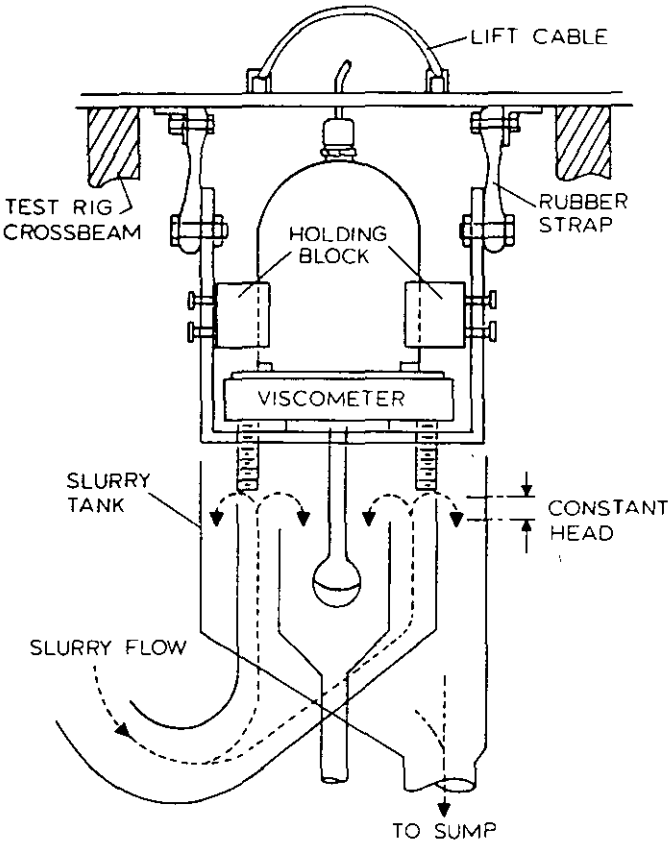

Figure 9. A method of mounting Nametre viscometer over an open slurry tank to eliminate problems with drifting zero setting and turbulence.

vibrations. This method of mounting has the additional advantage of easy removal of the sensor from the slurry presentation system via an overhead cable attached to the sensor. This feature was useful for cleaning or drying the sensor as well as checking the zero setting. A temperature sensor was inserted next to the viscometer probe to ensure that the slurry temperature was known accurately.

EXPERIMENTAL PROCEDURE

Equipment Description

The equipment used in this project consisted of a hydrocyclone test rig with a 4" diameter Krebs hydrocyclone. The viscometer was mounted to measure the viscosity of the recombined cyclone overflow and underflow products, which were kept well-mixed and had a consistent solids content in the course of each test Data was collected by an HP-85 microcomputer with an HP-3497A data acquisitior control unit. The computer was used to collect single data points, to collect data at specific time intervals, or to collect data after a specified change in slurry temperature had occurred.

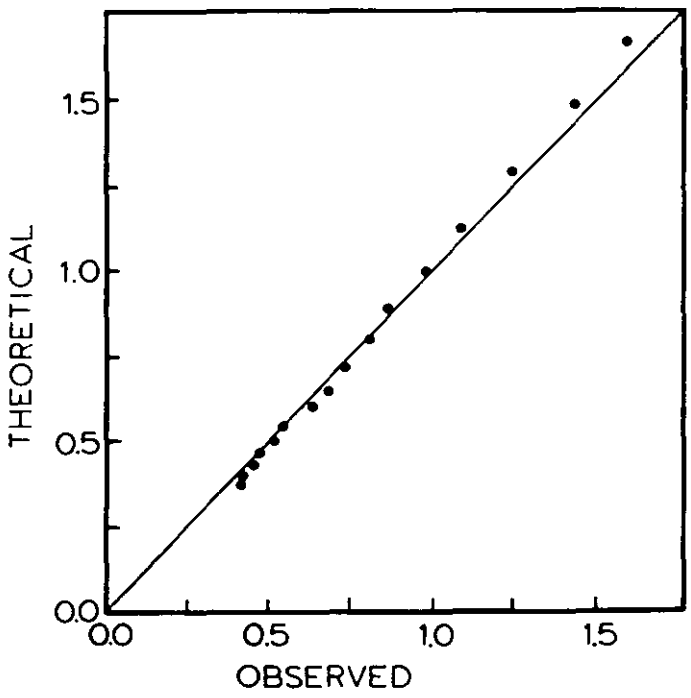

Figure 10. On-line test of viscometer installation on water viscosity after making improvements in the mounting arrangement. The viscosity of water is being varied by changing its temperature.

Experiments with Water

Initial tests with the slurry presentation system were run using water to compare measured values to those calculated from the formulas in the Handbook of Chemistry and Physics (CRC 1984)

$\log_{10}\eta = 1301/[998.333+8.1855(T-20)+0.00585(T-20)^2]-1.30233$ for 0°C to 20°C and

$\log_{10}\eta/\eta_{20} = [1.3272(20-T)-0.001053(T-20)^2]/(T+105)$ for 20°C to 100°C, where

η = viscosity, centipoise
T = Temperature, °C
η_{20} = Viscosity at 20°C, which is 1.002 centipoise

Tap water was circulated through the system while the temperature was varied between 10°C and 50°C. The results are shown in Figure 10. The stability of the slurry presentation system was then determined by allowing the system to measure the viscosity of water for 15 hours, while maintaining the temperature at 22.5°C to ± 0.3°C. Figure 11 shows the improvement between tests run on the initial installation as opposed to the improved system.

Experiments with Mineral Slurries

Following the initial tests with water, work was begun to determine the capabilities of the system with mineral slurries. A 99.9% pure silica provided by the Ottawa Sand Co. of Ottawa Illinois, with the size distribution shown in Table 1, was used in the mineral slurry experiments.

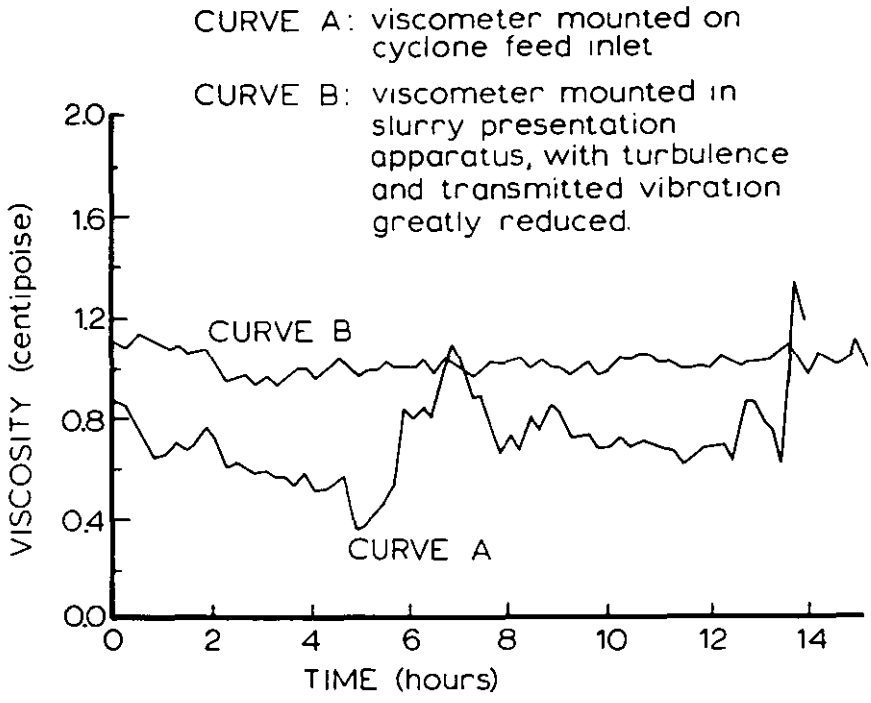

Figure 11. Stability check of on-line water viscosity measurements before and after making improvement in the mounting of the sensor with temperature controlled to 22.2°C ± 0.2°C.

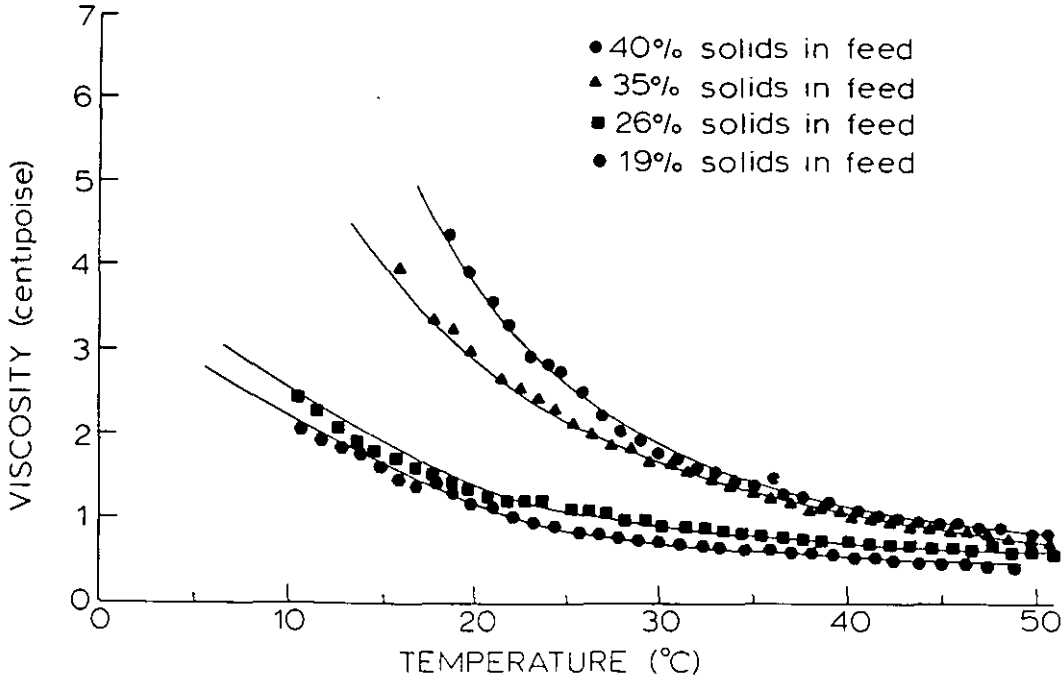

Figure 12. On-line viscosity measurements of silica/water slurries as a function of temperature at various solids concentrations.

Table 1. Size distribution of silica used for on-line tests of the viscometer system, as determined using a Leeds and Northrup Microtrac particle size analyzer.

Size, Micrometers	Cumulative % Passing
176	100
125	97.0
88	93.6
62	75.5
44	49.8
31	34.9
22	24.0
16	17.5
11	12.7
7.8	8.1
5.5	5.1
3.9	3.9
2.8	2.0

The experimental work was conducted at temperatures ranging from 10°C to 50°C, and percent solids ranging from 19% to 40%. For each experiment the cyclone test rig was filled with a known volume of water, the pump was started, and silica was added to the desired percent solids. Solids concentrations were checked by taking wet and dried sample weights after each test run. The temperature was controlled by the use of heating and refrigeration coils in the sump.

For initial experiments viscosity values were measured over a 40°C temperature range for solids concentrations of 19%, 26%, 35% and 40% solids. Figure 12 illustrates the dependence of viscosity on percent solids over this temperature range. The curves above 26% solids are noticeably steeper, which shows that increased interaction between particles is taking place.

To test the reproducibility of the system a second set of experiments at 15%, 25% and 40% solids were carried out. Samples to check percent solids were not removed until the completion of the experiments. This allowed the tests to be continued for an extended time through several temperature cycles without sampling introducing changes in the slurry composition or test rig operation. Each slurry was cycled through the temperature range from 50°C to 15°C. Viscosity measurements were made at 1°C intervals above 25°C, and 1/2°C intervals below 25°C. Each measurement is an average from 30 seconds of data acquisition.

RESULTS

Figures 13 through 15 show the temperature vs. viscosity data for three slurry solids concentrations. The second order polynomial curve fit was calculated from the total number of available points from the individual temperature runs, with the fitted polynomial equations, correlation coefficients, and standard errors for each percent solids given in Table 2.

From the results shown in Table 2, it is seen that the performance of the instrument is highly reproducible, with standard deviations less than 0.05 centipoise for all three percent solids. The average error, which is the standard deviation divided by the mean viscosity, is consistently under 4%, which, considering the difficulties with measuring slurry viscosity is completely acceptable for the goal of on-line control of grinding classification circuits.

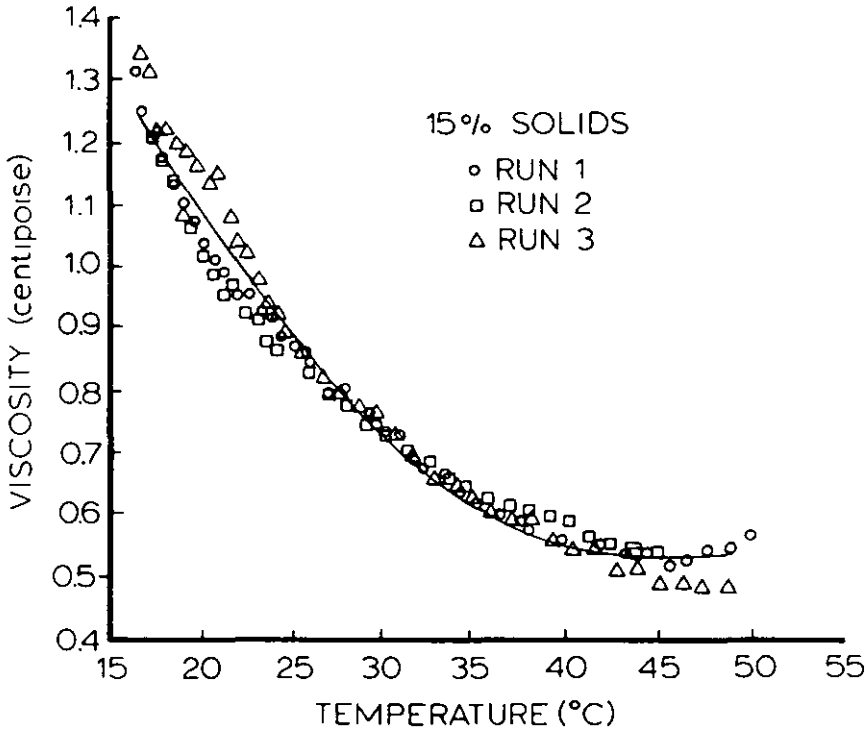

Figure 13. Viscosity measurements made during three runs of temperature between 50°C and 10°C on a 15 wt.% silica/water slurry.

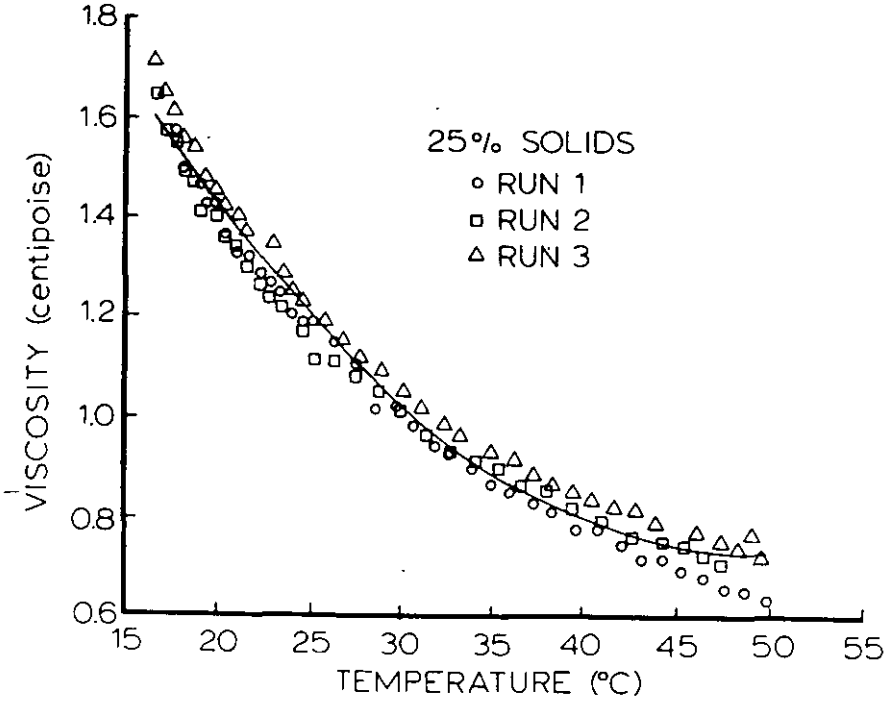

Figure 14. Viscosity measurements during three runs of temperature between 50°C and 10°C on a 25 wt.% silica/water slurry.

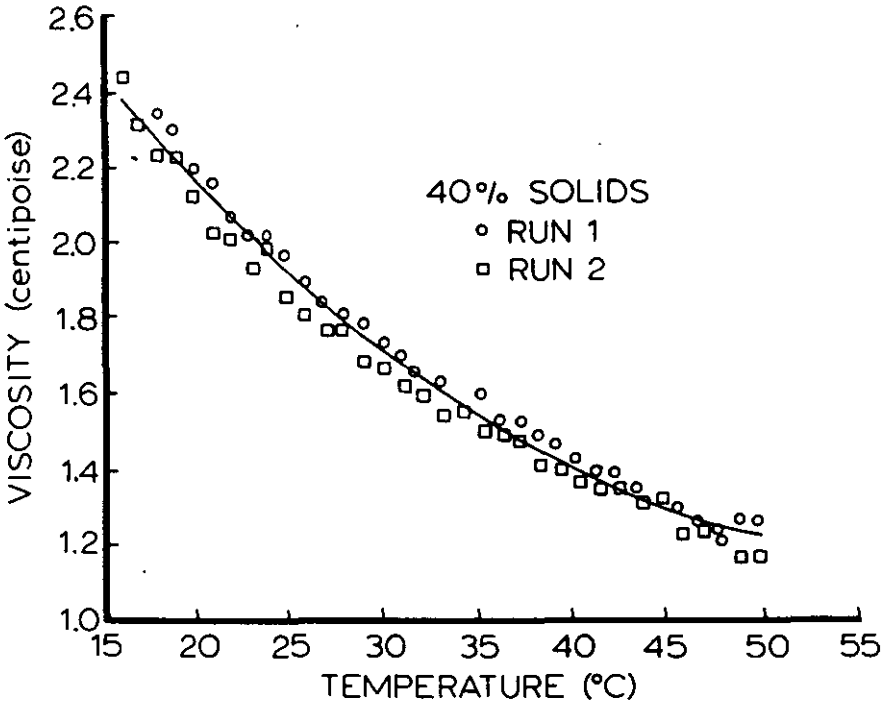

Figure 15. Viscosity measurements made during two runs of temperature between 50°C and 10°C on a 40 wt.% SiO_2/water slurry.

Table 2. Polynomial equations, correlation coefficients, and standard errors at 15% solids, 25% solids, and 40% solids. η = measured viscosity, centipoise; T = temperature, °C, and $\eta = A + BT + CT^2$.

%Solids	A	B	C	Mean η	Correlation Coefficient	Standard Deviation	Average % Error
15%	2.325	-0.079	0.001	0.81	0.979	0.03	3.70%
25%	2.725	-0.079	0.0008	1.09	0.981	0.04	3.67
45%	3.485	-0.079	0.001	1.66	0.986	0.04	2.41

CONCLUSION

It is well established that rheological control is important in the improvement of grinding efficiency in an operating plant. Such control has not been implemented primarily due to the lack of instrumentation. However an on-line apparent viscosity measuring system has been develped at Michigan Technological University which is capable of reproducible measurement of this parameter in mineral slurries. It is robust enough to be used on-line in grinding circuits, while still being precise enough to provide useful control data.

ACKNOWLEDGMENTS

This research has been supported by the Department of the Interior's Mineral Institute program administered by the Bureau of Mines through the Generic Mineral Technology Center for Comminution under grant number G1125149. Additional support was provided by Dow Chemical Co., Midland, Michigan.

REFERENCES

Agar, G. E. and Herbst, J. A., "The Effect of Fluid Viscosity on Cyclone Classification", Trans. AIME, vol. 235, 1966, pp. 145-149.

Austin, L. G., Klimpel, R. R., and Luckie, P.T., Process Engineering of Size Reduction: Ball Milling, SME-AIME, 1984.

Bradley, D., The Hydrocyclone, Pergamon Press, 1965.

Clarke, B., "Rheology of Coarse Settling Suspensions", Trans. of the Institution of Chem. Eng., vol. 45, pp. 251-256, 1967.

CRC Handbook of Chemistry and Physics 64th Ed., Weast, R. C., Chief Ed., Astle, M. J., and Beyer, W. A., Asst. Ed., CRC Press, Inc., Boca Raton, Fl., 1984.

DeVany, F. D. and Shelton, S. M., "Properties of Suspension Media for Float and Sink Concentration", U.S.B.M. Report of Investigations 3469, September 1939.

El-Shall, H., Somasundaran, P. "Physico-Chemical Aspects of Grinding: A Review of Use of Additives", Powder Technology, vol. 38, pp. 275-293, 1984.

Ferry, J. D., "Oscillation Viscometry-Effects of Shear Rate and Frequency", Measurements and Control, Sept.-Oct., vol. 11, no. 5, 1977.

Fuerstenau, D. W., Venkataraman, K. S. and Velamakanni, B. V., "Effect of Chemical Additives on the Dynamics of Grinding Media in Wet Ball Mill Grinding", Int. J. of Mineral Processing, vol. 15, no. 4, 1985, pp. 251-268.

Hemmings, C. E., and Boyes, J. M., "Plant Trial Evaluation of On-Stream Measurement System for Wet Grinding Mills", Int. Chem. Eng. Symposium Series, no. 63, 1977, pp. D4/EE/1-13.

Jeffery, D. J., and Acrivos, A., "The Rheological Properties of Suspensions of Rigid Particles", AiChE J., vol. 20, 1965, pp. 267-277.

Jinescu, V. V., "The Rheology of Suspension", Int. Chem. Eng., vol. 14, 1974, pp. 397-420.

Kawatra, S. K. and Eisele, T. C., "Rheology Effects in Grinding Circuits", Proceedings of the XVI International Mineral Processing Congress, Elsevier, New York, Part A, 1988, pp. 195-207.

Kawatra, S. K., Eisele, T. C., Zhang, D., and Rusesky, M. T., "Effects of Temperature on Hydrocyclone Efficiency", Int. J. of Min. Processing, vol. 23, 1988, pp. 205-211.

Klimpel, R. R., "Influence of Material Breakage Properties and Associated Slurry Rheology on Breakage Rates in Wet Grinding of Coal and Ores in Tumbling Media Mills", Reagents in the Minerals Industry, (M. J. Jones and R. Oblatt, eds.), Institution of Mining and Metallurgy, London, 1984, 265-270.

Oppliger, H. R., Matusik, F. J. and Fitzgerald, J. V., "New Technique Accurately Measures Low Viscosity On-Line", Control Eng., vol. 22, no. 7, 1975, pp. 39-40.

Reeves, T. J., "On-Line Viscometer for Mineral Slurries", Transactions of the Institution of Mining and Metallurgy: Section C: Mineral Processing and Extractive Metallurgy, vol. 94, 1984, pp. C201-C208.

Tadros, T., "Rheology of Concentrated Suspensions", Chem. and Industry, April 1985, pp. 210-219.

Tsai, S. C. and Knell, E. W., "Viscometry and Rheology of Coal-Water Slurry", Fuel, vol. 65, April 1986, pp. 566-571.

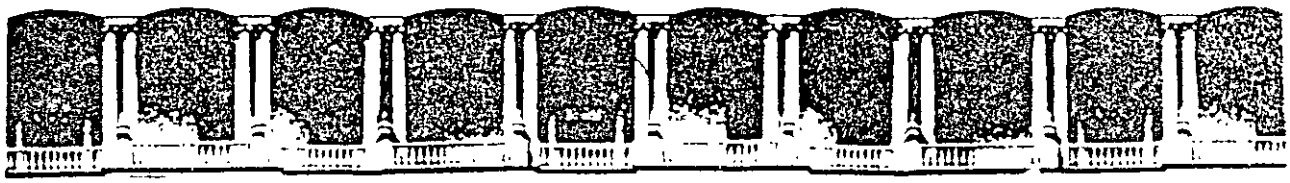

FACULTAD DE INGENIERIA U.N.A.M.
DIVISION DE EDUCACION CONTINUA

CURSOS ABIERTOS

DESARROLLO Y OPERACIÓN DE SENSORES PARA CONTROL DIRECTO Y CONTINUO EN PLANTAS DE BENEFICIO DE MINERALES Y EN LA RESTAURACIÓN DEL MEDIO AMBIENTE

Del 18 al 23 de mayo de 1998

TEMA: ON - LINE VISCOMETRY IN PARTICULATE PROCESSING

EXPOSITOR :DR. KOMAR KAWATRA

1998

Palacio de Mineria Calle de Tacuba 5 Primer piso Deleg. Cuauhtemoc 06000 Mexico, D.F. APDO. Postal M-2285
Telefonos. 512-8955 512-5121 521-7335 521-1987 Fax 510-0573 521-4020 AL 26

Mineral Processing and Extractive Metallurgy Review,
1995, Vol. 14, pp. 249–273
Reprints available directly from the publisher
Photocopying permitted by license only

© 1995 OPA (Overseas Publishers Association)
Amsterdam B.V. Published under license by
Gordon and Breach Science Publishers SA
Printed in Malaysia

On-Line Viscometry in Particulate Processing

S. K. KAWATRA and A. K. BAKSHI

*Department of Metallurgical and Materials Engineering, Michigan Technological University
Houghton, MI 49931*

(Received 23 Jun 1995, in final form 11 September 1995)

On-line viscometry of suspensions is very difficult compared to viscometry of pure liquids. The problem arises because of the unstable nature of the suspensions, particularly when coarse and fast settling particulates are present. Several attempts have been made in the past in which special mixing chambers have been designed to maintain slurry homogeneity while measuring viscosity. However, the credibility of these instruments are questioned by many authors, as quite often the same systems measure different rheological behavior for similar suspensions. In most of the designs suggested in the past, solving one of the problems of suspension viscometry introduces new problems. For example, agitation can keep the solids suspended, but it can also seriously affect the sensitivity of the viscometer. In this article the problems involved with three different types of viscometers (rotational, capillary, and vibrational), which have been used for measuring viscosity of suspensions, are discussed.

BACKGROUND

Unlike non-particulate fluids, rheological measurements of particulate fluids (suspensions) are very difficult. Since a suspension is a multi-phase system, its rheology depends upon the properties of both the liquid and the solids which constitute the suspension. During rheological measurement, the stability of the suspension must be maintained, so that the properties of the suspension will not change while they are being measured. Suspension stability is influenced by several interdependent parameters, such as: (i) Settling velocity of the particles, which depends upon the liquid viscosity, particle size, and particle density; and (ii) Coagulation and flocculation, which depend upon the surface properties of the particles, which in turn are influenced by the chemistry of the carrier liquid. Other parameters, such as particle concentration and particle packing, also influence interparticle interaction, and hence the rheology. The forces arising from all these parameters affect the movement of the fluid, and changes in these will change the rheology of the suspension. Unfortunately, most of the viscometers available to-day are not capable of keeping up with these complex mechanisms of suspension rheology.

Nevertheless, the importance of suspension rheology is widely felt in various industries. In the food industry, more and more attention is given to rheological properties to utilize modern technology for food production, handling, storage, and

quality improvement[1]. In injection molding (ceramic and metal casting) lower viscosities are needed to facilitate mixing, transportation, and enhance solids loading (to reduce shrinkage during sintering)[2]. In paint manufacturing, optimum rheology is needed for quality control. Similarly in the coal and mineral industries, a complete knowledge of rheology is necessary for optimum grinding[3-5,38,39] and efficient separations[6,7,40]. Slurry rheology is also important in the emerging coal slurry utilization technologies. A suitable yield value is needed to store the slurry without allowing the solids to settle, while lower viscosities are needed at intermediate and high shear rates for easier transportation and better atomization[8,9]. Similarly, examples of the importance of slurry rheology can be seen in many other industries, such as in paper and pulp making, waste treatment, cement manufacturing, and so on. Therefore, the need for a suitable rheometer for process control in these industry is always felt. The search for such an instrument was reported as early as 1940[10] and researchers are still working towards it in the 1990's[11-13]. This shows that until today a satisfactory on-line rheometer for suspensions has not been developed. In this article, a survey of viscometry systems for particulate fluids is provided. Since measurement of coarse suspensions is more difficult than measurement of suspensions containing submicron particles, emphasis is given to research work conducted on systems containing coarse, fast settling particles. Three different types of viscometers, the rotational type, the capillary type, and the vibrational type, are discussed whose use have been reported widely for suspensions.

ROTATIONAL VISCOMETERS

Operating Principle

Because of their control over shear rate, rotational viscometers are widely used among researchers. Most rotational viscometers used for suspensions are of the co-axial cylinder type. A line diagram of a simple co-axial cylinder viscometer is given in Figure 1. In this type of viscometer, the fluid is placed in the gap between two concentric cylinders for measurement. Then one of the cylinders is rotated by a motor at a particular r.p.m. while the other is kept stationary, and the torque required to rotate the cylinder is measured. As the viscosity of the fluid increases, the drag force on the surface of the rotating cylinder increases. This in turn increases the torque reading, from which viscosity of the fluid is determined.

Thus the only parameters which are measured by the instrument are the torque (T) and angular velocity (Ω) of the rotating cylinder. Then shear stress is calculated from torque, and shear rate is calculated from angular velocity. Viscosity is calculated by taking the ratio of shear stress and shear rate. The rheological type of the fluid is determined based on the variation of shear stress as a function of shear rate, as shown in Figure 2. A Newtonian fluid has the same viscosity at all shear rates, while the viscosity of a non-Newtonian fluid varies as the shear rate changes. Unless proper equations are used to calculate shear stress and shear rates from torque and angular velocity, an incorrect value of fluid viscosity will result. Calculation of shear stress from torque is straightforward and can be expressed by the following equation, which is valid for both Newtonian and non-Newtonian fluids:

$$\tau = T/(2\pi r^2 L) \qquad (1)$$

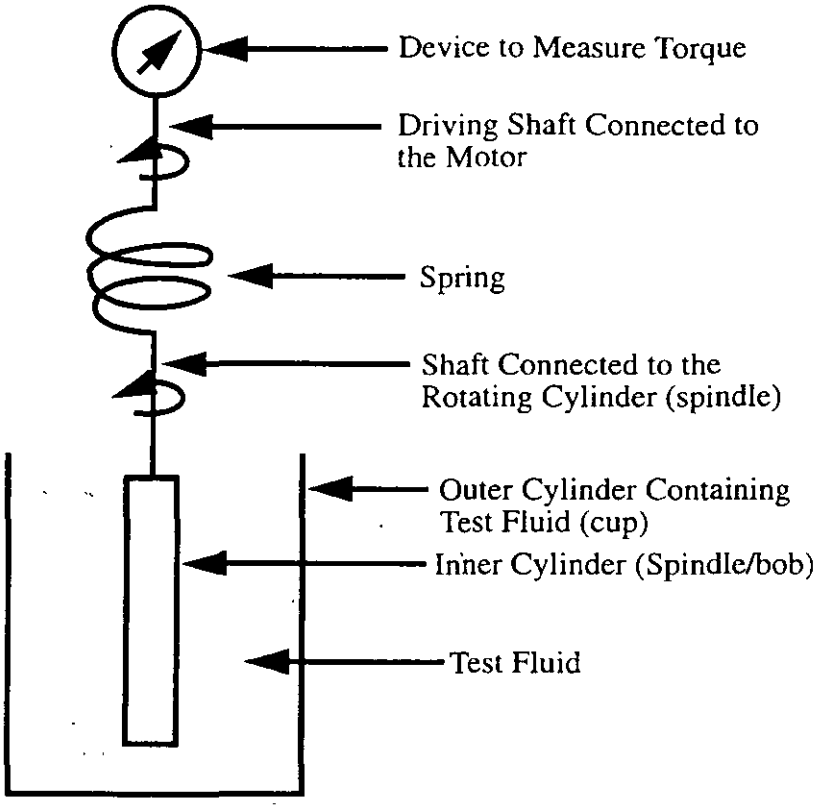

FIGURE 1 Line diagram showing the mechanism of a typical co-axial cylinder viscometer. The change in torque due to the drag force of the fluid on the rotating surface of the cylinder is the measure of viscosity.

Where, τ = shear stress
r = radial distance of the fluid from the axis of the inner cylinder
T = torque
L = length of the inner cylinder.

From this, it can be seen that the shear stress in the viscometer is not a constant, but decreases as one moves from the wall of the inner cylinder to the wall of the outer cylinder.

Calculation of the shear rate from the angular velocity is more complex, and depends upon both the type of fluid and the gap between the two cylinders. For Newtonian fluids:

$$\tau = \eta\dot{\gamma} \tag{2}$$

Where, τ = shear stress
$\dot{\gamma}$ = shear rate
η = viscosity

From this flow model it can be shown that[15],

$$\dot{\gamma} = [2R_2^2/(R_2^2-R_1^2)]\Omega \tag{3}$$

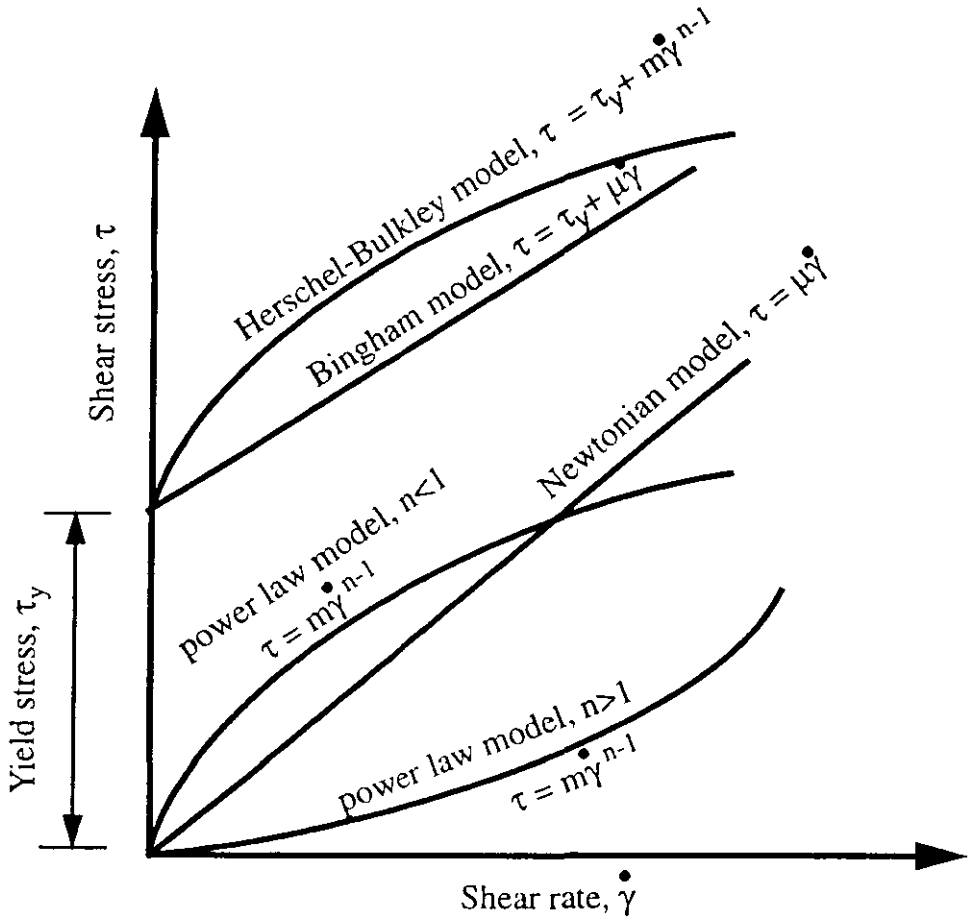

FIGURE 2 Flow curve models reported for suspensions.

where, $\dot{\gamma}$ = shear rate at the surface of the inner cylinder
R_1 = radius of the inner cylinder
R_2 = radius of the outer cylinder
Ω = angular velocity of the inner cylinder.

Quite often, Newtonian solutions of known viscosity are used to calibrate the torque scale of the viscometer to determine viscosity of non-Newtonian fluids. This is not correct because with different flow models different expression for shear rate will be obtained. For example, for a non-Newtonian fluid that obeys the power law (see Figure 2), the shear rate is given by the following equation:

$$\gamma = 2\Omega/n[1-(R_2/R_1)^{-2/n}] \quad (4)$$

where, $\dot{\gamma}$ = shear rate at the surface of the inner cylinder
R_1 = radius of the inner cylinder
R_2 = radius of the outer cylinder
Ω = angular velocity of the inner cylinder
n = flow index, from the power law equation.

From equations 3 and 4 it is seen that unless the appropriate equation is used to calculate shear rates of a particular fluid the viscosity measured by the viscometer will be wrong.

The measurement of the viscosity of a fluid with unknown flow behavior can be greatly simplified by using a coaxial cylinder viscometer whose annular gap is very narrow. If this gap is less than 1% of the diameter of the inner cylinder, then the velocity gradient of the fluid inside the annular gap will very closely approximate linearity for fluids of all types (Newtonian as well as non-Newtonian). In this case, the equation of the shear stress can be written as[15]:

$$\tau = T/(2\pi R_a^2 L) \tag{5}$$

Where, τ = shear stress at all points in the gap
R_a = average radial distance of the fluid from the axis of the inner cylinder
T = torque
L = length of the inner cylinder.
and the equation for shear rate can be simplified to[15]:

$$\dot{\gamma} = [R_a\Omega/(R_2-R_1)] \tag{6}$$

where, $\dot{\gamma}$ = shear rate at all points in the gap

From these values of shear stress and shear rates, flow curves of unknown fluid types can be determined.

While the narrow-gap coaxial-cylinder viscometers work well for liquids, they are unfortunately not suitable for coarse suspensions. This is because the narrow gap is prone to jamming and plugging by solid particles.

Critical Discussion of the Rotational Viscometers

Constant shear operation Rotational viscometers can be operated at a steady shear rate for a long time. This helps in taking precise measurements of viscosity at any particular shear rate, especially at low shear rates where yield stress can be calculated. By changing the rpm of the rotating spindle (or cylinder), the shear rate can be changed, thus a flow curve for non-Newtonian fluids can be determined with these instruments.

Wall slip The equations for shear stress and shear rates described in Equations 1 through 6 are derived under the assumption that the velocity of the fluid at the surface of each cylinder is the same as the velocity of the cylinder surface. This is the no slip condition or shear-flow condition. However, quite often slip occurs at the wall, and correct viscosity of a suspension cannot be obtained by using standard formulas. One of the reasons for such slippage in suspensions is believed to be migration of particles away from the cylinder wall[15,27]. This leaves a dilute suspension at the wall compared to the bulk of the fluids. This is often termed "apparent slippage," and it must be addressed while measuring suspension rheology. Corrections for slippage can be obtained experimentally by varying spindle dimensions, or theoretically by using correction factors suggested by various authors[15,27]. Some investigators have used cylinders with roughened surfaces (e.g., by cutting grooves on the surface) to avoid wall slip[16].

End effects Ideally the length of the cylinder in a co-axial cylinder viscometer should be infinite, to eliminate end effects. End effects are seen, because the fluid below the inner cylinder (and above the inner cylinder if it is submerged) will exert an additional torque on the spindle that is not included in Equations 1 through 6. End corrections are further complicated when different spindle shapes are used, such as the design shown in Figure 3(b) which has been used for eliminating solids build up on top of the spindle[11-13,20]. By changing this geometry, the direction of the velocity gradients will no longer be radially outwards at the ends. In some high precision laboratory viscometers, the bottom surface of the inner cylinder is made cup shaped to trap a layer of air below it, and so minimize the end effects. Also, by keeping the top surface of the inner cylinder above the fluid, torque exerted by the fluid on this surface can be eliminated. However, both these options cannot be practical in a flowing slurry line, and so cannot be used in on-line instruments. As far as end effects are concerned, the double gap design shown in Figure 3(c) is most suitable for suspensions, because it minimizes the end surfaces of the spindle.

Sensitivity Rotational viscometers are very sensitive and any disturbances associated with sample flow will offset the torque reading. In order to avoid settling of solids, many researchers have suggested top to bottom flow of slurry in the annular space. This arrangement will work if the flow is strictly vertical and has no component acting in the r (radial to spindle) or θ (tangential to spindle) directions. Otherwise the change in torque experienced by the spindle will not be solely from the molecular forces (shear) within the fluid, but will be supplemented by the fluid flow (see Figure 4). This also changes the shear rate experienced at the surface of the spindle because the flow interferes with its rotation[11,12].

Solids settling and centrifuging The most difficult suspensions for viscometers to deal with are those which contain fast settling particles. The solids settle during measurement, which not only destroys the homogeneity of the sample but also interferes with spindle

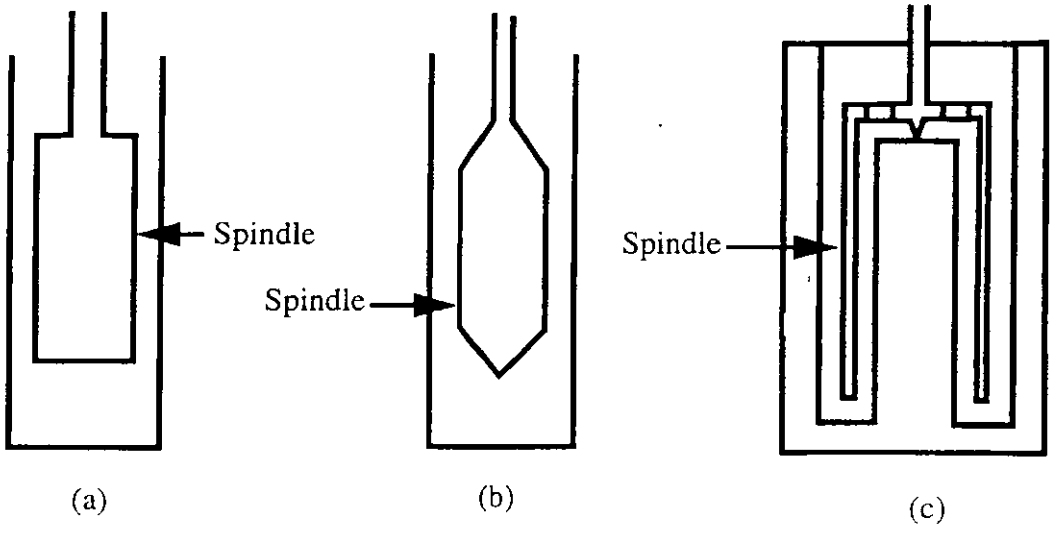

FIGURE 3 Different spindle designs adopted for suspension use.

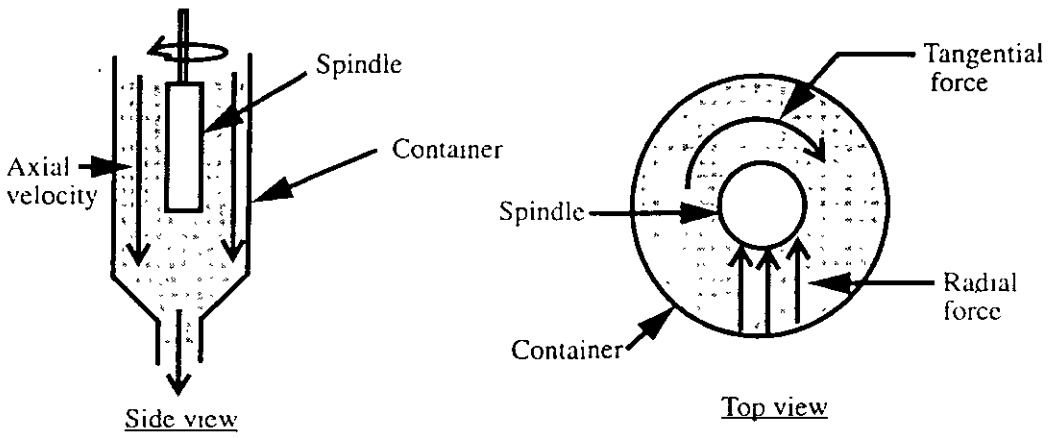

FIGURE 4 The axial flow (side view) prevents the solids from settling by continuously sweeping fresh slurry past the spindle. This component of the flowing slurry stream does not affect the rotation of the spindle. But any radial or tangential forces (Top view), arising from the flow, may put additional strain on the spindle resulting in erroneous viscosity readings. Unbalanced radial flows push the spindle to one side so that it does not spin uniformly and results in erratic readings. Tangential flows increase or decrease the torque on the spindle, making the fluid appear to be either more or less viscous then it really is.

rotation. For example, when the sample is taken in a beaker, solids start settling and slurry at the top of the beaker becomes dilute compared to the slurry at the bottom. Therefore, the spindle is no longer in contact with a representative sample. In this situation, the viscometer will read low viscosity if the compacted solids are below the spindle as shown in Figure 5(a) and a high viscosity if the compacted solids are touching the spindle as shown in Figure 5(b). Furthermore, when the rotational speed of the cylinder is increased to take measurements at high shear, the solids centrifuge outward towards the outer wall resulting in a poor measurement. These problems have been addressed by many past designs, and are discussed in the following section.

Solids plugging and the effect of annular gap For suspensions, the annular gap (the gap between the spindle and the sample holder) is usually large to avoid solids plugging. As a rule of thumb, this gap should be at least 10 times the largest particle size in the suspension[14]. Quite often liquids of known viscosity (Newtonian fluids like silicon oil or sucrose solution) are used to calibrate the torque scales which are then applied to calculate viscosity of non-Newtonian fluids. This is acceptable only when the annular gap is small (< 1% of the cylinder radius), and may not be correct when the gap is large. Therefore, for non-Newtonian suspensions, depending upon the flow model, proper equations (such as Equation 4) should be used to calculate the correct viscosity. Otherwise, the measurements will result in erroneous rheological characterization of the suspension.

Slurry Presentation Systems for Rotational Viscometers

Solids settling has been the major concern for most of the researchers who have used rotational viscometers for suspension viscometry. This has resulted in various designs of

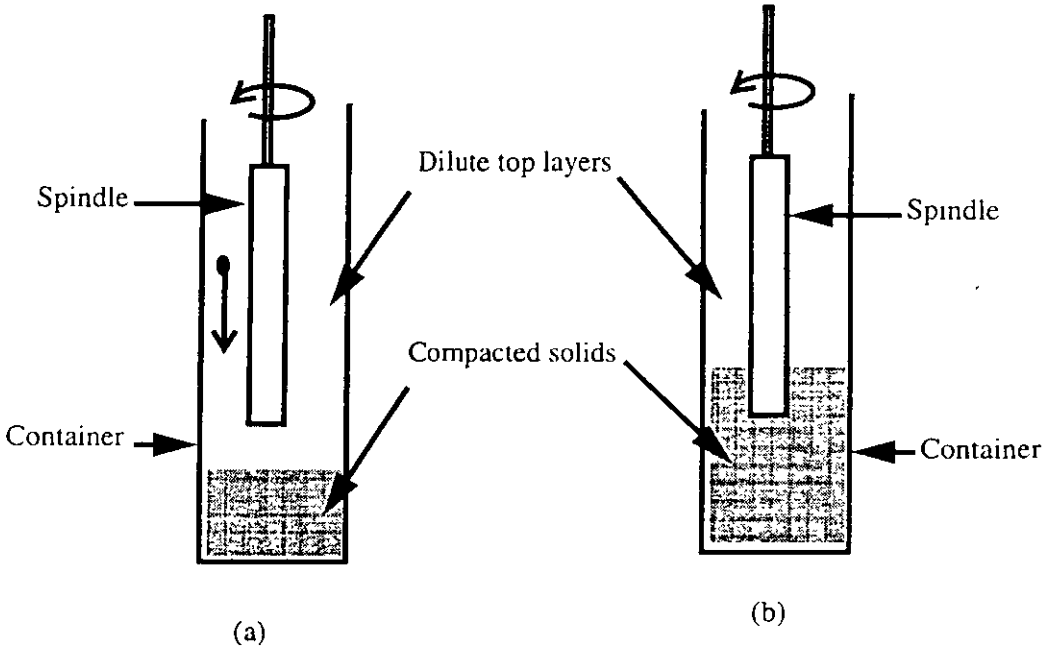

FIGURE 5 Solids settling leaves a dilute suspension on the top layers of the container. When the solids content is low (a) the solids gradually settle and are compacted below the spindle and the viscometer reads progressively lower viscosity as the solids settle At higher concentration of solids, the compacted solids can touch the spindle (b) resulting in higher readings

sample presentation systems to prevent solids settling during viscosity measurement. Some of these designs are discussed in this section.

Presentation systems in stirred tanks If proper precautions are taken, slurry viscosity can be measured by placing a rotational viscometer inside a stirred tank. One such arrangement has been reported by Clarke[16]. A line diagram of this measuring system is provided in Figure 6. He used a co-axial cylinder viscometer (Ferranti, Model VL), which could be operated between shear rates of 43 to 950 sec^{-1} with interchangeable spindles. The sample holder consisted of a 450 ml vessel with an eight bladed impeller at the bottom to keep the solids in dispersion. The impeller operated at 400 revolutions per minute. In order to prevent rotation of the sample inside the vessel, vertical baffles were fitted above the impeller. The whole arrangement was intended to encourage top to bottom flow of the solids so that the viscosity could be measured without obstructing the flow. Clarke tested suspensions of quartz, glass, and polymethacrylate in water with particle sizes up to 211 microns and concentrations up to 50% solids by volume. He measured apparent viscosity up to a shear rate of 350 sec^{-1}.

Clarke reported centrifuging of coarse particles (above 150 μm) because of the high speed of the impeller required to keep the solids in suspension. This offset the homogeneity of the suspension for many samples. In order to avoid centrifuging of solids, he took instantaneous measurements before the solids started outward movement. Clarke reported dilatancy of quartz suspensions at very low percent solids (10% by volume) which may have resulted from trapping of particles in the grooves which were made on the spindle surface to prevent slippage of the sample.

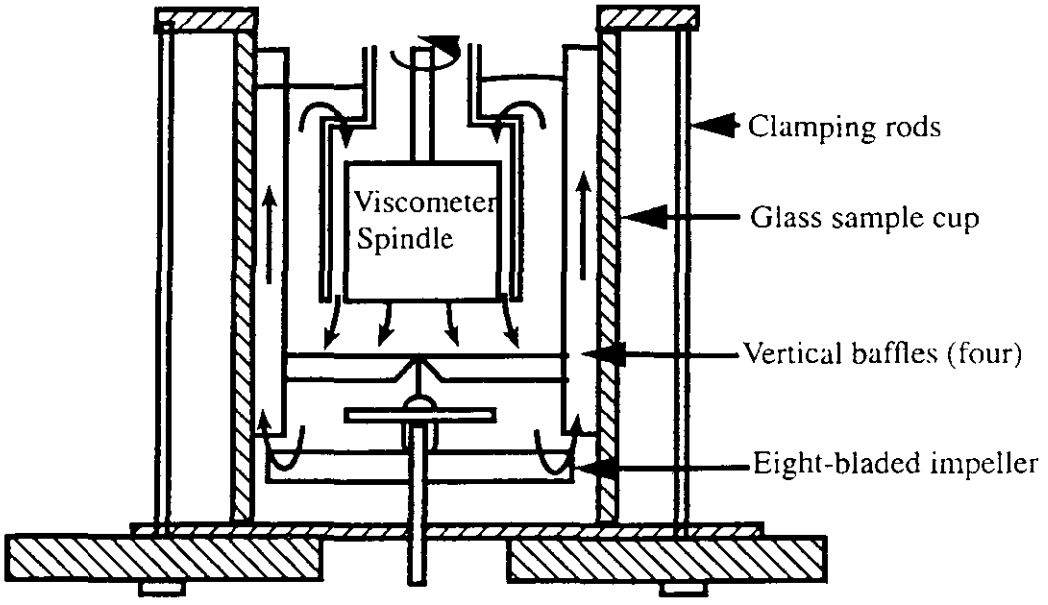

FIGURE 6 Sectional view of sample cup and measuring cylinders showing flow pattern (from Clarke 1967).

Similar designs were later reported by Lapasin[17] and Underwood[18] (Figure 7). In the Underwood design, a modified T-bar spindle (standard Brookfield spindles) was used The modified spindle had twelve cylindrical bars extending from a vertical shaft. The spindle was connected to a Brookfield model RVT viscometer. The sample was placed in a beaker which had an annular sleeve. A honeycomb of small diameter vertical cylinders was placed at the bottom. Below this honeycomb arrangement. a Teflon coated magnetic stir bar was placed. When the stir bar rotated, slurry ascended through the annular space. entered the beaker, flowed down past the spindle, and then drained through the honeycomb. The swirls and eddies created by the stirrer were prevented from reaching the spindle by this honeycomb arrangement.

Presentation systems in tanks with top to bottom flow Hemmings and Boyes[19] used a Brabender-Messtechnik Convimeter viscometer to measure apparent viscosity on the discharge line of a ball mill. The convimeter was mounted inside a column (Figure 8) and rotated in a gyratory motion at 120 revolutions per minute. Slurry from the ball mill flowed through this column. The level of slurry within the column was controlled by sensing the hydrostatic pressure and automatically controlling the slurry flow through the valve (by expanding or contracting an elastomeric flow restrictor). The operating range of the instrument was governed by the flowability of the slurry. This viscometer arrangement will not work for high solids concentrations when the slurry does not flow under gravity. Also, since the sensor moved in a gyratory motion, it did not have a well-defined shear rate. Therefore, at high percent solids when the slurry behaves in a non-Newtonian manner, the viscosity measured by the viscometer may not be the same as the viscosity experienced inside the mill.

Reeves[13,20] reported a rotational type viscometer for on-line use with slurries. He installed a specially designed spindle in a sample preparation and presentation system as

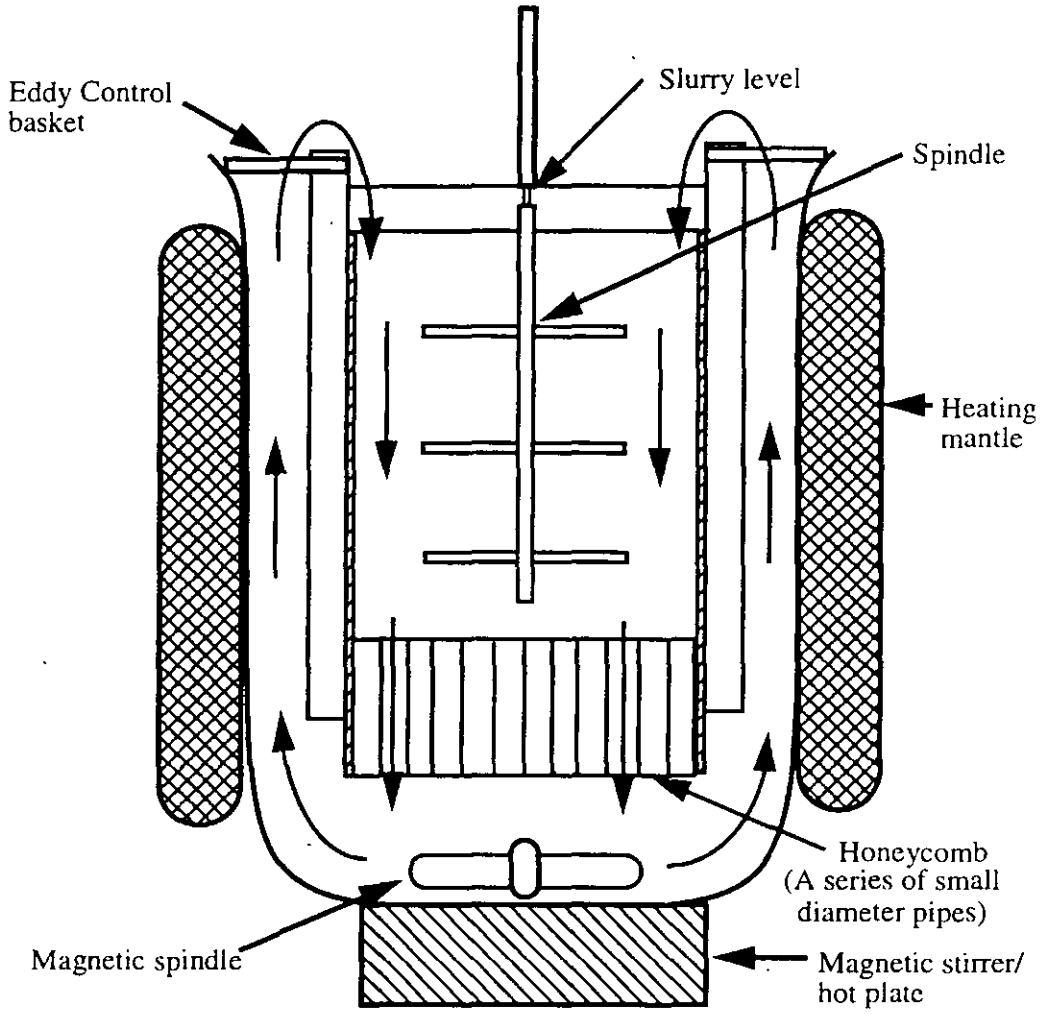

FIGURE 7 Viscometric assembly showing the spindle and eddy current basket (from Underwood 1976).

shown in Figure 9. The feed sample from the plant passed over a stationary screen (10–12 mm opening) to remove large particles and tramp materials. The instrument was capable of measuring viscosity within a shear rate range of 0 to 200 sec^{-1}, with the shear rate adjusted by changing the rotational speed of the bobbin. The viscometer operated at a constant shear rate by choosing a single rotational speed for the spindle. Reeves made on-line rheological measurements of ferro-silicon suspensions with 14–16% solid concentrations. In this design, baffles were installed in the measuring chamber to eliminate rotation of the sample in the container. Still he reported fluctuations in viscometer reading for fluids below 10 centipoise.

The Hemmings and Boyes design and the Reeves design were the only two rotational viscometer systems tried on-line for mineral slurries. These viscometers depend upon the flowability of the slurry[19], i.e. as long as the slurry flows under gravity through the sample presentation system, the associated viscometers can measure the viscosity. This may not be the case in many concentrated suspensions, where yield stresses are seen.

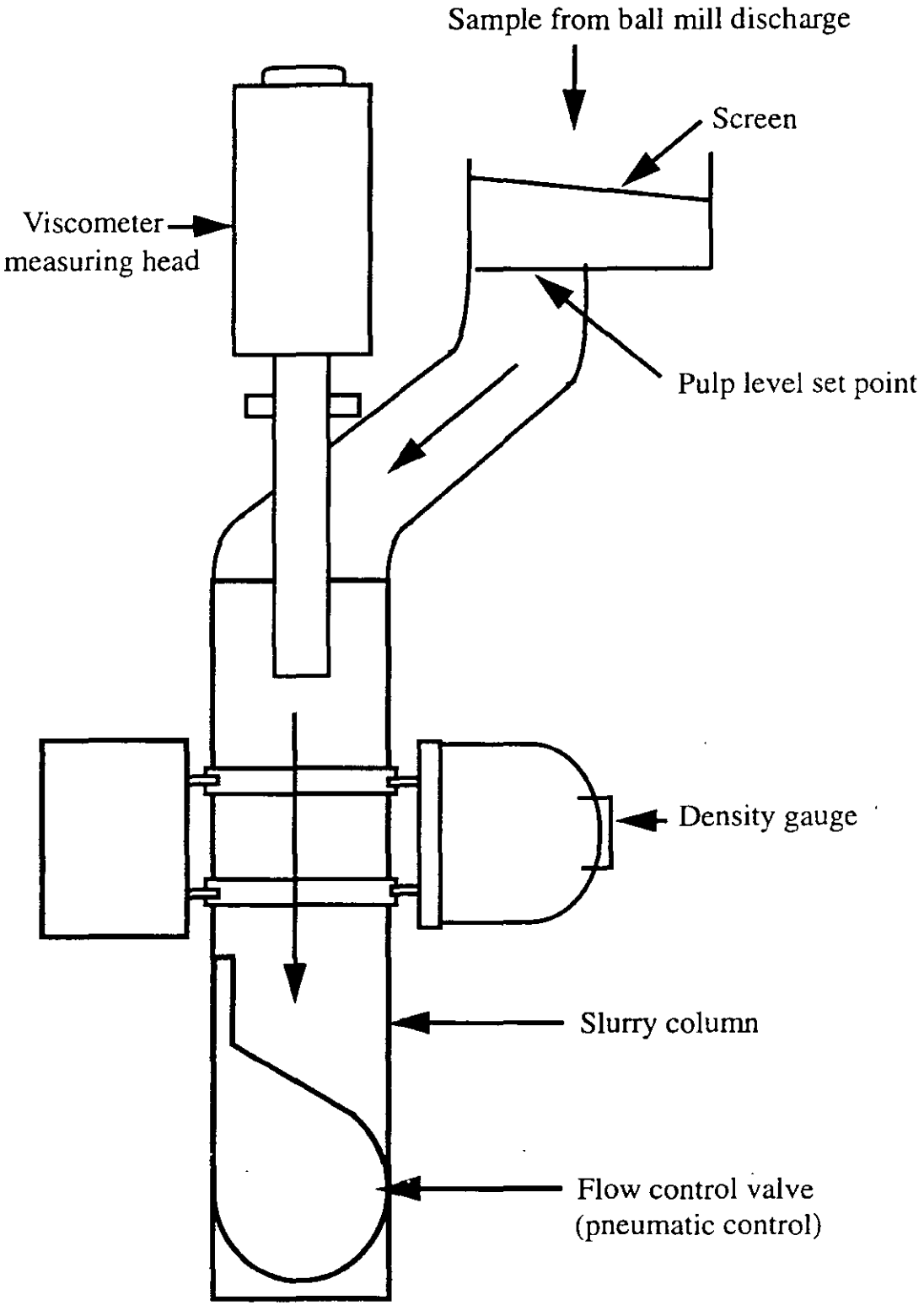

FIGURE 8 Viscosity sensing system designed by Hemmings and Boyes (from Hemmings and Boyes 1977)

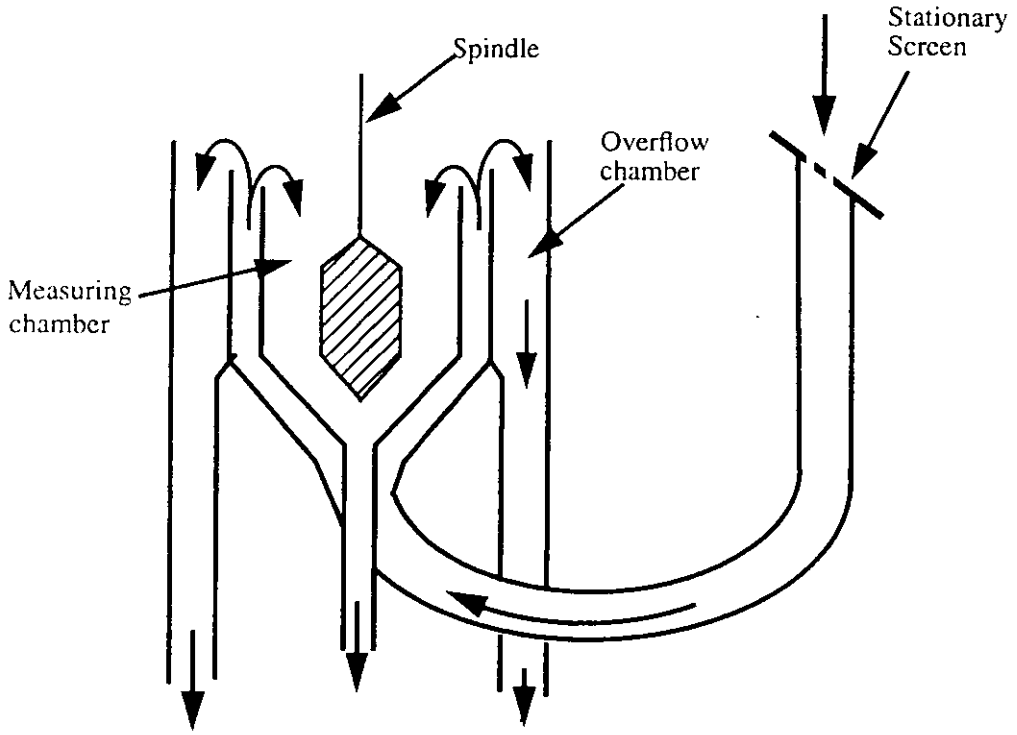

FIGURE 9 Viscometer arrangement developed by Reeves, 1984. The spindle, is made conical at the top and bottom surfaces to avoid solids deposition on top of it. (from Reeves 1984)

e.g., in grinding mills and concentrated coal slurries[4]. These slurries will be too viscous to flow properly through the gravity flow sample presentation systems.

Unless precautions are taken, the annular space in rotational viscometers can be plugged by coarse particles or tramp materials. In both the systems described above, it has been suggested that this problem be solved by pre-screening the sample before it entered the measurement chamber.

In general, the use of rotational viscometers in gravity fed sample presentation systems are questionable because the viscometer measures the drag from the fluid, and any tangential or radial forces on the spindle will affect this measurement (Figure 4). Most rotational viscometers are very sensitive to these forces, and the problem becomes severe when the instruments are used on-line. The use of baffles is aimed at reducing these effects. While evaluating the use of an eddy control basket[18] for measuring viscosity with a Brookfield viscometer, we realized that completely avoiding tangential or radial forces from fluid flow is a very difficult task. This is especially true for low viscosity fluids (such as water). Because of these concerns, Klien *et al.*[11] designed a different technique for measuring the rheology of unstable mineral suspensions which took advantage of the zone settling properties of some suspensions. They assumed that after the sample is placed in a container, solids settle and a constant density zone is created in the container. Then they constructed a double gap bob and cup arrangement. This bob and cup fixture was attached to a Haake Rotovisco RV 20 viscometer. They tried to place the bob in the constant density zone for shear stress and shear rate measurement (Figure 10). They measured rheograms of magnetite suspensions at solid

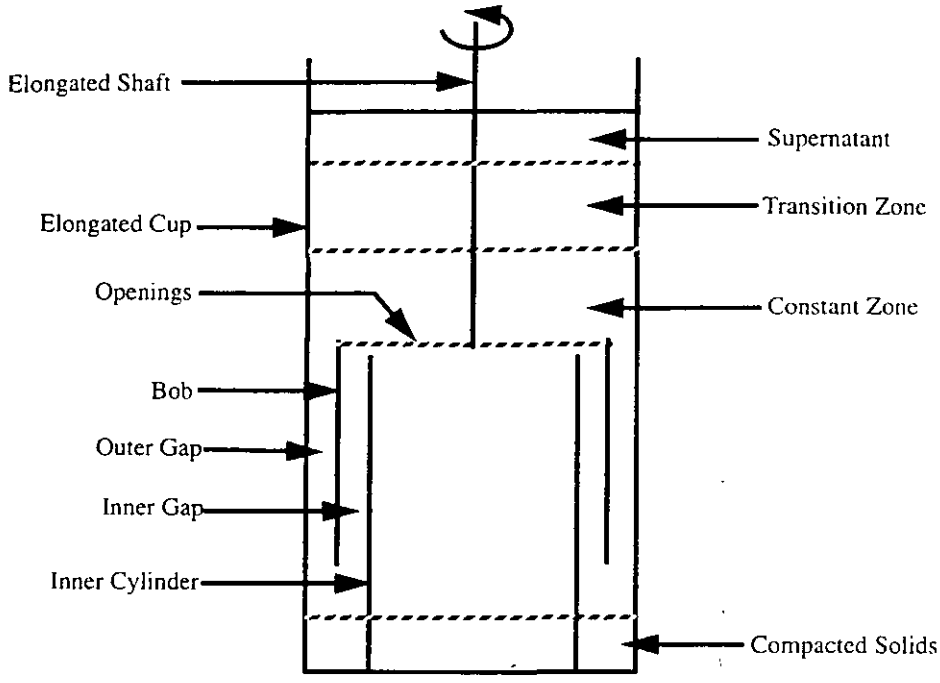

FIGURE 10 Line diagram of the double gap cup and bob arrangement for measuring the zone settling properties of suspensions (from Klien *et al.*, 1990).

concentrations of 11 to 25% by volume. In this way the undefined forces (tangential and radial) that could be generated by mixing arrangements were eliminated. However, since the coarse and fast settling particles were allowed to settle at the bottom of the container, the solids contents in the constant density zone must be different from the initial sample. Thus this arrangement cannot maintain a representative sample. Since solids concentration greatly influences the slurry rheology, this arrangement cannot be accepted for rheological measurements of suspensions.

The influence of undetermined forces generated by slurry flow (across the viscometer) is further reported by Kiljanski[12]. He too used a double gap coaxial fixture attached to the driving and measuring unit of a commercial rheometer (Figure 11). The viscometer operated at shear rates between 0.26 sec^{-1} and 870 sec^{-1}. The sample was pumped through the viscometer by a centrifugal pump, making a top to bottom flow (axial flow) of the fluid sample inside the viscometer. He used two samples of magnetite dense media, one at 34.5 vol% collected from the bottom of a drum separator which was contaminated with processed coal and the other was a 12.5 vol% suspension made out of pure magnetite dense medium. In his experiments, Kiljanski measured shear stress and viscosity at different shear rates at two different conditions, (i) while the sample was flowing through the instrument and (ii) after the flow was stopped. He noticed clear difference in readings between measurements made with circulation (when the suspension was flowing) and without circulation (when the flow was stopped). He argued that these differences in readings were (i) because of the additional shear rates imposed due to axial flow of sample, and (ii) because of an additional torque developed due to the inertia of the fresh, non-rotating fluid entering the viscometer, to which the rotation has to be imparted by the spindle (resulting in a higher shear stress). Kiljanski

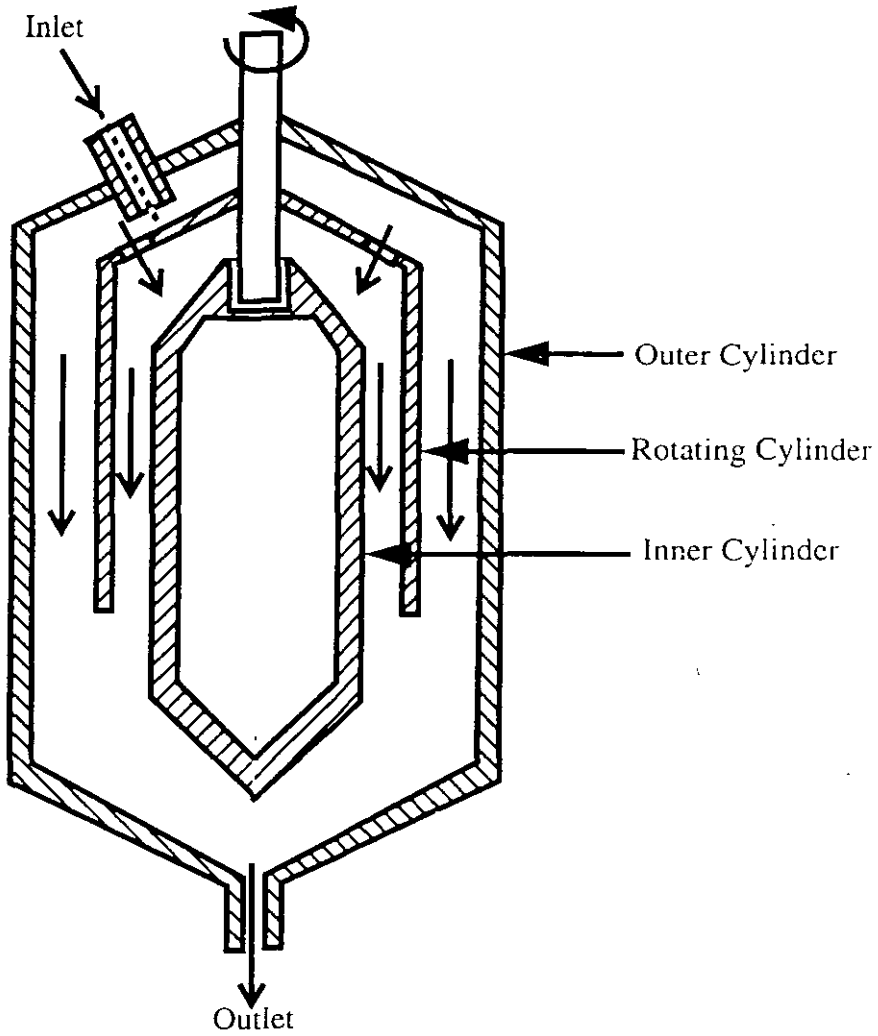

FIGURE 11 Simplified diagram of double gap rotational viscometer designed by Kiljansski, 1993. Both the outer and inner cylinders were held stationary. The diameters of the gaps outside and inside of the rotating cylinder (spindle) were designed such that the shear rates on both outer and inner surfaces were constant (from Kiljanski 1993).

also noticed differences in viscosity readings when the annular gap was increased. He argued that for smaller gap the axial shear rate originating from axial flow (top to bottom flow of the fluid) of fluid is higher than the axial shear rate for a wider gap, therefore viscosity measured at similar shear rates (calculated from the rotational speed of the spindle) were different. This shows how the undetermined forces from the sample circulation in the viscometer can generate misleading results.

Summary Solids settling has been the primary focus area for researchers working on rotational viscometers. Continuous agitation or top to bottom flow seems to be the answer to this problem. However, rotational viscometers are very sensitive and both these methods for keeping the solids in suspension create undue forces which seriously affects the viscometer readings.

Control of shear rate is the strongest point of rotational viscometers. This helps in measuring the rheology of non-Newtonian fluids, specially at low and medium shear rates. However, at higher shear rates (above 300 sec^{-1}) rotational viscometers are not suitable for suspensions because high rotational speed of the spindle produces a centrifugal force that segregates the solids

The annular gap between the cylinders must be at least 10 times larger than the largest particle in the suspension to avoid solids plugging. The sample must also be screened to remove any oversize and tramp material. Other problems which must be considered for rotational viscometers are wall slip and end effects.

CAPILLARY VISCOMETER

Operating Principle

In a capillary viscometer the fluid is passed through a tube under pressure. By measuring the flow rate and pressure drop across the tube shear stress and shear rate can be calculated. Although capillary viscometers are normally designed for Newtonian fluids, they are also extensively used for non-Newtonian fluids. These viscometers provide a simple and inexpensive method for rheological measurement, and when suitable for an application, capillary viscometers are more precise than rotational viscometers[15]. Specifically, these viscometers operate better at higher shear rates[22] which are common in many processing and manufacturing units.

For a fluid flowing through a tube (Figure 12) the shear stress at the wall can be calculated from the pressure difference across the tube by using the following formula:

$$\tau = R(P_1 - P_2)/(2L) \tag{7}$$

Where, τ = shear stress at the wall
P_1 = Pressure at the entry of the tube
P_2 = Pressure at the exit of the tube
L = Length of the tube
R = radius of the tube.

Shear rate at the wall for Newtonian fluids can be calculated by measuring the flow rate, Q through the tube by applying the following formula:

$$\dot{\gamma} = 32Q/\pi R^3 \tag{8}$$

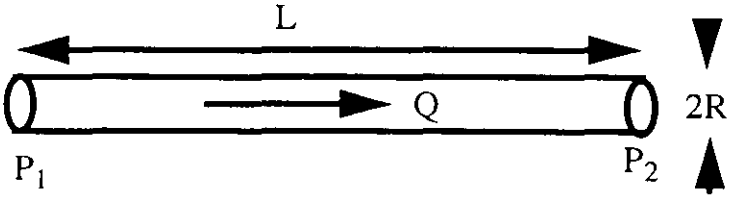

FIGURE 12 Line diagram of a capillary tube.

Where, $\dot{\gamma}$ = shear rate at the wall
Q = flow rate

Thus by using the measured pressure difference across the tube and the flow rate through the tube, shear stress, shear rate, and viscosity can be calculated. Equation 8 is derived from the Newtonian flow model. Therefore, for such fluids Equation 8 gives the true shear rate of the fluid. For non-Newtonian fluids the shear rate obtained from Equation 8 is called the apparent shear rate. True shear rate of non-Newtonian fluids can be obtained from $32Q/\pi R^3$(Equation 8) by the following formula which is derived by Metzner and Reed[23] after modifying the Rabinowitsch[24] equation:

$$\dot{\gamma} = (3n' + 1/4n'). (32Q/\pi R^3) \tag{9}$$

Where, $\dot{\gamma}$ = shear rate at the wall
n' = flow index given by the following formula

$$n' = \frac{d\log (\Delta P/4L)}{d\log (4Q/\pi R^3)} \tag{10}$$

Where, n'= flow index
ΔP = pressure difference across the tube = $P_1 - P_2$

n' can be determined graphically by plotting $\Delta P/4L$ vs. $32Q/\pi R^3$ on a log-log scale and measuring the slope of the resulting line. Equations 9 and 10 are valid for fluids with or without yield stress[23].

Necessary Conditions for Capillary Viscometers

The necessary conditions[25] (Bird *et al*., 1960), which must be satisfied in a capillary viscometer measurements are:

a) Laminar flow (Reynolds number < 2100)
b) Constant fluid density
e) Steady flow
d) End effects are negligible
e) No slip between the wall and the fluid
f) The fluid must be incompressible.

Common Capillary Viscometer Types

Common capillary viscometers are either constant flow type or constant pressure type viscometers. Piston viscometers are examples of the constant flow type. In these viscometers, fluid is pushed through the tube by a piston moving at a constant speed. Thus the flow rate through the tube remains constant. By measuring the pressure difference across the tube, viscometric functions can be calculated. In constant pressure

capillary viscometers a constant pressure is applied at the entry of the tube and the flow rate is measured by collecting the fluid flowing through the tube[15].

Discussion of the Capillary Viscometers

Capillary viscometers have several advantages as listed below.

- Since the flow is continuous and the sample stays inside the tube for a very short time, solid settling inside the viscometer is not a problem. However, the suspension should be kept well mixed before it enters the tube. This is usually done in an agitated system immediately before the sample enters the tube[28,29].
- Capillary viscometers are suitable for making measurements at high shear rates, where industrial operations such as pumping and spraying are carried out.
- They are simple to construct, and if they can be suitably used with a given fluid, can generate more accurate data than a rotational viscometer.

Many of the problems encountered in rotational viscometer are also common in capillary viscometers. Some of the examples are listed below.

- Similar to rotational viscometers, the diameter of the capillary viscometer should be at least 10 times larger than the top particle size of the suspended particles. Therefore, the sample must be screened to remove unusually coarse material before it is allowed to pass through the tube.
- Slippage at the wall is still a problem with capillary viscometers. This is mainly because of particle migration away from the wall[15,21]. As a result, a more dilute fluid is left in contact with the wall. The presence of wall slip can be detected by comparing flow curves of the same sample generated by tubes of different diameters[27]. This problem is minimized by selecting tubes with larger diameters with respect to the top particle size in the suspension, or by using any of several suggested correction factors[15,37].
- End effects are noticed in capillary tube viscometers, because of pinching of the slurry stream at the entry and exit of the tube[21]. Therefore, flow profiles at the ends are different than in the rest of the tube. This problem is eliminated by using tubes with high length to diameter ratio (above 300).
- Tubes must be calibrated at suitable intervals to compensate for any diameter changes resulting from abrasion or scaling.

Despite these problems, capillary viscometers are widely used by many investigators[15,21,23,27,28].

Selected Designs

Examples of the use of capillary viscometers for suspensions are abundant in the literature. Antonini *et al.*[28] measured rheological properties of a coal water slurry with 70 wt% solids content by using different dimension tubes. Their apparatus consisted of a 10 liter reservoir equipped with interchangeable tubes of different lengths and diameters.

The slurry was agitated by a pneumatic stirrer. For each pressure applied, they measured the flow rates by continuously weighing the slurry flowing through the tubes. Then from pressure gradient and flowrate, they generated flow curves for the coal slurry samples.

Turian *et al.*[29] reported a new design of capillary viscometer for measuring shear stress, shear rate, and yield stress of suspensions. The main body of the instrument consisted of a stainless steel container to hold the sample. The solids were kept in suspension by stirring the sample in the container. They used different dimension stainless steel tubes (with diameters from 2.4 to 8.8 mm) which could be connected to the bottom of the container. The sample flowing through the capillary tube was collected by a bucket placed on top of a electronic balance. The whole system was covered by a water jacket to maintain a constant temperature. Flow rate through the tube was determined by the balance whose signal was recorded by a computer. Shear stress (τ) and shear rate $\dot{\gamma}$ were calculated from pressure drop ΔP and flow rate Q.

Turian *et al.* determined yield stress by extrapolating the shear stress-shear rate curve to a shear rate of zero. They used pulverized Pittsburgh Seam (No. 8) coal to make the measurements over a shear rate range of 1 to 10^4 sec^{-1}. They also determined the yield stress of the slurry by the vane method[30] to verify the result obtained from the capillary tube, and reported that the yield stresses obtained by both the methods were similar.

Another way of measuring viscosity of a slurry is to drain a measured volume of slurry from an overhead container through a capillary tube and to measure the time taken for the material to drain completely. The slurry is kept in suspension in the tank by constant stirring. This method was first tried by DeVaney and Shelton[10], later it was reported by other authors[7,26]. The model used by Schack *et al.*[26] is shown in Figure 13. The authors measured the viscosity by measuring the time required for 100 ml. of

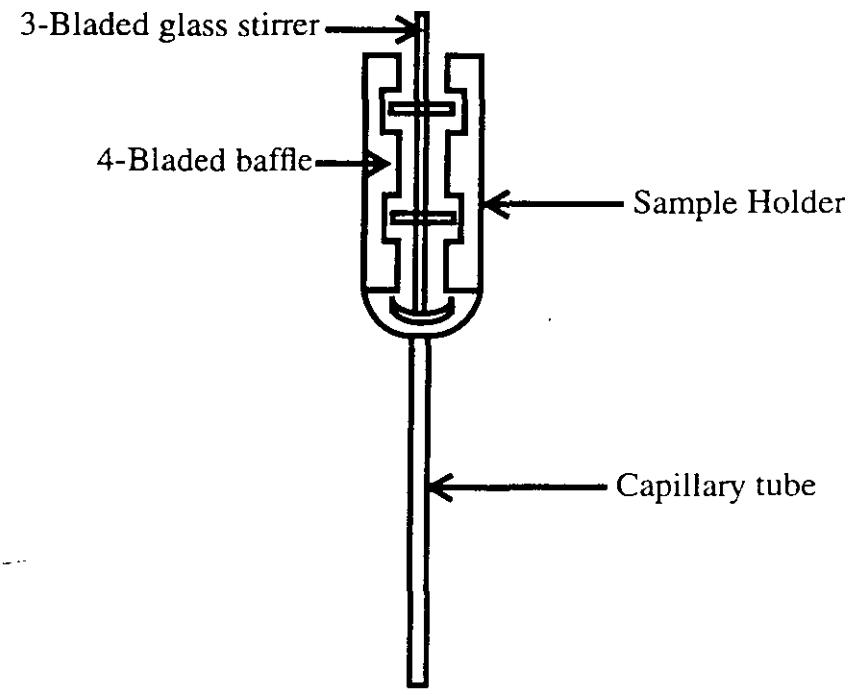

FIGURE 13 Diagram of consistometer chamber and capillary discharge tube used by Shack *et al.*, (from Schack *et al.*, 1957)

suspension to flow through the discharge tube. The major drawback of this instrument is that it does not determine whether the suspension is Newtonian or non-Newtonian. Also, it makes measurements at low shear rates, making it impossible to extrapolate to high shear rates (for hydrocyclone or pumping)[7].

Capillary viscometers are also used in plants to measure effective viscosity of fluids. This can be accomplished by measuring the pressure drop across a straight stretch of pipe. Shear stress and shear rate at the pipe wall can be calculated from pressure difference, flow rate and pipe dimensions. Apparent viscosity can be determined from the ratio of shear stress and shear rate at the wall. In this measurement, the fluid flow in the pipe must be laminar. In order for this method to work with suspensions, the suspension must be very stable (a high yield value), otherwise under laminar conditions a slow sedimentation process will take place at the bottom of the pipe[31].

Summary Compared to rotational viscometers, avoiding solids settling is relatively simpler in capillary viscometers, because the residence time of the sample inside the tube is very small. Measurements of non-Newtonian fluids can be made by changing different dimension tubes or by changing flow rates, which may not be an easy task in plants. For such measurements proper correction factors such as that suggested by Rabinowitsch[23,24] should be considered to obtain true viscosity of non-Newtonian fluids. As with rotational viscometers, wall slip and end effects must be considered while using capillary viscometers. Also, the sample must be pre-screened before allowing it to flow through the tube.

VIBRATING VISCOMETERS

Working Principle

Unlike rotational and capillary viscometers which are volume loading instruments, vibrating or oscillating viscometers are surface loading instruments, because they react only to a thin layer of fluid adjacent to the probe. The probe or sensor of the viscometer can be spherical (Figure 14), rod or plate shaped, or like a fork which vibrates in the fluid. The sinusoidal shear wave from the immersed probe is damped by the fluid, and

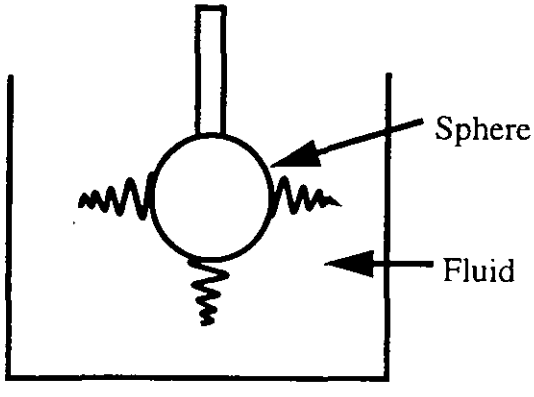

FIGURE 14 Vibrating sphere viscometer The probe oscillates in the fluid, and the power required to maintain a constant amplitude of oscillation is the measure of viscosity.

the damping is a function of the product of the viscosity and the density of the fluid. Usually the probe is oscillated at a constant amplitude and the force or power required to maintain this amplitude is measured. Rachman[33] derived the following formula for a vibrating rod viscometer to determine viscosity.

$$\eta = R_0^2/A^2\omega_0\rho[F_0x_{00}\omega_{00}/F_{00}x_0\omega_{00})-1]^2 \quad (11)$$

where, η = viscosity of the liquid
ρ = density of the fluid
ω_0 = resonant frequency
ω_{00} = free resonant frequency
x_0 = amplitude at resonance
x_{00} = amplitude in vacuum
F_0 = force at resonance
F_{00} = force required to maintain x_{00}
A = area of the surface in contact with the fluid
R_0 = transducer loss in the vacuum.

Thus by measuring the force F_0 which is required to maintain a constant amplitude x_0, and knowing the density ρ of the fluid one can measure the viscosity η. The remainder of the terms in Equation 13 will be constants for a particular instrument.

Discussion of the Vibrating Viscometers

Some of the advantages of vibrating viscometers over rotational and capillary viscometers are:

- Since the gap of fluid between the sensor and the container wall does not affect the reading, suspensions with coarse particles can be tested without the danger of plugging.
- Unlike rotational viscometers, oscillating viscometers are not affected by minor turbulences associated with slurry flow. Therefore, forces associated with slurry flow (see Figure 4) will not affect its readings.

The major disadvantage of this type of instrument is that the operator does not have any control over the shear rate. It is also difficult to measure the true viscosity of non-Newtonian fluid whose viscosity changes with shear rate. The shear rate $\dot{\gamma}$ will be a sinusoidal function of time. For a spherical probe, its peak value will be maximum at the equator and will be smaller by a factor cos ϕ at a sphere latitude of ϕ. Perry[34] derived the following equation for determining the maximum shear rate for the vibrating sphere viscometers:

$$\dot{\gamma} = k(\rho/\eta)^{1/2} \quad (12)$$

where, $\dot{\gamma}$ = maximum shear are
k = an instrument constant

From this equation we see that the maximum shear rate decreases as viscosity of the fluid increases. For a Newtonian fluid viscosity η is a constant, so maximum shear rate will remain constant. However, for viscoelastic fluids, the viscosity varies with shear rate, and computation of shear rate becomes complicated. Some investigators have suggested measuring the amplitude of vibration[33] and oscillating frequency as a means of measuring the apparent viscosity of viscoelastic fluids (non-Newtonian fluids)[35]. However, the reasoning provided for such measurements apply only to limited polymeric fluids, and the method does not work for suspensions[33,34].

Vibrating viscometers are sensitive to vibrations from supporting structures32,35. Unless precautions are taken to dampen these vibrations the instrument will pick up erroneous signals.

Selected Designs of Vibrating Viscometers

Vibrating rod viscometer for viscosity measurement Rachman[34] reported an assessment of vibrating viscometers in slurries. He utilized a vibrating plate transducer and a flexurally vibrating rod transducer in his research. However, for the suspension studies (with quartz slurries) only the flexurally vibrating rod transducer was used. In his initial experiment with 0.065 volume fraction solids in the slurry, Rachman experienced difficulty in measuring the viscosity because the solids settled quickly. In subsequent tests, the slurry was stirred vigorously by a motor driven pump to keep the solids in suspension. Then the stirrer was stopped and after 15 seconds, measurements were taken with the viscometer. In this way the investigator assumed that the slurry would have been in a similar state when each reading was taken. Similar measurements were taken with quartz-water slurries at 0.24 and 0.36 volume fraction solids. By changing the amplitude of vibration and transducer loading they showed that the denser slurries showed non-Newtonian flow whereas the dilute slurry with 0.065 volume fraction solids had Newtonian flow. However because of uncertain results, Rachman suggested use of this method only if no other simpler viscometer is obtained for measuring non-Newtonian slurry rheology.

Vibrating sphere viscometer for viscosity measurement Kawatra *et al.*[32] used a vibrating sphere viscometer manufactured by Nametre Co. along with a gravity flow sample presentation vessel as shown in Figure 15. Because of the basic design of the spherical oscillating probe (which oscillates at a high frequency and low amplitude rather than rotate in a single direction) and its durable construction, the flow of the slurry did not influence its reading. The solids settling problem was also eliminated because of the gravity flow arrangement of the slurry around the probe. Using this system Kawatra *et al.* were able to continuously measure viscosity of silica slurry at varying concentrations and temperatures in the feed line of a hydrocyclone.

However, the major difficulty in this type of instrument is that the operator has no control over the shear rate. The shear rate is a function of viscosity, higher in low viscosity fluids and lower in high viscosity fluids. Since most of the suspensions at higher solids contents show non-Newtonian flow their viscosity is highly dependent on shear rate. Thus for such suspensions, no logical conclusion can be drawn from viscosity measurements by these instruments unless they operate at the same shear rate as the process itself. Another problem with this type of instrument is that if the fluid velocity is very low, solids tend to settle in small layers over the top of the sphere (Figure 16)

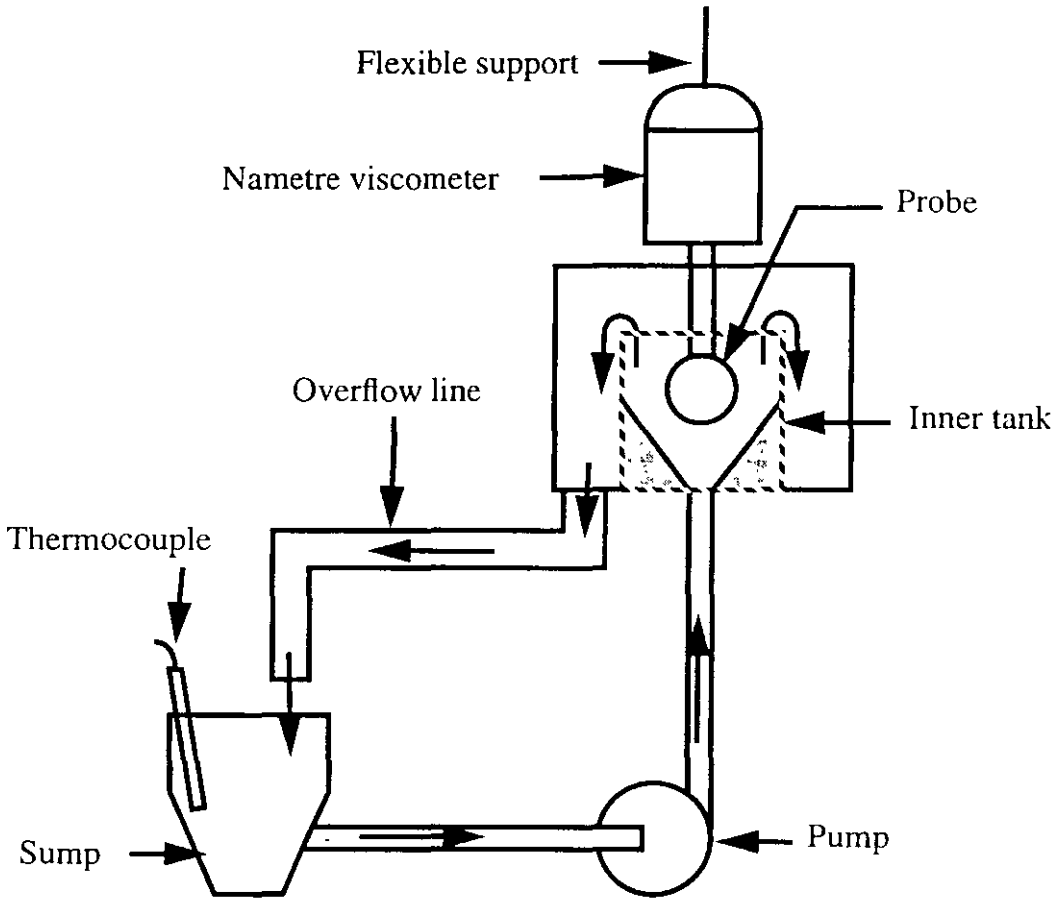

FIGURE 15 Nametre viscometer set-up. Sample is circulated through the system by a pump to keep the solids in suspension.

resulting in higher readings. These instruments are also affected by vibration from their surroundings, and special design is required to isolate from vibration. However, due to their ability to work in hostile plant environment, so far they are the most suitable instrument for making on-line viscosity measurements of Newtonian mineral slurries. The slurry used by Kawatra *et al.*[32] was Newtonian and therefore, good correlation could be established between the viscosity measured by this instrument and the hydrocyclone performance.

Vibrating sphere viscometer for distinguishing Newtonian and non-Newtonian suspensions Recently Kawatra and Bakshi[36] reported a system for classifying Newtonian and non-Newtonian suspensions in slurry streams. They used a vibrating sphere viscometer to measure apparent viscosity of slurries at high shear rates and a rotational viscometer to measure apparent viscosity of the same slurry at low shear rates. Since the shear rates were widely different, comparison of the apparent viscosities from the vibrating viscometer and the rotational viscometer allowed classification of the suspensions as either Newtonian or non-Newtonian flow types.

Summary The main advantages of vibrating viscometers over rotational and capillary

rheology of suspensions, their claims have been refuted later by other authors, because the instruments were not capable of repeating their performance. This shows that the particulate processing industry still needs a reliable viscometer which can work on-line under plant conditions.

References

1. R Lu and V. M. Puri, *J. Rheol.*, **36**(2), 303 (1992).
2. M K Agarwala, B. R. Patterson and P. E. Clark, *J. Rheol.*, **36**(2), 319 (1992).
3. D. W. Fuerstenau, K. S. Venkataramana, B. V. Velamakanni, *Inter. J. of Miner. Process.*, **15**, 251 (1984).
4. R. R. Klimpel, Part I, *Mining Engineering*, **34**(12), 1665 (1982), Part II, *Mining Engineering*, **35**(1), 21 (1983).
5. P. Tucker, *Trans. of Instn Min. Metall.*, Section C, Mineral Processing and Extractive Metallurgy, **91**, C117 (1982).
6. S. K. Kawatra, T. C. Eisele, Proceedings of the Sixteenth International Mineral Processing Congress, Elsevier Science Publishers B. V., *Amsterdam*, 1988, pp. 195–207.
7. F. F. Aplan and H. R. Spedden, Seventh International Mineral Congress, New York (Ed.) N. Arbiter, Gordon and Breach, New York, 1965, pp. 103–113.
8. R. B. Klose, Proceedings of the Sixth International Symposium on Coal Combustion and Technology, June 25–27, Orlando, Florida, 1984, pp 791–805.
9. S. C. Tsai and E. W. Knell, FUEL, **65**, 566 (1986).
10. F. D. DeVaney, S. M. Shelton, Rep. Invest. U. S. Bur. *Mines*, **3469R**., 24 (1940).
11. B. Klien, S. J. Partrigdge, J. S. Laskowski, *Coal Preparation*, **8**, 123 (1990).
12. T. Kiljanski, *Coal Preparation*, **13**, 107 (1993).
13. T. J. Reeves, *Coal Preparation*, **8**, 135 (1990).
14. J. Orban and P. Pacevaux, *Oil and Gas Journal*, **84**(26), 94 (1986).
15. R. W. Whorlow, Rheological Techniques, Chapter 2 and 3, Halsted Press, New York, 1980, pp. 57–191.
16. B. Clarke, *Trans. Inst. Chem. Engrs.*, **45**, T251 (1967).
17. R. Lapasin, *Coal Preparation*, **5**, 167 (1988).
18. W. M. Underwood, *Rev. Sci. Instrum.*, **47**(9), 1079 (1976).
19. C. E. Hemmings and J. M. Boyes, Twelfth International Mineral Processing Congress, Sao Paulo, 1977, pp. 46–64.
20. T. J. Reeves, *Trans. Instn. Min. Metall.*, Section C, Mineral Processing and Extractive Metallurgy, **94**, C201 (1985).
21. E. I. Shaheen and D. C Bogue, Rheological Study of Viscosities and Pipeline Flow of Concentrated Slurries, Selected Papers, Part 1, No. 58d, Sixty-Second Annual Meeting, AIChE, Washington, D.C., 1969, pp. 1–47.
22. S. C. Tsai and E. W. Knell, *FUEL*, **65**, 566 (1986).
23. A. B. Metzner and J. C. Reed, *AIChE Journal*, **1**(4), 434 (1955).
24. B. Rabinowitsch, *Physik. Chem.*, **1415A**, 1 (1929).
25. R. B. Bird, W. E. Stewart and E. N. Lightfoot, Transport Phenomena, Chapter 1 and 2, John Wiley & Sons Publication, Wiley International Edition, Singapore, 1960, pp. 3–70.
26. C. H. Schack, K. C. Dean and S. M. Molloy, Report of Investigations **5334**, U. S. Bureau of Mines, 1957, pp. 1–16.
27. R. J. Mannheimer, J. T. Park, T A. Grimley and T. B. Morrow, Fluids Engineering (Eds.) John Hyun Kim, Jae Min Hyun, Chung-Oh Lee, Hemisphere Pub. Corp., New York, 1991, pp. 513–535.
28. G. Antonini, O. Francois, P Gislais and A Touret, Proceedings of the Sixth International Symposium on Coal Combustion and Technology, June 25–27, Orlando, Florida 1984, pp. 266–281.
29. R. M. Turian, F. Hsu, K. S. Avramidis, D. Sung and R. K. Allerndorfer, *AIChE Journal*, **38**(7), 969 (1992).
30. K. S. Avramidis and R. M. Turian, *Journal of Colloidal Interf. Science.*, **143**(1), 54 (1991)
31. E. E. Cone, E/MJ, **169**(120), 82 (1968).
32. S K. Kawatra, T. C. Eisele and M T. Rusesky, Chapter 6, Comminution-Theory and Practice.

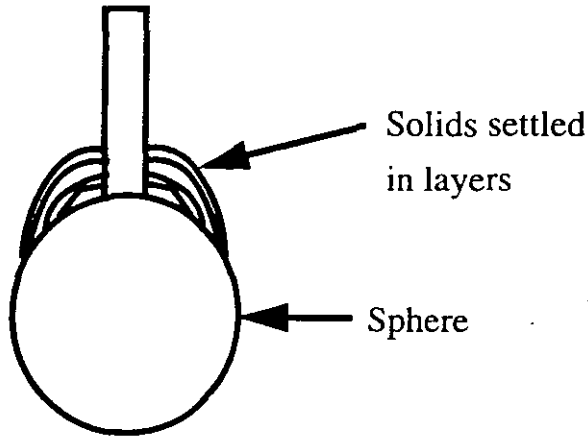

FIGURE 16 Vibrating sphere viscometer showing layers of solids settling on top of the sphere when the fluid velocity passing the spherical probe is small.

viscometers are, (i) these are less sensitive to plant disturbances, (ii) plugging is less of a problem, because these are surface loading instruments and the gap between the sensor and the container wall can be kept as large as required.

Vibrating viscometers still require some sort of agitation system to avoid solids settling. Since these viscometers are highly sensitive to vibrations from surrounding structures, steps must be taken to damp these vibrations. The main disadvantage of these instruments is their poorly defined shear rates which makes them highly unsuitable for measuring true viscosity of non-Newtonian suspensions.

CONCLUSIONS

Rotational and capillary viscometers are the most common viscometers which have been tried for measuring suspension rheology. Rotational viscometers have better control over shear rate which is essential for measuring the full rheology of non-Newtonian fluids. However, these instruments are very sensitive to disturbances in slurry flow. Because of this, many of the special designs studied in this report had baffle arrangements to inhibit unwanted forces like swirling and turbulence in the region of the measuring device. In capillary rheometers this problem is felt to a lesser extent because of the shorter residence time of the suspension inside the tube. However, the sample must be thoroughly mixed prior to its entry into the tube. Plugging is more of a problem in capillary tubes than in rotational viscometers. Slip at the walls is another problem felt by both the capillary and the rotational viscometers. In vibrating viscometers both plugging and wall slip can be eliminated easily, because vibrating viscometers are surface loading and the gap between the sensor and the container wall does not affect the measurement. Also, the vibrating viscometer can tolerate slight disturbance from slurry flow and is rugged enough for on-line use in suspensions. The main disadvantage of a vibrating viscometer is its inability to operate in a steady shear, which makes it unsuitable for non-Newtonian fluids. Otherwise, for Newtonian suspensions and for operations where a relative viscosity is needed vibrating viscometers are best suited for on-line use.

Although in the past many authors have claimed success in measuring on-line

(Ed.) S. K Kawatra, Society of Mining, Metallurgy, and Exploration, Littleton, 1992, pp. 529–545.
33. Y. A. Rachman, An Assessment of Vibrating Viscometers in Slurries, Report No. 2001, National Institute for Metallurgy, Private Bag X3015, Randburg, 2125 South Africa, 1979, pp. 1–20.
34. J. D. Perry, *Measurement and Control*, **143**(89), 89 (1977).
35. J. V. Fitzerald, F. J. Matusik and T. M. Walsh, *Measurement and Control*, December (1987).
36. S. K. Kawatra and A. K. Bakshi, *Coal Preparation*, **24**, 123 (1995).
37. M. Mooney, *J. Rheol.*, **2**(2), 210 (1931)
38. S. K. Kawatra, S. A. Moffat and K. A. DeLa'O, The effects of Freezing Conditions on Rock Breakage, Society of Mining, Metallurgy, and Exploration, Inc., Preprint Number 93–17, 1993.
39. K. J. Shoop and S. K. Kawatra, Effect of Rock Breakage Characteristics and Fines/Clay Content on the Autogenous Grinding of Iron Ore, Society of Mining, Metallurgy, and Exploration, Inc., Preprint Number 93–17, 1995.
40. A. K. Bakshi, K. J Shoop and S. K. Kawatra, Changes in Autogenous Grinding and Classification Performance due to Variation in Slurry Rheology, paper to be presented at the Society of Mining, Metallurgy, and Exploration, Inc. annual meeting 1996.

FACULTAD DE INGENIERIA U.N.A.M.
DIVISION DE EDUCACION CONTINUA

CURSOS ABIERTOS

DESARROLLO Y OPERACIÓN DE SENSORES PARA CONTROL DIRECTO Y CONTINUO EN PLANTAS DE BENEFICIO DE MINERALES Y EN LA RESTAURACIÓN DEL MEDIO AMBIENTE

Del 18 al 23 de mayo de 1998

TEMA: EFFECTS OF PULP RHEOLOGY ON AUTOGENOUS GRINDING PERFORMANCE

EXPOSITOR :DR. KOMAR KAWATRA

1998

Palacio de Mineria Calle de Tacuba 5 Primer piso Deleg. Cuauhtemoc 06000 México, D.F APDO. Postal M-2285
Telefonos. 512-8955 512-5121 521-7335 521-1987 Fax 510-0573 521-4020 AL 26

3 testing of core samples, however, will require samples because the core itself gives the proper ypes.

st offers the potential to implement mine planning oduction on a routine basis.

RECOMMENDATIONS

ower Index Test can be used to determine the o grind to 10 mesh. Additional power to give a d be added according to Bond ball mill grinding If Bond ball mill work index data is not available, igure 2 as a first estimate of SAG power required licated natural grain size.

Test for new projects to determine hardness varing the various rock types in several continuous rsections through an ore body. By knowing the n hardness, needed adjustments to pilot plant ade at the design stage. The SPI Test can be ations for mining pilot plant bulk samples for pilot

can be used as a problem solving tool at any opecially where ore hardness variance is causing ms due to lack of blending or other reasons.

ACKNOWLEDGMENTS

dgment is given to the six MITEC study spontheir support of the work described herein, but nission to publish this paper. Our thanks are Miramar Mining who have given permission to ng to the Delita Gold Project Feasibility Study paration.

REFERENCE

, G. and Kosick, G., "A New Tool For SAG . Proc. Canadian Mineral Processor's Confer-

SAG 1996
MINING AND MINERAL PROCESS ENGINEERING, UBC
Vancouver, B. C. Canada

EFFECT OF PULP RHEOLOGY ON AUTOGENOUS GRINDING PERFORMANCE

A. K. Bakshi, K. J. Shoop and S. K. Kawatra
Department of Metallurgical and Materials Engineering
Michigan Technological University
Houghton, MI 49931 U. S. A.

ABSTRACT

Autogenous grinding mill efficiency is affected by pulp rheology, which can change due to several factors such as ore composition, temperature, or chemical additions. In this study the effect of slurry viscosity on rock breakage characteristics and specific energy consumption were studied in a pilot scale autogenous mill. Rock breakage inside the mill was studied quantitatively by measuring the size stability of rocks on a scale of 0 to 100%, where a 100% size stability corresponds to zero rock breakage . Also, the effect of slurry viscosity on the production of critical size material was studied, where the "critical size" is material which is too large to be effectively ground in the mill, and too small to be effective for grinding other particles. The pulp rheology was altered by changing the initial clay/fines content of the feed and also by changing the initial temperature of both ore and water. It was observed that size stability, critical size material production, and specific energy consumption all increased as the slurry viscosity increased.

INTRODUCTION

The effect of slurry rheology on the performance of grinding ciruits has been well discussed in the literature (Hemmings and Boyes, 1977, Tucker 1982, Klimpel, 1982 and 1983, Fuerstenau

et al., 1984, Austin et al , 1984, Moys, 1989, Kawatra and Eisele, 1988, Kawatra and Bakshi, 1996) However, most of these studies dealt with ball mill grinding, where the grinding media are metal balls. In autogenous grinding, the media is the ore itself. Therefore, the efficiency of autogenous grinding also depends upon the way the media (larger size rocks) break inside the mill. Although the effect of rheology has been studied for various aspects of autogenous grinding (Moys, 1989), its effect on the breakage characteristics of the media is not discussed in the literature. This is an important problem, because small changes in the break-up rate of the media-sized rock will significantly affect the grinding efficiency of the mill

Another problem in autogenous grinding is the production of critical size material These are the particles that are too small to efficiently grind other particles, but too large to be easily ground themselves. Critical size particles tend to accumulate in the mill, and have to be removed and crushed separately as shown in Figure 1

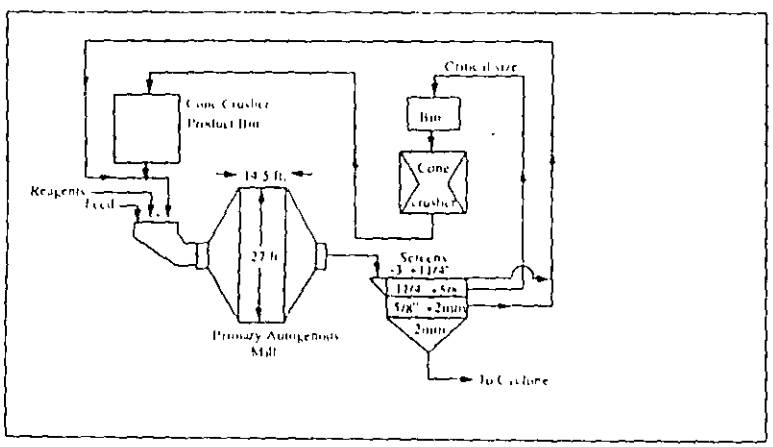

Figure 1. Typical autogenous circuit Critical size is crushed before feeding back to the autogenous mill

Therefore, production of critical size must be minimized to further save in energy consumption. Any changes in the slurry viscosity that result in a change in the rate of media break-up will also tend to change the amount of critical size material that is produced. This effect has been observed in an operating plant (Kawatra and Eisele, 1988) The plant personnel noted that in the winter the grinding efficiency was reduced, and the amount of critical size of

material produced was increased. These changes were linked to the seasonal temperature variations of the mill slurry. Two possible mechanisms were considered that could have been causing these effects: (1) The rock may have been becoming more brittle at low temperatures or (2) .The increasing slurry viscosity at low temperatures could have been affecting how the charge was lifted and tumbled in the mill. Past work by the authors has shown that the rocks were not becoming more brittle over the temperature range of interest (Kawatra et al., 1993), and so subsequent studies concentrated on the viscosity effects. In this article the impact of slurry rheology on the breakage characteristics of the rock and the overall energy consumption during autogenous grinding have been discussed. All tests were carried out using a pilot-scale mill so that the results would be relevant to what happens in a full-scale autogenous mill.

EXPERIMENTAL

Experimental Set-Up

Pilot Scale Autogenous Mill. Pilot plant tests were carried out in a 1 8 meter diameter by 0.6 meter long Hardinge cascade mill. The mill contained sixteen 2.5 cm high lifter bars. It was converted from continuous operation to batch operation by removing the grates on the discharge end of the mill and replacing them with liners made at Michigan Technological University. This mill was also insulated to maintain the initial charge temperatures, using 20 cm of fiberglass insulation applied to the circumference of the mill and 2.54 cm thick polystyrene foam insulation on the ends Energy consumption during each test was measured by a standard watt-hour meter

Viscometer Set-Up. Slurry viscosity was measured by a Brookfield viscometer. Since the slurry contained fast settling solids, it was necessary to modify the viscometer so that the solids would be kept in suspension while the reading was being taken. This was accomplished by the slurry presentation system shown in Figure 2. The slurry was mixed in an overhead tank and passed continuously through the annular space between a steel tube andthe spindle. After a steady state reading was displayed, flow w momentarily interrupted to eliminate any swirling motion d by flow at the inlet and a reading was taken immediately.

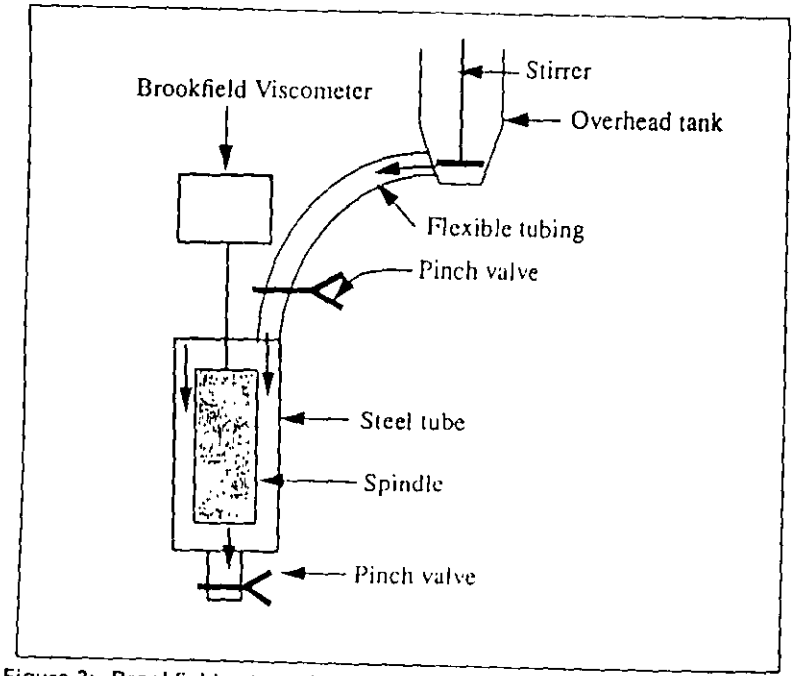

Figure 2: Brookfield set-up showing arrangement for measuring viscosities of rapidly-settling solids in slurries

This set-up is very suitable for measuring viscosity of slurries containing fast settling solids, and has been successfully used to characterize different slurries on the basis of their rheology (Kawatra and Bakshi, 1995).

Sample Preparation

An iron ore sample was collected from a local iron ore deposit. Each rock was sized and washed to (i) remove any fines that might be in the pores or fractures of the sample, and (ii) remove the visually detectable metamorphic clay material present in the sample. The washed ore was then dried. From this material, six samples were reconstituted according to the size distribution shown in Table 1. This was the original size distribution of the rocks in the pit from where the sample was collected. Samples prepared for cold tests were stored in a freezer at -25 °C, and samples prepared for tests at room temperature were stored in 55 gallon drums

Table 1: Size distribution of reconstituted feed sample for pilot scale AG tests.

Size Distribution, mm	Weight, kg	% Weight
-152.4 + 127.0	63.12	14.93
-127 0 + 101.6	65.83	15.59
-101.6 + 76.2	79 45	18.80
-76 2 + 50.8	82 17	19.47
-50.8 + 25.4	92.16	21.83
-25 4 + 12.7	39.50	9.38
Total	422.22	100.00

Test Procedure

Six tests were carried out in the pilot scale autogenous mill. The viscosity of the mill slurry in these tests was changed by changing the clay/fines content in the initial feed and by changing the temperature of both iron ore and water as shown in Table 2.

Table 2: Conditions for tests with pilot scale AG mill.

Test no.	Initial ore temp, °C	Feed composition	Slurry viscosity at end of test, mPa-sec
1	+25	Ore only	1.37
2	-25	Ore only	1.60
3	+25	Ore with 10% clay	1.42
4	-25	Ore with 10% clay	1 74
5	+25	Ore with 50% fines	5.24
6	-25	Ore with 50% fines	8 19

The clay material added during tests 3 and 4 was the same metamorphic clay which was washed from the initial ore collected from the mine pit During tests 5 and 6, 50% fines were added in the mill. The fines were prepared by grinding iron ore to pass 425 mm, and 59 5% of the resulting fines were finer than 150 mm. This was done because under plant conditions, a certain amount of fines (ground ore) is always present inside the mill due to

continuous operation. Since the tests were conducted as batch tests, the loads in the mill for tests 1-4 were initially devoid of these fines, and therefore had low slurry viscosities. The addition of a large amount of fine iron ore in tests 5 and 6 was expected to strongly show the effects that would occur in a plant situation due to the presence of fines.

The mill was chilled prior to the tests conducted at low temperatures. It was run empty for 30 minutes before each test to allow the bearings to warm up, so that bearing friction would be constant during the test. Then the mill was stopped, and solids charge was added to the mill A total of 423 kg solids were added for each test Then, 182 kg of water was added to keep the total solids content at 70% by weight The mill volume occupied by the charge was 26%. The initial temperature of water for the cold tests was maintained at 4 °C for test # 2, 4, and 6, and for other tests the water was at room temperature The slurry temperature was measured both at the beginning and the end of each test, to be sure that the mill did not warm significantly during the test

Once the mill was charged with solids and water, it was run for 15 minutes. A slurry sample for viscosity measurement was collected from the mill as soon as it stopped rotating. Energy consumption during the 15 minute grinding was measured using a watt-hour meter. The material from the mill was removed manually, and screened for size analysis

RESULTS AND DISCUSSION

Size Stability

Size stability vs slurry viscosity is shown in Figure 3. Size stability is a measure of the resistance of the media to impact breakage, and is expressed as follows (ASTM, 1991):

$$\% \text{ Size Stability} = \frac{\Sigma[(initialWt\%)x(avg.sievesize)]}{\Sigma[(finalWt\%)x(avg.sievesize)]} \times 100$$

Therefore, a size stability of 100% corresponds to a rock that did not break during grinding, and a size stability of 0% corresponds

to a rock that broke completely below the finest size measured (-12.5 mm in these tests).

As can be seen from Figure 3, size stability increased with increase in slurry viscosity, showing that at high viscosity the rocks had a higher resistance to breakage. This could be due to the fact that at higher viscosity the impact force between rocks was retarded by the viscous slurry which acted as a cushion, resulting in less breakage of the rock.

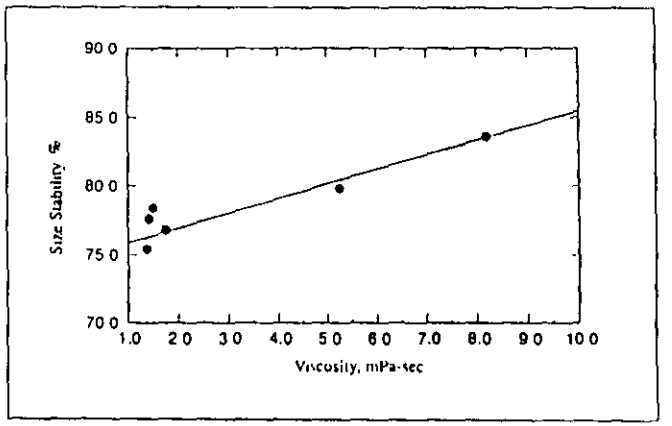

Figure 3: Size stability vs viscosity. At higher viscosity ore is less likely to be broken for all results.

Critical Size Material

The effect of slurry viscosity on critical size material is shown in Figure 4. Critical size material is the material which is too large to be effectively ground in the mill, and too fine to be effective for grinding other particles. This material is usually crushed outside the grinding mill (for example in a cone crusher as shown in Figure 1) before it can be sent back to the mill. In our tests, the change in the amount of material in the -25 4mm +12.7mm size fraction in the course of each test was small. Therefore, particles of this size were considered to be the critical size material.

The feed for each test initially contained 9.38% critical size material (see Table 1). The percentage of the critical size material was determined again at the end of each test As can be seen in

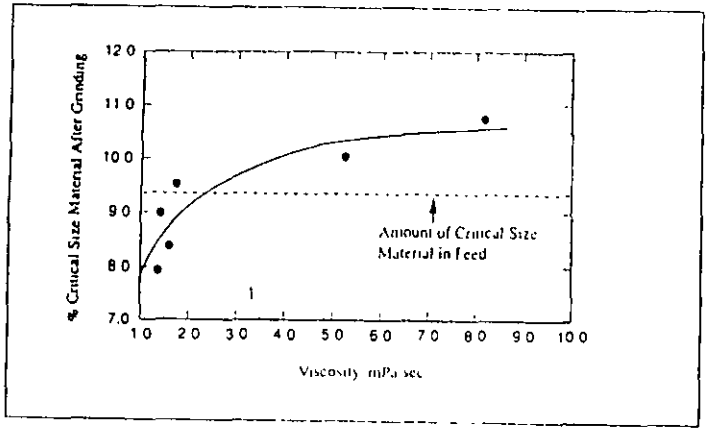

Figure 4: % critical size in mill after grinding vs viscosity. At high viscosity amount of critical was larger than at the start.

Figure 4, at low slurry viscosity the amount of critical size material in the mill after grinding was less than the amount of critical size material present before grinding However, at higher viscosity there was an increase in critical size material after grinding. During the first four tests, when the viscosity was low the slurry was more like water Therefore, in this condition the slurry did not leave a thick coating on the surfaces of both the media and the critical size particles This allowed some critical size material to be crushed upon impact. At higher viscosity, there was a thick coat of slurry on the media (large rocks) This retarded the energy of the impact collisions, and reduced the chances of a critical size particle to be broken up in the mill Therefore, during test No.6, when the viscosity was increased to 8 19 mPa-sec by adding fines and decreasing the temperature, the critical size content in the product increased by 1 37% to 10 8%

The results with added fines are most similar to the situation in full size plants, because due to continuous operation considerable amounts of fines are always present inside the mill which will keep the slurry viscosity in a higher range. For example Figure 5, shows the critical size material in a full-scale plant as a percentage of total feed during each month The data were collected over a period of two years from the local iron ore plant that provided the iron ore for the work reported herein As seen from the figure, critical size material production was at a minimum between April and September, and increased significantly duringDecember and January when the temperature was low (Kawatra and Eisele, 1992). It was originally believed that this change in

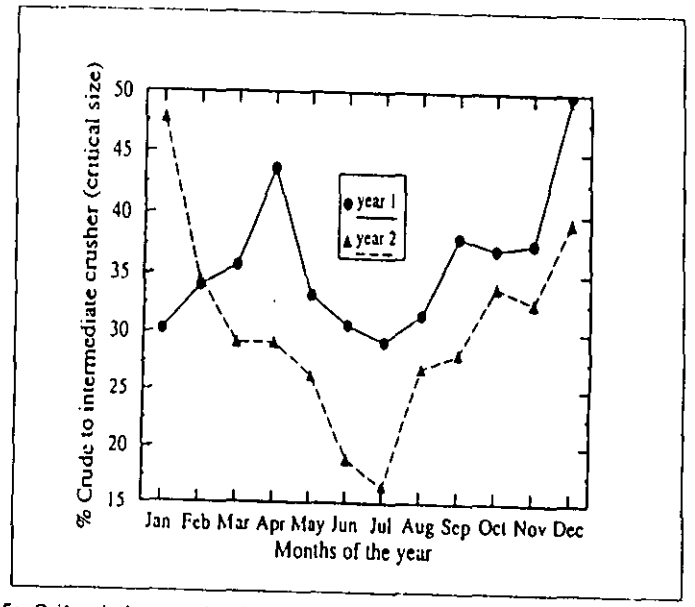

Figure 5: Critical size production in 8.2m x 4.4m primary AG mill for iron ore over 2 years.

critical size production was due to increased brittleness of the rock at low temperatures. However, drop tests conducted at Michigan Technological University showed that rocks did not become brittle over the temperature range of interest (+25 °C to -25 °C) (Kawatra et al., 1993). Therefore, these changes in critical size material production are due to viscosity changes caused by temperature variation.

Specific Energy Consumption

Specific energy consumptions at different slurry viscosities are shown in Figure 6 Specific energy consumption was calculated as the energy required to produce one kilogram of -150 micron material

As can be seen from Figure 6, the specific energy consumption of the mill increased with increasing slurry viscosity. The increase in specific energy from test 1 to test 4 was small, because the viscosity changes during these tests were also very small However, during tests 5 and 6 specific energy consumption increased significantly While comparing the specific energy con-

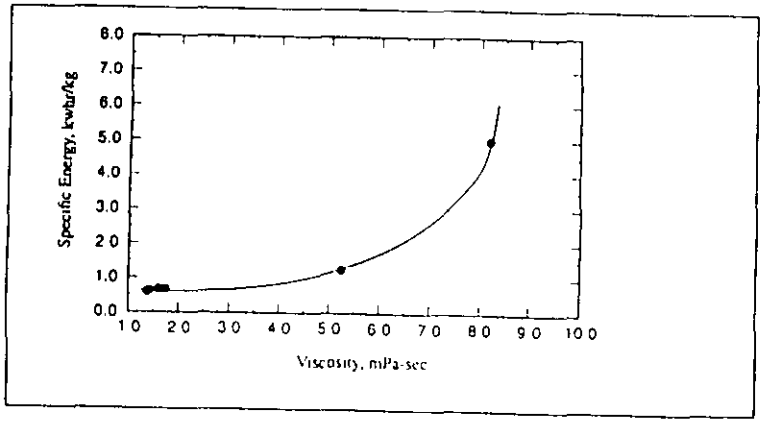

Figure 6: Specific energy vs viscosity. Note increase at high viscosities.

creased significantly While comparing the specific energy consumption between tests, the following observations were made:

(i) When the viscosity increased from 1.37 mPa-sec (test no.1) to 5.24 mPa-sec (test no. 5) due to fines addition, specific energy consumption increased from 0 63 kwhr/kg to 1 11 kwhr/kg.

(ii) When the viscosity increased from 5 24 mPa-sec (test no. 5) to 8.19 mPa-sec (test no. 6) due to decrease in temperature, specific energy consumption increased again, going from 1.11 kwhr/kg to 5.0 kwhr/kg. This trend agreed with the observations made in the local iron ore plant (Figure 7), where specific energy consumption increased by ~20% during winter months when the slurry temperature was very low (Kawatra and Eisele, 1992).

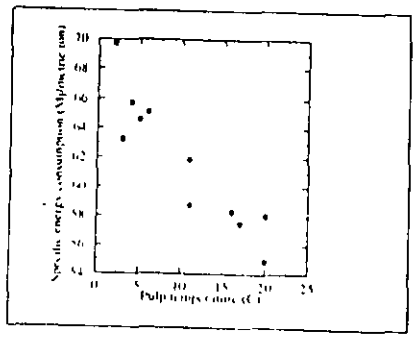

Figure 7: Specific energy consumption for 8.2m x 4 4m primary iron ore AG mill as function of temperature (see Kawatra and Eisele, 1992).

CONCLUSIONS

From our tests the following conclusions were made:

1. The resistance of the media-sized ore to breakage increased when the slurry viscosity was increased. This effect was prominent at higher viscosities.

2. Production of critical size material increased at higher slurry viscosity. These results agreed with plant observations reported by Kawatra and Eisele (1992), where critical size material production increased during winter months. It has already been determined that brittleness of the individual rocks does not change with temperature (Kawatra et al., 1993), and so the change must be due to changes in the behavior of the mill slurry as a whole. Since pulp viscosity increases at lower temperatures during winter months, such changes can be attributed to changes in pulp viscosity.

3. The specific energy consumption in the mill increased as the viscosity increased. This was a result of the increased viscosity reducing the grinding rate by cushioning of impacts, and by changing the motion of the charge in the mill. This explains the increased specific energy consumption in northern U.S. operations during winter months, when the temperature is very low.

ACKNOWLEDGEMENTS

This research has been supported by the Department of Interior's Mineral Institute program administered by the Bureau of Mines through the Generic Mineral Technology Center for Comminution under grant number G1115149.

REFERENCES

ASTM, 1991, Standard Method of Drop Shatter Tests for Coal, D440-86, Annual book of ASTM standards, Vol. 5.05, pp. 214.

Austin, L G., Klimpel, R. R., and Luckie, P. T., 1984, "What Laboratory Tests Tell Us About Breakage in Ball Mills," Chapter 5, Process engineering of Size Reduction: Ball Milling, Society of Mining Engineers, American Institute of Mining, Metallurgical , and Petroleum Engineers, Inc , New York, pp. 79-176.

Fuerstenau, D. W., Venkataramana, K. S., Velamakanni, B. V., 1984, "Effect of Chemical Additives on the Dynamics of Grinding Media in Wet Ball Mill Grinding," Inter. J. of Miner. Process., Vol. 15, pp. 251-267.

Hemmings, C E., and Boyes, J M , 1977, "An On-Line Viscometry Technique for Improved Operation and Control of Wet Grinding Circuits," Twelfth International Mineral Processing Congress, Sao Paulo, pp 46-64.

Klimpel, R. R., 1982 & 1983, "Slurry Rheology Influence on the Performance of Mineral/Coal Grinding Circuits," Part I, Mining Engineering, 34 (12), (1982), pp. 1665-1668, Part II, Mining Engineering, Vol 35, No. 1, (1983), pp. 21-26.

Kawatra, S K. and A. K. Bakshi, 1996, "The Effect of Slurry Viscosity on Hydrocyclone Classification," Inter. J of Miner. Process., paper accepted for publication.

Kawatra, S K. and A. K. Bakshi, 1995, "Determination of Changes in Rheological Properties of Coal Slurries in Process Streams," Coal Preparation, Vol. 15, pp. 165-175.

Kawatra, S. K., Moffat, S. A., DeLa'O, K. A., 1993, "The Effect of Freezing Conditions on Rock Breakage," Society for Mining, Metallurgy, and Exploration, Inc., Preprint Number 93-17.

SAG 1996

MINING AND MINERAL PROCESS ENGINEERI

Vancouver, B. C. Canada

THE INFLUENCE OF SLURRY TRANSPORT OI DRAW OF AUTOGENOUS AND SEMI-AUTOGI

Dr. S Morrell[1] and Dr. T. Kojovic[2]

1- Manager - Comminution Research, 2- Senior R
Julius Kruttschnitt Mineral Research Ce
Isles Road, Indooroopilly, Brisbane, Aus

ABSTRACT

In recent years there has been a trend in Australia circuiting autogenous and semi-autogenous mills clones. This has resulted in attention being focus relating to the ability of the grates and pulp lifters to move slurry from the mill. This paper describes the fects on power draw and mill performance tha observed to occur due to poor slurry transport. which explain these phenomena are described. Tl to develop mathematical models which link grate fl slurry hold-up and power draw. The model's ability capacity and its effect on power draw is illustrated u data.

INTRODUCTION

Recent experience with a number of autogenous (a autogenous (sag) mills in Australia has highlighted th of efficient slurry transport related to power draw and

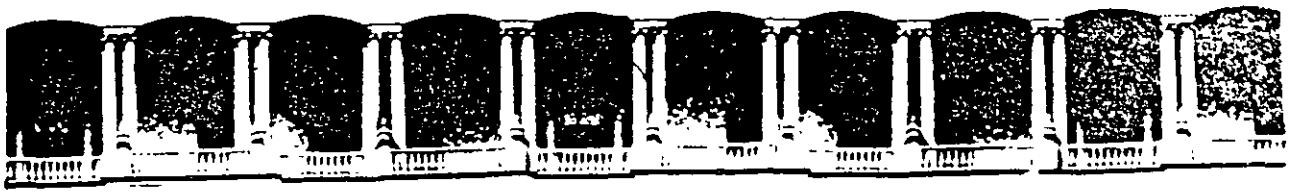

FACULTAD DE INGENIERIA U.N.A.M.
DIVISION DE EDUCACION CONTINUA

CURSOS ABIERTOS

DESARROLLO Y OPERACIÓN DE SENSORES PARA CONTROL DIRECTO Y CONTINUO EN PLANTAS DE BENEFICIO DE MINERALES Y EN LA RESTAURACIÓN DEL MEDIO AMBIENTE

Del 18 al 23 de mayo de 1998

TEMA: TEMPERATURE EFFECT ON GRINDING CIRCUIT PERFORMANCE

EXPOSITOR :DR. KOMAR KAWATRA

1998

Temperature effect on grinding circuit performance

S. K. Kawatra, T. C. Eisele, D. X. Zhang, and M. T. Rusesky

Abstract — *It has been observed in some mineral processing plants that grinding circuit efficiency varies seasonally, such as in some plants which are located in the northern US and Canada and undergo large seasonal temperature changes, with the grinding circuit efficiency different between summer and winter. This indicates that the temperature of grinding circuit slurry has a noticeable effect on grinding performance. The effect has rarely been studied. To this end, an investigation to examine the effects of changing temperature on efficiency and determination of the mechanism responsible has been carried out. Plant investigations and laboratory experiments have been conducted in order to study hydrocyclones. It was demonstrated that when the pressure drop is held constant, the $d_{50(c)}$ size decreased approximately linearly with increasing temperature, while the shape of the reduced efficiency curve remained nearly constant. This effect was determined to be due to changes in slurry viscosity with temperature.*

Introduction

As is well known, the single most energy intensive unit operation in mineral processing is comminution. Size reduction consumes approximately 25% of the total energy used in mineral concentrators, while typically less than 5% of this energy is consumed in the production of new mineral surface (NMAB, 1981). Thus, there is much room for improvement in grinding operations, and even a slight increase in efficiency would produce substantial energy savings. Such improvements are most readily obtainable by optimization and control of mill operating conditions.

A number of investigators (Austin, et al., 1984; El-Shall and Somasundaran, 1984; Klimpel, 1982, 1982a, 1983, 1984; Fuerstenau, et al., 1985) have determined that rheology has a large effect on the efficiency of grinding mills. Four parameters influence the rheology of slurry in a grinding mill: solids content, particle size distribution, chemical environment, and temperature. The effect of temperature is particularly significant in areas with large seasonal temperature variations such as the northern United States and Canada (Kampf, 1985). However, due to the unavailability of suitable viscometers and measurement techniques for mineral slurries, the control of mill rheology, especially the effects of temperature on efficiency of grinding mill and hydrocyclones, has been neglected or rarely studied. The investigation described here was therefore carried out to determine the magnitude and nature of temperature effects on hydrocyclone operation.

S.K. Kawatra, T.C. Eisele, members SME, D.X. Zhang, and M.T. Rusesky, member SME, are with Dept. of Metallurgical Engineering, Michigan Technological University, Houghton, MI. SME preprint 88-1, SME Annual Meeting, Phoenix, AZ, January. M&MP paper 88-639 Manuscript June 12, 1987. Discussion of this paper must be submitted, in duplicate, prior to July 31, 1989

Experimental Work

Plant Studies

The plant site that was chosen for obtaining the samples was an iron ore processing plant, which experiences substantial seasonal temperature variations. The plant has primary autogenous and secondary pebble mill grinding. The cyclones are operated in parallel banks of nine, with seven of the classifiers in use at any one time. The cyclones are Krebs model D15B-852-M271. This plant processes a very finely disseminated iron ore which requires grinding to -25 μm for liberation.

Sampling was carried out in the summer and in the winter in order to achieve the greatest temperature variation. Pulp temperature ranged from a high of 20°C (68°F) in the summer to a low of 3.3°C (38°F) in the winter. The resulting corrected efficiency curves for these conditions are shown in Fig. 1.

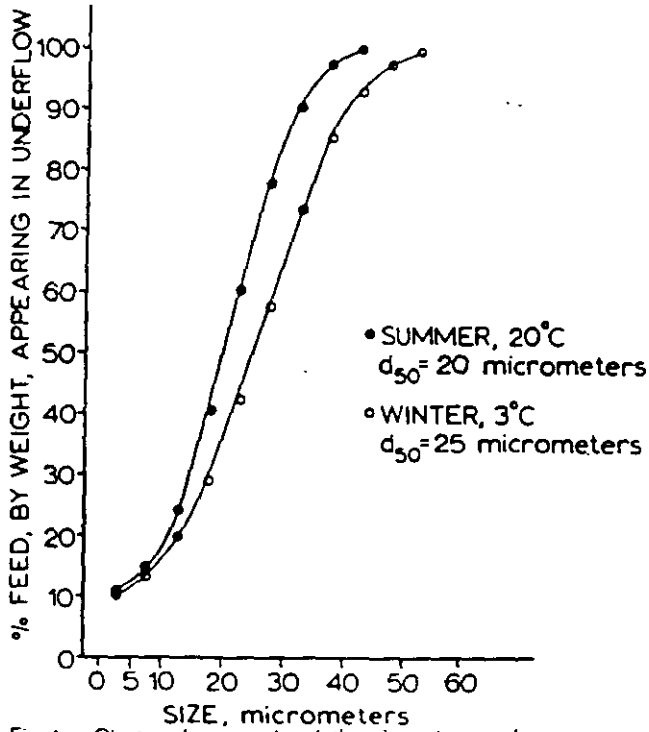

Fig 1 — Observed seasonal variations in cyclone performance in an iron ore processing plant

Laboratory Studies

Laboratory experiments were carried out using a Krebs hydrocyclone. The cyclone parameters were as follows: feed inlet diameter, 1.2 in. (3 cm); vortex finder diameter, 1 1/2 in. (3.8 cm); apex diameter, 7/8 in. (2.2 cm); cyclone diameter, 4 in. (10.2 cm); and pressure drop, 10 psi (69 kPa).

The cyclone was mounted on a laboratory test rig in closed circuit with a Warman centrifugal pump and a slurry tank. The cyclone overflow and underflow streams discharged freely into separate launders, which were used to either remove simultaneous samples from two streams or to recombine the streams before returning them to the slurry tank. The slurry temperature sensor was mounted in the feed sump, and a diaphragm-type pressure gage and an ultrasonic doppler flowmeter were both mounted on the cyclone inlet line. Apparent slurry viscosity was also measured at the cyclone feed inlet using a Namotre Model 810 vibrating sphere viscometer. Flowrate, viscosity, and temperature data were continuously collected and logged by a HP-85 computer.

The mineral used for these experiments was pure silica obtained from Ottawa Sand Co., Ottawa, IL. The particle size distribution was obtained using a Leeds and Northrup Microtrac particle size analyzer and is shown in Table 1. The temperature range was from 50 to 11°C.

Table 1 — Size Distribution of Ground Ottowa Sand

Size, μm	Cumulative Wt % Passing
176	100
125	97
88	93 6
62	75 5
44	49 8
31	34 9
22	24 0
16	17 5
11	12 7
7 8	8 1
5.5	5 1
3 9	3 9
2 8	2 0

Results and Discussion

A summary of the data collected in the laboratory cyclone experiments is presented in Table 2. The Rf is the water split, and α is the shape parameter from Lynch's equation,

$$y = \frac{e^{\alpha x} - 1}{e^{\alpha x} + e^{\alpha} - 2} \quad \text{where } x = \frac{d}{d_{50(c)}}.$$

Table 2 — Summary of Laboratory Cyclone Test Results

Test	Temperature °C	R_f, %	$d_{50(c)}$, μm	α	Viscosity Centipose
1	48 8	22 0	21 0	2 83	8 9
2	40 4	23 3	23 6	2 85	10 4
3	35 2	24 3	25 0	2 54	10 6
4	30 0	23 2	26 8	2 74	10 3
5	25 0	24 7	29 1	2 44	10 8
6	20 0	23 5	30 0	2 12	12 0
7	15 1	23 9	31 4	2 69	14 2
8	11 1	24 4	32 4	2 54	13 8

The values for α and $d_{50(c)}$ were determined by simplex optimization after the data was corrected for *Rf*.

It is clear from both plant and laboratory data that $d_{50(c)}$ does indeed decrease with increasing temperature in Figures 1 and 2. When $d_{50(c)}$ is plotted against temperature it is further observed that the relationship is essentially linear, as is illustrated by Fig. 3. From Fig. 2 it is clearly shown that increasing temperature shifts the efficiency curve towards finer sizes. However, the sharpness of the reduced efficiency curve for all of the temperatures is essentially unchanged, as shown by the curve in Fig. 4. This result is in agreement with the results of Lynch (1977), who stated that the reduced efficiency curve is a function only of cyclone geometry and particle characteristics in slurry and is largely unchanged by alterations in operating conditions.

From Table 2 it is shown that apparent slurry viscosity varies significantly with temperature.

The behavior of hydrocyclones as classifiers of mill output is dependent on slurry rheology (Austin et al, 1984, Agar and Herbst, 1966).

If the cyclone returns excessive amounts of fine material to feed, over-grinding will reduce mill efficiency and may cause difficulties in later separation processes as well.

Variations in temperature affect slurry viscosity by reducing the viscosity of the carrier water. A major effect of this is

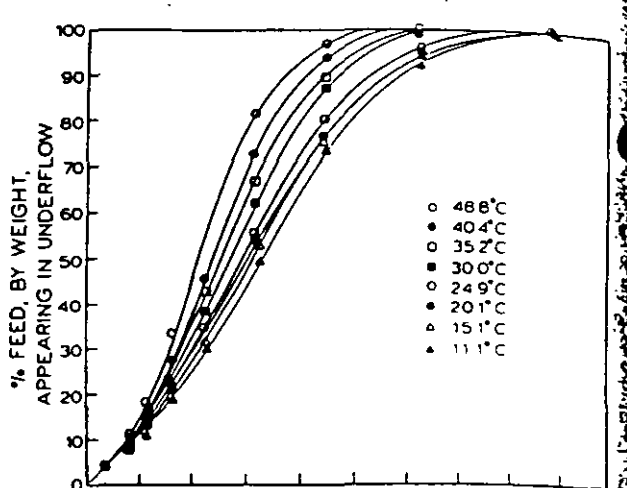

Fig. 2 — Effect of temperature on the efficiency curve of a 10.6 cm (4 in) hydrocyclone processing silica

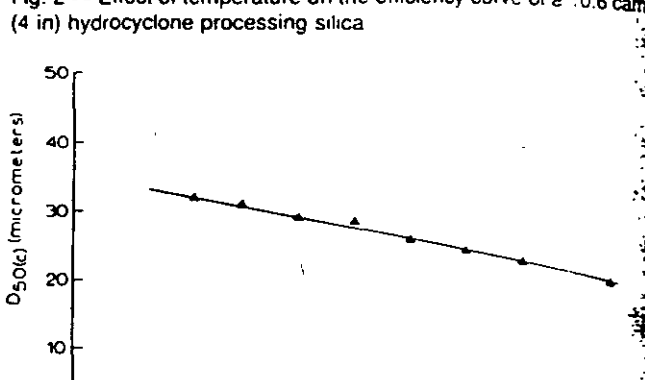

Fig 3 — Relationship of hydrocyclone corrected d_{50} size and slurry temperature for a 10.16 cm (4 in) hydrocyclone processing silica.

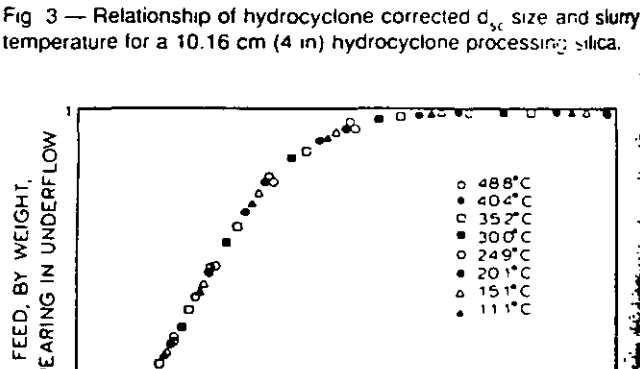

Fig. 4 — Reduced efficiency curve for varying percent solids and temperature for a 10.16 cm (4 in) hydrocyclone processing silica.

on hydrocyclone performance. The observed shift of the cyclone efficiency curve and reduction in $d_{50(c)}$ size arises from the reduced viscosity of water at elevated temperatures. Reduction of viscosity increases the settling velocity of the particles, which causes them to segregate more rapidly with fewer misplaced particles, thus improving efficiency. The increase in settling velocity also causes the apparent size of any given particle to increase which reduces the $d_{50(c)}$ size. This effect is amplified by an increase in flowrate at constant pressure as the viscosity is lowered, which increases centrifugal effects and hence raises the settling velocity. Similar conclusions can be drawn by analyzing the data obtained by Agar and Herbst (1966) where the water viscosity was altered with sucrose. It may be noted that viscosity reduction by increasing temperature, which reduces $d_{50(c)}$ size in cyclones, appears to conflict with Klimpel's data (1982), which predicts an increase in $d_{50(c)}$ size with a decrease in viscosity. This discrepancy may be explained by the difference in the mechanism of viscosity reduction. However, it should be kept in mind that direct comparisons of hydrocyclone results may be misleading due to the difficulty of ensuring that the same variables are held constant. For example, the results reported here are for constant pressure and varying throughput, while Klimpel's results may well have been for constant throughput and varying pressure.

Temperature changes have little effect on the interaction of water and solids, but produce a great alteration in the viscosity of water. It is the viscosity of the carrier liquid which controls the viscosity of the slurry under high shear conditions such as those encountered in the cyclone separating zone (Bradley, 1965), while the slurry viscosity at lower shear rates control the slurry flowrate and hence the magnitude of the centrifugal forces. Thus, increasing the temperature strongly influences both the centrifugal forces and the particle settling velocity, while viscosity reduction by chemical addition, which most strongly effects particle interactions and therefore the low-shear-rate apparent viscosity, has its greatest influence on centrifugal forces.

Conclusion

It has been shown that in both plant and laboratory environments, the temperature of the grinding circuit slurry has a noticeable effect on grinding and cyclone efficiency. The $d_{50(c)}$ size of a hydrocyclone is a function of the viscosity of the carrier liquid, which in turn is a function of temperature. The $d_{50(c)}$ size therefore decreases nearly linearly with increasing temperature. The sharpness of the separation is largely unaffected by temperature changes, as illustrated by the constant nature of the reduced efficiency curve.

Acknowledgments

The authors gratefully acknowledge the financial support for this project provided by the US Bureau of Mines through the Generic Center for Comminution at the University of Utah, and by the Dow Chemical Company. The authors also thank Krebs Engineers, Inc. for providing the hydrocyclone used in this project.

References

Agar, G. E. and Herbst, J. A., 1966. "The Effect of Fluid Viscosity on Cyclone Classification" *Trans. SME-AIME*, vol. 235, pp. 145-149.

Austin, L. G., Klimpel, R. R., and Luckie, P. T., 1984. *Process Engineering of Size Reduction: Ball Milling*. AIME, New York.

Bradley, D., 1965. *The Hydrocyclone*. Pergamon Press Ltd., London.

El Shall, H., Somasundaran, P., 1984. "Mechanisms of Grinding Modification by Chemical Additives: Organic Reagents". *Powder Technology*, Vol. 38, pp. 267-273.

Fuerstenau, D. W., Venkataraman, K. S., and Velamakanni, B. V., 1985. "Effect of Chemical Additives on the Dynamics of Grinding Media in Wet Ball Mill Grinding", *International Journal of Mineral Processing*, Vol. 15, no. 4, pp. 251-268.

Herbst, J. A., and Rajamani, K., 1979. "Control of Grinding Circuits", in *Computer Methods for the 80's*. A. Weiss, ed., AIME, New York, pp. 770-786.

Kampf, H. J., 1985, personal communication.

Klimpel, R. R., 1982. "The Influence of a Chemical Dispersant on the Sizing Performance of a 24-inch Hydrocyclone," *Powder Technology*, Vol. 31, pp. 255-262.

Klimpel, R. R., 1984. "Influence of Material Breakage Properties and Associated Slurry Rheology on Breakage Rates in Wet Grinding of Coal and Ores in Tumbling Media Mills," in *Reagents in the Minerals Industry*. M. J. Jones and R. Oblatt, eds., Institution of Mining and Metallurgy, London, pp. 265-270.

National Materials Advisory Board (NMAB), 1981. *Comminution and Energy Consumption*. NMAB-364.

Selective flotation of fossil resin from Wasatch Plateau high-volatile bituminous coal

J. D. Miller and Y. Ye

Abstract — *Certain bituminous coals are known to contain appreciable quantities of natural fossil or subfossil resin. Such resinous coals are found in the western US, particularly the Wasatch Plateau coalfield of UT. Some of the seams in this field contain an average of 5% resin. This fossil resin has been recovered by gravity and/or flotation processes since 1929. Resin concentrates thus produced are of low quality and are usually refined by solvent extraction. The purified resins are of commercial importance in the adhesive, coating, rubber, and ink industries, etc. An improved flotation technique has been developed which involves ozone conditioning to selectively float resin from high-volatile bituminous coal. With this flotation process, a concentrate product which contains 95%*

Y. Ye, and J.D. Miller, member SME are with Dept. of Metallurgy and Metallurgical Engineering, University of Utah, Salt Lake City, UT.

SME preprint 88-198. SME Annual Meeting, Phoenix, AZ, January 1988. M&MP paper 88-614. Manuscript January 1988. Discussion of this paper must be submitted, in duplicate, prior to July 31, 1989.

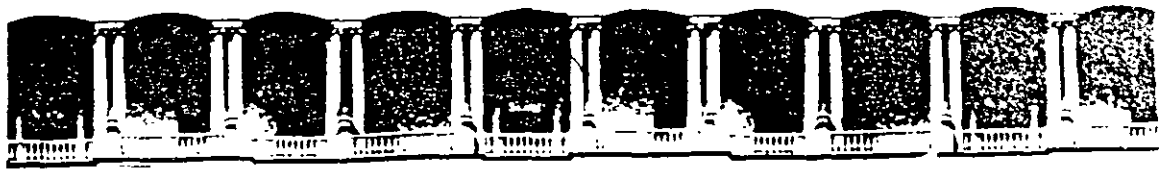

FACULTAD DE INGENIERIA U.N.A.M.
DIVISION DE EDUCACION CONTINUA

CURSOS ABIERTOS

DESARROLLO Y OPERACIÓN DE SENSORES PARA CONTROL DIRECTO Y CONTINUO EN PLANTAS DE BENEFICIO DE MINERALES Y EN LA RESTAURACIÓN DEL MEDIO AMBIENTE

Del 18 al 23 de mayo de 1998

TEMA: RHEOLOGY EFFECTS IN GRINDING CIRCUITS

EXPOSITOR :DR. KOMAR KAWATRA
1998

Palacio de Minería Calle de Tacuba 5 Primer piso Deleg. Cuauhtemoc 06000 Mexico, D.F. APDO. Postal M 2081
Telefonos: 512-8955 512-5121 521 7335 521-1987 Fax 510-0573 521-4020 AL 26

XVI International Mineral Processing Congress, edited by E. Forssberg
Elsevier Science Publishers B.V., Amsterdam, 1988 — Printed in The Netherlands

RHEOLOGY EFFECTS IN GRINDING CIRCUITS

S. K. KAWATRA and T. C. EISELE

Department of Metallurgical Engineering, Michigan Technological University, Houghton, Michigan 49931, U.S.A.

SUMMARY

A discussion of the effects of rheology on the performance of grinding circuits is presented, as well as a description of the major factors which influence the rheology of mineral slurries. One of these factors, slurry temperature, has long been discounted as unimportant to mill efficiency. The results of plant and laboratory investigations of the effects of temperature on grinding circuit performance are presented.

INTRODUCTION

Comminution is the single most energy-intensive and least efficient unit operation in mineral processing (Ref. 1). Although it has been known for some time that the efficiency of a wet grinding circuit is dependent on the rheological character of the mineral slurry (Ref. 2), no grinding circuits presently exist which use direct rheology control. This state of affairs is primarily due to the lack of a suitable sensor arrangement for on-line monitoring of mineral slurry rheology. For the same reason, there is a high degree of uncertainty concerning the responses of components such as mills and classifiers to changes in slurry rheology. As a result of the difficulties involved in actual rheology measurement, attention has been limited to readily measurable quantities such as pulp density, and to a lesser extent, particle size, which have a strong influence on rheology.

In general, it is unfortunately not feasible to assume that rheology can be predicted solely from the value of a single parameter such as percent solids. This is due to the strong influence of variables such as particle surface chemistry, particle size and shape, and temperature on rheology (Ref. 3). Of these factors, consideration of surface chemistry has been limited by the difficulty of determining the relevant parameters, and temperature has been largely ignored due to the common assumption that temperature effects are negligible.

THEORETICAL DISCUSSION

The rheology of mineral suspensions is highly complex and difficult to predict, with both time-dependent and time-independent components and a range

of possible variations from ideal behavior. Since time-dependent phenomena such as thixotropy and rheopexy depend on the development of a structure in a quiescent fluid (Ref. 4), the high-shear environment of the grinding circuits prevents such phenomena from occurring and only time-independent behavior need be considered (Ref. 5).

Time-independent behavior can be divided into four general categories, depending on how the shear stress developed in the fluid varies with shear rate, as shown in Figure 1. The slope of each of these curves represents the viscosity at a given shear rate. Thus, a Newtonian fluid exhibits a constant viscosity for all shear rates, the apparent viscosity of a dilatent fluid increases with shear rate, the apparent viscosity of a pseudoplastic fluid decreases with shear rate, and a Bingham plastic requires a minimum shear stress, or yield stress, before flow can begin. The empirical mathematical expressions for each type of behavior may be expressed as follows:

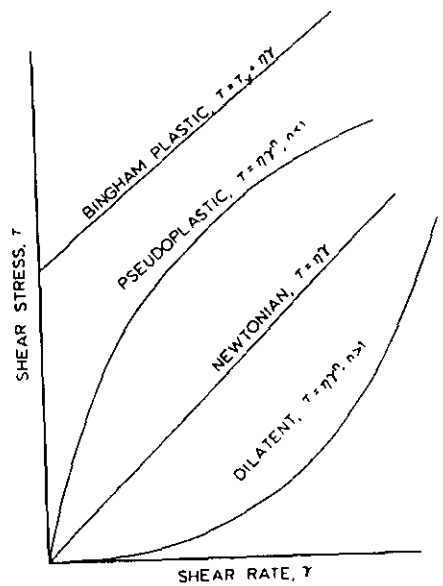

igure 1. Generalized time-independent rheology curves. The minimum shr stress required for flow of a Bingham plastic, τ_y, is the yie stress.

Newtonian: $\tau = \mu\gamma$

Dilatent: $\tau = \mu\gamma^n$, where $n>1$

Pseudoplastic: $\tau = \mu\gamma^n$, where $n<1$

Bingham plastic: $\tau = \tau_y + \mu\gamma$

where τ is the shear stress, γ is the shear rate, μ is the apparent viscosity, n is a dimensionless constant, and τ_y is the yield stress (Ref. 6). Although a slurry may exhibit any of these behaviors, very concentrated slurries are generally pseudoplastic or Bingham plastic. Indeed, in some cases it is very difficult to determine whether a slurry is pseudoplastic or Bingham plastic without very careful measurements at very low shear rates, as the curves obtained may be very similar otherwise (Ref. 6).

Known Effects in Grinding Circuits

The efficiency of closed circuit grinding is dependent on rheological effects both in the mill proper and in the classifiers used to close the circuit. Effects on mill performance have been extensively studied, largely in connection with studies of polymeric grinding aids (Refs. 2,7-10). The most notable result was that increasing the solids concentration of the slurry increased the fines production rate provided that the product slurry did not exhibit a non zero yield stress. Once a yield stress was exhibited, the breakage rate in the mill fell off (Ref. 8). In addition, decreasing the slurry viscosity frequently produced an increase in the fines production rate at a constant percent solids (Ref. 10). These effects are due to changes in the motion of the mill charge upon development of a non zero yield stress (Ref. 8), and to a decrease in the energy absorbed by the fluid at lower viscosities.

The effects of rheology on the performance of classifiers such as hydrocyclones is quite pronounced and fairly complex (Ref. 5). Although these effects have not been well studied due to the lack of suitable instrumentation, some data is available using sugar solutions to alter the medium viscosity. Also, several theoretical treatments of hydrocyclones include an explicit viscosity term. It is possible to divide the rheological influences into two categories for theoretical consideration; the effect on particle movement through the fluid, and the effect on flow patterns and velocities. However, it is not possible in practice to dissociate the two influences (Ref. 5).

At a constant cyclone inlet pressure, increasing the viscosity first decreases the centrifugal velocity, which results in a higher flowrate due to the lowered centrifugal force at the inlet. At viscosities greater than 50 centipoise, viscous drag causes the inlet flowrate to decrease again (Ref. 5). The decrease in centrifugal velocity will decrease the particle settling rate and the result will therefore be to increase the 50% cyclone cut size, d_{50}, and the particle by pass fraction, R_f, as the viscosity increases. In general, the effect of viscous drag will cause the cyclone to be ineffective as a classifier when the viscosity exceeds approximately 30 centipoise (Ref. 5).

Virtually no work has been done to determine the actual effect of slurry viscosity on the real performance of a hydrocyclone under plausible industrial conditions. In many cases, rheological effects have not been separated from the effects of percent solids, which is the most commonly used factor for controlling slurry viscosity (Ref. 10). The few experiments which have been carried out in the past, which have varied viscosity without varying percent solids, have produced contradictory results (Refs. 10,11), with the d_{50} size increasing with increasing viscosity in one case, and decreasing with increasing viscosity in the other. Additional, more carefully controlled experimentation is therefore needed to determine the true effect.

Factors Influencing Rheology

The rheology of a mineral suspension, consisting of particles fine enough to remain in suspension for more than a few seconds, is strongly influenced by the following four factors; solids concentration, particle size and shape, chemical environment, and temperature. Each factor has a characteristic effect on slurry rheology, which is described below:

(i) Solids Concentration. Solids concentration has a powerful effect on the apparent viscosity of a slurry, as shown by Figure 2. The effect is particularly strong at high percent solids, with slight changes in concentration producing large shifts in viscosity. In addition to affecting the viscosity, increasing the percent solids causes changes in the rheological curve for the slurry. In general, the rheology at very high solids content will shift from dilatent to pseudoplastic to Bingham plastic as the percent solids increases (Ref. 9), which will alter grinding mill operation.

(ii) Particle Size and Shape. For any given percent solids, a reduction in particle size will produce an increase in slurry viscosity. This is considered to be largely a result of increased particle surface area, which

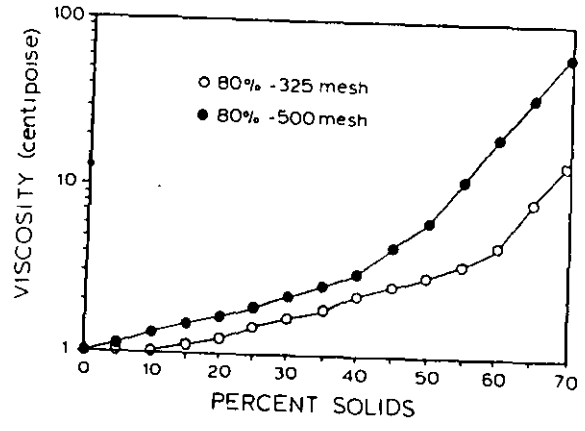

Figure 2. Effect of percent solids and particle size on slurry viscosity. Work described in this paper was carried out in the range of 20 to 40% solids by weight.

causes a greater proportion of the fluid phase to be bound up in particle boundary layers. The amount of free fluid is thus decreased, and the effective percent solids becomes greater. In addition to this effect, the manner in which the particles interact with the fluid changes with decreasing particle size. This causes an increase in viscosity through complex effects on both the manner in which the fluid flows and on interparticle friction. The net result is as shown by the two curves of Figure 2, with the finer particle size producing a substantially higher viscosity. Increasing the angularity of particles will also increase the viscosity, for reasons similar to those previously stated.

(iii) Chemical Environment. The chemical environment of the slurry includes a wide variety of factors such as particle surface chemistry and chemical effects on the viscosity of the fluid phase. These effects are highly complex and poorly understood, although the effects of surface-active agents on suspension rheology have been extensively studied empirically (Refs. 2,7-10). Chemical effects have been particularly studied in mill circuits in connection with the use of grinding aids, which are basically viscosity-reducing agents.

(iv) Temperature. The effect of temperature on slurry viscosity differs from that of the other three factors in that the slurry viscosity change results entirely from changes in the viscosity of

viscosity of water varies with temperature as shown in Figure 3 (Ref. 12). Changes in slurry viscosity with temperature obviously have a similar form, modified by the presence of particles.

While the effects of percent solids and particle size on mill and cyclone performance have been intensively studied, and chemical effects have been studied to a lesser extent, the influence of temperature on performance has been largely ignored. This is due to the widely held belief that temperature is of little consequence for the efficiency of grinding circuits. Nevertheless, it has been reported in several mills in Canada and the northern United States that seasonal shifts in grinding efficiency occur which are apparently due to the sizable temperature variation in these areas. This is borne out by the fact that when the mills take precautions to prevent chilling of the recycled water in the winter, the seasonal efficiency changes become less pronounced (Ref. 13). For this reason, an investigation was carried out to determine the effect of temperature on grinding circuit efficiency, particularly the effect on hydrocyclone performance.

PLANT STUDIES

An extensive campaign of plant sampling was carried out in an iron ore concentrator located in northern Michigan to monitor the effect of seasonal temperature changes on the performance of the grinding circuit.

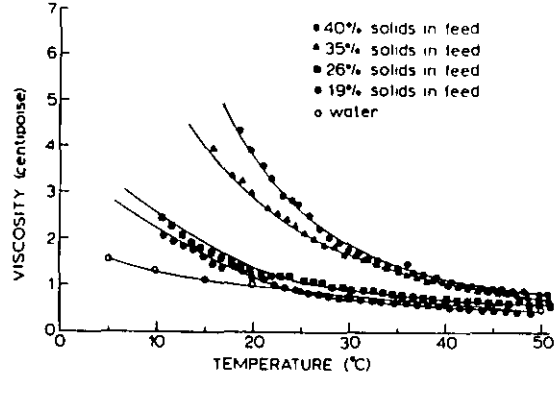

Figure 3. Effect of temperature variation on the viscosity of pure water and of fine silica slurries at four solids concentrations.

The plant selected for this investigation was specifically chosen due to its need to grind to a very fine particle size (80% passing 500 mesh) in order to achieve liberation. This ensured that the effects of seasonal temperature change would be most pronounced, as finer particles are more readily affected by rheology change than are coarser particles. In addition, since the plant used reverse flotation to remove quartz from hematite, downstream processing was highly sensitive to the size of grind. This ensured that the operation of the entire plant would be influenced by small changes in grinding performance, and that the temperature effect would be more likely to be of importance to plant operations.

The most notable seasonal effect observed in the grinding circuit was the change in the hydrocyclone efficiency curve. The representative data given in Figure 4 show that an increase in temperature from 4°C to 20°C produced a 20% decrease in the d_{50} size from 25 micrometers to 20 micrometers. Other data confirmed this trend. While the plant sampling was sufficient to show that an important effect exists, laboratory experimentation was necessary to properly measure the effect.

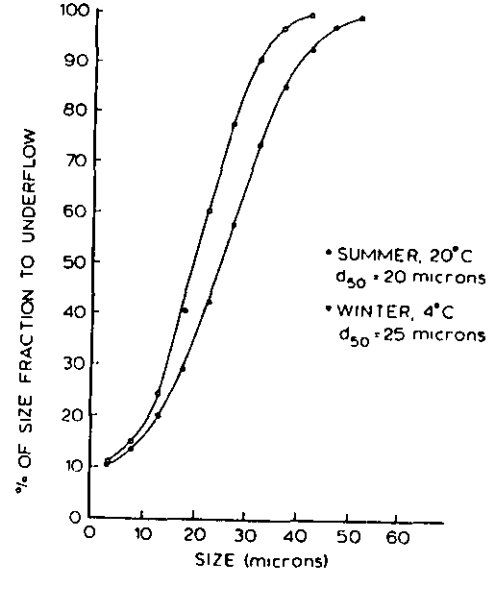

Figure 4. Effect of seasonal temperature changes on hydrocyclone performance in an operating iron ore concentrator.

LABORATORY STUDIES

Laboratory experiments were carried out using a 10.2 cm (4 inch) diameter Krebs hydrocyclone. The cyclone was mounted on a laboratory test rig, in closed circuit with a Warman centrifugal pump and a slurry tank. The cyclone overflow and underflow streams discharged freely into separate launders, which were used to either remove simultaneous samples from the two streams, or to recombine the streams before returning them to the slurry tank. Temperature was measured by a thermocouple mounted in the feed tank, and a diaphragm-type pressure gauge and an ultrasonic doppler flowmeter were mounted on the cyclone inlet line. Slurry viscosity was measured by a vibrating-sphere viscometer equipped with a specially designed sample presentation arrangement and receiving the recombined overflow and underflow slurries from the discharge launders when sampling was not being carried out. This instrument allowed the continuous monitoring of the viscosity, which had not previously been possible for mineral slurries in this size range. Data was collected and logged by an HP-85 computer and slurry temperature was controlled using an immersion heater and an immersion chiller.

Test Material

The mineral used for these experiments was pure silica, specific gravity = 2.65, obtained from the Ottawa Sand Co., Ottawa, Illinois. The size distribution of the silica is given in Table 1.

TABLE 1

Size distribution of ground Ottawa sand

Size (microns)	Cumulative wt. % passing
176	100
125	100
88	94
62	79
44	61
31	47
22	35
16	26
11	19
7.8	12
5.5	8
3.9	5
2.8	0.3

Experimental Procedures

The slurry tank was initially filled with hot water and sufficient silica to produce a slurry of the desired percentage solids. The cyclone inlet pressure was then set to 10 psi, and the immersion heater was used to maintain the slurry at 50°C. The system was allowed to stabilize for 10 minutes before the first overflow and underflow samples were taken, after which the slurry temperature was gradually decreased, with samples taken at approximately 5°C intervals. The use of the chiller allowed experiments over a temperature range of 50°C to 12°C.

The overflow and underflow samples were weighed, filtered, and dried. The dried samples were then weighed to allow the calculation of pulp densities, and the particle size distributions were determined with a Leeds and Northrup Microtrac particle size analyzer. The particle bypass fraction, R_f, was calculated from the fraction of the feed water which reported to the underflow, and cyclone efficiency values were corrected for R_f.

RESULTS AND DISCUSSION

A summary of the data collected in the laboratory cyclone experiments is presented in Table 2. The values of α and $d_{50(c)}$ in this table were determined from the equation (Ref. 14)

$$y' = (e^{\alpha x}-1)/(e^{\alpha x}+e^{\alpha}-1) \qquad (1)$$

where $x = d/d_{50(c)}$

y' = corrected fraction of feed to the coarse product

$d_{50(c)}$ = corrected 50% separation size

d = particle size

α = a measure of the sharpness of the separation, sharpness increases with increasing values of α.

A simplex optimization program was used to find the best-fit values of α and $d_{50(c)}$.

Plotting the corrected efficiency curves obtained at each temperature, as shown in the representative plot of Figure 5, shows the systematic shift in the curves towards finer sizes with increasing temperature.

It is clear from this data that $d_{50(c)}$ does indeed decrease with increasing temperature. When $d_{50(c)}$ is plotted against temperature, it is further observed that the relationship is nearly linear, as is illustrated by Figure 6. When the solids content of the slurry is increased, the line relating d_{50} to temperature is shifted upward, but the slope of the line remains constant over the range investigated. While the relationship of cut size to temperature is definite, the parameter α exhibits little dependence on temperature, which indicates that changing temperature has little if any effect on the sharpness of the separation. This is clearly shown by the reduced efficiency curve of Figure 7, which is essentially identical for all of the tests. This result is in agreement with the results of Lynch

TABLE 2

Summary of experimental results

Wt.% Solids	Temperature °C	Viscosity Centipoise	$D_{50(c)}$ Micrometers	R_f(%)	α
19.80	49.93	.53	13.02	19.30	2.80
19.30	44.85	.58	14.61	19.20	3.77
18.90	40.14	.65	14.87	21.50	3.87
18.80	35.72	.73	15.52	21.60	3.28
18.30	29.82	.82	15.65	23.80	2.89
18.10	25.42	.95	18.01	23.00	3.03
17.20	20.83	1.20	17.40	23.10	2.70
16.50	15.67	1.58	19.52	22.50	3.78
16.40	10.60	2.18	20.63	24.40	3.02
25.80	50.70	.69	17.40	18.60	3.48
26.60	41.00	.80	18.90	19.50	3.51
25.90	30.14	1.02	20.10	20.90	3.42
25.50	25.00	1.20	21.50	20.90	3.84
25.00	20.46	1.35	22.50	21.00	3.46
24.40	15.44	1.81	23.10	22.90	3.82
24.40	10.41	2.54	24.20	22.30	3.04
34.00	50.64	.89	24.04	21.20	3.26
34.60	40.01	1.20	26.15	25.10	3.48
35.50	30.61	1.84	28.56	24.00	3.09
34.90	25.31	2.31	29.91	23.40	2.88
36.20	14.75	4.15	30.71	27.50	2.47
40.20	50.62	1.01	27.62	22.70	2.62
41.20	40.54	1.25	29.69	23.90	2.36
40.90	30.85	1.90	32.46	24.00	2.78
41.00	25.75	2.70	32.76	24.70	2.69
40.70	20.84	3.75	35.83	24.50	2.87
40.90	14.38	6.22	36.06	25.00	3.03

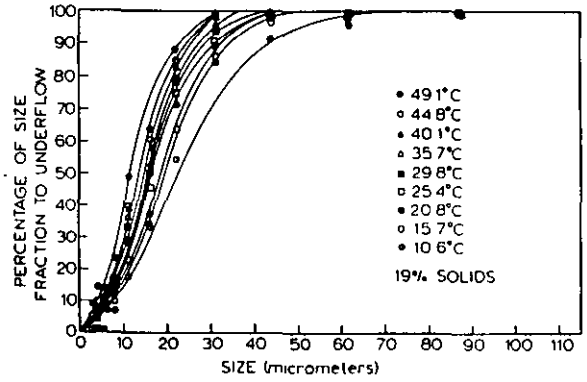

Figure 5. Effect of changing temperature on the corrected hydrocyclone efficiency curve for pure silica, as determined in laboratory experiments.

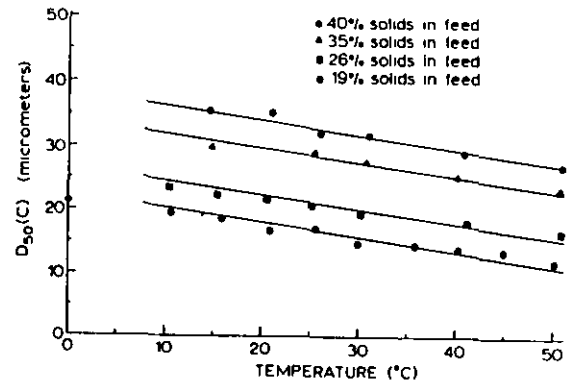

Figure 6. Experimentally determined relationship of corrected cyclone d_{50} size and slurry temperature for a 4" diameter hydrocyclone.

(Ref. 14), which show that the reduced efficiency curve is a function only of cyclone geometry and particle characteristics, and is largely unchanged by alterations in operating conditions.

It is known that increasing the fluid viscosity affects the cyclone performance both by slowing the settling rate of particles and by suppressing the tangential velocity of the fluid in the cyclone (Ref. 5). The net result is that increasing the viscosity of the slurry increases the cyclone $d_{50(c)}$ size. Since the viscosity of a fluid typically increases with decreasing temperature, the observed temperature dependence of $d_{50(c)}$ is primarily a result of changes in slurry viscosity.

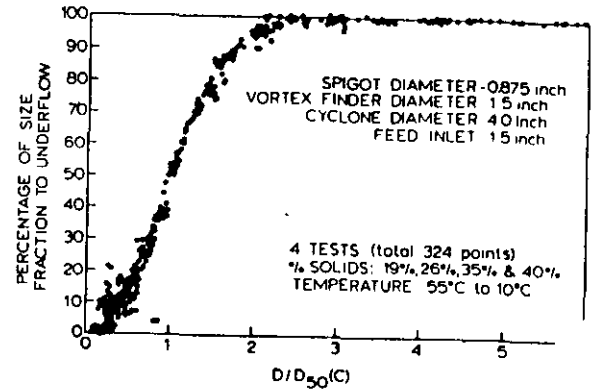

Figure 7. Reduced efficiency curve obtained for the classification of fine

CONCLUSIONS

From the available information concerning the effects of slurry rheology on mineral grinding circuits, it can be concluded that:

(i) The efficiency of the mill proper is maximized when the percent solids is held just below the level which will produce a yield value in the output slurry, and the viscosity is reduced as far as possible.

(ii) The d_{50} size for a hydrocyclone is expected to increase as the slurry viscosity increases, with d_{50} being roughly proportional to the square root of the viscosity.

(iii) In both plant and laboratory environments, the $d_{50(c)}$ size of a hydrocyclone is temperature dependent, with the cut size decreasing with increasing temperature. This effect is primarily due to the decreased slurry viscosity at elevated temperatures.

(iv) The dependence of $d_{50(c)}$ on temperature is very nearly linear, and the line is shifted to coarser $d_{50(c)}$ sizes with increasing percent solids, although the slope remains unchanged over the range investigated. The reduced efficiency curve for a given cyclone remains unchanged with changes in temperature or percent solids.

These results show the necessity for monitoring slurry viscosity in order to improve cyclone efficiency, and moreover, that the control strategies based on inferential sizing techniques (Ref. 15) must be modified to allow for the observed behavior. Further work must be done to improve the quality of on-line viscosity measurements of mineral slurries.

ACKNOWLEDGMENTS

The authors gratefully acknowledge the financial support for this project provided by the U. S. Bureau of Mines (through the Generic Centre for Comminution at the University of Utah), and the industrial support provided by the Dow Chemical Co., Midland, Michigan. The authors also thank Krebs Engineers, Inc. for providing the hydrocyclone used in this project.

REFERENCES

1. National Materials Advisory Board, Comminution and Energy Consumption, NMAB-364, 1981.

2. H. El-Shall, P. Somasundaran, "Mechanisms of Grinding Modification by Chemical Additives: Organic Reagents", Powder Technology, vol. 38, pp. 267-273, 1984.

3. C. H. Schack, K. C. Dean, S. M. Molloy, "Measurement and Nature of the Apparent Viscosity of Water Suspensions of Some Common Minerals", Report [illegible]

4. D. C.-H. Cheng, "Further Observations on the Rheological Behavior of Dense Suspensions", Powder Technology, vol. 37, pp. 255-273, 1984.

5. D. Bradley, The Hydrocyclone, Pergamon Press, 1965.

6. Parviz Shamlou, "Fine Solids Suspension and Rheology", The Chemical Engineer, May, 1984, pp. 31-34.

7. H. El-Shall and P. Somasundaran, "Mechanisms of Grinding Modification by Chemical Additives: Organic Reagents," Powder Technology, vol. 38, pp. 267-273, 1984.

8. D. W. Fuerstenau, K. S. Venkataraman, and B. V. Velamakanni, "Effect of Chemical Additives on the Dynamics of Grinding Media in Wet Ball Mill Grinding," Int. J. of Mineral Processing, vol. 15, no. 4, pp. 251-268, 1985.

9. R. R. Klimpel, "Influence of Material Breakage Properties and Associated Slurry Rheology on Breakage Rates in Wet Grinding of Coal and Ores in Tumbling Media Mills", in Reagents in the Minerals Industry, (M. J. Jones and R. Oblatt, eds.), Institution of Mining and Metallurgy, London, pp. 265-270, 1984.

10. L. G. Austin, R. R. Klimpel, and P. T. Luckie, Process Engineering of Size Reduction: Ball Milling, AIME, 1984.

11. G. E. Agar and J. A. Herbst, "The Effect of Fluid Viscosity on Cyclone Classification", Trans. AIME, vol. 235, pp. 145-149, 1966.

12. Handbook of Chemistry and Physics, 65th edition, CRC Press, 1984.

13. H. J. Kampf, Personal Communication, 1985.

14. A. J. Lynch, Mineral Crushing and Grinding Circuits, Elsevier, New York, 1977.

15. R. A. Seitz and S. K. Kawatra, "Further Studies on the Use of Classifiers for Control of Wet Grinding Circuits", International Journal of Mineral Processing, vol. 12, pp. 239-249, 1984.

FACULTAD DE INGENIERIA U.N.A.M.
DIVISION DE EDUCACION CONTINUA

CURSOS ABIERTOS

DESARROLLO Y OPERACIÓN DE SENSORES PARA CONTROL DIRECTO Y CONTINUO EN PLANTAS DE BENEFICIO DE MINERALES Y EN LA RESTAURACIÓN DEL MEDIO AMBIENTE

Del 18 al 23 de mayo de 1998

TEMA: CHANGES IN AUTOGENOUS GRINDING PERFORMANCE DUE TO VARIATION IN SLURRY RHEOLOGY

EXPOSITOR :DR. KOMAR KAWATRA

1998

Palacio de Minería Calle de Tacuba 5 Primer piso Deleg. Cuauhtemoc 06000 Mexico D.F. APDO. Postal M-2285
Telefonos: 512-8955 510-5121 521-7335 521-1987 Fax 510-0573 521-4020 AL 26

EXPERIMENTAL

Experimental set-up

Pilot scale autogenous mill: The pilot plant tests were done in a 1.8 meter diameter by 0.6 meter long Hardinge Cascade Mill. The mill contained sixteen, 2.5 cm high lifter bars. It was converted from continuous operation to batch operation by removing the grates on the discharge end of the mill and replacing them with liners made at Michigan Technological University. This mill was also insulated to maintain the initial charge temperatures, using 20 cm of Corning fiberglass insulation applied to the circumference of the mill and 2.54 cm thick polystyrene foam insulation on the ends. Energy consumption during each test was measured by a standard watt-hour meter.

Viscometer set-up. A Brookfield viscometer (DV-I model) was used to measure viscosity of the slurry collected immediately after each test. It was necessary to modify the viscometer so that the solids would be kept in suspension while the reading was being taken. This was accomplished by the slurry presentation system shown in Figure 1. The slurry was mixed in an overhead tank and passed continuously through the annular space between a steel tube and the spindle. After a steady state reading was displayed, flow was momentarily interrupted (to eliminate any swirling motion caused by the flow at the inlet) and the reading was taken immediately. This set-up is very suitable for measuring viscosity of slurries containing fast settling solids, and has been successfully used to characterize different slurries on the basis of their rheology (Kawatra and Bakshi, 1995)

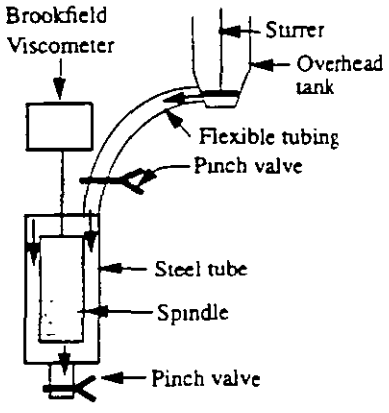

Figure 1 Brookfield set-up showing the special arrangement for measuring viscosity of slurries containing rapidly settling solids

Sample preparation

A 6500 kg iron ore sample was collected from a local iron ore deposit. Each rock was sized and washed to (i) remove any fines that might be in the pores or fractures of the sample, and (ii) remove the visually detectable clay material present in the sample. The washed ore was then dried. From the above material, six samples were reconstituted according to the size distribution shown in Table 1. This was the original size distribution of the rocks in the pit from where the sample was collected. Samples prepared for cold tests were stored in a freezer at -25°C, and samples prepared for tests at room temperature were stored in 55 gallon drums

Table 1: Size distribution of the reconstituted feed sample for the pilot scale autogenous tests.

Size Distribution (mm)	Weight (kg)	% Weight
-152.4 + 127.0	63.12	14.93
-127.0 + 101.6	65.83	15.59
-101.6 + 76.2	79.45	18.80
-76.2 + 50.8	82.17	19.47
-50.8 + 25.4	92.16	21.83
-25.4 + 12.7	39.50	9.38
Total	422.22	100.00

Test procedure

Six tests were carried out in the pilot scale autogenous mill. The viscosity of the mill slurry in these tests was changed by changing the clay/fines content in the initial feed and by changing the temperature of both iron ore and water. The mill was chilled prior to the tests conducted at low temperatures. The conditions for each test are given in Table 2.

The mill was run empty for 30 minutes before each test to allow the bearings to warm-up. Then the mill was stopped, and solids charge was added to the mill. A total of 423 kg solids were added for each test. Then, 182 kg of water was added to keep the total solids content at 70% by weight. The mill volume occupied by the charge was 26%. The initial temperature of water for the cold tests was maintained at 4°C (for test # 2, 4, and 6), and for other tests the water was at room temperature. The slurry temperature was measured both at the beginning and the end of each test, to be sure that the mill did not warm significantly during the test.

were done for ball

SOCIETY FOR MINING, METALLURGY, AND EXPLORATION, INC.

P.O. BOX 625002 • LITTLETON, COLORADO • 80162-5002

PREPRINT

96-144

CHANGES IN AUTOGENOUS GRINDING PERFORMANCE DUE TO VARIATION IN SLURRY RHEOLOGY

A.K. Bakshi
K. J. Shoop
S. K. Kawatra

Michigan Technological University
Houghton, Michigan

For presentation at the SME Annual Meeting
Phoenix, Arizona — March 11-14, 1996

Permission is hereby given to publish with appropriate acknowledgments, excerpts or summaries not to exceed one-fourth of the entire text of the paper. Permission to print in more extended form subsequent to publication by the Society for Mining, Metallurgy, and Exploration (SME), Inc. must be obtained from the Executive Director of the Society.

If and when this paper is published by the SME, it may embody certain changes made by agreement between the Technical Publications Committee and the author so that the form in which it appears is not necessarily that in which it may be published later.

Current year preprints are available for sale from the SME, Preprints, P.O. Box 625002, Littleton, CO 80162-5002 (303-973-9550). Prior year preprints may be obtained from the Linda Hall Library, 5109 Cherry Street, Kansas City, MO 64110-2498 (800)662-1545

PREPRINT AVAILABILITY LIST IS PUBLISHED PERIODICALLY IN MINING ENGINEERING

Table 2: Test conditions for each test conducted with the pilot scale autogenous mill.

Test No.	Initial Ore Temperature	Clay or Fines Content in the Feed
1	25°C	No clay No fines
2	-25°C	No clay No fines
3	25°C	10% clay No fines.
4	-25°C	10% clay No fines.
5	25°C	No clay 50% fines
6	-25°C	No clay 50% fines

Once the mill was charged with solids and water, it was run for 15 minutes. A slurry sample for viscosity measurement was collected from the mill as soon as it stopped rotating. Energy consumption during the 15 minute grinding was measured by the watt-hour meter. The material from the mill was removed manually, and screened for size analysis.

The clay material added was the same metamorphic clay which was washed from the initial ore collected from the mine pit. During tests 5 and 6, 50% fines were added in the mill. This was done to simulate the plant conditions, where due to the continuous operation a certain amount of fine (ground ore) is always present inside the mill. Since we conducted batch tests, the loads in the mill for tests 1-4 were initially devoid of these fines, which gave a low viscosity at the beginning. Thus by adding 50% iron ore fines, it was expected that the viscosity of the pulp would be comparable to the continuous operation in a plant. The size distribution of these fines is shown in Table 3.

Table 3: Size distribution of the fines which were added during tests 5 and 6 to simulate plant conditions.

Size Distribution (mm)	Weight (kg)	Weight Percent
-1.40 + 0.850	0.11	0.05
-0.850 + 0.600	8.88	4.20
-0.600 + 0.500	14.37	6.80
-0.500 + 0.425	21.85	10.34
-0.425 + 0.212	21.55	10.19
-0.212 + 0.150	18.77	8.88
-0.150	125.85	59.54
Total	211.38	100.00

RESULTS AND DISCUSSION

The effect of the viscosity of the slurry on size stability, critical size material production, and specific energy consumption were studied, and are discussed below.

Size stability

The resistance of the media to impact breakage was measured in terms of size stability. Size stability is expressed as (ASTM, 1991):

$$\% \text{ Size stability} = \frac{\Sigma(\text{initial wt\%}) \times (\text{avg. sieve size})}{\Sigma(\text{final wt\%}) \times (\text{avg. sieve size})} \times 100$$

Therefore, a size stability of 100% corresponds to a rock that did not break during grinding, and a size stability of 0% corresponds to a rock that broke completely below the finest size measured (-12.5 mm in these tests).

As it can be seen from Figure 2, size stability increased with increase in slurry viscosity, showing that at high viscosity the rocks had a higher resistance to breakage. This could be due to the fact that at higher viscosity the impact force between rocks was retarded by the viscous slurry which acted as a cushion, resulting in less breakage in the rock.

Critical size material

Critical size material is the material which is too large to be effectively ground in the mill, and too fine to be effecive for grinding other particles. In our tests, the change in the amount of material in the - 25.4mm + 12.7mm size fraction in the course of each test was small. Therefore, particles of this size were considered to be the critical size material. In a

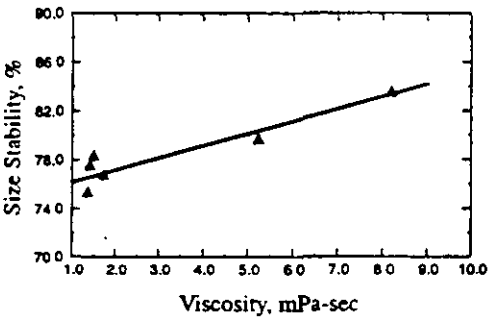

Figure 2 Size stability vs. viscosity The increased size stability shows that at higher viscosity the ore is less likely to be broken These are results of all six of the tests conducted

plant situation, the critical size material would typically be crushed in a cone crusher before it was recycled to the autogenous mill, as shown in Figure 3.

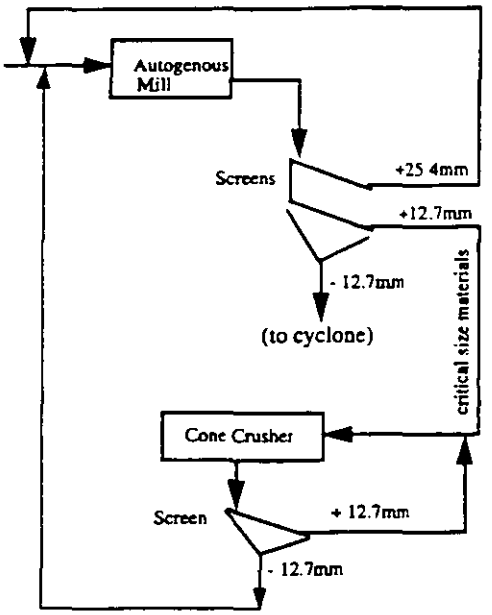

Figure 3. An autogenous grinding mill circuit, showing the treatment for critical size materials

The feed for each test contained 9.38% critical size material (see Table 1). The percentage of the critical size material was determined again after each test. As it can be seen in Figure 4, at low slurry viscosity the amount of critical size material in the mill after grinding was less than the amount of critical size material present before grinding At higher viscosity there was an increase in critical size material after grinding This is primarily due to the fact that higher viscosity reduces the energy of the impact collisions, which reduces the chances that a critical size particle will be broken up in the mill. Therefore, at a higher slurry viscosity an increase in critical size material production is expected.

During test No.6, when the viscosity was 8.2 mPa-sec, the critical size content in the product was found to be 10.75%, which is 1.37% higher than the amount of critical size material originally present in the feed. Under these conditions, if a mill is processing 1000 tones of ore per hour, then 107.5 tones of critical size material will need to be recycled through the cone crusher, which will make the circuit more energy consuming.

In the local iron ore plant which provided the material for this work, data collected over a period of two years showed that critical size material production was at a minimum between April and September, and increased significantly during December and January months when the temperature was low (Kawatra and Eisele, 1992). It was originally believed that this change in critical size production was due to increased brittleness of the rock at low temperatures However, drop tests conducted at Michigan Technological University showed that rocks did not become brittle over the temperature range of interest (+25°C to -25°C) (Kawatra et al., 1993). These changes in critical size material production can instead be attributed to viscosity changes, because viscosity of slurry increases at lower temperature.

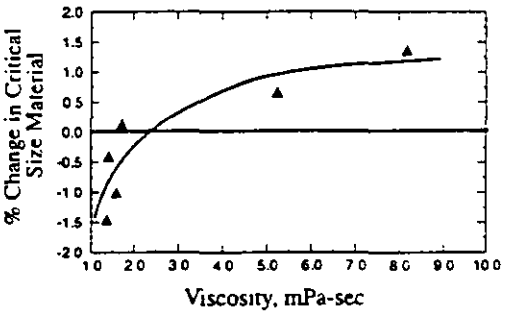

Figure 4. % change in critical size material vs viscosity. There was a net decrease in critical size material during grinding when slurry viscosity was low. At higher slurry viscosity amount of critical size material in the product was more than the amount of critical size material initially present in the feed

Specific energy consumption

Specific energy consumption was measured by calculating the energy required to produce one kilogram of material finer than 150 microns. As can be seen from Figure 5, the specific energy consumption of the mill increased with increasing slurry viscosity. The increase in specific energy from test 1 to test 4 was not significant because the viscosity changes during these tests were very small However, during tests 5 and 6 specific energy consumption increased significantly. While comparing the specific energy consumption between tests, the following observations were made:

(i) When the viscosity increased from 1.37 mPa-sec (test no. 1) to 5.24 mPa-sec (test no 5) due to fines addition, specific energy consumption increased from 0.63 kwhr/kg to 1.11 kwhr/kg

(ii) When the viscosity increased from 5.24 mPa-sec (test no. 5) to 8.19 mPa-sec (test no. 6) due to decrease in temperature, specific energy consumption increased again, going from 1.11 kwhr/kg to 5.0 kwhr/kg. This trend agrees with the observations made in the local iron ore plant, where specific energy consumption increased by ~20% during winter months when the slurry temperature was very low (Kawatra and Eisele, 1992).

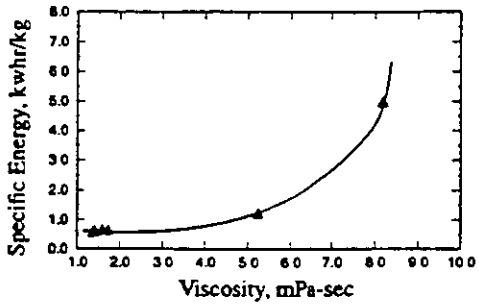

Figure 5 Specific energy vs. viscosity The increase in specific energy consumpuon is significant at higher viscosity values.

CONCLUSIONS

Viscosity of the pulp in the mill increased with addition of clay and fines content and also by decreasing the temperature. With each increase in viscosity there was a consistent increase in all three parameters measured during the tests; size stability values increased with viscosity, production of critical size material increased with viscosity, and specific energy consumption increased with viscosity. Therefore, we can say that viscosity had a definite influence during grinding and can conclude the following from this study;

1. The resistance of the media-sized ore to breakage increased when the slurry viscosity was increased. This effect was prominent at higher viscosities.

2. At lower slurry viscosity, there was a net decrease in the amount of critical size material present in the mill during grinding. However, as the viscosity increased, the amount of critical size material became higher than the amount of critical size material initially present in the feed. These results agree with plant observations reported by Kawatra and Eisele (1992), where specific energy consumption and critical size material production increased during winter months. It has already been determined that the breakage characteristics of the individual rocks do not change with temperature (Kawatra et al., 1993), and so the change must be due to changes in the behavior of the mill slurry as a whole. Since pulp viscosity increases at lower temperatures during winter months, such changes can be attributed to changes in pulp viscosity.

3. The specific energy consumption in the mill increased as the viscosity increased. This was a result of the increased viscosity reducing the grinding rate by cushioning of impacts, and by changing the motion of the charge in the mill.

ACKNOWLEDGEMENTS

This research has been supported by the Department of Interior's Mineral Institute program administered by the Bureau of Mines through the Generic Mineral Technology Center for Comminution under grant number G1115149.

REFERENCES

ASTM, 1991, Standard Method of Drop Shatter Tests for Coal, D440-86, Annual book of ASTM standards, Vol. 5.05, pp. 214.

Austin, L. G., Klimpel, R. R., and Luckie, P. T., 1984, "What Laboratory Tests Tell Us About Breakage in Ball Mills," Chapter 5, Process engineering of Size Reduction: Ball Milling, Society of Mining Engineers, American Institute of Mining, Metallurgical, and Petroleum Engineers, Inc., New York, pp. 79-176.

Fuerstenau, D. W., Venkataramana, K. S., Velamakanni, B. V., 1984, "Effect of Chemical Additives on the Dynamics of Grinding Media in Wet Ball Mill Grinding," Inter. J. of Miner. Process., Vol. 15, pp. 251-267.

Hemmings, C. E., and Boyes, J. M., 1977, "An On-Line Viscometry Technique for Improved Operation and Control of Wet Grinding Circuits," Twelfth International Mineral Processing Congress, Sao Paulo, pp 46-64.

Klimpel, R. R., 1982 & 1983, "Slurry Rheology Influence on the Performance of Mineral/Coal Grinding Circuits," Part I, Mining Engineering, 34 (12), (1982), pp. 1665-1668, Part II, Mining Engineering, Vol. 35, No. 1, (1983), pp. 21-26.

Kawatra, S. K. and A. K. Bakshi, 1995, "Determination of Changes in Rheological Properties of Coal Slurries in Process Streams," Coal Preparation, Vol. 15, pp. 165-175.

Kawatra, S. K., Moffat, S. A., DeLa'O, K. A., 1993, "The Effect of Freezing Conditions on Rock Breakage," Society for Mining, Metallurgy, and Exploration, Inc., Preprint Number 93-17.

Kawatra, S. K., and Eisele, T. C., 1992, "Influence of Temperature on the Energy Efficiency of an Industrial Circuit Processing Iron Ore," Minerals and Metallurgical Processing, Vol. 8, No. 1, pp 32-37.

Kawatra, S. K. and Eisele, T. C., 1988, "Rheology effects in Grinding Circuits," XVI International Mineral Processing Congress, Elsevier Science Publishers B. V., Amsterdam, pp. 195-207.

Moys, M. H., 1989, "Advances in Autogenous and Semi-autogenous Grinding Technology," Vol. 2, (Editors) A. L. Mular and G. E. Agar, Mining and Mineral Processing Engineering, University of British columbia, Vancouver, Canada, pp 713-728.

Tucker, P., 1982, "Rheological Factors that Affect the Wet Grinding of Ores," Trans. of Instn. Min. Metall., Section C, Mineral Processing and Extractive Metallurgy, Vol. 91, pp. 117-122.

FACULTAD DE INGENIERIA U.N.A.M.
DIVISION DE EDUCACION CONTINUA

CURSOS ABIERTOS

DESARROLLO Y OPERACIÓN DE SENSORES PARA CONTROL DIRECTO Y CONTINUO EN PLANTAS DE BENEFICIO DE MINERALES Y EN LA RESTAURACIÓN DEL MEDIO AMBIENTE

Del 18 al 23 de mayo de 1998

TEMA: INFLUENCE OF TEMEPERTURE ON THE ENERGY EFFICIENCY OF AN INDUSTRIAL CIRCUIT PROCESSING IRON ORE

EXPOSITOR :DR. KOMAR KAWATRA

1998

Influence of temperature on the energy efficiency of an industrial circuit processing iron ore

S.K. Kawatra and T.C. Eisele

Abstract—*In many mining operations, particularly northern open-pit mines, large seasonal variations in grinding slurry temperature can occur. It is shown in this paper that this temperature shift can cause a winter-time loss in autogenous grinding efficiency of as much as 20% if it is not controlled. Laboratory experimentation indicates that much of this effect is due to increases in slurry viscosity as the temperature is decreased. An additional effect may result from changes in rock strength upon freezing, for which possible mechanisms are discussed. However, no effect clearly resulting from rock strength changes has been definitely confirmed.*

Introduction

A great many excellent studies of the autogenous grinding process have been conducted since its development (Digre, 1979a and 1979b; Forssberg and Ekblom, 1979; Manlapig, Seitz and Spottiswood, 1979; Turner, 1979; Mokken, 1978; Stanley, 1974; Moys and Loveday, 1979; Rowland, 1981; Tangsathitkulchai and Austin, 1985, Austin, Klimpel and Luckie, 1984), allowing substantial improvements in autogenous milling performance. Nevertheless, the influence of temperature, viscosity and rheology on grinding circuit performance has largely been ignored, due both to the belief that it is of no consequence and to the expense of controlling the temperature of the mill feed. However, when the temperature approaches the freezing point of water, substantial changes in slurry rheology occur, and these changes would be expected to alter mill and hydrocyclone performance. This has been confirmed in the case of hydrocyclones (Kawatra et al., 1988 and 1989) and would be expected to be true for rod and ball mills as well (Austin, Klimpel and Luckie, 1984; Kawatra and Eisele, 1988). However, the rheology of mineral suspensions is difficult to measure (Cheng, 1984; Jinescu, 1974; Klimpel, 1982a and 1982b), particularly in real time and is therefore not used as a grinding circuit control parameter.

In addition to the rheological effects, any changes in the mechanical properties of the rock being ground, such as the hardness and fracture toughness, would also have an effect (Vitton, 1978). Mechanical changes in the rock would have the greatest effect on autogenous mill performance, as the grinding competency of the media-sized rock particles could be altered (Rowland, 1988). In extremely cold conditions, ice forms on the surface of the rock as it enters the mill, substantially changing the performance of the mill.

To understand the relative importance of each of these factors, and thus allow improved operating efficiency for grinding circuits, a study is being conducted at MTU of the effects of temperature on autogenous grinding. This study includes analysis of operating plant data, laboratory-scale experiments and pilot-scale grinding tests.

S.K. Kawatra and T.C. Eisele, members SME, are professor and graduate student, respectively, with Michigan Technical University, Metallurgy Dept., Houghton, MI. SME preprint 90-8, SME Annual Meeting, Salt Lake City, UT, Feb 26-March 1,1990. M&MP paper 90-606. Manuscript July 24, 1989. M&MP paper 90-606. Discussion of this paper must be submitted in duplicate, prior to June 1, 1991.

Theory

The effects of temperature on autogenous grinding can be immediately divided into rheological effects and mechanical effects. The rheological effects are a result of the substantial increase in the viscosity of water as the freezing point is approached. The change in apparent slurry viscosity that results from changing temperature is shown in Fig. 1. As can be seen, the effect at high percent solids is very pronounced, particularly when the temperature is quite low. This increased viscosity acts to cushion the impact of the media-sized particles, impede transport of slurry and in extreme cases cause the media to centrifuge at speeds well below the critical speed. The net result is decreased grinding rate and increased specific power consumption.

Effects resulting from changes in the mechanical properties of the rock are considerably more complicated, as they depend strongly on the specific characteristics of the rock. The major effect is a change in the mechanical strength, which alters the competency of the ore as grinding media.

One possible mechanism for strength changes with temperature is shown in Fig. 2. Here, the change is a result of water freezing in the pores and cracks of the rock, with the result depending on the degree of interconnections of the openings (Vitton, 1978). If the rock is very porous, as is the case with sandstone, the water can percolate freely through it and upon freezing form a continuous matrix that holds the rock together. This increases the fracture toughness of the rock and its competency as grinding media.

However, a hard, dense rock such as chert has relatively few, unconnected pores, which only collect water with difficulty. When the water in these pores freezes, frost cracking is likely to

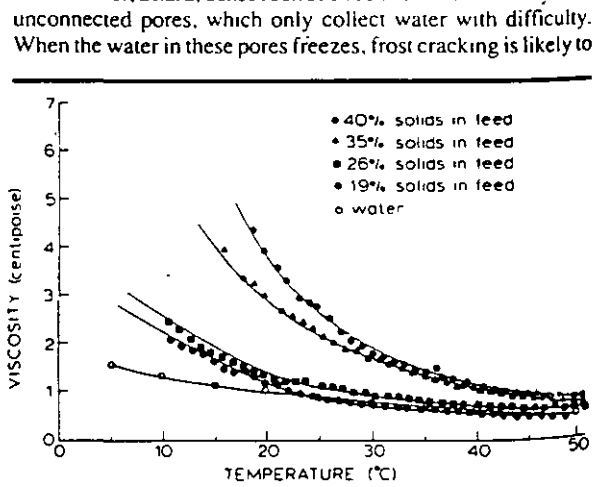

Fig. 1—Changes in apparent viscosity of fine silica slurries as a function of temperature. The viscosity was measured using a Nametre vibrating-sphere viscometer at an average shear rate of 4700 sec^{-1}, and the silica was 80% passing 270 mesh. The effect of temperature on apparent viscosity is most pronounced at high slurry solids contents and low temperatures.

occur around them, resulting in a slight weakening of the rock and a loss of grinding competency.

The effect of temperature on autogenous grinding is therefore highly variable and difficult to predict. No large effect is seen unless the water in the ore freezes, and this only occurs when the ore is exposed for some time before processing, as is the case in open-pit mines. An additional effect that can occur if the ore is seriously chilled is the formation of ice on the surface of the rock when it is added to the mill. The ice must then either melt or be ground away before grinding of the ore particle can commence, resulting in a reduced grinding rate. However, this requires both severely chilled ore and a near-freezing mill slurry, and should therefore not be a frequent problem.

For non-porous ores, each of these factors will result in a loss of autogenous milling efficiency. However, it has not been determined which of these phenomena is most important, or to what extent they reduce efficiency in real situations. In order to determine this, quantitative data are needed for both overall plant operation and for laboratory experiments designed to suppress all but one effect.

Plant studies

An iron ore processing plant that is subjected to large seasonal temperature variations was studied. This plant uses a fully autogenous grinding circuit, as shown in Fig. 3. Initially, plant personnel observed a significant seasonal variation in feed rate, as is illustrated in Fig. 4. This trend was observed for four years and so is unlikely to be entirely due to normal variations in ore characteristics. When com-

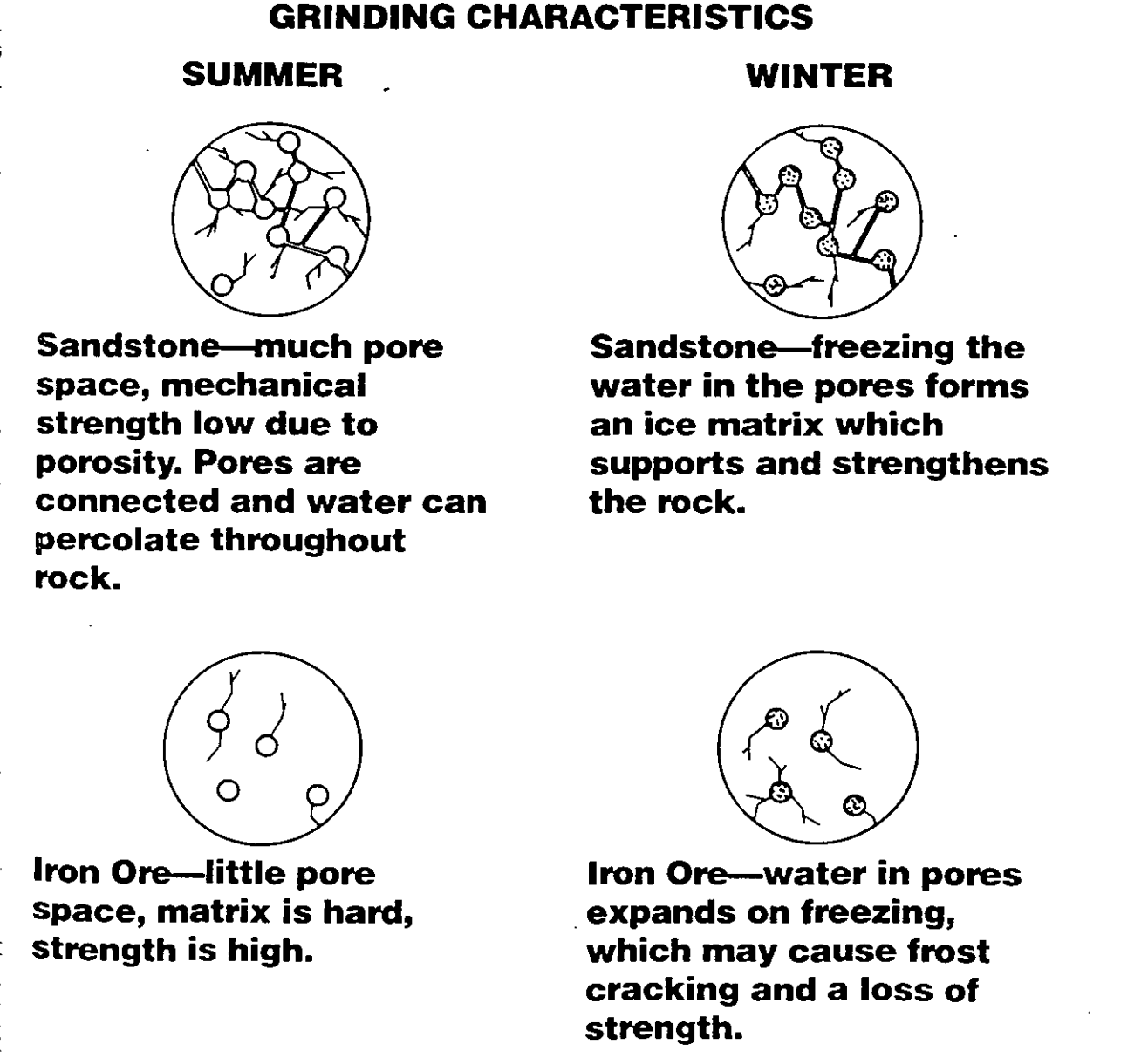

Fig. 2—Mechanism for changes in rock strength resulting from freezing of pore water. This effect is more important than changes in the hardness of the rock proper

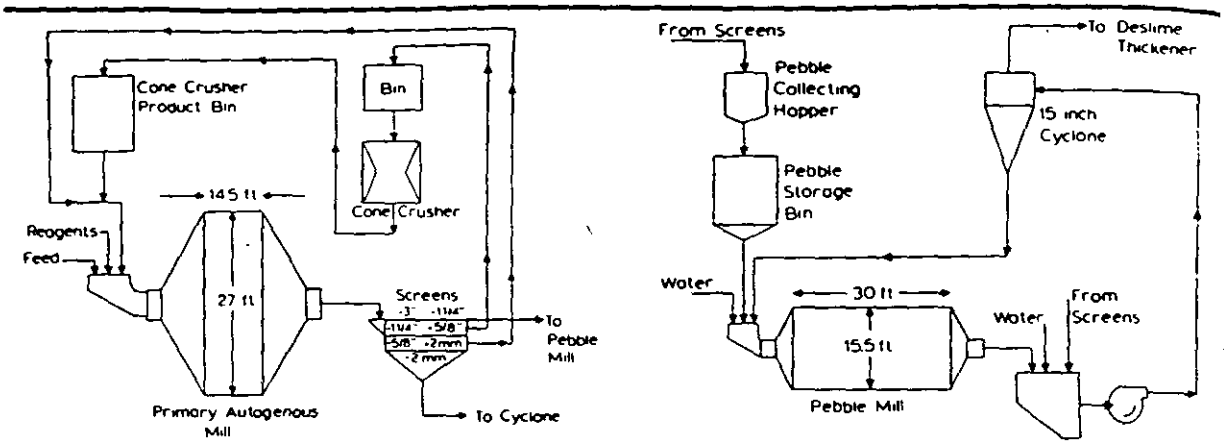

Fig. 3—Schematic of the grinding circuit discussed in this paper. The circuit is fully autogenous, with critical-size material crushed by a cone crusher to prevent buildup.

pared with measurements of the feed water temperature, which are also plotted in Fig. 4, it appears that the temperature effect is relatively slight until temperatures fall below 10° C. At temperatures below this value, the drop in throughput becomes quite pronounced.

Subsequently, the specific power consumption was computed for the primary, secondary and overall grinding circuits and plotted against the feed water temperature. Monthly averages were used to minimize the effects of variation in ore quality. The results for the primary autogenous mill are given in Fig. 5, where a pronounced decrease in specific energy consumption occurred as the temperature increased. A similar effect is shown in Fig. 6 for the pebble mill, although the trend is less pronounced. This is due to the warming of the pulp in the primary mill, which reduces the temperature fluctuation seen by the pebble mill. The overall result for the circuit is as shown in Fig. 7, which shows a total seasonal efficiency variation of 18% in the course of a year.

In addition to the efficiency measurements, plant personnel observed that the quantity of critical-size material circulated to the crusher increased in the winter, as indicated by Fig. 8 (Rowland, 1988; Kampe, 1988). This indicates that coarse rock may be more readily shattered at lower temperatures. Since large rocks are needed for effective autogenous grinding, the increased rate at which they are shattered into relatively ineffective critical-size material when the temperature is lowered results in reduced grinding efficiency. However, it is not clear whether this is due to changes in rock strength or to changes in the transport characteristics in the mill arising from rheological effects.

Laboratory studies

Laboratory tests were carried out primarily to determine the extent to which rheology alone would be expected to affect autogenous grinding. These experiments used a 20-cm-diam x 30-cm-long mill, rotating at 64 rpm with four 0.5-cm lifter bars. The mill and ore charge were heated in a forced-air drying oven for elevated temperature experiments and chilled using a freezer and an ice-water bath for low-temperature experiments. Polyurethane foam insulation was used to help keep the mill at a uniform temperature.

The results of initial experiments using Jacobsville sandstone have been previously reported (Kawatra et al., 1989). Further experiments were conducted using an iron ore sample from a local mine. The ore was crushed and mulled to the size

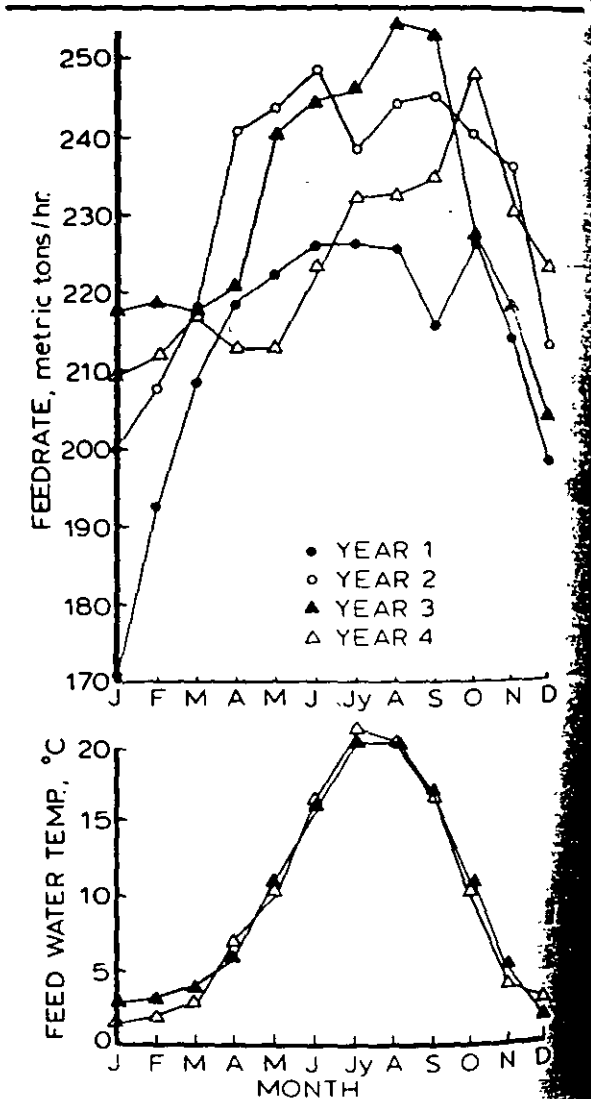

Fig. 4—Seasonal variations in grinding circuit throughput rate compared to average monthly feed water temperatures. A consistent seasonal trend is shown, with the greatest change in throughput exhibited during those months when the water temperature drops below approximately 10° C.

Table 1—Size Distribution of Charges for Laboratory Grinding Experiments

Size, millimeters	wt.%
50.8x38.1	41.5
38.1x25.4	25.2
25.4x19.0	15.1
19.0x12.7	13.1
12.7x 9.5	5.1
−9.5	0.0
	100.0

distribution given in Table 1, and each experiment used a 5.0-kg charge in 2 L of water. Six experiments were conducted consisting of three sets of duplicate tests at 2°-9° C, 24°-26° C, and 84°-62° C. For each experiment, the ore, water and mill were adjusted to temperature, and the ore was ground for 30 min. The slurry viscosity and quantity of -100 mesh material were then determined, the -100 mesh material was returned to the mill, the temperature was readjusted and the cycle was repeated. Viscosity was measured using a Brookfield viscometer fitted with a UL adapter for low viscosity measurements. Results of these experiments are given in Table 2.

Plotting these data as in Fig. 9 again shows a definite dependence of fines production on temperature. However, when grinding rate is plotted against viscosity, as in Fig. 10, it is evident that some factor other than viscosity is responsible for a portion of the change in grinding rate.

Discussion

In a plant situation, uncontrolled temperature changes can produce sizable changes in milling efficiency. The plant

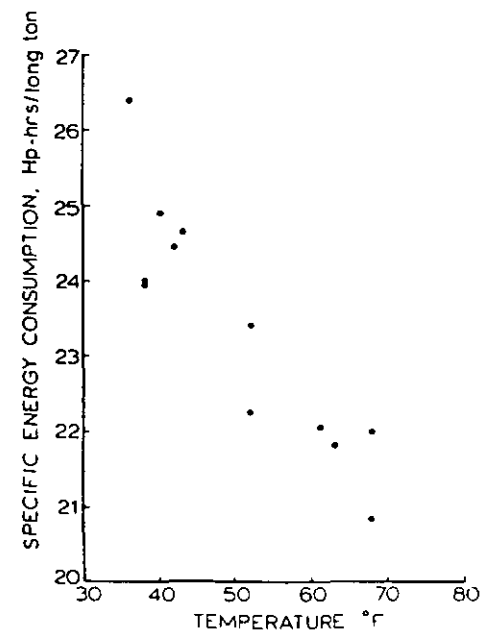

Fig. 5—Monthly change in specific energy consumption of the primary autogenous mill as a function of feed water temperature.

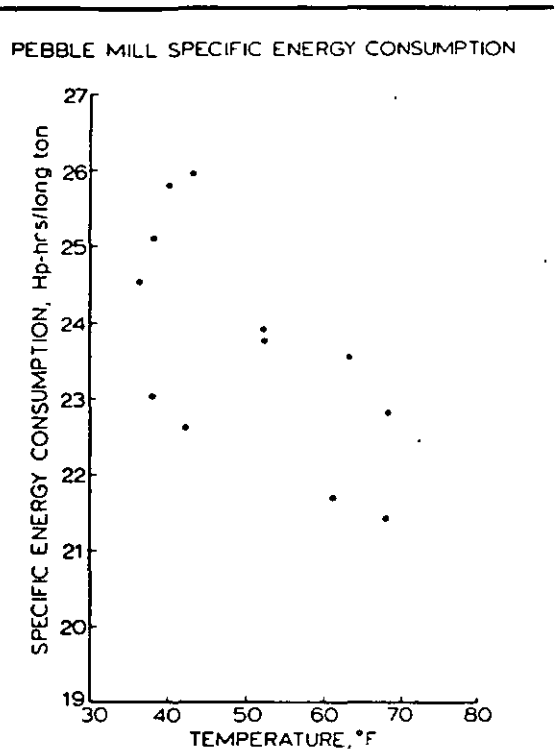

Fig. 6—Monthly change in specific energy consumption of the pebble mill as a function of feed water temperature

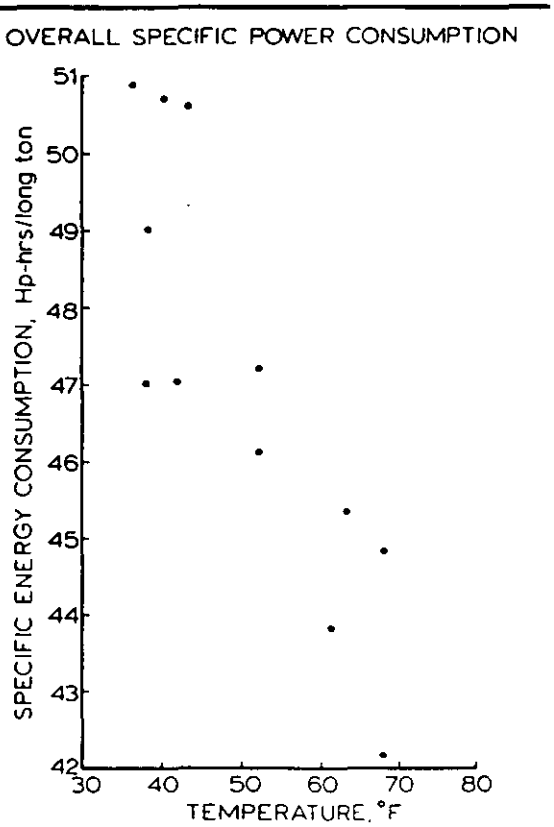

Fig. 7—Monthly change in specific energy consumption of the overall grinding circuit as a function of feed water temperature

Table 2—Results for Laboratory Grinding Experiements of Hematite Ore

	Grinding time (min.)	Temp. (°C)	Viscosity (cp)	Shear Rate (sec^{-1})	-100 mesh product (grams)
	30	4-9	1 57	73 42	69
	60	2-7	1.74	73 42	126
Test	90	2-9	1 82	73 42	178
1-1	120	2-7	1.93	73.42	206
	150	2-7	1.99	73 42	230
	180	2-6	2.18	73 42	248
	30	24-25	1.05	73 42	76
	60	26	1 23	73 42	145
Test	90	25	1 42	73.42	197
1-2	120	25	1.61	73 42	249
	150	25	1.78	73 42	289
	180	25	1.92	73.42	327
	30	83-64	0.83	73.42	85
	60	84-64	0.90	73 42	155
Test	90	84-64	0 97	73 42	218
1-3	120	84-64	1.02	73.42	281
	150	84-62	1 17	73 42	327
	180	84-63	1.28	73 42	366
	30	2-7	1.66	73 42	67
	60	2-8	1.72	73.42	122
Test	90	2-10	1 78	73.42	176
2-1	120	2-7	1.90	73 42	200
	150	2-6	2.02	73 42	227
	180	2-7	2 15	73.42	255
	30	24-25	1 06	73.42	79
	60	24-25	1 24	73 42	144
Test	90	25	1.43	73 42	195
2-2	120	25	1 62	73 42	248
	150	25	1 80	73 42	290
	180	25	1 94	73 42	329
	30	84-65	0 85	73.42	86
	60	84-65	0 90	73.42	157
Test	90	84-64	0 96	73 42	219
2-3	120	84-64	1.02	73 42	280
	150	84-63	1.15	73.42	325
	180	84-64	1 27	73 42	364

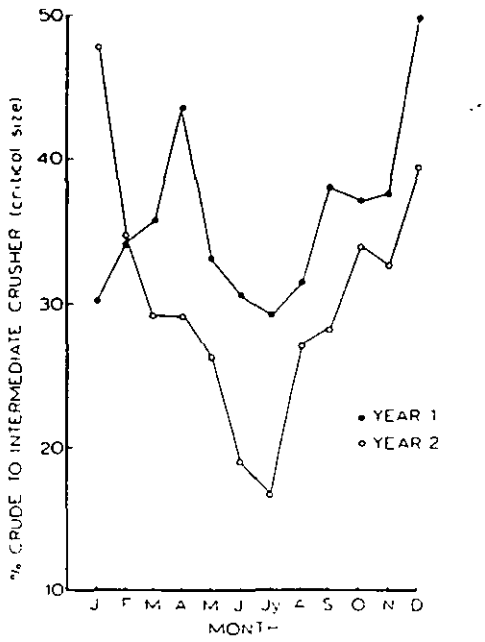

Fig 8—Monthly variation in critical-size production as measured by the tonnage of material circulated to the crusher

data presented here show a seasonal efficiency shift of approximately 18% for the overall circuit and more for the primary autogenous mill alone It is difficult to be completely certain of the precise mechanism, but it is likely that most of the effect is due to viscosity changes. It is seen that the temperature effect is much less pronounced in the pebble mill, but this is almost certainly due to the warming that occurs in the primary mill and not to inherently lower temperature sensitivity in the pebble mill. The change in production of critical-size material in the primary mill may be a result of changing rock strength, but it is possible that increasing viscosity forces the media-size particles to migrate to those portions of the charge where the impacts are most severe, causing them to break up more rapidly (Rowland, 1988). The seasonal shifts of mill throughput show clearly that the greatest change occurs at temperatures below about 10° C It is therefore evident that simply maintaining the temperature above this point will greatly reduce the seasonal throughput variation. This may be accomplished by prevent-

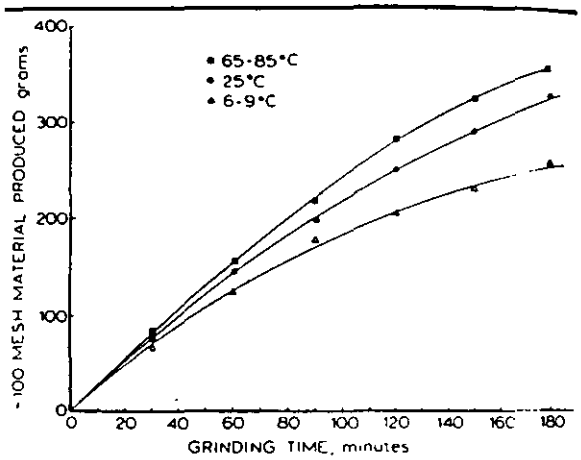

Fig 9—Variation in laboratory-scale fines production as a function of time and temperature for an iron ore The behavior of the non-porous iron ore is very similar to that of the porous sandstone.

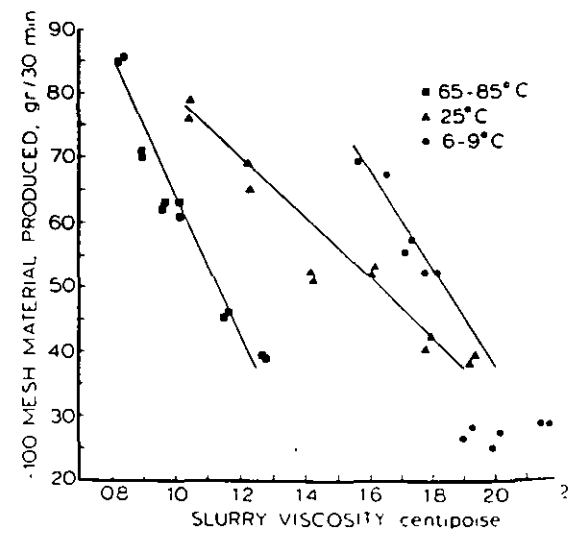

Fig 10—Grinding rate vs viscosity for the six laboratory-scale iron ore grinding experiments While decreasing the viscosity produces an increase in the grinding rate, this is obviously not the only effect occurring in these experiments

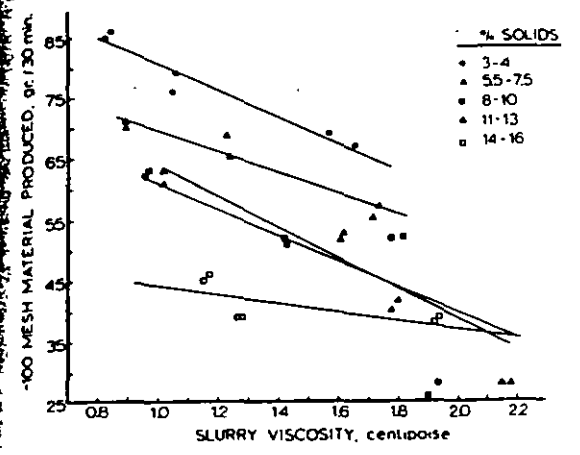

Fig. 11—Viscosity vs. grinding rate for the six laboratory-scale grinding experiments, correlating those measurements that contained similar amounts of -100 mesh fines. The listed percent solids ranges represent the ratio of -100 mesh material to water. The resulting lines are roughly parallel, indicating that buildup of fines is responsible for the drop in grinding rate with time.

ing the recycle water from being chilled and by thawing the ore before grinding.

From the laboratory experiments, it is readily seen that the changes in grinding rate are closely tied to slurry viscosity. However, in these experiments the viscosity was not the only factor influencing fines production, as shown in Fig. 10. If viscosity were the only relevant factor, tests for all three temperatures should have followed the identical grinding rate vs. viscosity curve. The second factor appears to be the quantity of fines in the suspension, as plotting grinding rate vs. viscosity for only those tests with similar quantities of fines generates a series of roughly parallel lines as in Fig. 11. It is likely that as the fines are accumulating, work is being expended to make the fines finer rather than generating additional fines. It is also possible that the increasing slurry density is cushioning the impacts due to increased buoyancy, thus further retarding the grinding rate.

Conclusions

From this investigation, the following conclusions are drawn:

1. In autogenous milling, temperature can significantly influence the grinding efficiency, particularly if the temperature falls below about 10° C. These efficiency changes can be reduced by preventing recycle water from becoming chilled, and by thawing frozen rock before grinding. Since the magnitude of the efficiency change is reduced at higher temperatures, heating the mill slurry to higher temperatures is unlikely to provide significant benefits.

2. Laboratory experiments indicate that the effect of slurry rheology changes with temperature is a significant factor in the grinding rate for both porous and non-porous rock types, with higher temperatures resulting in reduced viscosity and hence increased grinding rate.

Acknowledgements

This research has been supported by the Department of the Interior's Mineral Institute Program administered by the Bureau of Mines through the Generic Mineral Technology Center for Comminution under grant number G1175149.

References

Austin, L.G., Klimpel, R.R., and Luckie, P.T., 1984, *Process Engineering of Size Reduction Ball Milling*, SME-AIME, New York, pp. 385-406.

Cheng, D. C-H., 1984, "Further Observations on the Rheological Behavior of Dense Suspensions," *Powder Technology*, Vol. 37, pp. 255-273.

Degre, M., 1979a, "Autogenous Grinding in Relation to Abrasion Conditions and Mineralogical Factors," *Proceedings of the Autogenous Grinding Seminar*, Trondheim, Norway, Session A—Fundamentals, paper A1.

Degre, M., 1979b, "Autogenous Grinding Testing and Scale-Up," *Proceedings of the Autogenous Grinding Seminar*, Trondheim, Norway, paper F5.

Forssberg, E., and Ekblom, K., 1979, "Experience of Autogenous Grinding in Sweden," *Proceedings of the Autogenous Grinding Seminar*, Trondheim, Norway, Session A—Fundamentals, paper A2.

Jinescu, V.V., 1974, "The Rheology of Suspensions," *International Chemical Engineering*, Vol. 14, No. 3, pp. 397-420.

Kampe, H., 1988, personal communication.

Kawatra, S.K., and Eisele, T.C., 1988, "Rheological Effects in Grinding Circuits," *International Journal of Mineral Processing*, Vol. 22, pp. 251-259.

Kawatra, S.K., Eisele, T.C., Zhang, D.X., and Rusesky, M.T., 1988, "Effects of Temperature on Hydrocyclone Efficiency," *International Journal of Mineral Processing*, Vol. 23, pp. 205-211.

Kawatra, S.K., Eisele, T.C., Zhang, D.X., and Rusesky, M.T., 1989, "Effects of Seasonal Temperature Changes on Autogenous Milling Performance," SME-AIME Meeting, Las Vegas, Nevada, Feb. 27-March 2, 1989.

Klimpel, R.R., 1982a, "Slurry Rheology Influence on the Performance of Mineral/Coal Grinding Circuits," *Mining Engineering*, December 1982, pp. 1665-1668, and January 1983, pp. 21-26.

Klimpel, R.R., 1982b, "Laboratory Studies of the Grinding and Rheology of Coal-Water Slurries," *Powder Technology*, Vol. 32, pp. 267-277.

Manlapig, E.V., Seitz, R.A., and Spottiswood, D.J., 1979, "Analysis of the Breakage Mechanism in Autogenous Grinding," *Proceedings of the Autogenous Grinding Seminar*, Trondheim, Norway, Session A—Fundamentals, paper A3.

Mokken, A.H., 1978, "Progress in Run-of-Mine (Autogenous) Milling as Originally Introduced and Subsequently Developed in the Gold Mines of the Union Corporation Group," *Eleventh Commonwealth Mining and Metallurgical Congress*, Hong Kong, Institution of Mining and Metallurgy.

Moys, M.H., and Loveday, B.K., 1979, "Autogenous Milling Research at the South African National Institute for Metallurgy," *Proceedings of the Autogenous Grinding Seminar*, Trondheim, Norway, paper F2.

Rowland, C.A., 1981, "Pilot Plant Data for the Design of Primary Autogenous and Semi-Autogenous Mills," *CIM Bulletin*, November 1981.

Rowland, C.A., 1988, personal communication.

Stanley, G.G., 1974, "Mechanisms in the Autogenous Mill and Their Mathematical Representation," *Journal of the South African Institute of Mining and Metallurgy*, November 1974.

Tangsathitkulchai, C., and Austin, L.G., 1985, "The Effect of Slurry Design on Breakage Parameters of Quartz, Coal, and Copper Ore in a Laboratory Ball Mill," *Powder Technology*, Vol. 42, pp. 287-296.

Turner, R.R., 1979, "Primary Autogenous Grinding—A Study of Ball Charge Effects," *Proceedings of the Autogenous Grinding Seminar*, Trondheim, Norway, Session B—Mill and Mill Circuit Design, paper A4.

Vitton, S.J., 1978, "An Experimental Study of the Effects of Low Temperature on the Mechanical Properties of Iron Ore," unpublished M.S. thesis, Michigan Technological University.

FACULTAD DE INGENIERIA U.N.A.M.
DIVISION DE EDUCACION CONTINUA

CURSOS ABIERTOS

DESARROLLO Y OPERACIÓN DE SENSORES PARA CONTROL DIRECTO Y CONTINUO EN PLANTAS DE BENEFICIO DE MINERALES Y EN LA RESTAURACIÓN DEL MEDIO AMBIENTE

Del 18 al 23 de mayo de 1998

TEMA: RHEOLOGICAL CHARACTERIZATION OF MINERAL SUSPENSIONS USING A VIBRATING SPHERE AND A ROTATIONAL VISCOMETER

EXPOSITOR :DR. KOMAR KAWATRA

Palacio de Minería Calle de Tacuba 5 Primer piso Deleg. Cuauhtemoc 06000 Mexico D.F. APDO. M-2285
Teléfonos 512-8955 512-5121 521-7335 521-1987 Fax 510-0573 521-4020 AL 26

Reprinted from

INTERNATIONAL JOURNAL OF MINERAL PROCESSING

Int. J. Miner. Process. 44–45 (1996) 155–165

Rheological characterization of mineral suspensions using a vibrating sphere and a rotational viscometer

S.K. Kawatra [a], A.K. Bakshi [a], T.E. Miller Jr. [b]

[a] *Michigan Technological University, Department of Metallurgical and Materials Engineering, Houghton, MI 49931, USA*

[b] *The Dow Chemical Company, Dow Central Research, Midland, MI, USA*

ELSEVIER

INTERNATIONAL JOURNAL OF
MINERAL PROCESSING

Editors-in-Chief

J. Cases
CNRS/CRVM, P.O. Box 40,
54501 Vandoeuvre-lès-Nancy, Cedex,
France
Fax: +33 83 57 54 04
e-mail: ijmp@ensg.u-nancy.fr

D.W. Fuerstenau
Department of Materials Science and Mineral
Engineering, Hearst Mining Building,
University of California,
Berkeley, CA 94720, USA
Fax: +1 510 642 6623

Honorary Editor-in-Chief and Founder

Pierre M. Gy, Cannes

Associate Editors

A.M. Abouzeid, Giza
G. Adel, Blacksburg, VA
L.J. Cabri, Ottawa, Ont.
S. Chander, University Park, PA
J.A. Finch, Montreal, Que.
K.S.E. Forssberg, Luleå
R.D. Hagni, Rolla, MO
K.N. Han, Rapid City, SD
S. Heimala, Pori
J.A. Herbst, Salt Lake City, UT
R. Houot, Vandoeuvre
J. Hwang, Houghton, MI
C. Jin, Changsha
P.C. Kapur, Kanpur
R.P. King, Salt Lake City, UT
R. Klimpel, Midland, MI
J.S. Laskowski, Vancouver, B.C.
I.J. Lin, Haifa
A.M. Marabini, Rome
T.P. Meloy, Morgantown, WV
M.H. Moys, Johannesburg
T.J. Napier-Munn, Indooropilly, Qld.
S. Pignolet-Brandom, Grayslake, IL
B.J. Scheiner, Tuscaloosa, AL
P. Somasundaran, New York, NY
T. Wakamatsu, Kyoto
R. Woods, Port Melbourne, Vic.

Scope of the journal

The *International Journal of Mineral Processing* will cover all aspects of the processing of solid-mineral materials such as metallic and non-metallic ores, coals and other solid sources of secondary materials, etc. Topics dealt with include: comminution, sizing, classification (in air and water), gravity concentration, flotation, electric and magnetic separation, miscellaneous physical separation techniques, mixing and blending, thickening, filtering, drying, storage, transport, agglomeration, pyrometallurgy and hydrometallurgy (when applied to low-grade raw materials), biohydrometallurgy (when applied to low-grade raw materials), biometallurgy (use of bacteria and other living organisms), testing, control and automation, waste treatment and disposal and mineralogical studies (when related to beneficiation). In addition to research papers, the Journal will contain review articles, case histories and book reviews.

Publication information

International Journal of Mineral Processing (ISSN 0301-7516). For 1996 volumes 46–48 are scheduled for publication. Subscription prices are available upon request from the publisher. Subscriptions are accepted on a prepaid basis only and are entered on a calender year basis. Issues are sent by surface mail except to the following countries where air delivery via SAL is ensured: Argentina,

(see further inside back cover)

© 1996, ELSEVIER SCIENCE B.V. ALL RIGHTS RESERVED

0301-7516/96/$15.00

No part of this publication may be reproduced, stored in a retrieval system or transmitted in any form or by any means, electronic, mechanical, photocopying, recording or otherwise, without the prior written permission of the publisher, Elsevier Science B.V., Copyright & Permissions Department, P.O. Box 521, 1000 AM Amsterdam, Netherlands.
Upon acceptance of an article by the journal, the author(s) will be asked to transfer copyright of the article to the publisher. The transfer will ensure the widest possible dissemination of information.
Special regulations for readers in the USA – This journal has been registered with the Copyright Clearance Center, Inc. Consent is given for copying of articles for personal or internal use, or for the personal use of specific clients. This consent is given on the condition that the copier pays through the Center the per-copy fee stated in the code on the first page of each article for copying beyond that permitted by Sections 107 or 108 of the US Copyright Law. The appropriate fee should be forwarded with a copy of the first page of the article to the Copyright Clearance Center, Inc., 222 Rosewood Drive, Danvers, MA 01923, USA. If no code appears in an article, the author has not given broad consent to copy and permission to copy must be obtained directly from the author. The fee indicated on the first page of an article in this issue will apply retroactively to all articles published in the journal, regardless of the year of publication. This consent does not extend to other kinds of copying, such as for general distribution, resale, advertising and promotion purposes, or for creating new collective works. Special written permission must be obtained from the publisher for such copying.
No responsibility is assumed by the Publisher for any injury and/or damage to persons or property as a matter of products liability, negligence or otherwise, or from any use or operation of any methods, products, instructions or ideas contained in the material herein.
Although all advertising material is expected to conform to ethical (medical) standards, inclusion in this publication does not constitute a guarantee or endorsement of the quality or value of such product or of the claims made of it by its manufacturer.

♾ The paper used in this publication meets the requirements of ANSI/NISO Z39.48-1992 (Permanence of Paper).

PRINTED IN THE NETHERLANDS

ELSEVIER

Int. J. Miner. Process. 44–45 (1996) 155–165

INTERNATIONAL JOURNAL OF MINERAL PROCESSING

Rheological characterization of mineral suspensions using a vibrating sphere and a rotational viscometer

S.K. Kawatra [a], A.K. Bakshi [a], T.E. Miller Jr. [b]

[a] *Michigan Technological University, Department of Metallurgical and Materials Engineering, Houghton, MI 49931, USA*

[b] *The Dow Chemical Company, Dow Central Research, Midland, MI, USA*

Abstract

A new technique has been developed for the characterization of the rheology of mineral slurries into Newtonian and non-Newtonian flows. It utilizes a rotating type viscometer to measure apparent viscosity at a low shear rate, and a vibrating sphere type viscometer to measure the apparent viscosity at a high shear rate. Special precautions were taken to allow measurements of apparent viscosity of rapidly settling mineral suspensions. Both the viscometers are able to measure apparent viscosity as low as one mPa · s (millipascal-seconds) (1 mPa · s = 1 centipoise), which is the approximate room temperature viscosity of water. Because the vibrating sphere viscometer operates at a much high shear rate than the rotating viscometer, the two instruments together can determine the shear-rate dependency of the viscosity. Ground silica of −65 mesh size was used to prepare slurries in water at different percent solids. The apparent viscosity of each slurry sample was measured simultaneously by both viscometers, and the results were compared with each other. In this way, it was determined that silica slurries, for a given particle size distribution, between 0–70% solids by weight in distilled water have Newtonian flow behavior.

1. Introduction

It has long been observed that performance of grinding mills depends upon the rheological properties of the slurry (Klimpel, 1982). Several investigators (Klimpel, 1982; Fuerstenau et al., 1984; Tucker, 1982) have claimed improvement in grinding performance by altering the slurry rheology with grinding aids. These works suggest that by controlling the rheology of the slurry, the efficiency of a grinding mill can be improved. However, to accomplish this, it is first necessary to be able to monitor the slurry rheology.

0301-7516/96/$15.00 © 1996 Elsevier Science B.V. All rights reserved
SSDI 0301-7516(95)00026-7

Rheology of mineral suspensions is highly complex and difficult to predict. It depends upon several parameters, such as solids concentration, particle size and shape, chemical environment, and temperature (Schack et al., 1957). The flow behavior of these suspensions can be divided into different general categories depending upon the relationship between the shear stress developed in the fluid and its rate of shear (Fig. 1). The ratio of shear stress and shear rate is the viscosity. For a Newtonian fluid, the viscosity remains constant as the rate varies. But, for non-Newtonian fluids this ratio changes with shear rate, and is called the apparent viscosity of the fluid at any particular shear rate. The apparent viscosity increases with increase in shear rate for a dilatant fluid, and decreases with increase in shear rate for a pseudoplastic fluid. Dilatant and pseudoplastic fluids are also called shear thickening and shear thinning fluids respectively. Bingham plastics exhibit a yield stress, that is, they do not begin to flow until a critical shear stress is reached. Some suspensions also show yield stress with pseudoplastic flow. Among all the parameters, percent solids has the most visible effect on slurry rheology. At lower percent solids most slurries show Newtonian flow properties, but as the solids content increases, particle–particle interactions become important and the slurry changes to a non-Newtonian flow regime.

The importance of these rheological properties in mineral processing operations have been long realized (Klimpel, 1982). However, measuring slurry rheology is difficult with existing apparatus. The main difficulty of this measurement is rapid settling of the solid particles during measurement. The settling constantly changes the percent solids in the sample holder before the instrument can display a steady reading. This settling effect can be eliminated by measuring the viscosity of a constantly moving slurry in contact with the measuring device. Specially designed baffles (Clarke, 1967) and eddy control baskets (Underwood, 1976) have been used by several investigators to maintain a uniform suspension of solids and reduce the effect of fluid motion on viscometer readings. One of the promising designs for on-line application for slurry viscometry is the gravity flow system, in which the slurry flows through a conduit or a vessel under gravity (Hemmings and Boyes, 1977; Reeves, 1985). By constricting the out flow of slurry from this conduit, a constant hold-up of slurry can be maintained. Then the viscometer can be placed in this slurry to take viscosity measurements. In this way,

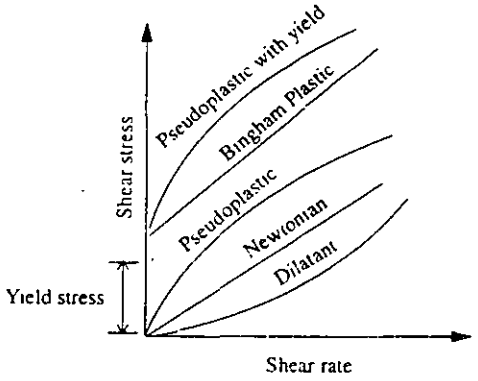

Fig. 1. Generalized time-independent rheology curves for mineral slurries.

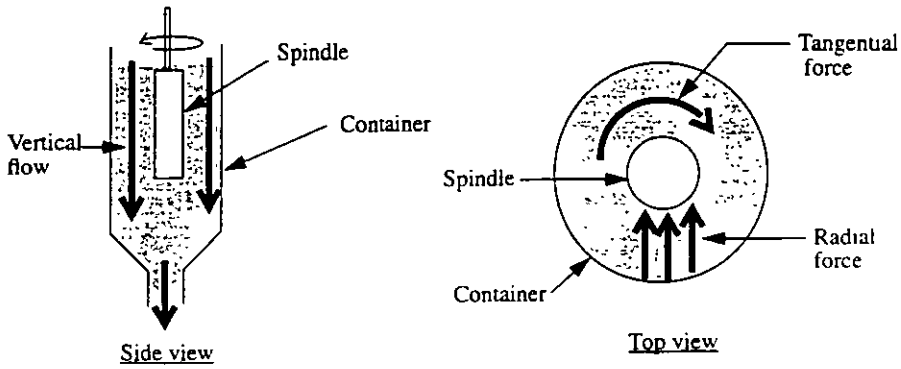

Fig. 2. The vertical flow (side view) prevents the solids from settling by continously sweeping fresh slurry past the spindle. This component of the flowing slurry stream does not affect the rotation of the spindle. But, any radial or tangenial forces (top view), arising from the flow, may put additional strain on the spindle resulting in erroneous viscosity readings. Unbalanced radial flows push the spindle to one side so that it does not spin uniformly and results in erratic readings. Tangential flows increase or decrease the torque on the spindle, making the fluid appear to be either more or less viscous then it really is.

solids settling can be avoided to obtain a homogeneous slurry sample. However, the problem with this method is to obtain a smooth laminar flow of slurry without causing any disturbances in the sample holder. This is particularly true for rotating viscometers, which measure viscosity by measuring the torque generated by the rotation of the spindle (see Fig. 2). The flow of the sample should be strictly vertical, because forces in any other direction will interfere in the rotation of the spindle. In this way, a small turbulence originating from the mixing or flow of slurry can produce a shift in the viscometer reading. Klien et al. (1990) and Kiljanski (1993) have discussed separately how the slurry flow in recirculation systems can change the effective shear rate, which results in different viscosity figures. Also, when one of these techniques (the Underwood design) was tried by the investigators with a Brookfield viscometer, erratic viscosity readings were obtained for suspensions, because the effect of eddies from fluid flow could not be eliminated. In the system described in this paper, suitable slurry handling systems have been designed to eliminate these problems. The details are discussed in the following sections.

2. Methods and materials

2.1. System development

Viscosity of a Newtonian fluid is not affected by shear rates, but for non-Newtonian fluids it changes with change in shear rate. Thus, by measuring the viscosity at two different shear rates sufficiently apart from each other, and comparing the two viscosity values, the fluid can be designated as Newtonian if both the viscosities are similar, and non-Newtonian if the viscosities are different. Based on this concept, a new system has been developed to determine the flow regimes of mineral slurries. Two viscometers were

used for this purpose: the first one was a Brookfield (rotating type) viscometer and the other was a Nametre (vibrating sphere type) viscometer. In this system the Brookfield viscometer operated at a much lower shear rate than the Nametre viscometer. Thus for Newtonian fluids readings from both the viscometers were the same; For pseudoplastic fluids the Brookfield reading was higher than the Nametre reading; and for dilatant fluids it was lower than the Nametre reading. The details of the Brookfield set-up and the Nametre set-up are discussed in the following sections.

2.2. *The Brookfield set-up*

A Brookfield viscometer (DV-I model) was used to measure apparent viscosity at low shear rates. It was a rotational viscometer (coaxial cylinder) and could operate at different shear rates. But, all of its spindles, except for the UL adaptor, were designed for high viscosity solutions and are not suitable for many mineral slurries. The UL adaptor consisted of a cylindrical spindle and a tube which housed the spindle. Sample was placed in the annular space between the spindle and the tube. Then, the viscosity was measured by measuring the torque required to rotate the spindle at a constant rotational speed. Although this arrangement could measure viscosity as low as 1 mPa · s, it failed to operate with slurry, because the solids settled quickly before the instrument could display a steady reading. Therefore, it was necessary to develop a system where the solids would be kept in suspension while the reading was taken. This was accomplished by the slurry presentation system described in Fig. 3. Slurry was mixed in a overhead tank and passed continuously through the annular space between the UL adapter and the tube. After a steady state reading was displayed, flow was stopped by both the pinch valves (to eliminate any swirling motion caused by the flow at the inlet) and the reading was taken immediately. This assembly operated at different shear rates depending upon the viscosity of the slurry. The range of viscosities which could be

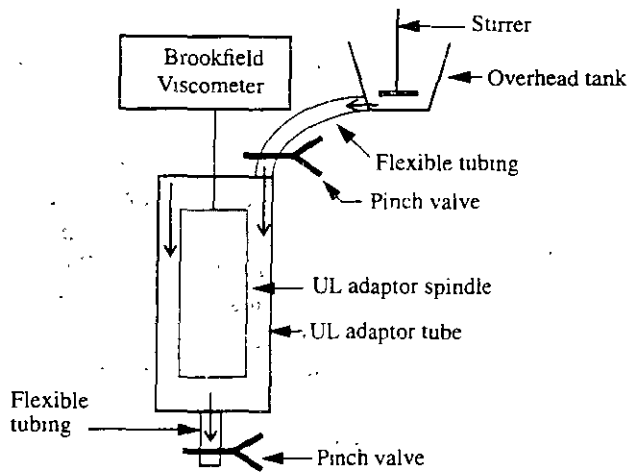

Fig. 3. Brookfield viscometer set-up showing the UL adaptor assembly and the slurry presentation system This arrangement is very suitable for dilute suspensions, and could measure viscosities of silica slurries up to 70% solids by weight in water without any difficulty.

Table 1
Range of apparent viscosities at any rate for the UL adaptor (Brookfield Engineering Laboratories, 1985)

R.P.M. of the spindle	Shear rate, sec^{-1}	Viscosity range, mPa·s	
		Minimum	Maximum
60.0	73.42	1	9.9
30.0	36.75	2	19.8
12.0	14.68	5	49.5
6.0	7.34	10	99
3.0	3.67	20	198
1.5	1.83	40	396
0.6	0.73	100	990
0.3	0.36	200	1980

measured at any shear rate are given in Table 1. Although the Brookfield viscometer could operate at different shear rates, it was not sufficient by itself to determine the rheological type, because for most of the slurries, readings could be taken only at a single shear rate. When the shear rate was changed by changing the r.p.m. of the spindle, the instrument went out of its operating range. Therefore, a Nametre viscometer was used to measure the viscosity of the fluid at another shear rate. The set-up for the Nametre viscometer is discussed in the next section.

2.3. The Nametre set-up

The Nametre viscometer consisted of a spherical probe, which oscillated along a vertical shaft at its resonant frequency of 750 Hz and a constant amplitude of 1 micron. This viscometer was selected because it operated at a much higher shear rate than the Brookfield viscometer and could measure viscosity as low as 1 mPa · s. When immersed in a fluid, the probe created a shear wave in the fluid, and the fluid dampened the oscillatory motion. The damping, or the power to restore constant amplitude, is a measure of the apparent viscosity of the fluid. Since the probe was vibrating rather than rotating in a single direction, the shear rate was a sinusoidal function of time. Also, the probe was spherical in shape, therefore its vibration had its maximum amplitude at the equator and gradually dropped to zero at the poles (Ferry, 1977). For these reasons, the Nametre viscometer did not operate at a specific shear rate but averaged the shear rates from zero to the maximum value. The maximum shear rate was not a definite constant for the instrument and it varied according to the velocity of propagation of the shear wave in the fluid, which in turn depended upon the fluid viscosity. Therefore, it was necessary to get an idea of its operating shear rate for fluids at different viscosities. This was done by measuring the apparent viscosity of non-Newtonian Methocel A4M (methylcellulose) solutions at different concentrations with the Nametre viscometer, and comparing these figures with the readings of a Bohlin viscometer (details of this test are discussed in the following sections). The shear rates for the Nametre viscometer obtained by this procedure are listed in Table 2. From Tables 1 and 2 it is seen that the Nametre viscometer operates at a much higher shear rate than the Brookfield viscometer with its UL adaptor.

Table 2
Apparent viscosities of Methocel solutions at different concentrations from the Nametre viscometer and their shear rates

Concentrations of Methocel A4M in water	Apparent viscosity from the Nametre viscometer, mPa·s	Shear rate, sec^{-1}
2.0%	212	1500
1.0%	49	3000
0.5%	13	3500

In earlier experiments, an attempt was made to install the Nametre viscometer on a T-joint and fit it to a pipe-line through which the sample was flowing (Kawatra et al., 1992). When the viscometer was bolted to the flange in this manner its response characteristics changed. The major problems encountered involved maintaining a constant tension on the mounting bolts, and dealing with vibration acting upon the instrument from the surrounding structure. The pumping system transmitted excessive vibration through the pipeline, loosening one or the other mounting bolts, which caused a drifting of the zero setting. This problem was eliminated by designing a special slurry presentation system as shown in Fig. 4. This was comprised of a vessel of two concentric cylinders made out of plexiglass. The bottom of the inner cylinder was made conical to avoid solids settling and had an inlet opening through which slurry from the pump entered the vessel. The outer cylinder was one inch taller than the inner cylinder and had a discharge opening on its side. Slurry overflowed from the inner cylinder and returned to the sump through this outlet. The viscometer was suspended from the top by a cable and the probe of the viscometer was immersed inside the inner cylinder. In this way the cable dampened any vibration from the surrounding structures. The weight of the viscometer kept the cable stretched, and the position of the viscometer was kept quite constant. A thermocouple was also placed inside the sump, so that both viscosity and temperature of the sample were recorded simultaneously.

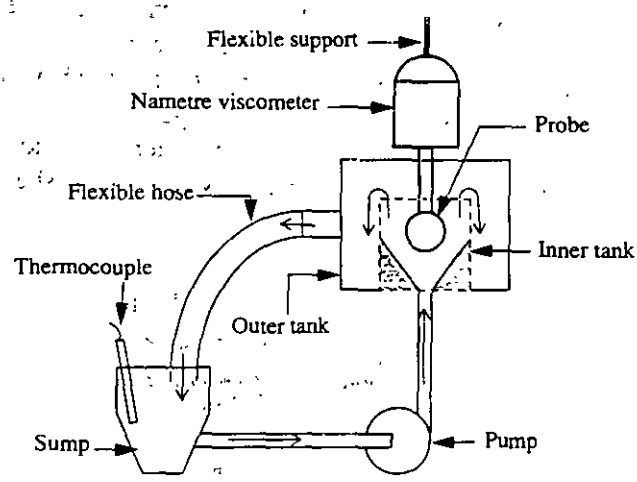

Fig. 4. Nametre viscometer set-up. Sample is placed in the sump and is circulated through the system by a centrifugal pump. Thus the probe of the viscometer comes in contact with a continously flowing slurry.

Table 3
Viscosity of sucrose solutions at different concentrations in water at room temperature (Weast, 1984)

Sucrose content, % by weight	10	20	30	40	50	60
Viscosity, mPa·s	1.33	1.94	3.18	6.15	15.40	58.37

2.4. Bohlin viscometer

A Bohlin viscometer was used to determine the shear rates of the Nametre viscometer for fluids of different viscosities. The Bohlin was a rotational viscometer, in which the spindle was held stationary and the outer cup, surrounding the spindle, rotated. The sample was placed in the annular space between the spindle and the cup, and measurements were taken at different rotational speeds of the cup. With this instrument, measurements of viscosity and shear stress could be taken at different shear rates within a range of 0–1450 sec^{-1}. However, this viscometer could not be used for slurries, because solids settled at the bottom and also on the wall of the cup because of gravity and centrifugal forces. Apparent viscosity vs. shear rate plots of three solutions of Methocel A4M were obtained from this instrument. From these plots, shear rates for the Nametre viscometer were determined.

2.5. Materials used

2.5.1. Sucrose solutions

Sucrose solutions show Newtonian flow properties, and were used to verify the system's ability to work with Newtonian fluids. Six different solutions at different sucrose concentrations were used, with the theoretical viscosities (Weast, 1984) of these solutions listed in Table 3.

2.5.2. Methocel A4M solutions

The molecular structure of Methocel A4M (methylcellulose), a water soluble polymer manufactured by The Dow Chemical Company, Midland, Michigan is given in Fig. 5. Four solutions of this product at 0.5%, 1.0%, 1.5% and 2.0% concentrations by weight in water were prepared. These solutions display pseudoplastic flow behavior (The Dow Chemical Company, 1988) and were used for the following purposes:

(1) To determine the shear rates for the Nametre viscometer for fluids at different viscosities. This was done by first obtaining the apparent viscosity vs. shear rate graph

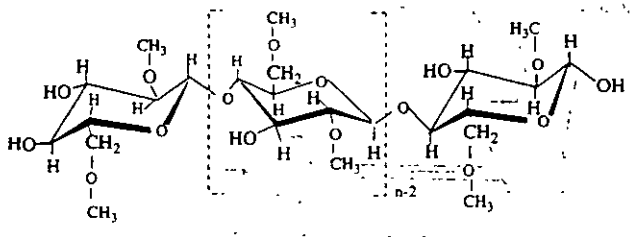

Fig. 5. Molecular structure of methylcellulose (The Dow Chemical Company, 1988).

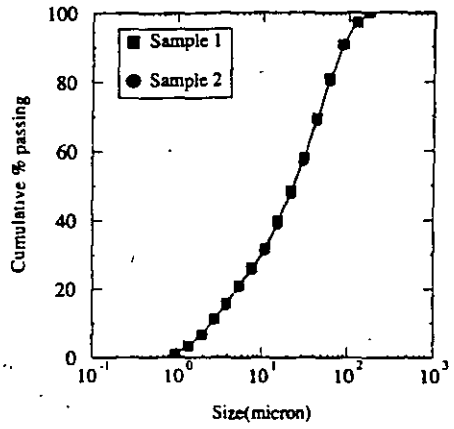

Fig. 6. Size distribution of the silica sample as determined by a Microtrac size analyzer. The sample was analyzed in duplicate, with excellent reproducibility.

for these solutions from the Bohlin viscometer and then finding the shear rates corresponding to the apparent viscosity values obtained from the Nametre viscometer.

(2) To verify the system's ability to detect non-Newtonian characteristics of fluids. This was accomplished by measuring the apparent viscosities of these solutions with the Nametre and the Brookfield viscometers respectively and then comparing the two apparent viscosity values.

2.5.3. Silica slurries

Ground silica at 99.9% purity was obtained from Ottawa Sands Company of Ottawa, Illinois. The size distribution as determined by a Microtrac size analyzer is given in Fig. 6. Several slurry samples were prepared, ranging from 0 to 70% silica by weight in distilled water.

3. Results and discussion

3.1. Determination of shear rates for the Nametre viscometer

Apparent Viscosity vs. shear rate plots obtained from the Bohlin viscometer were extrapolated to include the apparent viscosity values from the Nametre viscometer (Fig. 7). Then the shear rate corresponding to the apparent viscosity from the Nametre viscometer was obtained. As it can be seen from Fig. 7, this shear rate increases with a decrease in apparent viscosity. In this case the minimum shear rate corresponding to 2.0% Methocel solution (212 mPa·s) was 1500 sec^{-1}. This shows that even for high viscosity fluids, the Nametre viscometer operated at a very high shear rate compared to the Brookfield viscometer. Thus, readings from both the viscometers will give the viscosity values of any fluid at two extreme shear rates.

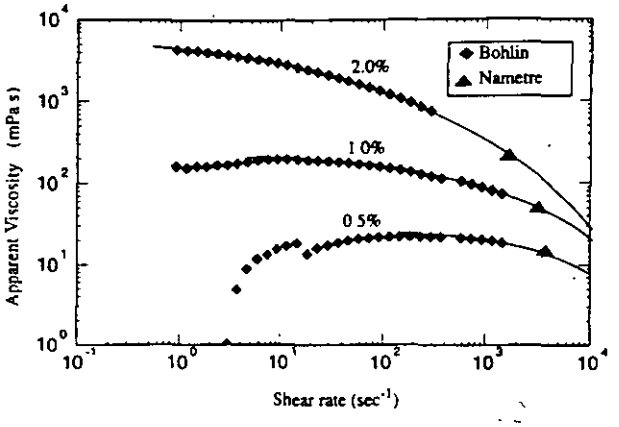

Fig. 7. Apparent viscosity vs. shear rate curves for Methocel A4M solutions at different concentrations, generated by the Bohlin viscometer. Apparent viscosity values from the Nametre viscometer plotted on these curves show that at higher viscosity the Nametre operates at lower shear rate. At very low shear rates, these solutions do not show pseudoplasticity (The Dow Chemical Company, 1988) and for solutions with lower concentrations, this shear rate above which the solutions show pseudoplasticity increases. That is why Methocel solution at a concentration of 0.5% and 1.0% did not show pseudoplasticity at low shear rates.

3.2. Calibration of the system with known solutions

Apparent viscosities of sucrose solutions at concentrations of 10–60 wt% in water and Methocel A4M Solutions at 0.5, 1.0, 1.5, and 2.0 wt% concentrations in water were measured first by the Nametre viscometer and then by the Brookfield viscometer. While measuring the apparent viscosity of Methocel at 2.0% concentration with the Brookfield viscometer, a different spindle (LV #1) was used. This was necessary because the apparent viscosity of 2% Methocel was above 2000 mPa · s, which is too high to be measured by the UL adaptor. For the rest of the samples, the UL adaptor was used. The viscosity readings from the Nametre viscometer were plotted against the viscosity readings from the Brookfield viscometer (Fig. 8). Since sucrose solutions are Newtonian, viscosity readings from both the Nametre (high shear rate) and the Brookfield (low shear rate) viscometers are similar for these solutions, as shown by the line drawn at a slope of 45° and passing through the origin, which coincides with these points. But, the points obtained from tests with Methocel solutions lie below this line, which shows that for these solutions, apparent viscosity values obtained from the Nametre (high shear rate) viscometer are less than their corresponding values from the Brookfield (low shear rate) viscometer. This is expected from Methocel solutions, because these are pseudoplastic fluids (The Dow Chemical Company, 1988). This proves that the system could distinguish between Newtonian and non-Newtonian fluids.

3.3. Viscosity measurements for silica slurries

After calibrating the system with known Newtonian (sucrose) and non-Newtonian (Methocel) solutions, tests were conducted with silica–water slurries at different percent solids ranging from 10–70% by weight in water. Apparent viscosities of these slurries

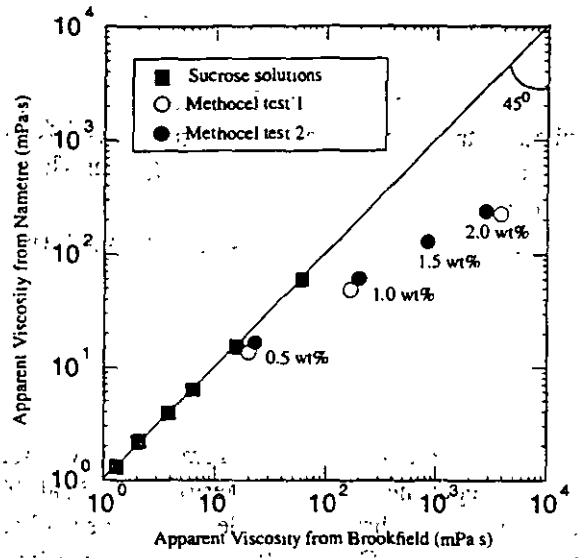

Fig. 8. Reading from Nametre viscometer vs. reading from Brookfield viscometer for sucrose solutions from 10 to 60 wt% and Methocel solutions from 0.5 to 2.0 wt% in water. Since sugar solutions have Newtonian flow properties, the points lie over a line drawn through the origin at a slope of 45°. Duplicate tests (test 1 and test 2) were conducted with Methocel solutions. These solutions are pseudoplastic and the points corresponding to these solutions lie below the line.

were measured by both the Nametre and Brookfield viscometers. The results are shown in Fig. 9. For all these slurries, viscosities obtained from both the viscometers are similar and a line drawn at a slope of 45° passes through these points. This shows that between 0–70% solids by weight the above slurries must have Newtonian flow properties.

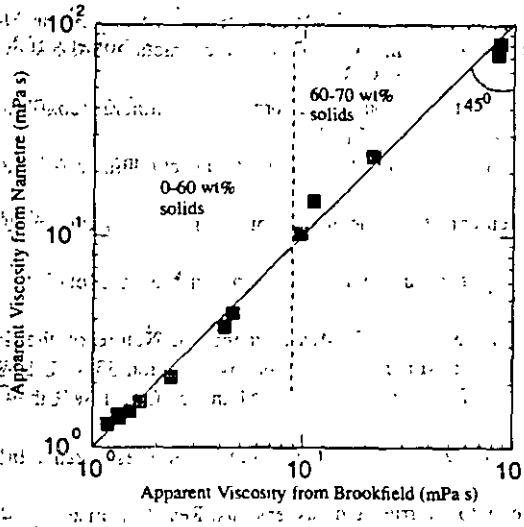

Fig. 9. Apparent viscosities of silica slurries at different % solids from Brookfield and Nametre viscometers. Since all the points lie over a line drawn through the origin at a slope of 45°, these slurries must have Newtonian flow properties.

4. Conclusions

The following conclusions were drawn from these tests:

(1) The system described in this article provides a simple method for characterizing mineral suspensions and liquids into Newtonian and non-Newtonian flow regions while also determining their viscosities.

(2) Between 0–70% solids by weight the slurry of ground silica (with the given size distribution) displayed Newtonian flow behavior.

Acknowledgements

Part of the funding for this project was obtained from the Dow Chemical Company, Midland, Michigan and the Department of the Interior's Mineral Institute program administered by the Bureau of Mines through the Generic Mineral Technology Center for Comminution under grant number G1125149. This paper was published without prior review by the Bureau of Mines.

References

Brookfield Engineering Laboratories, 1985. Assembly and Operating Instructions, UL Adaptor. Stoughton, MA 02072.

Clarke, B., 1967. Rheology of Coarse Settling Suspensions. Trans. Inst. Chem. Eng., 45: 7251–7256.

Fuerstenau, D.W., Venkataramana, K.S. and Velamakanni, B.V., 1984. Effect of chemical additives on the dynamics of grinding media in wet ball mill grinding. Int. J. Miner. Process., 15: 251–267.

Ferry, J.D., 1977. Oscillation viscometry — effects of shear rate and frequency. Meas. Control, 11(5): 89–91.

Hemmings, C.E. and Boyes, J.M., 1977. An on-line viscometry technique for improved operation and control of wet grinding circuits. In: 12th International Mineral Processing Congress, Sao Paulo, pp. 46–64.

Kawatra, S.K., Eisele, T.C. and Rusesky, M.T., 1992. Development of an on-line slurry viscosity monitoring system. In: S.K. Kawatra (Editor), Comminution—Theory and practice. Society of Mining, Metallurgy, and Exploration, Littleton, CO, Ch. 6, pp. 529–545.

Klimpel, R.R., 1982. Slurry rheology influence on the performance of mineral/coal grinding circuits. Parts I and II. Min. Eng., 34(12): 1665–1688; 35(1): 21–26.

Klien, B., Partrigdge, S.J. and Laskowski, J.S., 1990. Rheology of unstable mineral suspensions. Coal Prep., 8: 123–134.

Kiljanski, T., 1993. On the measurement of the rheological properties of unstable mineral suspensions. Coal Prep., 13: 107–112.

Reeves, T.J., 1985. On-line viscometer for mineral slurries. Trans. Inst. Min. Metall. Sect. C: Miner. Process. Extract. Metall., 94: C201–C208.

Schack, C.H., Dean, K.C. and Molly, S.M., 1957. Measurement and Nature of the Apparent Viscosity of Water Suspensions of Some Common Minerals. Report of Investigation 5334, U.S. Bureau of Mines.

The Dow Chemical Company, 1988. Technical Handbook, Methocel Cellulose Ether. The Dow Chemical Company, Midland, MI 48674.

Tucker, P., 1982. Rhelogical factors that affect the wet grinding of ores. Trans. Inst. Min. Metall., 91: 117–122.

Underwood, W.M., 1976. Viscometer for slurries and suspensions. Rev. Sci. Instrum., 47(9) 1079–1082.

Weast, R.C. (Editor), 1984. CRC Handbook of Chemistry and Physics, 65th Edition, CRC Press, Boca Raton, FL.

Australia, Brazil, Canada, Hong Kong, India, Israel, Japan, Malaysia, Mexico, New Zealand, Pakistan, PR China, Singapore, South Africa, South Korea, Taiwan, Thailand, USA. For all other countries airmail rates are available upon request. Claims for missing issues must be made within six months of our publication (mailing) date. Please address all your requests regarding orders and subscription queries to: Elsevier Science B.V., Journal Department, P.O. Box 211, 1000 AE Amsterdam, The Netherlands. Tel.: +31-20-4853642, fax: +31-20-4853598.

US mailing info – *International Journal of Mineral Processing* (ISSN 0301-7516) is published bimonthly by Elsevier Science B.V. (Molenwerf 1, P.O. Box 211, 1000 AE Amsterdam). Annual suscription price in the USA US$ 671.00 (valid in North, Central and South America), including air speed delivery. Application to mail at second class postage rate is pending at Jamaica, NY 11431.
USA POSTMASTERS: Send address changes to: *International Journal of Mineral Processing*, Publications Expediting, Inc., 200 Meacham Avenue, Elmont, NY 11003.
AIRFREIGHT AND MAILING IN THE USA by Publications Expediting, Inc., 200 Meacham Avenue, Elmont, NY 11003.

Advertising information
Advertising orders and enquiries may be sent to: Elsevier Science B.V., Advertising Department, P.O. Box 211, 1000 AE Amsterdam, The Netherlands, tel.: +31-20-4853796, fax: +31-20-4853810. Courier shipments to street address: Molenwerf 1, 1014 AG Amsterdam, The Netherlands. *In the UK*: TG Scott & Son Ltd., attn. Vanessa Bird, Portland House, 21 Narborough Road, Cosby, Leicestershire, LE9 5TA, UK, tel: 0116-2750521/2753333, fax: 0116-2750522. *In the USA and Canada*: Weston Media Associates, attn. Daniel Lipner, P.O. Box 1110, Greens Farms, CT 06436-1110, USA, tel: 203-2612500, fax: 203-2610101.

NOTE TO CONTRIBUTORS

A detailed Guide for Authors is available upon request. Please pay special attention to the following notes:

Language
The official language of the journal is English.

Preparation of the text
(a) The manuscript should preferably be prepared on a word processor and printed with double spacing and wide margins and include an abstract of not more than 500 words.
(b) Authors should use IUGS terminology. The use of S.I. units is also recommended.
(c) The title page should include the name(s) of the author(s), their affiliations, fax and e-mail numbers. In case of more than one author, please indicate to whom the correspondence should be addressed.

References
(a) References in the text consist of the surname of the author(s), followed by the year of publication in parentheses. All references cited in the text should be given in the reference list and vice versa.
(b) The reference list should be in alphabetical order.

Tables
Tables should be compiled on separate sheets and should be numbered according to their sequence in the text. Tables can also be sent as glossy prints to avoid errors in typesetting.

Illustrations
(a) All illustrations should be numbered consecutively and referred to in the text.
(b) Colour figures can be accepted providing the reproduction costs are met by the author. Please consult the publisher for further information.

Page proofs
One set of page proofs will be sent to the corresponding author, to be checked for typesetting/editing. The author is not expected to make changes or corrections that constitute departures from the article in its accepted form. To avoid postal delay, authors are requested to return corrections to the desk-editor, Mr. Herman E. Engelen, by FAX (+31-20-4852696) or e-mail (h.engelen@elsevier.nl), preferably within 3 days.

Reprints
Fifty reprints of each article are supplied free of charge. Additional reprints can be ordered on a reprint order form which will be sent to the corresponding author upon receipt of the accepted article by the publisher.

Submission of electronic text
Authors are requested to submit the final text on a 3.5" or 5.25" diskette. It is essential that the name and version of the word processing program, the type of computer on which the text was prepared, and the format of the text files are clearly indicated. Authors are requested to ensure that the contents of the diskette correspond exactly to the contents of the hard copy manuscript. If available, electronic files of the figures should also be included on a separate floppy disk.

Submission of manuscripts
Authors are requested to submit, with their manuscripts, the names and addresses of *four* potential referees. Manuscripts should be submitted in triplicate; those originating in North and South America should be sent to D.W. Fuerstenau, and all other manuscripts should be submitted to J. Cases (addresses are given on the inside front cover). Illustrations: Please note that upon submission of a manuscript that three sets of all photographic material printed sharply on glossy paper or high-definition laser prints must be provided to enable meaningful review. Photocopies and other low-quality prints will not be accepted for review.
The indication of a fax and e-mail number on submission of the manuscript could assist in speeding communications. The fax number for the Amsterdam office is +31-20-4852696.
Submission of an article is understood to imply that the article is original and unpublished and is not being considered for publication elsewhere.